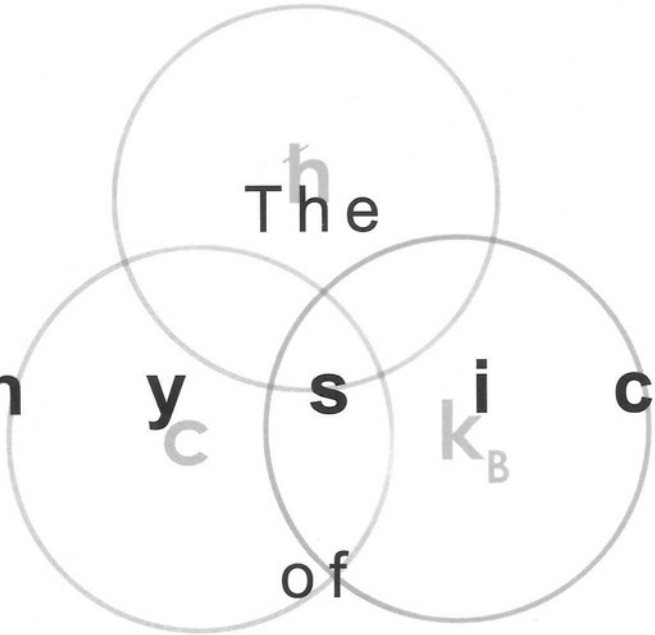

Physics of Communication

Proceedings of the XXII Solvay Conference on Physics

I Antoniou

V A Sadovnichy

H Walther

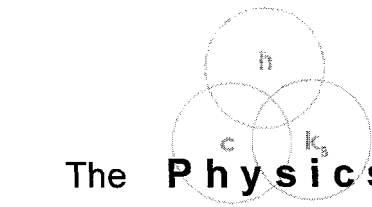

The Physics of Communication

XXII SOLVAY CONFERENCE ON PHYSICS

Delphi and Lamia, Greece, 24-29 November 2001

G. LEUCHS M. LUKIN R.Y. CHIAO S. METENS L. REICHL P. SIAFARIKAS L. STODOLSKY A. KARLSSON K. GUSTAFSON S.KIM V. KADYSHEVSKY G. ORDONEZ I. ZISIS G. DIMAKIS A. DIMAKIS

G. TSAKLIDIS R. PASSANTE S. DOLEV A. ELITZUR C. KARANIKAS S. PASCAZIO D. XOURIS M. COURBAGE E. YAREVSKY Yu. MELNIKOV A. SISSAKIAN G. ZENG

E. KARPOV V. LETOKHOV L. WANG W.S. SCHLEICH J.-M. RAIMOND A. STEINBERG G. NIMTZ E. POLZIK N. SOURLAS T. PETROSKY C. DASKALOYANNIS M. FLORATOS SI SI T. HIDA V.V. BELOKUROV

L. VAIDMAN Vi.. KOCHAROVSKY O. KOCHAROVSKAYA M. GADELLA A. BOHM G. PRONKO L. ACCARDI V. GURZADYAN S. LLOYD G. HEGERFELDT P. STAMP P. ZOLLER

Front row: A. ZEILINGER B. MISRA Y. NE'MAN E.C.G. SUDARSHAN I. PRIGOGINE J. SOLVAY H. WALTHER H.J. KIMBLE M. RAIZEN N. THEOFANOUS I. ANTONIOU T. DURT

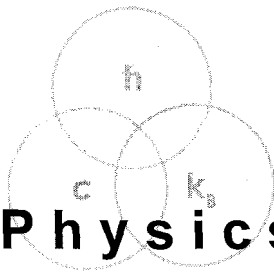

The Physics of Communication

Proceedings of the XXII Solvay Conference on Physics

Delphi Lamia, Greece 24 – 29 November 2001

edited by

I Antoniou
(International Solvay Institutes for Physics and Chemistry, Belgium & Aristotle University of Thessaloniki, Greece)

V A Sadovnichy
(Lomonosov Moscow State University, Russia)

H Walther
(University of Munich, Germany & Max-Planck-Institute for Quantum Optics, Germany)

World Scientific
New Jersey • London • Singapore • Hong Kong

Published by

World Scientific Publishing Co. Pte. Ltd.

5 Toh Tuck Link, Singapore 596224

USA office: Suite 202, 1060 Main Street, River Edge, NJ 07661

UK office: 57 Shelton Street, Covent Garden, London WC2H 9HE

British Library Cataloguing-in-Publication Data
A catalogue record for this book is available from the British Library.

THE PHYSICS OF COMMUNICATION
Proceedings of the XXII Solvay Conference on Physics

ISBN 981-238-449-9

Printed in Singapore by World Scientific Printers (S) Pte Ltd

CONTRIBUTORS TO THE PROCEEDINGS
OF THE XXII SOLVAY CONFERENCE ON PHYSICS

L. Accardi
University of Rome
Centro V. Volterra
Via di Tor Vergata
I-00133 Rome, Italy

I. Antoniou
Dept. of Mathematics
Aristoteles University of Thessaloniki
54006, Thessaloniki, Greece
and
International Solvay Institutes for Physics and Chemistry
ULB, Campus Plaine – CP 231
Boulevard du Triomphe
1050, Brussels, Belgium

V.V. Belokurov
Institute for Mathematical Study of Complex Systems
Lomonosov Moscow State University
Vorobievyi Gori
Moscow 119899, Russia

A. Bohm
University of Texas at Austin
Department of Physics
Center for Particle Theory, RLM 9.324A
Austin, Texas 78712-1081, USA

G. Casati
Dean
University of Insubria of Como
Via Valleggio 11
22100 Como, Italy

K. Chatzisavvas
Department of Physics
Aristotle University of Thessaloniki
54006 Thessaloniki, Greece

R. Chiao
Department of Physics
University of California at Berkeley
366 Le Conte Hall # 7300
Berkeley, CA 94720-7300, USA

I. Cirac
Max-Planck Institute fuer Quantenoptik
Hans-Kopfermann Str. 1
85748 Garching, Germany

C. Daskaloyannis
Department of Physics
Aristotle University of Thessaloniki
54006 Thessaloniki, Greece

S. Dolev
The Program for History and the Philosophy of the Sciences
Unit of Interdisciplinary studies
Bar-Ilan University
52900 Ramat-Gan, Israel

A. Ekert
Department of Physics
University of Oxford
Clarendon Laboratory
Parks Road
Oxford OX1 3PU, U.K.

A. Elitzur
Weizmann Institute of Science
PO Box 26
Rehovot 76100, Israel

D. Ellinas
Department of Sciences
Section of Mathematics
Technical University of Crete
GR-73 100 Chania Crete, Greece

M. Gadella
Departamento de Fisica Teorica
Facultad de Ciencias
University of Valladolid
Real de Burgos, s.n.
47011 Valladolid, Spain

V.G. Gurzadyan
ICRA, Dipartimento di Fisica
Universita di Roma "La Sapienza"
00185 Rome, Italy
and Yerevan Physics Institute
375036 Yerevan
Armenia

K. Gustafson
Department of Mathematics
University of Colorado
Campus Box 395
Boulder, Colorado 80309-0395, USA

G. Hegerfeldt
Institut für Theoretische Physik
University of Göttingen
Bunsenstrasse 9
D-37073 Göttingen, Germany

K. Imafuku
Centro Vito Volterra
Facolta di Economia
Universita di Roma "Tor Vergata"
Via Columbia 2
00133 Roma, Italy

L. Jacak
Institute of Physics
Technical University of Wroclaw
Wybrzeze Wyspianskiego 27
50-370 Wroclaw, Poland

I. Kanter
Department of Physics
Bar-Ilan University
Ramat Gan 52900, Israel

A. Karlsson
Department of Microelectronics and Information Technology
Laboratory of Quantum Electronics and Quantum Optics
Royal Institute of Technology (KTH)
Electrum 229
S-164 40 Kista, Sweden

S. Kim
University of Texas at Austin
Department of Physics
Austin, Texas 78712, USA

H. J. Kimble
California Institute of Technology, 12-33
Quantum Optics, Laboratory of Physics
Pasadena, CA 91125, USA

O. Kocharovskaya
Department of Physics
Mailstop 4242

Texas A&M University
College Station, TX 77843-4242, USA

Vi. Kocharovsky
Department of Physics
Texas A&M University
College Station, TX 77843-4242, USA

V. S. Letokhov
Institute of Spectroscopy of Russian Academy of Sciences
Troitsk, Moscow Region
142092 Russian Federation

G. Leuchs
University Erlangen-Nürnberg
Staudtstrasse 7 / B2
91058 Erlangen, Germany

S. Lloyd
Dept. of Mechanical Engineering
Massachusetts Institute of Technology
77 Massachusetts Avenue
Cambridge, MA 02139-4307, USA

M. Lukin
Physics Department
Lyman Laboratory
Harvard University
17 Oxford Street
Cambridge, MA 02138, USA

G. Metakides
Director IST - DG INFSO
European Commission
Avenue de Beaulieu 29 – 7/10
B-1160 Brussels, Belgium

S. Metens
Laboratoire de Physique Theorique de la Matiere Condensee
Université de Paris 7
Case Postale 7020
2, Place Jussieu
F-75231 Paris Cedex 05, France

B. Misra
International Solvay Institutes for Physics and Chemistry
ULB, Campus Plaine – CP 231
Boulevard du Triomphe
1050 Brussels, Belgium

K. Moelmer
University of Aarhus
Institute for Physics and Astronomy
Building 520
Ny Munkegade
DK-8000 Aarhus, Denmark

Y. Ne'eman
Professor Emeritus of Physics, TAU
Tel-Aviv University
Ramat Aviv
Tel Aviv 69978, Israel

G. Nimtz
University of Cologne
Institute of Physics
Zulpicher strasse 77
D-50937 Cologne, Germany

G. Ordonez
Center for Studies in Statistical Mechanics and Complex Systems, RLM 7.220
University of Texas at Austin
Austin, Texas 78712, USA

Ch. Panos
Department of Theoretical Physics
Aristoteles University of Thessaloniki
Thessaloniki 54006, Greece

S. Pascazio
Department of Physics
University of Bari
Via Amendola 173
I-70126 Bari, Italy

R. Passante
IAIF-CNR
Via Ugo La Malfa 153
I-90146 Palermo, Italy

T. Petrosky
Center for Studies in Statistical Mechanics and Complex Systems, RLM 7.220
University of Texas at Austin
Austin, Texas 78712, USA

E. Polzik
University of Aarhus
Institute of Physics and Astronomy
Building 520
Ny Munkegade

DK-8000 Aarhus, Denmark

I. Prigogine
International Solvay Institutes for Physics and Chemistry
ULB, Campus Plaine – CP 231
Boulevard du Triomphe
1050, Brussels, Belgium

J.-M. Raimond
Laboratoire Kastler Brossel
Département de Physique
Ecole Normale Supérieure
24, rue Lhomond
75005 Paris Cedex 05, France

M. Raizen
Department of Physics
The University of Texas at Austin
Austin, Texas 78712, USA

L. Reichl
Center for Studies in Statistical Mechanics and Complex Systems, RLM 7.220
University of Texas at Austin
Austin, Texas 78712, USA

W. P. Schleich
Abt. fuer Quantenphysik
Universitat Ulm
D-89069 Ulm, Germany

N. Sourlas
Departement de Physique
Ecole Normale Supérieure
24, rue Lhomond
75231 Paris Cedex 05, France

Prof. P. Stamp
Canadian Institute for Advanced Research and Physics Dept.
University of British Columbia
6224 Agricultural Rd.
Vancouver, B.C., Canada V6T 1Z1

A. Steinberg
Department of Physics
University of Toronto
60 George Street
Toronto, Ontario, Canada M5S 1A7

L. Stodolsky
Werner-Heisenberg-Institut

Fohringer Ring 6
80805 Munich, Germany

E.C.G. Sudarshan
Department of Physics, RLM 9.328A
University of Texas at Austin
Austin, Texas 78712, USA

L. Vaidman
Physics and Astronomy Faculty
Tel Aviv University
PO Box 39040
Tel Aviv 69978, Israel

H. Walther
Sektion Physik
University of Munich
Am Coulombwall 1
D-85748 Garching, Germany

L. Wang
NEC Research Institute Inc.
4 Independence Way
Princeton, New Jersey 08540, USA

A. Zeilinger
Institut für Experimentalphysik
University of Vienna
Boltzmanngasse 5
Wien 1090, Austria

G. Zeng
Theoretische Quantendynamic
Fakultat für Physik
Universitat Freiburg
H-Herder-Strasse 3
D-79104 Freiburg, Germany

P. Zoller
University of Innsbruck
Institut für Theoretische Physik
Technikerstrasse 25
A-6020 Innsbruck, Austria

ADMINISTRATIVE COUNCIL OF THE

INTERNATIONAL INSTITUTES FOR PHYSICS AND CHEMISTRY, FOUNDED BY E. SOLVAY A.S.B.L.

J. Solvay	President of the Administrative Board
F. Bingen	Vice-President of the Administrative Board
I. Prigogine	Director of the Solvay Institutes
I. Antoniou	Deputy Director of the Solvay Institutes
F. Lambert	Secretary of the Administrative Board
A. Bellemans	Secretary of the Scientific Committee of Chemistry
M. Henneaux	Secretary of the Scientific Committee of Physics
D. Janssen	
A. Jaumotte	
R. Lefever	
G. Nicolis	
J.-M. Piret	
I. Veretenicoff	
N. Schamp	Consultant for the Administrative Board

SCIENTIFIC COMMITTEE OF PHYSICS OF THE

INTERNATIONAL INSTITUTES FOR PHYSICS AND CHEMISTRY, FOUNDED BY E. SOLVAY A.S.B.L.

A. ABRAGAM
Professeur Honoraire au Collège de France
Rue d'Ulm, 3
75005 Paris, France

P. W. ANDERSON
Dept. of Physics
Princeton University
Princeton, NJ 08511, USA

F. T. ARECCHI
Directeur
Istituto Nazionale de Ottica Applicata
Large E. Fermi 6
I-50125 Florence, Italy

A. BOHM
University of Texas at Austin
Department of Physics
Center for Particle Theory, RLM 9.324A
Austin, Texas 78712-1081, USA

C. COHEN-TANNOUDJI
Laboratoire Kastler Brossel, Département de Physique
Ecole Normale Supérieure
24, rue Lhomond
75231 Paris Cedex 05, France

L. FADDEEV
Steklov Mathematical Institute
Fontanka 27
St. Petersburg 191011, Russia

M. HENNEAUX
Département de Physique
Université Libre de Bruxelles, CP 231
Bd. du Triomphe
1050 Bruxelles, Belgium

I. M. KHALATNIKOFF
Russian Academy of Sciences
Landau Institute of Theoretical Physics
2 Ul Kozygina, V 334
Moscow 117 940, Russia

Y. NE'EMAN
Sackler Institute for Advanced Study
Tel-Aviv University
Ramat Aviv
Tel Aviv 69978, Israel

R.Z. SAGDEEV
East West Place Science Center
(Room 3373)
University of Maryland
College Park, MD 20742, USA

G. SETTI
European Southern Laboraory
2, Karl-Schwarzschild-Strasse
D-8046 Garching-bei-München, Germany

E.C.G. SUDARSHAN
Department of Physics, RLM 9.328A
University of Texas at Austin
Austin, Texas 78712, USA

G. t'HOOFT
Spinoza Institute
Utrecht University
PO Box 80-195
NL 3508 TD Utrecht, Netherlands

S.C TONWAR
Tata Institute for Fundamental Research
Homi Bhabba Marg, Navy Nagar
Colaba, Bombay 400 005, India

H. WALTHER
Max-Planck-Institute für Quantenoptik
D-8046 Garching-bei-München, Germany

HONORARY COMMITTEE

E. Venizelos	Minister of Culture, Hellenic Republic
J. Solvay	President, International Solvay Institutes for Physics and Chemistry
I. Prigogine	Director, International Solvay Institutes for Physics and Chemistry
G. Mitsopoulos	President, Academy of Athens
T. Patrikios	President, Society for the Hellenic Cultural Inheritance
V. Exarchos	General Secretary for Central Greece
S. Alachiotis	Rector, University of Patras
G. Babiniotis	Rector, National and Kapodistrian University of Athens
P. Lazaridis	Rector, University of Thessalia
T. Lekkas	Rector, University of the Aegean
C. Massalas	Rector, University of Ioannina
M. Papadopoulos	Rector, Aristoteles University of Thessaloniki
K. Simopoulos	Rector, Demokritus University of Thrace
T. Xanthopoulos	Rector, National and Technical University of Athens

HELLENIC SCIENTIFIC COMMITTEE

Prof. I. Antonopoulos	Vice Rector Aristotle University of Thessaloniki
Prof. K. Daskaloyannis	Department of Physics Aristotle University of Thessaloniki
Prof. M. Floratos	Demokritos Research Center and Department of Physics University of Athens
Prof. C. Karanikas	Department of Mathematics Aristotle University of Thessaloniki
Prof. D. Kravvaritis	Chairman Department of Applied Mathematics and Physics National Technical University of Athens
Prof. N. Theofanous	Department of Informatics University of Athens
Prof. Th. Tomaras	Department of Physics University of Crete

LOCAL ORGANISING COMMITTEE

Mr. V. Exarchos	General Secretary of Central Greece Region
Mr. T. Bellos	Prefect of Fthiotida
Mrs. M. Karayanni	Prefecture of Fthiotida
Mr. G. Kotronias	Mayor of Lamia
Prof R. Kotronia	Lamia Town Hall
Mr. I. Zisis	Solon Cultural Center
Prof. K. Anastasiou	President Technological Education Institute of Lamia
Prof. Th. Kontogeorgos	Technological Education Institute of Lamia

THE SOLVAY CONFERENCES ON PHYSICS

The Solvay conferences started in 1911. The first conference on radiation theory and the quanta was held in Brussels. This was a new type of conference and it became the tradition of the Solvay conference; the participants are informed experts in a given field and meet to discuss one or a few mutually related problems of fundamental importance and seek to define the steps for the solution.

The Solvay conferences in physics have made substantial contributions to the development of modern physics in the 20th century.

1. (1911) "Radiation theory and the quanta"
2. (1913) "The Structure of the matter"
3. (1921) "Atoms and electrons"
4. (1924) "Electric Conductivity of Metals"
5. (1927) "Electrons and photons"
6. (1930) "Magnetism"
7. (1933) "Structure and properties of the atomic nuclei"
8. (1948) "Elementary particles"
9. (1951) "Solid state"
10. (1954) "Electrons in metals"
11. (1958) "The structure and evolution of the Universe"
12. (1961) "The quantum theory of fields"
13. (1964) "The structure and evolution of galaxies"
14. (1967) "Fundamental problems in elementary particle physics"
15. (1970) "Symmetry properties of nuclei"
16. (1973) "Astrophysics and gravitation"
17. (1978) "Order and fluctuations in equilibrium and non-equilibrium statistical mechanics"
18. (1982) "High energy physics. What are the possibilities for extending our understanding of elementary particles and their interactions to much greater energies?"
19. (1987) "Surface science"
20. (1991) "Quantum Optics"
21. (1998) "Dynamical systems and irreversibility"
22. (2001) "The Physics of Communication"

For more information, visit the website of the Solvay Institutes
http://solvayins.ulb.ac.be

This page intentionally left blank

PREFACE

This volume includes papers presented at the XXII Solvay Conference on Physics, which took place from the 24 to 29 November 2001 in the European Culture Centre of Delphi. The Castle of Lamia hosted the events of the last day.

The Physics of Communication was the selected theme of the conference. The 5 sessions reflected present challenging issues, namely Decoherence and Irreversibility, Non-locality and Superluminosity, Photonics, Quantum Information and Communication, Quantum Computation. The lively discussions, which followed the reports, have been recorded and are included after the presentations

The realisation of the XXII Solvay Conference was possible thanks to the complete spiritual and financial support of the Ministry of Culture of the Hellenic Republic and the personal interest of the Minister, Professor Evangellos Venizelos.

The excellent organisation is due to the professional and personal care of the personnel and the Director of the European Cultural Centre, Prof. V. Karasmanis, in collaboration with the administrative support and active interest of Dr. A. Soulogianni, Director of Educational Affairs of the Ministry of Culture.

The key catalyst for the organisation and success of the Conference was Mr. K. Gouvalas, Director of the Minister's office.

The idea to organise the XXII Solvay Conference in Central Greece came spontaneously during a friendly meeting of one of us (Ioannis Antoniou) with Mr. T. Bellos, prefect of Fthiotis, Mr. G. Kotronias, Mayor of Lamia, Prof. K. Anastasiou, President of the Technological Education Institute of Lamia and Mr. Y. Zisis, representative of "Solon" Cultural Foundation. Afterwards, they honoured their commitment with active interest, continuous support and personal involvement.

Thanks to the initiative and support of the Ministry of Culture, the internationally recognised pianist, Vinia Tsopela, Professor of the University of Macedonia, performed Hadjidakis and Chopin at the opening, thus creating a marvellous atmosphere.

V. Dimitropoulos, Professor of Mathematics, and his group of amateur dancers performed traditional Hellenic dances in an original way during the banquet.

Dr. E. Yarevsky and Dr. S. Metens kindly helped in the scientific aspects of the organisation.

The heavy organisational details were arranged thanks to the coordinated effort of several people. In particular we mention Mrs. Anne De Naeyer, from the Solvay Institutes, Mrs. A. Gotsi from the European Cultural Center, Mr. M. Kostakis and E. Tsekoura from the Ministry of Culture, Mrs. M. Karayanni from the Prefecture of Fthiotis, Prof. R. Kotronia, Director of the office of the Mayor of Lamia, Mrs. I. Moutsopoulou-Zisi, Mr. A. Belesis, Mr. I. Paraskevolakos, Mr. N. Theodorakis, Mr. P. Katsoulakos, Mr. D. Sarinakis and Mr. G. Mavrouleas from Solon Cultural Foundation.

The conference could be observed in real time, via the Internet, thanks to the kind sponsoring of the Hellenic Telecommunications Organisations (OTE and COSMOTE). Mr. A. Dimakis,

Mr. G. Dimakis and Mr. Y. Zisis coordinated the teleconference effort. During the conference, about 2000 visits have been registered.

The T.V. broadcasting and interviews were arranged by Mr. Y. Zisis (STAR Lamia Channel) and by Mr. P. Savidis (National Channel ET 3). The presentations in ET3 have been repeated more than 10 times during the following year at the request of the public. Mr. Y. Zisis, in addition to overall support, arranged also the press releases and the publicity. About 10 articles were devoted to the conference. The whole publicity effort was coordinated by Mr. A. Dimakis.

For the security of the conference, the Prefectural Police of Fokis and Fthiotis took special care. The Prefectural Hospitals of Fokis and Fthiotis were also especially available on a 24 hours basis. The General Secretary of Central Greece, Mr. V. Exarchos kindly arranged for that. We were very happy to know about these measures and most happy not to use them.

Finally, we gratefully acknowledge the enthusiastic support of Mr. J. Solvay and Prof. I. Prigogine.

I. Antoniou V. A. Sadovnichy H. Walther

PROLOGUE

by Minister E. Venizelos

It is with special pleasure to see that this edition completes the effort to prepare and realise the XXII Solvay Conference on Physics, which has been hosted by the Ministry of Culture in the European Cultural Centre of Delphi with great success.

We had the opportunity to attend leading scientists presenting and discussing the new impressive possibilities in Physics, which are expected to re-shape communication in the years to come. I was especially pleased to welcome Ilya Prigogine, Nobel Laureate, key founder of chaos theory and Mr. Jacques Solvay, President of the Solvay Institutes. It is well known that the Solvay conferences shaped the path of physics in the 20th century, as so many mythical personalities like Albert Einstein, Max Planck, Marie Curie, Niels Bohr, Werner Heisenberg, actively participated in these conferences. It is a common secret that the Solvay conferences have also served as a platform for the Nobel Prizes.

Progress in physics and chemistry in the 20th century has been intertwined during the last ninety years with the activities of the Solvay Institutes. The XXII Solvay Conference on Physics marks the passage and continuation of the Solvay Conferences into the 21st century. This edition will be one more stepping stone in the history of science. In this sense, the Ministry of Culture of the Hellenic Republic is specially satisfied to contribute to this important scientific progress, by organising and supporting the XXII Solvay Conference on Physics.

CONSEIL DE PHYSIQUE SOLVAY

BRUXELLES 1911

Photo Couprie, Bruxelles

GOLDSCHMIDT PLANCK RUBENS LINDEMANN HASENOHRL
NERNST BRILLOUIN SOMMERFELD DE BROGLIE HOSTELET
SOLVAY KNUDSEN HERZEN JEANS RUTHERFORD
LORENTZ WARBURG WIEN EINSTEIN LANGEVIN
PERRIN Madame CURIE POINCARÉ KAMERLINGH ONNES

OPENING ADDRESS BY J. SOLVAY

Ladies and Gentleman,

It is a great pleasure and honour to open the 22nd Solvay Conference on Physics. It is a special day for me. From October 30 till November 3, 1911, the first Solvay conference took place in Brussels nearly 90 years ago. The theme of the first conference was Radiation and Quanta. This is now the first Solvay conference in the XXI century. I am also very pleased that this conference takes place in Greece. Our presence here is a tribute to the role of Greek science and philosophy in the Western worldview.

Since 90 years, there has been an enormous change in science, as well as in the interaction between science and society. For a long time, science appeared as a highly specialized field, an elitistic occupation. For Einstein, scientists were people who wanted to escape the vicissitudes of every day life. Today science is permeating all our life, especially fields such as communication and molecular biology.

My great grand father, Ernest Solvay was confident that sciences will lead to an improvement of the human condition. He was a man of multiple interests, equally attracted by Physics, Chemistry, Physiology and Sociology. The possible role of science in the present society is a conflictual subject. Is this really an occasion for the improvement of human condition or is science bringing us closer to apocalypse? We can only guess what the future may be. It is still likely that science, communication especially, will permit us to reach a more multicultural and less conflicting society.

The Solvay conferences have been, in the past, exceptionally successful. Heisenberg has written: "The Solvay Meetings have stood as an example of how much well-planned and well-organised conferences can contribute to the progress of science". I am sure that this conference will be as successful as the preceding ones. It was often said that the people who came together at the Solvay conferences went then to Stockholm to receive the Nobel Prize. This is somewhat exaggerated, but there is some truth to it.

Here is the photograph of the first Solvay meeting, where we see Mrs Curie, Poincaré, Einstein, and many other famous people, who received indeed the Nobel Prize.

Thank you.

OPENING REMARKS BY I. PRIGOGINE

Dear colleagues, authorities, friends,

I first want to thank the Greek authorities for their magnificent hospitality we receive here. I specially want to thank my colleague and friend, Professor Ioannis Antoniou, who has organised the conference. I want also to thank the local committee, which has made the arrangements and all participants, who will, I am convinced, make this conference a success.

As Mr. Solvay mentioned, the first meeting was exactly ninety years ago in Brussels. The subject of this first conference was "electrons and photons". In a sense, the present conference continues the problems studied in the first conference as it deals largely again with interactions, with the matter, as light. In the 20th century, we have attended the birth of a new Physics. The progress realized is amazing. There was a feedback between progress in science and the Solvay conferences. Thanks to this progress, we had very interesting Solvay conferences and conversely the Solvay conferences contributed to the development of new results in science. The progress has been such that many physicists say "We are now at the end of the golden age, we are at the end of creative Physics. How could we imagine something else of comparable importance after the achievement of the 20th century?" The last frontiers would be the high-energy physics, cosmology or the brain. I have heard this suggested by a few very famous physicists. I personally don't believe it. I think there is a kind of autocatalytic character in the evolution of science. More we discover and more we are likely to discover. So much has been discovered in the 20th century. This is for me an indication that we shall all make, in the future again, new fundamental discoveries. Take the problem of communication. How many aspects have we missed? The first aspect, which I want to emphasize, is the relation between communication and irreversibility. It is clear that the situation, after we receive a message, is different from the one which was existing before the communication was established. We obtain new information and this new information will contribute to the decision we take for the future. Let me emphasize that, in my view, the flow of time, the arrow of time is not due to the fact that the communication is first prepared and then received, like we prepare breakfast and then we eat it. On the contrary, it is because there is an arrow of time in the universe that we first prepare our breakfast, to eat it later. In

this sense, of course, communication is closely related to the measurement problem and to the problem of the time symmetry breaking. There is still the dilemma how this universe, which is obviously an evolutionary universe, can be ruled by time reversible laws like classical dynamics or quantum theory. This problem is now more than 20 years old and still is discussed because of the dilemma between the static dynamical view, which was predominated as in Boltzmann's time, and the evolutionary view at the basis of thermodynamics. In most books you still find that the arrow of time is due to our approximations. I could never believe in this because if the arrow of time is a very fundamental property of our universe, which cannot be due to any approximation or to ignorance, then we should introduce it as a basic law of nature. Communication involves transmission of information. The discussions about information remain at the operational level. As far as I can see, only by understanding the dynamical foundation of entropy can we hope to give a sense to information. It is interesting that in many fields we encounter instabilities, manifesting in classical theory as chaos or in quantum theory as decoherence. Also there is a general movement from a static equilibrium view of nature to a fluctuating unstable evolutionary view. Communication is also a problem of great actuality because computer communication has, of course, been of great importance in recent times. Conversion to quantum computing has been expected by many scientists. Therefore, the problem of communication is far from being in a satisfactory state. Many aspects have to be elucidated. In general, my feeling is that we are not at the end of Physics. We are only at the beginning of developing new methods, which require new Physics and also new Mathematics. There is also something special about the problem of communication which is so close to human problems of our time. Professor Metakides will certainly say something about this in his address. Communication is at the basis of the evolution of civilization. An example in European history is communication between Islamic knowledge and European knowledge in the middle age. History has brought us to a stratified, stable world. Communication has hopefully to play a role in the various cultures, which are existing today, and bringing them closer together. Communication extends, of course, to larger and larger scales. Larger scales involve stronger and stronger non-linearities. Communication is both a basic scientific problem and a basic human problem. Let's hope that the human aspect of communication will improve the life of society in the 21st century.

It is difficult to imagine a more illustrious assembly. The discussions were passionate. Quantum theory and relativity were just born and had still to be incorporated in the general frame of science.

I would like to thank my friend, Ilya Prigogine, as well as Professor Antoniou, for having proposed, with the agreement of the scientific committee, the subject: "Physics of communication".

On one side, it corresponds to the technical interests of our time. There is a relation with non-linear optics and semi-conductors. On the other hand, over the last years, astonishing news has circulated in the scientific press. There is a new phenomenon called super luminosity which connects with the possibility of delaying or even stopping light. Information can be communicated by quantum teletransport. Quantum correlations lead to the creation of the quantum computers. This demonstrates that contrary to what has been stated in many places, we are far from being at the end of Science. But seen from my perspective, observing from the outside, we are at a new beginning of science in the sense of a different approach from that of 1911 and the personalities on the photograph.

There is also another aspect close to the heart of my friend, Professor Prigogine. Communication requires a distinction between before and after. There is an arrow of time involved. How this arrow of time brought us into the fundamental physics, is still a controversial subject. This is a favourite theme of the scientific research performed at the Solvay Institutes in Brussels. I shall not go into details, as Prigogine will undoubtedly develop this theme in his lecture.

In conclusion, I want to thank the participants for coming here. My gratitude goes also to the local organizing committee for their efforts. I would like also to thank the European Cultural Centre of Delphi for the traditional Hellenic hospitality we have received in this magnificent place, as well as the Ministry of Culture and the Government of the Hellenic Republic for their genuine interest and kind support, which have made this conference possible.

Thank you.

CHALLENGES IN AMBIENT INTELLIGENCE (A TRIBUTE TO CLAUDE SHANNON AND MICHAEL DERTOUZOS)

GEORGE METAKIDES

Director of Essential Information Society Technologies and Infrastructures, DG Information Society, European Commission

Introduction

I would like to outline in this paper a number of the reflections that are currently ongoing as part of the planning of the next phase of European research funding for what we called Information Society Technologies, or, if you prefer, Information and Communication Technologies (ICTs).

Support for Information Society Technologies is part of a broader political initiative that was launched by the Heads of the EU Member States at the summit of March 2000 in Lisbon. This date is significant because it was about two weeks before the collapse of the NASDAQ market, synonymous with the collapse of most of the technology stocks and much of the euphoria that surrounded all the related exuberant visions.

So, the first question to be asked is the following: is the general context still valid today or was it mostly hype, does it all still make sense?

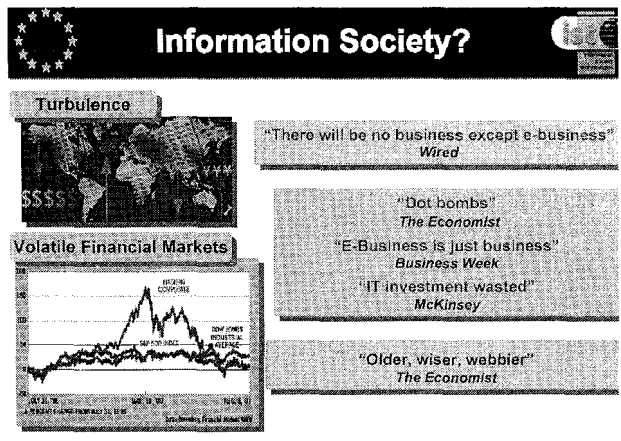

FIGURE 1

What happened in a very short period is that we went from this euphoria of the land of milk, honey and dot-coms to a land of turbulence and uncertainty. One may recall some famous adages of the period of euphoria (see Figure 1), like *"There will be no business except e-business"* (Wired magazine). And then, in the era of turbulence, dot-coms have turned themselves into *"dot-bombs"* and *"e-business"* has become *"just business"*. More recently, in early November 2001, McKinsey published a report even questioning whether many of the *"information technology investments"* by companies might have been *"wasted"*!

So, what happened to the vision, what happened to the expectations? Was it really all smoke? I do not think so. I believe that as the pendulum swings again now, the reality is

that: we are all becoming *"older"* (certainly true), *"wiser"* (debatable), (but certainly) *"webbier"*. If this is rephrased in Shannon's terms it becomes: there was a lot of noise in the channel, a lot of that noise was the hype, but the message is still there and it is as valid as ever.

In this paper, we argue the case for the validity of the message by looking at the intersection between the planning at the European level mentioned above and the topics of interest to this conference.

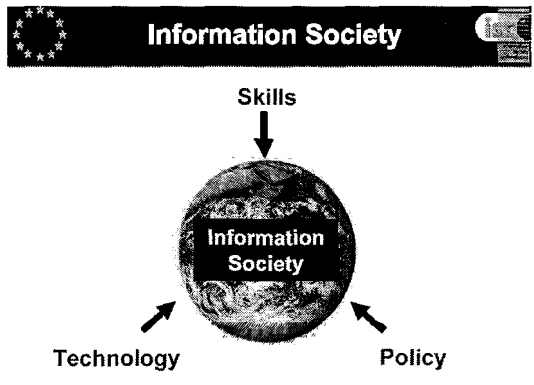

FIGURE 2

The general approach of the planning can be represented in the form of a triptych (see Figure 2).

Technology is one part of it, but it goes together with policy, and in the end, to make it all happen, with human resources and skills.

Policy initiatives

The main policy initiative addressing the development of the Information Society is "eEurope", which was launched by the Lisbon Summit in 2000 (see Figure 3). This has now been extended by the so-called "eEurope+" initiative to embrace all the Candidate Countries for accession in the EU as well. For research the approach is today realised through the

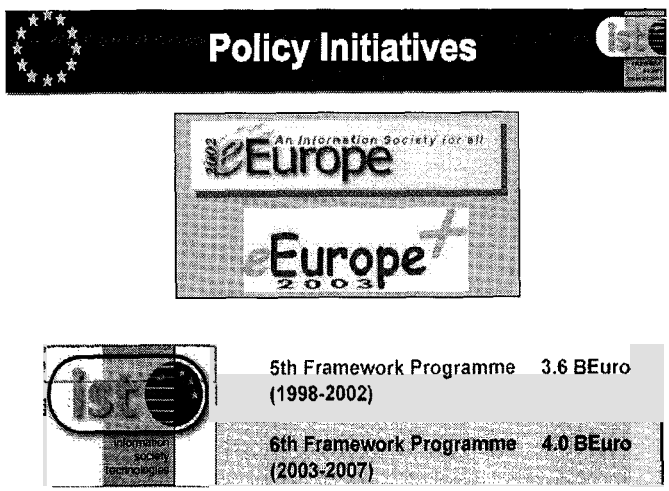

FIGURE 3

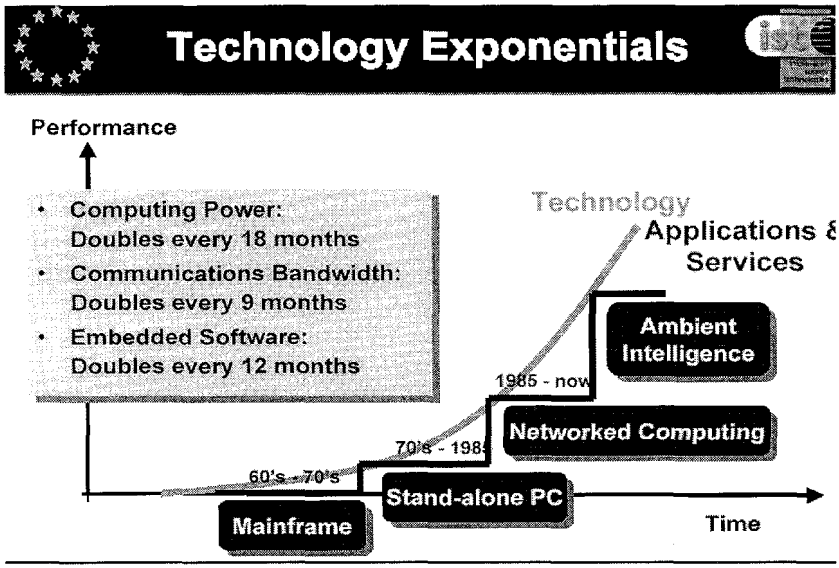

FIGURE 4

current Information Society Technologies Programme (running under the 5th EU Framework Programme for RTD, 1998-2002). It will be continued in the new Information Society Technologies Programme that will run for the period 2003-2006, as part of the 6th EU Framework Programme that is currently under preparation.

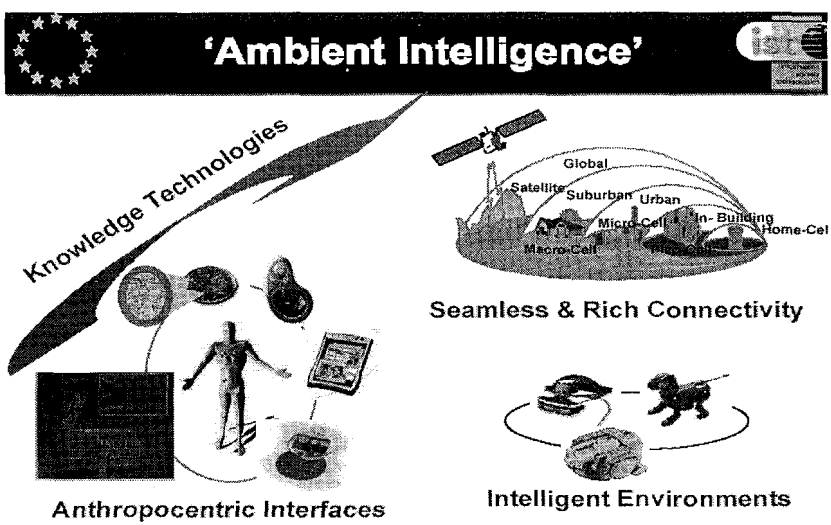

FIGURE 5

Technology

As far as ICT technology progress is concerned, I fully share here the view of Ilya Prigogine: we are not at the end, but at the very beginning of a digital revolution. Or, to quote Michael Dertouzos, "we haven't seen anything yet".

In particular, we are only at the very beginning of the digitalisation of the economy; this is indeed a revolution that will continue to bring changes through to the end of this decade and even much longer. The pace of technological advance will continue to gallop under the so-called "exponential laws" (e.g. Moore's Law), with computing, communication and storage capabilities doubling every 18, 9 & 12 months respectively (see Figure 4).

Whilst technology is advancing exponentially, applications and services follow much quicker than ever before, but they are developing in a step-wise fashion, in the shape of a series of alternating jumps and plateaux. The jumps are caused by the advent of disruptive technologies that change the rules of the game. Their cusps are synonymous with huge business opportunities for capturing new markets or extending existing ones through the development and deployment of whole new families of innovative products, applications and services. History shows that those who wait for the plateaux find only monopolised or commoditised marketplaces.

To illustrate the above, the following example from the IT sector can be used: the shrinking of processors permitted us to move from the mainframe era (60's and 70's), to the stand-alone PC era (from the 70's until 1985). Then came the shrinking of laser technology, which enabled the Internet as we know it. This gave rise to a new plateau, that of networked computing.

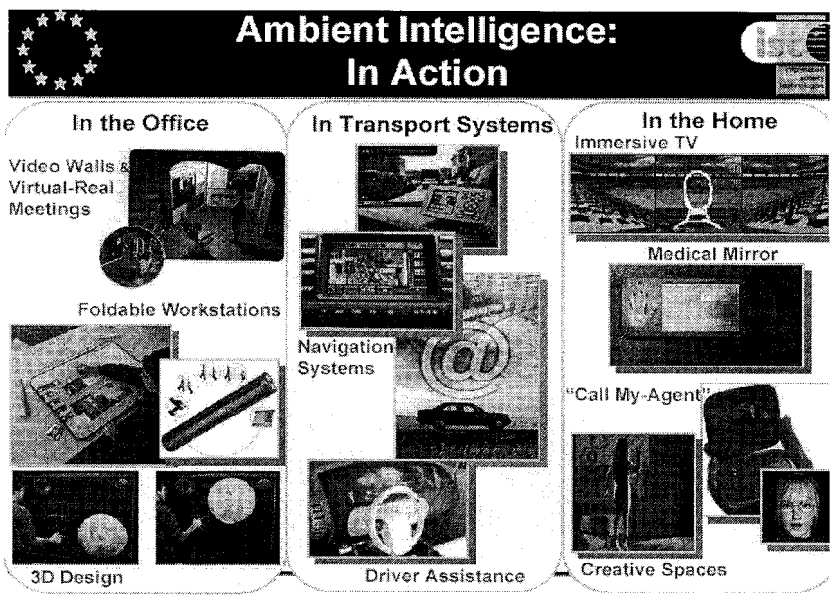

FIGURE 6

The plateau that is coming next is brought about by a new vision. It can be attributed again to a kind of shrinking, that is the shrinking of sensors and actuators of all kinds and to the recent advances in embedded software. Their combination will allow the creation of an environment of ambient intelligence (see Figure 5).

The main technology building blocks that are underneath this new environment of ambient intelligence are as follows.

- **Seamless communication networks**, spanning from the personal area to the regional and global area. Seamless communications, be that through fixed wired or wireless telephony, wireless LANs, mobile telephony or through satellites.
- A new generation of what Michael Dertouzos would call **anthropocentric interfaces**: interfaces that will enable us to communicate with computing and networking systems through our senses in a most intuitive and natural manner as opposed to artefacts that we have today. Interfaces that will increase the usability of such systems and enhance/substitute for our senses.
- **Intelligent environments** enabled by computing embedded in any/every physical object in our surroundings and with everything linked together through seamless communication networks.
- And a new family of *intelligent systems* based on a new generation of **knowledge technologies,** binding everything together and removing the complexity of human interaction with information technology.

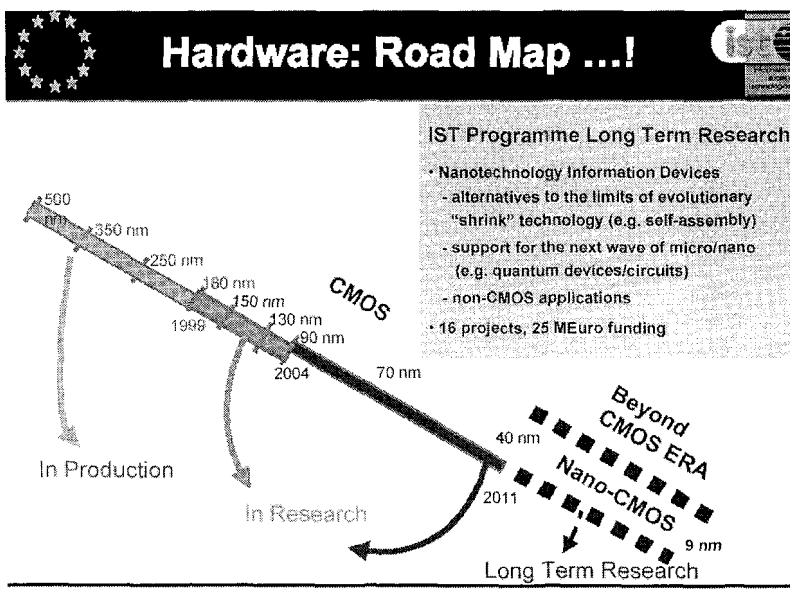

FIGURE 7

Given the above, how will this new vision of Ambient Intelligence materialise in practice? Some representative examples are shown in Figure 6. The illustrations of this figure are not an attempt to provide a futuristic vision, since each one of these items exist already today as prototypes in laboratories. The only thing that prevents many of these prototypes to go to the market is the business case, the business model, not the technology as such.

- *Video walls, virtual-real meetings*: a truly new generation of video conferencing technology. You are at a meeting table with people around in front of you. You are able to communicate with them effectively as if they are sitting next to you in the same room, in fact you are led to believe they are present in the same room, but they are actually located at several remote locations.
- *Foldable workstations*: by folding up the screen, they become your new computing and networking environment.
- *Navigation schemes* in all kinds of transport systems and *new driver assistance systems* for assisting car driving under difficult traffic or weather conditions or at night.
- *Immersive television.* For watching exhibitions and shows from your TV, as if you were physically present there and for choosing any viewing angle you wish.
- *The medical mirror* aimed in particular for handicapped or aged people that need health monitoring at home. Practically all the basic health measurements and monitoring can take place at home, without the patients staying in the hospital more than what is necessary.
- And then, the *Call-My-agent* sort of example, where you just order what you want to be done rather than keying it into the keyboard.

All the above examples support the message that scientific and technological advance and applications go now hand in hand, but also that we are still at the very primitive stage in these technologies.

But what is underneath these technologies to support their exponential advance? In the case of computing, there is a fairly clear roadmap – see Figure 7. This roadmap is based on what is known as Moore's law: the memory size or the number of transistors on chip is doubling every 18 months. In fact, the first part of the roadmap is based on the miniaturisation advances of CMOS technology. It is the world of the so-called *"shrinkers"*. But then, there comes a point around year 2010-2011 where a switch is expected to take place and to move from the shrinkers to the *"thinkers"*. Namely, this is at the stage where what before was considered as noise (in Shannon's terms) becomes now a useful signal: the quantum effects.

There is a lot of basic research that the Community is funding in the area of understanding quantum effects and using them to build the next generation of computing and networking. This is supported by the Future and Emerging Technologies part of the IST Programme and is expected to be strengthened even more in the IST Programme under the 6th Framework Programme.

But there exists a roadblock. It is not related to technology advances in hardware but to progress in software. As mentioned before, in microelectronics, according to the law of Moore, computing power is doubling every 18 months. This corresponds to a compound annual growth rate of 58 % (see graph of figure 8). In order to keep pace with this growth, geometric structures are getting so small that small-scale effects must be considered. Despite the use of advanced CAD tools, the growth in design productivity as measured by the International Technology Roadmap for Semiconductors is only 21 % CAGR, massively below the growth in system complexity. Another cause of design gaps is coming from shrinking product lifetimes. Time-to-market is becoming so important that now it alone can sometimes determine the economic success. The systems are more complex but have to be designed in shorter time. This again is shown in the productivity map of Figure 8. Bridging this productivity gap is one of the major challenges of this

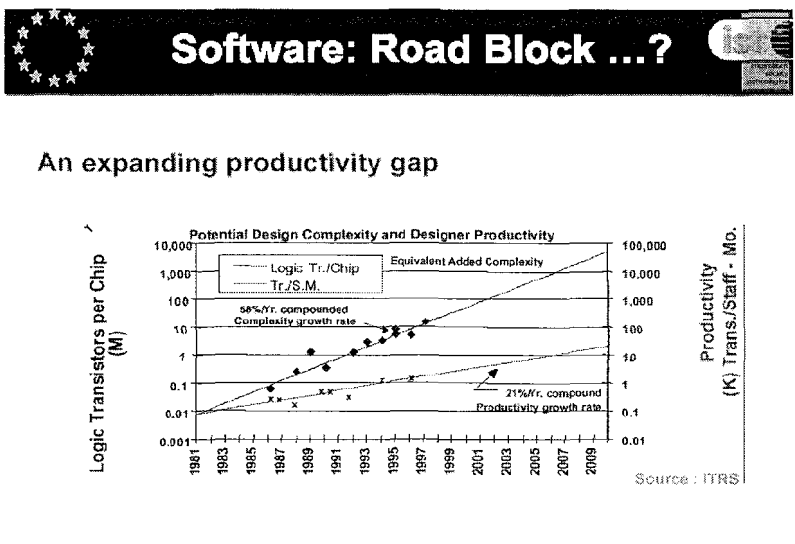

FIGURE 8

decade for realising the vision, especially when one also considers the advances expected by the next generation of computing, quantum computing: it will factor a 1000 digit number in a fraction of a second and is going to undo the whole basis of cryptography as we know it today.

All the above related to the computing side, but what is going to happen on the networking side? Seamless communications and broadband access everywhere: by meshing all sorts of different communication networks, whether these are fixed telephony networks, fixed wireless networks, 3rd generation mobile networks, wireless LANs or whatsoever. Indeed, within this decade, the integration of fixed and mobile, all-IP, communication infrastructures and their interconnection and interoperability will permit

the seamless roaming of data and services and their access from anywhere at anytime. These will be provided not only through PC-based but notably also through digital TV as well as through mobile communication platforms. This in its turn will contribute to opening up demand for a whole new generation of broadband applications and services.

The above do not represent just a quantitative advance but also a qualitative one, because then the network will become the computer, in the sense of **grids**. The easiest example one can use today is the sharing of computing power by some 3.5 million PC's to try and decipher space signals – that is the *SETI @ home* initiative. Similar efforts are also under way for environmental modelling and other "peer-to-peer" platforms.

And then there are all the activities which, in terms of complexity, one would call the tera-world, like protein folding that is foreseen to be at the origin of the next revolution in medicine. A protein folds in nature in about 20 milliseconds. To simulate it today using the most powerful computer may take 40 months. The interconnection and inter-working of the most advanced computing systems may permit to satisfy soon the requirements of the tera-world, like these computations in proteomics. This is expected to come, again, within this decade.

So, one aspect is that the network will become the computer, the other aspect is that the network will become the system, within a **distributed control architecture**. In this case, one is referring to complex non-linear systems, where control does not mean what it used to be, where it is impossible to control everything completely all the time, where

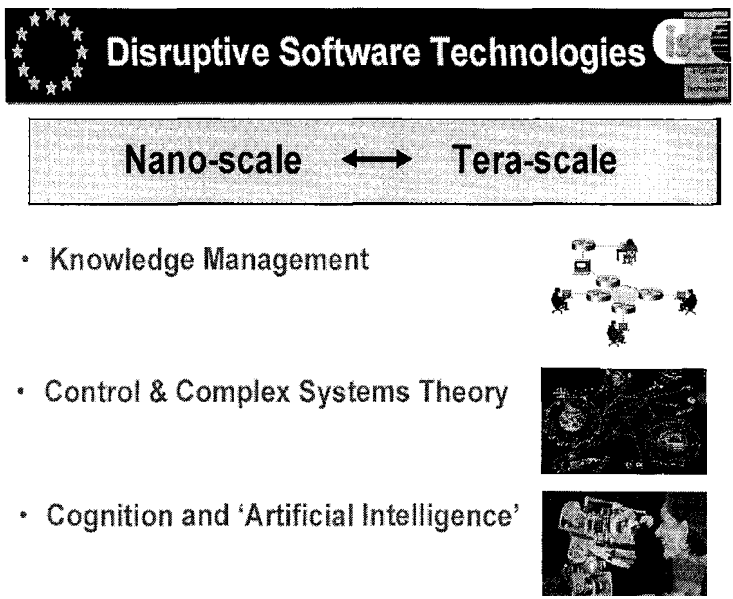

FIGURE 9

proceeding by model decomposition and model reduction techniques is no longer sufficient. There, totally new techniques mainly coming from the theory of complex systems must be devised to serve.

Once again, the roadblock is found in the underlying knowledge technologies, which are needed both for the nano-scale, in the case of nanotechnology, and for the tera-scale, in the case of networking. What is needed in fact is **disruptive software technologies**, in the sense that they represent the discontinuity with respect to what it is possible to do today (see Figure 9). Such disruptive software technologies will have to deal mainly with the following.

- *Knowledge management*: dealing with huge databases, efficient data representation and data handling, including intelligent data mining and data retrieval.
- *Complex non-linear hybrid dynamic systems*, capable of co-operating and interacting with each other.
- And finally, with so-called *cognition technologies*, perception and vision technologies and the new generation of **artificial intelligence**. A few years ago artificial intelligence was sort of swept away as itself a hype. Now it is coming back with a vengeance and, combined with new enabled cognition techniques, it will provide a third ingredient in what is needed to realise the vision of ambient intelligence, as a platform for all the applications to come.

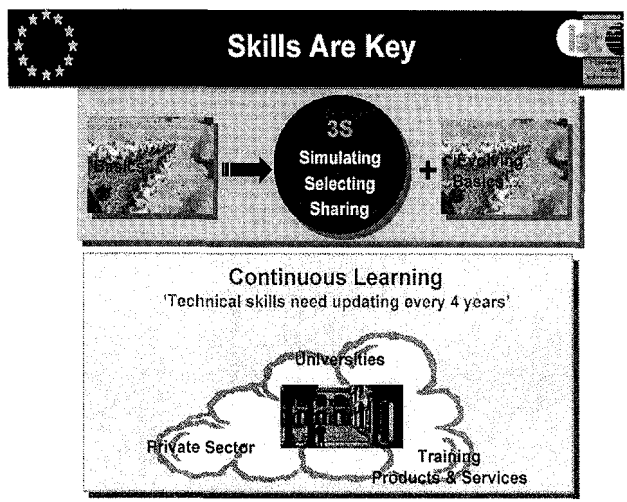

FIGURE 10

Skills

To make the above happen, it is clear that there is needed a generation of people having skills which is not at the moment available and producible by existing educational systems.

The simplest perhaps adjustment is going from the basics, be that scientific or as an engineer or as a citizen in the information society, to a set of evolved basics – these are the so-called 3Ss (see Figure 10):

- *simulation* in the sense of modelling physical and industrial processes and phenomena,
- *selection* of information out of plethora of what is available,
- and *sharing* information and communicating it in the basic human sense.

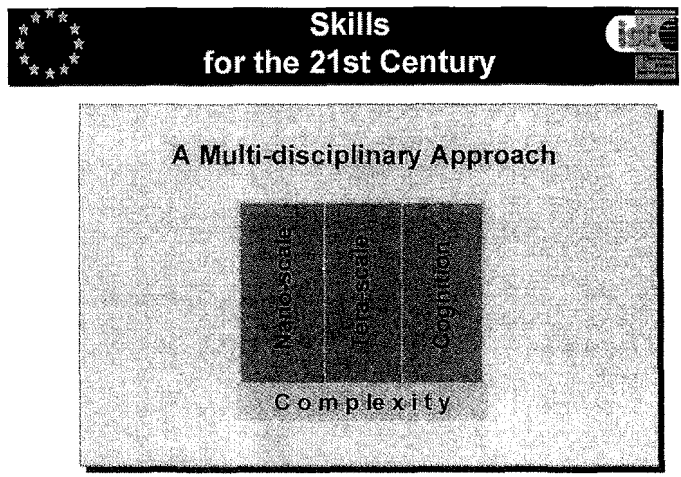

FIGURE 11

Furthermore, there is no single technology today where its underlying knowledge foundations – from the lower technician level to the most advanced computer science or microelectronics application – have not an expiration date of more than 4 years. As an example one can mention all those people who thought that, having learnt Oracle and C++ would provide a job for a life as a well-paid programmer. This was true five years ago but certainly it is not any more today.

We are now entering the world of continuous learning and training and one has to question what will happen. Can universities, as we know them today, remain the sole and exclusive portrayer of professional training? I do not believe so. Certainly, universities should and will remain the keepers of truth and beauty, and at the core of scientific research. But as far as professional and vocational training are concerned, there seem to be many other actors – the private sector and commercial services – that come, using the technologies themselves, to play a role.

So to caricature, the argument, we can say, is that the skills needed for the 21st century can be categorised in four areas (see Figure 11):

1. skills required for dealing with the nano-world,
2. skills for addressing the problems of the tera-world,
3. cognition skills providing the glue,

4. and finally, all the above must be underpinned by complex system theory and the techniques emanating from it, because in every single category such a context is valid.

Conclusions

At several points in this paper I made reference to Claude Shannon and Michael Dertouzos (Figure 12). This was done deliberately, because I wished to use this occasion to honour them. It is also because each one had a direct impact on my personal work and thinking:

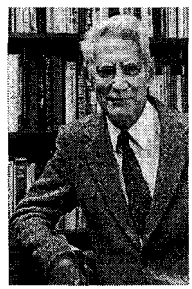

Michael Dertouzos
1936 - 2001

Claude Shannon
1916 - 2001

FIGURE 12

- Claude Shannon as my initiator in my student days to that most elegant foundation of digital communication theory.
- Michael Dertouzos as a spiritual brother and a visionary, who saw and anticipated the bridge between basic research and applications, and, perhaps more importantly, the bridge – a sort of luminous arc – between technology and humanism. He made extensive reference to this in his final book "The unfinished revolution": The enlightenment, some 300 years ago – perhaps unnecessarily, perhaps accidentally – separated technology and humanism. It is perhaps time to see if these two can be brought back together.

It was meant to be that both Claude Shannon and Michael Dertouzos left us in 2001. It is now up to us to carry their vision forward.

This page intentionally left blank

CONTENTS

Non-Locality and Superluminosity

Photonics

Quantum Information and Communication

Quantum Computation

STOCHASTICITY AND TIME SYMMETRY BREAKING IN HAMILTONIAN DYNAMICS

I. PRIGOGINE
S. KIM, G. ORDONEZ AND T. PETROSKY
Center for Studies in Statistical Mechanics and Complex Systems, The University of Texas at Austin, Austin, TX 78712 USA
and
International Solvay Institutes for Physics and Chemistry, CP231, 1050 Brussels, Belgium

In recent years, we have introduced a new type of transformation operator Λ, leading to irreversible kinetic equations from dynamics, both classical and quantum. In our approach we have no loss of information, since the Λ transformation is invertible. In this paper we consider classical mechanics. Our transformation is obtained by an extension of the canonical (unitary) transformation operator U that eliminates interactions. While U can be constructed for integrable systems in the sense of Poincaré, for nonintegrable systems there appear divergences in the perturbation expansion, due resonances. The removal of divergences leads to the Λ transformation. This transformation is "star-unitary". Star-unitarity for non-integrable systems is an extension of unitarity for integrable systems. In addition, Λ is non-distributive with respect to products of dynamical variables. This gives fluctuations usually associated with noise in phenomenological equations such as the Langevin equation.

1 Introduction

Communications play today a basic role. Communications require irreversibility and stochasticity. A part of our communication with the outside world involves the interaction between molecules and light. The emission and absorption of light quanta (photons) can be formulated as a superposition of irreversible processes (see the article "Microscopic entropy flow and entropy production in resonance scattering" in this issue).

Communication requires stochasticity as well. We distinguish good and bad communications. It is very often related to information, noise, entropy, and measured by bits. These two aspects, irreversibility and stochasticity, are not explicit in the fundamental equations of dynamics. Our aim has been to formulate a new form of dynamics that makes explicit irreversibility and stochasticity. The first question is to which form of dynamics this formulation may apply. Very briefly, the distinction is between integrable and non-integrable systems.

2 Integrable and non-Integrable systems

Suppose we have a system of particles with Hamiltonian

$$H = H_0 + \lambda V, \qquad H = H(p, q) \tag{1}$$

where H_0 is the unperturbed Hamiltonian describing non-interacting particles, and V is the interaction. We assume the coupling constant λ is dimensionless. We consider mainly classical systems, but our statements apply as well to quantum

systems. The Hamiltonian is a function of the momenta p and positions q of the particles. Often one introduces a new set of variables $J = J(p,q)$, $\alpha = \alpha(p,q)$ (action-angle variables) such that

$$H_0 = H_0(J), \qquad V = V(J,\alpha) \tag{2}$$

This means that when there is no interaction between the particles ($\lambda = 0$) the energy H only depends on the action variables J.

Integrable systems are systems for which we can go to a new representation $J \Rightarrow \bar{J}$, $\alpha \Rightarrow \bar{\alpha}$ such that

$$H = \bar{H}_0(\bar{J}) \tag{3}$$

The Hamiltonian can be written as a new function $\bar{H}_0$ depending only on the new actions. Typically, $\bar{H}_0$ will have the same form as H_0, but with renormalized parameters (such as frequencies).

The change of representation is expressed as a "canonical transformation" U,

$$\bar{J} = U^{-1}J, \qquad \bar{\alpha} = U^{-1}\alpha \tag{4}$$

The operator U is "unitary", $U^{-1} = U^{\dagger}$, where we define Hermitian conjugation through the inner product

$$\langle\langle f|\rho\rangle\rangle = \int d\Gamma f^*(\Gamma)\rho(\Gamma). \tag{5}$$

which is the ensemble average of f.[a] Here Γ is the set of all phase space variables, $d\Gamma$ is the phase-space volume element and $*$ means complex conjugate. The Hermitian conjugate is defined by

$$\langle\langle f|U\rho\rangle\rangle = \langle\langle \rho|U^{\dagger}f\rangle\rangle^* \tag{6}$$

The operator U is distributive with respect to products. For any two variables A and B we have [3]

$$UAB = (UA)(UB) \tag{7}$$

This property together with Eq. (3) lead to

$$UH(J,\alpha) = U\bar{H}_0(\bar{J}) = \bar{H}_0(U\bar{J}) = \bar{H}_0(J) \tag{8}$$

The transformed Hamiltonian UH is the unperturbed Hamiltonian $\bar{H}_0$ depending only on the original action variables. In other words, U eliminates interactions.

For non-integrable systems there exist, by definition, no transformation U. This happens, for example, when there appear divergences (divisions by zero) when we try to construct U as an expansion in the coupling constant λ (called "perturbation expansion"). Vanishing denominators appear when frequencies of the systems become equal. We have "Poincaré resonances" leading to divergences [4],

$$\frac{1}{\omega_1 - \omega_k} \to \infty \quad \text{for } \omega_1 \to \omega_k \tag{9}$$

We define now a transformation Λ with the following properties:

[a] One can introduce a Hilbert-space structure in classical mechanics through the Segal-Bargmann representation [1,2].

(1) The Λ transformation is obtained by analytic extension of the unitary operator U.
(2) When there are no resonances, Λ reduces to U.
(3) Λ is analytic with respect to the coupling constant λ at $\lambda = 0$.
(4) Λ preserves the measure of the phase space.
(5) Λ maps real variables to real variables.
(6) Λ leads to closed Markovian kinetic equations.

Our method corresponds to the elimination of Poincaré resonances on the level of distributions satisfying the Liouville equation

$$i\frac{\partial}{\partial t}\rho = i\{H, \} = L_H\rho \tag{10}$$

This extension of U is obtained by regularization of the denominators,

$$\frac{1}{\omega_1 - \omega_k} \Rightarrow \frac{1}{\omega_1 - \omega_k \pm i\epsilon} \tag{11}$$

where ϵ is an infinitesimal. As discussed below, the sign of $i\epsilon$ is determined by a time ordering depending on the correlations that appear as the particles interact. The regularization breaks time symmetry.

The Λ transformation permits us to find new units obeying kinetic equations. Indeed, applying the Λ transformation to the equations of motion, we discover irreversibility and stochasticity. Irreversibility appears because of the analytic continuation of U (from real to complex frequencies) and stochasticity because of the non-distributive property

$$\Lambda AB \neq (\Lambda A)(\Lambda B) \tag{12}$$

Hence we have fluctuations. Irreversibility and stochasticity are closely related to Poincaré resonances [5,6,7]. Non-distributivity also yields new uncertainty relations in quantum mechanics. For example, for the Hamiltonian we have, in general [8,9],

$$\Lambda H^2 \neq (\Lambda H)^2 \tag{13}$$

This leads to an uncertainty relation between energy and lifetime of unstable states.

We introduce the new distribution function $\tilde{\rho} = \Lambda\rho$ into Eq. (10). Then we obtain

$$i\frac{\partial}{\partial t}\tilde{\rho} = \tilde{\Theta}\tilde{\rho} \tag{14}$$

where

$$\tilde{\Theta} = \Lambda L_H \Lambda^{-1} \tag{15}$$

This is a kinetic equation describing irreversible stochastic phenomena. This equation in general contains diffusive terms, which map trajectories to ensembles. We have an intrinsically statistical formulation in terms of probabilities.

The next section will be devoted to a brief description of the main steps involved in the construction of the Λ transformation (more details can be found in Refs. [9,10] and references therein for quantum mechanics, and in Ref. [2] for classical mechanics).

3 Construction of the Λ transformation

Our formulation is based on the "dynamics of correlations" induced by the Liouville equation [11]. The Liouville operator $L_H = L_0 + \lambda L_V$ is separated into a part describing free motion $L_0 = i\{H_0, \}$ and an interaction $\lambda L_V = i\{\lambda V, \}$. We then define correlation subspaces by decomposing the density operator ρ into independent components

$$\rho = \sum_\nu P^{(\nu)}\rho \tag{16}$$

where $P^{(\nu)}$ are projectors to the orthogonal eigenspaces of L_0

$$L_0 P^{(\nu)} = P^{(\nu)} L_0 = w^{(\nu)} P^{(\nu)} \tag{17}$$

$w^{(\nu)}$ being the real eigenvalues of L_0. The projectors are orthogonal and complete:

$$P^{(\mu)}P^{(\nu)} = P^{(\mu)}\delta_{\mu\nu}, \qquad \sum_\nu P^{(\nu)} = 1 \tag{18}$$

The complement projectors $Q^{(\nu)}$ are defined by

$$P^{(\nu)} + Q^{(\nu)} = 1 \tag{19}$$

They are orthogonal to $P^{(\nu)}$, i.e., $Q^{(\nu)}P^{(\nu)} = P^{(\nu)}Q^{(\nu)} = 0$, and satisfy $[Q^{(\nu)}]^2 = Q^{(\nu)}$.

As seen in Eq. (17) the unperturbed Liouvillian L_0 commutes with the projectors. Therefore the unperturbed Liouville equation is decomposed into a set of independent equations,

$$i\frac{\partial}{\partial t}P^{(\nu)}\rho = L_0 P^{(\nu)}\rho = w^{(\nu)}P^{(\nu)}\rho \tag{20}$$

The interaction λL_V induces transitions from one subspace to another subspace. To each subspace $P^{(\nu)}$ we associate a "degree of correlation" d_ν: we first define the vacuum of correlation as the set of all distributions belonging to the $P^{(0)}$ subspace. This subspace by definition has a degree of correlation $d_0 = 0$. Usually this subspace has the eigenvalue $w^{(0)} = 0$, i.e., it contains the invariants of unperturbed motion. The degree of correlation d_ν of a subspace $P^{(\nu)}$ is then defined as the minimum number of times we need to apply the interaction L_V on the vacuum of correlations $P^{(0)}$ in order to make a transition to $P^{(\nu)}$. Dynamics is seen as a dynamics of correlations.

Our method involves the extension of U to Λ, from integrable to nonintegrable systems. This is applicable to systems, which, depending on certain parameters, can be either integrable or non-integrable in the sense of Poincaré. For example, a system contained in a finite box with periodic boundary conditions will have a discrete spectrum of frequencies. We can then avoid any resonances. The system is integrable, and we can construct U by perturbation expansions. However, when we take the limit of an infinite volume, the spectrum of frequencies becomes continuous and resonances are unavoidable. The system becomes non-integrable in Poincaré's sense, as the perturbation expansion of U gives divergent terms. We can remove the divergences by regularization of the denominators, obtaining the Λ transformation.

Let us consider first integrable systems, where we may introduce the canonical transformation U that eliminates the interactions. In the Liouvillian formulation the relation (8) gives

$$UL_HU^{-1} = \bar{L}_0 \tag{21}$$

Namely, the transformed Liouvillian is the unperturbed Liouvillian $\bar{L}_0 = i\{\bar{H}_0, \}$. Similar to L_0 we have

$$\bar{L}_0 P^{(\nu)} = P^{(\nu)} \bar{L}_0 = \bar{w}^{(\nu)} P^{(\nu)} \tag{22}$$

where $\bar{w}^{(\nu)}$ are renormalized eigenvalues. In the U representation there are no transitions from one degree of correlation to another.

We write U in terms of "kinetic operators" (we use bars for the integrable case)

$$\begin{aligned} \bar{\chi}^{(\nu)} &\equiv P^{(\nu)} U^{-1} P^{(\nu)} \\ \bar{C}^{(\nu)} \bar{\chi}^{(\nu)} &\equiv Q^{(\nu)} U^{-1} P^{(\nu)} \end{aligned} \tag{23}$$

We have as well the hermitian conjugate components

$$\begin{aligned} [\bar{\chi}^{(\nu)}]^\dagger &\equiv P^{(\nu)} U P^{(\nu)} \\ [\bar{\chi}^{(\nu)}]^\dagger \bar{D}^{(\nu)} &\equiv P^{(\nu)} U Q^{(\nu)} \end{aligned} \tag{24}$$

where $\bar{D}^{(\nu)} \equiv [\bar{C}^{(\nu)}]^\dagger$. The operators $\bar{C}^{(\nu)}$ and $\bar{D}^{(\nu)}$ are called, respectively, "creation" and "destruction" operators [6] as they can create or destroy correlations, leading to transitions from one subspace $P^{(\nu)}$ to a different subspace $P^{(\mu)}$. The $\bar{\chi}^{(\nu)}$ operator, on the other hand, is diagonal, as it leads to transitions within each subspace, i.e., it maps $P^{(\nu)}$ to $P^{(\nu)}$. Using Eq. (19) we obtain

$$U^{-1} P^{(\nu)} = (P^{(\nu)} + \bar{C}^{(\nu)}) \bar{\chi}^{(\nu)} \tag{25}$$

$$P^{(\nu)} U = [\bar{\chi}^{(\nu)}]^\dagger (P^{(\nu)} + \bar{D}^{(\nu)}) \tag{26}$$

Now, from the commutation relation in Eq. (22) we derive a closed equation for the $\bar{C}^{(\nu)}$ operators (see [12,9]):

$$\begin{aligned} \bar{C}^{(\nu)} = \sum_{\mu(\neq\nu)} P^{(\mu)} \frac{-1}{w^{(\mu)} - w^{(\nu)}} \\ \times [\lambda L_V P^{(\nu)} + \lambda L_V \bar{C}^{(\nu)} - \bar{C}^{(\nu)} \lambda L_V \bar{C}^{(\nu)}] \end{aligned} \tag{27}$$

We call Eq. (27) the *nonlinear Lippmann-Schwinger equation*. The $\bar{\chi}^{(\nu)}$ operators are obtained from the relation

$$P^{(\nu)} U U^{-1} P^{(\nu)} = P^{(\nu)} \tag{28}$$

which leads to [9]

$$\bar{A}^{(\nu)} = \bar{\chi}^{(\nu)} [\bar{\chi}(\nu)]^\dagger \tag{29}$$

where $\bar{A}^{(\nu)} \equiv (P^{(\nu)} + \bar{D}^{(\nu)} \bar{C}^{(\nu)})^{-1}$ (the inverse is defined in each subspace: $\bar{A}^{(\nu)} [\bar{A}^{(\nu)}]^{-1} = P^{(\nu)}$). The general solution of Eq. (28) is

$$\bar{\chi}^{(\nu)} = [\bar{A}^{(\nu)}]^{1/2} \exp(\bar{B}^{(\nu)}) \tag{30}$$

where $\bar{B}^{(\nu)} = -[\bar{B}^{(\nu)}]^\dagger$ is an arbitrary antihermitian operator. For the integrable case we have one more condition on U: the distributivity property Eq. (7). This condition fixes the operator $\bar{\chi}^{(\nu)}$ (see Appendix A). Note that for integrable systems the denominator in Eq. (27) is always non-vanishing: there are no Poincaré resonances.

Now we go to nonintegrable systems. Due to Poincaré divergence we cannot eliminate the interactions among particles through a canonical transformation. However we may still introduce a representation for which the dynamics is closed within each correlation subspace. We introduce the transformation Λ such that the transformed Liouvillian in Eq. (15) commutes with the projectors $P^{(\nu)}$

$$\tilde{\Theta} P^{(\nu)} = P^{(\nu)} \tilde{\Theta} \tag{31}$$

This allows us to obtain closed Markovian equations

$$i \frac{\partial}{\partial t} P^{(\nu)} \tilde{\rho} = \tilde{\Theta} P^{(\nu)} \tilde{\rho} \tag{32}$$

In contrast to the integrable case, the $P^{(\nu)}$ projectors are no more eigenprojectors of the transformed Liouvillian $\tilde{\Theta}$. Hence we can have transitions within each subspace. As we shall show, the Λ transformation makes a direct connection between dynamics and kinetic theory. The operator $\tilde{\Theta}$ is indeed a generalized "collision operator". Collision operators are familiar in kinetic theory. They are dissipative operators with complex eigenvalues, the imaginary parts of which give, for example, damping or diffusion rates. The Liouville operator is related to $\tilde{\Theta}$ through a similitude relation. This means that L_H itself has complex eigenvalues. This is possible because we are extending the domain of L_H to distributions outside the Hilbert space [13,14,9].

To construct Λ, the basic idea is to extend the canonical transformation U through analytic continuation. Similar to Eq. (25) we write Λ in terms of kinetic operators

$$\begin{aligned} \Lambda^{-1} P^{(\nu)} &= (P^{(\nu)} + C^{(\nu)}) \chi^{(\nu)} \\ P^{(\nu)} \Lambda &= [\chi^{(\nu)}]^\star (P^{(\nu)} + D^{(\nu)}) \end{aligned} \tag{33}$$

In order to avoid Poincaré divergences, Λ can no more be unitary. Instead, it is "star unitary"

$$\Lambda^{-1} = \Lambda^\star \tag{34}$$

where the $\star$ applied to operators means "star-hermitian" conjugation, defined below.

From the commutation relation Eq. (31) we arrive again at the equation (27) for the creation operator. But the denominator in Eq. (27) may now vanish due to Poincaré resonances. We regularize it by adding $\pm i\epsilon$. We obtain the equation

$$\begin{aligned} C^{(\nu)} = \sum_{\mu(\neq\nu)} P^{(\mu)} \frac{-1}{w^{(\mu)} - w^{(\nu)} - i\epsilon_{\mu\nu}} \\ \times [\lambda L_V P^{(\nu)} + \lambda L_V C^{(\nu)} - C^{(\nu)} \lambda L_V C^{(\nu)}] \end{aligned} \tag{35}$$

where the sign if $i\epsilon$ is chosen according to the "$i\epsilon$-rule:" [14,9]

$$\epsilon_{\mu\nu} = +\epsilon \text{ if } d_\mu \geq d_\nu \tag{36}$$
$$\epsilon_{\mu\nu} = -\epsilon \text{ if } d_\mu < d_\nu$$

where $\epsilon > 0$. This rule means, essentially, that transitions from lower to higher correlations are oriented towards the future and transitions from higher to lower correlations are oriented towards the past. We could also choose the other branch with $\epsilon < 0$, where the roles of past and future are exchanged. The main point is that regularization of the denominators breaks time symmetry.

For the $D^{(\nu)}$ operators we have

$$D^{(\nu)} = [P^{(\nu)}\lambda L_V + D^{(\nu)}\lambda L_V - D^{(\nu)}\lambda L_V D^{(\nu)}] \times \sum_{\mu(\neq\nu)} \frac{1}{w^{(\nu)} - w^{(\mu)} - i\epsilon_{\nu\mu}} P^{(\mu)} \tag{37}$$

The $i\epsilon$-rule leads to well defined perturbation expansions for $C^{(\nu)}$, $D^{(\nu)}$ and $A^{(\nu)} = [P^{(\nu)} + D^{(\nu)}C^{(\nu)}]^{-1}$. Recall that we have the relation $\bar{D}^{(\nu)} = [\bar{C}^{(\nu)}]^\dagger$ for the integrable case. For the non-integrable case, due to $i\epsilon$ rule, these operators are no more related by hermitian conjugation. They are related by star hermitian conjugation, which is obtained by hermitian conjugation plus the change $\epsilon_{\mu\nu} \Rightarrow \epsilon_{\nu\mu}$. Then we have

$$D^{(\nu)} = [C^{(\nu)}]^\star, \quad A^{(\nu)} = [A^{(\nu)}]^\star \tag{38}$$

Similar to the integrable case the χ operators are given by

$$\chi^{(\nu)} = [A^{(\nu)}]^{1/2} \exp(B^{(\nu)}) \tag{39}$$

where $B^{(\nu)} = -[B^{(\nu)}]^\star$ is an arbitrary anti-star-hermitian operator. In contrast to the integrable case we have no distributivity condition to derive $B^{(\nu)}$. However, as seen in the following section (see also the Appendices) the conditions on Λ stated in Sec. 2 lead to a well defined $\chi^{(\nu)}$ operator.

4 The Classical Friedrichs Model

To illustrate the construction of Λ, we shall consider a classical system that consists of a charged harmonic oscillator coupled with a classical scalar field in one-dimensional space [2]. We shall refer to the oscillator as "particle". The Hamiltonian of the system is given in terms of the normal coordinates a_1 and $a_k$sat isfying the Poisson bracket relation $i\{a_r, a_s^*\} = \delta_{r,s}$, where

$$i\{f,g\} = \sum_{r=1,k} \left[\frac{\partial f}{\partial a_r}\frac{\partial g}{\partial a_r^*} - \frac{\partial g}{\partial a_r}\frac{\partial f}{\partial a_r^*}\right] \tag{40}$$

We have

$$H = H_0 + \lambda V$$
$$= \omega_1 a_1^* a_1 + \sum_k \omega_k a_k^* a_k + \lambda \sum_k V_k (a_1^* a_k + a_1 a_k^*), \tag{41}$$

with a given constant frequency $\omega_1 > 0$ for the harmonic oscillator, $\omega_k = |k|$ for the field, and a dimensionless coupling constant λ. We have taken system in a one-dimensional box of size L, and imposed the usual periodic boundary conditions. Then the spectrum of the field is discrete, i.e., $k = 2\pi j/L$ where j is an integer. The volume dependence of the interaction V_k is given by

$$V_k = \sqrt{\frac{2\pi}{L}} v_k \tag{42}$$

where $v_k = O(1)$. We assume $v_k = v_{-k}$ and $v_k =$ real.

To deal with the continuous spectrum of the field we take the limit $L \to \infty$. In this limit we have

$$\frac{2\pi}{L}\sum_k \to \int dk, \quad \frac{L}{2\pi}\delta_{k,0} \to \delta(k). \tag{43}$$

The Liouville operator $L_H = L_0 + \lambda L_V$ is given by

$$L_0 = \sum_{s=1,k} \omega_s \Big[a_s^* \frac{\partial}{\partial a_s^*} - a_s \frac{\partial}{\partial a_s}\Big] \tag{44}$$

$$L_V = \sum_k V_k \Big[a_1^* \frac{\partial}{\partial a_k^*} - a_1 \frac{\partial}{\partial a_k} + a_k^* \frac{\partial}{\partial a_1^*} - a_k \frac{\partial}{\partial a_1}\Big] \tag{45}$$

The normal coordinates a_1^*, a_1 are related to the position x_1 and the momentum $p_1$of the particle as

$$a_1 = \sqrt{\frac{m\omega_1}{2}}(x_1 + \frac{ip_1}{m\omega_1}), \tag{46}$$

$$x_1 = \frac{1}{\sqrt{2m\omega_1}}(a_1 + a_1^*), \qquad p_1 = -i\sqrt{\frac{m\omega_1}{2}}(a_1 - a_1^*) \tag{47}$$

In terms of action-angle variables J_1, α_1w e have

$$a_1 = \sqrt{J_1} e^{-i\alpha_1} \tag{48}$$

The normal coordinates are eigenfunctions of the unperturbed Liouvillian. For example we have

$$\begin{aligned} L_0 a_r^* &= \omega_r a_r^*, \quad L_0 a_r = -\omega_r a_r \\ L_0 a_r^* a_s &= (\omega_r - \omega_s) a_r^* a_s \end{aligned} \tag{49}$$

where $r, s = 1$ or k. For the complete Liouvillian we have, e.g.,

$$\begin{aligned} L_H a_1^* &= \omega_1 a_1^* + \lambda \sum_k V_k a_k^* \\ L_H a_1 &= -\omega_1 a_1 - \lambda \sum_k V_k a_k \\ L_H a_1^* a_1 &= \lambda \sum_k V_k (a_k^* a_1 - a_1^* a_k). \end{aligned} \tag{50}$$

As long as the spectrum of frequencies ω_k is discrete and $\omega_1 \neq \omega_k$ for all ω_k, there are no Poincaré resonances and the system is integrable. We can construct the transformation U leading to new coordinates that diagonalize the Hamiltonian.

4.1 New particle modes

For instance we have the new normal coordinates of the particle (or "particle modes") [2],

$$\bar{A}_1 = U^{-1}a_1, \quad \bar{A}_1^* = U^{-1}a_1^* \tag{51}$$

given by the classical Bogoliubov transformation

$$\bar{A}_1 = \bar{N}_1^{1/2}[a_1 + \lambda \sum_k \bar{c}_k a_k], \tag{52}$$

$$\bar{c}_k = \frac{V_k}{(\bar{\omega}_1 - \omega_k)}, \quad \bar{N}_1 = (1 + \lambda^2 \sum_k \bar{c}_k)^{-1} \tag{53}$$

$$\tag{54}$$

where $\bar{\omega}_1$is the real pole of Green's function

$$[\eta^+(w)]^{-1} = [w - \omega_1 - \sum_k \frac{\lambda^2 V_k^2}{(w - \omega_k)}]^{-1}. \tag{55}$$

that reduces to $\omega_1$when $\lambda = 0$.

Note that in the perturbation expansion we have

$$\lambda \bar{c}_k = \frac{\lambda V_k}{\omega_1 - \omega_k} + O(\lambda^3) \tag{56}$$

As there is no Poincaré resonance, $\omega_1 \neq \omega_k$, the terms in the perturbation expansion are finite.

Since $\bar{L}_0$ is the unperturbed Liouvillian with renormalized frequencies we have (see Eq. (49))

$$\bar{L}_0 a_1^* = \bar{\omega}_1 a_1^*, \quad L_0 a_1 = -\bar{\omega}_1 a_1 \tag{57}$$

which implies that the new modes are eigenfunctions of the Liouvillian,

$$L_H \bar{A}_1 = -\bar{\omega}_1 \bar{A}_1, \qquad L_H \bar{A}_1^* = \bar{\omega}_1 \bar{A}_1^* \tag{58}$$

The transformation U is distributive with respect to products

$$U^{-1}a_1^* a_1 = (U^{-1}a_1^*)(U^{-1}a_1) \tag{59}$$

4.2 Gamow modes

Now we go to the continuous limit. There appear resonances and the system becomes non-integrable. The denominator in Eq. (56) may now vanish, giving divergences in the perturbation expansion of the renormalized modes. However, we can remove the divergences by regularization of the denominators. This means adding the infinitesimal $\pm i\epsilon$. We have now

$$\lambda c_k = \frac{\lambda V_k}{\omega_1 - \omega_k \pm i\epsilon} + O(\lambda^3) \tag{60}$$

In the continuous limit the solutions of the equations of motion break time symmetry, as we have damping of the particle either towards the future or towards the

past.[b] As we shall show below, this is connected to the choice of the sign of ϵ. The regularization in Eq. (60) is a special case of the regularization (36) (see Appendix B).

Continuing the regularization (60) to all orders in the perturbation expansion we obtain again exact eigenmodes of the Liouvillian. The eigenvalues are now complex. Choosing $+i\epsilon$ for the regularization we obtain [15]

$$\tilde{A}_1 = N_1^{1/2}[a_1 + \lambda \sum_k c_k a_k], \tag{61}$$

$$c_k = \frac{V_k}{(z-\omega_k)^+_{z_1}}, \quad N_1 = (1+\lambda^2 \sum_k c_k)^{-1} \tag{62}$$

and its complex conjugate, satisfying

$$L_H \tilde{A}_1 = -z_1 \tilde{A}_1, \qquad L_H \tilde{A}_1^* = z_1^* \tilde{A}_1^* \tag{63}$$

Here $z_1$is the complex pole of Green's function,

$$z_1 = \tilde{\omega}_1 - i\gamma, \quad \eta^+(z_1) = z_1 - \omega_1 - \int dk \, \frac{\lambda^2 v_k^2}{(z-\omega_k)^+_{z_1}} = 0 \tag{64}$$

where $2\gamma > 0$ is the damping rate of the particle and

$$\frac{1}{(z-\omega_k)^+_{z_1}} \tag{65}$$

is evaluated on the second Riemann energy sheet of z: we first integrate with z on the upper half plane and then substitute $z = z_1$ on the lower half plane.

The mode $\tilde{A}_1^*$ decays for $t > 0$ as

$$\exp(iL_H t)\tilde{A}_1^* = \exp(iz_1^* t)\tilde{A}_1^* = \exp[(i\tilde{\omega}_1 - \gamma)t]\tilde{A}_1^* \tag{66}$$

(and similarly $\tilde{A}_1$). We call these "Gamow modes" [2]. They correspond to the Gamow vectors in quantum mechanics [15,16,17,18,19,20]. The choice of $-i\epsilon$ gives the mode

$$A_1^* = N_1^{1/2}[a_1^* + \lambda \sum_k c_k a_k^*] \tag{67}$$

and its complex conjugate, satisfying

$$L_H A_1^* = z_1 A_1^*, \qquad L_H A_1 = -z_1^* A_1 \tag{68}$$

These modes decay for $t < 0$.

The modes we have introduced have quite different properties from the usual canonical variables. Their Poisson brackets vanish

$$i\{A_1, A_1^*\} = i\{\tilde{A}_1, \tilde{A}_1^*\} = 0 \tag{69}$$

However the modes $\tilde{A}_1$and $A_1^*$are duals; they form a generalized canonical pair

$$i\{\tilde{A}_1, A_1^*\} = 1 \tag{70}$$

This algebra corresponds to an extension of the usual Lie algebra including dissipation [2]. An analogue of this algebra has been previously studied in quantum mechanics [15,16,17,18,19,20].

[b] In the Friedrichs model the coupling constant should not be too strong in order to obtain a nonvanishing damping rate (see [9]).

4.3 Λ transformation

For single modes there is a simple relation between the Gamow modes and the Λ transformation (see Eq. (51))

$$\tilde{A}_1 = \Lambda^\dagger a_1, \quad \tilde{A}_1^* = \Lambda^\dagger a_1^*$$
$$A_1 = \Lambda^{-1} a_1, \quad A_1^* = \Lambda^{-1} a_1^* \tag{71}$$

Note that $\Lambda^\dagger \neq \Lambda^{-1}$ is not unitary. The difference between $\tilde{A}_1$ and A_1 is the change $\epsilon \Rightarrow -\epsilon$. This is precisely the difference between $\Lambda^\dagger a_1$ and $\Lambda^{-1} a_1 = \Lambda^* a_1$ (see Appendix B).

For products of modes the relation between the Gamow modes and Λ is slightly more involved. This is an important point. We have shown elsewhere [9] that there are difficulties inherent to the Gamow representation. The difficulties are connected to the fact that, as discussed below, products of Gamow modes lead to new Poincaré divergences. Hence the Λ-transformed products of particle modes cannot be expressed as products of Gamow modes alone [recall that Λ is analytic in λ]. We have

$$\Lambda^\dagger a_1^* a_1 \neq (\Lambda^\dagger a_1^*)(\Lambda^\dagger a_1) \tag{72}$$

and a similarly for Λ^{-1}. To understand why this is so, consider the product $(\Lambda^\dagger a_1^*)(\Lambda^\dagger a_1)$. We get (see Eqs. (61), (62))

$$\begin{aligned}
&(\Lambda^\dagger a_1^*)(\Lambda^\dagger a_1) \\
&= \tilde{A}_1^* \tilde{A}_1 = |N_1|(a_1^* + \lambda \sum_k c_k^* a_k^*)(a_1 + \lambda \sum_k c_k a_k) \\
&= |N_1|(a_1^* a_1 + \lambda a_1^* \sum_k c_k a_k + \lambda a_1 \sum_k c_k^* a_k^* \\
&+ \lambda^2 {\sum_{k,k'}}' c_k^* c_{k'} a_k^* a_{k'} + \lambda^2 \sum_k |c_k|^2 a_k^* a_k).
\end{aligned} \tag{73}$$

where the prime in the summation means $k \neq k'$. In Eq. (73), $|c_k|^2$ is not analytic in the coupling constant λ at $\lambda = 0$. The non-analyticity appears in the term $|c_k|^2$ due to the resonance. Indeed, to lowest order we have (see Eq. (60))

$$\begin{aligned}
\lambda^2 |c_k|^2 &= \frac{\lambda^2 V_k^2}{|\omega_1 - \omega_k + i\epsilon|^2} + \ O(\lambda^4) \\
&= \frac{\pi}{\epsilon} \lambda^2 V_k^2 \delta(\omega_1 - \omega_k) \to \infty.
\end{aligned} \tag{74}$$

This diverges when $\epsilon \to 0$. We have Poincaré's divergence. Hence $(\Lambda^\dagger a_1^*)(\Lambda^\dagger a_1)$ is not analytic in λ. This means that there are divergences in the perturbation series, i.e., we have Poincaré's nonintegrability. This nonanalyticity in λ is related to the vanishing of the Poisson brackets in Eq. (69) [15,19].

Going to the continuous limit the nonanalytic term in Eq. (73) may be written as

$$\int dk \frac{\lambda^2 v_k^2}{(z - \omega_k)_{z_1}^+ (z - \omega_k)_{z_1^*}^-} a_k^* a_k \tag{75}$$

When considering average values in phase space, this term is of $O(1)$ (in volume factors) if the average action $\langle J_k \rangle = \langle a_k^* a_k \rangle$ is $O(1)$ for every mode. This occurs in the thermodynamic limit, which corresponds to the infinite volume limit with a total energy proportional to the volume (we have a non vanishing energy density). Note that "thermodynamic limit" does not necessarily imply that we consider a system in thermal equilibrium; it just means that we have a finite energy density in the infinite volume limit.

In non-thermodynamic situations, we have $\langle J_k \rangle \sim O(1/L)$. The energy density goes to zero in the infinite volume limit. Here the appearance of the Poincaré divergence in Eq. (73) has no effect in the particle. This is consistent we the results we shall discuss below: the non-distributivity of Λ is related to the appearance of fluctuations in Brownian motion. And Brownian motion of the particle appears only when the particle is surrounded by a field described by the thermodynamic limit. As commented below, for quantum mechanics the situation is different. We can have fluctuations even in non-thermodynamic situations.[c]

Since we require that Λ is analytic in the coupling constant, we conclude that $\Lambda^\dagger a_1^* a_1$ cannot be expressed as the product Eq. (73). Using the formulation in terms of kinetic operators presented in the previous section, we obtain the result (see Appendix B)

$$\Lambda^\dagger a_1^* a_1 = \tilde{A}_1^* \tilde{A}_1 + \sum_k b_k a_k^* a_k \tag{76}$$

where

$$b_k = |N_1|(-|c_k|^2 + \xi_k), \quad \xi_k = r c_k^2 + \text{c.c.} \tag{77}$$

$$r = \frac{\exp(-ia/2)}{2\cos(a/2)}, \quad N_1 = |N_1| \exp(-ia) \tag{78}$$

Adding $\sum_k b_k a_k^* a_k$ to the product $\tilde{A}_1^* \tilde{A}_1$ we remove the non-analytic term containing $|c_k|^2$ and we replace it with the function ξ_k. Since ξ_k is an analytic function of λ, $\Lambda^\dagger a_1^* a_1$ becomes itself analytic in λ. The requirement of analyticity leads to non-distributivity.[d]

Similar to Eq. (76) we have (see Appendix B)

$$\Lambda^{-1} a_1^* a_1 = A_1^* A_1 + \sum_k b_k a_k^* a_k \tag{79}$$

When there is no Poincaré resonance, z_1b ecomes real, and we have $a = 0$ and $b_k = 0$ in Eq. (78). Then Λ reduces to U.

We first obtained results corresponding to (76) and (79) in a quantum mechanical model of a two-level atom (see Refs. [9,10]). We defined a dressed excited state through the Λ transformation. While in classical mechanics the term b_k leads to fluctuations in the particle only when the field is in a state corresponding to the thermodynamic limit, in quantum mechanics this term leads to fluctuations even

[c] In classical mechanics we can also obtain fluctuations in the *field* modes even in the non thermodynamic case. We shall discuss this elsewhere [21].

[d] Neglecting $O(1/L)$ corrections, the second term in Eq. (76) can be expressed in terms of renormalized field modes as $\sum_k b_k a_k^* a_k = \sum_k b_k \tilde{A}_k^* \tilde{A}_k + O(1/L)$.

in non-thermodynamic situations, due to vacuum effects. We obtain, for example, an energy fluctuation of the dressed excited state which is of the order of the decay rate. This gives the uncertainty relation between energy and lifetime mentioned in Sec. 2.

Coming back to classical mechanics, as we shall discuss next, the Λ transformation permits us to extract the damping and the Brownian motion of the particle due to the interaction with the field.

5 Brownian motion

We shall show that for the Friedrichs model in the thermodynamic limit, the time evolution in Λ representation of observables depending only on x_1 and p_1 coincides with the solution obtained through Langevin's equations for a damped harmonic oscillator. The results will be presented in detail in [22]. Here we shall show some of the main results.

Let us consider the equations of motion for $\Lambda^\dagger x_1$and $\Lambda^\dagger x_1^2$. Using Eq. (47) we have[e]

$$\Lambda^\dagger x_1 = \sqrt{\frac{1}{2m\omega_1}}(\tilde{A}_1 + \tilde{A}_1^*) \quad \Lambda^\dagger p_1 = -i\sqrt{\frac{m\omega_1}{2}}(\tilde{A}_1 - \tilde{A}_1^*). \tag{80}$$

The time evolution of $\tilde{A}_1$ is given by

$$\tilde{A}_1(t) = \tilde{A}_1(0)e^{-iz_1 t}. \tag{81}$$

This leads to

$$\frac{d}{dt}\Lambda^\dagger x_1 = -\gamma\Lambda^\dagger x_1 + \frac{1}{\tilde{m}}\Lambda^\dagger p_1. \tag{82}$$

where

$$\tilde{m} \equiv m\omega_1/\tilde{\omega}_1 \tag{83}$$

Next, we consider the equation for $\Lambda^\dagger x_1^2$. We have

$$\Lambda^\dagger x_1^2 = \Lambda^{-1}\frac{1}{2m\omega_1}(a_1^2 + a_1^{*2} + 2a_1^* a_1)$$
$$= \frac{1}{2m\omega_1}(\tilde{A}_1^2 + \tilde{A}_1^{*2} + 2\tilde{A}_1^*\tilde{A}_1 + 2\sum_k b_k a_k^* a_k). \tag{84}$$

Taking the time derivative we obtain

$$\frac{d}{dt}\Lambda^\dagger x_1^2 = -2\gamma\Lambda^\dagger x_1^2 + \frac{2}{\tilde{m}}\Lambda^\dagger x_1 p_1 + \frac{2}{\tilde{m}}\frac{\gamma}{\tilde{\omega}_1}\sum_k b_k a_k^* a_k. \tag{85}$$

[e]Here we use the $\Lambda^\dagger$ transformation, so that the transformed variables decay for $t > 0$ with evolution operator $\exp(iL_H t)$; see Eq. (66). In Refs. [9,10] we considered transformed *states* that decay for $t > 0$ with evolution operator $\exp(-iL_H t)$; see Eq. (68). For this reason in those papers we used the Λ^{-1} transformation.

Assuming that the field is at thermal equilibrium with temperature T we get the ensemble average

$$\sum_k b_k \langle a_k^* a_k \rangle = \sum_k b_k \frac{k_B T}{\omega_k} \approx \frac{k_B T}{\tilde{\omega}_1} \tag{86}$$

where the last relation is valid for weak coupling, where b_k may be approximated by $(\pi/L)\delta(\omega_k - \tilde{\omega}_1)$ [9] (see Appendix B).

In summary, we have the following equation for the ensemble averages of $\Lambda^\dagger x_1$ and $\Lambda^\dagger x_1^2$:

$$\frac{d}{dt}\langle \Lambda^\dagger x_1 \rangle = -\gamma \langle \Lambda^\dagger x_1 \rangle + \frac{1}{\tilde{m}} \langle \Lambda^\dagger p_1 \rangle \tag{87}$$

$$\frac{d}{dt}\langle \Lambda^\dagger x_1^2 \rangle = -2\gamma \langle \Lambda^\dagger x_1^2 \rangle + \frac{2}{\tilde{m}} \langle \Lambda^\dagger x_1 p_1 \rangle + D_x \tag{88}$$

where

$$D_x = \frac{2\gamma}{\tilde{m}\tilde{\omega}_1} \sum_k b_k \langle a_k^* a_k \rangle \approx \frac{2\gamma k_B T}{\tilde{m}\tilde{\omega}_1^2} \tag{89}$$

is the diffusion coefficient. Let's now write Langevin equations. For the particle position $x_1$and momentum p_1, we have [22f]

$$\frac{d}{dt} x_1 = -\gamma x_1 + \frac{p_1}{\tilde{m}} + A, \tag{90}$$

$$\frac{d}{dt} p_1 = -\gamma p_1 - \tilde{m}\tilde{\omega}_1^2 x_1 + B. \tag{91}$$

These equations describe the damped harmonic oscillator with random momentum and force terms $A(t)$ and $B(t)$. We assume that $A(t)$ and $B(t)$ have the Gaussian white noise properties [3,24]. The Gaussian property means that for noise averages of products we have

$$\langle A(t_1)A(t_2)...A(t_{2n+1}) \rangle = 0, \tag{92}$$

$$\langle A(t_1)A(t_2)...A(t_{2n}) \rangle = \sum_{\text{all pairs}} \langle A(t_{i_1})A(t_{i_2}) \rangle .... \langle A(t_{i_{2n-1}})A(t_{i_{2n}}) \rangle \tag{93}$$

The white noise property means that

$$\langle A(t)A(t') \rangle = A_c \delta(t - t') \tag{94}$$

where A_c is a constant to be determined. We assume the same for $B(t)$, i.e.

$$\langle B(t)B(t') \rangle = B_c \delta(t - t'). \tag{95}$$

[f] These Langevin equations with symmetrical random momentum and force terms are appropriate for comparison with our oscillator model since our Hamiltonian is symmetrical under rescaled position and momentum exchange. If the Hamiltonian is not symmetric for the position and momentum, e.g. if $q_1 q_k$ and $q_1^* q_k^*$ terms are included in the interaction, then Langevin equations with asymmetric random terms (as in the Ornstein-Uhlenbeck theory [23]) are more appropriate for the comparison.

The noise terms A and B are further assumed to be uncorrelated. The constants A_c and B_c may be obtained assuming that for $t \to \infty$ the Brownian particle reaches equilibrium with its medium, at temperature T. This leads to the following noise-average equations for $x_1$and x_1^2:

$$\frac{d}{dt}\langle x_1\rangle = -\gamma\langle x_1\rangle + \frac{\langle p_1\rangle}{\tilde{m}}, \tag{96}$$

$$\frac{d}{dt}\langle x_1^2\rangle = -2\gamma\langle x_1^2\rangle + \frac{2}{\tilde{m}}\langle x_1 p_1\rangle + \frac{2\gamma k_B T}{\tilde{m}\tilde{\omega}_1^2} \tag{97}$$

These equations coincide with the results obtained from the Λ transformation, Eqs. (87) and (88) together with Eq. (89).

Extending the construction of Λ for higher powers of the normal modes, $\Lambda^\dagger a_1^{*m} a_1^n$ one can show [22] that the Λ-transformed equations for x_1^n agree with the solutions of the Langevin equations for x_1^n for arbitrary integer n. This means that the Λ transformation can describe all the effects of the Gaussian white noise in Brownian motion.

In agreement with the results presented here, it can also be shown that the kinetic equation Eq. (14) leads to an exact form of the Fokker-Planck equation associated with the Brownian oscillator [22].

The Λ-transformed variables obey Markovian equations. In contrast, the original variables contain non-Markovian effects such as the Zeno effect and long tails [2]. These effects are connected to the appearance of a dressing field (or cloud) around the bare particle [9]. The transformed variables describe dressed objects. For this reason they do not include Zeno or long tail effects. They include only the Brownian motion and damping components of the motion of the particle.

6 Concluding Remarks

It is a quite remarkable conclusion that the extension of dynamics to nonintegrable systems allows to deduce stochastic formulations from dynamics. The main point is that the transformation operator Λ is not distributive. Therefore we obtain fluctuations for all variables which are in the domain of Λ. For irreversible nonintegrable systems we obtain a stochastic description of space-time, without the introduction of some new phenomenological constant.

This opens a wide field of research. Some applications to quantum and classical physics (unstable particles, radiation damping, interacting fields) are at present being prepared for publication.

Acknowledgements

We thank Prof. I. Antoniou, Prof. E. C. G. Sudarshan and Dr. E. Karpov for interesting comments. We acknowledge the International Solvay Institutes for Physics and Chemistry, the Engineering Research Program of the Office of Basic Energy Sciences at the U.S. Department of Energy, Grant No DE-FG03-94ER14465, the Robert A. Welch Foundation Grant F-0365, the European Commission Grant No.

HPHA-CT-2001-40002, the European Commission CEE Grant No. HPHA-CT-2000-00015, the National Lottery of Belgium and the Communauté Française de Belgique for supporting this work.

Appendix

A The U operator

In this appendix we give an example of the construction of the canonical transformation operator U using the kinetic formulation described in Sec. 3.

We consider the Friedrichs model presented in Sec. 4. In this model, we define the $P^{(\nu)}$ subspaces as consisting of monomials (or superposition of monomials) of field and particle modes. As discussed below Eq. (20) , we can associate a "degree of correlation" d_ν with each subspace. To define this, let us first note that if there are no interactions, diagonal monomials of the form $a_s^* a_s$ are invariants of motion. If the modes are initially uncorrelated, they will remain uncorrelated. The interaction L_V brings diagonal monomials to off diagonal ones, such as $a_s^* a_{s'}$. The modes become correlated. Hence the degree of correlation can be associated with the degree of off-diagonality of the modes [11]. The field modes play a special role. In order to have damping it is essential to have a continuous spectrum in the field. The degree of correlation is thus defined as the degree of off-diagonality of the field modes only. This gives a measure of the "number of times" that the particle has interacted with the field. In this specification the off-diagonality of the particle modes is irrelevant.

We define the degree of off-diagonality (i.e., d_ν) as the maximum number of unmatched field modes in a given monomial or polynomial [2]. Matched field modes are pairs $a_k^* a_k$ that depend only on the absolute value of the modes. For example, all the monomials a_1, $a_1^* a_1$, $a_k^* a_k$, $a_k^* a_k a_{k'}^* a_{k'}$ have zero degree of correlation, because there are no unmatched field modes. The monomial $a_1^* a_k$on the other hand, have degree of correlation 1, because the mode a_k is unmatched.

We shall consider the transformed product $U^{-1} a_1^* a_1$. The monomial $a_1^* a_1$ is an eigenfunction of L_0 with eigenvalue $w^{(0)} = 0$, so it belongs to the $P^{(0)}$ subspace with $d_0 = 0$. Using Eq. (25) we have

$$U^{-1} a_1^* a_1 = U^{-1} P^{(0)} a_1^* a_1 = (P^{(0)} + \bar{C}^{(0)}) \bar{\chi}^{(0)} a_1^* a_1 \tag{98}$$

The operator U^{-1} is a function of the Liouville operator. As seen in Eq. (45) this operator preserves the number of a^* and a modes in a given monomial: it will map a monomial with m modes a^* and n modes a to a superposition of monomials with the same numbers m, n of modes a^*, a, respectively. The same is true for the operators $\bar{C}$ and $\bar{\chi}$. So we have

$$\begin{aligned} \bar{\chi}^{(0)} a_1^* a_1 &= \sum_{s=1,k} a_s^* a_s \bar{\chi}^{(0)}_{ss;11} \\ \bar{C}^{(0)} a_1^* a_1 &= \sum_{s=1,k} \sum_{s'=1,k}{}' a_s^* a_{s'} \bar{C}^{(0)}_{ss';11} \end{aligned} \tag{99}$$

where $\bar{\chi}^{(0)}_{ss;11}$ and $\bar{C}^{(0)}_{ss';11}$ are coefficients, and the prime in the summation over s'

means $s \neq s'$ (recall that $\bar{\chi}^{(0)}$ is a diagonal operator, while $\bar{C}^{(0)}$ is off-diagonal). We have as well

$$\bar{C}^{(0)}\bar{\chi}^{(0)}a_1^*a_1 = \sum_s \bar{C}^{(0)}a_s^*a_s\bar{\chi}^{(0)}_{ss;11}$$
$$= \sum_{s=1,k}{\sum_{r,r'}}' a_r^*a_{r'}\bar{C}^{(0)}_{rr';ss}\bar{\chi}^{(0)}_{ss;11} \tag{100}$$

Note that each change from a mode a_k to a mode a_1 or viceversa involves an interaction of order $L^{-1/2}$ in volume. Hence each index change involves an $L^{-1/2}$ factor. For example we have

$$\bar{\chi}^{(0)}_{11;11} \sim O(L^0)$$
$$\bar{\chi}^{(0)}_{kk;11} \sim O(L^{-1})$$
$$\bar{C}^{(0)}_{1k;11} \sim O(L^{-1/2})$$
$$\bar{C}^{(0)}_{1k';kk} \sim O(L^{-3/2}), \text{ etc.} \tag{101}$$

Each summation over field modes gives an L factor. Taking all the volume factors into account we get

$$U^{-1}a_1^*a_1 = \sum_s a_r^*a_s\bar{\chi}^{(0)}_{ss;11} + {\sum_{s,s'}}' a_s^*a_{s'}\bar{C}^{(0)}_{ss';11}\bar{\chi}^{(0)}_{11;11} + O(1/L) \tag{102}$$

The $\bar{C}^{(0)}_{ss';kk}$ coefficients give $O(1/L)$ contributions. To determine the coefficients $\bar{C}^{(0)}_{ss';11}$ we use Eq. (27) [9]. This leads to (see Eq. (53))

$$\bar{C}^{(0)}_{1k;11} = \bar{C}^{(0)}_{k1;11} = \bar{c}_k, \quad \bar{C}^{(0)}_{kk';11} = \bar{c}_k\bar{c}_{k'} \tag{103}$$

For the operator $\bar{\chi}^{(0)}_{11;11}$ we have (see Eq. (30))

$$\bar{\chi}^{(0)}_{11;11} = [\bar{A}^{(0)}]^{1/2}_{11;11}[\exp(\bar{B}^{(0)})]_{11;11} + O(1/L)$$
$$= [\bar{A}^{(0)}]^{1/2}_{11;11} + O(1/L) \tag{104}$$

where in the second line we used the antihermiticity of $\bar{B}^{(0)}$, which leads to $\bar{B}^{(0)}_{11;11} = 0$. The second line in Eq. (104) may be explicitly evaluated [9] using Eq. (103). The result is

$$\bar{\chi}^{(0)}_{11;11} = \bar{N}_1 \tag{105}$$

With the results obtained so far we have

$$U^{-1}a_1^*a_1 = N_1(a_1^* + \sum_k \lambda\bar{c}_k a_k^*)(a_1 + \sum_{k'} \lambda\bar{c}_{k'}a_{k'}) + \sum_k(\bar{\chi}^{(0)}_{kk;11} - N_1\lambda^2\bar{c}_k^2)a_k^*a_k \tag{106}$$

Now, from the distributive property of U we conclude that the second term in the r.h.s. has to vanish, i.e.,

$$\bar{\chi}^{(0)}_{kk;11} = \bar{N}_1\bar{c}_k^2 \tag{107}$$

Indeed, if this is so we obtain the expected result $U^{-1}a_1^*a_1 = (U^{-1}a_1^*)(U^{-1}a_1)$ (see Eqs. (51), (53)). With this result we have completed the calculation of all the coefficients of the expansion of $U^{-1}a_1^*a_1$ using the formulation in terms of kinetic operators. The advantage of the method followed here is that it permits a straightforward extension to the nonintegrable case.

B Extension of U to Λ

In this appendix 1) we comment on the relations

$$A_1 = \Lambda^{-1}a_1, \quad A_1^* = \Lambda^{-1}a_1^* \tag{108}$$

$$\tilde{A}_1 = \Lambda^{\dagger}a_1, \quad \tilde{A}_1^* = \Lambda^{\dagger}a_1^* \tag{109}$$

and 2) we calculate the transformed products $\Lambda^{-1}a_1^*a_1$and $\Lambda^{\dagger}a_1^*a_1$.

1) Denoting the subspace consisting of a_1 and a_1^* as as $P^{(0;1)}$ and $P^{(1;0)}$, respectively, we have (see Eq. (33))

$$\begin{aligned}\Lambda^{-1}a_1 &= (P^{(0;1)} + C^{(0;1)})\chi^{(0;1)}a_1 \\ \Lambda^{-1}a_1^* &= (P^{(1;0)} + C^{(1;0)})\chi^{(1,0)}a_1^*\end{aligned} \tag{110}$$

Since the subspaces $P^{(0;1)}$ and $P^{(1;0)}$ are one-dimensional, the diagonal operators χ are simply constants, which may be found by the normalization condition (70). To find the C operators, we solve Eq. (35). In order to fix the analytic continuation, we note that the modes a_1 and a_1^* have zero degree of correlation. As any transition in Eq. (35) leads to a higher degree of correlation, we always have $\epsilon_{\mu 0} = +\epsilon$ in Eq. (36). Replacing the explicit forms of the operators C and χ we obtain the relations (108). To obtain $\Lambda^{\dagger}a_1$ we note that

$$\begin{aligned}\Lambda^{\dagger}a_1 &= [\Lambda^{\star}a_1]_{\epsilon\Rightarrow-\epsilon} = [\Lambda^{-1}a_1]_{\epsilon\Rightarrow-\epsilon} \\ &= [A_1]_{\epsilon\Rightarrow-\epsilon} = \tilde{A}_1\end{aligned} \tag{111}$$

(see the definition of star conjugation below Eq. (37); we have $\epsilon_{\mu 0} = -\epsilon_{0\mu} = -\epsilon$). This, and a similar argument for $\Lambda^{\dagger}a_1^*$, gives Eq. (109).

2) Similar to Eq. (102) we have

$$\Lambda^{-1}a_1^*a_1 = \sum_s a_r^*a_s\chi^{(0)}_{ss;11} + \sum_{s,s'}{}' a_s^*a_{s'}C'^{(0)}_{ss';11}\chi^{(0)}_{11;11} + O(1/L) \tag{112}$$

In Appendix A we obtained all the coefficients of the transformed product $U^{-1}a_1^*a_1$. We summarize the results, and we write already the extensions to the nonintegrable case (i.e. from U to Λ)

$$\bar{C}^{(0)}_{1k;11} = \bar{c}_k \Rightarrow C^{(0)}_{1k;11} = c_k^* \tag{113}$$

$$\bar{C}^{(0)}_{k1;11} = \bar{c}_k \Rightarrow C^{(0)}_{k1;11} = c_k \tag{114}$$

$$\bar{C}^{(0)}_{kk';11} = \bar{c}_k\bar{c}_{k'} \Rightarrow C^{(0)}_{kk';11} = c_kc_{k'}^* \tag{115}$$

$$\bar{\chi}^{(0)}_{11;11} = \bar{N}_1 \Rightarrow \chi^{(0)}_{11;11} = |N_1| \tag{116}$$

$$\bar{\chi}^{(0)}_{kk;11} = \bar{N}_1\bar{c}_k^2 \Rightarrow \chi^{(0)}_{kk;11} = |N_1|(rc_k^2 + \text{c.c.}) \tag{117}$$

Eqs. (113)-(116) are obtained along the same lines as the integrable case (for details see [9]). In particular, for the $C^{(0)}$ operator we use the equation Eq. (35) with analytically continued propagators. For the extension of $\bar{\chi}^{(0)}_{kk;11}$ we make the following argument: from Eqs. (113)-(115) we see that the analytic continuation of the function $\bar{c}_k$ (from real to complex frequency) is either c_k or c_k^*. Since we require that Λ maps real functions to real functions, we see that the extension of $\bar{c}_k^2$ in Eq. (117) should be a combination of both $c_k^2$and c_k^{*2}. In order that Λ reduces to U when there is no resonance, we impose the condition $r + r^* = 1$ for the r coefficient [g]. As we show now, this relation, plus the condition that Λ preserves the measure of phase space (equivalent to preservation of the trace in quantum mechanics) permit us to find r. Measure preservation means that

$$\int d\Gamma \Lambda^{-1} \rho = 1 \tag{118}$$

for any normalized ensemble ρ.

Consider the ensemble

$$\rho = C_1 a_1^* a_1 \exp(-J/J_0) \tag{119}$$

where $C_1$is the normalization factor given by

$$C_s = \Big[\int d\Gamma a_s^* a_s \exp(-J/J_0) \Big]^{-1} \tag{120}$$

with

$$J = \sum_{s=1,k} a_s^* a_s \tag{121}$$

and J_0 a constant that makes the argument of the exponential dimensionless. The factor $\exp(-J/J_0)$ ensures the existence of a finite norm of ρ, (see the "Segal-Bargmann representation" in [1,2]). The total action J is an invariant of motion, because we have $L_0 J = 0$ and $L_V J = 0$. Since Λ^{-1} can be expressed as a perturbation expansion, $\Lambda^{-1} = 1 + O(\lambda L_V)$, we get

$$\Lambda^{-1} J = J, \quad \Lambda^{-1} \exp(-J/J_0) = \exp(-J/J_0) \tag{122}$$

The operator $L_V$is a differential operator. Applying the chain rule of differentiation and Eq. (122) we conclude that

$$\Lambda^{-1} a_1^* a_1 \exp(-J/J_0) = (\Lambda^{-1} a_1^* a_1) \exp(-J/J_0) \tag{123}$$

Inserting the ensemble Eq. (119) in Eq. (118) and using Eqs. (112)-(117) we get

$$C_1 \int d\Gamma |N_1| [a_1^* a_1 + \sum_k (r c_k^2 + \text{c.c.}) a_k^* a_k] \exp(-J/J_0) = 1 \tag{124}$$

[g] In Ref. [9] we used the Λ transformation to define dressed unstable states in quantum mechanics. The derivation followed here is similar to the derivation followed in Ref. [9]. The only difference is that in [9] the relation $r + r^* = 1$ was derived from the requirement that the dressed unstable state has an energy fluctuation of the order of the lifetime. This fluctuation is a purely quantum effect. Here we are dealing with classical mechanics, so we postulate $r + r^* = 1$ as a basic condition. An alternative derivation, presented in Appendix A of Ref. [10], gives the same result.

where the off-diagonal terms such as $a_1^* a_k$ appearing in Eqs. (113)-(117) vanish due to the integration over angles in phase space. We can write Eq. (124) as

$$C_1|N_1|[C_1^{-1} + \sum_k (rc_k^2 + \text{c.c.})C_k^{-1}] = 1 \tag{125}$$

Since $C_1 = C_k$ for any k (see Eq. (120)), Eq. (124) leads to

$$|N_1|[1 + \sum_k (rc_k^2 + \text{c.c.})] = 1 \tag{126}$$

This equation plus the condition $r + r^* = 1$ yield the result Eq. (77).

Eqs. (113)-(117) lead to

$$\begin{aligned} &\Lambda^{-1} a_1^* a_1 \\ &= |N_1|\Big[a_1^* a_1 + \lambda a_1^* \sum_k c_k^* a_k + \lambda a_1 \sum_k c_k a_k^* + \lambda^2 {\sum_{k,k'}}' c_k c_{k'}^* a_k^* a_{k'} \\ &+ \lambda^2 \sum_k (rc_k^2 + \text{c.c.}) a_k^* a_k\Big] \end{aligned} \tag{127}$$

Since $\Lambda^{-1} = \Lambda^\star$, and (see Eq. (36) with $d_\nu = 0$ for $\nu = 0$)

$$\Lambda^\dagger a_1^* a_1 = \Lambda^\star a_1^* a_1|_{i\epsilon \Rightarrow -i\epsilon}, \tag{128}$$

we can find $\Lambda^\dagger a_1^* a_1$ by taking the complex conjugates of the propagators in Eq. (127):

$$\begin{aligned} &\Lambda^\dagger a_1^* a_1 \\ &= |N_1|\Big[a_1^* a_1 + \lambda a_1^* \sum_k c_k a_k + \lambda a_1 \sum_k c_k^* a_k^* + \lambda^2 {\sum_{k,k'}}' c_k^* c_{k'} a_k^* a_{k'} \\ &+ \lambda^2 \sum_k (rc_k^2 + \text{c.c.}) a_k^* a_k\Big] \end{aligned} \tag{129}$$

Eqs. (129) and (127) lead to the expressions (76) and (79), respectively.

For weak coupling we have [9]

$$b_k \approx \Big(\frac{2\pi}{L}\Big)\frac{1}{\pi}\frac{(\gamma)^3}{[(\omega_k - \tilde{\omega}_1)^2 + \gamma^2]^2} \approx \frac{\pi}{L}\delta(\tilde{\omega}_1 - \omega_k) \tag{130}$$

References

1. J. R. Klauder and E. C. G. Sudarshan, *Fundamentals of Quantum Optics*, (V. A. Benjamin, Inc., New York, 1968).
2. T. Petrosky, S. Kim, G. Ordonez and I. Prigogine, preprint (2002).
3. R. Balescu, *Equilibrium and Non Equilibrium Statistical Mechanics*, (Krieger Publishing Company, 1975).
4. T. Petrosky and I. Prigogine, Physica A **147**, 439 (1988).
5. I. Prigogine, Adv. Chem. Phys. **122**, 261 (2002).
6. I. Prigogine, C. George, F. Henin, L. Rosenfeld, Chemica Scripta **4**, 5 (1973).

7. I. Prigogine, *From being to becoming* (Freeman, New York, 1980).
8. I. Prigogine and T. Petrosky, Physica A **147**, 461 (1988).
9. G. Ordonez, T. Petrosky and I. Prigogine, Phys. Rev. A **63**, 052106 (2001).
10. T. Petrosky, G. Ordonez and I. Prigogine, Phys. Rev. A **64**, 062101 (2001).
11. I. Prigogine, *NonEquilibrium Statistical Mechanics*, (Wiley Interscience, 1962).
12. I. Antoniou and S. Tasaki, Int. J. Quantum Chemistry **46**, 425 (1993).
13. T. Petrosky and I. Prigogine, Physica A **175**, 146 (1991).
14. T. Petrosky and I. Prigogine, Adv. Chem. Phys. **99**, 1 (1997).
15. T. Petrosky, I. Prigogine and S. Tasaki, Physica A **173**, 175 (1991).
16. E.C.G. Sudarshan, C. Chiu and V. Gorini, *Phys. Rev.* **D18**, 2914 (1978).
17. N. Nakanishi, Prog. Theor. Phys. **19**, 607 (1958).
18. A. Böhm and M. Gadella, *Dirac Kets, Gamow Vectors and Gelfand Triplets*, (Springer Lecture Notes on Physics, Vol. 348, Springer, New York, 1989).
19. S. Tasaki, Phys. Reports **219**, 110 (1992).
20. I. Antoniou, M. Gadella, E. Karpov, I. Prigogine, and G. Pronko, Chaos, Solitons and Fractals **12**, 2757 (2001).
21. T. Petrosky, unpublished (2002).
22. S. Kim and G. Ordonez, preprint (2002).
23. E. Nelson, *Dynamical theories of Brownian motion,* (Mathematical notes, Princeton University Press, 1967)
24. P. Resibois, *Classical Kinetic Theory of Fluids*, (Wiley Interscience, 1977).

DISCUSSION

Chairman: H. Walther

W. Schleich: It seems that there are two kinds of probabilities: a subjective and an objective one. For example, when you trace the density matrix and average and your approach gives a unified treatment of different probabilities. The probability in quantum mechanics which is objective, and the probability in statistical mechanics which is subjective, reflecting our ignorance. Is your approach different?

I. Prigogine: It is a different approach. In the sense we do introduce, indeed as you stated, two types of probabilities: one due to ignorance and one due to laws of nature. The ignorance probability is true for integrable systems, because their solution is a deterministic solution, and therefore whenever we use probability it is because of our ignorance. But for the non-integrable systems, the solution is in terms of probability both in quantum and classical dynamics. We have shown that for a large class of non-integrable systems, we obtain a probability description, which is irreducible to a deterministic description. The future is not given. This has nothing to do with our ignorance.

G. Hegerfeldt: I come from a field where I was educated a long time ago. Some of these notions are there since that for example adjoint spaces, Lippman-Schwinger equations, and you break the symmetry between minus infinity and plus infinity, or you take the time depending Schrödinger equation and you break the symmetry by imposing a singularity at $t = 0$ where the decay starts. There is always a source

terms coming in, which breaks inevitably decay of the system and when you do that you always get non-exponential decay at least at the long end of the time. The point is, when you come and say I have define states which decay only exponentially this implies, experimentally at least, you should never see non-exponential decay for a long time. Is this the idea of a dressed exponential decay?

I. Prigogine: You are right. You observe deviations from the strictly exponential decay. What is new is that the decay can be separated in two different contributions. A universal contribution, which is strictly exponential and its characteristics of the unstable state or the unstable particle. Fortunately, this is so. If not, you would have, for example, old mesons and young mesons. In addition, the effects, which come from the mode of preparation, will perturb the exponential.

PRESERVATION OF A T-INVARIANT REDUCTIONIST SCAFFOLD IN "EFFECTIVE" INTRINSICALLY IRREVERSIBLE QUANTUM MECHANICS

YUVAL NE'EMAN

School of Physics and Astronomy, Tel Aviv University, Tel Aviv 69978, Israel

The recently developed *Irreversible Quantum Mechanics* formalism describes physical reality both at the statistical and the particle levels and voices have been heard suggesting that it be used in fundamental physics. Two examples are sketched in which similar steps were taken and proved to be terrible errors: Aristotle's rejection of the vacuum because "nature does not tolerate it", replacing it by a law of force linear in velocity and Chew's rejection of *Quantum Field Theory* because "it is not unitary off-mass-shell". In Particle Physics, I suggest using the new representation as an *"effective"* picture without abandoning the canonical background.

1 Apology and Introduction

The subject of the brief address I gave at the 22nd Solvay Congress was somewhat outside the conference's planned scope, as defined by the title of Quantum Communication, which is why I am including this apology for the apparent breach of intellectual discipline. I still think, however, that it was in place and might become very relevant in the sequel. This meeting was partly concerned with issues relating to the foundations of QM; so is the recently developed [1,2] Quantum Mechanical Irreversibility (QMI) formalism, devised by the Solvay Institutes and the Prigogine Center for Statistical Mechanics at UT Austin and basically following A. Bohm's introduction [3–6] of the appropriate mathematical tools - namely Rigged Hilbert Spaces, as induced by Gelfand triples. Bohm & collaborators have also applied the method [7–10] at the Particle level, beyond the Dissipative systems studied by the Prigogine School.

No doubt that the construction represents a useful and elegant addition to the methods by which Physical theory describes the Physical world. In the excitement that followed this advance, I have, however, come across suggestions which appeared to me over-enthusiastic and possibly even dangerous. The idea would be to use this picture directly and solely, make it the unique description, thereby *doing away altogether with the C, P, and T-invariant* (or CP and T- *invariant*, or even *just* CPT*-invariant*) *formalism of particle physics.* Somehow, I sensed a reawakening of a recurring *positivistic* and *anti-reductionist* tendency which, in the past, was very detrimental to the field's evolution. I shall refer to this tendency as the *on-mass-shell syndrome*, this being one modern set up which triggered it. In the spirit of the early Solvay meetings and their impact on the formatting of Quantum Mechanics, I believe these conferences do provide a unique opportunity for almost-philosophical discussions.

Returning to my issues, it is to forestall such positivistic suggestions that I shall relate two stories illustrating similar situations in the past and the lessons learned.

2 One Thousand Years of Greek Science

We start with the achievements of the First Age of Science, namely that of Greek Science from its birth around 600 BC to its agony and collapse between 400-550 AD - and study [11] more specifically the Dark Ages (for science) that followed and *why it took a thousand years to get back on track.*

Science in the full modern sense was born in Greece around 600 BC. It is thought that when the program of legislation arrived in Greece (Solon's laws) from the Middle East (Hammurabi, Moses, etc) it somehow occurred to the Greek scholars that a similar logical system (*"laws of nature"*) might describe and perhaps explain the behavior of the physical world. There was no guarantee that such a program would succeed, yet pragmatic considerations gradually brought about the idea that it could be done in *patches*, with several such patches coming together at some point and merging. The first polished piece was *geometry*, culminating in Euclid's systematics: a minimal number of *axioms* from which everything else can be derived - including *quantitative* "predictions" – by logical processes and, as later realized, by *mathematical proof*, considered as an extension of logic. This became the model for any science.

Both in that First Age and in the Second (which started with Galileo, Kepler etc. and is still on, though there are some indications that it might be heading for an unknown end [12]) the limits of what this *world-view* could encompass were not known. The Vitalists thought that the phenomena of *Life* are beyond science; there are others who even nowadays assume that *Consciousness* is off-science. In Cosmology, until the Nineteen-eighties, many assumed that the singularity at the Big Bang would screen anything prior to it; this was the issue that gave Hawking the title for his bestseller *"A Brief History of Time"*. Since 1986, however, we have A. Linde's "Eternal Inflation" and its sequel; in these models, *quantum tunneling* is assumed to do away with the singularity altogether and we have an infinite past for a *"multiverse"* with ever new Big Bangs. *As of 2002 AD, there does not appear to be any region or sector of the physical world which would have to be left out by science.*

The Pythagoreans contributed greatly between 600-400 BC and are responsible for the mathematical formulation of the end-product. Achievements in Mathematics itself were considerable, both in Geometry and in Number Theory - such as the proof that there is *no largest prime* and that of the existence of *irrationals*, both due to Pythagoras; the works of Archimedes, Appolonius of Perga, Diophantes of Alexandria, etc.. In Planetary science, Erathostenes (250 BC) measured the *radius of the Earth* with a 0.5 % precision and Hipparchos (150 BC) measured the *distance to the Moon* with a 1 % precision and also discovered the precession of the Equinoxes. Moreover, Heraclides of Pontos understood around 320 BC that the apparent daily rotation of the firmament really implies that the Earth spins on its axis once a day; Aristarchus of Samos explained the Solar System (250 BC), seventeen centuries before Copernicus.

In Physics, Archimedes made a good start in *Mechanics* (solid and fluid). Heron of Alexandria invented the steam-engine (100 AD). Prior to both, Aristotle had worked out some general physics in the presence of *friction*, the point we shall

return to.

All of this started decaying after Christianity became the State religion of the Roman Empire around 330 AD. The Greek Academies were gradually either closed or taken over by the Church. The last two turns of the key were the closure of the Academy of Alexandria after the lynching and death of its head, the woman mathematician Hypatia in 415 AD [13] – and Justinian's edict closing the Athens Academy in 529 AD. The latter event was followed by two developments which determined the profile of the next thousand years:

- (a) the incorporation of Aristotle's works in the body of the Church's Scholastic dogma – the Aristotelianism which ruled throughout the Middle Ages.

- (b) the intervention of the Sassanid emperor of Persia Khosru I, Anusharvan (beloved of the heavens), offering to take in the faculty of the closed Academy with their books and documentation and providing them with the means for a new start in Northern Mesopotamia. This gesture preserved the fruits of the First Age and saved science from having to "go back to square 1" in the XVIth Century AD.

3 The One-Thousand Years Gap

It is important to understand why scholasticism blocked any real advance in the sciences. After all, thanks to Emperor Khusru Anushirvan of Persia, the documentation of Greek science was saved. Why then weren't there any Galileos or Newtons between 550 AD and 1550 AD? The picture as generally drawn gives the impression that all that was missing was Copernicus' revival of Aristarchus of Samos' *solar-centered* model of the "solar-system"; but this was only one roadblock, important for the work of Kepler and his three "laws" – regularities. More important than that was the issue of the *vacuum.*

Plato was a reductionist and also liked geometry, so that he did discuss *empty space* and a *vacuum.* His student Aristotle, however, was a "practical" person and *did not believe in reductionism.* He therefore proclaimed that *"nature does not tolerate a vacuum"* a phrase often used in politics (mostly applied to a vacuum in leadership). Aristotle himself therefore developed *physics in the presence of friction* and obtained a law similar to more modern formulae dealing with friction-like phenomena, such as Ohm's Law etc. in which *velocity is proportional to the force applied.* This is indeed the correct result here too, provided one takes "velocity" here to mean the *final* velocity. Using Newtonian formalism, we note that friction and air-resistance forces $K(t)$ at any single instant t are proportional to the velocity $v(t)$ at that instant, and act in the opposite direction. Taking for instance the modern case of a parachutist dropping from a plane, we have $K(t) = -kv(t)$, k a constant. Let the weight of the paratrooper and his equipment be denoted by W, the force acting at any moment will then be $W + K = W - kv(t)$. Let g be the earth's average gravitational acceleration at these altitudes. At a certain instant T the friction or air resistance $K(T)$ will cancel the weight and the total force will be zero, $W - kv(T) = 0$, or, denoting $V := v(T)$ we get $W = kV$, which is indeed Aristotle's law of motion. The total force being zero, we know by Galileo's law

of Inertia (or Newton's first law) that from this instant on, the parachutist will continue to descend at this constant [final] velocity V.

Aristotle was thus right in his result, which we have just rederived from Newtonian mechanics; but the opposite situation would not have worked and one cannot reproduce other situations from Aristotle's formalism, i.e. from $W = kV$. For a Galileo and a Newton to emerge, we need to define *inertia* and *mass - and this requires starting from a vacuum.* Similarly, these physicists would not have concluded that all bodies on earth fall at a velocity $v(t) = gt$ without being able to experiment in the vacuum. As long as it was forbidden to think of a vacuum, there could be no progress! For a lecture I gave last year at a conference on *friction (tribology)*, I thus chose the title *"How friction slowed down the march of science".*

Returning to the question of why did the "dark" age last so long, note that all three religious (Christian, Muslim and Jewish) and cultural establishments (including the universities, after the XIIth Century) were totally Aristotelian, the only exceptions being the anti-science movements, i.e. in the opposite direction. Very few dared criticize anything related to Aristotle, and they generally were heavily punished and failed.

Hasdai Crescas (1350-1412) rabbi of Saragossa in Aragon was a man of courage and fought for his ideas. He came to rethink of the *vacuum* and Platonic ideas, ending up writing a book "Or Adonai" (Light of the Lord) which is one of the strongest expressions of well-reasoned anti-Aristotelianism. After excusing himself for having to include in his attack Maimonides, considered as the great master [and who was also a staunch Aristotelian], Crescas analyzes and *refutes Aristotle's arguments against the vacuum* and ends up reinstating it as a valid theater for the physical world. He discusses *empty space* and argues for its being *infinite.* Crescas' book was selected by Giovanni Pico della Mirandola (1463-1494), the great proto encyclopaedist (*"de omni re scibili"*) who had it translated in Latin. The next person in this story is Giordano Bruno (1548-1600) who was burned on the stake for his having quoted and championed Crescas' *infinite space*, as the theater in which the show played is the evolution of the physical world. The arguments for the vacuum were taken up by Regiomontanus, Kepler, Galileo and others – and opened the door to modern physics.

4 The (Rigged Hilbert Space) Time-Arrowed Formalism

Where is the analogy with the story of the vacuum? Bohm's construction of Rigged Hilbert Spaces with their complex eigenvalues naturally accommodates unstable states as described by the Breit-Wigner resonances' (complex) masses $E = E_R - i\gamma/2$. In the analytical S-matrix, E_R is the value of the peak in p, and γ is the width, or the inverse of the lifetime, $\tau = 1/\gamma$. *This certainly fits with the physical world*, in which *resonances* actually *decay* and the thermodynamical or statistical arrow of time is dominant.

But *throwing away the reductionist scaffolding is another matter.* At the particle physics level, it would have been fitting in the days of the S-Matrix and Dispersion Relations. It certainly provides a useful representation of phenomenological reality. *What is missing is the off-mass-shell* extended formalism, i.e. any Relativistic

Quantum Field Theory apparatus. Its existence requires at least explicit CPT invariance - which will fail due to the T-violating contribution of the thermodynamics. Moreover, CP-violating decays such as the $K_L^0 \to 2\pi$ lose their exceptional status and merge into the background of K-decays. Once before, in Particle Physics, *during the 1955-1971 "on-mass-shell physics" interlude*, working in a direct-realization formalism *caused RQFT to fall into desuetude and atrophy*, under the impact of the appealing positivism and negation of off-mass-shell physics as broadcast from Berkeley. Feynman had been working on the renormalization of the Yang-Mills gauge quantum field theory as a pilot-project for an attack on Gravity. He had encountered a difficulty, namely the loss of unitarity off-mass-shell, due to the misfit between the finite representations of $SL(4,R)$ which define tensorial fields (necessary in the classical transition to General Relativity, when these linear representations have to carry non-linear realizations of the diffeomorfisms) and the Unitary representations of the Poincare group determining the physical Hilbert space states' components.

Example: the Yang-Mills vector-meson field $\Phi_\mu^a(4)$ has 4 components for each value of the internal index a, whereas we know that massless fields have only two physical components. The rumour about this difficulty got to Berkeley, and G. Chew proscribed Quantum Field Theory as a methodology for Particle Physics. I recall arriving at Caltech in the Fall of 1963 and writing out a *Lagrangian* on the blackboard in a seminar, being asked by a distinguished colleague "What is that?"

Happily, the onus on Quantum Field Theory did not deter Feynman from his study of the loss of off-mass-shell unitarity in Yang-Mills theory and he went on to invent *ghost fields as restorers of unitarity.* Bryce De Witt belonged to the Gravity community and was unaware of - or unaffected by - the rejection of QFT in Particle Physics; he developed Feynman's concept, which was discussed at the Infeld Anniversary Conference in Relativity. Happily, communications had not reached the present ease and efficiency of the Internet and in some disconnected regions such as the USSR (Slavnov, Faddeev and Popov) or the Netherlands (Veltman and 't Hooft) RQFT wasn't yet discarded and the renormalization program was pursued to its happy ending in 1971. Within 6 months nobody was using the S-Matrix formalism any more.

Returning to canonical Relativistic Quantum Field Theory, we remind the reader that the resonances' width is produced by the interaction responsible for the decay and is related to the transition between several quantum pictures, namely from the Heisenberg to the Schrödinger or Dirac pictures. Moreover, in the "modern" approach based on *effective field theory* this philosophy is applied to all fermionic real mass terms (beyond the present discussion relating to the imaginary parts); these are assumed to be due to further interactions at higher energy beyond the cut-off of the effective treatment and involving additional field variables which have been integrated away. It should be possible to extend this approach so as to include the emergence of the Rigged Hilbert Space width (where relevant) within the context of Relativistic Effective Quantum Field Theory and thereby relate the reductionist and effective formalisms explicitly, preserving the basic formalism as the common background.

One last remark: my warning is directed only towards Particle physics; the issue

does not arise in statistical mechanics, which is an "effective" theory by definition, generating (effective) "collective" variables.

Acknowledgments

I would like to thank both Prof. A. Bohm and Dr. S. Wickramasekara for their help.

References

1. A. Bohm, I. Antoniou and P. Kielanowski, *Phys. Lett. A* **189** (1994) 442.
2. A. Bohm, S. Maxson, M. Loewe and M. Gadella, *Physica A* **236** (1997) 485.
3. A. Bohm, *J. Math. Phys.* **22** (1981) 2813.
4. A. Bohm and M. Gadella, *Dirac Kets, Gamow Vectors and Gelfand Triplets,* Lecture Notes in Physics, **V. 348** (Springer-Verlag, Berlin, 1989).
5. A. Bohm, M. Gadella and S. Wickramasekara, in Chapman and Hall/CRC Research Notes in Mathematics, **399;** *Generalized functions, operator theory, and dynamical systems,* Ioannis Antoniou and Gunter Lumer, Eds. (1999).
6. A. Bohm and N. L. Harshman, in Irreversibility and Causality, Lecture Notes in Physics **V. 504** (Springer-Verlag, 1998).
7. A. Bohm and S. Wickramasekara, *Foundations of Physics* **27** (1997) 969.
8. S. Wickramasekara and A. Bohm, "Symmetry Representations in the Rigged Hilbert Space Formulation of Quantum Mechanics", *J. Phys. A: Math. Gen.* **35** (2002) 807.
9. A. Bohm, N.L. Harshman, H. Kaldass, S. Wickramasekara, Eur. Phys. J. C. **18**, 333 (2000)
10. A. Bohm, H. Kaldass, P. Kielanowski, Phys. Lett. A **264**, 425 (2000)
11. Y. Ne'eman, "Pythagoreanism in Atomic, Nuclear and Particle Physics", in *Proc. of Wenner-Gren Inter. Symp. Symmetry 2000, Part 1,* I. Hargittai and T.C. Laurent, eds. (Portland Press, London, 2002) pp. 265-278.
12. Dzielska, M., Hypatia of Alexandria (Harvard University Press, Cambridge (Mass.) 1995).
13. Y. Ne'eman, "Are we nearing the End of the Second Scientific Era?" (Hebrew), in BaSha'ar *(Room for Thought),* #13 (January 2000) pp. 14-19.

DISCUSSION

Chairman: H. Walther

A. Bohm: I want to respond to two remarks of Professor Neeman. The first concerns the question of whether our Breit-Wigner resonance states with exponential time evolution fits better into the Aristotelean or the Pythagorean world view. Our state is an idealization, it describes the resonance per se, isolated from the background. Such a background is always present in a real experiment, like the

friction in the real world. We "reduce" the bump in the lineshape into an idealized Breit-Wigner resonance state and the background. For the idealized resonance state, we prove the exponential time evolution; the background does not allow such a simple law. It is like the particle with friction, if one does not "isolate" the particle from the friction, it does not evolve simply. Thus our resonance states represented by Gamow vectors are Pythagorean idealizations.

The second point concerns the quantum mechanical arrow of time of which time asymmetry of the quantum decay is just one manifestation. This arrow of time is not due to the effect of the environment, which one usually considers in quantum statistical mechanics, and which may bring to mind the effect of external friction and Aristotle. It is something that is intrinsic to the quantum system and it is described by boundary conditions, like the radiation arrow of time or the cosmological arrow of time. That is also why Professor Prigogine calls it intrinsic irreversibility. Boundary conditions are as fundamental as the dynamical equations. However, Hilbert space mathematics does not allow time-asymmetric boundary conditions for the Schrödinger or von Neumann equation and therefore one thinks of time asymmetry in quantum mechanics as an effect from the outside.

L. Reichl: I think that time irreversal shows up particularly in the modern quantum mechanics. It is still there, and this is a way to describe key problems.

ENTANGLEMENT, COMPLEMENTARITY AND DECOHERENCE

J.M. RAIMOND

Laboratoire Kastler Brossel, Département de Physique de l'Ecole Normale Supérieure, 24 rue Lhomond, F-75231 Paris Cedex 05, France

We review the ENS experiments performed with circular Rydberg atoms interacting, one at a time, with a high-quality superconducting cavity. The atom-cavity interaction makes it possible to engineer and manipulate complex entangled states. It also allows for an in-depth experimental exploration of basic quantum mechanics concepts, such as complementarity.

1 Introduction

The manipulation of complex entangled states has become a very active field since it has been recognized that the unique features of the quantum world make it possible to realize new information transmission and processing schemes. In this paper, I review briefly the experiments performed in our laboratory with a Cavity Quantum Electrodynamics (CQED) set-up. It makes use of circular Rydberg atoms and of superconducting millimeter-wave cavities to achieve a strong coupling regime, where the coherent atom-cavity interaction overwhelms the decoherence processes. These experiments demonstrate various aspects of entanglement, as well as the deep relationship between entanglement and complementarity. We give here only a very brief overview of this subject. A much more detailed account, as well as references to other cavity QED experiments, can be found in a recent review paper [1].

2 Experimental set-up

Our experimental set-up is sketched in Fig. 1. The atoms are prepared in a circular Rydberg state in box B, in a Rubidium atomic beam, velocity-selected by laser optical pumping. The atoms can be prepared either in level e (circular state with principal quantum number 51) or in state g (principal quantum number 50). Both levels have a long lifetime (about 30 ms). The $e \rightarrow g$ transition, at 51.1 GHz, is extremely strongly coupled to the millimeter-wave field. The circular atoms are protected from the blackbody background radiation by a 1 K cryogenic environment. The preparation process is time-resolved and the atomic samples have a well-defined velocity and initial position. The position of the sample at any time during its further travel in the apparatus is thus well-known, allowing us to apply selective transformations to different samples in the same experimental sequence.

The atoms interact with the superconducting cavity C, made of two spherical superconducting mirrors facing each other. It sustains two nearly degenerate gaussian modes M_a and M_b with orthogonal linear polarizations. The frequency difference between these modes, due to a slight mirrors asphericity, is $\delta/2\pi = 128$ kHz. Both modes store microwave photons for up to 1 millisecond. The cavity is tuned at or close to resonance with the $e \rightarrow g$ atomic transition. After the interaction with C, the final atomic state is measured in the selective field-ionization detector D. The number of atoms in a sample follows a Poisson statistical distri-

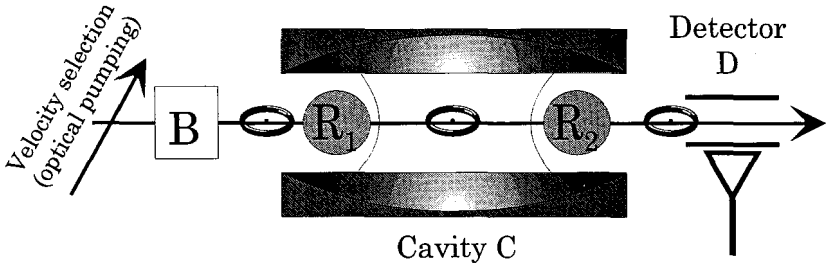

Figure 1. Scheme of the Rydberg atoms cavity QED set-up

bution, with an average value set around 0.1. When an atom is detected, there is thus a negligible probability for having an unwanted second atom in the sample.

Some experiments are performed by directly detecting the atomic final energy state in D. In others, atomic state superpositions are used. These superpositions are prepared, before the atom enters C, by applying to it an auxiliary microwave classical field pulse (produced in zone R_1, see Fig. 1). Another pulse, produced in R_2, is used to mix again the atomic energy states after the atom has interacted with C. The successive application of these two pulses constitutes a Ramsey interferometer. Interference fringes are obtained in the probability for finding the atom in a given final state either when the frequency of the $R_1 - R_2$ fields is swept across a transition between two Rydberg levels, or when the energy gap between these levels is tuned, using a Stark effect induced by a variable electric field applied across the cavity mirrors. We study how the fringe phase and amplitude is affected by the presence of photons in the cavity and we gain in this way useful information on the atom-photon interaction process.

3 Two-particle entanglement

Atom-field entanglement is achieved by exploiting the Rabi oscillation at frequency Ω which occurs when the atom interacts resonantly with one of the cavity modes containing 0 or 1 photon. Let us consider the simple situation of an atom entering the empty cavity in state e. The initial state, $|e,0\rangle$, is resonantly coupled to $|g,1\rangle$, describing an atom in the lower state g with one photon in the cavity. The Rabi oscillation between these states brings, after an interaction time t, the atom-field system in the linear superposition $\cos(\Omega t/2)|e,0\rangle + \sin(\Omega t/2)|g,1\rangle$. In our set-up, $\Omega/2\pi = 50$ kHz, so that the Rabi period is much shorter than the cavity field relaxation time [2]. The interaction time t is adjusted by Stark switching the $e \rightarrow g$ atomic transition out of resonance while the atom flies across the cavity, thus freezing the system evolution when the desired value of the "pulse area" Ωt has been achieved. When $\Omega t = \pi/2$, maximum atom-field entanglement is obtained [3]. When the pulse area is π, the atom and the field fully exchange their energies [4].

This process can be used to swap excitation between the atom and the field and to transform atom-field entanglement into an atom-atom one. The experiment

involves two atoms crossing the cavity one after the other, the first initially in level e, the second in g. The first atom undergoes a $\pi/2$ Rabi pulse and gets entangled with the cavity mode. The second is submitted to a π pulse, copying the cavity state and getting entangled in the process with the first atom. Note that the cavity is left in its initial vacuum state, disentangled from the atomic pair. It acts, in this process, as a "catalyst" for the atom-atom entanglement. This entanglement has been checked by performing various measurements on the final states of the two-atoms and analyzing their correlations [3]. This massive pair of particles, of the Einstein-Podolsky-Rosen (EPR) type, could be used for Bell's inequality tests.

The above atom-atom entangling procedure relies on the transient real emission of a photon in the cavity. It is also possible to entangle two atoms directly, via a collision process assisted by non-resonant cavity modes [5]. The first atom (A_1) is again initially in e and the second (A_2) in g. The atoms have now different velocities, so that the second catches up the first at cavity center, before exiting first from C. The two cavity modes are now detuned from the $e \rightarrow g$ transition frequency by amounts Δ and $\Delta+\delta$, greater than Ω. Due to energy non-conservation, no real photon emission can occur in this case. Atom A_1 can, however, virtually emit a photon immediately reabsorbed by A_2. This leads, as in the resonant case, to atom-atom entanglement. The system ends up in a superposition of the $|e,g\rangle$ and $|g,e\rangle$ states.

The quantum amplitudes associated to these states are periodic functions of the collision duration (which depends on the atoms velocities). The oscillation frequency associated to this second order collision process is $(\Omega^2/4)[1/\Delta + 1/(\Delta+\delta)]$. By repeating the experiment, we reconstruct the probabilities P_{eg} and P_{ge} for finding finally the atom pair in states $|e,g\rangle$ and $|g,e\rangle$. We plot these probabilities versus the dimensionless parameter $\eta = \omega[1/\Delta + 1/(\Delta+\delta)]$ (see Fig. 2). The oscillations of P_{eg} and P_{ge} as a function of η are well accounted for by theoretical models (solid and dashed lines in Fig. 2). We have realized the situation of maximum entanglement by adjusting η to the value corresponding to $P_{eg} = P_{ge} = 0.5$. We have also checked the coherent nature of the two-atom state prepared in this way by performing measurements of observables whose eigenstates are superpositions of energy states.

Since this new entanglement method implies only a virtual photon exchange with the detuned cavity mode, it is, in first order, insensitive to the cavity damping time or to a stray thermal field in the cavity mode. It thus opens interesting perspectives for demonstrating elementary steps of quantum logic with moderate Q cavities.

4 Quantum gates and non destructive measurement of photons

We now come back to the resonant atom-cavity case. After a full cycle of Rabi oscillation (2π pulse), the atom-field system comes back to its initial state, with a π phase shift of its wave function. If the system is initially in the $|g,1\rangle$ state, it ends up in the state $-|g,1\rangle = \exp(i\pi)|g,1\rangle$. This is reminiscent of the sign change of a spin state undergoing a 2π rotation. When the cavity is initially empty, the sign of the state is unaltered, the $|g,0\rangle$ state remaining unchanged. If we view the atom

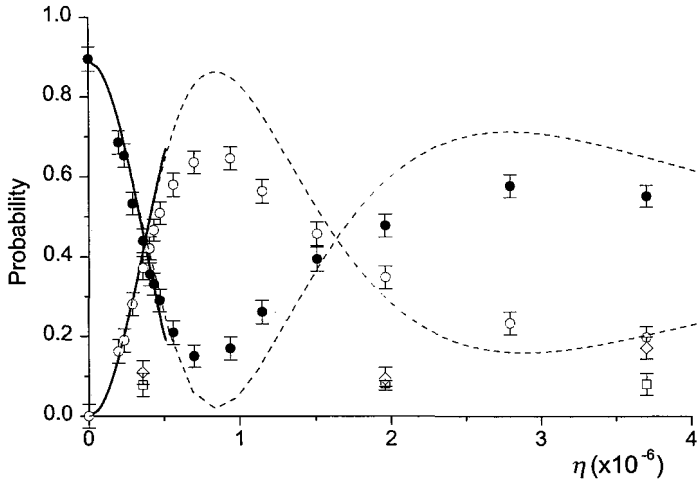

Figure 2. Joint detection probabilities P_{eg} and P_{ge} versus the parameter η. Points are experimental. Solid lines for small η values correspond to a simple analytical model based on second order perturbation theory. The dashed lines (large η) present the results of a numerical integration of the system evolution (adapted from [5])

and the field as qubits, the 2π Rabi pulse couples them according to the dynamics of a quantum phase gate. We have shown that this gate works in a coherent and reversible way [6]. We have also applied this gate to perform a non-destructive measurement of a single photon [7]. The phase change of the atomic wave function when it undergoes a 2π Rabi pulse in C can be translated into an inversion of the phase of the fringe pattern of the Ramsey interferometer sandwiching the cavity (see Fig. 1). By setting the interferometer at a fringe extremum, we correlate the photon number (0 or 1) to the final state of the atom. The atom is then a "meter" measuring, without destroying it, a single photon in C. The same photon can be measured repeatedly by successive atoms, without being absorbed. This is quite different from ordinary absorbing photon counting procedures. Note that this procedure leads also to a direct determination of the Wigner distribution at the origin of phase space for the vacuum or a one-photon field state [8].

5 Multiparticle entanglement

By combining quantum Rabi pulses of various durations and auxiliary Ramsey pulses on successive atoms, one can generate and analyse entangled states involving more than two particles. By applying a $\pi/2$ Rabi pulse on a first atom, one entangles it to a 0/1 photon field. A second atom then undergoes a 2π Rabi pulse combined to Ramsey pulses, in order to measure this field in a non destructive way. Before this atom is detected, a three-part entanglement involving the two atoms and the photon field is generated. The field state is finally copied on a third atom, initially

in the lower state of the transition resonant with the cavity mode (a π Rabi pulse is used for this copying procedure). The characteristics of this three-particle entangled state are analyzed by performing various measurements on the three atoms [9]. These measurements involve the application of auxiliary Ramsey pulses after the atoms have interacted with the cavity. The procedure could be generalized to situations of increasing complexity, with larger numbers of atoms.

6 Complementarity and entanglement at the quantum-classical boundary

We have also used our set-up to perform a complementarity test [10], very closely related in its principle to the double slit experiment described by Bohr in his 1927 discussions with Einstein. Bohr had analyzed a situation where particles are crossing a Young interferometer in which one slit is carried by a light assembly, free to move independently of the other. In an ordinary Young design with fixed slits, interference fringes reveal the wave nature of the particle. In this design, the momentum imparted to the moving slit by the deflected particle provides a "which path" information, suppressing the fringes and revealing the corpuscular aspect. In this experiment, the quantum moving slit and the particle are in fact the two components of a correlated EPR system. The trajectory of the particle gets entangled to the motion of the slit. Observing (really or virtually) this motion lifts the ambiguity of the particle path and suppresses the interferences. Intermediate situations can be considered, by varying for example the mass of the movable slit. There is a continuous transition from the quantum slit case (very small mass) to the classical one (infinite mass). In between, we expect fringes with a limited contrast, reflecting the partial degree of entanglement between the slit and the particle.

A Young double slit experiment with an ultra-light quantum slit would be very difficult to realize. This gedanken experiment can however be translated into an easier to perform cavity QED experiment, presenting the same conceptual features [10]. We use, instead of a Young device, our double oscillatory field Ramsey interferometer, in a slightly modified version. The field pulses, resonant on the $e \rightarrow g$ transition, act as atomic beam splitters transforming these states into superpositions. The first resonant field, instead of being produced by R_1, is now a small coherent field injected through a wave guide inside the long lived cavity mode C. Depending upon the average photon number n in this field, it can be considered either as a microscopic or macroscopic "beam splitter". The second pulse is produced downstream in R_2. This latter pulse, produced by photons fed into a low Q field mode and recycled at a very fast rate, can always be considered as macroscopic and classical. The first and second pulses are thus equivalent to the movable and fixed slits of Bohr gedanken experiment. If n is large, Ramsey fringes with maximum contrast are expected. When n gets smaller, the one photon change produced by the atomic transition from e to g leads to atom-field entanglement, in the same way as the recoil of the slit in the Young apparatus leads to slit-particle entanglement. Fringe contrast is then expected to be reduced. The experimental signals are shown in Fig. 3a. We observe that the fringe contrast becomes smaller and smaller as n decreases. At the limit where the field in C is the vacuum, the fringes vanish, re-

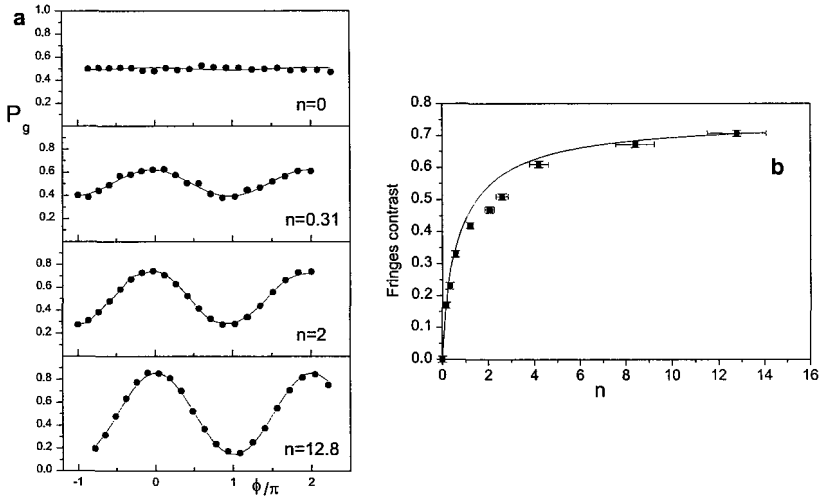

Figure 3. a) Ramsey fringes obtained for different mean photon numbers n in the first coherent field pulse. The phase Φ is swept by Stark tuning the atomic energy levels. b) Fringe contrast as a function of n. The points are experimental. The line represents the theoretical predictions corrected for the imperfections of the interferometer (adapted from [10])

vealing maximum atom-field entanglement in C. Fig. 3b shows the fringe contrast versus n. The points are experimental and the curve is a theoretical fit.

We have performed other entanglement experiments, based on the use of dispersive non-resonant atom-field interaction. Schrödinger cat like states of the field have been produced in this way and their decoherence studied [11]. All these experiments illustrate fundamental concepts of quantum theory and demonstrate the feasibility of elementary logical steps in quantum information processing. We are considering various improvements of our set-up and procedures, in order to be able to increase the number of atoms and photons involved in these experiments.

Acknowledgments

Laboratoire Kastler Brossel is a laboratory of Université Pierre et Marie Curie and ENS, associated to CNRS (UMR 8552). We acknowledge support of the European Community, of the Japan Science and Technology corporation (International Cooperative Research Project : Quantum Entanglement).

References

1. J.M. Raimond, M. Brune and S. Haroche, Rev. Mod. Phys. **73** , 565 (2001).
2. M. Brune *et al.*, Phys. Rev. Lett. **76**, 1800 (1996).
3. E. Hagley *et al.*, Phys. Rev. Lett. **79**, 1 (1997).

4. X. Maître *et al.*, Phys. Rev. Lett. **79**, 769 (1997).
5. S. Osnaghi *et al.* Phys. Rev. Lett. **87**, 037902 (2001).
6. A. Rauschenbeutel *et al.*, Phys. Rev. Lett. **83**, 5166 (1999).
7. G. Nogues *et al.*, Nature **400**, 239 (1999).
8. G. Nogues *et al.*Phys. Rev. A. **62**, 054101 (2000).
9. A. Rauschenbeutel *et al.*, Science **288**, 2024 (2000).
10. P. Bertet *et al.*, Nature (London), **411**, 166 (2001).
11. M. Brune *et al.*, Phys. Rev. Lett. **77**, 4887 (1996).

DISCUSSION

Chairman: A. Zeilinger

L. Stodolsky: I would like to make a couple of comments from the other field. I am not really an enemy of quantum optics, it is absolutely beautiful stuff, which we are hearing about. But there are other technologies which have been used, for example I will discuss in my talk so called Schrödinger cat, involving 10^{19} electrons using Josephson effect. Also under "which path" information, since I guess there is nobody here from the 2-dimensional electron gas community, there was a very beautiful experiment done by the Weizman Group, giving "which path" information when you observe the path by the so-called QPC (quantum point contact). By adjusting how strongly you look at the path you see the interference fringes disappearing. It is a very nice experiment.

J. Raimond: There are very beautiful experiments on Schrödinger cats in SQUIDs. However, there is not yet, I think, an extremely clear demonstration of the fact that these experiments really prepare a quantum superposition. More experiments are necessary to close this debate. Concerning the second part of your question, I would like to comment, of course, that we are very far from having made the first complementarity experiment. The one of the Weizman Institute is very remarkable. The main originality, I think, of our experiment is to have a continuous variation of the interferometer's slit from quantum to classical domains.

L. Stodolsky: A second point that I would like to comment is the question of whether decoherence can be viewed as a kind of standard relaxation phenomenon. In our original methodology for treating decoherence which we then called quantum damping around 1980, we have a certain formula for the decoherence rates, which in one limit does look like normal relaxation, in another limit, according to a certain parameter, it can describe these two-path experiments and it looks like a sort of collapse of the wave function. But it is actually one formula that describes both limits. I think in a sense in certain cases decoherence is just normal relaxation.

J. Raimond: I agree with you on the point that decoherence can be fully treated by standard relaxation theory. For instance, the results of our "Schrödinger cat" experiments are very well described by a simple calculation based on the standard tools of relaxation theory in quantum mechanics. They can also be cast, in an even simpler calculation, in terms of information leaking into the environment -in terms of complementarity if you prefer.

What is new in decoherence is the result of the application of standard relaxation theory to a macroscopic (or at least mesoscopic) system. If you apply relaxation theory to an ideal spin 1/2 system, you have one single relaxation time T_1, which governs everything (because T_2 is just proportional to T_1). Even if the spin is in a quantum superposition of states, it is always the same relaxation time that comes in. But if you have a macroscopic system, a big angular momentum for instance, then the relaxation time is not the same for all quantum states. Some "macroscopic" superpositions decay much faster than some other states. So, decoherence is standard relaxation theory in a situation where you have complex dynamics, which is reflected by this dependence of the relaxation time upon the state that you plug in initially.

L. Stodolsky: It is something that I will have to explain perhaps in my talk. It's actually one formula but which in certain limit looks like normal relaxation, and the other looks like collapse of the wave function.

G. Hegerfeldt: I would like to make a short remark about complementarity. You state it as a basic principle of quantum mechanics, and I do not quite agree with that. In your beautiful experiment, you show that it's useful principle, it is a very quick understanding of the experiment. But if you look at Bohr, then you will find continuous changes in what he means by complementarity. When I learn quantum mechanics from Dirac, he never uses complementarity. At least, in the Dirac sense you can do quantum mechanics without complementarity. But I agree that it is a useful concept to unify experimental designs.

A. Zeilinger: I have some interest in the discussion going on here. It's an old tradition in quantum mechanics that you have people who are just satisfied using the apparatus with working precision. That is perfectly legitimate. There are other people who think that there might be interesting notions, interesting philosophy notions behind, like for example complementarity or entanglement. These are different points of view and both are legitimate, and I don't understand why there is sometimes a battle between the two sides, because there are possibilities for new ideas. We all know that both sides are important. Dirac was absolutely not interested in philosophy, he just did great physics. Other people like Einstein, Schrödinger were very much interested in these questions. Both sides are important, you never know what leads to new ideas.

J. Raimond: Complementarity, at least in our experimental situation, is just the wave-particle duality It is clear that I cannot pretend I have understood fully what Bohr had in mind when he discussed complementarity and its far-reaching consequences. I use it in the most basic situation. Complementarity here basically states that the nature of your object depends on the question you ask. And I don't want to use or to push complementarity beyond this context.

W. Schleich: This one experiment with the fringes patterns changing, it is a beautiful realization of the old proposal by Scully if I remember.

J. Raimond: I am very much afraid I couldn't quote everybody on complementarity. An experiment closely related to ours was proposed in his paper. The basic proposal was to have a two-slit interference experiment and to put two cavities behind the slits. The atom deposits a photon when it crosses either cavity. A "which path" information is provided by the photon, finally stored in one cavity or in the

other. This is yet another experiment on complementarity, albeit there is not, in this case, a transition from quantum to classical behaviors as in our situation.

W. Schleich: I want just to say that in this paper, they said that complementarity is something deeper than just the uncertainty principle. My question now is if anyone knows anything going deeper than just wave-particle duality.

J. Raimond: In our case there is a simple interpretation of the fringe contrast loss in terms of photon number/phase uncertainty relations, at least in qualitative terms. The very interesting problem is: Is Heisenberg uncertainty necessary or not? My position is that any experiment on complementarity can be understood in more general terms by using the notion of entanglement. It gives a very general framework to discuss complementarity, either when it is based on Heisenberg relations or not.

PHASE DYNAMICS OF SOLID-STATE QUBITS: MAGNETS AND SUPERCONDUCTORS

P. C. E. STAMP[1,2]

[1] *Spinoza Institute, University of Utrecht, Leuvenlaan 4, 3584 CE Utrecht, Netherlands*
[2] *(from Jan. 2002) Canadian Institute for Advanced Research, and Physics Dept., University of British Columbia, 6224 Agricultural Rd., Vancouver, B.C., Canada V6T 1Z1*

It is widely believed that quantum information devices like quantum computers will be built from solid-state qubits. Making functioning networks of these will pose formidable challenges coming from decoherence, which is usually very strong in the solid state. Here I review theoretical progress in understanding the decoherence mechanisms in superconductors and magnetic systems, wherein we believe decoherence can be made extremely small, and for which experiments reporting large-scale coherence already exist. Our microscopic understanding of superconducting and magnetic qubits is reviewed – the way in which one arrives at a low-energy effective Hamiltonian is explained in detail for a magnetic system. The way in which decoherence enters the dynamics of solid-state qubits is then discussed, along with the connection to experiment. Finally, I discuss ways in which decoherence can be further suppressed, using for example applied transverse fields.

1 Introduction: Quantum Communication, and large-scale Quantum Phenomena

The following is a progress report on what has been done so far on the theory of solid-state qubits. I concentrate almost exclusively on nanomagnets and superconductors. Actually many other designs have been described for solid-state qubits. These include paramagnetic spins in semiconductors [1], nuclear spins in Fractional Hall states [2], and electronic spins in quantum dots [3]; and some experimental work has been done in these directions. So far, however, the most thorough work has been on superconductors and magnets – indeed a search for large-scale quantum phenomena has been going on in these systems for nearly 20 years now, since the original theoretical discussions for superconducting SQUIDs [4], and magnetic domain walls [5]. There has been very important recent experimental progress in this field in superconducting systems [6,7,8,9], which make it clear that we are well on the road to having superconducting qubits. It is puzzling that less success has so far been obtained in experiments on insulating magnetic systems – I will argue that this is mainly because experiments have not been looking in the right place, and that very high-Q coherent qubit dynamics should also be visible, in certain magnetic molecules, in strong transverse fields (see section 5A). Ultimately these experiments, and the theory which has led to them, will finally decide the old debate on whether quantum mechanics can truly be extrapolated to the macroscopic scale.

Most of the material reviewed here will be theoretical (for recent discussions of experiments on superconductors and nanomagnets, see refs. [8,9,7] and [10,11]). The main emphasis will be (i) on the underlying physics of magnetic and superconducting qubits, and the effective Hamiltonians describing them, and (ii) on decoherence, both the physical mechanisms responsible for it, and its dynamic effects at the

one-qubit level. Some ways of getting rid of decoherence are discussed at the end. The intended audience is the same as that at this 22nd Solvay conference, ie., a broad audience of physicists and some chemists, with no specialised knowledge of condensed matter theory assumed. Readers are also referred to recent theoretical reviews in the literature, including discussions of superconducting qubits [12], and discussions of decoherence and the dynamics of 2-level systems coupled to their surroundings [13,14,15,16]. Note that I will not really discuss quantum computation itself (for which see refs. [17,18]), nor try to review all theoretical work on decoherence; this is an article about hardware.

2 Magnets and superconductors: microscopic physics

The purpose of this section is to explain how at low energies (well below $1K$) the very complex physics of magnets and superconductors simplifies in such a way that one can build qubits from them, with only small sources of decoherence under appropriate conditions. The results described here exist already, for the most part, in specialised papers. However since the readership is assumed rather broad, I will try to give a more accessible picture.

As an illustration, I go into a little detail for the magnetic case. The procedure for superconductors is similar, so only the results will be described. The net result is an effective Hamiltonian for a single qubit (magnetic or superconducting) coupled to its environment. Multi-qubit systems are dealt with in the next section. The key results are embodied in equations (9) and (19), but these effective Hamiltonians are not meaningful until one knows where they come from.

The basic line of argument is conventional. It is a truism that *any* Hamiltonian in physics is an "effective" one, resulting from truncation of higher-energy "virtual" physics into effective couplings between low-energy modes. It is easy to forget this in fields like Quantum Optics or NMR, where the separation of energy scales between the energies of interest and higher energy/mass scales is large (as in, eg., the derivation from QED – another effective theory – of atomic Hamiltonians weakly coupled to photons, including relativistic corrections [19,20,21]). Things are not usually so simple in a condensed matter system – the separation of energy scales is not so clear cut, and interactions are not weak. Nevertheless the basic approach is the same – one begins with an effective Hamiltonian $\mathcal{H}(\Lambda_o)$ with ultraviolet cutoff Λ_o. This is assumed well understood and tested over some energy range less than Λ_o. One then truncates out those high-energy modes in $\mathcal{H}(\Lambda_o)$ which are irrelevant to the low-energy scale of interest, to give a new Hamiltonian $\mathcal{H}(\Omega_o)$ with UV cutoff Ω_o. There is of course nothing particularly quantum-mechanical about this – the same idea is involved in, eg., the derivation of classical hydrodynamics.

2.1 Magnetic systems

The sort of magnetic systems we are interested in include nanofabricated magnetic particles, and large-spin magnetic molecules – or, even smaller, paramagnetic or nuclear spins. These may be embedded in some matrix (eg., a semiconductor) or on a substrate, or self-organised into some array. The physics is usually complicated

– the spins inside a molecule or nanoparticle couple to each other via exchange or superexchange interactions, and to their surroundings in complex ways. One has high energy ($\sim O(eV)$) crystal field/spin orbit couplings, which at low energy give a magnetic anisotropy term acting on each spin. Then these spins couple to the surrounding EM field, and to nuclear spins via rather complex hyperfine interactions, involving many terms. Their real space motion also couples them to phonons, and if there are any mobile electrons around a rather complicated exchange coupling to these is involved. Finally, in any array of spins or nanomagnets, there will be long-range magnetic dipolar interactions between spatially separated spins. All of this makes for a messy hierarchy of interactions (Fig. 1). We want to know how this truncates to an effective low-energy Hamiltonian.

Truncation to a qubit

(i) Stage 1; eV energy scales: In an insulating magnetic system the spin-orbit, electromagnetic, and crystal field terms are closely linked with the dynamical electronic modes (electronic excitation energy gaps, electron-electron interaction strengths) at eV scales or higher – this is the main reason why magnetic phenomena are so complex and difficult to treat (see Fig. 1). However at lower energies much of this truncates to simpler forms – the resulting magnetic anisotropy terms are typically $\sim 1 - 10K$ per electronic spin, and the hyperfine terms $\sim 1 - 100mK$ per electron-nucleon coupling (NB: recall that $1eV \equiv 11,604K$; alternatively, $1K \equiv 20.83GHz$). Thus one has a very large separation of energy scales from the original electronic energies – more than 4 orders of magnitude. The same is less obviously true of the phonon terms, or the exchange/superexchange terms (arising from competing kinetic and potential terms in the high-energy atomic Hamiltonian). These each have characteristic energies $\sim 100 - 1000K$. However in an insulating magnet this is still ~ 100 times less than the electronic energies, except in unusual cases. One can therefore determine perturbatively the exchange and superexchange spin-spin interactions, magnetoacoustic couplings, and phonon and magnon spectra with some confidence – usually with help from experiment, and using symmetry arguments to determine their form.

All this procedure is standard (and exactly the same as that followed in, eg., high-energy theory or quantum optics). It gives a typically very messy effective theory for energy scales $\sim 100 - 1000\ K$, described in tens of thousands of papers and books (see, eg., ref. [22]). The exact quantitative values for all the different low-energy couplings (and there are many of these!) is not always easy to determine, mainly because the Hamiltonian at eV scales is uncertain (even if one knows the original atomic terms, the magnetic ions are very strongly perturbed versions of these). However their basic form can be determined, and the values of the couplings then extracted from experiment. Of course some terms (eg., phonon energies, and magnetoacoustic and dipolar hyperfine couplings) can be calculated from the higher energy theory, because accurate expansions in a small parameter can be made.

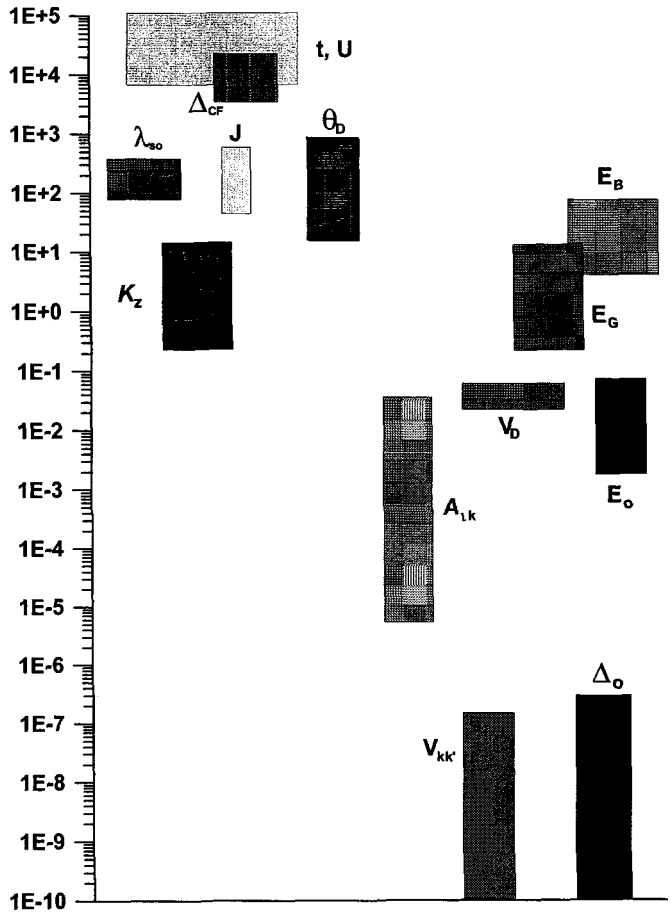

Figure 1: **Hierarchy of Magnetic Interactions.** The various energy scales existing in insulating magnetic systems – energies are measured in Kelvin, ranging from 10^5 K (i.e, roughly 8.6 eV), down to 10^{-10} K (ie., 2 Hz in frequency units). We show energy ranges typical of transition metal based magnets.

On the top left we have the energy scales important for bulk magnets. At eV scales are the electronic energies t (band kinetic energy), and U (on-site Coulomb repulsion), and the crystal field energies Δ_{CF}, followed at hundreds of Kelvin by superexchange energies $\mathcal{J}$, spin-orbit coupling λ_{so}, and phonon Debye energies θ_D. Easy axis anisotropy energies $\mathcal{K}_z$ come in at $1-10$ K (occasionally down to nearly 0.1 K).

On the right are shown energies relevant to magnetic nanomolecules and nanoparticles. In the rough range $1-100$ K we have the tunneling barrier E_B and the spin gap E_G. Around 0.1 K the intermolecular dipole interaction V_D sets in (for crystalline arrays of molecules/nanoparticles); the spread E_o of the nuclear multiplet around each electronic spin level is at somewhat lower energies. In zero applied field the tunneling amplitude $|\Delta_o|$is usually far below this (later we see how it can be dramatically increased using applied transverse fields). Finally one has the hyperfine couplings $\mathcal{A}_{ik}$ and the internuclear interactions $V_{kk'}$.

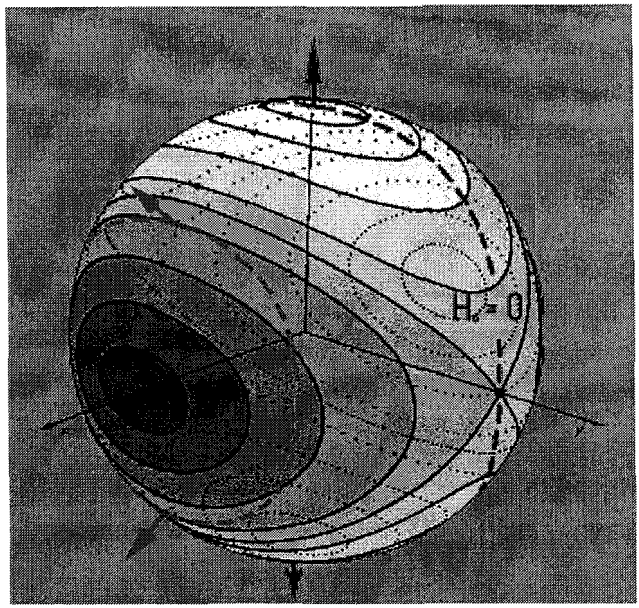

Figure 2: **Nanomagnetic Spin Dynamics on the Bloch Sphere.** Equipotential lines of an easy axis magnetic anisotropy potential are plotted on the Bloch sphere, with shaded areas representing higher energies. In zero applied field the minimum energies are found along the easy axis – the 2 lowest eigenstates are made from tunneling superpositions of the states $|\Uparrow\rangle$ and $|\Downarrow\rangle$, which have wave-functions concentrated around the 2 poles on the spin sphere (with the 2 possible tunneling paths, denoted by $H_o = 0$, crossing one or other saddle point in the potential). If a strong transverse field is applied along the hard axis (in the direction perpendicular to the saddle point paths) the 2 states $|\Uparrow\rangle$ and $|\Downarrow\rangle$ are pulled towards the field direction (and towards each other), and the tunneling paths are shortened. Interference takes place between these 2 paths (see section 5 for details of the behaviour with field.)

(ii) Stage 2; Intermediate energies: Things simplify when the UV cutoff is lowered to $1 - 10K$, well below superexchange energies. We then come to the picture which underlies the field of "nanomagnetism" (Fig. 1, right-hand side). The exchange/superexchange couplings lock the electronic spins in a nanomagnet together into a "giant spin" $\mathbf{S}$, with $|\mathbf{S}| = S = constant$ (electronic spin excitations, involving the superexchange couplings, can be ignored). This spin is of course coupled to crystal fields, which Means that its dynamics is described by a Hamiltonian $\mathcal{H}_o(\mathbf{S})$ which can be thought of as a simple potential on the Bloch spin sphere (Fig. 2). This potential obeys the relevant double point group symmetries in the problem, and its energy scale in $\sim KS$, where K is the energy scale of single spin magnetic anisotropy (typically $1 - 10K$). Typically there will be an easy axis (which we will take to be the $\hat{z}$-axis), with a barrier of height $\sim K_{\|}S$ between the potential wells at the poles (here $K_{\|}$ is the strength of the easy-axis anisotropy per electronic spin). Well-known examples include the magnetic nanomolecules Mn-12 and Fe-8, which are just two of thousands of magnetic molecules studied by chemists and

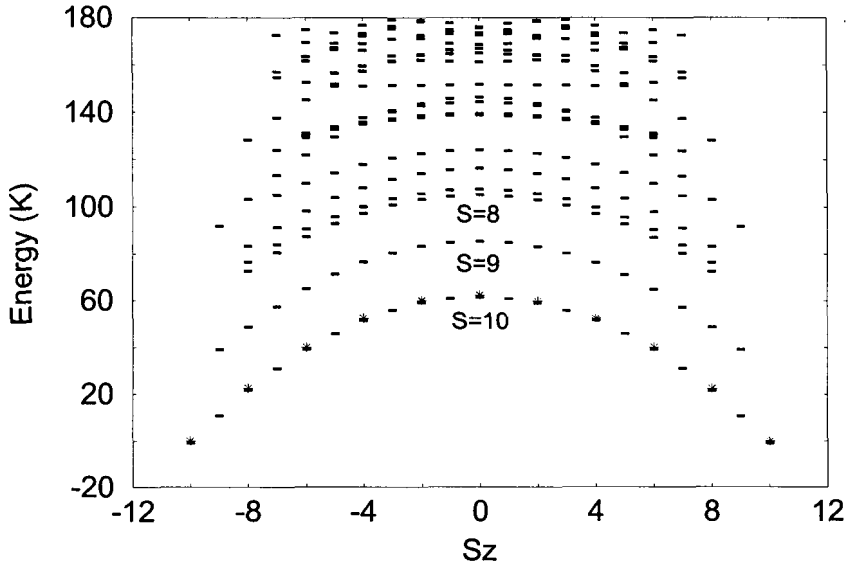

Figure 3: **Electronic spin excitations in a Nanomagnet.** Eigenfunctions of an approximate spin-spin Hamiltonian for a typical magnetic molecule (the spin-10 Mn-12 acetate molecule), shown as a function of the projection $S_z$on the easy axis. The lowest inverted parabola contains the 21 states of the $S = 10$ "giant spin" manifold, described by the Hamiltonian $\mathcal{H}_o(\mathbf{S})$. Higher states come from 'spin flip" excitations out of this manifold (courtesy of I.S.Tupitsyn, after ref.[11]).

physicists[23]. The rather typical Fe-8 molecule has a central core of 8 Fe^{+3} ions, which lock together via superexchange interactions to form a spin-10 "giant spin". The anisotropy potential is roughly[10]:

$$\mathcal{H}_o(\mathbf{S}) = \frac{1}{S}\left[-\mathcal{K}_z S_z^2 + \mathcal{K}_x S_x^2\right] + O(S_\alpha^4/S^3) \qquad (1)$$

where $\alpha = x, y, z$. In Fe-8 one has $\mathcal{K}_z \sim 2.3\ K$ and $\mathcal{K}_x \sim 0.94\ K$. Thus we have an easy $\hat{z}$-axis, and also an easy $\hat{z}\hat{y}$-plane (cf. Fig. 2). The longitudinal easy-axis term $\mathcal{K}_z$con trols the gross energy level structure, and the 2 lowest states are in potential wells of depth $\sim S\mathcal{K}_z$. If we ignore the transverse terms like $\mathcal{K}_x S_x^2/S$, then all states are eigenstates $|Sm\rangle$ of $\mathcal{H}_z = -\mathcal{K}_z S_z^2/S + ..$ with projection m along $\hat{z}$; the spin gap E_G between the 2 lowest states $|\pm 10\rangle$ and the next 2 states $|\pm 9\rangle$ is $E_G \sim \mathcal{K}_z$ (actually it is almost exactly $(2S-1)\mathcal{K}_z/S = 1.9\mathcal{K}_z \sim 4.4\ K$). These numbers are fairly typical of transition metal based high-spin molecules.

Higher magnetic excitations, not described by this simple model, lie above a threshold energy very roughly given by $\sim |\mathcal{J}|/S$, corresponding to spin flip or "magnon" excitations which are somewhat delocalised around the nanomagnet (in the case of Fe-8 this energy is roughly $15K$). The rough structure of these higher electronic spin states in energy space can be seen in Fig. 3 (actually computed by I.S. Tupitsyn[11] for the Mn-12 molecule, for which this energy is $\sim 40\ K$).

Although at intermediate energies these other electronic spin excitations have

gone away, we still have the gapless low energy phonons to contend with, as well as even lower energy nuclear spins – neither are included in (1). One can write down the forms for the spin-phonon and hyperfine interactions, but they are rather messy at this energy scale.

(iii) Quantum Regime: The final step is to energy scales way below $1K$. Then typically only *two* electronic energy levels are left, the two lowest levels of $\mathcal{H}_o(\mathbf{S})$ (with a splitting arising from the tunneling between the two lowest energy potential wells; cf. Fig. 2). Even though an accurate calculation of this splitting is difficult, it is obvious that the effective Hamiltonian now for the nanomagnet is just $\mathcal{H}_o(\hat{\tau}) = \mathbf{h}_o \cdot \hat{\tau}$, where $\mathbf{h}_o$ is some vector, and $\hat{\tau}$ a Pauli spin. Typically we write this as

$$\mathcal{H}_o(\hat{\tau}) = \Delta_o \hat{\tau}_x + \epsilon_o \hat{\tau}_z \tag{2}$$

using an appropriate rotation in Pauli space – Δ_o is the tunneling amplitude, and ϵ_o is called the longitudinal bias energy, since a field H_o^z along the $\hat{z}$-axis gives a bias energy $\epsilon_o = g\mu_B S H_o^z$. This is our *magnetic qubit*, which for shorthand we will call a "magbit". As we shall see the parameters Δ_o, ϵ_o are easily manipulated with applied fields.

I immediately emphasize that the 2 qubit eigenstates $|+\rangle$, $|-\rangle$ are not related in a simple way to the original electronic spin states. In fact the Hilbert space of even a small magnetic molecule is so enormous, and the electronic and other interactions are so complex (and strong) that one is dealing with a typical many-body problem here – with no hope of computing the total spin wave-function in terms of the individual electronic spin states (The results in Fig. 3 involve many approximations). This may seem utterly obvious, but it is useful to underline the point by clearing up a few misconceptions held in some quarters. In particular:

(a) Suppose a simple situation in which there is no applied field in the problem. We then write the eigenstates of $\mathcal{H}_o(\hat{\tau}) = \Delta_o \hat{\tau}_x$ as the superpositions $|\Rightarrow\rangle = (|\Uparrow\rangle + |\Downarrow\rangle])/\sqrt{2}$ and $|\Leftarrow\rangle(|\Uparrow\rangle - |\Downarrow\rangle)/\sqrt{2}$. What do these states look like? Consider first the eigenstates. One thing they do *not* look like is a giant spin pointing perpendicular to the easy axis! It is useful to consider the answer in terms of a distribution of spin density over the Bloch sphere. In zero applied field, the original giant spin $\mathbf{S}$ has 2 lowest eigenstates that are produced by tunneling between "coherent states" concentrated around the 2 poles of the sphere (the 2 potential wells in Fig. 2). The exponentially small overlap between these polar states (which, incidentally, very closely approximate $|\Uparrow\rangle$ and $|\Downarrow\rangle$, but are not identical with them) means that the state $|\Rightarrow\rangle$ is concentrated in 2 humps of equal weight around the 2 poles – with exponentially small weight around the equatorial regions.

(b) We should understand that this is even true if we have, say, a strong applied field $\mathbf{H}_o^x$ in the $\hat{x}$- direction. This field must overcome the strong anisotropy field – it has only a small effect until $|\mathbf{H}_o^x| \sim H_c^\perp$, where $g\mu_B H_c^\perp \sim K_z$, the anisotropy energy scale. The main result of the field will be to slowly move the 2 polar states around the sphere in the direction of $\mathbf{H}_o^x$ (see Fig. 2), to coherent states $|\Theta\rangle$and $|\pi - \Theta\rangle$, centred at polar angles $\theta(H_o^x)$ and $[\pi - \theta(H_o^x)]$. If the field is too strong, approaching the competing anisotropy field $H_c^\perp$, these 2 states start to have a strong

quantum overlap. Otherwise they still very closely approximate $|\Uparrow\rangle_{H_o^x}$ and $|\Downarrow\rangle_{H_o^x}$ (these latter defined as before by symmetric and antisymmetric combinations of the 2 lowest eigenstates – which are still tunneling combinations, with little weight around the equator). Of course the overlap increases with increasing H_o^x, which means that the tunneling amplitude Δ_o also increases. Actually the physics is often more interesting – tunneling can proceed by more than one path on the sphere, and interference between these paths then causes oscillations in Δ_o; this is discussed more below (section 5A).

Note as a corollary to these remarks that the effect of a transverse field $\mathbf{H}_o^\perp$ on these qubits is not to cause rapid flipping between $|\Uparrow\rangle$ and $|\Downarrow\rangle$, at a rate $\propto |\mathbf{H}_o^\perp|$ (as would be the case if we were dealing with spin-1/2 qubits). Actually low transverse fields have very little effect on the dynamics (see section 5A for more details).

(c) From these remarks it will also be obvious that whereas one may imagine, say, a system of N weakly-coupled 2-level atomic spins in a "Schrödinger's Cat" state like

$$|\Rightarrow\rangle_N \;=\; \frac{1}{\sqrt{2}}[|\uparrow\uparrow\uparrow\ldots\rangle + |\downarrow\downarrow\downarrow\ldots\rangle] \tag{3}$$

written in terms of the single atom states $|\uparrow\rangle$, $|\downarrow\rangle$, this state is utterly unlike the states we are talking about here. In the first place, the spins in the magnetic systems are extremely strongly correlated – the product states favoured by atomic physicists are about as far away as one can imagine from the correct low-energy states of a magnet. A second important difference appears if we imagine a generalisation of $|\Rightarrow\rangle_N$ to a superposition

$$|\Rightarrow\rangle_N \;\rightarrow\; \frac{1}{\sqrt{2}}[|\nearrow\nearrow\nearrow\ldots\rangle + |\searrow\searrow\searrow\ldots\rangle] \tag{4}$$

where the 2 states $|\nearrow\nearrow\nearrow\ldots\rangle$ and $|\searrow\searrow\searrow\ldots\rangle$ are products over spins pointing along "diagonal" directions at angles θ and $[\pi - \theta]$. Clearly these 2 states cannot be treated as qubit states since they are not orthogonal. However the apparently analogous states $|\Uparrow(H_o^x)\rangle$ and $|\Downarrow(H_o^x)\rangle$, described above for the case of a transverse field, *are* genuine qubit states, and are orthogonal by construction. Again we see the dangers of trying to use intuition gained from weakly-interacting systems, when discussing strongly-coupled spins.

So much for the 2 low-energy qubit states. However this is of course not the end of the story – we must include the remaining low energy excitations and couplings, associated with phonons and nuclear spins.

Phonons and Nuclear spins

There are of course phonons around at arbitrarily low energies. The nuclear bath is obviously very important as well – there are a lot of nuclear spins, and unlike the phonons all nuclear modes are still active (so they totally dominate the low-T entropy of the system). Moreover, the coupling of *each nuclear spin* to the magbit is usually much larger than the zero-field splitting Δ_o! Thus the full effective Hamiltonian at this energy scale must include the phonons and nuclear spins. To

give the discussion some concrete character I quote the general form:

$$\mathcal{H}_o^{\Omega_o} = \tilde{\Delta}\hat{\tau}^x + \epsilon\hat{\tau}^z + \mathcal{H}_{ph}(x_q) + \mathcal{H}_{NN}(\mathbf{I_k}) + \sum_q x_q[c_q^{\parallel}\hat{\tau}^z + (c_q^{\perp}\hat{\tau}^+ + H.c.)] + A_k^{\alpha\beta}\hat{\tau}^\alpha I_k^\beta \quad (5)$$

In this Hamiltonian the superscript Ω_o indicates the UV cutoff on the Hamiltonian – which is not properly defined until the UV cutoff (more generally, the Hilbert space) is specified. Here we assume that Ω_o is well above the energy separation of the 2 magbit states, but well below the "spin gap" energy E_G to the next highest states of the system (and $E_G \sim K_\parallel$, the anisotropy energy per spin). The first two terms on the right hand side are just the original magbit splitting and bias (except that Δ_o has been renormalised to $\tilde{\Delta}$). Then we have the standard phonon oscillator Hamiltonian $\mathcal{H}_{ph}(x_q)$ (where the $\{x_q\}$are the oscillators) and the Hamiltonian $\mathcal{H}_{NN}(\mathbf{I_k})$ of the nuclear spins. This latter includes both the very weak ($\sim 10^{-8} - 10^{-7}K$) pairwise internuclear interactions $\sum_{kk'} V_{kk'}^{\alpha\beta} I_k^\alpha I_{k'}^\beta$, and any other fields acting on the nuclear spins. Finally the last 2 terms describe the interactions between our 2-level qubit and the phonon and nuclear spins environments – both the "spin-phonon" couplings $\{c_q\}$ and the "hyperfine" couplings $\{A_k\alpha\beta\}$ sum the interactions, between phonons/nuclear spins and the electronic spins, over all electronic spins in the magnetic qubit.

Let us pause to consider where this renormalisation procedure has led us. First and foremost, it gives the correct form of the low-energy Hamiltonian, and flushes out irrelevant terms. The formal truncation calculation (for details of which see the literature [24,25,26]) will also try to derive the *size* of the couplings $c_q^{\parallel}$, $c_q^{\perp}$, $A_k^{\alpha\beta}$, and $V_{kk'}^{\alpha\beta}$, the phonon spectrum ω_q, and the qubit parameters $\tilde{\Delta}$ and ϵ, for a given magnetic system. It is in the nature of the procedure that it begins from the couplings in a higher-energy Hamiltonian – which are assumed known. If this can't be done (as is often the case – recall the simple example in QED of the basic fine structure coupling α, which we have no idea how to calculate, or even in terms of what), then these low-energy parameters must be *measured* if we are to have a predictive theory. The theory also defines *how* these parameters are to be measured, by showing how they enter into experiments. I emphasize again that this whole procedure is very traditional. What will perhaps be unfamiliar, to those not accustomed to strongly-correlated systems, is how it works when the important couplings are not weak.

For the magnetic systems of interest here, correlations are strong, and the truncation is not trivial. Thus $\tilde{\Delta}$ depends exponentially on poorly known high-energy parameters (it is a tunneling amplitude) and so is almost impossible to calculate accurately. The couplings $A_k^{\alpha\beta}$ between qubit and nuclear spins can usually be calculated straightforwardly from the hyperfine couplings between individual electronic spins and nuclear spins. However the hyperfine couplings themselves involve not only direct magnetic dipolar coupling between the nuclear moments (these determined experimentally!) and electronic spins, but also indirect high-energy "transfer hyperfine" couplings via other electronic clouds – not easy to calculate in such a complex system. The tiny internuclear couplings are trivial to calculate, knowing

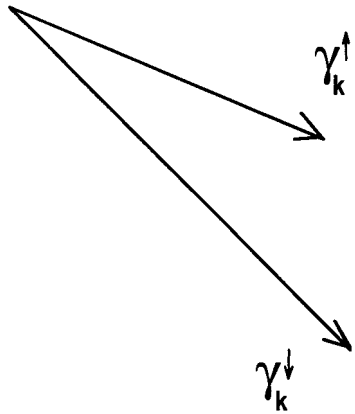

Figure 4: **Effective field acting on nuclear spin in a magnetic qubit.** The total effective field $\vec{\gamma}_k$ acting on the k-th nuclear spin in a nanomagnetic qubit changes according to whether the low-energy state of the qubit is $|\Uparrow\rangle$ or $|\Downarrow\rangle$ (for details see text).

the nuclear sites, if they only involve the magnetic dipolar coupling. However, again, there can be indirect high-energy couplings which compete with these, via polarisation of the electronic clouds. A proper calculation of spin-phonon couplings is also very messy, and beset by uncertainty about electron polarisation renormalisation effects.

However (and again this is typical), the situation is not so desperate as these remarks make it seem. Not only is the phonon spectrum fairly easy to calculate – also both it and the essential information about the spin-phonon couplings can be lumped into parameters measurable in neutron scattering and magnetoacoustic experiments [11]. Moreover, Δ_o can be determined from experiment [10], thereby allowing us to reverse the renormalisation procedure and infer important high-energy parameters! The longitudinal bias $\epsilon_o = g\mu_B S H_o^z$ is immediately given once the effective longitudinal g-factor of the nanomagnet is determined from susceptibility measurements. And NMR and ESR measurements can in principle give most of the essential information about the hyperfine and internuclear couplings.

Finally, some of the couplings just turn out to be negligible – we can throw them away, as we now see.

Simplification of the Hamiltonian: Deep in the quantum regime, when $kT << \Omega_o$, calculations using standard methods [26] show that inelastic spin-phonon processes occur over very long time scales, and elastic ones cause trivial renormalisations of parameters. Thus we can simply drop all phonon terms in this regime. A further simplification emerges if we rewrite the remaining magbit/nuclear bath terms in the form [27,25]

$$\mathcal{H}_o^{\Omega_o} = \left\{ \tilde{\Delta} \hat{\tau}_+ e^{i \sum_k \vec{\alpha}_k \cdot \hat{\mathbf{I}}_k} + H.c. \right\} + \hat{\tau}_z [\epsilon + \sum_k \omega_k^{\parallel} \hat{\mathbf{I}}_k \cdot \hat{\mathbf{I}}_k]$$

$$+ \sum_k \omega_k^{\perp} \hat{\mathbf{m}}_k \cdot \hat{\mathbf{I}}_k + \mathcal{H}_{NN}(\mathbf{I_k}) \qquad (6)$$

In this equation we have (i) replaced the tunneling term $\Delta_o \hat{\tau}_x$ by $\left\{ \tilde{\Delta} \hat{\tau}_+ e^{i \sum_k \vec{\alpha}_k \cdot \hat{\mathbf{I}}_k} + H.c. \right\}$, and (ii) defined the energies

$$\begin{aligned} 2\omega_k^{\parallel} &= |(\vec{\gamma}_k^{\uparrow} - \vec{\gamma}_k^{\downarrow})| \\ 2\omega_k^{\perp} &= |(\vec{\gamma}_k^{\uparrow} + \vec{\gamma}_k^{\downarrow})|. \end{aligned} \qquad (7)$$

in terms of the fields $\vec{\gamma}_k^{\uparrow}$, $\vec{\gamma}_k^{\downarrow}$ acting on the k-th nuclear bath spin $\mathbf{I}_k$ when the magbit is in its $|\Uparrow\rangle$, $|\Downarrow\rangle$ states respectively (cf. Fig. 4; note that $\hat{\mathbf{l}}_k$ and $\hat{\mathbf{m}}_k$ are unit vectors). Then $\omega_k^{\perp}$ defines the strength of the "static" fields acting on the k-th bath spin $\mathbf{I}_k$, including external fields, etc.; and $\omega_k^{\parallel}$ the strength of the "hyperfine" field, coupling $\mathbf{I}_k$ directly to the qubit dynamics.

To get (6) from (5) involves 2 moves. First, the straightforward separation of diagonal and non-diagonal (in $\hat{\tau}$) magbit-nuclear spin couplings, coming from $A_k^{\alpha\beta}$. Second, one recognises that the non-diagonal terms can be written as a coupling of the qubit flip operator to an operator acting on the nuclear spins – the general form of this comes if we write the effect of the qubit flip on the k-th nuclear spin in transfer matrix form. Let the relation between initial and final nuclear states (before and after a magbit transition) be $|\chi_k^{fin}\rangle \hat{T}_k |\chi_k^{in}\rangle$; then we can always write

$$\hat{T}_k = e^{-i \int d\tau H_{int}^k(\tau)} \quad \rightarrow \quad e^{-[\delta_k + i(\vec{\alpha}_k \cdot \mathbf{I}_k + \phi_k)]} \qquad (8)$$

where τ is a dummy time variable, integrated through a single magbit transition, and $H_{int}^k = A_k^{\alpha\beta} + g_N \mu_N \mathbf{I}_k \cdot \mathbf{H}_o^k$ (ie., the total Hamiltonian of the nuclear spin, including the Zeeman coupling to external fields – the internuclear couplings are dropped for simplicity, and because they are unimportant for this term). The integral over H_{int}^k is only defined once we know the trajectory of the magbit during the tunneling transition – which can be calculated knowing the anisotropy potential [25]. The scalar part δ_k of the exponent in $\hat{T}_k$, and the extra Berry phase ϕ_k, are then incorporated into a renormalised $\tilde{\Delta}$ in (6), and only the term involving α_k describes real transitions in the nuclear bath.

Why do we do things this way? Basically because it allows a further simplification. First, we notice that the parameter α_k, which tells us the importance of the non-diagonal terms, is usually very small. In most magnetic systems the hyperfine coupling $A_k^{\alpha\beta}$ is much smaller than the energy scale defined by the "bounce time" τ_o required for the nanomagnetic tunneling transition – this energy scale $\omega_o \sim 1/\tau_o$ is usually $\sim O(\mathcal{K}_z)$, the anisotropy energy (cf. Fig. 1), so that the nuclear spins are responding to a very fast change in the field acting on them. In this "sudden" limit it is obvious that $|\alpha_k| \sim |A_k^{\alpha\beta}|/\omega_o \ll 1$ (for a more precise discussion see refs. [26,27]). This does not immediately mean that we can replace the exponential term in (6) by unity, since the total physical effect of all the spins in the nuclear bath can still be large. It is parametrised by $\lambda \sum_k |\alpha_k|^2$, the average number of nuclear spin transitions accompanying each magbit flip, and unless it is also small, we get decoherence effects ("topological decoherence" [27]) from these transitions. However in almost all

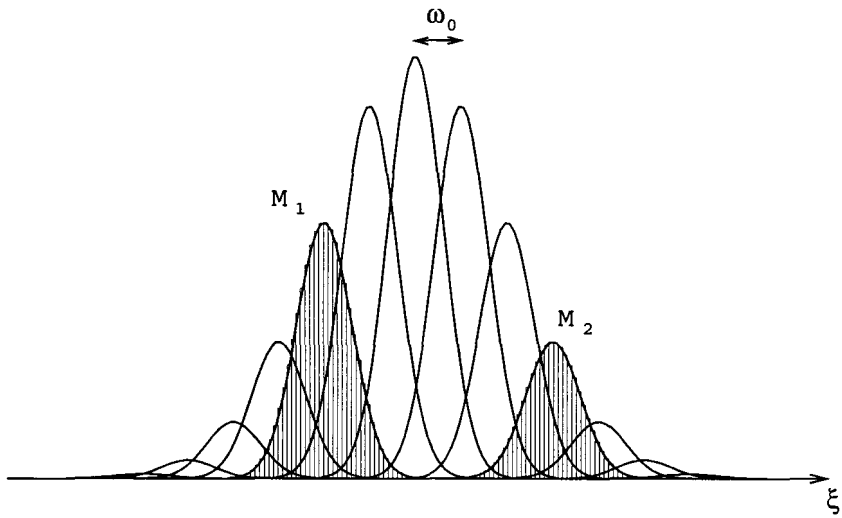

Figure 5: **Polarisation Groups in the Spin Bath.** Density of states $W(\xi)$ of the $\prod_k(2I_k+1)$ of nuclear states in a magnetic qubit, which form an envelope of half-width E_o (with $E_o^2 = \sum_k(\omega_k^{\|})^2$) around each qubit state. We assume $k = 1, 2, ..N$ (ie., N nuclear spins in each qubit), and zero applied field. The multiplet can be subdivided into "polarisation groups" [26,14], where the M-th polarisation group has a net spin $M = \sum_k I_k^z$ along the easy z-axis. These groups are separated by the mean value $\omega_o =< \omega_k^{\|} >$. Transitions between polarisation groups, which change the total spin projection, can only be mediated by T_1 processes coming from interaction with the environment, or stimulated by the qubit dynamics itself.

realistic cases, the number N of nuclear spins coupling to a nanomagnet is small, and $\lambda \ll 1$ as well; then we can simply drop all reference to nuclear flips.

The second simplification comes from a closer look at the internuclear interaction $V_{kk'}^{\alpha\beta}$, which gives the nuclear bath its "intrinsic dynamics" [28]. Again, one may use an argument based on time scales. In general the nuclear spin dynamics will involve a fast fluctuating component coming from the precession in the combination of external and hyperfine fields, already accounted for in our Hamiltonian, and then a much slower "nuclear spin diffusion" component coming from the internuclear interaction. If the timescale of the latter differs widely from that of the qubit dynamics, then we can treat it as a classical noise source, whose only effect will be to add a fluctuating bias acting on the qubit. Since the qubit is extremely sensitive to any longitudinal bias, which can push it off resonance, the most important term will be of form $\delta\mathcal{H}_{int} \sim \xi_z(t)\hat{\tau}^z(t)$, where the correlator $C_{zz}(t,t') = \langle\xi_z(t)\xi_z(t')\rangle$ can have a fairly complex form (detailed calculations for the Fe-8 molecule have recently been done [29]). The best way to understand the noise spectrum is via the picture shown in Fig.5., showing the spread of nuclear multiplets surrounding each qubit state. There is a huge number $\prod_k(2I_k+1)$ of nuclear states in each multiplet, which form an envelope of states in energy bias space, with half-width E_o, where $E_o^2 = \sum_k(\omega_k^{\|})^2$. The multiplet can be subdivided into "polarisation groups" [14,26],

where the M-th polarisation group has a net spin $M = \sum_k I_k^z$ along the easy z-axis (this classification is appropriate to low applied fields – in high fields, we will redefine the polarisation groups along the external field axis). These polarisation groups also contain a huge number of states, except for the extreme wings of the multiplet (where $M \sim \pm \sum I_k$, ie., near total nuclear polarisation), and have a corresponding width in energy bias space. Both the polarisation groups and the entire multiplet made from putting all the groups together will have a Gaussian lineshape.

From the point of view of the qubit, the bias appears to drift around inside this Gaussian umbrella. How it does this depends on various factors. In zero field the only way the nuclear system can change polarisation group is via a T_1 process, presumably mediated by impurities. Since such processes are rare at low T (ie., T_1 is very long), at very low fields the bias on a single nanomagnet will diffuse around *inside a single polarisation group only*, mediated by T_2 processes which change the spin distribution around the nuclear system, without changing M. However as soon as a field is applied, it can mediate transitions between different polarisation groups – thus the diffusion will rapidly spread over the whole multiplet. It is not possible to determine the energy bias diffusion characteristics directly, but indirect information is given by nuclear T_2 measurements. In previous papers where this kind of theory was applied to real nanomagnets [26,30,31], the effective energy bias width over which this diffusion occurred in experimental timescales was called ξ_o (sometimes called the "hole width" in experiments where it can be measured [32,33]). The theoretical assumption, that energy bias diffusion inside the nuclear multiplet is fairly fast, seems to have been justified by experiments so far (note that T_2 is typically a few *msec* in such systems [34], even at high T, and presumably considerably longer in the quantum regime).

Thus the net result of this discussion is that we can simplify all effects of the internuclear interactions, and the nuclear spin diffusion they cause, by assuming that they cause the nuclear bias field acting on the "central spin" to fluctuate fairly rapidly in a restricted random walk over a range ξ_o. In many cases $\xi_o \sim E_o$, except at very low field. Actually the same is obviously the case in very high applied fields, since such fields will not only force all nuclear spins to lie along the same axis, but also restrict nuclear spin diffusion – this point is further discussed in section 5A.

After these various simplifications one finally ends up with a low-energy effective Hamiltonian that can be used in practical discussions of magnetic qubit dynamics:

$$\mathcal{H}_o^{\Omega_o} = \tilde{\Delta}\hat{\tau}_x + \hat{\tau}_z \left[\epsilon + \sum_k \omega_k^{\parallel} \hat{\mathbf{I}}_k \cdot \hat{\mathbf{I}}_k \right] + \sum_k \omega_k^{\perp} \hat{\mathbf{m}}_k \cdot \hat{\mathbf{I}}_k + \hat{\tau}^z \xi_z(t) \qquad (9)$$

This Hamiltonian will be sufficient in most cases, provided we are at low enough T so that phonons are irrelevant. In some cases one can also imagine that there should be transverse fluctuation terms $\sim \hat{\tau}_x \xi^x(t)$, but these will usually be small – they correspond to fluctuations in $\tilde{\Delta}$, driven by the environment. We will return to this question later.

Let us anchor this long formal discussion in reality, by returning to the example discussed above, the Fe-8 molecule (cf. eqtn. (1)). First consider the zero-field

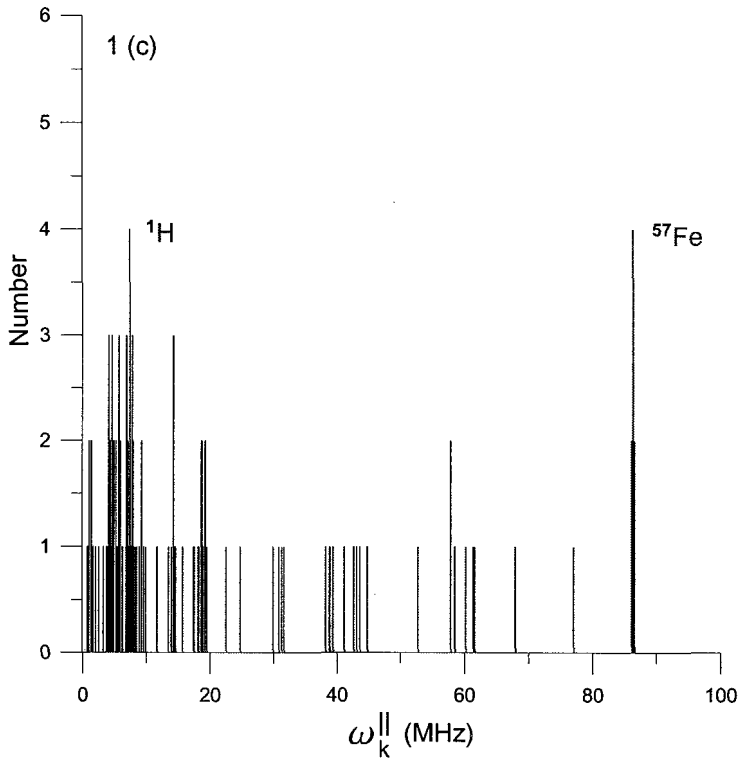

Figure 6: **Hyperfine Couplings in the Fe-8 molecule.** Histogram of the distribution of values of $|\omega_k^{\|}|$ in the Fe-8 molecule in zero applied field, measured in MHz units. Only the values for the protons and ^{57}Fe nuclear spins (both spin 1/2) are shown. The values are binned in 0.1 MHz intervals. The protonic couplings were calculated assuming dipolar hyperfine interactions (there are probably also weak transfer hyperfine couplings), and the contact hyperfine coupling to ^{57}Fe was calculated using a standard Hartree-Fock analysis (for details see ref. [35]).

qubit splitting Δ_o. This is found experimentally [10] to be $\sim 10^{-7}K$ in Fe-8, which is a fairly typical number (cf. Fig. 1; later we will see how application of transverse fields can make it far larger). This is a very small energy, corresponding to a frequency $\sim 2\ kHz$; it is so small because the qubit tunneling flip between states $|\Uparrow\rangle$ and $|\Downarrow\rangle$ is tunneling through a big barrier, and the transverse anisotropy terms driving it are appearing at very high order in perturbation theory (in the parameter $\mathcal{K}_x/\mathcal{K}_z$).

In comparison with this, the characteristic nuclear spin energies are actually very *large*. Fig. 6 shows the distribution of some of the hyperfine couplings $\omega_k^{\|}$ in the molecule – most of them are between $1 - 10MHz$ (ie., $0.05 - 0.5\ mK$), and the total spread E_o of the nuclear states is found expereimentally [33] and theoretically [35] to be $E_o \sim 7\ mK$ (although this can be varied a lot by isotopic substitution). The internuclear spin couplings are weaker – they range from $\sim O(1\ \mu K)$ for the closest

pairs of nuclear spins to $\sim O(1\ nK)$ for nuclei at opposite ends of the molecule [29] However this is enough to keep the nuclear spins fluctuating at low T.

Compared to the thermal energy kT in any experiment, all of these energies are very small – note that when the system is at temperature $kT \ll E_G$, so only the 2 qubit molecular states are active, it is *precisely because* the nuclear energies are so small that they cause most of the decoherence. All higher energy excitations are frozen out – only the nuclear degrees of freedom are still active (readers should however refrain from inferring that the decoherence rate has any relation to kT!). To freeze out the nuclear spin dynamics requires either going to extremely low temperatures ($T < 1\ nK$), or applying strong fields – this latter tactic is discussed in more detail in section 5.

We note in passing that in all experiments done so far on molecules like Fe-8, the molecules are not isolated but in crystalline arrays. This means that there are other interactions in the problem. Typical nearest neighbour intermolecular dipolar interactions are of order $0.05 - 0.1K$ in strength, ie., usually larger than the hyperfine interactions. One can incorporate these into a theoretical analysis in a fairly straightforward way [30,31], taking advantage of the slow variation in time of the dipolar fields compared to the rapid fluctuations of the hyperfine fields. There will also be other interactions between the molecules (eg., superexchange between them, via the outer ligands – these are usually argued to be negligible, for reasons that are not obvious to me) and between nuclear spins on different molecules (although these are very small, they are important in mediating nuclear spin diffusion [29]).

Finally, a word about conduction electrons. The treatment described above assumed a magnetic insulator – but if there are mobile electrons coupling to the nanomagnetic spin then these effectively act as an oscillator bath. One can also develop a detailed theory of this coupling [26]. I will largely ignore it here because mobile electrons are very bad for qubit coherence – they are gapless excitations with strong spectral weight at low energy. The "Kondo" physics of this is well understood [36], so when necessary we will take results from the literature – but most of the time we will assume that coupling to such excitations has been suppressed, by making the system either superconducting (see below) or insulating. It is perhaps interesting to remark, however, that in a sufficiently small nanomagnetic conductor, the mean spacing $\delta\epsilon$ between the quantized electronic levels can be quite large (it is $\sim D/N_s$, where D is the conduction electron bandwidth, and N_s the number of conduction electrons inside the nanomagnet). If the conduction electrons inside a nanomagnetic conductor are well decoupled from those outside, by an insulating coating, or the nanomagnetic conductor is on an insulating or semiconducting substrate, the broadening of these levels can be very small. In this case the decoherence from coupling of the qubit magnetisation to conduction electrons will be exponentially small ($\sim e^{-(\delta\epsilon/kT)}$ or $\sim e^{-(\delta\epsilon/\Delta_o)}$, whichever is larger). For more details on this see ref. [26].

Note finally that any residual weak coupling of the qubit to gapless electrons in external circuitry must be absorbed into an "Ohmic" coupling to an oscillator bath, and that this is also a decoherence source. This point is relevant for any kind of qubit [37,12].

2.2 Superconducting systems

There are two basic kinds of qubit design that have been discussed for superconducting qubits – with lots of variants in between. The first involves the flux coordinate of a SQUID ring, for which the "bare" effective Hamiltonian (considering only the inductive terms and the Josephson junction potential) is the well-known form [38]

$$\mathcal{H}_0 = \frac{p_\phi^2}{2C} + U_0 \left[\frac{(\phi - \phi_x)^2}{2} + g\cos\phi \right] , \tag{10}$$

where C is the junction capacitance, $\phi = 2\pi\Phi/\Phi_0$ with Φ_0 the flux quantum, $p_\phi = -i\hbar\partial/\partial\Phi$, and $\phi_x = 2\pi\Phi_x/\Phi_0$, where Φ_x is an externally applied flux. Then $U_0 = \Phi_0^2/4\pi^2 L$ and $g = 2\pi L I_c/\Phi_0$, for a ring inductance L and junction critical current I_c. For a SQUID qubit one uses more complex arrangements of junctions than this (see, eg., refs. [39,40]), but the basic idea is that flux tunnels between 2 potential wells, just as in the magnetic qubit design. The discussion of this kind of coherent tunneling goes back of course to Leggett et al. [41].

The other design involves transitions between 2 different charge states of a nanoscopic superconductor, as in the "Cooper pair box" design employed by Nakamura et al. [6,7]. A large superconductor already has superpositions of many different charge states (an important feature of the BCS wave-function). But once the capacitative energy gap E_c to add a Cooper pair to a nanoscopic superconductor (here, the Cooper box) becomes $\sim$ the Josephson energy E_J, both charge and flux tunneling must be considered [12] together. Adding the capacitative energy for n electrons on the Cooper box to the Josephson energy through a SQUID ring coupled to this box gives the very simple Hamiltonian

$$\mathcal{H}_o = \frac{1}{2}[E_c(n - Q/e)^2 + E_J\cos\phi] \tag{11}$$

where the Josephson term is equivalent to

$$E_J\cos\phi = \frac{E_J}{2}\sum_n |n\rangle\langle n+2| \; + \; |n+2\rangle\langle n| \tag{12}$$

and (12) and (10) are related by $E_J = 2gU_o$. The charge Q is a continuous variable – it is the charge induced on the box by fields coming from external gates, etc. Diagonalisation of (11) gives immediately a 2-level qubit system, provided we stay in the subspace corresponding to a given value of n, with a gap $\Delta_o = E_J$.

These Hamiltonians already assume a truncation to energy scales $\sim O(1K)$ or so. Of course when this truncation is done properly, using the same renormalisation techniques as before, things are more complicated than these simple forms suggest. Again, any starting high-energy Hamiltonian (at eV scales) is extremely complex, describing a set of electrons in a metal, interacting with each other and with photons (and thence to external circuitry), with the crystal lattice, and with nuclear spins and paramagnetic or charge defects, in both the superconductor and the surroundings (substrate, electrodes and gates, etc.). Again, however, truncation to lower energies simplifies things (see Fig. 7). At energies $\sim 1 - 10K$ in simple metallic systems, the electron-phonon interaction induces superconductivity. At temperatures well below the superconducting gap energy the gapped electronic

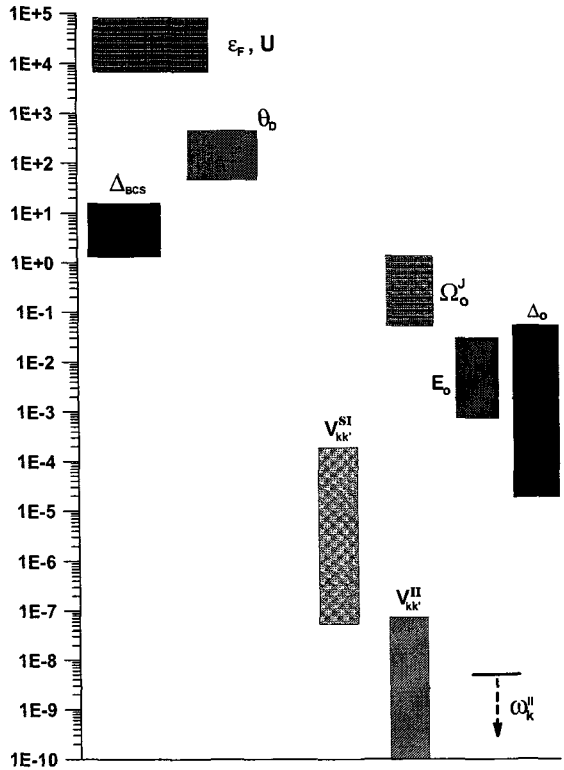

Figure 7: **Energy Scales in a SQUID.** Some of the energy scales in a superconducting SQUID (compare Fig. 1 for insulating magnets). At high energies the system is in the normal state, with electronic energy scales ϵ_F, U (Fermi energy and Coulomb interaction), and a phonon Debye energy θ_D. We assume a transition to an s-wave superconducting state at a temperature $T_c \sim \Delta_{BCS}$, the zero-T superconducting gap energy.
In the SQUID qubit the UV cutoff is Ω_o^J, the Josephson plasma energy, and current designs have a low energy barrier between the 2 SQUID wells, so that Δ_o may not be much smaller. The effective coupling to electron quasiparticles in the SQUID is gapped by the energy Δ_{BCS}; electrons in other parts of the circuit are gapless but very weakly coupled to the qubit. The characteristic energies of localised "spin bath" excitations include the nuclear-paramagnetic spin-spin couplings $V_{kk'}^{SI}$, the internuclear spin-spin interactions $V_{kk'}^{II}$, and the Zeeman coupling $\omega_k^{\parallel}$ between the SQUID flux and these spins (which is typically $< 10_8$ K for paramagnetic impurities and $< 10^{-11}$ K for nuclear spins). However the net effect of the coupling to all these spins is parametrised by E_o (defined as before) which is much larger.
In the case of Cooper boxes 2 other scales become relevant -- the charging energy E_c and the electrostatic coupling to charge defects (see text).

modes ("Bogoliubov quasiparticles") have an exponentially small effect on the dynamics of the superconducting order parameter – this is exactly the simplification mentioned in the introduction. Phonons are also largely irrelevant at these lower energies. What is left out of equations (10)-(12) are those "environmental" modes which are still active (and thence potential sources of decoherence). These include gapless electronic excitations in the surrounding circuitry and photons (both delocalised), and localised spin and charge modes.

All of the physics of the delocalised modes is described by the Caldeira-Leggett theory [4,37], in which these modes map at low energies to independent oscillators. Thus when one eventually truncates to mK temperatures, including the oscillators, both the Cooper box and the SQUID systems have an effective Hamiltonian of the well-known "spin-boson" form, in which the spin represents the qubit as before:

$$\mathcal{H}_{\rm SB}(\Omega_o) \;=\; \Delta\hat{\tau}_x + \epsilon\hat{\tau}_z + \sum_{q=1}^{N} c_q\hat{\tau}_z x_q \;\;+\;\; \frac{1}{2}\sum_{q=1}^{N}\left(\frac{p_q^2}{m_q} + m_q\omega_q^2 x_q^2\right)\,, \qquad (13)$$

As discussed extensively by Leggett et al. [4,41], the effect of the couplings c_q to the oscillator coordinates x_q can be entirely parametrised by a spectral function $J(\Omega)$ of form

$$J(\Omega) = \frac{\pi}{2}\sum_q \frac{|c_q|^2}{m_q\omega_q}\delta(\Omega-\omega_q) \qquad (14)$$

One can do this because the $\{c_q\}$ are all small, and all their effects are described perturbatively using this spectral function. The way to relate the spectral function to experimental properties of the system has also been widely discussed in the literature [37], as has the truncation of the microscopic SQUID Hamiltonian to this spin-boson form [42,43]; the reader may also refer to reviews [12].

However one still has to worry about the localised modes. For a SQUID, tunneling between different flux states, the most dangerous modes are spin modes – nuclear spins and paramagnetic impurities in SQUID and substrate, with their Zeeman coupling to the SQUID flux [44,45,46,47]. For a Cooper box qubit, the most dangerous coupling is to charge fluctuations, particularly in the surrounding substrate and circuitry [39]. Not so much work has been done on these couplings at the microscopic level – a pity, because the results are useful in understanding how to control decoherence. In the case of SQUIDs one can give a fairly detailed treatment of the Zeeman coupling of the SQUID flux to nuclear and paramagnetic spins [45,14,47]. The spins couple to a total field $\mathbf{B}(\mathbf{r})$ having 3 sources:

$$\mathbf{B}(\mathbf{r}) \;=\; \mathbf{B}_o + \mathbf{B}_\phi(\mathbf{r}) + \sum_k \mathbf{b}_k(\mathbf{r}) \qquad (15)$$

Here $\mathbf{B}_o$ is the external field, $\mathbf{B}_\phi(\mathbf{r})$ is the field generated by the electronic current, and $\mathbf{b}_k(\mathbf{r})$ is the field generated by the k-th bath spin at position $\mathbf{r}$. Since all current flow is in the supercurrent we have

$$\mathbf{B}_\phi(\mathbf{r}) = \mu_o\int_{R+J} d^3r' \frac{1}{|\mathbf{r}-\mathbf{r}'|^3}\cdot[\mathbf{j}_s^\phi(\mathbf{r})\times(\mathbf{r}-\mathbf{r}')] \qquad (16)$$

where $\mathbf{j}_s^{\phi}(\mathbf{r})$ is the supercurrent density, integrated over the junction and the bulk of the superconductor. When the SQUID qubit tunnels from one flux state to another, the field $\mathbf{B}_{\phi}(\mathbf{r})$ changes, but the field $\tilde{\mathbf{b}}(\mathbf{r}) = \sum_k \mathbf{b}_k(\mathbf{r})$ does not (at least not on the timescale of the SQUID transition). Thus yet again we see the separation between that part of the qubit/spin bath coupling that is static (and which can be incorporated into a term of form $\sum_k \omega_k^{\perp} \hat{\mathbf{m}}_k \cdot \hat{\mathbf{s}}_k$, where $\mathbf{s}_k$ is the k-th bath spin), and one which flips along with the SQUID flux transition, and which goes into the term $\hat{\tau}_z \sum_k \omega_k^{\parallel} \hat{\mathbf{l}}_k \cdot \hat{\mathbf{s}}_k$. The real work in the theory is to separate off the slowly fluctuating part of the field $\tilde{\mathbf{b}}(\mathbf{r})$ from the quasistatic part, and to evaluate the various fields and couplings in terms of microscopic parameters such as crystal field parameters for paramagnetic impurities, etc., in a real SQUID geometry. However since nothing very deep is involved we refer the interested reader back to the literature. It is perhaps interesting from a methodological point of view to note that because these Zeeman couplings are individually very weak, the spin bath modes map to oscillators (although the mapping is not as trivial as might be expected).

The effect of localised modes in the case of Cooper boxes is interesting because it is an example of a spin bath made not from spins but from charge defects, which couple electrostatically to the charge of the Cooper box. This would not be a problem if their dynamics was frozen – however, just as in the case of nuclear spins, this is not true even at very low temperatures. The tunneling dynamics of such charge defects has been very extensively studied and reviewed [48]. The mapping to a spin bath is not completely straightforward, since the 2-level tunneling charges also couple to the surrounding conduction electrons. To give a proper description of this, from the point of view of the charge defect, one usually begins by introducing an operator $B^{k\mu}$ which annihilates the k-th defect at site k_μ (where $\mu = 1, 2$ label the 2 available sites for this defect). If we ignore the electronic bath then we have the simple Hamiltonian (with UV cutoff $\sim 10 - 100\ K$):

$$\mathcal{H}_o^{(k)} = t_k^o (B_{k1}^{\dagger} B_{k2} + H.c.) + \epsilon_k (B_{k1}^{\dagger} B_{k1} - B_{k2}^{\dagger} B_{k2}) \tag{17}$$

which is just a 2-level Hamiltonian with bias energy ϵ_k between the 2 sites, and tunneling amplitude $\tilde{t}_k$. The position of the defect then couples to the charge of the Cooper pair box, which produces a different electric potential at the 2 defect sites. It is then obvious that we will end up with a low-energy effective Hamiltonian coupling the 2 qubit states to each defect state, having exactly the same form as (9); details of this have been worked out elsewhere [47]. The bare Hamiltonian (17) is equivalent to the term $\omega_k^{\perp} \mathbf{m}_k \cdot \hat{\sigma}_k$, where $\hat{\sigma}_k$ describes the defect. The parameter $\omega_k^{\parallel}$describ es the electric dipole coupling of $\hat{\sigma}_k$ to the qubit, and $\xi_z(t)$ is a residual noise term. Given that we can have a situation where both the flux and charge tunneling are active, it actually makes sense to have a vector noise coupling of form $g_\alpha \hat{\tau}_\alpha \xi_\alpha(t)$, where $\alpha(x, y, z)$, and the $\{g_\alpha\}$ are constants.

The only real complication to this simple mapping to a spin bath is that the defect also couples quite strongly to the surrounding conduction electrons. Thus one often replaces (17) by [48]

$$\mathcal{H}_{def}^k = \tilde{t}_k^{q,q';\sigma,\sigma'} (B_{k1}^{\dagger} B_{k2} c_{q\sigma}^{\dagger} c_{q'\sigma'} + H.c.) + \sum_{q\sigma} \epsilon_q c_{q\sigma}^{\dagger} c_{q\sigma} \tag{18}$$

where the electronic degrees of freedom are labelled by momentum index q and another internal index σ (usually angular momentum scattering channel). In this form the strict 2-level character of the defect dynamics is lost, to be replaced by a multi-channel Kondo dynamics – one can no longer map to a spin bath (actually an oscillator bath mapping can be made). More generally one can interpolate between (18) and (17).

We may summarize this discussion for superconducting qubits in the form of an effective Hamiltonian

$$\mathcal{H}_{eff}^{\Omega_o} = \mathcal{H}_{SB} + \hat{\tau}_z \sum_k \omega_k^{\parallel} \hat{\mathbf{l}}_k \cdot \hat{\mathbf{I}}_k + \sum_k \omega_k^{\perp} \hat{\mathbf{m}}_k \cdot \hat{\mathbf{I}}_k + g_\alpha \hat{\tau}_\alpha \xi_\alpha(t) \tag{19}$$

where $\mathcal{H}_{SB}$ describes the qubit coupled to oscillators, and the other terms are as before, with noise terms now coupling to all 3 components of $\hat{\tau}$. The oscillators represent electrons both inside and outside the SQUID, and the spin bath represents paramagnetic and nuclear spins, as well as charge defects coupling to the charge dynamics of the superconducting qubit.

3 Solid-state Qubit Hamiltonians

We have seen how at low energies, complex mesoscopic or nanoscopic superconducting and magnetic systems can be set up to behave like single qubits, albeit with some residual interactions with their environment. We now stand back a little and summarize the results from a more general standpoint. Most discussions of quantum circuitry either drop the decoherence-causing couplings to the environment, or treat them as a source of errors, quantified either as a noise field or as a simple error rate per qubit operation. While this may be useful for the development of algorithms, etc., and is in line with the well-developed ideas of classical error correction, such an approach is not quantum-mechanical, and a correct approach should include the environment on the same footing as the qubits. I will not belabour this point since it has been made repeatedly before in more general contexts [4,49].

I therefore summarize here what one finds for a real multi-qubit Hamiltonian, in a sold-state context. The first step is to write down a general Hamiltonian describing a set of interacting solid-state qubits. We have already seen how this is possible for a single superconducting or magnetic qubit – the step to a general solid-state qubit is not much farther. Second, we see how renormalisation goes through for this more complex system.

3.1 single solid-state qubits

We now see, by comparing the results of renormalisation for the magnetic and superconducting qubit systems, that the mathematical form one gets for the two is basically the same. The most important terms can all be included in the effective Hamiltonian

$$\mathcal{H}_o^{\Omega_o} = \tilde{\Delta}\hat{\tau}_x + \hat{\tau}_z \left[\epsilon + \sum_k \omega_k^{\parallel} \hat{\mathbf{l}}_k \cdot \hat{\mathbf{s}}_k \right]$$

$$+ \sum_k \omega_k^{\perp} \hat{\mathbf{m}}_k \cdot \hat{\mathbf{s}}_k + \mathcal{H}_{osc} + g_\alpha \hat{\tau}_\alpha \xi_\alpha(t) \qquad (20)$$

where the $\{\mathbf{s}_k\}$ represent the "spin bath" degrees of freedom, $\mathcal{H}_{osc}$ represents the oscillator bath and its coupling to the qubit, and $\vec{\xi}(t)$ is a noise field acting on the qubit, with components $\xi_\alpha = (\xi_x, \xi_y, \xi_z)$. As noted in section 2B, we do not need to deal directly with $\mathcal{H}_{osc}$, but can always deal with the Caldeira-Leggett spectral function $J(\omega)$ derived from it. Likewise (sections 2A and 2B), the only thing we need to know about the spin bath dynamics is how to characterise the noise $\vec{\xi}(t)$ it gives rise to. However we do need to know explicitly the couplings $\{\omega_k^{\parallel} \hat{\mathbf{l}}_k\}$ and $\{\omega_k^{\perp} \hat{\mathbf{m}}_k\}$, since these are often not small – they then compete directly with the qubit parameters $\tilde{\Delta}$ and ϵ.

Note that for a system described by (20) to be usable as a qubit, we must be able to control at least one of the basic qubit parameters $\tilde{\Delta}$ and ϵ as a function of time – moreover, this must be done without introducing further decoherence. Luckily for superconducting and magnetic qubits this does not pose any deep problems, since one can easily envisage schemes for doing this using external magnetic fields or, eg., gate voltages. Consider first the case of a magbit. The longitudinal bias ϵ is controlled directly and trivially by an external longitudinal field, and as we shall discuss in much more detail in section 5A, the tunneling term can be varied over many orders of magnitude by transverse external fields. Provided the field variation is done adiabatically (ie., at frequencies much less than the characteristic operating frequency of the qubit) no decoherence should arise here. The most important engineering problem will be to apply these fields locally, to a single magbit.

In the case of superconducting qubits various schemes have already been proposed and operated, in which both parameters can be varied – the reader is referred to the literature [6,8,9].

So far so good for magnetic and superconducting qubits. The expectation is that analogous derivations of low-energy Hamiltonians for other kinds of solid-state qubit will give the same form (in cases where such has been attempted, this is the case – compare, eg., the derivation for nuclear spin qubits in a Quantum Hall system [50]). One should not be surprised at this example of "universality" of effective Hamiltonians [51] at low T. There are 2 reasons for it. The first is mathematical – there is only a limited set of couplings one may write down for the interaction between a qubit and environments of spins or oscillators. The second reason is physical – at low energies the environmental modes always seem to map to spins or oscillators. These 2 points have been discussed extensively in the literature [13,14,4,52], so I will not reiterate them here.

There are, incidentally, 2 small provisos that should be added here to this assertion of generality for the low-T qubit Hamiltonian (20). The first is that the standard assumption of linearity in the oscillator coordinates, in the coupling of the oscillators to the qubit, can break down if the linear couplings are weak (or even zero for symmetry reasons). In this case one goes to higher-order couplings. However these can usually be mapped by a canonical transformation to T-dependent linear couplings – for more details and references on this see refs. [53,54,55].

The second proviso concerns the difference between oscillator and spin baths.

Although these can have markedly different effects on the dynamics of the qubit, if the qubit/spin bath couplings are sufficiently weak, the problem can be mapped to a spin-boson problem. This point has been studied in a general way [14,56,57], and also in detail for SQUIDs [47]. The mapping is not always simple, but I do not go into details here.

To summarize – for the problem of a single qubit coupled to its surroundings, we end up at low $T$with h the Hamiltonian (20), with couplings determined by a combination of experiment and theory (and with $\tilde{\Delta}$ and ϵ controllable parameters). This result is very handy, since it means that if we wish to understand the effect of a quantum environment on the dynamics of a qubit, we have a generic model we can use to do this. However our analysis is so far incomplete in one important respect – we need a corresponding model for a set of M interacting qubits.

3.2 multi-qubit systems

As already noted, in this article I will not go into much detail concerning multi-qubit systems – in any case, the variety and number of coupling terms that enter would make such a discussion too long. It is perhaps easiest to start with the desired final result. Consider the effective Hamiltonian

$$H_o^{QIP} = \sum_i^M \tilde{\Delta}_i \hat{\tau}_i^x + \epsilon_i \hat{\tau}_i^z + \sum_{i<j} U_{ij} \hat{\tau}_i^z \hat{\tau}_j^z \tag{21}$$

I immediately emphasize that this Hamiltonian, which describes a set of M qubits interacting only with external longitudinal fields ϵ_i, and with each other via diagonal interactions U_{ij} , is chosen specifically with solid-state qubits in mind. In other systems like NMR or optical cavity schemes, other couplings are also important. The important point for Quantum Information processing (QUIP) is that at least some of the couplings $\{\tilde{\Delta}_i, \epsilon_i, U_{ij}\}$ should be controllable by external means – and that this be done without introducing any further decoherence in the system. As a matter of fact, one can get away with having the control of only one set of parameters, eg., the $\{\epsilon_i\}$; a computation can be done with very little means [18]. However this tends to make QUIP very slow – the more parameters we can control, the better. In the case of magnetic and superconducting qubits, we saw that it is straightforward, at least in principle, to control $\tilde{\Delta}_i$ and ϵ_i using external fields (applied locally to each qubit). The couplings U_{ij}, which will usually be electromagnetic, are not so obviously controllable – here we will assume them constant and fixed by the real space geometry of the system (note however that in qubit designs where the coupling comes from the overlap of, eg., electron clouds associated with the qubit, it is very easy to control U_{ij} using external gate fields [1]).

It is of course obvious that the QUIP Hamiltonian in (21) is idealised. The first question to answer is what sort of form is produced by renormalisation to low energies for a real network of superconductors and/or magbits. Note that for a quantum computer to work, all information transmitted between the qubits must maintain coherence. This means that it is not permissible to arbitrarily replace effective inter-qubit interactions by simple instantaneous couplings – the full retarded

couplings must be kept, until it can be shown that they effectively reduce to constants. This is a standard problem in field theory (at least as far as the oscillator bath part of the environment is concerned), but one must be careful to keep all decoherence effects.

Let us then consider what sort of effective Hamiltonian describes the system at the low-energy level. Without going through the lengthy derivation for this (which of course parallels the derivation for a single qubit), we look at the answer at an energy stage where the qubits have all truncated to 2 levels, with an ultra-violet cut-off $\Omega_o \sim 0.1 - 1K$. The result, for both SQUID and magnetic qubits, is to replace (21) by $\mathcal{H}^{QIP} = \mathcal{H}_o^{QIP} + \mathcal{H}_{env}$, where now

$$\mathcal{H}_o^{QIP}(\Omega_o) = \sum_i^M \tilde{\Delta}_i \hat{\tau}_i^x + \epsilon_i \hat{\tau}_i^z + \sum_{i<j} \tilde{U}_{ij}^{(\Omega_o)} \hat{\tau}_i^z \hat{\tau}_j^z \tag{22}$$

and

$$\mathcal{H}_{env}(\Omega_o) = \sum_i \left\{ \hat{\tau}_i^z \sum_{k=1}^N \omega_{ik}^{\parallel} \vec{l}_{ik} \cdot \hat{\vec{\sigma}}_k + \sum_{k=1}^N \omega_{ik}^{\perp} \vec{m}_{ik} \cdot \hat{\vec{\sigma}}_k \right\} + \sum_{k=1}^N \sum_{k'=1}^N V_{kk'}^{\alpha\beta} \hat{\sigma}_k^{\alpha} \hat{\sigma}_{k'}^{\beta}$$
$$+ \sum_i \sum_q \left[c_{iq}^{\parallel} \hat{\tau}_i^z + (c_{iq}^{\perp} \hat{\tau}_i^- + h.c.) \right] x_q + \frac{1}{2} \sum_q \left(\frac{p_q^2}{m_q} + m_q \omega_q^2 x_q^2 \right), \tag{23}$$

This looks dreadful! However all these terms are entirely to be expected, and one has no right to drop any of them without good reason. This is another way of saying how difficult it will be to control decoherence for M interacting qubits. Note that all dynamics at frequencies above Ω_o is incorporated into the coupling terms here.

Consider first at the multi-qubit interaction $\tilde{U}_{ij}^{(\Omega_o)}$. This is defined as a static limit of a retarded propagator:

$$\tilde{U}_{ij}^{(\Omega_o)} = lim(\mathbf{q}, \mathbf{q}' \to 0;\ \omega \to 0;\ \frac{\omega}{\mathbf{q}}, \frac{\omega}{\mathbf{q}'} \to 0)\ \tilde{U}_{ij}^{(\Omega_o)}(\mathbf{q}, \mathbf{q}'; \omega) \tag{24}$$

This propagator includes the appropriate part of, eg., the electromagnetic propagator $\mathcal{D}_{\mu\nu}(\mathbf{q}, \mathbf{q}', \omega)$, calculated in this inhomogeneous geometry (but with all processes at energies $< \Omega_o$ omitted from internal lines). The "appropriate part" means the relevant channel – for example, in the case of coupling between Cooper pair boxes, it would just be the Coulomb part of $\mathcal{D}_{\mu\nu}$. However we also include in $\tilde{U}_{ij}^{(\Omega_o)}$ all effective couplings, generated down to energy ω_o via the electronic, photonic, etc., baths, which can be excited by the underlying bare EM coupling. Now it was understood long ago [37] how to include such terms as effective impedances in an effective Lagrangian for the system – allowing one to make the link to the macroscopic "electrical engineering" properties of the network, in the form of mutual inductances, capacitances, etc. (or the mutual susceptibility analogues for a magbit circuit). The imaginary part of these impedances can in principle be related to the decoherence arising in the coupling of the qubits (although this has never been explicitly done, to my knowledge). This then takes care of both the "bare" term (22) in the Hamiltonian, and the remaining oscillator terms in (23).

What of the spin bath terms? In the form (23) these are easy to understand – each qubit is coupled to the spin bath, in the same way as for a single qubit. There are no interactions mediated by the spin bath yet contained in $\tilde{U}_{ij}^{(\Omega_o)}$, simply because the UV cutoff is still well above the characteristic frequencies of the spins in the spin bath. If the qubit operating energy scales $\tilde{U}_{ij}^{(\Omega_o)}$ and Δ_i are always much higher than the spin bath frequencies, then we can simply stop at this point – our effective Hamiltonian is that given by equations (22) and (23). We can also think of converting some of the spin bath terms into noise terms, in the same way as done before.

If on the other hand the operating frequency of our qubit network is not high compared to the spin bath frequencies, we have to do a lot more work – to take account of effective retarded interactions via the spin bath. We do not do this here, simply because it would make little sense to operate a network of solid state qubits at such low energies (the spin bath decoherence would be too high).

4 Qubit Dynamics

We now come to the subject of decoherence – about which much has been written. Here we are interested in finding decoherence rates for real systems – obviously a delicate topic, given the often large discrepancy between theory and experiment! This means we need the decoherence dynamics for the models discussed in the last section.

One could write a whole book on the dynamics of the spin-boson model or the central spin model (indeed, books and very large reviews have been written [13,14,41,58,16]). Here instead I give a short summary of the results – enough to get a feeling for the mechanisms involved in single qubit decoherence. The way in which this applies to real magnetic and superconducting qubits is then discussed, along with the experimental progress so far.

In general, for a full-blooded quantum computation, one wishes to understand the dynamics of a multi-qubit system, with time-dependent inter-qubit couplings and control parameters – plus the coupling of each qubit to its surroundings. There is no space here to discuss this very complex topic (which has not yet been worked out in detail, and which is not yet relevant to solid-state qubit experiments).

4.1 Main features of Single qubit dynamics

This subject has been reviewed extensively in the past. The "spin-boson" problem, of a qubit coupled to a bath of oscillators, was reviewed in well-known articles by Leggett et al. [41] and in the book of Weiss [13]. The "central spin" problem, of a qubit coupled to a bath of spins, is reviewed in Prokof'ev and Stamp [14]. For a comparison between the two, see ref. [45]. Not so much has been done on the dynamics of a qubit coupled simultaneously to spin and oscillator baths (usually there is an obvious separation of time scales so that one bath is more important than the other); there is however a study in the context of nanomagnetic systems [26].

One is interested in the time-dependence of the diagonal and off-diagonal elements of the qubit reduced density matrix. The time decay of oscillations of the

diagonal elements gives us the analogue of a T_1 measurement. The most interesting quantity is the decay time of the off-diagonal elements, ie., the analogue of T_2, which tells us the decoherence timescale τ_ϕ (one often makes the identification $T_2 = \tau_\phi$, although this is only justified if the relaxation is rigourously exponential). What I will do here is describe in a semi-intuitive way the main results for the decoherence rate.

Spin-boson model

Intuitively the spin-boson model is easy to understand. The ground state of the system has the qubit weakly entangled with each oscillator. At $T = 0$ the qubit can relax to this ground state by giving up some energy to the bath – to do so requires that the bath have some spectral weight $J(\omega)$ at the characteristic energy $\omega = \tilde{\Delta}$ of the qubit (with $\tilde{\Delta}$ already renormalised by the adiabatic coupling to high-energy bath modes). Decoherence can only arise if phase information can be exchanged between qubit and bath. At $T = 0$ this can again only happen via energy exchange – there is no room in the theory for decoherence from "zero point motion of the oscillators". Thus decoherence and dissipation are intimately linked – this is actually inevitable in the limit where each bath mode couples weakly to the qubit. At finite T thermal transitions in the bath obviously cause both dissipation and decoherence.

In this model (recall eqtn. (13)) the worst source of decoherence is electrons, which cause "Ohmic" dissipation [13,4], having a Caldeira-Leggett spectral function $J(\omega) = \pi\alpha\omega$, where the dimensionless coefficient α can either be measured, or evaluated from circuit parameters if it is coming from circuitry [37,12] (in the case of magnetic qubits one could imagine measuring it in magnetic damping experiments, although the relevant theory has not been worked out). When α is small (weak decoherence) one has decay rates for the off-diagonal matrix elements given by [13]:

$$\Gamma_{12}(\tilde{\Delta}, \xi) = \frac{1}{2E^2}[2\xi^2\gamma(0) + \tilde{\Delta}^2\gamma(E)] \tag{25}$$

where the rate function $\gamma(E)$ is

$$\gamma(E) = \pi\alpha E \coth(E/k_B T) \tag{26}$$

and $E = (\xi^2 + \tilde{\Delta}^2)^{1/2}$ with a renormalised tunneling matrix element $\tilde{\Delta}$. The "decoherence Q-factor" (telling us roughly the number of coherent interference oscillations before decoherence sets in) is then just given by $Q_\phi = \pi\tilde{\Delta}/\Gamma_{12}$.

As already discussed in the case of SQUIDs and Cooper pair boxes, the Ohmic dissipation in these systems can be made very weak (recall that in the Delft experiments, $\alpha \sim 10^{-7}$, implying that if the Ohmic contribution was the only dissipation source, $Q_\phi \sim 10^{-7}$ also). There is no Ohmic dissipation at all in insulators, like magnetic molecules we have been discussing.

There are other "superOhmic" sources of decoherence (ie., with $J(\omega) \propto \omega^k$, with $k > 1$), coming from phonons and photons (where in this $k = 3$ in most cases). Generally in solid-state qubits $J(\omega)$ from this sources is very small at the GHz

operating frequencies we are interested in, but they may become important if other sources of decoherence can be suppressed.

To summarize – we see that if all we had to worry about were oscillator bath environmental modes, decoherence would be small, at least in well-designed SQUIDs or magnetic insulators.

Central Spin model

The easiest way to understand the dynamics of a qubit coupled to a spin bath is to go back to the effective Hamiltonian (see eqtn. (20)). There are then 2 main sources of phase decoherence.

(i) Noise decoherence: The first is the noise term $\hat{\tau}_z \xi_z(t)$, whose effect is standard and fairly trivial – it causes a diffusive drift of the phase from its coherent linear evolution in time, and is easily handled mathematically (see books on random noise, or ref. [14]. App. A). Two limiting cases are important. In the first, unimportant for qubits but important for many experiments on magnetic molecules, the tunneling matrix element Δ is so small that the noise bias $\xi_z(t)$ crosses the tunneling window (of energy width Δ) in a time $\ll 1/\Delta$, giving the system almost no time to tunnel. This "fast diffusion limit" [26,14] obtains when $\Delta_o^3 \ll \tilde{\Gamma}^2 T_2^{-1}$, where $\tilde{\Gamma}$ is the typical width of a polarisation group.The resulting 1-qubit dynamics is then slow and completely incoherent relaxation. The relaxation rate, for a qubit with no applied longitudinal bias (ie., with $\epsilon = 0$; for results for $\epsilon \neq 0$, see ref. [14]), is given by $\tau_N^{-1} \sim |\Delta_o|^2/\xi_o$. As discussed in section 2A, $\xi_o$is the range of energy bias over which the spin bath bias is effectively fluctuating, during the time scale of interest.

Much more important for the present discussion is the "slow diffusion" limit, when Δ_o is big, both much larger than ξ_o, and with the frequency Δ_o much higher than the fluctuation frequencies in the spin bath. In this case decoherence from the noise will be small, given by the slow phase wandering of the qubit caused by the slowly varying noise potential $\xi_z(t)$. We then have a contribution

$$Q_\phi^{-1} \sim \Gamma_N/\pi\tilde{\Delta} \tag{27}$$

to the inverse of the decoherence Q-factor, where we expect roughly that $\Gamma_N \sim N_{eff} T_2^{-1}$, where T_2 is the transverse nuclear relaxation time of the relevant nuclear spins (ie., those which are causing this noise), and N_{eff} the number of these relevant spins. In Fe-8 at low fields $T_2 \sim 1-5$ msec at $T\sim$ 2 K for the most relevant protons [34], and presumably much longer at low T. Thus we expect that $\Gamma_N \ll 10kHz$ (this is of course a rough estimate).

(ii) Precessional decoherence: In many papers it is assumed that all the decoherence can be described in terms of some noise term $\xi_z(t)$. In fact most of the decoherence usually comes from a quite different source, viz., the quasi-random precession of the bath spins in between transitions of the qubit, caused because the field on each bath spin flips between 2 orientations each time a qubit transition occurs.

To better understand this, consider what happens to the k-th bath spin when the qubit field flips between the 2 orientations $\vec{\gamma}_k^{\uparrow}$ and $\vec{\gamma}_k^{\downarrow}$(recall Fig. 5). Imagine a

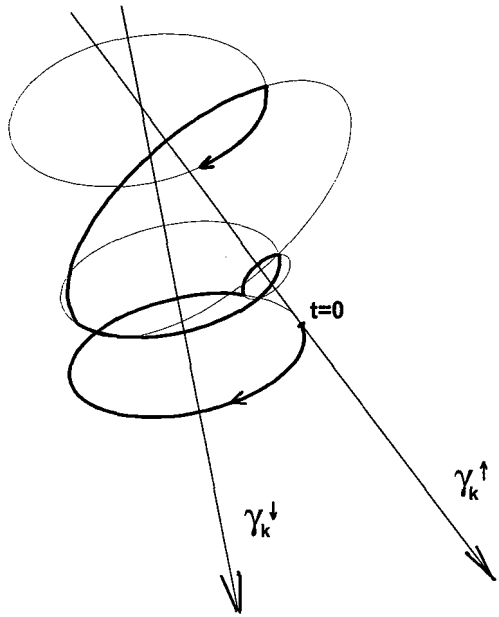

Figure 8: **Precessional dynamics in the spin bath.** One intuitive way to look at precessional decoherence comes from looking at the precessional motion of the k-th bath spin in a field $\vec{\gamma}_k$ which is flipping at random intervals between 2 orientations $\vec{\gamma}_k^{\uparrow}$ and $\vec{\gamma}_k^{\downarrow}$ (with the mean interval $\sim \Delta_o^{-1}$). Each time the field changes, the spin begins precessing around the new field – accumulating phase it goes. In a path integral formulation of quantum mechanics, we would sum over all possible paths of this kind – the result is an uncertain accumulated phase. Averaging over this gives phase decoherence.

path in a path integral for the motion of this pin, which for the sake of argument starts with the spin oriented along $\vec{\gamma}_k^{\uparrow}$. A typical path for the qubit will involve random flips between $|\Uparrow\rangle$ and $|\Downarrow\rangle$ (with average time interval $\sim 1/\Delta_o$ between flips). The effect on the bath spin dynamics is shown in Fig. 8. If we now integrate over paths, and sum over the bath spins, the result is lengthy to calculate [14,59] but not so hard to understand intuitively. The decoherence rate for this process is described by a parameter κ, which is related to the phase Q-factor of the qubit by $Q_\phi = \pi/\kappa$ (*provided* of course that there are no other sources of decoherence). One finds the following results:

(a) If either $\omega_k^{\parallel}$ or $\omega_k^{\perp}$ are $\gg \tilde{\Delta}$, ie., the qubit operating frequency is very low (as in, eg., Fe-8 in low applied transverse fields), then

$$\pi Q_\phi^{-1} \to \kappa = \tfrac{1}{2} \sum_k (\omega_k^{\parallel}/\omega_k^{\perp})^2 \qquad (if\ \ \omega_k^{\perp} \gg \omega_k^{\parallel}, \tilde{\Delta}\ )$$

$$\pi Q_\phi^{-1} \to \kappa = \tfrac{1}{2} \sum_k (\omega_k^{\perp}/\omega_k^{\parallel})^2 \qquad (if\ \ \omega_k^{\parallel} \gg \omega_k^{\perp}, \tilde{\Delta}\ ) \qquad (28)$$

One can get the second result from the first by a duality, switching the roles of $\omega_k^{\parallel}$

and $\omega_k^\perp$ in the derivation of the first (cf. ref. [14], App. 2B).

(b) If $\tilde{\Delta} \gg \omega_k^\parallel, \omega_k^\perp$, ie., high operating frequency (produced in Fe-8 by applying a strong transverse field, and in SQUIDs by using a low tunneling barrier), the problem is solvable either directly or, since we are now in the weak coupling regime, by mapping it to a spin-boson model [14,56]. If in addition $\tilde{\Delta} \gg E_o$, where $E_o = [\sum_k (\omega_k^\parallel)^2]^{1/2}$ is the linewidth of the multiplet of spin states surrounding each qubit line (recall Fig. 5), then

$$\pi Q_\phi^{-1} \to \kappa = (E_o/\tilde{\Delta})^2/2 \tag{29}$$

In the opposite case $\tilde{\Delta} \ll E_o$ the qubit dynamics is incoherent (ref. [14], eqtn. (4.21)).

The intuitive understanding of these results is as follows. The rapid changes of field acting on the k-th spin cause it to exhibit quasi-random precessional motion about a constantly changing axis. The decoherence rate is governed by κ because this parameter gives a measure of the amplitude of random angular displacement on the spin sphere per period of the qubit – this is small if $\vec{\gamma}_k^\uparrow$ and $\vec{\gamma}_k^\downarrow$ are either nearly parallel or nearly antiparallel (the 2 cases for which results were just given). In fact κ is measuring the accumulated random Berry phase of the spin, which when integrated out, gives decoherence.

I emphasize that this decoherence can not be parametrised in terms of the intrinsic environmental noise – it is a contribution to the environmental fluctuations caused by the coupling of the environment to the fluctuating qubit. Thus any calculation of decoherence starting from the intrinsic environmental fluctuation spectrum (eg., a response function calculation) will necessarily miss this contribution.

(iii) *Non-diagonal contributions*: Suppose that we were able to freeze out all intrinsic dynamics of the bath (thereby suppressing noise decoherence from the bath), and suppress precessional decoherence. Is there anything else left? The answer is yes – there is another kind of "off-diagonal" decoherence, arising purely from transitions in the environment induced *during* qubit transitions. To see how this works, consider again Fig. 5. As we saw, in general the motion of the qubit field acting on the k-th bath spin, between its two "static" orientations $\vec{\gamma}_k^\uparrow$and $\vec{\gamma}_k^\downarrow$, causes the bath spin to react – in doing so it will accumulate phase. Even if the 2 static orientations are the same, the bath will still be perturbed provided $\vec{\gamma}_k(t)$ makes some sort of excursion during the time period of interest. The extra phase accumulated must of course be averaged over ("integrated out"). The mathematical formulation of this (see refs. [14,27]) gives what we called "topological decoherence", since it involves averaging over the random topological phase of the bath spins. This decoherence can be parametrised by a number λ, such that the coherence Q-factor in the presence of only this decoherence source is $Q_\phi = \pi/\lambda$. In terms of the parameters of the original problem one has

$$\pi Q_\phi^{-1} \to \lambda = \frac{1}{2} \sum_k (\omega_k^\parallel/\Omega_o)^2 \tag{30}$$

in the usual case where $\omega_k^\parallel/\Omega_o \ll 1$.

Incidentally, one might guess by comparing (28) and (30) that there is a relation between topological decoherence and the precessional decoherence described

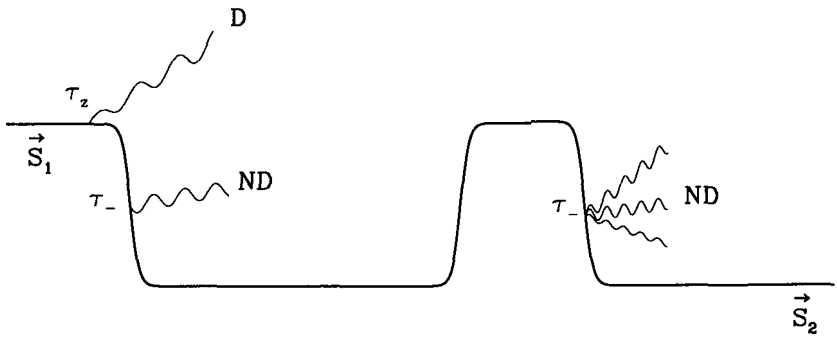

Figure 9: **Typical path for a tunneling Qubit.** A typical tunneling path for a qubit (shown here for a magnetic qubit, tunneling between states $|S_1\rangle$ and $|S_2\rangle$). These paths include coupling to the environment, shown as interaction vertices. Diagonal couplings (D) are defined as couplings to $\hat{\tau}_z$ (ie., taking place while the qubit is in one of the "stationary states" $|\Uparrow\rangle$ or $|\Downarrow\rangle$), and non-diagonal couplings (ND), occurring during transitions between the two, are to $\hat{\tau}_\pm$. The wavy lines represent either oscillator or spin bath modes.

by (28). Physically the connection is simple – precessional decoherence comes from bath transitions induced *in between* the qubit transitions, whereas topological decoherence comes from bath transitions induced *during* the qubit transitions (cf. Fig. 9). The mathematical connection is also straightforward [14,59]. In both cases the decoherence rate is coming from a product (over bath spins) of an "overlap squared" of form $|\langle\sigma_k^f|\sigma_k^{in}\rangle|^2$, for the k-th bath spin, where σ_k^{in} is an initial state for this spin, and σ_k^f a final state. The relation between the 2 states is given by $\sigma_k^f \hat{T}_k^{fi} \sigma_k^{in}$, where $\hat{T}_k^{fi} = e^{-i\vec{\alpha}_k \cdot \vec{\sigma}_k}$ in the case of topological decoherence (compare equation (8) and the discussion immediately following it). In the case of precessional decoherence one has $\hat{T}_k^{fi} = e^{-i\beta_k \hat{\sigma}_k^z}$ in the simplest case; the parameter β_k describes the angular mismatch between the vectors $\vec{\gamma}_k^\uparrow$ and $\vec{\gamma}_k^\downarrow$, so that $\beta_k \omega_k^\perp / \omega_k^\parallel$ when $\omega_k^\perp / \omega_k^\parallel \ll 1$, and the inverse of this when $\omega_k^\perp / \omega_k^\parallel \gg 1$.

These are the main points that arise in the calculation of single qubit decoherence dynamics. The detailed calculation of this dynamics [13,14,41] is complex because in general one has to deal with all the different decoherence mechanisms acting simultaneously – however in most cases one or other of them dominates. To get a better feeling for how things work it is useful to return to the examples of SQUIDs and magnetic qubits.

Note that the next obvious step would be to look at the dynamics of M coupled qubits, emphasizing the problem of "disentanglement dynamics", ie., the loss of coherence in that part of the M-qubit reduced density matrix which describes the qubit entanglement. The interest of this is that the whole enterprise of quantum information processing depends on preservation of N-qubit phase interference long enough for, eg., a computation to be done. However very little in the way of realistic calculations have been done on this problem, apart from a few calculations for 2-

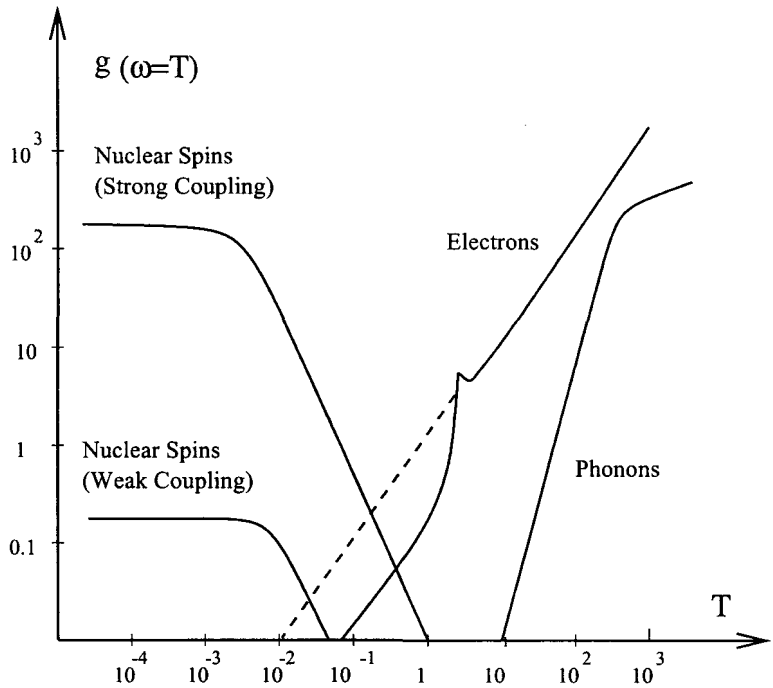

Figure 10: **Coupling to spin and oscillator bath modes.** The coupling strength $g(\omega, T)$ (discussed in detail in the text) between a qubit and various environmental modes – it is plotted here assuming $\omega = kT$, for a superconducting SQUID. The SQUID flux couples to phonons, (and photons), and electrons – a superconducting transition at $2K$ was assumed in this calculation (the residual Ohmic electronic term comes from a shunt resistance). The "nuclear spin" terms also include paramagnetic imputrities in the SQUID and substrate – for the purposes of this calculation we assumed $E_o = 3 \times 10^{-3}$ K. The difference between the strong and weak spin bath results is in the value of κ that was chosen.

qubit systems. This is undoubtedly one of the key theoretical problems facing the whole field – however I reluctantly leave it for another time.

4.2 Application to magnetic and superconducting Qubits

One important aspect of decoherence in solid-state qubits can be understood very quickly if we try to quantify the contributions to the decoherence rate coming from different energy scales. To do this we define a function $g(\omega, T)$ which takes the form

$$g(\omega, T) \rightarrow J(\omega) \coth(\hbar\omega/2kT) \tag{31}$$

for an oscillator bath, and

$$g(\omega, T) \rightarrow \sum_k (\omega_k^{\perp}/\omega_k^{\parallel})^2 \delta(\omega - \omega_k^{\parallel}) \qquad (\omega_k^{\perp} \ll \omega_k^{\parallel})$$

$$g(\omega, T) \to \sum_k (\omega_k^{\parallel}/\omega_k^{\perp})^2 \delta(\omega - \omega_k^{\perp}) \qquad (\omega_k^{\perp} \gg \omega_k^{\parallel}) \tag{32}$$

for a spin bath in he usual case where precessional decoherence dominates. The results are illustrated in Fig. 10, for the case $kT = \omega$, showing that decoherence from extended modes is worst at high energies, whereas the decoherence from localised modes is bad at low energies. As a general rule decoherence from extraneous noise sources (eg., $1/f$ noise) will also be worse at low frequencies. What this means is that there is typically going to be a "window" in energy space where decoherence is weak, at intermediate energies. We now look in more detail at this for superconductors and magnets – this is where we make contact with experiment.

Magnetic Systems

The best way to illustrate the results of the magnetic theory is to pick a model example. We consider the Fe-8 molecule again, which is apparently well understood (cf. end of section 2A). As we shall discuss in more detail in the next section, one can vary Δ_o over many orders of magnitude, going from completely incoherent behaviour for small Δ_o to highly coherent behaviour for sufficiently large Δ_o. In what follows I will simply discuss the precessional decoherence contribution from nuclear spins – a complete analysis of all decoherence contributions is beyond the scope of this article.

Taking over directly the results discussed in section 4A.2 for the central spin model, we see that to understand nuclear spin decoherence we must evaluate the noise decoherence from the fluctuating longitudinal nuclear bias, and the precessional decoherence from precession of the nuclear spins in between flips of the Fe-8 molecule. The former was already discussed (see paragraph following eqtn. (27). We estimated a noise decoherence rate $\Gamma_N \ll 10\ kHz$, *provided* the tunneling matrix element Δ_o was large. However in low fields in Fe-8, the opposite is true; $\Delta_o \sim 2\ kHz$ or less, and the dynamics is predicted to be completely incoherent [26,30,31]. Thus it makes little sense to look at the low-field precessional decoherence, except that in the detailed theory for an ensemble of tunneling molecules, the value of ξ_o depends on it. Since we are only here concerned with single tunneling molecules, we do not go into this.

In experiments in low fields on Fe-8, it is found that the molecular dynamics in the quantum regime is relaxational, and is clearly incoherent – relaxation rates are $\propto |\Delta_o|^2/\xi_o$. Detailed reviews of the low-field experiments on Fe-8, and other molecules in the quantum regime, have been given [10,11]. The results agree rather well with the theory of incoherent tunneling mediated by nuclear spins[26,30,31].

From these remarks it is clear that if one is to see coherent qubit behaviour in such molecules, one requires either a much bigger zero-field tunneling splitting Δ_o, or else Δ_o has to be increased using applied transverse fields. There are a couple of experiments which claim evidence for coherence in magnetic molecules – we look at these in section 5A, once we have had a chance to see how decoherence rates vary with applied field.

Superconducting systems

The experimental picture in superconducting qubits is evolving very quickly at the moment – anything I say here will certainly be out of date in the next year. Thus I simply give a quick look at the sort of numbers that appear, and what are believed to be the main decoherence mechanisms.

The first experiments to see qubit dynamics, with values of Q_ϕ eventually reaching several hundred, were those of Nakamura et al., in Cooper pair box systems [6,7]. In these experiments the charging energy $E_c \sim 1.3\ K$ and $E_J \sim 0.6\ K$, but both could be changed. The decoherence time for coupling to electrons could be fixed using a junction resistor to be $\sim 6-8$ nsecs, and the photon-mediated decoherence time was considered to be msecs. However it was found in "charge-echo" experiments (the analogue of spin-echo experiments for spin-1/2 nuclei) that the actual decoherence time was a few hundred psecs, roughly 30 times shorter. It was then shown that this could probably be correlated to $1/f$ noise in the system, which probably arose from coupling to charge defects [39], although in the absence of any direct knowledge of these defects or their concentration, it is hard to be quantitative.

Shortly after these experiments, indirect evidence was found in flux-tunneling SQUIDs for coherent dynamics [8]. In this case the tunneling matrix element $\Delta_o \sim 50\ mK$. Initial expectations were that very high Q coherence should be seen, because the coupling to electronic excitations was very weak – the dimensionless Ohmic coupling to electrons was $\alpha sim 10^{-7}$, implying $Q_\phi \sim 10^7$ for $kT < \Delta_o$. A very different result was found – although these experiments never measured T_2 directly, the linewidth in microwave absorption experiments indicated that Q_ϕ was more like 10-20, ie., a decoherence rate $\Gamma_\phi \sim 100\ MHz$.

This huge discrepancy may have several causes. Noise decoherence can arise from flux motion in, eg., the superconducting magnet, or from critical current fluctuations in the junction. One must also have decoherence from nuclear and paramagnetic spins in the SQUID and substrate. The parameters $\{\omega_k^\perp\}$ and $\{\omega_k^\parallel\}$ are defined for the SQUID in the same way as for magnetic systems, except that crystal fields acting on paramagnetic impurities must also be included – if these are strong, the impurity behaves as a 2-level system [28] at low T. The strengths of these couplings have been analysed elsewhere, for various geometries [14,45,46,47]. Unfortunately it is difficult to estimate them for a given sample – however we do know 2 things. First, $\omega_k^\perp \gg \omega_k^\parallel$, even in zero applied field – the quasi-static fields between spins ($\sim$ several Gauss) are much larger than the field generated by the SQUID supercurrent [14,45]. Second, the spins will be almost frozen – the paramagnetic spins by the much larger crystal fields, and the nuclear spins by the random fields from paramagnetic impurities – and so noise decoherence from the spin bath can be neglected. Then in low fields, where $\omega_k^\perp, \omega_k^\parallel \ll \tilde{\Delta}$, the decoherence rate can be calculated in terms of measurable parameters – one has $\kappa = (E_o/\Delta_o)^2/2$, provided $E_o \ll \Delta_o$ (otherwise there is no coherence at all); compare eqtn. (29). Application of this result to the Delft SQUID experiment [60], using the known sample geometry and concentration of nuclear spins and paramagnetic impurities in the system, indicates that one may account for $\sim 50\ MHz$ of this decoherence rate, mostly coming from paramagnetic impurities.

Very recently, a very interesting preprint has appeared[9] which combines various features of the Cooper pair box and SQUID designs, to give a very high Q-factor of roughly 25,000. The essential novelty here appears to be that one can remove the strictly linear couplings between the environment and both the charge and flux coordinates of the Q-bit, by sitting at a "symmetry point" in the combined space. This then leaves much less significant quadratic couplings, which do not appear in the theory discussed here. It seems likely that such designs will open up new experimental lines of investigation – note that such a high Q-factor may be enough for error correction to make multi-qubit computation feasible.

5 Suppressing Decoherence

Since the major problem facing any solid-state based quantum information processor is decoherence, what ways can one think of to suppress this? Various ideas have been discussed – they all rely in some way on the removal of environmental modes from the frequency range of operation of the qubits, and/or suppression of their coupling to the qubit. We consider first magnetic and superconducting systems, and then make some general observations on error correction and "decoherence free subspaces".

5.1 Decoherence Suppression in Magnetic Systems

There are several really obvious ways of suppressing decoherence in magnetic systems. The first thing to do is eliminate external noise sources – this is usually done with superconducting screening, but there is the risk here that random vortex motion in the superconductor will cause field fluctuations at the magbit sites. Since this kind of noise is *extrinsic*, I will not discuss it further here – the theorist can not say too much useful about its elimination.

Next on the list is decoherence from phonons and electrons. As indicated previously, even if a nanomagnet is conducting, the electronic energy levels will be strongly gapped if the nanomagnet is small enough, and decoherence from the spin-electron coupling exponentially suppressed (at least inside the nanomagnet). The coupling to any conduction electrons outside the nanomagnets is suppressed by having very high effective impedances for these electrons. Of course, if our magbit is an insulator, we can ignore electronic decoherence. The phonons can be a problem – their contribution to decoherence rises as the 3rd power[26] of the qubit operating frequency Δ_o, and should be included when Δ_o is large. In this pedagogical article we will ignore their contribution (but see ref. [35]).

Moving now to localised environmental modes, the most important source of intrinsic decoherence is nuclear spins. If isotopic purification is feasible, we may remove as many of the dangerous nuclear spins as possible. In some magnetic systems Nature has already done a lot of the work for us – only 2.21% of natural Fe nuclei are ^{56}Fe (with spin 1/2), and 1.14% of Ni is ^{61}Ni (again spin 1/2); all other stable isotopes are spinless. In nanostructured clusters or particles, made solely from magnetic elements, nuclear spins will then be fairly easy to remove. In many molecules the main problem will be H nuclei, none of which are spinless –

however there is no particular reason why one cannot find a high-spin insulating molecule without H ions.

Experimentalists may object here that isotopic purification is an expensive and imperfect technique – one can never completely expunge all nuclear spins from a sample. Since even a few nuclear spins can be very dangerous for multi-qubit coherence, let us consider the effect of applying a strong transverse field on spin bath decoherence [35]. It is important to consider a realistic example here, and so I give details for the well-studied Fe-8 molecule. Recall this system was already described at the end of section 2A (see also Fig. 6). We imagine applying a field $\mathbf{H}_o^x$ perpendicular to the easy axis and along the hard axis – as already noted, and shown in Fig. 2, the effect of this is to drag the 2 qubit states $|\Uparrow\rangle_{H_o^x}$ and $|\Downarrow\rangle_{H_o^x}$ towards each other on the Bloch sphere. The 2 lowest energy eigenstates of the system are produced by tunneling between these states.

A corollary to this has been the focus of some attention since it was first discussed by Bogachek and Krive[61]. As these authors noted, interference between the 2 tunneling paths shown in Fig. 2, means that there will be a kind of Aharonov-Bohm effect in spin space. This arises because, as is well known, the transition amplitude between 2 points on the spin sphere can be written in path integral language as equivalent to the dynamics of a particle of charge $q = \hbar S$ moving on its surface, along paths with unit vector coordinate $\hat{\mathbf{n}}(t)$. These are viewed as spin paths via the correspondence $\hat{\mathbf{n}}(t) = \mathbf{S}(t)/S$. The charge couples to a "potential" $\mathbf{H}_o(\mathbf{S})$ (the spin Hamiltonian) on the sphere, and also to a fake magnetic field from a unit monopole, situated at the centre of the sphere. The total tunneling amplitude is then the sum of that coming from the 2 tunneling paths, ie.,

$$\tilde{\Delta}_o(\mathbf{H}_o^x) = \Delta_o(\mathbf{H}_o^x)\cos\varphi(\mathbf{H}_o^x) \tag{33}$$

where $2\varphi = S\varpi$ is just the Berry phase enclosed by the tunneling paths, produced by the sum $(e^{i\varphi} + e^{-i\varphi})$. The term $\Delta_o(\mathbf{H}_o^x)$ is the tunneling amplitude along each path ignoring phase effects, and $\pm\varphi$ the phase along each path. The quantity ϖ is the *solid angle* enclosed by the tunneling paths on the sphere – the Aharonov-Bohm oscillations are occurring simply because this area is decreasing as we raise the transverse field (compare Fig. 2). If $\mathbf{H}_o^{\perp}$ is rotated away from $\hat{x}$, then the contributions from paths 1 and 2 are no longer equal, indeed $|\varphi_1| \neq |\varphi_2|$, and $|\Delta_o^{(1)} \neq \Delta_o^{(2)}$. Then one path is favoured over the other, and the oscillations are gradually lost as one rotates away from $\hat{x}$.

All of this physics is shown in Fig 11. We notice not only the oscillations in the tunneling splitting in low fields, but also the enormous rise in $|\tilde{\Delta}_o(\mathbf{H}_o^x)|$ as we increase the field above about 2 T. I emphasize that at such high fields this completely changes the picture we saw in Fig. 1 – instead of being very small, the qubit operating energy $\Delta_o$can now be much *larger* than the characteristic nuclear energy scales (this will certainly be the case in the Fe-8 system, as we see below), thereby radically altering the decoherence dynamics.

The other important thing that happens in a field is that we alter the dynamics of the nuclear spins. If all external fields are strictly zero, then $\omega_k^{\perp} = 0$ for all nuclear spins – this would imply no precessional decoherence at all! However even very small applied fields will change this, since they will compete with the very weak

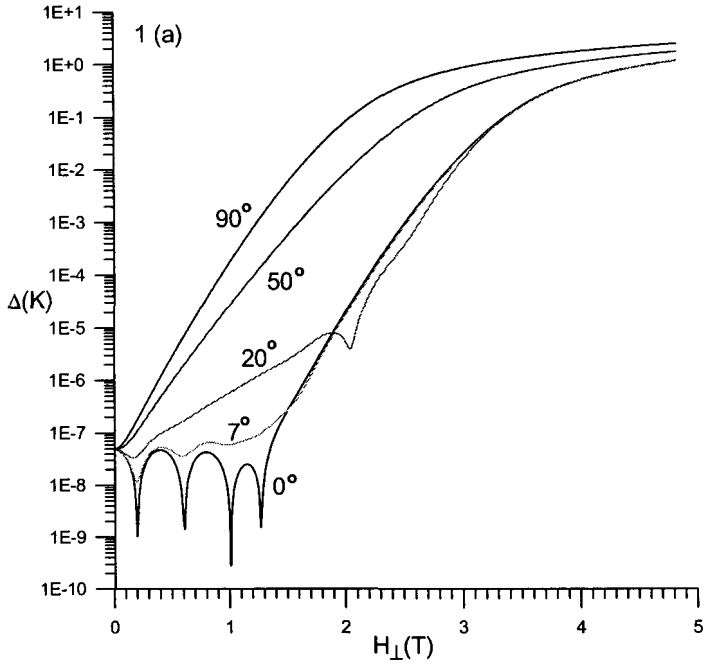

Figure 11: **Field variation of Tunneling splitting in *Fe*-8.** This plot is calculated by diagonalising the model Hamiltonian $\mathcal{H}_o\mathbf{S} = [-D\hat{S}_z^2 + E\hat{S}_x^2] + K_4^{\perp}(\hat{S}_+^4 + \hat{S}_-^4) - g\mu_B\mathbf{H}_o^{\perp} \cdot \mathbf{S}$, with the values of D, E, and $K_4^{\perp}$ taken from ref. [10]. The applied transverse field is at an angle ϕ to the in-plane hard axis. The modulus $|\Delta_o|$ of the tunneling splitting is given in Kelvin energy units, and field in Tesla (one should compare the results with the energy scales given in Fig. 1). Aharonov-Bohm oscillations for small ϕ are caused by phase interference between the 2 tunneling paths (see text).

hyperfine couplings of some of the far-flung nuclei in the molecule. As we continue to raise the field, more and more of the nuclei will start to give strong precessional decoherence contributions.

In much stronger fields, we slowly freeze the dynamics of the nuclear spins. The diagram in Fig. 4 shows what must happen – the strong field makes $\omega_k^{\perp}$ very large, and since $\omega_k^{\parallel}$ is only weakly affected, this forces the steadily increasing $\vec{\gamma}_k^{\uparrow}$ and $\vec{\gamma}_k^{\downarrow}$ to lie almost in the same direction, along the field. Actually $\omega_k^{\parallel}$ slowly *decreases* as H_o^x increases – it is a measure of the change in the hyperfine field on the k-th nucleus when the molecular spin flips between the 2 low energy states $|\Uparrow(H_o^x)\rangle$ and $|\Downarrow(H_o^x)\rangle$, but because the orientations of these states are approaching each other, the difference in these 2 hyperfine fields is correspondingly decreasing. The rapidly decreasing angular separation of $\vec{\gamma}_k^{\uparrow}$ and $\vec{\gamma}_k^{\downarrow}$ means that the essentially random phase precessional motion of the bath nuclear spins, caused by the tunneling dynamics of the molecule, is decreasing very rapidly in importance with increasing field, so that the decoherence from this is also rapidly decreasing (recall the discussion in

section 4).

We may then summarize the situation as follows. In a small field the precessional decoherence will quite rapidly switch on. Quite how fast this is can be seen in Fig 12(a), where we see that even in a field of $\sim 100\ G$, precessional decoherence will completely kill any coherent dynamics of an Fe-8 qubit. This merely substantiates the remark made in the last section, that in experiments conducted so far in low fields, the dynamics should be incoherent (in all low-field experiments on crystalline samples, intermolecular dipole fields were typically $\sim 200\ G$ at least; this quite apart from noise decoherence, which we saw was already sufficient at low fields to cause incoherent relaxation in these systems).

At much larger fields we now see that 2 effects will occur – a very rapid increase in the operating frequency Δ of the qubit, and a rapidly decreasing decoherence rate τ_ϕ^{-1}. Both of these effects operate in our favour, since the qubit coherence Q-factor is $Q_\phi \sim \tau_\phi \Delta$. The net result is a massive increase in Q_ϕ in transverse fields greater than $2-3\ T$, shown in Fig.12(b); in fact we see that for fields greater than $3\ T$, we have $Q_\phi \sim 10^6$, enough apparently for quantum computation to proceed.

At high fields we must also include noise decoherence, coming both from external noise sources and from internal spin diffusion in the nuclear spin subsystem. At this point I again assume that extrinsic noise has been suppressed by experimental tricks, and consider the effect of the nuclear spin diffusion. This problem is of some theoretical interest [29], particularly in a high applied field, where the nuclear spin diffusion will involve flip-flop processes amongst spins almost frozen by the field. In this case it makes sense to redefine the polarisation groups, introduced near the end of section 2A, by defining the polarisation along the external field rather than along the nanomagnetic easy axis. In sufficiently high field the nuclear system will then be confined to a single polarisation group of this kind.

The crucial question is then how fast is the diffusion inside one of these polarisation groups. This is a hard question to answer theoretically, and can only be definitively settled by experiments (eg., by measurements of the nuclear T_2 in Fe-8 in fields above $3\ T$). However our preliminary calculations [29] indicate that the characteristic timescale for nuclear diffusion at these fields may be as high as 1 sec. If this is true then it would give a contribution $\sim 10^{-10}$ to Q_ϕ^{-1}, and this can be completely ignored. Even if the fluctuation timescale were in the *msec* range, this would still give a contribution to Q_ϕ^{-1} in the range $10^{-7} - 10^{-6}$, which does not compete with the precessional decoherence just discussed.

Thus the theory indicates pretty clearly that a very good place to look for long-lived coherence in magnetic molecules is in high transverse fields. On the other hand there seems to be no point in looking for coherent dynamics at lower fields (at least not unless the field can be dropped to a small fraction of a Gauss – which rules out experiments on crystalline arrays of molecules, where the intermolecular dipolar fields are hundreds of Gauss).

We can also understand now why coherence should not have been seen in any experiments done so far on Fe-8; none of these have gone to high enough fields. Actually one experiment on a non-oriented powder of Fe-8 molecules [62] has claimed evidence for coherence, but this has not found general acceptance – no other experiments have confirmed it, and the averaging over orientations was done incorrectly

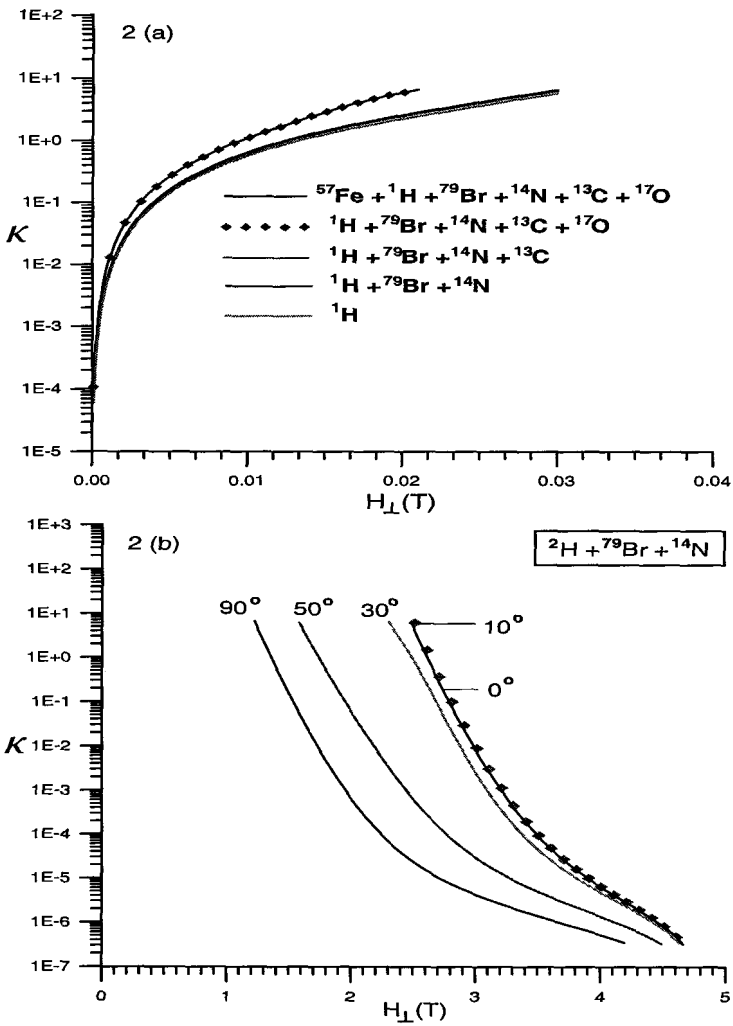

Figure 12: **Field dependence of $\kappa(H_o^\perp)$ in Fe-8.** In Fig. 12(a) the precessional decoherence parameter $\kappa(\mathbf{H}_o^\perp)$ is shown for small $\mathbf{H}_o^\perp$, where $H_o^\perp$ is applied transverse to the easy $\hat{z}$-axis, and the azimuthal angle ϕ is defined as in Fig. 11 relative to the hard axis. Results are computed from eqtn. (28). The different combinations of nuclear isotopes are as indicated.
In Fig. 12(b) we see the results in large transverse fields, calculated from (29), where the field is freezing the nuclear spin dynamics, and Δ_o is now large. The calculation is done for the *optimal* isotopic distribution, giving the lowest decoherence rate, with natural occurring isotopes, except that all the Fe is ^{56}Fe, and all protons are substituted by deuterium. Results now strongly depend on ϕ (via the angular dependence of $\Delta_o(\phi)$). Notice that in these high fields the 2 spin orientations $\mathbf{S}^\uparrow$ and $\mathbf{S}^\downarrow$ are pulled towards each other (compare Fig. 2). However even when $\mathbf{H}_o^\perp 4.7\ T$, these 2 orientations are separated by an angle $\sim 26^o$.

(see ref. 49 in ref. [15]). A more likely explanation of these results is that an ordinary EPR spectrum was being observed. One should also note the claim by Awschalom et al. [63] to have observed coherence in ferritin molecules. However this has been widely disputed, on theoretical and experimental grounds, in at least a dozen papers, and has not to my knowledge been confirmed by any other group.

5.2 Decoherence Suppression in Superconducting Systems

As discussed in section 4B.2, decoherence in superconducting qubits has many sources. Until very recently it looked as though it was going to be quite tough to control this. The most obvious strategy in SQUIDs, to suppress decoherence from paramagnetic and nuclear spins, is purification of the system. It can also be shown that reduction of the volume of both SQUID and substrate will cut down on this sort of decoherence [47]. Finally, if one is prepared to use *Nb* SQUIDs, the application of strong external field (which would be applied *transverse* to the ring plane, so as not to change the flux threading the ring) could be used. Then the paramagnetic impurity Zeeman energy $\omega_k^{\perp}$ can exceed $\tilde{\Delta}$ (eg. if $\tilde{\Delta} = 1GHz$, as in the Delft experiments, this happens when $|\mathbf{H}_o| > 500\ G$). If $\omega_k^{\perp} \gg \tilde{\Delta}$, we then have the very interesting situation where $\kappa(\mathbf{H}_o)$ is given by (28). In this case we see immediately that the paramagnetic impurity contribution to κ is $\kappa_p \sim N_p(h_\phi/H_o)^2/2 \sim (E_o/\omega_o(H_o))^2/2$, where h_ϕ is the field generated by the SQUID supercurrent on a typical impurity, ω_o the Zeeman energy of the impurity in H_o, and N_p the number of impurities. Thus consider a situation where ring and substrate yield a total $N_p \sim 10^{10}$, with $E_o \sim 100\ MHz$ in frequency units, and $\tilde{\Delta} = 1GHz$. In low fields one has $\kappa_p \sim 5 \times 10^{-3}$. However, once $|\mathbf{H}_o| \gg 500\ G$, we find $\kappa_p \sim 10^{-5}/B_o^2$, with $B_o = \mu H_o$ defined in Tesla units – i.e., if the external field exceeds $3\ T$ we have $\kappa_p < 10^{-6}$.

As already noted in the last section, a more interesting strategy for decoherence suppression in superconducting qubits has been devised in a recent preprint by Vion et al. [9]. It will be interesting how to see how this can be elaborated for superconducting multi-qubit networks.

5.3 General Remarks; Active decoherence suppression

A few years ago it was widely suspected that decoherence in solid-state systems would be prohibitively high, so high that quantum computation would be impossible. We now see that there is reason for some optimism – both theory and experiment indicate that decoherence can be understood and suppressed, at least at the single-qubit level.

Actually there are other reasons for optimism. So far I have only discussed "passive" forms of decoherence control – but work in quantum information theory has also come up with *active* schemes for either preventing or suppressing decoherence in quantum networks. The 2 schemes most relevant to solid-state qubits are (i) error correction protocols [64], and (ii) the isolation of "decoherence-free subspaces" [65,66]. Both of these are still largely untested experimentally (although there has been some work [67]), but hold great promise for the future.

Error correction has been discussed in some detail in the literature [17,18]; it is an active decoherence suppression mechanism in that the errors resulting from decoherence are rejected – the decoherence still takes place. As far as I know no attention has been given to its application to solid state systems. This will not be a trivial problem – although the formal description of error sources and correction is fairly straightforward, in reality it is obvious that any error correction must be implemented by some "circuit", whose time-dependent coupling to the information-processing system of interest will be itself a source of decoherence, and which must be understood. Moreover errors in a multi-qubit system cannot be understood by isolating errors in each qubit – decoherence in the M-qubit density matrix can only be fixed by correction schemes acting simultaneously on all M qubits.

For this reason the use of decoherence-free subspaces, before error correction routines are implemented, may well be quite important. The idea, somewhat familiar from NMR, is that the environment often couples very weakly to certain "quasi-conserved" combinations of operators referring to the qubits. Thus, if the system can be prepared so that it is in a subspace of the total Hilbert space where the environment acts trivially (or almost so), ie., as the unit operator, there will be little decoherence. The simplest way to implement this "decoherence prevention" idea arises if the relevant environmental decoherence mechanisms act in the same way on all qubits [65,66]. Then it is clear that the coupling of the environment to symmetric sums of operators acting on the qubits will be zero. The scheme is then implemented by preparing the multi-qubit system at $t = 0$ in a decoherence free subspace, so that it stays there during the computation. It is further argued that any residual coupling terms (which would cause this scheme to break down) can have their effects suppressed by pulse sequences [68], which in effect reverse the effects of the environment (an idea also familiar from NMR). Thus, eg., one can imagine schemes in which precessional decoherence from the spin bath (section 4A.2) is eliminated simply by reversing the applied field, so that the bath spins reverse their dynamics.

Of course things are not quite so simple. In the first place many environmental decoherence mechanisms will not act in the same way on each qubit (for example, different qubits will usually couple differently to the same spin bath, or even to different baths, and external noise sources may not couple symmetrically to all qubits). In this cause even elaborate (so-called "bang-bang" [68]) pulse sequences will not do the trick. However the idea is that one removes a lot of decoherence in this way, and then use "concatenation schemes" [69] in which such schemes prepare the way for active error correction. It is clear that a lot of work must be done to work out a realistic theory for such schemes (ie., a theory that applies to real solid-state qubits), but it seems very promising.

6 Future Prospects

Let me here stand back and address one of the more controversial issues that came up during this Delphi meeting.

From the technical point of view, there does not seem to be any fundamental obstacle in making a coherent solid-state qubit – it has already been done for

superconducting qubits, in several experiments [6,7,8,9], in one of which a very low decoherence rate was found. I am confident that when experiments probing the high frequency dynamics of magnetic molecules like Fe-8, or similar nanomagnets, are done at high transverse fields, the same success will be achieved. If one then believes the claim that, eg., error correction will then allow multiple qubit entanglement and computation, then we should be in business in perhaps a decade. Interestingly, at this conference the opinion was expressed by many from quantum optics that, although experiments on entanglement and quantum control in this field were "some 20 years ahead" of the work in solid-state physics, the scalability of solid-state designs meant that in the long run the future of quantum communication lay in this direction. It will be intriguing to see if this turns out to be the case.

However a much deeper question is quickly forced to the surface in discussions of quantum communication with solid-state systems, concerning the existence of genuine macroscopic quantum states. It is curious that this question should have been broached here in Delphi, since we are told that 2500 years ago, travellers from all over the Hellenic world came here in search of wisdom (apparently the nature of the advice varied from season to season, since some say that Apollo relinquished his oracle in the winter months to Dionysius). It is often asserted that modern science and philosophy are but footnotes to this legacy – that all modern ideas are just sophisticated elaborations on those of the ancient Greek philosophers.

However, as every physicist knows, just 76 years ago the discovery of quantum mechanics forced a completely new world-view upon us, involving non-locality of states and information, and entanglement (this being part of the legacy of Einstein and Schrodinger [70,71]). This revolution in our understanding, from sub-nuclear to cosmic scales, is frightening in its proportions, and surely unanticipated in all previous human thought. Could a latter-day Plato could also come to live with it? Perhaps – but my guess is that this would only be if entanglement and non-locality were assumed to exist solely at the atomic or molecular level (albeit over large distances), ie., far from the world of humanly sensible phenomena.

However this is not at all what the theory and experiments on solid-state qubits are telling us! Instead of ineffable massless photons, or tiny molecules, one is dealing with superpositions of macroscopic states of *large solid objects*. The problem of course is that such quantum superpositions at the human scale are felt by many (including some at this conference) to be fundamentally incompatible with our idea of physical reality, as understood at least since Hellenic times.

This issue is fundamental to the future of large-scale quantum computation and quantum communication. I should therefore like to emphasize one thing. This is that so far nothing has been found, either theoretically or in experiments on superconductors or magnets, to indicate that we cannot use quantum mechanics to discuss the entanglement of macrosocopic systems, including solid-state qubits, in quantum state superpositions, along the lines described in section 2A.1 (following eqtn. (2)). Given the deep questions raised by the extrapolation of quantum theory to large scales, it is obviously very interesting to search for deviations from the predictions of quantum mechanics [41]. However it is certainly incorrect to assert [72] that quantum theory does not permit such extrapolation – in fact the theory which has been used to predict large-scale quantum phenomena in superconductors and

magnets, including decoherence mechanisms, is entirely quantum-mechanical.

Acknowledgements

This work was supported by the Spinoza Institute in Utrecht, and by grants from the Dutch research council (FOM). I would particularly like to Dr. Igor Tupitsyn, and also Drs. Irinel Chiorescu, Boris Fine, Gerard 't Hooft, Boris Spivak, Caspar van der Wal, and Fei Zhou, for many discussions of the work in Utrecht. I also enjoyed stimulating exchanges in Delphi, particularly with Drs. Eugene Polzik, Jean-Michel Raimond, and Seth Lloyd.

References

1. B. Kane, Nature **393**, 133 (1998)
2. V. Privman, I.D. Vagner, G. Kventsel, Phys. Lett. **A236**, 141 (1998)
3. D. Loss, D. DiVincenzo, Phys. Rev. **A57**, 120 (1998)
4. A.O. Caldeira, A.J. Leggett, Ann. Phys. **149**, 374 (1983)
5. P.C.E. Stamp, Phys. Rev. Lett., **66**, 2802 (1991)
6. Y. Nakamura, Yu. A. Pashkin, J.S. Tsai, Nature **398**, 786 (1999)
7. Y. Nakamura et al., Phys. Rev. Lett. **88**, 047901 (2002)
8. C.H. Van der Wal, et al., Science **290**, 773 (2000)
9. D. Vion et al., Science **296**, 886 (2002)
10. W. Wernsdorfer, Adv. Chem. Phys. **118**, 99-190 (2001); /condmat 0101104
11. I.S. Tupitsyn, B. Barbara, pp. 109-168 in "*Magnetoscience – from Molecules to Materials*", ed. Miller and Drillon (Wiley, 2001)
12. Yu. Makhlin, G. Schon, A. Schnirman, Rev. Mod. Phys. **73**, 357 (2001)
13. U. Weiss, "*Dissipative Quantum Systems*" (World Scientific, 1999)
14. N.V. Prokof'ev, P.C.E. Stamp, Rep. Prog. Phys. **63**, 669 (2000)
15. M. Dubé, P.C.E. Stamp, Chem. Phys. 268, 257 (2001)
16. M. Grifoni, P. Hanggi, Phys. Rep. **304**, 229 (1998)
17. C.H. Bennett, D. DiVincenzo, Nature **404**, 247 (2000)
18. M.A. Nielsen, I.L. Chuang, "*Quantum Computation and Quantum Information*" (C.U.P., 2000)
19. V.B. Berestetskii, E.M. Lifshitz, L.P. Pitaevskii, *"Quantum Electrodynamics"*, vol. 4 of Landau-Lifshitz course (Pergamon, 1980)
20. C. Itzykson, J.-B. Zuber, *"Quantum Field Theory"* (McGraw-Hill, 1980)
21. L. Mandel, E. Wolf, *"Optical Coherence and Quantum Optics"* (C.U.P., 1995)
22. P. Fazekas, "*Electron Correlations and Magnetism*" (World Scientific, 1999)
23. O. Kahn, "*Molecular Magnetism*" (VCH, 1993)
24. P.Politi, A. Rettori, F. Hartmann-Boutron, J. Villain, Phys. Rev. Lett. **75**, 537 (1995)
25. I.S. Tupitsyn, N.V. Prokof'ev, P.C.E. Stamp, Int. J. Mod. Phys. **B11**, 2901 (1997)
26. N. V. Prokof'ev, P. C. E. Stamp, J. Low Temp. Phys. **104**,143 (1996)
27. N.V. Prokof'ev, P.C.E. Stamp, J. Phys. CM**5**, L663 (1993)
28. A. Abragam, "*The Principles of Nuclear Magnetism*" (O.U.P., 1961)

29. B.L. Fine, P.C.E. Stamp, I.S. Tupitsyn, unpublished
30. N.V. Prokof'ev, P.C.E. Stamp, Phys. Rev. Lett. **80**, 5794 (1998)
31. N.V. Prokof'ev, P.C.E. Stamp, J. Low Temp. Phys. **113**, 1147 (1998)
32. W. Wernsdorfer et al., Phys. Rev. Lett. **82**, 3903 (1999)
33. W. Wernsdorfer et al., Phys. Rev. Lett. **84**, 2965 (2000)
34. Y. Furukawa et al., Phys. Rev. **B62**, 14246 (2000); and Phys. Rev. **B64**, 094439 (2001)
35. P.C.E. Stamp, I.S. Tupitsyn, to be published
36. A.C. Hewson, "*The Kondo problem to Heavy Fermions*" (C.U.P. 1993)
37. A.J. Leggett, Phys. Rev. **B30**, 1208 (1984)
38. A. Barone, G. Paterno, "*Physics and Applications of the Josephson Effect*" (Wiley, 1982)
39. J. Mooij, T. Orlando, L. Levitov, L. Tian, C. H. van der Wal, S. Lloyd, Science **285**, 1036 (1999)
40. L.B. Ioffe, V.B. Geshkenbein, M.V. Feigelman, A.L. Fauchere, G. Blatter, Nature **398**, 679 (1999)
41. A.J. Leggett *et al.*, Rev. Mod. Phys. **59**, 1 (1987).
42. U. Eckern, G. Schon, V. Ambegaokar, Phys. Rev. **B30**, 6419 (1984)
43. A.I. Larkin, Y.N. Ovchinnikov, Phys. Rev. **B28**, 6281 (1983)
44. P.C.E Stamp, Phys. Rev. Lett. **61**, 2905 (1988)
45. P.C.E. Stamp, pp. 101-197 in *"Tunneling in Complex Systems"*, ed. S. Tomsovic (World Scientific, 1998)
46. L. Tian, et al., pp. 429-438 in "*Quantum Mesoscopic Phenomena and Mesoscopic Devices in Microelectronics*", ed. I.O.Kulik, R. Ellialtioglu (Kluwer, 2000)
47. N. V. Prokof'ev, P. C. E. Stamp, /cond-mat 006054 (May 2000); and P.C.E. Stamp, submitted to J. Low Temp. Phys.
48. D.L. Cox, A. Zawadowski, Adv. Phys. **47**, 599 (1998)
49. R. P. Feynman and A. R. Hibbs, "*Quantum Mechanics and Path Integrals*", (McGraw Hill, New York, 1965)
50. D. Mozyrsky, V. Privman, I.D. Vagner, Phys. Rev. B 63, 853131 (2001)
51. K.G. Wilson, Rev. Mod. Phys. **47**, 773 (1975)
52. R.P. Feynman, F.L. Vernon, Ann. Phys. **24**, 118 (1963)
53. P.C.E. Stamp, pp. 373-398 in *"Quantum Tunneling of Magnetisation-QTM'94"*, ed. L. Gunther, B. Barbara (Kluwer, 1995)
54. A. 0. Caldeira, A. H. Castro Neto, and T. 0. de Carvalho, Phys. Rev. B 48, 13974 (1993)
55. P.C.E. Stamp, E.M. Chudnovsky, and B. Barbara, Int. J. Mod. Phys. **B6**, 1355-1478 (1992)
56. A.O. Caldeira, A.H. Castro-Neto, T. Oliveira de Carvalho, Phys. Rev. **B48**, 13974 (1993)
57. J. Shao, P. Hanggi, Phys. Rev. Lett. **81**, 5710 (1998)
58. H. Grabert, P. Schramm, G-L. Ingold, Phys. Rep. **168**, 115 (1998)
59. N.V. Prokof'ev, P.C.E. Stamp, pp 347-371 in *"Quantum Tunneling of Magnetisation-QTM'94"*, ed. L. Gunther, B. Barbara (Kluwer, 1995)
60. I. Chiorescu, unpublished

61. E.N. Bogachek and I.V. Krive, Phys. Rev. B, **46**, 14559 (1992)
62. E. del Barco et al., Europhys. Lett. **47**, 722 (1999)
63. D.D. Awschalom et al., Science **258**, 414 (1992), S. Gider et al., Science **268**, 77 (1995). For the most recent experimental papers criticizing this work, see C. Gilles et al., Eur. Phys. J. B**17**, 417 (2000), and Physica **B304**, 237 (2001)
64. P.W. Shor, Phys. Rev. **A52**, 2493 (1995)
65. P. Zinardi, M. Rasetti, Phys. Rev. Lett. **79**, 3306 (1997)
66. D.A. Lidar, I.L. Chuang, K.B. Whaley, Phys. Rev. Lett. **81**, 2594 (1998)
67. D. Kielpniski et al., Science **291**, 1013 (2001)
68. L. Viola, S. Lloyd, Phys. Rev. **A58**, 2733 (1998)
69. D.A. Lidar, D. Bacon, K.B. Whaley, Phys. Rev. Lett. **82**, 4556 (1999)
70. A. Einstein, B. Podolsky, N. Rosen, Phys. Rev. **47**, 777 (1935)
71. E. Schrodinger, Naturwissenschaften **23**, 844 (1935)
72. N.G. van Kampen, Physica **A153**, 97 (1988)

DISCUSSION

Chairman: A. Zeilinger

L. Stodolsky: You didn't mention the experiment of Nakamura.

P. Stamp: I would have done if I had the time, I have a lot of slides and in fact I can spend a lot of time on it. Nakamura was the first to make a superconducting qubit that showed coherent oscillations in the off-diagonal density matrix elements and some of the work has not yet been published. He is the first to measure directly the noise decoherence rate in these systems and he has actually shown that it is $1/f$ noise, and seems to be coming from localized modes inside the Cooper pair box or in the surrounding circuitry, which are just charge defects. These are defects which can tunnel between two adjacent sites. Therefore the dipole moment associated with image couples to the charge in the Cooper pair boxes. These are really extraordinary experiments and the only point is, of course, that they are not doing it with macroscopic number of Cooper pairs. In the paper that I mention about the direct measurement of decoherence there is an analog with spin echo experiments, they see "charge echoes". Basically he is looking directly at the analog of the nuclear T_2 time. This is the design. We have here a superconducting box, and there are gates which allow Cooper pairs to tunnel on and off. The gates themselves are superconducting. The system is sufficiently small that its capacitance is very small, so the Coulomb charge gap is similar to the superconducting energy gap to excited pair states. Here is the level structure. Then by applying an external field you can essentially produce a qubit. What he did is, by applying pulse sequences analogous to what one does in a spin echo experiment, he observed directly decoherence. Here he shows that it is associated completely with $1/f$ noise, presumably associated with the charge defects.

I. Cirac: You mention the gap argument, could you quickly repeat the idea?

P. Stamp: Sure. Let me first start with an older argument, I am not sure from where it originated, but it has been around for a long time. This old argument

says you cannot have macroscopic superposition because no matter how precisely you define the Hilbert space of a macroscopic state, an enormous number of microscopic states are associated with it, say 10^{50}, which is what apparently David Bohm estimated in 1950 (although this is way too small, there are more nuclear spin states in a single magnetic nanomolecule!). Therefore, we are told, it is impossible to have such a superposition, because no way could one control the evolution of the system between all these microstates. Note that the old school argument suffers from a fatal weakness – it never tells you any details, it is a kind of a "bla-bla" argument. If you now have a look at superconductors or magnets, you find that the collective coordinates that you are interested in, say flux in a superconductor or total electronic spin in a magnet, are mostly coupled to degrees of freedom having an energy gap. For superconductors that obvious, that is the superconducting gap, and in magnetic systems you have the spin gap. Now you ask the following simple quantum mechanics question. Suppose I make a slow change in the effective potential acting on all those gap excitations, coming from the interaction with the slowly-changing collective mode. You can think of this collective mode as a kind of large soliton if you want. Think of the problem of a quantum soliton interacting with a gas of excitations which has a gap. You now see that the perturbation on those gap excitations is exponentially small in a parameter which is the ratio of gap energy over rate of change of the effective potential, in suitable units. That's one reason why the perturbation of the gapped excitations is so small, even though there is a huge number of them – that is what I mean by the "gap argument", which completely invalidates the earlier "old school" argument. Of course there are also some low-energy excitations below the gap- these are localised excitations which are described by the spin bath model, are not perturbed quasi-adiabatically, and which are potentially very dangerous. But to evaluate their effects you need a detailed theory, not vague remarks about the dimension of their Hilbert space. As I have discussed, it ought to be possible to suppress the decoherence from them as well, eg., by applying strong transverse fields.

L. Stodolsky: I want to make a remark and a question. About why decoherence is often not as bad as you think. As you'll see in the formulas represented in my talk, not all outside disturbances lead to decoherence. This is a common misconception, that every time you hit something it gets decoherent. If you have a two-states system, the external influence has to, in some way, disturb the two states differently. For instance, we find in our original work on optically active molecules at low temperature that only one in 10 000 collisions actually destroy the coherence. Our formula gives that qualitatively to show this. Therefore, don't think that every time something hits your system it will be decoherent.

P. Stamp: Well, I don't know who does think that! It is true that in the early days of discussions about quantum measurements, people talked naively in this way about decoherence. But I think it's fairly obvious from what I said that some kinds of interaction are much more dangerous than others – I mean, the point you made about them having to distinguish between the 2 states is of course well known. I guess I covered this in my last answer – there is no substitute for a proper calculation. It should also be a calculation applicable to real systems – I guess we all agree there are too many misleading toy models in the literature.

DECOHERENCE, PURIFICATION AND ENTANGLEMENT

E.C.G. SUDARSHAN

Department of Physics and Center for Particle Physics University of Texas, Austin, Texas 78712-1081 *

A pure quantum state is a projection on into linear space of quantum mechanics. But this may become, through a quantum stochastic map, a convex sum of projections (and hence an impure state) by decoherence. This is not a superposition. To get superposition we need to restore phase relations and that involves a fiducal projector. As this projector varies the various possible coherent combinations of the components of the mixture may be obtained. By a further application of this method the quantum entanglement between two subsystems can be restored. These methods can be used to maintain long term phase relations by the state being repeatedly processed by purification with possible applications to storage and processing information in quantum computing. In particular from separable or partially separable states we can obtain a purely entangled state.

1 Pure and Impure States: Density Matrices and Mappings

There are two ways of specifying a (pure) state of a quantum system. The first version associates with every quantum state a vector of unit norm in a complex inner-product space [1]. This is an overcomplete representation since the (absolute) phase of the state vector is irrelevant; we are in fact dealing with 'rays'. But if we have to superpose two pure states to form a pure state, the relative phase of the two state vectors is relevant (but their absolute phases are not). This method of representing states by vectors has another shortcoming in that it cannot represent mixed states. These can only be represented by assigning probabilities to a collection of states and averaging over all relative phases.

To surmount these shortcomings another method is to associate a pure state with projections in the complex inner product space [2]. There is no redundant phase. The impure states are formed by convex combinations of such projections. These states correspond to a normalized nonnegative linear operator called the density matrix rather than to rays. Any mechanism of corrupting the relative phases in a superposition is a process of 'decoherence'. The decoherence phenomenon of pure states into mixtures can be easily treated in terms of density matrices by looking at it as an instance of a broader class of linear maps acting on a pure density matrix. Such linear maps of density matrices has been studied under the title of (convex) stochastic maps and will be discussed in section 4.

Given a coherent superposition we can decohere it partly or totally to get an impure state density matrix. We may raise the reverse problem: given a mixed state, can we restore the relative phase? In particular, can we make a pure state but with the same probabilities?

*sudarshan@physics.utexas.edu

2 Purification

It is remarkable that this can be done by a simple protocol called 'purification' originally pointed out by Schrödinger [7]. We first illustrate it in the mixture of two orthogonal states:

$$\rho' = p_1\rho_1 + p_2\rho_2$$

$$\rho_1^2 = \rho_1 \ , \ \rho_2^2 = \rho_2 \ , \ \mathrm{tr}(\rho_1\rho_2) = 0 \ , \ \mathrm{tr}(\rho_1) = \mathrm{tr}(\rho_2) = 1.$$

Now we use the construction [6]

$$\rho = p_1\rho_1 + p_2\rho_2 + \sqrt{p_1p_2}\,\frac{\rho_1\Pi\rho_2}{\sqrt{\mathrm{tr}(\rho_1\Pi)\mathrm{tr}(\rho_2\Pi)}}. \tag{1}$$

It is easily verified that this is a pure state. Π is a projection which is *not* orthogonal to ρ_1 or ρ_2. As Π varies so does ρ, and the relative phase depends on the choice of Π. We can show that any desired phase can be so obtained.

For a mixture of more than two projections we need only to generalize the formula above:

$$\rho = \sum_{i,j}\sqrt{p_ip_j}\,\frac{\rho_i\Pi\rho_j}{\sqrt{\mathrm{tr}(\rho_i\Pi)\mathrm{tr}(\rho_j\Pi)}}. \tag{2}$$

We shall extend the purification of a separable density matrix of a bipartite system to restore full quantum entanglement.

3 Stochastic Maps from Hamiltonian Systems

Now that we have seen that there exists a simple way of restoring the coherence in a mixed state we can take a closer look at the process of decoherence itself. First let us consider how from a Hamiltonian system we could derive (irreversible) stochastic maps. For clarity we start with a two-level system with states $\mid 1\rangle$ and $\mid 2\rangle$ and a time-independent Hamiltonian

$$H = g(|1\rangle\langle 2| + |2\rangle\langle 1|) + \frac{\nu}{2}(|1\rangle\langle 1| - |2\rangle\langle 2|). \tag{3}$$

If we choose the term proportional to ν as the interaction part of the Hamiltonian, then in the interaction picture the Hamiltonian becomes time dependent

$$H_I = g(e^{i\nu t}|1\rangle\langle 2| - e^{-i\nu t}|2\rangle\langle 1|)\,. \tag{4}$$

Under this 'perturbation', the states $\mid 1\rangle$ and $\mid 2\rangle$ are no longer stationary but undergo Rabi oscillations. There is no decoherence. But if we take times *small* compared with ν^{-1} and compute only the *probabilities* for the states $\mid 1\rangle$ and $\mid 2\rangle$, we find a decoherent evolution. When we generalize this to a system with many frequencies which are small integral multiples of a single frequency, we get a collection of partial revivals reminiscent of Talbot's bands in optics. The problem of the time dependence of an arbitrary state of a free particle was studied by W. Schleich and collaborators (called a "quantum carpet") [9]. The relative phases endure naturally, and they are essential in the buildup of the Talbot resonances.

Qualitatively new features obtain when a discrete energy state is coupled to a continuum of energies. This is the model studied by Dirac [1] (which has had reincarnations as Friedrich's model, the Lee model and the Jaynes-Cummings model) to formulate the semiclassical theory of radiative deexcitation of an excited state of an atom. The amplitude for transition from the discrete state to the continuum is

$$h(\alpha'', \alpha') = \langle \alpha'' | V^*(t') | \alpha' \rangle = \langle \alpha'' | V | \alpha' \rangle \, e^{i(E''-E')t'}, \tag{5}$$

where $|\alpha''\rangle$ is the discrete state and $|\alpha'\rangle$ is a state belonging to the continuum. If we wait for a small time t the amplitude for transition is

$$\int_0^t dt' \langle \alpha'' | V^*(t') | \alpha' \rangle = \langle \alpha'' | V | \alpha' \rangle \, \frac{e^{i(E''-E')t} - 1}{i(E'' - E')}. \tag{6}$$

The discrete state at $t = 0$ becomes a superposition (*not* a mixture) of the continuum states.

$$|\alpha''\rangle \longrightarrow \left(\sqrt{1 - \int |h(\alpha'', \alpha')|^2 \, dE'} \right) |\alpha''\rangle + \int h(\alpha'', \alpha') \, e^{-iE't} \, |\alpha'\rangle \, . \tag{7}$$

This state is a pure state whether t is positive or negative. This transformation is unitary and reversible. If, following Dirac, we ask for the probability of a state with continuum energy and we have the probability density

$$\rho(\alpha'', \alpha') \, d\alpha' = |h(\alpha'', \alpha')|^2 \, d\alpha'.$$

By integrating over the frequency and making some approximation appropriate for not too small a time, he deduces a decay probability proportional to time t (with $t > 0$). So we see that the irreversible process is due to decoherence that is introduced when we look at the *probabilities* (with the relative phases being lost) rather than due to the interaction itself!

This conclusion is dramatically demonstrated if we start with a continuum superposition for $t = -\,|\,t'\,|$. In other words we take as our intial state corresponding to $t = 0$, that state which is obtained by evolving the original discrete state backwards in time for $|t'|$ seconds. Such a state would *recombine* to become the excited discrete state precisely when $t = |\,t'\,|$.

This remark about the relative phases and the role of decoherence in some (apparently irreversible) processes is seen in the time development of a free particle with an initial state minimum uncertainty wave function

$$\psi(x) = \pi^{\frac{1}{4}} e^{-x^2/2} \qquad \langle x^2 \rangle = \frac{1}{2}.$$

Then under free particle evolution this Gaussian packet spreads. The new mean square position is

$$\langle x^2(t) \rangle = \frac{1}{2\sqrt{1 + (t/m)^2}} = \frac{1}{2} \left[1 + \left(\frac{t}{m} \right)^2 \right]^{-1/2}$$

Does this mean that a Gaussian packet always expands? Yes, if the wave function was real at time $t = 0$. But if we had a suitable phase $e^{iH\tau}\psi(x, 0)$, then the mean square position variable will shrink from $t = 0$ to $t = \tau$ and then start expanding.

This may be seen even more clearly if we look at the wave function in the momentum space: the minimum uncertainty state is

$$\tilde{\psi}(p,0) = \pi^{-\frac{1}{4}} e^{-p^2/2}\,.$$

Then it will expand as time goes by since the wave function at time is

$$\tilde{\psi}(p,t) = e^{-i\frac{p^2}{2m}t} e^{-p^2/2}\,.$$

So the wave function at an earlier time $t = -\tau$ would have been

$$\tilde{\psi}(p,-\tau) = e^{+i\frac{p^2}{2m}\tau} e^{-p^2/2}\,.$$

This wave function *contracts* as time increases from $-\tau$ to 0 and then expands.

4 Decoherent Evolutions: Extremal Maps

The decoherent evolution of a quantum system leads to a stochastic map which is a contraction of the convex set of density matrices which converge to one (or more) fixed density matrices. In contrast, a unitary (reversible) evolution yields a map which takes the density matrices on to themselves, in particular a pure density matrix. The trace orthogonality of two density matrices ρ_1 and ρ_2 would not be preserved by a stochastic map

$$\mathrm{tr}(\rho_1'\rho_2') \neq \mathrm{tr}(\rho_1\rho_2)\,,$$

while the unitary evolutions preserve the trace orthogonality

$$\mathrm{tr}(\rho_1\rho_2) = 0 \;\longrightarrow \mathrm{tr}(\rho_1'\rho_2') = 0\,,$$

The stochastic maps themselves constitute a convex set [3]. It would be of interest to construct the extremal set of such dynamical maps. The maps themselves satisfy the following propertites (repeated indices are summed over).

$$\rho_{rs} \longrightarrow B_{rr',ss'}\rho_{r's'} \;>\; 0\,, \tag{8}$$

so that

$$x_r y_{r'}^* B_{rr',ss'} x_s^* y_{s'} \;>\; 0\,, \tag{9}$$

$$\sum B_{nr',ns'} = \delta_{r's'}\,, \tag{10}$$

and may be parametrized in terms of the eigenvectors of B in the form

$$B_{rr',ss'} = \mu(\alpha) C_{rr'}(\alpha) C^\dagger_{ss'}(\alpha)\,, \tag{11}$$

where $\mu(\alpha)$ may be positive or negative. If all the $\mu(\alpha)$ are positive, the map is said to be "completely positive" [4]. In this case the positive eigenvalue $\mu(\alpha)$ may be absorbed into the eigenmatrix $C(\alpha)$ so that a completely positive map may be described by a number $R \leq N$ matrices in the form

$$\rho' = \sum_{\alpha=1}^{R} C_\alpha\, \rho\, C_\alpha^\dagger\,, \qquad \sum_{\alpha=1}^{R} C_\alpha^\dagger C_\alpha = 1\,. \tag{12}$$

If we take the system S with density matrix ρ_{rs} to be coupled to an external 'reservoir' system R in the form

$$\rho_{rs} = \sum_a R_{ar,as} ,$$

then the evolution is by stochastic maps which are completely positive. The reservoir system is *not unique*, nor is the coupling between the concerned system and the reservoir.

We may write down the completely positive map as the contraction of a unitary map of an extended system as follows;

$$\rho_{jk} \longrightarrow V_{nj,a'j'}\, \rho_{j'k'} \tau_{a'b'} V^{\dagger}_{b'k',nk} , \tag{13}$$

with

$$V^{\dagger}_{aj,a'j'}\, V_{a'j',bk} = \delta_{ab}\, \delta_{jk} \quad ; \quad \tau_{aa} = 1 . \tag{14}$$

Such a map is completely positive. It will be extremal if τ is a projection

$$\tau_{ac}\, \tau_{cb} = \tau_{ab} . \tag{15}$$

The inverse construction also can be carried out to embed any stochastic map (which is completely positive) as the unitary evolution of the larger system [5]. Extremal maps corresponds to projection valued τ_{ab}.

It would be illustrative to construct all extremal maps of rank $R \leq 3$ for a 3×3 system: if $R = 1$, the condition

$$C^{\dagger} C = 1 ,$$

implies that the map is unitary. (Antiunitary maps are *not* completely positive.) The first nontrivial case is for $R = 2$. In this case we have

$$\rho \longrightarrow C^{\dagger}(1)\, \rho C(1) + C^{\dagger}(2)\, \rho C(2) \tag{16}$$

$$C(1)\, C^{\dagger}(1) + C(2)\, C^{\dagger}(2) = 1 .$$

We can always find unitary matrics U, V such that

$$C(1) = U^{\dagger}\, D(1)\, V ,$$

where $D(1)$ is a nonnegative diagonal matrix.

$$D^2(1) = U\, C(1)\, C^{\dagger}(1)\, U^{\dagger} = U\, [1 - C(2)\, C^{\dagger}(2)]\, U^{\dagger} = 1 - D^2(2). \tag{17}$$

We may choose

$$D(1) = \begin{pmatrix} \cos\theta_1 & 0 & 0 \\ 0 & \cos\theta_2 & 0 \\ 0 & 0 & \cos\theta_3 \end{pmatrix}$$

$$D(2) = \begin{pmatrix} \sin\theta_1 & 0 & 0 \\ 0 & \sin\theta_2 & 0 \\ 0 & 0 & \sin\theta_3 \end{pmatrix}$$

Then

$$C(2) = U^\dagger D(2) W$$

where W is an arbitrary unitary matrix. The generic map of rank 2 is

$$\rho \longrightarrow V^\dagger D(1) U \rho U^\dagger D(1) V + W^\dagger D(2) U \rho U^\dagger D(2) W . \tag{18}$$

For rank 3 ($R = 3$), the construction is as follows:

$$C(1) = U^\dagger D(1) V$$

$$C(2) C^\dagger(2) + C(3) C^\dagger(3) = 1 - U^\dagger D^2(1) U .$$

If $D(1)$ is chosen as

$$D(1) = \begin{pmatrix} \cos\theta_1 & 0 & 0 \\ 0 & \cos\theta_2 & 0 \\ 0 & 0 & \cos\theta_3 \end{pmatrix}$$

then

$$C(2) C^\dagger(2) + C(3) C^\dagger(3) = U^\dagger \begin{pmatrix} \sin^2\theta_1 & 0 & 0 \\ 0 & \sin^2\theta_2 & 0 \\ 0 & 0 & \sin^2\theta_3 \end{pmatrix} U .$$

We may write

$$C(2) = U^\dagger \begin{pmatrix} \sin\theta_1 & 0 & 0 \\ 0 & \sin\theta_2 & 0 \\ 0 & 0 & \sin\theta_3 \end{pmatrix} V \begin{pmatrix} \cos\phi_1 & 0 & 0 \\ 0 & \cos\phi_2 & 0 \\ 0 & 0 & \cos\phi_3 \end{pmatrix} W$$

$$C(3) = U^\dagger \begin{pmatrix} \sin\theta_1 & 0 & 0 \\ 0 & \sin\theta_2 & 0 \\ 0 & 0 & \sin\theta_3 \end{pmatrix} V \begin{pmatrix} \sin\phi_1 & 0 & 0 \\ 0 & \sin\phi_2 & 0 \\ 0 & 0 & \sin\phi_3 \end{pmatrix} X ,$$

where V, W and X are unitary matrices. Verify that

$$\begin{aligned} C(2) C^\dagger(2) + C(3) C^\dagger(3) = {} & U^\dagger \begin{pmatrix} \sin^2\theta_1 \cos^2\phi_1 & 0 & 0 \\ 0 & \sin^2\theta_2 \cos^2\phi_2 & 0 \\ 0 & 0 & \sin^2\theta_3 \cos^2\phi_3 \end{pmatrix} U \\ & + U^\dagger \begin{pmatrix} \sin^2\theta_1 \sin^2\phi_1 & 0 & 0 \\ 0 & \sin^2\theta_2 \sin^2\phi_2 & 0 \\ 0 & 0 & \sin^2\theta_3 \sin^2\phi_3 \end{pmatrix} U \\ = {} & U^\dagger \begin{pmatrix} \sin^2\theta_1 & 0 & 0 \\ 0 & \sin^2\theta_2 & 0 \\ 0 & 0 & \sin^2\theta_3 \end{pmatrix} U . \end{aligned}$$

Hence

$$C(1) C^\dagger(1) + C(2) C^\dagger(2) + C(3) C^\dagger(3) = 1 .$$

The map is

$$\rho \longrightarrow \quad X^\dagger \begin{pmatrix} \sin\phi_1 & 0 & 0 \\ 0 & \sin\phi_2 & 0 \\ 0 & 0 & \sin\phi_3 \end{pmatrix} V^\dagger \begin{pmatrix} \sin\theta_1 & 0 & 0 \\ 0 & \sin\theta_2 & 0 \\ 0 & 0 & \sin\theta_3 \end{pmatrix} U\rho$$
$$\times U^\dagger \begin{pmatrix} \sin\theta_1 & 0 & 0 \\ 0 & \sin\theta_2 & 0 \\ 0 & 0 & \sin\theta_3 \end{pmatrix} V \begin{pmatrix} \sin\phi_1 & 0 & 0 \\ 0 & \sin\phi_2 & 0 \\ 0 & 0 & \sin\phi_3 \end{pmatrix} X$$
$$+ \; W^\dagger \begin{pmatrix} \cos\phi_1 & 0 & 0 \\ 0 & \cos\phi_2 & 0 \\ 0 & 0 & \cos\phi_3 \end{pmatrix} V^\dagger \begin{pmatrix} \sin\theta_1 & 0 & 0 \\ 0 & \sin\theta_2 & 0 \\ 0 & 0 & \sin\theta_3 \end{pmatrix} U\rho$$
$$\times U^\dagger \begin{pmatrix} \sin\theta_1 & 0 & 0 \\ 0 & \sin\theta_2 & 0 \\ 0 & 0 & \sin\theta_3 \end{pmatrix} V^\dagger \begin{pmatrix} \cos\phi_1 & 0 & 0 \\ 0 & \cos\phi_2 & 0 \\ 0 & 0 & \cos\phi_3 \end{pmatrix} W$$
$$+ \; V^\dagger \begin{pmatrix} \cos\theta_1 & 0 & 0 \\ 0 & \cos\theta_2 & 0 \\ 0 & 0 & \cos\theta_3 \end{pmatrix} U\rho U^\dagger \begin{pmatrix} \cos\theta_1 & 0 & 0 \\ 0 & \cos\theta_2 & 0 \\ 0 & 0 & \cos\theta_3 \end{pmatrix} V \qquad (19)$$

No generality is lost by choosing an orthogonal transformation among $C(1)$, $C(2)$, $C(3)$ to make

$$\cos\theta_3 = 1 \quad , \quad \cos\phi_3 = 1 \, .$$

Hence the generic map is defined by the $SU(3)/Z_3$ matrices U, V, W, X and the angles $\theta_1, \theta_2, \phi_1, \phi_2$.

The indecomposable set $C(1)$, $C(2)$, $C(3)$ serve to preserve the trace but degrade some of the phases in ρ. The essential irreversibility is thus decoherence induced.

5 Entangled Systems, Decoherence and Purification

A closely related quantum property is that of 'quantum entanglement' [7]. If we have the density matrix R of a bipartite system AB, which may or may not be pure, then the partial traces

$$\mathrm{tr}_B \, R_{AB} = \rho_A \quad , \quad \mathrm{tr}_A \, R_{AB} = \rho_B$$

do not in general contain all the information in R. If R_{AB} is a pure state, ρ_A and ρ_B need not be pure, but they will have the same eigenvalues. If ρ_A is pure, so is ρ_B and R_{AB} is a direct product.

$$R_{AB} = \rho_A \otimes \rho_B \, .$$

So R_{AB} is separable. More generally if

$$R_{AB} = \sum_n p_n \, \rho_A(n) \otimes \rho_B(n) \quad , \quad \sum_n p_n = 1 \quad , \quad p_n \geq 0 \, , \qquad (20)$$

then R_{AB} is said to be separable. But for a generic pure state R_{AB}, ρ_A and ρ_B need not be pure. This obtains for example for the 'singlet' state

$$\Psi_{AB} = \frac{1}{\sqrt{2}} (\chi_A \varphi_B - \chi_B \varphi_A) \, ,$$

for which

$$R_{AB} = \Psi_{AB}\Psi_{AB}^{\dagger} \quad ; \quad \rho_A = \frac{1}{2}(\chi_A\chi_A^{\dagger} + \varphi_A\varphi_A^{\dagger});$$

the partial traces are not pure.

Thus the difference between the projection R_{AB} and $\rho_A \otimes \rho_B$ is the averaging over the phases of the interference terms $\chi_A\chi_B^{\dagger}$ and $\chi_B\chi_A^{\dagger}$. It follows that to restore the pure state from the separable impure state $\rho_A \otimes \rho_B$ is the restoration of the interference terms. But they are ambiguous since

$$R_{AB}(\theta) = \frac{1}{2}(\chi_A\varphi_B + e^{i\theta}\varphi_A\chi_B)(\chi_A^{\dagger}\varphi_B^{\dagger} + e^{-i\theta}\varphi_A^{\dagger}\chi_B^{\dagger}) \tag{21}$$

is a pure state giving the *same* marginal density matrices ρ_A and ρ_B . This indeterminateness of the relative phase angle was seen in the 'purification' of any impure density matrix.

It is not necessary that ρ_A and ρ_B are multiples of the unit matrix. For example

$$R_{AB} = \Psi_{AB}\Psi_{AB}^{\dagger}$$

$$\Psi_{AB} = (\cos\alpha\,\chi_A\varphi_B + \sin\alpha\, e^{i\theta}\,\chi_B\varphi_A)$$

leads to the partial density matrices

$$\rho_A = \cos^2\alpha\,\chi_A\chi_A^{\dagger} + \sin^2\alpha\,\varphi_A\varphi_A^{\dagger}$$

from which all information about θ has disappeared. We could generalize this to a more general Ψ_{AB} of the form

$$\Psi_{AB} = (c_1\chi_1\varphi_1 + c_2\chi_2\varphi_2 + c_3\chi_3\varphi_3 + \ldots)$$

$$\chi_j^{\dagger}\chi_k = \delta_{jk} = \varphi_j^{\dagger}\varphi_k \quad ; \quad |c_1|^2 + \ldots |c_n|^2 = 1\,.$$

The partial trace density matrices are

$$\rho_A = |c_1|^2\chi_1\chi_1^{\dagger} + |c_2|^2\chi_2\chi_2^{\dagger} + \ldots$$

$$\rho_B = |c_1|^2\varphi_1\varphi_1^{\dagger} + |c_2|^2\varphi_2\varphi_2^{\dagger} + \ldots\,.$$

The purification of either

$$R'_{AB} = \rho_A \otimes \rho_B$$

or

$$R''_{AB} = |c_1|^2\chi_1\chi_1^{\dagger}\varphi_1\varphi_1^{\dagger} + |c_2|^2\chi_2\chi_2^{\dagger}\varphi_2\varphi_2^{\dagger} + \ldots$$

can yield the same set of purified entangled density matrices

$$R_{AB} = \Psi_{AB}\Psi_{AB}^{\dagger}$$

with Ψ_{AB} as given above, but the relative phases of c_1, c_2... completely arbitrary.

The distinction between a 'simply separable' density matrix

$$R_{AB} = \rho_A \otimes \rho_B$$

and a 'generic separable' matrix

$$S_{AB} = \sum_n p_n \rho_A(n) \otimes \rho_B(n)$$

is this. The simply separable case has

$$R_{AB} = \sum_r p(r)\psi(r)\psi^\dagger(r).\phi(r)\phi^\dagger(r) \quad , \quad \sum_r p(r) = 1$$

with

$$\psi^\dagger(r)\psi(s) = \delta_{rs} = \phi^\dagger(r)\phi(s)$$

But

$$S_{AB} = \sum_s q(s)\psi(s)\psi^\dagger(s).\phi(s)\phi^\dagger(s) \quad , \quad \sum_s q(s) = 1$$

has the vectors $\{\psi(s)\}$ and $\{\phi(s)\}$ not being orthonormal. This decomposition is always possible since

$$\rho_A(r) \otimes \rho_B(n) = \sum_{n,r} p(n,r)\psi(n,r)\psi^\dagger(n,r).\phi(n,r)\phi^\dagger(n,r)$$

with

$$\psi^\dagger(n,r)\psi(n,r') = \delta_{rr'} = \phi^\dagger(n,r)\phi(n,r')$$

but no such restriction obtains for

$$\psi^\dagger(n,r)\psi(n',r') \ , \ \phi^\dagger(n,r)\phi(n',r') \, .$$

Purification in all cases involves the use of a projector Π which has nonzero overlap with any state involved in the decomposition of R_{AB}.

Purification [6] thus leads from a separable system, or any impure system to a pure state which automatically possessed quantum entanglement.

6 Concluding Remarks: Decoherence and Irreversibility.

We already saw that the coupling of a discrete state to a continuum does not lead to decay until the relative phases are averaged out. This insight answers an old puzzle: an accelerated charge radiates, but when does the radiation become independent of the accelerated charge? When does the photon really get emitted from the atom [8]? The answer is that when decoherence sets in, the processes have taken place.

But where does this decoherence come from? A finite closed system cannot have irreversible processes. If the system is not finite but is in the thermodynamic limit, no finite subsystem is closed. It is in this limit that we could obtain intrinsic decoherence.

I thank Anil Shaji for his assistance in the preparation of this paper.

References

1. PAM Dirac, "Principles of Quantum Mechanics", 4^{th}-edition, Oxford 1987.
2. J. von Neumann, "Mathematical Foundations of Quantum Mechanics", Princeton University Press, 1955.
3. E. C. G. Sudarshan, P. M. Mathews and Jayaseetha Rau, "Stochastic Dynamics of Quantum Mechanical Systems", Phys. Rev. **121**, 920-924 (1961).
4. M. D. Choi, "Positive Linear Maps on C^* Algebras", Canadian J. Math. **24**, 520 (1970).
5. E. C. G. Sudarshan, "Quantum Measurements and Dynamical Maps", in *From SU(3) to Gravity*, E. Gotsman and G. Tauber (eds), Cambridge University Press (1986).
6. V. I. Manko, G. Marmo, E. C. G. Sudarshan and F. Zaccaria, "Purification of Impure Density Operators and the Recovery of Entanglements" E-print, quant-ph/9910080 and "Inner Composition Law of Pure-Spin States" in *Spin-Statistics Connection and Commutation Relations*, R. C. Hilborn and G. M. Tino (eds), A.I.P. (2000).
7. E. Schrödinger, "Discussion of Probability Relations Between Separated Systems", Proc. Camb. Phil. Soc. **31**, 555 (1935).
8. M. Planck, "Theory of Heat Radiation", Dover reprint.
9. Berry, M., Marzoli, I., Schleich, W. Schleich, "Quantum carpets, carpets of light", Physics World, **14**, 39 (2001); C. Leichtle, I. Sh. Averbukh, and W. P. Schleich, "Multilevel quantum beats: An analytical approach", Phys. Rev. A **54**, 5299 (1996).

DISCUSSION

Chairman: A. Zeilinger

G. Pronko: Do you mean that irreversibility comes from interaction with some environment like radiation?

E. C. G. Sudarshan: You can call it interaction, intervention, hanging around. The point I'm trying to make is that, if you had an interaction of an atom with radiation field by itself, that leads only to a coherent state, coherent superposition. It is only when you disregard the phases then you get probabilities, and then you find the average of the problem.

G. Pronko: Thus it is anthropomorphic, subjective principle.

E. C. G. Sudarshan: Not subjective principle as Prigogine always tells. So irreversibility takes place but let us not say that the Hamiltonian produces the irreversibility.

What I said was that when we talk about the emission of light from an excited atom and write only that particular Hamiltonian, there is no irreversibility from that system. So therefore something has happened. Now if I have an external field which is driving the system having all complicated interactions, you still will get a coherent superposition and complicated coherent superposition. It becomes

a probabilistic distribution only when you have destroyed the phases, so you must destroy the phases by something. One mechanism is to couple this system with something outside. It doesn't matter what it is, anything outside, and then you eventually trace it out. It's partial tracing.

Therefore if you say that it interacts, for example you say that there are ambient photons which are going and disturbing something, and we are not paying enough attention to what happened with the photons. In that case you destroy the phases, but it is from the interaction only that you can destroy the phase, but there are many interactions with things which are not dynamical, but externally given, which would produce complicated time evolution but none of them would take your system in a pure state.

G. Pronko: In other words, only the environment with uncontrollable interactions will produce irreversibility.

E. C. G. Sudarshan: If you like to say, you put it that way.

G. Pronko: For closed systems, there will be no irreversibility.

E. C. G. Sudarshan: My statement is very clear and precise. For a finite dimensional system, because I talk about matrices, for a finite dimensional system coupled to other things, one finds that there is no irreversibility for the one simple case of radiation. Also, there is no irreversibility until you have said you will not taken into account the phases. And the reason for that thing is many: fact is that you are hanging around and looking at somebody else, photons are coming and hiding it and so on. But something happens and the mechanism of producing any kind of decoherence is — all believe it — in our competence and it does not require very complicated system. It needs only a finite number of states for the systems.

M. Courbage: *You need this phase destruction continuously in time or only* in the initial time?

E. C. G. Sudarshan: You need it continuously. It has to be thereof.

M. Courbage: You mean it is propagating by something.

I. Prigogine: I am not agree with you. When you have the photon which is emitted, you can go to many energies. That is a lineshape. There is typically the loss of information in the process.

E. C. G. Sudarshan: Only if you refuse to measure the relative phase between them.

I. Prigogine: No, I can measure the line shape, I can measure the propagation of the photons. Your point of view is that it is because we do not measure, because we are ignorant, that you obtain irreversibility. My point of view is that the irreversibility is a law of nature. And that can be seen in different situations because obviously in classical mechanics you see that there is no irreversibility in the two body problem but in the three body problem there is irreversibility. We don't know when the third body will be ejected away and at which time. You find that the basic difference are due to the Hamiltonian. And therefore I don't think that there will be difference between the case of quantum mechanics and I don't think it is because we make not enough measurements or something like that. I think, that comes out from the very foundation of quantum mechanics that you can have the situation when you have irreversibility. I agree with you that the irreversibility in quantum mechanics requires infinite systems because if you have finite box then

the spectrum of the Hamiltonian is not a continuous spectrum. We need a continuous spectrum and the continuous spectrum appears in the limit of large system. You have the same situation, expecting the same, when we have phase transitions. Phase transitions don't exist. Take a finite system - there are no phase transitions. If you go to the infinite system, you have phase transitions. And it is not because we want to have phase transitions. It is the fact that of course phase transitions are related to distributions, and with distribution you have somewhere a limit to have the distributions, and without this limit we cannot speak about the difference between soil and liquid.

E. C. G. Sudarshan: Professor Prigogine has pointed out something I should have specifically said. Namely that if you want to make a small system, with only finite number of degrees of freedom, not finite degree of states but finite number of the degrees of freedom, like for example a single atom emitting radiation. That is very different from a case in which you have an extensive system in which the thermodynamic limit is taken in which you have certain number of particles per volume but there is no limit to the size, it becomes larger and larger. So when you have this particular situation, the comments that I made do not apply, but as long as the system is what I write down Hamiltonian, the system at any state is obtained by unitary transformation. After finding unitary transformation you may say: look, I do measurements only on energy density distribution, not on the relative phases between the various things. That's perfectly fine. And if you do that then, of course, you will find that that particular thing is increasing. By the way, somebody mentioned Feynman-Wernan paper. That is an example of some situation in which a stochastic map is produced by taking a system which is perfectly legitimate and doing all the proper things. But then you will trace out the other variables, and then you get something of this kind.

I. Prigogine: The difference between finite system and infinite system is not so great, because, in fact, you can show that when we take a system, which is finite but with finite concentration, for some time it will behave like an infinite system. And that is, I think, the main problem because for most systems we have eigenvalue problem and it will take times long with respect to the duration of the particle going from one side to the other side. You have to take first the time large and then the volume starts to be large. When you want to have irreversibility you have to take first the volume to the infinity and then the time. And, in a sense, in the irreversibility problem you have never isolated system. And this is on of the mistakes of the Poincare's recurrence theorem because he says you will come back but after a long time you can never come back because the system will be submitted to other influence. Therefore there is no perfect reversibility.

E. C. G. Sudarshan: I'm completely agree with what you said, Professor Prigogine.

PROPAGATION OF DECOHERENCE IN A FIELD AND COMPLEX SPECTRAL REPRESENTATION

T. PETROSKY*,**AND C. O. TING*

*Center for Studies in Statistical Mechanics and Complex Systems
The University of Texas at Austin, Austin, TX 78712 USA

**International Solvay Institutes for Physics and Chemistry
CP231, 1050 Brussels, Belgium

The problem of decoherence in a system of a particle coupled with a field is studied by applying the Complex Spectral Representation of the Liouvillian that gives a rigorous approach to the irreversible processes without relying upon any anthropomorphic principle such as coarse-graining. We focus the time evolution of the field, which is commonly neglected in phenomenological approaches to the decoherence problem. In contrast to the usual hypothesis, our result shows that there is a non-negligible time evolution of the field. The decoherence in the field is an important consequence of the irreversible processes that leads dynamically to a mixed state from a pure state through a secular effect due to the resonance effect between the particle and the field.

1 Introduction

In this paper we shall study the problem of quantum decoherence as an application of the complex spectral representation of the Liouville-von Neumann equation. We consider a particle (such as a dipole molecule) coupled with a field through a bilinear interaction. This type of system has been repeatedly analyzed in the context of decoherence [1-5]. However, all arguments have a common phenomenological element, namely they have assumed that the field surrounding the particle is already in thermal equilibrium. Moreover, all assumed that the field as a thermal bath is so large that one can neglect the time evolution of the field.

However, this hypothesis is wrong. There is a non-negligible dressing cloud of field appears around the particle. In figure 1, we plot a numerical result of the number density $\langle n(x,t)\rangle$ of the quanta of the field in our system as a function of the coordinate x at a given time for the case the initial field is in a thermal equilibrium. More detailed discussion will be presented later in section 5. As one can see from this figure, indeed there appears a non-negligible dressing cloud around the particle as well as a non-negligible propagation of the field that do not die out in time.

Through these phenomenological hypotheses one can show that the reduced density matrix associated to the particle may approach to a mixed state even if it starts from a reduced pure state. However, this result is trivial since the surrounding field that is already in a mixed state may simply contaminate the pure state of the particle.

On the other side, a recent remarkable development on the complex spectral representation of the Liouville-von Neumann equations reveals the fact that irreversibility is a rigorous dynamical process of systems in the thermodynamic limit [6,7]. Irreversibility is the direct consequence of microscopic dynamical processes associ-

**PETROSKY@PHYSICS.UTEXAS.EDU

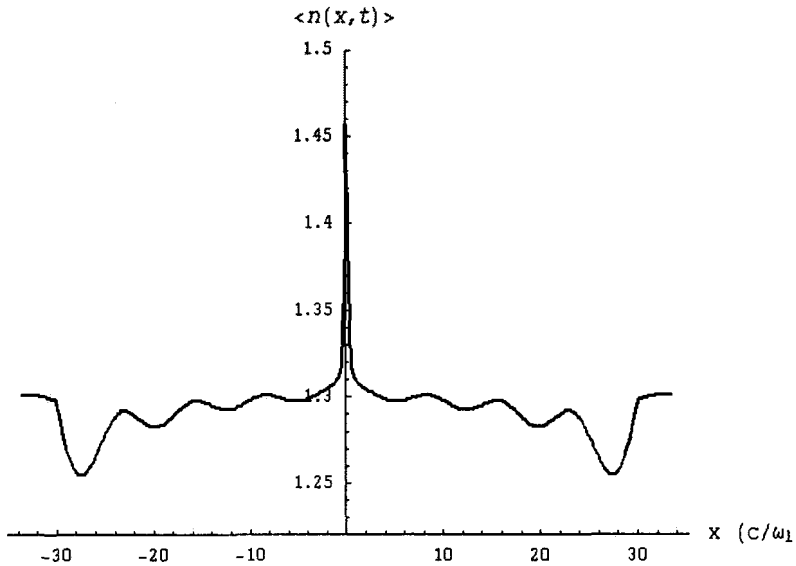

Figure 1. A numerical result of the number density $\langle n(x)\rangle$ in the x space at $t = 30$ for the initial $\langle n_1(0)\rangle = 0$ and $\langle n_k(0)\rangle = 1/(\exp(\beta\omega_k) - 1)$, with $\beta = 1/\omega_1$.

ated with resonance singularities, and does not come from the anthropomorphic principles, such as the incompleteness of our knowledge, coarse-graining approximations, or the so-called "environmental approach" that separates artificially a system into a subsystem and its surrounded environment that is already in thermal equilibrium. The appearance of decoherence is thus the result of irreversibility associated with the intrinsic instability inherited from the dynamics of the system itself.

The irreversible processes with which one deals in nonequilibrium statistical physics have two essential elements; the "extensivity" of the systems and the "non-integrability". In both equilibrium and nonequilibrium statistical mechanics, one deals with infinitely large systems which are characterized by extensive quantities that are proportional to the size of the system, such as the total number of particles or the total energy of the system. For this case, one can define the thermodynamic limit through the introduction of non-vanishing "intensive quantities", such as number density per volume. As we shall see later, an important consequence of the existence of the thermodynamic limit is that density matrices in quantum mechanics (or distribution functions in classical mechanics) do not belong to a Hilbert space. For this case, the Liouville-von Neumann operators (the Liouvillians in short) may have complex eigenvalues that break time-symmetry without adding any dissipative terms to the Hamiltonian or the Liouvillian.

However, the extensivity itself alone is not sufficient to have irreversibility as it

is well-known that the ideal gas is impossible to approach to equilibrium. This leads to the second ingredient of the irreversible processes, which is the non-integrability of the system. The interactions lead to the "small denominator" singularity (or resonance singularity) which prevents us from diagonalizing the Hamiltonian through a canonical (or unitary) transformation that is analytic with respect to a coupling constant (non-integrability in the sense of Poincaré) [8]. As a consequence, invariants of motion other than the total Hamiltonian are destroyed. Combining with the thermodynamic limit, the resonance singularities thus lead to contributions that break time-symmetry. In this situation, we have shown that one can obtain the irreversible dynamics through the complex spectral representation of the Liouvillian [6,7].

In section 2, we introduce our bilinear system. In order to deal with the thermodynamic situation, we adopt the box normalization with periodic boundary condition. Then we discuss the meaning of the thermodynamic limit. Indeed, this limit will naturally introduce some objects which do not belong to Hilbert space, hence one has to deal with a larger class of functions. We also demonstrate that the invariants of motion generated by the Bogoliubov transformation which diagonalize the Hamiltonian, are destroyed by the resonances in the thermodynamic limit. An important consequence of the failure of the Bogoliubov transformation is that one cannot reduce the time evolution of the state to the level of wave function in the thermodynamic limit.

In section 3, we overview the Liouvillian formulation of quantum mechanics. We introduce the projection operators associated to the correlation between the particle and the field, and solve the eigenvalue problem of the Liouvillian outside the Hilbert space, which gives us the complex spectral representation. We show the eigenvalue problem of the Liouvillian is reduced to the eigenvalue problem of the collision operator that commonly appears in the kinetic theory in non-equilibrium statistical physics. We also introduce the concept of subdynamics which enable us to evaluate the non-Markovian effect (i.e. memory effect) in a systematic way. As we shall see our method is based on the microscopic dynamics, which virtually implies no restriction on the class of initial conditions.

In section 4, we apply the complex spectral representation to our system. Our result shows that already in a weak coupling limit, there exists a signature of decoherence in the field that appears through the secular effect coming from the resonances. This effect can only be observed if we start from a non-equilibrium thermodynamic field. We also evaluate the non-Markovian effect that can be seen by going beyond the weak coupling limit (or the so-called $\lambda^2 t$ limit).

In section 5, we compare our theoretical results with the numerical simulations. The presentation of this paper is brief, we shall present a detailed paper elsewhere [9].

2 The System

We consider a one dimensional system which consists of a quantum harmonic oscillator linearly coupled to a bosonic massless scalar field. As a convention, we shall call the harmonic oscillator "particle" and the quanta of the field "photons". In the second quantized form and with units $\hbar = c = 1$, the Hamiltonian is defined by

a summation of the unperturbed part $H_0$and the interaction λV as

$$H = H_0 + \lambda V$$
$$= \omega_1 a_1^+ a_1 + \sum_k \omega_k a_k^+ a_k + \lambda \sum_k V_k (a_1^+ a_k + a_1 a_k^+) \quad (1)$$

where $\omega_1 > 0$, $\omega_k = |k| > 0$, and λ is positive dimensionless coupling constant. For simplicity we drop the virtual processes associated to the interaction proportional to $a_1 a_k$ or $a_1^+ a_k^+$, which is corresponding to the so-called the rotating wave approximation [10]. Due to this approximation, the total number of the unperturbed quanta is preserved in the time evolution. An extension of our argument including the virtual processes is straightforward [11,12]. Due to the periodic boundary condition, the spectrum of the field becomes discrete, i.e., $k = j/\Omega$ with a volume factor $\Omega \equiv L/2\pi$ and $j$is integer ranges from $-\infty$ to ∞. The volume dependence of the potential V_k is given by $V_k = v_k/\sqrt{\Omega}$, where v_k is independent of Ω.

In the Hamiltonian in (1), the creation and annihilation operators for the particle a_1^+, $a_1$and the field a_k^+, a_k obey the canonical commutation relations

$$[a_1, a_1^+] = 1, \quad [a_1, a_k^+] = 0, \quad [a_k, a_{k'}^+] = \delta_{k,k'} \quad (2)$$

where $\delta_{k,k'}$ is the Kronecker delta. In the continuous limit $\Omega \to \infty$, we have a continuous spectrum with

$$\sum_k \to \Omega \int dk, \quad \Omega \delta_{k,0} \to \delta(k) \quad (3)$$

where $\delta(k)$ is the Dirac delta function. We assume that the coupling is so weak $\lambda \ll 1$ that the interaction does not stabilize the particle by causing the negative renormalizing frequency.

Let us now specify the meaning of the thermodynamic limit. To this end, we focus our attention on a complete orthonormal basis of the unperturbed Hamiltonian H_0giv en by

$$H_0 |n_1, \{n_F\}\rangle = (\omega_1 n_1 + \sum_k \omega_k n_k) |n_1, \{n_F\}\rangle \quad (4)$$

where $\{n_F\} \equiv \{n_{k_1}, n_{k_2}, ...n_k\}$, and n_α is the occupation number for the state of particle ($\alpha = 1$) and field ($\alpha = k$), respectively. This basis spans a Hilbert space (Fock space) with the usual Hilbert norm $\| |n_1, \{n_F\}\rangle \|^2 = 1$, where $\|\Psi\|^2 \equiv \langle \Psi | \Psi \rangle$. Let us then consider an expectation value of the total Hamiltonian $\langle H \rangle$, where $\langle A \rangle \equiv Tr(A\rho)$ with a given density matrix ρ. For example, if the density matrix is diagonal in the number representation, we have in the limit $\Omega \to \infty$

$$\langle H \rangle = \omega_1 \langle n_1 \rangle + \Omega \int dk \omega_k \langle n_k \rangle \quad (5)$$

where we assume that $\int dk \omega_k \langle n_k \rangle < \infty$. We consider two different situations,

$$\langle n_k \rangle \sim O(\Omega^{-1}) \quad (6\text{-a})$$
$$\langle n_k \rangle \sim O(\Omega^0) \quad (6\text{-b})$$

In the first case in Eq.(6-a) with the condition $\langle H \rangle < \infty$, we have a situation which is considered in a problem of a stimulated or spontaneous emission of photon from the excited particle.

For the second case in Eq.(6-b), the total energy is an extensive quantity (as it is proportional to the volume) that characterizes the thermodynamic situations. We call that the limit $\Omega \to \infty$ with the condition Eq.(6-b) as the "thermodynamic limit". We note that in order to satisfy the condition of the thermodynamic limit it is not necessary for the density matrix ρ to be a mixed state. Indeed, we shall see later that one can construct a pure state that satisfies the condition of the thermodynamic limit by a super position of coherent states of the field.

An important consequence of the thermodynamic limit is that the time evolution of states cannot be described in terms of the states in the Hilbert space. Indeed, one can easily verify that the Hilbert norm of a state $|\Phi\rangle \equiv H|n_1, \{n_F\}\rangle$ diverges as $O(\Omega)$ in the thermodynamic limit $\Omega \to \infty$. Hence we have to solve the time evolution of the state in an extended space that lies outside the Hilbert space.

Another important consequence is that one cannot reduce the time evolution of the state to the level of wave functions. To see this let us first consider the case of the non-thermodynamic case Eq.(6-a). For this case it is well-known that one can diagonalize the Hamiltonian (1) in terms of the renormalized normal modes as (in the limit $\Omega \to \infty$) [13]

$$H = \int dk \omega_k \tilde{B}_k^+ \tilde{B}_k \tag{7}$$

with

$$[\tilde{B}_k, \tilde{B}_{k'}^+] = \delta(k - k') \tag{8}$$

Here $\tilde{B}_k$ is given by a linear transformation

$$\tilde{B}_k = \sqrt{\Omega} a_k + \lambda \frac{v_k}{\eta^-(\omega_k)} \left[a_1 - \int dk' \frac{\lambda v_{k'}}{\omega_{k'} - \omega_k + i\epsilon} \sqrt{\Omega} a_{k'} \right] \tag{9}$$

with

$$\eta(z) \equiv z - \omega_1 + \int dk' \frac{\lambda^2 |v_{k'}|^2}{\omega_{k'} - z} \tag{10}$$

where $\eta^{\pm}(\omega_k) \equiv \eta(\omega_k \pm i\epsilon)$ with a positive infinitesimal $\epsilon \to 0+$. We note that there is no renormalized particle such as $\tilde{B}_1$ in the new Hamiltonian (7), which is a characteristic property of the unstable system in the non-thermodynamic situation Eq.(6-a) [13]. Then we have an infinite set of invariants of motion $\langle \tilde{B}_k^+ \tilde{B}_k \rangle$.

However, this diagonalization of the Hamiltonian loses its meaning in the thermodynamic limit. Indeed, in the continuous spectrum limit the invariant $\langle \tilde{B}_k^+ \tilde{B}_k \rangle$ involves a singular product of the distribution $|\omega_k - \omega_{k'} + i\epsilon|^{-2}$. In the non-thermodynamic case Eq.(6-a), this product is negligible in the limit $\Omega \to \infty$ because of an extra volume factor Ω^{-1} in Eq.(6-a). However, in the thermodynamic limit Eq.(6-b) this singular product leads to a divergence as

$$\langle \tilde{B}_k^+ \tilde{B}_k \rangle \propto \int dk' \frac{\lambda^2 |v_{k'}|^2 \langle n_{k'} \rangle}{|\omega_{k'} - \omega_k + i\epsilon|^2} \propto \frac{1}{\epsilon} \longrightarrow \infty \tag{11}$$

The divergence comes from the contribution at the resonance $\omega_k = \omega_{k'}$, which destroys the invariant of motion.

Moreover, one can show through a direct calculation with the inverse transformation of Eq.(9) that the formal diagonalization of the Hamiltonian (7) leads to an inconsistent result to the conservation law of the total number of the unperturbed particle and photons in the thermodynamic limit. As a result one cannot follow the time evolution of the field through the diagonalization of the Hamiltonian as Eq.(7) in the thermodynamic limit.

Since the Hamiltonian (1) is bilinear in the annihilation and creation operators, the nonexistence of a diagonal form of the total Hamiltonian through a linear transformation in the thermodynamic limit is a nontrivial result. As a consequence of the failure of the diagonalization, one cannot reduce the time evolution of a given density matrix to an evolution of a product of the renormalized normal modes, or a product of wave functions. One has to deal with a non-factorizable evolution of the density matrix, even though one starts with a pure state as an initial condition.

3 Complex spectral representation of the Liouvillian

Since one cannot follow the time evolution of the system in terms of the wave functions in the thermodynamic limit, one has to directly deal with the evolution of the density matrices that is not in the Hilbert space. The density matrices obey the Liouville-von Neumann equation

$$i\frac{\partial}{\partial t}\rho(t) = L_H\rho(t) \tag{12}$$

where $L_H\rho \equiv H\rho - \rho H$. Corresponding to the decomposition of the Hamiltonian in (1), we have the Liouvillian decomposed into an unperturbed part L_0 and an interaction part L_V,

$$L_H = L_0 + \lambda L_V \tag{13}$$

Let us denote the complete orthogonal set of the eigenstates of the unperturbed Hamiltonian by $\{|\alpha\rangle\}$, i.e., $H_0|\alpha\rangle = \omega_\alpha|\alpha\rangle$. In our case $|\alpha\rangle = |n_1, \{n_F\}\rangle$ in Eq.(4). Then the complete orthogonal set of the eigenstates of the unperturbed Liouvillian in the "Liouville space" is given by the dyads $|\alpha;\beta\rangle\!\rangle \equiv |\alpha\rangle\langle\beta|$ as

$$L_0|\alpha;\beta\rangle\!\rangle = w^{(\alpha,\beta)}|\alpha;\beta\rangle\!\rangle \tag{14}$$

where $w^{(\alpha,\beta)} \equiv \omega_\alpha - \omega_\beta$. Here, the inner product in the Liouville space is defined by $\langle\!\langle A|B\rangle\!\rangle \equiv Tr(A^+B)$ where A^+ is the hermitian conjugate of the linear operator A in the wave function space. We note that the eigenstates of the unperturbed Liouvillian are infinitely degenerate as $L_0|\nu\rangle\!\rangle = w^{(\nu)}|\nu\rangle\!\rangle$ where $|\nu\rangle\!\rangle \equiv \sum_\alpha |\nu_\alpha\rangle\!\rangle$ and α is a degeneracy index. For example, all diagonal dyads $|\alpha;\alpha\rangle\!\rangle$ belong to zero eigenstate of L_0, i.e., we have $|0\rangle\!\rangle \equiv \sum_\alpha |\alpha;\alpha\rangle\!\rangle$. These degeneracies lead to a quite rich structure of the eigenvalue problem of the total Liouvillian L_H, as we shall see later.

The eigenstates of L_0defin e a complete orthogonal set of eigen-project-ion operators of L_0 as

$$P^{(\nu)} \equiv |\nu\rangle\!\rangle\langle\!\langle\nu| \tag{15}$$

that satisfies

$$\sum_{\nu} P^{(\nu)} = 1, \qquad P^{(\nu)} P^{(\mu)} = \delta_{\nu,\mu} P^{(\nu)} \tag{16}$$

We also introduce its complementary operator $Q^{(\nu)} \equiv 1 - P^{(\nu)}$ which satisfies

$$(Q^{(\nu)})^2 = Q^{(\nu)}, \qquad Q^{(\nu)} P^{(\nu)} = P^{(\nu)} Q^{(\nu)} = 0 \tag{17}$$

We recall that each projection operator $P^{(\nu)}$ defines the ν-th "correlation subspace" of the density matrix [7]. Of special interest is the "vacuum-of-correlation" subspace $P^{(0)}$ that extracts uncorrelated components of the density matrix among the particle and the field. Other components extract particle-field correlation components, field-field correlation components, and so on.

In the previous paper [7], I. Prigogine and one of us (T.P.) have extended the eigenvalue problem of the Liouvillian L_H to a class of density matrices that do not belong to the Hilbert space, and have shown that the Liouvillian may have complex eigenvalues that break time-symmetry. The complex spectral representation of the Liouvillian then leads to the "dynamics of correlations"[14]. In the correlation dynamics the non-Markovian evolution is described in terms of a set of infinite number of Markovian equations. This set includes the Pauli master equation. The detailed derivation of the solution of the eigenvalue problem of the Liouvillian as well as the derivation of the correlation dynamics has been given in [7]. Here we briefly summarize the complex spectral representation. For details the reader should consult the original article [7].

Let us now consider the eigenvalue problem of the Liouvillian[1]. Let us denote $|F_\alpha^{(\nu)}\rangle\!\rangle$, and $\langle\!\langle \tilde{F}_\alpha^{(\nu)}|$ as the right and left eigenstates of the total Liouvillian L_H respectively, [7],

$$L_H |F_\alpha^{(\nu)}\rangle\!\rangle = z_\alpha^{(\nu)} |F_\alpha^{(\nu)}\rangle\!\rangle, \qquad \langle\!\langle \tilde{F}_\alpha^{(\nu)}| L_H = \langle\!\langle \tilde{F}_\alpha^{(\nu)}| z_\alpha^{(\nu)} \tag{18}$$

where we assume that they satisfy bi-orthogonality and bi-completeness relations,

$$\langle\!\langle \tilde{F}_\alpha^{(\nu)} | F_\beta^{(\mu)} \rangle\!\rangle = \delta_{\nu,\mu}\delta_{\alpha,\beta}, \qquad \sum_{\nu}\sum_{\alpha} |F_\alpha^{(\nu)}\rangle\!\rangle \langle\!\langle \tilde{F}_\alpha^{(\nu)}| = 1 \tag{19}$$

The index α together with ν is a parameter characterizing the eigenfunctions. As mentioned before, since we consider the eigenvalue problem of the Liouvillian L_H outside Hilbert space, the left-eigenstate is generally different from the hermitian conjugate of the right-eigenstate. Moreover the eigenvalues $z_\alpha^{(\nu)}$ are complex, and the time evolution of the system splits into two semigroups. For the semigroup corresponding to $t > 0$, the eigenstates are associated with the eigenvalues with $\mathrm{Im} z_\alpha^{(\nu)} \leq 0$ and equilibrium is reached in our future for $t \to +\infty$, while for the other the eigenvalues are the complex conjugate of $z_\alpha^{(\nu)}$ and equilibrium is reached in our past. Experience shows that all irreversible processes have the same time orientation.

[1]We formulate the eigenvalue problem of L_H in the thermodynamic limit. In this limit, special care is necessary for a general Hamiltonian, as the perturbed Liouvillian L_V usually gives rise to divergence due to disconnected processes (see connected and disconnected diagrams in Refs.[14,7]). However, in the case of our Hamiltonian we do not encounter this divergence as all processes are connected to the tagged mode ω_1 through the specific form of interaction involving a_1 or a_1^+.

To be self-consistent, we have to choose the semigroup oriented towards our future. We consider the case where the eigenstates are analytic with respect to the coupling constant λ, i.e.,

$$\lim_{\lambda\to 0}|F_\alpha^{(\nu)}\rangle\!\rangle = \lim_{\lambda\to 0}P^{(\nu)}|F_\alpha^{(\nu)}\rangle\!\rangle, \qquad \lim_{\lambda\to 0}\langle\!\langle\tilde{F}_\alpha^{(\nu)}| = \lim_{\lambda\to 0}\langle\!\langle\tilde{F}_\alpha^{(\nu)}|P^{(\nu)} \tag{20}$$

and

$$\lim_{\lambda\to 0} z_\alpha^{(\nu)} = w^{(\nu)} \tag{21}$$

Using $P^{(\nu)}+Q^{(\nu)}= 1$ in Eq.(18) one can find the $Q^{(\nu)}$comp onent of the eigenstates as

$$Q^{(\nu)}|F_\alpha^{(\nu)}\rangle\!\rangle = \mathcal{C}^{(\nu)}(z_\alpha^{(\nu)})P^{(\nu)}|F_\alpha^{(\nu)}\rangle\!\rangle \tag{22}$$

where the "creation-of-correlation operator" (creation operator in short) is defined as

$$\begin{aligned}\mathcal{C}^{(\nu)}(z) &\equiv \frac{-1}{Q^{(\nu)}L_H Q^{(\nu)}-z}Q^{(\nu)}\lambda L_V P^{(\nu)} \\ &= Q^{(\nu)}\frac{-1}{L_0-z}\sum_{n=0}^{\infty}\left(Q^{(\nu)}\lambda L_V Q^{(\nu)}\frac{-1}{L_0-z}\right)^n Q^{(\nu)}\lambda L_V P^{(\nu)}\end{aligned} \tag{23}$$

This operator is an off-diagonal operator as it describes an "off-diagonal transition" between the different subspace $Q^{(\nu)}$ and $P^{(\nu)}$. Care has to be taken in the analytic continuation of z to have the time evolution approaching equilibrium in our future $t > 0$.

Substituting Eq.(22) into the eigenvalue equation (18), we obtain

$$\psi^{(\nu)}(z_\alpha^{(\nu)})|u_\alpha^{(\nu)}\rangle\!\rangle = z_\alpha^{(\nu)}|u_\alpha^{(\nu)}\rangle\!\rangle \tag{24}$$

where

$$|u_\alpha^{(\nu)}\rangle\!\rangle \equiv [N_\alpha^{(\nu)}]^{-1/2}P^{(\nu)}|F_\alpha^{(\nu)}\rangle\!\rangle \tag{25}$$

Here $N_\alpha^{(\nu)}$ is a normalization constant, and $\psi^{(\nu)}(z)$ are the *collision operators* defined by

$$\psi^{(\nu)}(z) \equiv P^{(\nu)}L_0P^{(\nu)} + P^{(\nu)}\lambda L_V\mathcal{C}^{(\nu)}(z)P^{(\nu)} \tag{26}$$

These operators are extension of the collision operators that appears in the kinetic theory in non-equilibrium statistical physics. The collision operator is a "diagonal operator" since it describes a "diagonal transition" within the same subspace $P^{(\nu)}$. As indicated in Eq.(24), the eigenvalue problem of the Liouville operator is then reduced to the eigenvalue problem of the collision operators which have the same eigenvalues $z^{(\nu)}$ as L_H. The eigenvalue equation Eq.(24) is "non-linear" as the eigenvalue appears in the collision operator.

Using Eq.(22), we obtain the right-eigenstates of L_H from the corresponding right-eigenstates of $\psi^{(\nu)}(z_\alpha^{(\nu)})$ as

$$|F_\alpha^{(\nu)}\rangle\!\rangle = [N_\alpha^{(\nu)}]^{1/2}(P^{(\nu)} + \mathcal{C}^{(\nu)}(z_\alpha^{(\nu)}))|u_\alpha^{(\nu)}\rangle\!\rangle \tag{27}$$

A construction parallel to the above, leads to the left-eigenstates of L_H with the same eigenvalues $z_\alpha^{(\nu)}$,

$$\langle\langle \tilde{F}_\alpha^{(\nu)}| = \langle\langle \tilde{v}_\alpha^{(\nu)}|(P^{(\nu)} + \mathcal{D}^{(\nu)}(z_\alpha^{(\nu)}))[N_\alpha^{(\nu)}]^{1/2} \tag{28}$$

where the "destruction operator" is defined by

$$\begin{aligned}\mathcal{D}^{(\nu)}(z) &\equiv P^{(\nu)}\lambda L_V Q^{(\nu)} \frac{1}{z - Q^{(\nu)} L_H Q^{(\nu)}} \\ &= P^{(\nu)}\lambda L_V Q^{(\nu)} \frac{1}{z - L_0} \sum_{n=0}^{\infty} \left(Q^{(\nu)}\lambda L_V Q^{(\nu)} \frac{1}{z - L_0} \right)^n \end{aligned} \tag{29}$$

and $\langle\langle \tilde{v}_\alpha^{(\nu)}| \equiv \langle\langle \tilde{F}_\alpha^{(\nu)}|P^{(\nu)} {N_\alpha^{(\nu)}}^{-1/2}$ are the left-eigenstates of the collision operator,

$$\langle\langle \tilde{v}_\alpha^{(\nu)}|\psi^{(\nu)}(z_\alpha^{(\nu)}) = \langle\langle \tilde{v}_\alpha^{(\nu)}|z_\alpha^{(\nu)} \tag{30}$$

Since the collision operator depends on the eigenvalue $z_\alpha^{(\nu)}$, the state $\langle\langle \tilde{v}_\alpha^{(\nu)}|$ is generally not bi-orthogonal to $|u_\alpha^{(\nu)}\rangle\rangle$. Assuming, however, bi-completeness of these states in each $P^{(\nu)}$ subspace, we may always construct sets of states $\{\langle\langle \tilde{u}_\alpha^{(\nu)}|\}$ and $\{|v_\alpha^{(\nu)}\rangle\rangle\}$ bi-orthogonal to $\{|u_\alpha^{(\nu)}\rangle\rangle\}$ and $\{\langle\langle \tilde{v}_\alpha^{(\nu)}|\}$, respectively,

$$\langle\langle \tilde{u}_\alpha^{(\nu)}|u_\beta^{(\mu)}\rangle\rangle = \delta_{\nu,\mu}\delta_{\alpha,\beta} \qquad \sum_\alpha |u_\alpha^{(\nu)}\rangle\rangle\langle\langle \tilde{u}_\alpha^{(\nu)}| = P^{(\nu)} \tag{31}$$

and similarly for $|v_\alpha^{(\nu)}\rangle\rangle$ and $\langle\langle \tilde{v}_\alpha^{(\nu)}|$.

In order to connect the kinetic theory to the eigenvalue problem of L_H, we introduce the "global" creation and destruction operators,

$$\mathbf{C}^{(\nu)} \equiv \sum_\alpha \mathcal{C}^{(\nu)}(z_\alpha^{(\nu)})|u_\alpha^{(\nu)}\rangle\rangle\langle\langle \tilde{u}_\alpha^{(\nu)}| \tag{32}$$

$$\mathbf{D}^{(\nu)} \equiv \sum_\alpha |v_\alpha^{(\nu)}\rangle\rangle\langle\langle \tilde{v}_\alpha^{(\nu)}|\mathcal{D}^{(\nu)}(z_\alpha^{(\nu)}) \tag{33}$$

Then, we can write the eigenstates as

$$|F_\alpha^{(\nu)}\rangle\rangle = [N_\alpha^{(\nu)}]^{1/2}(P^{(\nu)} + \mathbf{C}^{(\nu)})|u_\alpha^{(\nu)}\rangle\rangle \tag{34}$$

$$\langle\langle \tilde{F}_\alpha^{(\nu)}| = \langle\langle \tilde{v}_\alpha^{(\nu)}|(P^{(\nu)} + \mathbf{D}^{(\nu)})[N_\alpha^{(\nu)}]^{1/2} \tag{35}$$

The normalization constant can be found from the bi-orthonormality condition in Eq.(19) of the eigenstates,

$$[N_\alpha^{(\nu)}]^{-1} = \langle\langle \tilde{v}_\alpha^{(\nu)}|[(P^{(\nu)} + \mathbf{D}^{(\nu)}\mathbf{C}^{(\nu)})]|u_\alpha^{(\nu)}\rangle\rangle \tag{36}$$

The global collision operators associated with the creation operator $\mathbf{C}^{(\nu)}$ are given by

$$\theta^{(\nu)} \equiv \sum_\alpha \psi^{(\nu)}(z_\alpha^{(\nu)})|u_\alpha^{(\nu)}\rangle\rangle\langle\langle \tilde{u}_\alpha^{(\nu)}| \tag{37}$$

Then we have

$$\theta^{(\nu)}|u_\alpha^{(\nu)}\rangle\rangle = z_\alpha^{(\nu)}|u_\alpha^{(\nu)}\rangle\rangle \tag{38}$$

Substituting Eq.(26) into Eq.(29), we have

$$\theta^{(\nu)} = P^{(\nu)} L_0 P^{(\nu)} + P^{(\nu)} \lambda L_V \mathbf{C}^{(\nu)} P^{(\nu)} \tag{39}$$

Now we define the dressed projection operators in each subspace in terms of eigenstates Eqs.(34) and (35),

$$\Pi^{(\nu)} \equiv \sum_{\alpha} |F_{\alpha}^{(\nu)}\rangle\!\rangle \langle\!\langle \tilde{F}_{\alpha}^{(\nu)}|$$ (40)

This leads to the relation

$$\begin{aligned} e^{-iL_H t}\Pi^{(\nu)} &= \Pi^{(\nu)} e^{-iL_H t} \\ &= (P^{(\nu)} + \mathbf{C}^{(\nu)}) e^{-i\theta^{(\nu)} t} [(P^{(\nu)} + \mathbf{D}^{(\nu)}\mathbf{C}^{(\nu)})]^{-1} (P^{(\nu)} + \mathbf{D}^{(\nu)}) \end{aligned} \tag{41}$$

From Eq.(18) and Eq.(19) we have:

$$L_H \Pi^{(\nu)} = \Pi^{(\nu)} L_H, \qquad \sum_{\nu} \Pi^{(\nu)} = 1, \qquad \Pi^{(\nu)}\Pi^{(\mu)} = \Pi^{(\nu)} \delta_{\nu,\mu} \tag{42}$$

Hence, $\Pi^{(\nu)}$ is a generalization of $P^{(\nu)}$ for the total Liouvilian L_H, and each of the correlation subspace evolves independently in time under L_H. For this reason $\Pi^{(\nu)}$ is associated with *subdynamics*. However, Eq.(40) shows that $\Pi^{(\nu)}$ is not a hermitian superoperator. We call the component $P^{(\nu)}\rho^{(\nu)}$ as the "privileged" component of $\rho^{(\nu)} \equiv \Pi^{(\nu)}\rho$, which obeys the Markovian kinetic equation,

$$i\frac{\partial P^{(\nu)}\rho^{(\nu)}(t)}{\partial t} = \theta^{(\nu)} P^{(\nu)} \rho^{(\nu)}(t)$$ (43)

There is an infinite set of Markovian processes associated with each $\Pi^{(\nu)}$ subspace. Recall that we are interested in the weak coupling case. In that case, we apply series expansion in terms of λ up to $O(\lambda^2)$ which gives us

$$\theta^{(\nu)} = P^{(\nu)} L_0 P^{(\nu)} + \lambda^2 P^{(\nu)} L_V \frac{-1}{L_0 - (\omega^{(\nu)} + i\epsilon)} Q^{(\nu)} L_V P^{(\nu)} + O(\lambda^4)$$ (44)

where we have analytically continued $z_{\alpha}^{(\nu)}$ from the upper-half plane to ensure that the time evolution is oriented to our future $t > 0$. Similarly, we have the global creation and global destruction operators expanded up to $O(\lambda^2)$

$$\mathbf{C}^{(\nu)} = \lambda \mathcal{C}_1^{(\nu)}(w^{(\nu)}) + \lambda^2 \mathcal{C}_2^{(\nu)}(w^{(\nu)}) + O(\lambda^3)$$ (45)

$$\mathbf{D}^{(\nu)} = \lambda \mathcal{D}_1^{(\nu)}(w^{(\nu)}) + \lambda^2 \mathcal{D}_2^{(\nu)}(w^{(\nu)}) + O(\lambda^3)$$ (46)

with a suitable analytic continuation of $w^{(\nu)}$, where $\lambda^n \mathcal{C}_n^{(\nu)}$,$\lambda^n \mathcal{D}_n^{(\nu)}$ are the n-th order terms of the expansion of $\mathcal{C}^{(\nu)}$, and $\mathcal{D}^{(\nu)}$ in Eqs.(23) and (29), respectively.

An important consequence of the complex spectral representation of the Liouvillian is that non-Markov processes can be written as a superposition of the Markov process of each subspace. For example, let us consider a subspace $P^{(\nu_1)}$ with $\nu_1 \equiv (n_1, m_1)$ where the field components are diagonal so that it is associated to the eigenvalue of the unperturbed Liouvillian as

$$L_0 P^{(\nu_1)} = (n_1 - m_1)\omega_1 P^{(\nu_1)}$$ (47)

Then we have

$$
\begin{aligned}
&P^{(\nu_1)}e^{-iL_H t}\rho(0) \\
&= \sum_{\alpha} e^{-i\psi^{(\nu_1)}(z_\alpha^{(\nu_1)})t} P^{(\nu_1)}|F_\alpha^{(\nu_1)}\rangle\!\rangle\langle\!\langle \tilde{F}_\alpha^{(\nu_1)}|\rho(0)\rangle\!\rangle \\
&+ \sum_{\mu\neq\nu_1}\sum_{\alpha} P^{(\nu_1)}C^{(\mu)}(z_\alpha^{(\mu)})P^{(\mu)}e^{-i\psi^{(\mu)}(z_\alpha^{(\mu)})t}|F_\alpha^{(\mu)}\rangle\!\rangle\langle\!\langle \tilde{F}_\alpha^{(\mu)}|\rho(0)\rangle\!\rangle \qquad (48)
\end{aligned}
$$

The so-called Markov approximation corresponds to neglecting the second line in the right-hand side of (48). The decoherence of the particle occurs as a result of this Markov process. For the case where the expansion parameter of the perturbation analysis is the coupling constant λ, this approximation is valid only for the weakly coupling limit called as the "$\lambda^2 t$ limit"[14]. In this Markov approximation the first line in (48) obeys Eq.(43), which leads to the following set of equations

$$
\begin{aligned}
\frac{\partial}{\partial t}f_k(n_k,n_k,t) = \frac{\lambda^2\gamma_k}{\Omega}\big[&n_k\langle n_1\rangle_t f_k(n_k-1,n_k-1;t) \\
&-(\langle n_1\rangle_t + n_k + 2\langle n_1\rangle_t n_k)f_k(n_k,n_k,t) \\
&+(\langle n_1\rangle_t+1)(n_k+1)f_k(n_k+1,n_k+1,t)\big] \qquad (49)
\end{aligned}
$$

and

$$
\begin{aligned}
&\frac{\partial}{\partial t}f_{n_1,m_1}(t) - i\omega_1(m_1-n_1)f_{n_1,m_1}(t) \\
&= \lambda^2\int dk\gamma_k\big[\sqrt{n_1 m_1}\langle n_k\rangle_t f_{n_1-1,m_1-1}(t) \\
&-[(n_1+m_1+1)\langle n_k\rangle_t + \frac{1}{2}(n_1+m_1)]f_{n_1,m_1}(t) \\
&+\sqrt{(n_1+1)(m_1+1)}(\langle n_k\rangle_t+1)f_{n_1+1,m_1+1}(t)\big] \qquad (50)
\end{aligned}
$$

where

$$
\gamma_k \equiv 2\pi|v_k|^2\delta(\omega_k-\omega_1) \qquad (51)
$$

and $\langle n_\alpha\rangle_t$ is the average number of the particle for $\alpha=1$ and of the field for $\alpha=k$, where the frequency shift for the particle has been neglected. Here the reduced functions for the particle and the field, respectively, are defined by

$$
f_{n_1,m_1}(t) = \langle n_1|Tr_F[P^{(\nu_1)}\rho(t)]|m_1\rangle, \qquad (52)
$$

$$
f_k(n_k,n_k,t) \equiv \langle n_k|\mathrm{Tr}_{p,F_{(k)}}[P^{(0)}\rho(t)]\,|n_k\rangle \qquad (53)
$$

where Tr_F means that the partial trace is taken with respect to all field components, while $\mathrm{Tr}_{p,F_{(k)}}$ means that the partial trace is taken with respect to all component except for the kth-mode of the field. A detailed derivation of (49) and (50) has been presented in [11]. In the article [11] have shown that the Markov equation (49) together with (50) in the coordinate representation indeed describes the decoherence process as a result of the irreversible diffusion processes that come from the resonance effects between the particle and the field.

In the kinetic theory, to go beyond the $\lambda^2 t$ limit including memory effects (non-Markovian effects) has been a long standing extremely difficult problem. Our complex spectral representation gives a consistent description of the non-Markovian effects by systematically evaluating the second line in (48). For example, applying the expression (48) to our system, we have shown that the memory effect dies out in the time scale of the order $1/\omega_1 \ll \lambda^{-2}$ [11,12]. Therefore, $1/\omega_1$ gives a time scale of transition of the evolution from the non-Markovian regime to the Markovian regime. This transition time scale is called quantum Zeno time [17]. Only after the Zeno time does the first term in (48) dominate. Hence, the Zeno time serves as a lower bound for the decoherence time [11,12].

4 Time evolution of the system

As mentioned before, the decoherence process has been always investigated in the time evolution of the particle component alone [4-8]. In this section we shall focus our attention on the evolution of the field during the moment the decoherence in the particle is going on. To simplify our argument we shall consider here a special case of (48) with $\nu_1 = 0$. We first obtain a Pauli type of master equation in the weak coupling limit ($\lambda^2 t$ approximation). Later on, we shall go beyond this approximation by calculating the correction from non-Markovian effect in the second term of (48). By projecting Eq.(43) to $\langle\langle 1;1|$, and $\langle\langle k;k|$ in the case $\nu = 0$, we have in $\Pi^{(0)}$ subspace,

$$i\frac{\partial\langle n_1(t)\rangle_{\Pi^{(0)}}}{\partial t} = \theta^{(0)}_{11:11}\langle n_1(t)\rangle_{\Pi^{(0)}} + \sum_l \theta^{(0)}_{11:ll}\langle n_l(t)\rangle_{\Pi^{(0)}} \tag{54}$$

$$i\frac{\partial\langle n_k(t)\rangle}{\partial t} = \theta^{(0)}_{kk:11}\langle n_1(t)\rangle_{\Pi^{(0)}} + \sum_l \theta^{(0)}_{kk:ll}\langle n_l(t)\rangle_{\Pi^{(0)}} \tag{55}$$

where the matrix elements $\theta^{(0)}_{\alpha\beta:\alpha'\beta'} \equiv \langle\langle\alpha;\beta|\theta^{(0)}|\alpha';\beta'\rangle\rangle$, and we abbreviate $|1\rangle \equiv |1_1, 0_F\rangle$, and $|k\rangle \equiv |0_1, ...0_{k_{j-1}}, 1_{k_j}, 0_{k_{j+1}}\rangle$. The $\Pi^{(0)}$ component of the reduced probability density are defined as

$$\langle n_1(t)\rangle_{\Pi^{(0)}} \equiv \mathrm{Tr}(a_1^+ a_1 \Pi^{(0)}\rho(t)) \tag{56}$$

$$\langle n_k(t)\rangle_{\Pi^{(0)}} \equiv \mathrm{Tr}(a_k^+ a_k \Pi^{(0)}\rho(t)) \tag{57}$$

By using the expansion of $\theta^{(0)}$ in Eq.(44) up to $O(\lambda^2)$, we derive the Markovian kinetic equation under $\lambda^2 t$ approximation. This corresponds to the well-known Uhling-Unlenbeck equation for the average number of particles and the field for the case of nonlinear interaction, i.e.,

$$\frac{\partial}{\partial t}\langle n_1(t)\rangle_{\Pi^{(0)}} = \frac{\lambda^2}{\Omega}\sum_k \gamma_k[\langle n_k(t)\rangle_{\Pi^{(0)}} - \langle n_1(t)\rangle_{\Pi^{(0)}}] \tag{58}$$

$$\frac{\partial}{\partial t}\langle n_k(t)\rangle_{\Pi^{(0)}} = \frac{\lambda^2}{\Omega}\gamma_k[\langle n_1(t)\rangle_{\Pi^{(0)}} - \langle n_k(t)\rangle_{\Pi^{(0)}}] \tag{59}$$

The solutions of these equations up to $O(\Omega^{-1})$ are given by,

$$\langle n_1(t)\rangle_{\Pi^{(0)}} - \langle n_1(t)\rangle_{\Pi^{(0)}}$$
$$= (e^{-\gamma t} - 1)\langle n_1(0)\rangle_{\Pi^{(0)}} + \frac{1}{\gamma\Omega}\sum_l \gamma_l \langle n_l(0)\rangle_{\Pi^{(0)}}(1 - e^{-\gamma t}) \tag{60}$$

$$\langle n_k(t)\rangle_{\Pi^{(0)}} - \langle n_k(0)\rangle_{\Pi^{(0)}}$$
$$= \frac{1}{\Omega}\frac{\gamma_k}{\gamma}(1 - e^{-\lambda^2\gamma t})\langle n_1(0)\rangle_{\Pi^{(0)}}$$
$$+\lambda^2\frac{\gamma_k t}{\Omega}\left[\frac{1}{\gamma\Omega}\sum_l \gamma_l\langle n_l(0)\rangle_{\Pi^{(0)}} - \langle n_k(0)\rangle_{\Pi^{(0)}}\right]$$
$$-\frac{\gamma_k}{\gamma^2\Omega}\sum_l \gamma_l\langle n_l(0)\rangle_{\Pi^{(0)}}(1 - e^{-\lambda^2\gamma t}) + O(\frac{1}{\Omega^2}) \tag{61}$$

where $\gamma \equiv \Omega^{-1}\sum_k \gamma_k$.

Let us first focus on the decoherence of the particle by considering the initial background field which is in a thermal equilibrium, i.e. the photon probability density is given by Plank distribution with a fixed temperature. This situation has been well analyzed in the phenomenological approaches of decoherence problem. In figure 2, we compare our theoretical result in Eq.(60) with a numerical simulation of the total number of particle $\langle n_1(t)\rangle$. We choose the temperature of the background field $T = 1$ in the unit of ω_1/k_B where k_B is the Boltzman constant, and the dimensionless coupling constant $\lambda = 0.1$. The dotted line is the numerical result while another is the theoretical prediction from the solution of the Markovian kinetic equation. Both results show good agreement that the particle forgets its initial condition in the time scale $t \sim 1/\gamma$ obeying an exponential law and approaches to the final state which is solely determined by the temperature of the environment.

In figure 3, we show a magnification of the early stage of order $t \sim 1/\omega_1$ of the evolution in figure 2. The straight line is the theoretical result obtained only by taking into account a Markov process in a single $\Pi^{(0)}$ subspace. The deviation from the numerical result in figure 3 shows that we have a non-negligible memory effect coming from other subspaces. The deviation of exponential process is associated with the well-known "Quantum Zeno effect". In our previous paper [11], we showed that the memory effect follows a power law decay, then the time evolution undergoes a transition from non-Markovian regime to the Markovian regime. As a result, the time scale of this transition $t \sim 1/\omega_1$ serves as a lower bound for the decoherence time. Only after this time scale, the results obtained from the Markovian kinetic equation become valid.

Let us next consider the time evolution of the field. Our solution in Eq.(61) has two important aspects. First it gives non-vanishing time evolution of the field which is often neglected in the literature [4-8]. Indeed, by taking the summation over k that corresponds to evaluate the total number of photons, one cannot neglect the right-hand side of Eq.(61) in the thermodynamic limit. Therefore the neglecting of this time evolution leads to an inconsistency to the conservation law of the total number of the particle and photons. The second aspect of our solution is that

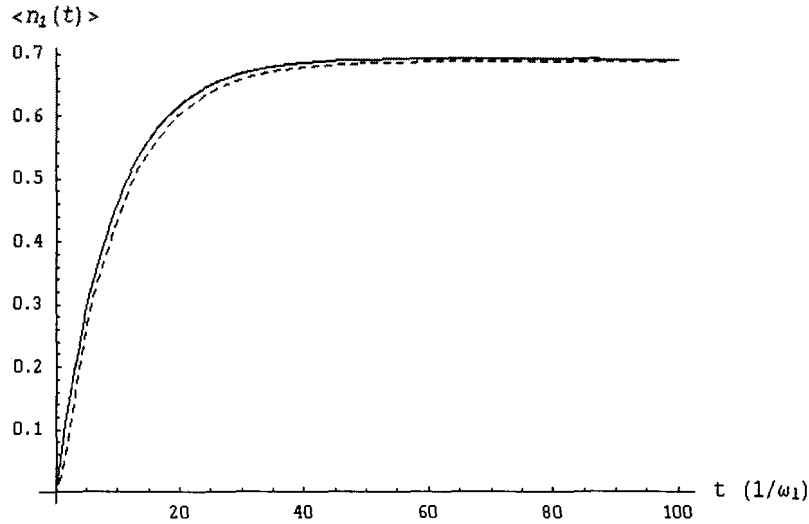

Figure 2. The time evolution of particle probability density $\langle n_1(t)\rangle$ under the same initial condition as Figure 1. The dotted line is numerical result, while the other one is theoretical result.

it shows the destruction of the wavefunction. As is well-known, the Pauli master equation leads the system to equlibrium so that evolution of the system cannot be reduced to the evolution of the wave functions. Under the thermodynamic limit Eq.(6-b), the second term of our solution in Eq.(61) has a non-negligible t-linear contribution as compared with the first term. This is a secular effect that appears through the resonance effect that destroys the factorizability to the evolution of the density matrix into the product of the wave functions. In fact, if we would apply the factorizable approach with the linear transformation in Eq.(9), we would obtain $\langle n_k\rangle$ with a diverging contribution as $\sim 1/\epsilon$ instead of the secular effect.

However, care has to be taken. Indeed, one has to make sure that the secular effect associated to the approach to equilibrium in the Pauli master equation does not disappear by adding non-Markov effects coming from components other than the vacuum-of-correlation component. This argument shows that only by going beyond the $\lambda^2 t$ approximation can one consistently discuss the decoherence process in the field evolution.

To analyze the secular effect in more detail, let us first note that if the initial condition of the field is in thermal equilibrium of the unperturbed system (which is a common setting of the phenomenological environmental approach [1-5]), the secular effect vanishes due to the symmetric dependence of $\langle n_k(0)\rangle$ with respect to an interchange of k to $-k$. In order to see this effect, we have to start with a field which is not in thermal equilibrium. As our theory of irreversibility is completely based on microscopic dynamics, we have an advantage to start with

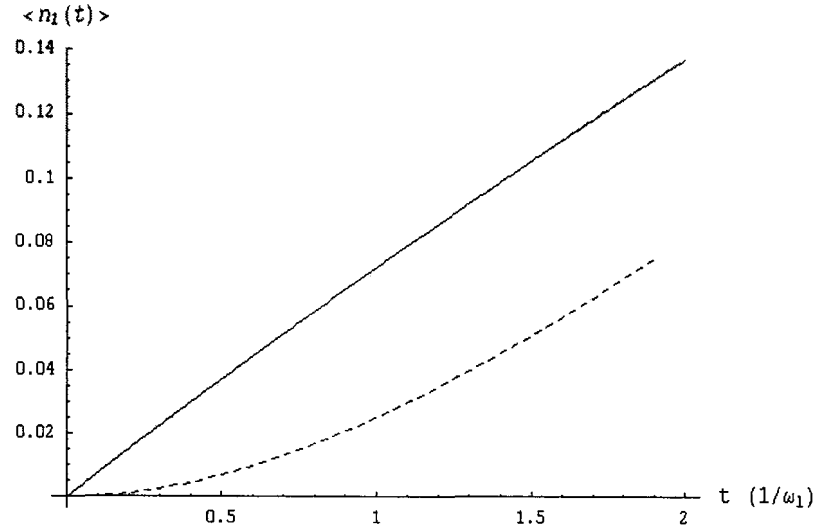

Figure 3. The Quantum Zeno effect in the time evolution of the particle. This is a magnification of an early state of the time evolution of the field in Figure 2. The dotted line is the numerical result, while the other one is theoretical result with Markovian approximation.

arbitrary initial condition. Indeed, this is the superiority of our approach over common phenomenological approaches of the decoherence problem which can only deal with the near equilibrium situation. Here we are especially interested in the extreme far from equilibrium situation that our initial field is a pure state given by

$$\rho(0) = |\Phi(0)\rangle\langle\Phi(0)| \tag{62}$$

To achieve the thermodynamic limit of the field in a pure state, we choose a large rectangular shaped wavepacket of the field with a size $L_{21} \equiv L_2 - L_1 > 0$ in one dimensional coordinate space that consists of a superposition of the coherent states of the field, i.e.,

$$|\Phi(0)\rangle = \sum_k^\infty \Phi_k |\hat{\alpha}_k\rangle \tag{63}$$

with

$$\Phi_k \equiv \frac{i}{\sqrt{L_{21}L}} \left[\frac{e^{-iL_2(k-k_0)} - e^{-iL_1(k-k_0)}}{k - k_0 - i\epsilon} \right] \tag{64}$$

and

$$|\hat{\alpha}_k\rangle = e^{-|\alpha_k|^2/2} \sum_{n_k=0}^\infty \frac{(\alpha_k a_k^+)^{n_k}}{\sqrt{n_k!}} |0_1, \{0_F\}\rangle \tag{65}$$

where 0_1 and $\{0_F\}$ denote the vacuums of the particle and the field, respectively. We assume that $\alpha_k = \sqrt{nL_{21}}$ for all modes k, where n is a number density of the photon per unit length. Then the total number of the photon in the initial wavepacket is proportional to the size of the wavepacket as $\sum_k \langle \Phi(0)|a_k^+ a_k|\Phi(0)\rangle = nL_{21}$.

To observe the spatial structure, we hereby introduce the x representation of creation operator a_k^+ by

$$a^+(x) \equiv \frac{1}{\sqrt{L}} \sum_k e^{-ikx} a_k^+ \tag{66}$$

The x representation of our wavepacket is then given by

$$\langle x|\Phi\rangle = \sqrt{n}\,[\theta_S(x - L_1) - \theta_S(x - L_2)]\, e^{ik_0 x} \tag{67}$$

where

$$|x\rangle \equiv \sum_{n_1} a^+(x)|n_1, \{0_F\}\rangle \tag{68}$$

and $\theta_S(x)$ is the step function, i.e., $\theta_S(x) = 0$ for $x < 0$ and $\theta_S(x) = 1$ for $x \geq 1$. For the case $L_{21} \sim L$, we have a wavepacket that satisfies the condition of the thermodynamic limit Eq.(6-b). For $L_1 = -L_2 = L/2$, Eq.(64) gives $\Phi_k = \delta_{k,k_0}$, i.e., we have a "plane wave".

By substituting our initial condition (64) into Eqs.(56) and (57), we obtain up to $O(\lambda^2)$

$$\langle n_1(0)\rangle_{\Pi^{(0)}} = 2\pi\lambda^2 n L_{21} L v_\omega^2 |\Phi_{\omega_1}|^2 \tag{69-a}$$

$$\langle n_k(0)\rangle_{\Pi^{(0)}} = |\Phi_k|^2 - 2\pi n L_{21}\lambda^2 v_k v_{\omega_k}\left[i\frac{\Phi_k^* \Phi_{\omega_k}}{(\omega_k - \omega_1 + i\epsilon)} + c.c\right] \tag{69-b}$$

The initial condition $\langle n_k(0)\rangle_{\Pi^{(0)}}$ is not symmetry under the changing from k to $-k$. Hence, there appears a non-vanishing t-linear term in the $\Pi^{(0)}$ component of the time evolution of the field density.

To be consistent, we have to calculate other contribution in $\Pi^{(1k)}$, $\Pi^{(k1)}$, $\Pi^{(lk)}$, and $\Pi^{(kl)}$ subspaces. The results are given up to $O(\lambda^2)$,

$$\langle n_k(t)\rangle_{\Pi^{(1k)}+\Pi^{(k1)}} = -\lambda^2 n L_{21} \frac{v_k \Phi_k^* e^{i(\omega_k - \omega_1)t - \gamma t}}{\Omega(\omega_k - \omega_1 + i\epsilon)} \sum_l \frac{v_l \Phi_l}{(\omega_1 - \omega_l + i\epsilon)} + c.c \tag{70}$$

$$\langle n_k(t)\rangle_{\Pi^{(lk)}+\Pi^{(kl)}} = -\lambda^2 n L_{21} \frac{v_k \Phi_k^* e^{i\omega_k t}}{\Omega} \sum_l \frac{v_l \Phi_l e^{-i\omega_l t}}{(\omega_k - \omega_l + i\epsilon)(\omega_1 - \omega_l + i\epsilon)} + c.c \tag{71}$$

These result shows that there is no secular effect in these subspaces contribution. As we shall see in next section, these results of non-Markovian contribution have a responsibility to Zeno effect which appeared in the early state of time evolution of the field, which can only be obtained by going beyond the $\lambda^2 t$ approximation.

5 Theoretical predictions v.s. numerical simulations

To verify our theoretical predictions, we have performed the numerical simulations. In the simulation, we consider the system of a finite box with size L. For this case our system is exactly diagonalizable through the linear transformation (the trouble due to the resonance singularity mentioned at Eq.(11) occurs only in the thermodynamic limit). By restricting our observation time to $t \ll L/c$, the numerical simulations give results which are not distinguishable from ones corresponding to the continuous spectrum case with $L \to \infty$. We have used the form factor v_k for the interaction as $v_k = \sqrt{\omega_k}\left[1 + (\omega_k/\omega_M)^2\right]^{-2}$ [15]. The cut-off frequency ω_M is introduced to avoid the ultraviolet divergence. We have used a unit system where the length is measured by the unit c/ω_1, while the time is measured by the unit $1/\omega_1$. We have fixed the size of box $L = 209$, the coupling constant $\lambda = 0.1$ and the cut-off frequency $\omega_M = 10$ in all cases.

In Figure 1, we plot the numerical result of the time evolution of the number density $\langle n(x,t)\rangle \equiv \mathrm{Tr}(a^+(x)a(x)\rho(t))$ of the photon at a given time $t = 30$, starting at $t = 0$ with $\langle n_1\rangle = 0$ and $\langle n_k\rangle \equiv 1/(\exp(\beta\omega_k) - 1)$ is the Plank distribution with the temperature $\beta_1 \equiv 1/k_B T_1 = 1/\omega_1$. The particle is located at $x = 0$. At $t = 0$ we have a constant density $\langle n(x,0)\rangle = 1.3$ in x space. About $t = 20$ a non-negligible steady cloud of field surrounding the particle with a size of c/ω_1 has been established. Generally the size of this cloud is much larger than the size of the molecule, and it causes the long-range van der Waals forces or Casimir-Polder forces [16]. At the distance $x = 30$, one can see the fronts of the propagation of the field. The shape of the fronts generally depends on the initial condition of $\langle n_1\rangle$. The fronts do not change their shape for the one-dimensional case, and propagate to an infinite large distance. In contrast to the assertion in the common approaches of the decoherence problem [1-5], the field has a non-negligible effect as time goes on.

In figure 2, we use the same initial setting as figure 1, that the particle is in the ground state at $t = 0$. We plot the time evolution of the number density of the particle. The solid line is the theoretical prediction in Eq.(60) obtained through Markovian approximation, while the dotted line is the numerical simulation. It shows that the Markovian approximation gives very good prediction in the time scale $t \sim O(1/\gamma)$ with $1/\gamma = 8.3$ in all of the simulations.

In figure 3, we magnify an early stage ($t \sim 1/\omega_1$) of the time evolution in Figure 2. In this regime, the non-Markovian effect dominates so that the Markov contribution alone is insufficient for prediction. Moreover, it is well-known that the so-called quantum Zeno effect [17] shall give the zero time derivative of $\langle n_k(t)\rangle$, and our numerical result which takes into account the non-Markovian effect, recovers this property. The Markovian effect itself cannot give rise to this non-exponential processes.

From figure 4-7, we consider the case where the initial condition of the field is given by the rectangular wavepacket in Eq.(64). In Figure 4, we plot the numerical simulation of the time evolution of the particle probability density by using $L_1 = -52$, $L_2 = 0$, and $k_0 = \omega_1$. The numerical results show the saturation of the particle and then decay exponentially after the passage of the wave packet.

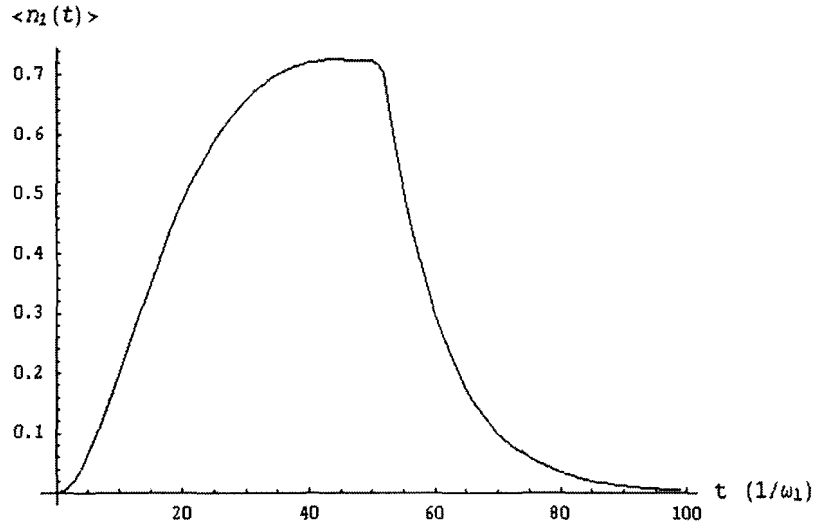

Figure 4. A numerical simulation of the time evolution of the particle $\langle n_1(t)\rangle$ with a rectangular wavepacket of size $L_{21} = 52$. After the wavepacket leaves at $t = 52$, $\langle n_1(t)\rangle$ starts to decay exponentially.

In Figure 5, we plot numerical results of the line shape $\langle n_k(t)\rangle$ for different times $t = 10$, 20, 30, and 40 as a function of k. In these results we have chosen a large wavepacket with the size $L_{21} = 35$, and $k_0 = \omega_1$. During the moment the wavepacket overlaps with the particle, the height of the line shape glows linearly in time in the negative direction as predicted by our theory, then the height is saturated when the wavepacket is dissociated from the particle.

In Figure 6, we plot theoretical results as well as a numerical result of $\langle n_k(t)\rangle$ at the mode $k = k_0$ as a function of time t for $\langle n_1(0)\rangle = 0$ and $\langle n_k(0)\rangle$ is the plane wave with $k_0 = 5$. The theoretical result due to the Markovian approximation Eq.(61) is plotted by the thick line, while the theoretical result including a dominant correction due to the non-Markov effects coming from the second line in Eq.(55) is plotted by the thin line. In the theoretical calculation the higher order effect of λ has been taken into account in such a way that the delta function $\delta(\omega_k - \omega_1)$ in Eq.(51) is replaced by the Lorentzian with the width of $\lambda^2\gamma$. The dotted line is the numerical result. After a time scale of a few oscillations of the particle, one can clearly see the t-linear secular effect.

In Figure 7, we magnify an early stage of the time evolution in Figure 6, where the numerical result (the dotted line) and the theoretical result (the solid line) with non-Markov effects included are shown. These results shows that the time derivative of $\langle n_k(t)\rangle$ vanishes at $t = 0$. This is the well-known quantum Zeno effect

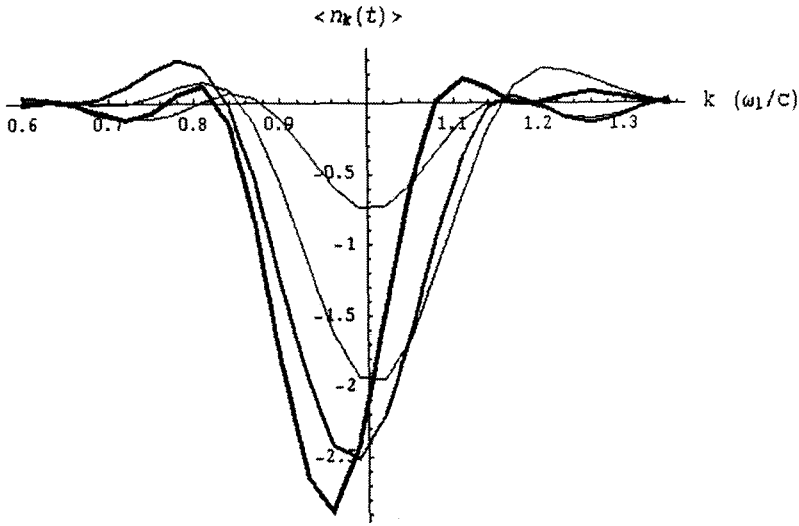

Figure 5. A numerical simulation of the linear growth of the line shape in time. We start with a wavepacket with size $L_{21} = 35$, and $k_0 = \omega_1$. The lines from thin to thick correspond to the different time $t = 10$, $t = 20$, $t = 30$, and $t = 40$, respectively.

in the evolution of the field [17]. Our theoretical result consistently recovers this well-known non-Markov effect.

6 Conclusion

As an application of the complex spectral representation of the Liouvillian that gives a rigorous approach to irreversible processes on the basis of microscopic dynamics, we have considered a problem of quantum decoherence for a particle coupled with a field that is in the thermodynamic limit. To deal with this problem we have emphasized that one has to go beyond the $\lambda^2 t$ approximation, the extension of which has been a long standing difficult problem in kinetic theory in non-equilibrium statistical mechanics.

In this article we have especially focused our attention on a time evolution of the field, which is commonly neglected in literature. As we have shown, this neglect misses an important signature of the decoherence in the field that may be measured in actual experiments. We have shown the decoherence in the field is a result of irreversible process that leads dynamically to a mixed state from a pure state through the secular effect due to the resonance effect between the particle and the field.

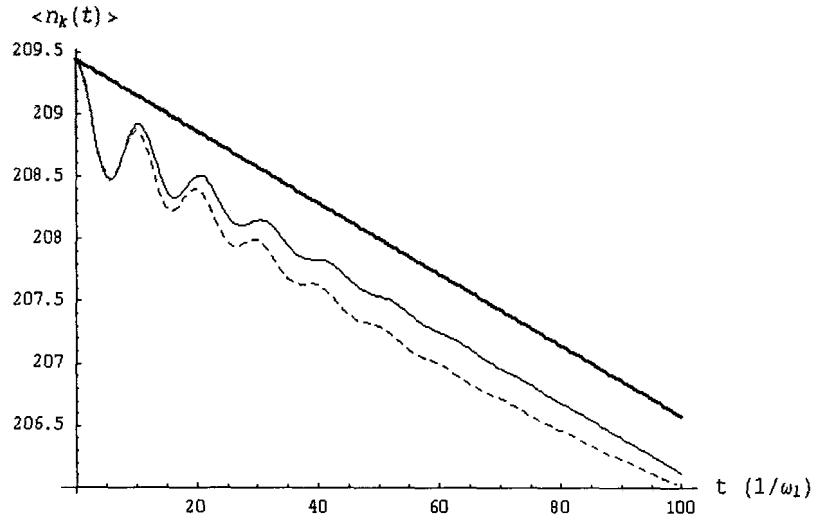

Figure 6. The time evolution of $\langle n_k(t) \rangle$. We start with a plane wave of the field with $k_0 = 1.5$. The dotted line is the numerical result, while the thin line is theoretical prediction including the non-Markovian contribution. The straight line is the Markovian approximation.

Acknowledgements

We would like to thank Professor I. Prigogine for his interest in this problem and stimulating discussion, as well as his constant support. We also like to thank Dr. V. Barsegov, Dr. G. Ordonez, and Dr. E. Karpov for useful comments. We acknowledge the Engineering Research Program of the Office of Basic Energy Sciences at the U.S. Department of Energy, Grant No DE-FG03-94ER14465, the Robert A. Welch Foundation Grant F-0365, the European Commission Project HPHA-CT-2001-40002, the National Lottery of Belgium and the Communautè Française de Belgique for support in this work.

References

1. W. G. Unruh and W. H. Zurek, Phys. Rev. D **40**, 1071 (1989).
2. D. Giulini *et al*, *Decoherence and the Appearance of a Classical World in Quantum Theory* (Springer-Verlag, New York, 1996).
3. A. O. Caldeira and A. J. Leggett, Physica A **121**, 587 (1983).
4. B. L. Hu, J. P. Paz, and Y. Zhang, Phys. Rev. D **45**, 2843 (1992).
5. B. L. Hu, J. P. Paz, and Y. Zhang, Phys. Rev. D **47**, 1576 (1993).
6. T. Petrosky and I. Prigogine, Chaos, Soliton and Fractals **7**, 441 (1996).
7. T. Petrosky and I. Prigogine, Adv. Chem. Phys. **99**, 1 (1997).

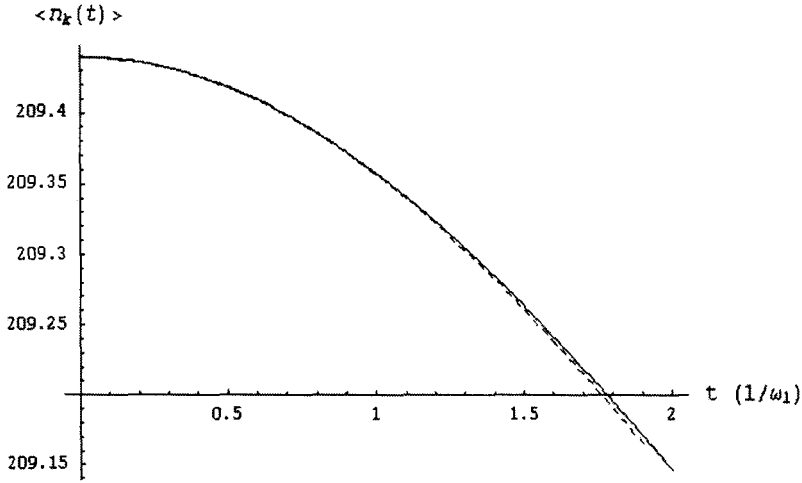

Figure 7. The Quantum Zeno effect in the time evolution of the particle. This is a magnification of an early state of the time evolution of the field in Figure 6. The dotted line is the numerical result, while the thin line is theoretical prediction including the non-Markovian contribution.

8. T. Petrosky and I. Prigogine, Physica A **147**, 461 (1988).
9. T. Petrosky and C. O. Ting, in preparation.
10. C. C. Tannoudji *et al*, *Atom-Photon Interactions* (John Wiley & Sons, 1998).
11. T. Petrosky and V. Barsegov, Phys. Rev. E **65**, 046102 (2002).
12. T. Petrosky and V. Barsegov, *in Advansed Studies in Astrophysics and Cosmology: The Chaotic Universe*, edited by V. Gurzadyan and R. Ruffini (World Scientific, Singapore, 1999).
13. E. C. G. Sudarshan, *Relativistic Particle Interactions*, Lecture Notes at University of Rochester (1962): See the subject on the Friedrichs model. In this article, the author did not present the model in the second quantization formalism. However, the extension to the second quantization formalism is straightforward.
14. I. Prigogine, *Non-Equilibrium Statistical Mechanics* (Wiley, New York, 1962).
15. P. Facchi and S. Pascazio, Physica A **271**, 133 (1999).
16. C. Compgano, R. Passante, and F. Persico, *Atom-Field Interactions and Dressed Atoms* (Cambridge University Press, 1995).
17. E. C. G. Sudarshan and B. Misra, J. Math. Phys. **18**, 756 (1977).

DISCUSSION

Chairman: L. Stodolsky

E.C.G. Sudarshan: I have two small questions. You choose exactly the same equilibrium solution for $-\epsilon$ and $+\epsilon$. So I would like you to tell me if you have chosen ii or if it was forced by the equation.

T. Petrosky: In order to obtain a well-separated expression for the Markov processes from the non-Markov processes (or memory effects), the initial condition forces us to choose a sign of ϵ. An advantage of the complex spectral representation of the Liouvillian is that this allows us to isolate contributions associated to Markov processes from the remaining contributions associated to non-Markov processes. Indeed, the Markov processes come from pole contributions, while the non-Markov processes come from the so-called background integral. For a given initial condition with a fixed direction of time (say $t > 0$), this decomposition is possible by choosing a suitable sign of ϵ. However, since both branches of the analytic continuation lead to complete sets of eigenstates of the Liouvillian, the evolution of the system does not depend on our choice of the sign of ϵ. In other words, we may use the opposite sign of ϵ to analyze the evolution of the system, if we wish. But if we would do that, we would obtain a theoretical expression of the evolution where the Markov processes and non-Markov processes are all mixed up, hence we lose the advantage of the complex spectral representation.

E.C.G. Sudarshan: What can you say in favor of the Bogoliubov transformation? It is well known that even for the free field, if you did canonical transformation of the field, almost all time there are non-equivalent representations. That does not mean that you cannot write down wave functions in that representation, but you cannot write down the wave functions in the original representation. Thus if you say that the wave function is not there, you mean that the wave function in the original variables is not there.

T. Petrosky: I think this indicates more than the non-equivalent representations. The divergence I have pointed out comes from a product of a bra-sate and a ket-state in the transformed states. This corresponds to a resonance interference between these bra and ket states. In the Pauli master equation this interference effect leads to secular terms with integer power of t and a delta function on energies that describes energy conservation in a collision process. Since there is no square root of delta function, the secular effects in the Pauli master equation destroy factorizability of the density matrix into a product of wave functions. As I have shown, contributions from the correlation subspace that give a correction to the Pauli master equation do not suppress these secular effects. Hence, the observation of the secular effects may indicate the destruction of the wave function.

TIME ASYMMETRIC QUANTUM THEORY. FOUNDATIONS AND APPLICATIONS

A. BOHM[1], M. GADELLA[2], M.J. MITHAIWALA[1].

[1] *Physics Department, The University of Texas at Austin, Austin, TX 78712, USA.*
[2] *Departamento de Física Teórica, Facultad de Ciencias, E-47011 Valladolid, Spain.*

It is shown that a slight modification of one axiom of Quantum Mechanics eliminates the conflicts between the standard mathematical theory and the phenomenological description of resonance scattering and decay. In addition, this modification leads to a quantum theory that incorporates time asymmetry in the quantum mechanical time evolution.

1 Introduction

In this presentation we want to give a brief description of the foundations of time asymmetric quantum theory (TAQT) and a summary of results which have also been applied or discussed in papers presented at this session [30] and other sessions [31,37] of this Conference.

The fundamental assumptions (or axioms) of TAQT are a slight modification of the standard axioms of Quantum Mechanics [29], basically of only one axiom. The resulting consequences are i.) a consistent theory of scattering and decay without the usual conflicts between phenomenological description (Weisskopf-Wigner approximation [38]) and mathematical methods [23,22,29,36] and ii.) the incorporation of time asymmetry in the quantum mechanical time evolution [18] of which the irreversibility of the (undisturbed or unobserved) decay of a resonance is a special case.

2 The fundamental assumptions of Quantum Mechanics

Most of discussions on the foundations of quantum theory start with two notions [25]:

A1.- States: described by a density operator ρ, W, or by a state vector ϕ for pure states, $W = |\phi\rangle\langle\phi|$.

A2.- Observables: described by self adjoint operators A $(= A^\dagger)$, Λ, or by vectors ψ if $\Lambda = |\psi\rangle\langle\psi|$.

All, ρ, W, A and Λ are defined as operators on some complex infinite dimensional vector spaces endowed with a scalar product and φ, ψ are elements of these vector spaces.

The quantity to be compared with experimental data is $\mathcal{P}_W(\Lambda(t))$, the probability to measure the observable Λ in state W at a time t. This probability is measured as a ratio of large numbers of detector counts, the relative frequencies $N(t)/N$. It is calculated in quantum theory as the Born probability. In the Heisenberg picture, it is calculated as:

$$\mathcal{P}_W(\Lambda(t)) \equiv \mathrm{Tr}[\Lambda(t)W_0] = |\langle\psi^-(t)|\phi^+\rangle|^2\,, \tag{1}$$

and in the Schrödinger picture it is calculated as:

$$\mathcal{P}_W(\Lambda(t)) = \mathrm{Tr}[\Lambda_0 W(t)] = |\langle\psi^-|\phi^+(t)\rangle|^2\,, \tag{2}$$

where "Tr" stands for trace. The last equalities hold for the special cases $W = |\phi^+\rangle\langle\phi^+|$ and $\Lambda = |\psi^-\rangle\langle\psi^-|$.

The comparison between theory and experiment is given by

$$\mathcal{P}_W(\Lambda(t)) \approx \frac{N(t)}{N} \tag{3}$$

The *almost equal* sign $\approx$ is to emphasize that the theoretical quantity in the left hand side of (3) is a continuous function of time, whereas the right hand side changes in discrete steps with time.

An axiom common to all formulations of Quantum Mechanics is that the dynamics is given by the dynamical differential equations, either in the Heisenberg picture by

$$i\hbar\frac{\partial}{\partial t}\psi^-(t) = -H\,\psi^-(t) \tag{4}$$

or in the Schrödinger picture by

$$i\hbar\frac{\partial}{\partial t}\phi^+(t) = H\,\phi^+(t)\,. \tag{5}$$

This means that one either uses the solutions of the Heisenberg equation (4) for the observables in (1) or one uses the solutions of the Schrödinger equation (5) for states in (2) to calculate the probabilities $\mathcal{P}_W(\Lambda(t))$ of (3)[a].

In addition to these basic assumptions (A1,A2) and (4,5), one uses rules for calculating the trace and the scalar product in (1,2). These rules are derived from a basis vector decomposition,

$$\phi = \sum_i |i\rangle\langle i|\phi\rangle \tag{8}$$

where $|i\rangle$ is a discrete set of eigenvectors of a prominent observable A:

$$A\,|i\rangle = a_i\,|i\rangle \tag{9}$$

or a continuous Dirac basis vector decomposition

$$\phi = \int d\lambda\,|\lambda\rangle\langle\lambda|\phi\rangle\,, \tag{10}$$

[a] For the more general observables Λ in the more general state W the Heisenberg equation of motion is

$$\frac{\partial\Lambda(t)}{\partial t} = -\frac{i}{\hbar}\,[H, \Lambda(t)]\,, \tag{6}$$

and the Schrödinger equation is

$$\frac{\partial W(t)}{\partial t} = \frac{i}{\hbar}\,[H, W(t)]\,, \tag{7}$$

and (4) and (5) is the special case $\Lambda = |\psi^-\rangle\langle\psi^-|$ and $W = |\phi^+\rangle\langle\phi^+|$, respectively.

where $|\lambda\rangle$ is a continuous set of eigenvectors,

$$A\,|\lambda\rangle = \lambda\,|\lambda\rangle\,. \tag{11}$$

Often one chooses for A in (9) and (11) the energy operator (Hamiltonian) of the system (or a complete system of commuting observables, $A \equiv \{H, B_1, B_2, \ldots, B_n\}$, e.g., $A \equiv \{H, \mathbf{J}^2, J_3\}$, where $\mathbf{J}$ is the total angular momentum and J_3 one of its components, so that $\lambda = (E, j, j_3)$ and $\int d\lambda = \sum_{j,j_3} \int dE$), so that (9) and (11) are the energy eigenvalue equations

$$H\,|i\rangle = E_i\,|i\rangle \quad \text{and} \quad H\,|E\rangle = E\,|E\rangle\,, \tag{11a}$$

respectively. The eigenvalue equations (9) and (11) are solved under some boundary conditions which specifies the space of allowed solutions. These boundary conditions are related to the boundary conditions of the dynamical equations (1,2).

Then, trace and scalar product in (1,2) are then calculated using (8) and (10) as

$$\mathrm{Tr}(\Lambda W) = \sum_i^{\infty} \langle i|\Lambda W|i\rangle \quad \text{or} \quad \mathrm{Tr}(\Lambda W) = \int d\lambda\, \langle\lambda|\Lambda W|\lambda\rangle \tag{12}$$

and

$$|\langle\psi|\phi\rangle|^2 = \left|\sum_{i=1}^{\infty} \langle\psi|i\rangle\langle i|\phi\rangle\right|^2 \quad \text{or} \quad |\langle\psi|\phi\rangle|^2 = \left|\int d\lambda\, \langle\psi|\lambda\rangle\langle\lambda|\phi\rangle\right|^2, \tag{13}$$

where obviously equations in the left hand side of (12) and (13) stand for the discrete case, whereas equations in the right hand side of (12) and (13) stand for the continuous case. In practical calculations, convergence of infinite sums and the meaning of integration (Lebesgue or Riemann) are usually not considered and the infinite sums and the integrals over infinite range are truncated to a finite range and restricted to continuous functions.

The basis vector decomposition formulas (8,9) and (10,11) can be proven under various mathematical assumptions, which are connected with the choice of the boundary conditions for (4,5) and (9,11). However, since the calculational rules (8,9) and (10,11) are of great practical importance, the boundary conditions, i.e., the choice of the space of solutions of (4,5) and (9, 11) must allow a proof of (8,9).

The boundary conditions, i.e., the conditions that select the set of allowed solutions of the dynamical differential equations (4,5) and of the eigenvalue (differential) equations (11), can be chosen in different ways.

In standard (von Neumann's) Quantum Mechanics, this is done by the Hilbert space axiom that says the following:

Axiom.- *The set of states* $\{\phi^+\}$ *is equal to the set of observables* $\{\psi^-\}$ *and both are equal to the whole Hilbert space* $\mathcal{H}$.

$$\{\phi^+\} \equiv \{\psi^-\} \equiv \mathcal{H} \tag{14}$$

From this axiom (14), it follows by the Stone-von Neumann theorem [36,29,1], that all solutions of the Heisenberg equations for the observable vector (4) are given by

$$\psi^-(t) = e^{itH}\,\psi^-(0)\,, \qquad -\infty < t < \infty \tag{15}$$

and in terms of the operator $|\psi^-(t)\rangle\langle\psi^-(t)|$ by

$$|\psi^-(t)\rangle\langle\psi^-(t)| = e^{itH}|\psi^-(0)\rangle\langle\psi^-(0)|e^{-itH}\,, \qquad -\infty < t < \infty\,. \tag{16}$$

For the solution $\phi^+(t)$ of the Schrödinger equation, it follows again by the Stone von-Neumann theorem [1,29,36]:

$$\phi^+(t) = e^{-itH}\,\phi^+(0)\,, \qquad -\infty < t < \infty \tag{17}$$

and for the operator[b] $|\phi^+(t)\rangle\langle\phi^+(t)|$:

$$|\phi^+(t)\rangle\langle\phi^+(t)| = e^{-itH}|\phi^+(0)\rangle\langle\phi^+(0)|e^{itH}\,, \qquad -\infty < t < \infty\,. \tag{20}$$

This is the unitary time evolution of standard Quantum Mechanics given by the unitary group. It is a mathematical consequence of the axiom (14) which predicts time symmetric dynamical evolution.

From (15) or (17) follows [22] that the probability to detect the observable $|\psi^-(t)\rangle\langle\psi^-(t)|$ in a state ϕ^+,

$$\begin{aligned}\mathcal{P}_{\phi^+}(|\psi^-(t)\rangle\langle\psi^-(t)|) &= |\langle\psi^-(t)|\phi^+\rangle|^2 = |\langle e^{itH}\psi^-|\phi^+\rangle|^2 \\ &= |\langle\psi^-|e^{-itH}\phi^+\rangle|^2 = |\langle\psi^-|\phi^+(t)\rangle|^2\,,\end{aligned} \tag{21}$$

is mathematically predicted to exist for all values of time, $-\infty < t < \infty$ and it is either different from zero for (almost) all values of t, or it is identically zero for all t. If it is identically zero at all t, for all observables $|\psi^-\rangle\langle\psi^-|$ and all states ϕ^+, then there are no transition probabilities and no decays. If it is different from zero for all $-\infty < t < \infty$, then there cannot be a state that has been prepared by a finite time $t_0 > -\infty$ and which decays after this time t_0. This is in conflict with causality supported by physical observations, according to which a state ϕ^+ has to be prepared first by the time $t = t_0$ *before* an observable $|\psi^-\rangle\langle\psi^-|$ can be measured. Thus the probabilities (21) can, for physical reasons (and causality), be different from zero only for times $t > t_0$. This must be so, independently of whether an apparatus is present to detect the observable or not [32].

Therefore, the solutions of the dynamical equations (4) and (5) must be such that (21) is *not* predicted, or at least *not predicted to be different from zero*, for $t \leq t_0$ where t_0 is an arbitrary finite time ($t_0 \geq -\infty$), which can then be called $t = 0$. It means that, in place of the unitary group solutions (15) and (17), one needs solutions for which the time t extends only over $0 \leq t < \infty$.

Although the solutions of the dynamical equations (4) (and (5)) are given by (15) and (17) for $-\infty < t < \infty$ as a consequence of the Axiom (14), one could

[b]For the general case of an observable Λ and a state W described by Hilbert space operators the solutions of the dynamical equations (6) and (7) are given by

$$\Lambda(t) = e^{itH}\Lambda(0)\,e^{-itH}\,, \qquad -\infty < t < \infty \tag{18}$$

and

$$W(t) = e^{-itH}W(0)\,e^{itH}\,, \qquad -\infty < t < \infty\,. \tag{19}$$

proclaim that (15) and (16) should be used for the time $t \geq 0$ as done e.g. in [18], but that is in conflict with Axiom (14). The right way is to modify the Axioms of Quantum Mechanics such that only solutions of (4), (5) with $0 \leq t < \infty$ result as the consequence of the new Axiom. Since the Axiom (14) has several troubling mathematical consequences [22,23] for a theory of resonance scattering and decay and since the heuristic description of these processes [21], in any case, makes use of notions that lie outside the frame set by the Hilbert space, like Dirac kets that fulfill Lippmann-Schwinger equations [3,16], we shall formulate below a new hypothesis that modifies the Hilbert space Axiom (14).

3 The fundamental hypothesis of time asymmetric Quantum Mechanics

In order to obtain time asymmetric solutions of the dynamical equations (4) and (5)− also of (6) and (7)− we change the boundary conditions. This means that we modify the Hilbert space Axiom (14) and leave all the other fundamental assumptions of Quantum Mechanics intact.

In Hilbert space quantum theory, one speaks of observables and one speaks of states, but Axiom (14) does not distinguish between observables and states in the mathematical theory. The set of prepared states $\{\phi^+\}$ and the set of detected observables $\{\psi^-\}$ are mathematically represented by the vectors in the same Hilbert space (or the same dense subspace $\mathbf{\Phi} \subset \mathcal{H}$ of the Hilbert space). We shall replace the Hilbert space Axiom (14) by a new hypothesis which also distinguishes mathematically between states and observables. This new hypothesis states:

The set of prepared states or in-states, defined by the preparation apparatus (e.g. accelerator), is described mathematically by

$$\{\phi^+\} \equiv \mathbf{\Phi}_- \subset \mathcal{H} \subset \mathbf{\Phi}_-^\times . \tag{22}$$

The set of observables, defined by the registration apparatus (e.g. detector), is described mathematically by

$$\{\psi^-\} \equiv \mathbf{\Phi}_+ \subset \mathcal{H} \subset \mathbf{\Phi}_+^\times . \tag{23}$$

The two triplets of spaces (22) and (23) form two different Rigged Hilbert Spaces [17], and the observables, state operators and transformations are represented in $\mathbf{\Phi}_\pm$ by continuous operators with respect to the topology on the space $\mathbf{\Phi}_\pm$[c]. The spaces of test vectors $\mathbf{\Phi}_\pm$ are realized by spaces of Hardy functions which can be analytically continued to the upper (for $\mathbf{\Phi}_+$) or lower (for $\mathbf{\Phi}_-$) complex energy plane [5,8].

The space of Hardy class functions[d] on the upper (lower) half plane is denoted by

[c]They cannot be continuous operators with respect to the Hilbert space topology because their commutation relations (e.g. $[Q, P] = iI$) cannot be represented by continuous operators on Hilbert space. But there exists no counterexample of observables represented by continuous operators in suitable constructed nuclear topological spaces $\mathbf{\Phi}$. Therefore, Dirac's hypothesis of an algebra of observables defined in whole space can be fulfilled with an algebra of continuous operators defined on the whole space $\mathbf{\Phi}$.

[d]A complex analytic function $f(z)$, $z = E + i\alpha$, $\alpha > 0$, defined on the upper half complex plane

$\mathcal{H}_+^2$ ($\mathcal{H}_-^2$). A Hardy function, $f(E)$, in $\mathcal{H}_+^2$ or in $\mathcal{H}_-^2$ is called *smooth* if, as a function on the real axis, it is infinitely differentiable and fast decreasing[e]. Therefore, smooth Hardy functions are the intersections of the Hardy spaces $\mathcal{H}_\pm^2$ with the Schwartz space S: $S \cap \mathcal{H}_\pm^2$.

The spaces $\mathbf{\Phi}_\pm$ are realized as follows: $\phi^+ \in \mathbf{\Phi}_-$ if and only if its wave function in the energy representation, $\phi^+(E) = \langle E^+|\phi^+\rangle$ (i.e., the expansion coefficients $\langle\lambda|\phi^+\rangle$ in (10)), is the restriction to the positive semiaxis $\mathbb{R}^+$ of a function in $S \cap \mathcal{H}_-^2$:

$$\phi^+(E) = \langle E^+|\phi^+\rangle \in S \cap \mathcal{H}_-^2\big|_{\mathbb{R}^+}\,. \tag{24}$$

Analogously, $\psi^- \in \mathbf{\Phi}_+$ if and only if

$$\psi^-(E) = \langle E^-|\psi^-\rangle \in S \cap \mathcal{H}_+^2\big|_{\mathbb{R}^+}\,. \tag{25}$$

This means that the spaces $\mathbf{\Phi}_\pm$ are realized by the spaces $S \cap \mathcal{H}_\mp^2\big|_{\mathbb{R}^+}$ respectively[f].

The new hypothesis (22,23) may look much more complicated than the Axiom (14), but it is really not much different.

The first part of (22), i.e., $\{\phi^+\} \equiv \mathbf{\Phi}_- \subset \mathcal{H}$ says that the space of apparatus prepared states is not the whole Hilbert space, but only a dense subspace thereof. The second part, $\mathcal{H} \subset \mathbf{\Phi}_-^\times$, says that there is in addition to the Hilbert space $\mathcal{H}$, the space of continuous antilinear functionals $\mathbf{\Phi}_-^\times$ over the space $\mathbf{\Phi}_-$. A similar statement holds for the spaces of observables (23).

To use a Rigged Hilbert Space in order to define Dirac kets $|\lambda\rangle$ (generalized eigenvectors of a self adjoint operator that belong to the absolutely continuous spectrum) is really nothing new. It is needed to justify mathematically the Dirac basis of vector decompositions (10) and is implicit in the Dirac bra and ket formalism of Quantum Mechanics.

However, the Dirac kets are usually defined (or presumed) to be functionals $|\lambda\rangle \in \mathbf{\Phi}^\times$, where

$$\mathbf{\Phi} \subset \mathcal{H} \subset \mathbf{\Phi}^\times \tag{26}$$

---

is a Hardy function if

$$\sup_{\alpha>0} \int_{-\infty}^{\infty} |f(E+i\alpha)|^2\, dE < K < \infty\,.$$

Boundary values of a Hardy function on the real positive semiaxis determine all the values of the function on the whole half plane. Therefore, we can identify the function with the function given by its boundary values $f(E)$. In addition, this function of the boundary values is square integrable, so that $\mathcal{H}_+^2 \subset L^2(\mathbb{R})$. Similar definitions and properties hold for Hardy functions on the lower half plane [12].

[e]This means that $f(E)$ has the following property

$$\lim_{E\mapsto\pm\infty} \left[E^n \frac{d^m f(E)}{dE^m}\right] = 0\,, \qquad n, m = 0, 1, 2, \ldots$$

Infinitely differentiable functions with this property form a vector space called the *Schwartz space*, here represented as S.

[f]Each function $f_\pm(E)$ in $S \cap \mathcal{H}_\pm^2\big|_{\mathbb{R}^+}$ determines one and only one function $F_\pm(E)$ in $S \cap \mathcal{H}_\pm^2$. Both are identical on the positive semiaxis, i.e., $F_\pm(E) = f_\pm(E)$ for all $E \in \mathbb{R}^+ \equiv [0, \infty)$. Thus, each function $f_\pm(E) \in S \cap \mathcal{H}_\pm^2\big|_{\mathbb{R}^+}$ can be uniquely extended to the function $F_\pm(E) \in S \cap \mathcal{H}_\pm^2$. This permits somehow identify the spaces $S \cap \mathcal{H}_\pm^2\big|_{\mathbb{R}^+}$ and $S \cap \mathcal{H}_\pm^2$.

is a rigged Hilbert space of Schwartz type, i.e., $\mathbf{\Phi}$ is either unitarily equivalent to the Schwartz space S or to a closed subspace of S^g dense in the Hilbert space of wave functions.

In general the space $\mathbf{\Phi}$ is realized by the space of smooth functions, which means that the energy wave functions $\phi(E) := \langle E|\phi\rangle$, in the Dirac basis vector expansion (10), are smooth rapidly decreasing functions:

$$\phi = \int_0^\infty dE\, |E\rangle\langle E|\phi\rangle \tag{27}$$

Often one uses the Axiom (14) in the form

$$\{\phi^+\} \equiv \{\psi^-\} \equiv \mathbf{\Phi} \subset \mathcal{H}\,, \tag{28}$$

which means that one restricts oneself to smooth energy wave functions $\phi^+(E) := \langle {}^+E|\phi^+\rangle$ and $\psi^-(E) = \langle E^-|\psi^-\rangle$ for states as well as for observables rather than using Lebesgue square integrable functions for both states and observables $\{\phi^+\} \equiv \{\psi^-\} \equiv \mathcal{H}$.

The new hypothesis (22,23) states that the set of wave functions, $\psi^-(E)$, of an observable $|\psi^-\rangle\langle\psi^-|$, is different from the set of wave functions, $\phi^+(E)$, for a state $|\phi^+\rangle\langle\phi^+|$[h]. Namely, for the observables, the set of wave functions is made of these smooth functions that can be analytically continued to the upper half plane. For states, the set of wave functions is made of these smooth functions that can be analytically continued to the lower half plane.

However, the new hypothesis (22, 23) is physically indistinguishable from Axiom (14) or (28).

The statement that the state $\phi^+ \in \mathbf{\Phi}_-$ means that the energy distribution of the accelerator beam is described by a smooth rapidly decreasing function, $|\phi^+(E)|^2$, where $\phi^+(E)$ can be analytically continued to the lower half complex energy plane.

The statement that the state $\psi^- \in \mathbf{\Phi}_+$ means that the energy resolution of the detector is described by a smooth rapidly decreasing function, $|\psi^-(E)|^2$, where $\psi^-(E)$ can be analytically continued to the upper half complex energy plane.

In contrast, (14) and (28) means that $\phi^+(E)$ and $\psi^-(E)$ are Lebesgue square integrable functions which in general cannot be analytically continued into the complex energy plane (see Appendix).

Thus, hypothesis (22,23) only differs from the Hilbert space Axiom (14) in that:

For **states** the wave function $\phi^+(E)$, describing the accelerator (preparation apparatus), can also be analytically continued to the lower half plane.

For **observables** the wave function $\psi^-(E)$, describing the detector (registration apparatus), can also be analytically continued to the upper half plane.

[g]This means that there exists a unitary operator U from $\mathcal{H}$ onto $L^2(\mathbb{R})$ (or $L^2(\mathbb{R}^n)$),

$$U : \mathcal{H} \longmapsto L^2(\mathbb{R})\,,$$

such that either the image of $\mathbf{\Phi}$ by U, $U(\mathbf{\Phi})$, is either the Schwartz space S or a closed subspace of S dense in $L^2(\mathbb{R})$.

[h]A more general state W^+ is given by $W^+ = \sum_n w_n\, |\phi_n^+\rangle\langle\phi_n^+|$, where $\phi_n^+ \in \mathbf{\Phi}_-$.

In Hilbert space Quantum Mechanics, every square integrable ($L^2(\mathbb{R}^+)$) function $f(E)$ can represent both a state and an observable. Not all functions $f(E)$ can be analytically continued to a half plane.

It is hard to imagine that a detector (or registration apparatus) can discriminate between the set of functions $\psi^-(E) \in S \cap \mathcal{H}^2_+\big|_{\mathbb{R}^+}$, which can be analytically continued to complex energies and the set of functions, $\psi(E) \in S\big|_{\mathbb{R}^+}$, which cannot be analytically continued to complex energies[i]. The same holds for the wave functions $\phi^+(E)$ that describe the accelerator.

In other words, the difference between Axiom (14) and the hypothesis (22,23) cannot be observed directly, but they are mathematically profound and they will lead to consequences which are physically significant. Some of these consequences will be discussed in the following section.

4 Consequences of the Hardy Space hypothesis

We suggest to consider a quantum theory which is based on the same fundamental assumptions and uses the same calculation rules as standard quantum mechanics, except that the general boundary condition (14) (the Hilbert space axiom of quantum mechanics or its modification (28) to include Dirac kets) is replaced by the new pair of general boundary conditions, (22) for states and (23) for observables.

All other axioms of quantum mechanics remain the same or are extended in a natural way to the new kets $|F^\pm\rangle \in \mathbf{\Phi}^\times_\mp$. For example, in addition to the $\mathcal{H}$-space functional

$$\psi^-(t) \longmapsto (\psi^-(t), \phi)\,, \qquad \phi \in \mathcal{H} \tag{29}$$

(where the brackets $(\cdot,\cdot)$ denote the scalar product on $\mathcal{H}$ and which is a function of all $\psi^- \in \mathcal{H}$), we also considers the $\mathbf{\Phi}_+$-space functional

$$\psi^-(t) \longmapsto \langle \psi^-(t)|F^-\rangle = F^-(\psi^-(t)) \tag{30}$$

(where the brackets $\langle\cdot,\cdot\rangle$ stands for the action of the functional $|F^-\rangle$ on the observable $\psi^-(t)$ and which is a function of all $\psi^- \in \mathbf{\Phi}_+$). In analogy to (1), one also interprets (30) as a probability amplitude. For instance for $F^- = |E^-\rangle$, where the $|E^-\rangle \in \mathbf{\Phi}^\times_+$ are solutions of the eigenvalue equation $H|E^-\rangle = E|E^-\rangle$, $E \in \mathbb{R}^+$, it is standard to interpret the $|\langle\psi^-|E^-\rangle|^2$ as the probability density for the energy E.

4.1 Time asymmetry

For the Hardy spaces one also has a general theorem, the Paley-Wiener theorem [12] that determines, like the Stone-von Neumann theorem of the Hilbert space the *general solution of the dynamical equations.* As a mathematical consequence of

[i]The continuation of $\psi^-(E) \in S \cap \mathcal{H}^2_+\big|_{\mathbb{R}^+}$ to the negative semiaxis is unique, whereas the continuation of a smooth rapidly decreasing function on $\mathbb{R}^+$ to the negative semiaxis as a Schwartz function can be done in infinite manners.

(22,23), one obtains for the solutions of the equations (4,5) semigroup solutions. These semigroup solutions are of two kinds:

1.- Solutions of the Heisenberg equation (4): For observables $\psi^- \in \mathbf{\Phi}_+$ one obtains

$$\psi^-(t) = \mathcal{U}(t)\psi^- = e^{itH}\psi^-, \qquad 0 \leq t < \infty \tag{31}$$

2.- Solutions of the Schrödinger equation (5): For states $\phi^+ \in \mathbf{\Phi}_-$, one obtains[j]

$$\phi^+(t) = e^{-itH}\phi^+, \qquad 0 \leq t < \infty \tag{32}$$

Thus, in place of the unitary group solution (15,17) of the dynamical equation (4,5) one obtains from the new hypothesis (22,23) the semigroup solution (31,32) of the same dynamical differential equation[k]. Therefore, one predicts for the probability of the observable $|\psi^-(t)\rangle\langle\psi^-(t)|$ in the state ϕ^+, using the Heisenberg picture:

$$\mathcal{P}(t) = |(\psi^-(t), \phi^+)|^2 = |(e^{iH_+t}\psi^-, \phi^+)|^2, \qquad \text{for } t \geq 0 \text{ only.} \tag{33}$$

Similarly, using the Schrödinger picture one predicts for the probability of the observable $|\psi^-\rangle\langle\psi^-|$ in the state $\phi^+(t)$[l]:

$$\mathcal{P}(t) = |(\psi^-, \phi^+(t))|^2 = |(\psi^-, e^{-iHt}\,\phi^+)|^2 = |\langle(e^{-iH_-t})^\times\psi^-|\phi^+\rangle|^2$$

$$= |\langle e^{iH_-^\times t}\psi^-|\phi^+\rangle|^2 = |(e^{iH_+t}\,\psi^-, \phi^+)|^2, \text{ for } t \geq 0 \text{ only} \tag{34}$$

where the above equalities follow because each $\psi^- \in \mathbf{\Phi}_+$ is also a functional $\psi^- \in \mathbf{\Phi}_-^\times$. Thus, the probabilities are the same, independently whether they are calculated in the Heisenberg or in the Schrödinger picture and they are calculable (or defined) for $t \geq 0$ only.

The time asymmetry $t \geq 0$ of (33) is the same time asymmetry $0 \leq t < \infty$ that we mentioned and whose heuristic meaning we discussed in section 2. Here this time asymmetry has been derived as a mathematical consequence of the new hypothesis (22,23). Thus, the empirical statement that the probability for an observable $\psi^-(t)$ in a state ϕ^+ makes sense only for times $t > t_0 = 0$ is a consequence of the new hypothesis (22,23).

[j] Precisely, the semigroup generator $H = (H_+)$ in (31) is the restriction of the self adjoint operator H to the (dense in $\mathcal{H}$) subspace $\mathbf{\Phi}_+$ and the generator $H = (H_-)$ in (32) is the restriction of H to $\mathbf{\Phi}_-$.

[k] But with the initial data values of the Cauchy problem restricted to the new boundary condition $\psi^-(0) = \psi^- \in \mathbf{\Phi}_+$.

[l] In order to make (35) precise, we have to be more accurate in our notation and use the notation of footnote (11). The semigroup $(e^{-itH_-})^\times$ acts on $\mathbf{\Phi}_-$ and has the generator $H_-^\times$. Analogously, the semigroup $(e^{-itH_+})^\times$ acts on $\mathbf{\Phi}_+$ and has the generator $H_+^\times$. In order to understand (34), we have to remark that $H_-^\times$ is not only an extension of H_-:

$$H_- \subset H = H^\dagger \subset H_-^\times,$$

but it is also an extension of H_+:

$$H_+ \subset H = H^\dagger \subset H_-^\times.$$

Whereas a group like (15,16) does not have a distinguished time since $-\infty < t < \infty$, the semigroups (31) and (32) introduce the time $t_0 = 0$. It is measured as the time t_0 at which the state has been prepared and at which the registration of an observable in this state can start. To clarify the meaning of this new notion, t_0, and to discuss whether it is a physically accessible quantity, we consider an example of quantum mechanical decay.

The observable in the decay of an excited quantum state is the projection operator on the space of out-states of the decay products $\Lambda^- = |\psi^-\rangle\langle\psi^-|$ (which we idealize here as a one dimensional projection operator on the vector $\psi^- \in \mathbf{\Phi}_+$). A detector, described by Λ^-, cannot register the decay products before the decaying state has been prepared.

Take as an example the decay

$$K_S^0 \longmapsto \pi^+ \pi^- . \tag{35}$$

We shall ignore here the K_L^0 and its CP violating $\pi^+\pi^-$ decay, this is discussed in terms of (52) below and does not affect our arguments here which deal just with the K_S^0. The decay products $\pi^+ \pi^-$ can be registered only after the decaying state K_S^0 has been prepared (this is independent of whether it has been prepared by the experimenter in a planned experiment or at random by cosmic rays) in e.g., the reaction pion π^- with proton p producing a K^0 and transforming the baryon state p into the baryon state Λ:

$$\pi^- p \longmapsto \Lambda K^0 \tag{36}$$

This means that the observable

$$|\psi^-(t)\rangle\langle\psi^-(t)| = e^{itH} |\pi^+ \pi^-\rangle\langle\pi^+ \pi^-| e^{-itH} \tag{37}$$

makes sense only for $t > t_0$, where t_0 is the time at which K_S^0 has been prepared. Since the neutral Kaon is created by the strong interaction, the time $t_0^{(i)}$ at which the i-th K^0 is produced at the proton target is very well defined within 10^{-23} seconds (the characteristic time of strong interaction). This i-th K_0 moves down the beam line for a time interval $t_{(i)} - t_0^{(i)}$ and decays at $t_{(i)}$ after it has moved a distance $d_{(i)} = \frac{\mathbf{T}}{m_K}(t_{(i)} - t_0^{(i)})$. Here $\mathbf{p}$ is the momentum of K^0, m_K its rest mass, $t_{(i)}$ is the time in the rest frame of the K^0 decay and $d_{(i)}$ is the distance in the laboratory frame from the proton target to the decay vertex of the i-th K^0. The distance $d_{(i)}$ of the decay vertex from the target position is measured by the detector and thus the lifetime for the i-th K_S^0 decay event $t_{(i)} - t_0^{(i)}$ can be calculated from $d_{(i)}$ and $\mathbf{p}$. It is of the order of 10^{-10} seconds. This time $t_0^{(i)}$, in the past of each individual $K_S^0 \longmapsto \pi^+ \pi^-$ event at $t_{(i)}$, is the mathematical time $t = 0$ for the state vector $\phi^+(t)$ describing the ensemble of individual K_S^0 that are created at different times $t_0^{(i)}$.

One counts the number of decay events (35) per time interval Δt (the counting rate) as a function of $d_{(i)}$, i.e., of a function of the travel time $t = t_{(i)} - t_0^{(i)} = \frac{m_k}{\mathbf{T}} d_{(i)}$ and obtains the exponential law $\frac{\Delta N(t)}{\Delta t} \approx e^{-Rt}$ from which one calculates the average travel time which is the average lifetime of the ensemble of K_S^0 that started traveling

at the proton target, τ = average $(t_{(i)} - t_0^{(i)}) = \frac{1}{R}$. This is the lifetime of the quantum mechanical K_S^0-state, whose state vector we denoted by ϕ^+. The K_S^0 state thus represents an ensemble of individual K_S^0 that are created in an experiment at quite arbitrary times $t_0^{(i)}$ and produce a decay vertex at the times $t_{(i)}$. All these times $t_0^{(i)}$, in the past of each individual $K_s^0 \longmapsto \pi^+ \pi^-$ event, are the initial time $t_0 = 0$ for the K^0 state, i.e., the time at which ϕ^+ has been created and after which one can count the decay products. This time t_0 of the K^0 state, i.e., the time $t = 0$ in the life of each individual K_S^0, is identified with the mathematical semigroup time $t = 0$. The vector ϕ^+ does not represent a bunch (wave packet) of K_S^0's moving down the beam line, but an ensemble of K^0 which are created at quite arbitrary times $t_0^{(i)}$ but have a well defined lifetime τ = average $(t_{(i)} - t_0^{(i)})$. In case of the K_S^0, the time t_0 at which the preparation of the state $\phi_{K^0}^+$ is completed and at which the registration can begin is experimentally very well defined (within 10^{-23} s.$\approx 10^{-13}\, \tau_{K_S^0}$). since K^0 in (36) is produced by the strong interaction with a time scale of 10^{-23} seconds and has a lifetime of the order of 10^{-10} seconds.

The existence of the time asymmetry in the decay process like (35) and others is independent of whether an experimentalist has set up an apparatus and whether the decay products, $\pi^+ \pi^-$ for (35) and others, have been registered or not. Quantum decay is a process for which it is impossible (or extremely improbable) to experimentally realize the time reversed quantum solution [26]. It has nothing to do with violation of time reversal invariance [7], which is the non-conservation of the time reversal transformation T (or of CP) by the total Hamiltonian H in the dynamical equations (4), (5), $[H, T] = 0$. It has also nothing to do with the apparatus affecting the quantum system and somehow collapsing or decohering its state [20]; that may be an effect which comes on top of this time asymmetry and may also contribute to irreversibility.

The time asymmetry that follows from the new hypothesis (22, 23) is a consequence of boundary conditions, not of the time reversal non-invariance in the dynamical equations (4, 5). The analogue in classical physics of our quantum mechanical time asymmetry is the radiation arrow of time (its quantum analogue is the radiative decay of an excited quantum state). This time asymmetry due to time asymmetric boundary conditions of a time symmetric differential equation, is also manifested in the big bang solution of the Einstein equations. And the realization in Nature of time asymmetric boundary conditions may well be attributable to the big bang [18]. Whatever its origin, time asymmetry is a law of this world and not a result of an experimentalist's manipulations [32].

4.2 Gamow vectors

Since the exponential law is very accurately fulfilled for the experimental counting rate in decay process as like (35), the probability rate, $\dot{\mathcal{P}}_{\phi^+}(t)$, calculated from (33) should also be exponential. That means that ϕ^+ should be an exponentially decaying state. Such a state cannot exist in the Hilbert Space[m] [13,15,23]. But we

[m] Because if such a normalizable state exists, then it must have a Lorentzian energy representation, which is in contradiction of the semibounded character of the Hamiltonian [13,15,23].

shall show now that the new hypothesis also provides a vector to represent an exponentially decaying state.

In addition to the apparatus prepared states $\phi^+ \in \mathbf{\Phi}_-$ with smooth wave function $\phi^+(E) = \langle {}^+E|\phi^+\rangle$, describing the energy distribution $|\phi^+(E)|^2$ of the accelerator beam and in addition to the detected observables $\psi^- \in \mathbf{\Phi}_+$ with smooth wave function $\psi^-(E) = \langle {}^-E|\psi^-\rangle$, describing the energy resolution of the detector, the RHS's (22,23) introduce new generalized vectors (functionals on the spaces $\mathbf{\Phi}_\pm$, $F^\mp \in \mathbf{\Phi}_\pm^\times$). Generally speaking in a RHS, $\mathbf{\Phi} \subset \mathcal{H} \subset \mathbf{\Phi}^\times$, the smaller the space $\mathbf{\Phi}$, the bigger the space $\mathbf{\Phi}^\times$. The spaces $\mathbf{\Phi}_\pm$ are restricted enough so that their (anti)duals, $\mathbf{\Phi}_\pm^\times$, contain not only the Dirac kets, but also more general kets.

For instance, they contain the scattering states (eigenvectors with eigenvalues in the continuous spectrum) $|E, j, \ldots^\mp\rangle \in \mathbf{\Phi}_\pm^\times$, with

$$H|E, j, \ldots^\mp\rangle = E|E, j, \ldots^\mp\rangle\,, \qquad 0 \le E < \infty\,, \tag{38}$$

which are the plane wave solutions of the Lippmann-Schwinger equations (where the sign + stands for incoming and the sign − for outgoing plane wave function). It is actually the pair of Lippmann-Schwinger equations of the heuristic description of scattering that suggests the need for the pair of the RHS's in the new hypothesis (22,23).

In addition to the eigenkets with real eigenvalues, the spaces $\mathbf{\Phi}_\pm^\times$ contain also eigenvectors with complex eigenvalues of the self-adjoint Hamiltonian H. For instance the vector ψ^G fulfilling[n]:

$$H\psi^G = (E_R - \frac{i\Gamma}{2})\psi^G \tag{39}$$

where $E_R - \frac{i\Gamma}{2}$ is the position of the resonance pole of the analytically continued S-matrix (or of the reduced resolvent of H) in the complex energy plane [3]. The vector $\psi^G = \sqrt{2\pi\Gamma}\,|E - i\Gamma/2, j, \ldots^-\rangle \in \mathbf{\Phi}_+^\times$ is called the Gamow vector of the resonance at $E - i\Gamma/2$. Here, $\sqrt{2\pi\Gamma}$ is an arbitrary "normalization" factor.

The state vectors $\phi^+ \in \mathbf{\Phi}_-$ are also elements of $\mathcal{H}$ and therefore of $\mathbf{\Phi}_+^\times$, according to (22,23). Therefore, it is natural to extend the interpretation of (33) also to all vectors $F^- \in \mathbf{\Phi}_+^\times$ and define the probability to measure an observable $|\psi^-(t)\rangle\langle\psi^-(t)|$ (or $\Lambda^-(t)$) in the generalized state $F^- \in \mathbf{\Phi}_+^\times$ as

$$\mathcal{P}_{F^-}(t) = |\langle\psi(t)|F^-\rangle|^2 = |\langle\psi^-|F^-(t)\rangle|^2\,. \tag{40}$$

[n] If the operator A has the property that $A\mathbf{\Phi} \subset \mathbf{\Phi}$, then $A^\dagger$ admits a unique extension to $\mathbf{\Phi}^\times$ called the conjugate operator $A^\times$. It is defined by the duality formula:

$$\langle A\varphi|F\rangle = \langle\varphi|A^\times F\rangle\,, \qquad \forall\varphi \in \mathbf{\Phi},\ F \in \mathbf{\Phi}^\dagger\,.$$

For a self adjoint $H = H^\dagger$ Dirac used the notation $H|E\rangle = |E\rangle$ in (38), whereas precisely one should write (38) as

$$H_\pm^\times\,|E, j, \ldots^\mp\rangle = E\,|E, j, \ldots^\mp\rangle\,, \quad |E, j, \ldots^\mp\rangle \in \mathbf{\Phi}_\pm^\times\,, \tag{38a}$$

and (39) as

$$H_+^\times\,\psi^G = \left(E_R - \frac{i\Gamma}{2}\right)\psi^G\,, \tag{39a}$$

where $H_\pm^\times$ are the conjugate of the operators $H_\pm$ and the $H_\pm^\times$ are defined in $\mathbf{\Phi}_\pm^\times$ (see footnote (10)). If one specifies to which space the vectors belong upon which the operators $H_\pm$ and $H_\pm^\times$ act, then one can omit the subscripts and write just H as done in (38, 39) and by Dirac.

Because of the semigroup property of the time evolution (31) the probability (40) is defined for $t \geq t_0 = 0$ only. The time evolution of F^- is defined by

$$\langle e^{iHt}\,\psi^-|F^-\rangle = \langle \psi^-|U^\times(t)|F^-\rangle \equiv \langle \psi^-|F^-(t)\rangle\,, \tag{41}$$

for all $\psi^- \in \mathbf{\Phi}_+$, where $U^\times(t) = e^{-iH^\times t}$ is the uniquely defined extension of $U^\dagger(t) = e^{-iHt}$ to $\mathbf{\Phi}_+^\times$ and $H^\times$ is the semigroup generator. But $U^\times(t)$ is defined for $t \geq 0$ only. If we omit the arbitrary ψ^- in (41), this equation can also be written, as a functional equation in $\mathbf{\Phi}_+^\times$:

$$F^-(t) \equiv U^\times(t)\,F^- = e^{-iH^\times t}\,F^-\,, \tag{41a}$$

valid for $t \geq 0$ only because only for $t \geq 0$ is $\mathcal{U}(t) = e^{iHt}$ a continuous operator in $\mathbf{\Phi}_+$ fulfilling $\mathcal{U}(t)\mathbf{\Phi}_+ \subset \mathbf{\Phi}_+$.

Choosing for F^- the vector ψ^G, we obtain:

$$\psi^G(t) = (e^{-itH})^\times \psi^G = e^{-iE_R t}\,e^{-\frac{\Gamma}{2}t}\,\psi^G\,, \qquad t \geq 0\,. \tag{42}$$

And for the probability to detect the decay products $\psi^- \in \mathbf{\Phi}_+$ in the state $\psi^G(t)$, one obtains

$$\mathcal{P}_{\psi^G(t)} = |\langle \psi^-(t)|\psi^G\rangle|^2 = e^{-\Gamma t}\,|\langle \psi^-|\psi^G\rangle|^2\,, \qquad \text{for } t \geq 0 \text{ only.} \tag{43}$$

This is the exponential law. Thus, the Gamow vector associated to the resonance pole at $E_R - i\Gamma/2$ represents an exponentially decaying state with lifetime $\tau = 1/\Gamma$ [8]. The Gamow vector, specified by resonance energy E_R and width Γ (and possibly some additional quantum numbers like angular momentum) is the idealized state vector that describes the resonance = decaying state independently of its mode of production and preparation. These other aspects are contained in the complex basis vector expansion of a prepared state that we shall turn to next.

4.3 Complex basis vector expansion

Another important consequence of the hypothesis (22,23) is the complex basis vector expansion (also called complex spectrum resolution), which has been applied in the work presented at the same session [30]. Since the spaces in (22,23) are Rigged Hilbert Spaces [RHS] [5], the generalized eigenvectors $|E, j, \ldots^\pm\rangle$ form complete basis systems[o]. That means that the Nuclear Spectral Theorem holds for the in-states $\phi^+ \in \mathbf{\Phi}_-$ and for the out-states (observables) $\psi^- \in \mathbf{\Phi}_+$ in the form[p]:

$$\mathbf{\Phi}_+ \ni \psi^- = \sum_b \int_0^\infty dE\,|E, b^-\rangle\langle {}^-E, b|\psi^-\rangle \tag{44}$$

$$\mathbf{\Phi}_- \ni \phi^+ = \sum_b \int_0^\infty dE\,|E, b^+\rangle\langle {}^+E, b|\phi^-\rangle\,. \tag{45}$$

[o] We are assuming the absence of bound states, i.e., we restrict ourselves to the space of scattering states.

[p] The Lippmann-Schwinger equations related generalized eigenvalues of the "free" Hamiltonian H_0 to the generalized eigenvectors of the total Hamiltonian $H = H_0 + V$ with respective eigenvectors in the same continuous spectrum. A study of these Lippmann-Schwinger equations in the context of RHS is given in [3] and [16].

These expansions are identical with the standard Dirac basis vector expansion used in scattering theory, where the $|E^{\pm}\rangle$ $(= |E, b^{\pm}\rangle)$ are the Dirac kets that fulfill the Lippmann-Schwinger equations (b are the degeneracy labels). These basis vector expansions are fulfilled in any RHS.

Here, the $|E, b^{\pm}\rangle$ are antilinear functionals on the space $\mathbf{\Phi}_{\mp}$ of (22,23) which are Hardy spaces. For Hardy RHS, i.e., under the hypothesis (22,23), one can prove in addition the following basis vector expansion [8]. For every vector $\phi^{+} \in \mathbf{\Phi}_{-}$,

$$\phi^{+} = \sum_{\text{bound states}} |E_n)(E_n|\phi^{+}) + \sum_{i=1}^{N} |\psi_i^G\rangle\langle\psi_i^G|\phi^{+}\rangle + \int_0^{\infty} dE\, |E^{+}\rangle\, b(E)\,. \qquad (46)$$

In here, the ψ_i^G, $i = 1, 2, \ldots, N$, represent N Gamow vectors with respective eigenvalues $E_{R_i} - i\Gamma_i/2$ and we have assumed that there are N first order resonance poles at the pole positions $z_{R_i} = E_{R_i} - i\Gamma_i/2$ of the analytically continued S-matrix (second Riemann sheet) or of the reduced resolvent. In (46) we have also assumed the existence of some stable bound states $|E_n)$ in order to show that the resonance states ψ_i^G appear in the complex basis expansion (46) in the same manner as the bound states. If there are no bound states, the first sum in (46) is omitted. The expansion (46) shows that the resonances appear in the basis vector expansion on the same footing with the bound states. However, (46) is not a complete analogue of the discrete basis vector decomposition (8) because, in addition to the superposition of resonance states ψ_i^G (and the sum over bound states $|E_n)$, which we shall omit since they are of no further relevance here) there appears an integral over the continuous basis vectors $|E^{+}\rangle$ with a weight function $b(E)$.

The complex basis vector expansion (46) — without the bound-state term — is obtained from the S-matrix element which with (44, 45) is written (suppressing the degeneracy index b)[q]

$$(\psi^{\text{out}}, S\,\phi^{\text{in}}) = (\mathbf{\Omega}^{-}\psi^{\text{out}}, \mathbf{\Omega}^{+}\phi^{\text{in}}) = (\psi^{-}, \phi^{+})$$

$$= \int_0^{\infty} dE\, \langle\psi^{-}|E^{-}\rangle\, S(E)\, \langle{}^{+}E|\phi^{+}\rangle\,. \qquad (47)$$

If the S-matrix $S(E)$ has N first order poles at $z_{R_i} = E_{R_i} - i\Gamma/2$ then, as a consequence of the new hypothesis in the form of (24,25) and the residue theorem, one can write the integral in (47) as a sum of residues corresponding to the N poles plus a background integral. As a result the S-matrix $S(E)$ can be represented as

$$S(E) = \sum_{i=1}^{N} \frac{R^{(i)}}{E - (E_{R_i} - i\Gamma/2)} + b(E)\,, \qquad (48)$$

where the $R^{(i)}$ is the residue at the pole z_{R_i}, which is a sum of Breit-Wigner amplitudes plus a background amplitude $b(E)$.

[q]Here, we define the Møller wave operators $\mathbf{\Omega}^{\pm}$ as the following limits in the strong operator sense:

$$\mathbf{\Omega}^{\pm} = \lim_{t \mapsto \mp\infty} e^{itH}\, e^{-itH_0}\,.$$

There is a one-to-one correspondence between a Breit-Wigner amplitude in (48) and a Gamow vector in (46) and the background amplitude corresponds to the continuous superposition over the $|E^+\rangle$ with weight function $b(E)$ in (46).

From the complex basis vector expansion (46) follows by applying the time evolution operator $U^\times(t) = e^{-itH^\times}$ to ϕ^+:

$$e^{-itH^\times}\phi^+ = \sum_{i=1}^{N} e^{-iE_R t}\, e^{-\frac{\Gamma_i}{2}t}\, |\psi_i^G\rangle\langle\psi_i^G|\phi^+\rangle + \int_0^\infty dE\, e^{-itE}\, |E^+\rangle\, b(E)\,, \qquad (49)$$

This expression is valid for $t \geq 0$ only, because only for $t \geq 0$ is the semigroup $e^{-itH^\times}$ defined.

The result (49) then shows that the time evolution of an apparatus prepared state ϕ^+ is given by a superpositions of exponentials plus a nonexponential background term. In case that there is only one resonance in the scattering system (and no bound state) the basis vector expansion (46) is

$$\phi^+ = C\,\psi^G + \int_0^\infty dE\, |E^+\rangle\, b(E) \qquad (50)$$

(where C is an arbitrary constant) and its time evolution is

$$\phi^+(t) = e^{-itH}\,\phi^+ = C\, e^{-iE_R t}\, e^{-\frac{\Gamma}{2}t}\,\psi^G + \int_0^\infty dE\, e^{-itE}\, |E^+\rangle\, b(E)\,. \qquad (51)$$

The first term of (50) representing the state of the resonance per se has its characteristic exponential time behavior. However, there is always the background term whose time evolution is not exponential and whose magnitude $b(E)$ depends upon the way the state ϕ^+ was prepared.

Therefore, a prepared in-state ϕ^+ cannot have a purely exponential time evolution. Only the Gamow vector which corresponds to the Breit-Wigner amplitude in the S-matrix (or in the scattering amplitude $a(E) := \frac{1}{2i}(S(E) - 1)$) (48), and represents the resonance per se, has a purely exponential decay. The resonance state is characterized by the resonance energy E_R and by the width Γ, or its inverse, the lifetime $\tau = 1/\Gamma$. These values do not vary from experiment to experiment, but the background $b(E)$ may. In resonance scattering experiments, in which the time scale for the preparation of the decaying state and the time scale for the decay are the same (e.g. resonance formation of hadrons) one always needs the slowly varying background term $b(E)$ for the fit of the cross section data. In this case, one expects deviations from the exponential decay given by the $e^{-itE}\, b(E)$ dependence in the second term of (51). This background term can thus account for the deviations from the exponential law reported in this conference [33]. It is the particular form of the complex basis vector expansion (50,46), that allows for deviations from the exponential law, though the ideal resonance state vector ψ^G has an exponential time evolution. The smaller one can make $b(E)$ in the experiment, the less important will be the deviations from the exponential law. And in those experiments in which the time scale for the preparation of the decaying state and the time scale for the observation of the decay products differ by orders of magnitudes like in the process (36,35) discussed above, the validity of the exponential law has been established to a high accuracy [19].

There is actually also some deviation from the exponential law observed in the neutral Kaon system of (35), but this has been known for a long time. It is well understood and can therefore be taken care of in the experimental analysis. It has its origin in the fact that the K^0 in (36) is not a K_S^0, but there are two K^0st ates (with different quantum numbers good for the strong interaction but not for the weak interaction), so that, for the neutral K-system, $N = 2$ in (46).

The complex basis system expansion (46) is an exact consequence of the hypothesis (22,23). But in the Lee-Oehme-Young theory for the K^0 system, one assumes that the prepared K^0 state in (36) is represented by its Weisskopf-Wigner approximation [26]:

$$\phi^+ = C_L \psi_L^G + C_S \psi_S^G \,, \tag{52}$$

The ψ_i^G in (52) are assumed to fulfill (39). The same result (52), one also obtains from (46) if one omits the continuum background of (46). This expansion (52) is thus a consequence of the hypothesis (22,23) but with the continuum (background term) omitted. The deviation from the exponential law, that one observes for the neutral Kaon system, is then explained by the interference between ψ_L^G and $\psi_S^G$and not by interference with the background term, which is small for the K^0-system.

The truncated complex basis vector expansion, i.e., (46) without the background integral, has also been used extensively in fitting experimental data by a superposition of resonance states in nuclear physics [14].

The application of the complex basis vector expansion (46) in atomic physics has been discussed in [24], where the interference of two or more Gamow vectors ψ^G and the continuum integral is used to explain the experimental data observed for the Na I dissociation process [10]. Consequences of (46) have also been discussed in another talk of this session [30].

5 Conclusions and general remarks

We have made minor modifications in the foundations of quantum mechanics, essentially we have replaced one axiom of quantum mechanics, the Hilbert space axiom (14), by the Hardy space hypothesis (22,23) and retained all other fundamental assumptions of quantum mechanics including the calculation rules, based on Dirac's continuous basis vector expansion. This modification of the axioms is so minimal that it cannot be observed directly, since this would require to discriminate between an apparatus resolution described by an energy wave function that can and an energy wave function that cannot be analytically continued into the complex energy plane. The important feature of our modification is that it distinguishes also mathematically between observables and states, describing them by the two different dense Hardy subspaces of the same Hilbert space. Experimentally one always makes this distinction attributing states and observables to different parts of the experiment; the preparation apparatus (accelerator) prepares the state and the registration apparatus (detector) registers the observable.

In the heuristic scattering theory, where one does not limit oneself to the Hilbert space [21], this discrimination between states and observables has already been done. In scattering theory, one describes the in and out plane waves by Dirac kets fulfill-

ing different Lippmann-Schwinger equations. The new hypothesis (22,23) provides the mathematical justification for this, which also allows for a generalization from the infinitesimal $\pm i0$, that appear in the Lippmann-Schwinger equations, to finite values (e.g. $i\Gamma/2$). Using the new hypothesis (22,23), one obtains a unified theory of resonance scattering and decay phenomena which is free of the problems that have their origin in the use of a mixture of the Hilbert space mathematical axiom and of calculational rules that are inconsistent with this axiom. One also obtains new results, like the complex basis vector expansion (46) whose truncation is the Weisskopf-Wigner approximation. It therewith justifies the finite dimensional effective theories of complex energy resonance states that have had successful applications in nuclear physics and the Lee-Oehme-Yang theory for the neutral Kaon system. On the more fundamental level, the new hypothesis leads to semigroup dynamics and provides a theoretical foundation for the concept of the time at which the preparation of a state has been done and the measurement of an observable can begin.

In the mathematical description of reality, we always have to make idealizations and one of the general lectures of this conference [28] discussed the question whether time-arrowed quantum mechanics (TAQM) is sufficiently idealistic and reductive enough to qualify as Pythagorean or whether it is Aristotelian, i.e., an empirical "effective" formalism like the theory of friction that slowed down the advance of physics. Time Asymmetric Quantum Theory does not describe the irreversibility due to the influence of the environment or of the measurement apparatus [20] upon an open quantum system [11]. The time evolution of open quantum systems is also given by a semigroup but its dynamical equations contains in addition the Hamiltonian term of (7) another term that describes the influence of the external reservoir or external environment. This may be the analogue of the friction term in Newton's equation in classical mechanics. TAQT attributes the "irreversibility", or better the time-asymmetry, to the time asymmetric boundary conditions (22,23) for the time-symmetric dynamical equations (6,7) or (4,5). Its classical analogue is the phenomenological law according to which nature favors the retarded over the advanced solution of the time symmetric Maxwell equations (radiation arrow of time), or the big bang over the big crunch solution of the Einstein equation. The standard Quantum Mechanics in Hilbert space does not allow time-asymmetric boundary conditions, however for stationary quantum systems - idealizations in which the excited states of atoms and molecules are considered stable - it does the job. However, resonance scattering and decay are time asymmetric phenomena and therefore using the Hilbert space boundary conditions leads to inconsistencies [22,23], whereas a more phenomenological approach has great empirical success [38,21]. Therefore, why not find the Pythagorean elements of this phenomenological approach, i.e., the mathematical idealizations that describe these phenomena?

These elements are the Gamow states, the vectors with exact exponential semigroup time evolution and idealized Breit-Wigner energy distribution. The Gamow vectors ψ^G are one of the end points of the reductive approach because they describe the resonance = decaying particle per se isolated from all background (which is represented by the integral of (50)). They may be difficult to isolate experimentally, (like the frictionless objects of classical mechanics) but they lead to a simple and consistent theory.

Acknowledgments

The authors wish to express their gratitude to the organizers of the Solvay Conference, in particular to Profs. I. Prigogine and I. Antoniou, for their support. Partial financial support is also acknowledged to the Junta de Castilla y León Project PC02/99, the DGCYT PB98-0370 and DGICYT PB98-0370 Projects from the Spanish Ministry of Education and the Welch Foundation.

Appendix: A note on Lebesgue integrals

Lebesgue square integrable functions on the real axis (or $L^2(\mathbb{R})$ functions) may be very weird to represent a physical state. The reader may have in mind square integrable functions of the type

$$f(x) = \begin{cases} 1 \text{ on the irrationals of the interval } [0,1] \\ 0 \quad \text{on the rationals of the interval } [0,1] \\ 0 \qquad\qquad\qquad\qquad \text{otherwise.} \end{cases}$$

We do not mean that kind: since $L^2(\mathbb{R})$ is a space of class of functions, and $f(x)$ is almost elsewhere identical to the function which is equal to one on the interval $[0,1]$ and zero elsewhere, we can choose the latter instead of $f(x)$ as a possible wave function. When we speak about weirdness, we are referring to functions of the type:

$$f(x) := \sum_{n=1}^{\infty} n\, \Delta_n(x)\,,$$

where

$$\Delta_n(x) = \begin{cases} 1 \text{ if } x \in [n - \frac{1}{2^n n^2}, n + \frac{1}{2^n n^2}] \\ 0 \qquad\qquad \text{otherwise.} \end{cases}$$

Note that $f(x)$ is neither bounded nor vanish at the infinity. In any neighborhood of infinity, $f(x)$ is different from zero almost elsewhere (a.e) and unbounded. Nevertheless, $f(x)$ is square integrable:

$$\int_{-\infty}^{\infty} |f(x)|^2\, dx = \sum_{n=1}^{\infty} \frac{2n^2}{2^n n^2} = \sum_{n=1}^{\infty} \frac{1}{2^{n-1}} = \sum_{n=0}^{\infty} \frac{1}{2^n} = 2\,.$$

One may argue that $f(x)$ is not continuous (in fact it is continuous a.e.). However, there are smooth functions that are square integrable but are neither bounded, nor having a limit at the infinite.

These functions can be constructed by using the following idea: Let

$$g(x) = \begin{cases} A > 0 \text{ if } \ x \in [a,b] \\ 0 \qquad\qquad \text{otherwise.} \end{cases}$$

Then, we can construct an indefinitely differentiable function *at all points*, $h(x)$, such that [9]:

a.) $h(x)$ has the value A on the interval $[c, d]$ with $a < c < d < b$.

b.) $h(x)$ has the value 0 outside $[a, b]$.

c.) $h(x)$ takes values between 0 and A smoothly on $[a, c]$ and $[d, b]$.

Let us make this construction on each of the intervals

$$[n - \frac{1}{2^n\, n^2}, n + \frac{1}{2^n\, n^2}]\,,$$

then, we have a function $\eta(x)$ such that:

1.- The function $\eta(x)$ admits continuous derivatives of all orders at all points of the real line.

2.- Since $0 \leq \eta(x) \leq f(x)$, $\forall\, x \in \mathbb{R}$, $\eta(x)$ is square integrable and $\eta(x)$ being non negative and non identically zero, we conclude that

$$0 < \int_{-\infty}^{\infty} |\eta(x)|^2\, dx < \infty\,.$$

3.- The function $\eta(x)$ is unbounded.

4.- The limit:

$$\lim_{x \mapsto \infty} \eta(x)$$

does not exist!

Therefore smoothness is not often a good enough property for functions in the space representing $\mathbf{\Phi}_{\pm}$. Thus, we need to impose in these functions some kind of behavior at the infinite. Often, rapid decreasing.

References

1. W.O. Amrein, J. Jauch and B. Sinha, *Scattering Theory in Quantum Mechanics*, Benjamin, Reading MA (1977).
2. J.P. Antoine, J. Math. Phys., **10**, 53 (1969); J. Math. Phys., **10**, 2276 (1969); also in *Quantum Mechanics Beyond Hilbert Space* in *Irreversibility and Causality*, A. Bohm, H-D Doebner, P. Kielanowski, Eds., Springer Lecture Notes in Physics vol **504**, Springer Verlag, Berlin and New York (1998), pp 3-33.
3. A. Bohm, *Quantum Mechanics: Fundations and Applications*, 3rd edition, 3rd printing, Springer Verlag (2002).
4. A. Bohm, *The Rigged Hilbert Space in Quantum Physics*, ICTP Report No 4, Trieste (1965); Boulder Lectures in Theoretical Physics (A.O. Barut, Editor), vol 9A (1966).
5. A. Bohm, M. Gadella, *Dirac Kets, Gamow Vectors and Gelfand Triplets*, Springer Lecture Notes in Physics, vol **348**, Springer Verlag, New York and Berlin (1989).
6. A. Bohm, N. L. Harshman, *Quantum Mechanics Beyond Hilbert Space* in *Irreversibility and Causality*, A. Bohm, H-D Doebner, P. Kielanowski, Eds., Springer Lecture Notes in Physics vol **504**, Springer Verlag, Berlin and New York (1998), pp. 181-237.
7. A. Bohm, P. Kielanowski, Acta Phys. Polonica, **27**, 2295, (1996).

8. A. Bohm, S. Maxon, M. Loewe, M. Gadella, Physica A **236**, 485 (1997).
9. W. M. Boothby, *An Introduction to Differentiable Manifolds and Riemannian Geometry*, Academic, New York (1975).
10. P. Cong, G. Roberts, J.L. Herek, A. Mohkatari, A.H. Zewail, J. Phys. Chem, **100**, 7832 (1996).
11. E. B. Davis, *Quantum Theory of Open Systems*, Academic Press, London (1976).
12. P. L. Duren, *Theory of H^p Spaces*, (Academic Press, New York, 1970); P. Koosis, *Introduction to H^p Spaces*, (Cambridge, UK, 1980); *The Logaritmic Integral*, (Cambridge, UK, 1990).
13. P. Exner, *Open Quantum Systems and Feynman Integrals*, Reidel, Dordrech (1985).
14. L. S. Ferreira, E. Maglione, *Resonances: Calculations and Observables*, Proceedings of the IV Workshop in Rigged Hilbert Spaces and Time Asymmetric Quantum Mechanics, to be published in the Int. J. Theor. Phys. (2002).
15. L. Fonda, G.C. Ghirardi, A. Rimini, Rep. Prog. Phys., **41**, 587 (1978).
16. M. Gadella, F. Gómez, *The Lippmann-Schwinger equations in RHS*, J. Phys. A: Math. Gen., (O'Raifeartaight Memorial Volume) (2002).
17. I. M. Gelfand, *Generalized Functions, Vol 4*, Academic, New York (1964); K. Maurin, *Generalized Eigenfunction Expansions and Unitary Representations of Topological Groups*, Polish Scientific Publishers, Warszawa (1968).
18. M. Gell-Mann and J.B. Hartle in *Physical Origins of Time Asymmetry*, J.J. Halliwell et al., Eds., Cambridge University Press (1994); also in *Complexity, Entropy and the Physics of Information*, SFI Studies in Science and Complexity, vol VIII, W. Zurek, Ed., (1990).
19. K.L. Gibbons, et al., Phys. Rev. D, **55**, 6625 (1997); V.L. Fitch, et al., Phys. Rev. B, **140**, 1088 (1965); N.N. Nikolaiev, Sov. Phys. Usp., **11**, 522 (1968) and references therein; E.B. Norman, Phys. Rev. Lett., **60**, 2246 (1988).
20. G.C. Ghirardi, A. Rimini, T. Weber, Phys. Rev. D, **34**, 470 (1986).
21. M.L. Goldberger, K.M. Watson, *Collision Theory*, Wiley, New York (1964).
22. C. G. Hegerfeldt, Phys. Rev. Lett., **72**, 596 (1994).
23. L. A. Khalfin, Sov. Phys. JETP, **6**, 1063 (1958); L. Fonda, G.C. Ghirardi, A. Rimini, Rep. Prog. Phys., **41**, 589 (1978).
24. I. Antoniou, E. Karpov, G. Pronko, E. Yarevsky, *Oscillating decay of an unstable system*, to be published in *Resonances, Time Asymmetry and Rigged Hilbert Spaces,* Kluwer A.P.
25. K. Kraus, *States, Effects and Operations*, Springer Lecture Notes in Physics, Vol 190, Springer, Berlin (1983).
26. T. D. Lee, *Particle Physics and Introduction to Field Theory*, Harwood Academic, New York (1981).
27. R. de la Madrid, *Rigged Hilbert Space Approach to the Schrödinger Equation*, J. Phys. A: Math. Gen., to appear (jan 2002); R. de la Madrid, A. Bohm, M. Gadella, Fort. Phys. (in press).
28. Y. Neeman, *Preservation of a T-invariant Reductionist Scaffold in "Effective" Intrinsically Irreversible Quantum Mechanics*, Proceedings of XXII Solvay Conference on Physics (in this volume).

29. J. von Neumann, *Mathematical Foundations of Quantum Mechanics*, Princeton University Press, Princeton, USA (1955).
30. T. Petrosky and C.O. Ting, *Propagation of Decoherence in a Field and Complex Spectral Representation*, Proceedings of XXII Solvay Conference on Physics (in this volume).
31. I. Prigogine, S. Kim, G. Ordonez and T. Petrosky, *Stochasticity and Time Symmetry Breaking in Hamiltonian Dynamics*, Proceedings of XXII Solvay Conference on Physics (in this volume).
32. I. Prigogine, remarks in this session of the XXII Solvay Conference on Physics.
33. M. G. Raizen, B. Gutiérrez-Medina, M.C. Fischer, *Observation of the Quantum Zeno and Anti-Zeno Effects in an Unstable System*, Proceedings of XXII Solvay Conference on Physics (in this volume); S.R. Wilkinson et al., Nature, **387**, 575 (1997); C.F. Barucha et al., Phys. Rev. A, **55**, R857 (1997).
34. M. Reed, B. Simon, *Functional Analysis*, Academic Press, New York (1972).
35. J.E. Roberts, J. Math. Phys, **7**, 1097 (1966); Comm. Math. Phys., **3**, 98 (1966).
36. M.H. Stone, *On one-parameter unitary groups in Hilbert space*, Ann. Math., **33**, 643-648 (1932).
37. E.C.G. Sudarshan, *Decoherence, Purification and Entanglement*, Proceedings of XXII Solvay Conference on Physics (in this volume).
38. E.P. Wigner, V.F. Weisskopf, Zs. Phys., **63**, 62 (1930).

DISCUSSION

Chairman: L. Stodolsky

L. Stodolsky: So if I understand, you say it's a better way of understanding what we already know, but it doesn't make way to any new experimental predictions. Can you propose an experiment which will come out different in a normal quantum mechanics?

A. Bohm: If you apply this to a relativistic theory, it gives you a criterion to choose the definition of the mass and the width of a relativistic resonance, which otherwise cannot be done. The particle data book gives two values for two different definitions of mass and width for a relativistic resonance. Our theory gives a third one, and for the Z-boson resonance, these values differ by about ten times the experimental error. The experimental lineshape cannot decide which are the right values. The fundamental axiom that we propose removes the ambiguity in the definition of mass and width for relativistic resonances using a theoretical criterion. This criterion is that the width must be defined such that it is the inverse lifetime. From that criterion, which you can only get from our axiom, you can predict precisely the value of the Z-boson mass and width. This is the only prediction I know at this time as far as experimental numbers are concerned.

I. Prigogine: You cannot separate the type of systems which you mentioned at the beginning from the system used in statistical mechanics. Because irreversibility is an obvious phenomenon which we see in many body systems. So you said

something which is certainly not correct, and that is the fact that you need to have a decaying particle. But that is not true. You have either zero trace or constant energy. Therefore you have a problem, and therefore I'm about to say that I object to this.

A. Bohm: Our time asymmetric quantum theory has one particular consequence, namely that preparation of the state must precede the observation of the decay products. That's only one of the many consequences. Of course, this arrow of time or irreversibility is also there without experimentalists performing any experiments. It has many manifestations and one can argue that ultimately it comes from the big bang, as you know so well. Whether it is connected with entropy increase I do not know. It is an irreversibility connected to boundary conditions.

W. Schleich: Can you use these two spaces that you have constructed in dynamic systems with higher poles?

A. Bohm: Higher order poles lead to Jordan blocks and density operators, not vector states. I have also tried to see if one can derive entropy increase from higher order poles, and have also not succeeded. But one can do something else, one can derive the complex basis vector expansion, and one can show that double poles or higher order poles of the S-matrix, are represented by vectors in the complex basis vector expansion. But they are not ordinary generalized eigenvectors, they are Jordan vectors. For a higher order resonance pole one does not get complex energy eigenvalues, but one gets Jordan block for the energy.

G. Pronko: Your irreversibility, it seems, was obtained from the fact that you chose the Hardy spaces.

A. Bohm: It is derived just from the Hardy space hypothesis.

G. Pronko: This is sufficient, but it is not necessary. To describe a resonance as a state you need the test function which could be continued to some region in the lower half-plane, not necessarily to the whole complex plane.

A. Bohm: For scattering theory using in- and out- plane wave solutions of the Lippmann-Schwinger equation, you need analytic continuation of the test functions only into a strip along the real axis, not the whole complex plane. But if you want to describe resonances with a Breit-Wigner energy distribution and an exponential time evolution, you need smooth Hardy functions. The best choice in the non-relativistic case is a space of Schwartz and Hardy functions. For the relativistic case, it is a little different but we always use the Hardy space property.

G. Pronko: In the non relativistic case, you do not need actually Hardy class, and you also do not need the continuation to the whole lower half-plane, plus some asymptotic conditions. This is the main reason why you receive a semi-group instead of a group.

A. Bohm: The semi-group, and this is not well-known, is already there for the Lippmann-Schwinger plane waves. Everybody thinks the Lippmann-Schwinger scattering states have a unitary Poincare group evolution, as stated in Weinberg's book. But one can show that they have only a semi-group evolution if one defines them properly as a functional over Hardy Spaces. Whether other asymptotic decay properties than those of Hardy functions would lead to a semigroup, I do not know.

ON PHONON MEDIATED DECOHERENCE OF ORBITAL DEGREES OF FREEDOM IN QUANTUM DOT

LUCJAN JACAK[1]*, JURIJ KRASNYJ[2], DOROTA JACAK[3], PAWEL MACHNIKOWSKI[1]

[1] *Institute of Physics, Wrocław University of Technology, Wybrzeże Wyspiańskiego 27, 50-370 Wrocław, Poland*

[2] *Institute of Mathematics, University of Opole, Oleska 48, 45-051 Opole, Poland, (on leave from Institute of Physics, Odessa University, Ukraine)*

[3] *Institute of Mathematics, Wrocław University of Technology, Wybrzeże Wyspiańskiego 27, 50-370 Wrocław, Poland*

In the state-of-the-art strain induced InAs/GaAs quantum dots, the polaron lifetime due to the anharmonic LO-TA phonons interaction was recently estimated numerically to be several picoseconds. This time, treated as the upper limit for the decoherence of orbital degrees of freedom in quantum dots, is too short for successful application of the error correction procedures necessary to create a scalable optically driven quantum computer in self-assembled dot technology, even when using ultrafast, of femtosecond scale, information processing. In the present report, we rediscuss the polaron relaxation in a quantum dot using the Davydov diagonalization method; we show that the previous estimations were too sever and argue that the relevant relaxation channel is slower by one order of magnitude. The increase of the estimation results from taking into account the coherent renormalization of the appropriate anharmonic term. We give also the explanation of the strong enhancement of the electron-LO phonon ineraction for electrons confined in the dot, which can be expressed via renormalization of the Fröhlich constant.

1 Introduction

Due to the continuous development of nanotechnology, quantum dots (QDs) are believed to be in the center of the imminent technological revolution e.g. in laser technology [1] or in quantum computing [2,3]. QDs offer a nanometer-scale confinement for carries (electrons and holes) in the field of well technically recognized semiconductor-solid-state technology. The techniques used for manufacturing of QDs include epitaxy, lithography and self-assembling methods[4]. The so-called self-assembled QDs, obtained by Stranski-Krastanow method [4], are particularly promising, as the strain-induced growth in multilayer structures allows for creation of dot-molecules[5] or dot-chains [6], which are expected to be helpful for implementation of quantum gates. The other advantages of QDs for potential application in quantum information processing consist also in possible integration with the existing microelectronic technology, scalability and available manipulation techniques including magnetic field (in a reasonable range of magnitudes) and sub-picosecond optical techniques [7]. Both the orbital[3] and spin [2] degrees of freedom of the carriers trapped in a QD are considered for the definition of a qubit. The advantage of spin degrees of freedom consists in relatively long decoherence time for the spin of a single electron in a QD (of order of μs) and in the very effective method of implementation of double-qubit operations (e.g. CNOT) by exploiting the exchange

*EMAIL: JACAK@RAINBOW.IF.PWR.WROC.PL

interaction [2] (singlet-triplet transition in magnetic field; time of operation can be of order of ps as the singlet-triplet energy seperation is of the scale of meV for realistic fields). There are, however, certain problems with single-qubit operations – they are very slow for single spin qubit (as the Zeeman splitting is small, e.g. 0.03 meV/T for GaAs). Moreover, operating with a single electron in a QD is rather outside the reach of the state-of-the-art technology, whereas coupling of spin to the orbital degrees of freedom in multielectron QDs (via Hund-like rules) efficiently enhances decoherence. Therefore the orbital degrees of freedom in a QD are currently considered as more feasible for practically setting up a quantum gate (an excitonic entanglement in QD molecule has already been demonstrated [8]). Since the electronic (or excitonic) states in a system of QDs are designed to play the role of qubits which must be manipulated with great precision, the exact knowledge of the energetic spectrum of a QD is of major importance. Moreover, because of the necessary quantum coherence during quantum computing processes, the interaction between the localized electron and the surrounding medium must be well understood.

The electronic properties of QDs were widely analyzed [4]. In particular, it has been confirmed that the 2-dimensional harmonic oscillator description for electron states is a relatively good approximation e.g. in the case of self-assembled InAs/GaAs lens-shaped dots [9]. In the case of polar medium of QDs, the electron–longitudinal optical (LO) phonon interaction must be taken into account in a reliable description. The theoretical investigation of this issue was performed by e.g. the standard perturbation techniques [10], by the variational Lee-Low-Pines method [11], by numerical diagonalization[12,13] or by Green function methods [14]. The experimental data [12] show, in particular, a large splitting width near the one-phonon and two-phonon resonance in a InAs/GaAs QD. This was accounted for by the theoretical model via a numerical diagonalization of the Fröhlich interaction[12]. The required value of the Fröhlich constant was much larger (by a factor of two[12]) than measured in bulk.

The recent proposal of a fully optically driven quantum gate for a scalable quantum computer on the system of QDs employing excitonic states [3] is one of the most promising ideas for quantum information processing due to the possibility of application of ultrafast resonant optical methods [7]. The feasibility of this idea depends, however, crucially on the decoherence ratio, i.e. the ratio of the characteristic decoherence time to the time needed for elementary operations. The error correction schemes need this ratio to be not smaller than 10^5. As the optical techniques allow for even femtosecond scale for one-qubit operations, the nanosecond scale of the typical exciton lifetime in quantum dots was originally recognized as a promising opportunity. A serious objection appears, however, when the electron-phonon interaction in InAs/GaAs quantum dots was identified to be much stronger in comparison to bulk semiconductor [12] and to lead to dressing of electrons (holes) with LO phonons, i.e. to the creation of effective quasiparticles, polarons, even at energies relatively far from the resonant energy [19,14].

The polarons decohere very quickly due to the scattering of the optical phonons from the coherent cloud via anharmonic interaction with the continuum of acoustical phonons. For GaAs-bulk the most efficient anharmonic process (of picosecond

timescale) is the zone-center LO phonon decay into a zone-edge LO phonon and a transversal acoustical (TA) phonon with the opposite momentum[17]. The theoretical analysis based on a phenomenological approach[23] leads to a similar, picosecond lifetime for confined LO phonons: for InAs/GaAs dots with size larger than 15 nm, the anharmonic decay lifetime of the confined LO phonons was estimated to be $7 - 2.5$ ps for temperatures from 0 K to 300 K [23].

The LO-TA phonon decay in GaAs gives rise to an anharmonicity-induced relaxation of a polaron in the self-assembled InAs/GaAs quantum dots. The corresponding relaxation time, treated as the upper limit for the decoherence time of the polaron state was estimated to be of order of 3 ps for a dot with ≈ 10 nm radius [19].

In Refs [12,19], the polarons were analyzed by direct (numerical) diagonalization of the Hamiltonian containing terms for confined electrons in a quantum dot, free phonons and the Fröhlich electron-phonon interaction. The anharmonic third order term (LO-TA), was further included perturbatively. The question is whether including the coherent effect of phononic dressing in the anharmonic term changes the relaxation time or not. The purpose of the present report is to verify this possibility via application of the analytical method of the Davydov canonical transformation, i.e. by the approximate but explicit diagonalization of the Fröhlich interaction. This method allows for simultaneous accounting for anharmonic phonon interaction including its coherent renormalization.

2 Model

The system under investigation consists of electrons confined in a QD and phonons. We take into account longitudinal optical (LO) and longitudinal and transversal acoustical (LA and TA) bulk branches of phonons. The electron-phonon interactions via the LO and LA channels are included as well as the anharmonic third order LO–TA channel of phonon interaction (the most efficient channel for decay of LO phonons in GaAs bulk [17] – the medium of the self-assembled InAs/GaAs quantum dot).

The system is described by the Hamiltonian

$$H = H_e(\mathbf{r}) + \hbar\Omega \sum_{\mathbf{k}} b_{\mathbf{k}}^\dagger b_{\mathbf{k}} + \sum_{\mathbf{q},s} \hbar\omega_s(\mathbf{q}) c_{\mathbf{q}s}^\dagger c_{\mathbf{q}s} - \frac{1}{\sqrt{N}} \sum_{\mathbf{k}} \frac{e}{k} \sqrt{\frac{2\pi\hbar\Omega}{v\tilde{\epsilon}}} \left(b_{\mathbf{k}} + b_{-\mathbf{k}}^\dagger\right) e^{i\mathbf{k}\cdot\mathbf{r}}$$
$$+ \frac{1}{\sqrt{N}} \sum_{\mathbf{q}} \sigma \sqrt{\frac{\hbar q}{2MC_l}} \left(c_{\mathbf{q}l} + c_{-\mathbf{q}l}^\dagger\right) e^{i\mathbf{q}\cdot\mathbf{r}} \qquad (1)$$
$$+ \sum_{\mathbf{k}_1,\mathbf{k}_2,\mathbf{q}} W(\mathbf{k}_1,\mathbf{k}_2,\mathbf{q}) \delta_{\mathbf{k}_1-\mathbf{q},\mathbf{k}_2} b_{\mathbf{k}_1}^\dagger b_{\mathbf{k}_2} \left(c_{\mathbf{q}t} + c_{-\mathbf{q}t}^\dagger\right),$$

where $b_{\mathbf{k}}$ is the bosonic annihilation operator for LO phonon with quasi-momentum $\mathbf{k}$ and with the dispersionless (for simplicity) frequency Ω, $c_{\mathbf{q}s}$ is the bosonic annihilation operator for the acoustical phonon with quasi-momentum $\mathbf{q}$ and polarization s (t – transversal or l – longitudinal) with frequency $\omega_s(\mathbf{q})$, C_l is the sound velocity for the longitudinal phonons, M is the mass of ions in the elementary cell, σ is the deformation constant (for GaAs $\sigma \simeq 6$ eV), v is the volume of the elementary cell, N is the number of cells in the crystal and $\tilde{\epsilon} = (1/\epsilon_\infty - 1/\epsilon_0)^{-1}$ is

the effective dielectric constant. $H_e(\mathbf{r})$ is the Hamiltonian for electrons confined in the QD. The electron-LO phonon interaction is given by the Fröhlich term, the electron-acoustical phonon interaction term includes only LA phonons; the last term describes the third order anharmonic LO–TA phonon interaction.

We will consider the simplified model for the self-assembled, shallow, disc-shaped, weakly elliptical in-plane, InAs/GaAs QD[12]. We will assume that the dot is strongly confined in the z direction (the results do not depend on the actual potential shape in this direction; we assume a strong parabolic confinement). The in-plane electron dynamics is governed by the anisotropic harmonic potential $V(x,y)$ with eigen-frequencies $\omega_\pm = \omega_0^2(1 \pm \lambda)$, $\lambda \ll 1$, i.e. $V(x,y) = \frac{1}{2}m^*\omega(x^2+y^2) + \frac{\lambda}{2}m^*\omega(x^2-y^2)$. This lateral potential describes the weakly elliptical in-plane QD. The external magnetic field (which can additionally enhance confinement) is assumed to be applied in the z direction and described by the potential in the symmetric gauge. Thus, the single-electron Hamiltonian may be written as

$$H_e(\mathbf{r}) = -\frac{\hbar^2}{2m^*}\left[\frac{1}{r_\perp}\frac{\partial}{\partial r_\perp}\left(r_\perp\frac{\partial}{\partial r_\perp}\right) + \frac{1}{r_\perp^2}\frac{\partial^2}{\partial\varphi^2} + \frac{\partial^2}{\partial z^2}\right] + \frac{1}{2}m^*\omega^2 r_\perp^2 + \frac{\hbar\omega_c}{2}\left(-i\frac{\partial}{\partial\varphi}\right) + U(z) + W(\mathbf{r}_\perp), \tag{2}$$

where $\mathbf{r} = (r_\perp\cos\varphi, r_\perp\sin\varphi, z)$, $\omega^2 = \omega_0^2 + \omega_c^2/4$, $\omega_c = \frac{eB}{m^*c}$, $U(z) = \frac{1}{2}m^*\omega_z z^2$, $\omega_z \gg \omega_0$. The last term describes the anisotropy,

$$W(\mathbf{r}_\perp) = \frac{\lambda}{2}m^*\omega_0^2 r_\perp^2\cos 2\varphi,$$

and can be treated as a perturbation.

Let us now consider the ground and the lowest excited states for the single electron in the dot. For the unperturbed electron Hamiltonian [i.e. neglecting $W(\mathbf{r}_\perp)$], we deal with the cylindrical symmetry and thus with the usual n_r and m quantum numbers (the Fock-Darwin states [4]). We consider states with $n_r = 0$, $m = 0, \pm 1$. The energies and wavefunctions including the perturbation caused by the term W have the following form (we use indices $0, \pm$, for perturbed states $(0,0)$ and $(0,\pm 1)$, respectively):

$$\epsilon_0 = \hbar\omega, \tag{3a}$$

$$\Psi_0(\mathbf{r}) = \psi_0(r_\perp)\phi(z), \tag{3b}$$

$$\epsilon_\pm = 2\hbar\omega \pm \hbar\sqrt{\omega_c^2 + (\lambda\omega_0)^2}, \tag{3c}$$

$$\Psi_\pm(\mathbf{r}) = [c_+\psi_{\pm 1}(\mathbf{r}_\perp) \pm c_-\psi_{\mp 1}(\mathbf{r}_\perp)]\,\phi(z), \tag{3d}$$

where

$$c_\pm = \frac{1}{\sqrt{2}}\left[1 \pm \frac{\omega_c}{\sqrt{(\lambda\omega_0)^2 + \omega_c^2}}\right]^{1/2},$$

ψ_0 and $\psi_{\pm 1}$ stand for the wavefunctions for the two-dimensional isotropic harmonic potential,

$$\psi_m(\mathbf{r}_\perp) = \left[\frac{n_r!}{(n_r+|m|)!}\right]^{1/2}\frac{1}{l_B\sqrt{\pi}}\left(\frac{r_\perp}{l_B}\right)^{|m|} e^{\frac{1}{2}(r_\perp/l_B)^2}e^{im\varphi}, \quad m = 0, \pm 1,$$

where $l_B = \sqrt{\frac{\hbar}{m^*\omega}}$, and $\phi(z)$ is the ground-state harmonic oscillator wavefunction in the z direction.

If we introduce the second quantization representation in the electron Hamiltonian $H_e(\mathbf{r})$, then the entire Hamiltonian (1) can be rewritten as follows:

$$H = H_0 + H_1, \tag{4}$$

$$H_0 = \sum_n \epsilon_n a_n^\dagger a_n + \hbar\Omega \sum_{\mathbf{k}} b_{\mathbf{k}}^\dagger b_{\mathbf{k}} + \sum_{\mathbf{q},s} \hbar\omega_s(\mathbf{q}) c_{\mathbf{q}s}^\dagger c_{\mathbf{q}s} + \frac{1}{\sqrt{N}} \sum_{n_1,n_2,\mathbf{k}} F^{\mathrm{o}}_{n_1n_2}(\mathbf{k}) a_{n_1}^\dagger a_{n_2} \left(b_{\mathbf{k}} + b_{-\mathbf{k}}^\dagger\right),$$

and

$$H_1 = \frac{1}{\sqrt{N}} \sum_{n_1,n_2,\mathbf{q}} F^{\mathrm{a}}_{n_1n_2}(\mathbf{q}) a_{n_1}^\dagger a_{n_2} \left(c_{\mathbf{q}l} + c_{-\mathbf{q}l}^\dagger\right) + \sum_{\mathbf{k}_1,\mathbf{k}_2,\mathbf{q}} W(\mathbf{k}_1,\mathbf{k}_2,\mathbf{q}) \delta_{\mathbf{k}_1-\mathbf{q},\mathbf{k}_2} b_{\mathbf{k}_1}^\dagger b_{\mathbf{k}_2} \left(c_{\mathbf{q}t} + c_{-\mathbf{q}t}^\dagger\right),$$

where

$$F^{\mathrm{o}}_{n_1n_2}(\mathbf{k}) = \frac{e}{k}\sqrt{\frac{2\pi\Omega\hbar}{v\tilde{\epsilon}}} \mathcal{F}_{n_1n_2}(\mathbf{k}), \quad F^{\mathrm{a}}_{n_1n_2} = \sigma\sqrt{\frac{\hbar q}{2MC_l}} \mathcal{F}_{n_1n_2}(\mathbf{k}), \tag{5}$$

with

$$\mathcal{F}_{n_1n_2}(\mathbf{k}) = \int d^3r \Psi_{n_1}^*(\mathbf{r}) \exp(i\mathbf{k}\cdot\mathbf{r}) \Psi_{n_2}(\mathbf{r}). \tag{6}$$

The formfactors (6) for the states $\Psi_{0,\pm}$ given by (3b,3d) have the form:

$$\mathcal{F}_{nn'} = g_{nn'}(k_\perp, \varphi_0) e^{-\left(\frac{k_\perp l_B}{2}\right)^2} e^{-\left(\frac{k_z l_z}{2}\right)^2}, \tag{7}$$

where $l_z = \sqrt{\hbar/(m^*\omega_z)}$ is the confinement length in the z direction and the functions $g_{nn'}$ are given by the formulae

$$\begin{aligned} g_{00} &= 1, \\ g_{0\pm} = -g_{\pm 0}^* &= i\xi\left(c_+ e^{\pm i\varphi_0} \pm c_- e^{\mp i\varphi_0}\right), \\ g_{\pm\pm} &= 1 - \xi^2 \left|c_+ e^{i\varphi_0} \pm c_- e^{-i\varphi_0}\right|^2, \\ g_{\pm\mp} &= -\xi^2\left(|c_+|^2 e^{-2i\varphi_0} + |c_-|^2 e^{2i\varphi_0}\right) \\ &\quad \pm (1-\xi^2)(c_-^* c_+ - c_+^* c_-), \end{aligned}$$

where $\xi = \frac{k_\perp l_B}{2}$.

3 Diagonalization of electron–LO phonon interaction

Due to the interaction between the electron localized in the QD and the LO phonons in the polar medium, the electron is dressed in a polarization cloud, forming a polaron — a superposition of electronic and phononic states. The spectrum of the polaron may be found using the canonical transformation introduced by Davydov and Pestryakov [15].

This transformation is defined by the unitary operator $\mathsf{U} = e^{\mathsf{S}}$, where S is an anti-hermitean operator

$$\mathsf{S}(a,b) = \sum_{n_1,n_2,\mathbf{k}} \Phi_{n_1,n_2}(\mathbf{k}) a^+_{n_1} a_{n_2} (b_{\mathbf{k}} - b^+_{-\mathbf{k}}), \tag{8}$$

with the scalar function $\Phi_{n_1,n_2}(\mathbf{k})$ chosen suitably for the diagonalization demands. The Hamiltonian H_0 (Eq.(4)) may be written as

$$H_0(a,b) = \mathsf{U}^\dagger[\mathsf{U}H_0\mathsf{U}^\dagger]\mathsf{U} = \mathsf{U}^\dagger H_0(\alpha,\beta)\mathsf{U},$$

where $H_0(\alpha,\beta)$ is H_0 Hamiltonian with the operators a, b replaced by operators $\alpha = \mathsf{U}a\mathsf{U}^\dagger$, $\beta = \mathsf{U}b\mathsf{U}^\dagger$, respectively (note that $U(a,b) = U(\alpha,\beta)$).

The function Φ may be chosen in such a way that $\mathsf{U}^\dagger H(\alpha,\beta)\mathsf{U}$ does not contain terms linear in β. Neglecting residual multi-polaron and multi-phonon interaction terms [15] (these terms are of higher order in the Fröhlich constant, $\alpha << 1$, thus are small),

$$e^{-\mathsf{S}} H_0(\alpha,\beta) e^{\mathsf{S}} \approx \sum_n E_n \alpha^\dagger_n \alpha_n + \hbar\Omega \sum_{\mathbf{k}} \beta^\dagger_{\mathbf{k}} \beta_{\mathbf{k}} + \sum_{\mathbf{q},s} \hbar\omega_s(\mathbf{q}) c^\dagger_{\mathbf{q}s} c_{\mathbf{q}s} \tag{9}$$

with

$$\Phi_{n_1 n_2}(\mathbf{k}) = \frac{1}{\sqrt{N}} \frac{F^{\circ}_{n_1 n_2}(\mathbf{k})}{E_{n_2} - E_{n_1} + \hbar\Omega}. \tag{10}$$

and

$$E_n = \epsilon_n - \sum_{n'} \frac{J_{n'n}}{E_{n'} - E_n + \hbar\Omega}, \tag{11}$$

where

$$J_{n'n} = \frac{1}{N} \sum_{\mathbf{k}} |F^{\circ}_{n'n}(\mathbf{k})|^2.$$

The equation (11) is the self-consistent non-perturbative equation for the energy $E_n$of the polaron, derived and applied for bulk semiconductor by Davydov and Pestryakov [15].

Note also that in our case of the electron confined in the QD, similarly as for an unconfined electron [15], the polaron states are highly distinct from the original electron states, while the phonon states are almost not modified by coherent effects. This follows from the formulae:

$$\alpha^+_n|0\rangle \simeq a^+_n|0\rangle - \frac{1}{2} \sum_{n_1,n_2,\mathbf{k}} \Phi_{n_1 n}(\mathbf{k}) \Phi_{n_2 n_1}(-\mathbf{k}) a_{n_2}|0\rangle - \sum_{n_1,\mathbf{k}} \Phi_{n_1 n}(-\mathbf{k}) b^+_{\mathbf{k}} a^+_{n_1}|0\rangle$$

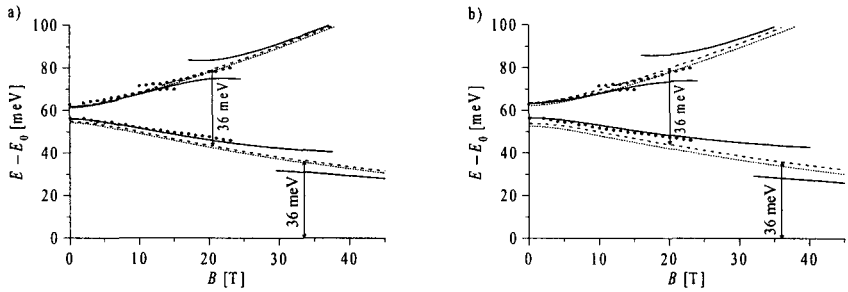

Figure 1. Polaron resonances in a weakly elliptical quantum dot in the presence of magnetic field for (a) $\alpha = 0.07$ and (b), $\alpha = 0.15$ (the other system parameters are fitted to the experimental data of Ref.[12]). Bare electron levels $\epsilon_n(\mathbf{B}) - \epsilon_0(\mathbf{B})$ (3a,3c) (dotted lines), the shifted polaron levels $E_n^{(1)}(\mathbf{B}) - E_0^{(1)}(\mathbf{B})$ (12) (dashed lines), branches of polaron levels split in the vicinity of resonances $E_n(\mathbf{B}) - E_0(\mathbf{B})$ (solid lines), and the experimental data[12] (dots).

and

$$\beta_{\mathbf{k}}^{+}|0\rangle \simeq b_{\mathbf{k}}^{+}|0\rangle$$

($|0\rangle$ is the state without particles and the vacuum is defined by the formulae: $\Psi_0 = a_0^{+}|0\rangle$ and $a_n\Psi_0 = b_{\mathbf{k}}\Psi_0 = c_{\mathbf{q}s}\Psi_0 = 0$ for all $\mathbf{k}$, $\mathbf{q}$ and $n \neq 0$).

Let us denote for future convenience

$$E_n^{(1)} = \epsilon_n - \frac{1}{\hbar\Omega} J_{nn} \tag{12}$$

(these entities are approximations to the polaron energy levels, but they are insensitive to polaron-phonon resonances; see Fig. 1).

The factors $J_{nn'}$ in the harmonic approximation are

$$J_{nn'} = j_{nn'} \frac{\sqrt{\pi}}{2} \alpha\hbar^2\Omega\sqrt{\omega\Omega}, \tag{13}$$

where the values of the coefficients $j_{nn'}$ for the our weakly elliptical quantum dot are given below.

n	0	+	−
0	1	$\frac{1}{4}$	$\frac{1}{4}$
+	$\frac{1}{4}$	$\frac{11}{16} + \frac{2}{8}\lvert c_+c_-\rvert^2$	$\frac{3}{16} - \frac{5}{8}\lvert c_+c_-\rvert^2$
−	$\frac{1}{4}$	$\frac{3}{16} - \frac{5}{8}\lvert c_+c_-\rvert^2$	$\frac{11}{16} + \frac{2}{8}\lvert c_+c_-\rvert^2$.

For GaAs, with $\hbar\Omega \simeq 36$ meV and $\alpha \sim 0.1$ (for electrons confined in the QD with diameter of order of 20 nm[12]), we have

$$\frac{J_{nn'}}{(\hbar\Omega)^2} \ll 1,$$

which highly simplifies the further analysis.

First, let us consider the non-resonant situation, i.e. when

$$E_n^{(1)} - E_{n'}^{(1)} - \hbar\Omega \neq 0 \quad (\sim \hbar\Omega).$$

In this case the eigenvalues E_n differ only slightly from $E_n^{(1)}$ and one can replace the former with the latter in the denominator of Eq. (11). Thus, outside the resonance region we have

$$E_n \approx E_n^{(1)} + \sum_{n' \neq n} \frac{J_{nn'}}{E_n^{(1)} - E_{n'}^{(1)} - \hbar\Omega}.$$

Now we can proceed to the examination of the Eq. (11) near the one-phonon resonance between the levels n_1 and n_2, i.e. in the case of

$$E_{n_1}^{(1)} - E_{n_2}^{(1)} - \hbar\Omega = 0. \tag{14}$$

Let us introduce the following notation for the energy level shifts: $\Delta E_n = E_n - E_n^{(1)}$, $\Delta E_{n_1 n_2} = \Delta E_{n_1} - \Delta E_{n_2}$ and $E_{n_1 n_2} = \frac{1}{2}(\Delta E_{n_1} + \Delta E_{n_2})$. Then we find from the self-consistent Eq. (11)

$$\Delta E_{n_1 n_2} = \frac{J_{n_1 n_2}}{\Delta E_{n_1 n_2} + f_{n_1 n_2}} - \frac{J_{n_1 n_2}}{-\Delta E_{n_1 n_2} + f_{n_2 n_1}} + \sum_{n' \neq n_1, n_2} \left(\frac{J_{n_1 n'}}{\Delta E_{n_1 n'} + f_{n_1 n'}} - \frac{J_{n_2 n'}}{\Delta E_{n_2 n'} + f_{n_2 n'}} \right),$$

where $f_{n_1 n_2} = E_{n_1}^{(1)} - E_{n_2}^{(1)} - \hbar\Omega$. As $|f_{n_2 n_1}| \simeq 2\hbar\Omega \gg \sqrt{J_{n_1 n_2}}$, $|f_{n_1 n_2}| \simeq 0$ (near the resonance) and $|f_{n_1 n'}| \sim |f_{n_2 n'}| \sim \hbar\Omega \gg \sqrt{J_{n_{1,2} n'}}$, then

$$\Delta E_{n_1 n_2} \simeq \frac{J_{n_1 n_2}}{\Delta E_{n_1 n_2} + f_{n_1 n_2}}.$$

The above equation has the simple solution

$$\Delta E_{n_1 n_2}^{\pm} = -f_{n_1 n_2}/2 \pm \sqrt{(f_{n_1 n_2}/2)^2 + J_{n_1 n_2}}$$

(at the resonance point $f_{n_1 n_2} = 0$). The $\pm$ pair of the solutions corresponds to the usual splitting of the polaron energy near the resonance. In order to find E_{n_1} and E_{n_2} it is necessary to find also $E_{n_1 n_2}$ via solution of the equation:

$$E_{n_1 n_2} = \frac{1}{2}\left(\frac{J_{n_1 n_2}}{\Delta E_{n_1 n_2} + f_{n_1 n_2}} + \frac{J_{n_1 n_2}}{-\Delta E_{n_1 n_2} + f_{n_2 n_1}} \right) + \frac{1}{2} \sum_{n' \neq n_1, n_2} \left(\frac{J_{n_1 n'}}{\Delta E_{n_1 n'} + f_{n_1 n'}} + \frac{J_{n_2 n'}}{\Delta E_{n_2 n'} + f_{n_2 n'}} \right).$$

From this equation one finds

$$E_{n_1 n_2} \simeq \frac{1}{2}\Delta E_{n_1 n_2} + \Delta E_{n_1 n_2} \frac{J_{n_1 n_2}}{(2\hbar\Omega)^2} + \frac{J_{n_1 n_2}}{2\hbar\Omega} + \sum_{n' \neq n_1, n_2} \frac{J_{n_2 n'}}{\Delta E_{n_2 n'} + f_{n_2 n'}}.$$

Hence, one can write out the splittings for both states:

$$\Delta E_{n_1}^{+} - \Delta E_{n_1}^{-} = 2\sqrt{(f_{n_1 n_2}/2)^2 + J_{n_1 n_2}}$$

and

$$\Delta E_{n_2}^{+} - \Delta E_{n_2}^{-} = 2\frac{J_{n_1 n_2}}{(2\hbar\Omega)^2}\sqrt{(f_{n_1 n_2}/2)^2 + J_{n_1 n_2}}$$

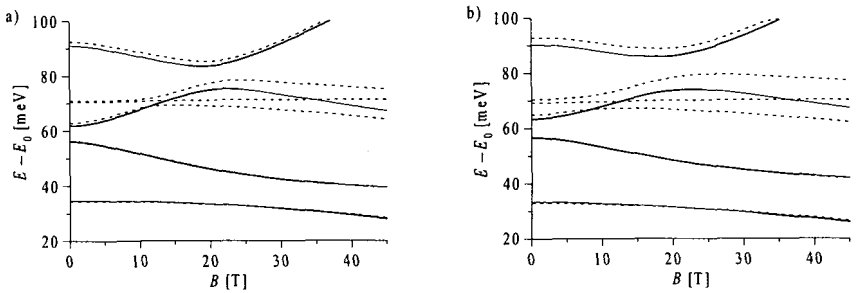

Figure 2. Polaron spectrum in a weakly elliptical quantum dot in the presence of magnetic field for (a) α=0.07 and (b) $\alpha = 0.15$. In both cases the approximate analytical results (solid lines) are compared to the exact numerical ones (dashed lines).

We see that only the upper state (i.e. n_1 as $E_{n_1} > E_{n_2}$) splits. The splitting of the lower one has to be neglected due to the small factor $\frac{J_{n_1 n_2}}{(2\hbar\Omega)^2}$. This behavior is depicted in the Fig. 1 for two resonances in our model three-state system. The first resonance takes place between the states '$-$' and '0' (at the magnetic field $B_1 \simeq$ 36 T) and the second one between the states '+' and '$-$' (at the field $B_2 \simeq 20$ T).

The diagonalization of the Hamiltonian H_0 was also performed numerically for the phononic occupation numbers limited to $0, \ldots, 3$. We have checked that allowing higher occupation numbers does not affect the obtained spectrum within the interesting energy range. The results, after deleting purely phononic modes, are shown in the Fig. 2. We find out that the exact numerical diagonalization confirms the picture found by the Davydov method. For the lower resonance (between the '0' and '$-$' states) the coincidence between the two treatments is excellent, while for the other resonances, the exact behavior is reproduced with satisfactory accuracy, slightly decreased by the approximate methods of analytical solution of the Davydov equation (11).

4 Relaxation rates for polaron

Apart from the system spectrum, the Davydov transformation allows also for a convenient description of the relaxation processes, including the coherent polaronic effects. Let us study the second term in the Hamiltonian (4), i.e. H_1, responsible for the electron–LA phonon interaction and for the anharmonic phonon decay. Upon the canonical transformation e^{S} the two terms of H_1 attain the following form:

$$H_1 = \frac{1}{\sqrt{N}} \sum_{n_1 n_2, \mathbf{q}} F^{\mathrm{a}}_{n_1 n_2}(\mathbf{q}) \alpha^\dagger_{n_1} \alpha_{n_2} (c_{l,\mathbf{q}} + c^\dagger_{l,-\mathbf{q}}) \qquad (15)$$
$$+ \sum_{\mathbf{k}_1, \mathbf{k}_2, \mathbf{q}} W(\mathbf{k}_1, \mathbf{k}_2, \mathbf{q}) \delta_{\mathbf{k}_1, \mathbf{k}_2 + \mathbf{q}} \beta^\dagger_{\mathbf{k}_1} \beta_{\mathbf{k}_2} (c_{\mathrm{t},\mathbf{q}} + c^\dagger_{\mathrm{t},-\mathbf{q}})$$
$$+ \sum_{n_1 n_2, \mathbf{q}, \mathbf{k}, s} \tilde{W}^s_{n_1 n_2}(\mathbf{q}, \mathbf{k}) \alpha^\dagger_{n_1} \alpha_{n_2} \beta_{\mathbf{k}} (c_{s,\mathbf{q}} + c^\dagger_{s,\mathbf{q}}) + h.c.,$$

where

$$\tilde{W}^{\rm t}_{n_1n_2}(\mathbf{q},\mathbf{k}) = -\frac{1}{\sqrt{N}}\frac{F^{\rm o}_{n_1n_2}(\mathbf{k}+\mathbf{q})W(\mathbf{k}+\mathbf{q},\mathbf{k},\mathbf{q})}{E_{n_2}-E_{n_1}+\hbar\Omega}, \tag{16}$$

and

$$\tilde{W}^{\rm l}_{n_1n_2}(\mathbf{q},\mathbf{k}) = -\frac{1}{N}\sum_{n_3}\left[\frac{F^{\rm o}_{n_1n_3}(\mathbf{k})F^{\rm a}_{n_3n_2}(\mathbf{q})}{E_{n_3}-E_{n_1}+\hbar\Omega} - \frac{F^{\rm o}_{n_3n_2}(\mathbf{k})F^{\rm a}_{n_1n_3}(\mathbf{q})}{E_{n_2}-E_{n_3}+\hbar\Omega}\right]. \tag{17}$$

The first term in the transformed Hamiltonian H_1 (15) describes the polaron–LA phonon interaction (note that it has the same coupling energy as it was for electron-LA phonon interaction), the second term describes anharmonic interaction of LO phonons (almost unaffected by the canonical transformation) with TA phonons (again with the same energy as without the coherent effects), whereas the last term describes the relaxation of the polaron. The LO–TA anharmonicity induced relaxation channel corresponds to Eq. (16) while the LO–LA channel to Eq. (17). Both these channels lead to a change of the polaron state accompanied by the creation or annihilation of a pair of phonons: the optical and the acoustical one. There are four possibilities for this process with probabilities (according to the Fermi golden rule)

$$w^{x,y;s}_{n_1n_2}(\mathbf{q},\mathbf{k}) = \frac{2\pi}{\hbar}|\tilde{W}^s(n_1n_2,(x\cdot y)\mathbf{q},\mathbf{k})|^2(N_{\mathbf{k}}+\eta_x)(\nu_{s,\mathbf{q}}+\eta_y)\delta(E_{n_1}-E_{n_2}-x\hbar\Omega-y\hbar\omega_{s,\mathbf{q}}), \tag{18}$$

where x (y) $= \pm$ and $+$ corresponds to emission and - to absorption of an optical (acoustical) phonon, respectively, and $\eta_+ = 1$, $\eta_- = 0$ ($N_{\mathbf{k}}$, $\nu_{\mathbf{q},s}$ - temperature dependent occupation numbers of LO phonons in the $\mathbf{k}$ state and of acoustical phonons in the state $\mathbf{q}$ and polarization s, respectively).

At sufficiently low temperatures (for GaAs at $T < 11$ K [17]), the phonon occupation numbers are negligible and the only contribution is from the process of polaron transition with simultaneous emission of two phonons; the corresponding probability is $w^{++}_{n1,n2}(\mathbf{q},\mathbf{k})$. The relaxation probability for this process is given by the sum

$$w_{n_1\to n_2} = \sum_{\mathbf{k},\mathbf{q},s} w^{++}_{n_1n_2}(\mathbf{q},\mathbf{k}).$$

For the third order phonon–phonon coupling strength with one long-wavelength acoustical phonon involved we have [18]

$$|W(\mathbf{k}+\mathbf{q},\mathbf{k},\mathbf{q})|^2 = \frac{\gamma^2}{N}q.$$

Thus, assuming that γ is independent of $\mathbf{k}$ (as $\mathbf{k}$ are near the Γ point for GaAs[19]), the relaxation probability via the LO–TA channel may be written as

$$w^{(\rm t)}_{n_1\to n_2} = \frac{2}{\pi}\frac{J_{n_1n_2}\gamma^2 q_{\rm t} v}{\hbar^4 C_{\rm t}^3}, \tag{19}$$

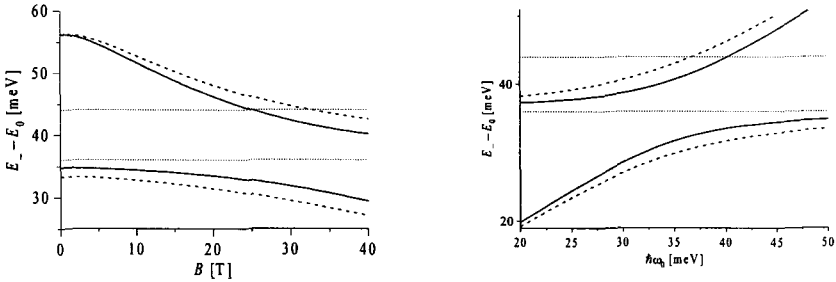

Figure 3. Two branches of the $E_- - E_0$ polaron energy difference compared with the energy sector where the LO-TA polaron relaxation is possible (shown by dotted lines) ($T = 0$) for $\alpha = 0.07$ (solid lines) and $\alpha = 0.15$ (dashed lines): (a) for various magnetic fields; (b) at $B = 0$, for various confinement energies $\hbar\omega_0$.

where C_t is the sound velocity for the transversal phonons and $q_t = (E_{n_1} - E_{n_2} - \hbar\Omega)/\hbar C_t$ (limited by the maximal frequency for TA phonons).

Let us now estimate the polaron relaxation rate for this anharmonicity induced LO–TA channel. We restrict ourselves to the polaron relaxation from the '$-$' state to the ground state 0. For the LO–TA process at low temperatures only phonon emission is possible. The energy conservation restricts this process to a certain energy range, related to the maximum energy of the TA phonon, ~ 8 meV (indicated by the dotted lines in the Fig. 3). Thus, this channel of polaron relaxation is ineffective for magnetic fields $B < 33$ T and $B < 25$ T for $\alpha = 0.15$ and $\alpha = 0.07$, respectively. This situation is characteristic of a dot with the confinement energy $\hbar\omega_0$ exceeding the phonon energy $\hbar\Omega$ by several meV. For comparison, the same two branches of the first excited state at $B = 0$ for various dot confinements are shown in the inset in the Fig. 3. The relaxation channel by the LO–TA phonon emission from the physically important, stable polaronic branch is possible only if $\hbar\omega_0 < 40$ meV. Similarly, the process with TA phonon absorption at non-zero temperatures is also possible only in a relatively narrow sector of confinement energies.

For a quantitative estimation of the corresponding relaxation rate the value of the anharmonic phonon–phonon coupling constant is needed; it can be fitted using the experimental data for GaAs bulk [17]. For GaAs, the dominant anharmonic process involves TA phonons with $\mathbf{q}$ in the vicinity of the L point in the Brillouin zone [17]. At low temperatures, for GaAs bulk, we find for the LO phonon lifetime

$$\tau_{\mathrm{LO}} = w^{-1} = \frac{\pi\hbar^2\tilde{c}}{\gamma^2 v q_0^3 \mu},$$

where the factor μ accounts for anisotropy effects and q_0 corresponds to the vicinity of the L point. From the experimental data for phonon dispersions in GaAs[20] one can notice that the energy conservation needed for the considered channel of LO phonon decay is satisfied along the L–W line on the hexagonal zone wall but it is violated towards the Σ line. It therefore seems reasonable to assume that $\mu \approx 0.4$. From the phonon dispersion curves it also results that on the Γ–L line near L point

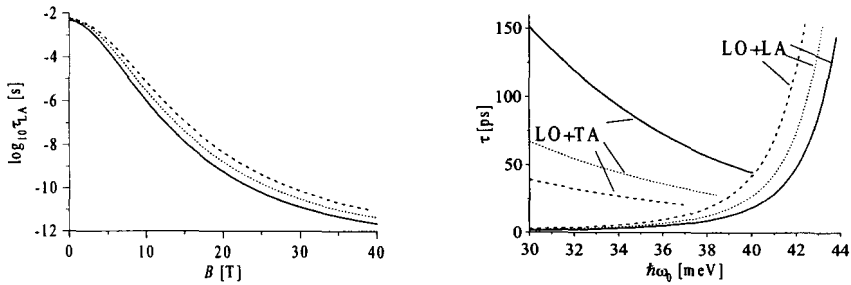

Figure 4. (a) Polaron relaxation time from the '−' level with respect to the LO-LA emission ($T = 0$) for $\alpha = 0.07$ (solid line), $\alpha = 0.11$ (dotted line) and $\alpha = 0.15$ (dashed line). (b) Relaxation times with respect to the LO-TA anharmonicity induced channel and to the LO–LA channel for various dots at $B = 0$. For strong confinements the LO–TA channel is forbidden by energy conservation.

one has the group velocity of longitudinal phonons $\tilde{c} \approx 0.6C_{\rm t}$. Using the lifetime $\tau_{\rm LO} = 9.2$ ps at $T = 6$ K reported in Ref. [17], one can thus estimate the γ factor. Using this value, the lifetime for the polaron in a GaAs self-assembled quantum dot with respect to the LO–TA relaxation channel can be estimated. The polaron relaxation times obtained in this way are even of order of 10 ps (but only in the region of very high magnetic fields - cf. Fig. 4).

The LO–LA channel may be responsible for polaron relaxation in a wider range of magnetic fields due to the much higher energies of the LA phonons in GaAs (up to 24 meV[20]). The probability of relaxation has the form [retaining only the largest terms in $\tilde{W}^{1}_{n_1 n_2}(\mathbf{q}, \mathbf{k})$]:

$$w^{(\rm l)}_{n_1 \to n_2} = \frac{\sigma^2 J_{n_1 n_2}}{4\pi\varrho\hbar^3 C_{\rm l}^4 q_{\rm l} l_{\rm B}^2} \mathcal{J}_{n_1 n_2}, \tag{20}$$

where $q_{\rm l} = (E_{n_1} - E_{n_2} - \hbar\Omega)/\hbar C_{\rm l}$ (limited by the maximal frequency for LA phonons) and

$$\mathcal{J}_{n_1 n_2} = l_{\rm B}^2 \int d^3\mathbf{q} |\mathcal{F}_{n_2 n_2}(\mathbf{q}) - \mathcal{F}_{n_1 n_1}(\mathbf{q})|^2 \delta(q - q_{\rm l}).$$

For the initial state '−' and the final state 0 one has

$$\mathcal{J}_{-0} = \left(1 + 2|c_+ c_-|^2\right) \frac{(q_{\rm a} l_{\rm B})^6}{15} M\left(3, \frac{7}{2}, -\frac{1}{2}(l_{\rm B}^2 - l_z^2) q_{\rm l}^2\right) e^{-\frac{1}{2}(q_{\rm l} l_z)^2}, \tag{21}$$

where M is the degenerated hypergeometric function [21].

The polaron relaxation time with respect to the LO-LA channel for various magnetic fields and dot sizes is plotted in the Fig. 4. It is clear that for the self-assembled dot discussed here, with $\hbar\omega_0 \simeq 58$ meV, the initial state is very long-living for any practically attainable magnetic field. This is due to the well-known bottleneck mechanism [22], where the emission of short-wavelength phonons is strongly suppressed in a confined system. It is essential to note that, unlike the bare

electronic levels, the polaronic energy levels never approach the resonant LO phonon energy (anti-crossing effect). The combined LO-LA phonon emission/absorption is therefore less probable than that obtained by the perturbation theory methods[14,19] and the polaron lifetimes are long at realistic magnetic fields (cf. Fig 4). A rather unexpected effect is also related to the fact that increasing the electron-phonon coupling (the Fröhlich constant) broadens the anti-crossing and thus strengthens the bottleneck mechanism [due to the exponential factor in (21)].

The efficiency of the bottleneck mechanism crucially depends, however, on the dot size (i.e. its confinement energy). The lifetime becomes very short when the confinement energy is close to the resonance with LO phonons (cf. Fig. 4b). Only when the confinement becomes stronger (roughly $\hbar\omega_0 > 40$ meV, cf. Fig. 3b), the LO–TA channel is excluded by the energy conservation and the LO–LA channel is strongly suppressed due to the geometrical confinement (bottleneck) effects (see Fig. 4b).

5 Fröhlich constant for electron confined in the quantum dot

In the definition of $F^{\mathrm{o}}_{n_1 n_2}(\mathbf{k})$ [in Eq. (6)] it is customary to rearrange the coefficients, namely $F^{\mathrm{o}}_{n_1 n_2}(\mathbf{k}) = \sqrt{4\pi\alpha}\hbar\Omega\frac{1}{\sqrt{vQ_0^3}}\frac{Q_0\mathcal{F}}{k}{}_{n_1 n_2}(\mathbf{k})$, where $Q_0 = \sqrt{\frac{2m^*\Omega}{\hbar}}$ and α is the dimensionless Fröhlich constant,

$$\alpha = \frac{e^2}{\tilde{\epsilon}}\sqrt{\frac{m^*}{2\hbar^3\Omega}}, \quad \frac{1}{\tilde{\epsilon}} = \frac{1}{\epsilon_\infty} - \frac{1}{\epsilon_0}. \tag{22}$$

If we take (as for bulk GaAs) $\epsilon_0 = 12.9$, $\epsilon_\infty = 10.9$, $m^* = 0.067\,m_e$, and $\hbar\Omega = 36$ meV, then $\alpha = 0.071$, and this value has been verified experimentally in bulk GaAs[24]. However, for the electrons confined on the nanometer scale, as in a InAs/GaAs self-assembled dot with a radius of order of 10 nm, the recent experimental data on far-infrared attenuation[12] indicated that $\alpha \approx 0.15$.

The enhancement of the electron-LO phonon interaction for QDs manifests itself also via a significant increase of the Huang–Rhys factor[25] for satellite LO phonon-assisted photoluminescence features in III–V quantum dots (InAs/GaAs)[26,27,29], as well as in spherical nanocrystals II–VI[28]. This phenomenon concerns the exciton–LO phonon interaction and the geometrical separation of e-h charges in localized exciton states turns out to be insufficient[26,29] to explain it. Some effects beyond e–h charges separation were invoked, for spherical II-VI dots – the nonadiabaticity[28] and for pyramid-shaped III-V, InAs/GaAs dots – piezoelectricity[29].

It is possible to account for the enhancement of the LO phonon-electron interaction for QDs in phenomenological terms using description by *inertial* and *non-inertial* parts of local crystal polarization. For the electron-LO phonon interaction only the *inertial* part of the local polarization is important. The *non-inertial* part, accompanying the moving electrons, is included into the crystal field which defined both the electron and phonon states. Therefore, the *inertial* polarization of the crystal acting on the free-lattice electrons equals: $\mathbf{P}(\mathbf{r}) = \mathbf{P}_0(\mathbf{r}) - \mathbf{P}_\infty(\mathbf{r})$, where $\mathbf{P}_0 = \frac{\epsilon_0 - 1}{4\pi\epsilon_0}\mathbf{D}$ and $\mathbf{P}_\infty = \frac{\epsilon_\infty - 1}{4\pi\epsilon_\infty}\mathbf{D}$ ($\mathbf{D}$ is the electrical induction) are the static and the high-frequency (of atomic-scale) polarizations, respectively. This formula leads, in a standard manner, to the Fröhlich constant given by Eq.(22) [15].

For the localized electron in a QD, the *inertial* part of the polarization is greater in comparison with the free-moving lattice electron since the quasiclassical velocity of the confined electron ($\sim \frac{\hbar}{m^* d}$) is greater than the velocity of the conducting band electrons (especially near the Γ point). The *inertial* part of polarization acting on electron quickly moving within the dot can thus be written in the form: $\mathbf{P}'(\mathbf{r}) = \mathbf{P}_0(\mathbf{r}) - \eta \mathbf{P}_\infty(\mathbf{r})$, with some factor $0 \leq \eta \leq 1$, depending on the localization scale (given by d - the diameter of the dot). It is clear that $\eta = 1$ when $d \to \infty$ and $\eta = 0$ when d attains dimensions of atoms, i.e. when $d \sim a$ (a - diameter of a unit cell). Therefore, within the linear approximation with respect to the small parameter $\frac{a}{d}$ (or equivalently, linear with respect to the quasiclassical velocity of the confined electron), $\eta = \frac{d-a}{d}$. Hence for the confined electron we have

$$\mathbf{P}'(\mathbf{r}) = \frac{\mathbf{D}}{4\pi\tilde{\epsilon}'}, \tag{23}$$

where

$$\frac{1}{\tilde{\epsilon}'} = \frac{1 - a/d}{\epsilon_\infty} - \frac{1}{\epsilon_0} + \frac{a}{d}. \tag{24}$$

This formula leads to the renormalized Fröhlich constant in the form

$$\alpha' = \frac{e^2}{\tilde{\epsilon}'} \sqrt{\frac{m^*}{2\hbar^3 \Omega}}. \tag{25}$$

For QD with $d \approx 25$ nm, as was reported in Ref. [12], we have $d \approx 40a$ (for GaAs $a \simeq 0.56$ nm), which yields the desired value the of the Fröhlich constant: $\alpha' \approx 0.15$. The formula (25) would also be helpful for the understanding of the enhancement of the Huang-Rhys parameter [26,27,28,29], which scales as α (some further corrections result from the different Fröhlich constant for electrons and holes due to distinct effective mass). For dots of diameter of $\sim 5 - 9$ nm, as reported in Ref. [26], the corresponding $\alpha' \sim 0.4 - 0.3$, and for dots with diameter $\sim 15 - 19$ nm (cf. Ref. [29]), $\alpha' \sim 0.25 - 0.18$. In the former case it gives the factor $6 - 5$ and in the latter $4 - 3$ for the Huang-Rhys parameter, which coincides well with experimental data[26,29].

An additional small renormalization of the Fröhlich constant can also be connected with a change of the effective mass due to localization and strain effects in InAs/GaAs dot. It was theoretically estimated[30] that for the strain-induced InAs/GaAs QD, similar in size to that discussed above, the effective mass $\simeq 0.05\, m_e$. However, this correction does not cause any important change in α as the shift from the bulk value, $\simeq 0.06\, m_e$, is rather small. Additionally, $\alpha \propto \sqrt{m^*}$ resulting in renormalization factor ~ 0.9. Thus, the renormalization due to the change of the effective dielectric constant $\tilde{\epsilon}'$ suggested above is dominant. Note also that for $d > 100a$, the parameter α' does not differ significantly from its bulk value, while for smaller d it increases up to ~ 0.45 at atomic scale.

6 Conclusions

The realistic model of a weakly elliptical InAs/GaAs quantum dot was considered including coupling of electrons to phonons in the presence of magnetic field. The

resulting magneto-polarons were analyzed in details by application of the approximate Davydov diagonalization method. The accuracy of this method was further verified by exact numerical diagonalization of the relevant Fröhlich Hamiltonian. Within the model three-level system, the polaron resonances were found. The relaxation of polarons via the LO–TA anharmonicity induced channel and via the LO–LA channel was investigated. The decay rates were discussed for various magnetic fields and dot dimensions. The appearance of windows of relative inefficiency of relaxation processes was indicated. This can be helpful in optimizing decoherence in semiconductor dot implementations of quantum gates.

The enhancement of the polaron relaxation time, treated as the growth of the upper limit for the decoherence time of polarons, even though significant (at least of one order), is however too small for the need of the error correction procedures for fully optically driven gates in InAs/GaAs quantum dot systems unless the windows of effectiveness of the LO–TA (and LO–LA) channels are avoided. The relatively lower decoherence can be achieved by proper utilizing of dimension dependent bottleneck-like effects and polaronic effects. As the technology of the self-assembled dots imposes strong restrictions on dot dimensions, other quantum dots would be more convenient for implementation of excitonic quantum information processing. The electric field defined dots in ultra-narrow quantum wells might be more promising candidates. They offer much more flexible electronic structure than self-assembled dots including also dots with greater d, i.e. with not so strong phonon-electron coupling. Moreover the metastable excitonic states in electric field defined dots would allow for new methods of their manipulation by magnetic field [31]. The problem consists, however, in technological difficulties of preparation of sufficiently small electrode systems for such structures.

We analyzed the relaxation rates for transitions of polaron from an excited to a ground state, but the phonon mediated effects in QDs can cause also some decoherence of the ground polaron state. If one creates an exciton (the electron–hole pair) in QD within time scale of fs then only the bare electron, rather than the polaron, is tranferred from valence-band-state localized in the QD to the localized conduction-band-state, since the dressing with coherent phonon cloud is an inertial proccess and takes time of order of ps (the adiabatic limit for inclusion of electron-phonon interaction). Thus within this latter, relatively long time the initially bare excited electron (and hole) is being dressed with phonons and finally becomes a polaron, with corresponding significant rearrangement of the wave function even for the ground state – this is a source of an additional decoherence.

Supported by E.E.C. Project No. IST-1999-11311 (SQID) and KBN Project No. PB 2 PO3B 055 18.

References

1. M. Grundmann, *Physica E* **5**, 167 (2000); S. Fafard, K. Hinzer, S. Raymond, M. Dion, J. Mc.Caffrey, Y. Feng, and S. Charbonneau, Science **274**, 1350 (1996).
2. D. Loss and D. P. DiVincenzo, *Phys. Rev. A* **57**, 120 (1998); Ch. Bennet and

D. DiVincenzo, Nature **404** 247 (2000).
3. P. Zanardi and F. Rossi, *Phys. Rev. B* **59**, 8170 (1999); E. Biolatti, R. C. Iotti, P. Zanardi, and F. Rossi, Phys. Rev. Lett. **85**, 5647 (2000).
4. for review e.g. L. Jacak, P. Hawrylak, A. Wojs, *Quantum Dots.* Springer Verlag, Berlin, (1998).
5. T. Lundstrom, W. Schoenfeld, H. Lee, P.M. Petroff, *Science* **286**, 2312 (1999).
6. S. Fafard, *Physica E* **8**, 107 (2000).
7. J. M. Kikkawa and D. D. Awschalom, Phys. Rev. Lett. **80**, 4313 (1998).
8. M. Bayer, P. Hawrylak, K. Hinzer, S. Fafard, M. Korkusinski, Z. R. Wasilewski, O. Stern, A. Forchel, *Science* **291**, 451 (2001).
9. A. Wójs, P. Hawrylak, S. Fafard, and L. Jacak, Phys. Rev. B **54**, 5604 (1996).
10. K. D. Zhu and S. W. Gu, Phys. Lett. A **163**, 435 (1992).
11. A. Chatterjee and S. Mukhopadhyay, Acta Phys. Polon. B **32**, 473 (2001).
12. S. Hameau, Y. Guldner, O. Verzelen, R. Ferreira, G. Bastard, J. Zeman, A. Lemaître, and J. M. Gerard, Phys. Rev. Lett. **83**, 4152 (1999)
13. T. Stauber, R. Zimmermann, and H. Castella, Phys. Rev. B **62**, 7336 (2000).
14. T. Inoshita, H. Sakaki, Phys. Rev. B **46**, 7260 (1992); **56**, R4355 (1997).
15. A. Davydov, G. Pestryakov, Phys. Stat. Sol. (b), **49**, 505 (1972); A. Davydov, *Solid state theory.* Nauka, Moscow, (1976) (in Russian).
16. L. Jacak, J. Krasnyj, D. Jacak, P. Machnikowski, Anharmonicity induced relaxation of polaron in self-assembled InAs/GaAs quantum dot. To appear in Phys. Rev. B, March 2002.
17. F. Vallée, F. Bogani, Phys. Rev. B **43**, 12049 (1991); F. Vallée, Phys. Rev. B **49**, 2460 (1994).
18. E. Lifshitz, L. Pitaevskii, *Physical Kinetics.* Butterworth-Heinemann, Oxford, (1997).
19. O. Verzelen, R. Ferreira and G. Bastard, Phys. Rev. B **62**, R4809 (2000).
20. D. Strauch and B. Dorner, J. Phys: Cond. Matt. **2**, 1457 (1990).
21. M. Abramovitz and I. A. Stegun, *Handbook of Mathematical Functions.* National Bureau of Standards, (1964).
22. U. Bockelmann and G. Bastard, Phys. Rev. B **42**, 8947 (1990).
23. X. Q. Li, Y. Arakawa, Phys. Rev. B **57**, 12285 (1998).
24. S. Adachi, J. Appl. Phys. **58** R1 (1985).
25. K. Huang and A. Rhys, Proc. R. Soc. London (A) **204**, 406 (1950).
26. A. García-Cristóbal, A. W. E.Minnaert, V. M. Fomin, J. T. Devreese, A. Yo. Silov, J. E. M. Haverkort, and J. H. Wolter, Phys. Stat. Sol. (b) **215**, 331 (1999).
27. A. Lemaître, A. D. Ashmore, J. J. Finley, D. J. Mowbray, M. S. Skolnick, M. Hopkinson, T. F. Krauss, Phys.Rev. B **63**, 161309(R) (2001).
28. V. M. Fomin, V. N. Gladilin, J. T. Devreese, E. P. Pokatilov, S. N. Balaban, and S. N. Klimin, Phys.Rev. B **57**, 2415 (1998).
29. R. Heitz, I. Mukhametzhanov, O. Stier, A. Madhukar, and D. Bimberg, Phys. Rev. Lett. **83**, 4654 (1999).
30. C. Pryor, Phys. Rev. Lett. **80**, 3579 (1998).
31. L. Jacak, J. Krasnyj, M. Korkusinski, A. Wojs, Phys. Rev. B **57**, 9069 (1998).

DISCUSSION

Chairman: L. Stodolsky

R. Chiao: I want to ask how these experiments of Awschalom, which show very long spin decoherence times, drives with what you are saying.

L. Jacak: Sorry, because I am not sure that I understand well what you mean. I think that Awschalom results are connected with experiments with extremely quick coherent optical or spin manipulations and are not addressed directly to decoherence in quantum dots which we consider.

Concerning quantum dots, I would like to mention an experiment with observation of exciton entanglement in quantum dots. It is an experiment done by the Forchel group from Würzburg together with Hawrylak from Ottawa and our Ph.D. student Korkusinski. They published these results in January in "Science". They reported an optically observed entanglement of excitons in two vertically stacked quantum dots for various separation of the dots.

R. Chiao: It is true that Awschalom's experiment is not in quantum dots, but the question is, when you did the calculation, and if you apply that to bulk materials as Awschalom has done, what will be values for the spin decoherence time?

L. Jacak: We did not address here the spin decoherence, and I expect that some already known estimations of spin decoherence in quantum dots, up to even microseconds scale, would be very probable for a spin of a single electron, at least. But in the case of the real state-of-the-art quantum dots, that are rather multi-electrons systems, we deal with the effective spin in the last shell, therefore the coupling of spin to orbital degrees of freedom, via Hund-like rules, would preclude these optimistic estimations.

P. Stamp: Why are phonons most important for decoherence?

L. Jacak: It is certainly connected as we are dealing with crystalline medium and in such a situation phonons are a dominating source of disorder, at least for structures like well separated quantum dots, or low level of doping. Moreover, the nanometer scale of confinement in dots leads to the electron energy scale close to the resonance with optical phonons, which results in the strong coupling regime for interaction with optical phonons.

P. Stamp: People suggested a lot of other mechanisms of decoherence in quantum dots, for example coupling to paramagnetic impurities.

L. Jacak: Yes, of course, I agree that various admixtures will result in an additional decoherence.

P. Stamp: And also an obvious question: what about an electron-electron interaction?

L. Jacak: Electron-electron interaction for a quantum dot with a single electron, which we consider, is rather not a problem with respect to the relaxation or decoherence, especially for a dot well separated from the others. Thus the most quick relaxation process is connected with optical phonons, at least in a gallium arsenide medium, which is a weakly polar material. In other materials, nonpolar in particular, the situation would be different.

P. Stamp: According to some experiments, there are relaxation processes as-

sociated with phonons, and they are rapid. Is that right?

L. Jacak: Relaxation induced by phonons is indeed very quick in bulk semiconductors. With respect to the experimental observations of phonon induced relaxations I would refer to the presentation of Professor Raimond.

L. Stodolsky: I would like to make a quick comment about the question of temperature. In our work on SQUIDs we also find surprisingly long decoherence times, around 40 or 50 mK. We use some standard calculations, and if we make a straightforward application we find rather surprisingly long times.

L. Jacak: With respect to the temperature I would like to comment that the measurements of phonons decay in gallium arsenide–bulk, to which we have referred, were done at temperature of order of 10 K, and at this temperature the occupation numbers of phonons were treated as negligible. Thus, to the similar temperature range we can address the zero temperature limit of our calculus, with channels corresponding to emission and not to absorption of phonons. If we go into higher temperature regions, certainly the decoherence and relaxation rates start to be significantly shorter, due to the absorption.

S. Lloyd: Since you take the opportunity to say that you calculate very long decoherence time in SQUIDs, I should emphasize that in the experiments they are very short ones.

P. Stamp: In SQUIDs you have a gap, and in this system you have no gap at all.

L. Jacak: I would like to say that the scale of relaxation time, estimated by us, say of order of 50 or even of 100 picoseconds instead of single picoseconds, seems to be however still insufficient for quantum processing needs and this time scale also probably precludes a chance for successful implementation of error correction procedures in optically driven quantum dot gates.

STIMULATED EMISSION WITH NON-EQUILIBRIUM STATE OF RADIATION

L. ACCARDI*, K. IMAFUKU†, S.V. KOZYREV[1]‡

Centro Vito Volterra, Università di Roma Tor Vergata, 00133 Rome, Italy
N.N. Semenov Institute of Chemical Physics, Russian Academy of Science, 117334 Moscow, Russia[1]

The stimulated emission from an atom interacting with radiation in a non–equilibrium state is considered. The stochastic limit, applied to the non–relativistic QED Hamiltonian, shows that the state of the atom, driven by a non–equilibrium state of the field, approaches a stationary state which can continuously emit photons, unlike the case with an equilibrium state. Non equilibrium states of the radiation field are characterized by a single function of the energy. The Gibbs states are precisely those for which this function is linear. The nonlinearity of the generalized (inverse) temperature function can account for effects previously attributed to so–called "negative temperatures". It also allows to deduce a nonlinear, non-equilibrium, generalization of Einstein's formula describing the detailed balance of the radiation at each frequency in an equilibrium state. We conclude the present paper with the introduction of a general notion of "local KMS condition" as a characterization of local equilibrium states and with the proof of the fact that the non equilibrium states (both for field and atom) considered in the first part of the paper satisfy this condition.

1 Introduction

The basic idea of control of a quantum system is: to drive a system to a pre-assigned state in a given interval of time. For the requirements of quantum information the additional requirement of stability is essential: it is not only required that at time T the system is in a given quantum state, but also that it remains in this state sufficiently long time to allow the manipulations required by quantum computation. One possible way to achieve this goal is to exploit a general principle of the stochastic limit [1,2], namely: *the interaction of a quantum field with a discrete system (e.g. an N-level atom) drives the system to a stationary state which is uniquely determined by the state of the field.* The condition of stationarity guarantees stability, i.e. if no other interaction is switched on, the state of the system will not change. Already now many manipulations on microscopic objects are achieved through their interaction with appropriate fields. This the scenario we are proposing, simply integrates this approach with the additional requirement of stability. The advantage of the stochastic limit approach is that it gives a quite explicit description of the parameters which control the final state of the system. Therefore, if we are able to act on these parameters by suitably choosing the initial state of the field and the interaction, we could drive the system, in a stable way, to a large class of pre-assigned states.

This program leads to an interesting connection between quantum information and non equilibrium physics. In fact the "driving of a system to a stable stationary

*ACCARDI@VOLTERRA.MAT.UNIROMA2.IT
†IMAFUKU@VOLTERRA.MAT.UNIROMA2.IT
‡KOZYREV@MI.RAS.RU

state" is one of the basic topics of analysis in non equilibrium physics. Up to now this problem has been investigated for a rather narrow class of states of the field (mainly vacuum or equilibrium). However we will show that there are also other states of the quantum field which probably are experimentally realizable with contemporary technology, and which can considerably enrich the class of stable atomic states which can be obtained under their driving action. In the following we shall illustrate this idea by analyzing the interaction of a 3–level atom with electromagnetic field. In order to give us not only a good prospect for computation but also a deep insight into the physics, we briefly review the stochastic limit of quantum theory [1,2] and, by applying it to the study of an atom interacting with a radiation field in a non equilibrium state, we show that it can lead to some interesting new results in non–equilibrium physics as well as to a practical implementation of the program described above.

Since Einstein applied Planck's radiation theory to describe the equilibrium state between an atom and field [6], it is well-known that such an equilibrium state can be realized through the detailed balance condition, i.e. the balance in each mode between spontaneous emission and the emission stimulated by the field.

Einstein's detailed balance condition gives the clearest insight into the origin of Planck's radiation formula because, with this approach, we can understand Planck's law on the density of states of the photons as an equilibrium condition on the field, i.e.

$$\rho(\omega)d\omega = \frac{\hbar\omega^3}{\pi^2 c^3}\frac{1}{\exp\left(\frac{\hbar\omega}{kT}\right)-1}d\omega. \tag{1}$$

With the development of nanotechnologies, a controlled emission with a controlled stimulating field has been realized in many experiments. However, in spite of the importance of this technology for the new and most active application of quantum physics, that is quantum communication and computation, the fundamental understanding of the physics is not as clear as the equilibrium case. In this paper we apply the stochastic limit technique to investigate stimulated emission of matter under the influence of a radiation field which is in a non–equilibrium (neither Fock) state.

The general idea, which we illustrate in this paper with a simple but physically interesting example, can be described as follows.

The most commonly used states in quantum field theory are the Fock (vacuum) or Gibbs (equilibrium) states. When a field in such a state interacts with a discrete system (e.g. an atom) in the stochastic limit one obtains a master equation for the system whose stationary state is the ground state of the atom, if the field was originally in the Fock state the Gibbs state of the atom at inverse temperature β, if the field was originally in its equilibrium state at inverse temperature β. The systematic development of the theory of stochastic limit [1] has revealed that the above described phenomenon is quite universal namely: for a large class of states (including many concrete examples which are neither Fock nor equilibrium) the stochastic limit procedure allows deducing master equations whose associated Markov semigroup drives the system to a stationary state ρ_∞ in the sense that,

independently of the initial state ρ_0, one has

$$\lim_{t\to+\infty} P^t\rho_0 = \rho_\infty$$

(P^t is the Markov semigroup).

This fact allows us to give a dynamical characterization of ground (or equilibrium) states of the system (atom) in terms of their response to an interaction with the environment (field) in the weak coupling regime.

From the above considerations it is natural to conjecture that the analysis of stationary states of master equations associated to non equilibrium states of the environment should lead to the introduction of a new class of states, of discrete quantum systems, which should play for non–equilibrium phenomena, a role analogue to that played by Gibbs states for equilibrium phenomena. In the present paper we show that this program can lead to interesting and non trivial physical conclusions even in the case of a single 3–level system interacting with radiation.

The fact that interesting physical phenomena can emerge from relatively simple systems should justify the attempt to produce experimentally these states of the field, just as one has produced vacuum, equilibrium, squeezed,... states. The problem of concretely constructing these non equilibrium states of the EM field will be discussed in a forthcoming paper.

The rest of this paper is arranged as follows: In Sec. 2, we apply the stochastic limit to the non-relativistic QED Hamiltonian and derive two types of equations: one is the so–called rate equation for the atom and the other is a new equation describing the time evolution of the number of photons. This equation cannot be deduced by standard techniques using master equations and requires the full power of the stochastic limit. In Sec. 3, we investigate the radiation emitted from an atom interacting with a non–equilibrium field and discuss its connection with the non–equilibrium current. In Sec. 4, we deduce a formula for the stationary state of a 3-level atom interacting with non-equilibrium EM field. Since this formula is nonlinear (quadratic) generalization of the well known Einstein formula describing the equilibrium of matter with thermal radiation (cf. formula (38) below), we call it the Double Einstein formula. In the second part of the paper, starting from Sec. 5, we try to abstract from the concrete examples of non-equilibrium states, described in the first part of the paper, a general property which should play for (at least a large class of) non equilibrium states, a role analogue to the Kubo-Martin-Schwinger (KMS) characterization of equilibrium states. We individuate the natural candidate for this property in the "local KMS condition" introduced in Sec. 6. The non equilibrium stated introduced in Sec. 2 are shown to satisfy this local KMS condition in Sec. 5. (This is in fact our motivation for the definition given in Sec. 6). Finally, in Sec. 7 we prove that also the atomic stationary state satisfies the local KMS condition with non-linear temperature function which is uniquely expressed by the non-linear temperature function of the field. In other words: a radiation field in local equilibrium function drives the atom to a local equilibrium stationary state. If this function is linear we recover the known fact that a thermal field at inverse temperature β drives the atom to a stationary state which is the Gibbs state (for the free atomic Hamiltonian) at the same temperature.

2 Application of stochastic limit to non-relativistic QED

In this section, we apply the stochastic limit to the non–relativistic QED Hamiltonian and derive two types of equations: one is the so–called rate equation for the atom and the other is a new equation describing the time evolution of the number of photons.

We shall consider an atom interacting with the EM-filed described with the standard non-relativistic QED Hamiltonian

$$H = H_0 + \lambda\, V, \quad H_0 = H_A + H_F \tag{2}$$

where

$$H_A = \frac{p^2}{2m} + V(q) \qquad , \qquad [q,p] = i \tag{3}$$

$$H_F = \int \omega(k) a^\dagger_{k,\sigma} a_{k,\sigma} \qquad , \qquad [a_{k,\sigma}, a^\dagger_{k',\sigma'}] = \delta_{\sigma\sigma'}\delta(k-k') \tag{4}$$

σ is the polarization index ($\sigma = \leftrightarrow, \updownarrow$) and

$$V = \sum_\sigma \int dk \frac{1}{|k|^{1/2}} \varepsilon_{k,\sigma} \left(a_{\sigma,k} e^{ik\cdot q} + a^\dagger_{\sigma,k} e^{-ik\cdot q} \right). \tag{5}$$

In the following discussion we assume that H_A has discrete spectrum: $H_A|\epsilon_a\rangle = \epsilon_a|\epsilon_a\rangle$. The interaction Hamiltonian $V(t)$ in interaction picture can be written as [7]

$$V(t) = \sum_{\omega\in F} \sum_{a,b} \int dk \left(\overline{g_{ab}(k,\sigma)} E^\dagger_\omega \Big(|\epsilon_a\rangle\langle\epsilon_b| \Big) a_{k,\sigma} e^{-i(\omega(k)-\omega)t} + h.c \right) \tag{6}$$

where

$$\overline{g_{ab}(k,\sigma)} = \frac{1}{|k|^{1/2}} \langle\epsilon_a| e^{ik\cdot q} p\cdot\varepsilon_\sigma |\epsilon_b\rangle \tag{7}$$

$$E^\dagger_\omega(X) = \sum_{\epsilon_r \in F_\omega} P_{\epsilon_r} X P_{\epsilon_r - \omega} \qquad , \quad P_{\epsilon_r} := |\epsilon_r\rangle\langle\epsilon_r| \tag{8}$$

$$F = \{\omega = \epsilon_r - \epsilon'_r;\ \epsilon_r, \epsilon'_r \in Spec\ H_A\}, \quad \text{(Bohr frequencies)} \tag{9}$$

$$F_\omega = \{\epsilon_r \in Spec\ H_s;\ \epsilon_r - \omega \in Spec\ H_A\} \tag{10}$$

The stochastic limit describes the quantum dynamics in the regime of weak coupling ($\lambda \to 0$) and large times ($t \to t/\lambda^2$). The main result of this theory is expressed by the stochastic golden rule [1,2] according to which the time rescaling $t \to t/\lambda^2$ induces a frequency dependent rescaling of the quantum field

$$a_{k,\sigma} \to \frac{1}{\lambda} e^{-i\frac{t}{\lambda^2}(\omega(k)-\omega)} a_{k,\sigma} \tag{11}$$

and, in the limit $\lambda \to 0$, for each Bohr frequency ω, the rescaled field (11) becomes a quantum white noise (or master field) $b_{\omega,\sigma}(t,k)$ satisfying the commutation relations

$$[b_{\omega,\sigma}(t,k), b^\dagger_{\omega',\sigma'}(t',k')] = \delta_{\sigma\sigma'}\delta_{\omega\omega'} 2\pi\delta(t-t')\delta(\omega(k)-\omega)\delta(k-k') \tag{12}$$

Moreover, if the initial state of the field is the mean zero gauge invariant Gaussian state (cf. section (2.3) of [1] for this notion) with correlations

$$\langle a_k^\dagger a_{k'} \rangle = N(k)\delta(k-k')$$

then the state of the limit white noise will be of the same type with correlations

$$\langle b_{\omega,\sigma}(t,k) b^\dagger_{\omega',\sigma'}(t',k') \rangle = \delta_{\sigma\sigma'}\delta_{\omega\omega'} 2\pi\delta(t-t')\delta(\omega(k)-\omega)\delta(k-k')N_\sigma(k) \tag{13}$$

$$\langle b^\dagger_{\omega,\sigma}(t,k) b_{\omega',\sigma'}(t',k') \rangle = \delta_{\sigma\sigma'}\delta_{\omega\omega'} 2\pi\delta(t-t')\delta(\omega(k)-\omega)\delta(k-k')(N_\sigma(k)+1) \tag{14}$$

Moreover, in the stochastic limit, the Schrödinger equation becomes a quantum white noise equation which, after having been put in causal normal order (which is different from the usual normal order), takes the form [1,2,7]

$$dU_t = (-idH(t) - Gdt)U_t \quad ; \quad t > 0 \tag{15}$$

with the initial condition $U_0 = 1$ and where $dH(t)$, *called the martingale term*, is the stochastic differential:

$$dH(t) = \sum_{\omega\in F} \sum_{a,b} \int dk \left(\overline{g_{ab}(k,\sigma)} E^\dagger_\omega \left(|\epsilon_a\rangle\langle\epsilon_b| \right) dB_{\omega,\sigma}(t) + E_\omega \left(|\epsilon_a\rangle\langle\epsilon_b| \right) dB^\dagger_{\omega,\sigma}(t) \right) \tag{16}$$

driven by the quantum Brownian motions

$$dB_{\omega,\sigma} = \sum_{\epsilon_a - \epsilon_b = \omega} \int_t^{t+dt} d\tau \int dk \overline{g_{ab}(k,\sigma)} b_{\omega,\sigma}(\tau,k) \tag{17}$$

and the operator G, *called the drift term*, is given by

$$G = \sum_\sigma \sum_{\omega\in F} \left((g|g)^-_{\omega,\sigma} E^\dagger_\omega \left(|\epsilon_a\rangle\langle\epsilon_b| \right) E_\omega \left(|\epsilon_a\rangle\langle\epsilon_b| \right) + \overline{(g|g)}^+_{\omega,\sigma} E_\omega \left(|\epsilon_a\rangle\langle\epsilon_b| \right) E^\dagger_\omega \left(|\epsilon_a\rangle\langle\epsilon_b| \right) \right) \tag{18}$$

$$(g|g)^-_{\omega,\sigma} = \sum_{\epsilon_a - \epsilon_b = \omega} \int dk |g_{ab}(k,\sigma)|^2 \frac{-i(N_\sigma(k)+1)}{\omega(k) - \omega - i0} \tag{19}$$

$$(g|g)^+_{\omega,\sigma} = \sum_{\epsilon_a - \epsilon_b = \omega} \int dk |g_{ab}(k,\sigma)|^2 \frac{-iN_\sigma(k)}{\omega(k) - \omega - i0} \tag{20}$$

With this quantum stochastic differential equation, we can always derive equations for the atom and field, that is, (i) master equation for reduced density operator for the atom [1,2,7], and (ii) equation for the field [8,9].

One should notice that we do not assume the state of the field to be equilibrium. Therefore $N_\sigma(k)$ in (13) and (14) has not necessarily the form

$$N_\sigma(k) = \frac{1}{e^{\beta\omega(k)} - 1}, \quad \left(\beta = \frac{1}{kT} \right)$$

but can be a general positive function (even a positive distribution). In the present paper we will assume that, for some general nonlinear functions $\beta_\sigma(\omega)$, called a "nonlinear temperature function"

$$N_\sigma(k) = \frac{1}{e^{\beta_\sigma(\omega(k))} - 1} \tag{21}$$

Conditions (13) (14), (21) uniquely specify a mean zero gauge invariant Gaussian state which in particular, is invariant under the free evolution (4). Such a state will be called a local equilibrium state in (here the term "local" is referred to the momentum space) of the field. The physical meaning of such a state will be considered in the following sections.

2.1 Rate equation for 3-level atom

In the following we consider a 3-level atom ($\epsilon_1 < \epsilon_2 < \epsilon_3$) whose matrix elements satisfy the conditions (forbidden transitions):

$$\langle \epsilon_1 | e^{ikq} p \cdot \varepsilon_{\updownarrow} | \epsilon_2 \rangle = 0, \quad \langle \epsilon_2 | e^{ikq} p \cdot \varepsilon_{\leftrightarrow} | \epsilon_3 \rangle = \langle \epsilon_1 | e^{ikq} p \cdot \varepsilon_{\leftrightarrow} | \epsilon_3 \rangle = 0, \quad others \neq 0. \tag{22}$$

Notice that condition (22) requires the preparation of the atom in a situation in which the longitudinal ($\updownarrow$) and transverse ($\leftrightarrow$) polarization do not enter symmetrically. This means that the state in Λ-configuration [3,4,5] for the $\updownarrow$-field which the transition $2 \to 1$ is highly privileged for the $\leftrightarrow$-field. We believe that atoms, satisfying condition (22), can be experimentally prepared. In addition, for simplicity, we restrict ourselves to a generic system [7]: this means in our case that the 3 Bohr frequencies ω_{21}, ω_{31}, ω_{32} ($\omega_{jk} = \epsilon_j - \epsilon_k$) are all different among themselves.

Within this setup, the physical meaning of the interaction with non-equilibrium is made clear by the following considerations.

First of all we derive the so-called rate equation for the atom

$$\begin{aligned}
\frac{d}{dt}P_1(t) &= -\left\{2(\gamma^{(+)}_{21,\leftrightarrow} + \gamma^{(+)}_{31,\updownarrow})P_1(t) - 2(\gamma^{(-)}_{21,\leftrightarrow}P_2(t) + \gamma^{(-)}_{31,\updownarrow}P_3(t))\right\} \\
\frac{d}{dt}P_2(t) &= -\left\{2(\gamma^{(-)}_{21,\leftrightarrow} + \gamma^{(+)}_{32,\updownarrow})P_2(t) - 2(\gamma^{(-)}_{32,\updownarrow}P_3(t) + \gamma^{(+)}_{21,\leftrightarrow}P_1(t))\right\} \\
\frac{d}{dt}P_3(t) &= -\left\{2(\gamma^{(-)}_{32,\updownarrow} + \gamma^{(-)}_{31,\updownarrow})P_3(t) - 2(\gamma^{(+)}_{31,\updownarrow}P_1(t) + \gamma^{(+)}_{32,\updownarrow}P_2(t))\right\}
\end{aligned} \tag{23}$$

where $P_j(t) = Tr\Big(\rho_{tot}(0)U_t^\dagger |\epsilon_j\rangle\langle\epsilon_j| U_t\Big)$ with eigenvectors $|\epsilon_j\rangle$ of the system Hamiltonian H_A. It can be proved that the diagonal and off–diagonal terms of the reduced density matrix evolve separately, and that the off–diagonal part vanishes exponentially, cf. [7]. It can be proved that, as $t \to +\infty$, the probability distribution $(P_1(t), P_2(t), P_3(t))$ converges to the unique stationary solution $(P_1(\infty), P_2(\infty), P_3(\infty))$ of equation (23) independently of the initial distribution. The explicit form of $(P_1(\infty), P_2(\infty), P_3(\infty))$ is given in subsection 3 below and shows that it cannot be a Gibbs distribution, at any temperature, associated to the 3–level atomic Hamiltonian. In this sense we say that the radiation field drives the atom to a stationary non equilibrium state.

2.2 Number operator for the Field

The most important addition of the stochastic limit approach to the information deduced from the usual master equations, such as (23), is that it allows to describe the dynamical behavior not only of the system, but also of the environment.

Therefore it is natural to expect that, using this additional information, a more satisfactory description of the non-equilibrium currents could be obtained [8]. To illustrate this idea we consider the time evolution of the number operator of the field:

$$n_\sigma(k) = a^\dagger_{k,\sigma} a_{k,\sigma}, \quad (\sigma = \leftrightarrow, \updownarrow).$$

This operator has constant free evolution (slow degrees of freedom of the field):

$$e^{itH_0} n_\sigma(k) e^{-itH_0} = n_\sigma(k)$$

and therefore it does not change in the stochastic limit. In fact it can be proven (cf. [5,6]) that in the noise space, which is different from the original field space there exists an operator, still denoted $n_\sigma(k)$ which satisfies the following commutation relations with the master fields is as follows

$$\begin{aligned}[b_{\omega,\sigma}(t,k), n_{\sigma'}(k')] &= \lim_{\lambda\to 0} \frac{1}{\lambda} e^{-\frac{it}{\lambda^2}(\omega(k)-\omega)} [a_{\sigma,k}, n_{\sigma'}(k)] \\ &= \lim_{\lambda\to 0} \frac{1}{\lambda} e^{-\frac{it}{\lambda^2}(\omega(k)-\omega)} a_{\sigma,k}\delta_{\sigma\sigma'}\delta(k-k') = b_{\omega,\sigma}(t,k)\delta_{\sigma\sigma'}\delta(k-k'). \qquad (24)\end{aligned}$$

This means that the new number operator, which is different from the usual number operators $b^\dagger_{\omega,\sigma}(t,k)$ of the noise fields, extends the quantum noise algebra. The time evolution of this new number operator is given by:

$$\frac{d}{dt} n_\leftrightarrow(t) = 2\left(\gamma^{(-)}_{21,\leftrightarrow} P_2(t) - \gamma^{(+)}_{21,\leftrightarrow} P_1(t)\right) \qquad (25)$$

$$\frac{d}{dt} n_\updownarrow(t) = 2\left(\gamma^{(-)}_{31,\updownarrow} P_3(t) - \gamma^{(+)}_{31,\updownarrow} P_1(t) + \gamma^{(-)}_{32,\updownarrow} P_3(t) - \gamma^{(+)}_{32,\updownarrow} P_2(t)\right) \qquad (26)$$

where

$$P_j(t) = Tr\Big(\rho_{tot}(0) U_t^\dagger |\epsilon_j\rangle\langle\epsilon_j| U_t\Big), \quad n_\sigma(t) = Tr\Big(\rho_{tot}(0) U_t^\dagger \int dk a^\dagger_{k,\sigma} a_{k,\sigma}\, U_t\Big) \qquad (27)$$

$$\gamma^{(\pm)}_{ij,\sigma} = \mathrm{Re}(g|g)^\pm_{\omega_{ij},\sigma}, \qquad (28)$$

and the $(g|g)^\pm_{\omega_{ij},\sigma}$ are given by (19) and (20).

3 Radiation from the non-equilibrium stationary state

Now let us investigate the radiation from the stationary but non-equilibrium state of the atom. From equation (23), one can easily find that the stationary solution $(t \to \infty)$ is characterized by the following relations:

$$\frac{P_2(\infty)}{P_1(\infty)} = \frac{\gamma^{(-)}_{31,\updownarrow}\gamma^{(+)}_{21,\leftrightarrow} + \gamma^{(-)}_{32,\updownarrow}\gamma^{(+)}_{21,\leftrightarrow} + \gamma^{(+)}_{31,\updownarrow}\gamma^{(-)}_{32,\updownarrow}}{\gamma^{(-)}_{31,\updownarrow}\gamma^{(-)}_{21,\leftrightarrow} + \gamma^{(-)}_{31,\updownarrow}\gamma^{(+)}_{32,\updownarrow} + \gamma^{(-)}_{32,\updownarrow}\gamma^{(-)}_{21,\leftrightarrow}} =: A$$

$$\frac{P_3(\infty)}{P_1(\infty)} = \frac{\gamma^{(+)}_{31,\updownarrow}\gamma^{(-)}_{21,\leftrightarrow} + \gamma^{(+)}_{32,\updownarrow}\gamma^{(+)}_{21,\leftrightarrow} + \gamma^{(+)}_{31,\updownarrow}\gamma^{(+)}_{32,\updownarrow}}{\gamma^{(-)}_{32,\updownarrow}\gamma^{(-)}_{21,\leftrightarrow} + \gamma^{(-)}_{31,\updownarrow}\gamma^{(-)}_{21,\leftrightarrow} + \gamma^{(-)}_{31,\updownarrow}\gamma^{(+)}_{32,\updownarrow}} =: B$$

$$\frac{P_3(\infty)}{P_2(\infty)} = \frac{\gamma^{(+)}_{32,\updownarrow}\gamma^{(+)}_{21,\leftrightarrow} + \gamma^{(+)}_{31,\updownarrow}\gamma^{(-)}_{21,\leftrightarrow} + \gamma^{(+)}_{32,\updownarrow}\gamma^{(+)}_{31,\updownarrow}}{\gamma^{(-)}_{31,\updownarrow}\gamma^{(+)}_{21,\leftrightarrow} + \gamma^{(-)}_{32,\updownarrow}\gamma^{(+)}_{21,\leftrightarrow} + \gamma^{(+)}_{31,\updownarrow}\gamma^{(-)}_{32,\updownarrow}} =: C \tag{29}$$

Notice that the compatibility condition $AC = B$ is automatically satisfied by the coefficients so that

$$P_1(\infty) = \frac{1}{1+A+B}\,;\; P_2(\infty) = \frac{A}{1+A+B}\,;\; P_3(\infty) = \frac{B}{1+A+B}$$

On the other hand, the equation (25) shows that, if $\gamma^{(-)}_{21,\leftrightarrow}P_2(t) - \gamma^{(+)}_{21,\leftrightarrow}P_1(t) > 0$, i.e. if

$$\frac{P_2(t)}{P_1(t)} > \frac{\gamma^{(+)}_{21,\leftrightarrow}}{\gamma^{(-)}_{21,\leftrightarrow}} \tag{30}$$

then, $n_{\leftrightarrow}(t)$ must increase. Now suppose that equations (25), (26) are referred to an initial time in which the atom is essentially stable in its stationary state. Then we can replace in them $P_j(t)$ by $P_j(\infty)$ and therefore *also in the stationary state of the atom*, $n_{\leftrightarrow}(t)$ must keep increasing if

$$\frac{P_2(\infty)}{P_1(\infty)} > \frac{\gamma^{(+)}_{21,\leftrightarrow}}{\gamma^{(-)}_{21,\leftrightarrow}} \tag{31}$$

is satisfied. This means that, when the stationary state satisfies condition (31), then we observe a continuous emission of $\leftrightarrow$-photon from the atom, stimulated by the initial non–equilibrium state of the field. Notice that, using (29), condition (31) can be written as

$$\frac{\gamma^{(+)}_{21,\leftrightarrow}}{\gamma^{(-)}_{21,\leftrightarrow}} < \frac{\gamma^{(-)}_{31,\updownarrow}\gamma^{(+)}_{21,\leftrightarrow} + \gamma^{(-)}_{32,\updownarrow}\gamma^{(+)}_{21,\leftrightarrow} + \gamma^{(+)}_{31,\updownarrow}\gamma^{(-)}_{32,\updownarrow}}{\gamma^{(-)}_{31,\updownarrow}\gamma^{(-)}_{21,\leftrightarrow} + \gamma^{(-)}_{31,\updownarrow}\gamma^{(+)}_{32,\updownarrow} + \gamma^{(-)}_{32,\updownarrow}\gamma^{(-)}_{21,\leftrightarrow}} \quad \Leftrightarrow \quad \frac{\gamma^{(+)}_{21,\leftrightarrow}}{\gamma^{(-)}_{21,\leftrightarrow}} < \frac{\gamma^{(+)}_{31,\updownarrow}}{\gamma^{(-)}_{31,\updownarrow}}\frac{\gamma^{(-)}_{32,\updownarrow}}{\gamma^{(+)}_{32,\updownarrow}}. \tag{32}$$

Now suppose that the initial photon densities (21) do not depend on polarization i.e., for some nonlinear function $\beta(\omega)$, they are given by:

$$N_{\leftrightarrow}(\omega) = N_{\updownarrow}(\omega) = \frac{1}{e^{\beta(\omega)} - 1}$$

Then condition (32) becomes equivalent to

$$\beta(\omega_{31}) < \beta(\omega_{32}) + \beta(\omega_{21}). \tag{33}$$

Notice that, this process respects the energy-conservation law, in fact one can easily check that

$$\frac{d}{dt}\left(\sum_{j=1}^{3}\epsilon_j P_j(t) + \sum_{\sigma}\int dk\ \omega(k) Tr\Big(\rho_{tot}(0)U_t^{\dagger}a^{\dagger}_{k,\sigma}a_{k,\sigma}\ U_t\Big)\right) = 0, \tag{34}$$

and in the stationary state of the atom this becomes

$$\frac{d}{dt}\varepsilon_{31,\updownarrow}(t) = -\frac{d}{dt}\Big(\varepsilon_{32,\leftrightarrow}(t) + \varepsilon_{21,\leftrightarrow}(t)\Big) \tag{35}$$

where

$$\varepsilon_{ij,\sigma}(t) = \int dk\ \omega(k) Tr\left(\rho_{tot}(0) U_t^\dagger a_{k,\sigma}^\dagger a_{k,\sigma} U_t\right) \delta(\omega(k) - \omega_{ij}). \tag{36}$$

If (33) is satisfied, then the left hand side of (35) is negative and this means that the energy of the $\updownarrow$-field is converted to the energy of the $\leftrightarrow$-field through the stationary state of the atom. This conversion can be considered as an energy current in the non–equilibrium stationary state and this current is consistent with the naive thermodynamical interpretation of $\beta(\omega)$ as temperature in (33). (Similar but more direct considerations on the non-equilibrium thermodynamic current with the stochastic limit are discussed in [9].)

This property is peculiar to the stimulated emission from a non-equilibrium state of the field. In fact the usual Gibbs states are characterized by the fact that the function β in (21) is linear, i.e. $\beta(\omega) = \beta\omega$, and in this case condition (33) can never be satisfied. The non-equilibrium field can therefore drive the atom to a stationary state which can continuously emit photons, and this means that this stationary state gives an example of dissipative structure in the sense of Prigogine [10].

4 The Double Einstein formula

Now let us discuss another aspect of the radiation from the atom with non-equilibrium stationary state. Consider the quotient

$$\frac{\gamma_{ij,\sigma}^{(-)}}{\gamma_{ij,\sigma}^{(+)}} = \frac{N_\sigma(\omega_{ij}) + 1}{N_\sigma(\omega_{ij})}. \tag{37}$$

Recalling that $N_\sigma(\omega)$ is the density of the field quanta at the frequency ω, and comparing formula (37) with the well known formula of radiation theory (Einstein formula)

$$\frac{W_{\text{emission}}}{W_{\text{absorption}}} = \frac{\bar{n}_\omega + 1}{\bar{n}_\omega} \tag{38}$$

giving the quotient of the probability of emission and absorption of a light quantum by an atom[11], we gain some physical intuition of the meaning of the generalized susceptibility. In fact the quotient (38) *...is just that which is necessary to preserve the correct thermal equilibrium of the radiation with the gas...* ([11], p.180).

In the stochastic limit approach this statement can be proven. One can prove that, if the initial state of field is equilibrium, then the dynamics of the atom describes the relaxation to equilibrium state if the atom satisfying the detailed balance condition, i.e.;

$$\frac{P_i}{P_j} = \frac{\bar{n}_{\omega_{ij}} + 1}{\bar{n}_{\omega_{ij}}} \tag{39}$$

In the case of a non-equilibrium state of the field, one sees some interesting phenomena in terms of this formula. In order to make them clear, we consider the extreme case in which the assumptions of Sec.2-1 are satisfied and moreover

$$N_\leftrightarrow(\omega) \ll N_\updownarrow(\omega). \tag{40}$$

In this situation, the relation (29), defining the stationary solution, becomes approximately

$$\frac{P_2}{P_1} \sim \frac{\gamma^{(+)}_{31,\updownarrow}\gamma^{(-)}_{32,\updownarrow}}{\gamma^{(-)}_{32,\updownarrow}\gamma^{(+)}_{31,\updownarrow}} = \frac{N_\updownarrow(\omega_{32})}{N_\updownarrow(\omega_{32})+1}\frac{N_\updownarrow(\omega_{31})+1}{N_\updownarrow(\omega_{31})} \tag{41}$$

$$\frac{P_3}{P_1} \sim \frac{\gamma^{(+)}_{31,\updownarrow}}{\gamma^{(-)}_{31,\updownarrow}} = \frac{N_\updownarrow(\omega_{31})}{N_\updownarrow(\omega_{31})+1} \tag{42}$$

$$\frac{P_3}{P_2} \sim \frac{\gamma^{(+)}_{32,\updownarrow}}{\gamma^{(-)}_{32,\updownarrow}} = \frac{N_\updownarrow(\omega_{32})}{N_\updownarrow(\omega_{32})+1}. \tag{43}$$

The crucial difference between the equilibrium and the non equilibrium situation is the identity

$$\frac{N_\updownarrow(\omega_{32})}{N_\updownarrow(\omega_{32})+1}\frac{N_\updownarrow(\omega_{31})+1}{N_\updownarrow(\omega_{31})} = \frac{N_\updownarrow(\omega_{21})}{N_\updownarrow(\omega_{21})+1} \tag{44}$$

is true if and only if the initial state of the field is equilibrium. In fact, since $\omega_{32} - \omega_{31} = \omega_{21}$, we conclude that the validity of the Einstein relation (38) is equivalent to the linearity of β ($\beta(\omega) = \beta\omega + \mu$) and this characterizes Gibbs states.

The relation (41) for the considered system is natural, since the transition from level 2 to level 1 is supposed to be extremely smaller than the other transitions with the conditions (22) and (40). In this case to jump from level 2 to level 1 the system has to make two consequent jumps: from level 2 to level 3 and then from 3 to 1. Therefore it is natural to represent (41) in the following form:

$$\frac{P_1}{P_2} = \frac{W_{\text{absorption}}}{W_{\text{emission}}}|_{2-3}\frac{W_{\text{emission}}}{W_{\text{absorption}}}|_{1-3} = \frac{N_\updownarrow(\omega_{32})+1}{N_\updownarrow(\omega_{32})}\frac{N_\updownarrow(\omega_{31})}{N_\updownarrow(\omega_{31})+1}. \tag{45}$$

We might call this formula the Double Einstein formula. From (21) we see that (45) is equal to $\exp[\beta(\omega_{32}) - \beta(\omega_{31})]$.

It is obvious that we need at least a 3-level atom to get such a distorted balance state because, since detailed balance means balance at each transition frequency, it follows that, if there is only one such frequency as in a 2-level atom, then every stationary state is a detailed balance state. This distorted balance state should play the role of the *negative temperature* state introduced in the phenomenology of laser systems [12]. Within our setup, the $\updownarrow$-field can be interpreted as the *pumping field* which realizes the so-called inverse population state of atom and the $\leftrightarrow$-field as a *stimulating field* which stimulates the emission from 2 to 1.

5 The non equilibrium Gibbs factor

Definition 1 *For a mean zero gauge invariant (MZGI) stationary process*

$$a^\dagger(t,k')\ ,\ a(t,k) \tag{46}$$

with expectation value $\langle \cdot \rangle$*, the time (auto–)correlation (or 2–point) functions are the distributions*

$$\langle a(0,k)a^\dagger(t,k')\rangle \quad , \quad \langle a^\dagger(t,k')a(0,k)\rangle \tag{47}$$

their Fourier (resp. causal Fourier) transform define the spectral resp. causal spectral functions:

$$\int_{-\infty}^{+\infty} e^{i\omega t}dt\langle a(0,k)a^\dagger(t,k')\rangle \quad , \quad \int_{-\infty}^{+\infty} e^{i\omega t}dt\langle a^\dagger(t,k')a(0,k)\rangle \tag{48}$$

(resp. causal spectral) functions:

$$\int_{-\infty}^{0} e^{i\omega t}dt\langle a(0,k)a^\dagger(t,k')\rangle \quad , \quad \int_{-\infty}^{0} e^{i\omega t}dt\langle a^\dagger(t,k')a(0,k)\rangle \tag{49}$$

In the case of a free evolution

$$a^\dagger(t,k) = e^{it\omega_k}a_k^\dagger \tag{50}$$

and of a δ–correlated state (on the $a_k^\dagger, a_k$–algebra) with *density of particles* $n(k)$

$$\langle a_k^\dagger a_{k'}\rangle =: n(k)\delta(k-k') \tag{51}$$

and *anti–density of particles* $m(k)$

$$\langle a_k a_{k'}^\dagger\rangle =: m(k)\delta(k-k') \tag{52}$$

the Fock spectral function becomes

$$\int_{-\infty}^{+\infty} e^{it(\omega_k-\omega)}dt\langle a_k^\dagger a_{k'}\rangle = 2\pi\delta(\omega_k-\omega)n(k)\delta(k-k') \tag{53}$$

The $a^\dagger a$–(resp $aa^\dagger$–)correlation is also called the Fock (resp. anti–Fock) correlation and the anti–Fock spectral function is

$$\int_{-\infty}^{+\infty} e^{it(\omega_k-\omega)}dt\langle a_k a_{k'}^\dagger\rangle = 2\pi\delta(\omega_k-\omega)m(k)\delta(k-k') \tag{54}$$

Similarly, using the known identity of distribution theory

$$\int_{-\infty}^{0} e^{it\omega}dt = \frac{-i}{\omega - i0} = \pi\delta(\omega) - i\,\mathrm{P.P.}\,\frac{1}{\omega} \tag{55}$$

the causal Fock spectral function becomes

$$\int_{-\infty}^{0} e^{it(\omega_k-\omega)}dt\langle a_k^\dagger a_{k'}\rangle = \pi\delta(\omega_k-\omega)n(k)\delta(k-k') - i\,\mathrm{P.P.}\,\frac{n(k)}{\omega_k-\omega}\delta(k-k') \tag{56}$$

and the causal anti–Fock spectral function

$$\int_{-\infty}^{0} e^{it(\omega_k-\omega)}dt\langle a_k a_{k'}^\dagger\rangle = \pi\delta(\omega_k-\omega)m(k)\delta(k-k') - i\,\mathrm{P.P.}\,\frac{m(k)}{\omega_k-\omega}\delta(k-k') \tag{57}$$

Notice that, both in the Fock and anti–Fock case, the spectral function is equal to twice the real part of the causal spectral function.

Definition 2 *A δ–correlated MZGI state with density of particles $n(k)$ and anti–density of particles $m(k)$ will be called compatible with the evolution (50) if both the density of particles $n(k)$ and the anti–density of particles $m(k)$ are functions of the energy density ω_k:*

$$n(k) = n_0(\omega_k) \qquad ; \qquad m(k) = m_0(\omega_k) \tag{58}$$

for some functions $n_0, m_0 : \mathbb{R} \to \mathbb{R}_+$.

States (MZGI) compatible with an evolution (50) have an important universal property, expressed by the following

Theorem 1 *Let $\langle \cdot \rangle$ be a MZGI δ–correlated state on the $a_k^\dagger, a_k$–algebra with correlations (51), (52) and compatible with the evolution (50). For any pair of test functions f, g, define the smeared creations and annihilation operators*

$$a^\dagger(t,f) := \int dk f(k) e^{it\omega_k} a_k^\dagger \qquad ; \qquad a(t,g) := \int dk \overline{g}(k) e^{-it\omega_k} a_k \tag{59}$$

their Fock and anti–Fock time correlations

$$\langle a(0,g) a^\dagger(t,f) \rangle \qquad ; \qquad \langle a^\dagger(t,f) a(0,g) \rangle \tag{60}$$

and their spectral functions

$$\int dt e^{-it\omega} \langle a^\dagger(t,f) a(0,g) \rangle =: (g|f)_\omega^- \quad ; \quad \int dt e^{-it\omega} \langle a(0,g) a^\dagger(t,f) \rangle =: (g|f)_\omega^+ \tag{61}$$

Then for any real number ω such that both spectral functions are different from zero the quotient $(g|f)_\omega^- / (g|f)_\omega^+$ does not depend on the test functions f, g and the following identity holds:

$$\frac{(g|f)_\omega^-}{(g|f)_\omega^+} = \frac{n(\omega)}{m(\omega)} \tag{62}$$

Remark. The quantities $(g|g)_\omega^\pm$ are called *generalized susceptibilities (or susceptivities)* and contain a great deal of information on the field and its interactions. They play an important role in the stochastic limit.

Proof. Using the forms (53) and (54) for the spectral functions and (61), we find

$$(g|f)_\omega^- = 2\pi \int dk \overline{g}(k) f(k) \delta(\omega_k - \omega) n(\omega_k) = 2\pi n(\omega) \int dk \overline{g}(k) f(k) \delta(\omega_k - \omega) \tag{63}$$

$$(g|f)_\omega^+ = 2\pi \int dk \overline{g}(k) f(k) \delta(\omega_k - \omega) m(\omega_k) = 2\pi m(\omega) \int dk \overline{g}(k) f(k) \delta(\omega_k - \omega) \tag{64}$$

and from this the thesis follows.

Notice that the right hand side of (62) is well defined whenever

$$m(\omega) \neq 0 \tag{65}$$

We will use the notation

$$\frac{n(\omega)}{m(\omega)} =: e^{-\beta(\omega)} \tag{66}$$

and the right hand side of (66) will be called *the non equilibrium Gibbs factor*. It is a natural generalization of the usual Gibbs factor to which it reduces when $\beta(\omega)$ is an affine function of ω:

$$\beta_k = \beta\omega_k + \mu \tag{67}$$

More generally, the following fact is true.

6 The local KMS condition

Recall that, if $\beta > 0$ is a constant, then the β–KMS condition for the two point function is

$$\langle a(0,k)a^\dagger(t+i\beta,k')\rangle = \langle a^\dagger(t,k')a(0,k)\rangle \tag{68}$$

where the identity is meant in the distribution sense. In the case of a free evolution of the form (50) it becomes

$$e^{i(t+i\beta)\omega_{k'}}\langle a_k a_{k'}^\dagger\rangle = e^{it\omega_{k'}}\langle a_{k'}^\dagger a_k\rangle \tag{69}$$

or equivalently

$$e^{-\beta\omega_{k'}}\langle a_k a_{k'}^\dagger\rangle = \langle a_{k'}^\dagger a_k\rangle \tag{70}$$

For a q–Gaussian MZGI equilibrium state this uniquely fixes the 2-point correlations (cf. [1] section (2.10)) to be of the form:

$$\langle a_k^\dagger a_{k'}\rangle =: n(k)\delta(k-k') = \frac{1}{e^{\beta\omega_k} - q}\delta(k-k') \tag{71}$$

$$\langle a_k a_{k'}^\dagger\rangle =: m(k)\delta(k-k') = \frac{e^{\beta\omega_k}}{e^{\beta\omega_k} - q} = (qn(k)+1)\delta(k-k') \tag{72}$$

From (71) and (72) one sees that, in the Bose case ($q=1$) the non equilibrium Gibbs factor

$$\frac{n(k)}{n(k)+1} =: e^{-\beta_k} \tag{73}$$

is well defined whenever $n(k)$ is a function (it might be a distribution).

Using the above remarks and Theorem (3.2.1) of [1] we see that the stochastic limit of a q–Gaussian MZGI thermal field

$$\lim_{\lambda\to 0} \frac{e^{i(\omega_k-\omega)t/\lambda^2}}{\lambda} a_k =: b_t(k) = b_\omega(t,k) \tag{74}$$

is the q–white noise with covariance

$$\langle b_t^\varepsilon(k) b_{t'}^{\varepsilon'}(k')\rangle = \delta(t-t')\int_{-\infty}^{+\infty} e^{i(\omega_k-\omega)\tau}d\tau\langle a_k^\varepsilon a_{k'}^{\varepsilon'}\rangle = \delta(t-t')\delta(\omega_k-\omega)\langle a_k^\varepsilon a_{k'}^{\varepsilon'}\rangle \tag{75}$$

and causal covariance

$$\langle b_t^\varepsilon(k) b_{t'}^{\varepsilon'}(k')\rangle = \delta(t-t')\int_{-\infty}^{0} e^{i(\omega_k-\omega)\tau}d\tau\langle a_k^\varepsilon a_{k'}^{\varepsilon'}\rangle = \delta(t-t')\frac{-i\langle a_k^\varepsilon a_{k'}^{\varepsilon'}\rangle}{\omega_k-\omega-i0} \tag{76}$$

Using (70) and (71), we see that the q–white noise correlations satisfy

$$e^{-\beta\omega}\langle b_t(k)b_{t'}^\dagger(k')\rangle = \langle b_{t'}^\dagger(k')b_t(k)\rangle \tag{77}$$

which corresponds to the β–KMS condition for the trivial evolution

$$b_t(k) \mapsto e^{-i\tau\omega}b_t(k) \qquad \forall t,k \tag{78}$$

For the physical meaning of the evolution (78), cf. [1]section (4.26).

A possible formulation of the local KMS condition is the following

Definition 3 *A state $\langle\cdot\rangle$ on the polynomial algebra a_k, $a_k^\dagger$, is said to satisfy the local KMS condition with temperature function $\beta : \mathbb{R}^d \to \mathbb{R}$ if, for every m, $n \in \mathbb{N}$, $\varepsilon_1,\ldots,\varepsilon_n$, $\eta_1,\ldots,\eta_m \in \{0,1\}$, and with the convenction $x^0 = x^\dagger$, $x^1 = x$ for any operator x, the following identities hold in the sense of distributions.*

$$\langle a_{k_1}^{\eta_1}(0)\ldots a_{k_m}^{\eta_m}(0)a_{h_n}^{\varepsilon_n}(t+i\beta_{h_n})a_{h_{n-1}}^{\varepsilon_{n-1}}(t+i\beta_{h_{n-1}})\ldots a_{h_1}^{\varepsilon_1}(t+i\beta_{h_1})\rangle$$

$$= \langle a_{h_n}^{\varepsilon_n}(t)\ldots a_{h_1}^{\varepsilon_1}(t)a_{k_1}^{\eta_1}(0)\ldots a_{k_m}^{\eta_m}(0)\rangle \tag{79}$$

Lemma 1 *Define the local inverse temperature function by*

$$-\beta(k) := \left(\log\frac{n(k)}{m(k)}\right)\frac{1}{\omega_k} \tag{80}$$

Then the local KMS condition is satisfied by the 2–point functions:

$$\langle a_k(0)a_{k'}^\dagger(t+i\beta(k'))\rangle = \langle a_{k'}^\dagger(t)a_k\rangle \tag{81}$$

$$\langle a_k^\dagger(0)a_{k'}(t+i\beta(k'))\rangle = \langle a_{k'}(t)a_k^\dagger(0)\rangle \tag{82}$$

Proof. In the above notations, one has

$$\langle a_k(0)a_{k'}^\dagger(t+i\beta(k'))\rangle = e^{i(t+i\beta(k'))\omega_{k'}}\langle a_k a_{k'}^\dagger\rangle = e^{-\beta(k')\omega_{k'}}e^{it\omega_{k'}}\langle a_k a_{k'}^\dagger\rangle$$

$$= e^{it\omega_k}\frac{m(k)}{n(k)}n(k)\delta(k-k') = e^{it\omega_{k'}}m(k')\delta(k'-k) = e^{it\omega_{k'}}\langle a_{k'}^\dagger a_k\rangle = \langle a_{k'}^\dagger(t)a_k\rangle$$

and this proves (81). In a similar way one verifies that (82) holds.

Proposition 1 *If the state $\langle\cdot\rangle$ is mean zero gauge invariant and Boson Gaussian then condition (79) is satisfied.*

Proof. By Gaussianity both sides of (79) are reduced to weighted sums of pair correlation functions. Since in both sides of (79) we can distinguish the (h,ε)–terms from the (k,η)–terms and since the pair correlations preserve the order, there will be 3 types of pair correlations:

(i) those of type (h,k)

(ii) those of type (h,h)

(iii) those of type (k,k)

In case (i), due to gauge invariance, the only non zero combinations are of the form $\langle aa^\dagger \rangle$ or $\langle a^\dagger a \rangle$ so we can apply (81) and (82).

In case (ii) the terms are already in the correct order.

In case (iii), again by gauge invariance, the only possibilities are

$$\langle a_h(t+i\beta_h)a^\dagger_{h'}(t+i\beta_{h'})\rangle = e^{-(t+i\beta_h)\omega_h} e^{i(t+i\beta_{h'})\omega_{h'}} \langle a_h a^\dagger_{h'}\rangle$$

$$= e^{it(\omega_{h'}-\omega_h)+(\beta_h\omega_h-\beta_{h'}\omega_{h'})}\delta(h-h')$$

$$= \langle a^\dagger_h(t)a_{h'}(t)\rangle \tag{83}$$

and similarly for the other term.

Since in the Boson case the weight of each pair partition is equal to 1, after the replacements (81), (82), (83) the pair–partition expansion of the left hand side of (79) becomes the pair–partition expansion of the right hand side.

Remark. The validity of the local KMS condition for more general Gaussian states as well as for quantum Markov states is now under investigation.

7 The local KMS condition for discrete Hamiltonians

The following considerations show that, for discrete Hamiltonians, the Local KMS condition allows to distinguish between those general density matrices which commute with a given Hamiltonian and those which are functions of the given Hamiltonian.

Given a discrete specrum Hamiltonian H_s:

$$H_s = \sum_\epsilon \epsilon P_\epsilon \quad , \quad P_\epsilon = |\epsilon\rangle\langle\epsilon| \quad , \quad H_s|\epsilon\rangle = \epsilon|\epsilon\rangle \tag{84}$$

For any complex valued Borel function $f : \mathbb{R} \to \mathbb{C}$ the map $x \mapsto e^{itf(H_s)}xe^{-itf(H_s)}$ is defined by the spectral theorem and one has

$$x(t) := e^{itf(H_s)}xe^{-itf(H_s)} = \sum_{\epsilon,\epsilon'} e^{it(f(\epsilon)-f(\epsilon'))}P_\epsilon x P_{\epsilon'} = \sum_{\delta\in B_f} e^{it\delta}E^f_\delta(x) \tag{85}$$

where

$$B_f := \{f(\epsilon)-f(\epsilon');\ \forall\epsilon,\epsilon'\} \quad , \quad E^f_\delta(x) := \sum_{\epsilon,\epsilon'\ :\ f(\epsilon)-f(\epsilon')=\delta} P_\epsilon x P_{\epsilon'} \tag{86}$$

Theorem For a density matrix ρ and the corresponding state $\langle\ \cdot\ \rangle$ the following are equivalent: (i) There exists a real valued Borel function $\beta : \mathbb{R} \to \mathbb{R}$ such that $\exp -\beta(H_s)H_s$is trace class and

$$\rho = \frac{1}{Z}e^{-\beta(H_s)H_s} \tag{87}$$

(ii) There exists a real valued Borel function $\beta : \mathbb{R} \to \mathbb{R}$ such that $\exp -\beta(H_s)H_s$ is trace class and ρ satisfies the following local KMS condition with respect to the Heisenberg dynamics $x \mapsto e^{itH_s}xe^{-itH_s}$:

$$\forall x, y, t, \quad \langle xy(t+i\beta(H_s))\rangle = \langle y(t)x\rangle \tag{88}$$

where the meaning of $y(t+i\beta(H_s))$ is given by (85).
Proof. (87) $\Rightarrow$ (88)

$$\langle xy(t+i\beta(H_s))\rangle = \mathrm{Tr}\left(\rho x e^{-\beta(H_s)H_s} y(t) e^{+\beta(H_s)H_s}\right) = \frac{1}{Z}\mathrm{Tr}\left(x e^{-\beta(H_s)H_s} y(t)\right) = \tag{89}$$

$$= \mathrm{Tr}\left(y(t)x\rho\right) = \langle y(t)x\rangle \tag{90}$$

(88) $\Rightarrow$ (87). (88) means that for all x, y and for all t

$$\mathrm{Tr}\left(e^{-\beta(H_s)H_s} y(t) e^{+\beta(H_s)H_s}\rho x\right) = \mathrm{Tr}\left(\rho y(t) x\right) \tag{91}$$

Therefore for all y and for all t

$$e^{-\beta(H_s)H_s} y(t) e^{+\beta(H_s)H_s}\rho = \rho y(t) \tag{92}$$

or equivalently, putting $t=0$ and replacing y by $ye^{-\beta(H_s)H_s}$

$$e^{-\beta(H_s)H_s} y\rho = \rho e^{\beta(H_s)H_s} y \tag{93}$$

hence, putting $y=1$

$$e^{\beta(H_s)H_s}\rho = \rho e^{\beta(H_s)H_s} \tag{94}$$

(93),(94) imply that, for all y

$$y e^{\beta(H_s)H_s}\rho = e^{\beta(H_s)H_s}\rho y \tag{95}$$

and this implies that, for some scalar λ

$$e^{\beta(H_s)H_s}\rho = \lambda 1 \tag{96}$$

Since $\mathrm{Tr}(\rho)=1$, (96) implies that

$$\rho = \frac{1}{Z} e^{-\beta(H_s)H_s} \tag{97}$$

Remark 1 When $\beta(H)=\beta$, the state (87) is the Gibbs state with temperature β^{-1} and (88) becomes the KMS condition.
Remark 2 The factor $\beta(\epsilon)$ can be interpreted as a (local) inverse temperature for each eigenstate with the energy eigenvalue ϵ. In this sense condition (88) is a local KMS condition in the sense of energy. The stationary state of the 3-level atom interacting with the non equilibrium state of the field, which has been discussed in the first part of this paper, is exactly of this kind, i.e. it satisfies the local KMS condition.

Acknowledgments

Kentaro Imafuku and Sergei Kozyrev are grateful to Centro Vito Volterra and Luigi Accardi for kind hospitality. This work was partially supported by INTAS 9900545 grant. Kentaro Imafuku is supported by an overseas research fellowship of Japan Science and Technology Corporation. Sergei Kozyrev was partially supported by RFFI 990100866 grant.

References

1. L. Accardi, Y. G. Lu, and I. V. Volovich, *Quantum Theory and Its Stochastic Limit* Springer-Verlag (2002)
2. L. Accardi, A. Frigerio, and Y. G. Lu, Commun. Math. Phys. **131**, 537 (1990); L. Accardi, J. Gough, and Y. G. Lu, Rep. Math. Phys. **36**, 155 (1995); L. Accardi, S. V. Kozyrev, and I. V. Volovich, Phys. Lett. A **260**, 31 (1999)
3. A. Imamoğlu, Phys. Rev. A **40**,2835 (1989); A. Imamoğlu, J.E. Field, and S.E. Harris, Phys. Rev. Lett. **69**, 1154 (1991)
4. O.A. Kocharovskaya and Ya. I. Khanin, Pis'ma Zh. Eksp. Teor. Fiz **48**, 581 (1988). [JETP Lett. **48**, 630 (1988)]; O. Kocharovskaya and P. Mandel, Phys. Rev. A **42**, 523 (1990); O. Kocharovskaya, R-D. Li, and P. Mandel, Opt. Commun. **77**, 36 (1990)
5. Martin Graf and Ennio Arimondo, Phys. Rev. A **51** 4030 (1995); Ennio Arimond, Phys. Rev. A **54** 2216 (1996)
6. Einstein, A. Phys. Z. **18**, 121 (1917)
7. L. Accardi, S.V. Kozyrev, *Quantum interacting particle systems*, Lecture Note of Levico school, September 2000, Preprint Centro Vito Volterra N. 431; World Scientific (2002)
8. L. Accardi, K. Imafuku, and Y. G. Lu, in preparation
9. L. Accardi, K. Imafuku, and Y. G. Lu, Proceedings of the Japan-Italy Joint Waseda Workshop on "Fundamental Problems in Quantum Mechanics", 27-29 September, 2001, Tokyo, Japan. (To be published from World Scientific, 2002)
10. I. Prigogine "Nonequilibrium statistical mechanics" New York, Wiley(1962), P. Glansdorff, I. Prigogine, *Thermodynamic theory of structure, stability and fluctuations* (Wiley-Interscience, London, 1971)
11. W. Heitler, *The quantum theory of radiation*, Oxford University Press, London, 1954
12. See, e.g. H. Haken, In *Encyclopedia of Physics, Vol. XXV/2c, Laser theory* (Springer, Berlin-Heidelberg-New York 1970)

DISCUSSION

Chairman: A. Bohm

B. Misra: What is stochastic limit?

L. Accardi: Stochastic limit, roughly speaking, means the following. You rescale time according to the van Hove prescription $t \to \frac{t}{\lambda^2}$. I underline that this is the only thing which we put by hand. Everything else follows from the fundamental laws of physics. Because of the duality time-energy, this rescaling of time is equivalent to an energy rescaling and, as you can see with some easy calculations, this leads to the fact that the original field in the interaction representation will go into

$$\frac{1}{\lambda} e^{-i\omega_k \frac{t}{\lambda^2}} a_k.$$

So, the rescaling of time is equivalent to this rescaling of the field. And the theorem is this object converges to the quantum white noise. In other words: the rescaled field becomes, in the limit, a white noise. That is why we call it "stochastic limit". It should not be confused with the old "Markovian limit" where you only obtain the master equation. The limit evolution we find is unitary and only after averaging over the noise (i.e. the limit field) we recover the master equation. For the study of nonequilibrium phenomena, such as currents, this additional information is absolutely crucial.

Of course, this is not a fundamental theory. This is an approximation. One might ask: what is the advantage of this approximation? The answer is that, in this approximation, you can read a lot of physics which is hidden in the original Hamiltonian.

For example, if you tried to read in the original Hamiltonian such phenomena like the structure of the non-equilibrium stationary states, or the quadratic Einstein relation, you would find that this is absolutely impossible because the irrelevant scales complicate the picture beyond tractability.

Since we start from the basic laws of physics, the original Hamiltonian describes a huge amount of phenomena belonging to totally different scales of magnitude. We are using a kind of magnification lens to isolate only the scale pertaining to the phenomena we are interested in.

What is new, in my opinion, is that we are not isolating this scale by hand, with vague plausibility arguments, but it is the dynamics itself that isolates the correct order of magnitude of the phenomena.

M. Courbage: When you consider the third level do you mean that the Hamiltonian of the system has continuous spectrum?

L. Accardi: Yes. Discrete spectrum of the system Hamiltonian is typical of the first level. A typical example is the Friedrichs model where discrete spectrum is embedded in the continuum. The first model, which was solved in the level three, was quantum electrodynamics without dipole approximation and the second was the quantum Anderson model, i.e. not the usual model involving classical random potentials but the real quantum Anderson model. And in both cases, very interesting and exciting new phenomena come out. The diagrams are no longer the Gaussian diagrams of the field. We get the non crossing diagrams but not the semicircle law. The noise is not Gaussian in the usual sense. Physics leads to a new probability which is not free probability. The vacuum distribution of the field has the same diagrams of the semicircle law but does not coincide with it. Just as the diagrams for Bose and Fermi fields are the same, but the distributions are quite different.

This also means that the phenomenological models built with random matrices have a deep explanation in real physics, through the stochastic limit.

The new statistics (e.g. new photon statistics) are a consequence of the breaking of the usual commutation relations under strong nonlinearity. It is what we call entanglement. Usually the term entanglement is used just as a synonym of the superposition of composite systems but this use may be not so appropriate. What we call entanglement is the expression of a deeper phenomenon: originally, the atom and the field are kinematically completely independent - the atom variables and

the field variables commute. However, after the stochastic limit, the non-linearity obliges them to take a non-trivial commutation relation.

T. Petrosky: You are partly using the Wigner solution. You said that this is an approximation. Now, you are going already into the regime of the Markov process, so you do not have memory effect.

L. Accardi: Concerning the first comment I want to emphasize that what is usually called the Wigner distribution has nothing to do with the Wigner semi–circle law and the associated noncrossing diagrams. My statement is that the noncrossing diagrams emerge naturally from the dynamics in the third level of the stochastic limit.

My answer to the second comment is: Yes.

G. Pronko: If we consider the same model but with an infinite number of levels, this model may be solved by the Bogolubov transformation because this is a quadratic interaction. Then the property, which you find, is not true.

L. Accardi: First of all let me emphasize again that the stochastic limit is applicable also to a wide class of non quadratic models. But even in the quadratic case there are a lot of interesting phenomena which you can describe with the stochastic limit but not with the original Hamiltonian. In this connection I would like to recall a sentence, which I found in Gordon's 1964 lectures on quantum optics at the Varenna School. He said, in some sense, quantum optics (in dipole approximation) is itself an explicitly solvable model because the equations are linear. The problem is however that you cannot do any physics with them. For more than 40 years the art of quantum optics has been to devise clever approximations of these equations from which one can say something non-trivial.

For example studying the non equilibrium states of a 3–level system we found, with K. Imafuku and S. Kozyrev, an interesting phenomenon and, after some time, we discovered that several papers in the most recent experimental literature on quantum optics were discussing precisely this phenomenon, which is called "amplification without inversion". Facts like this suggest that our approach really captures some hidden physical properties.

EFFECTS OF STATIC IMPERFECTIONS FOR QUANTUM COMPUTING

GIULIANO BENENTI[(a)] and GIULIO CASATI[(a,b)]
[(a)] *International Center for the Study of Dynamical Systems, Università degli Studi dell'Insubria and*

Istituto Nazionale per la Fisica della Materia, Unità di Como, Via Valleggio 11, 22100 Como, Italy

[(b)] *Istituto Nazionale di Fisica Nucleare, Sezione di Milano, Via Celoria 16, 20133 Milano, Italy*

We model the quantum computer hardware as a two-dimensional lattice of qubits with static imperfections, i.e. fluctuations in individual qubit energies and residual short-range inter-qubit couplings. We show that these imperfections can lead to the emergence of quantum chaos and dynamical thermalization also in a quantum computer ideally decoupled from the environment. We discuss their effect on the stability of (i) the quantum computer hardware and (ii) an efficient quantum algorithm simulating a physical model with rich and complex dynamics described by the quantum sawtooth map.

1 Introduction

A quantum computer can perform some computational tasks much more efficiently than a classical computer (for a review see, e.g., [1,2]). Shor [3] constructed a quantum algorithm which performs integer factorization into prime factors exponentially faster than any known classical algorithm. It was also shown by Grover [4] that the search of an item in an unstructured list can be done with a square root speedup over any classical algorithm. These results motivated a great body of experimental proposals for the construction of a realistic quantum computer (see [2] and references therein). While the technological challenge to develop scalable, fault tolerant quantum processors is highly demanding, it is nowadays widely recognized that decoherence, due to the coupling with the environment, will be the ultimate obstacle to the realization of such devices. In addition, even in the ideal case in which the quantum computer is isolated from the external world, a proper operability of the computer is not guaranteed. Internal and unavoidable imperfections in the quantum computer hardware are another source of errors. For example, the energy spacing between the two states of each qubit can fluctuate, e.g., due to magnetic field inhomogeneities in nuclear magnetic resonance quantum processors [2]. Moreover, since qubit interactions are required to operate two-qubit gates and generate entangled states, unwanted residual interactions will appear.

The quantum computer hardware can be modeled as a qubit lattice[5] and one has to consider a quantum many-body (-qubit) interacting system. These systems have been widely investigated in the field of quantum chaos [6] and it is now well known that residual interactions can lead to quantum chaos characterized by ergodicity of the eigenstates and level spacing statistics described by Random Matrix Theory [7]. This means that the properties of the wave functions and energy spectra become so complicated that statistical considerations can be applied to them.

To summarize, it is important to study the stability of quantum information processing in the presence of realistic models of quantum computer hardware imperfections. In the following we discuss two main problems [8,9]:

A) The onset of chaos in the quantum computer hardware, which may lead to occupation number statistics given by the Fermi-Dirac distribution. This means that a strong enough interaction plays the role of a heat bath, thus leading to dynamical thermalization for an isolated system. In such a regime, a quantum computer eigenstate is composed by an exponentially large (with the number of qubits) number of noninteracting multi-qubit states representing the quantum register states. As a result, exponentially many states of the computational basis are mixed after a chaotic time scale [5]. This sets an upper time limit to the stability of a generic superposition of states coded in the quantum computer wave function. In addition, it is clear that a necessary requirement for quantum computer operability and fault tolerant computation schemes is the possibility to operate many quantum gates inside the chaotic time scale.

B) The effect of hardware imperfections on the stability of an efficient quantum algorithm which computes the time evolution of a well known dynamical system – the quantum sawtooth map – exponentially faster than any known classical computation. Since one of the main applications of computers is the simulation of physical systems, it is desirable to find efficient quantum algorithms which describe physical models with rich and complex dynamics. The sawtooth map is a paradigm of classical and quantum chaos and exhibits a variety of different behaviors, from anomalous diffusion to quantum ergodicity and dynamical localization. As we will see, the quantum algorithm which solves the quantum sawtooth map has certain advantages over, e.g., the Shor algorithm, since complex dynamics can be investigated already with less than 10 qubits, making it interesting for the first generation of quantum processors working with a small number of qubits [10,11]. Moreover, this algorithm would provide information inaccessible to classical simulations already with about 40 qubits whereas the Shor algorithm becomes useful only for more than 1000 qubits. Therefore quantum computers could become useful devices for the simulation of important physical problems much before than they can afford basic problems like integer factoring. Our investigations also show a certain stability of quantum computing with respect to imperfection effects.

In Section 2 we discuss a model for the quantum computer hardware; in Section 3 we study the statistical properties of the eigenvalues of this model; in Section 4 we investigate the occupation number distribution and compare different definitions for the effective temperature of the system; in Section 5 we review the main properties of the sawtooth map model; in Section 6 we discuss a quantum algorithm for the sawtooth map and its stability in the presence of static imperfections in the quantum computer hardware; in Section 7 we present our conclusions.

2 The model

We consider a model of n qubits on a two-dimensional lattice with nearest neighbors inter-qubit coupling. The Hamiltonian of this model, introduced in [5], reads:

$$H = \sum_i \Gamma_i \sigma_i^z + \sum_{i<j} J_{ij} \sigma_i^x \sigma_j^x, \quad (1)$$

where the σ_i are the Pauli matrices for the qubit i and the second sum runs over nearest-neighbor qubit pairs on a two-dimensional lattice with periodic boundary conditions applied. The energy spacing between the two states of a qubit is determined by $\Gamma_i = \Delta_0 + \delta_i$, with δ_i randomly and uniformly distributed in the interval $[-\delta/2, \delta/2]$. Therefore the detuning parameter δ gives the width of the Γ_i distribution around its average value Δ_0. For generality we choose the couplings J_{ij}, which represent the residual interaction, randomly and uniformly distributed in the interval $[-J, J]$. The model (1) can be considered as a model for the quantum computer hardware, in which the unavoidable system imperfections generate residual inter-qubit couplings and energy fluctuations. We note that similar Hamiltonian models, but without coupling/detuning fluctuations, have been discussed in different experimental proposals, based, for example, on optical lattices [12], arrays of quantum dots [13] or chains of nuclear spins [14] embedded in a two-dimensional electron system. Fluctuations in the values of δ_i appear due to imperfections, e.g., local magnetic field fluctuations in the proposals [13,14]. Since an inter-qubit coupling is required to operate two-qubit quantum gates, some residual static interaction J between qubits will be unavoidably present. This coupling can originate from spin-exciton exchange [14], exchange interaction between spins of electrons trapped in neighboring quantum dots [13], dipole-dipole interaction between electrons trapped near the surface of liquid helium [15], etc. When the inter-qubit coupling is switched off, for example via a potential barrier created by a point contact gate in the quantum dots proposal [13], some unavoidable residual interaction still remains. Therefore, the model (1) describes the quantum computer hardware, while to study the gate operations in time one should include additional time-dependent terms in the Hamiltonian (see Section 6 below).

At $J = 0$, the noninteracting eigenstates of the model can be written as $|\psi_k\rangle = |\alpha_1, ..., \alpha_n\rangle$, where $\alpha_i = 0, 1$ marks the polarization of qubit i. These are the ideal multi-qubit eigenstates of a quantum computer, the quantum register states used for computer operations. For $J \neq 0$, these states are no longer eigenstates of the Hamiltonian, and the new multi-qubit eigenstates are now linear combinations of different quantum register states.

Here we focus on the case $\delta \ll \Delta_0$, which corresponds to the situation where fluctuations induced by imperfections are relatively weak. In this case, the unperturbed energy spectrum of (1) (corresponding to $J = 0$) is composed of $n + 1$ well separated bands, with interband spacing $2\Delta_0$. Since the δ_i's randomly fluctuate in an interval of size δ, the $J = 0$ bands have a Gaussian shape of width $\Delta_B \approx \sqrt{n}\delta$. The average number of states inside a band N_B is of the order of $N_H/n = 2^n/n$, so that the energy spacing between adjacent multi-qubit states inside one band is

exponentially small in the number of qubits:

$$\Delta_n = \frac{\Delta_B}{N_B} \sim n^{3/2} 2^{-n} \delta. \tag{2}$$

In the presence of a residual interaction $J \sim \delta$, the spectrum still has the above band structure with an exponentially large density of states. For $J, \delta \ll \Delta_0$, the interband coupling is very weak and can be neglected. We concentrate our studies on the central band. It corresponds to the highest density of states, and in a sense represents the quantum computer core. On the other hand, quantum chaos and ergodicity first appear in this band, which therefore sets the limit for the stability of quantum computer hardware. Inside this band, the system properties depend only on the number of qubits n and the dimensionless coupling J/δ.

3 Spectral statistics

As shown in Refs.[5], the quantum chaos border in (1) corresponds to a critical interaction J_c given by:

$$J_c \approx \frac{C\delta}{n}, \tag{3}$$

where C is some numerical constant. Indeed, since the interaction is of a two-body nature, each noninteracting multi-qubit state $|\psi_k\rangle$ has nonzero coupling matrix elements only with about n other multi-qubit states. Therefore, the number of directly coupled states is much smaller than the number of multi-qubit states inside the central band, $N_B = n!/([n/2]!(n - [n/2])!)$ (we consider the band with the number of spins up given by the integer part of $n/2$). These couplings induce transitions in an energy interval of order δ (we assume that J is of the order of or smaller than δ). Therefore the energy spacing between directly coupled states is

$$\Delta_c \sim \delta/n. \tag{4}$$

The transition to chaos takes place for $J = J_c \approx \Delta_c$, which leads to the relation (3).

The border (3) is exponentially larger than the energy spacing between multi-qubit states Δ_n. This is in agreement with previous studies of complex interacting many-body systems [6], in which the transition to quantum chaos takes place when the interaction matrix elements between directly coupled states become larger than their energy spacing.

The transition to quantum chaos and ergodic eigenstates can be detected in the change of the spectral statistics of the system. A convenient way is to look at the level spacing statistics $P(s)$, which gives the probability to find two adjacent levels whose spacing, normalized to the average level spacing, is in $[s, s + ds]$. In fact, $P(s)$ goes from the Poisson distribution $P_P(s) = \exp(-s)$ for nonergodic states to the Wigner-Dyson distribution $P_W(s) = (\pi s/2)\exp(-\pi s^2/4)$, corresponding to Random Matrix Theory, for ergodic states [7].

In Fig.1 we show the level spacing statistics near the band center ($\pm 5\%$ of levels around it) at different coupling strengths J for $n = 16$. The transition from the Poisson to the Wigner-Dyson statistics is evident.

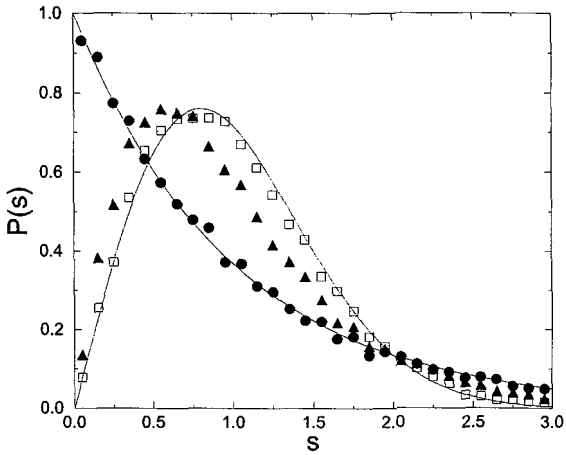

Figure 1: Level spacing statistics at $n = 16$, $J = 0.05\delta$ (circles), $J = 0.2\delta$ (triangles), and $J = 0.4\delta$ (squares). Full curves show Poisson and Wigner-Dyson distributions.

To analyze the change of $P(s)$ with the coupling J one can conveniently use the parameter $\eta = \int_0^{s_0}(P(s) - P_W(s))ds / \int_0^{s_0}(P_P(s) - P_W(s))ds$, where $s_0 = 0.4729...$ is the first intersection point of $P_P(s)$ and $P_W(s)$. In this way $P_P(s)$ corresponds to $\eta = 1$ and $P_W(s)$ to $\eta = 0$. Fig.2 gives the dependence of the parameter η on the scaled coupling Jn/δ at different system sizes, for states near the middle of the energy spectrum [16]. The Poisson to Wigner-Dyson crossover becomes sharper when n increases, suggesting a sharp transition in the thermodynamic limit. One can see that the minimum spreading of curves is for $\eta(J_c) \approx 0.2$, corresponding to $J_c n/\delta \approx 3.7$. We stress that, since the chaos border (3) drops only algebraically with n, it is *exponentially larger* than the multi-qubit energy level spacing, e.g., for $n = 18$, $J_c \approx 0.2\delta \gg \Delta_n \approx 7 \times 10^{-5}\delta$. Therefore a relatively large coupling strength is required for the emergence of quantum chaos: this constitutes a very positive result for quantum computing.

4 Dynamical thermalization

The transition in the level spacing statistics reflects a qualitative change in the structure of the eigenstates [5]. While for $J \ll J_c$ the eigenstates are very close to the quantum register states, for $J > J_c$ each eigenstate $|\phi_m\rangle$b ecomes a superposition of an exponentially large number of noninteracting eigenstates $|\psi_k\rangle$. The mixing takes place inside a Breit-Wigner energy width Γ given by the Fermi golden rule: $\Gamma \sim J^2/\Delta_c \sim J^2 n/\delta$ [5]. As a result, the residual interaction spreads a quantum register state over an exponentially large number of states after a chaotic time scale [5,17]:

$$\tau_\chi \approx \frac{1}{\Gamma} \sim \frac{\delta}{J^2 n}. \qquad (5)$$

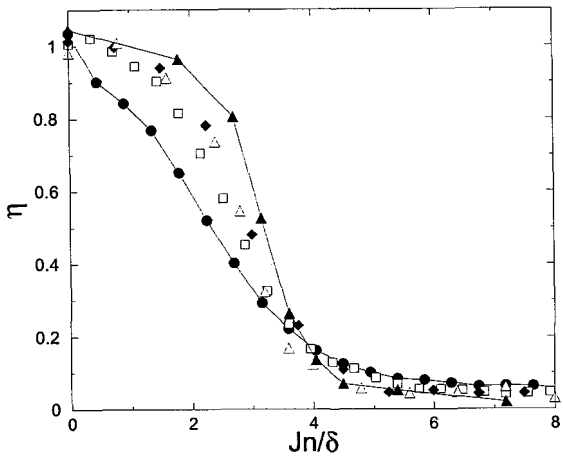

Figure 2: Dependence of η on the scaled coupling Jn/δ, for $n = 9$ qubits (circles), $n = 12$ (squares), $n = 15$ (diamonds), $n = 16$ (empty triangles), and $n = 18$ (filled triangles)

After this time the quantum computer hardware stability is certainly destroyed, unless one can apply quantum error-correcting codes (see [1,2] and references therein) operating on a shorter time scale. We stress that this destruction takes place in an isolated system, without any external decoherence process. It happens due to inter-qubit coupling, which can mimic the effect of a coupling with the external world.

In the following we show that in the quantum chaos regime a statistical description of our isolated n-qubit system is indeed possible, similarly to results found for other physical systems in [18]. We concentrate on the distribution of the occupation numbers n_i, defined as the probability that the qubit (spin) at the site i is in its up polarization state. Given an eigenfunction $|\phi_m\rangle$ with eigenvalue E_m, one can write:

$$n_i(m) = \sum_{k=1}^{N_B} W_{km} \langle \psi_k | \hat{n}_i | \psi_k \rangle, \tag{6}$$

where $\hat{n}_i$ is the occupation number operator, and the term $\langle \psi_k | \hat{n}_i | \psi_k \rangle$ equals 1 or 0 depending on whether the spin at the site $i$is up or down.

For noninteracting qubits one can write, e.g. for the central band,

$$\sum_{i=1}^{n} n_i(m) = \left[\frac{n}{2}\right],$$

$$\sum_{i=1}^{n} n_i(m)\delta_i = E_m^{'}, \quad (n_i(m) = 0, 1), \tag{7}$$

where $E_m^{'} = E_m/2 + \sum_i \delta_i/2$ ($E_m = \sum_i (2n_i(k) - 1)\delta_i$). As $n_i(m) = 0, 1$, the relations (7) are the usual ones used to derive the Fermi-Dirac distribution for an ideal

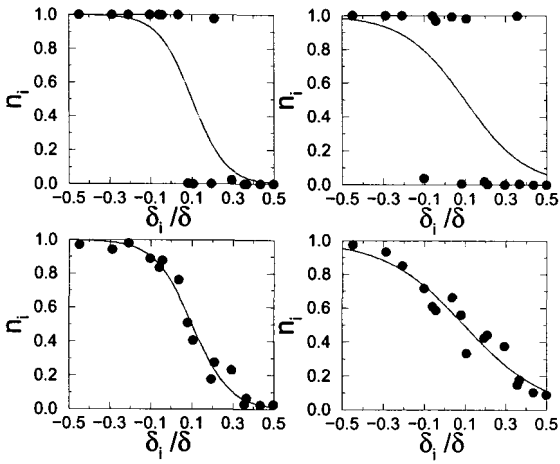

Figure 3: Distribution of the occupation numbers n_i as a function of the qubit detunings δ_i, for a given random realization and a single eigenstate for $n = 16$ qubits. Left: level number $m = 5$; right: $m = 100$ (the levels are ordered by increasing energy, $m = 1$ being the ground state). Top: $J = 0.03\delta$; bottom: $J = 0.3\delta$.

gas of many noninteracting particles in contact with a thermostat. However, here we consider an isolated system of relatively few interacting particles. Nevertheless, recent studies[18] have demonstrated that interaction can play the role of a heat bath, thus allowing one to use a statistical description even in an isolated system with few particles. The Fermi-Dirac statistics appears due to the fact that the number of spins up/down is fixed and in this way they become equivalent, for the purposes of a statistical description, to electrons/holes.

In Fig. 3 we show the occupation numbers *for a single eigenstate* of a given random realization. In the upper figures ($J = 0.03\delta << J_c \approx 0.2\delta$) a given eigenstate significantly projects only over a single quantum register state and therefore half of the occupation numbers is close to 1, half close to 0, and the Fermi-Dirac distribution (8) is very far from the actual distribution. On the contrary, in the quantum chaos regime (lower figures, $J = 0.3\delta > J_c$), where a large number of quantum register states are mixed in a single eigenstate, there is a good agreement between the occupation number distribution and the Fermi-Dirac distribution:

$$n_i^{FD} = \frac{1}{\exp(\beta(\delta_i + \delta/2 - \mu)) + 1}, \tag{8}$$

where μ is the chemical potential and $\beta = 1/T_{FD}$ is the inverse temperature (we set the Boltzmann's constant $k_B = 1$). Taking into account the constraint set by the fixed number of spins up ($\sum_i n_i^{FD} = [n/2]$), T_{FD} is the only fitting parameter.

In order to make quantitative the comparison with the Fermi-Dirac distribution, we introduce a parameter which measures the root mean square deviation of the

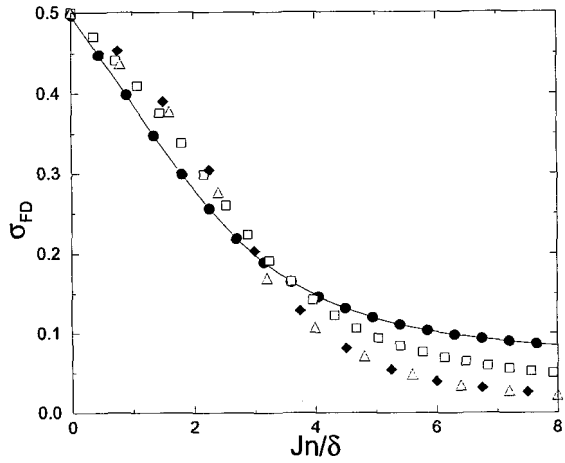

Figure 4: Dependence of σ_{FD} on the scaled coupling Jn/δ, for $n = 9$ (circles), $n = 12$ (squares), $n = 15$ (diamonds), and $n = 16$ (triangles).

actual distribution from (8):

$$\sigma_{FD}(m) = \sqrt{\frac{1}{n}\sum_{i=1}^{n}(n_i(m) - n_i^{FD}(m))^2}. \qquad (9)$$

The maximum value $\sigma_{FD}^{max} = 0.5$ is obtained at the band center ($T_{FD} = \infty$) for $J = 0$, when $n_i = 1$ for $[n/2]$ spins and $n_i = 0$ for the remaining ones.

The dependence of the thermalization parameter σ_{FD} on the scaled coupling Jn/δ at different system sizes is shown in Fig.4. Our data show that the crossover to a thermalized distribution sharpens when the number of qubits increases, in a way consistent with a sharp thermalization border J_t in the thermodynamic limit, at $J_t n/\delta \approx 3.2$. The similarity between the results of Fig.1 ($J_c n/\delta \approx 3.7$) and Fig.4 leads us to surmise that the chaos border coincides with the thermalization border. This looks quite natural since the Poisson level spacing statistics indicates the existence of uncoupled parts in the whole system, thus preventing thermalization. On the contrary, in the chaotic regime each eigenfunction spreads over an exponentially large number M of quantum register states, resulting in the Wigner-Dyson statistics. In this regime the fluctuations of eigenstate components are Gaussian [18] and therefore, according to the central limit theorem, the fluctuations of the occupation numbers are small: $\Delta n_i \propto M^{-1/2} \ll 1$. For this reason eigenstates close in energy give similar n_i-distributions, which means that there is equilibrium in the statistical sense.

Finally, it is interesting to compare the temperature T_{FD} obtained from the

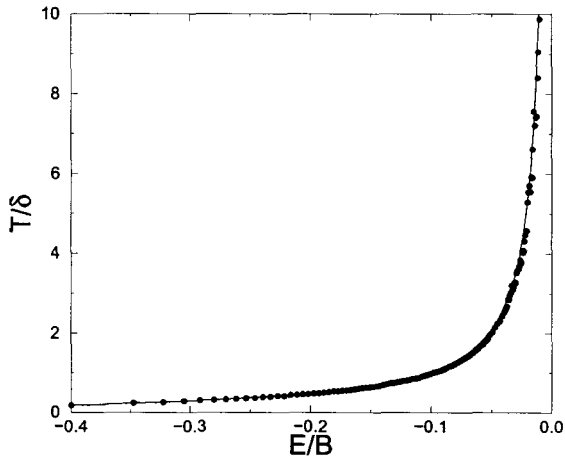

Figure 5: Dependence of the Fermi-Dirac temperature T_{FD} (circles) and the canonical temperature T_{can} (full curve) on the scaled energy E/B (B band width), for $n = 16$, $J = 0.3\delta$.

Fermi-Dirac fit with the canonical temperature T_{can}, defined as follows:

$$E(T_{can}) = \frac{\sum_{m=1}^{N_B} E_m \exp\left(-\frac{E'_m}{T_{can}}\right)}{\sum_{m=1}^{N_B} \exp\left(-\frac{E'_m}{T_{can}}\right)}, \tag{10}$$

where E_m are the exact eigenenergies of the interacting system. The very good agreement between T_{FD} and T_{can} (see Fig.5) supports the validity of a statistical description for our isolated quantum computer model. This means that in such closed system inter-qubit residual interactions play the role of a heat bath in an open system.

5 The sawtooth map

We now describe a quantum algorithm which computes the time evolution of a well known quantum system – the so-called sawtooth map, *exponentially faster* than any known classical computation. This model is very relevant in the theory of dynamical systems, has a rich and complex dynamics and finds various applications, e.g., for dynamical localization in billiards [19].

The classical sawtooth map is given by

$$\overline{n} = n + k(\theta - \pi), \quad \overline{\theta} = \theta + T\overline{n}, \tag{11}$$

where (n, θ) are conjugated action-angle variables ($0 \leq \theta < 2\pi$), and the bars denote the variables after one map iteration. Introducing the rescaled momentum

variable $p = Tn$, one can see that the classical dynamics depends only on the single parameter $K = kT$, so that the motion is stable for $-4 < K < 0$ and completely chaotic for $K < -4$ and $K > 0$. For such a discontinuous map the Kolmogorov-Arnold-Moser (KAM) theorem does not apply and, for any $K \neq 0$, the motion is not bounded by KAM tori. The map (11) can be studied on the cylinder ($p \in (-\infty, +\infty)$), which can also be closed to form a torus of length $2\pi L$, where L is an integer. For any $K > 0$, one has normal diffusion: $< (\Delta p)^2 > \approx D(K)t$, where t is the discrete time measured in units of map iterations and the average $< \cdots >$ is performed over an ensemble of particles with initial momentum p_0 and random phases $0 \leq \theta < 2\pi$. It is possible to distinguish two different dynamical regimes: for $K > 1$, the diffusion coefficient is well approximated by the random phase approximation, $D(K) \approx (\pi^2/3)K^2$, while for $0 < K < 1$ diffusion is slowed down, $D(K) \approx 3.3K^{5/2}$, due to the sticking of trajectories close to broken tori (cantori). For $-4 < K < 0$ the motion is stable, the phase space has a complex structure of elliptic islands down to smaller and smaller scales, and we observed anomalous diffusion, $< (\Delta p)^2 > \propto t^{\alpha}$, (for example, $\alpha = 0.57$ when $K = -0.1$).

The quantum evolution on one map iteration is described by a unitary operator $\hat{U}$ acting on the wave function ψ:

$$\overline{\psi} = \hat{U}\psi = e^{-iT\hat{n}^2/2} e^{ik(\hat{\theta}-\pi)^2/2} \psi, \tag{12}$$

where $\hat{n} = -i\partial/\partial\theta$ (we set $\hbar = 1$). The classical limit corresponds to $k \to \infty$, $T \to 0$, and $K = kT = \text{const}$. In this quantum model one can observe important physical phenomena like dynamical localization [19]. Indeed, due to quantum interference effects, the chaotic diffusion in momentum is suppressed, in a way similar to Anderson localization in disordered solids. Also in the vicinity of a broken KAM torus, cantori localization takes place, since a cantorus starts to act as a perfect barrier to quantum wave packet evolution, if the flux through it becomes less than $\hbar$ [20,19].

6 The quantum algorithm

The algorithm which we will now describe, is based on the Quantum Fourier Transform (QFT) [21], and simulates the dynamics of a system with N levels in $O((\log_2 N)^2)$ operations per map iteration, while a classical computer, which performs Fast Fourier Transforms (FFT), requires $O(N \log_2 N)$ operations. A further striking advantage of the algorithm is the *optimum utilization* of qubits: one needs only $n_q = \log_2 N$ qubits (without any extra work space). We demonstrate that complex phase space structures can be simulated with less that 10 qubits, while about 40 qubits would allow one to make computations inaccessible to present-day supercomputers. This is particularly important, since experiments with few qubits are being performed at present [10,11]. For this reason the investigation of this interesting physical system will be accessible to the first quantum computers, operating with few qubits and for which large-scale computations like integer factoring are not possible.

The most efficient way to simulate the quantum dynamics (12) on a classical computer is based on forward/backward FFT between θ and n representations.

This is advantageous because the evolution operator $\hat{U}$ is the product of two unitary operators, $\hat{U}_k = \exp(ik(\hat{\theta} - \pi)^2/2)$ (kick) and $\hat{U}_T = \exp(-iT\hat{n}^2/2)$ (free rotation), which are diagonal in the θ and n representation, respectively. Therefore, for a system with N levels, the one map iteration (12) requires two FFT and two diagonal multiplications and can be performed in $O(N \log_2(N))$ operations. The dynamics (12) can be simulated exponentially faster on a quantum computer with $n_q = \log_2 N$ qubits by means of the following quantum algorithm:
(i) the wave function $|\psi\rangle = \sum_{n=0}^{N-1} a_n |n\rangle$ (given in the n representation) is multiplied by $\hat{U}_T$, so that $\hat{U}_T|\psi\rangle = \sum_n a_n \exp(-iTn^2/2)|n\rangle$. This step can be done in n_q^2 controlled-phase shift gates, as explained in [22];
(ii) one can get the wave function in the θ representation via the QFT [21], which requires n_q single-qubit (Hadamard) gates and $n_q(n_q - 1)/2$ two-qubit gates (controlled phase-shifts);
(iii) the action of $\hat{U}_k$ is diagonal in the angle representation and can be simulated in a way similar to (i) in n_q^2 two-qubit gates (we note that this is possible thanks to the particular form of $\hat{U}_k$ for the sawtooth map);
(iv) we go back to the momentum basis performing backward QFT in $n_q(n_q + 1)/2$ gates.
Therefore the whole algorithm requires $n_g = 3n_q^2 + n_q$ quantum gates per map iteration.

We study numerically the many-body dynamics of the quantum computer (1) running the quantum algorithm described above. The algorithm is realized by a sequence of instantaneous and perfect one- and two-qubit gates, separated by a time interval τ_g, during which the Hamiltonian (1) gives unwanted phase rotations and qubit couplings [23]. We assume that the average phase accumulation given by Δ_0 is eliminated, e.g. by means of refocusing techniques [24].

We study the sawtooth map in the anomalous diffusive regime, with $K = -0.1$, $-\pi \leq p < \pi$ (torus geometry). The classical limit is obtained by increasing the number of qubits n_q, with $T = 2\pi/N$ ($k = K/T$, $-N/2 \leq n < N/2$). We consider as initial state at time $t = 0$ a momentum eigenstate, $|\psi(0)\rangle = |n_0\rangle$, with $n_0 = [0.38N]$. Such a state can be prepared in $O(n_q)$ one-qubit rotations starting from the ground state $|0, \ldots, 0\rangle$. The dynamics of the sawtooth map reveals the complexity of the phase space structure, as shown by the Husimi functions [25] in Fig.6, taken after 1000 map iterations. We note that $n_q = 6$ qubits are sufficient to observe the quantum localization of the anomalous diffusive propagation through hierarchical integrable islands. At $n_q = 9$ one can see the appearance of integrable islands, and at $n_q = 16$ the quantum Husimi function already explores the complex hierarchical structure of the classical phase space down to small scales. The effect of static imperfections for the operability of the quantum computer is shown in Fig.6 (right column). The data are shown for $J = 0$ (we observed similar structures for $J = \delta$). The main features of the wave packet dynamics remain evident even in the presence of significant imperfections, characterized by the dimensionless strength $\epsilon = \delta\tau_g$. The main manifestation of imperfections is the injection of quantum probability inside integrable islands. This creates characteristic concentric ellipses, which follow classical periodic orbits moving inside integrable islands. These structures become more and more pronounced with the increase of n_q. Thus quantum errors strongly

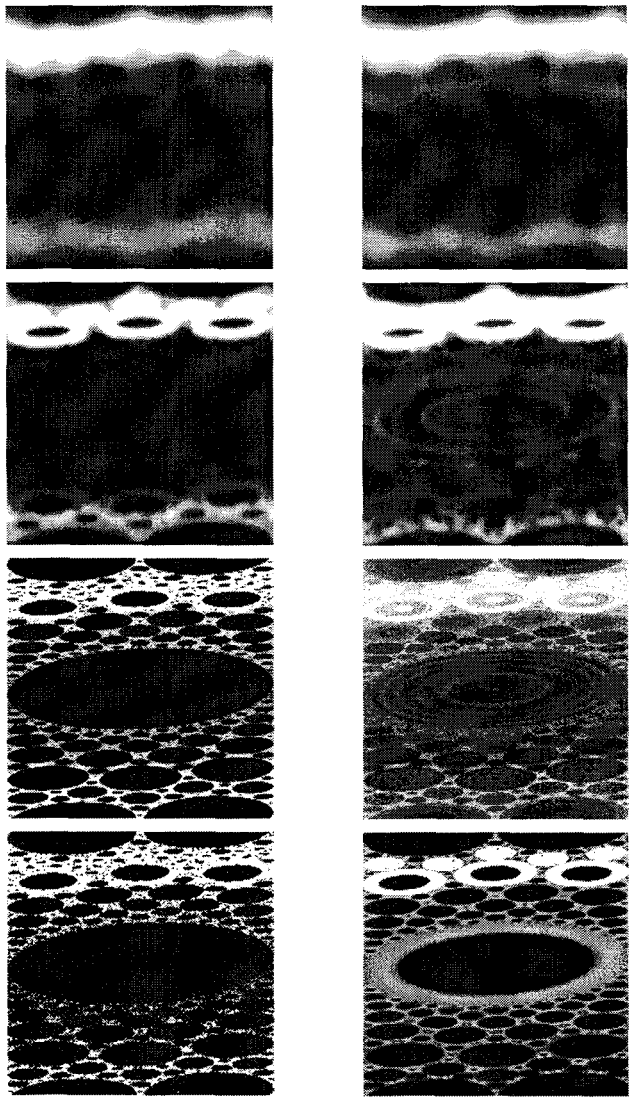

Figure 6: Husimi function for the sawtooth map in action angle variables (p, θ), with $-\pi \leq p < \pi$ (vertical axis) and $0 \leq \theta < 2\pi$ (horizontal axis), for $K = -0.1$, $T = 2\pi/2^{n_q}$, $n_0 = p_0/T = [0.38 \times 2^{n_q}]$, averaged in the interval $950 \leq t \leq 1000$. From top to bottom: $n_q = 6, 9, 16$ and classical density plot, obtained from an ensemble of 10^8 trajectories, with initial momentum $p_0 = 0.38 \times 2\pi$ and random angles. Left and right columns show the case without and with imperfections: in the quantum case the imperfection strength $\epsilon = \delta\tau_g$sc ales $\propto n_q^{-3}$, where $\epsilon = 2 \times 10^{-3}$ $(n_q = 6)$, $\epsilon = 6 \times 10^{-4}$ $(n_q = 9)$, $\epsilon = 10^{-4}$ $(n_q = 16)$, at $J=$ 0; in the classical case round-off errors are of amplitude 10^{-3}. We choose the ratio of the action-angle uncertainties $s = \Delta p/\Delta\theta =$ 1 $(\Delta p \Delta\theta = T/2)$. Black corresponds to the minimum of the probability distribution and white to the maximum.

affect the quantum tunneling inside integrable islands, which in a pure system drops exponentially ($\propto \exp(-CN)$, C =const). It is interesting to stress that the effect of quantum errors is qualitatively different from the classical round-off errors, which produce only slow diffusive spreading inside integrable islands (see Fig.6 bottom right). This difference is related to the fact that spin flips in quantum computation can make direct transfer of probability on a large distance in phase space.

It is clear from Fig. 6 that the main structures inside the localization domain turn out to be rather stable in the presence of static imperfections (see also Ref. [9]). It should be stressed that, obviously, it is not possible to extract all exponentially large information hidden in the wave function with 2^{n_q} states. However, it is possible to have access to coarse grained information. For example from a polynomial number of measurements one can obtain the probability distribution over momentum (or angle) states. This allows one to study the anomalous diffusion in the deep semiclassical regime. Such an information is not accessible for classical computers which cannot simulate more than 2^{40} quantum states. Moreover, we note that an efficient algorithm was proposed in Ref. [26], which allows one to measure the value of the Wigner function at a chosen phase space point. This can also provide important new information about quantum states in systems with hierarchical phase space structures.

7 Conclusions

In this paper we have discussed the effects of static imperfections on the stability of (i) the quantum computer hardware and (ii) an efficient quantum algorithm for the quantum sawtooth map. From these studies, a certain robustness of quantum computation emerges. We also outline that interesting phenomena like dynamical localization can be observed in the above described algorithm already with less than 10 qubits. Therefore quantum algorithms for the simulation of interesting physical models [27,9] may constitute the ideal software for the first generation of quantum computers operating with a small number of qubits and the most suitable testing ground for investigating the effects of decoherence and imperfections for quantum information processing.

The authors wish to acknowledge the fruitful collaboration with Simone Montangero and Dima Shepelyansky. Support from the ARO contract No. DAAD19-02-1-0086 and the PRIN-2000 "Chaos and localization in classical and quantum mechanics" is gratefully acknowledged.

References

1. A. Steane, Rep. Progr. Phys. **61**, 117 (1998).
2. M.A. Nielsen and I.L. Chuang, *Quantum Computation and Quantum Information* (Cambridge University Press, Cambridge, 2000).
3. P. Shor, in *Proceedings of the 35-th Annual Symposium on Foundations of Computer Science*, edited by S. Goldwasser (IEEE Computer Society Press, Los Alamitos, CA, 1994), p. 124.
4. L.K. Grover, Phys. Rev. Lett. **79**, 325 (1997); *ibid.* **80**, 4329 (1998).

5. B. Georgeot and D.L. Shepelyansky, Phys. Rev. E **62**, 3504 (2000); **62**, 6366 (2000).
6. S. Åberg, Phys. Rev. Lett. **64**, 3119 (1990); Ph. Jacquod and D.L. Shepelyansky, Phys. Rev. Lett. **79**, 1837 (1997); D.Weinmann, J.-L. Pichard, and Y. Imry, J. Phys. I France **7**, 1559 (1997).
7. For a review see, e.g., T. Guhr, A. Müller-Groeling, and H.A. Weidenmüller, Phys. Rep. **299**, 189 (1998).
8. G. Benenti, G. Casati, and D.L. Shepelyansky, Eur. Phys. J. **D 17**, 265 (2001).
9. G. Benenti, G. Casati, S. Montangero, and D.L. Shepelyansky, Phys. Rev. Lett. **87**, 227901 (2001).
10. Y.S. Weinstein, M.A. Pravia, E.M. Fortunato, S. Lloyd, and D.G. Cory, Phys. Rev. Lett. **86**, 1889 (2001).
11. L.M.K. Vandersypen, M. Steffen, G. Breyta, C.S. Yannoni, M.H. Sherwood and I.L. Chuang, Nature 414, 883 (2001).
12. G.K. Brennen, C.M. Caves, P.S. Jessen, and I.H. Deutsch, Phys. Rev. Lett. **82**, 1060 (1999); D. Jaksch, H.-J. Briegel, J.I. Cirac, C.W. Gardiner, and P. Zoller, Phys. Rev. Lett. **82**, 1975 (1999); A. Sorensen and K. Molmer, Phys. Rev. Lett. **83**, 2274 (1999).
13. D. Loss and D.P. Di Vincenzo, Phys. Rev. A **57**, 120 (1988).
14. B.E. Kane, Nature **393**, 133 (1998); V. Privman, I.D. Vagner, and G. Kventsel, Phys. Lett. A **239**, 141 (1998).
15. P.M. Platzman and M.I. Dykman, Science **284**, 1967 (1999).
16. In order to reduce statistical fluctuations, we use $3 \leq N_D \leq 10^4$ random realizations of δ_i, J_{ij}. In this way the total number of spacings N_S is varied in the interval $1.4 \times 10^4 \leq N_S \leq 1.2 \times 10^5$.
17. V.V. Flambaum, Aust. J. Phys. **53**, 489 (2000).
18. V. Zelevinsky, B.A. Brown, N. Frazier, and M. Horoi, Phys. Rep. **276**, 85 (1996); V.V. Flambaum, F.M. Izrailev, and G. Casati, Phys. Rev. E **54**, 2136 (1996); V.V. Flambaum and F.M. Izrailev, Phys. Rev. E **56**, 5144 (1997); F. Borgonovi, I. Guarneri, F.M. Izrailev, and G. Casati, Phys. Lett. A **247**, 140 (1998).
19. F. Borgonovi, G.Casati, and B. Li, Phys. Rev. Lett. **77**, 4744 (1996); F. Borgonovi, Phys. Rev. Lett. **80**, 4653 (1998); G. Casati and T. Prosen, Phys. Rev. E **59**, R2516 (1999); R.E. Prange, R. Narevich, and O. Zaitsev, Phys. Rev. E **59**, 1694 (1999).
20. T. Geisel, G. Radons, and J. Rubner, Phys. Rev. Lett. **57**, 2883 (1986); R.S. MacKay and J.D. Meiss, Phys. Rev. A **37**, 4702 (1988).
21. See, e.g., A. Ekert and R. Jozsa, Rev. Mod. Phys. **68**, 733 (1996).
22. B. Georgeot and D.L. Shepelyansky, Phys. Rev. Lett. **86**, 2890 (2001).
23. We consider the case of short range inter-qubit interaction, in which two-qubit gates can be performed only between nearest neighbor pairs (we also assume nearest neighbors residual interactions). As a result, for a square lattice of n_q qubits, we make $O(n_q^{1/2})$ swap gates to obtain a generic two-qubit gate. Therefore a single iteration of the map (12) requires $n_g = O(n_q^{5/2})$ gates.
24. See, e.g., N.A. Gershenfeld and I.L. Chuang, Science **275**, 350 (1997).

25. The computation of Husimi function is described in S.-J. Chang and K.-J. Shi, Phys. Rev. A **34**, 7 (1986).
26. C. Miquel, J.P. Paz, M. Saraceno, E. Knill, R. Laflamme, and C. Negrevergne, quant-ph/0109072.
27. A quantum algorithm for the quantum baker's map was proposed by R. Schack, Phys. Rev. A **57**, 1634 (1998), and a first experimental implementation has been realized in Y.S. Weinstein, S. Lloyd, J.V. Emerson, and D.G. Cory, quant-ph/0201064.

DISCUSSION

Chairman: A. Bohm

L. Reichl: How do you choose the form of the Hamiltonian, and how can you distinguish different states of the qubits?

G. Casati: We have considered the simplest model in which system imperfections generate energy fluctuations and residual inter-qubit couplings. In principle, the different states of the qubits can be distinguished by means of standard projective spin measurements.

L. Reichl: The model you choose doesn't necessarily model an actual quantum computer?

G. Casati: Other models of quantum computation can be devised, it is still not clear what will be the actual architecture of a quantum computer.

L. Reichl: Can you make a comment about the ability of a quantum computer to function, if it is constructed according to this model?

G. Casati: The preferred regime is below the thermalization border. Above this border, a generic state stored in the quantum computer is destroyed after a "decoherence" time scale determined by the width of the Breit-Wigner distribution.

W. Schleich: Is there something to say about the approach of classical limit? Because somehow you say you go much faster, you go exponentially faster, and we see that with this, your Husimi function goes pretty much to the classical map already.

G. Casati: We have simulated a quantum model in which the approach to the classical limit goes exponentially fast with the number of qubits. When you plot the Husimi function, already with 16 qubits you obtain something which is very close to the classical distribution.

LESSONS OF COHERENCE AND DECOHERENCE – FROM NEUTRINOS TO SQUIDS

L. STODOLSKY
Max-Planck-Institut für Physik (Werner-Heisenberg-Institut), Föhringer Ring 6, 80805 München, Germany

We indicate some of the lessons learned from our work on coherence and decoherence in various fields and mention some recent work with solid state devices as elements of the "quantum computer", including the realization of simple logic gates controlled by adiabatic processes. We correct a commonly held misconception concerning decoherence for a free particle.

The subject of "quantum information" and in particular its realization in terms of real devices revolves in large measure around the problems of coherence and decoherence. Thus it may be of interest here to review the origins of the subject and see what has been learned in applications to various areas. We first got involved in these issues through the attempt to see the effects of parity violation ("weak neutral currents") in handed molecules [1]. The method we found – an analogy to the famous neutral K meson behavior with chiral molecules – seemed too good to be true: we had a way of turning 10^{-15} eV into a big effect! There must be some difficulty, we felt. Indeed there was; it turned out to be what we called "quantum damping" and what now-a-days is called "decoherence".

The lessons from this work were several and interesting. First, concerning parity violation, we realized that this could solve Hund's "paradox of the optical isomers" as to why we observe handed molecules when the true ground state should be parity even - or - odd linear combinations. We realized that for molecules where tunneling between chiral isomers is small, parity violation dominates and the stationary state of the molecule becomes a handed or chiral state, and not a 50-50 linear combination of chiral states.

This holds for a perfectly isolated molecule, and in itself has nothing to do with decoherence. However, and this is very related, even a very small interaction with the surroundings suffices to destroy the coherence necessary for the aforesaid linear combination, in effect the environment can stabilize the chiral states. This now goes under the catch-word "decoherence by the environment". The limit of strong damping or stabilization is often called the Zeno or "watched pot" effect, an idea which as far as I can tell, goes back to Turing. We were able to show how this just arises as the strong damping limit of some simple "Bloch-like" equations [2,3].

1 The Unitarity Deficit Formula

A result of this work is that there is a simple and illuminating formula for the decoherence rate. There is a quantity Λ, given by the flux of the surrounding particles or excitations, and the S matrix for the interaction of our system (e.g. the chiral molecule) with these surroundings:

$$\Lambda = i(flux) < i|(1 - S_L S_R^\dagger)|i > \quad (1)$$

The imaginary part gives the decoherence rate or loss of phase coherence per unit time D:

$$D = Im\ \Lambda \quad (2)$$

(The real part also has a significance, a level shift induced by the surroundings. This turns out to be a neat way to find the index of refraction formula for a particle in a medium [6,7].)

The labels (L,R) on the S refer to which state of the molecule (or other system) is doing the interacting with the surroundings. Here with (L,R) we have taken the case of the simplest non-trivial system, the two-level system.

These equations may be derived[3,6]b y thinking of the S-matrix as the operator which transforms the initial state of an incoming object into the final state. If the different states (L,R) of our system scatter the object differently, a "lack of overlap" or "unitarity deficit" as given by Eq [1] arises. These intuitive arguments can also be supported by more formal manipulations [7].

An important point that we see here, in Eq [1], is that the environment "chooses a direction in hilbert space"[6]. That is, there is some direction (here L,R) in the internal space of the system under study (the molecule) that is left unchanged – is not "flipped" – by the interaction with the surroundings. Such states however get a phase factor by the interaction, and this is the decoherence . If the interaction did not distinguish some direction, if we had $S_L = S_R$ then the formula tells us there would be no decoherence . This is intuitively correct in accord with one's ideas about "measurement". If the probe does not distinguish any state there are no "wavefunction collapses" and no decoherence takes place. (This is not meant to imply sanctioning of "wavefunction collapses" in any way.)

Another simple limit for the formula occurs when only one state interacts, say no interaction for L, or $S_L = 1$. Then one finds that the decoherence rate is $1/2$ the scattering rate for the interacting component [3]. Thus Eqs [1,2] have two interesting limits:

$$S_L = S_R \qquad D = 0\ ,\ \ no\ decoherence \quad (3)$$

and

$$S_L = 1 \qquad D = 1/2\ (scattering\ rate\ of\ R) \quad (4)$$

The latter followed from an application of the optical theorem. With appropriate evaluation of the S-matrices, Eqs [1,2] can be applied to many types of problems, like quantum dots [11] or neutrinos [4], or even gravity [8].

Eq [3] is quite interesting in that it says the system can interact but nevertheless retain its internal coherence. A lesson here is that one shouldn't think that every interaction or disturbance "decoheres" or "reduces" the system. The system can interact quite a bit as long as the interactions don't distinguish the different internal states.

2 A common misconception

The fact that the interaction responsible for the decoherence must "choose a direction in hilbert space" has some interesting implications. One of these has to do with the decoherence of a free particle in some background environment.

Eq [1] was for a two-state system, and the extension to a larger number of states, as long as it is a finite number, can be easily envisioned as following the logic[2,3,6] used in finding Eq [1]. However if we go to the continuum, that is if we have a infinite number of states, the problem becomes more subtle. The most common example of this is the free particle which, say in the limit of an infinitely large "box", is described as system of continuous, dense, levels.

A number of authors, in talking about this system, have automatically assumed, as indeed first seems plausible, that at long times the particle under the influence of some continually interacting environment becomes totally "decohered"; in the sense that the density matrix of the particle $\rho(x, x')$ approaches the situation of no off-diagonal elements, that ρ approaches a δ function.

Although this may seem plausible, that under the repeated bombardment by the surroundings the particle becomes more and more "decohered", it is in fact wrong

$$\rho(x, x') \rightarrow\sim \delta(x - x') \qquad wrong \qquad (5)$$

Consider the simplest case, that of a thermal environment. On general grounds we expect the particle in a thermal environment to be described by the boltzmann factor, to be given by a density matrix operator $\rho \sim e^{-H/T}$, where T is the temperature and H the hamiltonian, say $p^2/2m$ for a non-relativistic particle. Now evaluate this operator in the position representation:

$$\rho(x, x') =< x|e^{-p^2/2mT}|x' >\sim \int d^3p\ e^{i\mathbf{p}(\mathbf{x}-\mathbf{x}')-p^2/2mT} \sim e^{-(x-x')^2MT/2} \qquad (6)$$

This is the stationary, long time value of ρ. It applies for nearly any state we care to initially throw into the medium. Evidently it shows no signs of changing and certainly no sign of turning into a δ function. Of course at high temperature our expression will resemble a delta function. The practical importance of this will depend on the other length scales in the problem at hand. The point we wish to make, however, is of a conceptual nature, namely that repeated interactions with the environment don't necessarily lead to more "decoherence". Indeed Eq [6] says if we were initially to put $\delta(x - x')$ or some other "highly incoherent" density matrix into the medium, the density matrix of the particle would become *more coherent* with time — until it reached the value Eq [6]. Apparently the medium can "give coherence" to a state that never had any to start with.

"Creating coherence" by an outside influence is not as mysterious as it may sound, there are familiar cases where we know this already. For example, using a high resolution detector can "create a long wavepacket" [5] or in particle physics neutral K oscillations and the like may be enhanced or "created" by using some subset of our total event sample, such as a "flavor tag".

Where did the seemingly plausible argument or feeling about the indefinitely increasing decoherence go wrong? It's the question of the "direction chosen in hilbert space". The feeling is right, but we must know where to apply it. As we can see from the boltzmann factor, thermodynamics likes to work in momentum (actually energy) space. The intuition would have been right there, – in momentum space – but this then means something non-trivial in position space. The lesson here is that the notion of "decoherence by the environment" must be understood to include a statement about the "direction chosen in hilbert space" by that environment [6].

3 Mesoscopic systems

The interest in these issues has had a revival with the advances made possible by the technologies of mesoscopic systems. In one such system, the "quantum dot observed by the QPC", one has a complete model of the measurement process, including the "observer", "who" in this case is a quantum point contact (QPC) [10]. In a slight generalization of the original experiment [9] one can see how not only the density matrix of the object being observed is "reduced" by the observing process, but also see how the readout current–the "observer" responds. In particular one may see how effects looking very much like the "collapse of the wavefunction", that is sequences of repeated or "telegraphic" signals indicating one or another of the two states of the quantum dot, arise. All this without putting in any "collapses" by hand [11].

We should stress that what we are not only talking about a reduction of fringe contrast due to "observing" or disturbing an interference experiment, as in [9]; and also in interesting experiments in quantum optics where an environment is simulated [12] or different branches of the interferometer [13] interact differently and adjustably with the radiation in a cavity (like our two S-matrices). By the "collapses" however, we are referring not so much to the interferometer itself as to the signal from some "observing" system, like the current in the qpc. With repeated probing of the *same* object (say electron or atom), in the limit of strong "observation" this signal repeats itself — this is the "collapse". For not too strong observation there is an intermediate character of the signal, and so on. All this may be understood by considering the amplitude for the interference arrangement and the readout procedure to give a certain result [11]. The properties of the readout signal naturally stand in some relation to the loss of coherence or "fringe contrast" of the interference effect under study.

Following this line of thought we come to the idea that there should be some relation between the fluctuations of a readout signal and decoherence. Indeed the decoherence rate, the imaginary part of Eq [1] is a dissipative parameter in some sense; it characterizes the rate of loss of coherence. Now there is the famous "dissipation-fluctuation theorem", which says that dissipative parameters are related to fluctuations in the system. Is there some such relationship here? Indeed, one is able to derive a relation between the fluctuations of the readout current and the value of D[14]. The interesting and perhaps practical lesson here is that the decoherence parameter can be observed in two ways. One is the direct way, just observe the damping out of the coherent oscillations of the system in question. Experimentally,

this involves starting the system in a definite, selected state. However, as just explained, there is a second way; namely, observe the fluctuations of the readout. This can be done even if the system is in the totally "decohered" $\rho \sim I$ state.

Another mesoscopic system, the SQUID and in particular the rf SQUID, has been long discussed[15] as a candidate for showing that even macroscopic objects are subject to the rules of quantum mechanics. The rf SQUID, a Josephson device where a supercurrent goes around a ring, can have two distinct states, right- or left- circulation of the current. These two conditions apparently differ greatly, since a macroscopic number of electrons change direction. It would be a powerful argument for the universality of the quantum rules if one could demonstrate the meaningfulness of quantum linear combinations of these two states.

Such linear combinations can in principle be produced since there is some amplitude for a tunneling between the two configurations. In fact this was recently manifested through the observation of the "repulsion of levels" to be anticipated if the configurations of opposite current do behave as quantum states[16].

Another approach, where we would directly "see" the meaningfulness of the relative quantum phase of the two configurations, is the method of "adiabatic inversion" [17,18]. This method also offers the possibility of a direct measurement of the decoherence time. In adiabatic inversion the "spin" representing a two-level system [3,4] is made to "follow" a slowly moving "magnetic field" (meant symbolically, as an analogy to spin precession physics), which is swept from "up" to "down". In this way the system can be made to invert its direction in "spin space", that is to reverse states and go from one direction of circulation of the current to the other. This inversion is an intrinsically quantum phenomenon. If it occurs it shows that the phases between the two configurations were physically meaningful and that they behave quantum mechanically . This may be dramatically manifested if we let decoherence destroy the phase relation between the two configurations. Now the configurations act classically and the inversion is blocked.

We thus predict that when the decoherence rate is low the inversion takes place, and when it is high it does not. Figs 1 and 2 show the idea of this procedure.

Since in such an experiment we have the sweep speed at our disposal, we have a way of determining the decoherence time. It is simply the slowest sweep time for which the inversion is successful. We must only be sure that for the sweep speeds in question the conditions remain adiabatic.

Setting up the adiabatic condition and taking some estimates for the decoherence time, it appears that the various requirements can be met [17,18] when operating at low temperature. Hence it may be realistically possible to move between the classical and quantum mechanical worlds–to turn quantum mechanics "on and off" in one experiment. This would be a beautiful experiment, the main open question being if the estimates of the decoherence rate are in fact realistic, since we are entering a realm which has not been explored before.

4 Adiabatic logic elements and the quantum computer

A two-state system behaving quantum mechanically can serve as the physical embodiment of a quantum mechanical bit, the "qbit". Furthermore, the adiabatic

inversion procedure just described amounts to a quantum realization of one of the basic elements of computer logic: the NOT. If one configuration is identified as 1 and the other as 0, then the inversion turns a linear combination of 1 and 0 into a linear combination of 0 and 1 with reversed weights.

We can try to push this idea of "adiabatic logic" a step further. NOT was a one bit operation. The next most complicated logic operation is a two bit operation, which we may take to be "controlled not" or CNOT. In CNOT the two bits are called the control bit and the target bit, and the operation consists of performing or not performing a NOT on the target bit, according to the state of the control bit.

To realize CNOT, an idea which suggests itself[17] as a generalization of adiabatic inversion is the following. We have a two bit operation and so two SQUIDS. These are devices with magnetic fields. Now if one SQUID, the target bit, is undergoing a NOT operation, it can be influenced by the control bit, a second nearby SQUID, through its linking flux. We could imagine that this linking flux can be arranged so that it helps or hinders the NOT operation according to the state of the second SQUID. This would amount to a realization of "controlled not", again by means of an adiabatic sweep.

To analyze this proposal we must set up the two-variable Schrödinger equation describing the two devices and their interaction. The result is a Hamiltonian with the usual kinetic energy terms and a potential energy term in the two variables, which in this case are the fluxes in the SQUIDS, ϕ_1, ϕ_2:

$$V = \frac{1}{2}V_0\{[l_1(\phi_1-\phi_1^{ext})^2+l_2(\phi_2-\phi_2^{ext})^2-2l_{12}(\phi_2-\phi_2^{ext})(\phi_1-\phi_1^{ext})]+\beta_1 f(\phi_1)+\beta_2 f(\phi_2)\} \tag{7}$$

The ϕ^{ext} are external biases which in general will be time varying. The $l's$ are dimensionless inductances and l_{12} represents the coupling between the two devices. The $f(\phi)$ are symmetric functions starting at one and decreasing with increasing ϕ so as to produce a double well potential when combined with the quadratic term; in the SQUID $f(\phi) = cos(\phi)$. Fig. 3 shows this "potential landscape" for some typical values of the parameters.

Given the hamiltonian, we must search for values of the control parameters ϕ^{ext}, the "external fields", which can be adiabatically varied in such a way as to produce CNOT. Preliminary analysis indicates favorable regimes of the rather complex parameter space where this can in fact be done[19].

5 Some Experimental Proposals

Finally we would like to recall that there are still some fundamental and beautiful experiments waiting to be done in these areas.

A) One is the demonstration of the large effects of parity violation for appropriately chosen and contained handed molecules [1]. Because of what we now call decoherence this seemed very remote at the time. But now with the existence of single atom/molecule traps and related techniques, perhaps it's not so hopeless.

B) Another, concerned with fundamentals of quantum mechanics, could be called the "adjustable collapse of the wavefunction" where the "strength of observ-

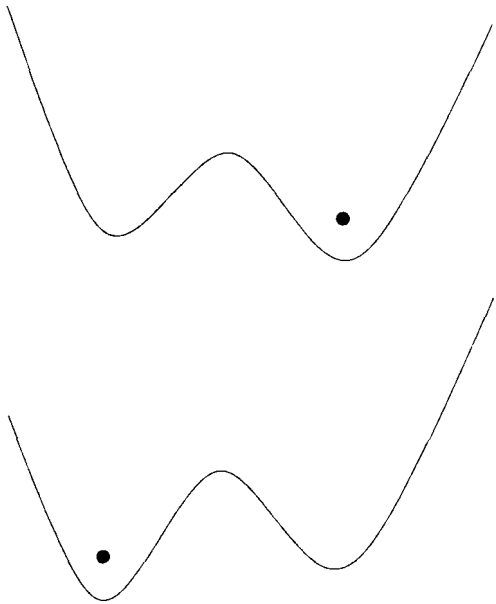

Figure 1: A successful inversion, starting from the upper figure and ending with the lower figure. The black dot indicates which state is occupied. The system starts in the lowest energy level and by staying there, reverses states. It behaves as a quantum system with definite phase relations between the two configurations.

ing" can be varied, leading to effects like washing out of interferences, as already seen in [9] and a number of further predictions where we vary the qualities of the "observer" [11], or slowing down of relaxation according to the rate of probing of the object [3].

C) Then there is the second way of measuring D, through the fluctuations in the readout signal, even for a fully "decohered" system.

D) Finally there is the direct demonstration of quantum linear combinations of big objects by the method of adiabatic inversion; "turning quantum mechanics on and off" [17,18].

Many of the questions we have briefly touched upon had their origins in an unease with certain consequences of quantum mechanics, often as "paradoxes" and "puzzles". It is amusing to see how, as we get used to them, the "paradoxes" fade and yield to a more concrete understanding, sometimes even with consequences for practical physics or engineering. If we avoid overselling and some tendency to an inflation of vocabulary, we can anticipate a bright and interesting future for "applied fundamentals of quantum mechanics".

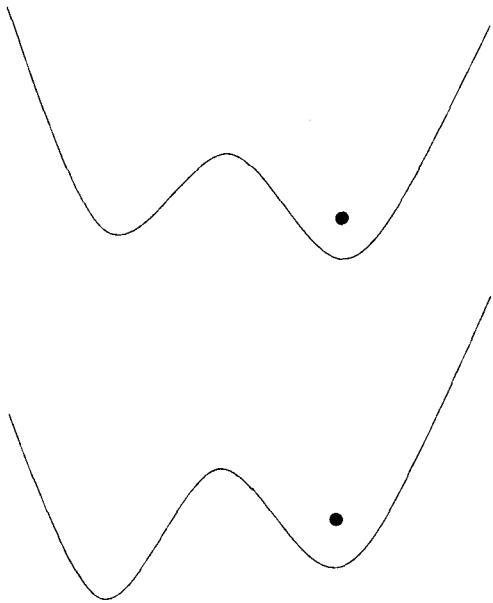

Figure 2: An inhibited inversion, starting from the upper figure and ending with the lower figure. Due to the lack of phase coherence the system behaves classically and stays in the same state, the current is not reversed.

References

1. Quantum Beats in Optical Activity and Weak Interactions, R.A. Harris and L. Stodolsky, Phys Let B78 (1978) 313. [Molecular tunneling and parity violation, need to understand decoherence.]
2. On the Time Dependence of Optical Activity, R.A. Harris and L. Stodolsky, J. Chem. Phys. **74** (4), 2145 (1981). [Decoherence by environment, formula for decoherence rate, application to chiral molecules.] The notion that handed molecules could "decohere" or be stabilized by the environment somehow was raised by H.D. Zeh, Found. Phys. 1, 69 (1970), M. Simonius, Phys Rev. Lett. 40, 980 (1978).
3. Two Level Systems in Media and 'Turing's Paradox', R.A. Harris and L. Stodolsky, Phys. Let. B 116 (1982) 464. [Decoherence by environment, formula for decoherence rate, quantitative explanation of "Zeno", prediction of anti-intuitive relaxation, application to neutrinos.]
4. On the Treatment of Neutrino Oscillations in a Thermal Environment, L. Stodolsky, Phys. Rev. D 36 (1987) 2273 .[Method for decoherence in neutrino oscillations. Spin precession picture for neutrinos.] See chapter 9 of G.G. Raffelt, *Stars as Laboratories for Fundamental Physics* (Univ. Chicago Press, 1996)

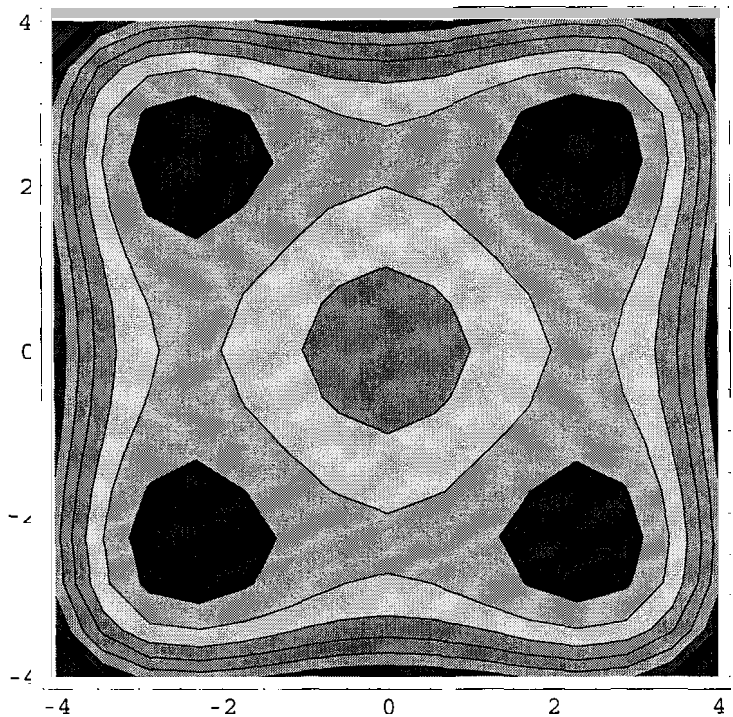

Figure 3: Potential landscape for CNOT

5. When the Wavepacket is Unnecessary, L. Stodolsky, Phys. Rev. **D58** 036006, 1998 and hep-ph/9802387.
6. Quantum Damping and Its Paradoxes, L. Stodolsky, in *Quantum Coherence*, J. S. Anandan ed. World Scientific, Singapore (1990) [Review and historical background to 1989.]
7. Non-Abelian Boltzmann Equation for Mixing and Decoherence G. Raffelt, G. Sigl and L. Stodolsky, Phys Rev Let. **70 (1993) 2363.** [Derivation of decoherence rate formula in neutrino applications]
8. Decoherence Rate of Mass Superpositions, L. Stodolsky, Acta Physica Polonica **B27**, 1915 (1996). [Decoherence in gravitational interactions.]
9. S. Gurvitz, quant-ph 9607029. E. Buks, R. Schuster, M. Heiblum, D. Mahalum and V. Umanksy, Nature **391**, 871 (1998).
10. M. Field, C.G. Smith, M. Pepper, D. A. Ritchie, J. E. F. Frost G.A. C. Jones and D.G. Hasko, Phys. Rev. Lett. **70**, 1311 (1993).
11. Measurement Process In a Variable-Barrier System, L. Stodolsky, Phys. Lett. **B459** pages 193-200, (1999). [Formalism for quantum dot-QPC system. Prediction of novel phase effect. Prediction of "collapse-like" behavior of readout.]

12. Myatt et al. Nature 403, 269 (2000).
13. Brune et al. Phys. Rev. Lett. 77, 4887 (1996).
14. Decoherence-Fluctuation Relation and Measurement Noise, L. Stodolsky, Physics Reports **320** 51-58 (1999), quant-ph/9903075. [Suggestion of Decoherence-Fluctuation Relation connecting decoherence rate and fluctuations of readout signal.]
15. See A. J. Leggett, Les Houches, session XLVI (1986) *Le Hasard et La Matiere*; North-Holland (1987), references cited therein, and introductory talk, Conference on Macroscopic Quantum Coherence and Computing, Naples, June 2000, Proceedings published by Academic-Plenum.)
16. J. Friedman, V. Patel, W.Chen, S.K. Tolpygo and J.E. Lukens, Nature **406**, 43 (2000). C.S. van der Wal, A.C. ter Haar, F. K. Wilhelm, R. N. Schouten, C.J.P.M. Harmans, T.P. Orlando, Seth Lloyd, and J.E. Mooij, in MQC2: Conference on Macroscopic Quantum Coherence and Computing, Naples, June 2000, Proceedings published by Academic-Plenum.
17. Study of Macroscopic Coherence and Decoherence in the SQUID by Adiabatic Inversion, Paolo Silvestrini and L. Stodolsky, Physics Letters **A280** 17-22 (2001). [Linear Combinations of macroscopic states. Measuring decoherence time. Relation to NOT operation.] cond-mat/0004472
18. Adiabatic Inversion in the SQUID, Macroscopic Coherence and Decoherence, Paolo Silvestrini and L. Stodolsky, *Macroscopic Quantum Coherence and Quantum Computing*, pg.271, Eds. D. Averin, B. Ruggiero and P. Silvestrini, Kluwer Academic/Plenum, New York (2001). [Linear Combinations of macroscopic states. Measuring decoherence time.]cond-mat/0010129. D.V. Averin, Solid State Communications **105**, 659 (1998), has discussed related ideas using adiabatic operations on the charge states of small Josephson junctions.
19. Adiabatic Methods for a Quantum CNOT Gate, Valentina Corato, Paolo Silvestrini, L. Stodolsky, and Jacek Wosiek, cond-mat/0205514, and contribution to *Macroscopic Quantum Coherence and Quantum Computing 2002.* [Principles of quantum gates using adiabatic inversion. Design parameters for CNOT.]

DISCUSSION

Chairman: A. Bohm

G. Hegerfeldt: The final form of these off-diagonal matrix elements depends, of course, on the basis you choose.

L. Stodolsky: Exactly. This was the way I explained why the environment answers the question of what happened to the "democracy" of Hilbert space.

G. Hegerfeldt: The other point, I was going to make, is that the measurement problem is very difficult. If at the exponential fall of the non-diagonal matrix elements the decomposition of the density matrix is not unique, for instance, if we had one density matrix we can decompose the density matrix one in one half

and one half, and many different superpositions. If you have degeneracy then the decomposition is not unique.

L. Stodolsky: Afraid I haven't understood the question, perhaps we can discuss this privately.

R. Chiao: How is it related to the Zurek's work on the "pointer basis"? Is it the same thing?

L. Stodolsky: Yes. However, since I don't believe in the "measurement problem", in our old work we stressed the "decoherence by the environment" more than "the measurement question".

R. Chiao: Another question I have for you. You solve only one half of the problem. The off-diagonal elements of the density matrix go away. There is still the remaining problem, which outcome will you actually get, zero or one? Do you have any answer to this second half of the problem?

L. Stodolsky: I think there's a misunderstanding or I don't understand the question. The density matrix represents the result of many repeated experiments and not of just one trial. If we don't see this difference we are going to be confused.

S. Pascazio: Have you looked at the adiabatic corrections?

L. Stodolsky: Yes. Here are two plots addressing this point. (See Figs 4 and 5.) These were done for a neutrino problem, but it's independent of the kind of system. This first plot (Fig 4) is for a very slow adiabatic sweep, the second (Fig 5) for a faster, somewhat non-adiabatic sweep. The various panels in each figure are for different values of the decoherence rate D. With D=0 we see with the slow sweep that we get a perfect adiabatic inversion: P_3 reverses direction, it starts from one and goes to minus one. In Fig 5, when we make the sweep faster, we see that even with decoherence zero, P_3 does not quite get all the way around since it is not adiabatic. Note, incidentally, for very large D (last panel on either plot) P_3 is practically unchanging. This is the "Zeno" effect (see ref. 2).

S. Pascazio: Yes, I understand, the neutrino is a simple system and the MSW theory is a rather simple theory. I am interested in non-adiabatic corrections when you have SQUIDs. Do they depend on the size of the system or not?

L. Stodolsky: Well, you can write down the analogy of this for the SQUID and you can write down what the adiabatic condition is (see refs 17 and 18). We have also studied non-adiabatic effects by computer simulations for these systems. So we can simulate it and we have some results but I don't believe them yet, we are still playing with the program. Anyway, it is a perfectly straightforward problem. [*Note added in proof by LS*: More extensive simulations for the SQUID have given reasonable agreement with the theoretical estimate for the adiabatic condition. Also, in answer to the question that was asked: No, the size of the system has no direct influence on the adiabaticity.]

P. Stamp: I have a problem. You study the so-called Landau-Zener problem with dissipation by using models which you have, precisely your time reversible problem, and they couple it to some bath of oscillators for example. My guess is that you haven't done the simulation in a way they can agree with this and the reason is very simple. Once you have gone past to avoid the crossing, if you have strong decoherence it implies that you, in fact, have strongly coupled your system to some bath. Then the probability that you have the spontaneous emission is rather

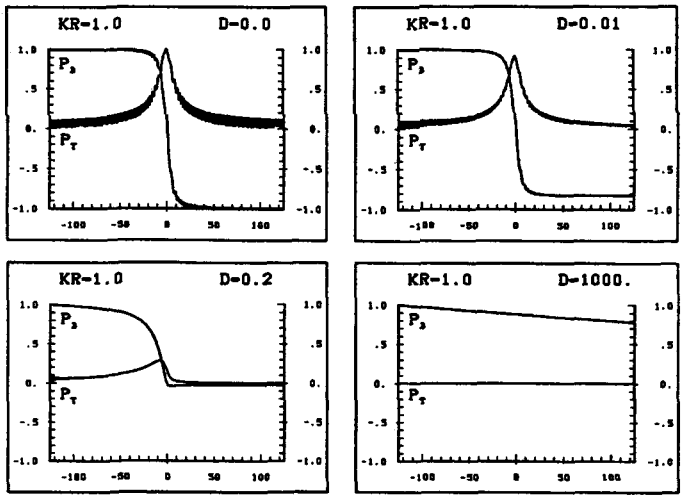

Figure 4: Behavior of the "polarization vector" representing the density matrix for a slow, adiabatic sweep of an applied "psuedo- magnetic field"(see refs. 2,3,4 for definitions). From the Diploma Thesis of J. Flaig, Munich, 1989.

strong.

L. Stodolsky: In this level crossing language, you're asking about what happens when there's a spontaneous jump down by emitting something as the levels pass each other. This could even happen off-resonance where it is more favourable because you have more phase space. Of course for neutrinos we can forget this problem because of the lack of neutrino coupling to the photon. So it depends very much which system you are talking about.

So, coming to SQUIDs, we did some simulations for the SQUIDs and we just took results in the literature for the various time scales involved: the relaxation rate, which you are asking about, as well as the decoherence rate and the tunnelling rate between the two wells. All these frequencies seem to be well separated and, in particular, what impressed me, was that the relaxation rate seems to be quite slow, so we can forget it when we are talking about sweeping in microseconds. I should point out that we are speaking of working at forty milli-Kelvin. Maybe this is below what you are used to thinking about.

P. Stamp: The real question is what is the amplitude of your sweeps, because as you have pointed out, the farther you are from resonance the larger is the probability.

L. Stodolsky: The amplitude of the sweep has to be large compared to the level splitting induced by the tunneling process, but small compared to distance to the next principal set of levels. These are the conditions we used in the simulations.

E. Polzik: Let me ask you about your macroscopic superposition. Let me give an example from atomic physics. I have an atom with two states. I can put it in a superposition of these two states. Then I have many atoms like that. Will you

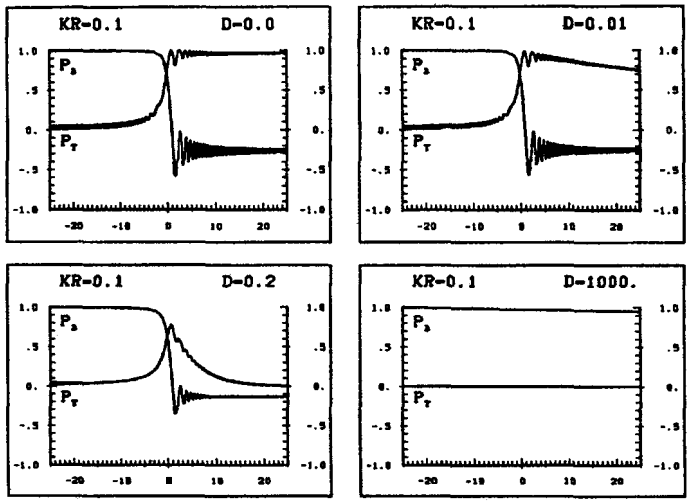

Figure 5: Same as previous figure with a faster, somewhat non- adiabatic sweep.

call it the same macroscopic superposition that you have for all electrons going this way and all electrons going that way?

L. Stodolsky: No, because in the system I am talking about they (the electrons) all reverse at the same time and are not separate atoms. They are highly correlated.

E. Polzik: The Rabi oscillations can be observed for arbitrary large number of atoms.

L. Stodolsky: But I can also do them one at a time. Here you cannot do them one at a time. The whole superconductor is reversed at the same time.

E. Polzik: It is in a sense the same kind of problem. You cannot look at them one at a time, but it does not prove that it is a macroscopic superposition.

L. Stodolsky: Well, in a sense, I agree with your tendency to doubt because I also feel that people talking about "macroscopic systems" are suffering from a fundamental conceptual error because really there is no objective definition what is a macroscopic system. From the point of view of field theory, for example even an electron contains an infinite number of degrees of freedom, if you think of the photons attached to it. But on the other hand, if you have a system where some macroscopic current, of say microamperes, changes its direction, I think most of us would consider this in some intuitive way as a macroscopic change. But I agree it is not an objective definition.

E. Polzik: The superposition of states of a macroscopic system is nothing unusual. What can be unusual here is the sort of entanglements you can observe, the correlation between various parts of the system.

KOLMOGOROV COMPLEXITY, COSMIC BACKGROUND RADIATION AND IRREVERSIBILITY

V.G. GURZADYAN

Yerevan Physics Institute and Garni Space Astronomy Institute, Armenia
ICRA, Department of Physics, University of Rome La Sapienza, Rome, Italy

We discuss the algorithmic information approach to the analysis of the observational data on the Universe. Kolmogorov complexity is proposed as a descriptor of the Cosmic Microwave Background (CMB) radiation maps. An algorithm of computation of the complexity is described, applied, first, to toy models and then, to the data of the Boomerang experiment. The sky maps obtained via the summing of two independent Boomerang channels reveal threshold independent behavior of the mean ellipticity of the anisotropies, thus indicating correlations present in the sky signal and possibly carrying crucial information on the curvature and the non-Friedmannian, i.e. accelerated expansion of the Universe. Similar effect has been detected for COBE-DMR 4 year maps. Finally, as another application of these concepts, we consider the possible link between the CMB properties, curvature of the Universe and arrows of time.

1 Introduction

In the process of the study of the Nature we are dealing not with photons, atoms, planets, galaxies and so on, but with the information that we are obtaining on them. If one can succeed to get a 'complete' information (in bits) on a given object, then, in principle, one can recover that object. Obviously, the main problem is whether one can define a universal device, so that the coding and decoding of the information will be independent on the device. The complexity or algorithmic information [12] carries this idea, i.e. invariant description of an object with respect to a universal computer. The existence of a universal computer was proven by Kolmogorov.

Invariant descriptors have always been of outstanding importance in any research. One can recall the discovery by De Moivre, Laplace and Gauss of the independence of the behavior of errors on the phenomena, among the latter, the coin tossing, human birth rates and observations of planetary motions.

In the present article we apply the concepts of algorithmic information theory in the studies of the properties of the Universe, via the analysis of the Cosmic Microwave Background (CMB) radiation data.

CMB provides one of the key windows to the early history of the Universe. In accordance with the currently held views, the expanding and cooling Universe at certain moments of time after the Big Bang at redshifts $z \simeq 1100$, becomes transparent for photons which we detect now, at $z = 0$, as CMB with highly isotropic temperature and accurate Planckian spectrum. The discovery of the quadruple anisotropy of the CMB by Cosmic Background Explorer (COBE) satellite in 1992 marked an important phase for cosmological studies. The next generation of experiments, Boomerang, Maxima, DASI, CPI, measured the peaks of the power spectrum (angular autocorrelation function). Existence of such peaks was predicted decades ago as a consequence of the interplay of the periods of the compression waves and the decoupling time at the epoch of the last scattering. On the one hand, this

supports the basic paradigms of the Big Bang cosmology, on the other hand, the existence of over 10 free parameters shows the necessity of extreme care in the determination of unambiguous values of the key cosmological parameters. Among the latter parameters which are evaluated only in combination with others, is the curvature of the Universe. Such degeneracy makes it hard to get an empirical proof of the precise flatness of the Universe.

CMB sky maps, i.e. the distribution of the temperature anisotropies over the sky, have been studied via various descriptors mainly to trace possible departures of the noise from the Gaussian one. The use of Kolmogorov complexity to extract cosmological information from the CMB maps has been proposed in [3]. It was motivated by the possibility of tracing of the geometry of the Universe by means of the effect of geodesic mixing. The effect of geodesic mixing, which is absent at precisely flat and positively curved spaces, can therefore open a way to distinguish the curvature.

Our broader aim here however, is to illustrate the efficiency and universality of complexity in the analysis of profound astrophysical problems. We complete our discussion with consideration of even older problem, the irreversibility and arrows of time.

We start with a brief account of the effect of geodesic mixing, definition and properties of complexity and then move to the description of algorithm of computations for CMB maps, with subsequent application to the Boomerang data [4].

2 Geodesics

Let us first inquire, when the geodesic defined on a 4–dimensional manifold W with Lorentzian metric ${}^4\mathbf{g}$ which is oriented and time–oriented, will be a geodesic of a 3–dimensional manifold M of Riemannian metric ${}^3\mathbf{h}$ with respect to the operation of projection.

The projection π is defined uniquely as

$$\begin{array}{ccc} W & \overset{\jmath^{-1}}{\rightarrow} & M \times R \\ & \searrow & \downarrow \pi_M \\ & \pi & M \end{array} \qquad \pi = \pi_M \circ \jmath^{-1},$$

where

$$\pi_M : M \times R \rightarrow M : (x,t) \mapsto x.$$

This reduces the curve γ in W to a curve c in $U \in M$ as represented below

$$\begin{array}{ccc} W & \overset{\pi}{\rightarrow} & M \\ & \searrow & \\ \gamma \uparrow & \overset{\phi}{} & \uparrow c \\ R & \overset{\sigma}{\rightarrow} & R \end{array} \qquad \begin{array}{l} \sigma = \phi \circ \gamma : R \rightarrow R \text{ is a diffeomorphism} \\ c = \pi \circ \gamma \circ \sigma^{-1} : R \rightarrow M : \lambda \mapsto c(\lambda). \end{array}$$

The search of the conditions to be satisfied in order for the projection of any null geodesic on W to be a geodesic on M in general case is a complicated problem. For homogeneous-isotropic spaces this can be traced via the problem of "internal time" considered initially in [5] where the corresponding sufficient conditions have

been obtained. For any null geodesics on W to be a geodesic on M the conditions include

$$\mathbf{g} = a^2(t) \cdot \mathbf{h}, \tag{1}$$

$$\phi(x,t) = \phi_0 + \int_{t_0}^{t} a^{-1}(s)ds, \tag{2}$$

$$\lambda(t) = \int_{t_0}^{t} a^{-1}(s)ds = \eta(t) - \eta(t_0), \tag{3}$$

where ${}^3\mathbf{h}$ is one of the metrics of maximally symmetric 3–dimensional manifold.

Thus the geodesic flow $W = U \times R$ be $(3+1)$–dimensional manifold with Robertson–Walker metric can be reduced to a geodesic flow on three–dimensional closed manifold $M = U$ with metric $a_0^2\mathbf{h}$ and affine parameter λ (for details see [6]).

If the Friedmann-Robertson-Walker universe has a negative curvature, the flow of null geodesics which describes the free motion of photons, represents an Anosov system [7] (locally, if U is not compact), a class of dynamical systems with maximally strong statistical properties. Anosov systems are characterized by exponential divergence of initially close trajectories, positive KS-entropy, countable Lebesgue spectrum, exponential decay of time correlation functions and K-mixing.

One of the significant properties of Anosov systems is the structural stability (coarseness) as proved by Anosov in 1967, roughly, the robustness of properties with respect to perturbations. This is a crucial property also in our context, since we live not in a FRW Universe with strongly constant curvature but with small perturbations of metric, and moreover, we know the magnitude of their smallness from the same CMB measurements.

The deviation of two geodesics in 3–manifold implies that

$$l(\lambda) = l(0)\exp(\chi\lambda), \tag{4}$$

where Lyapunov exponent $\chi = a_0^{-1}$ and $\chi = 0$ when $k = 0$ or $k = +1$. Hence

$$\lambda_c^l = \frac{1}{\chi}.$$

For the geodesic flows in W we have

$$L(t) = L(t_0)\frac{a(t)}{a(t_0)}\exp(\chi\lambda(t)). \tag{5}$$

The time correlation function of those geodesic flows for $d = 3$

$$b_{A_1,A_2}(\lambda) = \int_{SM} A_1 \circ f^\lambda \cdot A_2 d\mu - \int_{SM} A_1 d\mu \int_{SM} A_2 d\mu,$$

decreases by exponential law, i.e., $\exists c > 0$ such that for all $A_1, A_2 \in L^2(SM)$ but a finite-dimensional space in $L^2(SM)$ [8]

$$|b_{A_1,A_2}(\lambda)| \leq c\|A_1\| \cdot \|A_2\| \cdot e^{-h\lambda}\ , \tag{6}$$

where $d\mu$ is the Liouville measure, h is the KS-entropy of the geodesic flow $\{f^\lambda\}$, and

$$\|A\| = \left[\int_{SM} A^2 d\mu\right]^{1/2}\ .$$

One may readily see that if

$$A_1(u) = T(u) \ ,$$

and

$$A_2(u) = \chi_{\mathcal{K}(v)}(u) \ ,$$

where T is the temperature of sky at u, $\mathcal{K}(v)$ is a Cartesian product of $3D$ ball and $2D$ rigid angle at the point v, and $\chi_{\mathcal{K}(v)}$ is the characteristic function of the set $\mathcal{K}(v)$, then

$$T_\lambda(u) = \frac{1}{\mu(\mathcal{K}(u))} \int_{\mathcal{K}(u)} T \circ f^\lambda d\mu \tag{7}$$

and

$$T_\lambda(u) - \bar{T} = \frac{1}{\mu(\mathcal{K}(u))} \cdot b_{A_1,A_2}(\lambda) \ ,$$

where

$$\bar{T} = \int_{SM} T d\mu \ .$$

Therefore

$$\left| \frac{T_\lambda(u)}{\bar{T}} - 1 \right| \leq \frac{c}{[\mu(\mathcal{K}(u))]^{1/2}} \cdot e^{-h\lambda} \ . \tag{8}$$

In particular, for any u we have

$$\lim_{\lambda \to \infty} T_\lambda(u) = \bar{T} \ ,$$

i.e. the isotropic state is the final state.

Thus the non-zero negative curvature will lead to the decrease of perturbations of the geodesic flows, i.e. of the amplitude of anisotropy of CMB, while the strong statistical properties of Anosov systems will lead to the complexity of the anisotropy areas [9].

3 Kolmogorov Complexity

A crucial concept for definition of the complexity is that of the universal computer. A computer is considered *universal*, if for any computer C there exists a constant S_C which can be added to any program p, so that $S_C p$ should execute the same operation on computer U as the program p on computer C. The computer is a device performing only deterministic operations, so that the Turing machine can be considered as an example of universal computer, as well as the probabilistic computers of Shennon, which are using *the random rules* to reduce the time of computation for problems with unique solution.

The *algorithm* is the set of instructions defining which operations have to be executed by the computer and when. Since the computer must halt, the program cannot be a prefix for some other program; a word a is called prefix for a word b

if $b = ac$ with some other word c. Hence, the set of accessible programs should be *prefix-free.*

The *complexity* $K_U(x)$ of the sequence x with respect to a universal computer U is defined as the length in bits of the smallest algorithm p by which the computer U starting with some *initial fixed state* calculates the object x as its *only output*, and *halts.* The complexity was introduced by Kolmogorov, Solomonoff and Chaitin [1,2]. The sequence is called complex if its complexity is comparable with its length. Note, that the time of calculation is not entering this definition.

The complexity is related with another basic concept, *random sequences.* The most general definition by Martin-Löf [10] is formalizing the idea of Kolmogorov that random sequences have very small number of rules comparing to its length; the rule is defined as an algorithmically testable and rare property of a sequence. Though correlated for typical objects, the properties of complexity and randomness are not identical, however.

Chaotic systems which are non-compressible therefore possess higher complexity than regular ones which are compressible. As shown by Martin-Löf, the complexity of finite sequences varies between N and $N - log_2 N$, since even random sequences can have extended non-random subsets. In such cases the *specific complexity* introduced by Alekseev

$$k(A) = \frac{K_A}{|A|}, \tag{9}$$

enables to distinguish the random sequences and hence algorithmically complex systems, i.e. when at large N a finite limit does exist

$$k(N) \to k \neq 0,$$

from the non-random sequences when this limit is zero. Random sequences are indistinguishable (for all practical purposes) from the ones generated by the proper stochastic process [11].

In certain trivial cases low-complexity objects can be distinguished easily, for example, (0,...,0) or (1,...,1). In some other cases, the object could have a complex binary representation, such as π, though actually being again of low-complexity. In the general case, however, the situation is much less simple. Moreover, it is proved that there is no short algorithm to decide whether a given complex-looking sequence is really complex [2,11]. Fortunately, though in general the shortest program cannot be reached, i.e. the exact complexity cannot be calculated, in certain problems the obtained results cannot be too far from that value.

If the length of a sequence x is N then the obvious upper limit can be established [a]

$$K_U(x) < N. \tag{10}$$

Let us estimate the fraction of such sequences among all N-bit sequences, for which

$$K_U(x) < N - m.$$

[a] Note that, if x is the binary representation of some integer N_0, then $N \approx \log_2 N_0$.

This means that there exists a program of length $N - m$ which computes x. The total number of programs of such a length cannot be larger than 2^{N-m+1}; this is the upper limit without taking into account the prefix-free condition. Thus, we have the following upper limit

$$(2^{N-m+1} - 1)/2^{-N} \approx 2^{-m+1}.$$

This value is small if m is sufficiently large. Thus a more general relation than (10) can be established

$$K_U(x) \approx c(x)\, N, c(x) \approx 1 \tag{11}$$

Thus, the calculation of the relative complexity of an object and of a perturbed object via given computer and developed code (though the latter cannot be proved to be the shortest possible), has to reflect the complexity introduced by the perturbation. Since in our problem the complexity is a result of the propagation of photons after the last scattering surface (if k=-1), one can thus 'measure the perturbation' caused by the curvature of the space as it was performed while measuring the elongation of the CMB anisotropy areas in [13].

The complexity of a dynamical system can be determined by means of the representation of the trajectory via a symbolic language [12]. Then a trajectory of the considered dynamical system can be viewed as a sequence of symbols which can be translated into the language of bits. The dynamics can be called chaotic (for fixed initial conditions) if the corresponding symbolic sequence is algorithmically complex. Note that the partition should be detailed enough because algorithmic complexity is well-defined only for sufficiently long sequences of symbols. The CMB digitized maps when given values of averaged temperature are assigned to the pixels covering a region of sky is a proper example for symbolic dynamics, and hence can be linked not only with complexity but also random sequences.

Below we describe an algorithm of estimation of the complexity for anisotropy areas of computer-imitated CMB maps. Similarly, one can formulate the problem for definition and study of the random sequences of CMB maps.

4 The Complexity Algorithm

Strictly speaking we can estimate only the upper limit of K corresponding to a given algorithm. By algorithm we will understand the computer program in PASCAL [14], along with the data file, describing the coordinates of the pixel of the anisotropy area (spot). Namely, the data file includes compressed information about the string of digits. The program is a sequence of commands performing reconstruction of the string and calculations of the corresponding lengths. Since at the analysis of various areas we use the same code, the only change will be in the data files. Hence the complexity of the figure will be attributed to the file containing the information on the position of the pixels.

The code describing the area works as follows. As an initial pixel we fix the upper left pixel of the area and move clockwise along its boundary. Each step – a 'local step' – is a movement from a current pixel to the next one in above given direction. This procedure is rigorously defining the 'previous' and 'next' pixels.

Table 1.

first 2 bits	next bits
0 1	1
1 0	2
1 1	3

Two cases are possible. First, when the next pixel (or several pixel areas) after the initial one is in the same row: we write down the number of pixels in such a 'horizontal step'. The second case is when the next pixel is in a vertical direction; then we perform the local steps in vertical direction ('vertical step') and record the number of corresponding pixels. Via a sequence of horizontal and vertical steps we, obviously, return to the initial pixel, thus defining the entire figure via a resulting data file.

The length of the horizontal step cannot exceed the number of columns, i.e. N, while the vertical step cannot exceed M, requiring $log_2 M$ and $log_2 N$ bits of information, correspondingly. For the configurations we are interested in, the lengths of the horizontal and vertical steps, however, are much less than $log_2 M$ and $log_2 N$ and therefore we need a convenient code for definition of the length of those steps. The code realized in [14] was for $M = N = 256$; apparently for each value of M and N one has to choose the most efficient code.

Thus, after each step, either horizontal or vertical, a certain amount of bits of information is stored. The first two bits will contain information on the following bits defining the length of the given step in a manner given in Table 1. The case when the first two bits are zero, denotes: if the following digit is zero than the length of the step is $l_s = 0$, and hence no digits of the same step exist; if the next digit is 1, then 8 bits are following, thus defining the length of the step. If $l_s = 1$, then after the combination 0 1 the following digit will be either 0 or 1 depending whether the step is continued to the left or to the right with respect to the direction of the previous step.

Thus, the complexity is a calculable quantity for CMB digitized sky maps [14]. Its values correlate also with the values of the fractal dimension of the areas.

5 Cosmic Background Maps

The available CMB maps such as of COBE and even Boomerang, are not accurate enough for the meaningful calculation of the Kolmogorov complexity. However, its simplified descriptor can be used for those maps, namely, the mean elongation-ellipticity of the anisotropy spots. This aim also needs the development of special algorithms and careful runs to distinguish correlations from the foreground effects.

We now briefly describe the special purpose adaptive software MAP08 [16], which was used for the analysis of the Boomerang data. The code enabled to reveal the hot and cold anisotropy areas, determine their coordinates, sizes in pixel numbers, analysis of their shapes, of the spatial correlation functions, etc. The software runs in interactive regime with two input datasets A and B obtained at measurements

at two channels, via the sum and difference maps, as well as Gaussian and any simulated map.

After the definition of the temperature threshold interval, for example, from -2000 μK up to +2000 μK, with step 25 μK, the choice of the minimal and maximal number of pixels per area (e.g. 3-200), of the step of the input matrix (e.g. 1 arc min), the mode SkyMap enables the visualization of the map and a creation of a matrix MM containing the pixel data for positive (negative) thresholds of areas of equal or higher (lower) the given threshold. For parameters of the Boomerang data, the following choice was efficient: 1 Pix 2×2 pixels, Sqw - a square of $8' \times 8'$ (approximately), Dia - a circle of diameter 11.2'.

The matrix MM [x, y] of a unit step and given size, e.g. 1692×1296 cells for Boomerang data of $1'$ cell size, defined by the following formula

$$X = round(60.0 * (XY[n, 1] - 237.11))$$

$$Y = round(60.0 * (XY[n, 2] + 41.61)); MM[x, y] = 1,$$

is determining the anisotropy areas via the choice of pixels with temperatures equal to and higher/lower than the given threshold. The non-equal size of the pixels and some other input inhomogeneities are taken into account here, while using both Cartesian or curvilinear coordinates. The scheme of the regularization can be performed for each coordinate frame, with the subsequent check of its efficiency by means of the least number of the abandoned (non-regularized) pixels.

The matrix MM is then scanned, e.g. a field of ± 11 pixels in vertical and horizontal directions at a step $1'$, and ± 1 cell with a step $7.5'$ (in both cases within a field $22' \times 22'$) with the center in x_0 and y_0. The points of the array with a given code and current coordinates x_t and y_t are chosen and the determination of the center and other characteristics of the revealed (anisotropy) areas can be performed readily. For example, the condition $r_t <= rw$ has to be checked for each pixel, where r_t is the distance between the current point and the central one, and $r_w = 9'$, while the parameters and the definition of assignment of a point to a given area can be modified if necessary.

Thus upon fixing the modes of operation and the CMB temperature threshold range and the step, the geometrical descriptors of the sum, difference, Gaussian or other simulated map can be estimated. All input parameters, auxiliary and temporary data e.g. the numbers of pixels in any given area, and extreme and average values of various parameters can be displayed.

6 Boomerang Maps

The experiment BOOMERanG - Balloon Observations Of Millimetric Extragalactic Radiation and Geomagnetism - measured temperature fluctuations of the Cosmic Microwave Background at multipole numbers corresponding to the range of the predicted so-called acoustic oscillations at the epoch of the last scattering [4]. The measurements have been performed by means of a millimetric telescope with bolometric detectors located on a balloon borne platform. It was flown in Antarctica in 1998/99 and produced maps covering 4% of the sky with high resolution, $\sim 10'$, at

four bands from 90 to 410 GHz. The rms fluctuation of the anisotropy areas was $\sim 80\mu K$. The detected fluctuations were spectrally consistent with the derivative of a 2.735 K blackbody. Masi et al. [15] had shown that contamination from local foregrounds was negligible in the maps at 90, 150 and 240 GHz, and that the 410 GHz channel is a good monitor for dust emission. The maps have been obtained from the time ordered data using an iterative procedure, which properly takes into account the system noise and produces a maximum likelihood map. Structures larger than 10^o have been removed, to avoid the dominating effects of instrument drifts and 1/f noise. The map has also been convolved with a Gaussian kernel to obtain a final FWHM resolution of 22.5 arcmin.

The study of the Boomerang maps at 150 GHz covering around 1% of the sky have been performed by means of the MAP08 code together with P.De Bernardis and the Boomerang team [17].

The anisotropy areas have been revealed at each temperature threshold. MAP08 enabled the analysis of the properties of various subsets of areas, with given number of pixels, within given interval of pixel numbers, e.g. from 3 to 200 pixel ones, the distribution of the areas vs number of pixels, etc. The mean ellipticity of the areas has been estimated via a procedure of double averaging, first, over the areas at given temperature threshold, then, over the threshold interval. The dependence of the mean ellipticity of the anisotropy areas vs the temperature threshold obtained during that study are shown in Figures 1 and 2.

The presence of a threshold interval where the ellipticity is independent on the threshold is seen from Figure 1. Such behavior was shown to be robust with respect to the pointing reconstruction procedure accuracy. The ellipticity due to the noise on the other hand, has to depend on the threshold. Therefore this indicates correlations existing in the sky signal. Similar elongation has been detected also for COBE-DMR 4-year maps. The mean elongation for COBE data was around 1.9 [13], for Boomerang data it is close to 2.2 [17]. This is remarkable since COBE-DMR and Boomerang data are quite different by their angular resolution and noise level.

The described CMB ellipticity (see Figure 3), in principle, can arise due to still unknown processes. However, if such correlations in the sky signal are due to geodesic mixing, as was predicted, then this can be interpreted as model-independent indication of two effects, of negative curvature and the non-Friedmannian expansion of the Universe [18].

The further work on simulated maps and especially the search of this effect at forthcoming more accurate experiments is of particular interest.

7 Arrows of Time

Let us mention another aspect of the effect of geodesic mixing which may provide a condition necessary for emergence of the thermodynamic arrow of time. This mechanism can also explain why CMB contains the major fraction of the entropy of the Universe.

The thermodynamical arrow for a statistical system can be formulated as a consequence of the following conditions (see e.g. [19,20,21,22]):

1) Decorrelated (special) initial conditions;

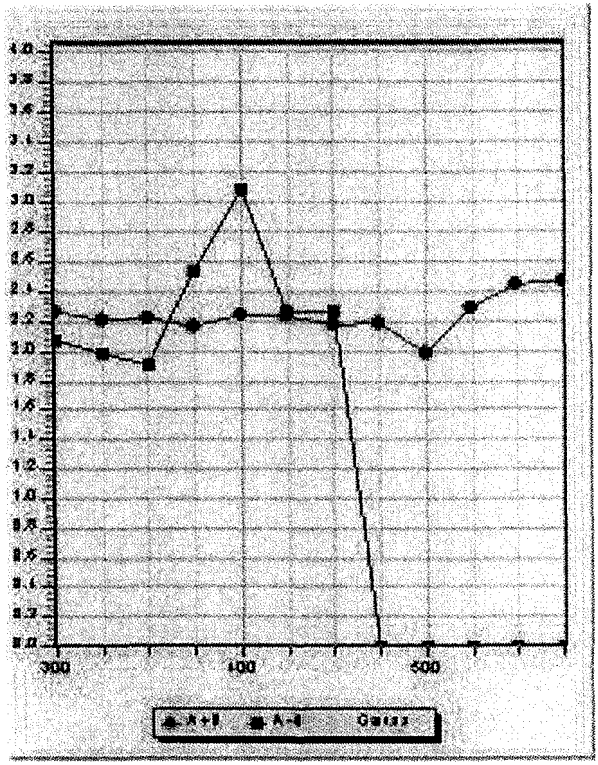

Figure 1. The adaptive software MAP08 revealed the dependence of mean ellipticity of anisotropy areas in the Boomerang sum, A+B (circles), and difference, A-B (squares), maps created from independent channels, on the CMB temperature in μK; positive thresholds. A+B maps contain a cosmological signal, while A-B maps contain mainly the noise. From 3 to 200-pixel areas are taken into account, the step of the matrix MM is 0.6 arc min, (for details see [17]).

2) No memory dynamics.

It should be emphasized that both these conditions are necessary and they appear already in Boltzmann's derivation of his kinetic equation, though not explicitly. They can be traced clearly in Zwanzig's derivation of master-equation [23] or Jaynes' information-theoretical approach to irreversibility [24]. A usual discussion about possible relations between cosmological and thermodynamical arrows of time concentrates mainly on the first condition [19,22,25]. However, one can show [26] that this is not sufficient, since *special initial conditions alone can generate only a thermodynamical pre-arrow of time.*

We then point out that, along with the initial conditions the second ingredient of the thermodynamical arrow can have a cosmological context as well, due to mixing of null trajectories in hyperbolic spaces.

If this is indeed the mechanism of the origin of the thermodynamic arrow,

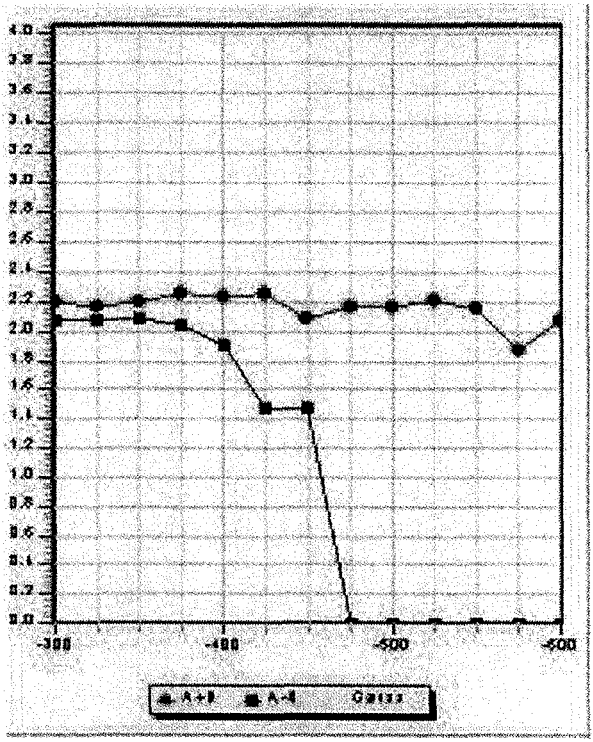

Figure 2. The same as in Fig 1. Negative thresholds.

then the thermodynamics in a flat and positively curved universe is not necessarily strongly time asymmetric. Time asymmetry is observed since we happened to live in a Universe with negative curvature. In other words, the symmetry of the Newtonian mechanics, electrodynamics, quantum mechanics might purely survive in some universes. On the other hand, a recent activity devoted to the foundations of thermodynamics allows to disentangle time-asymmetric elements from the remained basis.

In this context the essence of thermodynamical arrow must be understood as not the mere increase of entropy of an almost closed system, but the fact that this arrow has the universal direction in the entire Universe (see [27]). In the light of the suggested explanation of the emergence of this arrow, it follows that the negative curvature is the very mechanism unifying all local thermodynamical arrows. While in the flat or positively curved universes, i.e. at the absence of a global unification mechanism, there can be local thermodynamical arrows with various directions.

This enabled us to formulate the *curvature anthropic principle*, to reflect the difference of conditions for life in the hyperbolic Universe and hence with unified

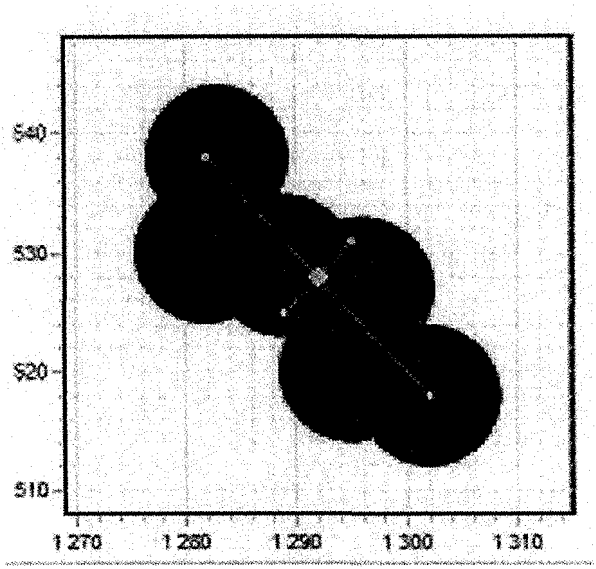

Figure 3. An example of an anisotropy area in Cosmic Microwave Background map observed by Boomerang [4]. The semi-axes defined for the estimation of the ellipticities are shown.

arrows, and in flat or positively curved spaces, i.e. at the absence of such unification mechanism [26].

Often the thermodynamical arrow of time is identified with the second law of thermodynamics, and the appearance of Gibbs distribution. We show [26] that the second law, and the Gibbs distribution can be obtained from purely time-symmetric arguments, and need not be consequences of the thermodynamical arrow.

Thus CMB has to carry the direct signature of the thermodynamical and cosmological arrows.

8 Conclusion

We showed that the algorithmic information approach can enable not only qualitative but also quantitative study of astrophysical problems. The estimation of the Kolmogorov complexity for computer-generated CMB maps and detection of threshold independent ellipticity in the COBE and Boomerang sum maps, geodesic mixing and possible model-independent indication of the non-zero negative curvature and the accelerated expansion of the Universe, show the efficiency of the approach.

One may expect the further use of algorithmic information concepts not only in fundamental problems but also in various applications. The seeds of such developments are seen already now, considered as fiction several decades ago. For example, instead of sending a letter by post, now it is enough to send a binary

coded signal which then is transfered to a hardcopy. The same is true for a color image, music, movie. In principal the same operation can be performed, say with an apple, via sending the relevant complete information. One may think that, in future, even human beings can travel via transfer of information, thus realizing the speed-of-light travels.

I am grateful to many colleagues. Thus, many of the mentioned results have been obtained together with my collaborators A. Kocharyan, A. Allahverdyan and A. Kashin. The Boomerang data have been analyzed together with P. de Bernardis and the Boomerang team. Numerous discussions with R. Penrose were of particular importance.

References

1. Kolmogorov A.N., Probl.Inform.Transmis. 1, 3, 1965; UMN, 38, 27, 1983.
2. Chaitin G.J., *Algorithmic Information Theory*, Cambridge University Press, 1987.
3. Gurzadyan V.G., Europhys.Lett., 46, 114, 1999.
4. De Bernardis P., et al, Nature, 404, 955, 2000; New Astronomy Rev., 43, 289, 1999; Astrophys.J. 564, 559, 2002.
5. Lockhart C.M., Misra B., Prigogine I., Phys.Rev., D25, 921, 1982.
6. Gurzadyan V.G., Kocharyan A.A., *Paradigms of the Large-Scale Universe*, Gordon and Breach, 1994.
7. Anosov D.V., Comm. Steklov Math.Inst., 90, 1, 1967.
8. Pollicott M., J.Stat.Phys., 67, 667, 1992.
9. Gurzadyan V.G., Kocharyan A.A., Astr.Astrophys., 260, 14,1992; Europhys.Lett. 22, 231, 1993.
10. Martin-Löf K., Inform. & Control, 9, 602, 1966.
11. Zvonkin A.K., Levin L.A., UMN, 25, 85, 1970.
12. Arnold V.I., *Mathematical Methods of Classical Mechanics*, Nauka, Moscow, 1989.
13. Gurzadyan V.G., Torres S., Astr.Astrophys. 321, 19, 1997.
14. Allahverdyan A.E., Gurzadyan V.G., Soghoyan A.A., Int.Journ.Mod.Phys.D., 8, 383, 1999.
15. Masi S., et al, Astrophys.J. 553, L93, 2001.
16. Gurzadyan V.G., Kashin A.L., in Proc.IX Marcel Grossmann Meeting, World Scientific, 2002.
17. Gurzadyan V.G., Ade P.A.R., de Bernardis P., et al, 2002 (in preparation).
18. Gurzadyan V.G. 2002, (in preparation).
19. Penrose R., *The Emperor's New Mind*, Oxford University Press, 1989; J. Stat.Phys. 77, 217, 1994.
20. Petrosky T., Prigogine I., Advances in Chem. Phys. XCIX, 1, 1997.
21. Zurek W., in *Physical Origins of Time Asymmetry*, ed. J.J.Halliwell, J.Perez-Mercader, W.H.Zurek, p.175, Cambridge University Press, 1996.
22. Zeh H.D., *The Physical Basis of the Direction of Time*, Springer, Berlin, 1992; C. Kiefer, H.D. Zeh, Phys. Rev. D, 51, 4145, 1995.
23. Zwanzig R., J. Chem. Phys., 33, 1338, 1960.

24. Jaynes E.T., in *Papers on Probability, Statistics, and Statistical Physics*, ed. R.D. Rosenkrantz, Kluwer, Dordrecht, 1983.
25. Mackay M.C., Rev.Mod.Phys., 61, 981, 1989.
26. Allahverdyan A.E., Gurzadyan V.G., in *The Chaotic Universe*, ed. V.G.Gurzadyan, R.Ruffini, p.218, World Scientific, 2000; J.Phys.A, 2002 (in press).
27. Gell-Mann M., Hartle J.B., in *Physical Origins of Time Asymmetry*, ed. J.J. Halliwell, J. Perez-Mercader, W.H. Zurek, p.311, Cambridge University Press, 1996.

DISCUSSION

Chairman: A. Bohm

L. Reichl: Do you have a result? Does the universe have negative curvature?

V. Gurzadyan: We have seen an effect in cosmic background radiation maps from the analysis of experimental data of COBE and Boomerang without any model dependent approach. It is not a fitting of data by a curve of a given model. The recent models contain 11-13 free parameters describing the content of the matter in the universe, of the dark matter, the initial fluctuation spectrum, etc. To fit an empirical curve by a model with so many free parameters is not as difficult. The problem is to prove that this is the only possible model. Our approach is model independent. We can say that we have a new effect, which would exist in a non-flat universe. Therefore either we have a new physical effect or this effect is due to non-zero curvature of the universe.

I. Khalatnikoff: Non zero, negative or positive?

V. Gurzadyan: Negative.

I. Khalatnikoff: Closed or open?

V. Gurzadyan: I prefer not to use the words "closed" or "open" because Einstein equations define the geometry but not the topology of the universe. For example, at zero curvature one can have a sheet, a cylinder, a torus. We can speak only on the negative curvature $k = -1$, but topologically the universe can be both compact (closed) or non-compact (open).

L. Stodolsky: The usual opinion in astrophysical circles is that the curvature is equal to zero. So, you have found it different?

V. Gurzadyan: Yes, at present flat models are preferred, in part as inflationary motivated, though there are claims for other models as well. Precise flatness cannot be proved however, not only due to the observational errors, but due to the degeneracy and dependence on a number of free parameters.

M. Courbage: Does the complexity depend on the stage of the evolution of the universe?

V. Gurzadyan: Of course. I have shown a formula where the complexity depends on the time from the last scattering epoch. The effect of geodesic mixing could be observed, in principle, from quasars. But there is not enough time (distance) for photons from quasars to feel the geometry. Cosmic background photons

are moving too long. The problem comes to the numerical measurement of the tiny effect, whether it is possible or not. It appears that it can be possible.

I. Khalatnikoff: You have shown us different geometry of spots. Have you concluded about the curvature from the analysis of these spots?

V. Gurzadyan: The analysis was motivated by the predicted effect and we have found its signature. It may be a signature of another effect.

P. Stamp: It is a way of calculation of multiple correlations between the densities of radiation and matter. This was calculated since 1962. Can you, from these correlation functions, which you can simply extract from measurements, deduce the curvature k?

V. Gurzadyan: If you mean the correlations in the angular power spectrum, the acoustic peaks, they were indeed predicted long time ago, most clearly by Doroshkevich, Sunyaev and Zeldovich in 1978. They are now measured by Boomerang and at other experiments. The autocorrelation function indeed depends on the curvature but also on many other parameters and though provides important constraints on the curvature, the deduction of the precise value of k is not as simple. Here I discussed correlations in the sky maps.

OBSERVATION OF THE QUANTUM ZENO AND ANTI-ZENO EFFECTS IN AN UNSTABLE SYSTEM

BRAULIO GUTIÉRREZ-MEDINA, MARTIN C. FISCHER, AND MARK G. RAIZEN[a]
Center for Nonlinear Dynamics and Department of Physics,
The University of Texas at Austin, Austin, Texas 78712-1081, USA

We report the first observation of the Quantum Zeno effect (QZE) and Anti-Zeno effect (AZE) in an unstable system. These effects are the inhibition or enhancement of decay by frequent measurement during the non-exponential time. The experiment builds on our earlier observation of short-time deviations from exponential decay in the tunneling of atoms from accelerating lattices. Recent improvements in the experiment and development of the measurement method have now allowed us to observe both the QZE and the AZE.

1 Introduction

From its foundations, quantum mechanics assigns a special role to the observer of any physical system. The fact that any measurement of a quantum system projects it to one particular eigenstate has counter-intuitive consequences. One observable effect is the prediction that repeated observations on an unstable system can slow down its evolution to the point that, for frequent enough observations, decay can be completely inhibited [1,2]. This is known as the Zeno effect. More recently, it was predicted that under more general conditions repeated measurement can enhance the decay [3,4,5], a phenomenon which was called Anti-Zeno (or Inverse-Zeno) effect. The experimental observation of these effects relies on the ability to reset the evolution of the system during the non-exponential time of the decay. Unstable systems like a radioactive nucleus or an atom in an excited state possess non-exponential times so short that are currently inaccesible to experiment. This is why the observation of these effects has been elusive until now. We overcame this experimental difficulty by studying the tunneling of ultracold atoms in an accelerating optical lattice [6], a system that can be shown to be unstable. The importance of this system is that it exhibits non-exponential decay on time scales that are accessible to experiment.

In this paper we first review the main aspects of non-exponential decay, an effect predicted more than forty years ago and only observed recently experimentally in our group [7]. The possibility of the existence of the Zeno and Anti-Zeno effects will follow the discussion. The third part describes the main features of our quantum system, consisting of neutral atoms transported in an accelerating optical lattice. The experimental realization and our results are described in the last section.

2 Non-exponential decay, and the Zeno and Anti-Zeno effects

2.1 Non-exponential decay

An exponential decay law is the universal hallmark of unstable systems and is observed in all fields of science. This law is not, however, fully consistent with

[a]Correspondence to: raizen@physics.utexas.edu

quantum mechanics and deviations from exponential decay have been predicted for short as well as long times [8,9,10]. In 1957 Khalfin showed that if the Hamiltonian of the system, H, has a spectrum bounded from below, the survival probability P is not a pure exponential but rather of the form

$$\lim_{t\to\infty} P(t) \approx \exp(-ct^q) \qquad q < 1, c > 0. \tag{1}$$

Winter examined the time evolution in a simple barrier-penetration problem [9]. He showed that the survival probability begins with a non-exponential, oscillatory behavior. Only after this initial time does the system start to evolve according to the usual exponential decay of an unstable system. Finally, at very long times, it decays like an inverse power of the time.

The initial non-exponential decay behavior is related to the fact that the coupling between the decaying system and the reservoir is reversible for short enough times. Moreover, for these short times, the decayed and undecayed states are not yet resolvable, even in principle.

For very short times the time evolution of the survival probability can be determined explicitly. Given that the mean energy of the decaying state is finite, it can be shown that [10]

$$\left.\frac{dP(t)}{dt}\right|_{t\to 0} = 0. \tag{2}$$

This is a general property independent of the details of the interaction. However, the time scale over which the deviation from exponential behavior is apparent depends on the particular time scales of the decaying system. Greenland and Lane point out a number of time scales which are relevant [11]. The first time scale τ_e is given by the time that it takes the decay products to leave the bound state region. This time can be estimated as

$$\tau_e = \frac{\hbar}{E_0}, \tag{3}$$

where E_0 is the energy released during the decay. It determines the amount of time required to pass before the decayed and undecayed states can be resolved. The second time scale τ_w is related to the bandwidth ΔE of the continuum to which the state is coupled

$$\tau_w = \frac{\hbar}{\Delta E}. \tag{4}$$

The phases of all states in the continuum evolve at a rate corresponding to their energy. Thus after the time τ_w the phases of these states have spread over such a wide range as to prevent the reformation of the initial undecayed state. After this dephasing time, the coupling is essentially irreversible.

Although these predictions are of a general nature and applicable in every unstable system, deviations from exponential decay have not been observed experimentally in any other system than the one described here [7]. As mentioned earlier, the primary reason is that these characteristic time scales in most naturally occurring systems are extremely short. For the decay of a spontaneous photon, the time τ_e it takes a photon to traverse the bound state size is approximately an optical period, 10^{-15} s. For a nuclear decay this time scale is orders of magnitude shorter,

about 10^{-21} s. By contrast, the dynamical time scale for an atom bound in an optical lattice is just the inverse band gap energy, which in our experiments is on the order of several microseconds.

2.2 Quantum Zeno and Anti-Zeno effects

The universal phenomenon of non-exponential decay of unstable systems led Misra and Sudarshan in 1977 to the prediction that frequent measurements during the non-exponential period could inhibit decay entirely [1,2,12]. They named this effect the *Quantum Zeno effect* after the Greek philosopher, famed for his paradoxes and puzzles. In his most famous paradox, Zeno considers an arrow flying through the air. The time of flight can be subdivided into infinitesimally small intervals during which the arrow moves only by infinitesimal amounts. Assuming the summation of infinitesimal terms amounts to nothing led Zeno to believe that motion is impossible and is merely an illusion. The version put forth by Misra and Sudarshan is the quantum mechanical version of the paradox. One can take advantage of the slow initial decay in order to inhibit the decay altogether just by performing frequent observations on the system at very short time intervals. Each observation made during this time not only stops but resets the evolution of the system.

Reviews of the Quantum Zeno effect can be found in modern textbooks of quantum mechanics [13]. Even though measurement-induced suppression of the dynamics of a two-state driven system has been observed [14,15], no such effect was ever measured on an unstable system.

The original prediction of the quantum Zeno effect has been recently revisited [3,4,5]. The studies focused on the frequency of observations, and on the decay of an unstable system as a consequence of a reservoir of possible states. The result was the prediction of the opposite effect. It was found that, under more general conditions, repeated observations must shorten the lifetime of the unstable system, which was called 'Anti-Zeno' or 'Inverse-Zeno' effect. Because of the characteristic features of decay of our system, we were able to observe both effects just by adjusting the interruption interval, as it will be described later.

3 Quantum transport in an optical lattice

The system of ultra-cold atoms in a periodic optical potential offers unique means of studying solid state effects with quantum optics tools [16]. In order to gain insight into our experiment, some of the basic properties of this system will be reviewed. A thorough treatment of the fundamental properties can be found in many solid state textbooks [17]. The specifics of our system are described in detail in [7].

3.1 An atom in an optical lattice

A neutral atom and light far detuned from atomic resonance interact via the dipole potential. The interaction is directly proportional to the intensity of the laser light and inversely proportional to the detuning from atomic resonance. The number of spontaneous emissions can be made negligible, therefore making the system conservative. The optical potential can be created by spatially overlapping two counter-

propagating traveling light beams of the same frequency. The system, consisting of an atom in the presence of the interference pattern, has the effective Hamiltonian

$$H = \frac{p^2}{2M} + V_0 \cos\left(2k_{\mathrm{L}}x\right), \tag{5}$$

assuming that beam propagation is along the x-axis. Here, M is the mass of the atom and k_{L} is the laser wavenumber.

This form of the Hamiltonian is a textbook example for a particle placed in a spatially periodic potential, that results in a band structure energy spectrum. The study of the band structure in the optical lattice can reveal information about the behavior of electrons in a crystal lattice [16].

For electrons in a crystal the most commonly encountered perturbation is an applied static electric field. This seemingly simple perturbation leads to a very rich system, whose properties were controversial for quite some time. Experimental tests in the field of solid state physics were hindered by decohering processes which are negligible in our atom optics system. A static electric field, which exerts a strong force on the electrons in a crystal, does not have the desired effect on a neutral atom in an optical potential. However, we can simulate the corresponding force by introducing an appropriate time dependence of the optical lattice. Let us consider an optical lattice composed of two counterpropagating light beams that do not possess the same frequency. The effective Hamiltonian for this system is given by

$$H = \frac{p^2}{2M} + V_0 \cos\left(2k_{\mathrm{L}}x - \phi(t)\right). \tag{6}$$

A constant acceleration of the 'standing' wave pattern is generated by linearly chirping the frequency difference of the counterpropagating beams. This is described by $\phi(t) = k_{\mathrm{L}}at^2$, where a is the acceleration. Inserting this into the equation above yields

$$H = \frac{p^2}{2M} + V_0 \cos\left[2k_{\mathrm{L}}\left(x - \frac{1}{2}at^2\right)\right]. \tag{7}$$

To make the connection to the solid state system, one can transform Eq. (7) to the accelerating reference frame. Applying this transformation yields

$$\tilde{H} = \frac{p^2}{2M} + V_0 \cos(2k_{\mathrm{L}}x) + Ma\,x. \tag{8}$$

The last term containing the mass M of the atom is an inertial term, resulting from the transformation. It mimics the role of the interaction potential between an electric field $\mathcal{E}$ and the electron

$$U_{el} = \mathcal{E}\,e\,x, \tag{9}$$

where e is the electric charge of the electron.

Having established this connection, we can directly apply the results for the solid state system to an atom in the accelerated optical potential. One remarkable consequence of the equations of motion resulting from the above Hamiltonian is

that particles exposed to a static field are predicted to oscillate in space rather than increase their velocity steadily. The period of oscillation τ_B is known as the Bloch period, and is the time it takes for a particle to traverse the Brillouin zone of width $K = 2k_L$:

$$\tau_B = \frac{2\hbar k_L}{Ma} = \frac{2v_r}{a}, \tag{10}$$

where v_{rec} denotes the single photon recoil velocity.

3.2 Landau-Zener tunneling

The problem of atoms in an accelerated optical lattice can be treated using a Landau-Zener tunneling process based on diabatic transitions in momentum space[18]. An alternative description can be derived in the position representation[20].

A particle approaching an avoided level crossing between energy bands might not be able to follow the dispersion curve adiabatically, in which case it continues its motion and diabatically changes levels across the energy gap. The expression for the probability P of diabatic transfer between two repelled levels[19] is

$$P = \exp\left(-\frac{\pi}{2\hbar}\frac{E_g^2}{\frac{d}{dt}(\epsilon_1 - \epsilon_2)}\right), \tag{11}$$

where E_g is the minimum energy separation of the perturbed levels and $\epsilon_{1,2}$ are the unperturbed energy eigenvalues of level 1 and 2, respectively.

Let N denote the number of particles populating the lowest band within the first Brillouin zone. Applying formula (11) to our case[18] yields an exponential decay of the population N as

$$N = N_0\, e^{-\Gamma_{LZ}\, t}, \tag{12}$$

with the Landau-Zener (LZ) decay rate Γ_{LZ} given by

$$\Gamma_{LZ} = \frac{a}{2v_r}\, e^{-a_c/a}. \tag{13}$$

The critical acceleration a_c is

$$a_c = \frac{\pi}{4}\frac{E_g^2}{\hbar^2 k_L}. \tag{14}$$

Experimental studies of the tunneling rates out of the lowest band were performed in our group and the decay rates were compared to the Landau-Zener prediction[21,22].

As mentioned earlier, deviations from exponential decay are expected in our system. Niu and Raizen[23] performed a detailed investigation of a two-band model, and found an initial non-exponential regime that starts with a quadratic time dependence, then becomes a damped oscillation, and finally settles into an exponential decay. The time scale for which the coherent oscillations damp out and the exponential decay behavior sets in is identified as the crossover time t_c equal to

$$t_c = \frac{E_g}{a}\frac{1}{2\hbar k_L}. \tag{15}$$

For a typical value for the acceleration of $a = 10,000\,\mathrm{m/s^2}$ and a band gap of $E_g/h = 80$ kHz the crossover time is $t_c = 2\,\mu$s. This time is accesible experimentally, and is the key feature that allowed us to observe non-exponential decay [7].

Access to the non-exponential time in our system also made possible the observation of both Zeno and Anti-Zeno effects. By repeatedly resetting the evolution while the system was decaying we managed to alter the dynamics and show the existence of these novel quantum effects.

4 Experimental realization

In order to prepare the initial condition, well developed techniques of laser cooling and trapping of neutral atoms were employed. We started by cooling and trapping approximately $3 \cdot 10^5$ sodium atoms in a magneto-optical trap, followed by a stage of molasses cooling [24]. After this stage the distribution had a typical Gaussian width of $\sigma_x = 0.3$ mm in position and $\sigma_v = 6\,v_{rec}$ in velocity, where $v_{rec} = 3$ cm/s is the single-photon recoil velocity. After switching off the cooling and trapping fields the interaction beams were turned on. The interaction potential was a standing wave created by two linearly polarized counter-propagating laser beams with parallel polarization vectors. The light was far detuned from the $(3S_{1/2}) \leftrightarrow (3P_{3/2})$ transition in order to avoid electronic excitation and the resulting spontaneous emission. Detunings typically ranged from 40 to 60 GHz and the power in each of the beams was adjusted up to 150 mW. The beams were spatially filtered and focused to a beam waist of 1.8 mm at the position of the atomic cloud, providing a relatively uniform intensity distribution over the cloud. Due to the larger initial momentum spread of the atomic distribution, switching on the interaction potential populated several of the lower energy bands. Atoms projected into the lowest band are trapped within the potential wells whereas atoms in the second band are only partially trapped. Atoms in even higher bands have energies well above the potential and hence are effectively free. In order to have a well defined initial condition we emptied all but the lowest band. We achieved this by accelerating the standing wave with an acceleration a_{trans} to a velocity of $v_0 = 35\,v_{rec}$ by linearly chirping the frequency of one of the counter-propagating beams while keeping the frequency of the other beam fixed. The acceleration of the potential leads to a loss of population in the lower bands due to Landau-Zener tunneling of atoms into higher untrapped bands. Energy gaps between successive energy bands decrease rapidly (as an increasing power of the well depth). Therefore, the transport acceleration a_{trans} was chosen to maximize tunneling out of the second band while minimizing losses from the first trapped band. This ensured that after the initial acceleration only the first band still contained a significant number of atoms. After reaching the velocity v_0 the acceleration was suddenly increased to a value a_{tunnel} where appreciable tunneling out of the first band occurred. The beginning of this large acceleration period determined the start of the experiment, or $t = 0$, and was maintained for a period of time t_{tunnel}. At the end of this tunneling period we continued the frequency chirping at the decreased rate corresponding to a_{trans}. During this segment atoms that escaped the potential were left behind while atoms still trapped at the end of tunneling were taken to higher velocities. After reaching a final velocity of $75\,v_{rec}$

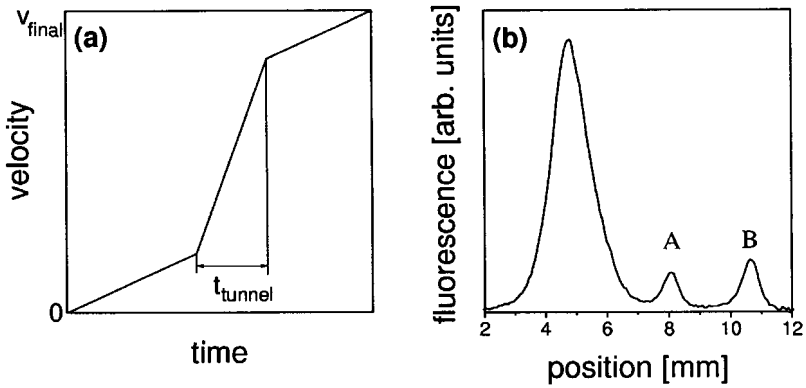

Figure 1: Part (a) shows a diagram of the acceleration sequence. Part (b) displays a typical integrated spatial distribution of atoms after the time of ballistic expansion. The large peak on the left shows atoms that were lost during the preparation of the initial condition, first segment of the acceleration sequence. The peak with label A indicates the atoms that escaped the potential during the tunneling time. The atoms that remained trapped the entire sequence correspond to label B. The survival probability is therefore equal to A over A + B.

the interaction beams were switched off suddenly. A diagram of the velocity profile versus time is shown in Fig. 1(a).

The quantity to be measured in our experiment was the fractional number of atoms that remained trapped in the first band after the tunneling time. At the end of the acceleration sequence the atoms were separated in momentum space but overlapped in position space. To distinguish the two classes of atoms a period of ballistic expansion was implemented. After an atom tunneled out of the potential during the sequence, it would maintain the velocity it had at the moment of tunneling. Turning off the light beams allowed the atoms to expand freely. During this period each atom moved a distance proportional to its velocity. Due to the difference in final velocity, trapped and tunneled atoms separated and could be spatially resolved. In the detection phase the resonant cooling beams were turned back on with no magnetic field gradient present. This temporarily restricted movement of the atoms in a 'freezing molasses'. The fluorescence of the atoms in the presence of the laser beams was imaged onto a charge-coupled-device camera. Since the potential is one-dimensional we integrated the two-dimensional image in the direction perpendicular to the transport. A typical integrated distribution is shown in Fig. 1(b). For this trace, about one third of the initially trapped atoms have tunneled out of the well during the fast acceleration period.

We measured the decay of the unstable system by repeating the experiment for various tunneling durations t_{tunnel}, holding the other parameters of the sequence fixed. In the past, our group observed deviations from exponential decay[7] following a similar procedure. In our case we focused on the effect of measurements on the system decay rate. There are two key facts used towards the observation of both Zeno and Anti-Zeno effects. The first one corresponds to the possibility of having experimental access to the non-exponential time of decay. The second concerns the

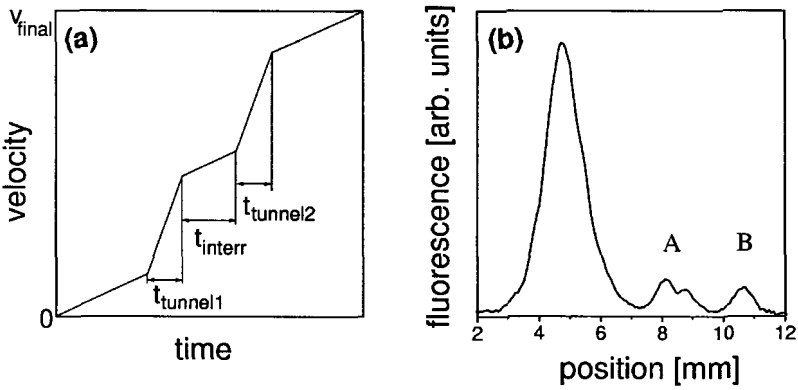

Figure 2: Part (a) shows a diagram of the interrupted acceleration sequence. The total tunneling time is the sum of all the tunneling segments. Part (b) shows a typical integrated spatial distribution of atoms after the time of ballistic expansion. One interruption was implemented in this case. The peaks can be identified as in Fig. 1. However, the area A containing the tunneled fraction of the atoms is now composed of two peaks. Atoms that left the well during the first tunneling segment are offset in velocity from the ones having left during the second period of tunneling. The amount of separation is equal to the velocity increase of the well during the interruption segment.

resetting of the evolution during the non-exponential region. As mentioned before, the quantity to be measured is the fraction of atoms remaining trapped in the potential after some tunneling time. This measurement could be realized, as before, by suddenly interrupting the tunneling duration by a period of reduced acceleration a_{interr}, as indicated in Fig. 2(a). During this interruption tunneling was negligible and the atoms were therefore transported to a higher velocity without being lost out of the well. This separation in velocity space enabled us to distinguish the remaining atoms from the ones having tunneled out up to the point of interruption, as can be seen in Fig. 2(b). At the end of the measurement the acceleration is switched back to a_{tunnel}, and the system can then be returned to its unstable state where it continues its decay. This procedure defined a new initial state with the remaining number of atoms as the initial condition. Since the 'clock' was reset, the system starts its evolution again with the same non-exponential decay features. It is important to note that the requirements for this interruption section were very similar to those during the transport section, namely the largest possible acceleration while maintaining negligible losses for atoms in the first band. This ensured that the only effect of the measurement was the separation in velocity space of trapped and untrapped atoms. This is why a_{interr} was chosen to be the same as a_{trans}. The sequence tunneling-measurement-tunneling can be repeated many times, and only the short tunneling segments contribute to the total tunneling time.

The result of such a series of frequent measurements can be seen in Figure 3. The hollow squares indicate the decay curve without interruption. The solid circles in Fig. 3 depict the measurement of the survival probability in which after each tunneling segment of 1 μs an interruption of 50 μs duration was inserted. The survival probability clearly shows a much slower decay than the corresponding system

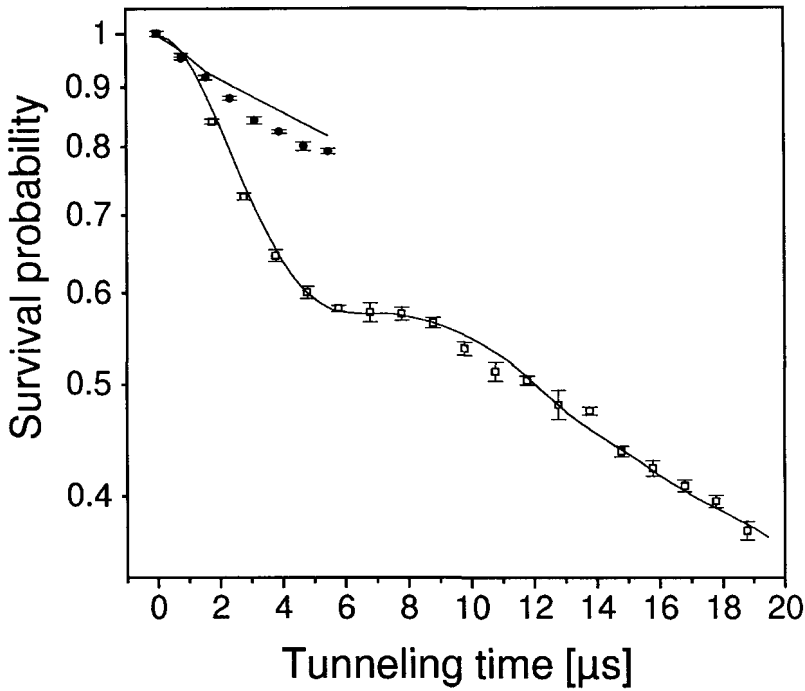

Figure 3: Probability of survival in the accelerated potential as a function of duration of the tunneling acceleration. The hollow squares show the non-interrupted sequence, the solid circles show the sequence with interruptions of 50 μs duration every 1 μs. The error bars denote the error of the mean. The data have been normalized to unity at $t_{\text{tunnel}} = 0$ in order to compare to the simulations. The solid lines are quantum mechanical simulations of the experimental sequence with no adjustable parameters. For these data the parameters were: $a_{\text{tunnel}} = 15,000\,\text{m/s}^2$, $a_{\text{interr}} = 2,000\,\text{m/s}^2$, $t_{\text{interr}} = 50\,\mu$s and $V_0/h = 91$ kHz, where h is Planck's constant.

measured without interruption. This constitutes the first observation of the Zeno effect in an unstable system, following the spirit of the original proposal by Misra and Sudarshan. It is important to note that our experimental setup had a limited time response, and care was taken to include this into the analysis of the data. The response time was limited by electronic and electro-optic devices used in the experiment. The frequency response was measured and the resulting transfer function was used to calibrate the response of the optical potential to a desired change in acceleration. This ensured that only sections were included for which tunneling was substantial and established a lower bound for the actual tunneling duration. This effect was taken into account for the curves in Fig. 3. Quantum mechanical simulations of the decay were performed by numerically integrating Schrödinger's equation for the experimental sequence and determining the survival probability numerically. The results are indicated as solid lines in Fig. 3. These simulations contained no adjustable parameters and are in good agreement with the experimental data. The seemingly larger decay rate for the Zeno experiment as compared to the simulation

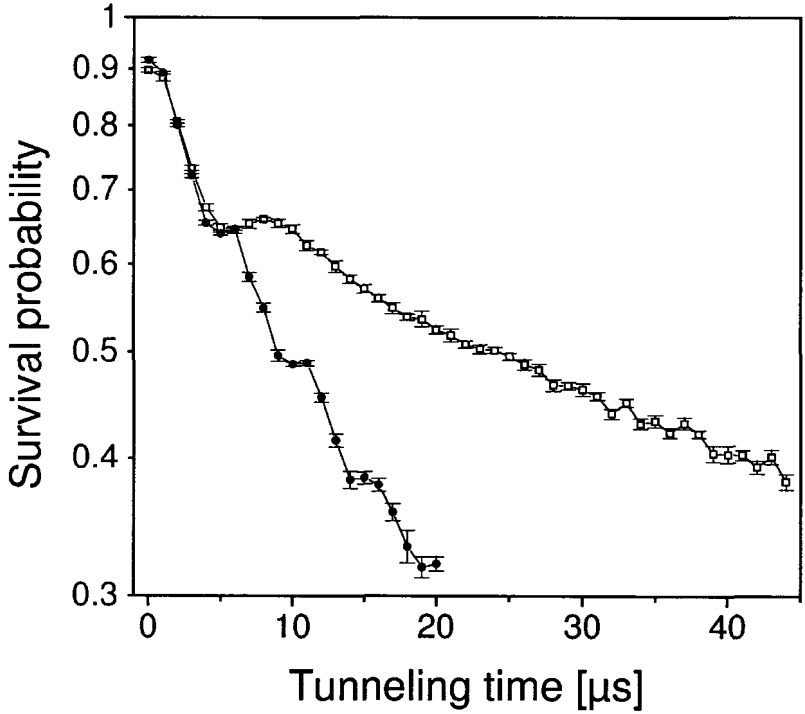

Figure 4: Survival probability as a function of duration of the tunneling acceleration. The hollow squares show the non-interrupted sequence, the solid circles show the sequence with interruptions of 40 μs duration every 5 μs. The error bars denote the error of the mean. The experimental data points have been connected by solid lines for clarity. For these data the parameters were: $a_{\text{tunnel}} = 15,000\,\text{m/s}^2$, $a_{\text{interr}} = 2,800\,\text{m/s}^2$, $t_{\text{interr}} = 40\,\mu$s and $V_0/h = 116$ kHz.

may be attributed to an under-estimate of the actual tunneling time.

During the non-exponential time, the uninterrupted decay curve shows two very distinct features. For acceleration times less than one microsecond the decay is much slower as compared to the exponential decay. This was used in observing the Zeno effect by realizing the observations after such short times of tunneling. The other feature, however, is the complete opposite. After the initial period of slow decay the curve shows a steep drop as part of an oscillatory feature, which for longer time damps away to show the well-known exponential decay. Therefore, interrupting the decay right after the steep drop would lead the system to an overall decay that is faster than the uninterrupted decay[4]. This is the predicted Anti-Zeno effect. The solid circles in Fig. 4 show such a decay sequence, where after every 5 μs of tunneling the decay was interrupted by a slow acceleration period. The length of the tunneling segments between the measurements are chosen in such a way as to include the periods exhibiting fast decay. As in the Zeno-case, these interruption segments force the system to repeat the initial non-exponential decay behavior after

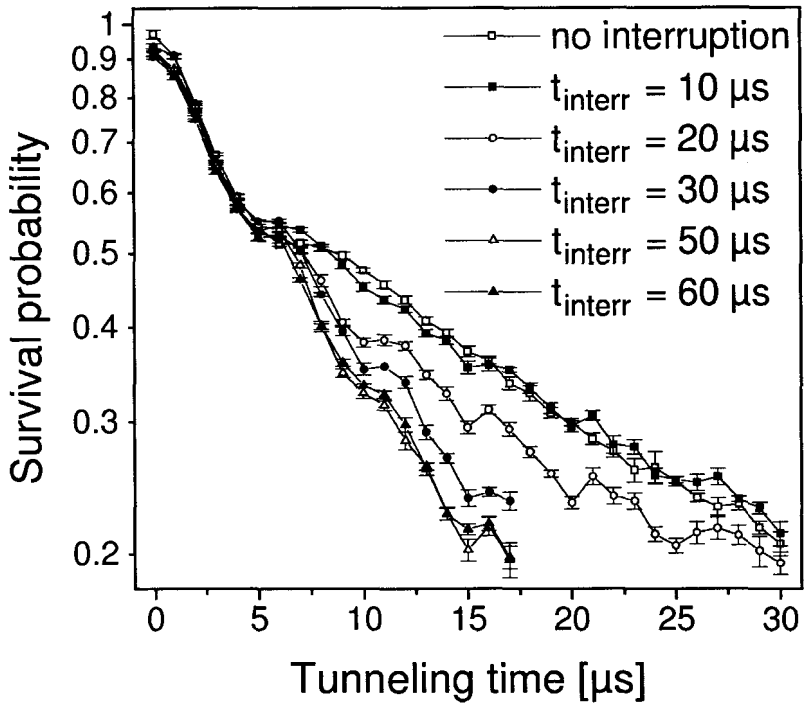

Figure 5: Survival probability as a function of duration of the tunneling acceleration. The hollow squares show the non-interrupted sequence, other symbols indicate the sequence with a finite interruption duration after every 5 μs of tunneling. The error bars denote the error of the mean. A further increase of the interruption duration than as indicated does not result in a further change of the decay behavior. The experimental data points have been connected by solid lines for clarity. For these data the parameters were: $a_{\text{tunnel}} = 15,000\,\text{m/s}^2$, $a_{\text{interr}} = 2,000\,\text{m/s}^2$ and $V_0/h = 91$ kHz.

every step. The interrupted curve of Fig. 4, indicated by hollow squares, clearly shows such a reproduction. The result is a dramatic decay that is much faster than for the uninterrupted case, namely the Anti-Zeno effect.

The ability to restart the quantum evolution translates to the ability to separate the two classes of atoms in momentum space. However, the atoms trapped in the lowest band of the optical lattice have some distribution, which in our case is the width of the first Brillouin zone, $\delta p = 2mv_{\text{rec}}$. This is the reason behind our procedure not being instantaneous, for it takes some time for an atom to be accelerated in velocity by this amount, corresponding to the Bloch period $\tau_{\text{B}} = 2v_{\text{rec}}/a_{\text{interr}}$. An interruption shorter than this time will not resolve the tunneled atoms from those still trapped in the potential and therefore results in an incomplete projection of the atom number. To investigate the effect of the interruption duration we repeated a sequence to measure the Anti-Zeno effect for varying interruption durations while holding all other parameters constant. Fig. 5 displays the results

of this measurement, interrupting the decay every 5 μs with an acceleration of a_{interr} of 2000 m/s^2. The hollow squares show the uninterrupted decay sequence as a reference. For an interruption duration smaller than the Bloch period of 30 μs the procedure is incomplete and has little or no effect. For a duration longer than the Bloch period the effect saturates and results in a complete restart of the decay behavior after every interruption.

References

1. B. Misra and E. C. G. Sudarshan, J. Math. Phys. **18**, 756 (1977).
2. C. B. Chiu, E. C. G. Sudarshan, and B. Misra, Phys. Rev. D **16**, 520 (1977).
3. W. C. Schieve, L. P. Horwitz, and J. Levitan, Phys. Lett. A **136**, 264 (1989).
4. A. G. Kofman and G. Kurizki, Nature **405**, 546 (2000).
5. P. Facchi, H. Nakazato, and S. Pascazio, Phys. Rev. Lett. **86**, 2699 (2001).
6. M. C. Fischer, B. Gutiérrez-Medina, and M. G. Raizen, Phys. Rev. Lett. **87**, 040402 (2001).
7. S. R. Wilkinson, C. F. Bharucha, M. C. Fischer, K. W. Madison, P. R. Morrow, Q. Niu, B. Sundaram, and M. G. Raizen, Nature **387**, 575 (1997).
8. L. A. Khalfin, JETP **6**, 1053 (1958).
9. R. G. Winter, Phys. Rev. **123**, 1503 (1961).
10. L. Fonda, G. C. Ghirardi, and A. Rimini, Rep. Prog. Phys. **41**, 587 (1978).
11. P. T. Greenland and A. M. Lane, Phys. Lett. A **117**, 181 (1986).
12. P. Valanju, E. C. G. Sudarshan, and C. B. Chiu, Phys. Rev. D **21**, 1304 (1980).
13. J. J. Sakurai, *Modern Quantum Mechanics* (Addison-Wesley, 1994).
14. W. M. Itano, D. J. Heinzen, J. J. Bollinger, and D. J. Wineland, Phys. Rev. A **41**, 2295 (1990).
15. P. Kwiat, H. Weinfurter, T. Herzog, A. Zeilinger, and M. A. Kasevich, Phys. Rev. Lett. **74**, 4763 (1995).
16. Mark G. Raizen, Christophe Salomon, and Quian Niu, Physics Today, p. 30 (july 1997).
17. Neil W. Ashcroft and N. David Mermin, *Solid State Physics* (Saunders College, Philadelphia, 1976).
18. Q. Niu, X. Zhao, G. A. Georgakis, and M. G. Raizen, Phys. Rev. Lett. **76**, 4504 (1996).
19. C. Zener, Proc. R. Soc. London A **137**, 696 (1932).
20. C. Zener, Proc. R. Soc. London A **145**, 523 (1934).
21. C. F. Bharucha, K. W. Madison, P. R. Morrow, S. R. Wilkinson, B. Sundaram, and M. G. Raizen, Phys. Rev. A **55**, R857 (1997).
22. K. W. Madison, C. F. Bharucha, P. R. Morrow, S. R. Wilkinson, Q. Niu, B. Sundaram, and M. G. Raizen, Appl. Phys. B **65**, 693 (1997).
23. Q. Niu and M. G. Raizen, Phys. Rev. Lett. **80**, 3491 (1998).
24. C. Cohen-Tannoudji, in *Fundamental Systems in Quantum Optics* edited by J. Dalibard, J. M. Raimond, and J. Zinn-Justin (Elsevier, New York, 1992).

DISCUSSION

Chairman: T. Petrosky

L. Stodolsky: Of course, this pure exponential decay, for example, in the radioactivity, means that the particle escaped to infinity gets totally away from any influence of the initial state they came from. Your initial wiggles, do they have any remnants of Rabi oscillations?

M. Raizen: No, those initial wiggles can be interpreted as a tunnelling time through the forbidden barrier as I discussed with Rolf Landauer. This problem is identical to Zener break-down.

L. Stodolsky: But still these particles are not really escaping to infinity like in radioactivity.

M. Raizen: They are escaping in the sense that there is no possibility for return.

L. Stodolsky: You always have both non-exponential and true decay processes.

M. Raizen: Why is that?

A. Bohm: Because you always have the background. I agree fully.

M. Raizen: That is the problem of time resolution and "setting the clock".

L. Stodolsky: No, because you have a true continuum. In all this problems you are never getting out of the source.

M. Raizen: I disagree with that statement. As far as I understand it is really just a question of the time scale.

T. Petrosky: You are using the word "measurement", but your measurement is not in the sense of von Neumann. You are actually disturbing the system therefore the system starts to change the behaviour.

M. Raizen: Yes, that is presumably, what is happening.

S. Pascazio: I have a question and a comment. My question is technical: how large is your wave packet, how many wells do you have? And my comment is that I completely disagree with two previous comments. There is a coupling to a continuum, the continuum is not flat therefore there is the deviation from the exponential decay.

M. Raizen: I can say that the extent of the wave packet oscillations during the Bloch oscillations become larger as the tilt becomes smaller, typically the extent is two or three wells, to be more precise.

H. Walther: Can you tell us some more about last items, the recent results of slowing molecular beams? Is it slowing or is it rather cooling?

M. Raizen: It is slowing. Cooling is a much harder problem than slowing. But the first step is to make the big jump from room temperature to sub Kelvin. The way we are planning to do this is to start from a supersonic beam with very high expansion ratios to get extremely monochromatic beams. We are working on slowing the beam by reflection off a cold single-crystal surface. These crystals have high enough Debye temperature so that the probability of elastic reflection is very large at low temperatures. And then if you just translate the crystal you can slow the beam.

L. Vaidman: What I see here is, probably, the best Zeno effect experiment because in the earlier experiments, they changed the oscillator evolution. The Zeno

effect was first proposed for decay. It works for everything but if we try to have an original name, it is decay. And this is, probably, the first experiment on something like decay because tunnelling is decay. I think your worries about measurement are not grounded. At the end of your measurement you see the atoms, and this is really the irreversible measurement. It is true that until you saw the atoms there is no measurement. These atoms at the end, plus the idea giving the time between the accelerations, give exactly the right effect. So, I think it is a beautiful example of the Zeno effect, according to the name, as it was proposed originally.

M. Raizen: In fact, the question is really whether we have to observe those atoms. I could also argue that, in principle, once you have the atoms resolved in velocity space we could in principle do velocity-selective Raman transitions that would distinguish them.

L. Vaidman: Until you see them nothing happens.

M. Raizen: I am not sure because they are in principle distinguishable in this space.

L. Stodolsky: Could you show the first transparency? The fact that the mass in the last term is the same as the mass in the first term is a kind of equivalence principle result. And if by this sensitive quantum measurement we shall be able to control things, we could have very simple analogue of what we have seen this morning.

M. Raizen: I think it is an interesting comment. I don't see yet how to do this sensitive measurement, but in principle, you are right. If we could, for example, run an atomic clock in the accelerating frame that might be interesting.

I. Antoniou: I have two questions which will help us to understand what is happening. You realize the von Neumann projection by modifying the Hamiltonian. Have you estimated to what extent this modification of the Hamiltonian is close to the ideal von Neumann projection? This is the first question. The second question is: can you give us some detailed estimation of the error at the very short time?

M. Raizen: Yes. Let me answer the second question, as I don't have a good answer for the first one. The second question is what is the time scale for switching and the answer is under three hundred nanoseconds. That settles the limit on how short a time we can look at. In practice that meant that we could only interrupt with about a microsecond. On the time scale shorter than that we just start to see the ramp of acousto-optic modulators which cause this switching. In principle, it can be made shorter. I don't think that it is a fundamental limit.

I. Antoniou: I think these interesting estimations can be done, so we can see how close you are and decide the issue.

M. Raizen: Right.

T. Petrosky: If you really can make it very short, really continuous observation, as was proposed by Sudarshan and Misra, maybe you can really distinguish the von Neumann arguments.

M. Raizen: My feeling is that in our problem there is no possibility, even in principle, of determining whether the atom has tunnelled or not on such a short time scale.

QUANTUM ZENO EFFECT

B. MISRA[1] AND I. ANTONIOU[1,2]

[1] *International Solvay Institutes for Physics and Chemistry, ULB-CP 231, Bd. du Triomphe, 1050 Brussels, Belgium*

[2] *Department of Mathematics, Aristotle University of Thessaloniki, 54006 Thessaloniki, Greece (E-mail: iantonio@vub.ac.be)*

1 Introduction

Quantum Zeno effect predicts that the decay of an unstable system will be inhibited by sufficiently frequent measurements. If the frequency of measurements is further increased inhibition of decay will be more pronounced. This conclusion holds also for transitions between general non stationary states, for example coherent oscillations. The general formulation of this conclusion is given in [1]. An earlier work attributed to Turing by Yourgrau, which is based on second order perturbation formula for transition probability, suggests such a conclusion [2]. The relation between Zeno effect and the existence of an initial period of "slow decay" is made explicit in [3]. Existence of such a period (the short time deviation from "exponential decay law") follows from quite general arguments [4-8].

The Zeno effect is concerned with the behaviour of survival or "non decay" probability under successive measurements, when the time interval between successive measurements becomes sufficiently small. We have based the consideration of such probabilities on the validity of state collapse, for obtaining the probabilities of outcomes of subsequent measurements (§2).

A more fundamental approach should perhaps be based on a theory of measurement process. Problems of measurement theory are, however, well known since Von Neumann's initial analysis of the question [9]. The measurement problem has not yet received any definitive solution, but attempted solutions tend to show the validity of state collapse. For a thorough and critical examination of issues related to measurement problem and more general issues concerning the interpretation of Quantum Mechanics, the reader may see [10, 11]. It seems to us that at the present stage the validity of state collapse, which is consistent with the properties of measurement, is the only general principle for considering Quantum effects involving successive measurements, like the Zeno effect.

This does not, of course, imply that particular experiments showing Zeno-type effect should not be subjected to critical examination to see, if a purely dynamical explanation of the observed effect can be given.

We shall not discuss in detail several reported observations of Zeno effect except to make some preliminary remarks. One of the first reported observations of Zeno effect is that of Itano et al [12] realizing an experiment proposed by Cook [13]. This experiment has been widely discussed and differing opinions have been expressed as to whether it demonstrates Zeno effect [14-22 to cite only a few]. What is striking is that different approaches reproduce the same result as would be expected from the validity of state collapse. This, of course, does not show the invalidity of

state collapse interpretation of the experiment [12] and supports even less the view advocated in the "ensemble interpretation" of quantum mechanics, which denies the validity of state collapse for all predictions pertaining to the outcome of successive measurements. Even before the experiment [12], it has been remarked that in some cases appropriate modification of the Hamiltonian may mimic the effect of repeated measurements [23]. But the need for other experiments, which would show more convincingly the effect of repeated measurements, as emphasized in [14], remained. There is also a much older remarkable effect, which seems at first sight as some kind of Zeno effect, namely the **narrowing** of resonance line in NMR experiments in gaseous or liquid samples [24]. It seems unlikely that it is some kind of Zeno effect, although no detailed consideration of this experiment from the point of view of Zeno effect has been made.

The recent experiment by Raizen and co-workers [25] discussed in this conference [26] shows more convincingly the effect of repeated measurements on the decay of an unstable system. The repeated selective measurements are sufficiently "non invasive" and both Zeno effect and anti Zeno effect are observed depending on the interval between successive measurements. Interpretation of both Zeno and anti Zeno effects is based on the validity of state collapse (§4). The word state collapse is not used in [25], but the idea of state collapse in this case is very simply expressed by saying that repeated measurements repeatedly redefine a new initial state, which must start evolution again with the initial non exponential decay feature. The problem of making "instantaneous" measurements is ingeniously bypassed in this experiment. Therefore, it seems that in this experiment one can observe stronger inhibition of decay by making repeated measurements at shorter intervals. Moreover, as mentioned in §4, inhibition of decay can be seen even in the period when "exponential decay law" holds by allowing the system to evolve up to time to uninterrupted and then performing repeated measurements. These will not only show even more convincingly the effect of repeated measurement but will also raise conceptual questions about the significance of "exponential decay law" for unstable quantum systems.

Some final brief remarks on the implications of consideration on Zeno effect. Experimental observation of Einstein-Podolsky-Rosen correlation violating Bell's inequality, has excluded the possibility of "local" hidden variable theory. But "non local" hidden variable formulation of Quantum Mechanics by Bohm or its variation is still of some interest [27, 28]. It is doubtful whether quantum Zeno effect, e.g. for the tunnelling, from a potential, will survive within this formulation. If this is investigated, an appropriate experiment of Zeno effect will help to decide the tenability of "non local" hidden variable theories.

The Zeno effect exists in principle for actually decaying systems such as the excited levels of atoms or unstable particles. Although it cannot probably be observed for such systems, its existence raises conceptual questions. Can one meaningfully speak of **occurrence** of Quantum Jump? Can one meaningfully say that such systems survive **up to** time t and decay during a subsequent period, even in a probabilistic sense? Can one assign meaning to "time of decay" and relate it to "life time"? The initial motivation of the work on Zeno effect was partly to study these questions. But all theoretical descriptions of unstable systems, begin-

ning with Weiskopf-Wigner theory, deal with survival probability at time t or the related probability of transition to the continuum. One cannot strictly speak of survival **up to time t**, although one often uses such expressions when thinking of transition of an unstable system.

Even Dirac reverts to such expressions, e.g. when he starts with perturbation expression for transition probability at time t and then makes the well-known approximations to obtain the so-called golden rule and speaks of transition probability per unit time [29]. But Dirac emphasizes that this approximation is not valid for times too small or too large. Existence of Zeno effect even in the period when "exponential decay law" holds, shows that one cannot strictly speak of survival probability or transition probability **up to time t**. Theory of unstable particles cannot, of course, be based only on general principles of Quantum Mechanics. It involves considerations of Quantum Field Theory. Moreover, the fact that "decay products" have "outgoing character" has to be incorporated in theories of unstable particles. How these will affect the consideration of Zeno effect remains to be seen. Exponential decay law was formulated before quantum theory, based on classical probability applied to **occurrence of events**. There are in general no quantum events independent of observation. How to account for **occurrence of events** in a purely quantum world, is the main problem of interpretation of quantum theory. It seems that the notion of unstable particle and "life time" attributed to it as an intrinsic property, has not yet received a completely satisfactory quantum theoretical description. Consideration of Zeno effect for the neutral K-meson, raises further intriguing issues. We will not discuss these questions further here.

The rest of this communication is a straightforward brief account of Zeno effect with occasional comments. It should be stressed that we do not adhere to interpretations of quantum theory which involve partial tracing upon degrees of freedom of a larger system. At the same time we do not take a too realistic view of Quantum states, and state collapse, but rely only on the validity of state collapse for predicting probabilistic outcome pertaining to successive measurements. We hope to discuss issues related to Zeno effect in greater detail in a future communication. There is a fairly large literature on issues related to Zeno effect. This communication is, however, not intended to be even a partially comprehensive review of the subject.

2 Survival probability under repeated measurements and "wave-packet reduction"

Consider a quantum system. Its states are represented by density operators ρ of a Hilbert space $\mathcal{H}$. If ρ is the one-dimensional projection $|M><M|$ (Dirac's notation [29]) on the vector $|M>$ of $\mathcal{H}$ then ρ corresponds to the pure state $|M>$. More general density operators represent (weighted) "mixtures" of pure states. Dynamical evolution of the system is described by the unitary group e^{-iHt}, where H is the time-independent Hamiltonian of the system. An initial state ρ evolves in time t to the state $\rho_t = e^{-iHt}\rho e^{iHt}$. Consider now a projection E onto a non- stationary subspace $\mathcal{H}_E$ of $\mathcal{H}$: $[H, E] \neq 0$. Although we are considering a general non-stationary subspace we shall use the language of decay and non-

decay of unstable systems. The subspace $\mathcal{H}_E$will thus be called the subspace of undecayed states and its orthogonal subspace $\mathcal{H}_E^{\perp}$ will be called the subspace of decayed products. A measurement of the observable E has only two possible outcomes: "yes" or "no" corresponding to finding the system to be undecayed or decayed. In general measurement of a projection corresponds to determining if certain property of the system, e.g. the system being "localized" in given region of space, holds. If the initial state of the system is ρ, the probability $Q(t)$ of finding the system undecayed (survival probability) **at time t** is given by

$$Q(t) = \mathrm{tr}(e^{-iHt}\rho e^{iHt}E). \tag{1}$$

In the situation that E is a one-dimensional projection $|M><M|$ and ρ is the pure state $|M><M|$, the survival probability (1) reduces to $|<M|e^{-iHt}M>|^2$. The formulation of Quantum Zeno effect starts from the consideration of the probability that a sequence of measurements at times 0, $\frac{t}{n}$, $\frac{2t}{n}$ $\ldots$ $\frac{n-1}{n}t$ and t, with yield the result "yes" (undecayed) for each of these measurements. Such probabilities concerning the outcomes of a sequence of successive measurements, have not been considered widely in the literature. A general formula concerning the outcomes of successive measurement was first stated by Wigner [30]. Wigner's expression for the probability that each of the sequence of measurements of (possibly different) projections E_1, E_2, $\ldots E_k$, $\ldots E_n$ at successive instants t_1, t_2, $\ldots t_k$, $\ldots t_n$ (respectively) yields the result "yes" when the initial state is ρ is:

$$\mathrm{tr}[E_n(t_n)\ldots E_k(t_k)\ldots E_1(t_1)\rho E_1(t_1)\ldots E_k(t_k)\ldots E_n(t_n)]. \tag{2}$$

Here $E_k(t_k) \equiv e^{iHt_k}E_k e^{-iHt_k}$.

In the special case that one repeats the measurement of the same projection E at times 0, $\frac{t}{n}$, $\frac{2t}{n}$ $\ldots t$, the expression (2) for the probability of finding the result "yes" for each of these measurements reduces to

$$\mathrm{tr}[W_n(t)\rho W_n^*(t)] \equiv Q(n,t;\rho), \tag{3}$$

where $W_n(t) = [Ee^{-iHt/n}E]^n$. If the undecayed subspace is one-dimensional with corresponding projection $|M><M|$and ρ corresponds also to the undecayed state $|M>$, then the probability (3) reduces to:

$$Q(n,t;\rho) = Q(t/n)^n \tag{4}$$

where $Q(t/n) = |<M|e^{-iHt/n}M>|^2$, the survival probability of $|M>$ **at time** t/n.

The probability $Q(n,t;\rho)$ given by (3) or its special case (4) will be called **survival probability under repeated measurements**. Unlike the survival probability at a given t, the expressions (2), (3), (4), which refer to the probability of outcomes of a sequence of measurements, do not result from Schrödinger time evolution and Born's probability rule alone. Their justification involves the validity of "wave-packet reduction" or state collapse upon measurement.

To see this let us briefly consider the meaning of survival probability under repeated measurements. For this we need to consider only two measurements of E at t/n and $2t/n$ when the initial state is the "undecayed" state $\rho \equiv E\rho E$. The meaning of survival probability under these repeated measurements is then

the following: one considers an ensemble of a very large number m_1 of identically prepared systems corresponding to the state ρ, which evolve in time t/n to form the ensemble C_1 of m_1 systems in the state $\rho_{t/n} \equiv e^{-iHt/n}\rho e^{+iHt/n}$. Theoretically, one then makes independent measurements of E on each system in $C_1$and retain only the systems that give the result "yes" (undecayed). In practice, the experimental procedure should be such that it selects effectively from systems in C_1, only those giving the result undecayed. In principle, this selective experimental procedure need not be instantaneous. Let C_2 be the ensemble of systems that are retained by such a selective measurement device. The systems in C_2 are then allowed to evolve under Schrödinger evolution for a further period t/n and then a similar selective measurement is made on the resulting ensemble. Let C_3b e the ensemble resulting from this second selective measurement of E and m_3 be the number of systems in it. Then the survival probability under repeated measurements of E at t/n and $2t/n$ is m_1/m_3 or more precisely $\lim_{m_1\to\infty} m_1/m_3$. The probability, in the more general situation to which formula (2) refers, has similar meaning. From Born's probability rule, we know that the number m_2 of systems in the ensemble C_2 is $m_1\mathrm{tr}(\rho_{t/n}E)$ (when m_1 is very large). But to calculate the number m_3 of systems in C_3 on the basis of Schrödinger evolution law and Born's probability rule, we need to know the state, which should be attributed to (the systems in) the ensemble C_2 that has resulted from a selective measurement of E on the ensemble C_1. This raises the question of state collapse, namely, if the state of the system prior to measurement is ρ what state $[\rho]_E$ should be attributed to the system after the measurement of E, if the measurement gives the result "yes". One may be reluctant to attribute a state ρ to individual systems. In that case, ρ, refers to an ensemble of identically prepared systems and $[\rho]_E$ to the ensemble that results from the selective measurement of E corresponding to the result "yes". Since there is no satisfactory Quantum theory of measurement, this question cannot be answered on the basis of quantum dynamics and additional hypothesis must be made about $[\rho]_E$ which is consistent with the quantum formalism and certain general properties of quantum measurement. Before considering the specific types of measurements and their implications for $[\rho]_E$, let us note that the probability $\lim_{m_1\to\infty} m_1/m_3$ is given by

$$\mathrm{tr}(\rho_{t/n}E)\mathrm{tr}[e^{-iHt/n}[\rho_{t/n}]_E e^{+iHt/n}E] = \mathrm{tr}(\rho_{t/n}E)\mathrm{tr}[[\rho_{t/n}]_E E(t/n)] \qquad (5)$$

It may be asked if Heisenberg picture and Schrödinger picture are equivalent for the consideration of survival probability under repeated measurements. In the preceding discussion we have adopted the Schrödinger picture. In the Heisenberg picture the successive measurements of E at t/n and at $2t/n$ correspond to (immediately) successive measurements of $E(t/n)$ and $E(2t/n)$ on the state ρ. Similar argument will give the survival probability under these two measurements:

$$\mathrm{tr}[\rho E(t/n)]\mathrm{tr}[[\rho]_{E(t/n)}E(2t/n)] \qquad (6)$$

Equivalence of Schrödinger picture and Heisenberg picture (i.e. the equality of (5) and (6) obviously implies strong restriction on the form of the "collapsed" state $[\rho]_E$ that "results" from a selective measurement of E on ρ.

While considering the survival probability under repeated measurements or the probability in the more general case referred to by (2), it is natural to consider only

measurements of the **first kind**. An immediate repetition of such a measurement gives the same result without any indeterminacy. Requiring the measurement of E to be of first kind means that the state $[\rho]_E$ will give the result "yes" with **certainty** under the measurement of E. Thus

$$\mathrm{tr}[[\rho]_E E] = 1 \text{ or equivalently } E[\rho]_E E = [\rho]_E \tag{7}$$

When E is a one-dimensional projection $|M><M|$, (7) immediately implies that

$$[\rho]_E = \frac{E\rho E}{\mathrm{tr}(E\rho E)} \tag{8}$$

When the subspace corresponding to E is not one-dimensional, more general forms of state collapse than that given by (8) are possible and are considered in [31]. The general form of state collapse allows the possibility that even if ρ is an eigenstate corresponding to the eigenvalue 1 (yes) the "collapsed" state $[\rho]_E$ is different from ρ. If one considers the measurement to be such that it leaves the eigenvectors of E unchanged, the form of $[\rho]_E$ is again given by (8). In a sense, such a measurement affects the state in a minimal way, and is called ideal measurement.

Under ideal (selective) measurement, then state collapse proceeds according to the scheme:

$$\rho \rightarrow \frac{E\rho E}{\mathrm{tr}(E\rho E)} \tag{9}$$

This hypothesis about state collapse is due to Von Neumann [9] and Lüders [32]. It is interesting to recall that Dirac has found the notion of state collapse to be a natural consequence of the formalism of Quantum theory. Starting from the property of measurement (of first kind), he comes to the conclusion that "a measurement always causes the system to jump into an eigenstate of the dynamical variable that is being measured, the eigenvalue this eigenstate belongs to, being equal to the result of measurement" [29]. Obviously, Dirac is thinking of the system being in a pure state prior to measurement and collapse (9) is in accord with Dirac's conclusion. When the observed eigenvalue is degenerate, Dirac's conclusion is ambiguous about the eigenstate to which the system would "jump". This ambiguity is removed by considering ideal measurements.

It is easy to see that expressions (3) or (4) for survival probability under repeated measurements as well as expression (2) for probability pertaining to a more general sequence of measurements follow from the state collapse hypothesis (9). It should be noted that under state collapse [9], the Schrödinger picture and Heisenberg picture are equivalent for consideration of probabilities pertaining to outcomes of successive measurements. Under more general form of state collapse this equivalence can fail to hold. Moreover, the probabilities will not be uniquely determined only by the outcomes of successive measurements and initial state. It may be mentioned that Wigner, after stating formula (2), passingly suggested that it may be accepted as part of interpretative rule of Quantum theory; for one can then avoid talking about state collapse!

3 Quantum Zeno effect: general formulation

Although in almost all theoretical discussion as well as reported experimental observations of Zeno effect since its general formulation in [1], the relevant non stationary or undecayed subspace is one-dimensional, we begin with a brief review of the general formulation.

Zeno effect concerns the behaviour of survival probability under repeated measurements given by relation (3) when the interval t/n between successive measurements decreases. It is found that for any given time t, $\lim_{n\to\infty} Q(n,t;\rho) = \mathrm{tr}(\rho E)$, so that if the initial state ρ is undecayed ($\mathrm{tr}(\rho E) = 1$), then $\lim_{n\to\infty} Q(n,t;\rho) = 1$. Thus for **any given** t, if n is sufficiently large $Q(n,t;\rho)$ will be close to 1, which is the prediction that sufficiently frequent measurements will inhibit decay and if the frequency of measurement is further increased this inhibition will be more pronounced. This general conclusion is based on the following three assumptions, which can be either verified or dispensed with in special cases.

1) The existence of $\lim Q(n,t;\rho)$ as $n \to \infty$ is assumed without specifying what this limit is. This can be assured by requiring that the strong limit

$$\lim_{n\to\infty} (Ee^{-iHt/n}E)^n = W(t) \tag{10}$$

exists for $t \geq 0$. Verifying the existence of $W(t)$ for general E and H poses non trivial mathematical problems which we shall not discuss here. But if $E = |M><M|$, a very mild condition on $|M>$ leads to Zeno effect (Section 4).

2) One also adopts the natural assumption that the Hamiltonian H is bounded from below. This assumption seems unavoidable if one wants to establish the general formulation of Zeno effect. But if E is one-dimensional even this assumption can be dispensed with (Section 4).

3) Further, on grounds of physical continuity, one assumes that $\lim_{t\to 0+} W(t) = E$. This assures the desirable continuity property that $\lim_{n\to\infty} Q(n,t;\rho) \to 1$ as $t \to 0+$ if the initial state ρ is undecayed. From a purely mathematical point of view, however, this is an additional assumption and implies certain restrictions on E. The continuity of $W(t)$ as well as its semigroup property for $t > 0$, follow from general results in [33] but its continuity at $t = 0$ although expected is not known to follow from any general argument.

Under these assumptions it is shown that $W(t)$ is of the form: $W(t) = Ee^{-iAt}E$, where A is a non negative self adjoint operator commuting with the projection E: $EA = AE = A$. Hence, $W^*(t)W(t) = E$, and $\lim_{n\to\infty} Q(n,t;\rho) = \mathrm{tr}(W(t)\rho W^*(t)) = \mathrm{tr}(\rho E)$, for any given t. The form of $W(t)$ shows also that $W(t)$ is a unitary group in the subspace corresponding to E. The group property of $W(t)$ has been discussed in some detail for specific H and E recently in connection with question as to whether "Quantum Zeno dynamics" $W(t)$ is reversible or irreversible [34]. The argument in [1] relied also on an additional assumption, which was a weak formulation of time reversal or CPT invariance. An important unpublished remark of Chernoff shows that this assumption is not necessary [35].

The above general formulation for the multidimensional projection E shows that sufficiently frequent measurements of E will stabilize states which may be **unknown** to remain within the subspace corresponding to the projection E. This may have applications for error prevention in Quantum computing devices.

4 Quantum Zeno effect, Anti Zeno effect and deviation from exponential decay law

The general formulation of Zeno effect in [1] did not directly appeal to short time deviation from exponential decay law. However short time deviation follows from the Corollary in [1]. The connection between short time deviation from exponential decay and the Zeno effect is explicitly shown in a subsequent work [3] where Zeno effect is discussed in the case when there is exactly one (undecayed) unstable state $|M>$, i.e. the "undecayed" subspace is one-dimensional. The unstable state $|M>$, being non stationary, must remain orthogonal under dynamical evolution to all bound states of the Hamiltonian H associated with the discrete spectrum. Hence, without loss of generality, we may consider H to have only absolutely continuous spectrum. The survival probability $Q(t)$ of $|M>$ at time t is the absolute square of the survival amplitude $< M|e^{-iHt}M >\equiv a(t)$ and $< M|e^{-iHt}|M >= \int_{-\infty}^{\infty} e^{-i\lambda t} w(\lambda) d\lambda$ where $w(\lambda)$ is the energy distribution function of $|M>$ [6]. Mathematically, $w(\lambda) = \frac{d}{d\lambda} < M|E_\lambda|M >$, where E_λ (λ real) denotes the spectral projections of the Hamiltonian H. Physically, the quantity $\int_E^{E+\Delta E} w(\lambda) d\lambda$ is the probability that the energy of the system in the state $|M>$ lies in the interval $[E, E+\Delta E]$.

In theoretical descriptions of unstable systems, it is the survival probability $Q(t)$ at time t is shown to be exponentially decreasing, $e^{-i\Gamma t}$, with $\Gamma > 0$. But this exponential decay law is not exact because "approximations" involved in obtaining this law are not valid for very short and very large times. A model independent argument showing short time deviation from exponential decay law, results if one puts a mild condition on the state $|M>$:

$$\int_{-\infty}^{\infty} |\lambda| w(\lambda) d\lambda < \infty \tag{11}$$

If the Hamiltonian H is bounded from below, this condition simply says that the expectation value of the energy for the state $|M>$ is finite. If H is not semibounded, condition (11) puts a slightly stronger restriction on $|M>$. The argument given in [3,4] shows that if $|M>$ satisfies (11), then the survival probability $Q(t) = |a(t)|^2$ is a differentiable function of t, its derivative $\dot{Q}(t)$ is a continuous function of t and

$$\dot{Q}(t)|_{t=0} = 0 \tag{12}$$

The continuity of $\dot{Q}(t)$ and property (12) obviously imply that the decay for short time must be slower than that expected from exponential decay law. It may be mentioned that in [3] it was unduly emphasized that for obtaining short time deviation from exponential decay law, H should be semibounded. It is condition (11), which is needed for the validity of the argument and it is independent of whether H is semibounded or not. Short time deviation from exponential decay law has been studied in detail in the problem of decay from a potential barrier by Winter [7].

The survival probability $Q(n,t) \equiv Q(n,t,|M>< M|)$ under repeated measurement at intervals t/n is now given by (4): $Q(n,t) = [Q(t/n)]^n$. The Zeno effect,

i.e. the conclusion that $\lim_{n\to\infty} Q(n,t) = 1$ for any given t, follows from the continuity of $\dot{Q}(t)$ and (12). The popular argument for Zeno effect assumes survival probability $Q(t)$ at time t to be given by

$$Q(t) \approx 1 - < \Delta H >^2 t^2 \tag{13}$$

for **small times** t. However, the validity of (12) requires restrictive conditions on $|M>$ when the Hamiltonian H is not bounded. This approximation for $Q(t)$ can fail for states $|M>$ of physical interest. The Zeno effect depends only on the existence of a short initial interval during which decay is slow as implied by the continuity of $\dot{Q}(t)$ and relation (12).

Recently, it has been suggested that for an unstable state $|M>$, after the initial period of slow decay, called the Zeno period, there can be a period ("anti-Zeno period") when $Q(t)$ will show a faster decay than eventual exponential decay to which $Q(t)$ settles for longer time [36-38]. This has indeed been verified by the numerical integration of relevant Schrödinger equation in the recently reported observation of Zeno effect [25]. This possibility has suggested that if repeated measurement is performed at intervals in this period of faster decay, then overall decay will be faster than uninterrupted exponential decay. This effect has been called anti-Zeno effect or inverse Zeno effect [36-38] and it has been observed in the recently reported experiment [25].

In fact, if τ is a time in this period of faster decay, then

$$Q(\tau) \equiv e^{-\Gamma(\tau)\tau}$$

with $\Gamma(\tau) > \Gamma$, where Γ is the uninterrupted "decay rate". The survival probability under repeated measurements at τ, $2\tau \ldots n\tau = t$ will be given as before by

$$[Q(\tau)]^n = e^{-\Gamma(\tau)t}.$$

The "effective decay rate" $\Gamma(\tau)$ shows therefore enhancement of decay. But a somewhat different interpretation of anti-Zeno effect is given in [37], which seems to be questionable. In [37], $[Q(\tau)]^n$ is taken to be the survival probability under n repeated measurement at intervals with duration τ. Then no matter how large n may be, the "effective decay rate" is the same $\Gamma(\tau)$ for given τ. Of course, $\Gamma(\tau)$ is different for different choices of τbu t $\Gamma(\tau)$ is completely determined by the Hamiltonian H and the state $|M>$ because

$$Q(\tau) = |< M|e^{-iH\tau}M >|^2 \equiv e^{-\Gamma(\tau)\tau}.$$

There is no "measurement induced level width" as this interpretation of Zeno effect and anti-Zeno effect seems to imply. Repeated measurements do not "create" a new unstable state with larger or smaller life time depending on the interval τ between measurements. The state of the system after repeated (selective) measurements is still the same state $|M>$ with the same energy distribution function $w(\lambda)$. Invoking time-energy uncertainty relation for the interpretation of Zeno and anti-Zeno effect seems also to be questionable. Although the time-energy uncertainty relation has been discussed since the early days of Quantum mechanics, its precise interpretations and theoretical basis are still a subject of controversy. It will be outside the scope of the present communication to go into this discussion but it

seems to us that there is no valid interpretation of time-energy uncertainty relation which forbids sufficiently frequent measurements considered here even in the case of "genuine" decay such as nuclear β-decay. If Zeno effect cannot be observed for such systems, it is only because the "Zeno Period" is too small for making measurements at intervals in this period.

It may be mentioned that Zeno effect exists even in the period when "exponential decay law" holds. In fact, the unstable (undecayed) state $|M>$ may be allowed to evolve uninterrupted for a period T when "exponential decay law" holds and measurements are done at T, $T+\Delta t$, $\ldots T+n\Delta t = T+t$ with $\Delta t = t/n$. The survival probability under these repeated measurements will be given as before by:

$$Q(T)[Q(t/n)]^n = e^{-\Gamma(T)}[Q(t/n)]^n \tag{14}$$

which approaches the limiting value $e^{-\Gamma(T)}$ as $n \to \infty$, for any given t. Therefore if n is large, it will be significantly larger than $e^{-\Gamma(T+t)}$. Since "**exponential decay law**" holds for times smaller than the "lifetime", the fraction $Q(T)$ of the initial number of systems in the undecayed state $|M>$ which will be found to survive by the measurement at T, will be appreciable if T is not too large than the "lifetime" $1/\Gamma$. Such an observation of Zeno effect in the period of "exponential decay" seems possible in the recently reported experiment [25]. For similar reasons it is also possible to observe anti-Zeno effect in the period of "exponential decay" in this experiment.

5 Estimation of Zeno period for unstable state

Estimation of Zeno period has to depend, of necessity, on model theoretic descriptions of unstable states. We shall briefly present here the results of two such attempts. The first one is a "resonance model" considered in [3].

One starts with the representation of survival amplitude of the state $|M>$ given by:

$$a(t) \equiv < M|e^{-iHt}|M> | = \frac{1}{2\pi i}\int_C e^{-izt}\beta(z)dz \tag{15}$$

with $\beta(z) =< M|R(z)|M >$, $R(z) = (H-z)^{-1}$ the resolvent of H and C the contour in the complex plane shown in the figure 1.

The function $\beta(z)$ is analytic and free of Zeros in the complex plane except for the cut along the spectrum of H, which is taken to be continuous and extending from 0 to $+\infty$. In terms of the energy distribution function $w(\lambda)$ of $|M>$, $\beta(z)$ is given by:

$$\beta(z) = \int_{-\infty}^{\infty}\frac{w(\lambda)}{\lambda - z}d\lambda \tag{16}$$

Introducing the function $\gamma(z) \equiv \frac{1}{\beta(z)}$ which is also analytic and free of Zeros, we can write:

$$a(t) = \frac{1}{2\pi i}\int_C \frac{e^{-izt}}{\gamma(z)}dz \tag{17}$$

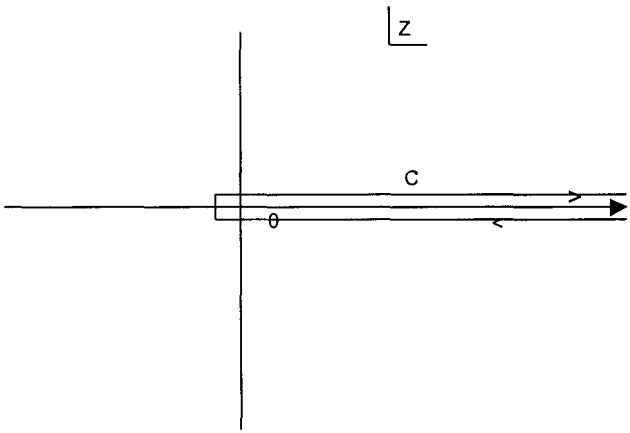

Figure 1.

The representation (16) of survival amplitude $a(t)$ holds for quite general states $|M>$. In order that $|M>$ represents an unstable state with a "characteristic lifetime", $\gamma(z)$ should satisfy certain "resonance condition", viz. the condition that analytic continuation of $\gamma(z)$ to the second sheet has a Zero at $E_0 - i\Gamma/2$ with $E_0 \gg \Gamma > 0$. Under this condition the survival amplitude $a(t)$ will receive a contribution $e^{-iE_0 t} e^{-\Gamma/2}$ from the pole of $1/\gamma(z)$ and a contribution from the "background integral" of the deformed contour, which leads to the deviation from exponential decay. Estimation of Zeno period thus amounts to an estimation of the time T_z so that for $t < T_z$ the contribution from the "background integral" is significant compared to exponential contribution from the pole of $1/\gamma(z)$. To achieve the estimation, one makes specific choice of $\gamma(z)$. In making this choice, one is guided by certain (suitably subtracted) dispersion relation, which $\gamma(z)$ should satisfy and also by the form of $\gamma(z)$ occurring in the theoretical description of unstable states in the Lee model [39]. Two such choices of $\gamma(z)$ are considered in [3].

For both choices, it was found that for $t \ll T_z \approx 25/E_0$, the "background contribution" to survival amplitude is significant. For one of these choices, it was found that for $t \ll T_z$:

$$\dot{Q}(t) \propto -t^{1/2} \text{ with } \dot{Q}(t) = 0 \text{ for } t = 0. \tag{18}$$

This choice corresponds to the form of $\gamma(z)$ occurring in Lee Model. For this choice, the energy expectation $< M|H|M >$ of the unstable state is finite. This shows that $1 - Q(t)$ is not always proportional to t^2, for small times t. But T_z is very small and in fact of the order of 10^{-21} sec, when estimated for the decay of charged pion $\pi \to \mu\nu$ with $E_0 \approx m_\pi - m_\mu$.

The other choice corresponds to a state $|M>$ whose energy expectation value

is **not** finite. In this case, for $t \ll T_z$,

$$\dot{Q}(t) \propto -\frac{1}{\sqrt{t}} \to \infty, \text{ as } t \to \infty. \tag{19}$$

There is no Zeno period but an initial anti-Zeno period! But because the energy expectation value of the state is infinite, $|M>$ represents an unphysical situation.

For very long time, the background contribution again dominates over the exponential contribution and the expected long time deviation from exponential decay law holds.

The other estimation of Zeno time and anti-Zeno time [40] starts with the second quantized version of Friedrichs model. The Hamiltonian $H = H_0 + \lambda V$ is given by:

$$H_0 = \omega_1 a^\dagger a + \int d\omega \omega b_\omega^\dagger b_\omega, \text{ and } V = \int d\omega f(\omega)(a b_\omega^\dagger + a^\dagger b_\omega) \tag{20}$$

Here, $a^\dagger$ and a are creation and annihilation operators of the harmonic oscillator. The energy eigenstates are the discrete levels $n\omega_1$, n, integer corresponding to the excited levels of the atom. $b_\omega^\dagger$ and b_ω are the corresponding creation and annihilation operators for photons of frequency ω. The unperturbed Hamiltonian H_0 has continuous spectrum with discrete levels $n\omega_1$ embedded in the continuum ($\omega_1 > 0$). The interaction V makes the discrete levels unstable and causes transitions between the unstable states of the atom and the continuum of photon states. The survival probability $Q(t)$ at time t of the first discrete state $a^\dagger|0> \equiv |1>$ is given by

$$Q(t) = |<0|a(t)a^\dagger|0>|^2, \text{ where } a(t) = e^{iHt} a e^{-iHt}. \tag{21}$$

From dimensional argument, one writes the form factor $f(\omega)$ in the form:

$$f^2(\omega) = \Lambda \Phi(\omega/\Lambda) \tag{22}$$

where $\Phi(x)$ is a dimensionless function and Λ a parameter with the dimension of energy. The model can be exactly solved to give

$$Q(t) = |A(t)|^2 \tag{23}$$

with

$$A(t) = \frac{1}{2\pi i} \int_{-\infty}^{\infty} d\gamma \frac{e^{i\Lambda y t}}{\gamma_-(y)}$$

$$\gamma(z) = \frac{\omega_1}{\lambda} - z - \lambda^2 \int_0^\infty dx \frac{\Phi(x)}{x - z}, \qquad \gamma_-(y) \equiv \gamma(y - i0)$$

Three choices of $\Phi(x)$ with corresponding choice of parameters Λ, ω_1 and λ^2 are made to correspond to models of photo detachment [41], quantum dot [42] and hydrogen atom [43]. They are (respectively):

$$\Phi_1(x) = \frac{\sqrt{x}}{1+x}, \quad \Phi_2(x) = \frac{x}{(1+x^2)^2}, \quad \Phi_3(x) = \frac{x}{(1+x^2)^4} \tag{24}$$

For these choices, the behaviour of $Q(t)$ as a function of t is analysed and T_z is estimated to be respectively of the order:

$$\frac{1}{\Lambda}, \qquad \frac{\sqrt{6}}{\Lambda\sqrt{\ln\left(\frac{2\sqrt{6}\omega_1}{\Lambda}\right)}}, \qquad \frac{2\sqrt{6}}{\Lambda} \tag{25}$$

With appropriate values of Λ, ω_1 and λ^2, T_z turns out to be 10^{-10}s, 10^{-17}s, and 10^{-19}s respectively. It is also shown that for the choice $\Phi_1(x)$, the short time behaviour of $Q(t)$ is given by $Q(t) \approx 1 - Kt^{3/2} + K't^2$, where K and K' are constants depending on the parameters Λ and λ. This shows again that $Q(t)$ is not necessarily analytic near $t = 0$ for physically interesting states. For the models corresponding to $\Phi_2(x)$ and $\Phi_3(x)$ the existence of an anti-Zeno period is also found.

Acknowledgements

Thanks are due to Prof. I. Prigogine for his interest and support and to Profs. E. Karpov, G. Pronko and E. Yarevsky for critical discussions. This work was supported by the International Solvay Institutes for Physics and Chemistry and by the European Commission Project no. IST-1999-11311 (SQID).

References

1. B. Misra, E.C.G. Sudarshan, J.Math.Phys. 18 756 (1977)
2. W. Yorgrau in *Problems in philosophy in science* ed. I. Lakatos, A. Musgrave, North Holland pp. 191-192 (1968)
3. C. Chiu, E.C.G. Sudarshan, B. Misra, Phys. Rev. D 16 520 (1977)
4. L. Khalfin, JETP Lett. 8 65 (1968)
5. L. Mandelstam, I. Tamm, J. Phys. (USSR) 9 249 (1945)
6. V. Fock, N. Krylov, J. of Phys. (USSR) 11 112 (1947)
7. R. G. Winter, Phys. Rev. 123 1503 (1961)
8. B. Misra, K. Sinha, Helv. Phys. Acta 50 99 (1977)
9. J. von Neumann, *Die Mathematische Grundlagen der Quantenmechanik*, Springer, Berlin (1932); English translation by E.T. Beyer, *Mathematical Foundation of Quantum Mechanics*, Princeton Univ. Press, New Jersey (1955)
10. B. d'Espagnat, *Conceptual Foundations of Quantum Mechanics*, Addison-Wesley, Reading, 2nd edition (1976)
11. B. d'Espagnat, *Veiled reality*, Addison-Wesley (1995)
12. W.H. Itano, D.J. Heinzen, J.J. Bollinger and D.J. Wineland, Phys. Rev. A 41 2295 (1990)
13. R. Cook, Phys. Scrip. T21 49 (1988)
14. T. Petrosky, S. Tasaki and I. Prigogine, Phys. Lett. A 151 109 (1990); Phys. A 170 306 (1991)
15. A. Peres and A. Ron, Phys. Rev. A 42 5720 (1990)
16. L. Ballentine, Rev. A 43 5165 (1991)
17. W. Itano et al, Phys. Rev. A 43 5168 (1991)
18. W. Itano et al, Phys. Rev. A 44 3340 (1991)

19. E. Block, P. Berman, Phys. Rev. A 44 1466 (1991)
20. M. G. Gagan and G.J. Milburn, Phys. Rev. A 47 1467 (1993)
21. P. Knight, Nature 344 493 (1990)
22. A. Biege, G. Hegerfeldt, Phys. Rev. A 53 53 (1996)
23. A. Peres, Am. J. Phys. 48 931 (1980)
24. A. Abragam, *The principle of nuclear magnetism*, Clarendon, Oxford (1962)
25. M. Raizen et al, Phys. Rev. Lett. 87 040402 (2001)
26. B. Gutiérrez-Medina, M.C. Fischer and M.G. Raizen, *Observation of the Quantum Zeno and Anti-Zeno effects in an unstable system*, Proceedings of the XXII Solvay Conference on Physics, "The Physics of Communication", Journal of Quantum Computing and Computation and World Scientific
27. D. Bohm, Phys. Rev. 85 166, 180 (1952)
28. D. Bohm, J. Bub Rev. Mod. Phys., 453 (1966)
29. P. A. M. Dirac, *The Principles of Quantum Mechanics*, Oxford University Press, London (1958), first edition (1930)
30. E. P. Wigner in *Foundations of Quantum Mechanics*, ed. B. d'Espagnat, Academic Press, New York p. 16 (1971)
31. G. Ludwig, *Foundations of QM* Vol I., Springer, Berlin (1983); K. Kraus, *States, Effects and Operations*, Springer (1983)
32. G. Luders, Ann. Phys 8, 323 (1951)
33. P. R. Chernoff, Mem. Am. Math. Soc. 140 (1974)
34. P. Facchi, V. Gorini, G. Marmo, S. Pascazio, E.C.G. Sudarshan, *Quantum Zeno dynamics*, Phys. Lett. A 275 12-19 (2000); P. Facchi, S. Pascazio, A. Scardicchio, L.S. Schulman, *Zeno dynamics yields ordinary constraints*, Phys. Rev. A 65 012108 (2002)
35. P. Chernoff, private communication
36. W. Schieve, L. Horwitz, J. Levitan, Phys. Lett A 136 264 (1998)
37. A. G. Kofman and G. Kurizski, Nature 405 546 (2000)
38. P. Facchi, H. Nakazato, S. Pascazio, Phys. Rev. Lett 86 2699 (2001)
39. T. D. Lee, Phys.Rev. 95 1329 (1954)
40. I. Antoniou, E. Karpov, G. Pronko and E. Yarevsky, Phys. Rev. A 63 062110 (2001)
41. M. Lewenstein and K. Rzazewski, Phys. Rev. A 61 022105 (2000); K. Rzazewski, M. Lewenstein and J.H. Eberly, J. Phys. B 15 L661 (1982); S.L. Haan and J. Cooper, J. Phys. B 17 3481 (1984)
42. L. Jacak, P. Hawrylak, A. Wojs, *Quantum Dots*, Springer, Berlin (1998); D. Steinbach et al, Phys. Rev. B 60 12079 (1999)
43. P. Facchi and S. Pascazio, Phys. Lett. A 241 139 (1998)

DISCUSSION

Chairman: T. Petrosky

T. Petrosky: I will use my privilege of the chairman to ask the first question. 10 years ago, when Itano did the first experiment in order to check the Zeno effect,

he tried to drive all these formulae from von Neumann's postulate. Together with Tasaki and Prof. Prigogine, we have shown that during the measurement one disturbs the system by sending a signal from the "outside world", which corresponds to use of the time dependent Hamiltonian. In this way, you can drive the same result without using the von Neumann postulate.

B. Misra: Yes. I know this. Itano's experiment used an externally driven system and "measurement pulses" were in a sense too "invasive". So it was not as clear indication of the Zeno effect as the experiment of Prof. Raizen is. Secondly, measurements usually disturb the system. There is no satisfactory theory of measurement, but several proposals for such a theory tend to show the validity of "state collapse" when subsequent measurements are involved. If in some cases one can do without it using the time dependent Hamiltonian, well, it is very interesting, but it is not the general situation.

L. Reichl: I believe that in Prof. Raizen's experiment the continuous spectrum has no lower bound because it is equivalent to the presence of a constant field. So the explanation in terms of the branch point would not hold. This is one comment. A question now about the anti Zeno effect. There is an oscillation, which comes from, I would guess, the interference of several complex poles. Is the anti Zeno effect due to the fact that the oscillation starts negative that brings you below what you would expect if you had a sequel pole?

B. Misra: The anti Zeno effect was found in several models of decaying states. It does not follow as the Zeno effect from very general principles. Regarding the lower bound for the spectrum of the Hamiltonian, it is sufficient and perhaps unavoidable for proving Zeno effect in the general case, where the subspace of "undecayed" states is multidimensional. In particular cases, and specially if the "undecayed" subspace is one-dimensional, the Zeno effect occurs even if the Hamiltonian is not bounded from below. So there is no difficulty in explaining Prof. Raizen's experiment as Zeno effect.

E. C. G. Sudarshan: I want to emphasize the points that Prof. Misra has made. First of all, it is with regard to a certain system, in which to talk about the projection postulate is really very bad. One must distinguish one-dimensional projection from multidimensional. I am anticipating Prof. Pascazio's talk. When you have more than one dimension some time dependence can happen but not going outside of the system. The second comment that I wanted to make is that Prof. Misra emphasized that it is conventional quantum mechanics. When I used the analytic continuation and the complex vector states it was not to go outside the quantum mechanics it was to repeat the calculations but using a different method. There are people who followed me but who have invented a new kind of systems in which one departs from the quantum mechanical systems. In particular, the pole by itself, is not a state which is available in the physical Hilbert space. The physical state is the pole plus the background integral. The background integral gives the corrections, which may be very important for short times. This enables the Zeno effect to come. The Zeno effect may be thought of as a reinsurance of whether you calculate with complex variables or with the real variables, you should do the same physics, which is reflected in the fact that in the region of the pole you must have the background integral.

B. Misra: I have not much to add to Prof. Sudarshan's comments. Only some more remarks about the feeling of some people that state collapse (projection postulate) is very bad, which he has mentioned. Even in the case of Itano's experiment, several different theories of the experiment, of which that of Profs. Petrosky, Tasaki and Prigogine was one of the first, obtained the same result as that of Itano based on the validity of state collapse. Thus, these different theories do not show the invalidity of Itano's account of his experiment but show only that in this case "state collapse" may not be needed, and these do not, of course, prove the invalidity of state collapse in general. For various reasons it seems to me that Prof. Raizen's experiment shows the validity of state collapse. The word "collapse" evokes a too realistic view and a more neutral language as used in Prof. Raizen's paper should be used. Too realistic a view of state collapse and in fact of quantum states leads one, as some authors have advocated, to change the linear nature of dynamics or to "many world Interpretation" of quantum mechanics. I rely only on predictive validity of state collapse consistent with certain general properties of measurement and general formalism of quantum theory. As mentioned before this predictive validity is shown in several attempted theories of measurement including the one developed in the more recent "consistent history theory" of quantum mechanics. Some authors desire and attempt to develop a theory of "dynamical Zeno effect". It seems to me that such a theory is not possible at the present stage and any such theory should be able to explain Prof. Raizen's experiment and other such conceivable Zeno-type experiments.

L. Stodolsky: Let me show you a very simple argument, which Michael Berry explained me when we were discussing these things. Why the Zeno effect will occur in a two level system and more general in any finite level system but not for the true decay to the continuum. Consider some typical two level system with some tunnelling between the two levels. The Zeno effect occurs when you have some random noise, which makes these levels move back and forth. So you don't have exactly the degeneracy which you need for good tunnelling. Obviously, this random noise will slow down the tunnelling because you remove the perfect degeneracy between the two levels. On the other hand, if you are decaying to the true continuum you may move this level but, of course, you are always degenerate with somebody. This is the physical explanation of what you get from mathematics, why you don't have the flat perturbative beginning when you decay to the continuum. That is why it works for the two level system and not for the continuum.

B. Misra: I do not feel that noise has anything to do with Zeno effect although I know that some authors tend to interpret measurement as introducing noise or random phasing. The effect of "noise" is not always similar. Let me mention a much older "effect, the **narrowing** of resonance line in NMR experiment in gaseous or liquid sample. Existing theory considers it as the effect of fluctuating field considered as random classical signals. In this case "noise" inhibits transition to the continuum. Also Prof. Raizen's experiment is **not** the inhibition of "tunneling" between two or finite levels. I also do not understand the relevance of removing "degeneracy" for Zeno effect. Zeno effect can occur only if the state or subspace of states is non stationary and that is the case for unstable systems including excited levels of atoms or unstable particles which decay into the "continuum" of

decay products. The existence of initial flat beginning (short time deviation) does not follow **only** from perturbative argument but follows from quite general model independent argument. Of course, the period of short time deviation is very small for unstable particles or excited levels of atom and therefore Zeno effect can not probably be observed for such systems. But this limitation has nothing to do with Berry's and your argument.

S. Pascazio: You should put the form factor to the decaying state.

B. Misra: It is a simple quantum mechanical problem, everybody can do it.

L. Reichl: We have looked at the system with the constant field. This is not your mechanism but there is something like the Zeno effect.

B. Misra: In the **general** proof, the positivity of the Hamiltonian is sufficient condition. But as I said before, the Zeno effect can be obtained in special cases, specially for a single unstable state, even when Hamiltonian is not bounded from below.

C. Nicolaides: The Zeno effect of the short time breakdown of the exponential law has nothing to do with the lower bound, because the lower bound is just a cut off of the Fourier integral, which gives you really necessarily the long time deviation. The short time deviation is simply the result of the expansion of e^{-iHt} for short times. You can have it no matter how the Hamiltonian is. In all these works in the past thirty years, people have been using form factors that are models. I wanted just to point out that in a couple of papers, which recently appeared in Physical Review, we have solved for multiparticle real atoms the time evolution and in fact it does come out the t^2 evolution for short times rather than any other stages of the evolution. If you have an excitation with the femtosecond, you have a wave packet and the question is how do you really know where the unstable state is formed so as to be able to clock the decay and really pinpoint where the deviation might occur. Another question is related to people who propagate the Zeno effect blindly have in mind a real nucleus that decays not in femtosecond but each hour, so you can clock it. Then by clocking it, no matter how fast or slow you can do it, can you stop the nucleus from decaying? What does the Zeno effect in this regime imply? Perhaps, this experiment with nucleus is easier to prepare because the femtosecond decay is too fast.

B. Misra: I agree with you that short time deviation does not depend on the semiboundedness of Hamiltonian. But the **general** reason for this is not the expansion of e^{-iHt} which may fail for unstable states of physical interest. The deviation is also not always given by "t^2la w". It may behave as $t^{3/2}$for example. We (Chiu, Sudarshan and I) have estimated the Zeno time for proton decay which was predicted in the GUT. We found the Zeno time to be of the order of 10^{-12} s although proton lifetime was about 10^{31} years. The fact that lifetime is longer does not imply that the Zeno time will also be longer.

T. Petrosky: I have the same comment. When you consider the problem in the language of generalized master equation, even in classical mechanics, you can see the same effect: the evolution for short times is flat and then the exponential decay starts. Therefore, the boundedness of the Hamiltonian from below is not necessary for the Zeno effect.

B. Misra: I have said before about this. It is true that you can have deviation from exponential relaxation even in classical mechanics. But in classical mechanics you cannot take advantage of this to **inhibit** relaxation by frequent measurements. In that sense there is no Zeno effect in classical mechanics.

L. Stodolsky: We should not forget the question. Where is the time equal to zero?

B. Misra: It is when you prepare your initial unstable state. Moreover, it is not necessary to know exactly the time when the unstable state is prepared. In experiments like that of Prof. Raizen you can see inhibition of (further) decay by starting frequent measurements at any time t, provided t is not too large compared to "lifetime".

L. Stodolsky: When you prepare a wave packet you have to define where really the $t = 0$ is.

L. Accardi: Something I don't understand. You speak about Zeno time. Then you speak about the connection to the standard von Neumann quantum mechanics. But in your arguments of the standard quantum mechanics there is privilege of time. You have to take short intervals but your argument applies to any interval of time. You have to take short intervals in order to have the t^2 but the whole interval which you divide can be totally arbitrary. There is no scale of time. There is not any privilege of time. Why do you speak about short time effects?

B. Misra: Zeno time is the short time where the deviation from exponential decay holds. The whole interval $[0, T]$ can be arbitrary but n (the number of measurements) should be large in order that T/N is smaller than the Zeno time.

QUANTUM ZENO SUBSPACES AND DYNAMICAL SUPERSELECTION RULES

PAOLO FACCHI AND SAVERIO PASCAZIO
Dipartimento di Fisica, Università di Bari
and Istituto Nazionale di Fisica Nucleare, Sezione di Bari
I-70126 Bari, Italy

The quantum Zeno evolution of a quantum system takes place in a proper subspace of the total Hilbert space. The physical and mathematical features of the "Zeno subspaces" depend on the measuring apparatus: when this is included in the quantum description, the Zeno effect becomes a mere consequence of the dynamics and, remarkably, can be cast in terms of an adiabatic theorem, with a dynamical superselection rule. We look at several examples and focus on quantum computation and decoherence-free subspaces.

1 Introduction

The quantum Zeno effect has a curious history. It was first understood by von Neumann, in 1932 [1]: while analyzing the thermodynamic features of quantum ensembles, at page 195 of his book on the Mathematical Foundations of Quantum Mechanics (page 366 of the English translation), von Neumann proved that any given state ϕ of a quantum mechanical system can be "steered" into any other state ψ of the same Hilbert space, by performing a series of very frequent measurements. If ϕ and ψ coincide (modulo a phase factor), the evolution is "frozen" and, in modern language, a quantum Zeno effect takes place.

This remarkable observation did not trigger much interest, neither in the mathematical, nor in the physical literature. It took 35 years before Beskow and Nilsson [2] applied the same ideas to a rather concrete physical problem (a particle in a bubble chamber) and wondered whether it is possible to influence the decay of an unstable system by performing frequent "observations" on it (a bubble chamber can be thought of as an apparatus that "continuously" checks whether the particle has decayed). This interesting idea was subsequently physically analyzed by several authors [3,4,5,6]. The classical allusion to the sophist philosopher Zeno of Elea is due to Misra and Sudarshan [4], who were also the first to provide a consistent and rigorous mathematical framework. During those years it was also realized that the formulation of the "Zeno effect" (or "paradox" as people tended to regard it) hinged upon difficult mathematical issues [7,8,9], most of which are yet unsolved.

The interest in the quantum Zeno effect (QZE) was revived in 1988, when Cook [10] proposed to test it on oscillating (mainly, two-level) systems, rather than on *bona fide* unstable ones. This was an interesting and concrete idea, that led to experimental test a few years later [11]. The discussion that followed [12,13] provided alternative insight and new ideas [14], eventually leading to new experimental tests. The QZE was successfully checked in experiments involving photon polarization [15], chiral molecules [16] and ions [17] and new experiments are in preparation with neutron spin [18]. One should emphasize that the first experiments were not free from interpretational criticisms. Some of these criticisms could be successfully

countered (e.g., the serious problem related to the so-called "repopulation" of the initial state [19,20] was avoided in [17]), but some authors insisted in arguing that the QZE had not been successfully demonstrated on *bona fide* unstable systems, as in the seminal proposals.

Fortunately (or unfortunately, depending on the perspective) the recent experiments by Raizen and collaborators are conclusive, in our opinion: the presence of a short-time quadratic region for an unstable quantum mechanical system (particle tunnelling out of a confining potential) was experimentally confirmed in 1997 [21] and then, a few years later, the existence of the Zeno effect (hindered evolution by frequent measurements) was demonstrated [22]. This last experiment is of great conceptual interest, for it also proved the occurrence of the so-called inverse (or anti) Zeno effect (IZE) [23,24,25]), first suggested in 1983 (!), according to which the evolution can be *accelerated* if the measurements are frequent, but not *too* frequent.

The QZE is a direct consequence of general features of the Schrödinger equation that yield quadratic behavior of the survival probability at short times [26,20]. According to the standard formulation, the hindrance of the evolution is due to very frequent measurements, aimed at ascertaining whether the quantum system is still in its initial state. We call this a "pulsed measurement" formulation [20], according to von Neumann's projection postulate [1]. However, from a physical point of view, a "measurement" is nothing but an interaction with an external system (another quantum object, or a field, or simply a different degree of freedom of the very system investigated), playing the role of apparatus. If the apparatus is included in the quantum description, the QZE can be reformulated in terms of a "continuous" measurement [20,27,25], without making use of projection operators and non-unitary dynamics, obtaining the same physical effects. It is important to stress that the idea of a "continuous" formulation of the QZE is not new [5,6], but a *quantitative* comparison with the "pulsed" situation is rather recent [28].

Nowadays, it seems therefore more appropriate to frame the Zeno effects in a dynamical scenario [13] by making use of a continuous-measurement formulation [20,27,28,29,30]. Also, it is important to focus on additional issues, in view of possible applications. For instance, it is interesting to notice that a quantum Zeno evolution does not necessarily freeze the dynamics. On the contrary, for frequent projections onto a multidimensional subspace, the system can evolve away from its initial state, although it remains in the subspace defined by the "measurement" [31]. By blending together these three ingredients (dynamical framework, continuous measurement and Zeno dynamics within a subspace) the quantum Zeno evolution can be cast in terms of an adiabatic theorem [32]: under the action of a continuous measurement process (and in a strong coupling limit to be defined in the following) the system is forced to evolve in a set of orthogonal subspaces of the total Hilbert space and an *effective superselection rule* arises. The dynamically disjoint *quantum Zeno subspaces* are the eigenspaces (belonging to different eigenvalues) of the Hamiltonian that describes the interaction between the system and the apparatus: in words, they are those subspaces that the measurement device is able to distinguish.

This paves the way to possible interesting applications of the QZE: indeed, if the coupling between the "observed" system and the "measuring" apparatus can

be tailored in order to slow (or accelerate) the evolution, a door is open to control unwanted effects, such as decoherence and dissipation. It is therefore important to understand in great detail when an external quantum system can be considered a good "apparatus," able to yield QZE and IZE, and why.

We have organized our discussion as follows. We first review in Sec. 2 some notions related to the (familiar) "pulsed" formulation of the Zeno effect and summarize the celebrated Misra and Sudarshan theorem in Sec. 3. This theorem is then extended in Sec. 4, in order to accommodate multiple projectors, and the notion of continuous measurement is introduced in Sec. 5, by looking at several examples. We propose in Sec. 6 a broader definition of QZE (and IZE) [20] and prove in Sec. 7 an adiabatic theorem, defining the Zeno subspaces [32,33]. Finally, in Secs. 8-12, we elaborate on some interesting examples, focusing in particular on quantum computation and applications. We conclude in Sec. 13 with a few comments.

2 Notation and preliminary notions: pulsed measurements

Let H be the total Hamiltonian of a quantum system and $|a\rangle$ its initial state at $t = 0$. The survival probability in state $|a\rangle$ is

$$p(t) = |\mathcal{A}(t)|^2 = |\langle a|e^{-iHt}|a\rangle|^2 \tag{1}$$

and a short-time expansion yields a quadratic behavior

$$p(t) \sim 1 - t^2/\tau_{\rm Z}^2, \qquad \tau_{\rm Z}^{-2} \equiv \langle a|H^2|a\rangle - \langle a|H|a\rangle^2, \tag{2}$$

where $\tau_{\rm Z}$ is the Zeno time [34]. Observe that if the Hamiltonian is divided into a free and an (off-diagonal) interaction parts

$$H = H_0 + H_{\rm int}, \qquad \text{with} \quad H_0|a\rangle = \omega_a|a\rangle, \quad \langle a|H_{\rm int}|a\rangle = 0, \tag{3}$$

the Zeno time reads

$$\tau_{\rm Z}^{-2} = \langle a|H_{\rm int}^2|a\rangle \tag{4}$$

and depends only on the interaction Hamiltonian.

Perform N (instantaneous) measurements at time intervals $\tau = t/N$, in order to check whether the system is still in state $|a\rangle$. The survival probability after the measurements reads

$$p^{(N)}(t) = p(\tau)^N = p\left(t/N\right)^N \sim \exp\left(-t^2/\tau_{\rm Z}^2 N\right) \stackrel{N\to\infty}{\longrightarrow} 1. \tag{5}$$

If $N = \infty$ the evolution is completely hindered. For very large (but finite) N the evolution is slowed down: indeed, the survival probability after N pulsed measurements ($t = N\tau$) is interpolated by an exponential law [24]

$$p^{(N)}(t) = p(\tau)^N = \exp(N \log p(\tau)) = \exp(-\gamma_{\rm eff}(\tau)t), \tag{6}$$

with an *effective decay rate*

$$\gamma_{\rm eff}(\tau) \equiv -\frac{1}{\tau}\log p(\tau) = -\frac{2}{\tau}\log|\mathcal{A}(\tau)| = -\frac{2}{\tau}\,{\rm Re}\left[\log \mathcal{A}(\tau)\right] \geq 0\,. \tag{7}$$

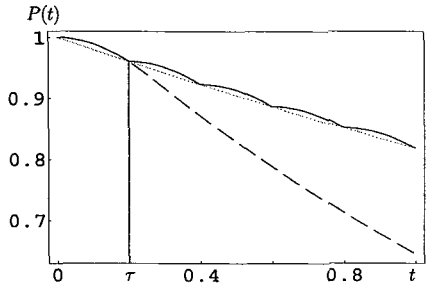

Figure 1. Evolution with frequent "pulsed" measurements: quantum Zeno effect. The dashed (full) line is the survival probability without (with) measurements. The gray line is the interpolating exponential (6).

For $\tau \to 0$ (i.e. $N \to \infty$) one gets $p(\tau) \sim \exp(-\tau^2/\tau_Z^2)$, whence

$$\gamma_{\text{eff}}(\tau) \sim \tau/\tau_Z^2. \qquad (\tau \to 0) \tag{8}$$

Increasingly frequent measurements tend to hinder the evolution. The *physical* meaning of the mathematical expression "$\tau \to 0$" is a subtle issue [34,24,20,35], involving quantum field theoretical considerations [36,30,25] that will not be considered here. The Zeno evolution for "pulsed" measurements is pictorially represented in Figure 1. The notion of "continuous" measurement will be discussed later (Sec. 5).

3 Misra and Sudarshan's theorem

We briefly sketch Misra and Sudarshan's theorem and introduce more notation. Let Q be a quantum system, whose states belong to the Hilbert space $\mathcal{H}$ and whose evolution is described by the unitary operator $U(t) = \exp(-iHt)$, where H is a time-independent lower-bounded Hamiltonian. Let P be a projection operator and $\text{Ran}P = \mathcal{H}_P$it s range. We assume that the initial density matrix ρ_0 of system Q belongs to $\mathcal{H}_P$:

$$\rho_0 = P\rho_0 P, \qquad \text{Tr}[\rho_0 P] = 1. \tag{9}$$

Under the action of the Hamiltonian H (i.e., if no measurements are performed in order to get information about the quantum state), the state at time t reads

$$\rho(t) = U(t)\rho_0 U^\dagger(t) \tag{10}$$

and the *survival probability*, namely the probability that the system is still in $\mathcal{H}_P$ at time t, is

$$p(t) = \text{Tr}\left[U(t)\rho_0 U^\dagger(t)P\right]. \tag{11}$$

No distinction is made between one- and multi-dimensional projections.

The above evolution is "undisturbed," in the sense that the quantum systems evolves only under the action of its Hamiltonian for a time t, without undergoing

any measurement process. Assume, on the other hand, that we do perform a *selective measurement* at time τ, in order to check whether Q has survived inside $\mathcal{H}_P$. By this, we mean that we select the survived component and stop the other ones. (Think for instance of spectrally decomposing a spin in a Stern-Gerlach setup and absorbing away the unwanted components.)

The state of Q changes (up to a normalization constant) into

$$\rho_0 \to \rho(\tau) = PU(\tau)\rho_0 U^\dagger(\tau)P \tag{12}$$

and the survival probability in $\mathcal{H}_P$ is

$$p(\tau) = \mathrm{Tr}\left[U(\tau)\rho_0 U^\dagger(\tau)P\right] = \mathrm{Tr}\left[V(\tau)\rho_0 V^\dagger(\tau)\right], \qquad V(\tau) \equiv PU(\tau)P. \tag{13}$$

The QZE is the following. We prepare Q in the initial state ρ_0 at time 0 and perform a series of (selective) P-observations at time intervals $\tau = t/N$. The state of Q at time t reads (up to a normalization constant)

$$\rho^{(N)}(t) = V_N(t)\rho_0 V_N^\dagger(t), \qquad V_N(t) \equiv [PU(t/N)P]^N \tag{14}$$

and the survival probability in $\mathcal{H}_P$ is given by

$$p^{(N)}(t) = \mathrm{Tr}\left[V_N(t)\rho_0 V_N^\dagger(t)\right]. \tag{15}$$

In order to consider the $N \to \infty$ limit, one needs some mathematical requirements: assume that the limit

$$\mathcal{V}(t) \equiv \lim_{N\to\infty} V_N(t) \tag{16}$$

exists (in the strong sense) for $t > 0$. The final state of Q is then

$$\rho(t) = \lim_{N\to\infty} \rho^{(N)}(t) = \mathcal{V}(t)\rho_0 \mathcal{V}^\dagger(t) \tag{17}$$

and the probability to find the system in $\mathcal{H}_P$ is

$$\mathcal{P}(t) \equiv \lim_{N\to\infty} p^{(N)}(t) = \mathrm{Tr}\left[\mathcal{V}(t)\rho_0 \mathcal{V}^\dagger(t)\right]. \tag{18}$$

By assuming the strong continuity of $\mathcal{V}(t)$ at $t = 0$

$$\lim_{t\to 0^+} \mathcal{V}(t) = P, \tag{19}$$

Misra and Sudarshan proved that under general conditions the operators

$$\mathcal{V}(t) \quad \text{exist for all real } t \text{ and form a semigroup.} \tag{20}$$

Moreover, by time-reversal invariance

$$\mathcal{V}^\dagger(t) = \mathcal{V}(-t), \tag{21}$$

one gets $\mathcal{V}^\dagger(t)\mathcal{V}(t) = P$. This implies, by (9), that

$$\mathcal{P}(t) = \mathrm{Tr}\left[\rho_0 \mathcal{V}^\dagger(t)\mathcal{V}(t)\right] = \mathrm{Tr}\left[\rho_0 P\right] = 1. \tag{22}$$

If the particle is very frequently observed, in order to check whether it has survived inside $\mathcal{H}_P$, it will never make a transition to $\mathcal{H}_P^\perp$ (QZE). In general, if N is sufficiently large in (14)-(15), all transitions outside $\mathcal{H}_P$ are inhibited.

We emphasize that close scrutiny of the features of the survival probability has clarified that if N is not *too* large the system can display an inverse Zeno effect [23,24,25], by which decay is accelerated. Both effects have recently been seen in the same experimental setup [22]. We will not elaborate on this here.

Notice also that the dynamics (14)-(15) is not reversible. On the other hand, the dynamics in the $N \to \infty$ limit is often time reversible [31] (although, in general, the operators $\mathcal{V}(t)$ in (20) form a *semi*group).

The theorem just summarized *does not* state that the system *remains* in its initial state, after the series of very frequent measurements. Rather, the system *evolves* in the subspace $\mathcal{H}_P$, instead of evolving "naturally" in the total Hilbert space $\mathcal{H}$. The features of this evolution will be the object study of the following sections.

4 Multidimensional measurements

We now analyze the (most interesting) case of multidimensional measurements. We will apply the von Neumann-Lüders [1,37] formulation in terms of projection operators, by adopting some definitions given by Schwinger [38].

4.1 Incomplete measurements

We will say that a measurement is "incomplete" if some outcomes are lumped together. This happens, for example, if the experimental equipment has insufficient resolution (and in this sense the information on the measured observable is "incomplete"). See, for example, [39]. The projection operator P, which selects a particular lump, is therefore multidimensional. Let us first consider a *finite* dimensional $\mathcal{H}_P = \mathrm{Ran}P$,

$$\dim\mathcal{H}_P = \mathrm{Tr}P = s < \infty. \tag{23}$$

The resulting time evolution operator is a finite dimensional matrix and has the explicit form

$$\mathcal{V}(t) = \lim_{N\to\infty} V_N(t) = \lim_{N\to\infty} [PU(t/N)P]^N = P\exp(-iPHPt). \tag{24}$$

It is easy to show that if $\mathcal{H}_P \subset D(H)$, the domain of the Hamiltonian H, then $\mathcal{V}(t)$ in (24) is unitary within $\mathcal{H}_P$ and is generated by the self-adjoint Hamiltonian PHP (an example is given in [40]). Reversibility is recovered in the $N \to \infty$ limit.

For infinite dimensional projections, $s = \infty$, one can always formally write the limiting evolution in the form (24), but has to define the meaning of PHP. In such a case the time evolution operator $\mathcal{V}(t)$ may be not unitary and one has to study the self-adjointness of the limiting Hamiltonian PHP [31,7,8,9].

In general, for incomplete measurements, system Q does *not* remain in its initial state. Rather, it is confined in the subspace $\mathcal{H}_P$ and evolves under the action of $\mathcal{V}(t)$, instead of evolving "naturally" in the total Hilbert space $\mathcal{H}$.

4.2 Nonselective measurements

We will say that a measurement is "nonselective" [38] if the measuring apparatus does not "select" the different outcomes, so that all the "beams" (after the spectral decomposition [41,13,42]) undergo the whole Zeno dynamics. In other words, a nonselective measurement destroys the phase correlations between different branch waves, provoking the transition from a pure state to a mixture.

We now consider the case of nonselective measurements and extend Misra and Sudarshan's theorem in order to accommodate multiple projectors and build a bridge for our subsequent discussion. Let

$$\{P_n\}_n, \qquad P_n P_m = \delta_{mn} P_n, \qquad \sum_n P_n = 1, \tag{25}$$

be a (countable) collection of projection operators and $\mathrm{Ran} P_n = \mathcal{H}_{P_n}$ the relative subspaces. This induces a partition on the total Hilbert space

$$\mathcal{H} = \bigoplus_n \mathcal{H}_{P_n}. \tag{26}$$

Consider the associated nonselective measurement described by the superoperator [1,37]

$$\hat{P}\rho = \sum_n P_n \rho P_n. \tag{27}$$

The free evolution reads

$$\hat{U}_t \rho_0 = U(t)\rho_0 U^\dagger(t), \qquad U(t) = \exp(-iHt) \tag{28}$$

and the Zeno evolution after N measurements in a time t is governed by the superoperator

$$\hat{V}_t^{(N)} = \hat{P}\left(\hat{U}\left(t/N\right)\hat{P}\right)^{N-1}. \tag{29}$$

This yields the evolution

$$\rho(t) = \hat{V}_t^{(N)}\rho_0 = \sum_{n_1,\ldots,n_N} V^{(N)}_{n_1\ldots n_N}(t)\ \rho_0\ V^{(N)\dagger}_{n_1\ldots n_N}(t), \tag{30}$$

where

$$V^{(N)}_{n_1\ldots n_N}(t) = P_{n_N} U\left(t/N\right) P_{n_{N-1}} \cdots P_{n_2} U\left(t/N\right) P_{n_1}, \tag{31}$$

which should be compared to Eq. (14). We follow Misra and Sudarshan [4] and assume, as in Sec. 3, the time-reversal invariance and the existence of the strong limits ($t > 0$)

$$\mathcal{V}_n(t) = \lim_{N\to\infty} V^{(N)}_{n\ldots n}(t), \qquad \lim_{t\to 0^+} \mathcal{V}_n(t) = P_n, \quad \forall n\ . \tag{32}$$

Then $\mathcal{V}_n(t)$ exist for all real t and form a semigroup [4], and

$$\mathcal{V}_n^\dagger(t)\mathcal{V}_n(t) = P_n. \tag{33}$$

Moreover, it is easy to show that

$$\lim_{N\to\infty} V^{(N)}_{n\ldots n'\ldots}(t) = 0, \qquad \text{for} \quad n' \neq n. \tag{34}$$

Notice that, for any *finite* N, the off-diagonal operators (31) are in general non-vanishing, i.e. $V^{(N)}_{n\ldots n'\ldots}(t) \neq 0$ for $n' \neq n$. It is only in the limit (34) that these operators become diagonal. This is because $U(t/N)$ provokes transitions among different subspaces $\mathcal{H}_{P_n}$. By Eqs. (32)-(34) the final state is

$$\rho(t) = \hat{\mathcal{V}}_t \rho_0 = \sum_n \mathcal{V}_n(t)\rho_0 \mathcal{V}_n^\dagger(t), \quad \text{with} \quad \sum_n \mathcal{V}_n^\dagger(t)\mathcal{V}_n(t) = \sum_n P_n = 1. \tag{35}$$

The components $\mathcal{V}_n(t)\rho_0\mathcal{V}_n^\dagger(t)$ make up a block diagonal matrix: the initial density matrix is reduced to a mixture and any interference between different subspaces $\mathcal{H}_{P_n}$is destroyed (complete decoherence). In conclusion,

$$p_n(t) = \mathrm{Tr}\,[\rho(t)P_n] = \mathrm{Tr}\,[\rho_0 P_n] = p_n(0), \quad \forall n. \tag{36}$$

In words, probability is conserved in each subspace and no probability "leakage" between any two subspaces is possible: the total Hilbert space splits into invariant subspaces and the different components of the wave function (or density matrix) evolve independently within each sector. One can think of the total Hilbert space as the shell of a tortoise, each invariant subspace being one of the scales. Motion among different scales is impossible. (See Fig. 4 in the following.)

If $\mathrm{Tr}P_n = s_n < \infty$, then the limiting evolution operator $\mathcal{V}_n(t)$ (32) within the subspace $\mathcal{H}_{P_n}$has the form (24),

$$\mathcal{V}_n(t) = P_n \exp(-iP_nHP_nt). \tag{37}$$

If $\mathcal{H}_{P_n} \subset D(H)$, then the resulting Hamiltonian P_nHP_n is self-adjoint and $\mathcal{V}_n(t)$ is unitary in $\mathcal{H}_{P_n}$.

The original limiting result (22) is reobtained when $p_n(0) = 1$ for some n, in (36): the initial state is then in one of the invariant subspaces and the survival probability in that subspace remains unity. However, even if the limits are the same, notice that the setup described here is conceptually different from that of Sec. 3. Indeed, the dynamics (31) allows transitions among different subspaces $\mathcal{H}_{P_n} \to \mathcal{H}_{P_m}$, while the dynamics (14) completely forbids them. Therefore, for *finite* N, (31) takes into account the possibility that a given subspace $\mathcal{H}_{P_n}$ gets repopulated [19,20] after the system has made transitions to other subspaces, while in (14) the system must be found in $\mathcal{H}_{P_n}$ at every measurement.

5 Continuous observation

The formulation of the preceding sections hinges upon von Neumann's concept of "projection" [1]. A projection is (supposed to be) an *instantaneous* process, yielding the "collapse" of the wave function, whose physical meaning has been debated since the very birth of quantum mechanics [42]. Repeated projections in rapid succession yield the Zeno effect, as we have seen.

A projection *à la* von Neumann is a handy way to "summarize" the complicated physical processes that take place during a quantum measurement. A measurement

process is performed by an external (macroscopic) apparatus and involves dissipative effects, that imply an interaction and an exchange of energy with and often a flow of probability towards the environment. The external system performing the observation need not be a *bona fide* detection system, namely a system that "clicks" or is endowed with a pointer. It is enough that the information on the state of the observed system be encoded in the state of the apparatus. For instance, a spontaneous emission process is often a very effective measurement process, for it is irreversible and leads to an entanglement of the state of the system (the emitting atom or molecule) with the state of the apparatus (the electromagnetic field). The von Neumann rules arise when one traces away the photonic state and is left with an incoherent superposition of atomic states. However, it is clear that the main features of the Zeno effects would still be present if one would formulate the measurement process in more realistic terms, introducing a physical apparatus, a Hamiltonian and a suitable interaction with the system undergoing the measurement. Such a point of view was fully undertaken in [20], where a novel and more general definition of QZE and IZE was given, that makes no explicit use of projections *à la* von Neumann. It goes without saying that one can still make use of projection operators, if such a description turns out to be simpler and more economic (Occam's razor). However, a formulation of the Zeno effects in terms of a Hamiltonian description is a significant conceptual step. When such a formulation is possible and when the Hamiltonian has (at most) a smooth dependence on time, we will speak of QZE (or IZE) realized by means of a *continuous* measurement process.

A few examples will help us clarify these concepts.

5.1 *Non-Hermitian Hamiltonian*

The effect of an external apparatus can be mimicked by a non-Hermitian Hamiltonian. Consider a two-level system

$$\langle 1| = (1,0), \quad \langle 2| = (0,1), \tag{38}$$

with Hamiltonian

$$H_K = \begin{pmatrix} 0 & \Omega \\ \Omega & -i2K \end{pmatrix} = \Omega(|1\rangle\langle 2| + |2\rangle\langle 1|) - i2K|2\rangle\langle 2|. \tag{39}$$

This yields Rabi oscillations of frequency Ω, but at the same time absorbs away the $|2\rangle$ component of the Hilbert space, performing in this way a "measurement." Due to the non-Hermitian features of this description, probabilities are not conserved.

Prepare the system in the initial state $|1\rangle$. An elementary calculation [20] yields the survival probability

$$p^{(K)}(t) = \left|\langle 1|e^{-iH_K t}|1\rangle\right|^2 = \left|\frac{1}{2}\left(1 + \frac{K}{\sqrt{K^2-\Omega^2}}\right)e^{-(K-\sqrt{K^2-\Omega^2})t} + \frac{1}{2}\left(1 - \frac{K}{\sqrt{K^2-\Omega^2}}\right)e^{-(K+\sqrt{K^2-\Omega^2})t}\right|^2, \tag{40}$$

which is shown in Fig. 2 for $K = 0.4, 2, 10\Omega$. As expected, probability is (exponen-

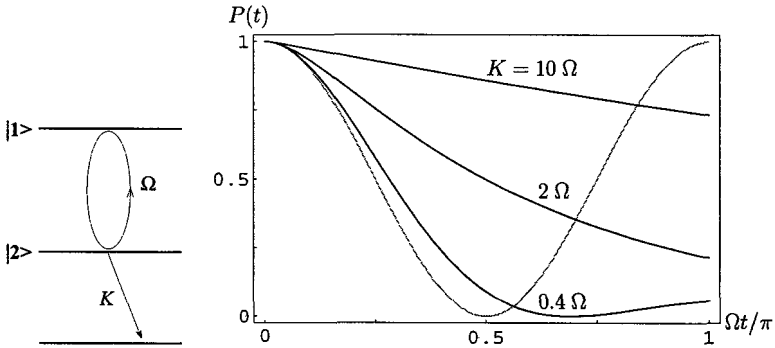

Figure 2. Survival probability for a system undergoing Rabi oscillations in presence of absorption ($K = 0.4, 2, 10\Omega$). The gray line is the undisturbed evolution ($K = 0$).

tially) absorbed away as $t \to \infty$. However, as K increases, the survival probability reads

$$p^{(K)}(t) \sim \left(1 + \frac{\Omega^2}{2K}\right) \exp\left(-\frac{\Omega^2}{K}t\right), \qquad (t \gtrsim K^{-1}) \tag{41}$$

and the effective decay rate $\gamma_{\text{eff}}(K) = \Omega^2/K$ becomes smaller, eventually halting the "decay" (and consequent absorption) of the initial state and yielding an interesting example of QZE: a larger K entails a more "effective" measurement of the initial state. Notice that the expansion (41) is not valid at very short times (where there is a quadratic Zeno region), but becomes valid very quickly, on a time scale of order K^{-1} (the duration of the Zeno region [20,34,35]).

The (non-Hermitian) Hamiltonian (39) can be obtained by considering the evolution engendered by a Hermitian Hamiltonian acting on a larger Hilbert space and then restricting the attention to the subspace spanned by $\{|1\rangle, |2\rangle\}$: consider the Hamiltonian

$$\tilde{H}_K = \Omega(|1\rangle\langle 2| + |2\rangle\langle 1|) + \int d\omega\, \omega |\omega\rangle\langle\omega| + \sqrt{\frac{2K}{\pi}} \int d\omega\, (|2\rangle\langle\omega| + |\omega\rangle\langle 2|), \tag{42}$$

which describes a two-level system coupled to the photon field $\{|\omega\rangle\}$ in the rotating-wave approximation. It is not difficult to show [20] that, if only state $|1\rangle$ is initially populated, this Hamiltonian is "equivalent" to (39), in that they both yield the *same* equations of motion in the subspace spanned by $|1\rangle$ and $|2\rangle$. QZE is obtained by increasing K: a larger coupling to the environment leads to a more effective "continuous" observation on the system (quicker response of the apparatus), and as a consequence to a slower decay (QZE). The quantity $1/K$ is the response time of the "apparatus."

5.2 Continuous Rabi observation

The previous example might lead one to think that absorption and/or probability leakage to the environment (or in general to other degrees of freedom) are funda-

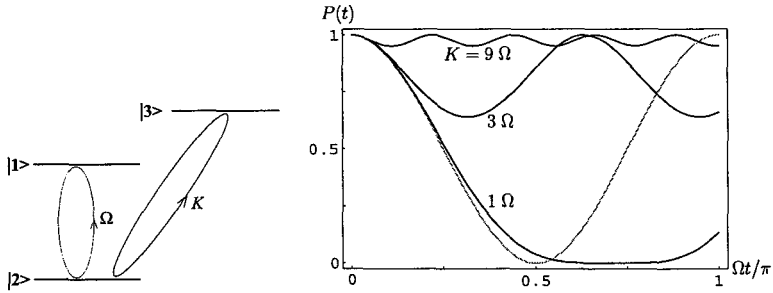

Figure 3. Survival probability for a continuous Rabi "measurement" with $K = 1, 3, 9\Omega$: quantum Zeno effect. The gray line is the undisturbed evolution ($K = 0$).

mental requisites to obtain QZE. This expectation would be incorrect. Even more, *irreversibility is not essential.* Consider, indeed, the 3-level system

$$\langle 1| = (1,0,0), \quad \langle 2| = (0,1,0), \quad \langle 3| = (0,0,1) \tag{43}$$

and the (Hermitian) Hamiltonian

$$H_{3\text{lev}} = \Omega(|1\rangle\langle 2| + |2\rangle\langle 1|) + K(|2\rangle\langle 3| + |3\rangle\langle 2|) = \begin{pmatrix} 0 & \Omega & 0 \\ \Omega & 0 & K \\ 0 & K & 0 \end{pmatrix}, \tag{44}$$

where $K \in \mathbb{R}$ is the strength of the coupling between level $|2\rangle$ ("decay products") and level 3 (that will play the role of measuring apparatus). This model, first considered by Peres [5], is probably the simplest way to include an "external" apparatus in our description: as soon as the system is in $|2\rangle$ it undergoes Rabi oscillations to $|3\rangle$. We expect level $|3\rangle$t o perform better as a measuring apparatus when the strength K of the coupling becomes larger.

A straightforward calculation [20] yields the survival probability in the initial state $|1\rangle$

$$p^{(K)}(t) = \left|\langle 1|e^{-iH_{3\text{lev}}t}|1\rangle\right|^2 = \frac{1}{(K^2+\Omega^2)^2}\left[K^2 + \Omega^2\cos(\sqrt{K^2+\Omega^2}t)\right]^2. \tag{45}$$

This is shown in Fig. 3 for $K = 1, 3, 9\Omega$. We notice that for large K the state of the system does not change much: as K is increased, level $|3\rangle$ performs a better "observation" of the state of the system, hindering transitions from $|1\rangle$ to $|2\rangle$. This can be viewed as a QZE due to a "continuous," yet Hermitian observation performed by level $|3\rangle$.

In spite of their simplicity, the models shown in this section clarify the physical meaning of a "continuous" measurement performed by an "external apparatus" (which can even be another degree of freedom of the system investigated). Also, they capture and elucidate many interesting features of a Zeno dynamics.

6 Novel definition of quantum Zeno effect

The examples considered in the previous section call for a broader formulation of Zeno effect, that should be able to include "continuous" observations as well as other situations that do not fit into the scheme of the "pulsed" formulation. We proposed such a definition in Ref. [20]. It comprises all possible cases (oscillating as well as unstable systems) and situations (quantum Zeno effect as well as inverse quantum Zeno effect). Although in this article we are mostly concerned with the QZE for oscillating systems, we give here all definitions for the sake of completeness.

Consider a quantum system whose evolution is described by a Hamiltonian H. Let the initial state be ρ_0 (not necessarily a pure state) and its survival probability $p(t)$. Consider the evolution of the system under the effect of an additional interaction, so that the total Hamiltonian reads

$$H_K = H + H_{\rm meas}(K), \tag{46}$$

where K is a set of parameters (such as coupling constants) and $H_{\rm meas}(K=0)=0$. Notice that H is not necessarily the free Hamiltonian; rather, one should think of H as a full Hamiltonian, containing interaction terms, and $H_{\rm meas}(K)$ should be viewed as an "additional" interaction Hamiltonian performing the "measurement." If K is simply a coupling constant, then the above formula simplifies to

$$H_K = H + KH_{\rm meas}. \tag{47}$$

Notice that if a projection is viewed as a shorthand notation for a (generalized [13]) spectral decomposition [41], the above Hamiltonian scheme includes, for all practical purposes, the usual formulation of quantum Zeno effect in terms of projection operators. In such a case the scheme (46) is more appropriate, for a fine tuning of K might be required [13].

All the examples considered in the previous sections (for both "pulsed" and "continuous" measurements) can be analyzed within the scheme (47) and *a fortiori* (46). We can now define all possible Zeno effects.

6.1 *Oscillating systems*

We shall say that an oscillating system displays a QZE if there exist an interval $I^{(K)} = [t_1^{(K)}, t_2^{(K)}]$ such that

$$p^{(K)}(t) > p(t), \qquad \forall t \in I^{(K)}, \tag{48}$$

where $p^{(K)}(t)$ and $p(t) = p^{(0)}(t)$ are the survival probabilities under the action of the Hamiltonians H_K and H, respectively. We shall say that the system displays an IZE if there exist an interval $I^{(K)}$ such that

$$p^{(K)}(t) < p(t), \qquad \forall t \in I^{(K)}. \tag{49}$$

The time interval $I^{(K)}$ must be evaluated case by case. However,

$$t_2^{(K)} \leq T_{\rm P}, \tag{50}$$

where T_P is the Poincaré time of the system. Obviously, in order that the definition (48)-(49) be meaningful from a physical point of view, the length of the interval $I^{(K)}$ must be of order T_P.

The above definition is very broad and includes a huge class of systems [even trivial cases such as time translations $p(t) \to p(t - t_0)$]. We would like to stress that we have not succeeded in finding a more restrictive definition and we do not think it would be meaningful: many phenomena can be viewed or reinterpreted as Zeno effects and this is in our opinion a fecund point of view [20].

In order to elucidate the meaning of the above definition, let us look at some particular cases considered in the previous sections. The situations considered in Figs. 2 and 3 are both QZEs, according to this definition: one has $t_1^{(K)} = 0$ and $t_2^{(K)} \leq T_P = \pi/\Omega$ [and $(t_2^{(K)} - t_1^{(K)}) = O(T_P)$]. The case outlined in Fig. 1 is also a QZE, with $t_1^{(K)} = 0$ and $t_2^{(K)} \leq T_P$ (notice that T_P may even be infinite).

6.2 *Unstable systems*

In this paper we mostly deal with few-level systems. However, for unstable systems, the definition of Zeno effect can be made more stringent and expressed in terms of a single parameter, the decay rate. In fact, in such a case, one need not refer to a given interval $I^{(K)}$, but can consider the *global* behavior of the survival probability.

Let us consider Eqs. (3) and (47). For an unstable system, the off-diagonal interaction Hamiltonian $H_{\rm int}$ in Eq. (3) is responsible for the decay. Let

$$\gamma = 2\pi \langle a|H_{\rm int}\delta(\omega_a - H_0)H_{\rm int}|a\rangle \tag{51}$$

be the decay rate (Fermi "golden" rule [43], valid at second order in the decay coupling constant), $|a\rangle$ being the initial state, which is an eigenstate of H_0wit h energy ω_a. We define the occurrence of a QZE or an IZE if

$$\gamma_{\rm eff}(K) \lesseqgtr \gamma, \tag{52}$$

respectively, where $\gamma_{\rm eff}(K)$ is the new (effective) decay rate under the action of H_K,

$$\gamma_{\rm eff}(K) = 2\pi \langle a|(H_{\rm int} + KH_{\rm meas})\,\delta(\omega_a - H_0)\,(H_{\rm int} + KH_{\rm meas})|a\rangle. \tag{53}$$

Notice that this case is in agreement with the definitions (48)-(49). Moreover, $t_2^{(K)} \to \infty$ for IZE, while $t_2^{(K)} \leq t_{\rm pow}$ for QZE, where $t_{\rm pow}$ is the time at which a transition from an exponential to a power law takes place. (Such a time is of order log(coupling constant), at least for renormalizable quantum field theories [44].)

It is worth noticing that (52) is of general validity when it refers to physical decay rates, even when the perturbative expressions (51) and (53) are not valid. In such a case the decay rate is simply given by the imaginary part of the pole $E_{\rm pole}$ of the resolvent nearest to the real axis in the second Riemann sheet of the complex energy plane [26]. The pole is the solution of the equation

$$E_{\rm pole} = \omega_a + \Sigma_{\rm II}(E_{\rm pole}), \qquad \gamma = -2\,{\rm Im}\,[E_{\rm pole}], \tag{54}$$

where $\Sigma_{\rm II}(E)$ is the determination of the proper self-energy function

$$\Sigma(E) = \langle a|H_{\rm int}\frac{1}{E - H_0}H_{\rm int}|a\rangle \tag{55}$$

on the second Riemann sheet. Analogously for $\gamma_{\rm eff}(K)$, with the substitution $H_{\rm int} \to H_{\rm int} + KH_{\rm meas}$ in Eq. (55). For a more detailed discussion, see [20].

7 Dynamical quantum Zeno effect

The broader formulation of quantum Zeno effect (and inverse quantum Zeno effect) elaborated in Sec. 6 triggers a spontaneous question about the form of the interaction Hamiltonian $H_{\rm meas}$ between system and apparatus [Eq. (47)]. In the case of pulsed measurements, in order to get a Zeno effect one has to prepare the system in a state belonging to the measured subspace $\mathcal{H}_P$ as in Eq. (9) [or to any subspace $\mathcal{H}_{P_n}$ of the partition (26) for nonselective measurements]. On the other hand, in the case of a continuous measurement it is not clear which relation must hold between the initial state of the system ρ_0 and the structure of the interaction Hamiltonian $H_{\rm meas}$ in order to get a Zeno effect. We have introduced two paradigmatic examples in Sec. 5, but we still do not know *why* they work. It is therefore important to understand in more detail which features of the coupling between the "observed" system and the "measuring" apparatus are needed to obtain a QZE. In other words, one wants to know when an external quantum system can be considered a good apparatus and why. We shall try to clarify these issues and cast the dynamical quantum Zeno evolution in terms of an adiabatic theorem. We will show that the evolution of a quantum system under the action of a continuous measurement process is in fact similar to that obtained with pulsed measurements: the system is forced to evolve in a set of orthogonal subspaces of the total Hilbert space and an effective superselection rule arises in the strong coupling limit. These *quantum Zeno subspaces* [32] are just the eigenspaces (belonging to different eigenvalues) of the Hamiltonian describing the interaction between the system and the apparatus: they are subspaces that the measurement process is able to distinguish.

7.1 A theorem

Our answer to the afore-mentioned question is contained in a theorem [33,32], which is the exact analog of Misra and Sudarshan's theorem for a general dynamical evolution of the type (47). Consider the time evolution operator

$$U_K(t) = \exp(-iH_K t). \tag{56}$$

We will prove that in the "infinitely strong measurement" ("infinitely quick detector") limit $K \to \infty$ the evolution operator

$$\mathcal{U}(t) = \lim_{K\to\infty} U_K(t), \tag{57}$$

becomes diagonal with respect to $H_{\rm meas}$:

$$[\mathcal{U}(t), P_n] = 0, \qquad \text{where} \quad H_{\rm meas}P_n = \eta_n P_n, \tag{58}$$

P_n being the orthogonal projection onto $\mathcal{H}_{P_n}$, the eigenspace of $H_{\rm meas}$ belonging to the eigenvalue η_n. Note that in Eq. (58) one has to consider distinct eigenvalues, i.e., $\eta_n \neq \eta_m$ for $n \neq m$, whence the $\mathcal{H}_{P_n}$'s are in general multidimensional.

Moreover, the limiting evolution operator has the explicit form

$$\mathcal{U}(t) = \exp[-i(H_{\rm diag} + KH_{\rm meas})t], \tag{59}$$

where

$$H_{\rm diag} = \sum_n P_n H P_n \tag{60}$$

is the diagonal part of the system Hamiltonian H with respect to the interaction Hamiltonian $H_{\rm meas}$.

In conclusion, the generator of the dynamics is the *Zeno Hamiltonian*

$$H^{\rm Z} = H_{\rm diag} + KH_{\rm meas} = \sum_n (P_n H P_n + K\eta_n P_n)\,, \tag{61}$$

whose diagonal structure is explicit, and the evolution operator is

$$\mathcal{U}(t) = \exp(-iH^{\rm Z}t). \tag{62}$$

7.2 Dynamical superselection rules

Before proving the theorem of Sec. 7.1 let us briefly consider its physical implications. In the $K \to \infty$ limit, due to (58), the time evolution operator becomes diagonal with respect to $H_{\rm meas}$,

$$[\mathcal{U}(t), H_{\rm meas}] = 0, \tag{63}$$

a superselection rule arises and the total Hilbert space is split into subspaces $\mathcal{H}_{P_n}$ which are invariant under the evolution. These subspaces are simply defined by the P_n's, i.e., they are eigenspaces belonging to distinct eigenvalues η_n: in other words, they are *subspaces that the apparatus is able to distinguish.* On the other hand, due to (61)-(62), the dynamics within each Zeno subspace $\mathcal{H}_{P_n}$ is essentially governed by the diagonal part $P_n H P_n$ of the system Hamiltonian H (the remaining part of the evolution consisting in a (sector-dependent) phase). The evolution reads

$$\rho(t) = \mathcal{U}(t)\rho_0\mathcal{U}^\dagger(t) = e^{-iH^{\rm Z}t}\rho_0 e^{iH^{\rm Z}t} \tag{64}$$

and the probability to find the system in each $\mathcal{H}_{P_n}$

$$\begin{aligned} p_n(t) &= {\rm Tr}\,[\rho(t)P_n] = {\rm Tr}\,[\mathcal{U}(t)\rho_0\mathcal{U}^\dagger(t)P_n] = {\rm Tr}\,[\mathcal{U}(t)\rho_0 P_n\mathcal{U}^\dagger(t)] \\ &= {\rm Tr}\,[\rho_0 P_n] = p_n(0) \end{aligned} \tag{65}$$

is constant. As a consequence, if the initial state of the system belongs to a specific sector, it will be forced to remain there forever (QZE):

$$\psi_0 \in \mathcal{H}_{P_n} \to \psi(t) \in \mathcal{H}_{P_n}. \tag{66}$$

More generally, if the initial state is an incoherent superposition of the form $\rho_0 = \hat{P}\rho_0$, with $\hat{P}$ defined in (27), then each component will evolve separately, according to

$$\begin{aligned} \rho(t) &= \mathcal{U}(t)\rho_0\mathcal{U}^\dagger(t) = \sum_n e^{-iH^{\rm Z}t}P_n\rho_0 P_n e^{iH^{\rm Z}t} \\ &= \sum_n e^{-iP_nHP_nt}P_n\rho_0 P_n e^{iP_nHP_nt} = \sum_n \mathcal{V}_n(t)\rho_0\mathcal{V}_n^\dagger(t), \end{aligned} \tag{67}$$

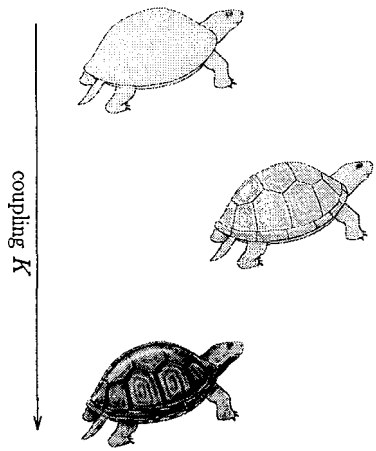

Figure 4. The Hilbert space of the system: a dynamical superselection rule appears as the coupling K to the apparatus is increased.

with $\mathcal{V}_n(t) = P_n \exp(-iP_nHP_nt)$, which is exactly the same result (35)-(37) found in the case of nonselective pulsed measurements. This bridges the gap with the description of Sec. 4.2 and clarifies the role of the detection apparatus: it defines the Zeno subspaces. In Fig. 4 we endeavored to give a pictorial representation of the decomposition of the Hilbert space as K is increased.

Notice, however, that there is one important difference between the dynamical evolution (64) and the projected evolution (35). Indeed, if the initial state ρ_0 contains coherent terms between any two Zeno subspaces $\mathcal{H}_{P_n}$ and $\mathcal{H}_{P_m}$, $P_n\rho_0P_m \neq 0$, these vanish after the first projection in (35), $P_n\rho(0^+)P_m = 0$, and the state becomes an incoherent superposition $\rho(0^+) \neq \rho_0$, whence $\mathrm{Tr}\rho(0^+)^2 < \mathrm{Tr}\rho_0^2$. On the other hand, such terms are preserved by the dynamical (unitary) evolution (64) and do not vanish, even though they wildly oscillate. For example, consider the initial state

$$\rho_0 = (P_n + P_m)\rho_0(P_n + P_m), \qquad P_n\rho_0P_m \neq 0. \tag{68}$$

By Eq. (64) it evolves into

$$\begin{aligned}\rho(t) = {} & \mathcal{V}_n(t)\rho_0\mathcal{V}_n^\dagger(t) + \mathcal{V}_m(t)\rho_0\mathcal{V}_m^\dagger(t) \\ & + e^{-iK(\eta_n-\eta_m)t}\mathcal{V}_n(t)\rho_0\mathcal{V}_m^\dagger(t) + e^{iK(\eta_n-\eta_m)t}\mathcal{V}_m(t)\rho_0\mathcal{V}_n^\dagger(t),\end{aligned} \tag{69}$$

at variance with (67) and (35). Therefore $\mathrm{Tr}\rho(t)^2 = \mathrm{Tr}\rho_0^2$ for any t and the Zeno dynamics is unitary in the *whole* Hilbert space $\mathcal{H}$. We notice that these coherent terms become unobservable in the large-K limit, as a consequence of the Riemann-Lebesgue theorem (applied to any observable that "connects" different sectors and whose time resolution is finite). This interesting aspect is reminiscent of some results on "classical" observables [45], semiclassical limit [46] and quantum measurement theory [47,38].

It is worth noticing that the superselection rules discussed here are *de facto* equivalent to the celebrated "W[3]" ones [48], but turn out to be a mere consequence of the Zeno dynamics. For a related discussion, but in a different context, see [49].

7.3 Proof of the theorem

We will now use perturbation theory and prove [33] that the limiting evolution operator has the form (59). Property (58) will then automatically follow. In the next subsection we will give a more direct proof of (58), which relies on the adiabatic theorem.

Rewrite the time evolution operator in the form

$$U_K(t) = \exp(-iH_K t) = \exp(-iH_\lambda \tau) = U_\lambda(\tau) \tag{70}$$

where

$$\lambda = 1/K, \qquad \tau = Kt = t/\lambda, \qquad H_\lambda = \lambda H_K = H_{\rm meas} + \lambda H, \tag{71}$$

and apply perturbation theory to the Hamiltonian $H_\lambda$for small λ. To this end, choose the unperturbed degenerate projections $P_{n\alpha}$

$$H_{\rm meas} P_{n\alpha} = \eta_n P_{n\alpha}, \qquad P_n = \sum_\alpha P_{n\alpha}, \tag{72}$$

whose degeneration α is resolved at some order in the coupling constant λ. This means that by denoting $\widetilde{\eta}_{n\alpha}$ and $\widetilde{P}_{n\alpha}$ the eigenvalues and the orthogonal projections of the total Hamiltonian H_λ,

$$H_\lambda \widetilde{P}_{n\alpha} = \widetilde{\eta}_{n\alpha} \widetilde{P}_{n\alpha}, \tag{73}$$

they reduce to the unperturbed ones when the perturbation vanishes

$$\widetilde{P}_{n\alpha} \stackrel{\lambda\to 0}{\longrightarrow} P_{n\alpha}, \qquad \widetilde{\eta}_{n\alpha} \stackrel{\lambda\to 0}{\longrightarrow} \eta_n. \tag{74}$$

Therefore, by applying standard perturbation theory [50], we get the eigenprojections

$$\begin{aligned} \widetilde{P}_{n\alpha} &= P_{n\alpha} + \lambda P^{(1)}_{n\alpha} + {\rm O}(\lambda^2) \\ &= P_{n\alpha} + \lambda \left(\frac{Q_n}{a_n} H P_{n\alpha} + P_{n\alpha} H \frac{Q_n}{a_n} \right) + {\rm O}(\lambda^2), \end{aligned} \tag{75}$$

where

$$Q_n = 1 - P_n = \sum_{m\neq n} P_m, \qquad \frac{Q_n}{a_n} = \frac{Q_n}{\eta_n - H_{\rm meas}} = \sum_{m\neq n} \frac{P_m}{\eta_n - \eta_m}. \tag{76}$$

The perturbative expansion of the eigenvalues reads

$$\widetilde{\eta}_{n\alpha} = \eta_n + \lambda \eta^{(1)}_{n\alpha} + \lambda^2 \eta^{(2)}_{n\alpha} + {\rm O}(\lambda^3) \tag{77}$$

where

$$\begin{aligned} &\eta^{(1)}_{n\alpha} P_{n\alpha} = P_{n\alpha} H P_{n\alpha}, \qquad \eta^{(2)}_{n\alpha} P_{n\alpha} = P_{n\alpha} H \frac{Q_n}{a_n} H P_{n\alpha}, \\ &P_{n\alpha} H P_{n\beta} = P_{n\alpha} H \frac{Q_n}{a_n} H P_{n\beta} = 0, \qquad \alpha \neq \beta. \end{aligned} \tag{78}$$

Write now the spectral decomposition of the evolution operator (70) in terms of the projections $\widetilde{P}_{n\alpha}$

$$U_\lambda(\tau) = \exp(-iH_\lambda\tau)\sum_{n,\alpha}\widetilde{P}_{n\alpha} = \sum_{n,\alpha}\exp(-i\widetilde{\eta}_{n\alpha}\tau)\widetilde{P}_{n\alpha} \tag{79}$$

and plug in the perturbation expansions (75), to obtain

$$\begin{aligned} U_\lambda(\tau) = &\sum_{n,\alpha} e^{-i\widetilde{\eta}_{n\alpha}\tau}P_{n\alpha} \\ &+\lambda\sum_{n,\alpha}\left(\frac{Q_n}{a_n}HP_{n\alpha}e^{-i\widetilde{\eta}_{n\alpha}\tau} + e^{-i\widetilde{\eta}_{n\alpha}\tau}P_{n\alpha}H\frac{Q_n}{a_n}\right) + \mathrm{O}(\lambda^2). \end{aligned} \tag{80}$$

Let us define the operator

$$\begin{aligned} \widetilde{H}_\lambda &= \sum_{n,\alpha}\widetilde{\eta}_{n\alpha}P_{n\alpha} \\ &= H_{\mathrm{meas}} + \lambda\sum_n P_nHP_n + \lambda^2\sum_n P_nH\frac{Q_n}{a_n}HP_n + \mathrm{O}(\lambda^3), \end{aligned} \tag{81}$$

where Eqs. (77)-(78) were used. By plugging Eq. (81) into Eq. (80) and making use of the property

$$\sum_n P_nH\frac{Q_n}{a_n} = -\sum_n \frac{Q_n}{a_n}HP_n, \tag{82}$$

we finally obtain

$$U_\lambda(\tau) = \exp(-i\widetilde{H}_\lambda\tau) + \lambda\left[\sum_n\frac{Q_n}{a_n}HP_n,\ \exp(-i\widetilde{H}_\lambda\tau)\right] + \mathrm{O}(\lambda^2). \tag{83}$$

Now, by recalling the definition (71), we can write the time evolution operator $U_K(t)$ as the sum of two terms

$$U_K(t) = U_{\mathrm{ad},K}(t) + \frac{1}{K}U_{\mathrm{na},K}(t), \tag{84}$$

where

$$U_{\mathrm{ad},K}(t) = e^{-i\left(KH_{\mathrm{meas}}+\sum_n P_nHP_n+\frac{1}{K}\sum_n P_nH\frac{Q_n}{a_n}HP_n+\mathrm{O}(K^{-2})\right)t} \tag{85}$$

is a diagonal, *adiabatic* evolution and

$$U_{\mathrm{na},K}(t) = \left[\sum_n\frac{Q_n}{a_n}HP_n,\ U_{\mathrm{ad},K}(t)\right] + \mathrm{O}\left(K^{-1}\right) \tag{86}$$

is the off-diagonal, *nonadiabatic* correction. In the $K\to\infty$ limit only the adiabatic term survives and one obtains

$$\mathcal{U}(t) = \lim_{K\to\infty}U_K(t) = \lim_{K\to\infty}U_{\mathrm{ad},K}(t) = e^{-i\left(KH_{\mathrm{meas}}+\sum_n P_nHP_n\right)t}, \tag{87}$$

which is formula (59) [and implies also (58)]. The proof is complete. As a byproduct we get the corrections to the exact limit, valid for large, but finite, values of K.

Notice that in our derivation we assumed that the eigenprojections and the eigenvalues of the perturbed Hamiltonian H_λ admit the asymptotic expansions (75) and (77) up to order $O(\lambda^2)$ and $O(\lambda^3)$, respectively. With these assumptions we have been able to exhibit also the first corrections to the limit. However, it is apparent that in order to prove the limit (87), it is sufficient to assume that the eigenprojections and the eigenvalues admit the expansions

$$\widetilde{P}_{n\alpha} = P_{n\alpha} + o(1), \qquad \widetilde{\eta}_{n\alpha} = \eta_n + \lambda\eta^{(1)}_{n\alpha} + o(\lambda), \qquad \text{for} \quad \lambda \to 0, \tag{88}$$

whence

$$U_K(t) = e^{-i\left[KH_{\rm meas} + \sum_n P_n H P_n + o(1)\right]t} + o(1), \qquad \text{for} \quad K \to \infty. \tag{89}$$

Notice however that in such a case, unlike in (84), we have no information on the approaching rate and the first-order corrections.

7.4 Zeno evolution from an adiabatic theorem

We now give an alternative proof [and a generalization to time-dependent Hamiltonians $H(t)$] of Eq. (58). We follow again [33]. The adiabatic theorem deals with the time evolution operator $U(t)$ when the Hamiltonian $H(t)$ slowly depends on time. The traditional formulation [50] replaces the physical time t by the scaled time $s = t/T$ and considers the solution of the scaled Schrödinger equation

$$i\frac{d}{ds}U_T(s) = TH(s)U_T(s) \tag{90}$$

in the $T \to \infty$ limit.

Given a family $P(s)$ of smooth spectral projections of $H(s)$

$$H(s)P(s) = E(s)P(s), \tag{91}$$

the adiabatic time evolution $U_{\rm A}(s) = \lim_{T\to\infty} U_T(s)$ has the intertwining property [51,50]

$$U_{\rm A}(s)P(0) = P(s)U_{\rm A}(s), \tag{92}$$

that is, $U_{\rm A}(s)$ maps $\mathcal{H}_{P(0)}$ onto $\mathcal{H}_{P(s)}$.

Theorem (58) and its generalization,

$$\mathcal{U}(t)P_n(0) = P_n(t)\mathcal{U}(t), \tag{93}$$

valid for generic time dependent Hamiltonians,

$$H_K(t) = H(t) + KH_{\rm meas}(t), \tag{94}$$

are easily proven by recasting them in the form of an adiabatic theorem [32]. In the H interaction picture, given by

$$i\frac{d}{dt}U_{\rm S}(t) = HU_{\rm S}(t), \qquad H^{\rm I}_{\rm meas}(t) = U^\dagger_{\rm S}(t)H_{\rm meas}U_{\rm S}(t), \tag{95}$$

the Schrödinger equation reads

$$i\frac{d}{dt}U^{\rm I}_K(t) = KH^{\rm I}_{\rm meas}(t)\, U^{\rm I}_K(t). \tag{96}$$

The Zeno evolution pertains to the $K \to \infty$ limit: in such a limit Eq. (96) has exactly the same form of the adiabatic evolution (90): the large coupling K limit corresponds to the large time T limit and the physical time t to the scaled time $s = t/T$. Therefore, let us consider a spectral projection of $H^{\rm I}_{\rm meas}(t)$,

$$P^{\rm I}_n(t) = U^\dagger_{\rm S}(t) P_n(t) U_{\rm S}(t), \tag{97}$$

such that

$$H^{\rm I}_{\rm meas}(t) P^{\rm I}_n(t) = \eta_n(t) P^{\rm I}_n(t), \qquad H_{\rm meas}(t) P_n(t) = \eta_n(t) P_n(t). \tag{98}$$

The limiting operator

$$\mathcal{U}^{\rm I}(t) = \lim_{K\to\infty} U^{\rm I}_K(t) \tag{99}$$

has the intertwining property (92)

$$\mathcal{U}^{\rm I}(t) P^{\rm I}_n(0) = P^{\rm I}_n(t) \mathcal{U}^{\rm I}(t), \tag{100}$$

i.e. maps $\mathcal{H}_{P^{\rm I}_n(0)}$ onto $\mathcal{H}_{P^{\rm I}_n(t)}$:

$$\psi^{\rm I}_0 \in \mathcal{H}_{P^{\rm I}_n(0)} \to \psi^{\rm I}(t) \in \mathcal{H}_{P^{\rm I}_n(t)}. \tag{101}$$

In the Schrödinger picture the limiting operator

$$\mathcal{U}(t) = \lim_{K\to\infty} U_K(t) = \lim_{K\to\infty} U_{\rm S}(t) U^{\rm I}_K(t) = U_{\rm S}(t) \mathcal{U}^{\rm I}(t) \tag{102}$$

satisfies the intertwining property (93) [see (97)]

$$\begin{aligned} \mathcal{U}(t) P_n(0) &= U_{\rm S}(t) \mathcal{U}^{\rm I}(t) P_n(0) = U_{\rm S}(t) \mathcal{U}^{\rm I}(t) P^{\rm I}_n(0) \\ &= U_{\rm S}(t) P^{\rm I}_n(t) \mathcal{U}^{\rm I}(t) = P_n(t) U_{\rm S}(t) \mathcal{U}^{\rm I}(t) = P_n(t) \mathcal{U}(t), \end{aligned} \tag{103}$$

and maps $\mathcal{H}_{P_n(0)}$ onto $\mathcal{H}_{P_n(t)}$:

$$\psi_0 \in \mathcal{H}_{P_n(0)} \to \psi(t) \in \mathcal{H}_{P_n(t)}. \tag{104}$$

The probability to find the system in $\mathcal{H}_{P_n(t)}$,

$$\begin{aligned} p_n(t) &= {\rm Tr}\left[P_n(t) \mathcal{U}(t) \rho_0 \mathcal{U}^\dagger(t)\right] = {\rm Tr}\left[\mathcal{U}(t) P_n(0) \rho_0 \mathcal{U}^\dagger(t)\right] \\ &= {\rm Tr}\left[P_n(0) \rho_0\right] = p_n(0), \end{aligned} \tag{105}$$

is constant: if the initial state of the system belongs to a given sector, it will be forced to remain there forever (QZE).

For a time-independent Hamiltonian $H_{\rm meas}(t) = H_{\rm meas}$, the projections are constant, $P_n(t) = P_n$, hence Eq. (93) reduces to (58) and the above property holds *a fortiori* and reduces to (65).

Let us add a few comments. It is worth noticing that the limiting evolutions (57), (99) and (102) are understood in the sense of the intertwining relations (58), (100) and (103), that is

$$\lim_{K\to\infty} \Big(U_K P_n - P_n U_K \Big) = 0, \tag{106}$$

while, strictly speaking, each single addend has no limit, due to a fast oscillating phase. In other words, one would read Eq. (103) as

$$U_K(t) P_n(0) - P_n(t) U_K(t) = {\rm o}(1), \qquad \text{for} \quad K \to \infty. \tag{107}$$

As a matter of fact, there is no single adiabatic theorem [52]. Different adiabatic theorems follow from different assumptions about the properties of $H^{\mathrm{I}}_{\mathrm{meas}}(t)$ and $P^{\mathrm{I}}_n(t)$, the notion of smoothness, what are the optimal error estimates, and so on. But all these theorems have the structure of Eq. (107) and only differ in their respective approaching rates [for example, for noncrossing energy levels, o(1) is in fact $\mathrm{O}(1/K)$, while for crossing levels the rate is $\mathrm{O}(1/\sqrt{K})$]. The theorem we have shown must therefore be understood in this variegated framework.

The formulation of a Zeno dynamics in terms of an adiabatic theorem is powerful. Indeed one can use all the machinery of adiabatic theorems in order to get results in this context. An interesting extension would be to consider time-dependent measurements

$$H_{\mathrm{meas}} = H_{\mathrm{meas}}(t), \tag{108}$$

whose spectral projections $P_n = P_n(t)$ have a nontrivial time evolution. In this case, instead of confining the quantum state to a fixed sector, one can transport it along a given path (subspace) $\mathcal{H}_{P_n(t)}$, according to Eqs. (104)-(105). One then obtains a dynamical generalization of the process pioneered by Von Neumann in terms of projection operators [1,53].

8 Example: three-level system

In the present and in the following sections we will elaborate on some examples considered in [20,27,25]. Our attention will be focused on possible applications in quantum computation.

Reconsider (and rewrite) Peres' Hamiltonian (44)

$$H_{3\mathrm{lev}} = \begin{pmatrix} 0 & \Omega & 0 \\ \Omega & 0 & K \\ 0 & K & 0 \end{pmatrix} = H + KH_{\mathrm{meas}}, \tag{109}$$

where

$$H = \Omega(|1\rangle\langle 2| + |2\rangle\langle 1|) = \Omega \begin{pmatrix} 0 & 1 & 0 \\ 1 & 0 & 0 \\ 0 & 0 & 0 \end{pmatrix}, \tag{110}$$

$$H_{\mathrm{meas}} = |2\rangle\langle 3| + |3\rangle\langle 2| = \begin{pmatrix} 0 & 0 & 0 \\ 0 & 0 & 1 \\ 0 & 1 & 0 \end{pmatrix}. \tag{111}$$

Let us reinterpret the results of Sec. 5.2 in the light of the theorem proved in Sec. 7. As K is increased, the Hilbert space is split into three invariant subspaces (eigenspaces of H_{meas}) $\mathcal{H} = \bigoplus \mathcal{H}_{P_n}$

$$\mathcal{H}_{P_0} = \{|1\rangle\}, \quad \mathcal{H}_{P_1} = \{(|2\rangle + |3\rangle)/\sqrt{2}\}, \quad \mathcal{H}_{P_{-1}} = \{(|2\rangle - |3\rangle)/\sqrt{2}\}, \tag{112}$$

corresponding to the projections

$$P_0 = \begin{pmatrix} 1 & 0 & 0 \\ 0 & 0 & 0 \\ 0 & 0 & 0 \end{pmatrix}, \quad P_1 = \frac{1}{2}\begin{pmatrix} 0 & 0 & 0 \\ 0 & 1 & 1 \\ 0 & 1 & 1 \end{pmatrix}, \quad P_{-1} = \frac{1}{2}\begin{pmatrix} 0 & 0 & 0 \\ 0 & 1 & -1 \\ 0 & -1 & 1 \end{pmatrix}, \tag{113}$$

with eigenvalues $\eta_0 = 0$ and $\eta_{\pm 1} = \pm 1$. The diagonal part of the system Hamiltonian H vanishes, $H_{\rm diag} = \sum P_n H P_n = 0$, and the Zeno evolution is governed by

$$H^{\rm Z}_{\rm 3lev} = H_{\rm diag} + KH_{\rm meas} = KH_{\rm meas} = \begin{pmatrix} 0 & 0 & 0 \\ 0 & 0 & K \\ 0 & K & 0 \end{pmatrix}. \tag{114}$$

Any transition between $|1\rangle$ and $|2\rangle$ is inhibited: a watched pot never boils. This simple model has a lot of nice features and will enable us to focus on several interesting issues. We will therefore look in detail at its properties and generalize them in the following sections.

9 Zeno dynamics in a tensor-product space

In the preceding example the initial state of the apparatus (namely the initial population of level $|3\rangle$) has a strong influence on the free evolution of the system (levels $|1\rangle$ and $|2\rangle$). Such an influence entails also unwanted spurious effects: the apparatus is, in some sense, "entangled" with the system, even if $K = 0$. In other words, the evolution of the system has an unpleasant dependence on the state of the apparatus: the system can make Rabi transitions (between states $|1\rangle$ and $|2\rangle$) only if the "detector" is not excited (i.e. state $|3\rangle$ is not populated). If, on the other hand, state $|3\rangle$ is initially considerably populated, the dynamics of the system is almost completely frozen. This is not a pleasant feature (although one should not be too demanding for such a simple toy model).

In a certain sense the QZE is counterintuitive in this case just because, if the initial state is $\simeq |1\rangle$, although the interaction strongly tends to drive the system into state $|3\rangle$, the system remains in state $|1\rangle$. On the other hand, one wonders whether such an effect would take place if the initial state of the apparatus would have little or no influence on the system evolution. This would give a better picture of the QZE: the interaction Hamiltonian should be chosen in such a way that the measured system modifies the state of the apparatus without significant back reaction. In other words, the dynamics of the system should not depend on the state of the apparatus: the apparatus should simply "register" the system evolution (performing a spectral decomposition [41,13]) without "affecting" it.

The most convenient scheme for describing such a better notion of measurement is to consider the system and the detector as two different degrees of freedom living in *different* Hilbert spaces $\mathcal{H}_{\rm s}$ and $\mathcal{H}_{\rm d}$, respectively. The combined total system evolves therefore in the tensor-product space

$$\mathcal{H} = \mathcal{H}_{\rm s} \otimes \mathcal{H}_{\rm d} \tag{115}$$

according to the generic Hamiltonian

$$H_{\rm prod} = H_{\rm s} \otimes 1_{\rm d} + 1_{\rm s} \otimes H_{\rm d} + KH_{\rm meas}. \tag{116}$$

The theorem of Sec. 7.1 is naturally formulated in the total Hilbert space $\mathcal{H}$, without taking into account its possible tensor-product decomposition. On the other hand, one would like to shed more light on the Zeno evolution of the system

and the apparatus in their respective spaces, $\mathcal{H}_{\rm s}$ and $\mathcal{H}_{\rm d}$, in order to understand whether there is such a simple prescription as (61) and (62) in each component space.

9.1 Three-level system revisited

Let us first reconsider the example of Sec. 8. The (3-dimensional) Hamiltonian (109) is expressed in terms of a direct-sum Hilbert space $\mathcal{H} = \mathcal{H}_{\rm s} \oplus \mathcal{H}_{\rm d}$, but can be readily reformulated in terms of the tensor-product Hilbert space of two 2-dimensional Hilbert spaces, i.e. in terms of two coupled qubits $|i)_{\rm s}$ and $|i)_{\rm d}$ $(i = 0, 1)$, as

$$H_{\rm 3lev} = \Omega\, \sigma_{1\rm s} \otimes P_{0\rm d} + K\, P_{1\rm s} \otimes \sigma_{1\rm d}, \tag{117}$$

where $\sigma_1 = |0)(1| + |1)(0|$ and $P_i = |i)(i|$. Indeed, it is easy to show that, by identifying

$$|1\rangle = |00), \quad |2\rangle = |10), \quad |3\rangle = |11), \tag{118}$$

where $|ij) = |i)_{\rm s} \otimes |j)_{\rm d}$, the Hamiltonian (117) becomes the Hamiltonian (109). The fourth available state $|4\rangle = |01)$ of the tensor-product space is idle and decouples from the others.

The unwanted features of the apparatus discussed at the beginning of this section are apparent in Eq. (117): the system-Hamiltonian $\Omega\sigma_{1\rm s}$ is effective *only* if the detector is in state $|0)_{\rm d}$. It is also apparent that the minimal modification that fits the general form (116) is simply

$$H'_{\rm 3lev} = \Omega\, \sigma_{1\rm s} \otimes 1_{\rm d} + K\, P_{1\rm s} \otimes \sigma_{1\rm d}. \tag{119}$$

Note that $H_{\rm meas} = P_{1\rm s} \otimes \sigma_{1\rm d} = |2\rangle\langle 3| + |3\rangle\langle 2|$ is not changed, whence its three eigenspaces are still

$$\begin{aligned} \mathcal{H}_{P_0} &= \{|1\rangle, |4\rangle\} = \{|10), |11)\}, \\ \mathcal{H}_{P_1} &= \{(|2\rangle + |3\rangle)/\sqrt{2}\} = \{|1)_{\rm s} \otimes |+x)_{\rm d}\}, \\ \mathcal{H}_{P_{-1}} &= \{(|2\rangle - |3\rangle)/\sqrt{2}\} = \{|1)_{\rm s} \otimes |-x)_{\rm d}\} \end{aligned} \tag{120}$$

[remember that the enlarged product space contains also a fourth idle state $|4\rangle = |01)$], with eigenprojections

$$P_0 = P_{0\rm s} \otimes 1_{\rm d}, \qquad P_1 = P_{1\rm s} \otimes P_{+x\rm d}, \qquad P_{-1} = P_{1\rm s} \otimes P_{-x\rm d}, \tag{121}$$

where $|\pm x) = [|0) \pm |1)]/\sqrt{2}$ and $P_{\pm x} = |\pm x)(\pm x|$. As a consequence, the Zeno evolution is the same as before

$$H'^{\rm Z}_{\rm 3lev} = \sum_{n=-1}^{+1} P_n H_{\rm 3lev} P_n = K\, P_{1\rm s} \otimes \sigma_{1\rm d} = K H_{\rm meas} = H^{\rm Z}_{\rm 3lev}, \tag{122}$$

see (114). This proves that the answer to the implicit question at the beginning of this section is affirmative: it is indeed possible to design the apparatus in such a way that its initial state has little or no influence on the system evolution (so that the apparatus can be properly regarded as a sort of "pointer"); nevertheless, the measurement is as effective as before and yields QZE.

9.2 Two coupled qubits

In order to understand better the role of $H_{\rm meas}$ in a product space, we study two coupled qubits (system and detector), living in the product space

$$\mathcal{H} = \mathbb{C}^2 \otimes \mathbb{C}^2, \tag{123}$$

whose evolution is engendered by the Hamiltonian (116), with an interaction of the same type as (119)

$$H_{\rm meas} = P_{1\rm s} \otimes V_{\rm d}. \tag{124}$$

This describes an ideal detector, with no "false" events: the detector never clicks when the system is in its initial "undecayed" state $|0)_{\rm s}$.

The spectral resolution of the interaction reads

$$V_{\rm d} P_{\eta_n {\rm d}} = \eta_n P_{\eta_n {\rm d}}, \qquad (n = 1, 2)\ , \tag{125}$$

that is,

$$H_{\rm meas} = P_{1\rm s} \otimes (\eta_1 P_{\eta_1 {\rm d}} + \eta_2 P_{\eta_2 {\rm d}}), \tag{126}$$

where the two eigenvalues η_1 and η_2 are not necessarily different and nonvanishing. Therefore, the Hilbert space is at most split into three Zeno subspaces: a two-dimensional one, corresponding to $\eta_0 = 0$,

$$H_{\rm meas} P_0 = 0, \qquad P_0 = P_{0\rm s} \otimes 1_{\rm d}, \tag{127}$$

and two one-dimensional ones

$$H_{\rm meas} P_n = \eta_n P_n, \qquad P_n = P_{1\rm s} \otimes P_{\eta_n {\rm d}}, \quad (n = 1, 2) \tag{128}$$

corresponding to η_1 and η_2. There are three different cases.

9.2.1 Nondegenerate case $0 = \eta_0 \neq \eta_1 \neq \eta_2 \neq \eta_0$

In the nondegenerate case $0 = \eta_0 \neq \eta_1 \neq \eta_2 \neq \eta_0$ the apparatus is able to distinguish the three subspaces and the total Hilbert space is split into

$$\begin{aligned} &\mathcal{H} = \mathcal{H}_0 \oplus \mathcal{H}_1 \oplus \mathcal{H}_2 \\ &\mathcal{H}_0 = \{|00), |01)\}, \quad \mathcal{H}_1 = \{|1)_s \otimes |\eta_1)_d\}, \quad \mathcal{H}_2 = \{|1)_s \otimes |\eta_2)_d\}. \end{aligned} \tag{129}$$

Therefore (116) yields (for large K) the Zeno Hamiltonian

$$\begin{aligned} H^{\rm Z}_{\rm prod} &= \sum_{n=0}^{2} P_n H_{\rm prod} P_n \\ &= (P_{0\rm s} H_{\rm s} P_{0\rm s} + P_{1\rm s} H_{\rm s} P_{1\rm s}) \otimes 1_{\rm d} \\ &\quad + P_{0\rm s} \otimes H_{\rm d} + P_{1\rm s} \otimes (P_{\eta_1 {\rm d}} H_{\rm d} P_{\eta_1 {\rm d}} + P_{\eta_2 {\rm d}} H_{\rm d} P_{\eta_2 {\rm d}}) + K H_{\rm meas}. \end{aligned} \tag{130}$$

One should notice that the resulting effect on the system Hamiltonian $H_{\rm s} \otimes 1_{\rm d}$ is simply the replacement

$$H_{\rm s} \to H^{\rm Z}_{\rm s} = P_{0\rm s} H_{\rm s} P_{0\rm s} + P_{1\rm s} H_{\rm s} P_{1\rm s}, \tag{131}$$

satisfying our expectations (QZE). On the other hand, for the detector Hamiltonian $1_{\rm s} \otimes H_{\rm d}$ such a simple replacement is not possible, for the resulting dynamics

is entangled. This is a consequence of the fact that the interaction is able to distinguish between different detector states [P_n in (128)] in the subspace of the decay products $P_{1s} \otimes 1_d$. If the interaction Hamiltonian (124) commutes with the detector Hamiltonian,

$$[V_d, H_d] = 0, \tag{132}$$

then the above-mentioned entanglement does not occur, for the detector Hamiltonian $1_s \otimes H_d$ remains unchanged. In such a case, if H_d is nondegenerate, i.e. if it is not proportional to the identity operator 1_d, then $V_d$is not a good measurement Hamiltonian. Indeed, for any value of the coupling constant K, the detector qubit does not move and remains in its initial pointer eigenstate (eigenstate of H_d). Nevertheless, the QZE is still effective. See also the next case.

On the other hand, a good detector has an interaction Hamiltonian V_d which is a complementary observable [1,38] of its free Hamiltonian H_d. For example, if we set, without loss of generality, $H_d = b\sigma_{3d}$, the interaction should be $V_d = \sigma_{1d}$ (or $V_d = \sigma_{2d}$). In such a case, the diagonal part of an observable with respect to the other vanishes, i.e. $P_{\eta_1 d} H_d P_{\eta_1 d} + P_{\eta_2 d} H_d P_{\eta_2 d} = 0$, and the Zeno Hamiltonian (130) reads

$$H^Z_{prod} = (P_{0s} H_s P_{0s} + P_{1s} H_s P_{1s}) \otimes 1_d + P_{0s} \otimes H_d + K H_{meas}. \tag{133}$$

It is therefore apparent that, in the case of a good detector, not only the system evolution, but also the detector evolution is hindered (QZE). Indeed, in the large-K limit, if the system qubit starts (and remains) in $|0)_s$, then the pointer qubit is frozen as well in one of its eigenstates (the eigenstates of H_d).

9.2.2 Degenerate interaction $0 = \eta_0 \neq \eta_1 = \eta_2$

In this case there are only two projections

$$P_0 = P_{0s} \otimes 1_d, \quad \tilde{P}_1 = P_1 + P_2 = P_{1s} \otimes 1_d \tag{134}$$

and two 2-dimensional Zeno subspaces

$$\begin{aligned} &\mathcal{H} = \mathcal{H}_0 \oplus \tilde{\mathcal{H}}_1 \\ &\mathcal{H}_0 = \{|00), |01)\}, \quad \tilde{\mathcal{H}}_1 = \{|10) + |11)\}. \end{aligned} \tag{135}$$

The Zeno Hamiltonian reads

$$\begin{aligned} H^Z_{prod} &= P_0 H_{prod} P_0 + \tilde{P}_1 H_{prod} \tilde{P}_1 \\ &= (P_{0s} H_s P_{0s} + P_{1s} H_s P_{1s}) \otimes 1_d + 1_s \otimes H_d + K H_{meas} \end{aligned} \tag{136}$$

and the QZE occurs again according to (131), leaving the detector Hamiltonian unaltered and without creating entanglement. Notice that in this case the interaction (124) reduces to

$$H_{meas} = \eta_1 P_{1s} \otimes 1_d \tag{137}$$

and does not yield an evolution of the detector qubit. In spite of this, the Hilbert space is split into two Zeno subspaces and a QZE takes place. This happens because some information is stored in the phase of the detector qubit.

9.2.3 Imperfect measurement $0 = \eta_0 = \eta_1 \neq \eta_2$

In this last situation, there are again two projections,

$$\tilde{P}_0 = P_0 + P_1 = P_{0\mathrm{s}} \otimes 1_{\mathrm{d}} + P_{1\mathrm{s}} \otimes P_{\eta_1 \mathrm{d}}, \quad P_2 = P_{1\mathrm{s}} \otimes P_{\eta_2 \mathrm{d}}, \tag{138}$$

and two Zeno subspaces,

$$\begin{aligned} &\mathcal{H} = \tilde{\mathcal{H}}_0 \oplus \mathcal{H}_2 \\ &\tilde{\mathcal{H}}_0 = \{|00), |01), |1)_{\mathrm{s}} \otimes |\eta_1)_{\mathrm{d}}\}, \quad \mathcal{H}_2 = \{|1)_{\mathrm{s}} \otimes |\eta_2)_{\mathrm{d}}\} : \end{aligned} \tag{139}$$

a 3-dimensional one, corresponding to the eigenvalue $\eta_0 = 0$ and a 1-dimensional one, corresponding to $\eta_2 \neq 0$. However, in this case the measuring interaction is not able to perform a clear-cut distinction between the initial state $|0)_{\mathrm{s}}$ of the system and its decay product $|1)_{\mathrm{s}}$, i.e. it yields an *imperfect* measurement.

The Zeno Hamiltonian reads

$$\begin{aligned} H^{\mathrm{Z}}_{\mathrm{prod}} &= \tilde{P}_0 H_{\mathrm{prod}} \tilde{P}_0 + P_2 H_{\mathrm{prod}} P_2 \\ &= H_{\mathrm{s}} \otimes P_{\eta_1 \mathrm{d}} + (P_{0\mathrm{s}} H_{\mathrm{s}} P_{0\mathrm{s}} + P_{1\mathrm{s}} H_{\mathrm{s}} P_{1\mathrm{s}}) \otimes P_{\eta_2 \mathrm{d}} \\ &\quad + P_{0\mathrm{s}} \otimes H_{\mathrm{d}} + P_{1\mathrm{s}} \otimes (P_{\eta_1 \mathrm{d}} H_{\mathrm{d}} P_{\eta_1 \mathrm{d}} + P_{\eta_2 \mathrm{d}} H_{\mathrm{d}} P_{\eta_2 \mathrm{d}}) + K H_{\mathrm{meas}}. \end{aligned} \tag{140}$$

Notice that $H^{\mathrm{Z}}_{\mathrm{prod}}$ displays an interesting symmetry between the system and the apparatus. The origin of this symmetry is apparent by looking at the interaction Hamiltonian H_{meas}:

$$H_{\mathrm{meas}} = \eta_1 P_{1\mathrm{s}} \otimes P_{\eta_2 \mathrm{d}}. \tag{141}$$

A partial QZE is still present. In fact, the evolution of the system is frozen only if the detector is in state $|\eta_2)_{\mathrm{d}}$, while it is not hindered if the latter is in state $|\eta_1)_{\mathrm{d}}$ (and a similar situation holds for the detector evolution).

The three cases analyzed in this subsection are paradigms for examining the rich behavior of the Zeno dynamics engendered by Hamiltonian (116) in a generic tensor-product space (115). In particular, one can show that, by considering a good detector (whose free and interaction Hamiltonians, H_{d} and V_{d}, are two generic complementary observables [54]), the Zeno Hamiltonian (133) admits a straightforward natural generalization to the N-dimensional case. We shall elaborate further on this issue in a future paper.

10 A watched cook can freely watch a boiling pot

Let us look at another interesting model. Consider

$$H_{4\mathrm{lev}} = \Omega\sigma_1 + K\tau_1 + K'\tau_1' = \begin{pmatrix} 0 & \Omega & 0 & 0 \\ \Omega & 0 & K & 0 \\ 0 & K & 0 & K' \\ 0 & 0 & K' & 0 \end{pmatrix}, \tag{142}$$

where states $|1\rangle$ and $|2\rangle$ make Rabi oscillations,

$$\Omega\sigma_1 = \Omega(|2\rangle\langle 1| + |1\rangle\langle 2|) = \Omega \begin{pmatrix} 0 & 1 & 0 & 0 \\ 1 & 0 & 0 & 0 \\ 0 & 0 & 0 & 0 \\ 0 & 0 & 0 & 0 \end{pmatrix}, \tag{143}$$

while state $|3\rangle$ "observes" them,

$$K\tau_1 = K(|3\rangle\langle 2| + |2\rangle\langle 3|) = K \begin{pmatrix} 0 & 0 & 0 & 0 \\ 0 & 0 & 1 & 0 \\ 0 & 1 & 0 & 0 \\ 0 & 0 & 0 & 0 \end{pmatrix} \tag{144}$$

and state $|4\rangle$ "observes" whether level $|3\rangle$ is populated,

$$K'\tau_1' = K'(|4\rangle\langle 3| + |3\rangle\langle 4|) = K' \begin{pmatrix} 0 & 0 & 0 & 0 \\ 0 & 0 & 0 & 0 \\ 0 & 0 & 0 & 1 \\ 0 & 0 & 1 & 0 \end{pmatrix}. \tag{145}$$

If $K \gg \Omega$ *and* K', then (142) must be read

$$H_{4\text{lev}} = H + KH_{\text{meas}}, \qquad \text{with} \quad H = \Omega\sigma_1 + K'\tau_1', \quad H_{\text{meas}} = \tau_1, \tag{146}$$

and the total Hilbert space splits into the three eigenspaces of H_{meas} [compare with (112) and (120)]:

$$\mathcal{H}_{P_0} = \{|1\rangle, |4\rangle\}, \quad \mathcal{H}_{P_1} = \{(|2\rangle + |3\rangle)/\sqrt{2}\}, \quad \mathcal{H}_{P_{-1}} = \{(|2\rangle - |3\rangle)/\sqrt{2}\}. \tag{147}$$

Moreover, $H_{\text{diag}} = \sum_n P_n H P_n = 0$ and the Zeno evolution is governed by

$$H_{4\text{lev}}^{\text{Z}} = K\tau_1 = \begin{pmatrix} 0 & 0 & 0 & 0 \\ 0 & 0 & K & 0 \\ 0 & K & 0 & 0 \\ 0 & 0 & 0 & 0 \end{pmatrix}. \tag{148}$$

The Rabi oscillations between states $|1\rangle$ and $|2\rangle$ are hindered.

On the other hand, if $K' \gg K$ and Ω (and even if $K \gg \Omega$), then (142) must be read

$$H_{4\text{lev}} = H + K'H_{\text{meas}}, \qquad \text{with} \qquad H = \Omega\sigma_1 + K\tau_1, \quad H_{\text{meas}} = \tau_1', \tag{149}$$

the total Hilbert space splits into the three eigenspaces of H_{meas} [notice the differences with (147)]:

$$\mathcal{H}_{P_0'} = \{|1\rangle, |2\rangle\}, \quad \mathcal{H}_{P_1'} = \{(|3\rangle + |4\rangle)/\sqrt{2}\}, \quad \mathcal{H}_{P_{-1}'} = \{(|3\rangle - |4\rangle)/\sqrt{2}\} \tag{150}$$

and the Zeno Hamiltonian reads

$$H_{4\text{lev}}^{\text{Z}\,\prime} = \Omega\sigma_1 + K'\tau_1' = \begin{pmatrix} 0 & \Omega & 0 & 0 \\ \Omega & 0 & 0 & 0 \\ 0 & 0 & 0 & K' \\ 0 & 0 & K' & 0 \end{pmatrix}. \tag{151}$$

The Rabi oscillations between states $|1\rangle$ and $|2\rangle$ are fully *restored* (even if and in spite of $K \gg \Omega$) [55]. A watched cook can freely watch a boiling pot.

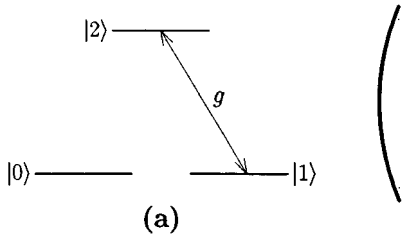

Figure 5. Schematic view of the system described by the Hamiltonian (152).

11 Quantum computation and decoherence-free subspaces

We now look at a more realistic example, analyzing the possibility of devising decoherence-free subspaces [56], that are relevant for quantum computation. The Hamiltonian [57]

$$H_{\rm meas} = ig \sum_{i=1}^{2} \left(b \, |2\rangle_{ii}\langle 1| - b^\dagger \, |1\rangle_{ii}\langle 2| \right) - i\kappa b^\dagger b \tag{152}$$

describes a system of two ($i = 1, 2$) three-level atoms in a cavity. The atoms are in a Λ configuration with split ground states $|0\rangle_i$ and $|1\rangle_i$ and excited state $|2\rangle_i$, as shown in Fig. 5(a), while the cavity has a single resonator mode b in resonance with the atomic transition 1-2. See Fig. 5(b). Spontaneous emission inside the cavity is neglected, but photons leak out through the nonideal mirrors with a rate κ.

The excitation number

$$\mathcal{N} = \sum_{i=1,2} |2\rangle_{ii}\langle 2| + b^\dagger b, \tag{153}$$

commutes with the Hamiltonian,

$$[H_{\rm meas}, \mathcal{N}] = 0. \tag{154}$$

Therefore we can solve the eigenvalue equation inside each eigenspace of $\mathcal{N}$ (Tamm-Duncoff sectors).

A comment is now in order. Strictly speaking, the Hamiltonian (152) is non-Hermitian and we cannot directly apply the theorem of Sec. 7.1. (Notice that the proof of the theorem heavily hinges upon the hermiticity of the Hamiltonians and the unitarity of the evolutions.) However, we can apply the technique outlined at the end of Sec. 5.1 and enlarge our Hilbert space $\mathcal{H}$, by including the photon modes outside the cavity a_ω and their coupling with the cavity mode b. The enlarged dynamics is then generated by the *Hermitian* Hamiltonian

$$\tilde{H}_{\rm meas} = ig \sum_{i=1}^{2} \left(b \, |2\rangle_{ii}\langle 1| - b^\dagger \, |1\rangle_{ii}\langle 2| \right) + \int d\omega \, \omega a_\omega^\dagger a_\omega + \sqrt{\frac{\kappa}{\pi}} \int d\omega \left[a_\omega^\dagger b + a_\omega b^\dagger \right] \tag{155}$$

and it is easy to show that the evolution engendered by $\tilde{H}_{\rm meas}$, when projected back to $\mathcal{H}$, is given by the effective non-Hermitian Hamiltonian (152), provided the field outside the cavity is initially in the vacuum state. Notice that any complex eigenvalue of $H_{\rm meas}$ engenders a dissipation (decay) of $\mathcal{H}$ into the enlarged Hilbert space embedding it. On the other hand, any real eigenvalue of $H_{\rm meas}$ generates a unitary dynamics which preserves the probability within $\mathcal{H}$. Hence it is also an eigenvalue of $\tilde{H}_{\rm meas}$ and its eigenvectors are the eigenvectors of the restriction $\tilde{H}_{\rm meas}|_{\mathcal{H}}$. Therefore, as a general rule, the theorem of Sec. 7.1 can be applied also to non-Hermitian measurement Hamiltonians $\mathcal{H}_{\rm meas}$, provided one restricts one's attention *only* to their *real* eigenvalues.

The eigenspace $\mathcal{S}_0$ corresponding to $\mathcal{N}=0$ is spanned by four vectors

$$\mathcal{S}_0 = \{|000\rangle, |001\rangle, |010\rangle, |011\rangle\}, \tag{156}$$

where $|0j_1j_2\rangle$ denotes a state with no photons in the cavity and the atoms in state $|j_1\rangle_1|j_2\rangle_2$. The restriction of $H_{\rm meas}$ to $\mathcal{S}_0$is the null operator

$$H_{\rm meas}|_{\mathcal{S}_0} = 0, \tag{157}$$

hence $\mathcal{S}_0$ is a subspace of the eigenspace $\mathcal{H}_{P_0}$ of $H_{\rm meas}$ belonging to the eigenvalue $\eta_0 = 0$

$$\mathcal{S}_0 \subset \mathcal{H}_{P_0}, \qquad H_{\rm meas}P_0 = 0. \tag{158}$$

The eigenspace $\mathcal{S}_1$ corresponding to $\mathcal{N}=1$ is spanned by eight vectors

$$\mathcal{S}_1 = \{|020\rangle, |002\rangle, |100\rangle, |110\rangle, |101\rangle, |021\rangle, |012\rangle, |111\rangle\}, \tag{159}$$

and the restriction of $H_{\rm meas}$ to $\mathcal{S}_1$is represented by the 8-dimensional matrix

$$H_{\rm meas}|_{\mathcal{S}_1} = \begin{pmatrix} 0 & 0 & 0 & ig & 0 & 0 & 0 & 0 \\ 0 & 0 & 0 & 0 & ig & 0 & 0 & 0 \\ 0 & 0 & -i\kappa & 0 & 0 & 0 & 0 & 0 \\ -ig & 0 & 0 & -i\kappa & 0 & 0 & 0 & 0 \\ 0 & -ig & 0 & 0 & -i\kappa & 0 & 0 & 0 \\ 0 & 0 & 0 & 0 & 0 & 0 & 0 & ig \\ 0 & 0 & 0 & 0 & 0 & 0 & 0 & ig \\ 0 & 0 & 0 & 0 & 0 & -ig & -ig & -i\kappa \end{pmatrix}. \tag{160}$$

It is easy to prove that the eigenvector $(|021\rangle - |012\rangle)/\sqrt{2}$ has eigenvalue $\eta_0 = 0$ and all the other eigenvectors have eigenvalues with negative imaginary parts. Moreover, all restrictions $H_{\rm meas}|_{\mathcal{S}_n}$ with $n > 1$ have eigenvalues with negative imaginary parts. Indeed they are spanned by states containing at least one photon, which dissipates through the nonideal mirrors, according to $-i\kappa b^\dagger b$ in (152). The only exception is state $|0,2,2\rangle$of $\mathcal{S}_2$, but also in this case it easy to prove that all eigenstates of $H_{\rm meas}|_{\mathcal{S}_2}$ dissipate. In conclusion, blending these results with (156), one infers that the eigenspace $\mathcal{H}_{P_0}$ of $H_{\rm meas}$ belonging to the eigenvalue $\eta_0 = 0$ is 5-dimensional and is spanned by

$$\mathcal{H}_{P_0} = \{|000\rangle, |001\rangle, |010\rangle, |011\rangle, (|021\rangle - |012\rangle)/\sqrt{2}\}, \tag{161}$$

If the coupling g and the cavity loss κ are sufficiently strong, any other weak Hamiltonian H added to (152) reduces to P_0HP_0 and changes the state of the

system only *within* the decoherence-free subspace (161). This corroborates the conclusions of [57] and completely characterizes the decoherence-free subspaces in this example. This could be relevant for practical applications.

12 Spontaneous decay in vacuum

Our last example deals with spontaneous decay in vacuum. Let

$$H_{\rm decay} = H + KH_{\rm meas} = \begin{pmatrix} 0 & \tau_{\rm Z}^{-1} & 0 \\ \tau_{\rm Z}^{-1} & -i2/\tau_{\rm Z}^2\gamma & K \\ 0 & K & 0 \end{pmatrix}. \tag{162}$$

This describes the spontaneous emission $|1\rangle \rightarrow |2\rangle$ of a system into a (structured) continuum, while level $|2\rangle$ is resonantly coupled to a third level $|3\rangle$ [20]. The quantity γ represents the decay rate to the continuum and $\tau_{\rm Z}$ is the Zeno time (convexity of the initial quadratic region). This case is also relevant for quantum computation, if one is interested in protecting a given subspace (level $|1\rangle$) from decoherence by inhibiting spontaneous emission. A somewhat related example is considered in [58]. Model (162) is also relevant for some examples analyzed in [56] and [57], but we will not elaborate on this point here.

Notice that, in a certain sense, this situation is complementary to that in (152); here the measurement Hamiltonian $H_{\rm meas}$ is Hermitian, while the system Hamiltonian H is not. Again, one has to enlarge the Hilbert space, as in Secs. 5.1 and 11, apply the theorem to the dilation and project back the Zeno evolution. As a result one can simply apply the theorem to the original Hamiltonian (162), for in this case $H_{\rm meas}$ has a complete set of orthogonal projections that univocally defines a partition of $\mathcal{H}$ into Zeno subspaces. We shall elaborate further on this interesting aspect in a future paper.

As the Rabi frequency K is increased, one is able to hinder spontaneous emission from level $|1\rangle$ (to be "protected" from decay/decoherence) to level $|2\rangle$. However, in order to get an effective "protection" of level $|1\rangle$, one needs $K > 1/\tau_{\rm Z}$. More to this, if the initial state $|1\rangle$ has energy $\omega_1 \neq 0$, an inverse Zeno effect takes place [25] and the requirement for obtaining QZE becomes even more stringent [24], yielding $K > 1/\tau_{\rm Z}^2\gamma$. Both these conditions can be very demanding for a real system subject to dissipation [20,24,27]. For instance, typical values for spontaneous decay in vacuum are $\gamma \simeq 10^9 {\rm s}^{-1}$, $\tau_{\rm Z}^2 \simeq 10^{-29}{\rm s}^2$ and $1/\tau_{\rm Z}^2\gamma \simeq 10^{20}{\rm s}^{-1}$ [34].

We emphasize that the example considered in this subsection is not to be regarded as a toy model. The numerical figures we have given are realistic and the Hamiltonian (162) is a good approximation at short (for the physical meaning of "short", see [20,24,27]) and intermediate times.

13 Conclusions

The usual formulation of the QZE (and IZE) hinges upon the notion of pulsed measurements, according to von Neumann's projection postulate. However, as we pointed out, a "measurement" is nothing but an interaction with an external system (another quantum object, or a field, or simply another degree of freedom of

the very system investigated), playing the role of apparatus. This remark enables one to reformulate the Zeno effects in terms of a (possibly strong or finely-tuned) coupling to an external agent and to cast the quantum Zeno evolution in terms of an adiabatic theorem. We have analyzed several examples, which might lead to interesting applications. Among these, we have considered in some detail the possibility of tailoring the interaction so as to obtain decoherence-free subspaces, useful also for quantum computation.

References

1. J. von Neumann, *Die Mathematische Grundlagen der Quantenmechanik* (Springer, Berlin, 1932). [English translation by E. T. Beyer: *Mathematical Foundation of Quantum Mechanics* (Princeton University Press, Princeton, 1955)].
2. A. Beskow and J. Nilsson, *Arkiv für Fysik* **34**, 561 (1967).
3. L. A. Khalfin, *JETP Letters* **8**, 65 (1968).
4. B. Misra and E. C. G. Sudarshan, *J. Math. Phys.* **18**, 756 (1977).
5. A. Peres, *Am. J. Phys.* **48**, 931 (1980).
6. K. Kraus, *Found. Phys.* **11**, 547 (1981); A. Sudbery, *Ann. Phys.* **157**, 512 (1984).
7. C. N. Friedman, *Indiana Univ. Math. J.* **21**, 1001 (1972).
8. K. Gustafson, *Irreversibility questions in chemistry, quantum-counting, and time-delay*, in *Energy storage and redistribution in molecules*, edited by J. Hinze (Plenum, 1983), and refs. [10,12] therein. See also K. Gustafson and B. Misra, *Lett. Math. Phys.* **1**, 275 (1976).
9. K. Gustafson, *A Zeno story*, in *Proceedings of the 22nd Solvay Conference*, quant-ph/0203032 (2002).
10. R. J. Cook, *Phys. Scr.* T **21**, 49 (1988).
11. W. M. Itano, D. J. Heinzen, J. J. Bollinger, and D. J. Wineland, *Phys. Rev.* A **41**, 2295 (1990).
12. T. Petrosky, S. Tasaki, and I. Prigogine, *Phys. Lett.* A **151**, 109 (1990); *Physica* A **170**, 306 (1991); A. Peres and A. Ron, *Phys. Rev.* A **42**, 5720 (1990); S. Pascazio, M. Namiki, G. Badurek, and H. Rauch, *Phys. Lett.* A **179**, 155 (1993); T. P. Altenmüller and A. Schenzle, *Phys. Rev.* A **49**, 2016 (1994); J. I. Cirac, A. Schenzle, and P. Zoller, *Europhys. Lett.* **27**, 123 (1994); A. Beige and G. Hegerfeldt, *Phys. Rev.* A **53**, 53 (1996); A. Luis and J. Peřina, *Phys. Rev. Lett.* **76**, 4340 (1996).
13. S. Pascazio and M. Namiki, *Phys. Rev.* A **50**, 4582 (1994).
14. M. V. Berry, "Two-State Quantum Asymptotics", in *Fundamental Problems in Quantum Theory*, eds. D. M. Greenberger and A. Zeilinger (*Ann. N.Y. Acad. Sci.* **755**, New York, 1995), p. 303; B. Kaulakys and V. Gontis, *Phys. Rev.* A **56**, 1131 (1997); P. Facchi, S. Pascazio and A. Scardicchio, *Phys. Rev. Lett.* **83**, 61 (1999); J. C. Flores, *Phys. Rev.* B **60**, 30 (1999); B **62**, R16291 (2000); S. A. Gurvitz, *Phys. Rev. Lett.* **85**, 812 (2000); J. Gong and P. Brumer, *Phys. Rev. Lett.* **86**, 1741 (2001); A. Luis, *J. Opt.* B **3**, 238 (2001).
15. P. Kwiat, H. Weinfurter, T. Herzog, A. Zeilinger, and M. Kasevich, *Phys. Rev.*

Lett. **74**, 4763 (1995).
16. B. Nagels, L. J. F. Hermans, and P. L. Chapovsky, *Phys. Rev. Lett.* **79**, 3097 (1997).
17. C. Balzer, R. Huesmann, W. Neuhauser, and P. E. Toschek, *Opt. Comm.* **180**, 115 (2000); P. E. Toschek and C. Wunderlich, *Eur. Phys. J.* D **14**, 387 (2001); C. Wunderlich, C. Balzer, and P. E. Toschek, *Z. Naturforsch.* **56a**, 160 (2001).
18. E. Jericha, D. E. Schwab, M. R. Jäkel, C. J. Carlile, and H. Rauch, *Physica* B **283**, 414 (2000); H. Rauch, *Physica* B **297**, 299 (2001).
19. H. Nakazato, M. Namiki, S. Pascazio, and H. Rauch, *Phys. Lett.* A **217**, 203 (1996).
20. P. Facchi and S. Pascazio, *Progress in Optics*, edited by E. Wolf (Elsevier, Amsterdam, 2001), Vol. 42, Ch. 3, p. 147.
21. S. R. Wilkinson, C. F. Bharucha, M. C. Fischer, K. W. Madison, P. R. Morrow, Q. Niu, B. Sundaram, and M. G. Raizen, *Nature* **387**, 575 (1997).
22. M. C. Fischer, B. Gutiérrez-Medina, and M. G. Raizen, *Phys. Rev. Lett.* **87**, 040402 (2001).
23. A. M. Lane, *Phys. Lett.* A **99**, 359 (1983); W. C. Schieve, L. P. Horwitz, and J. Levitan, *Phys. Lett.* A **136**, 264 (1989); A. G. Kofman and G. Kurizki, *Nature* **405**, 546 (2000); B. Elattari and S. A. Gurvitz, *Phys. Rev.* A **62**, 032102 (2000).
24. P. Facchi, H. Nakazato, and S. Pascazio, *Phys. Rev. Lett.* **86**, 2699 (2001).
25. P. Facchi and S. Pascazio, *Unstable systems and quantum Zeno phenomena in quantum field theory*, quant-ph/0202127 (2002).
26. H. Nakazato, M. Namiki, and S. Pascazio, *Int. J. Mod. Phys.* B **10**, 247 (1996); D. Home and M. A. B. Whitaker, *Ann. Phys.* **258**, 237 (1997).
27. P. Facchi and S. Pascazio, *"Quantum Zeno effects with "pulsed" and "continuous" measurements"*, in *Time's arrows, quantum measurements and superluminal behavior*, edited by D. Mugnai, A. Ranfagni, and L. S. Schulman (CNR, Rome, 2001) p. 139; *Fortschr. Phys.* **49**, 941 (2001).
28. L. S. Schulman, *Phys. Rev.* A **57**, 1509 (1998).
29. R. A. Harris and L. Stodolsky, *Phys. Lett.* B **116**, 464 (1982); A. Venugopalan and R. Ghosh, *Phys. Lett.* A **204**, 11 (1995); M. P. Plenio, P. L. Knight, and R. C. Thompson, *Opt. Comm.* **123**, 278 (1996); M. V. Berry and S. Klein, *J. Mod. Opt.* **43**, 165 (1996). E. Mihokova, S. Pascazio, and L. S. Schulman, *Phys. Rev.* A **56**, 25 (1997); A. Luis and L. L. Sánchez–Soto, *Phys. Rev.* A **57**, 781 (1998); K. Thun and J. Peřina, *Phys. Lett.* A **249**, 363 (1998); A. D. Panov, *Phys. Lett.* A **260**, 441 (1999); J. Řeháček, J. Peřina, P. Facchi, S. Pascazio, and L. Mišta, *Phys. Rev.* A **62**, 013804 (2000); P. Facchi and S. Pascazio, *Phys. Rev.* A **62**, 023804 (2000); B. Militello, A. Messina, and A. Napoli, *Phys. Lett.* A **286**, 369 (2001); A. Luis, *Phys. Rev.* A **64**, 032104 (2001).
30. A. D. Panov, *Ann. Phys.* (NY) **249**, 1 (1996).
31. P. Facchi, V. Gorini, G. Marmo, S. Pascazio, and E. C. G. Sudarshan, *Phys. Lett.* A **275**, 12 (2000); P. Facchi, S. Pascazio, A. Scardicchio, and L. S. Schulman, *Phys. Rev.* A **65**, 012108 (2002).
32. P. Facchi and S. Pascazio, *Quantum Zeno subspaces*, quant-ph/0201115 (2002).

33. P. Facchi, *Quantum Time Evolution: Free and Controlled Dynamics*, PhD Thesis (Univ. Bari, Italy, 2000); *Quantum Zeno effect, adiabaticity and dynamical superselection rules*, quant-ph/0202174 (2002).
34. P. Facchi and S. Pascazio, *Phys. Lett.* A **241**, 139 (1998).
35. I. Antoniou, E. Karpov, G. Pronko, and E. Yarevsky *Phys. Rev.* A **63**, 062110 (2001).
36. C. Bernardini, L. Maiani, and M. Testa, *Phys. Rev. Lett.* **71**, 2687 (1993); L. Maiani and M. Testa, *Ann. Phys.* (NY) **263**, 353 (1998); I. Joichi, Sh. Matsumoto, and M. Yoshimura, *Phys. Rev.* D **58**, 045004 (1998); R. F. Alvarez-Estrada and J. L. Sánchez-Gómez, *Phys. Lett.* A **253**, 252 (1999); A. D. Panov, *Physica* A **287**, 193 (2000).
37. G. Lüders, *Ann. Phys.* (Leipzig) **8**, 322 (1951).
38. J. Schwinger, *Proc. Nat. Acad. Sc.* **45**, 1552 (1959), reproduced in J. Schwinger, *Quantum kinematics and dynamics* (Perseus Publishing, New York, 1991), p. 26.
39. A. Peres, *Quantum Theory: Concepts and Methods* (Kluwer Academic Publishers, Dordrecht, 1998).
40. K. Machida, H. Nakazato, S. Pascazio, H. Rauch, and S. Yu, *Phys. Rev.* A **60**, 3448 (1999).
41. E. P. Wigner, *Am. J. Phys.* **31**, 6 (1963).
42. M. Namiki, S. Pascazio and H. Nakazato, *Decoherence and Quantum Measurements* (World Scientific, Singapore, 1977).
43. E. Fermi, *Rev. Mod. Phys.* **4**, 87 (1932); *Nuclear Physics* (University of Chicago, Chicago) pp. 136, 148 (1950); *Notes on Quantum Mechanics. A Course Given at the University of Chicago in 1954*, edited by E Segré (University of Chicago, Chicago) Lec. 23 (1960).
44. P. Facchi and S. Pascazio, *Physica* A **271**, 133 (1999).
45. J. M. Jauch, *Helv. Phys. Acta* **37**, 293 (1964).
46. M. V. Berry, "Chaos and the semiclassical limit of quantum mechanics (is the moon there when somebody looks?)," in *Quantum Mechanics: Scientific perspectives on divine action* (eds: Robert John Russell, Philip Clayton, Kirk Wegter-McNelly and John Polkinghorne), Vatican Observatory CTNS publications, p. 41.
47. S. Machida and M. Namiki, *Prog. Theor. Phys.* **63**, 1457; 1833 (1980); H. Araki, *Einführung in die Axiomatische Quantenfeldtheorie I, II* (ETH-Lecture, ETH, Zurich, 1962); *Prog. Theor. Phys.* **64**, 719 (1980).
48. G. C. Wick, A. S. Wightman, and E. P. Wigner, *Phys. Rev.* **88**, 101 (1952); *Phys. Rev.* D **1**, 3267 (1970).
49. D. Giulini, E. Joos, C. Kiefer, J. Kupsch, I.-O. Stamatescu, and H.-D. Zeh, *Decoherence and the Appearance of a Classical World in Quantum Theory* (Springer, Berlin, 1996).
50. A. Messiah, *Quantum mechanics* (Interscience, New York, 1961).
51. M. Born and V. Fock, *Z. Phys.* **51**, 165 (1928); T. Kato, *J. Phys. Soc. Jap.* **5**, 435 (1950).
52. J. E. Avron and A. Elgart, *Comm. Math. Phys.* **203**, 445 (1999), and references therein.

53. Y. Aharonov and M. Vardi, *Phys. Rev.* D **21**, 2235 (1980); P. Facchi, A. G. Klein, S. Pascazio, and L. S. Schulman, *Phys. Lett.* A **257**, 232 (1999).
54. J. Schwinger, *Quantum mechanics. Symbolism of atomic measurements* (Springer, Berlin, 2001).
55. B. Militello, A. Messina, and A. Napoli, *Fortschr. Phys.* **49**, 1041 (2001).
56. G. M. Palma, K. A. Suominen, A. K. Ekert, *Proc. R. Soc. Lond.* A **452**, 567 (1996); L. M. Duan and G. C. Guo, *Phys. Rev. Lett.* **79**, 1953 (1997); P. Zanardi and M. Rasetti, *Phys. Rev. Lett.* **79**, 3306 (1997); *Mod. Phys. Lett.* B **11**, 1085 (1997); P. Zanardi, *Phys. Rev.* A **57**, 3276 (1998); D. A. Lidar, I. L. Chuang, and K. B. Whaley, *Phys. Rev. Lett.* **81**, 2594 (1998); L. Viola, E. Knill, and S. Lloyd, *Phys. Rev. Lett.* **82**, 2417 (1999).
57. A. Beige, D. Braun, B. Tregenna, and P. L. Knight, *Phys. Rev. Lett.* **85**, 1762 (2000).
58. G. S. Agarwal, M. O. Scully, and H. Walther, *Phys. Rev. Lett.* **86**, 4271 (2001).

DISCUSSION

Chairman: T. Petrosky

T. Petrosky: The mechanism seems to be very simple, but the result is surprising.

G. Leuchs: My comment is about the use of the decoherence-free subspaces in quantum computing. Back in 1994, among the works on quantum error correction, the first proposal for protecting quantum information was to use the Zeno effect to consequently project to a symmetric subspace and thereby preventing the quantum qubit from getting out of that.

S. Pascazio: Yes. Thank you. Since I am not very familiar with these old ideas in quantum computing, I am not sure that what I am going to say makes sense in that context. Assume that you are interested in the evolution in a given subspace and want to perform quantum computing in that subspace, but that subspace is leaking out, namely is decohering towards something else. This is a kind of exponential decay towards the environment. I can describe this situation by the Hamiltonian H in (162), which is not a bad approximation. I perform the evolution with the Hamiltonian H in its own subspace and find that this subspace leaks out with a certain decay rate. How could I perform a measurement in the Zeno sense? I simply take H, couple it to $H_{\rm meas}$ and look at the evolution. The idea is that due to the strong coupling K between levels #2 and #3, the decay is suppressed. Even the experiment performed by Mark Raizen fits into this scheme. In the large coupling limit you get a superselection rule. The decaying subspace is isolated and the other subspace is also isolated (they're both "Zeno" subspaces), but the time scales involved turn out to be extremely short. You need an extremely strong coupling of order $1/\tau^*$, where $\tau^* = \tau_Z^2\gamma$ is the transition time introduced in Ref. [24], in order to freeze your quantum state. The real problem is therefore the following. When the coupling is very strong I don't trust my Hamiltonian anymore.

In the strong coupling regime you should go back to your theory and look at the Hamiltonian you started with. If you can trust your Hamiltonian, you can be sure that you obtain Zeno at those timescales. If you don't trust it anymore, you'd better look at your theory again and find a better Hamiltonian. As a general rule you have to be careful, because your mathematics might not describe well your physics. For example, counter-rotating effects might become important and could not be neglected. I hope I have answered your question.

I. Antoniou: I would like to understand the superselection rule, which appears when you change the coupling parameter. In order to have these quantum transitions you must have a continuous spectrum and resonances. If you have a continuous spectrum and resonances, you have spectral instabilities. How does this superselection rule appear?

S. Pascazio: You are right. I did not give enough details. The theorem is proved by transforming the evolution in the interaction picture and rephrasing the theory in terms of an adiabatic evolution. In the limit of large coupling K the total space adiabatically splits into the Zeno subspaces and a superselection rule appears. Of course one is assuming a discrete spectrum for the "measurement" Hamiltonian H_{meas}. When K is not too large, transitions between the different sectors are still allowed. So the point is to evaluate the mistakes you make, which are the same as in adiabatic theory. You are often able to evaluate the non-adiabatic transitions between subspaces and you can also look at the problems arising from crossings and from other details of your Hamiltonian. I completely agree that in general the problem of the appearance of superselection rules can be a very serious one, but in this case many factors can be efficiently controlled.

L. Stodolsky: I would like to comment on the argument about $1 - t^2$ at short times. This is a perfectly fine argument, of course. We never find the finite number of levels, but there is a problem when you go to the continuum with a singular limit. As we all know, when you do scattering theory there are infinities that you have to deal with. It is not obvious whether you can take off your arguments, which you have for the two level system and apply them to the continuum. It is a mathematical problem. The argument of Michael Berry shows that this is different.

E. C. G. Sudarshan: I completely disagree with what he said because we have exact solutions without any approximations.

S. Pascazio: This question is a delicate one. Michael Berry's argument is of general validity, when the coupling to the continuum is flat. However, when you study physical systems in greater details, you have to look at the exact coupling and form factors, yielding the *exact* survival amplitude. We looked in particular (in Ref. [34]) at the hydrogen atom with the exact relativistic QED matrix elements, without any assumptions and free parameters (the only constants are the electron charge and mass). How do you compute the evolution? The survival amplitude is expressed as an inverse Fourier-Laplace transform in the complex energy plane. You cut the plane, you go to the second Riemann sheet and uncover the pole. The pole gives you the Weisskopf-Wigner term, while the contribution of the cut, which is of second order in the coupling constant, yields all deviations from the exponential law. The self-energy function in this case can be computed *exactly*. For the $2P \rightarrow 1S$ transition in the hydrogen atom this is a ratio of two known

polynomials plus a logarithmic term.

A. Bohm: What is the pole? What is the vector that corresponds to the pole?

S. Pascazio: If you take the contribution of the pole plus the contribution of the cut, the exact evolution exhibits deviation from the exponential law and in particular a short-time quadratic region (see Ref. [34]). When you take only the pole contribution into account, the evolution is given by a pure exponential. Notice that this exponential is *renormalized.* The renormalization of the wave function yields Z, which is $1-\mathrm{O}(g^2)$, where g is the coupling constant. By looking carefully at the renormalization procedure you get a Zeno region also for a decaying atom. I should also say (I agreed with Leo Stodolsky on this point) that the duration of the short-time Zeno region for the hydrogen atom is very short, about 10^{-18} seconds. This is too short to be *directly* observed, but has important observable consequences at the level of the inverse Zeno effect, see P. Facchi and S. Pascazio, *Phys. Rev.* A **62**, 023804 (2000).

W. Schleich: I want to stimulate the discussion during the coffee break by the following comment. As you have said already, this effect exists in many other fields of physics. In classical Newtonian statistical physics for short times if you take a larger number of particles you consider the Liouville equation. If you propagate it a little bit in time, you see that the average position always changes quadratically while the first moment changes linearly. This is the same effect.

S. Pascazio: I agree that there is also a *classical* Zeno effect.

FASTER-THAN-LIGHT PROPAGATIONS, NEGATIVE GROUP DELAYS, AND THEIR APPLICATIONS

RAYMOND Y. CHIAO

Department of Physics, University of California, Berkeley, CA 94720-7300, U. S. A.
(E-mail: chiao@physics.berkeley.edu)

Conceptual tensions between the three pillars of physics consisting of quantum mechanics, relativity, and statistical mechanics, will be reviewed. Relativity is not violated by our earlier experiments showing that quantum tunneling is superluminal, nor by the recent observations of faster-than-c group velocities, including the recent Princeton NEC experiments, nor by our electronic circuit experiments, which demonstrate the existence of negative group delays. In fact, relativity does not forbid the group velocity in transparent optical media from exceeding c, nor the occurrence of seemingly anti-causal negative group delays in any other linear-response media. We have observed such counter-intuitive behaviors in electronic circuits, in particular, the occurrence of negative group delays of analytic signals, in which the peak of an output pulse leaves the exit port of the circuit *before* the peak of the input pulse enters the input port. Moreover, we predict that similar negative group delays will occur for atomic wavepackets incident at low energies on an atomic BEC. Some applications of these counter-intuitive effects, including the speeding up of computers, will be discussed.

1 Introduction

For this 22nd International Solvay Conference in Physics, let us begin by broadening the discussion that Einstein and Bohr had during the 20th century Solvay Conferences, which concerned mainly quantum mechanics, to include a discussion of the three pillars of physics, as they stand at the beginning of the 21st century, viz., quantum mechanics, relativity, and statistical mechanics. These three pillars correspond to the three 1905 papers of Einstein, and can be represented by three circles in a Venn-like diagram (see Figure 1). Even today, there exist conceptual tensions at the intersections of these three circles.

Why examine conceptual tensions? A brief answer is that they often lead to new experimental discoveries. It suffices to give just one example from 19th and early 20th century physics: the clash between the venerable concepts of *continuity* and of *discreteness*. Since this conference is being held in Greece, it is appropriate to trace these concepts back to their early Greek roots. The concept of continuity, which goes back to the Greek philosopher Heraclitus ("everything flows"), clashed with the concept of discreteness, which goes back to Democritus ("everything is composed of atoms"). Eventually, Heraclitus' concept of continuity, or more specifically that of the *continuum*, was embodied in the idea of *field* in the classical field theory associated with Maxwell's equations. The atomic hypothesis of Democritus was eventually embodied in the kinetic theory of gases in statistical mechanics.

Experiments on blackbody radiation in the 19th century were exploring the intersection, or borderline, between Maxwell's theory of electromagnetism and statistical mechanics, where this conceptual tension was most acute, and eventually led to the discovery of quantum mechanics through the work of Planck. The concept of *discreteness* was thereby embodied in the concept of the *quantum*. This led in

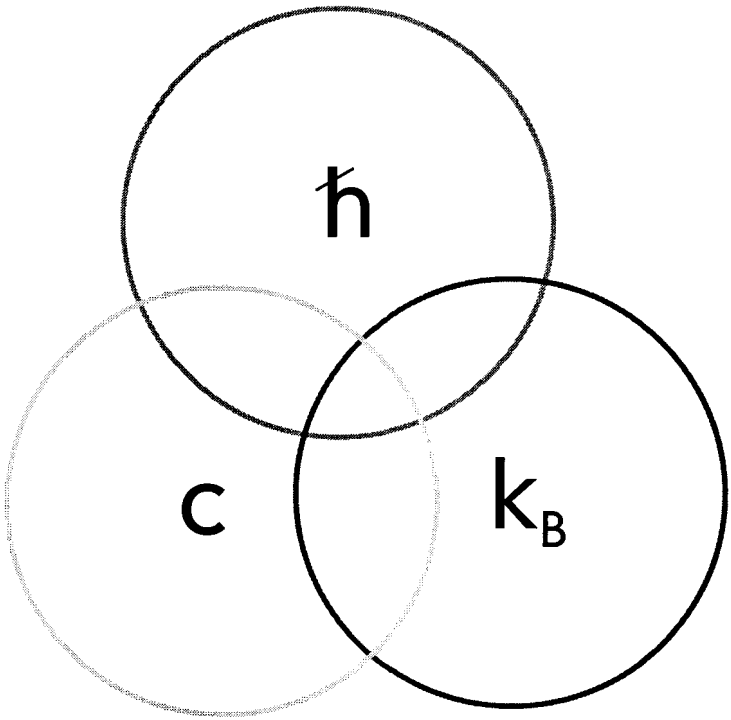

Figure 1. Three pillars of physics at the beginning of the 21st century, represented in a Venn-like diagram: Quantum Mechanics, represented by Planck's constant $\hbar$; Relativity, represented by the speed of light c; Statistical Mechanics and Thermodynmics, represented by Boltzmann's constant k_B. At the beginning of the 20th century, Planck, working at the intersection of these three circles, discovered quantum mechanics. That his discovery involved all three fields of physics is indicated by the fact that his formula for blackbody radiation involved all the three fundamental constants, $\hbar$, c, and k_B.

turn to the concept of *discontinuity* embodied in Bohr's *quantum jump* hypothesis, which was necessitated by the *indivisibility* of the quantum. Experiments, such as Millikan's measurements of h/e, were in turn motivated by Einstein's heuristic theory of the photoelectric effect based on the quantum hypothesis. This is a striking example showing that many fruitful experimental consequences can come out of one particular conceptual tension.

Now it may at once be objected that in drawing Figure 1, one is assuming that statistical mechanics is on an equal footing with quantum mechanics and relativity. One common viewpoint is that statistical mechanics is not as fundamental as quantum mechanics, from which it can in principle be derived, nor is it as fundamental as relativity, since the notion of spacetime underlies all statistical mechanical and thermodynamic phenomena. However, this may not be not so. For example, it may turn out to be the case that the concept of spacetime itself is valid only in the

thermodynamic limit.

Furthermore, it is well known that in the problem of measurement in quantum mechanics, one must introduce the notion of *irreversibility*, which is fundamentally a thermodynamic concept arising from the second law, into the description of all observable quantum phenomena, before they can become physically meaningful. Wheeler, following Bohr, has emphasized the important role played by irreversibility in the process of quantum measurement in the following statement [1]:

> "A phenomenon is not yet a phenomenon until it has been brought to a close by an *irreversible* act of amplification such as the blackening of a grain of silver bromide emulsion or the triggering of a photodetector." [*Italics mine.*]

Moreover, the irreversible arrow of time of statistical mechanics also enters in a fundamental way into relativity, at the point where Einstein introduced into the light-cone structure of spacetime the important distinction between past and future light-cones. This distinction is based on a common-sense notion of causality, in which only *past* events can be causally connected to *future* events, a notion which fundamentally requires the existence of an irreversible arrow for time. This step taken by Einstein in special relativity is quite similar in spirit to the *ad hoc* step in classical electrodynamics, in which, again on the basis of common sense, one discards the *advanced* Green function solution, in favor of the *retarded* solution. However, Wheeler and Feynman have shown that one can retain both advanced and retarded solutions in such a way as to be consistent with relativistic causality [2].

At the intersections of these fields, there exist certain deep conceptual tensions such as:

(I) Reversibility versus irreversibility of time.

(II) Objectivity versus subjectivity of probabilities.

(III) Locality versus nonlocality of space.

(I) First, there is the profound problem of the "arrows of time," that is, the apparent irreversibility of time, versus the reversibility of most of the fundamental processes of microscopic physics. However, there exists a very fundamental microscopic process in which a breakdown of time-reversal symmetry occurs, which has been observed in the weak decays of the K (and, according to preliminary data, the B) mesons. It is unclear how this microscopic arrow of time is related to the other arrows of time, but some physicists argue that in any case, in any eventual hierarchy for the arrows of time, this arrow must be the most fundamental one, since it is the most microscopic one. In two recently proposed views concerning the hierarchy of the various arrows of time [3], both place this microscopic arrow at the most fundamental level, from which all the other arrows of time must somehow originate. According to these viewpoints, any theory which ignores the existence of this microscopic arrow of time must be regarded with suspicion as being not truly fundamental.

At the macroscopic level, it is well known that the phenomenon of irreversibility originates from the second law of thermodynamics. Closely connected with this

thermodynamic arrow of time are the physiological and psychological arrows of time. The question naturally arises: Is the irreversibility of time observed in the macroscopic world a fundamental feature of the physical world, or is it a law that appears only as a *practical necessity* in describing the macroscopic world, or in the words of Bell, true only "For All Practical Purposes (FAPP)"?

There also exist two other closely related, macroscopic arrows of time, namely, the cosmological arrow arising from the expansion of the universe, and the electromagnetic arrow of time, imposed by the boundary conditions for the radiation field at infinity (i.e., "black-universe" boundary conditions [2]). For example, the use of these boundary conditions implies that a spontaneously emitted photon from an atom escapes into a black universe, never to return, FAPP. This suggests that there may be a nested hierarchy of arrows of time, starting from the microscopic to the macroscopic [3]. However, this problem is still far from a satisfactory solution, in my opinion.

(II) Second, the concepts of probability in quantum mechanics and in statistical mechanics are quite different in nature. In statistical mechanics, probabilities are *subjective*, in the sense that it is *our ignorance* of all the microscopic physical conditions necessary to specify completely a system, which is the source of an *apparent* randomness in these systems. For example, in the kinetic theory of gases in classical statistical mechanics, if we have all the necessary information for the positions and velocities as initial data for all the particles in a box, we could *in principle* follow all the Newtonian trajectories of each particle with complete certainty, and there would be no *fundamental* randomness in system at all. In quantum mechanics, by contrast, probabilities are *objective*, since it is not *our* ignorance, but an *in-principles unknowability* arising from the uncertainty principle, which is the origin of a truly *fundamental* randomness in physical systems. Closely related to the problem of the nature of probabilities is the problem of the nature of information. Is information truly physical, as indicated by Landauer's principle for computers, and therefore objective, or is it merely a measure of the subjective state of *our* knowledge or *our* ignorance of system?

(III) Third, *locality* is a fundamental notion in relativity and all of classical physics, whereas *nonlocality*, in the sense of the *spatial nonseparability* of physical systems, is a ineluctable consequence of the quantum mechanics. This is best illustrated by the Einstein-Podolsky-Rosen (EPR) effects for two particles in an entangled state. Experiments have shown that such systems violate Bell's inequalities, so that physical systems are, in general, fundamentally nonseparable.

2 Experiments on superluminal group velocities

I shall examine the outgrowth of one particular conceptual tension between quantum mechanics and relativity, namely, the one connected with the question: How fast does a particle traverse a tunnel barrier? Our experiments at Berkeley have shown that the particle tunnels *superluminally* through the barrier. For earlier reviews of this subject, see [4] and [5], in which the data showing the phenomena of superluminal tunneling times of photons, the various theories of tunneling times, and the theoretical predictions of superluminal light pulse propagation in transpar-

ent media, were critically reviewed. Here, I shall discuss some other recent experimental and theoretical developments concerning faster-than-light propagation phenomena in optics, electronics, and condensed matter physics. I hope thereby to be able to help and correct the commonly held, but mistaken, belief that only the phase velocity in a medium can exceed c, but not the group velocity. Several situations in which the group velocity in fact exceeds c will be discussed, and some applications of these phenomena, such as to speed-up of computer circuits by using negative group delays to cancel out deleterious positive group delays, will be pointed out. These ideas will then be applied to novel situations in condensed matter physics, such as to the transmission of helium atoms through a slab of superfluid helium, or of atoms identical to those in a condensate, through an atomic Bose-Einstein condensate. The transmission times of such atoms, under the appropriate experimental conditions, can be negative, and should be clearly observable [7].

2.1 *Phasor description of superluminal propagation*

A simple phasor picture (see Figure 2) helps explain how such superluminal group velocities can occur for all kinds of waves (e.g., for light and for matter waves), in complete generality. The peak of a Gaussian wave packet, indicated by point B in Figure 2, is the moment when all the phasors which represent the various Fourier components of the wave packet, line up in a straight line, so that the resultant phasor has a maximum amplitude. Therefore, the peak of the wave packet represents a point of maximum constructive interference. By the same token, a point in the early part of the wave packet where the amplitude is small, represented by point A in Figure 2, is a moment of almost total destructive interference, in which the same phasors curl up to form a polygon which almost closes in on itself. Hence, the resultant amplitude at point A in the early tail of the Gaussian wave packet, is small.

After propagation through a dispersive medium, there is no physical reason why the phasors at the early point A cannot precess due to dispersion, in such a way that the curled-up polygon becomes uncurled, forming a large resultant phasor at point A'. The phasors at this point are now aligned in constructive interference, and the peak occurs *earlier* in time in the wave packet compared with what would have happened in the vacuum. By the same reasoning, the aligned phasors at point B now curl up to form a polygon which almost closes in on itself, leading to almost total destructive interference at point B' in the trailing tail of the wave packet. The result is an *advancement* of the entire Gaussian wave packet relative to vacuum propagation; this occurs whenever the spectrum of this wave packet lies in a region of negative wave-number dispersion relative to that of the vacuum. In the case of optics, this can occur in a spectral region of anomalous dispersion.

Furthermore, if the dispersion in the group velocity vanishes at the carrier frequency, the entire wave packet can propagate superluminally with negligible change in shape. Moreover, by the superposition principle, one can add up many such wave packets to form an arbitrary, analytic waveform, which can propagate faster than c with negligible distortion.

Much more commonly, the medium possesses a *positive* dispersion, and the pha-

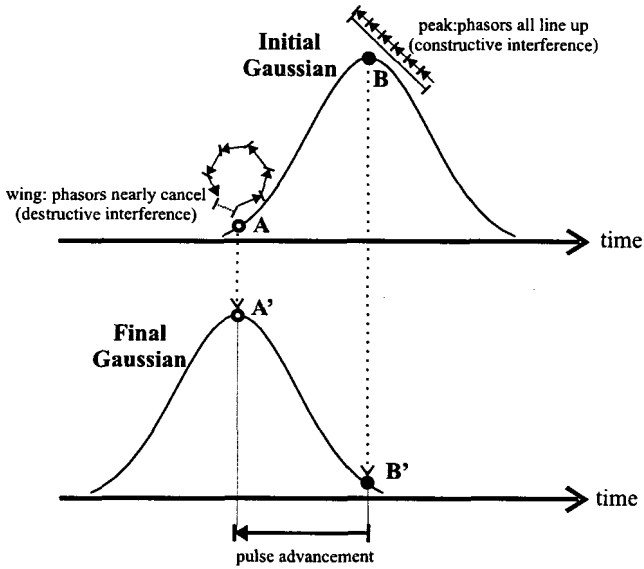

Figure 2. Phasor description of superluminal propagation.

sors precess in the opposite sense from the above case of *negative* dispersion. There results a *retardation* of the Gaussian wave packet relative to vacuum propagation, rather than an *advancement*. For example, in optical media such as ordinary glass, one normally observes *subluminal* pulse propagation in spectral regions of normal dispersion. Nevertheless, the underlying physical mechanisms for both the retardation and the advancement of the wave packet are identical, apart from the *sign* of the precession of the phasors, and both are possible in principle.

However, it should be emphasized that there are conditions on the above phasor-precession processes, which must be fulfilled before they can be physically significant. In general, the group advancements or retardations of an incident wave packet will be destroyed by the *decoherence* of the system. For example, in the optical case it is necessary to maintain the phase coherence of a light pulse during the phasor-precession process which produces the advanced peak; otherwise, the constructive interference will be destroyed. In particular, for an optical medium with gain, stimulated emission must always be accompanied by spontaneous emission. Hence, spontaneous emission will lead to phasor decoherence, and this will limit the maximum possible amount of superluminal advancement [8]. One possible definition of a signal velocity in terms of a signal-to-noise ratio which is limited by amplified spontaneous emission, leads to a velocity which is less than c [9]. Thus, signals so defined cannot propagate faster than c.

Why do such superluminal pulse propagation phenomena not violate relativity? The answer can be seen in Figure 3, where the Gaussian wave packet is multiplied by a step function, such that there results a *front* in its early tail, ahead of which

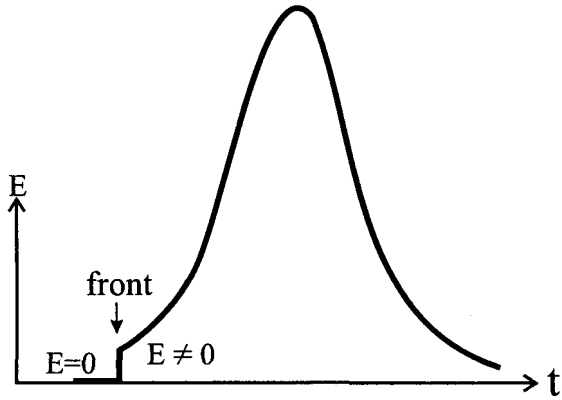

Figure 3. Front defined by discontinuity.

the electromagnetic field is strictly zero. Here, all phasors representing the field ahead of the front have strictly zero length. Since the discontinuity at the front contains Fourier components of infinite frequency, where the index of refraction of any dispersive medium approaches unity, it follows that the front velocity is exactly c, as was pointed out by Sommerfeld and Brillouin [10]. Although the peak of the Gaussian wave packet moves at the group velocity, which may exceed c, this peak can never overtake the front. The reason is that there is no way that phasors of zero length ahead of the front can ever produce a resultant phasor of finite length. Thus, no signal can overtake the front, and this sets a fundamental limit on superluminal pulse propagation, in agreement with the principle of causality in special relativity.

It is important to distinguish between two kinds of signal waveforms: *analytic* waveforms, such that of a Gaussian wave packet, and *nonanalytic* wave forms, such as that of a step function. Any small but finite piece of the the early part of an analytic wave form can be extrapolated into the future by means of a Taylor series; therefore, there is no surprise associated with the arrival of any of the features of the subsequent waveform, including its peak. Conversely, the same extrapolation of the signal ahead of the Sommerfeld front would predict that the waveform would remain identically zero for all time. When the front arrives, there is a genuine surprise associated with its arrival [11]. This suggests another definition of signal velocity in terms of discontinuities [5]. Again, signals so defined cannot travel faster than c.

However, other definitions of "signal velocities" that differ from this one have been proposed. Perhaps the oldest definition is that the signal velocity is simply the group velocity. For a discussion of this possibility, see the article by Nimtz in this volume, and also the earlier review [6]. One of the earliest other alternative definitions of "signal velocity" was formulated in Brillouin's book *Group Velocity and Wave Propagation* [10] in terms of the half-maximum amplitude velocity. Both of these alternate definitions suffer from the fact that under the circumstances of

Wang's experiment, "signals" so defined travel faster than light, which leads to the false impression that relativistic causality is somehow violated.

An important special case of superluminal propagation occurs when the group velocity becomes negative. Recent optical experiments at Princeton NEC [12] have verified my prediction that superluminal pulse propagation, in particular, propagation even with a negative group velocity, can occur in transparent media with optical gain [13]. These experiments have shown that a laser pulse can indeed propagate with little distortion in an optically pumped cesium vapor cell with a *negative* group velocity [14]: The peak of the output laser pulse left the output face of the cell *before* the peak of the input laser pulse entered the input face of the cell. This implies a *negative time of flight* of the pulse through the cell. A negative-time-of-flight process is represented in Figure 4 by a zigzag world-line for the motion of the peak of the wave packets. Note that a time slice through the middle of the zigzag world-line shows that at that moment, *three* wave packets are simultaneously present in the system: the input wave packet propagating to the right, whose peak is about to enter the input face of the cell, a wave packet propagating to the left, which is in the middle of the cell, and an output wave packet propagating to the right, whose peak has already left the output face of the cell.

The question immediately arises as to how energy can be conserved in such a process. One answer is that there can be optical gain, for example, through the population inversion of an atomic system: the atoms can then possess enough extra energy which can then be "loaned" to the light in order to produce the two extra pulses at point β at the output face of the medium, in a process reminiscent of "pair creation" (in the sense of the creation of a pair of wave packets). The borrowed energy is later restored to the inverted atomic system at point α at the input face of the medium, in the process reminiscent of "pair annihilation" (in the sense of the annihilation of a pair of wave packets). Note that for this zigzag process, if one were to *double* the cell length, the output laser pulse would have to come out *twice* as early.

This process is reminiscent of the zigzag world line introduced by Feynman in quantum electrodynamics shown in Figure 5(b). In this diagram, Feynman interpreted the backwards-in-time propagation of a particle (an electron) as the forwards-in-time propagation of an antiparticle (a positron). Point b, which corresponds to electron-positron pair creation in the vicinity of a nucleus of charge +Ze, occurs *earlier* in time than point a, which corresponds to pair annihilation in the vicinity of the nucleus. The net result of this Feynman process is that the peak of the scattered electron wave packet comes out *earlier* from the scattering region than when it entered [15]. This is in contrast to the more intuitive process shown in Figure 5(a), where the electron wave packet comes out *later* from the scattering region than when it entered. Both processes are possible, and must be added coherently when the final states are indistinguishable. However, there is a fundamental limit on the magnitude of the wave packet advancement associated with the counter-intuitive zigzag diagram. Note that the intermediate state consisting of the positron portion of the zigzag is a *virtual state*. The energy-time uncertainty principle

$$\Delta E \Delta t \sim \hbar, \tag{1}$$

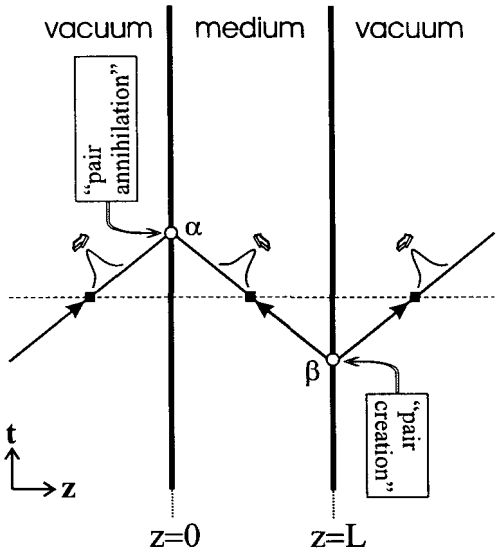

Figure 4. Zigzag world-line diagram.

allows the temporary borrowing of the energy ΔE from the nuclear Coulomb field at point b, as long as the borrowed energy is paid back later at point a after a short time Δt, where Δt is the duration of the intermediate state during which the positron exists. The resulting negative group delay for the scattered electron wave packet is plotted schematically in Figure 6. Note that there results a "negative Hartman effect," in which a negative group delay saturates at a value given by the above uncertainty principle. This behavior is analogous to the positive Hartman effect seen for wave packets which tunnel through a barrier. In this effect, the tunneling particle experiences a positive group delay, which saturates for thick barriers at a positive value given by the uncertainty principle. The Hartman effect [16] represents the thick-barrier limit of the Wigner tunneling time [17], which is also plotted in Figure 6, for the sake of comparison.

We performed some early experiments on the speed of the quantum tunneling process [18]. We found that a photon tunneled through a barrier at an effective group velocity which was faster than c. In these experiments, spontaneous parametric down-conversion was used as a light source which emitted randomly, but simultaneously, two photons at a time (i.e., photon "twins"). These photons were detected by means of two equidistant Geiger counters (silicon avalanche photodiodes), so that the time at which a "click" was registered was interpreted as the time of arrival of the photon. Coincidence detection was used to detect these photon twins. One photon twin traverses a tunnel barrier, whilst the other traverses an equal distance in the vacuum.

The idea of the experiment was to measure the time of arrival of the tunneling photon with respect to its twin, by measuring the time difference between

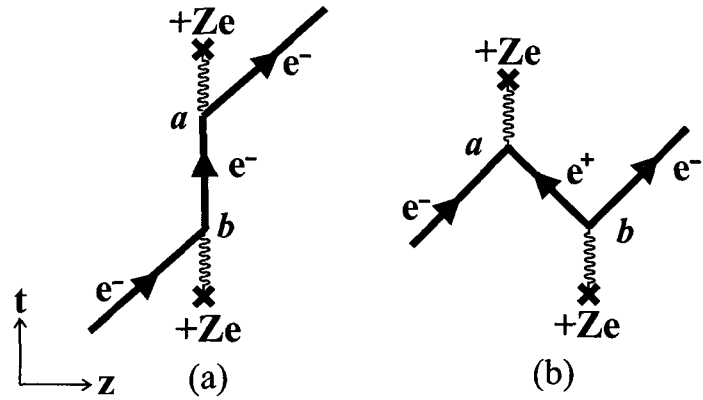

Figure 5. Feynman processes in QED for multiple scattering of an electron from a nuclear (+Ze) Coulomb field. In the zigzag process (b), pair creation occurs at point b before pair annihilation occurs at point a. Lorentz transformations leave the interval between a and b space-like, and hence "superluminal."

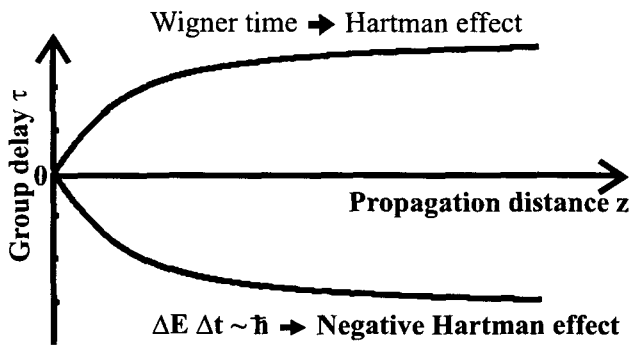

Figure 6. Positive group delays in Wigner tunneling time lead to a positive Hartman effect; negative group delays (see Figure 5(b)) lead to a negative Hartman effect.

the two "clicks" of their respective Geiger counters. (We employed a two-photon interference effect in the Hong-Ou-Mandel interferometer [19] in order to achieve sufficient time resolution.) The net result was surprising: On the average, the Geiger counter registering the arrival of the photon which tunneled through the barrier clicked *earlier* than the Geiger counter registering the arrival of the photon which traversed the vacuum. This indicates that the process of tunneling in quantum physics is superluminal.

The earliest experiment to demonstrate the existence of faster-than-c group velocities was performed by Chu and Wong at Bell Labs. They showed that picosecond laser pulses propagated superluminally through an absorbing medium

in the region of anomalous dispersion inside the strong optical absorption line [20]. This experiment was reproduced in the millimeter range of the electromagnetic spectrum by Segard and Macke [21]. These experiments verified the prediction of Garrett and McCumber [22] that Gaussian pulses of electromagnetic radiation could propagate with faster-than-c group velocities in regions of anomalous dispersion associated with an absorption line. Negative group velocities were also observed to occur in these early experiments. However, these kinds of superluminal pulse propagation phenomena were not known to occur in *transparent* optical media at the time.

Subsequently, we observed these counter-intuitive pulse sequences in experiments on electronic circuits [23]. In the first of these experiments, we used an electronic circuit which consisted of an operational amplifier with a negative feedback circuit containing a passive RLC network. This circuit produced a negative group delay similar to that observed in the recent optical pumping experiment [12]: The peak of the output voltage pulse left the output port of the circuit *before* the peak of the input voltage pulse entered the input port of the circuit. Such a seemingly anti-causal phenomenon does not in fact violate the principle of causality, since there is sufficient information in the early portion of any analytic voltage waveform to reproduce the entire waveform earlier in time. We showed that causality is solely connected with the occurrence of discontinuities, such as "fronts" and "backs" of signals, and not with the peaks of voltage waveforms, and, therefore, that causal loop paradoxes could never arise [24]. Since there was gain in these electronic circuits, the output signal was not strongly attenuated, in contrast to the earlier optical experiments.

I believe that these counter-intuitive ideas can be applied to the design of microelectronic devices, in particular, computer chips [25]. This is timely, since it is widely believed that Moore's law for microprocessor performance will fail to hold in the next decade due to a "brick wall" arising from fundamental physical limitations [26]. Therefore, there have been many proposals for new transistor technologies to try to solve this problem [27][28]. At the present time, the "transistor latency" problem is one of the main factors limiting computer performance, although the "propagation delays" due to the RC time constants in the interconnects between individual transistors on a computer chip are beginning to be another serious limiting factor. As the scale of microprocessor circuits fabricated on a silicon wafer is reduced to become ever smaller in size, the transistor switching time becomes increasingly faster, but the propagation delay from transistor to neighboring transistor becomes increasingly longer [29]. This will still be true even after new technologies to replace MOSFETS with faster devices are implemented.

3 General principles for negative group delays in electronic circuits

We now begin our discussion of superluminal effects in electronic circuits, using the concept of negative group delays as the starting point. Electronic circuits are usually very small in size compared with the wavelengths corresponding to the typical frequencies of operation of these circuits; thus, the retardation due to the speed of light across these circuits is usually negligible. Nevertheless, a concatena-

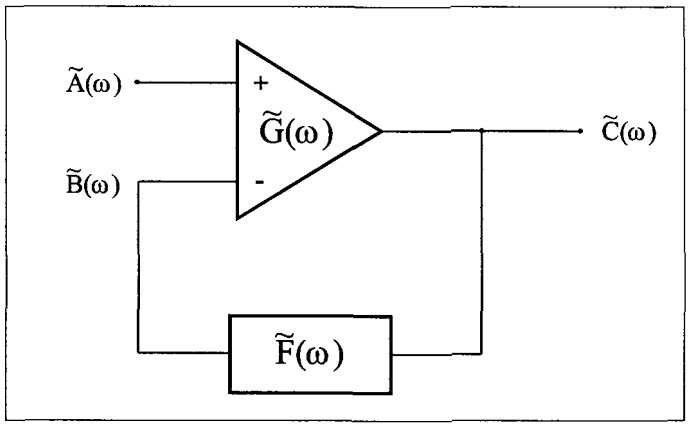

Figure 7. Operational amplifier circuit with negative feedback.

tion of such negative-delay circuits interspersed periodically along a transmission line, could lead to superluminal propagation of pulses with a negative group velocity. Hence, we focus here only on how a negative group delay can be generated in general.

3.1 Negative group delays necessitated by the "Golden Rule" for operational amplifier circuits with negative feedback

In Figure 7, we show an operational amplifier with a signal entering the noninverting (+) port of the amplifier. The output port of the amplifier is fed back to the inverting (−) port of the amplifier by means of a black box, which represents a passive linear circuit with an arbitrary complex transfer function $\widetilde{F}(\omega)$ for a signal at frequency ω. We thus have a linear amplifier circuit with a negative feedback loop containing a passive filter. In general, the transfer function of any passive linear circuit, such as a RC low-pass filter, will always lead to a *positive* propagation delay through the circuit.

However, for operational amplifiers with a sufficiently high gain-feedback product, the voltage difference between the two input signals arriving at the inverting and noninverting inputs of the amplifier must remain small at all times. The operational amplifier must therefore supply a signal with a *negative* group delay at its output, such that the *positive* delay from the passive filter is exactly canceled out by this negative delay at the inverting (−) input port. The signal at the inverting (−) input port will then be nearly identical to that at the noninverting (+) port, thus satisfying the "Golden Rule" which demands small voltage differences at all times. The net result is that this negative feedback circuit will produce an output pulse whose peak leaves the output port of the circuit *before* the peak of the input pulse arrives at the input port of this circuit.

In Figure 8, we show experimental evidence for this counter-intuitive behavior

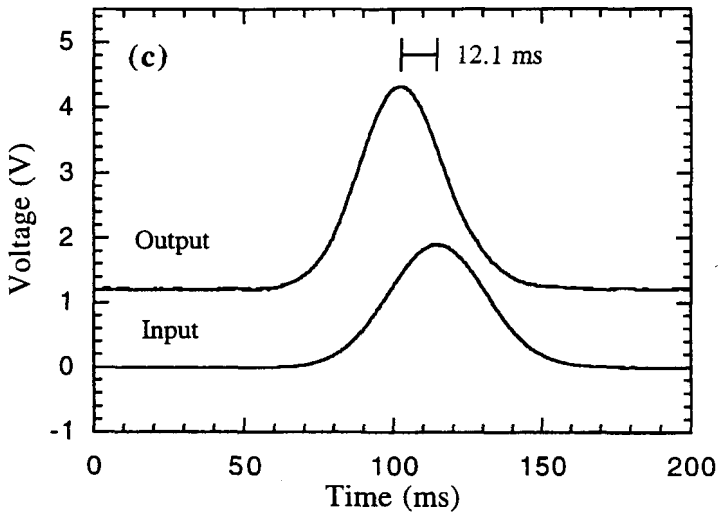

Figure 8. Experimental results showing the pulse advancement.

for the special case of an RLC tuned bandpass circuit in the negative feedback loop [23]. The peak of an output pulse is *advanced* approximately by 12 milliseconds relative to the input pulse. The output pulse has obviously not been significantly distorted with respect to the input pulse by this linear circuit, apart from a slight amplification factor. Also, note that the size of the advance of the output pulse is comparable in magnitude to the width of the input pulse. At these very low frequencies, the role of spontaneous emission is entirely negligible, and the pulse advance can obviously satisfy Rayleigh's criterion for pulse resolution, as can be seen by inspection of the data shown in Figure 8.

That causality is not violated is demonstrated in a second experiment, in which the input signal voltage is very suddenly shorted to zero the moment it reaches its maximum. The result is shown in Figure 9. By inspection, we see that the output signal is also very suddenly reduced to zero voltage at essentially the same instant in time that the input signal has been shorted to zero. This demonstrates that the circuit cannot advance in time truly *discontinuous* changes in voltages: These are the only points on the signal waveform which are directly connected by the principle of causality [24]. However, for the *analytic* changes of the input signal waveform, such as those in the early part of the Gaussian input pulse which we used, the circuit evidently has the ability to extrapolate the input waveform into the future, in such a way as to reproduce the output Gaussian pulse peak *before* the input pulse peak has arrived. In this sense, the circuit *anticipates* the arrival of the Gaussian pulse.

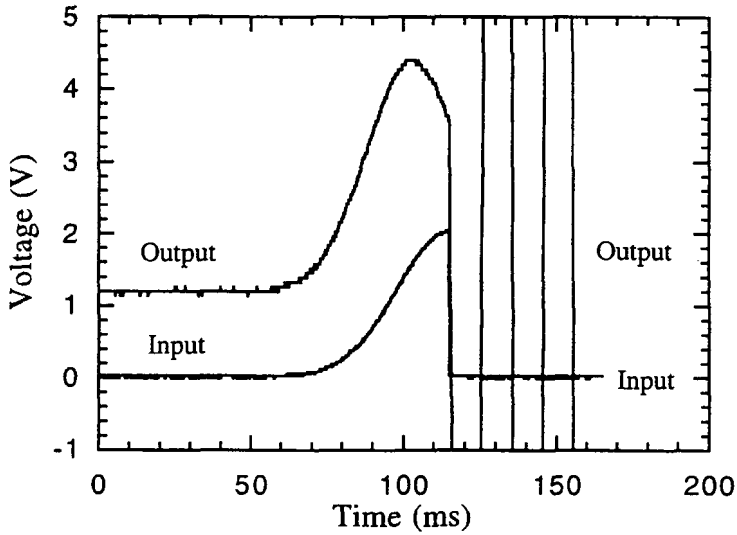

Figure 9. Experimental results showing that discontinuities cannot be advanced.

3.2 *The "Golden Rule" and the inversion of the transfer function of any passive linear circuit*

Now we shall analyze under what conditions the "Golden Rule" holds and negative group delays are produced. In Figure 7, $\widetilde{A}(\omega)$ denotes the complex amplitude of an input signal of frequency ω into the noninverting $(+)$ port and $\widetilde{B}(\omega)$ refers to that of the feedback signal into the inverting $(-)$ port of the amplifier. The output signal $\widetilde{C}(\omega)$ is then related to the feedback signal $\widetilde{B}(\omega)$ by means of the complex linear feedback transfer function $\widetilde{F}(\omega)$ (the black box) as follows:

$$\widetilde{B}(\omega) = \widetilde{F}(\omega)\widetilde{C}(\omega). \tag{2}$$

The voltage gain of the operational amplifier is characterized by the active complex linear transfer function $\widetilde{G}(\omega)$, which amplifies the difference of the voltage signals at the $(+)$ and $(-)$ inputs to produce an output signal as follows:

$$\widetilde{C}(\omega) = \widetilde{G}(\omega)\left(\widetilde{A}(\omega) - \widetilde{B}(\omega)\right). \tag{3}$$

Defining the total complex transfer function $\widetilde{T}(\omega) \equiv \widetilde{C}(\omega)/\widetilde{A}(\omega)$ as the ratio of the output signal $\widetilde{C}(\omega)$ to input signal $\widetilde{A}(\omega)$, we obtain for the total transfer function,

$$\widetilde{T}(\omega) = \frac{\widetilde{G}(\omega)}{1 + \widetilde{F}(\omega)\widetilde{G}(\omega)}. \tag{4}$$

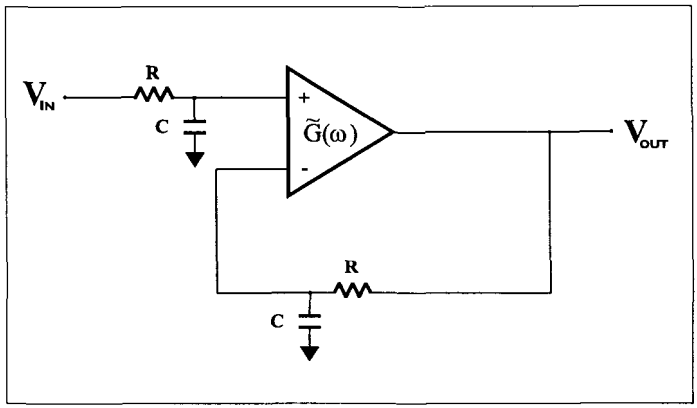

Figure 10. Circuit with RC filter placed before the negative feedback circuit.

If the gain-feedback product is very large compared to unity, i.e.,

$$\left|\widetilde{F}(\omega)\,\widetilde{G}(\omega)\right| >> 1, \tag{5}$$

we see that to a good approximation this leads to the inversion of the transfer function of any passive linear circuit by the negative feedback circuit, i.e.,

$$\widetilde{T}(\omega) \approx 1/\widetilde{F}(\omega) = \left(\widetilde{F}(\omega)\right)^{-1}. \tag{6}$$

This also implies through Eq. (2), that the "Golden Rule,"

$$\widetilde{A}(\omega) \approx \widetilde{B}(\omega), \tag{7}$$

holds under these *same* conditions. Equation (6) also implies that the negative feedback circuit shown in Figure 7 can completely undo any deleterious effects, such as propagation delays, produced by a linear passive circuit (whose transfer function is identical to $\widetilde{F}(\omega)$) when it is placed before this active device.

In Figure 10, we show one example, where an RC low-pass filter is placed before the negative feedback circuit. The positive propagation delay $\tau_{\widetilde{F}(\omega)}$ due to this RC low-pass circuit, can in principle be completely canceled out by the negative group delay produced by the active circuit with the same RC circuit in its feedback loop. This will be true in general for any linear passive circuit, if an identical copy of the circuit is placed inside the negative feedback loop of the active device. The group delay of the negative feedback circuit in the high gain-feedback limit is then given by

$$\tau_{\widetilde{T}(\omega)} = \frac{d\arg\widetilde{T}(\omega)}{d\omega} \approx \frac{d\arg\left(1/\widetilde{F}(\omega)\right)}{d\omega} = -\frac{d\arg\widetilde{F}(\omega)}{d\omega} = -\tau_{\widetilde{F}(\omega)}. \tag{8}$$

This shows that the positive group delay from any linear passive circuit can in principle be completely canceled out by the negative group delay from a negative feedback circuit.

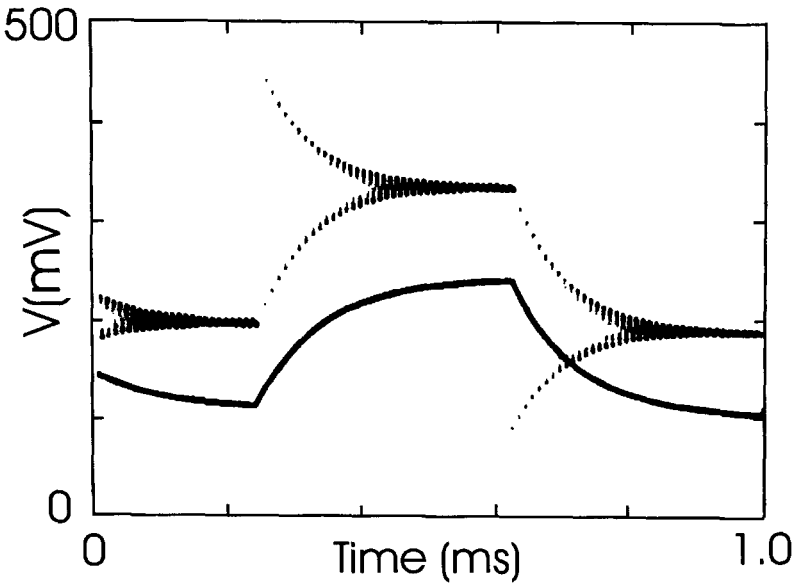

Figure 11. V_{out} with (upper) and without (lower) the negative feedback.

It is important to note that this negative feedback scheme places a requirement on the gain-bandwidth product of the amplifier. For this active circuit to advance the waveform, it must have a large gain at all of the frequency components present in the signal. In particular, if we want to counteract a particular RC time delay, the amplifier must have a large gain at frequencies greater than $1/RC$.

3.3 Data demonstrating the elimination of propagation delays from RC time constants by means of negative group delays

In a recent, simple experiment with the circuit shown in Figure 10, we obtained the data shown in Figure 11, of the outputs from a square wave input into an RC low-pass circuit, with (in the upper trace), and without (in the lower trace) negative feedback. It is clear by inspection of the data in Figure 11, that the propagation delays due to the RC time constant on both the rising and falling edges of the square wave have been almost completely eliminated by means of the negative feedback circuit. However, there is a ringing or overshoot phenomenon accompanying the restoration of the rising and falling edges. Since the CMOS switching levels between logic states occur within 10% of zero volts for LO signals, and within 90% of volt-level HI signals [25], the observed ringing or overshoot phenomenon is not deleterious for the purposes of computer speedup.

It is clear from these data that not only the RC time constants associated with transistor gates (the "latency" problem), but also the RC "propagation delays" from the wire interconnects between transistors on a computer chip, can in principle be

eliminated by means of the insertion of negative feedback elements. In particular, the finite rise time of a MOSFET arising from its intrinsic gate capacitance can be eliminated.

3.4 Energy transport by pulses in the optical and electronic domains

In the optical domain, there has been a debate concerning whether or not the velocity of energy transport by the wave packet can exceed c when the group velocity of a wave packet exceeds c. In the case of anomalous dispersion inside an absorption line, Sommerfeld and Brillouin showed that the energy velocity defined as follows:

$$v_{energy} \equiv \frac{\langle S \rangle}{\langle u \rangle}, \tag{9}$$

where $\langle S \rangle$ is the time-averaged Poynting vector and $\langle u \rangle$ is the time-averaged energy density of the electromagnetic wave, is *different* from the group velocity [1033]. Whereas the group velocity in the region of absorptive anomalous dispersion exceeds c, they found that their energy velocity is less than c. Experiments on picosecond laser pulse propagation in absorptive anomalous dispersive media, however, show that these laser pulses travel with a superluminal group velocity, and not with the subluminal energy velocity of Sommerfeld and Brillouin [20]. Hence, the physical meaning of this energy velocity is unclear.

When the optical medium possesses gain, as in the case of laser-like media with inverted atomic populations, there arises ambiguities as to whether or not to include the energy stored in the inverted atoms in the definition of $\langle u \rangle$ or not [3435]. However, in regions of anomalous dispersion well outside of the gain line, and, in particular, in a spectral region where the group-velocity dispersion vanishes, a straightforward application of Sommerfeld and Brillouin's definition of the energy velocity would imply that the group and energy velocities both exceed c. The equality of these two kinds of wave velocities arises because the pulses of light are propagating inside a transparent medium with little dispersion. In particular, in the case when the energy velocity is negative, the maximum in the pulse of energy leaves the exit face of the optical sample *before* the maximum in the pulse of energy enters the entrance face. A recent paper defined the energy velocity in terms of a time expectation integral over the Poynting vector without any use of the concept of "energy density," and therefore avoids the above ambiguities associated with the definition of the energy density of the optical medium [36]. The result is that the energy velocity so defined can be superluminal.

In the case of the electronic circuit with negative feedback which produces negative group delays, the question of when the peak of the energy arrives, can be answered by terminating the output port of Figure 7 by a load resistor, which connects the output to ground. The load resistor (not shown) will be heated up by the energy in the *output* pulse. It is obvious that the load resistor will then experience the maximum amount of heating when the peak of the Gaussian output pulse arrives at this resistor, and that this happens when the peak of the output voltage waveform arrives. For negative group delays, the load resistor will then heat up earlier than expected. However, there is no mystery here: The operational

amplifier can supply the necessary energy to heat up the load resistor ahead of time. The negative group delay and the negative energy delay are identical to each other in this case, and likewise the negative group and energy velocities are equal.

3.5 Kramers-Kronig relations imply faster-than-c group velocities, and the Bode relations necessitate negative group delays

These counter-intuitive results also follow quite generally from the Kramers-Kronig relations for optical media [30], and the Bode relations for electronic circuits [31]. For optical media, we have proved two theorems starting from the principle of causality, along with the additional assumption of linearity of the media, that superluminal group velocities in any optical medium must generally exist in some spectral region, and that for an amplifying medium, this spectral region must exist outside of the regions with gain, i.e., in the transparent regions outside of the gain lines [32]. Negative group delays for electronic circuits similarly follow quite generally from the Bode relations. These dispersion relations can also be generalized to apply to the transmission of atoms through the quantum many-body systems which we shall discuss below. Negative group delays in this case means negative transmission times of atomic wave packets through the many-body system. Thus, the principle of causality itself *necessitates* the existence of these counter-intuitive, superluminal phenomena.

4 Anomalous transmission times in condensed matter systems

So far, we have considered examples from optics and electronics. The quantum-mechanical tunneling process is another example of a superluminal phenomenon; however, this example involved only single-particle propagation. Here we consider other quantum mechanical examples taken from condensed matter physics. Unusual many-body systems, such as superfluid helium and atomic Bose-Einstein condensates (BECs), might also exhibit anomalous transmission times. These effects arise from Bose exchange symmetry and macroscopic quantum coherence. In such systems, one cannot know, even in principle, which identical particle of the many-body system was involved in a particular collision process. The Bose symmetrization of the total wavefunction leads to a long-range, macroscopic entangled state of the entire many-body system, and thus to off diagonal long range order.

4.1 Condensate-mediated transmission of helium atoms through superfluid helium slabs

We first focus on superfluid helium. Solving the scattering problem of ^{4}He atoms from a superfluid helium surface is not an easy task. Several approaches have been taken to reproduce the experimental data on quantum evaporation and condensation obtained by Wyatt and Tucker [37], and others. These approaches include semiclassical treatments (Mulheran and Inkson [38]), time-dependent density functional theory using a phenomenological density functional (Dalfovo et al. [39]) and the correlated basis function method used by Campbell et al. [40]. The difficulty of

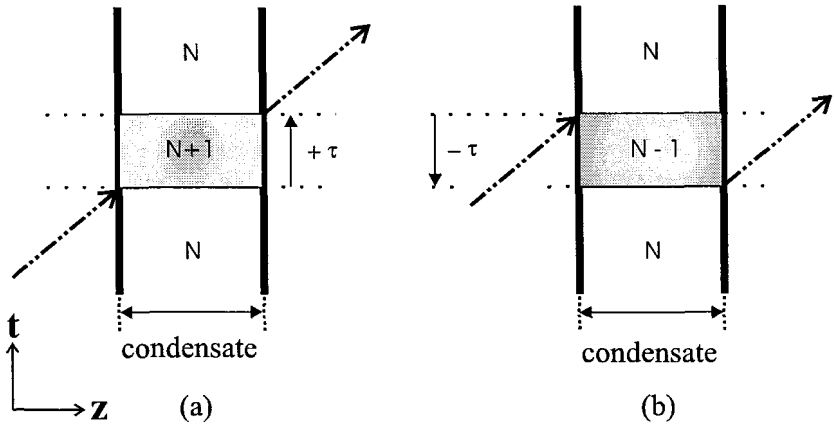

Figure 12. Condensate-mediated processes associated with the coherent transmission of an incoming atom.

the problem arises from the necessity of a self-consistent many-body solution for a system of strongly interacting bosons.

Circumventing all these difficulties, we give here some general arguments for why there can in principle be anomalous transmission times in the transmission of a helium atom through a superfluid helium slab, if measurements with sufficiently high time resolution are performed.

Halley *et al.* [41] proposed the possibility of the transmission of helium atoms through a superfluid helium slab due to a condensate-mediated process with transmission time delays independent of the slab thickness. Consider a superfluid helium slab in an N particle ground state. In the Halley *et al.* process, the transmission of an incoming helium atom through the slab occurs via a virtual transition of the N particle ground state plus the incident particle, to the $N+1$ particle ground state, followed by the coherent reemission of one particle on the opposite side of the superfluid (see Figure 12(a)). Following the steps of the paper first suggesting this process [41], we consider the transfer Hamiltonian

$$H_T = \sum_{\mathbf{k}'} (T^L_{\mathbf{k}'} b_{\mathbf{k}',L} a_0^\dagger + T^R_{\mathbf{k}'} b^\dagger_{\mathbf{k}',R} a_0 + h.c.) \tag{10}$$

The $b^\dagger$ and b operators are creation and annihilation operators of particles with momentum $\mathbf{k}'$ at the left (L) and right (R) surfaces; the $a_0^\dagger$ and a_0 operators create and annihilate the particles in the condensate part of the fluid. The coefficients T depend on the microscopic structure of the fluid surface and must be determined by experiment.

We assume that $|left\rangle = |N, N_0\rangle|\mathbf{k}\rangle_L|vac\rangle_R$ is the initial state of the system with a total number of N atoms in the fluid, out of which N_0 particles are in the condensate; one helium atom with momentum $\mathbf{k}$ is incident from the left. A transmission of an atom from the left to the right side of the slab can occur in

the second-order process shown in Figure 12(a), for which the transition matrix element is the following:

$$\frac{\langle right|H_T|i\rangle\langle i|H_T|left\rangle}{E - E_i}. \tag{11}$$

Here $|i\rangle = |N+1, N_0+1\rangle|vac\rangle_L|vac\rangle_R$ is the intermediate state, E_i its energy, and $|right\rangle = |N, N_0\rangle|vac\rangle_L|\mathbf{k}\rangle_R$ the final state.

Using the standard definitions for the creation and annihilation operators, it is easy to show that the numerator of Eq. (11) is

$$(N_0+1)T^L_{\mathbf{k}}T^R_{\mathbf{k}}. \tag{12}$$

In this scattering process, the energy in the initial and the final state is given by the sum of the kinetic energy of the incoming particle plus the energy of the N particle ground state

$$E = \epsilon_{\mathbf{k}} + E_N \tag{13}$$

The energy in the intermediate state is

$$E_i = E_{N+1}. \tag{14}$$

This leads to an energy denominator in second-order perturbation theory of

$$\Delta E = \epsilon_{\mathbf{k}} + E_N - E_{N+1} = \epsilon_{\mathbf{k}} + |\mu|. \tag{15}$$

Here, μ is the chemical potential (-7.16 K in the case of superfluid helium). Thus, the transition matrix element for this process is

$$\frac{(N_0+1)T^L_{\mathbf{k}}T^R_{\mathbf{k}}}{\epsilon_{\mathbf{k}} + |\mu|}. \tag{16}$$

If the intermediate state used above were the only one coupling the initial and final states, a transition rate in the form of Fermi's golden rule could be given by squaring the transition amplitude [41]. However, a *coherent* sum of the transition amplitudes over all possible intermediate states has to be performed, and there is another process which was not taken into account in Ref. [41]. This process is equally important and leads to *negative* time delays in transmission. It is pictured in Figure 12(b), and we will refer to it as the primed process. A helium atom approaches the slab, and, before the atom reaches the superfluid, the condensate coherently emits another atom on the other side of the slab. In this intermediate state there are two atoms outside of an $N-1$ particle ground state. Finally, the atom on the left side of the superfluid gets absorbed into the condensate, and the fluid is brought back into the N particle ground state.

The energy for the intermediate state in the primed process is

$$E_i' = 2\epsilon_{\mathbf{k}} + E_{N-1}. \tag{17}$$

The energy difference between the initial and the intermediate state is

$$\Delta E' = \epsilon_{\mathbf{k}} + E_N - (2\epsilon_{\mathbf{k}} + E_{N-1}) = -\epsilon_{\mathbf{k}} - |\mu| = -\Delta E. \tag{18}$$

The numerator of Eq. (11) is now

$$N_0 T_{\mathbf{k}}^R T_{\mathbf{k}}^L, \tag{19}$$

so that the transition matrix element for the primed process is

$$-\frac{N_0 T_{\mathbf{k}}^R T_{\mathbf{k}}^L}{\epsilon_{\mathbf{k}} + |\mu|}. \tag{20}$$

For plane waves, the final states of these two condensate-mediated processes are indistinguishable. Therefore the two transition matrix elements must be added up coherently. Comparison of Eq. (16) with Eq. (20) shows that the two processes destructively interfere with each other, and that they almost cancel out in the large N_0 limit. This implies that the transmission probability for very long, single-particle wave packets via a condensate-mediated process becomes vanishingly small.

The energy-time uncertainty relation restricts the durations of the intermediate states, so that the transmission times will be of the order of $\pm\hbar/|\Delta E|$ for the unprimed and primed processes, respectively. For low energy incident atoms the transmission times are approximately given by $\pm\hbar/|\mu|$, which is of the order of a picosecond in the system considered. In order to detect either one of these processes experimentally, the final states have to be made distinguishable. This could be achieved by temporal resolution, i.e., the formation of atomic wave packets with a duration comparable to the lifetimes of the respective intermediate states, so that the transmitted wave packets would be Rayleigh resolved, and an actual measurement of the time sequence of events could be performed. A wave packet this short in time will have an energy uncertainty comparable to the size of the chemical potential, so that Rayleigh resolution will only barely be possible.

It should be noted that both of the processes considered here depend in the same way on the macroscopic coherence and on the off diagonal long range order of this quantum system. Both processes will lead to faster-than-light effects. In the primed process this is due to the intrinsic negativity of the transmission time. In the unprimed process faster-than-light effects can be achieved by the choice of a sufficiently thick slab, since the transmission time, although positive, is independent of the slab thickness, similar to the case of the Hartman effect in tunneling discussed earlier.

4.2 Transmission times of atoms through an atomic BEC

In connection with condensate-mediated transmission of atoms, it is simpler to consider the recently observed atomic BECs [42], which are weakly-interacting Bose

gases, than superfluid helium, which is a strongly-interacting Bose liquid. The microscopic theory of a dilute, weakly-interacting Bose gas is well characterized in terms of the Bogoliubov theory [43], which has been verified by experiment. In the case of the atomic BECs, the chemical potential sets the energy scale for the uncertainty-principle lifetime or duration of the intermediate state, and hence for the transmission times (either positive or negative) through the condensate of low-energy incident atoms identical to the atoms of the BEC. The chemical potential μ in the condensate can be calculated in the Bogoliubov approximation, and is given by

$$\mu \approx N_0 \frac{2\pi\hbar^2 a}{mV}, \tag{21}$$

where N_0 is the number of atoms in the condensate, a is the S-wave scattering length, m is the mass of the atom, and V is the volume of the condensate. The typical experimental parameters for a BEC consisting of sodium atoms are $a = 2.75$ nm, $N_0/V = 1.5 \times 10^{14}$ cm^{-3}, and $D = 10$ μm for the typical size of the condensate [44]. The speed of sound for such a condensate has been observed to be $v_s \approx 1.0$ mm/s, which is close to that predicted by the Bogoliubov theory. From these numbers, we infer that the chemical potential for an atom in the typical sodium BEC is $\mu \approx 7.4 \times 10^{-24}$ erg ≈ 54 nK. The typical time scale associated with condensate-mediated processes is therefore $\hbar/\mu$, which is two orders of magnitude shorter than the transmission time due to sound wave propagation across the condensate. Hence it should be easy to distinguish the condensate-mediated processes from sound-wave mediated processes. Note that the time scale $\hbar/\mu$ is independent of the size D of the condensate, and leads to a Hartman-like effect, which resembles the Hartman effect in tunneling. The positive and negative condensate-mediated transmission times, or group delays, which correspond to the two processes depicted in Figure 12(a) and (b), respectively, are

$$\tau_{\pm} \approx \pm \frac{\hbar}{\varepsilon_{\mathbf{k}} + \mu} \lesssim \pm \frac{\hbar}{\mu} \approx \pm 0.14 ms. \tag{22}$$

These times are much larger than those observed in the photon tunneling experiments. Again, as in the case of superfluid helium, it should barely be possible to distinguish, by Rayleigh's resolution criterion, a negative group delay from a positive group delay, for cold atoms whose incident kinetic energy is comparable to the chemical potential. Nevertheless, this effect should be experimentally observable with a sufficiently high signal-to-noise ratio, as has already be done in the case in the measurement of the tunneling times for photons. Furthermore, each atomic transmission event detected in an experiment would result in a definite *sign* for the transmission time for that event. The post-selection of rare, condensate-mediated transmission events leads to a "weak measurement" of this post-selected subensemble in the sense of Aharonov [45], and results, as in the case of tunneling [46], in surprising "weak values," such as *negative* transmission times. Thus, not only can light pulses be slowed to a stop in atomic BECs [47], but atoms can also be transmitted superluminally through such BECs.

5 Conclusions

There is a widespread view among electrical engineers and physicists that although the phase velocity can exceed the vacuum speed of light, the group velocity can never do so. Otherwise, signals would be able to propagate faster than light, since conventional wisdom equates the group velocity with the signal velocity. From this conventional point of view, the group velocity is essentially the same as the energy velocity in transparent media, and the latter could never exceed c. Several generations of students have been taught this. Many of the standard textbooks and handbooks state this conventional viewpoint, some, however, with qualifications which unfortunately are not strong enough, so that the net result is still misleading. For example, *The Electrical Engineering Handbook* in its discussion concerning the group velocity states the following [48]:

> "When traveling in a medium, the velocity of energy transmission (e.g. a light pulse) is less than c, and is given by [the group velocity]."

This statement, and other similar statements in many of the early standard textbooks in optics and classical electrodynamics, are misleading. As a result, we have been blinded by our misconceptions, and thereby have been prevented from exploring and discovering many new, interesting, and possibly important, phenomena, which could have been discovered long ago. Some of these are only now being uncovered, and some of these phenomena may in fact lead to important applications, such as the speed-up of computers.

The effects reported in this paper do not violate relativity. The front velocity of Sommerfeld and Brillouin, which is strictly c, is the only velocity which is relevant to relativity. However, the group, the energy, and Brillouin's "signal," velocity can all exceed c, without violating the principle of relativistic causality [5].

Returning to the larger picture of physics in Figure 1 discussed of this lecture depicted, I believe that there still exist many conceptual tensions at the intersections of quantum mechanics, statistical mechanics, and relativity. The most fruitful method to proceed from here is not to speculate on these matters, but to perform experiments to probe these tensions.

Acknowledgements

This work was supported by the ONR, NSF, and NASA. I thank C. Ropers, D. Solli, and J. M. Hickmann for their contributions as co-authors to an earlier version of this paper [7], and S. Coen, J. C. Garrison, M. Haakestad, C. McCormick and M. Mojahedi for helpful discussions.

References

1. J. A. Wheeler in *Quantum Theory and Measurement*, edited by J. A. Wheeler and W. H. Zurek (Princeton University Press, Princeton, 1983), p. 184.
2. J. A. Wheeler and R. P. Feynman, Rev. of Mod. Phys. **17**, 157 (1945); ibid. **21**, 425 (1949).

3. S. W. Hawking, Phys. Rev. D **32**, 2489 (1985); J. G. Cramer, Rev. Mod. Phys. **58**, 647 (1986); Int. J. Th. Phys. **27**, 227 (1988); 'The Plane of the Present and the New Transactional Paradigm of Time' in *Time and the Instant*, Robin Durie, ed., (Clinamen Press, Manchester, 2000), Chap. 8.
4. R. Y. Chiao and A. M. Steinberg, in the *Proceedings of the Nobel Symposium No. 104* held in Gimo, Sweden on June 13-17, 1997 on 'Modern Studies of Basic Quantum Concepts and Phenomena,' edited by E. B. Karlsson and E. Braendas, Physica Scripta T**76**, 61 (1998).
5. R. Y. Chiao and A. M. Steinberg, Progress in Optics **37**, 345 (1997).
6. G. Nimtz and W. Heitmann, Progress in Quantum Electronics **21**, 81 (1997).
7. R. Y. Chiao, C. Ropers, D. Solli, and J. M. Hickmann, *Proceedings of the VIIIth International Conference on Coherence and Quantum Optics* held in Rochester, NY in June 2001 (to be published).
8. B. Segev, P. W. Milonni, J. F. Baab, and R. Y. Chiao, Phys. Rev. A **62**, 022114 (2000).
9. A. Kuzmich, A. Dogariu, L. J. Wang, P. W. Milonni, and R. Y. Chiao, Phys. Rev. Lett. **86**, 3925 (2001).
10. *Wave Propagation and Group Velocity* by L. Brillouin (Academic Press, New York, 1960).
11. I thank J. C. Garrison for pointing out to me the importance of the idea of "surprise" in discontinuous signals.
12. L. J. Wang, A. Kuzmich, and A. Dogariu, Nature **406**, 277 (2000); A. Dogariu, A. Kuzmich, and L. J. Wang, Phys. Rev. A **63**, 053806 (2001).
13. R. Y. Chiao, Phys. Rev. A**48**, R34 (1993); A. M. Steinberg and R. Y. Chiao, Phys. Rev. A **49**, 2071 (1994); R. Y. Chiao in *Amazing Light: A Volume Dedicated to Charles Hard Townes on his 80th Birthday* edited by R. Y. Chiao (Springer Verlag, New York, 1996), p. 91.
14. E. L. Bolda, J. C. Garrison, and R. Y. Chiao, Phys. Rev. A **49**, 2938 (1994).
15. *Quantum Electrodynamics* by R. P. Feynman (W. A. Benjamin, New York, 1961), p. 75. The zigzag process of Fig. 5(b) involves a fermionic system in a *microscopic* effect. Bosonic systems allow *macroscopic* effects, which can arise because they can exhibit off diagonal long range order with little decoherence. In Compton scattering also, there is a process in which a photon leaves the scattering region *before* it enters. I thank C. McCormick for pointing this out to me.
16. T. E. Hartman, J. Appl. Phys. **33**, 3427 (1962).
17. E. P. Wigner, Phys. Rev. **98**, 145 (1955).
18. A. M. Steinberg, P. G. Kwiat, and R. Y. Chiao, Phys. Rev. Lett. **71**, 708 (1993); A. M. Steinberg and R. Y. Chiao, Phys. Rev. A **51**, 3525 (1995).
19. C. K. Hong, Z. Y. Ou, and L. Mandel, Phys. Rev. Lett. **59**, 2044 (1987).
20. S. Chu and S. Wong, Phys. Rev. Lett. **48**, 738 (1982); **49**, 1293.
21. B. Segard and B. Macke, Phys. Lett. A **109**, 213 (1985).
22. C. G. B. Garrett and D. E. McCumber, Phys. Rev. A **1**, 305 (1970).
23. M. W. Mitchell and R. Y. Chiao, Phys. Lett. A **230**, 133 (1997); M. W. Mitchell and R. Y. Chiao, Am. J. Phys. **66**, 14 (1998).
24. J. C. Garrison, M. W. Mitchell, R. Y. Chiao, E. L. Bolda, Phys. Lett. A**245**,

19 (1998).
25. *Microelectronic circuits* by A. S. Sedra and K. C. Smith (4th edition, Oxford University Press, Oxford, 1998).
26. P. A. Packan, Science **285**, 2079 (1999).
27. Y. Taur, IEEE Spectrum **36**, 25 (1999).
28. L. Geppert, IEEE Spectrum **37**, 46 (2000).
29. D. A. B. Miller, Proceedings of the IEEE **88**, 728 (2000).
30. *Electrodynamics of Continuous Media* by L. D. Landau and E. M. Lifshitz (Pergamon Press, Oxford, 1960), p. 256.
31. *Fields and Waves in Communication Electronics* by S. Ramo, J. R. Whinnery, and T. van Duzer (John Wiley & Sons, New York, 1965), p. 623.
32. E. L. Bolda, R. Y. Chiao, and J. C. Garrison, Phys. Rev. A **48**, 3890 (1993).
33. R. Loudon, J. Phys. A **3**, 233 (1970).
34. E. O. Schulz-Dubois, Proc. IEEE **57**, 1748 (1969).
35. K. E. Oughstun and S. Shen, J. Opt. Soc. Am. B **5**, 2395 (1988).
36. J. Peatross, S. A. Glasgow, and M. Ware, Phys. Rev. Lett. **84**, 2370 (2000).
37. M. A. H. Tucker and A. F. G Wyatt, Science **283**, 1150 (1999).
38. P. A. Mulheran and J. C. Inkson, Phys. Rev. B **46**, 5454 (1992).
39. F. Dalfovo , A. Fracchetti, A. Lastri, L. Pitaevskii , S. Stringari, Phys. Rev. Lett. **75**, 2510 (1995).
40. C. E. Campbell, E. Krotscheck, and M. Saarela, Phys. Rev. Lett. **80**, 2169 (1998).
41. J. W. Halley, C. E. Campbell, C. F. Giese, and K. Goetz, Phys. Rev. Lett. **71**, 2429 (1993); A. K. Setty, J. W. Halley, and C. E. Campbell, Phys. Rev. Lett. **79**, 3930 (1997).
42. M. H. Anderson, J. R. Ensher, M. R. Matthews, C. E. Wieman, and E. A. Cornell, Science **269**, 198 (1995); C. C. Bradley, C. A. Sackett. J. J. Tollett, and R. G. Hulet, Phys. Rev. Lett. **75**, 1687 (1993); K. B. Davis, M.-O. Mewses, M. R. Andrews, N. J. van Druten, D. S. Durfee, D. M. Kurn, and W. Ketterle, Phys. Rev. Lett. **75**, 3969 (1995); D. Kleppner, Physics Today **49**, 11 (1996); A. S. Parkins and D. F. Walls, Physics Reports **303**, 1 (1998).
43. N. Bogoliubov, J. Phys. (USSR) **11**, 23 (1947); R. Y. Chiao, Opt. Comm. **179**, 157 (2000).
44. W. Ketterle and S. Inouye, arXiv:cond-mat/0101424 29 Jan 2001.
45. Y. Aharonov, D. Z. Albert, and L. Vaidman, Phys. Rev. Lett. **60**, 1351 (1988); Y. Aharonov and L. Vaidman, Phys. Rev. A **41**, 11 (1990).
46. A. M. Steinberg, Phys. Rev. A **52**, 32 (1995); A. M. Steinberg, Phys. Rev. Lett. **74**, 2405 (1995).
47. C. Liu, Z. Dutton, C. H. Behroozi, L. V. Hau, Nature **409**, 490 (2001).
48. *The Electrical Engineering Handbook* edited by R. C. Dorf (2nd edition, CRC Press/IEEE Press, Boca Raton, 1997), p. 812.

DISCUSSION

Chairman: G. Leuchs

W. Schleich: Great. Coming back to the Compton scattering where you end up with the probability amplitude because you cannot decide which of the pulses came first or you cannot distinguish between these processes. In your example, in order to decide you would need a sharp wave front. Is it your argument?

R. Chiao: What you say is absolutely true. If we have monochromatic wave planes these two processes are completely indistinguishable and you must add the two processes coherently and then square to find the transmission probability. But if you have a superposition of various frequency components to construct a Gaussian wave packet such that the wave packet becomes comparable to the delay given by the uncertainty principle, then you are beginning to resolve these two processes one from the other and that is an interesting situation. In fact, in all experiments that I know with atomic Bose condensate, it is extremely difficult to put a sharp front on the pulses. This is an easy experiment and also the most spectacular result.

T. Petrosky: One question is about this two photons case. I don't see the original explanation of the anomalous reflection coefficient. Another comment is that in the second experiment, the existence of evanescent modes is essential. At the boundary there is a resonate component that can travel to the infinity. And also there is a sticking evanescent mode. This is a place, I suppose, where the effect appears. And as the evanescent modes are related to the non-pole (cut) effect problem which is related to the Zeno's phenomenon, therefore these evanescent modes should be related to the quantum Zeno's effect.

R. Chiao: Let me first answer the first question. There is no anomalous dispersion in the tunnelling experiment. It is the evanescent wave phenomenon that gives rise to the positive group delays, not negative group delays. But still, group delays, which are so short that they violate the naive Einstein causality. The apparent group velocity is faster than the speed of light and the peak appears behind the tunnel barrier earlier then light would come through air. This is due to the exponential tail of tunnelling. Concerning the second question, I haven't even thought in terms of quantum Zeno effect for the explanation of this phenomenon but one can explain it in terms of Aharonov's ideas of weak values or weak measurements. If you postulate only a small subensemble of all possible events, namely, the ones which succeeded in tunnelling, they will have unusual values like faster than light velocities.

M. Raizen: In your talk you gave two extreme examples. One is the discontinuous pulse and the other is analytic pulse. Do you have anything in between?

R. Chiao: Yes. It is a good point. Let me look at Fourier decomposition in the intermediate case and ask the following question: are the Fourier components above or below the resonance of the system? If they are above you are going to get something like front velocities. If they are below you can get something like group velocity, which is superluminal.

M. Raizen: From the information point of view, I would say that whatever the receiver can predict, can be very far from the speed of light because it does not carry anything new. From this point of view, it is not just a front but also the

non-analytic part of the signal. Is there any possibility to test not just a front but the discontinuity?

R. Chiao: That is an excellent point. I took a very simple extreme example where the front has this discontinuity in the amplitude of the signal but the front may have discontinuity in the slope or in second derivative and in any derivative as you like and still you cannot apply Taylor series. In that case you should also see the non-analytic points going at the front velocity at the speed of light. The experiment has not been done because it is very difficult to do. The only one that has been done is the discontinuous front, which I have just shown to you.

L. Stodolsky: I have a conceptual question. Maybe you can clear it up. In your first discussion with Sommerfeld and the front and the peak, the examples involve just Fourier transforms and classical mathematics, no quantum mechanics. On the other hand in your Wigner delay time I saw some $\hbar$'s. Is it quantum mechanics or Fourier transforms?

R. Chiao: Excellent question. This is a Fourier transform plus, when we go to the quantum level, we use the Born interpretation. The wave's form is interpreted as a probability amplitude for finding the particle. That is the "click" of the particle. With this interpretation of the classical wave's forms you have the whole story.

L. Stodolsky: So, if you did some other quantum optics experiment not involving photon counting but something else you might see some other kind of effect. Photon is a quantum concept involving $\hbar$. There should be something you can do like the (EPR), which would not involve $\hbar$.

R. Chiao: Yes. In fact, that is what we did. The (EPR) experiments do not involve $\hbar$.

L. Stodolsky: But I mean even with light.

R. Chiao: This experiment for tunnelling was verified by the group in Vienna using femtosecond laser pulses, which are completely classical. I have just presented our results, which are at the quantum level.

L. Stodolsky: So, the Wigner formula should be interpreted as a classical formula?

R. Chiao: Yes.

O. Kocharovskaya: There is a recent paper by Brandel, which stated that the result of the beautiful experiment by Dr. Wang is the same as in a two level amplifying system. It is due to the reshaping of the pulse. Could you comment on it?

R. Chiao: No. I don't agree with that at all. I know the paper and it is wrong.

A. Steinberg: I want to come back to the Bose condensation experiment which is obviously incredibly interesting to see. In your final result you really wrote down 0.4 milliseconds. I did not see plus or minus 0.4 milliseconds. Because, you know, you can observe one of those processes or the other. You can distinguish them and can translate with the limit of the short enough wave packet. As you know if the wave packet is short, all these effects go away. That is what happens for the short front. If you are in one of the intermediate regimes this implies for both of them. How have you calculated whether the peak of that wave packet will move at plus 0.4 milliseconds or minus or something in between?

R. Chiao: Excellent question. The question is how can we really resolve the advance of the wave packet. If we construct a wave packet out of many Fourier components, whether we can resolve the delayed wave packet with respect to the advanced wave packet.

A. Steinberg: You have actually a negative time.

R. Chiao: Oh, yes, you do have negative time. If you like I can show my calculation, which I skipped in my talk.

G. Ordonez: You mentioned sharp fronts. Sharp fronts in quantum mechanics, are they compatible with the Heisenberg principle?

R. Y. Chiao: This is an excellent question. I think I would refer this also to Prof. Hegerfeldt's talk. He will answer your question.

E.C.G. Sudarshan: The interpretation of Pendry about the diffraction is conceptually wrong. There is a group in Texas (I am not an author) who has shown that the group velocity is just as would normally be expected and there is no faster than light propagation. I am fond of faster than light propagation but in this case it apparently does not work.

R. Chiao: OK.

G. Nimtz: Two brief comments. You are claiming always that the signal is not defined. In fact, the signal is well defined, otherwise we could not communicate to mobile phones and to computers. The engineers know very well what they want from signal. A well-defined effect, that is a signal. The second comment is you are always talking about Hegerfeldt, about the front. If you read the books for engineers, we don't have in physics unlimited frequencies. In this case, we don't have front. The engineers are talking about the envelope of signal.

R. Chiao: Of course, I agree with you, this is a matter of definition what we call signal. In fact, there are different definitions of signal and the one, which is more natural in the light of special relativity and causality is the front. This is what I am saying. In that sense, I am very conservative.

G. Nimtz: We have just heard that the front is not defined by Heisenberg.

R. Chiao: That is not true. It is defined and we will hear talks about it later. We have done experiments where we have seen that the front velocity is well defined. It is a question of the Fourier components present in the discontinuity whether they are below or above the resonance frequency of your circuit or your amplifying medium. So, it is a practical definition, which works in experiment. We have done the front velocity experiment.

SIGNAL VELOCITY OF SUPERLUMINAL LIGHT PULSES

L. J. WANG
NEC Research Institute, 4 Independence Way, Princeton, NJ 08540, USA
Email: Lwan@research.nj.nec.com

We review the recent work on producing a transparent, linear, anomalously dispersive medium. Experimentally, a light pulse propagating through the atomic vapor cell has its peak reaching the exit side before entering it, resulting in a negative transit time, and negative group velocity. We further review a recently proposed operational definition of the velocity of information transport based on a close analysis of quantum fluctuations.

1 Introduction

In the process of light propagation through a transparent medium, it is well known that a number of velocities are involved. First, there is the "wave (phase) velocity," c/n, determined by the refractive index n of the medium. The envelope of the pulse, however, travels at the group velocity $v_g = c/n_g$, determined by the group index: $n_g = n + \nu dn/d\nu$. In a dispersive medium where the wave velocity depends on the frequency, i.e., $dn/d\nu \neq 0$, the group velocity can be very different from the phase velocity. The topic has been extensively discussed in the past [1,2]. Furthermore, Sommerfeld and Brillouin considered to define a "signal velocity," and have concluded that it is impossible to do so for a noiseless "classical" analytical signal. Hence, they concluded that the proper definition of a signal is the propagation of an abrupt discontinuity; the resulting "front velocity" should be considered the velocity of signal transfer. And finally, there is the problem of defining the velocity of energy transfer[1-4]. Of course, in vacuum, all five velocities are equal to c. In this paper, we will summarize our recent study of the superluminal group velocity in a transparent anomalously dispersive medium. We also discuss the definition of the signal velocity for a smoothly-varying optical pulse. The discussion of energy velocity is beyond the scope of this present paper.

A pulse of light propagates at the group velocity in a dispersive medium. In recent years, much attention has been paid to the case where an artificial steep normal dispersion is realized in an EIT medium. Consequently, very slow or vanishingly small group velocity can be achieved. To the opposite, if a medium can be obtained to be both transparent and anomalously dispersive, i.e., $n + dn/d\nu < 1$, the group velocity $v_g = c/n_g$ will exceed c ("superluminal" group velocity), or even become negative. Of course,it is well known that inside an absorption line, the dispersion is anomalous, resulting in a superluminal group velocity [1,2,5-7]. However, when absorption is large, the medium becomes opaque.

Generally, for all passive, transparent matter such that it is absorptive at all frequencies in the electromagnetic spectrum, the medium's optical dispersion is normal. Landau and Lifshitz [2] showed that under the condition

$$\Im\left[\chi(\nu)\right] \geq 0, \text{ for any } \nu \tag{1}$$

and in the special case for media with a magnetic permeability $\mu(\nu) = 1$, two

inequalities hold simultaneously:

$$n_g(\nu) = \frac{d[n(\nu)\nu]}{d\nu} > n(\nu),$$
$$\text{and} \quad n_g(\nu) = \frac{d[n(\nu)\nu]}{d\nu} > \frac{1}{n(\nu)}. \tag{2}$$

Here n_g is the group index. Obviously, we have $n_g > 1$.

However, for media with gain, the general assumption in Eq.(1) no longer holds. In a series of papers [8,9,10,11,12,13,14], Chiao and coworkers showed theoretically that anomalous dispersion can occur inside a transparent material. It was predicted that, by using a gain doublet [13], it is possible to obtain a transparent anomalous dispersion region where the group velocity of a light pulse exceeds c.

Here we use gain-assisted linear anomalous dispersion to demonstrate superluminal light pulse propagation with a negative group velocity through a transparent atomic medium [15,16,17]. We place two Raman gain peaks closely to obtain an essentially lossless anomalous dispersion region that results in a superluminal group velocity. The group velocity of a pulse in this region exceeds c and can even become negative, while the shape of the pulse is essentially preserved. We measured [15,16] a negative group velocity index of $n_g = -315(\pm 5)$. Experimentally, a light pulse propagating through the atomic vapor cell exits from it earlier than propagating through the same distance in vacuum by a time difference that is 315 times of the vacuum light propagation time L/c.

The experimental situation invites the question of what the velocity of a light signal is. And it is fitting to address this question in the Solvay conference in Physics where the topic is the physics of information.

As noted many years ago by Sommerfeld and Brillouin [1], group velocity is not the velocity of signal transmission. For a smoothly varying pulse that is described by an analytic function, the signal velocity cannot be defined. Because an analytic signal is entirely determined by its very small leading edge, there is no new information being carried by the peak. Furthermore, this leading edge of the pulse can in principle extend infinitely far back in time, making it impossible to assign a point marking the onset of a signal. They noted that the "front velocity," the velocity at which an infinitely sharp step-function-like disturbance of the light intensity propagates, should be used as the velocity of information transmission [1].

These ingenious arguments, however, are not immediately applicable in practice. First, it is impossible even in principle to realize the infinite bandwidth associated with a step-function "front." But more subtle questions arise when one considers a smoothly-varying pulse, where a tiny leading edge of a smooth pulse determines the entire pulse. In practice, one cannot extend the "arrival time" to any time before the detection of the *first* photon. Furthermore, if the tiniest leading edge of a smooth "superluminal" pulse determines the entire pulse, we must account for the effect that quantum fluctuations at the leading edge might have on the detection of the pulse [18,19].

Recently, we suggested [20] an operational definition of the signal velocity and applied it to the observed superluminal propagation of a light pulse in a gain medium [15,16]. Previous considerations of quantum noise in this context focused on the

motion of the peak of a wave packet, and on the observability of the superluminal velocity of the peak at the one- or few-photon level [18,19]. Here we showed that quantum noise associated with the amplifying medium can act in effect to retard the observed signal. In order to achieve a given signal-to-noise ratio (SNR) at the output of an amplifying medium, a larger signal is required, resulting in a retardation of the signal. This retardation is found in numerical simulation to be larger than the propagation time reduction due to anomalous dispersion, leading to a signal velocity $\leq c$. The operational definition given and the conclusions reached here are independent of the intensity of the input pulse.

The paper is organized as the following. We first summarize the realization of a transparent, linear, anomalously dispersive medium. Pulse propagation and the "rephasing" process in such a medium is then reviewed. The experimental details and observational results are left out and can be found in references [15,16]. Finally, we review the operational approach to defining a signal velocity for a smooth pulse propagating through such an anomalously dispersive medium [20].

2 Transparent Anomalous Dispersion

Let us start by considering a classical Lorentz oscillator model of the refractive index. The electric displacement is given by:

$$D = \varepsilon_0 E + P = \varepsilon_0(1+\chi)E = \varepsilon_0 E(1+N\alpha), \tag{3}$$

where N is the atomic density and α is the atomic polarizability. The polarization density $P = -Ne\,x = \varepsilon_0 N\alpha E$ can be obtained using a simple Lorentz model.

In order to obtain the dipole polarization $p = -e\,x$ for a bound charge with an intrinsic angular frequency ω_0 and an angular damping rate $\Gamma = 2\gamma$, we start from the equation of motion of the electron:

$$\ddot{x} + \Gamma\dot{x} + \omega_0^2 x = -\frac{eE}{m} = -\frac{eE_0}{m}\,e^{-i\omega t}. \tag{4}$$

Hence, one obtains that,

$$x = \frac{eE}{m}\,\frac{1}{\omega^2 - \omega_0^2 + i\omega\Gamma} \approx \frac{eE}{2m\omega_0}\,\frac{1}{\omega - \omega_0 + i\Gamma/2}, \tag{5}$$

where the approximation is good as long as $\omega_0 \gg \Gamma$. We further obtain for the polarizability,

$$\alpha = -\frac{e^2}{2\varepsilon_0 m\omega_0}\,\frac{1}{\omega - \omega_0 + i\gamma}. \tag{6}$$

The dielectric susceptibility of the medium thus can be written:

$$\chi(\nu) = -\frac{Ne^2}{2\varepsilon_0 m\omega_0} \times \frac{1}{\omega - \omega_0 + i\gamma} = -f \times \frac{M}{\omega - \omega_0 + i\gamma}, \tag{7}$$

where $M = \omega_P^2/\omega_0$ with ω_P being the effective plasma frequency and f being the oscillator strength. When two absorption lines of frequencies ω_1 and ω_2 are placed

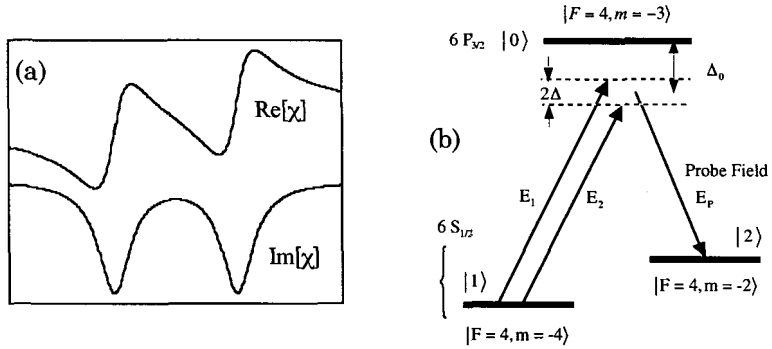

Figure 1: Gain-assisted anomalous dispersion. (a) frequency-dependent gain coefficient and refractive index, (b) schematic atomic level diagram.

nearby with equal oscillator strengths $f_1 = f_2 = 1$, the dielectric susceptibility can be written:

$$\chi(\nu) = -\frac{M}{\omega - \omega_1 + i\gamma} - \frac{M}{\omega - \omega_2 + i\gamma}. \tag{8}$$

For a narrow frequency region in the middle between the two absorption lines, a steep normal dispersion region occurs resulting in an ultra-slow group velocity [21].

Conversely, for gain lines, a negative oscillator strength $f = -1$ is assigned [9]. Hence between two closely placed gain lines, the effective dielectric constant can be obtained:

$$\epsilon(\omega) = 1 + \chi(\omega) = 1 + \frac{M}{\omega - \omega_1 + i\gamma} + \frac{M}{\omega - \omega_2 + i\gamma}. \tag{9}$$

For dilute gaseous medium, we obtain from Eq.(9) for the refractive index $n(\omega) = n'(\omega) + i\,n''(\omega) = 1 + \chi(\omega)/2$ and the real and imaginary parts of the refractive index are plotted in Fig.1(a). It is evident from Fig.1(a) that a steep anomalous dispersion region appears without the heavy absorption present. In fact, a residual gain persists. Furthermore, with the correct choice of experimental parameters, the steep drop of refractive index as a function of frequency can be made a mostly linear one in this region. Thus a light pulse with a frequency bandwidth within this narrow linear anomalous dispersion region will experience almost no change in pulse shape upon propagating through such a medium.

While the details of the experimental realization and parameters can be found in references [15,16], here we review the basics of the experiments. Illustrated in Fig.1(b), in a gaseous medium of atoms each of which has three levels: an excited state $|0\rangle$ and two ground states $|1\rangle$ and $|2\rangle$, we first prepare all atoms to be in a ground state $|1\rangle$ via optical pumping. For simplicity, let us first ignore the Doppler shift and assume that the atoms are at rest. We apply two strong continuous-wave (CW) Raman pump light beams E_1 and E_2 that propagate through the atomic medium. The frequencies of E_1 and E_2, ν_1 and ν_2, are different by a small amount 2Δ and both fields are detuned from the atomic transition frequency ν_{01} ($|1\rangle$ to $|0\rangle$) by a large average amount Δ_0. Since the Rabi frequencies associated with the

fields E_1 and E_2 are small compared with the common detuning Δ_0, the atoms mostly remain in state $|1\rangle$. When a probe light beam E_P is introduced, a Raman transition can occur causing an atom to absorb a Raman pump photon from the fields E_1 or E_2 and emit a photon into the field E_P while in the mean time making a transition from $|1\rangle$ to $|2\rangle$. Obviously, there are two frequencies where the gain in the probe field is maximized. The maximum gain occurs when the probe field is resonant with the Raman transitions caused by either of the two pump fields E_1 and E_2. We hence obtain a medium whose optical susceptibility for the probe field is described by Eq.(9). Here we have

$$M_{1,2} = \frac{|\mu_{02}|^2}{2\hbar\varepsilon_0} \frac{|\Omega_{1,2}|^2}{|\Delta_0|^2} N, \tag{10}$$

with μ_{02}, $\Omega_{1,2}$, and N being the dipole moment of the $|0\rangle$ to $|2\rangle$ atomic transition, the Rabi frequencies of the Raman pump fields E_1 and E_2, and the effective atomic density difference of states $|1\rangle$ to $|2\rangle$, respectively. The quantum mechanical treatment of atomic polarization that yields Eq.(10) and discussion related to the Doppler broadening, as well as linewidth of the gain lines can be found in reference [15,16].

3 Pulse Propagation in an Anomalously Dispersive Medium, Pulse "rephasing" versus "reshaping"

Now, we consider the propagation of a light pulse of an arbitrary shape but of long duration (important to have a limited bandwidth within the anomalously dispersive region between the two gain lines) through a transparent anomalous dispersing medium of a length L as illustrated in Fig.2. For a scalar light pulse that can be decomposed into its positive and negative frequency parts:

$$E(z,t) = E^{(+)}(z,t) + E^{(-)}(z,t), \tag{11}$$

we have for its Fourier decomposition:

$$E^{(+)}(z,t) = \frac{1}{\sqrt{2\pi}} e^{-i\,[\omega_0 t - k(\omega_0) z]} \times \int d\Omega\, E^{(+)}(\Omega)\, e^{-i\,\{\Omega\, t - [k(\omega_0+\Omega) - k(\omega_0)] z\}}, \tag{12}$$

where ω_0 is the carrier frequency of the light pulse. Inside the transparent anomalous dispersion medium, if over the narrow bandwidth of the incident light pulse $E(\omega - \omega_0)$, the gain is essentially constant, the propagation is largely governed by the wave vector $k(\omega)$. We can expand the wave vector in a Taylor series:

$$k(\omega) = k(\omega_0) + \frac{1}{v_g}(\omega - \omega_0) + \frac{1}{2} \left.\frac{d^2 k}{d\omega^2}\right|_{\omega_0} \cdot (\omega - \omega_0)^2 + \cdots. \tag{13}$$

When the higher order terms in Eq.(13) are negligible, i.e., the dispersion is essentially linear, from Eqs.(12) and (13) we obtain:

$$E^{(+)}(L,t) = g \cdot e^{-i\,(\omega_0 t - k_0 \cdot L)}\, E^{(+)}(0, t - L/v_g), \tag{14}$$

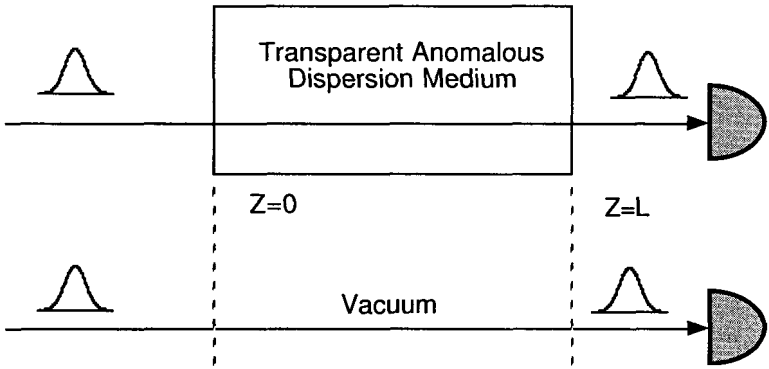

Figure 2: Pulse propagation through a medium of a length L at a group velocity $v_g = c/(n + \nu\, dn/d\nu)$. and through vacuum for the same length.

where $g \approx 1$ is a gain factor. Hence, the intensity of the light pulse as a function of time measured with a detector, $I(L,t)$, is related to the incident pulse's time-dependent intensity by:

$$I(L,t) = I(0, t - L/v_g). \tag{15}$$

Ordinarily, in a normal dispersion medium, the group velocity $v_g < c$. Hence, the output intensity of a pulse propagating through the medium is retarded by the propagation time L/v_g, resulting in a delay longer than the vacuum transit time L/c. In a transparent anomalous dispersion medium, the group velocity $v_g = c/[n+\nu\, dn/d\nu]$ can exceed c provided the anomalous dispersion is sufficiently strong such that: $n + \nu\, dn/d\nu < 1$. In this case, the group velocity becomes superluminal: $v_g > c$, resulting in a "*superluminal transit time*:" $L/v_g < L/c$.

Furthermore, when the transparent anomalous dispersion becomes stronger to yield: $n + \nu\, dn/d\nu = 0$, the group velocity $v_g = c/[n + \nu\, dn/d\nu]$ approaches infinity, resulting in a "*zero transit time*", such that Eq.(11) gives $I(L,t) = I(0,t)$. In this case, the output pulse and the input pulse vary the same way in time and there is no time delay experienced by the pulse propagating through the medium.

Finally, when the transparent anomalous dispersion becomes very steep, the dispersive term $\nu\, dn/d\nu$ which is negative becomes very large in its magnitude such that $|\nu\, dn/d\nu| \gg 1$, resulting in a negative group velocity $v_g = c/[n + \nu\, dn/d\nu] < 0$. In this case, Eq.(11) gives $I(L,t) = I(0, t + |L/v_g|)$, where the quantity $|L/v_g| = |n_g|\, L/c$ is positive and can becomes very large compared to the vacuum transit time L/c. This means that the intensity at the output of the medium of length L, $I(L,t)$, will vary in time *earlier* than that of the input pulse $I(0,t)$. Thus in this case, a "*negative transit time*" can be observed. The time difference between the output pulse and the input pulse in the form of a pulse advance, is $|n_g|$ fold of the vacuum transit time L/c. Practically, since the shape of the pulse is not changed, this results in a rather counterintuitive phenomenon where a certain part of the light pulse has already exited the medium before the corresponding part of the incident light pulse even enters, by a time difference that is $|n_g|$ times of the

vacuum transit time L/c.

This rather counterintuitive effect is a result of the wave nature of light.

To bring about a physical insight of the phenomenon, we have analyzed the behavior of pulse propagation by examining the phase change of the various frequency components of the pulse [17]. In fact, Lord Kelvin first pointed out [1] that the peak of a light pulse is merely the point in space where at a given time, all of its various frequency components are "in-phase." Inside a medium at a time t, the phase of a frequency component becomes $\phi(\omega) = \omega t - k(\omega)z$. Hence, the space-time point where phases of all the frequency components "line-up" is the point where the phase is independent of the frequency:

$$\ell = c \cdot \frac{\partial \phi}{\partial \omega} = c \cdot [t - \frac{z}{U}] = 0, \tag{16}$$

where $U = c/n_g$ is the group velocity.

In the special case where $U < 0$, one can find that a "rephasing" peak of the pulse exits the medium before the incoming pulse arrives at the input port. A detailed description and an animation of the pulse behavior can be found in reference [17].

In some quarters [22], however, it was insisted that our experimental results must be attributed to a "reshaping" or "differential-gain" effect. In their lines of reasoning, the medium is so adaptive such that it can selectively "'amplify' the front of a pulse and 'absorb' its tail." Thus came the argument of the "differential gain," where the medium can respond to the derivatives of the pulse intensity variation [22]. Here we simply point out an experimental fact that this type of theory cannot explain. Namely, in the experiments reported in references [15,16], the pulses used had a typical duration of about 4 μsec, and the typical atomic dwell-time inside the beam is merely 1 μsec. Hence, the 'front' and the 'tail' of the pulse see the same ground-state inverted atoms and the same steady-state CW-Raman pump beams. Consequently, it can never be that the 'front' is amplified while the 'tail' is absorbed. If the argument of reference [22] is correct, both the front and the tail will be amplified.

4 Signal velocity and quantum fluctuation

In order to properly analyze the signal velocity of light, let us start by considering the detection of a signal carried by a light pulse shown in Fig.2. We assign a time window T centered about a pre-arranged time t_0 at the detector and monitor the photo-current produced by the detector. We assume that there is a background level of irradiation that causes a constant photo-current i_0 when no light pulse was sent. We further assume that an increased photo current $i_1(t)$ is registered as a result of a light pulse being received. If the detector's integrated photo current rises $\int dt\, i_1(t)$ rises above the background level during that time by a certain number of the level of noise fluctuation, we can confidently determine that a signal has been received. The time when this preset level of confidence is reached in the detection is to be defined as the time the signal has arrived, assuming perfect detectors allowed by physical laws.

Hence, the realistic observable that should be considered for the definition of the arrival of the signal carried by a light pulse is the time-dependent integrated photon number in the pulse

$$\hat{S}(L,t) = \eta \int_{t_0-T/2}^{t} dt_1 \hat{E}^{(-)}(L,t_1)\hat{E}^{(+)}(L,t_1) \ , \tag{17}$$

where $\hat{E}^{(+)}(L,t_1)$ and $\hat{E}^{(-)}(L,t_1)$ are respectively the positive- and negative-frequency parts of the reduced electric field operator at the exit point ($z = L$) of the medium. $t_0 = T_c + L/c$ where T_c is the time corresponding to the pulse peak. $T/2$ is half the time window assigned to the pulse, typically a few times the pulse width. η is a constant containing the quantum efficiency and will be taken as unity for the rest of the analysis. The expectation value $\langle \hat{S}(L,t) \rangle$ is proportional to the number of photons that have arrived at the detector at the time t. If $\langle \hat{S}_1(L,t) \rangle$ and $\langle \hat{S}_0(L,t) \rangle$ are respectively the expectation values of $\hat{S}(L,t)$ with and without an input pulse, then the photocurrent difference for an ideal detector is $\langle \hat{S}_1(L,t) \rangle - \langle \hat{S}_0(L,t) \rangle$. Since the second-order variance of the integrated photon number, $\langle \Delta^2 \hat{S}(L,t) \rangle$, characterizes the noise power due to quantum fluctuations, we define an optical signal-to-noise ratio in accord with standard signal detection practice[23]

$$SNR(L,t) = \frac{(\langle \hat{S}_1(L,t) \rangle - \langle \hat{S}_0(L,t) \rangle)^2}{\langle \Delta^2 \hat{S}(L,t) \rangle} \ . \tag{18}$$

As discussed above, we define the arrival time t_s of a signal as the time at which $SNR(L,t)$ reaches a prescribed threshold level determined by the allowed error rate.

The positive-frequency part of the reduced electric field operator can be written as [24]

$$\hat{E}^{(+)}(z,t) = \frac{e^{-i\omega_o(t-z/c)}}{\sqrt{2\pi}} \int_{-\infty}^{\infty} d\omega \, \hat{a}(\omega) e^{-i\omega(t-z/v_g)}, \tag{19}$$

where ω_o is the carrier frequency of the pulse, and $[\hat{a}(\omega), \hat{a}^\dagger(\omega')] = \delta(\omega - \omega')$. Eq.(19) assumes plane-wave propagation in the z direction and that the group-velocity approximation is valid.

In the experiment discussed above the anomalously dispersive medium is a phase-insensitive linear amplifier for which [25]

$$\hat{a}_{\rm out}(\omega) = g(\omega)\hat{a}_{\rm in}(\omega) + \sqrt{|g(\omega)|^2 - 1}\hat{b}^\dagger(\omega) \ , \tag{20}$$

where $\hat{a}_{\rm in}$ and $\hat{a}_{\rm out}$ refer respectively to the input ($z = 0$) and output ($z = L$) ports of the amplifier and the operator $\hat{b}(\omega)$ is a bosonic operator ($[\hat{b}(\omega), \hat{b}^\dagger(\omega')] = \delta(\omega - \omega')$) that commutes with all operators $\hat{a}_{\rm in}(\omega)$ and $\hat{a}^\dagger_{\rm in}(\omega)$ and whose appearance in Eq.(20) is required among other things to preserve the commutation relations for the field operators $\hat{a}_{\rm out}$ and $\hat{a}^\dagger_{\rm out}$. $|g(\omega)|^2$ is the power gain factor given by Eq.(1).

We first consider the case of propagation over the distance L in a vacuum where $g(\omega) = 1$. We assume that the initial state $|\psi\rangle$ of the field is a coherent state such that $\hat{a}(\omega)|\psi\rangle = \alpha(\omega)|\psi\rangle$ for all ω, where $\alpha(\omega)$ is a c-number. For such a state we may write $\hat{E}^{(+)}(0,t)|\psi\rangle = \alpha(t)|\psi\rangle$, where $\alpha(t) \equiv \pi^{-1/4}(N_p/\tau)^{1/2} \exp(-(t-T_c)^2/2\tau^2)$,

N_p is the average number of photons in the initial pulse of duration τ. We obtain after a straightforward calculation that

$$SNR_{\rm vac}(L,t) = \langle \hat{S}_1(L,t)\rangle_{\rm vac} = SNR_{\rm vac}(0, t - L/c). \tag{21}$$

Clearly, the point $SNR_{vac}(L,t) = $ const. propagates at the velocity c without excess noise.

Next we treat the case of pulse propagation over the distance L in the anomalously dispersive medium, using Eq.(20) with $g(\omega) \neq 1$ and the same initially coherent field. We obtain in this case

$$\langle \hat{S}_1(L,t)\rangle - \langle \hat{S}_0(L,t)\rangle = |g(0)|^2 \langle \hat{S}_1(0, t - L/v_g)\rangle_{\rm vac} \tag{22}$$

where $\langle \hat{S}_0(L,t)\rangle = (1/2\pi)\int_{t_0-T/2}^{t} dt_1 \int d\omega[|g(\omega)|^2 - 1]$ is the photon number in the absence of any pulse input to the medium. The fact that $\langle \hat{S}_0(L,t)\rangle > 0$ is due to amplified spontaneous emission (ASE) [23]; in the experiment of interest the ASE is due to a spontaneous Raman process.

For a probe pulse with sufficiently small bandwidth, the gain factor becomes

$$|g(0)|^2 = e^{4\pi M\gamma/(\Delta\nu^2+\gamma^2)\cdot L/\lambda}\ , \tag{23}$$

and the effective signal $\langle \hat{S}_1(L,t)\rangle - \langle \hat{S}_0(L,t)\rangle$ is proportional to the input signal $\langle \hat{S}_1(0, t - L/v_g)\rangle_{\rm vac}$ with time delay L/v_g determined by the group velocity v_g. In the anomalously dispersive medium $v_g = c/(n + \nu dn/d\nu)$ and can be $> c$ or even negative, resulting in a time delay

$$\frac{L}{v_g} = \left[1 - \nu_o M \cdot \frac{\Delta\nu^2 - \gamma^2}{(\Delta\nu^2 + \gamma^2)^2}\right]\frac{L}{c}\ , \tag{24}$$

which is shorter than the time delay the pulse would experience upon propagation through the same length in vacuum, or can become negative. In other words, the effective signal intensity defined here can be reached sooner than in the case of propagation in vacuum.

In order to determine with confidence when a signal is received, however, one must evaluate the SNR. Again using the commutation relations for the field operators, we obtain for the fluctuating noise background

$$\begin{aligned}\langle \Delta^2 \hat{S}(L,t)\rangle &\equiv \langle \hat{S}^2(L,t)\rangle - \langle \hat{S}(L,t)\rangle^2 \\ &= |g(0)|^2 \langle \hat{S}_1(0, t - L/v_g)\rangle_{\rm vac} + \langle \hat{S}_0(L,t)\rangle \\ &+ 2|g(0)|^2 {\rm Re}[\int_{t_0-T/2}^{t} dt_1 \int_{t_0-T/2}^{t} dt_2 \\ &\times \alpha^*(t_1 - L/v_g)\alpha(t_2 - L/v_g)F(t_1 - t_2)] \\ &+ \int_{t_0-T/2}^{t} dt_1 \int_{t_0-T/2}^{t} dt_2 |F(t_1 - t_2)|^2\ .\end{aligned} \tag{25}$$

Here

$$F(t) = \frac{1}{2\pi}\int_{-\infty}^{\infty} d\omega[|g(\omega)|^2 - 1]e^{-i\omega t} \tag{26}$$

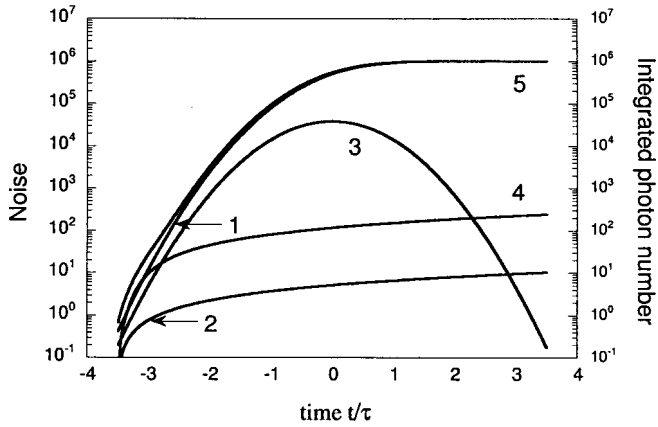

Figure 3: Evolution of quantum noise terms. Curves 1 to 5 indicate noises associated with terms 1 to 4 in Eq.(10), and the total noise, respectively. Parameters used in the figure are adopted from the experiments reported in References [15] and [16]. There are 10^6 photons per pulse. Noise retards the detection of the signal by reducing the SNR. (Fig. adopted from reference [20]).

is a correlation function for the amplified spontaneous emission noise. The four terms in Eq. (25) can be attributed to amplified shot noise, spontaneous emission noise, beat noise, and ASE self-beat noise, respectively [26]. Fig.3 shows the evolution of these noise terms within the time window T. Clearly, amplified shot noise dominates when the input pulse is strong.

Using Eqs. (22) and (25), we compute $SNR_{(\mathrm{med})}(L,t)$ for the propagation through the anomalously dispersive medium. In Fig.4 we plot the results of such computations for $SNR_{(\mathrm{med})}(L,t)$ as a function of time on the output signal. For reference we also show SNR for the identical pulse propagating over the same length in vacuum. It is evident that the pulse propagating in vacuum always maintains a higher SNR. In other words, for the experiments of interest here [15,16], the signal arrival time defined here is delayed, even though the pulse itself on average is advanced compared with propagation over the same distance in vacuum.

To further examine the signal velocity, we require that at a time t' the SNR of a pulse propagating through the medium be equal to that of the same pulse propagating through a vacuum at a time t:

$$SNR_{(\mathrm{med})}(L,t') = SNR_{(\mathrm{vac})}(L,t)\,. \tag{27}$$

Hence, we obtain a time difference $\delta t = t' - t$ that marks the retardation due to quantum noise. $\Delta t = t' - t + L/c$ gives the propagation time of the light signal, and $L/\Delta t$ gives the signal velocity.

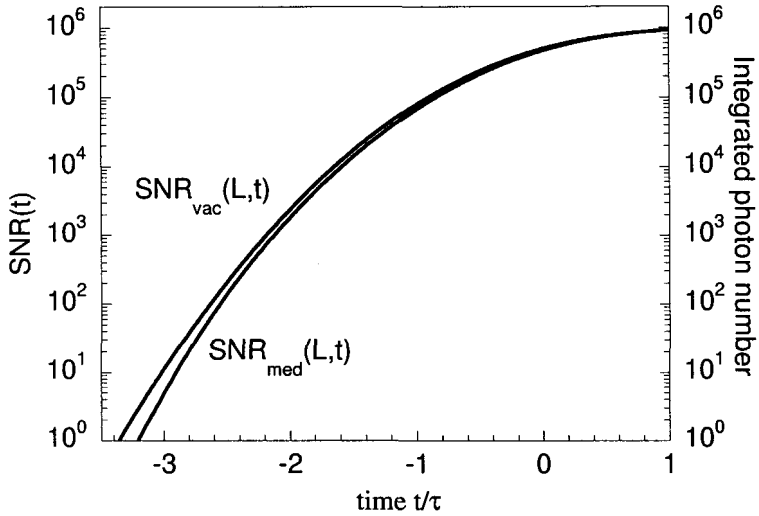

Figure 4: Signal-to-noise ratios for light pulses propagating through the gain-assisted anomalous dispersion medium $SNR_{\rm med}(L,t)$, and through the same distance in a vacuum $SNR_{\rm vac}(L,t)$. Parameters used are appropriate to the experimental situation of reference [15,16,20].

It is useful to further examine the optical noise figure [23] defined as the ratio of the input SNR to that of the output: $F_o = SNR_o^{(in)}/SNR_o^{(out)}$.

It is apparent from the result we derived that transparent anomalous dispersion medium not only is not able to improve the noise figure F_0 but actually increases it. This should come as no surprise: it is well known that a phase-insensitive amplifier (PIA) at large gains has at its best the noise figure of 2.

5 Summary

In conclusion, we note that the observed superluminal and negative group velocity is a result of the wave nature of light. The measured negative and superluminal group velocity of a light pulse propagating through a transparent anomalous dispersion medium is due to the physical effect of "rephasing" [20,22]. Specifically, inside a medium with refractive index n, the effective wavelength of a light ray is modified: $\lambda' = \lambda/n$, where λ is the vacuum wavelength. It is easy to derive:

$$\frac{d(\lambda/n)}{d\lambda} = \frac{n_g}{n^2}. \tag{28}$$

Under the condition $n_g < 0$, we have $d(\lambda/n)/d\lambda < 0$. Hence a longer wavelength (redder) component of the incident pulse becomes a shorter wavelength ray inside the medium, and vice versa. This results in an unusual situation where the phases

of the different frequency components of a pulse become aligned at the exit surface of the medium earlier than even in the case of the same pulse propagating through the same distance in a vacuum.

Finally, we note that a superluminal group velocity is not at odds with causality or special relativity [1–4,8–20]. Simply put, causality only requires that the signal velocity, instead of the group velocity, be limited by c; the signal velocity is different from the group velocity, as first noted again by Sommerfeld and Brillouin [1]. We further reviewed an operational definition of the signal velocity [20]. In the experimental cases where the medium is transparent, we must consider the excess noise due to the gain lines. We found that, in these cases the excess spontaneous emission noise from the gain resonances retards the onset of the signal by retarding the time at which a prescribed signal-to-noise ratio (SNR) is reached [20]. Hence, it was concluded that the quantum noise associated with an amplifier (which is related to the "no-cloning" theorem and the linear nature of quantum mechanics) is associated with the basic requirement of causality that states that no "signal" can be transmitted faster than c.

Acknowledgements

The author wishes to thank A. Dogariu, A. Kuzmich, P. W. Milonni, and R. Y. Chiao for helpful discussion.

References

1. L. Brillouin, *Wave Propagation and Group Velocity* (Academic, New York, 1960).
2. L. D. Landau and E. Lifshitz, *Electrodynamics of Continuous Media*, Chapter 9, 10, (Pergamon, Oxford, 1960).
3. G. Diener, Phys. Lett. A **223**, 327 (1996).
4. G. Diener, Phys. Lett. A **235**, 118 (1997).
5. C. G. B. Garrett and D. E. McCumber, Phys. Rev. A **1**, 305 (1970).
6. S. Chu and S. Wong, Phys. Rev. Lett. **48**, 738 (1982); A. Katz and R. R. Alfano, Phys. Rev. Lett. **49**, 1292 (1982), and S. Chu and S. Wong, *ibid.*, 1293.
7. B. Segard and B. Macke, Phys. Lett. **109A**, 213 (1985).
8. R. Y. Chiao, in *Amazing Light: A Volume Dedicated to Charles Hard Townes on His 80th Birthday*, edited by R. Y. Chiao (Springer-Verlag, New York, 1996), p. 91.
9. R. Y. Chiao, Phys. Rev. A **48**, R34 (1993).
10. R. Y. Chiao, J. Boyce, and J. C. Garrison, Phys. Rev. A **48**, 3890 (1993).
11. M. W. Mitchell and R. Y. Chiao, Phys. Lett. A**245**, 133 (1997); M. W. Mitchell and R. Y. Chiao, Am. J. Phys. **66**, 14 (1998).
12. E. L. Bolda, J. C. Garrison, and R. Y. Chiao, Phys. Rev. A **49**, 2938 (1994).
13. A. M. Steinberg and R. Y. Chiao, Phys. Rev. A **49**, 2071 (1994).
14. R. Y. Chiao, et. al. in *Proceeding of the 8th Conference on Coherence and Quantum Optics*, edited by N. P. Bigelow, J. H. Eberly, and E. Wolf (Planum,

New York, *to be published*).
15. L. J. Wang, A. Kuzmich, and A. Dogariu, Nature (London) **406**, 277 (2000).
16. A. Dogariu, A. Kuzmich, and L. J. Wang, Phys. Rev. A, **63** 053806 (2001).
17. A. Dogariu, A. Kuzmich, H. Cao, and L. J. Wang, Opt. Express **8**, 277 (2001).
18. Y. Aharonov, B. Reznik, and A. Stern, Phys. Rev. Lett. **81**, 2190 (1998).
19. B. Segev, P. W. Milonni, J. F. Babb, and R. Y. Chiao, Phys. Rev. A**62**, 022114 (2000).
20. A. Kuzmich, A. Dogariu, L. J. Wang, P. W. Milonni, and R. Y. Chiao, Phys. Rev. Lett., **86** 3925 (2001).
21. S. E. Harris, Phys. Today **50 (7)**, 36 (1997), and references therein.
22. P. Sprangle, J. R. Penano, B. Hafizi, Phys. Rev. E. **64**, 026504 (2001),
23. E. Desurvire, *Erbium-Doped Fiber Amplifiers: Principles and Applications* (Wiley, New York, 1994), Chapter 2. B. E. A. Saleh and M. C. Teich, *Fundamentals of Photonics* (Wiley, New York, 1991), Chapter 16.
24. L. Mandel and E. Wolf, *Optical Coherence and Quantum Optics* (Cambridge, 1995).
25. H. A. Haus and J. A. Mullen, Phys. Rev. **128**, 2407 (1962). See also C. M. Caves, Phys. Rev. D**26**, 1817 (1982).
26. Y. Yamamoto, IEEE J. Quantum Electron. **16**, 1073 (1980).

DISCUSSION

Chairman: G. Leuchs

L. Stodolsky: My question is whether quantum mechanics is involved or not. In non-relativistic quantum mechanics there is no problem with defining position operator, so you can make eigenstates of **x**. However, it is well known that in the field theory there is no position operator for the position of a photon. So, maybe, we are really reaching the limit that we cannot say where the particle is.

L. Wang: I think this is also related to the localization problem.

E. C. G. Sudarshan: The statement that the position operator is not defined for photon is a little confusing. The Newton-Wigner position operator is defined with point eigenvalues. This does not exist because the photon must be transverse. However you can take a final packet as small as you want and define a series of states which are zero outside and one inside a finite region. The only thing to do is to take a function vanishing with all its derivatives at the boundaries and there are a lot of such test functions.

W. Schleich: My question goes back to your argument. You said that quantum fluctuations protect causality. How does this argument really work?

L. Wang: The statement is a very loose way of saying that it is due to quantum fluctuations. Even the bulk of the energy in the pulse comes out earlier but the energy in your detector fluctuates more, so you are not even sure at the onset of the pulse that the signal has actually been sent. In other words, if you don't send anything your fluctuation is so large that you miss the moment where the level goes up.

W. Schleich: Are you speaking about shot noise?

L. Wang: Various kinds of noise. At the beginning the amplified shot noise is not so important because the pulse itself is small. The shot noise is photon number in the pulses, which you have detected. At the beginning it is the amplifier noise, which overtakes everything. The amplified shot noise is not a major problem because the amplification is very small in between the peaks.

W. Schleich: Is this a fundamental limit or just an experimental limitation?

L. Wang: I cannot prove it. My "math" is not so good. That is why I became experimentalist.

L. Vaidman: Is it the same argument as in the Aharonov's paper on superluminal propagation?

L. Wang: There are many questions, which I didn't read too well but the language is fine. Maybe we can discuss afterwards.

A. Steinberg: I find the operational definition of the signal to noise ratio very interesting. But I still want to take issue with the idea that it is the way to protect causality, because if you even ignore the quantum noise and just write down the classical impulse response function as you did that already demonstrates that at no time does the output have any dependence whatsoever on the input. So, I don't believe in a need for quantum fluctuations to protect causality.

L. Wang: Certainly, theory must fit reality and when you do the experiment you are going to see the quantum fluctuations. It is the fact that the impulse response function itself merely stays classical and the classical theory works pretty well. But if you do real experiment trying to measure that you are going to see fluctuations.

MATTER-WAVE DIFFRACTION OFF NANO GRATINGS: QUANTUM EFFECTS

GERHARD C. HEGERFELDT
Institut für Theoretische Physik
Universität Göttingen

In recent years it has become possible to carry optical diffraction experiments over to atoms and molecules, in particular diffraction by double slits and transmission gratings. However, small deviations from the usual wave-optical theory occur, and a fully quantum mechanical theory yields new surprising insights on the interaction of atoms with surfaces and on the size of molecules.

1 Introduction

In 1923 de Broglie introduced the idea of the wave nature of subatomic particles, an idea which later led Schrödinger to his wave equation. The simple idea of de Broglie has been very fruitful and suffices to explain many diffraction experiments in complete analogy to wave optics. However, as shown in this contribution, in many cases this analogy is not sufficient. To describe and evaluate more sophisticated recent experiments, full quantum mechanics is necessary.

Only recently have advances in micro-technology made atomic diffraction experiments possible. For usual beam velocities of a few hundred meters per seconds the de Broglie wavelength λ of light atoms is only about 1 Å, where $\lambda = \hbar/p$, with p the particle momentum. Therefore very small slit widths and slit distances are needed to obtain diffraction angles which can be resolved experimentally. As a consequence, for atoms the simple but fundamental double slit experiment has been just a thought experiment for a long time.

When a classical wave passes through a transmission grating of period d with N slits of width $s$one observes behind it and outside the original direction an intensity with characteristic directional modulation. For a perpendicularly incident plane wave the diffraction maxima are at the angles

$$\sin\vartheta_n = n\lambda/d \quad (n = 0, \pm 1, \pm 2, \cdots) \,, \tag{1}$$

with the intensity

$$I_n \equiv I(\theta_n) \propto \frac{\sin^2(n\pi s_0/d)}{(n\pi s_0/d)^2} \,. \tag{2}$$

For many purposes this simple wave-optical approach gives a good description of matter diffraction also.

The typical experimental setup for atomic and molecular diffraction consists of a beam of particles with very small velocity distribution which pass through a transmission grating or double slit [1,2,3]. The setup of the Toennies group in Göttingen is shown in Fig. 1 with a transmission grating of period $d = 100$ nm. Fig. 2 shows a picture of the grating bars [4]. For helium atoms a high resolution diffraction picture provided by the Toennies group is shown in Fig. 3. A spectacular diffraction pattern is shown in Fig. 4 [3,5]. In the inset in the upper right hand corner

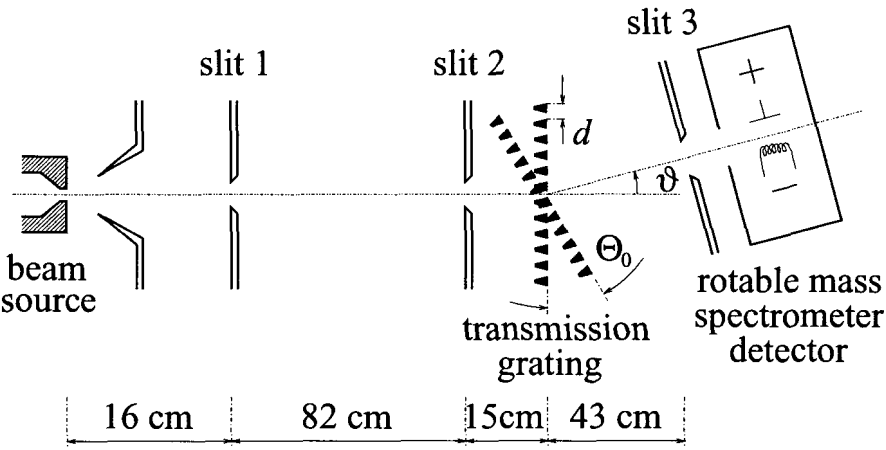

Figure 1. Experimental setup for diffraction of atoms and molecules [3].

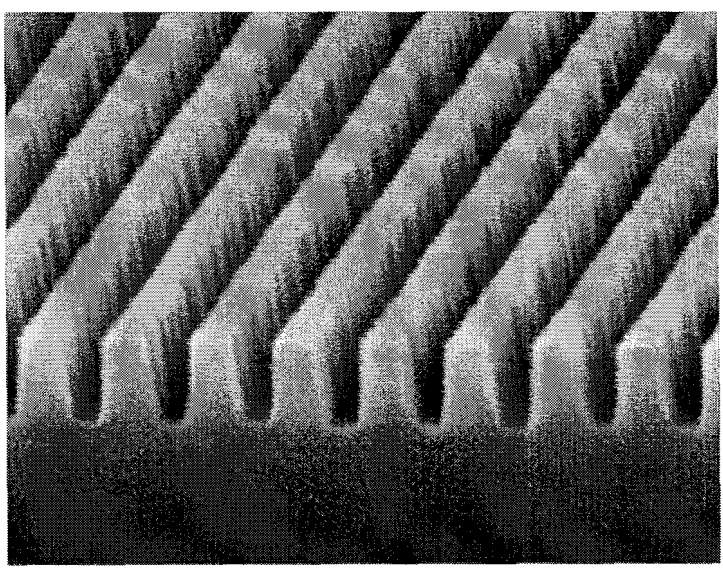

Figure 2. Bars of the transmission grating [4]. Period $d = 100$ nm. The substrate below the bars is later removed. Note the trapezoidal form of the bars.

one observes the first helium diffraction order and left of it at half the angle another small maximum. The latter provided the first direct evidence of the exotic helium dimer molecule $^4He_2$. In the atomic beam there can be helium clusters, all moving with the same velocity. Therefore their de Broglie wavelengths and their diffraction

angles are inversely proportional to their mass. The main part of the figure shows diffraction maxima of higher clusters up to He_{26}. Diffraction of the fullerenes C_{60} and C_{70} was also recently observed [6].

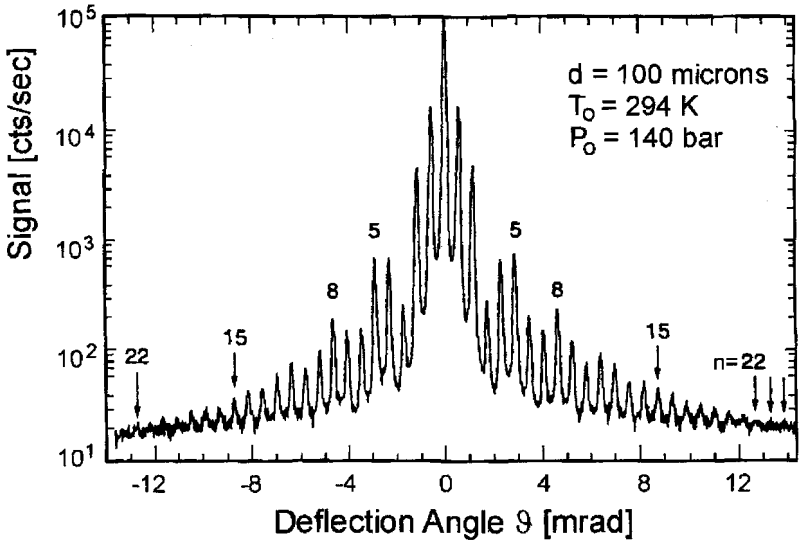

Figure 3. Diffraction pattern of helium atoms up to 22nd order.

Deviations from the simple wave-optical diffraction theory are expected to occur [7]due to

1. the inner structure of the particles and surface van der Waals potentials
2. the spatial size of the particles
3. the breakup of weakly bound molecules.

These deviations are not just "dirt effects" but contain surprises with useful information. This information can be extracted from experimental data by means of a full quantum theory.

2 Quantum theoretical description

In principle, matter diffraction off a grating is not a classical wave phenomenon but a quantum mechanical scattering problem. The diffraction is not caused by the slits but by scattering of the particles off the grating bars. This is depicted in Fig. 5. In addition to the reflective particle-surface interaction one also has to take an attractive van der Waals surface interaction into account.

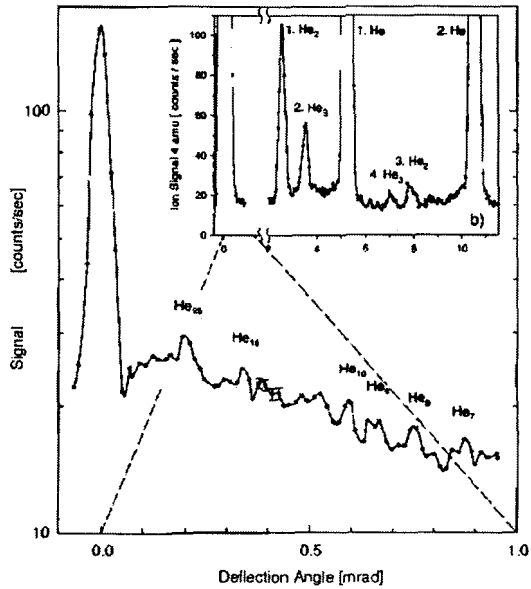

Figure 4. Diffraction pattern of helium atoms and molecules up to He_{26}, yielding the first definite detection of these exotic molecules (cf. Refs. [3] and [5]).

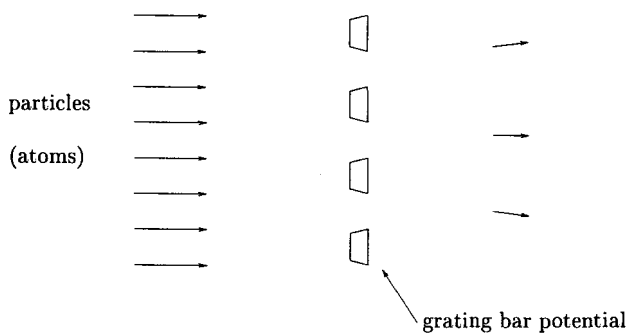

Figure 5. Matter diffraction as scattering off grating bars.

In the context of diffraction and for usual beam velocities, an atom with tightly bound electrons can be considered as a single point particle. However, diffraction of a weakly bound molecule, such as the helium dimer, has to be treated by multichannel scattering theory since there may be breakups or excitations. We have carried the Faddeev scattering theory in the formulation of Alt, Grassberger and Sandhas [8] over to bound particles with an external potential [9] and starting from the Schrödinger equation we have obtained a general expression for the diffraction

intensity I_n of atoms or extended molecules off a grating with an additional *weak* attractive interaction in the form [10]

$$I_n \propto e^{-(2\pi n\sigma/d)^2} \left[\frac{\sin^2(n\pi s_{\text{eff}}/d) + \sinh^2(n\pi\delta/d)}{(n\pi s_{\text{eff}}/d)^2 + (n\pi\delta/d)^2} \right] \quad (3)$$

where s_{eff} denotes an effective slit width which is smaller than s. The term δ diminishes the contrast and the exponential term takes into account that the number of molecules in the individual diffraction orders may decrease due to breakups at the bars and that small variations in the bar widths may occur. All these parameters may depend on the particle-grating interaction, on the spatial extent of the particles and on their velocity.

3 Effects of the atom-surface van der Waals interaction

During the passage through a slit an atom experiences an additional attractive surface van der Waals potential $V = -C_3/l^3$ where l denotes the distance from the surface of a grating bar and where C_3 depends on the particle species. Quite recently we have found the as yet unpublished result that for rare gas atoms in the groundstate s_{eff} behaves as $s_{\text{eff}} \propto 1/\sqrt{v}$ where v is the particle velocity. Therefore we have plotted $s_{\text{eff}}(v)$ obtained from experimental diffraction patterns for variable helium beam velocities as a function of $1/\sqrt{v}$ in Fig. 6. From the slope one can determine C_3. The intersection with the ordinate axis yields the true slit width. The result agrees with an alternative procedure we have used before [10]. The method is so sensitive that the geometrical trapeze form of the grating base has to be taken into account. Fig. 7 shows results for the interaction strength of various groundstate atoms with the surface material of the grating.

For atoms in a highly excited metastable state the situation is very different. In this case the surface van der Waals interaction is much stronger than for atoms in the groundstate. As a consequence Eq. (3) no longer holds and the notion of an effective slit width is no longer adequate. The strength of the surface interaction can still be obtained from diffraction data, but now a much more complicated expression for the diffraction intensity in terms of phase integrals involving C_3 as a parameter has to be numerically fitted to the experimental data. This requires many runs and is more prone to experimental and numerical errors than the approach by means of effective slit width. Recently, measurements for the metastables He* and Ne* have been evaluated by this method [11] and the results are shown in Fig. 8.

4 Determination of the helium-dimer size

Quantum effects in matter diffraction become important when size and breakups become relevant [7] and when excitations of higher levels occur [12]. Size and breakup effects are particularly interesting for the exotic He_2 which is fifty times larger than a hydrogen molecule and whose binding energy is a hundred million times smaller than that of an electron in a hydrogen atom. Therefore He_2 is extremely fragile and thus very difficult to investigate by conventional methods. But at small diffraction angles most helium dimers arrive at the detectors unbroken so that deviations of

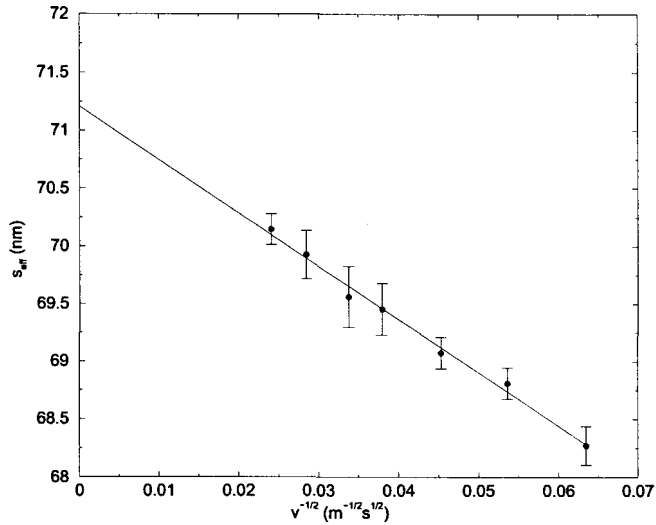

Figure 6. Plot of s_{eff} over $1/\sqrt{v}$ for helium. From the slope of the straight line one can calculate C_3. The ordinate intersection gives the true slit width of $s = 71.2$ nm.

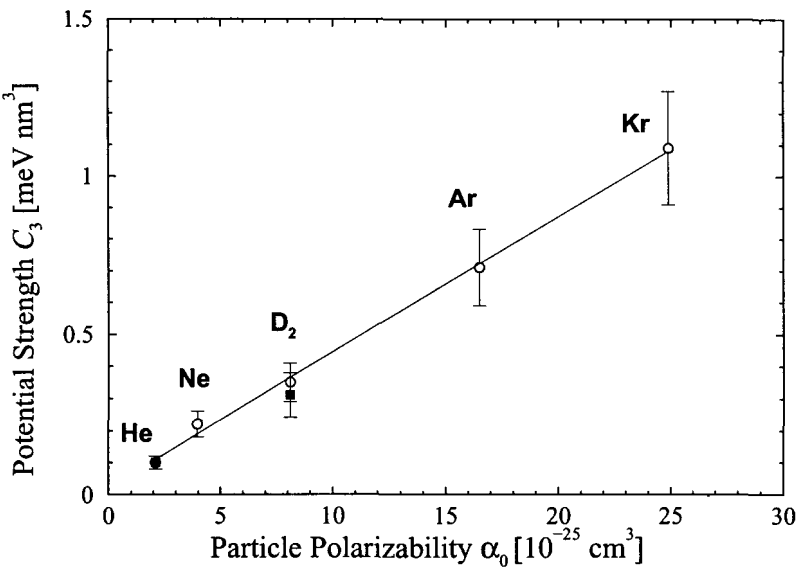

Figure 7. Strength of grating surface potential for various atoms in the groundstate.

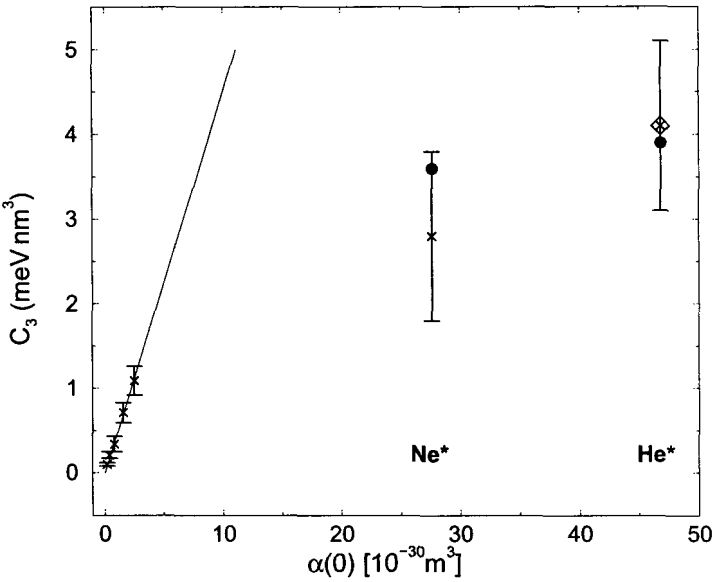

Figure 8. Comparison of measured (×) and theoretical (•, ◊) values for C_3. The data points on the straight line are for the groundstate atoms He, Ne, D_2, Ar, Kr of the previous figure.

the diffraction pattern from the predictions of wave optics can be measured and analyzed.

To do this the van der Waals surface interaction of the dimer constituents has to be taken into account. Again one can use Eq. (3). In Ref. [13] experimental dimer diffraction intensities up to 7th order have been measured and fitted to the expression I_n from Eq. (3). From this s_{eff} was determined. Now multi-channel scattering theory enters. It was possible to express the effective slit width in the form

$$s_{\text{eff}} = \left[2\text{Re}\int_0^{\frac{s}{2}} d\zeta\tau(\zeta)\tau(\zeta + \langle r\rangle/2)\right] - \frac{\langle r\rangle}{2}, \tag{4}$$

where $\tau(\zeta)$ is the slit function for the diffraction of He atoms and $\langle r\rangle$ is the interatomic distance of the dimer constituents. The first term on the right hand side of Eq. (4) accounts for the reduction of the true slit width s by the van der Waals interaction of each atomic constituent with the grating bars. The bond length $\langle r\rangle$ is determined from Eq. (4) by calculating $\tau(\zeta)$ with the measured s and the C_3 value for He from Ref. [10] and then fitting the experimentally determined effective slit widths of $^4He_2$ to Eq. (4) with $\langle r\rangle$ as a parameter. A least-squares fit yields $\langle r\rangle = 52 \pm 4$ Å.

5 Conclusions and future developments

Matter diffraction has developed from a textbook experiment to a new tool in atomic, molecular and surface physics. Its most direct use is that of a mass spectrometer, and this has led to a direct verification of the exotic helium molecules and higher clusters. Quantum effects in matter diffraction, i.e. deviations from the simple wave-optical theory, have been used to determine particle-surface interactions. This has been achieved both for rare gas atoms in the groundstate as well as for highly excited metastable atoms. For the latter alternative methods are practically not available since usually the metastables immediately ionize when interacting with a surface. In diffraction the angle of incidence is essentially zero and therefore sufficiently many metastables survive.

The influence of particle size on the diffraction pattern has been used to determine the size of the delicate helium dimer molecule. Again, its small binding energy and the absence of excited states make it very difficult to use alternative methods.

In Ref. [12] it was proposed to use diffraction to verify the existence of an excited state of the helium trimer, believed to be a long sought Efimov state. Alternative methods are also difficult in this case, due to the small binding energy.

Interferometers for atoms and molecules will allow an even more precise study. External fields in one arm of the interferometer can be used for polarizability measurements, and in principle surface interactions could be investigated with interferometric precision.

References

1. D. W. Keith, M. L. Schattenburg, H. I. Smith, D. E. Pritchard, Phys. Rev. Lett. **61**, 1580 (1988)
2. O. Carnal and J. Mlynek, Phys. Rev. Lett. **66**, 2689 (1991)
3. W. Schöllkopf, J. P. Toennies, Science **266**, 1345 (1994)
4. T. A. Savas, S. N. Shah, M. L. Schattenburg, J. M. Carter, and H. I. Smith, J. Vac. Sci. Technol. B **13**, 2732 (1995)
5. W. Schöllkopf, Doctoral Dissertation, University of Göttingen (1998)
6. M. Arndt, O. Nairz, J. Vos-Andreae, C. Keller, G. van der Zouv, and A. Zeilinger, Nature (London), **401**, 680 (1999)
7. G. C. Hegerfeldt, T. Köhler, Phys. Rev. A **57**, 2021 (1998); Phys. Rev. A **61**, 023606 (2000)
8. E. O. Alt, P. Grassberger, and W. Sandhas, Nucl. Phys. B **2**, 167 (1967)
9. G. C. Hegerfeldt, T. Köhler, Few Body Systems Suppl. **10**, 263 (1999)
10. R. E. Grisenti, W. Schöllkopf, J. P. Toennies, G. C. Hegerfeldt, T. Köhler, Phys. Rev. Lett. **83**, 1755 (1999)
11. R. Brühl, P. Fouquet, R. E. Grisenti, J. P. Toennies, G. C. Hegerfeldt, T. Köhler, M. Stoll, and C. Walter, preprint quant-ph/0112173
12. G. C. Hegerfeldt, T. Köhler, Phys. Rev. Lett. **84**, 3215 (2000)
13. R. E. Grisenti, W. Schöllkopf, J. P. Toennies, G. C. Hegerfeldt, T. Köhler, M. Stoll, Phys. Rev. Lett. **85**, 2284 (2000)

DISCUSSION

Chairman: G. Leuchs

M. Raizen: It seems that your calculation has to take into account the detailed structure of grating.

G. Hegerfeldt: When I showed the slide with the grating I was insisting on the slope of the grating bars. If you neglect that you will never be able to fit the experimental data to the theory. It is very sensitive to this angle.

M. Raizen: I also wanted to point out that various measurement on sodium atoms were done. Instead of diffraction, which is very small in general they very accurately determined correlations.

G. Hegerfeldt: I am sorry for not giving all the references here, but they will be in the proceedings, in particular the early work by Mlynek (with He*) and by Pritchard (with sodium).

A. Zeilinger: I was very intrigued by your result that the C_3 values for excited atoms are not on the line. The reason for us being intrigued is that we only understand our C_{70} interferometer results if we assume that C_3 is much smaller than what polarizability indicates.

G. Hegerfeldt: This is in line with our results.

L. Stodolsky: Experimental question. How big a molecule can I diffract in practice?

G. Hegerfeldt: I am a theorist but Prof. Zeilinger hopes to have bacteria diffracted. I cannot comment on that.

A. Zeilinger: This is a question of money available.

L. Stodolsky: Is this because the grating has to be very good and you need a high angular resolution? What is the experimental problem?

A. Zeilinger: The grating is not a problem because you can use steady light or whatsoever. I don't think that it is a serious problem, just a matter of knowledge, experience and work.

G. Hegerfeldt: With larger particles there may be more what I call dirt effects, so the theory becomes more complicated. But in principle, it would be interesting to probe the limit.

W. Schleich: I have two remarks. The first remark. I know that about 50 years ago in Göttingen, Weizsäcker and Heisenberg discussed what could happen if you take a big molecule and send it through a slit that is more than the molecule and the question was whether it is just a geometric size that determines how many atoms are going to get through or rather whether any wave effects are involved. That was the first step towards what you are doing here. Well they couldn't do a calculation but the author does obviously the calculation. Why is this complicated? Because if you model, as you are doing, this grating by potentials you now have to solve the two-particle problem of going through the slit with interaction. Obviously, this system is even classically not separable anymore. Even on the classical level there are scales.

G. Hegerfeldt: Thank you for this question, because now I can give a theoretical remark why it is so difficult. You all know that the three-body problem is very complicated. This here is only a two-body problem. Why is that so complicated?

The reason is because the grating effectively acts as a third body although it is treated as an external potential, but mathematically it introduces the same singularities in your perturbation theory as in three-body problem. What we did is we looked at the three-body problem and then saw how we could carry that over to the two-body problem with an external potential. People doing few body problems are excited because they seem to have never thought about introducing an interesting external potential like this one.

L. Stodolsky If I saw the graph correctly this is the He_{26} complex detected. How can this get through the grating if the He_2 is already almost too big?

G. Hegerfeldt: The He_2 is very big because it is weakly bound, but the higher clusters are much more tightly bound, and so they are smaller. Here, He_{26} is not 26 times or 13 times larger that He_2. It is much smaller than He_2. Similarly, the diameter of C_{60} is only about 10Å while that of He_2 is about 50Å.

SUPERLUMINAL TUNNELING DEVICES

GÜNTER NIMTZ
II. Physikalisches Institut, Universität Köln

Photonic tunneling permits superluminal group velocity. The principle of causality is not violated but the time duration between cause and effect can be shortened compared with an interaction exchange with velocity of light. This outstanding property can be applied to speed-up photonic modulation and transmission as well as to improve micro-electronic devices. Superluminal photonic pulse transmission has been presented at microwave and infrared frequencies already. Presumably superluminal photonic and electronic devices can become reality having in mind the experimental evidence of the universal tunneling time of photons and of electrons.

1 Introduction

In 1992 Enders and the author have demonstrated that photonic tunneling takes place with superluminal group velocity [1]. The experiments were carried out with microwaves. At that time any application of superluminal tunneling was not expected in spite of the popular semiconductor tunneling diode. A decade later I am going to present some potential applications of superluminal tunneling in photonics and electronics.

The special features of evanescent modes and wave mechanical tunneling are presented in this chapter. In the following chapters the essential properties of a technical signal as well as the universal tunneling time are introduced. There are chapters devoted to applications of the tunneling process as well as finally to a summary of the strange tunneling properties.

Tunneling is the wave mechanical presentation of evanescent modes [2,3]. Evanescent modes are predominantly found in undersized waveguides, in the forbidden frequency bands of periodic dielectric heterostructures, and with double prisms in the case of frustrated total reflection [4,5]. These prominent examples of photonic tunneling barriers are sketched in Fig. 1. The dielectric lattice is equivalent to the electronic lattice of semiconductors with forbidden energy gaps.

Evanescent modes and tunneling wave functions are characterized by a purely *imaginary* wave number. For instance the wave equation yields for the electric field $E(z)$

$$E(z) = E_0\, e^{i(\omega t - kx)} \quad \Rightarrow \quad E(z) = E_0\, e^{i\omega t - \kappa x}, \tag{1}$$

where ω is the angular frequency, t the time, x the distance, k the wave number, and κ the *imaginary* wave number of the evanescent mode.

In the three introduced examples the modes are characterized by an exponential attenuation of transmission due to reflection by tunneling barriers and by a lack of a phase shift inside the barrier. The latter means a zero time barrier traversal according to the phase time approach

$$\tau = d\phi/d\omega, \tag{2}$$

where τ, ϕ, ω are the phase-time, the phase, and the angular frequency, respectively. The observed very short tunneling time is caused at the barrier front boundary. In

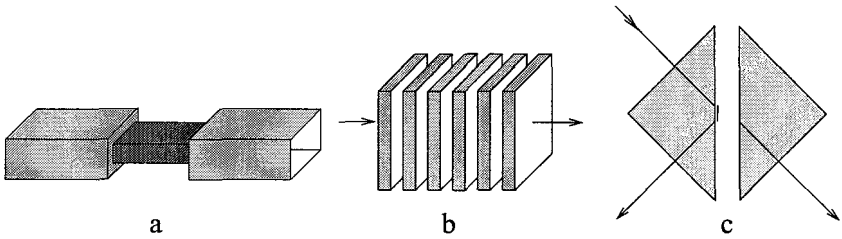

Figure 1. Sketch of three prominent photonic barriers. a) illustrates an undersized wave guide (the central part of the wave guide has a cross-section being smaller than half the wavelength in both directions perpendicular to propagation), b) a photonic lattice (periodic dielectric hetero structure), and c) the frustrated total internal reflection of a double prism, where total reflection takes place at the boundary from a denser to a rarer dielectric medium.

this report the tunneling time is defined as the time a group or a pulse spent traversing a barrier. The time is measured outside the barrier with detectors positioned at the front and the back of the barrier.

This time corresponds to the phase-time or group delay, see Refs. [6,7,8] for example.

In Fig.2 a pulse (i.e. a wavepacket) is sketched which represents a digital signal. The front of the envelope is very smooth corresponding to a narrow frequency band width. The frequency band is choosen with respect to the barrier in question in such a way that the pulse contains essentially evanescent frequency components. Such an evanescent pulse travels in zero time through opaque barriers, which in turn results in an infinite velocity in the phase-time approach neglecting the phase shift at the barrier front [4,9].

In the review on *The quantum mechanical tunnelling time problem - revisited* by Collins et al. [10], the following statement has been made: *the phase-time-result originally obtained by Wigner and by Hartman is the best expression to use for a wide parameter range of barriers, energies and wavepackets.* The experimental results of photonic tunneling have confirmed this statement [4].

Einstein causality prohibits superluminal signal velocity in vacuum and in media with a finite real component of the refractive index. (The general principle of causality prohibits only the exchange of cause and effect [11].) Einstein causality does not hold for media characterized by a purely imaginary refractive index, where the phase shift is zero as in the case of evanescent modes. A zero phase shift corresponds to an instantaneous field spreading, i.e. represents an action at a distance.

In order to avoid signal reshaping due to the dispersion of the special media the signal has to be frequency band limited. Frequency band limitation and finite time duration are found in technical signals and have been discussed and analyzed in Refs.[6,12,13] for example. The energy problem of unlimited frequency bands of signals has been solved by quantum mechanical arguments [14,11]. Actually, technical signals of limited frequency band and limited time duration have been transmited in the multiplex telephony for more than a hundred years. The theory for these technical signals and more general for all physical signals, presents the sampling

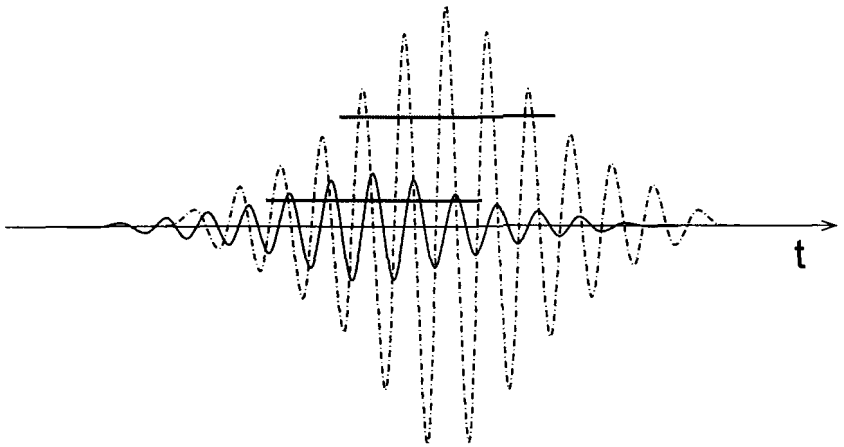

Figure 2. Sketch of two wave packets (i.e. pulses), amplitude vs time. The larger packet travelled slower than the attenuated one. The horizontal bars indicate the half width of the packets which do not depend on the packet's magnitude. The figure illustrates the gradually beginning of the packets [12]. The forward tail of the smooth envelope may be described by the relation $[1 - exp(-t/\tau)][sin(\omega t)]$ for instance, where τ is a time constant.

theorem, which has been introduced by Shannon around 50 years ago [15]. More details about signal properties are presented in the Chapter on Signals.

Evanescent modes are solutions of the classical Maxwell equations, however, they display some nonclassical properties as for instance:

1. The evanescent modes seem to be represented by nonlocal fields as was predicted and later shown by transmission and partial reflection experiments [4,9,16]. Tunneling and reflection times are equal and independent of barrier length [16,17].

2. Evanescent modes have a negative energy, thus they cannot be measured [17,18].

3. Evanescent modes can be described by virtual photons [19].

4. Evanescent modes are not Lorentz invariant as $(v_\varphi/c)^2 \rightarrow \infty$ holds, where $v_\varphi = x/\tau$ is the phase time velocity and c the velocity of light in vacuum. x represents the barrier length.

Obviously, evanescent modes are not fully describable by the Maxwell equations and quantum mechanics has to be taken into consideration. This is similar to the photoelectric effect which is explained by quantum mechanics, i.e. by photons. In general, electric fields are only detectable by a quantized energy exchange.

The tunneling time raised at the front of opaque barriers is constant, i.e. it is independent of barrier length. Thus with increasing barrier length the group velocity increases at the same rate as the length. This phenomenon is often called Hartman effect [20,21].

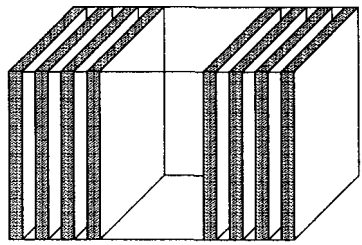

Figure 3. An example of a resonant electromagnetic tunneling structure with evanescent mode solutions (forbidden frequency bands) at microwave frequencies. Two periodic quarter wavelength hetero–structures of perspex and air which are separated by a distance of 18.9 cm forming a resonant cavity with a total length of 28 cm.

The effective barrier length can be significantly lengthened by resonant barrier structures without decreasing the transmission. Resonant tunneling structures with forbidden frequency bands are advantageous to speed-up signals with a narrow frequency band width [4,22]. Figure 3 displays a resonant barrier built of two photonic lattices. The dispersion relations of the respective transmission coefficients and the group velocity of the periodic dielectric quarter wavelength heterostructure are displayed in Fig.4. For narrow frequency band limited signals there is no significant dispersion effect if the carrier frequency is placed in the centre of a forbidden frequency gap.

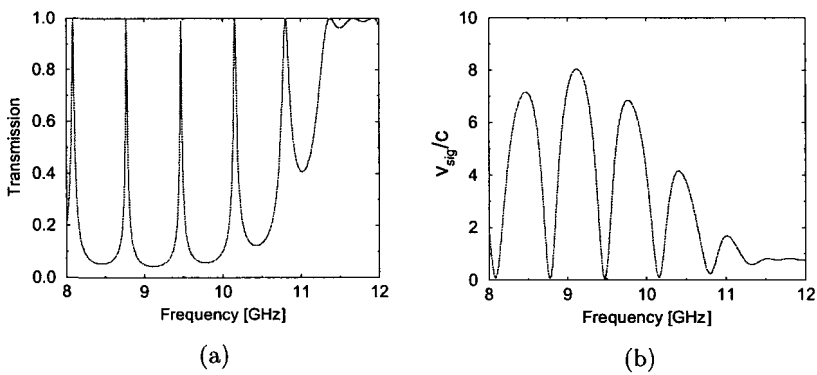

Figure 4. The graph (a) shows the dispersion relation for the resonant heterostructure vs frequency (Fig.3(a)). The transmission dispersion of the periodic heterostructure displays forbidden gaps separated by resonant peaks. The forbidden frequency gaps correspond to the tunneling regime, for details see Ref. [4]. The evanescent regime is characterized by a strong attenuation due to reflection. In (b) the group velocity v_{sig} in units of c is displayed for the resonant periodic dielectric quarter wavelength heterostructure vs frequency.

The three barriers introduced in Fig.1 have different dispersion relations. A simple one describes the frustrated total internal reflection of a double prism. In

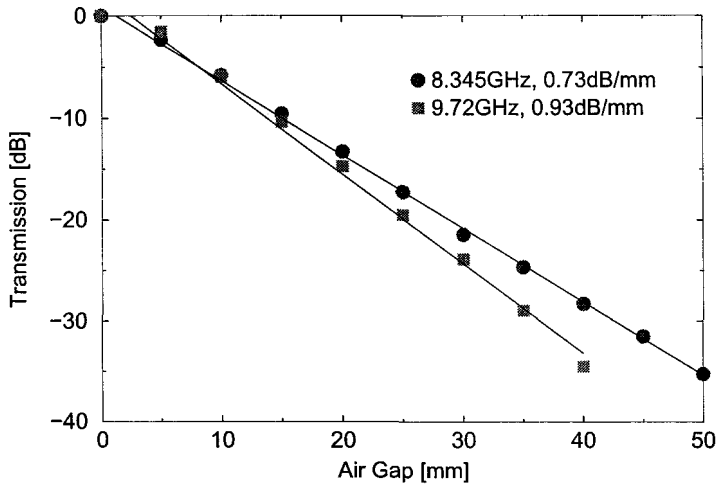

Figure 5. Transmission vs air gap measured at two frequencies [25]. The data follow the theoretical relation of Eqs.3,4. $n_1 = 1.6, n_2 = 1$. $\theta = 45°$, (critical angle of total reflection $\theta_c = 38.5°$).

this case the transmitted electric field E_t and the imaginary wave number κ are given by the relations [3]:

$$E_t = E_0 e^{(i\omega t - \kappa z)} \tag{3}$$

$$\kappa = [\frac{\omega^2}{c^2}((\frac{n_1}{n_2})^2 - 1)sin^2\theta)]^{1/2}, \tag{4}$$

where θ is the angle of the incident beam, E_0 the electric field at the barrier entrance, n_1 and n_2 are the refractive indices, and $(n_1/n_2)\ \sin\theta > 1$. The transmission $t = E_t/E_0$ as a function of air gap of a double prism was measured with microwaves and is shown in Fig. 5. The displayed data are in agreement with Eqs. 3, 4.

The tunneling time in the case of frustrated total internal reflection (FTIR) has been revisited recently [23,24,25]. There is a theoretical shortcoming in describing the time behaviour of FTIR which is based on the approach with ideal plane waves. This approach holds for an unlimited beam diameter, but is not mimicking properly the experimental procedure with limited beam diameters [25,26].

In this report two experiments are introduced, which demonstrate superluminal group velocity in photonic barriers. The signal is represented by a pulse as used in digital communication systems [14,18]; one example was measured with microwaves and one in the infrared frequency range as shown in Figs. 6, 7.

The digital signal displayed in Fig. 6 tunneled with a frequency band width of less than 10^{-2} at a speed of 8 c. The carrier frequency was 9.15 GHz. The starting of detecting the envelope of the tunneled pulse is about 0.8 ns earlier than that of the airborne pulse. The signal frequency band contained essentially evanescent components only.

The experimental set-up to determine and to demonstrate superluminal group

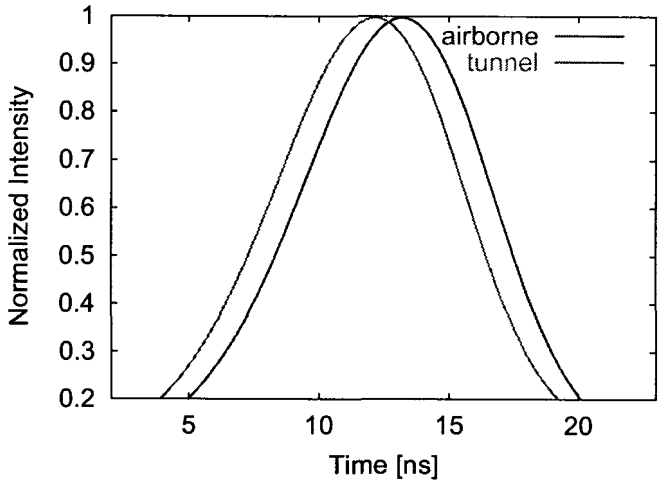

Figure 6. Measured propagation time of two pulses. The faster one has tunneled in the forbidden gap of the photonic barrier of the length of 28 cm. The pulses magnitudes are normalized. The tunneled signal (the half–width of the pulse, representing one bit) traversed the barrier more than 800 ps faster than the airborne pulse. The corresponding velocity of the tunneled pulse was 8·c .

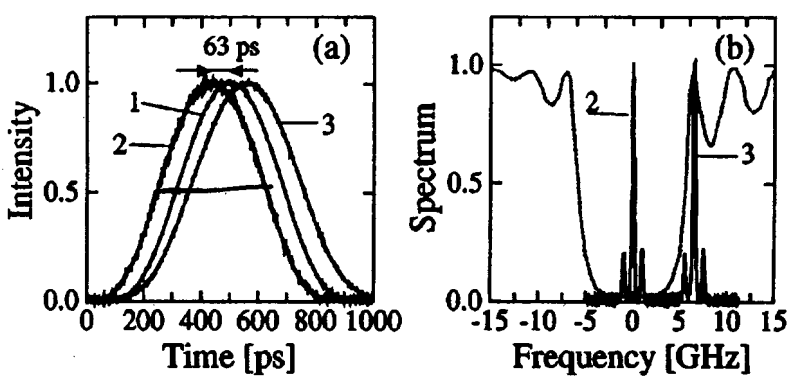

Figure 7. Measured propagation time of three digital signals [37]. (a) Pulse trace 1 was recorded in vacuum. Pulse 2 traversed a photonic lattice in the center of the frequency band gap (see part (b) of the figure), and pulse 3 was recorded for the pulse travelling through the fiber outside the forbidden band gap. The photonic lattice was a periodic dielectric hetero-structure fiber.

velocity is shown in Figs. 8 and 9. The group arrival was measured in vacuum where group, energy, and signal velocities are equal to c [12,27], (actually, a signal does not depend on its magnitude as illustrated in Fig. 2). Amplitude modulated

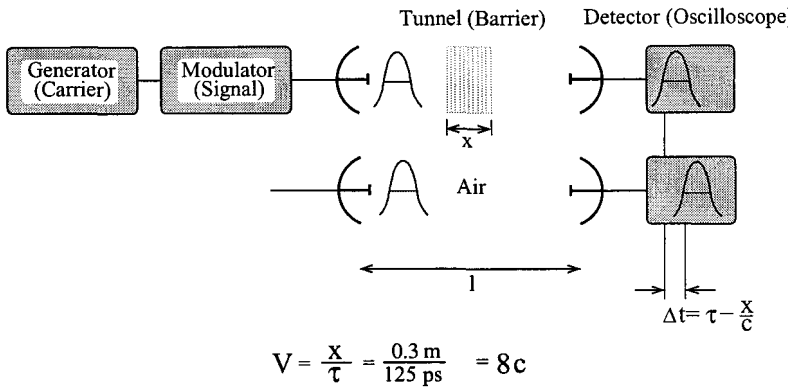

Figure 8. Experimental set-up for the periodic dielectric quarter wavelength heterostructure to measure the group velocity, i.e. the pulse velocity.

microwaves with a frequency of 9.15 GHz (λ = 3.28 cm) are generated with an HP 8341B synthesized sweeper (10 MHz - 20 GHz). A parabolic antenna transmitted parallel beams. The transmitted signal has been received by another parabolic antenna, rectified by a diode (HP 8472A (NEG)) and displayed on an oscilloscope (HP 54825A).

The propagation time of a pulse was measured across the air distance between transmitter and receiver and across the same distance but partially filled with the barrier of 28 cm length. The barrier structure is formed by quarter wavelength slabs of perspex and is introduced and analyzed in Figs. 3, 4. Each slab is 0.5 cm thick and the distance between two slabs is 0.85 cm. Two structures are separated by an air distance of 18.9 cm forming a resonant tunneling structure [4]. Comparing the two travelling times we see that the tunneled pulse arrived the detector about 900 ps earlier than that pulse which travelled the same distance through air. The result corresponds to a signal velocity of the tunneled pulse of 8·c.

The performed measurements are asymptotic. There is no coupling between the generation process, the detection process, and the photonic barrier. In addition the experiment is not stationary and the pulse is measured in the dispersion free vacuum. The experimental situation is the same as that performed in the Hong-Ou-Mandel interferometer, in which the measurement is also asymptotic and yields the group velocity, the energy and the signal velocity at the same time [11,28]. An infrared example of superluminal pulse velocity is displayed in Fig. 7.

So far we have discussed transmission experiments only. An experimental set-up for measuring the partial reflection by photonic barriers at microwave frequencies is presented in Fig. 9. The procedure of varying the barrier length in such an experiment is sketched in Fig. 10.

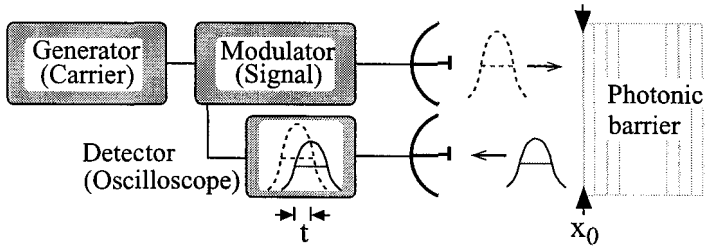

Figure 9. Experimental set–up for the periodic dielectric quarter wavelength heterostructure to measure partial reflection as a function of barrier length.

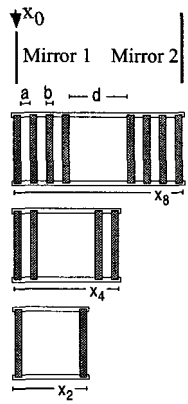

Figure 10. Experimental procedure to measure partial reflection depending on photonic lattice structure.

2 Signals

For instance, a signal may be a photon, which excites an atom with a well defined energy and polarization or it may be a word, which informs the receiver. Both examples are described by wavepackets of limited frequency band width and of limited time duration. The envelope of such a signal is travelling at the speed of light in vacuum, however, the front and the end are continuous rather than discontinuous like in the case of an ideal signal [12].

Technical signals like those displayed in Figs. 6,7,11 are frequency band limited. Technical signals are either amplitude modulated (AM) or frequency modulated (FM). Definitions of the frequency bandwidth, of the time duration, and of the bandwidth-time interval product are introduced and explained in Ref. [13,30] for example. Frequency components of a signal outside the band width in charge of a hypothetical signal front are usually smaller than -60 dB compared with the signal peak component.

The Fourier transform yields for frequency band limited signals an unlimited time extension and hence a noncausal behaviour. However, the noncausal time components have never been detected. In the case of an unlimited frequency band the wave packet is presented by an analytic function and the information contained in the forward tail of the packet determines the whole packet [32]. This is mathematically correct but not relevant for signals from the physical point of view.

As mentioned above engineers have transmitted frequency band and time duration limited signals with the multiplex technology already a hundred years ago. An historic picture of such a multiplex transmission system is shown in Fig. 12. Obviously, the five signals transmitted over one guide are frequency band limited and time duration limited. In this example the frequency band width has been 2 kHz and the time length about 0.3 ms. Shannon's and many other's theoretical investigations yielded the result that the product of frequency band and of time duration represents the amount of information. The Fourier transform of such a multiplex technique yields a noncausal behaviour. This indicates that noncausal time components obtained from Fourier transform are not detectable [14,11].

3 Universal Tunneling Time

An analysis of different experimental tunneling time data obtained with opaque barriers (i.e. $\kappa\, z > 1$) pointed to a universal time [33]. The relation

$$\tau \approx 1/\nu = T \tag{5}$$

$$\tau \approx h/W, \tag{6}$$

was found independent of frequency and of the type of barrier studied [33,34], where τ , ν and T are the tunneling time, the carrier frequency or a wave packet's energy W divided by the Planck constant h, and T the oscillation time of the wave. The microwave experiments near 10 GHz displayed a tunneling time of about 100 ps, experiments in the optical frequency regime near 427 THz a tunneling time of 2.2 fs for instance. In Ref. [33] it was conjectured that the relation holds also for wave packets with a rest mass having in mind the mathematical analogy between the Helmholtz and the Schrödinger equations. Quantum mechanical studies point to this conjecture [9,10,35]. Recently electron tunneling time was measured in a field emission experiment [36]. The measured tunneling times are between 6 fs and 8 fs. Assuming an electron energy of 0.6 eV (the barrier height was 1.7 eV) the empirical relation Eq. (5) yields a tunneling time of 7 fs.

4 Photonic Applications

Tunneling transmission has an exponential decrease with barrier length, the transmission loss is due to reflection. Actually, the transmission loss is not converted into heat and may be recycled in a special circuit design.

4.1 Tunneling

a) Recently Longhi et al. [37] performed tunneling of narrow band infrared pulses over a distance of 20 000 wavelenghts corresponding to 80 000 quarter wavelengths layers. Experimental results are presented in Fig. 7. The overall distance of the photonic fiber lattice was 2 cm. (Scaling the barrier length to 10 GHz microwaves the barrier would be 400 m long.) The periodic variation of the refractive index along the fiber between the two different quarter wavelength layers is only of the order of 10^{-4}. The measured group velocity was 2 c and the transmission intensity of the barrier was 1.5 %.

b) An analogous tunneling barrier of 16.81 m length is under construction at the University of Koblenz. The long structure is designed for microwave signals at a frequency of 9.15 GHz, i.e. at a wavelength of 3.28 cm. 159 dielectric layers differing in the refractive index between 1.00 (air) and 1.05 of a plastic material. The transition time of the huge barrier will be 14 ns compared with a vacuum time of 56 ns. The expected group velocity will be 4 c at a transmitted intensity of 0.16 % [38]. The tunneled pulse will arrive at the detector 49 ns earlier than the airborne one.

4.2 Partial Reflection By Photonic Barriers

a) Photonic barrier reflection is used at 1.5 μm wavelength in fiber optics. Barriers are performed by a 20 mm long piece of glass fiber with a weakly periodically changed refractive index similar to the barrier used in the superluminal transmission experiment by Longhi et al. mentioned above [37]. The losses of reflection by a photonic barrier (imaginary impedance) are less than that of a metal. Photonic barriers represent more effective mirrors than metallic ones. For example photonic barriers are profitably used to stabilize infrared laser diodes in optoelectronics.

b) Figure 13 shows time dependent reflection data by two mirrors at different positions and by photonic barriers of different lengths. Only the magnitude of the reflected pulse is changed but not the reflection time by the barrier length. The observed reflection time of about 100 ps equals the tunneling time in transmission of the barrier. The nonlocal behavior of tunneling modes gives the information on barrier length within one oscillation time at the barrier front.

We have designed an ultrafast modulator on the basis of partial reflection. The effective barrier length is modulated by an electric field induced change of the refractive index at half of the total barrier length. This results in an amplitude change of reflection, see Fig. 13. Another type of modulation can be achieved due to a local change of refractive index by signals exciting an optical active dielectric medium. For example this principle has been applied in experiments on negative group velocity, see e.g. Ref. [40]. In the case of the above microwave experiment the modulations at the distance of 150 mm away from the barrier entrance appears at the barrier front within 100 ps, whereas the corresponding luminal propagation time is five times longer.

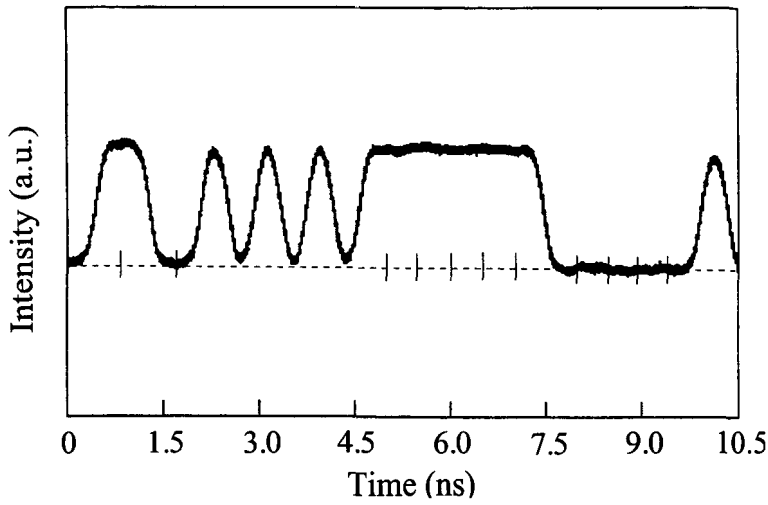

Figure 11. Signals: Measured signal in arbitrary units. The half width in units of 0.2 ns corresponds to the number of bits. From left to right: 1,1,0,0,1,0,1,0,1,0,1,1,1,1,1,1,1,..... The infrared carrier frequency of the signal is $2 \cdot 10^{14}$ Hz (wavelength 1.5 μm). The frequency-band-width of the signal is about $2 \cdot 10^{10}$ Hz corresponding to a relative frequency-band-width of 10^{-4} [29].

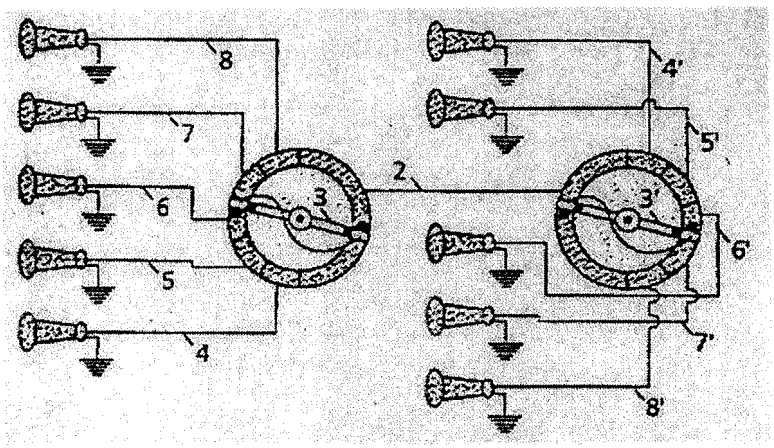

Figure 12. Historical picture of a multiplex transmission system Ref. [31].

5 Electronic Applications

5.1 The Tunneling Diode

The first man-made tunneling device was the tunneling diode. It was invented by Esaki around 1960. This nonlinear electronic device is more and more used since

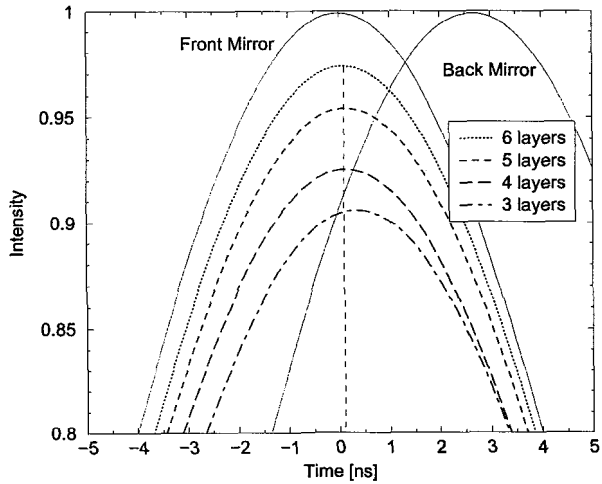

Figure 13. Measured partial reflected microwave pulses vs time. Parameter is the barrier composition as shown in Fig. 10. The signal reflections from metal mirrors either substituting the barrier's front or back position are displayed [16]. In this example the wavelength has been 3.28 cm and the effective barrier length was 41 cm.

that time. However, the tunneling time which would give the ultimate dynamical specification of such a diode has never been measured yet. Our conjecture is: the universal photonic tunneling time Ref. [33] is valid also for the electronic tunneling process. Actually, recent electronic tunneling time experiments support the conjecture [36]. The experimental data is in agreement with relation Eq. 6.

5.2 Superluminal Electron Transport

It was shown in several quantum mechanical studies by Low and Mende for instance that *a particle suitably localized in space and time, which is transmitted through a long, high barrier, travels as if it tunneled it in zero time.* [35]. Of course, the time spent inside the barrier was considered only. Again as in the case of photonic tunneling the barrier traversal velocity was superluminal even in the case of relativistic approaches [10,35,39].

The electronic transport in a semiconductor is rather slow compared with the velocity of light. The utmost highest electron velocity is given by the ballistic electron transport like in the case of an electron microscope or some semiconductor nano-device structures. Bias voltages of electronic devices are of the order of 1V. This results in a ballistic electron velocity of the order of magnitude of 10^6 m/s, which is two orders of magnitude smaller than c.

5.2.1 Electronic Lattice Structures

We propose an electronic lattice structure with alternating quarter wavelength lay-

ers of slightly different bandgaps, which can be traversed at superluminal speeds. The conduction band electron wavelength is of the order of magnitude of 1 nm. Ultrafast coupling of electronic device elements in a circuit could be performed and accelerate the speed of computers. For instance a periodic structure of Si/SiGe quarter wavelength layers represents an electronic lattice. Such a doping of a Si-semiconductor structure with the SiGe alloy yields a weak variation of the band gap analogous to the periodic dielectric fiber structure mentioned above. The electronic structure could have extensions up to more than 1 μm and could be used to perform ultra-fast interconnections between device elements.

5.2.2 pn-Tunnel Junctions

Interband tunneling the basis of the classical tunneling diode can also be used for fast electronic interconnections. By an appropriate doping profile the tunneling path can be adjusted between some 100 nm up to several 1000 nm.

There is a problem left with all the tunneling applications: the high reflection at the barrier entrance. However, tunneling is not a dissipative process with energy loss. As mentioned above the reflected electronic power should be recycled by a smart circuit design.

6 Summing up

The tunneling process shows amazing properties in the case of opaque barriers which we are not used to from classical physics. The tunneling time is universal and arises at the barrier front. It equals approximately the reciprocal frequency of the carrier frequency or of the wave packet energy divided by the Planck constant h. Inside a barrier the wave packet does not spend any time. Another strange experience is that evanescent fields are solutions of the Maxwell equations, but they are not fully describable by them. They carry a *negative* energy for instance which makes it impossible to detect them [17,18,41] and they are nonlocal. Incidentally, the properties are in agreement with the wave mechanical tunneling. This is a situation similar to the Hydrogen atom and the photoelectric effect, where quantum mechanics is necessary to explain the atom's stability and the photon-electron interaction.

The energy of signals is always finite resulting in a limited frequency spectrum. This is a consequence of Planck's quantization of radiation with an energy minimum of $\hbar\omega$. An electric field cannot be measured directly. All detectors need at least one energy quantum $\hbar\omega$ in order to respond. This is a fundamental deficiency of classical physics, which assumes any small amount of field and charge is measurable.

The front and the end of a frequency band limited signal are continous rather than discontinuous as an ideal signal [6,12]. The latter would need infinite high frequency components with an accordingly high energy [11]. In addition, signals are not presented by an analytical function, otherwise the complete information would be contained in the forward tail of the signal [32].

According to Collins et al. [10] the disputes on zero tunneling time (the time spent inside a barrier) are redundant after reading the papers by Wigner and Hartman. The discussions about superluminal tunneling remind me the problem of multiplex

transmission displayed in Fig. 12. Here a signal's finite time duration and frequency band limitation violate causality according to Fourier transform. However, no one had a ringing-up before the other phone was switched on. This indicates the crucial role of finite frequency bands and finite time duration of technical signals without violating the principle of causality [11].

In spite of so much arguing about violation of Einstein causality, all the properties introduced above are useful for novel fast devices, for both fields of photonics and electronics.

Acknowledgments

I gratefully acknowledge discussions with A. Haibel, A. Stahlhofen, and R.-M. Vetter.

References

1. A. Enders and G. Nimtz, J. Phys. I France **2**, 1693 (1992)
2. A. Sommerfeld, Vorlesungen über Theoretische Physik, Band IV, Optik Dieterchsche Verlagsbuchhandlung (1950)
3. R. P. Feynman, Lectures on Physics **II**, 33–12, Addison–Wesley (1970)
4. G. Nimtz and W. Heitmann, Prog. Quantum Electronics **21**, 81 (1997)
5. R. Chiao and A. Steinberg, Progress in Optics **XXXVII**, 345 (1997)
6. A. Papoulis, The Fourier Integral And Its Applications, McGraw-Hill, New York (1962), Secs. 7.5 and 7.6
7. The IEEE Standard Dictionary of Electrical and Electronics Terms, IEEE Std 100-1996
8. NTIA 2000, National telecommunication and information Administration (USA), American National Standard of Telecommunication Terms.
9. Th. Hartman, J. Appl. Phys. **33**, 3427 (1962); A. Enders and G. Nimtz, Phys. Rev. E **48**, 632 (1994)
10. S. Collins, D. Lowe and J. Barker, J. Phys. C **20**, 6213 (1987)
11. G. Nimtz and A. Haibel, Ann. Phys. (Leipzig) **11**, 163 (2002)
12. L. Brillouin, Wave propagation and group velocity, Academic Press New York (1960)
13. Berkeley physics course, Vol.3, waves, chap.6, McGraw-Hill Book Company, Inc. New York and London (1968)
14. G. Nimtz, Eur. Phys. J., B. **7**, 523 (1999)
15. C. E. Shannon, Bell Sys. Tech. J. **27**, 379, and 623 (1948)
16. R.-M. Vetter, A. Haibel and G. Nimtz, arXiv. physics/0103073 (23 Aug 2001)
17. O. Bryngdahl, Progress in Optics **11**, 167 (1973)
18. G. Nimtz, General Relativity and Gravitation, **31**, 737 (1999)
    G. Nimtz, Ann. Phys. (Leipzig) **7**, 618 (1998)
19. C. K. Carniglia and L. Mandel, Phys. Rev. D **3**, 280 (1971)
20. V. Olkhovsky and E. Recami, Phys. Rep. **214**, 339 [1992)
21. A. Enders and G. Nimtz, Phys. Rev. E **48**, 632 (1994)
22. S. Longhi, P. Laporta, M. Belmonte, and E. Recami, arXiv:physics/0201013

v1 (9 Jan 2002)
23. Ph. Balcou and L. Dutriaux, Phys. Rev. Lett. **78**, 851 (1997)
24. A. A. Stahlhofen, Phys. Rev. **A 62**, 12112 (2000)
25. A. Haibel, G. Nimtz, and A. A. Stahlhofen, Phys. Rev. E **63**, 047601 (2001)
26. J. J. Hupert, Appl. Phys. **6**, 131 (1975)
27. J. A. Stratton, Electromagnetic Theory, McGraw-Hill Book Company, Inc. New York and London (1941)
28. A. Steinberg, P. Kwiat, R. Chiao, Phys. Rev. Lett. **68**, 2421 (1992)
29. E. Desurvivre, Scientific American, **266** January, 96 (1992)
30. D. Leeper, Scientific American, **268** May, 46 (2002)
31. H. D. Lüke, IEEE Commun. Magazine, April 1999, p. 106-108
32. F. Low, Annalen der Physik (Leipzig), **7**, 660 (1998)
33. A. Haibel and G. Nimtz, Ann. Phys. (Leipzig), **10**, 707(2001)
34. S. Esposito, Phys. Rev. E **64**, 026609 (2001)
35. F. E. Low and P. F. Mende, Ann. Phys. NY **210**, 380 (1991)
36. S. K. Sekatskii and V. S. Letokhov, Phys. Rev. B **64**, 233311 (2001)
37. S. Longhi, M. Marano, P. Laporta, and M. Belmonte, Phys. Rev. E **64**, 055602 (2001)
38. R.-M. Vetter, design of tunneling barriers, Dissertation 2002, University of Cologne, Physics Department.
39. C. R. Leavens and G. C. Aers, Phys. Rev. B **40**, 5387 (1989); C. R. Leavens and W. R. McKinnon, Phys. Lett. A **194**, 12 (1994)
40. L. Wang, A. Kuzmich and A. Dogariu, Nature, **406**, 277 (2000)
41. S. Gasiorowicz, Quantum Physics, Second Edition, John Wiley & Sons, New York (1996)

DISCUSSION

Chairman: R. Chiao

A. Steinberg: I understand your operational definition of a signal. In very different cases there are different ways of defining a signal. What I would ask is if you really think about the information received and you ask yourself if someone equidistant from the two of us sends me a signal through the air, and you a signal through a tunnel barrier, at a given time t is there any function you can calculate based on what you received that I am incapable of calculating at the same time? And the answer is "no" precisely because of this impulse response function that Dr. Wang shown you.

G. Nimtz: I have shown a graph with a multiplex transmission system. This example is used to discuss that a signal has a well-defined effect whether it is a digital or a frequency modulated signal. Remember Shannon's sampling theorem. The frequency components are shifted with superluminal velocity and the signal does not depend on its magnitude. For instance, a cellular phone has a dynamical signal range of 9 orders of magnitude.

G. Hegerfeldt: I think there is confusion in terminology between what I call a signal and what you call a signal. You cannot argue about definitions. What you should argue about is what Einstein used and Einstein used another definition not the engineering definition. I will just show a figure, which summarizes one of his (Nimtz) beautiful experiments. This is a pulse through the air and this is the tunnelling pulse, which is always smaller in the amplitude than the transmitted pulse. Here you see clearly how the peak velocity is larger for the tunnelling pulse but still lower in amplitude than the transmitted envelope. Only after the amplification you can compare. You have superluminal peak velocity.

G. Nimtz: No. He is calculating with infinite frequency band. It is mathematically correct what he did but it does not describe the physical signal.

T. Petrosky: You said that you don't know how to construct the evanescent modes for Maxwell equation. Actually, the evanescent modes are the result of the boundedness of the frequency from below. Therefore, even in the free wave equation if you construct a wave packet with only the positive frequency you can find the evanescent mode at the level of Maxwell equation. We have such kind of paper for free wave equation.

G. Nimtz: Having a negative energy, you cannot measure an evanescent mode. The impedance is imaginary corresponding to a reactive power.

S. Pascazio: I found Prof. Hegerfeldt's explanation convincing. If the amplitude of tunnelled pulse is below the amplitude of "free" pulse gives the perfect explanation. Can you tell me in a few words why you don't agree with Prof. Hegerfeldt?

G. Nimtz: The importance of the information is its envelope. Professor Hegerfeldt is always discussing the front velocity, which is not defined nor carries information in the case of frequency band limitation and physical signals are frequency band limited. In the experiments the detector made "click", i.e. it measured the signal travelled at a superluminal speed.

G. Leuchs: You said that the evanescent wave has negative energies. If your wave is under some angle like you present it, the evanescent wave will be locked and you have quantum vector parallel to the surface with perfectly positive energy. What do you mean by the evanescent wave has negative energy?

G. Nimtz: The dielectric function is negative in the case of an evanescent mode. This means the energy of the evanescent mode is negative and the impedance is purely imaginary. As I mentioned, you cannot measure it. It is the same, like you cannot measure a particle inside a tunneling barrier in quantum mechanics.

G. Leuchs: Then you cannot separate the evanescent modes. You cannot scatter it out.

G. Nimtz: Yes. This is the reason why we cannot measure it.

E. C. G. Sudarshan: I have two brief questions. One refers to the measurement by a double prism. We also did it. We thought we could calculate how much is the evanescent wave, what is the polarization, what is the amplitude as a function of distance. You seem to say something to the contrary. Is that right?

G. Nimtz: Yes certainly, as we published last year in Physical Review. The theories do not describe correctly the polarization and do not properly take into account the influence of the beam diameter. All these parameters have an influence

on the tunnelling process as recent experiments revealed.

E. C. G. Sudarshan: Another question is with regard to scalar waves, the quantum mechanical waves. When you are in the domain of evanescent waves, the wave number is purely imaginary but the energy density is not negative and the energy transport is zero.

G. Nimtz: No, it is negative.

E. C. G. Sudarshan: OK. I will trust you.

W. Schleich: I also have problems with this evanescent wave concept because in experiments in quantum optics this evanescent wave is used to reflect atoms and you see very clearly that evanescent wave and you measure it really, because if you change the intensity of the field you see this reflection.

G. Nimtz: I like these experiments because they represent an example to explain that you don't reflect particles by evanescent modes but by the surface mode and this mode has a real wave number or reflection takes place by destroying the evanescent mode.

W. Schleich: These are different experiments. I am talking about the experiment of Cohen-Tannoudji.

G. Nimtz: It is the same situation. In all these total reflection experiments, you always have a surface component with a real wave number (Goos-Hänchen shift) and a component with an imaginary wave number. The component with an imaginary wave number is the evanescent mode and there is no interaction with an evanescent mode without its annihilation, i.e. the total energy of the process must be positive.

MEASUREMENTS OF NONLOCAL VARIABLES

LEV VAIDMAN

School of Physics and Astronomy
Raymond and Beverly Sackler Faculty of Exact Sciences
Tel-Aviv University, Tel-Aviv 69978, Israel

Nonlocal variables are briefly reviewed and it is shown that all nonlocal variables related to two or more separate sites can be measured instantaneously, provided we restrict ourselves to verification measurements. The method is based on quantum teleportation.

Seventy years ago Landau and Peierls [1] claimed that the measurability of nonlocal variables contradicts relativistic causality. Twenty years ago, Aharonov and Albert [2] showed that some nonlocal variables can be measured and that this does not contradict causality. The question: "What are the *observables* of relativistic quantum theory?" remains topical even today [3]. In the thriving field of quantum communication this question is relevant for quantum cryptography and quantum computation performed with distributed systems. Here, using the techniques of the process of teleportation [4], I will show that *all* nonlocal variables related to two or more separate sites are measurable.

Although there are many papers on nonlocal measurements, there is no clear and unique definition of the concept of *nonlocal variable.* I will start with the discussion of a *nonlocal variable* of a compound quantum system consisting of several separated parts. One possible definition is:

Definition 1
Variable O of a compound system is nonlocal if it cannot be measured (in a nondemolition way) using measurements of local variables of all separate parts of the system.

According to this definition, for a system of two separated spin-$\frac{1}{2}$ particles, variable $\sigma_{Az}+\sigma_{Bz}$ is nonlocal, while $\sigma_{Az}+2\sigma_{Bz}$ is local. Indeed, measurements of σ_{Az} and σ_{Bz} separately yield values of both variables of the composite system, but an eigenstate of $\sigma_{Az}+\sigma_{Bz}$, $\frac{1}{\sqrt{2}}(|\uparrow\rangle|\downarrow\rangle+|\downarrow\rangle|\uparrow\rangle)$ is disturbed by local measurements while all four eigenstates of $\sigma_{Az}+2\sigma_{Bz}$ are not.

The requirement that the measurement is *nondemolition* might not be relevant for some considerations. Then we can modify the definition:

Definition 2
Variable O of a compound system is nonlocal if it cannot be verified (maybe in a demolition way) using measurements of local variables of all separate parts of the system.

According to this definition, the above variables are both local, but there are other variables of two spin-$\frac{1}{2}$ particles which are nonlocal. Probably the most popular example is the Bell operator which is defined by its four nondegenerate

eigenstates:

$$
\begin{aligned}
|\Psi_-\rangle &= \frac{1}{\sqrt{2}}(|\uparrow\rangle_A|\downarrow\rangle_B - |\downarrow\rangle_A|\uparrow\rangle_B), \\
|\Psi_+\rangle &= \frac{1}{\sqrt{2}}(|\uparrow\rangle_A|\downarrow\rangle_B + |\downarrow\rangle_A|\uparrow\rangle_B), \\
|\Phi_-\rangle &= \frac{1}{\sqrt{2}}(|\uparrow\rangle_A|\uparrow\rangle_B - |\downarrow\rangle_A|\downarrow\rangle_B), \\
|\Phi_+\rangle &= \frac{1}{\sqrt{2}}(|\uparrow\rangle_A|\uparrow\rangle_B + |\downarrow\rangle_A|\downarrow\rangle_B).
\end{aligned} \tag{1}
$$

It is interesting that entanglement of the eigenstates is not a necessary condition for the nonlocality. The variable with the following set of eigenstates which are all product states is also nonlocal [6]:

$$
\begin{aligned}
|\Psi_1\rangle &= |\uparrow_z\rangle_A|\uparrow_z\rangle_B, \\
|\Psi_2\rangle &= |\uparrow_z\rangle_A|\downarrow_z\rangle_B, \\
|\Psi_3\rangle &= |\downarrow_z\rangle_A|\uparrow_x\rangle_B, \\
|\Psi_4\rangle &= |\downarrow_z\rangle_A|\downarrow_x\rangle_B.
\end{aligned} \tag{2}
$$

The question I want to discuss here is the measurability of nonlocal variables. I consider instantaneous von Neumann measurements relaxing the requirement of repeatability, i.e., as in Definition 2, the requirement that the measurement is nondemolition. The existence of a measurement which yields the eigenvalue of a variable with certainty, if prior to the measurement the quantum system was in the corresponding eigenstate, gives the physical meaning for such a variable. (The need to relax the requirement of repeatability was clear before [7], when it has been shown that measurements of some nonlocal variables erase local information and, therefore, cannot be nondemolition.)

The meaning of "instantaneous measurement" is that in a particular Lorentz frame, at time t, we perform local actions for a duration of time which can be as short as we wish. At the end of the procedure (arbitrary small period of time after t) there are local records which together yield the outcome of the measurement of the nonlocal variable. The question I ask: "Is it possible to measure nonlocal variables (defined by Definition 2) in instantaneous measurements of this type?" We assume that it is allowed to perform, beyond local measurements, arbitrary local interactions and to use *prior entanglement* between the sites of different parts of the system.

In fact, it was known before [8] that the Bell operator variable can be measured, and even in a nondemolition way. The variable (2) cannot be measured in a nondemolition way: its measurability would allow superluminal communication. The question of measurability (in a demolition way) of nonlocal variable of all types has been answered only recently [9]. Here I will report this result, showing that *all* nonlocal variables related to two or more separate sites are measurable.

I will start explaining the method by describing the measurement of a nonlocal variable with nondegenerate eigenstates (2). The first step of the measurement is the teleportation of the state of the spin from B (Bob's site) to A (Alice's site). Bob

and Alice do not perform the full teleportation (which invariably requires a finite period of time), but only the Bell measurement at Bob's site which might last, in principle, as short a time as we wish. (I will continue to use the term "teleportation" just for this first step of the original proposal [4].) This action teleports the state of particle B except for a possible rotation by π (known to Bob) around one of the axes of teleportation: $\hat{x}_1$, $\hat{x}_2$, or $\hat{x}_3$.

The second step is taken by Alice. She can perform it at time t without waiting for Bob. She measures the spin of her particle in the z direction. If the result is "up", she measures the spin of the particle teleported from Bob in the z direction and if the result is "down", she measures the spin in the z direction. This completes the measurement. Indeed, the eigenstates of the spin in the z direction are teleported without leaving the z line and the eigenstates of the spin in the x direction are teleported without leaving the x line. Thus, Bob's knowledge about possible flip together with Alice's results distinguish unambiguously between the states Ψ_i.

Next, consider the measurement of a nonlocal variable of two spin-$\frac{1}{2}$ particles located in separate locations A and B, whose eigenstates are the following generalization of (2):

$$\begin{aligned} |\Psi_1\rangle &= |\uparrow_z\rangle_A \, |\uparrow_z\rangle_B, \\ |\Psi_2\rangle &= |\uparrow_z\rangle_A \, |\downarrow_z\rangle_B, \\ |\Psi_3\rangle &= |\downarrow_z\rangle_A \, |\uparrow_\theta\rangle_B, \\ |\Psi_4\rangle &= |\downarrow_z\rangle_A \, |\downarrow_\theta\rangle_B, \end{aligned} \tag{3}$$

where $|\uparrow_\theta\rangle$ is an eigenstate of a spin pointing in a direction $\hat{\theta}$ making angle θ with the z axis. The method of measurement of this variable was found recently using a different approach [10] and this result inspired the current work.

The first step is, again, the Bell measurement at Bob's site which teleports the state of the spin from B to A except for a possible rotation by π (known to Bob) around one of the axes of teleportation: $\hat{x}_1$, $\hat{x}_2$, or $\hat{x}_3$. This time Bob modifies the axes of teleportation (which define the eigenstates of the Bell measurement) in the following way: $\hat{x}_3 = \hat{z}$ and $\hat{x}_1$ is such that $\hat{\theta}$ lies in the plane of $\hat{x}_3$ and $\hat{x}_1$, see Fig. 1.

The second step is taken by Alice at time t. As in the previous case, she measures the spin of her particle in the z direction.

If the result is "up", she measures the spin of the particle teleported from Bob in the z direction and this completes the measurement since the eigenstates of the spin in the z direction are teleported without leaving the z line and, therefore, Bob's knowledge about possible flip together with Alice's results distinguish unambiguously between $\Psi_1$and Ψ_2.

If the result is "down", Alice cannot perform a measurement on Bob's teleported particle because it has spin either along the line of $\hat{\theta}$ (corresponding to teleportation without rotation or rotation around $\hat{x}_2$) or along the line of $\hat{\theta}'$ obtained from the line of $\hat{\theta}$ by π rotation around $\hat{x}_1$ (or $\hat{x}_3$). In this case, Alice teleports Bob's teleported state back to Bob using a new teleportation axes defined by $\hat{x}'_3 = \hat{\theta}$ and $\hat{x}'_2 = \hat{x}_2$.

In the third step, Bob performs an action similar to that of Alice in step 2. He knows whether the spin state in θ direction was teleported to Alice along the $\hat{\theta}$ line

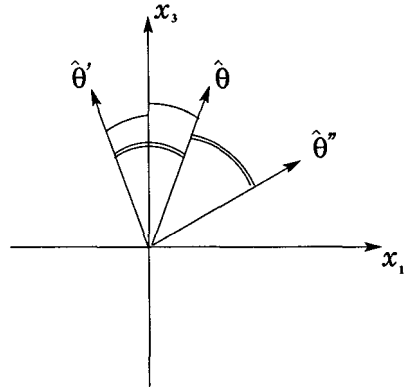

Figure 1. The axes of teleportations. Bob starts with teleportation choosing $\hat{x}_3$ and $\hat{x}_1$ such that $\hat{\theta}$ lies in the plane defined by the axes. Alice teleports back with $\hat{x}'_3 = \hat{\theta}$. Bob continues with $\hat{x}''_3 = \hat{\theta}'$, etc.

or along the $\hat{\theta}'$ line. In the former case, the state teleported to him is still along the $\hat{\theta}$ line, so he completes the procedure by spin measurement in this direction. In the latter case, he receives the spin either along the $\hat{\theta}'$ line or along the $\hat{\theta}''$ line obtained by π rotation around the $\hat{\theta}$ axis. In this case, he teleports the particle back with the teleportation axes $\hat{x}''_3 = \hat{\theta}'$ and $\hat{x}''_2 = \hat{x}_2$.

Alice and Bob continue this procedure. If $\theta = \frac{k}{2^n}\pi$, the line $\hat{\theta}^{(n)}$ coincides with the line $\hat{\theta}^{(n-1)}$ because the angle between the lines is: $\theta^{(n)} - \theta^{(n-1)} = (2^n\theta) \mathrm{mod} \pi$. In this particular case the process is guaranteed to stop after n teleportation steps. If the lines do not coincide, the probability that after n teleportations the result of the measurement is not known is 2^{-n}, so the probability of success can be made as large as we wish. There is no minimal time for performing all the steps of this procedure. Bob and Alice need not wait for each other: they only have to specify before the measurement the teleportation channels they will use. Note, that usually Alice and Bob will use only a small number of teleportation channels: they stop when both Alice and Bob make teleportations which do not change the line of the spin. Thus, this method requires less resources than the alternative approach [10].

Groisman and Reznik [10] showed also how to measure other nonlocal variables of two spin-$\frac{1}{2}$ particles. The method I presented above can be modified for these variables too. However, I will turn now to another, universal, method which is applicable to any nonlocal variable $O(q_A, q_B, ...)$, where q_A belongs to region A, etc. I will not try to optimize the method or consider any realistic proposal: my task is to show that, given unlimited resources of entanglement and arbitrary local interactions, any nonlocal variable is measurable.

I will start with the case of a general variable of a composite system with two parts. First, (for simplicity), Alice and Bob perform unitary operations which swap the states of their systems with the states of sets of spin-$\frac{1}{2}$ particles. In this way Alice and Bob will need the teleportation procedure for spin-$\frac{1}{2}$ particles only.

Teleporting the states of all individual spins teleports the state of the set, be it entangled or not.

The general protocol is illustrated in Fig. 2. Bob teleports his system to Alice. Again, he does not send to Alice the results of his Bell measurements, but keeps them for his further actions; we signify the possible outcomes of these measurements by $i = 1, ...N$. The outcome $i = 1$ corresponds to finding singlets in all Bell measurements and in this case the state of Bob's system is teleported without distortion.

Alice performs a unitary operation on the composite system of her spins and the teleported spins which, under the assumption of non-distorted teleportation, transforms the eigenstates of the nonlocal variable (which now actually are fully located in Alice's site) to product states in which each spin is either "up" or "down" along the z direction. Then she teleports the *complete* composite system consisting of her spins and Bob's teleported spins to Bob. From now on this is the system which will be teleported back and forth between Bob and Alice. In all these teleportations the usual z, x, y basis is used. Hence, if the state is in the one of the product states in spin z basis, then it will remain in this basis.

If, indeed, Bob happened to teleport his spins without any distortion, i.e., $i = 1$ (the probability for which is $\frac{1}{N}$), Bob gets the composite system in one of the spin z product states and his measurements in the spin z basis that he now performs, complete the measurement of the nonlocal variable. If $i \neq 1$, Alice's operation does not bring the eigenstates of the nonlocal variable to the spin z basis, so Bob cannot perform the measurement and he teleports the system back to Alice following a protocol that we explain below.

Alice and Bob have numerous teleportation channels arranged in $N - 1$ clusters numbered from 2 to N. Each cluster consists of two teleportation channels capable to teleport the complete system and $M - 1$ clusters of a similar type, where M is the number of possible outcomes of the Bell measurement for teleportation of the complete system. In turn, each of the $M - 1$ clusters consists of two teleportation channels and $M - 1$ further nested clusters, etc.

If in his first teleportation the result of Bob's Bell measurements is i, he teleports now the composite system back to Alice in the teleportation channel of cluster i. Alice does not know in which channel she gets the system back (if she gets it back at all). So she must work on all of them. She knows that if she does get the system in channel i, the result of the Bell measurement in Bob's first teleportation was i. Thus, she knows all the transformations performed on this system except for the last teleportation. Alice performs a unitary operation that transforms eigenstates of the nonlocal variable to product states under the assumption that the last teleportation was without distortion and teleports the system back to Bob.

Let us denote the result of the Bell measurement in Bob's last teleportation by i', $i' = 1, ..., M$. Again, for $i' = 1$ which corresponds to finding singlets for all Bell measurements, Bob performs the spin z measurement on the system which he receives in the teleportation channel of the cluster i. This then completes the nonlocal measurement. Otherwise, he teleports the system back in the channel of the sub-cluster i'. Alice and Bob continue this procedure. The nonlocal measurement is completed when, for the first time, Bob performs a teleportation without

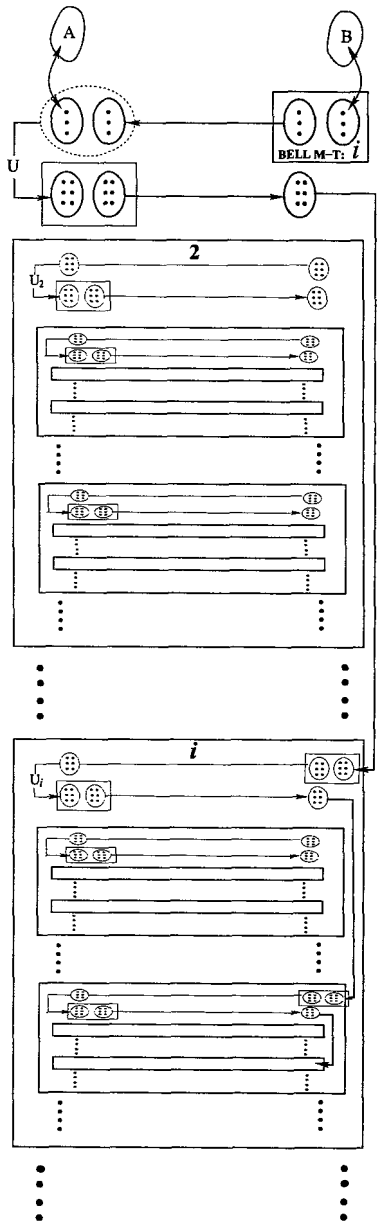

Figure 2. The scheme of the measurement of a nonlocal variable of a two-part system.

distortion. Since, conceptually, there is no limitation for the number of steps, and each step (starting from the second) has the same probability for success, $\frac{1}{M}$, the measurement of the nonlocal variable can be performed with probability arbitrarily close to 1.

The generalization to a system with more than two parts is more or less straightforward. Let us sketch it for a three-part system. First, Bob and Carol teleport their parts to Alice. Alice performs a unitary transformation which, under the assumption of undisturbed teleportation of both Bob and Carol, transforms the eigenstates of the nonlocal variable to product states in the spin z basis. Then she teleports the complete system to Bob. Bob teleports it to Carol in a particular channel i_B depending on the results of the Bell measurement of his first teleportation. Carol teleports all the systems from the teleportation channels from Bob back to Alice in the channels (i_B, i_C) depending on her Bell measurement result i_C. The system corresponding to $(i_B, i_C) = (1, 1)$ is not teleported, but measured by Carol in spin z basis. Alice knows the transformation performed on the system which arrives in her channels (i_B, i_C) except for corrections due to the last teleportations of Bob and Carol. So she again assumes that there were no distortions in those, and teleports the system back to Bob after the unitary operation which transforms the eigenstates of the variable to product states in the spin z basis. Alice, Bob and Carol continue the procedure until the desired probability of successful measurement is achieved.

The required resources, such as the number of teleportation channels and required number of operations are very large, but this does not concern us here. We have shown that there are no relativistic constraints preventing instantaneous measurement of any variable of a quantum system with spatially separated parts, answering the above long standing question.

Can this result be generalized to a quantum system which itself is in a superposition of being in different places? The key to this question is the generality of the assumption of the possibility to perform any local operation. If a quantum state of a particle which is in a nonlocal superposition can be locally transformed to (an entangled) state of local quantum systems, then any variable of the particle is measurable through the measurement of the corresponding composite system. However, while for bosons it is clear that there are such local operations (transformation of photon state to entangled state of atoms has been achieved in the laboratory [11]), for fermion states the situation is different [12]. If the transformation of a superposition of a fermion state to local variables is possible, then these local separated in space variables should fulfill anti-commutation relations. This is the reason to expect super-selection rules which prevent such transformations.

It is a pleasure to thank Yakir Aharonov, Shmuel Nussinov and Benni Reznik for helpful discussions. This research was supported in part by grant 62/01 of the Israel Science Foundation and by the Israel MOD Research and Technology Unit.

References

1. L. Landau and R. Peierls, Z. Phys. **69**, 56 (1931).
2. Y. Aharonov, and D. Z. Albert, Phys. Rev. D **24**, 359 (1981).

3. D. Beckman *et al.*, Phys. Rev. A **64**, 052309 (2001).
4. C. H. Bennett *et al.*, Phys. Rev. Lett. **70**, 1895 (1993).
5. C. H. Bennett *et al.*, Phys. Rev. A **59**, 1070 (1999).
6. B. Groisman and L. Vaidman, J. Phys. A **34**, 6881 (2001).
7. S. Popescu and L. Vaidman, Phys. Rev. A **49**, 4331 (1994).
8. Y. Aharonov, D. Albert and L. Vaidman, Phys. Rev. D **34**, 1805 (1986).
9. L. Vaidman, quant-ph/0111124.
10. B. Groisman and B. Reznik, Phys. Rev. A, to be published [quant-ph/0111012] (2002).
11. X. Maitre, *et al.*, Phys. Rev. Lett. **79**, 769 (1997).
12. Y. Aharonov, and L. Vaidman, Phys. Rev. A **61**, 052108 (2000).

DISCUSSION

Chairman: R. Chiao

G. Hegerfeldt: I have a very simple question. As I understand you are working in non-relativistic quantum mechanics. Then you are using the finite velocity of light. How can you bring them together?

L. Vaidman: The context of the work is following. We have non-relativistic quantum mechanics and then, when people talk about relativistic quantum mechanics, they usually go to field theory, string theory and so on. The question is: Can we go and use the concept of non-relativistic quantum mechanics correctly in relativistic quantum mechanics? If we have a variable of the form $O(q_a, q_b, q_c, t)$, does it have meaning in relativistic quantum mechanics? The claim is that it does have a meaning. It is clearly physical and it is measurable in Nature. There is a procedure, which will tell us exactly what it is. It will transform accordingly from one Lorentz frame to another because it is measurable. So, this variable has a meaning in relativistic quantum mechanics.

E. Polzik: Your results imply that if there is an entanglement shared between two particles, the presence of this entanglement can be verified instantaneously.

L. Vaidman: No. When you make a quantum measurement, you measure an operator. You find an eigenvalue. You don't know that before the measurement the state was the eigenstate with this eigenvalue. You know that the state was not orthogonal to this eigenstate. So, if I found an entangled state $\frac{1}{\sqrt{2}}(|\uparrow\rangle_A|\downarrow\rangle_B - |\downarrow\rangle_A|\uparrow\rangle_B$ it might be that before the measurement it was just $|\uparrow\rangle_A|\downarrow\rangle_B$. I had a 50% chance to find it entangled.

NONLOCAL GROSS-PITAEVSKII EQUATION COUPLED TO THE NONCONDENSATE QUANTUM KINETIC EQUATIONS IN THE THEORY OF BOSE-EINSTEIN CONDENSATE FORMATION, FLUCTUATIONS, AND DECOHERENCE

V. V. KOCHAROVSKY [1,2,3], VL. V. KOCHAROVSKY [1,3], M. O. SCULLY [1,2,4]

[1] *Institute for Quantum Studies,*
Texas A & M University, College Station, TX 77843-4242, USA
[2] *Department of Physics,*
Texas A & M University, College Station, TX 77843-4242, USA
[3] *Institute of Applied Physics of the Russian Academy of Sciences,*
46 Ulyanov str., Nizhny Novgorod 603600, Russia
[4] *Max-Planck Institut fur Quantenoptik, 85748 Garching, Germany*

We study kinetics of the formation, quantum fluctuations, and decoherence of Bose-Einstein condensate (BEC) in a weakly interacting Bose gas. These processes determine, in particular, the properties of the atom lasing and quantum information processing based on BEC. We develop the method of the canonical ensemble quasiparticles in the theory of interacting Bose gases that solves the problem of uncontrollable particle-number non-conservation of the standard grand canonical ensemble approximations, e.g., Bogoliubov-Popov approximation. It yields a solution to the problem of the non-Gaussian anomalously large fluctuations of the ground state occupation in a condensed interacting Bose gas at all temperatures below the critical value.

This method allows us also to derive a time-dependent equation for a coherent order parameter in a partially condensed weakly interacting Bose gas, i.e., a generalized Gross-Pitaevskii equation, that takes a form of a nonlocal nonlinear Schrodinger equation coupled to the equation for the noncondensate excitations via nonlocal inhomogeneous source term responsible for an exchange of particles between condensate and noncondensate. In this way we make gapless approximations particle-number-conserving and provide a well-grounded basis for the analysis of the formation and decoherence of a coherent condensate due to coupling with an incoherent noncondensate.

1 Introduction

Standard techniques in the theory of Bose-Einstein condensation in the interacting gases, such as the Green's function methods and diagram technique, utilize a grand canonical ensemble approach and approximations that often do not conserve exactly a total number of particles in the system but control only an average number of particles [1-6]. In a series of problems, it is important to avoid the uncontrollable effects of the non-conservation of the number of particles. One of such problems is the kinetics of a condensate growth from an incoherent noncondensate, especially at an early stage of the condensate formation since fluctuations of the ground state occupation are extremely sensitive to the particle number constraint $N = const$ [7,8]. In particular, grand canonical fluctuations of the ground state occupation are much stronger than canonical or microcanonical fluctuations. Another example is a well-known dilemma of "conserving versus gapless approximations" [9]. In many respects, it is essential to work within the approximations that preserve the conservation laws of the number of particles, energy, and momentum. These features are important for the dynamics and fluctuations of an atom laser that emits coherent matter

waves from a partially condensed Bose gas and holds promise for the applications in gyroscopes and other supersensitive gauge systems.

This paper is a brief outline of our presentation at the XXII Solvay Conference in Physics (Delphi, Greece, 24-29 November, 2001) and is devoted to a convenient method of an explicit account for a particle-number conservation in the partially condensed interacting Bose gases and its applications to the kinetics of the formation, quantum fluctuations, and decoherence of the BEC. In particular, it allows one to upgrade usual approximations, such as a Bogoliubov-Popov approximation, in order to ensure a conservation of the number of particles. A careful analysis of these problems is necessary to resolve an unprecedented discrepancy (up to about 400%) between the existing theory and the experimental growth curves for the BEC [6,11]. The method is based on the concept of the canonical ensemble quasiparticles described in [7,8].

2 The Concept of Canonical Ensemble Quasiparticles

This concept utilizes the operators

$$\hat{\beta}_{\mathbf{k}}^{+} = \hat{a}_{\mathbf{k}}^{+}\hat{c}_0, \qquad \hat{\beta}_{\mathbf{k}} = \hat{c}_0^{+}\hat{a}_{\mathbf{k}}, \qquad \hat{c}_0 = (1+\hat{N}_0)^{-1/2}\hat{a}_0, \tag{1}$$

introduced by Girardeau and Arnowitt [10].

Two main ideas stand behind this concept. First idea is to use everywhere only particle-number-conserving creation and annihilation operators (1) that describe transitions between ground ($\mathbf{k}=0$) and excited ($\mathbf{k}\neq 0$) states. (For the sake of simplicity, throughout this paper, we write down formulas for a case of a homogeneous gas. A generalization to the case of a trap with arbitrary external potential $U_{ext}(\mathbf{x})$ is straightforward.) Any approximation in these terms automatically conserves the total number of particles, $N = const$. Standard approximations replaced the creation-annihilation operators of the actual particles in the ground state by the c-numbers, $\hat{a}_0^{+}, \hat{a}_0 \to \sqrt{\bar{N}_0}$, that introduced suspicious particle-number non-conserving terms $\bar{N}_0\hat{a}_{\mathbf{k}}\hat{a}_{-\mathbf{k}}$ and $\bar{N}_0\hat{a}_{\mathbf{k}}^{+}\hat{a}_{-\mathbf{k}}^{+}$ in the Hamiltonian and even some difficulties in the physical interpretation. For instance, the very coherent order parameter, i.e., the macroscopic wave function $\bar{\Psi} = \langle N|\hat{\Psi}|N+1\rangle$, where $\hat{\Psi} = V^{-1/2}\sum_{\mathbf{k}=0}^{\infty}\hat{a}_{\mathbf{k}}e^{i\mathbf{kx}}$, turned out to be a transition matrix element related to two different physical systems (with N and $N+1$ particles in a trap) and not just a quantum-mechanical average for a given physical system of N particles. (For a standard discussion of this subtlety, see [1].)

Our method of the canonical ensemble quasiparticles (they could be named also by phonon excitations, or phonons) cures both the non-conserving terms and interpretation. In particular, the coherent order parameter is determined now by a canonical $\hat{\Psi}_{N_0}$-operator which is related to a standard $\hat{\Psi}$-operator by a simple formula

$$\hat{\Psi} = \hat{c}_0\hat{\Psi}_{N_0} \equiv (1+\hat{N}_0)^{-1/2}\hat{a}_0[(\hat{N}_0/V)^{1/2} + \hat{\beta}_{\mathbf{x}}], \tag{2}$$

where

$$\hat{\beta}_{\mathbf{x}} = V^{-1/2}\sum_{\mathbf{k}\neq 0} e^{i\mathbf{kx}}\hat{\beta}_{\mathbf{k}}, \qquad \int_V \hat{\beta}_{\mathbf{x}}d^3x = 0. \tag{3}$$

Now the macroscopic wave function $\bar{\Psi}_{N_0} = \langle N|\hat{\Psi}_{N_0}|N\rangle$, or, for a general mixed state with a density matrix $\hat{\rho}$,

$$\bar{\Psi}_{N_0} = Tr\hat{\Psi}_{N_0}\hat{\rho} \equiv \langle(\hat{N}_0/V)^{1/2}\rangle + \bar{\beta}_{\mathbf{x}}, \tag{4}$$

is exclusively related to a given physical system of N particles.

The second main idea is to approximate a canonical ensemble Hilbert space $\mathcal{H}^{CE}$ by a subspace with non-zero ground-state occupation $\mathcal{H}^{CE}_{N_0\neq 0}$ where the canonical ensemble quasiparticles obey the Bose canonical commutation relations exactly

$$[\hat{\beta}_{\mathbf{k}}, \hat{\beta}_{\mathbf{k}'}] = 0, \qquad [\hat{\beta}_{\mathbf{k}}, \hat{\beta}^{+}_{\mathbf{k}'}] = \delta_{\mathbf{k},\mathbf{k}'}, \qquad \text{for} \qquad \mathbf{k},\mathbf{k}' \neq 0 \qquad \text{on} \quad \mathcal{H}^{CE}_{N_0\neq 0}. \tag{5}$$

This allows us to use the usual many-body techniques for Bose operators, including the diagram techniques. The canonical $\hat{\Psi}_{N_0}$-operator has the following Fourier decomposition (see also Eq.(2)),

$$\hat{\Psi}_{N_0}(\mathbf{x}) = V^{-1/2}\sum_{\mathbf{k}=\mathbf{0}}^{\infty} e^{i\mathbf{k}\mathbf{x}}\hat{\beta}_{\mathbf{k}} = \sqrt{\hat{N}_0/V} + \hat{\beta}_{\mathbf{x}}. \tag{6}$$

It is important that the constant in space, i.e. $\mathbf{k} = 0$, contribution to the canonical $\hat{\Psi}_{N_0}(\mathbf{x})$-operator is completely determined by the fluctuation operator $\hat{\beta}_{\mathbf{x}}$.

An incorrect attempt of a particle-number-conserving modification of the standard theory of Bose-Einstein condensation [11] was criticized by Girardeau [12].

3 Equation of Motion for the Canonical $\hat{\Psi}_{N_0}$-operator and Generalized Gross-Pitaevskii Equation

Similarly to a well-known Heisenberg equation for the standard $\hat{\Psi}$-operator [1]

$$-i\hbar d\hat{\Psi}/dt = (\hbar^2/2m)\Delta\hat{\Psi} - (U_0/V)\hat{\Psi}^{+}\hat{\Psi}^2, \tag{7}$$

we derive a Heisenberg equation for the canonical $\hat{\Psi}_{N_0}$-operator

$$-i\hbar d\hat{\Psi}_{N_0}/dt = [(\hbar^2/2m)\Delta + \hat{H} - \hat{c}^{+}_0\hat{H}\hat{c}_0 - (U_0/V)\hat{c}^{+}_0\hat{\Psi}^{+}_{N_0}\hat{\Psi}_{N_0}\hat{c}_0]\hat{\Psi}_{N_0} \tag{8}$$

in the coordinate $\mathbf{x}$-representation where $\hat{H}$ is the Hamiltonian of an interacting Bose gas.

It yields coupled equations for the noncondensate fluctuations $\Delta\hat{\Psi}_{N_0} = \hat{\Psi}_{N_0} - \bar{\Psi}_{N_0}$ and for the quantum-mechanical average of an operator wave function $\bar{\Psi}_{N_0}(\mathbf{x})$. The latter equation, by definition, is the Gross-Pitaevskii equation for a coherent order parameter. In our analysis it has a form of a nonlocal nonlinear Schrodinger equation

$$-i\hbar d\bar{\Psi}_{N_0}(\mathbf{x})/dt = ((\hbar^2/2m)\Delta + \mu - (U_0/V)|\bar{\Psi}_{N_0}(\mathbf{x})|^2)\bar{\Psi}_{N_0}(\mathbf{x}) + F(\mathbf{x}). \tag{9}$$

The explicit expressions for the effective chemical potential μ and for the source term $F(\mathbf{x})$ include integral, nonlocal contributions due to the particle number constraint $N = const$. We can analyze the related effects in different approximations.

4 Continuity Equation and Exchange of Particles between Condensate and Noncondensate

The most important effect is an exchange of particles between condensate and noncondensate. It can be seen most clearly from the continuity equation for the average density and current of particles,

$$d\langle\hat{n}\rangle/dt = -div\langle\hat{\mathbf{j}}\rangle. \tag{10}$$

Being split into the condensed and noncondensed parts, it yields two coupled equations with a source terms of opposite signs,

$$d\langle\hat{n}_s\rangle/dt = -div\langle\hat{\mathbf{j}}\rangle_s + S(\mathbf{x}), \tag{11}$$

$$d\langle\hat{n}_{nc}\rangle/dt = -div\langle\hat{\mathbf{j}}\rangle_{nc} - S(\mathbf{x}).$$

It is related to the source term in the Gross-Pitaevskii equation as follows

$$S(\mathbf{x}) = -(2/\hbar)Im(F(\mathbf{x})\bar{\Psi}^*_{N_0}(\mathbf{x})). \tag{12}$$

The generalized Gross-Pitaevskii equation (9) is coupled to the quantum kinetic equations for the noncondensate which can be derived in a way similar to that used in [3,4,13,14] but with additional nonlocal contributions. (They will be presented elsewhere.) On this basis, we can discuss different physical mechanisms responsible for a growth or decay of the Bose-Einstein condensate in the canonical or microcanonical ensembles and resolve a huge discrepancy between the experiment and the existing standard theory of the BEC formation [6,11]. A simple Gross-Pitaevskii equation for a pure coherent condensate alone preserves the norm of the coherent order parameter in the volume of a trap, $\int_V |\bar{\Psi}_{N_0}(\mathbf{x})|^2 d^3x = const$, and, hence, cannot give an account for a condensate growth or decay. It describes only the dynamics of the existing condensate, e.g., modifications or oscillations of a superfluid flow pattern.

5 Conclusions

The method of the canonical ensemble quasiparticles efficiently improves the standard analysis of the Bose-Einstein condensation in all aspects that concern the conservation of the number of particles. Hence, it is preferable for the studies of the canonical and microcanonical ensembles and such effects in the condensate formation and in the spectral, decaying, and dynamical behavior of a partially condensed interacting Bose gases where many-particle correlations induced by the particle-number constraint $N = const$ are important. In particular, it yields explicitly nonlocal coupled equations for the condensate wave function and noncondensate fluctuations that preserve the continuity equation for the total density and current of particles and describe an exchange of particles between the condensate and noncondensate.

The concept of the canonical ensemble quasiparticles yields also a very transparent solution to the problem of calculation of the anomalously large non-Gaussian

fluctuations of the ground state occupation in a partially condensed interacting Bose gas in the canonical or microcanonical ensembles at all temperatures below the critical value [7,8].

Acknowledgements

We acknowledge stimulating discussions with L.P. Pitaevskii. The support of NSF and DARPA is gratefully acknowledged.

References

1. E.M. Lifshitz and L.P. Pitaevskii, *Statistical Physics, Part 2*, Pergamon, Oxford (1981).
2. F.Dalfovo, S.Giorgini, L.P.Pitaevskii, and S.Stringari, Rev. Mod. Phys. **71**, 463 (1999).
3. E.Zaremba, T.Nikuni, and A.Griffin, J. Low Temp. Phys. **116**, 227 (1999).
4. M.Imamovic-Tomasovic and A.Griffin, cond-mat/0010107 (2000).
5. Y.Pomeau, M.-E.Brachet, S.Metens, and S.Rica, C.R.Acad.Sci.Paris **327**, Serie II b, 791 (1999).
6. M.J.Bijlsma, E.Zaremba, and H.T.C.Stoof, cond-mat/0001323 (2000).
7. V.V.Kocharovsky, Vl.V.Kocharovsky, M.O.Scully, Phys. Rev. Lett. **84**, 2306 (2000).
8. V.V.Kocharovsky, Vl.V.Kocharovsky, M.O.Scully, Phys. Rev. **A 61**, 53606 (2000).
9. A. Griffin, Phys. Rev. **B 53**, 9341 (1996-II).
10. M. Gerardeau and R. Arnowitt, Phys. Rev. **113**, 755 (1959).
11. C.W. Gardiner et al., Phys. Rev. **A 56**, 1414 (1997); **A 55**, 2902 (1997); **A 56**, 575 (1997); M.J.Davis, C.W.Gardiner, and R.J.Ballagh, cond-mat/9911017 (1999).
12. M.D. Girardeau, Phys. Rev. **A 58**, 775 (1998).
13. U.Eckern, J. Low Temp. Phys. **54**, 333 (1984).
14. T.R.Kirkpatrick and J.R.Dorfman, J. Low Temp. Phys. **58**, 301, 399 (1985).

DISCUSSION

Chairman: R. Chiao

R. Chiao: Are you talking about the depletion when you say "non-condensate"?

V. Kocharovsky: Yes. The depletion of the ground state contributes to the non-condensate if the condensate, i.e., the average value of the canonical-ensemble quasiparticle field operator decreases and the fluctuation component increases. In other words, the non-condensate is everything except of the average value of the canonical-ensemble quasiparticle field operator.

R. Chiao: Does it mean that there will be some dissipation in the non-condensate because of this coupling between condensate and non-condensate, which

means that, for example, sound waves in the superfluid will be dissipated?

V. Kocharovsky: This coupling between the condensate and the non-condensate components can contribute to the dissipation, for example, of the oscillations in the condensate. This dissipation was discussed usually in terms of the processes like Landau damping or Belyaev process. We analyze this coupling and the full quantum kinetic equations for the non-condensate in the canonical or microcanonical ensemble.

W. Schleich: You have mentioned non-locality. How does it emerge here?

V. Kocharovsky: Non-locality emerges here due to this kind of non-local term, which is the integral over the trap volume, and the reason for this non-locality is exactly the conservation of the total number of particles in the trap. A process where the non-condensate particles go from some excited levels to the condensate is non-local because the condensate is spread over the trap in accord with a macroscopic wave function. Finally, the particle-number constraint is an integral condition, this results in a non-local behaviour of the condensate.

W. Schleich: Is there a similar effect in laser theory?

V. Kocharovsky: If we have a mode in the resonator then the mode is also distributed over the whole volume of a laser. It is a similar effect. In a laser we usually have a kind of non-local contribution to the generating mode.

A. Steinberg: It seems to me that the contribution in the laser will only come up if the other mode in the laser cavity is the lasing mode. The lasing mode consequently is the condensate here and you need interaction with the other kinds of modes.

V. Kocharovsky: If you have different active atoms distributed along the laser cavity, they just go from an upper energy level to a lower energy level and emit photons in the lasing mode. This is equivalent to some extent to the transformation of the non-condensate component to the condensate component in the Bose gas.

MICROSCOPIC ENTROPY FLOW AND ENTROPY PRODUCTION IN RESONANCE SCATTERING

G. ORDONEZ, T. PETROSKY AND I. PRIGOGINE

Center for Studies in Statistical Mechanics and Complex Systems, The University of Texas at Austin, Austin, TX 78712 USA

and International Solvay Institutes for Physics and Chemistry, CP231, 1050 Brussels, Belgium

A microscopic dynamical entropy (or $\mathcal{H}$ function) for a two-level atom interacting with a field is introduced. The excitation process of the atom due to the resonance scattering of a wave packet is discussed. Three stages of scattering process (before, during and after the collision) are described in terms of entropy production and entropy flow. The excitation of the atom may be considered as the construction of a non-equilibrium structure due to entropy flow. The emission of photons distributes the energy of the unstable state among the field modes, leading to an increase of microscopic entropy. In this process, instability in dynamics associated with resonances plays a central role. The $\mathcal{H}$ function is constructed outside the Hilbert space, which allows strictly irreversible time evolution, avoiding probabilistic arguments associated with ignorance.

1 Introduction

Irreversible processes can be characterized by the existence of an entropy or $\mathcal{H}$ function with monotonic behavior in time. One of the simplest models where we can find irreversible processes is a two-level atom interacting with a field (the Friedrichs model [1,2]). The excited state is unstable and decays to the ground state emitting a photon. Conversely, the ground state may absorb a photon and go to the excited state. Both processes include an exponentially decaying component $\exp(-2\gamma t)$ in the excitation probability, associated with the lifetime $(2\gamma)^{-1}$of the excited state. This component breaks time symmetry.

As shown in [2,3] for the Friedrichs model one can introduce an $\mathcal{H}$ function, which is the microscopic analogue of Boltzmann's $\mathcal{H}$ function in statistical mechanics. In our earlier work [4,5,6,7] we have shown that if there exists a microscopic entropy it must be an operator. In the Friedrichs model we can construct an $\mathcal{H}$ function in terms of the operator [4,2]

$$\mathcal{H} = |\tilde{\phi}_1\rangle\langle\tilde{\phi}_1|, \tag{1}$$

where $|\tilde{\phi}_1\rangle$ is "Gamow state" outside the Hilbert space. We do not go here to a detailed discussion on a general aspect of entropy. Let us only notice that there have always been two points of view: the point of view of Planck, relating entropy to dynamics and the point of view of Boltzmann, relating entropy to probabilities (ignorance) [8]. We understand now that Planck could not realize his program as he worked in the usual representation of dynamics, equivalent to a Hilbert space representation.

The Heisenberg evolution of Eq. (1) is given by

$$\mathcal{H}(t) = e^{iHt}\mathcal{H}e^{-iHt} = e^{-2\gamma t}\mathcal{H}. \tag{2}$$

In this paper we consider the relation between dynamics and the monotonic decrease of $\mathcal{H}$. We consider a scattering process, where a localized wave packet is sent to collide with the atom in its ground state. For simplicity we consider scattering in a one-dimensional space.

In this process we identify three periods: 1) before the collision, 2) during the collision, and 3) after the collision. All the three periods can be understood in terms of microscopic entropy production and entropy flow, which added together give a positive entropy production for the whole system, given by

$$\frac{d_i S(t)}{dt} = -\frac{\langle \mathcal{H}(t) \rangle}{dt} \geq 0. \tag{3}$$

where $d_i S$ is the total internal entropy production, and $\langle\ \rangle$ means an expectation value for a given state. Before the collision we have to target the wave packet towards the atom in order to have scattering. This introduces a long range correlation that makes the value of $\mathcal{H}$ higher (the entropy lower). The $\mathcal{H}$ function decreases as the "precollisional correlation" decreases, leading to a positive entropy production.[a]

During the collision, the atom is excited. There appears an entropy flow from the field to the atom. This flow makes the atom component of the entropy lower, in spite of the total entropy production always being positive. Hence, the excitation of the atom may be considered as a construction of a non-equilibrium structure due to entropy flow.

After the collision, the atom decays back to the ground state. In this moment the dominant part of the entropy production is due to the decay of the atom. The emitted field, moving away from the atom, now has a very small correlation component (postcollisional correlation) that gives a small correction of the entropy production.

In Secs. 2 and 3 we discuss the model and the Gamow states, which are used to define the $\mathcal{H}$ function in Sec. 4. In Sec. 5 we describe the scattering of the wave packet. In Sec. 6 we introduce a decomposition of the wave packet into two nonlocal components, one moving away from the atom, the other towards the atom [10]. As shown in Sec. 7, they give very different behavior of the $\mathcal{H}$ functions. This corresponds to the distinction between precollisional and postcollisional correlations. In Sec. 8 we analyze the scattering process in terms of entropy production and entropy flow. Finally, in Sec. 9 we discuss the effects of momentum inversion on $\mathcal{H}$.

2 The Friedrichs model

We consider the Friedrichs model in one-dimensional space. The Hamiltonian of this model is given by

$$\begin{aligned} H &= H_0 + \lambda V \\ &= \omega_1 |1\rangle\langle 1| + \sum_k \omega_k |k\rangle\langle k| + \lambda \sum_k V_k (|k\rangle\langle 1| + |1\rangle\langle k|). \end{aligned} \tag{4}$$

[a] The question of the meaning of the decrease of $\mathcal{H}$ before the collision has been raised in Ref. [9].

We use units with $\hbar = 1$ and $c = 1$. The state $|1\rangle$ represents a bare atom located at the origin $x = 0$ of space in its excited level and no field present, while the state $|k\rangle$ represents a bare field mode of momentum k together with the atom in its ground state. Hereafter we will refer to the states $|k\rangle$ as "photon" states as a convention. For $\alpha, \beta = 1, k$ we have

$$\langle\alpha|\beta\rangle = \delta_{\alpha,\beta}, \qquad \sum_{\alpha=1,k} |\alpha\rangle\langle\alpha| = 1. \tag{5}$$

The energy of the ground state is chosen to be zero; ω_1 is the bare energy of the excited level and $\omega_k \equiv |k|$ is the photon energy. The coupling constant λ is dimensionless. We put the system in a "box" of size L and eventually take the limit $L \to \infty$. As usual, we assume periodic boundary conditions. For L finite the momenta k are discrete. In the limit $L \to \infty$ they become continuous, i.e.,

$$\sum_k \to \frac{L}{2\pi} \int dk. \tag{6}$$

The summation sign is written with the understanding that the limit (6) is taken at the end. The potential V_k is of order $L^{-1/2}$. To indicate this we write

$$V_k = (2\pi/L)^{1/2} v_k, \tag{7}$$

where v_k is of order 1 in the continuous spectrum limit $L \to \infty$. We assume that $\omega_1 > 0$. We consider the situation where the state $|1\rangle$ is unstable due to the interaction with the field, i.e., the interaction is weak enough ($\lambda \ll 1$) so that it does not lead to a stable solution for the dressed atom.

The survival probability of the excited state $|1\rangle$ decays in an approximately exponential way. The exponential behavior is given by the complex pole at

$$z_1 \equiv \tilde{\omega}_1 - i\gamma, \tag{8}$$

of Green's energy function $[\eta^+(\omega)]^{-1}$ where $\tilde{\omega}_1 > 0$ is the renormalized energy of the excited state, $2\gamma > 0$ is the decay rate, and

$$\eta^{\pm}(\omega) \equiv \omega - \omega_1 - \int dl \, \frac{\lambda^2 v_l^2}{(z - \omega_l)_{\tilde{\omega}}^{\pm}}. \tag{9}$$

The pole z_1 is the solution of $\eta^+(z_1) = 0$ that reduces to ω_1 when $\lambda = 0$. In Eq. (9) the superscript "+" (or $-$) indicates analytic continuation of z from the upper (or lower) half plane to $z = \omega$ [11,2].

In addition to the exponential component the survival probability contains non-exponential components related to the "Zeno" effect [12,3] and long time tails [13]. These components come from the branch cut contribution of Green's function.

3 Gamow states

The complex pole z_1 can be associated with a generalized eigenstate (the so-called "Gamow state") of the Hamiltonian H [2,14-16]

$$H|\phi_1\rangle = z_1|\phi_1\rangle, \qquad \langle\tilde{\phi}_1|H = \langle\tilde{\phi}_1|z_1. \tag{10}$$

The left eigenstates $\langle\tilde{\phi}_1|$ are different from the Hermitian conjugates of the right eigenstates $|\phi_1\rangle$. Both the left and right eigenstates do not belong to the Hilbert space, since these states have no Hilbert norm. This allows the Hamiltonian H to have complex eigenvalues.

For the field modes there are also right and left eigenstates,

$$H|\phi_k\rangle = \omega_k|\phi_k\rangle, \quad \langle\tilde{\phi}_k|H = \langle\tilde{\phi}_k|\omega_k. \tag{11}$$

The eigenstates are given by [11,2]

$$|\phi_1\rangle = N_1^{1/2}\Big[|1\rangle + \sum_k |k\rangle \frac{\lambda V_k}{(z-\omega_k)^+_{z_1}}\Big], \tag{12}$$

$$|\tilde{\phi}_1\rangle = [N_1^{c.c}]^{1/2}\Big[|1\rangle + \sum_k |k\rangle \frac{\lambda V_k}{(z-\omega_k)^-_{z_1^{c.c.}}}\Big], \tag{13}$$

$$|\phi_k\rangle = |k\rangle + \frac{\lambda V_k}{\eta_d^+(\omega_k)}\Big[|1\rangle + \sum_p |p\rangle \frac{\lambda V_p}{\omega_k - \omega_p + i\epsilon}\Big], \tag{14}$$

$$|\tilde{\phi}_k\rangle = |k\rangle + \frac{\lambda V_k}{\eta^+(\omega_k)}\Big[|1\rangle + \sum_p |p\rangle \frac{\lambda V_p}{\omega_k - \omega_p + i\epsilon}\Big]. \tag{15}$$

where

$$\frac{1}{\eta_d^+(\omega_k)} \equiv \frac{1}{\eta^+(\omega_k)} \frac{z_1 - \omega_k}{(z-\omega_k)^+_{z1}}. \tag{16}$$

The eigenstates of H form a bi-complete and bi-orthonormal set in the wave function space as

$$\langle\tilde{\phi}_\alpha|\phi_\beta\rangle = \delta_{\alpha,\beta}, \quad \sum_{\alpha=1,k} |\phi_\alpha\rangle\langle\tilde{\phi}_\alpha| = 1. \tag{17}$$

They give a complex spectral representation of H,

$$H = |\phi_1\rangle z_1 \langle\tilde{\phi}_1| + \sum_k |\phi_k\rangle\omega_k\langle\tilde{\phi}_k|. \tag{18}$$

In addition to this complex representation, there also exists a real representation of H in terms of the states $|\tilde{\phi}_k\rangle$ (called "Friedrichs eigenstates") [2]. These states, by themselves form a complete set

$$\sum_k |\tilde{\phi}_k\rangle\langle\tilde{\phi}_k| = 1, \tag{19}$$

and give the real spectral representation

$$H = \sum_k |\tilde{\phi}_k\rangle\omega_k\langle\tilde{\phi}_k|. \tag{20}$$

4 $\mathcal{H}$ function

Because of the instability due to the resonance effect, one can introduce a microscopic analog of Boltzmann's $\mathcal{H}$-theorem through the operator $\mathcal{H} = |\tilde{\phi}_1\rangle\langle\tilde{\phi}_1|$ defined at Eq. (1). This quantity is defined outside the Hilbert space.

Our definition of $\mathcal{H}$ through Gamow vectors is closely related to the microscopic $\mathcal{H}$ operator in the Liouville space that has been first introduced many years ago by one of the authors (I.P.) [5,6]. The relation between this operator and the one defined in Eq. (1) is briefly discussed in Appendix A.

Let us consider the time evolution of the expectation value of $\mathcal{H}$ with an initial state $|\xi\rangle$,

$$\langle\mathcal{H}(t)\rangle \equiv \langle\xi|\mathcal{H}(t)|\xi\rangle = \langle\xi(t)|\tilde{\phi}_1\rangle\langle\tilde{\phi}_1|\xi(t)\rangle, \tag{21}$$

where

$$|\xi(t)\rangle \equiv e^{-iHt}|\xi\rangle. \tag{22}$$

Since $\langle\tilde{\phi}_1|$ is an eigenstate of H, we have the exponential behavior

$$\langle\tilde{\phi}_1|\xi(t)\rangle = e^{-\gamma - i\tilde{\omega}_1}\langle\tilde{\phi}_1|\xi(0)\rangle, \tag{23}$$

which leads to

$$\langle\mathcal{H}(t)\rangle = e^{-2\gamma t}\langle\mathcal{H}(0)\rangle. \tag{24}$$

This shows that $\langle\mathcal{H}(t)\rangle$ is a Lyapounov function [5,6] (or the $\mathcal{H}$ function) that decays monotonically for all times.

5 Scattering of a wave packet

The monotonic decrease of the $\mathcal{H}$ function can be understood as a balance between entropy production and entropy flow. We will show this for the scattering process where a wave packet of the field collides with the atom.

As an initial condition at $t = 0$ we assume that the atom is in its ground state and the localized wave packet $|\xi\rangle$is away from the atom, as shown in Fig. 1. To simplify calculations, we choose a rectangular shape for the wave packet with an initial momentum k_0 and a width b in x,

$$\langle x|\xi\rangle = \frac{e^{ixk_0}}{(Wb)^{1/2}}[\theta(x - x_1) - \theta(x - x_2)], \tag{25}$$

where W is a normalization constant,

$$x_1 = x_0 + b/2, \qquad x_2 = x_0 - b/2, \tag{26}$$

and the state $\langle x|$ is defined through the momentum state $|k\rangle$ by

$$\langle x|k\rangle \equiv (2\omega_k L)^{-1/2}\exp(ikx). \tag{27}$$

The packet is centered at $x = x_0 < 0$. We assume that

$$b \gg |k_0|^{-1}. \tag{28}$$

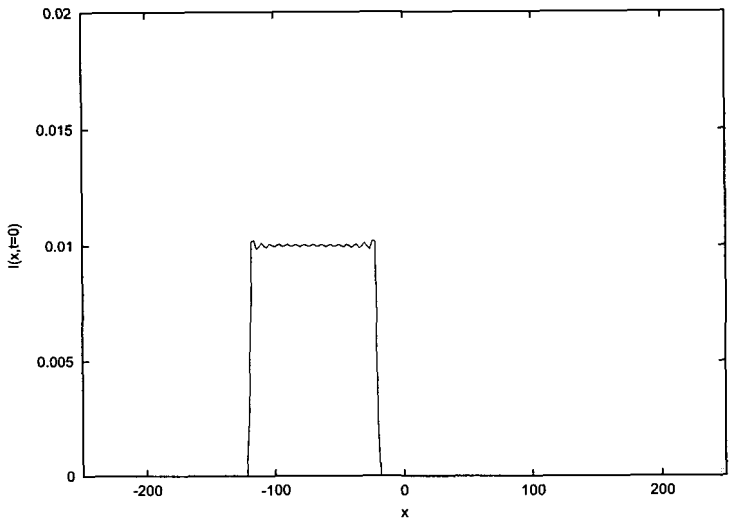

Figure 1. Field intensity $I(x,t)$ for a rectangular wave packet at $t = 0$. The wave packet is approaching the atom located at $x = 0$ from the left hand side. Parameters are $b = 100$, $x_0 = -70$, $k_0 = \tilde{\omega}_1 = 0.95$, $\gamma = 0.02$.

As we will see, this condition ensures a small distortion of the wave packet during free motion.

The momentum representation of the state is given by $\langle k|\xi\rangle \equiv (2\pi/L)^{1/2}\xi_k$ with

$$\xi_k = i\sqrt{\frac{\omega_k}{\pi bW}}\,\frac{\exp[-ix_2(k-k_0)] - \exp[-ix_1(k-k_0)]}{k-k_0}. \tag{29}$$

For the purpose of evaluating contour integrals, we may add an infinitesimal $i\epsilon$ to the denominator:

$$\frac{1}{k-k_0} \Rightarrow \frac{1}{k-k_0-i\epsilon}. \tag{30}$$

As $k = k_0$ is not a singular point in Eq. (29), we may choose the sign of ϵ at our convenience.

For $k_0 > 0$ the main part of the wave packet moves to the right towards the atom located at $x = 0$, while for $k_0 < 0$ it moves towards the left, away from the atom. Actually, as we will see later, there is a more detailed structure in the motion, which can be seen by decomposing the wave packet into two nonlocalized components moving in opposite directions.

In Figs. 1–3 we show numerical plots of the field intensity for the case $k_0 > 0$. The numerical plots are obtained by solving the Schrödinger equation through

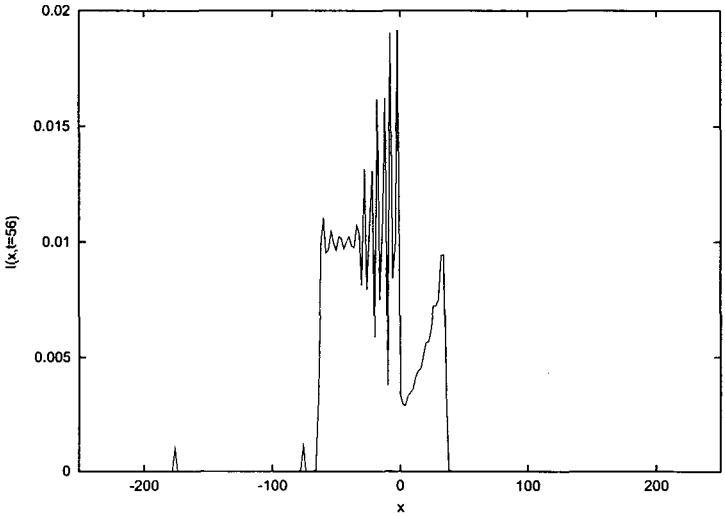

Figure 2. Wave packet during the collision with the atom at $t = 56$.

diagonalization of the Hamiltonian (see [17] for a description of the numerical method; we have used a 2500 × 2500 Hamiltonian matrix). In these figures the parameters have been chosen as $\omega_1 = 1$, $\lambda = 0.1$. For the numerical plots we have introduced a cutoff $k_{\max}$ for the momenta that leads to a discreteness Δx of space. We have $k_{\max} = \pi/\Delta x$. For the potential we have used $V_k = (2\omega_k/L)^{1/2}\theta(k_{\max} - |k|)$ with $L = 1250$ and $k_{\max} = 2\pi$. With these parameters we have obtained $\tilde{\omega}_1 = 0.95$ and $\gamma = 0.02$ by the numerical solution of $\eta^+(z_1) = 0$ (see Eq. (9)). We have chosen the value of k_0 at the resonance point $k_0 = \tilde{\omega}_1$ to maximize absorption of the wave packet by the atom.

In Fig. 2 one can see the interaction between the incident wave packet and the atom at a intermediate time $t_1 < t < t_2$ when the wave packet is passing through the atom (with $t_1 = |x_1|$ and $t_2 = |x_2|$). During this period the atom is excited. The interference pattern to the left of the atom is due to the interference between the incident wave packet and the emitted photons. To the right of the atom we have the part of the incident wave packet that has been transmitted. It presents a dip towards the origin as a result of absorption by the excited atom. For $t > t_2$ (Fig. 3) the excited state decays with an emission of resonant photons. The transmitted wave packet is seen to the right of the atom. The distant profile to the left of the atom (in the region $x < -Q$, where $Q \equiv t - t_2$) represents the photons that were emitted as soon as they were absorbed (i.e. the reflected photons). Around the atom at $x = 0$ we see the cloud and the field emitted after $t = t_2$ in the region

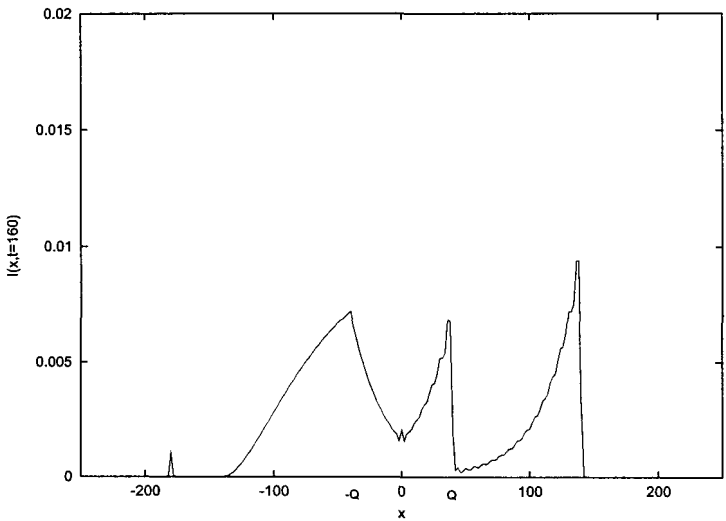

Figure 3. Field intensity after the collision with the atom at $t = 160$. The field emitted after the excitation of the atom appears in the region $|x| < Q \equiv t - t_2$. The transmitted wave packet is in the region $x > Q$ and the reflected wave packet is in the region $x < -Q$.

$|x| < Q$. In this region there is a universality in the structure of the field around the decaying atom. Indeed, if we prepare the initial atom in a bare excited state without field, the same cloud and emitted field appear in the time evolution [3].

6 Nonlocality in the wave packet

To study the motion of the wave packet, we introduce a decomposition of the initial wave packet into two nonlocal wave packets.

In the lowest order approximation of λ, the time evolution of the wave packet is given by the free motion. In x representation we have

$$\xi(x,t) \equiv \langle x|e^{-iHt}|\xi\rangle \approx \langle x|e^{-iH_0t}|\xi\rangle. \tag{31}$$

Inserting a complete set of momentum states we have

$$\xi(x,t) \approx \frac{1}{\sqrt{2\pi}} \int_{-\infty}^{\infty} \frac{dk}{\sqrt{2\omega_k}} e^{-i\omega_k t} e^{ikx} \xi_k. \tag{32}$$

Using $\omega_k = |k|$ and decomposing the wave packet into the two components,

$$\xi_k = \theta(k)\xi_k + \theta(-k)\xi_k = \xi_k^+ + \xi_k^-, \tag{33}$$

we have

$$\xi(x,t) \approx \frac{1}{\sqrt{2\pi}} \sum_{s=\pm} \int_{-\infty}^{\infty} \frac{dk}{\sqrt{2\omega_k}} e^{ik(x-st)} \varsigma_k^s$$
$$= \xi^+(x-t) + \xi^-(x+t). \tag{34}$$

Under free motion, the two components move undistorted in opposite directions. As shown in [10] both components are nonlocal, i.e., they have long tails in space. The long tails decrease as an inverse power law of the distance from the center of the wave packet. At $t = 0$ the long tails cancel to obtain the rectangular shape of $|\xi\rangle$. For $t > 0$, as the two components move away from each other, the long tails no longer cancel (we have called this the "curtain" effect [10]). The long tails may excite the atom immediately after $t = 0$. This nonlocal effect does not violate causality, because the components move with the finite speed $c = 1$ (the wave packet $|\xi^-\rangle$ moves to the left and $|\xi^+\rangle$ to the right). We note that nonlocal tails appear even if the initial wave packet is not strictly localized. For example, if it is a Gaussian wave packet, there will appear tails that extend over a much larger range than the Gaussian tails.

The relative intensity of the nonlocal wave packets depend on the initial momentum k_0. For $k_0 > 0$, with the condition (28), the intensity of the nonlocal wave packet moving towards the atom is large while the nonlocal wave packet away from the atom is small. The latter can be seen in Fig. 2. It corresponds to the two small peaks on the left hand side. The central part of the wave packet $|\xi^-\rangle$, as well as the tails extending to the sides are too small to be seen. In this figure the wave packet $|\xi^+\rangle$ (which is much larger) is already interacting with the atom.

For $k_0 < 0$ we have the opposite situation: the intensity of the nonlocal wave packet moving away from the atom is large while the nonlocal wave packet moving towards the atom is small.

As we will see in the next section, the two nonlocal wave packets give very different behavior of the $\mathcal{H}$ functions.

7 $\mathcal{H}$ functions of the nonlocal wave packets

The $\mathcal{H}$ functions associated with the two nonlocal wave packets $|\xi^+\rangle$ and $|\xi^-\rangle$ are given by

$$\langle \mathcal{H}^{\pm}(t) \rangle \equiv \langle \xi^{\pm} | \mathcal{H}(t) | \xi^{\pm} \rangle = |\langle \tilde{\phi}_1 | e^{-iHt} | \xi^{\pm} \rangle|^2. \tag{35}$$

Inserting a complete set of unperturbed states we write the amplitude as

$$\langle \tilde{\phi}_1 | e^{-iHt} | \xi^{\pm} \rangle = A_1^{\pm}(t) + A_f^{\pm}(t), \tag{36}$$

where

$$A_1^{\pm}(t) \equiv \langle \tilde{\phi}_1 | 1 \rangle \langle 1 | e^{-iHt} | \xi^{\pm} \rangle, \qquad A_f^{\pm}(t) \equiv \sum_k \langle \tilde{\phi}_1 | k \rangle \langle k | e^{-iHt} | \xi^{\pm} \rangle. \tag{37}$$

Restricting our interest to the weak coupling case $\lambda \ll 1$, we keep only the lowest order terms in λ. In the limit $L \to \infty$, with the relation between $\xi_k$and $\xi_k^{\pm}$ given

by Eq. (33) we have (note that $\xi_{\pm k} \neq \xi_k^{\pm}$)

$$A_f^{\pm}(t) \approx \int_0^{\infty} dk \frac{\lambda v(k)}{(z-k)_{z_1}^{+}} e^{-ikt} \xi_{\pm k}$$
$$= A_{f,\text{pole}}^{\pm}(t) + A_{f,\text{cut}}^{\pm}(t), \tag{38}$$

where

$$A_{f,\text{pole}}^{\pm}(t) \equiv \int_{-\infty}^{\infty} dk \frac{\lambda v(k)}{(z-k)_{z_1}^{+}} e^{-ikt} \xi_{\pm k},$$
$$A_{f,\text{cut}}^{\pm}(t) \equiv -\int_0^{\infty} dk \frac{\lambda v(-k)}{z_1 + k} e^{ikt} \xi_{\mp k}. \tag{39}$$

Similarly we have (using Eqs. (15) and (20))

$$A_1^{\pm}(t) \approx \int_0^{\infty} dk \frac{\lambda v(k)}{k - z_1} (e^{-ikt} - e^{-iz_1 t}) \xi_{\pm k}$$
$$= A_{1,\text{pole}}^{\pm}(t) + A_{1,\text{cut}}^{\pm}(t) \tag{40}$$

where

$$A_{1,\text{pole}}^{\pm}(t) \equiv \int_{-\infty}^{\infty} dk \frac{\lambda v(k)}{k - z_1} (e^{-ikt} - e^{-iz_1 t}) \xi_{\pm k},$$
$$A_{1,\text{cut}}^{\pm}(t) \equiv \int_0^{\infty} dk \frac{\lambda v(-k)}{z_1 + k} (e^{ikt} - e^{-iz_1 t}) \xi_{\mp k}. \tag{41}$$

For the "pole" contributions we evaluate the integrals by closing the integration path in the upper or lower infinite semicircle of complex k, respectively. The choice depends on the sign of the coefficient C in the exponential $\exp(iCk)$ in the integrand: upper for $C > 0$ and lower for $C < 0$ (see Eq. (29)). Neglecting any singularities of $v(k)$, the pole contribution is then given by the residue at the poles $k = z_1$ and $k = k_0 \pm i\epsilon$, if these are enclosed by the integration contour. Taking into account the explicit form of ξ_k in Eq. (29) we get

$$A_{f,\text{pole}}^{+}(t) \approx \pi \lambda v(\omega_1) e^{-iz_1 t} f(z_1) \Big(\theta[t_2 - t] e^{it_2(z_1 - k_0)} - \theta[t_1 - t] e^{it_1(z_1 - k_0)} \Big),$$
$$- \pi \lambda v(k_0) e^{-ik_0 t} f(z_1) \Big(\theta[t_2 - t] - \theta[t_1 - t] \Big) \tag{42}$$
$$A_{f,\text{pole}}^{-}(t) = 0, \tag{43}$$

and

$$A_{1,\text{pole}}^{+}(t) \approx \pi \lambda v(\omega_1) e^{-iz_1 t} f(z_1) \Big(\theta[t - t_2] e^{it_2(z_1 - k_0)} - \theta[t - t_1] e^{it_1(z_1 - k_0)} \Big),$$
$$- \pi \lambda v(k_0) e^{-ik_0 t} f(z_1) \Big(\theta[t - t_2] - \theta[t - t_1] \Big) \tag{44}$$
$$A_{1,\text{pole}}^{-}(t) = 0, \tag{45}$$

where

$$f(z_1) \equiv -2\sqrt{\frac{\omega_1}{\pi b W}} \frac{1}{z_1 - k_0}, \tag{46}$$

and $t_j \equiv |x_j|$ for $j = 1, 2$. Putting all the terms together we have

$$\langle \tilde{\phi}_1 | e^{-iHt} | \xi^+ \rangle \approx \pi \lambda v(z_1) f(z_1) e^{-iz_1 t} [e^{it_2(z_1 - k_0)} - e^{it_1(z_1 - k_0)}] + A(t)^+_{\rm cut}, \quad (47)$$

$$\langle \tilde{\phi}_1 | e^{-iHt} | \xi^- \rangle \approx A(t)^-_{\rm cut}, \quad (48)$$

where

$$A^{\pm}_{\rm cut}(t) = A^{\pm}_{1,{\rm cut}}(t) + A^{\pm}_{f,{\rm cut}}(t) = -\int_0^\infty dk \frac{\lambda v(-k)}{z_1 + k} e^{-iz_1 t} \xi_{\mp k}. \quad (49)$$

Inserting this in Eq. (35) we obtain the $\mathcal{H}$ functions of the nonlocal wave packets.

Now suppose that we start with the component $|\xi^-\rangle$ alone. In this case the excitation of the state is caused by off-resonance photons, since it involves the "cut" term, containing no pole contributions. Then, we have

$$\langle \mathcal{H}^-(t) \rangle = |A(t)^-_{\rm cut}|^2 \quad (50)$$

One can show that as a function of the initial distance x_0, this decreases as an inverse power law of x_0 for large $|x_0|$. On the other hand, it decays exponentially as a function of time. This is due to the excitation of the atom by the tails of the wave packets and the subsequent decay of the excited atom.

If we start with the component $|\xi^+\rangle$ alone, we have

$$\langle \mathcal{H}^+(t) \rangle = \left| \pi \lambda v(z_1) f(z_1) e^{-iz_1 t} [e^{it_2(z_1 - k_0)} - e^{it_1(z_1 - k_0)}] + A(t)^+_{\rm cut} \right|^2. \quad (51)$$

We again have a cut contribution due to the tails of the wave packet. But in addition we have the much larger pole contribution coming from resonant photons. This grows exponentially with the distances x_1 and x_2 as $t_j = |x_j|$. For $|x_0| \gg \gamma^{-1}$ we may neglect the cut contribution. Approximating $x_1 \sim x_2 \sim x_0$ we have

$$\langle \mathcal{H}^+(t) \rangle \propto e^{2\gamma(|x_0| - t)} \quad (52)$$

This shows that for larger distances $|x_0|$ from the atom we have larger values of $\langle \mathcal{H}^+(t) \rangle$ that come from the nonlocal wave packet $|\xi^+\rangle$ moving towards the atom. In order to have a *resonance* scattering process the wave packet has to be targeted towards the atom. In other words, there exists a long range "precollisional" correlation between the wave packet and the targeted atom. The increase of $\langle \mathcal{H}^+(t) \rangle$ with the distance $|x_0|$ implies that there is a stronger precollisional correlation for larger $|x_0|$.

8 Entropy production and entropy flow

We focus our attention on the scattering of the $|\xi^+\rangle$ wave packet. During the time the wave packet overlaps with the atom, the atom is excited. For a large enough wave packet one can keep the atom in a steady excited state. One may consider this as a nonequilibrium steady state, since it decays after the wave packet dissociates from the atom. This indicates that there is an entropy flow from the field to the atom. The $\mathcal{H}$ function associated with the atom must increase during the excitation process in spite of the fact that the total $\mathcal{H}$ function decreases.

To see this in more detail, let us write our $\mathcal{H}$ function as

$$\langle \mathcal{H}^+(t) \rangle = \langle \mathcal{H}^+(t) \rangle_{11} + \langle \mathcal{H}^+(t) \rangle_{1f} + \langle \mathcal{H}^(t) \rangle_{ff}, \tag{53}$$

where

$$\begin{aligned}
\langle \mathcal{H}^+(t) \rangle_{11} &= \langle \xi^+(t)|1\rangle\langle 1|\mathcal{H}|1\rangle\langle 1|\xi^+(t)\rangle, \\
\langle \mathcal{H}^+(t) \rangle_{1f} &= \sum_k \langle \xi^+(t)|1\rangle\langle 1|\mathcal{H}|k\rangle\langle k|\xi^+(t)\rangle + \text{c.c.}, \\
\langle \mathcal{H}^+(t) \rangle_{ff} &= \sum_{k,k'} \langle \xi^+(t)|k\rangle\langle k|\mathcal{H}|k'\rangle\langle k'|\xi^+(t)\rangle.
\end{aligned} \tag{54}$$

The $\mathcal{H}^+$ function is expressed as a superposition of the atom component $\langle \mathcal{H}^+ \rangle_{11}$, the atom-field correlation component $\langle \mathcal{H}^+ \rangle_{1f}$ and the field-field correlation component $\langle \mathcal{H}^+ \rangle_{ff}$. Using the results obtained in the previous section we have

$$\begin{aligned}
\langle \mathcal{H}^+(t) \rangle_{11} &\approx |A^+_{1,\text{pole}}(t)|^2, \\
\langle \mathcal{H}^+(t) \rangle_{1f} &\approx A^+_{1,\text{pole}}(t)[A^+_{f,\text{pole}}(t)]^{\text{c.c.}} + \text{c.c.}, \\
\langle \mathcal{H}^+(t) \rangle_{ff} &\approx |A^+_{f,\text{pole}}(t)|^2.
\end{aligned} \tag{55}$$

In Figs. 4 we plot the total $\mathcal{H}$ function as well as the individual correlation components. For easier visualization we have chosen here a smaller decay rate $\gamma = 0.005$ than in the previous figures. We discuss now the behavior of the different correlation components during the three stages of the scattering process.

1) Before the collision

For $t < t_1 = 20$ (i.e., before the moment when the wave packet touches the atom for the first time), all the decrease of the $\mathcal{H}$ function is due to the decrease of the field-field component $\langle \mathcal{H}^+(t) \rangle_{ff}$. During this period the precollisional correlation is destroyed.

2) During the collision

For $t_1 < t < t_2 = 120$, all the components contribute to the $\mathcal{H}$ function. This is the period during which the atom is excited. As we have expected, the atom component $\langle \mathcal{H}^+(t) \rangle_{11}$ increases monotonically due to the entropy flow from the field. The field-field component decreases as the wave packet dissociates during the collision. The atom-field correlation component $\langle \mathcal{H}^+(t) \rangle_{11}$ first increases and then decreases. This is due to the competition between the increase of the atom component and the decrease of the field component. As a whole the total $\mathcal{H}$ function maintains its monotonic decrease, because the increase in $\langle \mathcal{H} \rangle_{11}$ and $\langle \mathcal{H} \rangle_{1f}$ components are compensated by the decrease due to the field-field component.

3) After the collision

For $t > t_2$ the contribution to the $\mathcal{H}$ function comes, essentially, only from the atom component. The decrease of $\mathcal{H}$ is associated with the decay process of the atom. Note that the emitted photons move away from the atom and hence they only give a small contribution to the $\mathcal{H}$ function. They play the same role as the $|\xi^-\rangle$ wave packet moving away from the atom. The scattered field has a long range "postcollisional" correlation. The existence of this long range correlation is

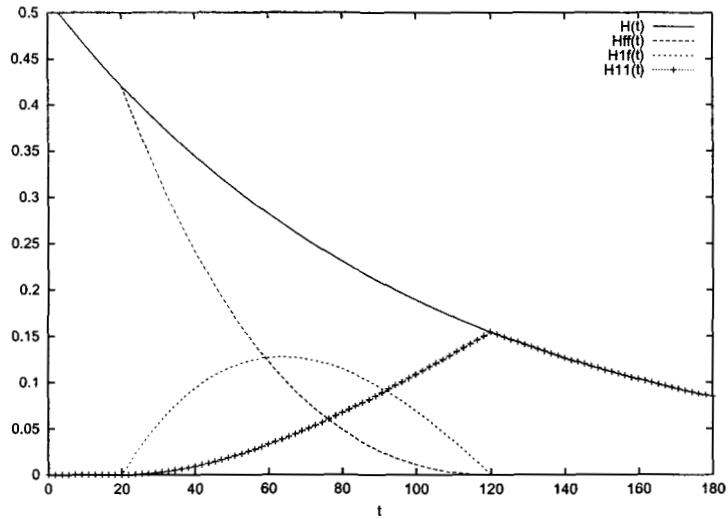

Figure 4. Total $\mathcal{H}^+(t)$ function, field component $\mathcal{H}^+_{ff}(t)$, atom-field component $\mathcal{H}^+_{1f}(t)$, and atom component $\mathcal{H}^+_{11}(t)$ in units of $C = |\pi\lambda v(\omega_1)f(z_1)|^2$. Time t is in units of ω_1^{-1}. Parameters are $t_1 = 20$, $t_2 = 120$, $\gamma = 0.005$, $k_0 = \bar{\omega}_1$.

obvious, since if at $t = t_3 > t_2$w e perform a momentum inversion of the scattered wave packet that dissociates from the atom, we should find the atom again in the ground state at a time $t = 2t_3 - t_1$. Some details of the momentum inversion will be discussed in the next section.

Let us now define more precisely the microscopic entropy production and entropy flow [5] in this scattering process. In thermodynamic systems, the entropy contains two components [18]

$$dS = d_iS + d_eS. \tag{56}$$

The term d_iS is the total internal entropy production, while d_eS is the entropy flow, coming from the interaction with the environment.

The second law of thermodynamics takes the form

$$d_iS \geq 0. \tag{57}$$

The entropy flow d_eS can be either negative or positive.

If we view the the atom-field system as a single isolated system, then the entropy flow is zero. We define the microscopic internal entropy production as

$$\frac{d_iS(t)}{dt} = -\frac{\langle\mathcal{H}(t)\rangle}{dt} \geq 0. \tag{58}$$

The total entropy production is a sum of the entropy productions coming from the field-field, the atom and the atom-field components,

$$\frac{d_i S(t)}{dt} = \left[\frac{dS(t)}{dt}\right]_{ff} + \left[\frac{dS(t)}{dt}\right]_{11} + \left[\frac{dS(t)}{dt}\right]_{1f}. \tag{59}$$

Neglecting the small correction coming from $|\xi^-\rangle$, we have

$$\left[\frac{dS(t)}{dt}\right]_{ij} = -\left[\frac{\langle \mathcal{H}^+(t)\rangle}{dt}\right]_{ij}. \tag{60}$$

As mentioned before, for the wave packet moving towards the atom the last two terms in Eq. (59) may be negative during the excitation period. During this period the atom is going further away from the ground state that corresponds to "equilibrium" in thermodynamic systems. But as a whole the total entropy production remains positive, because of the strong entropy production by the field-field component.

We can also view the atom as a subsystem interacting with its environment (the field). We have

$$\left[\frac{dS(t)}{dt}\right]_{11} = \frac{d_i S(t)}{dt} + \frac{d_e S(t)}{dt} \tag{61}$$

where

$$\frac{d_e S(t)}{dt} = -\left[\frac{dS(t)}{dt}\right]_{ff} - \left[\frac{dS(t)}{dt}\right]_{1f} \tag{62}$$

The first term in the r.h.s. is again the positive entropy production of the global scattering-absorption-emission process. The second term is the entropy flow due to the interaction of the atom with the field. This can be either positive or negative. As a whole the entropy change of the atom can be either negative or positive. In nonequilibrium thermodynamics, entropy flow can lead to self organization and the appearance of nonequilibrium structures (or dissipative structures) [19,20]. Our result shows that the excited state of the atom may be considered as an example of a nonequilibrium structure obtained from microscopic dynamics.

9 Momentum inversion

As far as the system is governed by dynamics, the $\mathcal{H}$ function should decrease monotonically in time. However, this is not the case when we perform some non-dynamical operation to the system. For example, if we perform a momentum inversion of the system at a given time t, the $\mathcal{H}$ function may jump to a higher or lower value. As we now show, the direction of the jump depends on the moment when we perform the momentum inversion. To some extent, we may say that the momentum inversion gives a positive or negative "injection" of correlations [5,6,2].

Momentum inversion is achieved by the antilinear time inversion operator T_I. Suppose that at time t_3 we perform a momentum inversion. Then the states $|\xi^\pm(t_3)\rangle$ change as

$$\begin{aligned} |\xi^\pm(t_3)\rangle &\equiv e^{-iHt_3}|\xi^\pm\rangle \\ &\Rightarrow T_I e^{-iHt_3}|\xi^\pm\rangle = e^{+iHt_3}|\xi^\mp\rangle = |\xi^\mp(-t_3)\rangle \end{aligned} \tag{63}$$

The ratio of the $\mathcal{H}$ function after the inversion to the one before the inversion is given by

$$j_r^{\pm}(t_3) \equiv \frac{\langle \xi^{\mp}(-t_3)|\mathcal{H}|\xi^{\mp}(-t_3)\rangle}{\langle \xi^{\pm}(t_3)|\mathcal{H}|\xi^{\pm}(t_3)\rangle} = \frac{\exp(2\gamma t_3)|\langle \tilde{\phi}_1|\xi^{\mp}\rangle|^2}{\exp(-2\gamma t_3)|\langle \tilde{\phi}_1|\xi^{\pm}\rangle|^2} \tag{64}$$

Suppose that at $t = 0$ we start with the component $|\xi^+\rangle$alone. The wave packet moves to the right. We perform momentum inversion at a time when the wave packet has excited the atom and the atom is emitting the decay products, as in Fig. 3. The momentum inversion (point A in Fig. 5) causes the $\mathcal{H}$ function to jump up, as the decay products start to move towards the atom (we have an increase of "order" due to the injection of the correlations from outside [2]). After the inversion, we have a "backwards" evolution and we follow the inverse sequence, from Fig. 3 to 1. The decay products move towards the atom, which subsequently absorbs them. Eventually the field collects itself back into the initial wave packet, which then moves away from the atom. We may interpret the continued decrease of $\mathcal{H}$ (solid line in Fig. 5) as due to the disappearance of the "anomalous" correlations that were injected to the system at point A to ensure that all the emitted field is re-absorbed by the atom. The $\mathcal{H}$ function continues to decrease as the wave packet moves away and the atom decays to the ground state.

Note that the larger t_3 is in Eq. (64) the higher is the entropy jump. There is an "entropy barrier." The more we wait, the more "difficult" it is to bring the system back to its initial state after momentum inversion. For $t \to \infty$ we have an infinite entropy barrier.

A different situation occurs if we perform the momentum inversion earlier, at a time when the wave packet is still far from the atom. The wave packet then changes to $|\xi^-\rangle$ and moves to the left. At the moment of inversion (point B in Fig. 5) we have [cf. Eq. (52)] $j_r(t) \propto \exp(-2\gamma|x_3|)$. The $\mathcal{H}$ function jumps down, due to the change of the direction of motion (dotted line in Fig. 5). The momentum reversal turns the precollisional correlations into postcollisional correlations.

If we start at $t = 0$ with the component $|\xi^-\rangle$ alone and perform a momentum inversion some time later, then the $\mathcal{H}$ function jumps up, because the wave packet, which was moving away from the atom, now moves towards the atom. After the inversion the $\mathcal{H}$ function decreases in time as described previously (see Fig. 6).

10 Concluding remarks

We have described resonance scattering in terms of entropy production and entropy flow. During the collision there is an entropy flow from the field to the atom. As a result, we can interpret the excited state as a nonequilibrium structure in our microscopic dynamical system. To ensure the resonance scattering occurs, we have to target the wave packet to the atom at the initial time. This gives a large value of the $\mathcal{H}$ function given by a precollisional correlation. In contrast, we have a small value of the $\mathcal{H}$ function for wave packets moving away from the atom, given by a postcollisional correlation. The momentum inversion turns precollisional correlations into postcollisional correlations or vice versa, making the $\mathcal{H}$ function

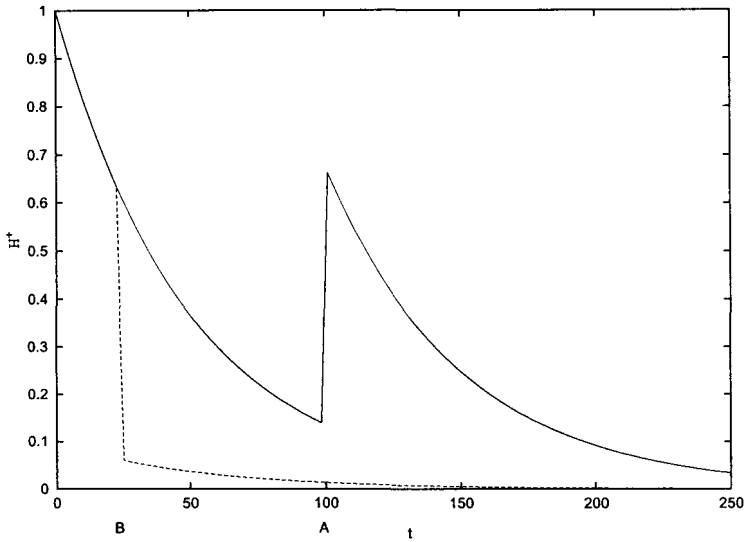

Figure 5. Schematic plot of the Lyapounov function $\langle \mathcal{H}^+(t) \rangle / \langle \mathcal{H}^+(0) \rangle$. The time inversion at A (after the wave packet collides with the atom) creates correlations; at B (before the wave packet collides with the atom) it destroys correlations. In this figure and in Fig. 6 time t is measured in units of the inverse frequency $\omega_1^{-1} = 1$ of the unstable state.

jump in a positive or negative direction depending on the moment of the momentum inversion.

The absorption and emission processes are part of a global process going from an "ordered" situation (the distribution of the field being not symmetric, as the field is concentrated on one side of the atom) to a "disordered" situation (the field distributed more symmetrically on both sides of the atom, due to the emission process). This is analogous to the increase of the entropy in statistical mechanics, associated with the approach to equilibrium. Here "equilibrium" means the atom in the ground state and the field emitted away to infinity. The $\mathcal{H}$ function gives an indication of how far the system is to its final asymptotic state [2]. A large class of initial conditions, including ones giving rise to a temporary "backwards" evolution (e.g. after a momentum inversion) eventually end up with the atom relaxing to the ground state and all the field moving away from the atom to infinity.[b]

The relation between the value of the $\mathcal{H}$ function and the direction of the wave packet (on target or off target) is more interesting when we consider systems in

[b] An exception is given by initial conditions where a wave packet is at an infinite distance from the atom, and is directed towards the atom. Such states take an infinite amount of time to reach the "equilibrium" asymptotic state. This corresponds to the existence of an infinite entropy barrier mentioned before.

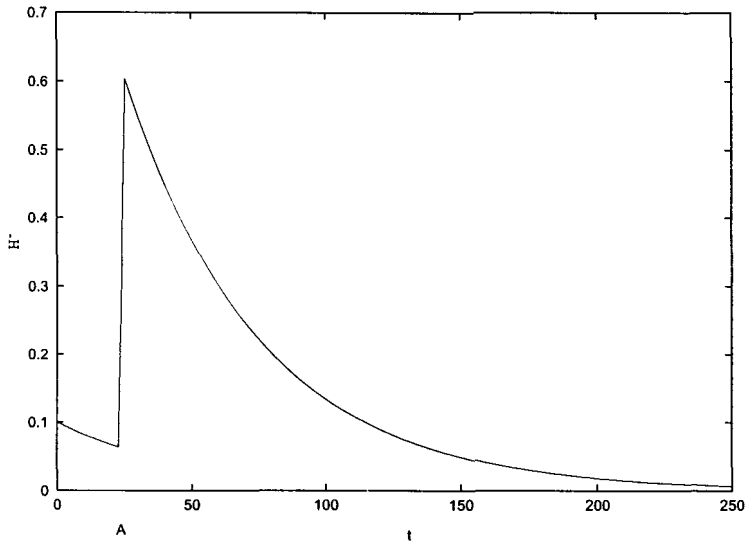

Figure 6. Schematic plot of the Lyapounov function $\langle \mathcal{H}^-(t) \rangle / \langle \mathcal{H}^+(0) \rangle$. The time inversion at A creates correlations and causes $\mathcal{H}^-$ to jump up.

more that one-dimensional space. We will present the detailed description of three-dimensional scattering elsewhere [21].

Many elements found in the microscopic $\mathcal{H}$ function can be included on the macroscopic level. Our example supports the view that the second law of thermodynamics can be formulated on a dynamical basis, avoiding additional probabilistic arguments [6]. The origin of irreversible behavior is rooted in the microscopic level. Here instability in dynamics coming from resonances plays a central role.

Acknowledgments

We thank Prof. I. Antoniou, Dr. E. Karpov, Prof. R. Passante and Prof. G. Pronko for helpful suggestions and interesting discussions. We acknowledge the International Solvay Institutes for Physics and Chemistry, the Engineering Research Program of the Office of Basic Energy Sciences at the U.S. Department of Energy, Grant No DE-FG03-94ER14465, the Robert A. Welch Foundation Grant F-0365, European Commission Grant No. HPHA-CT-2001-40002, the National Lottery of Belgium and the Communauté Française de Belgique for supporting this work.

Appendix

A $\mathcal{H}$ function in the Liouville space

We introduce the superoperator $M = \Lambda^\dagger \Lambda$ (see [5,3]), where Λ is a "star-unitary" transformation that puts dynamics in a "kinetic representation." Λ is an extension (to nonintegrable systems) of unitary transformations diagonalizing the Hamiltonian in integrable systems. It maps bare particles to dressed unstable particles or quasiparticles [11]. Λ-transformed density operators obey Markovian kinetic equations, that to lowest order agree with the usual kinetic equations, e.g., the Pauli master equation.

M is similar to a Gibbs entropy with the replacement of unitary transformations U by Λ [for unitary transformations the Gibbs entropy is an invariant of motion, while with Λ the entropy evolves monotonically].

To connect the operator M with our present $\mathcal{H}$ function, we note that for systems with many particles or field modes we may introduce a reduced Lyapounov operator

$$M_\alpha = \Lambda^\dagger |\hat{n}_\alpha\rangle\rangle\langle\langle \hat{n}_\alpha | \Lambda, \tag{65}$$

where $\hat{n}_\alpha$ is a one-particle observable corresponding to the bare particle α and $\Lambda^\dagger |\hat{n}_\alpha\rangle\rangle$ is the transformed observable associated with particle α dressed by the interactions (quasiparticle). In Eq. (65) we use the notation $|A\rangle\rangle$ and $\langle\langle B|$ for kets and bras in the Liouville space, where A and B are ordinary quantum mechanical operators. The inner product is defined as

$$\langle\langle B|A\rangle\rangle = \mathrm{Tr}(A^\dagger B) \tag{66}$$

We use as well the notation

$$|a;b\rangle\rangle = |a\rangle\langle b|, \quad \langle\langle a;b| = |b\rangle\langle a| \tag{67}$$

for dyadic operators.

The Lyapounov function is the expectation value $\langle\langle M_\alpha(t)\rangle\rangle \equiv \langle\langle \rho(t)|M_\alpha|\rho(t)\rangle\rangle$, where $|\rho(t)\rangle\rangle \equiv \exp(-iL_H t)|\rho\rangle\rangle$, and $L_H = [H, \,]$ is the Liouville operator. For N-particle systems, $\langle\langle M_\alpha(t)\rangle\rangle$ is a generalized Boltzmann $\mathcal{H}$ function [7]. We will present more details elsewhere. Here we restrict ourselves to the Friedrichs model. As shown in [3], for states with no diagonal singularity in momentum representation, there is a simple relation between this Lyapounov function M_α and the $\mathcal{H}$ operator in Eq. (21). For example, if ρ is a pure state $\rho = |\xi\rangle\langle\xi|$ normalized as $\mathrm{Tr}(\rho) = 1$, we have for $|\hat{n}_1\rangle\rangle = |1;1\rangle\rangle$,

$$\langle\langle M_1(t)\rangle\rangle \equiv \langle\langle \rho(t)|\tilde{\rho}_1^0\rangle\rangle\langle\langle \tilde{\rho}_1^0|\rho(t)\rangle\rangle. \tag{68}$$

where

$$|\tilde{\rho}_1^0\rangle\rangle = \Lambda^\dagger |1;1\rangle\rangle \tag{69}$$

In Eq. (68) the state $\langle\langle\rho(t)|$ plays the role of a test function with no diagonal singularity. This allows us to write $\langle\langle \rho(t)|\tilde{\rho}_1^0\rangle\rangle = \langle\langle \rho(t)|\tilde{\phi}_1;\tilde{\phi}_1\rangle\rangle$ [3]. Thus we obtain

$$\langle\langle M_1(t)\rangle\rangle = \langle\langle \rho(t)|\tilde{\phi}_1;\tilde{\phi}_1\rangle\rangle\langle\langle \tilde{\phi}_1;\tilde{\phi}_1|\rho(t)\rangle\rangle. \tag{70}$$

or

$$\langle\langle M_1(t)\rangle\rangle = [\langle\mathcal{H}(t)\rangle]^2, \tag{71}$$

where $\langle\mathcal{H}(t)\rangle = \langle\xi|\mathcal{H}(t)|\xi\rangle$. This shows the relation between M and the $\mathcal{H}$ function considered in this paper.

For states with diagonal singularities the M_1op erator is no longer factorizable in terms of Gamow states. States with diagonal singularities occur naturally in systems in the thermodynamic limit, e.g., for a particle coupled to a heat bath.

References

1. K. Friedrichs, Commun. Pure Appl. Math. **1**, 361 (1948).
2. T. Petrosky, I. Prigogine and S. Tasaki, Physica A **173**, 175 (1991).
3. T. Petrosky, G. Ordonez and I. Prigogine, Phys. Rev. A **64**, 062101 (2001).
4. M. de Haan, C. George, and F. Mayne, Physica A **92**, 584 (1978).
5. I. Prigogine, C. George, F. Henin, L. Rosenfeld, Chemica Scripta **4**, 5 (1973).
6. I. Prigogine, *From being to becoming* (Freeman, New York, 1980).
7. T. Petrosky and I. Prigogine, Adv. Chem. Phys. **99**, 1 (1997).
8. J. Mehra and H. Rechenberg, *The Historical Development of Quantum Theory. Vol. 1, Part 1* (Springer Verlag, New York 1982).
9. M. de Haan and C. George, J. Plasma Phys. **59** (part 4), 619 (1998).
10. E. Karpov, G. Ordonez, T. Petrosky, I. Prigogine, and G. Pronko, Phys. Rev. A **62**, 012103 (2000).
11. G. Ordonez, T. Petrosky and I. Prigogine, Phys. Rev. A **63**, 052106 (2001).
12. B. Misra and E.C.G. Sudarshan, J. Math. Phys. **18**, 756 (1977).
13. L. A. Khalfin, Zh. Eksp. Theor. Fiz. **33**, 1371 (1957) [Sov. Phys. JETP **6**, 1053 (1958).
14. N. Nakanishi, Prog. Theor. Phys. **19**, 607 (1958).
15. E.C.G. Sudarshan, C. B. Chiu and V. Gorini, Phys. Rev. D **18**, 2914 (1978).
16. A. Böhm and M. Gadella, *Dirac Kets, Gamow Vectors and Gelfand Triplets*, (Springer Lecture Notes on Physics, Vol. 348, Springer, New York, 1989).
17. T. Petrosky, G. Ordonez and I. Prigogine, Phys. Rev. A **62**, 042106 (2000).
18. I. Prigogine, *Thermodynamics of irreversible processes* (John Wiley Interscience, 3rd edition, 1967).
19. G. Nicolis and I. Prigogine, *Self-organization in nonequilibrium systems* (John Wiley Interscience, 1977).
20. D. Kondepudi and I. Prigogine, *Modern thermodynamics* (John Wiley and Sons, Ltd., 1998).
21. E. Karpov, G. Ordonez, T. Petrosky and I. Prigogine, unpublished.

NONLOCALITY AND CAUSALITY IN QUANTUM ELECTRODYNAMICS

G. COMPAGNO[1], G.M. PALMA[1], R. PASSANTE[1,2]A ND F. S. PERSICO[1,2]
[1] *Istituto Nazionale di Fisica della Materia and Dipartimento di Scienze Fisiche ed Astronomiche, Universitá degli Studi di Palermo, Via Archirafi 36, I-90123 Palermo, Italy*
[2] *Istituto per le Applicazioni Interdisciplinari della Fisica, Consiglio Nazionale delle Ricerche, Via Ugo La Malfa 153, I-90147 Palermo, Italy*

The problem of relativistic causality in atom-radiation interacting systems is investigated. The excitation transfer in the Fermi problem is considered and it is shown that, independently from the initial state of the two atoms, it is causal, as well as the propagation of the electromagnetic field emitted by an excited atom. Nonlocal interatomic correlations and nonlocal spatial field correlations however appear in the evolution of the systems considered. These nonlocal correlations are shown to be compatible with relativistic causality. Our results are discussed with reference to questions recently raised in the literature about possible violations of relativistic causality.

1 Introduction

The problem of relativistic causality in quantum field theory has received much attention since the beginning of quantum electrodynamics in connection with the so-called Fermi problem, that is the excitation transfer between two atoms [1,2,3,4,5,6,7,8]. This and related problems have been investigated until very recently [9,10,11]. In the Fermi problem there are two atoms separated by a distance r; one of them (atom A) is initially in an excited state and the other (atom B) in its ground state. Relativistic causality requires that the excitation probability of atom B must vanish before the causality time $t = r/c$. Recently, a series of papers by Hegerfeldt have questioned, on the basis of very general arguments, about a possible violation of the relativistic causality in this system [3,12,13]. Hegerfeldt's considerations are based on a general theorem stating that any quantum system described by a Hamiltonian with a spectrum bounded from below, instantaneously develops tails of the wavefunction spreading all over the space . Apparently, this may yield an instantaneous nonvanishing excitation probability of atom B, and thus a possible violation of relativistic causality. Also, it is known that the field emitted by a field source usually has nonlocal spatial correlations [14] and that instantaneous interatomic correlations may appear in matter-radiation interacting systems [15]. On the other hand, the energy density of the electromagnetic field emitted by an excited atom propagates causally [16,17,18] and specific calculations have proved causality for the excitation transfer in the Fermi problem, within the approximations used [5,9]. Thus, the causality problem is still controversial and the relation between causality and the emergence of nonlocal correlations seems worth deeper investigation.

In this paper we consider the problem of causality in quantum electrodynamics and its relation with the appearance of nonlocal atomic and field correlations. We consider two two-level atoms (A and B) in vacuo, separated by a distance r and interacting with the electromagnetic radiation field in the multipolar coupling

scheme and within dipole approximation. By solving the Heisenberg equations of motion for the atomic operators, we show that, independently from the initial state of the two atoms, the evolution of single-atom operators is not affected by the presence of the other atom until the "causality time" r/c, even if instantaneous interatomic correlations develop. We also show that the energy density of the field emitted by an excited two-level atom propagates causally, but nonlocal spatial correlations of the emitted field appear. Finally, we give some arguments indicating that our results, which show a strict causal behaviour of "local" quantities such as single-atom operators or field energy densities, are not in contradiction with the Hegerfeldt theorem.

2 Atomic and field dynamics

The Hamiltonian describing two identical two-level atoms A and B, localized at points 0 and $\mathbf{r}$, respectively, interacting with the electromagnetic radiation field in the multipolar coupling scheme and in the dipole approximation, is [19]

$$\begin{aligned} H = {} & \hbar\omega_0 \left(S_z^{(A)} + S_z^{(B)}\right) + \sum_{\mathbf{k}j} \hbar\omega_k a_{\mathbf{k}j}^\dagger a_{\mathbf{k}j} \\ & + \sum_{\mathbf{k}j} \left\{ \epsilon_{\mathbf{k}j} a_{\mathbf{k}j} \left(S_+^{(A)} + e^{i\mathbf{k}\cdot\mathbf{r}} S_+^{(B)}\right) + \epsilon_{\mathbf{k}j}^\star a_{\mathbf{k}j}^\dagger \left(S_-^{(A)} + e^{-i\mathbf{k}\cdot\mathbf{r}} S_-^{(B)}\right) \right. \\ & \left. - \epsilon_{\mathbf{k}j} a_{\mathbf{k}j}^\dagger \left(S_+^{(A)} + e^{-i\mathbf{k}\cdot\mathbf{r}} S_+^{(B)}\right) - \epsilon_{\mathbf{k}j}^\star a_{\mathbf{k}j} \left(S_-^{(A)} + e^{i\mathbf{k}\cdot\mathbf{r}} S_-^{(B)}\right) \right\} \end{aligned} \tag{1}$$

where S_z, S_+, S_- are the atomic pseudospin operators, ω_0 is the transition frequency of the atoms, and the coupling constant $\epsilon_{\mathbf{k}j}$ is given by

$$\epsilon_{\mathbf{k}j} = i\sqrt{\frac{2\pi\hbar\omega_k}{V}}\mathbf{e}_{\mathbf{k}j} \cdot \boldsymbol{\mu}_{21} \tag{2}$$

($\mathbf{e}_{\mathbf{k}j}$ are real polarization vectors, $\boldsymbol{\mu}_{21}$ is the real matrix element of the transition dipole moment and V the quantization volume).

The Heisenberg equation for the atomic operator $S_z^{(A)}$ in the second Born approximation can be put in the form [6]

$$\dot{S}_z^{(A)} = \dot{S}_z^{(AA)} + \dot{S}_z^{(AB)} \tag{3}$$

where $\dot{S}_z^{AA}$ is the same term which would be obtained in the absence of the atom B and $\dot{S}_z^{AB}$ is the contribution of atom B to the evolution of atom A. Because we are interested in causality issues, the first contribution is not relevant for our purposes. The second contribution can be evaluated and the result is

$$\begin{aligned} \dot{S}_z^{(AB)} = {} & -\frac{i}{\hbar} \left(\mu_{21}\right)_m \left(\mu_{21}\right)_n e^{i\omega_0 t} D_{mn}^r \left\{ \left(\left(S_+^{(A)} S_-^{(B)}\right)_{t=0} e^{i\omega_0(r/c-t)} \right. \right. \\ & \left. \left. + \left(S_+^{(A)} S_+^{(B)}\right)_{t=0} e^{-i\omega_0(r/c-t)} \right) \Theta(ct-r) \right\} + \text{h.c.} \end{aligned} \tag{4}$$

where we have defined the differential operator

$$D_{mn}^r = \frac{1}{r}\left(\left(\delta_{mn} - \hat{r}_m\hat{r}_n\right)\frac{\partial^2}{\partial r^2} + \left(\delta_{mn} - 3\hat{r}_m\hat{r}_n\right)\left(\frac{1}{r^2} - \frac{1}{r}\frac{\partial}{\partial r}\right)\right) \tag{5}$$

A similar result is obtained for $\dot{S}_+^{(A)} = \dot{S}_+^{(AA)} + \dot{S}_+^{(AB)}$, and the contribution of atom B to the time evolution of $S_+^{(A)}$ is

$$\dot{S}_+^{(AB)} = -\frac{2i}{\hbar}\left(\mu_{21}\right)_m \left(\mu_{21}\right)_n D^r_{mn} \left\{ \left(\left(S_z^{(A)} S_+^{(B)} \right)_{t=0} e^{-i\omega_0(r/c-t)} + \left(S_z^{(A)} S_-^{(B)} \right)_{t=0} e^{i\omega_0(r/c-t)} \right) \Theta(ct-r) \right\} \tag{6}$$

The presence of the Heaviside function $\Theta(ct-r)$ in equations (4,6) ensures a causal behaviour of the atomic operators. There is no influence of atom B on the evolution of the operators of atom A before the causality time $t = r/c$. Because (4,6) are operator equations, this is valid independently of the initial state. We expect that the evolution of any combination of operators of only one atom (i.e. excluding quantities containing products of operators relative to different atoms such as interatomic correlations) behaves similarly.

The situation changes when products of operators pertaining to different atoms are considered, as in the case of atomic correlations. Let consider the specific case of an initial state of two uncorrelated atoms, in the vacuum state of the field, of the form [15]

$$|\Psi\rangle = \frac{1}{2}\left(|\uparrow_A\rangle + |\downarrow_A\rangle\right)\left(|\uparrow_B\rangle + |\downarrow_B\rangle\right) \tag{7}$$

At $t = 0$, we have $\langle S_z^{(A)} S_z^{(B)} \rangle_{t=0} = 0$. At time t, the average value of the correlation between the operators $S_z^{(A)} S_z^{(B)}$ is given by (for $r \gg ct$)

$$\langle S_z^{(A)} S_z^{(B)} \rangle_t = -\frac{8c\left(\mu_{21}\right)_m \left(\mu_{21}\right)_n}{\pi\hbar\omega_0} \left(\frac{1-\cos\omega_0 t}{\omega_0} - \frac{1-\cos 2\omega_0 t}{4\omega_0} \right) \times \frac{1}{r^4}\left(\delta_{mn} - 2\hat{r}_m\hat{r}_n\right) \tag{8}$$

Thus, instantaneous interatomic correlations develop in the system, in spite of the fact that the dynamics of local quantities, i.e. quantities pertaining to a single atom, is causal.

A similar situation occurs when field observables are considered. For example, if we evaluate the electric energy density of the field emitted by an initially excited two-level atom located at $\mathbf{r} = 0$ in the vacuum state of the field and described by the multipolar Hamiltonian, we find [17]

$$\langle \uparrow \{0_{\mathbf{k}j}\} \mid \mathcal{H}(\mathbf{r},t) \mid \uparrow \{0_{\mathbf{k}j}\} \rangle = -\frac{1}{V}\sum_{\mathbf{k}j} \mathbf{e}_{\mathbf{k}j} \cdot \boldsymbol{\mu}_{21} \left(\mathbf{e}_{\mathbf{k}j}\right)_m \left(\boldsymbol{\mu}_{21}\right)_n \frac{\omega_k}{\omega_k - \omega_0} \times \Re\left\{ e^{i\mathbf{k}\cdot\mathbf{r}} D^r_{mn} \left(e^{-i\omega_k r/c} - e^{i(\omega_0-\omega_k)t} e^{-i\omega_0 r/c} \right) \Theta(ct-r) \right\} \tag{9}$$

where $\mathcal{H}(\mathbf{r},t)$ is the electric field energy density operator and the space- and time-uniform zero-point energy density has been subtracted. The presence of the Θ function ensures causality in the propagation of the electric energy density. It should be noted that the energy density of the total electric field (transverse plus

longitudinal) appears in eq. (9). However, similarly to the atomic operators case, a nonlocal behaviour is found when the average value of the spatial correlation of equal time field operators is evaluated. For example, the following equal-time correlation function of the (total) electric field emitted by an atom located at $\mathbf{R} = 0$ during spontaneous emission

$$\langle \uparrow \{0_{\mathbf{k}j} \, | \mathbf{E}_i(\mathbf{r}, t) \mathbf{E}_j(\mathbf{r}', t) \, | \uparrow \{0_{\mathbf{k}j}\} \rangle \tag{10}$$

is different from zero even if $|\mathbf{r} - \mathbf{r}'| > ct$, provided $r > ct$ and $r' > ct$ [20].

Thus the examples discussed above show that the propagation of local field observables such as the field energy density (that is, observables expressed in terms of field operators at the same point of space) is causal, while expectation values of quantities containing field operators at different points of space show a nonlocal behaviour.

3 Conclusions

In this paper we have investigated some specific examples of atom-radiation interacting systems, and shown that: i) the evolution of single-atom observables, as well as of local field observables such as the field energy density, is strictly causal; ii) nonlocal interatomic correlations and nonlocal spatial field correlations emerge in the evolution of matter-radiation systems. These two statements on the evolution of the interacting system may appear incompatible, but this is not the case. The point is that, in order to evaluate the correlation between atomic or field observables at two points 1 and 2, separated by a distance r, two local measures are necessary. The two observers must then communicate to each other the result of their measures. This requires at least a time equal to the "causality" time $t = r/c$. Therefore the existence of nonlocal correlations does not imply a violation of relativistic causality. Naturally, in principle we cannot exclude that one could envisage some other procedure for using the correlations' nonlocal behaviour to transmit some kind of information at superluminal velocity. This, however, would appear to violate relativistic causality. We can only say that the nonlocality we find is compatible with relativistic causality.

Finally, we wish to stress that the causal result for the Fermi problem we obtained in eqs. (4,6) is not necessarily inconsistent with Hegerfeldt theorem, as Hegerfeldt himself suggested [3]. This theorem states that any quantum system described by a Hamiltonian with a spectrum bounded from below instantaneously develops infinite tails of the wavefunction. In quantum field theory, the definition of a Hamiltonian with interactions and bounded from below implies renormalization. The eigenstates of a renormalized Hamiltonian are dressed states, in our case a superposition of atomic and photon states. These states are not localized in space, due to their photon part. In the case of the Fermi problem, this means that the two "dressed" atoms have some overlap since the beginning. In other words, a part of dressed atom A is already present at $t = 0$ at the position of bare atom B. In view of this fact, the nonvanishing excitation probability found by Hegerfeldt for $t < r/c$ is not surprising, and it is not due to an instantaneous influence of one atom on the other, but only to the instantaneous effect of one (delocalized) dressed atom on the

other dressed atom. Thus it does not yield a violation of causality. Our method based on the partition (3) of the (bare) atomic operators allows an unambiguous identification of which contribution to the evolution of one atom comes from the other (bare) atom, and indeed our results show a strict causality for the excitation transfer between the two atoms.

The authors acknowledge partial financial support by the European Commission under Contract No. HPHA-CT-2001-40002, by Comitato Regionale di Ricerche Nucleari e di Struttura della Materia and by Ministero dell'Universitá e della Ricerca Scientifica e Tecnologica.

References

1. E. Fermi, Rev. Mod. Phys. **4**, 87 (1932)
2. P.W. Milonni, P.L. Knight, Phys. Rev. A **10**, 1096 (1974)
3. G.C. Hegerfeldt, Phys. Rev. Lett. **72**, 596 (1994)
4. D. Buchholtz, J. Yngvason, Phys. Rev. Lett. **73**, 613 (1994)
5. P.W. Milonni, D.F.V. James, H. Fearn, Phys. Rev. A **52**, 1525 (1995)
6. G. Compagno, G.M. Palma, R. Passante, F. Persico, Chem. Phys. **198**, 19 (1995)
7. L. Maiani, M. Testa, Phys. Lett. B **356**, 319 (1995)
8. P.R. Berman, B. Dubetsky, Phys. Rev. A **55**, 4060 (1997)
9. E.A. Power, T. Thirunamachandran, Phys. Rev. A **56**, 3395 (1997)
10. E. Karpov, G. Ordonez, T. Petrosky, I. Prigogine, G. Pronko, Phys. Rev. A **62**, 012103 (2000)
11. T. Petrosky, G. Ordonez, I. Prigogine, Phys. Rev. A **62**, 042106 (2000)
12. G.C. Hegerfeldt, quantum-ph/9707016
13. G.C. Hegerfeldt, quantum-ph/9806036
14. A. La Barbera, R. Passante, Phys. Lett. A **206**, 1 (1995)
15. A.K. Biswas, G. Compagno, G.M. Palma, R. Passante, F. Persico, Phys. Rev. A **42**, 4291 (1990)
16. V.P. Bykov, A.A. Zadernovskii, Opt. Spektr. **48**, 229 (1980); Opt. Spectrosc. [USSR] **48**, 130 (1980)
17. G. Compagno, R. Passante, F. Persico, J. Mod. Opt. **37**, 1377 (1990)
18. G. Compagno, G.M. Palma, R. Passante, F. Persico, J. Phys. B **28**, 1105 (1995)
19. G. Compagno, R. Passante, F. Persico, *Atom-Field Interactions and Dressed Atoms*, Cambridge University Press, 1995
20. R. Passante, F. Persico, L. Rizzuto, to be published

DISCUSSION

Chairman: O. Kocharovskaya

G. Pronko: You said that in the two atoms problem the interaction be-

tween two atoms spreads with the velocity of light and there is no contradiction to Hegerfeldt's theorem because of renormalization. Correct?

R. Passante: In the time evolution of one atom, there is no influence of the other atom before the causality time. This is the result of our calculations. Now, my question is how this is related to Hegerfeldt's theorem, which apparently says that we should have an instantaneous effect on the other atom. The point is that Hegerfeldt's theorem can be applied only to renormalized Hamiltonians, because it requires an Hamiltonian bounded from below. Both atoms are therefore dressed because we perform a renormalization, and the renormalization procedure includes some part of the dressing into the physical object. All atoms are now extended objects and there is some component of atom 1 in all space. For example, there is a photon cloud of atom 1 also in the place where atom 2 is located. But this photon cloud is already there when we prepare the initial state. Thus, the evolution of atom 2 is not due to an instantaneous propagation from atom 1 to atom 2, but to the photon cloud of atom 1 which was already present at the position of atom 2, because we are considering a dressed atom. So, if we look carefully at the problem, there is no contradiction at all with Hegerfeldt's theorem.

G. Hegerfeldt: What I have shown is that if one atom is in the ground state here and another atom is excited over there then the transition probability of the ground state atom to excited state will be immediately non zero under some spectral conditions. Nothing more. The question is how does this excitation arise on the second atom? I completely agree with you that the excitation arises spontaneously. What he has done, he has separated the influence of this spontaneous part from the influence of the second atom which is causal and I completely agree with it.

E. C. G. Sudarshan: There is a distinction between the whole field being equal to zero or non-zero and the positive frequency part of the field. When you talk about an atom emitting a photon you want to create a photon of positive energy, which is the creation part of the field, and that leads to quantities, which are not related to what we look. This is one part. The other part of the thing is that whenever you have an interacting system, an interacting field, the interacting field is never local with regard to the asymptotic field. If it is local then according to the theorem it is trivial. In both these cases when we talk about this locality and non-locality one has to be careful about this. I think, Dr. Passante was very careful.

SUPERLUMINAL LIGHT PULSE PROPAGATION IN ACTIVE NONLINEAR MEDIA

V.S. LETOKHOV

Institute of Spectroscopy, Russian Academy of Sciences, Troitsk, Moscow region, 142190, Russia

"Only darkness propagates faster than the light"
(from Greek mythology)

The advent of lasers and novel experimental techniques have made it possible to conduct experiments on the already solved but ever "intriguing" problem of the "superluminal velocity of light pulses" [1,2] in various experimental situations (see review [3]): anomalous dispersion near an absorption line [4], linear gain spectral lines [5-11], and tunneling barriers [12,13]. In essence, these experiments have only confirmed the usefulness of the five different kinds of wave velocity, namely, the *phase* velocity, the *group* velocity, the *energy* velocity, the "*signal*" velocity, and the "*front*" velocity, introduced by L. Brillouin [2] for absorptive dispersion media. In this connection, I would like to return to the discussion of this problem for the interesting case of propagation of a short laser pulse in a *nonlinear* (saturable) amplifying medium in the wider context of propagation of instability autowaves in an active nonlinear medium.

1 Early Works

In 1964-65, at the laboratory headed by N.G. Basov (P.N. Lebedev Physical Institute), who had just received, together with A.M. Prokhorov and C.H. Townes, a Nobel Prize in physics, there were conducted very advanced, at the time, investigations into the enhancement of the power of nanosecond pulses generated by a Q-switched ruby laser by means of a chain of ruby crystal amplifiers. In the course of these experiments, performed by R.V. Ambartzumian, P.G. Kryukov, and V.S. Zuev, it was planned to raise the pulse energy to a few tens of joules and reduce the pulse duration from a few tens of nanoseconds down to sub-nanosecond values. They aimed at achieving a power density of a few hundreds of gigawatts per square centimeter, a record-high value at the time. Such pulse powers and energies were believed to be necessary for the observation of laser-induced thermonuclear fusion. In the course of these experiments, the experimenters met with difficulties typical of multiple-stage laser amplifiers: (1) damage caused to laser crystals and optical elements by a strong light field and (2) unwanted lasing, i.e., the transformation of laser amplifiers into laser oscillators as a result of any scattered light reflection. When studying this phenomenon, they developed incoherent scattering feedback lasers and also observed a new effect - the running of the pulse peak being amplified far ahead of the leading edge [14,15].

In the experiments, a Q-switched laser pulse was passed through a laser amplifier

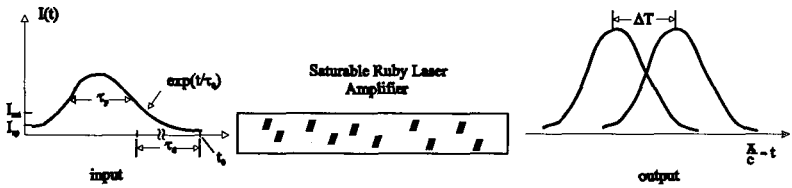

Figure 1. Effect of laser pulse reshaping in saturable laser amplifier with observable superluminal velocity of pulse propagation. Shape of initial pulse of Q-switched laser with exponential leading edge expanding to the time of Q-switching is shown on left side. The ordinate scale is highly compressed ($I_{sat}/I_{sp} = 10^{12} - 10^{15}$).

with a length of L and arrived at the registering oscillator ahead of time, the advance being equal to ΔT (Fig. 1). This corresponded to the pulse propagation through the amplifier with a velocity of $v \simeq 9c$, where c is the velocity of light in the medium (crystal) free from active particles (ions). I took part in these experiments as a graduate student-theoretician. The observed superluminal propagation of the laser pulse was at once interpreted [14,15] as being the result its *nonlinear reshaping* in the laser amplifier due to the preferential amplification of its exponentially rising leading edge. The point is that the leading edge of the input Q-switched laser pulse stretches, by virtue of the dynamics of such lasers, far ahead of the pulse maximum and has a nonzero, though negligible, intensity. This exponentially small leading edge is of principal importance in the subsequent superluminal reshaping of the pulse in the nonlinear amplifier, which was analyzed in detail in [16–18].

2 Theoretical consideration

I described the amplifying medium by the Boltzmann equation for the density matrix $\hat{\rho}$ with longitudinal and transverse relaxation, and the field $\mathbf{E}$ by Maxwell's equation in a medium having also a linear nonresonant radiation losses:

$$\frac{\partial^2 \mathbf{E}}{\partial t^2} + c^2 \mathrm{rotrot}\mathbf{E} + \gamma c \frac{\partial \mathbf{E}}{\partial t} = -4\pi N_i \frac{\partial^2}{\partial t^2} \mathrm{Sp}(\mu\hat{\rho}), \tag{1}$$

$$i\hbar \frac{\partial \hat{\rho}}{\partial t} = [H_0 - \mu\mathbf{E}, \hat{\rho}] - i\hbar\Gamma\hat{\rho}, \tag{2}$$

where γ is the coefficient of nonresonant linear radiation losses per unit length in the medium, N_i is the particle density, H_0 is the unperturbed Hamiltonian of the particle, and μ is the operator the electric dipole moment of the transition. The term $\Gamma\hat{\rho}$ describes phenomenologically the relaxation of the elements of the

density matrix: the diagonal elements $(\Gamma\rho)_{nn} = \left(\rho_{nn} - \rho_{nn}^0\right)/T_1$, describing the level population, relax within the longitudinal relaxation time T_1, and the non-diagonal elements $(\Gamma\rho)_{mn} = \rho_{mn}/T_e$ (m, n=1,2), which describe the high-frequency dipole moment, relax within the transverse relaxation time T_2.

In the representation in which H_0 is diagonal, the equation for the density matrix can lead to equations for the polarization $\mathbf{P} = N_i Tr(\mu\hat{\rho})$ and for the inverted-population density $N = N_i(\rho_{22} - \rho_{11})$:

$$\begin{cases} \frac{\partial^2 \mathbf{P}}{\partial t^2} + \frac{2}{T_2}\frac{\partial \mathbf{P}}{\partial t} + \omega_0^2 \mathbf{P} = -2N\mathbf{E}\frac{\omega_0}{\hbar}|\mu|^2, & (3) \\ \frac{\partial N}{\partial t} + \frac{1}{T_1}(N - N_0) = \frac{2}{\hbar\omega_0}\mathbf{E}\frac{\partial \mathbf{P}}{\partial t}, & (4) \end{cases}$$

where $N_0 = N_i\left(\rho_{22}^0 - \rho_{11}^0\right)$ is the density of the inverted population in the absence of a field, $\omega_0 = \omega_{21}$, and small terms have been omitted under the assumption that $\omega_0 \gg 1/T_2$.

The field equations (1) and the material equations (3) and (4), together with the initial conditions, describe completely the propagation of a light pulse in a resonantly amplifying medium. In luminescent crystals and practically in all other amplifying media, the variation of the light-wave parameters over distance on the order of the light wavelength and within times on the order of the light period is very small. We can therefore go over to "slow" variables $\mathcal{E}$, $\mathcal{P}$, φ, and ψ.

$$\begin{aligned} E &= \tfrac{1}{2}\mathcal{E}(t,x)\exp\{i[\varphi(t,x) + \omega t - kx]\} + c.c. \\ P &= \tfrac{1}{2}\mathcal{P}(t,x)\exp\{i[\psi(t,x) + \omega t - kx]\} + c.c. \end{aligned} \quad (5)$$

where a light pulse is in the form of a linear polarized plane wave, moving in the positive direction of the x axis. Then the equation for the field and the material equation reduced to the following system of equations:

$$\frac{\partial \mathcal{E}}{\partial t} + c\frac{\partial \mathcal{E}}{\partial x} + \frac{\gamma}{2}c\mathcal{E} = 2\pi\omega\mathcal{P}\sin(\psi - \varphi), \quad (6)$$

$$\mathcal{E}\left(\frac{\partial \varphi}{\partial t} + c\frac{\partial \varphi}{\partial x}\right) = -2\pi\omega\mathcal{P}\cos(\psi - \varphi), \quad (7)$$

$$\frac{\partial \mathcal{P}}{\partial t} + \frac{1}{T_2}\mathcal{P} = \frac{\mu^2}{\hbar}N\mathcal{E}\sin(\psi - \varphi), \quad (8)$$

$$\frac{\partial N}{\partial t} + \frac{1}{T_1}(N - N_0) = -\frac{1}{\hbar}\mathcal{P}\mathcal{E}\sin(\psi - \varphi). \quad (9)$$

In the envelope approximation, Eqs. (6-9) are exact, and take into account the effects of *coherent interaction* of the pulse with the medium. They become much simpler, however, in the case of *incoherent interaction.*

Incoherence of the interaction can arise either as a result of the incoherent state of the medium during the pulse time, or as a result of an incoherent state of the field. The condition for incoherent interaction between a coherent pulse and a medium is of the form

$$\tau_p \gg T_2. \quad (10)$$

However, even if $\tau_p \sim T_2$, the interaction can be incoherent if the coherence time of the field t_{coh} is much shorter than T_2:

$$T_2 \gg \tau_{coh}. \tag{11}$$

If the interaction is incoherent as a result of the incoherent state of the medium ($\tau_p \gg T_2$) then, as follows from the equation of (7), the polarization "follows" the field amplitude to quasistatically:

$$\mathcal{P} = \frac{\mu^2}{\hbar} T_2 N \mathcal{E} \sin(\psi - \varphi). \tag{12}$$

Taking this into account and changing over to the radiation flux density

$$I = \frac{1}{\hbar\omega_0} \frac{c}{8\pi} \mathcal{E}^2 [\text{photons/cm}^2 \text{sec}] \tag{13}$$

we can reduce (6-8) to the following three equations:

$$\begin{cases} \frac{\partial I}{\partial T} + c\frac{\partial I}{\partial x} = c(\sigma N - \gamma) I, & (14) \\ \frac{\partial N}{\partial t} + \frac{1}{T_1}(N - N_0) = -2\sigma I N, & (15) \end{cases}$$

$$\frac{\partial \varphi}{\partial t} + c\frac{\partial \varphi}{\partial x} = (\omega_0 - \omega)\frac{T_2}{2} c\sigma N, \tag{16}$$

where $\sigma = \sigma(\omega)$ is the cross section of the radiative transition at the frequency ω, defined by the expression

$$\sigma(\omega) = \frac{4\pi T_2 \omega_0 \mu^2}{\hbar c} \frac{T_2^{-2}}{(\omega - \omega_0)^2 + T_2^{-2}}. \tag{17}$$

The first two equations are the usual transport equations that follow from the energy conservation law. The third phase equation describes the effect of variation of the phase velocity as a result of the anomalous dispersion within the limits of the negative-absorption line.

3 Nonlinear Reshaping of a Laser Pulse During Propagation in an Amplifying medium

Stationary pulse propagation in nonlinear (saturable) media occurs with both modes of interaction (coherent and incoherent) between laser pulses and amplifying media: (1) in the propagation of an ultrashort laser pulse with a duration of $\tau_p \ll T_2$, where T_2 is the transverse relaxation time (phase memory relaxation time in the amplifier medium), that interacts with the amplifying medium in a coherent fashion and (2) in the propagation of a short laser pulse with a duration of $\tau_p \gg T_2$ that interacts with the amplifying medium in an incoherent fashion. In both cases, account should be taken of the linear, nonsaturable absorption γ that is inevitably present in any chain of amplifiers. This loss is much smaller than the linear amplification, but once saturation is reached, it becomes substantial for the tailing part of the pulse and thus limits its maximum energy.

Under *coherent* interaction conditions, the propagating ultrashort pulse is transformed into a stationary "π-pulse" of specified shape and duration that pushes all

the excited particles down to the lower level, i.e., extracts all the energy stored in the amplifying medium [19]. The propagation velocity of such a pulse does not differ from the velocity of light, c. This propagation mode is difficult to realize experimentally in luminescent crystals, because the energy the ultrashort pulse ($\tau_p \ll T_2 \tilde{-} 10^{-12}$s) must have for its nonlinear amplification to take place, i.e., the saturation energy flux $E_{sat} \tilde{-} \hbar\omega/\sigma_0$ (for the ruby crystal, $\sigma_0 \tilde{-} 10^{-20}$cm^2), corresponds to its intensity of $I \tilde{-} E_{sat}/\tau_p = 10^{12}$-$10^{13}$ W/cm^2, which is above the damage threshold of the ruby crystal.

The evolution of the nanosecond pulse propagating under incoherent interaction conditions is described by simple rate equations (14) and (15). The character of this deformation depends substantially on the shape of the leading edge of the laser pulse at the entrance to the amplifying medium [17].

The effect of preferential amplification of the leading edge of the pulse leads to a gradual "shift" of the pulse maximum over the leading front, and the magnitude of the shift is determined essentially by the character of the leading front of the initial pulse. If the magnitude of the shift is characterized by the relation $W = d\tau/dx$, where $d\tau$ is the shift of the pulse over the leading front on passing through a layer of medium with thickness dx, then the following expression holds [17]:

$$W = \frac{d\tau}{dx} = -(\sigma N_0 - \gamma) \frac{\int_{-\infty}^{\tau_s} I_0(\tau)\, d\tau}{I_0(\tau_s)}, \tag{18}$$

where $\tau = t - (x/c)$, and t_s is the point of the leading front of the pulse corresponding to a definite (say, 10%) level of gain saturation.

The shift of the maximum of the pulse prevents its compression. Therefore, in nonlinear amplification, only the pulses for which $W = 0$ (pulses with a step-wise leading front) or $W \to 0$ are shortened as the pulse is shifted over the leading front. The condition

$$\lim_{\tau \to -\infty} \left[\frac{1}{I_0(\tau)} \int_{-\infty}^{\tau} I_0(\tau')\, d\tau' \right] = 0 \tag{19}$$

is satisfied, for example, by the leading front of a pulse of Gaussian shape $I_0(\tau) \sim \exp\left(-\tau^2/\tau_0^2\right)$. In spite of the infinite length of the leading front, a Gaussian pulse is shortened when propagating in a nonlinearly amplifying medium. Figure 2a shows the results of a computer solution of Eqs. (14, 15) for a Gaussian initial pulse.

Pulses for which $W = \text{const}$ or $W \to \text{const}$ as the pulse propagates, i.e.,

$$\lim_{\tau \to -\infty} \left[\frac{1}{I_0(\tau)} \int_{-\infty}^{\tau} I_0(\tau')\, d\tau' \right] = \text{const}, \tag{20}$$

tend to a stationary shape $I[t - (x/u)]$ without a decrease in duration. In particular, this condition is satisfied by pulses with an exponential growth of the leading front, $I_0(\tau) \sim \exp(\tau/\tau_0)$. Numerical solutions of the equation (14,15) for a pulse with an exponential leading edge are shown in Fig. 2b, where the approach of the stationary state can be seen.

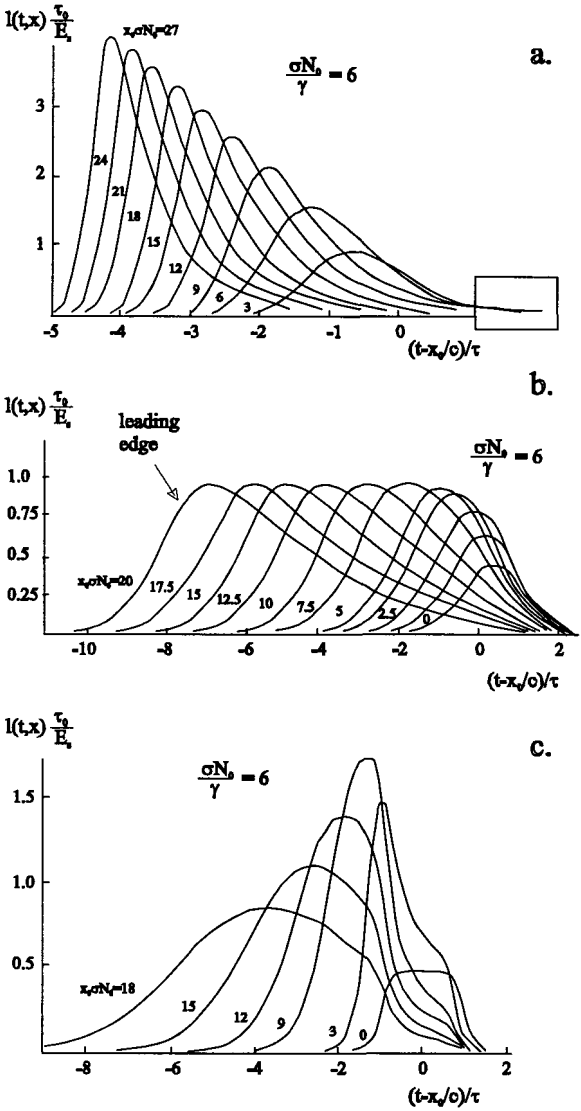

Figure 2. Reshaping of light pulse in nonlinear laser amplifier: (a) Gaussian pulse; (b) light pulse with exponential wings; (c) light pulse with a leading edge having a power-law growth. x_0 is the length of the amplifier (from [17]).

Finally, pulses satisfying the condition $|W| \to \infty$, i.e.

$$\lim_{\tau \to -\infty} \left[\frac{1}{I_o(\tau)} \int_{-\infty}^{\tau} I_0(\tau')\, d\tau' \right] = \infty, \tag{21}$$

experience an infinite lengthening of duration. Since the total energy of the pulse, regardless of its form, is limited, the intensity of such pulses tends to zero. Including among the "broadening" pulses are initial pulses with power-law growth of the leading front, $I_0(\tau) \sim |\tau_0/\tau|^n, n > 1$. Figure 2c shows the results of a numerical integration of Eq. (14-15) for an initial pulse with a leading front of the type $|\tau_0/\tau|^8$.

4 Superluminal Stationary (Autowave) Pulse Propagation

Most interesting is the stationary propagation of a pulse with an *exponential leading edge*, which is practically realized in the amplifying medium due to stimulated emission. This is a rather general principle: the evolution of spontaneous emission in the amplifying medium of a laser oscillator or amplifier always obeys an exponential law.

The input Q-switched laser pulse in the experiments [14,15] has the shape shown in Fig. 1. The shape of the pulse is determined by the operating principle of this laser. The development of generation begins with the level of spontaneous noise in the oscillation modes I_{sp} at the instant of Q switching ($t = t_0$). The exponential growth of the power $I_{sp} \exp(t/\tau_0)$ continues for a relatively long time τ_d (50 – 500nsec), called the delay time until the power reaches the level I_{sat} ($I_{sat} \approx 10^{15} I_{sp}$), sufficient to start saturation of the gain of the active medium. After this period, the energy stored in the laser is emitted, and this emission lasts for a short time, $\tau_p \approx 5 - 50$ nsec, which is smaller by approximately one order of magnitude than the delay time. During that time, the giant radiation pulse proper is emitted. It is clear that the leading front of such a pulse satisfies the condition (20). Therefore the pulse of the Q-switched laser should not be shortened but tend to a certain stationary shape. However, a similar displacement of the pulse over the leading front continues until the maximum of the pulse reaches the start of the pulse ($t = 0$). Fig. 2b illustrates the numerical solution of equations (14,15) for the initial pulse with experimental rise of the leading front.

The shift of the maximum of the pulse over the leading front can lead to a motion of the pulse in the medium with a velocity exceeding the velocity of light. Indeed, the velocity of a point on the leading front $t_s(x)$ with definite saturation level is determined by the relation

$$u = \left[\frac{dt_s(x)}{dx} \right]^{-1}, \tag{22}$$

and the connection between the velocity u and the displacement of the pulse over the leading front W is determined by differentiating the relation $\tau_s(x) = t_s(x) - (x/c)$.

As a result, the velocity of the pulse u is satisfies the relation

$$\frac{1}{u} - \frac{1}{c} = W = -(\sigma N_0 - \gamma) \frac{\int_{-\infty}^{\tau_s} I_0(\tau)\, d\tau}{I_0(\tau_s)}. \tag{23}$$

For pulses with an exponential leading front $\exp(\tau/\tau_0)$, expression (23) takes the form

$$\frac{1}{u} - \frac{1}{c} = -\chi_0 \tau_0, \tag{24}$$

where $\chi_0 = (\sigma N_0 - \gamma)$ is the initial gain of the medium per unit length. It is easy to see that when $\chi_0 \tau_0 < 1$ the velocity of propagation of the maximum pulse $u > c$, and when $c\chi_0\tau_0 > 1$, the velocity is negative ($u < 0$) [18].

The condition for the existence of the stationary state then takes the form

$$\chi_0 \tau_0 c < 1. \tag{25}$$

Physically condition (25) is due to the exponential spatial growth of the intensity of the leading front in the amplifying medium. This is illustrated in Fig. 3, which shows the instantaneous distribution of the intensity of the pulse inside and outside a layer of an amplifying medium, for three values of the parameter $\chi_0\tau_0 c$. From Figs. 3b and 3c it follows that intensity at infinity (as $\tau \to -\infty$) is not satisfied when $\chi_0\tau_0 c \geq 1$ in an unbounded medium. It follows from Fig. 3c that when $\chi_0\tau_0 c > 1$ the saturation of the gain begins at the output boundary of the layer, and then moves towards the input boundary in a direction opposite to the propagation of the light ($u < 0$). In this case there is not stationary state of the pulse in an infinite medium, but if we consider a medium of finite length, then the expression (24) for the velocity u is meaningful in this case, too.

The pulse stationary form $I_{st}(t)$, i.e., pulses that do not change their form as they propagate through a nonlinear amplifying medium, after passing through a layer of amplifying medium of thickness L, is given by

$$I_{st}\left(t - \frac{L}{c} + L\chi_0\tau_0\right), \tag{26}$$

where τ_0 is the slope of the exponential leading front of the given stationary pulse. Actually this effect of movement of the maximum of the pulse toward the leading edge was observed experimentally [14,15], and the theoretical magnitude of the movement $\Delta T = \tau_0\chi_0 L$ agrees with the experimental data. Measurements of the magnitude of the movement ΔT versus the length of the nonlinear amplifier lead to a linear dependence in agreement with the theory.

In accordance with expression (24), at $\chi_0\tau_0 c > 1$ the propagation velocity of the maximum of the pulse becomes negative because of the reshaping of its exponential leading edge. The meaning of this conclusion can be understood from Fig. 4 illustrating the deformation of a stationary pulse in the course of its passage through an amplifying medium of a finite length T. The change of the coordinate of the pulse maximum x_m in the course of time is shown for three values of the parameter $\chi_0\tau_0 c$. The regions $x < x_0$ and $x > x_0 + L$ are occupied by a transparent medium where the velocity of propagation of the maximum is u. When $\chi_0\tau_0 c < 1$, the pulse

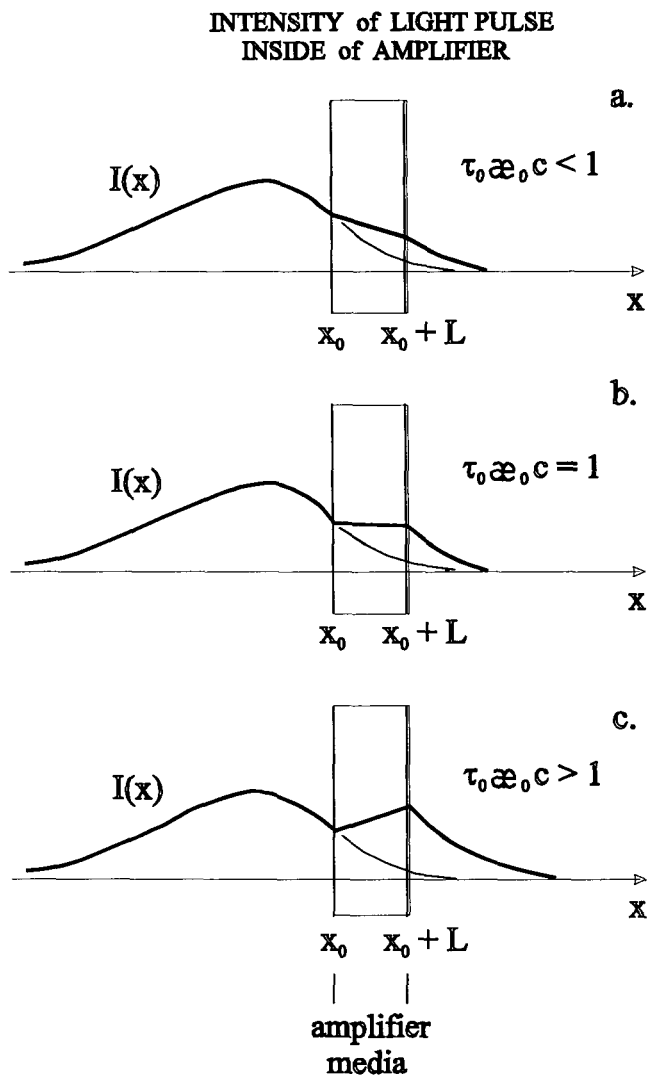

Figure 3. Spatial distribution of the intensity of a light pulse passing through a saturable amplifier for different parameter $\chi_0\tau_0 c$ (from [18]).

maximum in the medium is propagated with a velocity exceeding that of light ($u > c$). When $\chi_0\tau_0 c = 1$, the velocity u increases without limit. When $\chi_0\tau_0 c > 1$, the change in the position of the maximum is highly singular. At the instant of

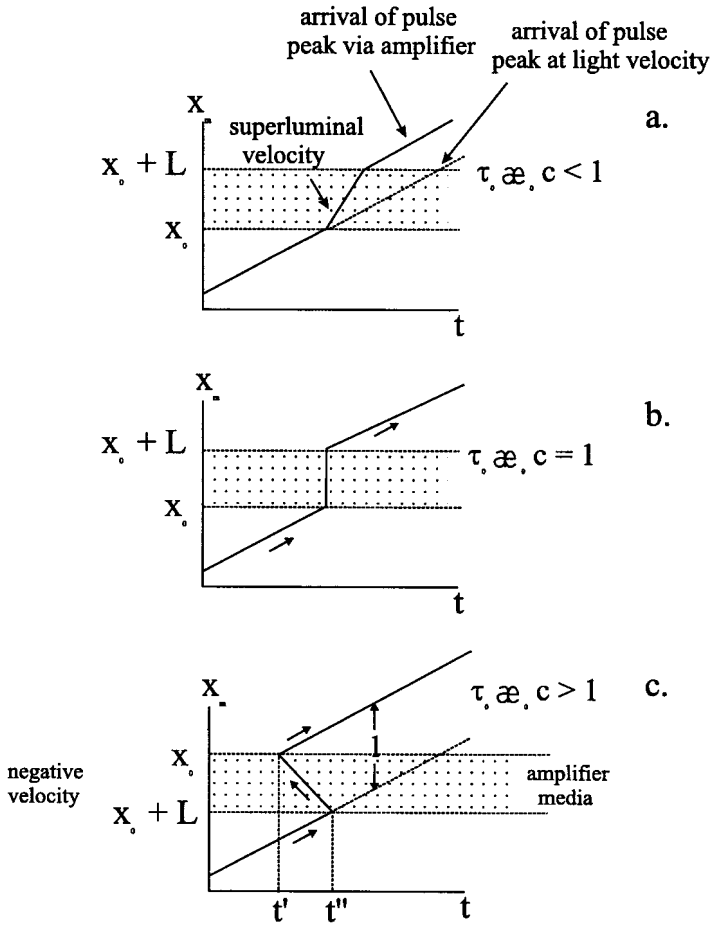

Figure 4. The position of maximum of a light pulse during passage through a layer of the amplifying medium of the thickness L, for different values of the parameter $\chi_0 \tau_0 c$ (from [18]).

time t' when the pulse maximum has not yet reached the entrance boundary of the medium ($x_m < x_0$), the leading edge of the pulse is already causing saturation of the amplifier at the exit boundary of the medium. As a result, the intensity at the exit boundary reaches a maximum, but then this maximum begins to move along with the saturation boundary toward the entrance boundary of the medium with the velocity u. Simultaneously, the maximum "breaks away" from the exit boundary and moves in the region $x > x_0 + L$ with the velocity c. During the

interval of time $t' < t < t''$, there exist simultaneously three peaks of the pulse at various points in space. This deformation of the pulse is possible because of the transfer of excitation energy from the particles of the medium to the pulse. In describing the deformation of a pulse with the three peaks, it has no meaning to speak of the velocity of propagation of the pulse as a whole.

There are two experiments on nonlinear amplification of the light of a Q-switched laser [14,20]. In the experiments of [14,15] the steepness of the leading edge $\tau_0 \simeq 4 \cdot 10^{-9}$sec, and the amplification of the medium $\chi_0 \sim 0.12\text{cm}^{-1}$. In this case the parameter $\chi_0\tau_0 c \simeq 8$ (the velocity of light in ruby, $c = 1.7 \cdot 10^{10}$ cm/sec) and, as stated, it is impossible to speak of the velocity of propagation of the pulse maximum in the medium. However, in the order experiment [20], the pulse had a duration of $2 \cdot 10^{-9}$ sec, and the steepness of the leading edge was $\tau_0 \simeq 4 \cdot 10^{-10}$sec in the last stage of the amplifier. The energy density of the pulse, equal to 7 J/cm^2, was sufficient for saturation of the amplification in the ruby. For such a pulse, $\chi_0\tau_0 c \simeq 0.7$ ($\chi_0 \simeq 0.1\text{cm}^{-1}$) and, consequently, it is possible to speak of a velocity exceeding the speed of light for propagation of the pulse maximum in the medium. With the conditions of the experiment in [20] the velocity of propagation of the pulse maximum in the final stage is $u \simeq 3c$. For observation of effects arising because of the propagation of the pulse maximum with velocity exceeding that of light a still shorter pulse with energy exceeding the energy for saturation of the amplification of the medium is required.

The theoretical results obtained in [17,18] and the interpretation of the superluminal velocity effect [14,15] were confirmed in independent calculations performed in [21], where the modeling of the nonlinear amplification of a laser pulse was extended to the case of inhomogeneous Doppler broadening of an amplification spectral line.

To study nonlinear amplification in extended media became possible with the advent of fiber laser amplifiers. The elegant experiments were performed in [22] at $\chi_0\tau_0 c \ll 1$, when u was only slightly over c.

5 Prospects

So, the effect of superluminal velocity of a laser pulse in a nonlinear amplifying medium due to its being reshaped to have an elongated exponential leading edge does not violate the relativity principle [1]. The physics of this effect differs entirely from that of the superluminal group velocity in linear media with an anomalous dispersion [2], both two-level [4–9] and three-level [10,11] ones. Though the history of this effect is long, but with the present-day experimental possibilities being what they are, it is, in my opinion, of undoubted interest, at least in two respects.

First, the strong field region also moves with a superluminal velocity, and so there must occur new effects, some of which attracted special attention in the early work published in [23].

1) *Electromagnetic radiation by a light pulse.* The motion of a space-limited light pulse is accompanied by the displacement of a bunch of an averaged polarization of the medium moving with the same velocity and generated by a gradient force acting on the electrons in the medium. If the velocity polarization buch exceeds the phase velocity of electromagnetic waves in the medium a Cherenkov radiation can

occur. As the light pulse propagates in a nonlinear amplifying medium the velocity of the pulse peak may be higher then the velocity of light in a vacuum, so that the above condition is met. If the pulse peak generates a breakdown, the motion of an ionization front with a velocity higher than that of light also may cause intensive Cherenkov radiation. The light pulse may also radiate during accelerated motion of the average polarization bunch or breakdown front, for example, in motion along a circular trajectory. Ring amplifiers of fiberglass can be used conveniently for experiments of this type. The generated radiation will be analogous to the synchrotron radiation by an electron bunch. An attempt at analyzing this effect was made in [24], but it should also be considered for the case of nonlinear propagation.

2) *Relativistic "mirrors"*. The leading edge of an intensive light pulse generates a gradient of dielectric permittivity caused by a discontinuity in population inversion, light field intensity and ionization breakdown by strong field. The moving discontinuity in dielectric permittivity can serve as a relativistic "mirror" for electromagnetic waves whose wavelength exceeds the dimensions of the discontinuity of dielectric permittivity. Experiments carried out to observed the Doppler effect of such mirrors can make use of media whose refraction index coefficient changes in strong light field. This avenue of inquiry is associated with the "photon acceleration" problem [25].

Secondly, this effect can be treated as a manifestation of an autowave propagating pulsed instability in *any active medium* with amplification due to stimulated emission. It corresponds to the superluminal-velocity propagation of the very transformation region (and not of the photon!) of the energy stored in the amplifying medium into radiation on account of stimulated emission, as illustrated in Fig. 5. At first glance this seems a fairly "artificial laboratory effect". In actual fact, this can give rise to the "superluminal" effects observed, for example, under astrophysical conditions. The interstellar space is filled with radiation occupying an extremely broad spectral range. If nonequilibrium conditions with an inverted population are produced in some region of space, the boundary of transformation of the energy stored in the inverted medium into stimulated emission can propagate with a superluminal velocity in the form of inverted population "spills of" autowaves. On the Earth this can be observed from the side, because of the scattering of radiation (optical, microwave), as a superluminal "propagation" process. In my opinion, this effect can be considered in addition to the well-known "kinematic" effect of superluminal objects in the form of relativistic jets in astrophysics [26], when the relativistic jet model is inapplicable, for example, in the case of *perpendicular* propagation with a superluminal velocity.

Acknowledgments

I wish to express my deep gratitude to the International Solvay Institutes and particularly Professor I. Antoniou and I. Prigogine for their kind invitation to this Conference and their remarkable hospitality in the lovely stimulating Delphi landscape and environment.

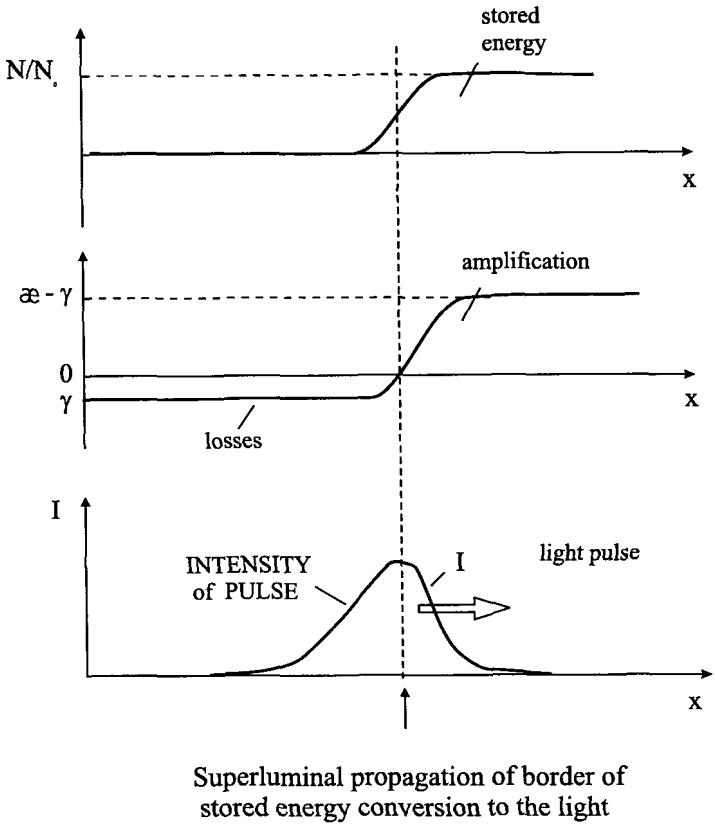

Figure 5. Superluminal propagation of conversion border of stored energy in amplifying medium to light pulse due to stimulated emission: $N(x)$ is the spatial distribution of population inversion, $\chi - \gamma$ is net gain and I is intensity of light pulse.

References

1. Einstein, A., Lorentz, H.A., Minkowski, H. & Weyl, H. *The Principle of Relativity. Collected Papers.* (Dover, New York, 1952).
2. Brillouin, L. *Wave Propagation and Group Velocity.* (Academic, New York, 1960).
3. Chiao, R.Y. Population inversion and superluminality. In *Amazing Light, a Volume Dedicated to C.H. Townes on His Eightieth Birthday* (ed. Chiao, R.Y.) 91-108 (Springer, New York, 1996).

4. Chu, S. & Wong, S. Linear pulse propagation in an absorbing medium. *Phys. Rev. Lett.* **48**, 738-741 (1982).
5. Segard, B., Macke, B. Observation of negative velocity pulse propagation. *Phys. Lett.* **A109**, 213-216 (1985).
6. Picholle, E., Montes, C., Leycuras, C., Legrand, O. & Botineau. J. Observation of dissipative superluminous solutions in a Brillouin fiber ring laser. *Phys. Rev. Lett.* **66**, 1454-1457 (1991).
7. Fisher, D.L. & Tajima, T. Superluminous laser pulse in an active medium. *Phys. Rev. Lett.* **71**, 4338-4341 (1993).
8. Chiao, R.Y. Superluminal (but causal) propagation of wave packets in transparent media with inverted atomic populations. *Phys. Rev.* **A48**, R34-R37 (1993).
9. Steinberg, A.M. & Chiao, R.Y. Dispersionless, highly superluminal propagation in a medium with a gain doublet. *Phys. Rev.* **A49**, 2071-2075 (1994).
10. Wang, L.J., Kuzmich, A., Dogariu, A. Gain-assisted superluminal light propagation. *Nature* **406**, 277-279 (2000).
11. Dogariu, A., Kuzmich, A., Wang, L.J. Transparent anomalous dispersion and superluminal light propagation at a negative group velocity. *Phys. Rev.* **A63**, 053806 (2001).
12. Steinberg, A.M., Kwiat, P.G. & Chiao, R.Y. Measurement of the single-photon tunneling time. *Phys. Rev. Lett.* **71**, 708-711 (1993).
13. Chiao, R.Y., Steinberg, A.M. Tunneling times and superluminality in *Progress in Optics*, XXXVII, ed. by Wolf, E. (Elsevier Science, B.V. Amsterdam, 1997), pp. 346-405.
14. Basov, N.G., Ambartzumian, R.V., Zuev, V.S., Kryukov, P.G., Letokhov, V.S. Propagation velocity of powerful laser pulse in inverted population medium. Proceed. USSR Acad. Sci. (Doklady) 165, 58-60 (1965); [*Sov. Phys. Doklady* **10**, 1039-1041 (1966)].
15. Basov, N.G., Ambartzumian, R.V., Zuev, V.S., Kryukov, P.G. & Letokhov, V.S. Nonlinear amplification of light pulses. *Sov. Phys. JETP* **23**, 16-22 (1966).
16. Kryukov, P.G., Letokhov, V.S. Propagation of light pulse in a resonantly amplifying (absorbing) medium. *Soviet Physics Uspekhi* **12**, 641-672 (1970).
17. Basov, N.G., Letokhov, V.S. Reshaping of light pulse in nonlinear amplifier. Proceed. Of USSR Acad. Sci. 167, 73-76 (1966); [*Sov. Phys. Doklady* **11**, 222-224 (1966)].
18. Letokhov, V.S. Nonlinear amplification of light pulses. II. Velocity of propagation. *Soviet Physics - Technical Physics* **13**, 644-649 (1968).
19. Basov, N.G., Letokhov, V.S. Resonance interaction of light pulse with inverted population medium. *Preprint A-2*, P.N. Lebedev Physical Institute, 1965 (results were published in [15]).
20. Ambartzumian, R.V., Basov, N.G., Zuev, V.S., Kryukov, P.G. Letokhov, V.S. Propagation of light pulse in a nonlinearly amplifying and absorbing medium. *JETP Lett.* **4**, 12-14 (1966).
21. Icsevgi, A. & Lamb, W.E. Propagation of light pulses in a laser amplifier. *Phys. Rev.* **185**, 517-545 (1969).

22. Ströker, D., Hüve, J., Mitschke, F. Superluminal pulse propagation in the erbium fiber laser. *Appl. Phys.* **B69**, 323-326 (1999).
23. Ambartzumian, R.V., Basov, N.G, Zuev, V.S., Kryukov, P.G., Letokhov, V.S. Short-pulse Q-switched laser with variable pulse length. *IEEE J. of Quant. Electr.* **QE-2**, 436-441 (1966).
24. Klimov, V.V., Letokhov, V.S. Radio emission of an optical solution propagating in a ring laser. *Optics Comm.* **100**, 437-442 (1993).
25. Mendonca, J.T. *Theory of Photon Acceleration.* (IOP Publ., Bristol, 2001).
26. Zensus, A., Pearson, T.J. Eds. *Superluminal Radiosources* (Cambridge Univ. Press, 1987).

DISCUSSION [a]

Chairman: O. Kocharovskaya

W. Schleich: It i a fascinating idea, employing nanotubes. How are you going to do mirrors for this laser?

V. Letokhov: No, there is no feedback there is only spontaneous emission. We don't discuss the stimulated emission, which is possible. In case of a high intensity, we can come to the range of stimulated emission and saturation. It will be one pass saturable amplifier and one Frennel zone for X-ray or gamma ray. It is a very interesting question because when we are talking about spontaneous emission for very short wave lengths, we have in mind the Rayleigh-Jezus formula for the density of modes. However, we should consider the relativistic compression, which changes the density of modes. That is why the relativistic particles are very promising for X-rays and even for γ-rays. It seems to me the real future for the shortwave length laser based on relativistic particles.

R. Chiao: I would like to ask about Larmor time. They are very fascinating, the experiments that you did measuring the tunnelling time for the electron using the field emission from the point. Are you aware of the work of Buttiker, who modified the Larmor time? When you are talking about Larmor time, are you talking about the Buttiker-Larmor time or about the original Baz-Rybachenko?

V. Letokhov: Yes, our consideration is based on all early theoretical works.

R. Chiao: Is it a tunnelling through an opaque barrier?

V. Letokhov: Yes, for the classical electron.

G. Nimtz: I would like to make a comment about the tunnelling time between one and zero in optical and macro experiments. According to my calculations, which I did not have time to present in my talk this afternoon, the result was that the tunnelling time in the first order of approximation is reciprocal to the frequency of the particle or photon. Exactly the same time we get for electronic tunnelling,

[a] The oral presentation covered the number of subjects including the measurement of femtosecond tunneling time of electron through the electric field barrier (published separately by S.K. Sekatskii and V.S. Letokhov, Phys. Rev. **B64**, 233311 (2001)) and the possibility of $\chi - \gamma$- ray production by relativistic electrons or positrons moving in the carbone nanotube (see V.V. Klimov and V.S. Letokhov, Phys. Lett. **A226**, 244 (1997); Physica Scripta **56**, 480 (1997)). Some part of the discussions concerns these subjects which are not presented in this paper.

a couple of femtoseconds. It is in agreement with Hartman and Wigner concept of the phase time approximation for the tunnelling. I am happy with this result.

V. Letokhov: With the current state of the femtosecond technology it is relatively easy to study this effect because we can measure the time of excitation and detection so precisely as 0.1 femtosecond.

M. Raizen: Could you comment on the proposal from Technion, who proposed that one could do higher harmonic generation with carbon nanotubes. He argues by very simple arguments, which seem to be very different from yours, because he could cancel out everything except highest order harmonics.

V. Letokhov: Yes, I know this work. In our case, I do not consider to use X-rays for nonlinear effects. I consider to use relativistic electron in order to produce γ-rays. What you have mentioned is an alternative possibility to the one where people use a capillary filled by noble gas to produce higher harmonics. Instead of the capillary with noble gas in the proposal you mentioned the carbon nanotube is used. This is an interesting possibility.

L. Stodolsky: I have a comment for people interested in measuring tunnelling times. I do not know if it is known. It is an old method from nuclear physics. It was an idea, which was used in the fifties of the bremsstrallung of the reaction to determine the lifetime of the nuclear level. A proton goes in, makes nuclear level, hangs around for a while, and leaves again. And now, you can show that the bremsstrallung from this reaction reflects the time that the proton spent in the nucleus. I know one reference on this effect. This is a way of measuring delay times.

A. Steinberg: I am also really struck by these marvellous experiments and I have a few questions about them. I am curious whether you are able to measure the dependence of that spreading the Larmor time on the distance of the tip to the surface which should saturate to a constant value according to the Baz-Rybachenko predictions. And Buttiker's modifications, basically the second component to the Larmor time, was also mentioned earlier. It seems to me that the physical meaning of this component would be that in addition to the spreading of the wave packet, the tunnelling should preferentially select out certain momentum components, so we should be able to observe the change in the transverse momentum spread. If it is feasible to measure such things?

V. Letokhov: Yes. I think that in the case of deviation from the spherical symmetry of the electric field near tip it will be some contribution to the transversal momentum and it is secondly measurable, no doubt, because at present, it is possible to prepare nanotips of various configurations, not only spherical. Actually we introduced a parameter correction to the spherical field because it is not a sphere. Our parameter correction is $\gamma = 1.5$. The shape of the nanotip is controlled very well by the electron transmission microscopy in our experiment.

R. Chiao: Did you see the Hartman effect? The Hartman effect is that if you increase the tunnel barrier width, the tunnelling time saturates.

V. S. Letokhov: No, not in our case. We have a tip with radius about fifty nanometres. Actually, $CaNa_2$ material has anomalous transmission escaping depth for low energy electrons. For $CaNa_2$, the escaping depth is more than fifty nanometres. It is about hundred to two hundred nanometres. In principle, yes, in the case of another material the saturation can be observed.

GENERATION AND DETECTION OF PHOTON NUMBER STATES ON DEMAND[a]

HERBERT WALTHER
Max-Planck-Institut für Quantenoptik and
Sektion Physik der Universität München,
85748 Garching, Germany
fax: +49/89-32905-710; e-mail: herbert.walther@mpq.mpg.de

The widely discussed applications in quantum information and quantum cryptography require radiation sources capable of producing a fixed number of photons. This paper reviews the work performed in our laboratory to produce these fields on demand. Two different methods are discussed. The first is based on the one-atom maser or the micromaser operating under the conditions of the so-called trapping states. In this situation the micromaser stabilises to a photon number state. The second device uses a single ion in an optical cavity. The latter setup was recently realised in our laboratory.

1 Introduction

Single photon sources are a necessary requirement for secure quantum communication [1,2,3], for quantum cryptography [4] and in special cases also for quantum computing [5]. Photon fields with fixed photon numbers are also interesting from the point of view of fundamental physics since they represent the ultimate non-classical limit of radiation. When the photon number state is produced by strong coupling of excited-state atoms, a corresponding number of ground-state atoms is simultaneously populated. Such a system therefore produces a fixed number of atoms in the lower state as well. This type of atom source is a long sought after *gedanken* device as well [6]. Single photons have been generated by several processes such as single-atom fluorescence [7] (see also Refs. [28,29]), single-molecule fluorescence [8], two-photon down-conversion [9], and Coulomb blockade of electrons [10], and one- and two-photon Fock states have been generated in the micromaser [11] (see also [12]). As these sources do not produce the photons on demand, they are better described as "heralded" photon sources, because they are stochastic either in the emission direction or in the time of creation. A source of single photons or, more generally, of Fock states generated on demand has not yet been demonstrated. Cavity quantum electrodynamics (QED) provides us with the possibility of generating a photon both at a particular time and with a predetermined direction. To this end there have been several proposals making use of high-Q cavities, which are basically capable of serving as sources of single photons [3,13,14,15]. The current paper reviews the work on a microwave source capable of producing a preset number of photons and lower state atoms. The principle of the source and the first experimental demonstration will be described. It is based on the One-Atom Maser or micromaser and allows generation of a specified photon Fock state ($n \geq 1$) *on demand*, without need of conditional measurements, thus making it independent of detector efficiencies.

The second part of the paper describes the work towards a new single-photon source in the visible spectral range. This source uses a single trapped ion placed in

[a] in collaboration with S. Brattke, G.R. Guthöhrlein, M. Keller, W. Lange and B. Varcoe

a cavity. The realization of this source will be reported.

Steady-state operation of the One-Atom Maser has been extensively studied both theoretically [16] and experimentally, and has already been used to demonstrate many quantum phenomena of the radiation field such as sub-Poissonian statistics [17], collapse and revival of Rabi oscillations [18], and entanglement between the atoms and cavity field [19]. More recently, two experiments demonstrated that Fock states (i.e. states with a fixed photon number) can be readily created in the normal operation of the maser, by means of either state reduction [11] or steady-state operation of the micromaser in a trapping state [12]. The trapping states in the micromaser are the quantum states of the radiation field produced in the maser cavity. They are described in detail below. State reduction is possible owing to the entanglement between the state of the outgoing atoms and the cavity field; detection of a lower state atom means that a field originally in an n-photon Fock state is projected onto the $n+1$ state [20]. As a source of single photons, such a source can be compared to two-photon down-conversion, in which an idler beam is used to prove the creation of a photon in the signal beam. Both are subject to the same limitation in that the creation of the Fock state is unpredictable, and imperfect detectors further reduce the probability of a state, once created, also being detected. In contrast, it is shown here that the micromaser can be used to prepare *on demand* Fock states with small photon numbers in the cavity, this having the great advantage of making the process independent of detection efficiencies. Simultaneously, an equal number of ground state atoms are produced with an efficiency of up to 98%.

Trapping states are a feature of low-temperature-operation of the micromaser, for which the steady-state photon distribution closely approximates a Fock state under certain conditions. They are typical of strongly coupled systems. They occur when atoms perform an integer number, k, of Rabi cycles under the influence of a fixed photon number n:

$$\sqrt{n+1}gt_{\mathrm{int}} = k\pi, \tag{1}$$

where g is the effective atom-field coupling constant and t_{int} is the interaction time. Trapping states are characterized by the number of photons n and the number of Rabi cycles k. The trapping state $(n, k)=(1, 1)$ therefore refers to the one-photon, one-Rabi-oscillation trapped field state. In other words, trapping states occur when the interaction time is chosen such that the emission probability becomes zero for certain operating parameters of the maser. When the trapping state is reached in steady-state operation, the micromaser field will therefore enter a Fock state and become stabilised. The particular Fock state is known and is determined by the interaction time between the atom and cavity as given by the trapping state formula (Eq. 1). The Fock state, once prepared, is preserved owing to the trapping condition with a minimum probability of photon emission. Following preparation of the state, the beam of pump atoms can be turned off and the Fock state remains in the cavity for the duration of the cavity decay time. For simplicity, we concentrate in the following on preparation of a one-photon Fock state, but the method can also be generalised to generation of fields of higher photon numbers.

The micromaser setup used for the experiments is shown in Fig. 1 and is operated in the same way as described in [12]. Briefly, a ^{3}He-^{4}He dilution refrigerator houses the closed superconducting microwave cavity. A rubidium oven provides two

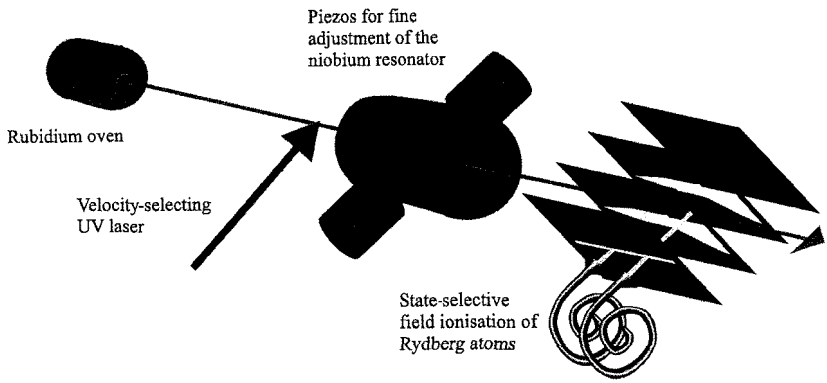

Figure 1: The atoms leaving the rubidium oven are excited into the $63P_{3/2}$ Rydberg state by means of a UV laser at an angle of 11°. After the cavity the atoms are detected by state-selective field ionisation. The cavity is tuned with two piezo translators. An auxiliary atomic beam (not shown) is used to stabilise the laser frequency. The laser is locked to a Stark-shifted atomic resonance of the auxiliary beam, thus allowing the velocity subgroup selected by excitation to be continuously changed within the range of the velocity distribution of the atoms.

collimated atomic beams: the main beam passing directly into the cryostat and the second being used to stabilise the laser frequency [12]. (This second beam is for simplicity not shown in Fig. 1). A frequency-doubled dye laser ($\lambda = 297$ nm) was used to excite rubidium (^{85}Rb) atoms to the Rydberg $63P_{3/2}$ state from the $5S_{1/2}$(F = 3) state. The cavity is tuned to the 21.456 GHz transition from the $63P_{3/2}$ state to the $61D_{5/2}$ state, which is the lower or ground state of the maser transition. For this experiment a cavity with a Q-value of 4×10^{10} was used, this corresponding to a field decay time of 0.6 s or a photon lifetime of 0.3 s. This Q-value is the largest ever achieved in this type of experiments and the photon lifetime is more than two orders of magnitude higher than that of related setups [21]. This cavity is used to study micromaser operation in great detail. To realise the Fock state, it is necessary to switch the excitation of the Rydberg atoms on and off in a predefined pulse sequence; this was achieved by means of an intensity-modulating electro-optical modulator triggered by control software. The pulse duration and pulse separation can both be tailored to the conditions required for the particular experiment.

To demonstrate the principle of this source, Fig. 2 shows a sequence of twenty successive pulses obtained by Monte Carlo simulation [22] of the micromaser operating in the (1, 1) trapping state. In each pulse there is a single emission event, producing a single lower state atom and leaving a single photon in the cavity. In the case of loss of a photon by dissipation, one of the next incoming excited state atoms will restore the single-photon Fock state. This condition was observed in [12] when sub-Poissonian atom statistics was measured with the maser operating in a trapping state. The influence of thermal photons and variations in interaction time or cavity tuning further complicates this picture, resulting in reduced visibility of steady-state Fock states [12]. Pulsed excitation as discussed here, however, reduces these

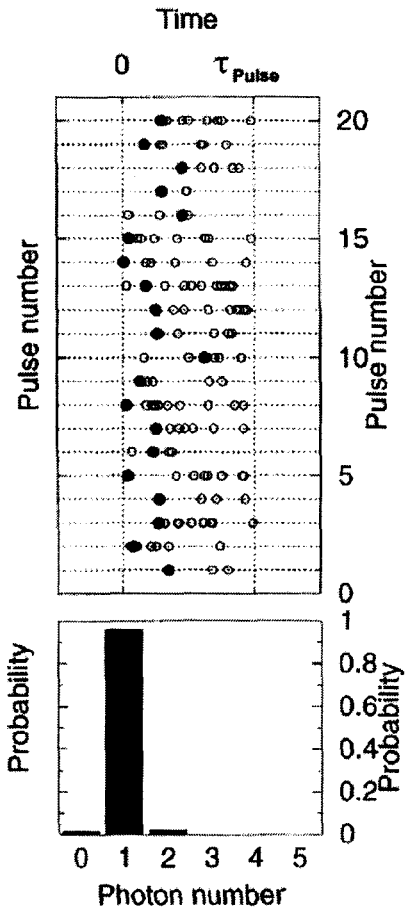

Figure 2: Simulation of a subset of twenty successive atom bunches after the cavity and the associated probability distribution for photons or lower-state atom production (solid circles represent lower-state atoms and open circles represent excited-state atoms). The start and finish of each pulse are indicated by the vertical dotted lines marked 0 and τ_{pulse}, respectively. The operating conditions are the (1,1) trapping state ($gt_{int} = 2.2$) conditions. The size of the atoms in this figure is exaggerated for clarity. With the real atomic separation, there is 0.06 atom in the cavity on average (i.e. the system operates in the one-atom regime). The other parameters are $\tau_{pulse} = 9,92 \times \tau_{cav}$, $n_{th} = 10^{-4}$ and $N_a = 7$ (see also Refs. [23] and [24]).

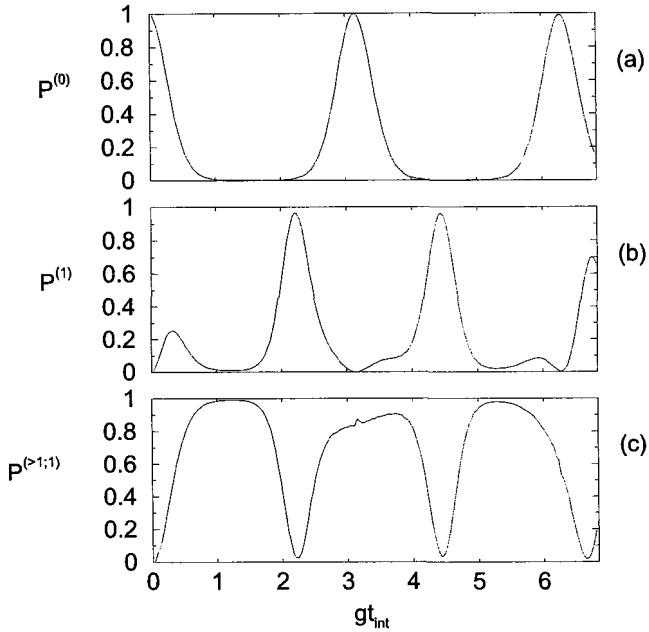

Figure 3: The probability of finding (a) no lower-state atoms per pulse, $P^{(0)}$, (b) exactly one lower-state atom per pulse $P^{(1)}$, and (c) a second lower-state atom, if one has already been detected, $P^{(>1;1)}$. The parameters are $\tau_{\text{pulse}} = 0.02\ \tau_{\text{cav}}$, $N_{\text{a}} = 7$ atoms and $n_{\text{th}} = 10^{-4}$. The maximum value of $P^{(1)}$ is 98% for the (1, 1) trapping state.

perturbations present in the case of a continuous operation of the atomic beam and the Fock state maintains a high probability [24].

Figure 3 shows three curves again obtained from a computer simulation that illustrate the behaviour of the maser under pulsed excitation as a function of the interaction time for more ideal (but achievable) experimental parameters. The simulations show the probability of finding no ground-state atom per pulse ($P^{(0)}$) and exactly one ground-state atom per pulse ($P^{(1)}$); and the conditional probability of finding a second ground-state atom in a pulse, if one has already been detected ($P^{(>1;1)}$). It is shown below that the latter plot of the conditional probability, $P^{(>1;1)}$, has the advantage of being especially suitable for comparing theory and experiment since it is relatively insensitive to the detection probability for atoms in the upper and lower maser levels.

From the simulations it follows that with an interaction time corresponding to the (1, 1) trapping state, both one photon in the cavity and a single atom in the lower state are produced with a 98% probability. In order to maintain an experimentally verifiable quantity, most of the simulations presented relate to the production of lower-state atoms rather than to the Fock state left in the cavity. Pulse lengths, on the other hand, are rather short ($0.01\tau_{\text{cav}} \leq \tau_{\text{pulse}} \leq 0.1\tau_{\text{cav}}$), and so there is little

dissipation and the one photon state in the cavity following the pulse is very close to the probability of finding an atom in the lower state. Note that at no time in this process is a detector event required to project the field; the field evolves to the trapping state as a function of time when the suitable interaction time has been chosen.

The variation of the time when an emission event occurs during an atom pulse in Fig. 2 is due to the variable time spacing between the atoms as a consequence of Poissonian statistics and the stochasticity of the quantum process. The atomic rate therefore has to be high enough to ensure a sufficient number of excited atoms per laser pulse, so as to maintain the 98% probability of an atom emitting. To guarantee single-atom single-photon operation, the duration of the preparation pulses must be short in relation to the cavity decay time. For practical purposes, the pulse duration should be smaller than $0.1\tau_{\rm cav}$ for dissipative losses to be less than 10%. Apart from reducing the fidelity of the Fock state produced, losses increase the likelihood of a second emission event leading to a larger number of lower-state atoms than photons in the field; the 1:1 correspondence between the two would thereby be lost. Shorter atom pulses reduce the dissipative loss, but the number of atoms per cavity decay time (usually labelled $N_{\rm ex}$) must be larger than ten times the threshold value of the atomic flux to realise the Fock source with significant fidelity. Since a minimum atom number is required to produce the desired state, care must also be taken to avoid atom beam densities violating the one-atom-at-a-time condition.

For a large range of operating conditions, the production of Fock states of the field and single lower-state atoms is remarkably robust against the influence of thermal photons, variations of the velocity of atoms and other influences such as mechanical vibrations of the cavity; much more so than the steady-state trapping states, for which highly stable conditions with low thermal photon numbers are required [12,23].

An obvious side-effect of the production of a single photon in the mode is, as already mentioned, that a single atom in the lower state is produced. This atom is in a different state when it leaves the cavity, and is therefore distinguishable from the pump atoms. Under these operating conditions, the micromaser thus also serves as a source of single atoms in a particular state, a requirement for many experiments proposed [6,25].

Although the distribution of lower-state atoms leaving the cavity will be maximally sub-Poissonian, the arrival time of an atom within the pumping pulse still shows a small uncertainty, the upper limit of which is determined by the pump pulse duration in the range of $0.01 - 0.1\tau_{\rm cav}$ for the parameters used in this paper. The separation of the pulses is $\geq 3\tau_{\rm cav}$,leadin g to a small relative variation in the arrival times. If the pump rate were to be increased still further, the pulse lengths could be further reduced and the arrival of an atom would become even more predictable.

The present micromaser setup was specifically designed for steady-state operation and is therefore not ideal for the parameter range presented here. However, the current setup does permit comparison between theory and experiment in a relatively small parameter range. The experimental test relies on measurement of an absolute number of atoms and although the operation of the Fock source is independent of detector efficiencies, the experimental test is blurred by the fact that

the state-selective field ionisation detectors for the Rydberg atoms do not reach an efficiency of 100%. Atoms in a particular state will therefore be missed, leading to wrong or misleading results. In order to circumvent this disadvantage, it is useful to measure population correlations between successive atoms instead. Owing to the strong coupling between the atoms and cavity, the cavity field and the state of the pumping atom are entangled following the interaction. A subsequent pumping atom will thereby also become entangled with any previous one, and thus the population correlations between successive atoms are determined by the particular dynamics of the atom-cavity interaction. The connection between population correlations and the micromaser dynamics has been studied in detail in previous papers [19,26]. It is important to note that even in the presence of lost counts the correlations between successively detected atoms are maintained. Conditioning the experimentally measured parameter to the detection of atom pairs that contain at least one lower-state atom provides a value both appropriate to the existent correlation and - at the same time - directly related to the total probability of finding one atom per pulse.

By means of an extremely high cavity Q factor (4×10^{10}) an $N_{\rm ex}$ of approximately 60 was accessible for a short range of interaction times around the maximum in the Maxwell-Boltzmann velocity distribution, which happens to correspond to the interaction time for the (1, 1) trapping state. A pulse length of $\tau_{\rm pulse} = 0.066\ \tau_{\rm cav}$ leading to an average of 4 atoms per pulse was chosen as a compromise between the effects of dissipation and external influences, while still providing a pump rate above the threshold for single-photon Fock state production. Figure 4 shows the results of a comparison of theory and experiment for a scan over the (1, 1) trapping state. Plotted here is the ratio of two-atom events to the total number of two-atom events detected that contain at least one lower state. That is,

$$P^{(>1;1)} = \frac{N_{\rm gg}}{N_{\rm gg} + N_{\rm eg} + N_{\rm ge}}, \tag{2}$$

where, for example, $N_{\rm eg}$ is the probability of detecting a two-atom event containing first an upper-state atom (e) and then a lower-state atom (g) in any given pulse. The number of three-atom events detected is negligible and can be ignored as a contributing factor. Constructing the parameter in this way ensures that there is a one-to-one correspondence between the correlation parameter and the maximum probability of finding exactly one atom per pulse. That is, to a good approximation for pump rates and pulse durations employed in this experiment, the difference between the upper bound $P^{\rm max}$ and the measured correlation $P^{(>1;1)}$ gives the probability of finding exactly one atom per pulse ($P^{(1)}$). $P^{(>1;1)}$ in Eq. 2 is independent of the absolute detector efficiency and depends only on the relative detector efficiencies and the miscount probability (the probability that a given atomic level is detected in the wrong detector), each of which has been measured experimentally. The theoretical curves of Fig. 4 represent an evaluation of the probability of finding exactly one atom per pulse and the conditional probability introduced in Fig. 3. The curves are evaluated both for the ideal situation of no detector miscounts and for the measured detector miscounts of 7% in the lower-state detector and 2% in the excited-state detector. When the miscounts are incorporated into the data, there is an excellent match between the experimental points and the theoretical curve.

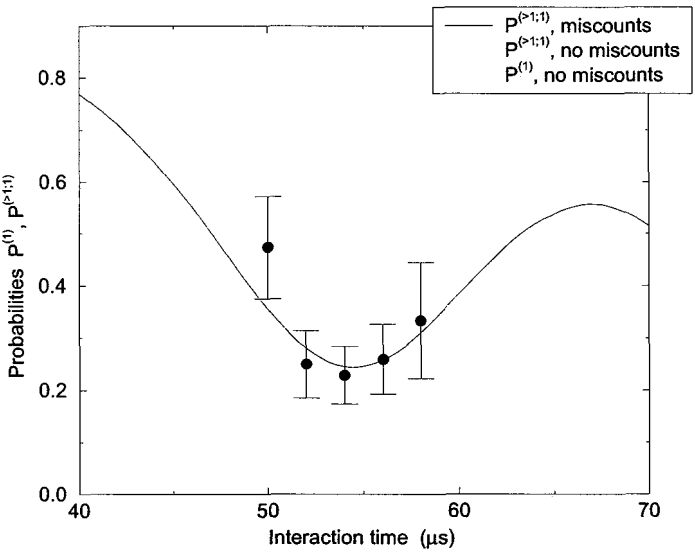

Figure 4: Comparison between theory and experiment. Investigated here are the probabilities also shown in Fig. 3. The experimental data are evaluated according to Eq. 2. This ratio is independent of the absolute detector efficiency and is dependent only on the relative detector efficiencies of the upper and lower state detectors and on the miscount probability, which can be measured experimentally. The relative detector efficiencies can be considered to be approximately equal to one. On the other hand, a calculation of the probability of finding one lower-state atom per pulse is highly dependent on the absolute detector efficiency. The two theoretical curves presented for $P^{(>1;1)}$ are a theoretical prediction of Fock state creation and a theoretical result which takes into account the experimentally measured miscounts of 7% in the lower-state detector and 2% in the excited-state detector. Given the extreme conditions for operation of the apparatus, there is excellent agreement between theory and experiment. The single-atom probability is evaluated to be 83.2%. The parameters for the experiment were, τ_{cav} = 300 ms, $\tau_{\rm pulse} = 0.066\,\tau_{cav}$, pulse spacing of 1 s, $n_{\rm th} = 0.03$, $N_{\rm a} = 4$.

As the present apparatus was designed for operating the micromaser under steady-state conditions, the current results were obtained with non-ideal operating parameters of the apparatus. In order to overcome this disadvantage, future developments will incorporate two improvements to increase the atomic flux and introduce a second pulse of atoms with variable velocity to act as a field probe. With these changes it will be easier to arrive at the optimum conditions for the Fock source and, in addition, will allow direct measurement of the cavity photon number by means of Rabi oscillations of the probe atom [11] and further studies of quantised field effects.

In relation to our previous method of Fock state creation [11], the source presented here has the significant advantage of being unconditional and therefore significantly faster in preparing a target quantum state. Previously, the state was prepared by the dynamics of the interaction of excited state atoms with the cavity field. State reduction occurred on detection of a lower-state atom, indicating preparation of the

desired cavity field. In the current experiment, however, the cavity field is correctly prepared in 83.2% of the pulses, independently of state reduction and hence atomic detection efficiency. Simply detecting the lower-state atom as it emerges from the cavity increases the fidelity of the one-photon Fock state to $\geq 95\%$ at the moment of detection (incorporating both dissipative losses and detector miscounts). Assuming 40% detector efficiency, detection of a lower-state atom within any given preparation pulse will occur with a 36.8% probability. This should be compared with the 95% fidelity of the measured Fock state in [11], in which there was a $\leq 1\%$ probability of detecting the correctly prepared state. Along with the first observation of the operation of a single-photon Fock state source on demand, we thus also have an order-of -magnitude improvement of Fock state creation over our previous experiment.

The second part of this paper reports on the progress of our work on ions in optical cavities. The interaction of a single atom with a single field mode of a high-finesse cavity has been the subject of a number of experiments in the field of cavity QED (see, e.g. Ref. [15]). However, most of these investigations suffer from a lack of control over the position of the atom, which results in non-deterministic fluctuations of the coupling between atoms and the field. In this context, the strong localisation and position control available when an ion trap is combined with an optical cavity would be a big step forward and would become a key technology for future progress in cavity QED in the optical range. We are now implementing two experiments exploiting localisation of an ion in a cavity. By pulsed excitation of a maximally coupled ion, single-photon wave packets may be emitted from the cavity on demand [14,15,27] (single-photon gun). Under conditions of strong coupling, a single calcium ion in the cavity provides sufficient gain to build up a laser field [13]. Like a single ion in free space, which was previously shown to be an excellent source of antibunched light [28,29], radiation from a single-ion laser has nonclassical photon statistics and correlations.

An equally attractive goal in the area of cavity QED is the simultaneous interaction of two or more ions with a single-cavity mode. Due to the linear geometry of our trap several ions can be stored within the mode volume. As a first test, we placed an array of two ions in the cavity field and observed the total fluorescence. We succeeded in matching the ion crystal to the two maxima of the TEM_{01} mode of the cavity. In such a configuration the cavity field may be used to entangle the two ions [30,31]. This is a promising alternative to schemes involving the ions' motional degrees of freedom, since there is no need for cooling the vibrational modes of the string below the Doppler temperature. Using a cavity to perform quantum operations on adjacent pairs of ions in a long string is a viable route to a scalable quantum computer.

In the following, we now give a progress report of our experiment. (For details see also Ref. [32].) We are using a linear trap with Ca ions (see Fig. 5). As an initial test of the setup for the above-mentioned cavity QED experiments, we used the trapped Ca ions to probe the optical field in the cavity. The Ca ion is sensitive to radiation close to the resonance line $4^2S_{1/2} - 4^2P_{1/2}$ at a wavelength of $\lambda = 397$ nm. The fluorescent light emitted by the ion is collected with a lens (numerical aperture $= 0.17$) and detected with a photomultiplier tube (overall detection efficiency $\eta \approx$

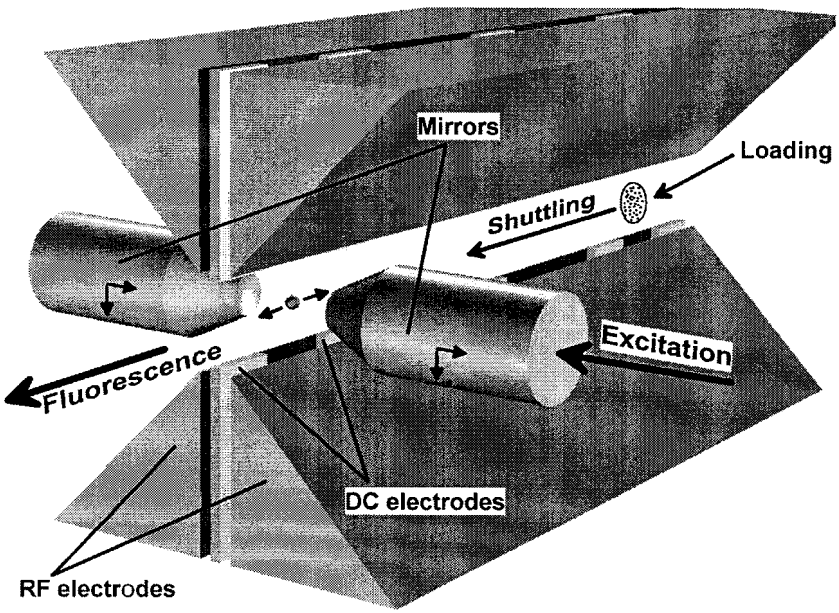

Figure 5: Experimental arrangement of trap electrodes and cavity mirrors. The ion is loaded at the rear end of the trap and shuttled to the mirror region. Fluorescence is observed from the side of the cavity. For scans in the direction of the trap axis, the ion is moved with DC electrodes. In all other directions, the cavity is translated relative to the ion's position, as indicated by arrows.

10^{-4}). The observed fluorescence rate R is proportional to the local intensity of the optical field at the position $\vec{r}$ of the ion, i.e. $R \propto I(\vec{r})$, provided there is no saturation of the atomic transition. By scanning the position of the ion in the field and detecting the fluorescence rate at each point, a high-resolution map of the optical intensity distribution is obtained. It should be noted that a single ion can also probe the amplitude distribution $\vec{E}(\vec{r})$ of the light field and hence measure its phase. To this end, heterodyne detection of the fluorescent light must be used, with the exciting laser as a local oscillator [7,29].

With the single ion as a probe, we investigated the eigenmodes of a Fabry-Perot resonator formed by two mirrors (radius of curvature = 10 mm) at a distance of L = 6 mm (Fig. 5). The transverse mode pattern is described by Hermite-Gauss functions with a beam waist $w_0 \approx 24\,\mu$m, while in the direction of the cavity axis a standing wave builds up. In the experiment, a particular cavity mode is excited by a laser beam with a power of a few hundred nanowatts at 397 nm. The length of the cavity is actively stabilised to this mode.

An ion is loaded in the trap after electron-impact ionisation of calcium atoms. Since the electron beam and the calcium beam would degrade the optical mirrors and make stable trapping difficult, we use a linear trap and load it in a region spatially separated from the observation zone, as shown in Fig. 5. Subsequently,

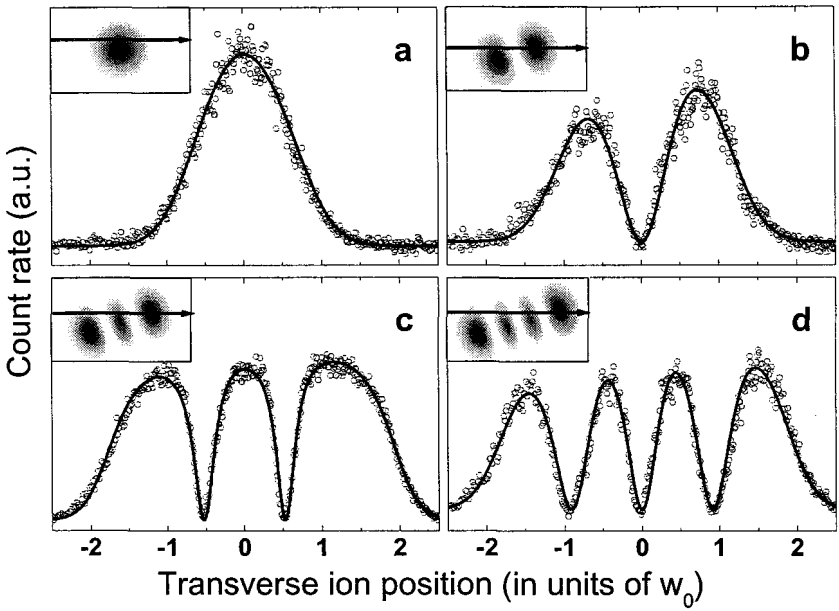

Figure 6: Transverse profiles of the Hermite-Gauss modes of the cavity, obtained by monitoring the ion's fluorescence while scanning over a range of 120 μm. The solid line is a fit including saturation of the transition. The inset shows the calculated intensity distribution of the mode and indicates the scan path. The modes are a) TEM_{00}, b) TEM_{01}, c)TEM_{02}, d) TEM_{03}.

DC electrodes along the axis are employed to shuttle the ion over a distance of 25 mm to the uncontaminated end of the trap, where the cavity is located, oriented at right angles to the trap axis. Residual DC fields in the radial direction must be carefully compensated with correctional DC voltages to place the ion precisely on the nodal line of the RF field (coinciding with the trap axis), so as to prevent the trapping field from exciting the micromotion of the ion.

In the direction of the trap axis, the ion is confined in a DC potential well which is approximately harmonic with an oscillation frequency of $\omega_z \approx 300$ kHz. By applying asymmetric voltages, the minimum of the potential well and thus the equilibrium position of the ion is moved along the trap axis. By simultaneously monitoring the fluorescence, we sampled one-dimensional cross-sections of the cavity mode. The width of the ion's wave function in the axial potential well is a few hundred nanometres, which provides sufficient resolution to map the transverse mode pattern with an intensity distribution varying on a scale given by the cavity waist w_0.

Figure 6 shows scans of the first four TEM_{0n} modes of the cavity obtained in this way. The fluorescence data are not entirely symmetric because of a small displacement and rotation of the cavity eigenmodes with respect to the trap axis. In each plot, an inset indicates the path along which the ion is scanned. The solid

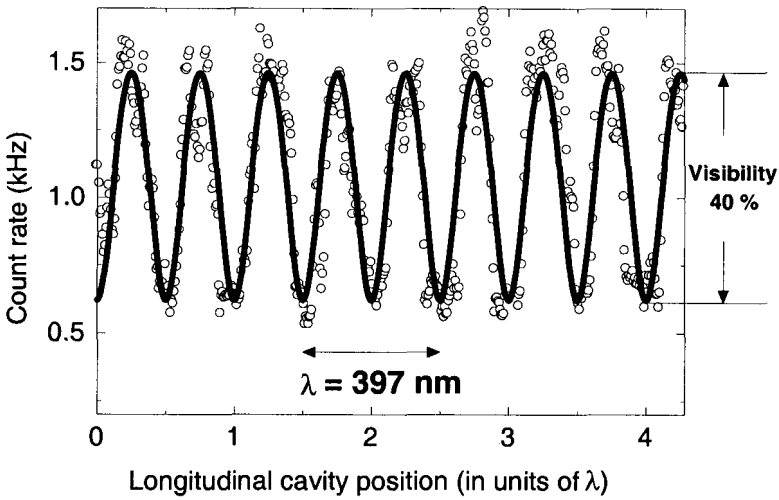

Figure 7: Single-ion mapping of the longitudinal structure of the cavity field. The visibility is determined by the residual thermal motion of the Doppler-cooled ion. It corresponds to a resolution of 60 nm. The localisation of the ion's wave packet in this measurement is 16 nm.

curves in Fig. 6 are obtained from a fit using Hermite-Gauss functions and take into account saturation of the ion's transition. The influence of saturation is apparent in Fig. 6c, where a slightly higher intensity was injected into the cavity. In all cases, the correspondence with the measured fluorescence is excellent.

The ion's motion must be restrained to the trap axis, since off the axis the radio–frequency field of the trap would lead to micromotion. To scan other dimensions of the field, the sample must be moved. In our experiment this is done by piezoelectrically translating the entire cavity assembly perpendicularly to the trap axis. In this way complete three-dimensional mapping of the mode field can be obtained [32].

RF confinement of the ion perpendicular to the trap axis is also harmonic, but the corresponding oscillation frequency $\omega_r \approx 1.1\,\mathrm{MHz}$ is larger than the axial frequency so that field structures in the radial direction of the trap are better resolved. The resolution achieved by our method may be determined most accurately by probing the standing-wave field created between the cavity mirrors, which varies on a scale of $\lambda/2$. To this end, the cavity was moved parallel to its axis while keeping the ion stationary and monitoring its fluorescence. Figure 7 shows the mapping of the cavity field obtained in this way. A pronounced standing-wave pattern is observed with a visibility of 40 %. For details see also Ref. [32].

Taking advantage of the excellent localisation in ion traps, we performed the hitherto most precise measurement of a three-dimensional spatial structure of an optical field over a range of up to 100 μm. As a demonstration, we scanned modes of a low-loss optical cavity. The precise positioning we achieve implies deterministic

control of the coupling between the ion and field. At the same time, the field and the internal states of the ion are not affected by the trapping potential. What we have realised, therefore, is an ideal system for cavity QED with a single particle.

2 Conclusion

This paper reviews our work on the generation of photon number states on demand using the micromaser. In addition, it describes first experiments using a single trapped ion in conjunction with an optical cavity. The system described in the second part of the paper shows a great promise and will open a series of new interesting applications.

References

1. H. Zbinden, N. Gisin, B. Huttner, and W. Tittel, J. Cryptol. **13**, 207 (2000); H.-K. Lo and H. F. Chau, Science **283**, 2050 (1999).
2. K. M. Gheri, C. Saavedra, P. Törmä, J. I. Cirac, and P. Zoller, Phys. Rev. A **58**, R2627 (1998); S. J. van Enk, J. I. Cirac, and P. Zoller, Phys. Rev. Lett. **78**, 4293 (1997); S. J. van Enk, J. I. Cirac, and P. Zoller, Science **279**, 205 (1998).
3. J. I. Cirac, P. Zoller, H. J. Kimble, and H. Mabuchi, Phys. Rev. Lett. **78**, 3221 (1997); A. S. Parkins, P. Marte, P. Zoller, and H. J. Kimble, Phys. Rev. Lett. **71**, 3095 (1993); S. Parkins and H. J. Kimble, J. Opt. B. **1**, 496 (1999).
4. T. Jennewein, C. Simon, G. Weihs, H. Weinfurter, and A. Zeilinger, Phys. Rev. Lett. **84**, 4729 (2000); D. S. Naik, C. G. Peterson, A. G. White, A. J. Berglund, and P. G. Kwiat, Phys. Rev. Lett. **84**, 4733 (2000); W. Tittel, J. Brendel, H. Zbinden, and N. Gisin, Phys. Rev. Lett. **84**, 4737 (2000).
5. The error-tolerant quantum computing proposal by D. Gottesman, I. L. Chuang, Nature **402**, 390 (1999) requires that a "quantum resource" be supplied *on demand* to facilitate computation. Such a source can be provided by the apparatus considered here. See also J. Preskill, Nature **402**, 357 (1999); D. Johnathon and M. B. Plenio, Phys. Rev. Lett., **83**, 3566 (1999).
6. Sources of single atoms, such as that described in this paper, are routinely employed for hypothetical tasks such as creation of an atomic beam with arbitrary timing sequence or for stabilisation of cavity states. See, for example, D. Vitali, P. Tombesi, and G. Milburn, Phys. Rev. A **57**, 4930 (1998).
7. J. T. Höffges, H. W. Baldauf, W. Lange, and H. Walther, J. Mod. Opt. **44**, 1999 (1997).
8. C. Brunel, B. Lounis, P. Tamarat, and M. Orrit, Phys. Rev. Lett. **83**, 2722 (1999).
9. C. K. Hong and L. Mandel, Phys. Rev. Lett. **56**, 58 (1986).
10. J. Kim, O. Benson, H. Kan, and Y. Yamamoto, Nature **397**, 500 (1999).
11. B. T. H. Varcoe, S. Brattke, M. Weidinger, and H. Walther, Nature **403**, 743 (2000).
12. M. Weidinger, B. T. H. Varcoe, P. Heerlein, and H. Walther, Phys. Rev. Lett. **82**, 3795 (1999).

13. G. M. Meyer, H.-J. Briegel, and H. Walther, Europhys. Lett. **37**, 317 (1997).
14. C. K. Law and J. H. Eberly, Phys. Rev. Lett. **76**, 1055 (1996); C. K. Law and H. J. Kimble, J. Mod. Opt. **44**, 2067 (1997); P. Domokos, M. Brune, J. M. Raimond, and S. Haroche, Eur. Phys. J. D **1**, 1 (1998).
15. A. Kuhn, M. Hennrich, T. Bondo, and G. Rempe, Appl. Phys B **69**, 373 (1999); P. W. H. Pinkse, T. Fischer, P. Maunz, and G. Rempe, Nature **404**, 365 (2000); J. Ye, D. W. Vernooy, and H. J. Kimble, Phys. Rev. Lett. **83**, 4987 (2000); C. J. Hood, T. W. Lynn, A. C. Doherty, A. S. Parkins, and H. J. Kimble, Science **287**, 1447 (2000).
16. See, for example, M.O. Scully and M. S. Zubairy, *Quantum Optics* (Cambridge University Press, 1997).
17. G. Rempe, F. Schmidt-Kaler, and H. Walther, Phys. Rev. Lett. **64**, 2783 (1990).
18. G. Rempe, H. Walther, and N. Klein, Phys. Rev. Lett. **58**, 353 (1987).
19. B. Englert, M. Löffler, O. Benson, M. Weidinger, B. Varcoe, and H. Walther, Fortschr. Phys. **46**, 897 (1998).
20. J. Krause, M.O. Scully, and H. Walther, Phys. Rev. A **36**, 4547 (1987).
21. G. Nogues, A. Rauschenbeutel, S. Osnaghi, M. Brune, J. M. Raimond, and S. Haroche, Nature **400**, 239 (1999).
22. A detailed account of the simulations used in this paper and a comparison with ideal micromaser theory can be found in S. Brattke, B.-G. Englert, B. T. H. Varcoe, and H. Walther, J. Mod. Opt. **47**, 2857 (2000).
23. S. Brattke et al., Optics Express **8**, 131 (2001).
24. S. Brattke, B. T. H. Varcoe, and H. Walther, Phys. Rev. Lett. **86**, 3534 (2001).
25. Proposals such as teleportation of an atomic state using multiple atomic beams would be substantially enhanced if atoms arrived on demand rather than by chance. See, for example, L. Davidovich, M. Zagury, M. Brune, J. M. Raimond, and S. Haroche, Phys. Rev. A **50**, R895 (1994); J. I. Cirac and A. S. Parkins, Phys. Rev. A **50**, R4441 (1994); M. H. Y. Moussa, Phys. Rev. A **55**, R3287 (1997).
26. H. J. Briegel, B. G. Englert, N. Sterpi, and H. Walther, Phys. Rev. A **49** 2962 (1994).
27. M. Hennrich, T. Legero, A. Kuhn, and G. Rempe, Phys. Rev. Lett. **85**, 4872 (2000).
28. F. Diedrich and H. Walther, Phys. Rev. Lett. **58**, 203 (1987).
29. J. T. Höffges, H. W. Baldauf, T. Eichler, S.R. Helmfrid, and H. Walther, Opt. Comm. **133** 170 (1997).
30. T. Pellizzari, S. A. Gardiner, J. I. Cirac, and P. Zoller, Phys. Rev. Lett. **75**, 3788 (1995).
31. S. B. Zheng and G. C. Guo, Phys. Rev. Lett. **85**, 2392 (2000).
32. G. R. Guthöhrlein, M. Keller, K. Hayasaka, W. Lange, and H. Walther, Nature **414**, 49 (2001).

DISCUSSION

Chairman: W. Schleich

L. Stodolsky: In the mapping of the position of the ion there will be oscillations. But the oscillations, which we are seeing, are they due to the electromagnetic modes or due to de Broglie wave packets?

H. Walther: So far we do not yet see the de Broglie wave. We have achieved this limit in other experiments, however, not yet in the one I described. But you can reach that, of course, if you really go down to the quantum ground state of the trapped ion then one can probe the overlap between the electromagnetic wave and the probability function of the trapped ion in a harmonic potential. We have a standing electromagnetic mode and the laser exciting this mode is stabilized to the cavity, so that we know the mode which we are exciting. The uncertainty in the field probing by means of the ion is determined by the rest motion of the ion due to its temperature.

S. Pascazio: I think this idea of combining the ion trap with an optical cavity is a very nice idea. I was wondering what are the future prospects you have in mind and, in particular, can you look at quantum jumps of a single particle?

H. Walther: Quantum jumps have already been seen without cavity. But you can, of course, also look for them in combination with a cavity. You can do cavity QED experiments on the basis of quantum jumps. This possibility opens up as soon as you have a single particle in a high Q-cavity. There is also an application to quantum computing, which I did not mention here. If you can combine an ion with a cavity you can use the optical field as a control parameter for the Qbit. Instead of using the ion's vibration, you can use the optical radiation as a control bit. This gives you the advantage that the ion has not to be cooled down to the vibrational ground state. Klaus Mølmer has proposed a method which uses vibrational excitation without the requirement of low temperatures for the trapped ions. This is an alternative way to the use of optical interaction. In the optical coupling, of course, you have to think about methods to bring more than one ion into the cavity and how you combine them, but there are ideas around on how to realize that.

G. Leuchs: With regard to the total number of photons on demand, you were explaining this self-stabilization. Where are the limits?

H. Walther: There is a problem if the photon number gets too high then the dynamics of photon exchange in the cavity gets very complicated so that the feedback mechanism in a trapping state does not work any more. This limits the process described. Low photon numbers are fine. However, as soon as you go to very high photon numbers, the method does not work any more. You are relying on the Jaynes-Cummings dynamics. The Jaynes-Cummings dynamics and the condition that you have to have a single atom in the cavity.

Y. Ne'eman: I will not comment on this beautiful work, just tell this story, which was prompted by Rydberg's name. In 1964 I published a paper about $SU(3)$. And I got a letter from Stockholm, not from the Nobel Foundation. The letter came from Rydberg's daughter. She compared the excitement of the formula that her father had worked out with the ones that are in particle physics now.

L. Accardi: You are speaking about number states. What do you precisely mean? How do you recognize that your number state is a pure state and not a

mixture? Do you measure statistical parameters?

H. Walther: The field is probed by Rydberg atoms. The dynamics is determined by the Rabi-flopping frequency depending on the photon number. Analysing the Rabi cycle gives the accurate composition of the field.

L. Stodolsky: You see that an excited atom comes in and a deexcited atom comes out. So you know you will have a single photon.

H. Walther: This is what we measure in the experiment producing the number state. Afterwards the photon is stored in the cavity and by a subsequent atom the field is probed. From this probing you get another proof, so we do a double check of the outcome of the experiment.

W. Schleich: How do you really measure the wave function, not just a photon statistics?

H. Walther: This is a different topic. This you can do also. Both our group and the Paris group are doing experiments in this direction. We are preparing experiments to measure the Wigner function of the one photon state.

W. Schleich: Then you would really know it is one photon state and not a mixture.

L. Wang: Do you measure the phase properties of the number state?

H. Walther: At the moment we have not yet measured the phase. However, this is the experiment one would like to do. This is a more difficult experiment since you have to measure the photon number and the phase as well. We know how to do that and we have published the method. The measurement will give the connection between phase and amplitude of the field and leads to the Wigner function of the field.

S. Lloyd: It is a really nice design for a quantum computer, just to have a line of atoms or ions, which are brought sequentially into a cavity. And if you can store a photon in there and bring it from one ion to the next then than you can actually build a universal quantum computer in this way. I was wondering how the cavity lifetime for this setup compares with the time taken to move one ion, take it out of this cavity.

H. Walther: In the moment the cavity lifetime is still much shorter than the time you need to shift the ions. In the moment we can only entangle ions which interact with the same mode.

L. Stodolsky: I want to comment on this beautiful result. You have this very long dissipation time that we are getting to the region where you might see weak interaction effects due to the Rabi oscillations. We could not see the weak interaction effects twenty-thirty years ago, because we got no more than one second. Now it is possible.

G. Leuchs: My question is a follow up of the third question. When you bring your ion to the cavity, can you bring an ion that is in a superposition of these states without disturbing this state, which is in the centre of the cavity? The process of bringing it into the cavity, will that introduce phase randomisation?

H. Walther: You have to study the interaction inside the cavity. It means that you must have the ions there from the beginning and study their interaction with a common mode.

QUANTUM PROPERTIES OF SOLITONS IN OPTICAL FIBERS FOR OPTICAL COMMUNICATION

N. KOROLKOVA, F. KÖNIG, S. LORENZ, M. MEISSNER, CH. SILBERHORN, G. LEUCHS

Zentrum für Moderne Optik, Universität Erlangen-Nürnberg, Staudtstr. 7 / B2, D-91058 Erlangen, Germany

Coherent quantum solitons show a characteristic evolution when propagating through an optical fiber, unlike their classical counterparts which are stable solutions to the nonlinear Schrödinger equation. The dynamical properties of quantum solitons as well as their use in quantum interferometry and in high-bit rate, long distance and secure optical communication are discussed.

In the last decade, quantum noise engineering of light fields has definitely experienced the change from purely fundamental research to applications in optical communication, information processing and measurements at the quantum limit. Specifically, the present contribution shows the latest achievements and prospects in optical techniques using stable intense short optical pulses, fiber solitons for these purposes.

The vision of quantum-assisted high-bit rate, long-distance and/or secure information exchange is gradually turning into reality. In the present paper, we are dealing with intense light beams, thus being in the domain of optical communication using continuous variables [1]. Conventional concerns in the field of continuous variable quantum information are the achievable degree of quantum entanglement and always only finite quantum noise reduction which are limited as a matter of principle. However, it is important to keep in mind the ultimate goal of the protocol under consideration while discussing the particular tasks arising in this context. Most of the protocols relevant for optical communication actually start and end with classical data. The quantum-mechanical properties in between allow to generate certain types of correlations between such classical data (like using quantum key distribution for secure communication) or to reach high precision in data transmission or acquisition not achievable with pure classical means (e.g. high bit rate long distance fiber-optical communication, back action evading quantum measurements, quantum interferometry). We would like to emphasize, that what counts at the very end is the quality of classical data. Thus quantum-assisted optical communication can beat its purely classical counterpart also with non-perfect quantum resources. The particular advantage of such quantum-assisted classical protocols is the fact that they can be fitted into existing, classical communication network structures [2].

Quantum subroutines of the complete classical protocols mentioned above [2] are protocols contributing within the quantum mechanical domain, accepting quantum mechanical input and delivering quantum mechanical output, such as e.g. quantum teleportation or entanglement swapping protocols. We are implementing these subroutines using optical continuous variable techniques, conventional tools in quantum optics taking advantage of efficient quantum sources and efficient and fast detection techniques.

In this paper we address classical quantum-assisted protocols which exploit

the quantum properties of fiber solitons. These are in the first line the methods for noise reduction and bit rate enhancement in modern telecommunication systems [3,4] and secure communication using quantum distributed secret key [5,6]. As useful quantum subroutines for different communication and measurement applications using intense optical soliton one can name quantum non-demolition and back-action evading measurements [7,8], quantum noise reduction (squeezing of the quantum uncertainty) [3], generation of quantum entanglement [9] and various quantum communication protocols based on it [10,11]. Our main tools to implement all these tasks are signal processing using linear optical elements and quantum noise engineering using non-linear interferometers and the multi-mode quantum structure of soliton pulses. Some of these techniques can be easily extended to any kind of optical signals, continuous-wave (CW) or pulsed. The application of fiber solitons to implement such schemes is motivated by the fact that short pulses are taking full advantage of the optical non-linearity in a fiber to generate non-classical light and by the stability of a soliton during the propagation which allows one to achieve high visibility in interferometric measurements. Other schemes, which hinges directly to the complex internal quantum structure of optical pulses [12,7], rely explicitly on quantum properties of fiber solitons.

Long distance telecommunication lines are affected by different pulse distortions and noise processes. For example, the amplifiers used to compensate for the signal depletion by losses inevitably introduce intensity noise, thus reducing the signal to noise ratio by typically 5 dB the quantum limit being 3 dB. Such effects give rise to inter-symbol interference and to fluctuations in the signal level at a receiving station and hence limit bit rates. Moreover, the high bit rate telecommunication systems are approaching gradually the border line to the quantum regime where the quantum noise of the transmitted light comes into play.

To circumvent this problem, we have investigated a highly asymmetric Sagnac interferometer [3,13], a nonlinear optical fiber-loop mirror with a beam splitting ratio of around 90:10, to reduce the amplifier noise. The Sagnac interferometer has a nonlinear input-output characteristic with regions of slope larger and smaller than one. Using the regions of slope smaller than one, in an ideal case of slope zero, the amplitude noise can be reduced. First experimental results were now achieved using an erbium-glass laser, emitting 738 fs pulses at about telecommunication wavelength of 1535nm with a repetition rate of 130MHz. The laser beam is attenuated to $3\mu W$ of average power before it is directed into the amplifier, which is used as a noise source. The gain of the amplifier is about 400 for the power of the "1" bit. The used Sagnac interferometer consists of 250m of polarization-maintaining FS-PM7811 fiber (manufacturer: 3M) and a variable-ratio fiber-coupler. The experimental setup is depicted in Figure 1.

In this experiment the variance of the intensity probability-distribution was measured using a single AC-Detector and a spectrum analyzer. The noise power, proportional to the intensity variance, was measured directly at the amplifier-output and at the output port of the Sagnac interferometer. Multiple measurements were done varying the coupling-ratio of the fiber-loop. A maximum noise-reduction of -5,45dB on the "1" bit below the amplifier output level was achieved. The noise suppression on the "0" bit is still good enough for pedestal suppression [14]. With this

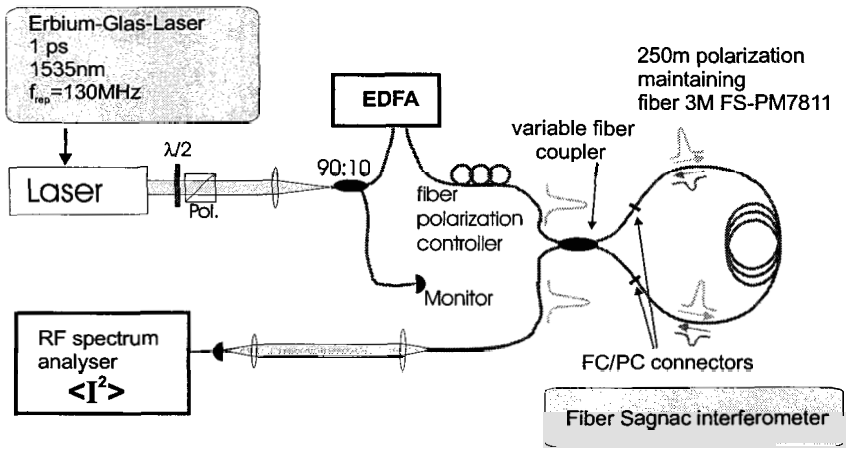

Figure 1: The experimental setup for the measurements of amplifier noise reduction.

setup bit error rate measurements have already been done and show an improvement of approximately 3 dB in terms of receiver sensitivity [15]. The asymmetric fiber Sagnac interferometer has exhibited simultaneously noise reduction and pulse shape stabilization representing a new emerging technology for fiber optical telecommunication.

The asymmetric fiber Sagnac interferometer can operate in the regime of both classical and quantum noise reduction [16,13,9]. The photon number noise reduction can be achieved due to the fiber Kerr nonlinearity, squeezing the quantum uncertainty of the light beam [17], and linear interference of the strong and weak pulses at the output of the Sagnac interferometer, realigning the minimum uncertainty along the amplitude direction [3,18]. The theoretically predicted limit of measured squeezing reaches -11 ± 1dB [19] without taking into account the Raman effect. The best observed values are -5.1 ± 0.3dB [20] and -5.7 ± 0.1dB [21] with the asymmetric interferometer and recently -6.1 ± 0.2dB [22] with the symmetric interferometer. This system does not resolve the internal quantum structure of the soliton pulse and can be explained qualitatively in a single mode picture. This complex internal structure is nevertheless of significant importance to understand and use the optical pulses, particularly in quantum communication.

If one considers the evolution of different spectral components of a travelling pulse, there is a mixing between various components during propagation due to nonlinear refractive index and chromatic dispersion. This mixing leads to correlations between different spectral components of the pulse. Such correlations also exist if quantum mechanical aspects are taken into account [12,11]. By filtering out certain spectral components of the pulse, these quantum correlations can be used to produce noise reduced or noise enhanced pulses [23,24,25,26] and to perform quantum non-demolition measurement of photon number [7].

Both schemes for generation of non-classical pulsed beams, spectral filtering and fiber Sagnac interferometer, can be implemented using a novel fiber type, the microstructured fiber[26], which allows for the control of the zero dispersion wavelength. It was demonstrated to deliver a quantum source at 800 nm which is advantageous for free space communication in the low absorption window of the atmosphere[26]. The microstructured fibre evolved from experiments with photonic band gap materials. It consists of pure silica, with a bulk core and a cladding which has a pattern of holes, oriented in longitudinal direction. Due to these holes, the cladding has a lower effective refractive index than the pure silica core. The guiding effect is the same as in standard silica fibres. By adjusting the air-hole/silica geometry, fibres with anomalous dispersion in the near infrared can be produced. The soliton in such a holey fiber can exist in a wide wavelength range between 0.8 and 1.5 μm and the nonlinear effects are much stronger even at very low pulse powers. Thus the internal quantum structure of the soliton can be studied with high accuracy.

As mentioned above, the internal structure of the soliton can be used to realize a quantum nondemolition measurement scheme. Since quantum nondemolition (QND) interactions couple two quantum systems in a specific and deterministic way, they can be exploited in the context of quantum information processing.

In our scheme for QND measurement based on the multimode correlation structure of solitons[12,11], a soliton collision is used to couple a signal soliton to a second soliton, which is labeled 'probe'. The QND observable is the photon number of the signal soliton. It transiently couples to the frequency of the collision partner such that spectral components of the two solitons are mutually quantum correlated during the soliton interaction (Fig. 2). This results in a novel scheme: the signal soliton undergoes half a collision with a probe soliton such that the transient spectral correlations are established. Then the solitons are separated and the probe soliton is spectrally filtered and directly measured. This new QND technique provides several advantages. It is immune to phase noise, a problem in previous experiments. The scheme requires merely two pulses since no phase reference pulse is needed. Since the photon numbers are correlated, only direct detection is required. The idea of coupling to a completely different degree of freedom in the probe, neither conjugate nor identical to the corresponding QND observable, may also be utilized to improve other back-action evading or quantum nondemolition measurements in $\chi^{(3)}$ and $\chi^{(2)}$ systems.

Among possible applications are noiseless optical tapping, entanglement creation, entanglement purification, and quantum state control. Using the optical fiber as $\chi^{(3)}$ nonlinear medium is perfectly compatible with subsequent quantum transport and communication purposes. In optical communication using wavelength-division multiplexing the investigation of quantum properties of soliton collisions explores ultimate bounds of channel crosstalk.

Many quantum communication protocols which were initially proposed for single photons, can be extended from discrete to continuous variable systems, for example to intense fiber soliton pulses. The implementation of continuous variable communication schemes with bright light fields has the advantage of a highly efficient, experimentally easy to handle entanglement generation, which does not rely on any spontaneous, and therefore probabilistic process. Continuous variable en-

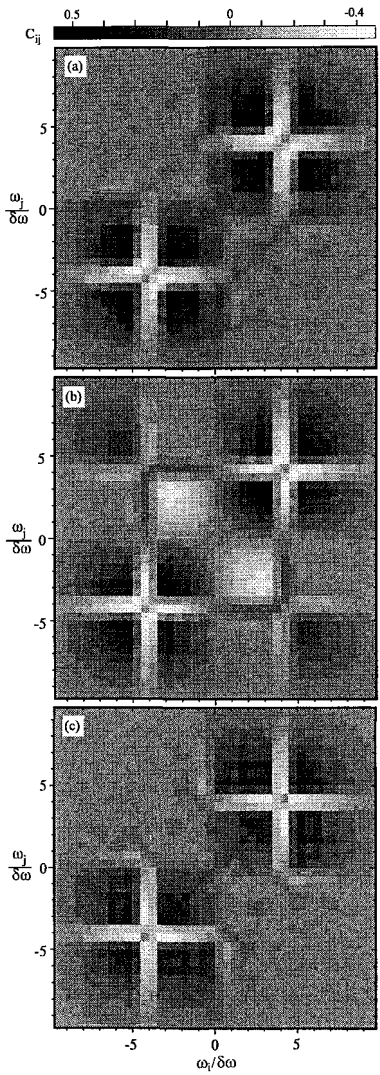

Figure 2: Quantum spectral intensity correlations of two solitons before (a), during (b) and after a collision (c) (compare to [12]). The correlation matrices in the bottom left and top right corners of each figure represent the intra-pulse spectral correlation structure within an individual probe or signal soliton. The correlation matrices in top left and bottom right show the transient inter-pulse quantum correlation between the colliding solitons. The grey scale encodes the degree of correlation between two given spectral intervals: dark grey marks the regions of positive correlation and light grey to white - those of negative correlation. For more details and explanations on formalism of correlation matrices see [7,8,12].

tanglement is characterized by the quantum correlations of two conjugate variables, like the amplitude X and phase Y quadratures of optical fields and can be generated via superimposing two amplitude squeezed beams on a 50:50 beam splitter [9]. In our experiments, the squeezed light is generated in a double fiber Sagnac interferometer [13,9] delivering two amplitude squeezed beams of orthogonal polarization simultaneously.

Along with quantum-quantum subroutines of complete protocols with fiber optical solitons mentioned above, like QND measurements, squeezing and entanglement generation, quantum teleportation, etc [11,10], it is possible to perform complete protocols such as quantum-assisted secret key distribution. Quantum key distribution (QKD) allows two communicating parties Alice and Bob to generate a shared secret bit string for secure information transfer. Several protocols for QKD with continuous variables have been published recently [27].

In our approach we exploit the quantum correlations in two conjugate quadratures X and Y of a pair of entangled Gaussian beams, for example entangled optical solitons [5]. The binary bits are encoded by the independent and completely random choice of Alice and Bob to detect either the quadrature X or Y for prearranged time slots Δt. This choice will later determine to the bit value, e. g. $X \rightarrow 0$ and $Y \rightarrow 1$. Therefore both Alice and Bob never have to publish the type of measurements they do. Instead Alice discloses the results of the measurement of X or Y to Bob by ways of a classical channel. Thus by taking Alice's information into account Bob can estimate Alice's choice by testing correlations of his and Alice's measurement results and derive her encoded bit value 0 or 1. He will tell Alice to keep time intervals, where he could find valid correlations and exclude eavesdropping. Figure 3 illustrates the appropriate experimental setup.

Currently it is thought that the use of continuous variable techniques does not allow quantum key distribution (QKD) beyond a loss of 3 dB. The argument leading to this limit is based on an optimal cloning approach for Gaussian states that correspond to a symmetric beam-splitting attack on the beams. The 3 dB loss limit [28], which corresponds to an 50/50 beam splitter, is ascertained by the fidelity an eavesdropper Eve can maximally achieve for an optimal cloned signal, if she replaces a lossy channel by a perfect one with an adapted beam splitter to mimic the losses. In the case of the 3 dB loss, the mutual information of all data between Alice and Bob becomes smaller than the maximum amount of information Eve shares with either of the communicating parties.

To analyze the security with respect to the losses one can rephrase the QKD presented above as a prepare-and-measure scheme. Alice's measurements on her entangled beam in one of two orthogonal quadratures X and Y yield the results Δx or Δy for the deviation of the mean field amplitude. By these measurements Alice effectively prepares squeezed conditional states from the entangled beam she sent to Bob. In this view Alice's results Δx or Δy play the role of a basis similar to the polarization basis in the BB84 protocol, whereas the measurement type encodes the bit value. It determines the direction of squeezing of the conditional states Alice prepared.

For the generation of a shared key Bob tries to figure out the direction of squeezing of Alice's conditional states, and thus the encoded bit, by quadrature

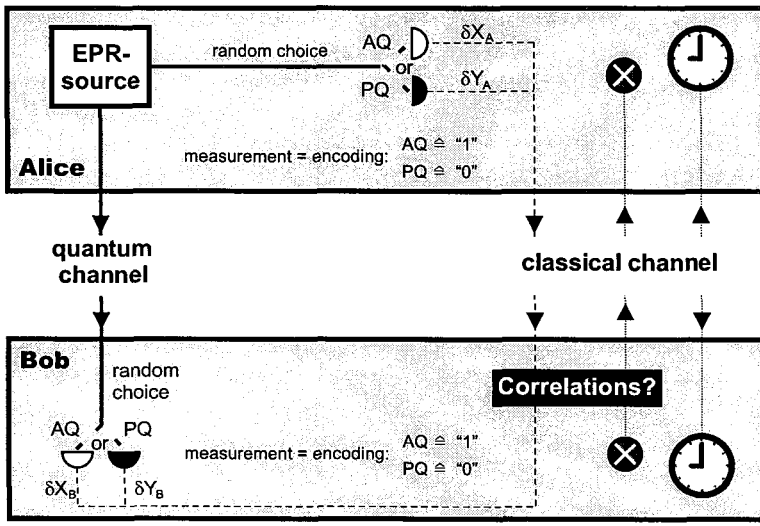

Figure 3: Setup for quantum key distribution with entangled Gaussian beams

measurements in X or Y. To prove the secrecy of the key one detects the correlations between measurement results for a subset of random selected bits. In this setting we studied the statistics that will occur near the apparent 3 dB limit and have recently shown that the secure quantum key distribution with intense fields is also possible in the presence of high loss [6].

In conclusion, in this paper we have highlighted the potential of quantum continuous variables for the realization of complete communication protocols. The quantum properties of fiber solitons can be exploited to meet the growing requirements set on bit rates, security, accuracy and efficiency of classical optical communication systems. In the quantum domain, generation of nonclassical light beams and quantum measurement techniques contribute to the solution of this task. This pushes the quantum-assisted optical communication with intense pulses closer to practical applications.

This work was supported by the Deutsche Forschungsgemeinschaft, by the EU grant under QIPC, project IST-1999-13071 (QUICOV) and by Bundesministerium für Bildung und Forschung under VDI-AZ0155/00.

References

1. S. L. Braunstein and A. K. Pati, eds., *Quantum Information Theory with Continuous Variables*, Kluwer Academic, Dodrecht, in print; D. Bouwmeester, A. Ekert, and A. Zeilinger, eds., *The Physics of Quantum Information*, Springer, Berlin, 2000.

2. Our special thank goes to Norbert Lütkenhaus for the fruitful discussions on practical quantum communiction and putting the relevant accents in the development of practical protocols.
3. A. Sizmann and G. Leuchs, *The optical Kerr effect and quantum optics in fibers*, Progress in Optics **34**, 373 (1999).
4. M. Meißner, A. Wietfeld, N. Korolkova, B. Schmauß, A. Sizmann, and G. Leuchs, "The assymetric fiber-Sagnac interferometer in high bitrate telecommunication system", Conference on Laser and Electro-Optics CLEO/Europe - European Quantum Electronics Conference EQEC Focus Meeting, *CLEO/Europe-EQEC Focus Meeting Conference Digest*, p. 235, European Physical Society, Munich, Germany, June 18-22 (2001).
5. Ch. Silberhorn, N. Korolkova, and G. Leuchs, *Phys. Rev. Lett.* **88**, 167902 (2002).
6. Ch. Silberhorn, T. C. Ralph, N. Lütkenhaus, and G. Leuchs, "Continuous variable quantum cryptography - beating the 3 dB loss limit", arXiv:quant-ph/0204064 (2002).
7. F. König, M. Zielonka, and A. Sizmann, "Transient photon-number correlations of interacting solitons", *Phys. Rev.* A, in print (2002).
8. F. König, "QND Measurement of Photon Number", PhD Thesis, Universität Erlangen-Nürnberg (2001).
9. Ch. Silberhorn, P. K. Lam, O. Weiß, F. König, N. Korolkova, and G. Leuchs, *Phys. Rev. Lett.* **86**, 4267 (2001).
10. N. Korolkova, Ch. Silberhorn, O. Glöckl, S. Lorenz, Ch. Marquardt, and G. Leuchs, *Eur. Phys. J. D* **18**, 229 (2002).
11. G. Leuchs and N. Korolkova, *Optics & Photonic News*, February 2002, p. 64-69.
12. S. Spälter, N. Korolkova, F. König, A. Sizmann, and G. Leuchs, *Phys. Rev. Lett.* **81,** 786 (1998).
13. N. Korolkova, G. Leuchs, S. Schmitt, C. Silberhorn, A. Sizmann, M. Stratmann, O. Weiß, and H. A. Bachor, *Nonlinear Optics* **24**, 223 (2000).
14. N. J. Smith et al, *J. Opt. Soc. Am. B* **12**, 1117 (1995).
15. R. Ludwig et al, 27th European Conference on Optical Communication ECOC'01, **2**, 178 (2001).
16. S. Schmitt, J. Ficker, M. Wolff, F. König, A. Sizmann, and G. Leuchs, *Phys. Rev. Lett.* **81,** 2446 (1998).
17. M. Kitagawa, and Y. Yamamoto, *Phys. Rev. A* **34,** 3974 (1986).
18. H. A. Haus, *Electromagnetic Noise and Quantum Optical Measurements*, Springer-Verlag, Berlin Heidelberg 2000.
19. M. J. Werner, *Phys. Rev. Lett.* **81**, 1432 (1998).
20. S. Schmitt, J. Ficker, A. Sizmann, and G. Leuchs, "Investigation of strongly photon-number squeezed solitons from an asymmetric fiber-Sagnac interferometer", Annual Report, Chair for Optics, University of Erlangen-Nuremberg, 1998, p. 63.
21. D. Krylov, and K. Bergman, *Optics Lett.* **23,** 1390 (1998).
22. C. X. Yu, H. A. Haus, and E. P. Ippen, *Opt. Lett.* **26**, 669 (2001).
23. S.R. Friberg, S. Machida, M.J. Werner, A. Levanon, and T. Mukai, *Phys.*

Rev. Lett. **77,** 3775 (1996).
24. S. Spälter, M. Burk, U. Strößner, A. Sizmann, and G. Leuchs, *Optics Express* **2,** 77 (1998).
25. F. König, S. Spälter, I. L. Shumay, A. Sizmann, Th. Fauster, and G. Leuchs, *J. Mod. Opt.* **45,** 2425 (1998).
26. S. Lorenz, Ch. Silberhorn, N. Korolkova, R.S. Windeler, and G. Leuchs, *Appl.Phys.B* **73**, 855-859 (2001).
27. T. C. Ralph, *Phys. Rev.* **A 61**, 010303(R) (2000); M. Hillery, *Phys. Rev.* **A 61**, 022309 (2000); M. D. Reid, *Phys. Rev.* **A 62**, 062308 (2000); T. C. Ralph, *Phys. Rev.* **A 62**, 062306 (2000); N. J. Cerf, M. Levy, and G. Van Assche, *Phys. Rev.* **A 63**, 052311 (2001); D. Gottesman *et al*, *Phys. Rev.* **A 63**, 022309 (2001); K. Bencheikh et al, *J. Mod. Opt.* **48**, 1903 (2001); F. Grosshans and Ph. Grangier, *Phys. Rev. Lett.* **88**, 057902 (2002); A. C. Funk and M. G. Raymer, *Phys. Rev.* **A 65**, 042307 (2002).
28. F. Grosshans and P. Grangier, *Phys. Rev.* **A 64**, 010301(R) (2001).

DISCUSSION

Chairman: W. Schleich

W. Schieve: How do you quantize your equation?

G. Leuchs: This is the non-linear Schrödinger equation. The calculations were done using the Bethe-Ansatz and the Hartree approximation assuming that the nonlinearity of each photon experiences depends only on its own coordinate in the pulse and not on the coordinates of the other photons.

G. Nimtz: You mentioned that you can measure in a non-demolition way the intensity of one soliton by the second soliton using phase shift. Could you comment on the mechanisms underlying this process?

G. Leuchs: Yes. I think the best thing is to look back at this picture. Due to the Kerr effect, a single soliton experiences the intensity dependent phase shift. If we have two solitons, which are separated in terms of the spectral frequency, and if they overlap in time, the presence of the one will give rise to the phase shift of the other through the intensity dependent refractive index, i.e. through the Kerr effect. This shift can be of the order of the width of the soliton which consist of 10^9 photons. The shift is sensitive enough to make measurements in the quantum regime.

H. J. Kimble: Can I comment before I put in a question. Of course, those conditions in 1994 that have been virtually champions in the quantum optic squeezing were not at all sufficient and necessary. As a result several published experiments satisfy these conditions but are not generally regarded as QND measurements.

G. Leuchs: That is right. I agree.

H. J. Kimble: Now, my question. In your wild imagination, could you imagine making a soliton gathering one or ten photons?

G. Leuchs: That is of course something we are thinking about. You need a phase shift per photon which is close to unity. But such a high nonlinear phase

shift would not only be interesting for a pulse of a few photons but also for pulses with millions of photons. In this way one could generate macroscopic cat states. However, this seems to be out of reach at the moment. It is a question of the relation between non-linearity and losses. People have started to make fibers with much higher non-linearity but so far they are much more lossy and you do not get any advantage. This is primarily a technological problem. Standard optical fibers were also much more lossy twenty years ago. There will possibly be an improvement also for highly non-linear fibers such as photonic crystal fibers. We have started to do experiments with such fibers. There you have a much stronger confinement, which also enhances the effective non-linearity, and maybe there are some other beneficial effects. At the moment, in terms of technology, I do not know whether it will be possible to reach the regime with the phase shift per photon of order of unity and with negligible losses. One could also think of using a material with a resonance and of working close to resonance, e.g. by using fibers made out of semiconductor material. So, I think there is a lot to do on the material side, and I think the prospects are high. The few photon soliton will probably become real in the future.

PRACTICAL CREATION AND DETECTION OF POLARIZATION BELL STATES USING PARAMETRIC DOWN-CONVERSION

K. J. RESCH, J. S. LUNDEEN, AND A. M. STEINBERG
Department of Physics, University of Toronto
60 St. George Street, Toronto ON M5S 1A7
CANADA

The generation and detection of maximally-entangled two-particle states, 'Bell states', are crucial tasks in many quantum information protocols such as cryptography, teleportation, and dense coding. Unfortunately, they require strong inter-particle interactions lacking in optics. For this reason, it has not previously been possible to perform complete Bell state determination in optical systems. In this work, we show how a recently developed quantum interference technique for enhancing optical nonlinearities can make efficient Bell state measurement possible. We also discuss weaknesses of the scheme including why it cannot be used for unconditional quantum teleportation.

1 Introduction

The new science of quantum information builds on the recognition that entanglement, an essential but long underemphasized feature of quantum mechanics, can be a valuable resource. Many of the headline-grabbing quantum communication schemes (including quantum teleportation [1,2,3], dense coding [4,5], and quantum cryptography [6,7]) are based on the maximally-entangled two-particle quantum states called Bell states. Using the polarization states of a pair of photons in different spatial modes, the four Bell states are written as:

$$\begin{aligned} |\psi^{\pm}\rangle &= \frac{1}{\sqrt{2}}\left(|V\rangle_1 |H\rangle_2 \pm |H\rangle_1 |V\rangle_2\right) \\ |\phi^{\pm}\rangle &= \frac{1}{\sqrt{2}}\left(|H\rangle_1 |H\rangle_2 \pm |V\rangle_1 |V\rangle_2\right), \end{aligned} \tag{1}$$

where $|H\rangle$ and $|V\rangle$ describe horizontal- and vertical-polarization states, and the subscripts 1 and 2 are spatial mode labels. These four states form a complete, orthonormal basis for the polarization states of a pair of photons. In each Bell state, a given photon is completely unpolarized but perfectly correlated with the polarization of the other photon. Photon Bell states were produced in atomic cascades for the first tests of the nonlocal predictions of quantum mechanics [8]. Since that time, parametric down-conversion sources [9,10,11,12,13] have replaced cascade souces due to their ease of use, high brightness, and the high-purity states they produce. However, down-conversion sources do not deterministically prepare photon Bell states, but rather states in which the Bell state component is in a coherent superposition with a dominant vacuum term; coincidence detection of photon pairs projects out only the two-photon component of the state.

While optical Bell state source technology has shown marked improvement, methods of distinguishing these states has proven a difficult challenge. Perhaps the most well-known example of why distinguishing Bell states is important comes from quantum teleportation. A general projective measurement is required for

unconditional teleportation; experimental teleportation was originally limited to a maximum efficiency of 25% since only the singlet state, $|\psi^-\rangle$, could be distinguished from the triplet states [2]. The challenge for measuring Bell states stems from the requirement for a strong inter-particle interaction, which is usually nonexistent for photons. Without such a nonlinearity, only two of the four states can be distinguished [14]. It was realized that a strong enough optical nonlinearity, typically $\chi^{(3)}$, could be used to mediate a photon-photon interaction. Unfortunately, even the nonlinearities of our best materials are far too weak. An experiment using standard nonlinear materials to demonstrate a scheme for unconditional teleportation was limited to extremely low efficiencies (on the order of 10^{-10}) by the tiny nonlinearities involved [15]. Proposals for extending optical nonlinearities to the quantum level include schemes based on cavity QED [16], electromagnetically-induced transparency [17], photon-exchange interactions [18], and quantum interference techniques [19,20]. Using the latter, we have recently demonstrated a conditional-phase switch [20] which is similar to the controlled-phase gate in quantum computation. In this work, we show how to apply the conditional-phase switch to the problem of Bell state detection. It should be noted that if recently published schemes for performing quantum computing with linear optics [21,22] could be experimentally realized, then the problem of distinguishing all four Bell states could be performed without the need for strong optical nonlinearities. Theoretical work has also shown that if the Bell state is embedded appropriately in a higher-dimensional Hilbert space, all of the Bell states can be distinguished [23].

Strong optical nonlinearities are desired so that one can construct a controlled-π, a specific case of the controlled-phase gate for photons. Such a gate and all one-qubit rotations form a universal set of gates for the more general problem of quantum computation – just as the NAND gate is universal for classical computation. The controlled-π transformation [24] is described by:

$$\begin{aligned} |0\rangle_1 |0\rangle_2 &\longrightarrow |0\rangle_1 |0\rangle_2 \\ |0\rangle_1 |1\rangle_2 &\longrightarrow |0\rangle_1 |1\rangle_2 \\ |1\rangle_1 |0\rangle_2 &\longrightarrow |1\rangle_1 |0\rangle_2 \\ |1\rangle_1 |1\rangle_2 &\longrightarrow -|1\rangle_1 |1\rangle_2 , \end{aligned} \tag{2}$$

in which the two qubit states are $|0\rangle$and $|1\rangle$ and the subscript is the qubit label. This transformation does nothing to the input state unless both qubits have a value of $|1\rangle$, in which case it applies a phase-shift of π. On the surface this transformation appears to do nothing since an overall phase in quantum mechanics is meaningless. However, it is clearly nontrivial when applied to superpositions of states.

The polarization of the photon makes an ideal two-level system for encoding a qubit largely due to its relative immunity to environmental decoherence. A large enough $\chi^{(3)}$ nonlinearity could be used to effect the c-π transformation on a pair of photons. Given a polarization-dependent $\chi^{(3)}$, or through the use of polarizing beam-splitters, only photon pairs with, say, horizontal polarization would experience the nonlinear interaction and pick up the additional phase shift. Such a gate could then be incorporated into the optical implementation of the quantum circuits shown in Fig. 1a. and 2a. (similar circuits are discussed in [14,25]). The circuit in Fig. 1a. converts, through unitary transformation, a state in the rectilinear

product state basis (i.e. $|0\rangle_1|0\rangle_2$, $|0\rangle_1|1\rangle_2$, $|1\rangle_1|0\rangle_2$, and $|1\rangle_1|1\rangle_2$) to the Bell basis. The circuit in Fig. 2a. performs the opposite function converting a Bell state via unitary transformation to the rectilinear basis. In essence, these circuits allow for the creation and removal of entanglement between pairs of qubits. If the qubit states $|0\rangle$ and $|1\rangle$ are encoded into the polarization states $|H\rangle$ and $|V\rangle$ in two different spatial modes 1 and 2, then an optical realization of the circuit in Fig. 2a. allows for the conversion of a photon pair in a Bell state to a rectilinear basis state. These four rectilinear basis states are easily distinguishable using the simple optical setup shown in Fig. 3. Thus, after passing the photon pair in a Bell state through the optical realization of the circuit in Fig. 2a., the subsequent detection of the rectilinear state is equivalent to determination of the Bell state.

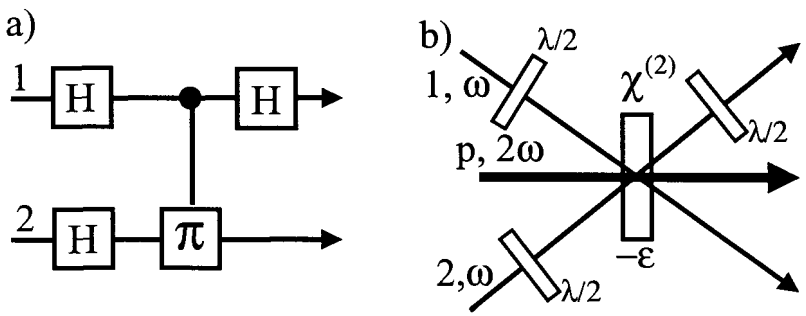

Figure 1. a) A quantum circuit and b) its optical analogue for the creation of Bell states from product states. a) The quantum circuit acts on a pair of input modes 1 and 2. The circuit uses one-qubit Hadamard gates, and a two-qubit controlled-π gate. This circuit performs a unitary transformation on the inputs and takes each of the four possible qubit product states to a different Bell state. b) The optical analogue of the quantum circuit. In the diagram, $\lambda/2$ are half-wave plates oriented at 22.5 degrees and $\chi^{(2)}$ is a nonlinear material. The device is capable of converting the state of a photon pair in a product state of polarization to one of the Bell states, provided that the input is in the correct superposition with the vacuum.

The conditional-phase switch we propose is related to the controlled-phase gate of quantum computation and is described in the theory section of this work. The switching effect occurs in a $\chi^{(2)}$ nonlinear material that is pumped by a strong, classical beam. This pump beam is capable of creating pairs of down-converted photon pairs into a pair of output modes. Pairs of photons, in a coherent superposition with the vacuum, pass through the crystal into those same output modes. It is the interference between the amplitudes for multiple paths leading to a photon pair that greatly enhances the effective nonlinearity; since the down-converted light is only created in pairs, the interference only affects the amplitude for photon pairs. However, since the switching effect is based on an interference effect, it is intrinsically dependent on the phase and amplitude of the incoming beams. This has two consequences. First, the switch requires an input which is in a coherent superposition with the vacuum. In this way, the input has the required *uncertain* number of photons, since photon number and phase are conjugate quantities. And

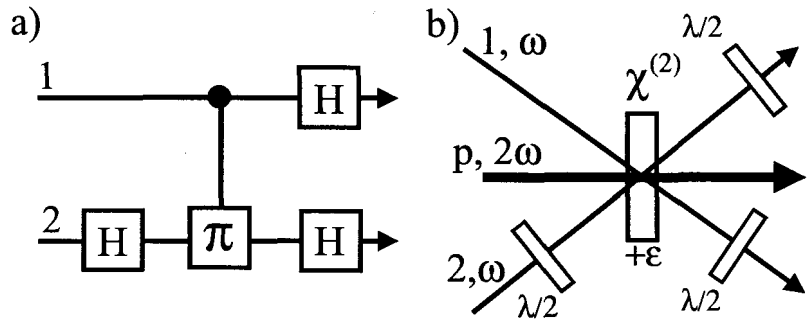

Figure 2. a) A quantum circuit and b) its optical analogue for the conversion of Bell states to product states. a) This quantum circuit takes a pair of qubits in input modes 1 and 2 and performs a unitary transformation that will convert a Bell state to a product state. b) The optical analogue of the quantum circuit takes a photon pair in a Bell state to a rectilinear product state, provided the photon pair is in the correct superposition with the vacuum.

second, the switch works as described only for states in the correct superposition with the vacuum, not a general input state. As we will show, these conditions do allow for one to distinguish between the four Bell states provided they are in the correct superposition with the vacuum. Nonetheless, the conditions are too stringent to allow for unconditional teleportation using this method.

First, we describe the effective nonlinearity. Then we show how the nonlinearity can be used to construct optical devices analogous to the quantum computation circuits shown in Fig. 1a. and Fig. 2a.

2 Theory

2.1 Effective Nonlinearity

The general down-conversion state can be written as

$$|\psi\rangle = |0\rangle + \varepsilon \left(|H\rangle_1 |H\rangle_2 \quad |H\rangle_1 |V\rangle_2 \quad |V\rangle_1 |H\rangle_2 \quad |V\rangle_1 |V\rangle_2 \right) \begin{pmatrix} \alpha \\ \beta \\ \gamma \\ \delta \end{pmatrix}, \qquad (3)$$

where the part of the state describing photon pairs has been written as an inner product. The amplitudes for the polarization states $|H\rangle_1 |H\rangle_2$, $|H\rangle_1 |V\rangle_2$, $|V\rangle_1 |H\rangle_2$, and $|V\rangle_1 |V\rangle_2$ are $\varepsilon\alpha$, $\varepsilon\beta$, $\varepsilon\gamma$, and $\varepsilon\delta$, respectively. Again, the subscripts 1 and 2 describe two different spatial modes. Throughout this theory section, we adopt a 4-dimensional vector representation to describe the polarization state of the photon pairs. In this more compact notation, the general state is written

$$|\psi\rangle = |0\rangle + \varepsilon \begin{pmatrix} \alpha \\ \beta \\ \gamma \\ \delta \end{pmatrix}, \qquad (4)$$

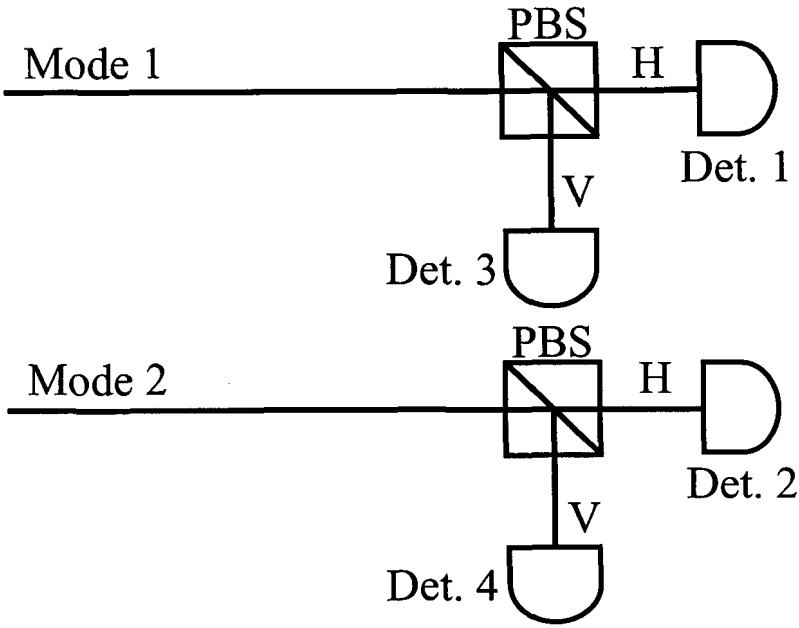

Figure 3. An optical device for distinguishing rectlinear basis states. This simple device can distinguish between the product states for the polarization of a pair of photons $|H\rangle_1 |H\rangle_2$, $|H\rangle_1 |V\rangle_2$, $|V\rangle_1 |H\rangle_2$, and $|V\rangle_1 |V\rangle_2$, where the subscripts 1 and 2 are mode labels. The device consists of a pair of polarizing beam-splitters (PBS) and 4 photon counting detectors monitoring their outputs. For example, the detection of a photon at detector 1 and detector 4 corresponds to the state $|H\rangle_1 |V\rangle_2$.

In both cases, we have suppressed the normalization factor for clarity, and for the discussion here we will restrict ourselves to the case where the probability of having a photon pair at any given time is small, i.e. $|\varepsilon|^2 \ll 1$ (as is always the case in real down-conversion experiments).

The effective nonlinearity [20] can be described as follows. Modes 1 and 2 are of frequency ω and pass through a $\chi^{(2)}$ nonlinear crystal that is simultaneously pumped by a strong classical laser beam of frequency 2ω in mode p. The modes are so chosen such that the nonlinear crystal can create degenerate horizontally-polarized photon pairs in spatial modes 1 and 2 via spontaneous parametric down-conversion, as shown in Fig. 4. The nonlinear process is mediated by the interaction Hamiltonian,

$$\mathcal{H} = g a^\dagger_{1,H} a^\dagger_{2,H} a_{p,V} + g^* a_{1,H} a_{2,H} a^\dagger_{p,V}, \tag{5}$$

where g is the coupling constant and $a_i^{(\dagger)}$ is the field annihilation (creation) operator for the i^{th} mode, and the subscripts H and V are the polarizations of the relevant modes for the type-I phase-matching. The pump laser is intense enough that we

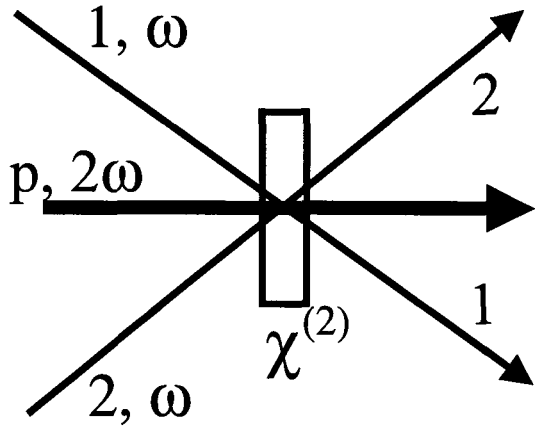

Figure 4. Schematic for the conditional-phase switch. A strong, classical, laser in mode p, of frequency 2ω, pumps a $\chi^{(2)}$ nonlinear material such that it can create down-conversion pairs in modes 1 and 2. A pair of input beams, of frequency ω, pass through the nonlinear material into modes 1 and 2. Interference between the multiple paths leading to photon pairs at the output can be used to introduce a large phase shift on the amplitude for a photon pair.

treat it classically by replacing its field operators with c-number amplitudes, ζ and ζ^*:

$$\mathcal{H} = g\zeta a^\dagger_{1,H} a^\dagger_{2,H} + g^*\zeta^* a_{1,H} a_{2,H}. \tag{6}$$

Due to phase-matching constraints, the nonlinear crystal can only produce horizontally-polarized photon pairs. In the weak coupling regime, we can use first-order perturbation theory to propagate our state under the interaction to,

$$|\psi(t)\rangle = \left(1 - \frac{it}{\hbar}\mathcal{H}\right)|\psi\rangle \tag{7}$$

$$= |0\rangle + \varepsilon \begin{pmatrix} \alpha \\ \beta \\ \gamma \\ \delta \end{pmatrix} - \frac{it}{\hbar} g\zeta \begin{pmatrix} 1 \\ 0 \\ 0 \\ 0 \end{pmatrix} \tag{8}$$

$$= |0\rangle + \varepsilon \begin{pmatrix} \alpha - \frac{it}{\hbar}\frac{g\zeta}{\varepsilon} \\ \beta \\ \gamma \\ \delta \end{pmatrix}. \tag{9}$$

To first order, this Hamiltonian simply creates an amplitude for a horizontally-polarized pair of photons. This new down-conversion amplitude interferes with the preexisting amplitude for the HH term.

The transformation, as described here, does not appear unitary. This is due to a few approximations. We assume that the vacuum term in our state is unchanged, and neglect terms describing more that one pair of photons. These approximations

are only valid in the relevant limit where $|\varepsilon| \ll 1$, where we can also suppress the normalization term for clarity. However, the exact propagator follows from a hermitian Hamiltonian and is of course unitary.

As was shown in the "railcross experiment" [26] and in our subsequent work with photon pairs from coherent state inputs [19], interference between the amplitudes for existing pairs and for down-conversion can modulate the rate of pair production. Given the phase-matching scheme presented here, only the amplitude for HH pairs is affected. Accompanying this modulation of the photon pair production rate is a shift in the phase of the horizontally-polarized photon pair term. The down-conversion crystal impresses a π phase-shift on the HH term if the down-conversion amplitude, $-itg\zeta/\hbar$ to be $-2\varepsilon\alpha$. To implement a tranformation analogous to the c-π (Eq. 2) in the coincidence basis, this is the only condition that must be enforced; the values for the coefficients α, β, and γ are free. This condition takes the place of the more usual normalization condition on α, β, γ, and δ to describe our state space. It can be enforced experimentally by controlling the amplitude and phase of the pump laser and/or the overall pair amplitude ε. Unfortunately, this means that the gate cannot be utilized on arbitrary inputs without some prior information. Under these conditions, the crystal implements

$$|0\rangle + \varepsilon \begin{pmatrix} \alpha \\ \beta \\ \gamma \\ \delta \end{pmatrix} \longrightarrow |0\rangle + \varepsilon \begin{pmatrix} -\alpha \\ \beta \\ \gamma \\ \delta \end{pmatrix}. \tag{10}$$

If horizontal polarization is used to represent a logical '0', this performs a transformation analogous to a c-π within the state space defined by our constraint on α. We do not use the conventional c-π so that we can use the common convention for the Hadamard gate later on without the need for additional quantum gates. We will now describe how this operation can be used to perform Bell state creation under certain conditions.

2.2 *Bell state creation*

The circuit in Fig. 1a. is capable of converting each rectilinear basis state to a different Bell state. To give a concrete example, we begin with the qubit pair in the state $|0\rangle_1 |0\rangle_2$ represented as the 4-vector

$$|\psi\rangle = \begin{pmatrix} 1 \\ 0 \\ 0 \\ 0 \end{pmatrix}, \tag{11}$$

where the rows now contain the amplitudes for the states $|0\rangle_1 |0\rangle_2$, $|0\rangle_1 |1\rangle_2$, $|1\rangle_1 |0\rangle_2$, and $|1\rangle_1 |1\rangle_2$. The circuit contains one-qubit Hadamard transformations which are defined by the 2×2 matrix,

$$H = \frac{1}{\sqrt{2}} \begin{bmatrix} 1 & 1 \\ 1 & -1 \end{bmatrix} \tag{12}$$

and the two-qubit c-π gate whose operation has already been discussed. The circuit then takes the input state, $|\psi\rangle$, to the output state $|\psi'\rangle$ given by

$$|\psi'\rangle = (H_1 \otimes I_2)\,(c\text{-}\pi)\,(H_1 \otimes H_2)\,|\psi\rangle \tag{13}$$

$$= \frac{1}{2\sqrt{2}} \begin{bmatrix} 1&0&1&0 \\ 0&1&0&1 \\ 1&0&-1&0 \\ 0&1&0&-1 \end{bmatrix} \begin{bmatrix} 1&0&0&0 \\ 0&1&0&0 \\ 0&0&1&0 \\ 0&0&0&-1 \end{bmatrix} \begin{bmatrix} 1&1&1&1 \\ 1&-1&1&-1 \\ 1&1&-1&-1 \\ 1&-1&-1&1 \end{bmatrix} \begin{pmatrix} 1 \\ 0 \\ 0 \\ 0 \end{pmatrix} \tag{14}$$

$$= \frac{1}{\sqrt{2}} \begin{pmatrix} 1 \\ 0 \\ 0 \\ 1 \end{pmatrix}. \tag{15}$$

This final state is the Bell state $|\phi^+\rangle$. Each different rectilinear state input will produce a different Bell state output through this circuit.

The conditional-phase operation can be incorporated into the optical device schematically represented in Fig. 1b that can perform a very similar transformation. Instead of using a state describing a pure photon pair as input, this device requires the input pair to be in a coherent superposition with the vacuum. As discussed previously, this is merely the output from a parametric down-conversion source (Eq. 3). Here we assume the coefficients are normalized according to $|\alpha|^2 + |\beta|^2 + |\gamma|^2 + |\delta|^2 = 1$, such that $|\varepsilon|^2$ is the probability of a photon pair of any polarization being present. The photons have been created into spatial modes 1 and 2 by an initial down-conversion crystal (not shown) to serve as input to the optical device in Fig. 1b. Hadamard operations are accomplished via half-wave plates at 22.5 degrees, and the c-π has been replaced by the conditional-phase switch. The initial state will evolve as follows through the device. The pair of Hadamard gates changes the general state, $|\psi_1\rangle$, to $|\psi_2\rangle$,

$$|\psi_2\rangle = (H_1 \otimes H_2)\,|\psi_1\rangle \tag{16}$$

$$= |0\rangle + \frac{\varepsilon}{2} \begin{bmatrix} 1&1&1&1 \\ 1&-1&1&-1 \\ 1&1&-1&-1 \\ 1&-1&-1&1 \end{bmatrix} \begin{pmatrix} \alpha \\ \beta \\ \gamma \\ \delta \end{pmatrix} \tag{17}$$

$$= |0\rangle + \frac{\varepsilon}{2} \begin{pmatrix} \alpha+\beta+\gamma+\delta \\ \alpha-\beta+\gamma-\delta \\ \alpha+\beta-\gamma-\delta \\ \alpha-\beta-\gamma+\delta \end{pmatrix}. \tag{18}$$

This state passes through the conditional-phase shift, which is phase-matched to contribute an amplitude of $-\varepsilon$ for horizontally-polarized photon pairs. It will

evolve to $|\psi_3\rangle$,

$$|\psi_3\rangle = |0\rangle + \frac{\varepsilon}{2}\begin{pmatrix}\alpha+\beta+\gamma+\delta\\ \alpha-\beta+\gamma-\delta\\ \alpha+\beta-\gamma-\delta\\ \alpha-\beta-\gamma+\delta\end{pmatrix} - \varepsilon\begin{pmatrix}1\\0\\0\\0\end{pmatrix} \tag{19}$$

$$= |0\rangle + \frac{\varepsilon}{2}\begin{pmatrix}\alpha+\beta+\gamma+\delta-2\\ \alpha-\beta+\gamma-\delta\\ \alpha+\beta-\gamma-\delta\\ \alpha-\beta-\gamma+\delta\end{pmatrix}. \tag{20}$$

The final Hadamard gate acts only on mode 1, and converts $|\psi_3\rangle$ to the output state $|\psi'\rangle$,

$$|\psi'\rangle = (H_1 \otimes I_2)\,|\psi_3\rangle \tag{21}$$

$$= |0\rangle + \frac{\varepsilon}{2\sqrt{2}}\begin{bmatrix}1&0&1&0\\0&1&0&1\\1&0&-1&0\\0&1&0&-1\end{bmatrix}\begin{pmatrix}\alpha+\beta+\gamma+\delta-2\\ \alpha-\beta+\gamma-\delta\\ \alpha+\beta-\gamma-\delta\\ \alpha-\beta-\gamma+\delta\end{pmatrix} \tag{22}$$

$$= |0\rangle + \frac{\varepsilon}{\sqrt{2}}\begin{pmatrix}\alpha+\beta-1\\ \alpha-\beta\\ \gamma+\delta-1\\ \gamma-\delta\end{pmatrix}. \tag{23}$$

If, for example, the input state to this device had only an amplitude for a horizontally-polarized photon pair (i.e. $\alpha = 1$ and $\beta, \gamma, \delta = 0$), then the output state would be,

$$|\psi'\rangle = |0\rangle + \frac{\varepsilon}{\sqrt{2}}\begin{pmatrix}0\\1\\-1\\0\end{pmatrix} \tag{24}$$

$$= |0\rangle - \varepsilon\,|\psi^-\rangle. \tag{25}$$

The other 3 possible rectilinear basis inputs would each evolve to a different Bell state in a coherent superposition with the vacuum state. The resulting transformations on four possible rectilinear input states are

$$\begin{aligned}
|0\rangle + \varepsilon\,|H\rangle_1\,|H\rangle_2 &\longrightarrow |0\rangle - \varepsilon\,|\psi^-\rangle\\
|0\rangle + \varepsilon\,|H\rangle_1\,|V\rangle_2 &\longrightarrow |0\rangle - \varepsilon\,|\psi^+\rangle\\
|0\rangle + \varepsilon\,|V\rangle_1\,|H\rangle_2 &\longrightarrow |0\rangle - \varepsilon\,|\phi^-\rangle\\
|0\rangle + \varepsilon\,|V\rangle_1\,|V\rangle_2 &\longrightarrow |0\rangle - \varepsilon\,|\phi^+\rangle.
\end{aligned} \tag{26}$$

2.3 *Bell state detection*

The method just described for creating polarization Bell states is much more experimentally difficult than the elegant methods of doing so in a cleverly-oriented crystal or crystal pair [11,12]. What is unique about this method is that this device performs a one-to-one transformation between rectilinear basis states and Bell basis states. This device for creating the Bell states can, in fact, be run in reverse to distinguish between the four Bell states provided, again, that they are in a superposition with vacuum. Fig. 2a. shows a quantum circuit for transforming Bell states to the rectilinear basis, that is very similar in structure to the circuit shown in Fig. 1a. To give a concrete example, we can trace the evolution of the singlet state, $|\phi^-\rangle$, through the device. The singlet state can be written in 4-vector notation as,

$$|\psi^-\rangle = \frac{1}{\sqrt{2}} \begin{pmatrix} 0 \\ -1 \\ 1 \\ 0 \end{pmatrix}. \tag{27}$$

The circuit transforms the input state to the output $|\psi'\rangle$ in the following way,

$$|\psi'\rangle = (H_1 \otimes H_2)\,(c\text{-}\pi)\,(H_1 \otimes I_2)\,|\phi^-\rangle \tag{28}$$

$$= \frac{1}{2} \begin{bmatrix} 1 & 1 & 1 & 1 \\ 1 & -1 & 1 & -1 \\ 1 & 1 & -1 & -1 \\ 1 & -1 & -1 & 1 \end{bmatrix} \begin{bmatrix} 1 & 0 & 0 & 0 \\ 0 & 1 & 0 & 0 \\ 0 & 0 & 1 & 0 \\ 0 & 0 & 0 & -1 \end{bmatrix} \frac{1}{\sqrt{2}} \begin{bmatrix} 1 & 0 & 1 & 0 \\ 0 & 1 & 0 & 1 \\ 1 & 0 & -1 & 0 \\ 0 & 1 & 0 & -1 \end{bmatrix} \frac{1}{\sqrt{2}} \begin{pmatrix} 0 \\ -1 \\ 1 \\ 0 \end{pmatrix} \tag{29}$$

$$= \begin{pmatrix} 0 \\ 0 \\ 0 \\ 1 \end{pmatrix}. \tag{30}$$

The output state is the product state $|1\rangle_1\,|1\rangle_2$.

The optical device that performs the analogous transformation is shown in Fig. 2b. The device, again, uses half-wave plates to implement the Hadamard transformations, and the conditional-phase switch which is set to contribute an amplitude of $+\varepsilon$ for a horizontally-polarized photon pair. The input state to this device, $|\psi_1\rangle$, is again described by the general down-conversion state,

$$|\psi_1\rangle = |0\rangle + \varepsilon \begin{pmatrix} \alpha \\ \beta \\ \gamma \\ \delta \end{pmatrix}. \tag{31}$$

This state passes through the polarization rotator in mode 1 and will evolve to the

state $|\psi_2\rangle$,

$$|\psi_2\rangle = (H_1 \otimes I_2)\,|\psi_1\rangle \tag{32}$$

$$= |0\rangle + \frac{\varepsilon}{\sqrt{2}} \begin{bmatrix} 1 & 0 & 1 & 0 \\ 0 & 1 & 0 & 1 \\ 1 & 0 & -1 & 0 \\ 0 & 1 & 0 & -1 \end{bmatrix} \begin{pmatrix} \alpha \\ \beta \\ \gamma \\ \delta \end{pmatrix} \tag{33}$$

$$= |0\rangle + \frac{\varepsilon}{\sqrt{2}} \begin{pmatrix} \alpha+\gamma \\ \beta+\delta \\ \alpha-\gamma \\ \beta-\delta \end{pmatrix}. \tag{34}$$

This state is subsequently passed through the conditional-phase switch where the pump laser is set to the appropriate amplitude and phase to add an amplitude of $+\varepsilon$ for a vertically-polarized photon pair. The state evolves to $|\psi_3\rangle$ where

$$|\psi_3\rangle = |0\rangle + \frac{\varepsilon}{\sqrt{2}} \begin{pmatrix} \alpha+\gamma \\ \beta+\delta \\ \alpha-\gamma \\ \beta-\delta \end{pmatrix} + \varepsilon \begin{pmatrix} 1 \\ 0 \\ 0 \\ 0 \end{pmatrix} \tag{35}$$

$$= |0\rangle + \frac{\varepsilon}{\sqrt{2}} \begin{pmatrix} \alpha+\gamma+\sqrt{2} \\ \beta+\delta \\ \alpha-\gamma \\ \beta-\delta \end{pmatrix}. \tag{36}$$

Finally, this state passes through a pair of half-wave plates. The final state, $|\psi'\rangle$, is

$$|\psi'\rangle = |0\rangle + \frac{1}{2} \begin{bmatrix} 1 & 1 & 1 & 1 \\ 1 & -1 & 1 & -1 \\ 1 & 1 & -1 & -1 \\ 1 & -1 & -1 & 1 \end{bmatrix} \frac{\varepsilon}{\sqrt{2}} \begin{pmatrix} \alpha+\gamma+\sqrt{2} \\ \beta+\delta \\ \alpha-\gamma \\ \beta-\delta \end{pmatrix} \tag{37}$$

$$= |0\rangle + \sqrt{2}\varepsilon \begin{pmatrix} \alpha+\beta+\frac{1}{\sqrt{2}} \\ \alpha-\beta+\frac{1}{\sqrt{2}} \\ \gamma+\delta+\frac{1}{\sqrt{2}} \\ \gamma-\delta+\frac{1}{\sqrt{2}} \end{pmatrix}. \tag{38}$$

If, for example our input state has $\alpha = \delta = -1/\sqrt{2}$ and $\beta = \gamma = 0$ (i.e. the input is $|0\rangle - \varepsilon\,|\phi^+\rangle$– one of the outputs of the previous device), then the output state

would be,

$$|\psi'\rangle = |0\rangle + \sqrt{2}\varepsilon \begin{pmatrix} 0 \\ 0 \\ 0 \\ \sqrt{2} \end{pmatrix} \tag{39}$$

$$= |0\rangle + \varepsilon \begin{pmatrix} 0 \\ 0 \\ 0 \\ 1 \end{pmatrix}. \tag{40}$$

That is, the output contains only an amplitude for a photon pair in the product state $|V\rangle_1 |V\rangle_2$. The results for all of the input states are simply stated:

$$\begin{aligned} |0\rangle - \varepsilon |\psi^-\rangle &\longrightarrow |0\rangle + \varepsilon |H\rangle_1 |H\rangle_2 \\ |0\rangle - \varepsilon |\psi^+\rangle &\longrightarrow |0\rangle + \varepsilon |H\rangle_1 |V\rangle_2 \\ |0\rangle - \varepsilon |\phi^-\rangle &\longrightarrow |0\rangle + \varepsilon |V\rangle_1 |H\rangle_2 \\ |0\rangle - \varepsilon |\phi^+\rangle &\longrightarrow |0\rangle + \varepsilon |V\rangle_1 |V\rangle_2 , \end{aligned} \tag{41}$$

and are the inverse of the transformation the previous device performed.

In order to complete the measurement of the Bell state, the output of this device is passed through an optical device like the one in Fig. 3. The detection of a photon pair constitutes a successful measurement and will occur with probability $|\varepsilon|^2$ – the probability of having a Bell state in our input state. This probability ignores issues of detector and path efficiency.

3 Discussion

We have proposed a way of implementing a transformation capable of converting the polarization state of a pair of photons from the rectilinear basis to the Bell state basis and vice versa provided the photon pairs are in a known coherent superposition with the vacuum. This transformation relies on a recently reported effective nonlinearity at the single-photon level [20]. Requiring the photon pair to be in a superposition with the vacuum seems unusual, but this type of superposition exists in all down-conversion sources of entangled photons. It is only upon performing a photon-counting coincidence measurement that the maximally-entangled behaviour is projected out. While these down-conversion sources of Bell states exist and are practical in the lab, the creation mechanism does not suggest how one might try to measure those Bell states. In the device discussed here, the Bell state creator and Bell state analyzer look very similar. The creator can essentially be run in reverse to make the analyzer.

This device cannot be used for performing unconditional quantum teleportation. The device is only capable of distinguishing the four Bell states; it is not capable of performing a general projective measurement in the Bell basis. This is due to the conditional-phase shifter's dependence on the magnitude and phase of the amplitude for the Bell state component in the input state; the gate does not operate properly on arbitrary superpositions of Bell states. Nevertheless, the device discussed herein

constitutes a novel way of manipulating the degree of entanglement between a pair of photons, and may find a use in other quantum optics applications, such as dense coding [4,5]. The ability to entangle and disentangle photon pairs is a crucial step toward building scalable all-optical quantum computers.

We would like to thank Andrew White and Ray Laflamme for valuable discussions. We are grateful for the financial support of Photonics Research Ontario, NSERC, and the US Air Force Office of Scientific Research (F49620-01-1-0468).

References

1. C. H. Bennett, G. Brassard, C. Crépeau, R. Jozsa, A. Peres, and W. K. Wootters, *Phys. Rev. Lett.*, **70**, 1895 (1993).
2. D. Bouwmeester, J.-W. Pan, K. Mattle, M. Eibl, H. Weinfurter, A. Zeilinger, *Nature*, **390**, 575 (1997).
3. D. Boschi, S. Branca, F. De Martini, L. Hardy, and S. Popescu, *Phys. Rev. Lett.*, **80**, 1121 (1998).
4. C. H. Bennett and S. J. Wiesner, *Phys. Rev. Lett.*, **69**, 2881 (1992).
5. K. Mattle, H. Weinfurter, P.G. Kwiat, and A. Zeilinger, *Phys. Rev. Lett.*, **76**, 4656 (1996).
6. Bennett, C. H. & Brassard, G., *Proceedings of the IEEE International Conference on Computers, Systems & Signal Processing, Bangalore, India* (IEEE, New York, 1984), p. 175-179.
7. A. K. Ekert, *Phys. Rev. Lett.*,**67**, 661 (1991).
8. S. J. Freedman and J. F. Clauser, *Phys. Rev. Lett.*, **28**, 938 (1972); J. F. Clauser, Phys. Rev. D, **9**, 853 (1974); A. Aspect, P. Grangier, and G. Roger, *Phys. Rev. Lett.*, **47**, 460 (1981).
9. Z. Y. Ou and L. Mandel, *Phys. Rev. Lett.*, **61**, 50 (1988); Y. H. Shih and C. O. Alley, *Phys. Rev. Lett.*, **61**, 2921 (1988); T. E. Kiess, Y. H. Shih, A. V. Sergienko, and C. O. Alley, *Phys. Rev. Lett.*, **71**, 3893 (1993).
10. Optical tests of quantum mechanics, R.Y. Chiao, P.G. Kwiat, and A.M. Steinberg, in *Advances in Atomic, Molecular, and Optical Physics*, edited by B. Berson and H. Walther (Academic Press, New York, 1994), Vol. 34.
11. P. G. Kwiat, K. Mattle, H. Weinfurter, and A. Zeilinger, *Phys. Rev. Lett.*, **75**, 4337 (1995)
12. P. G. Kwiat, E. Waks, A. G. White, and P. H. Eberhard, *Phys. Rev. A*, **60**, R773 (1999).
13. J. H. Shapiro and N. C. Wong, J. Opt. B: Quant. and Semiclass. Opt. **2**, L1 (2000).
14. N. Lutkenhaus, J. Calsamiglia, and K.-A. Suominen, *Phys. Rev. A*, **59**, 3295 (1999).
15. Y.-H. Kim, S. P. Kulik, and Y. Shih, *Phys. Rev. Lett.*, **86**, 1370 (2001).
16. Q. A. Turchette, C. J. Hood, W. Lange, H. Mabuchi, and H. J. Kimble, *Phys. Rev. Lett.*, **75**, 4710 (1995); A. Rauschenbeutel, G. Nogues, S. Osnaghi, P. Bertet, M. Brune, J. M. Raimond, and S. Haroche, *Phys. Rev. Lett.*, **83**, 5166 (1999).

17. S. E. Harris, and L.V. Hau, *Phys. Rev. Lett.*, **82**, 4611 (1999); M. M. Kash, V. A. Sautenkov, A. S. Zibrov, L. Hollberg, G. R. Welch, M. D. Lukin, Y. Rostovtsev, E. S. Fry, and M. O. Scully, *Phys. Rev. Lett.*, **82**, 5229 (1999).
18. J. D. Franson, *Phys. Rev. Lett.*, **78**, 3852 (1997).
19. K. J. Resch, J. S. Lundeen, and A. M. Steinberg, *Phys. Rev. Lett.*, **87**, 123603 (2001); K. J. Resch, J. S. Lundeen, and A. M. Steinberg, *Journal of Modern Optics*, **49**, 487 (2002).
20. K. J. Resch, J. S. Lundeen, and A. M. Steinberg, pre-print: quant-ph/0205109, submitted to *Phys. Rev. Lett.* (2002).
21. E. Knill, R. Laflamme, and G. Milburn, *Nature*, **409**, 46 (2001).
22. D. Gottesman, A. Kitaev, and J. Preskill, *Phys. Rev. A*, **64**, 012310 (2001).
23. P. G. Kwiat and H. Weinfurter, *Phys. Rev. A*, **58**, R2623 (1998).
24. M. A. Neilsen and I. L. Chuang, Quantum Computation and Quantum Information (Cambridge University Press, Cambridge, 2000), p. 294.
25. M. A. Neilsen and I. L. Chuang, Quantum Computation and Quantum Information (Cambridge University Press, Cambridge, 2000), p. 26.
26. T. J. Herzog, J. G. Rarity, H. Weinfurter, and A. Zeilinger, *Phys. Rev. Lett.*, **72**, 629 (1994); H. Weinfurter, T. Herzog, P. G. Kwiat, J. G. Rarity, A. Zeilinger, and M. Zukowski, *Ann. N.Y. Acad. Sci.*, **755**, 61 (1995).

DISCUSSION

Chairman: W. Schleich

L. Stodolsky: Why did you say the photons are entangled in your down conversion experiment?

A. Steinberg: Because the total energy of the output is equal to the total energy in the input. If I have one photon "in" at 2ω then I either get an "out" photon at 2ω or two photons at ω and nothing at 2ω. The different field modes are entangled. I cannot describe the state of the ω field independently of the state of the 2ω field, because there is no way that I can find a pair at ω each *and* a photon left at 2ω if I have a single photon at 2ω coming "in".

L. Wang: An alternative explanation of what we saw could be that the input classical signal as a local oscillator is producing stimulated emission, which interferes with the local oscillator in that. Is there any evidence to hear this oscillator?

A. Steinberg: That is exactly correct. There is an alternate classical picture that, as usual, explains the singles rates. It cannot explain the coincidence rates. We have a paper coming out in the Journal of Modern Optics that goes through the theory in detail connecting the classical and quantum pictures. The idea is that certainly the strong classical beam and a weak quantum beam will generate some difference frequency, which will then beat against the other mode. One percent modulation in intensity, the classical theory would predict. However, the fact that we can see 60% visibility in coincidence is a purely quantum effect.

L. Stodolsky: You have explained in the introduction that in the parametric down conversion the energy and momentum are conserved. Do I make any mistake

by thinking that in quantum mechanics this is as the decay of a particle into two photons like π^0deca y?

A. Steinberg: Yes; I mean the constraints are due to the fact that momentum and energy need to be conserved. In a crystal with a particular dispersion relation, it is by playing tricks with choosing the polarisations that you are able to create these conditions, but at the end the conservation laws are the same. Obviously, there are small corrections due to the fact that the crystal can actually recoil, so the conservation laws are approximate. The frequency sum you can treat as exact.

G. Pronko: What kind of crystal do you use to split the photon? If we literally understand this process this is forbidden by the charge-parity conservation.

A. Steinberg: We use β-Barium Borate, in particular, but the general property is that in order to have this non-linearity the crystals have to lack inversion symmetry, because by turning one photon into two you are not conserving the parity quantum number.

G. Pronko: So, it means you are using some anisotropic crystal.

A. Steinberg: Yes, it is an anisotropic crystal.

TIME-REVERSED EPR AND THE CHOICE OF HISTORIES IN QUANTUM MECHANICS

AVSHALOM C. ELITZUR *, SHAHAR DOLEV †
Unit for Interdisciplinary Studies, Bar-Ilan University, 52900 Ramat-Gan, Israel.

ANTON ZEILINGER ‡
Institut für Experimentalphysik, Universität Wien, Boltzmanngasse 5, 1090 Wien, Austria.

When a single photon is split by a beam splitter, its two "halves" can entangle two distant atoms into an EPR pair. We discuss a time-reversed analogue of this experiment where two distant sources cooperate so as to emit a single photon. The two "half photons," having interacted with two atoms, can entangle these atoms into an EPR pair once they are detected as a single photon. Entanglement occurs by creating indistinguishabilility between the two mutually exclusive histories of the photon. This indistinguishabilility can be created either at the end of the two histories (by "erasing" the single photon's path) or at their beginning (by "erasing" the two atoms' positions).

1 Introduction

As peculiar as quantum measurement is known to be, its strangeness is even greater when one tries to determine not merely the state of a system, but its entire *history*. Past events are supposed to be unchangeable, and as such the most essential aspect of reality. And yet, when a quantum measurement traces a certain history, it seems to take an active part in the very formation of that history.

So far, however, this assertion has been merely philosophical. The most notable experiment supporting it, namely, the Einstein-Wheeler "delayed choice" experiment (see Sec. 2), is equally open to other, less radical interpretations. Could there be a more straightforward experiment, showing that the history observed is retroactively affected by observations carried out much later? In this article we propose a few experiments of this type and discuss their implications.

2 The Delayed Choice Experiment

We shall begin with the "delayed choice" experiment. Discussing its limitations will later highlight the advantage of our proposed demonstration of "choosing history."

Let a Mach-Zehnder Interferometer (MZI) be large enough such that it takes light a long time to traverse it (Fig. 1). Due to interference, every single photon traversing this MZI must hit detector C. Suppose, however, that, at the last moment, the experimenter decides to pull out BS_2. In this case the photon hits either C or D with equal probability.

What concerned Einstein about this experiment was that the two options given to the experimenter's choice seem to entail two mutually exclusive histories. In the

*AVSHALOM.ELITZUR@WEIZMANN.AC.IL
†SHAHAR_DOLEV@EMAIL.COM
‡ANTON.ZEILINGER@UNIVIE.AC.AT

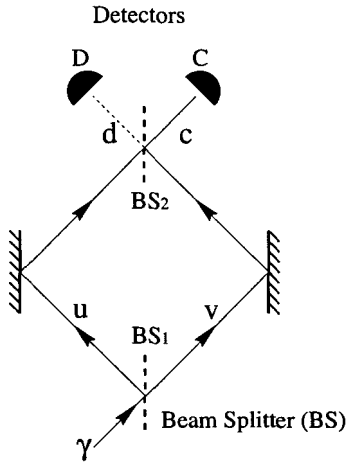

Figure 1. Mach-Zehnder Interferometer.

former case the photon seems to have been, *all along,* a wave that has traversed both MZI arms and then gave rise to interference. In the latter case the photon must have been – again, *all along* – a particle: if it has hit D it must have traversed only the right arm, and conversely for C. To make the result more impressive, Wheeler [1] proposed to perform the experiment on photons coming from outer space, whereby the history thus "chosen" is millions-years long.

However, the delayed choice experiment is not scientific in the full sense of the word, as other explanations are possible within interpretations that do not invoke backward causation. One could, for example, just stick to the observed facts, refrain from any statement about the unobserved past and explain the experiment strictly in terms of wave mechanics or "collapse."

Can there be an experiment that indicates more strongly that past events are susceptible to the effect of future observation?

3 Interference between Independent Sources

Even more striking than the delayed-choice experiment is an effect that was still unknown to Einstein, namely, the interference of light coming from different sources. It was first discovered by Hanbury-Brown and Twiss [2,3], and later demonstrated at the single-photon level [4,5] (Fig. 2). It is odd that, although this experiment offends classical notions more than most other experiments known today, it has not yet received appropriate attention. When the radiation involved is of sufficiently low intensity, then even a single particle seems to "have originated" from two distant sources.

We shall first point out two variations of this experiment that highlight its peculiar nature. First, it can have a delayed-choice variant: If the experimenter

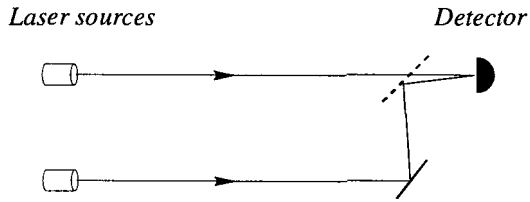

Figure 2. A schematic description of Pfleegor-Mandel experiment for interference between two distinct sources.

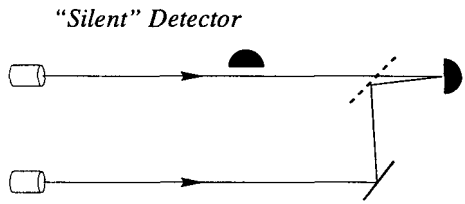

Figure 3. A variation of Pfleegor-Mandel experiment, implementing Interaction-Free Measurement.

chooses at the last moment to pull out the BS, a click at detector C will indicate that a single photon has emerged from only one source, namely, the one facing the detector that clicked. If, on the other hand, she leaves the BS in its place, the interference will again indicate that the photon "has been emitted" by both sources.

Next consider an Interaction-Free Measurement [6] variant of this setting (Fig. 3). Assuming that the phase between the sources is fixed for the time of the experiment, it can be arranged that all the photons will reach detector C. Now, if an object is placed next to one of the sources, it will occasionally absorb the photon. Therefore, when a photon eventually hits the detector, it is obvious that it has been emitted only from the other, unblocked source. But then, in 50% of the cases, that photon will emerge from the BS towards the "dark" detector D, thereby indicating that, although it could have originated from only one source, it has somehow sensed the object blocking the other source!

How can two distant sources emit together a single photon? It is instructive to study this effect as a time-reversed version of the familiar case where a single photon is split by a BS and then goes to two distant detectors. In that case, there is an uncertainty as to which detector *will* absorb the photon. Similarly, in our case, there is an uncertainty as to which source *has* emitted the photon.

This time-symmetry suggests constructing a new experiment. Consider first the familiar, V-shaped case (one source, two detectors). Such a split photon can entangle two unrelated particles so as to create an EPR pair. For example, two atoms positioned across its two possible paths will become entangled due to the correlation between their ground and excited states. Can the more peculiar, Λ-

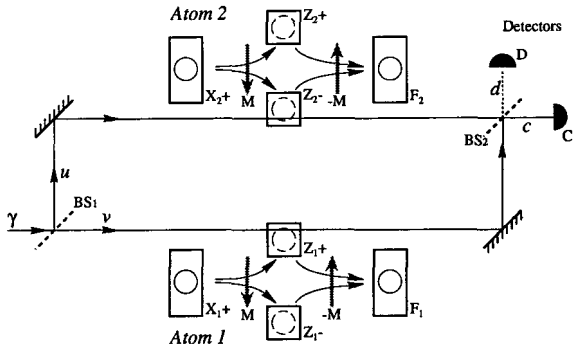

Figure 4. Hardy's experiment.

shaped case (two sources, one detector) be similarly used to create an inverse EPR?

4 Hardy's Hybrid Experiment

Before we show how to do that, let us study an experiment due to Hardy [7], in which he has elegantly integrated the peculiarities of the EPR experiment, single-particle interference and the interaction-free measurement – all in one simple setting (Fig. 4).

Let a single photon traverse a MZI. Let two spin $\frac{1}{2}$ atoms be prepared in the following way: Each atom is first prepared in an up spin-x state (x^+) and then split by a non-uniform magnetic field M into its spin-z components. The two components are then carefully put into two boxes z^+ and z^- while keeping their superposition state:

$$\Psi = |\gamma\rangle \cdot \frac{1}{\sqrt{2}}(iz_1^+ + z_1^-) \cdot \frac{1}{\sqrt{2}}(iz_2^+ + z_2^-). \tag{1}$$

The boxes are transparent for the photon but opaque for the atoms. Atom 1's (2's) z_1^+ (z_2^-) box is positioned across the photon's v (u) path in such a way that the photon can pass through the box and interact with the atom inside in a 100% efficiency. Now let the photon be transmitted by BS_1:

$$\Psi = \frac{1}{\sqrt{2}^3}(i|u\rangle + |v\rangle) \cdot (iz_1^+ + z_1^-) \cdot (iz_2^+ + z_2^-). \tag{2}$$

After the photon was allowed to interact with the atoms, we discard the cases in which absorption occurred (50%), to get:

$$\begin{aligned}\Psi = \tfrac{1}{\sqrt{2}^3}(&-i|u\rangle z_1^+ z_2^+ - |u\rangle z_1^- z_2^+ \\ &+i|v\rangle z_1^- z_2^+ + |v\rangle z_1^- z_2^-).\end{aligned} \tag{3}$$

Now, let photon parts u and v pass through BS_2, following the evolution:

$$|v\rangle \xrightarrow{BS_2} \frac{1}{\sqrt{2}} \cdot (|d\rangle + i|c\rangle), \qquad |u\rangle \xrightarrow{BS_2} \frac{1}{\sqrt{2}} \cdot (|c\rangle + i|d\rangle),$$

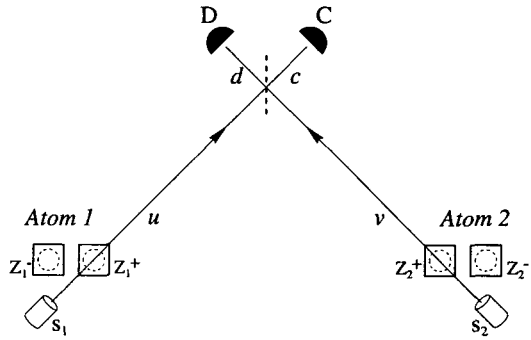

Figure 5. Entangling two atoms.

giving:

$$\Psi = \tfrac{1}{4}(\,|d\rangle z_1^+ z_2^+ + |d\rangle z_1^- z_2^- + i|c\rangle z_1^- z_2^- - i|c\rangle z_1^+ z_2^+ - 2|c\rangle z_1^- z_2^+). \tag{4}$$

If we now post-select only the experiments in which the photon was surely disrupted along its way, thereby hitting detector D, we get:

$$\Psi = \frac{1}{4}|d\rangle(z_1^+ z_2^+ + z_1^- z_2^-). \tag{5}$$

Consequently, the atoms, which have never met in the past, become entangled in an EPR-like relation. Unlike the ordinary EPR, where the two particles have interacted earlier, here the only common event in the past is the single photon that has "visited" both of them.

In the next section we shall show how to achieve this result even without any common past. Then, the measurement's effect on past evolution will become even more striking.

5 Inverse EPR ("RPE")

Let two coherent photon beams be emitted from two distant sources as in Fig. 5. Let the sources be of sufficiently low intensity such that, on average, one photon is emitted during a given time interval. Let the beams be directed towards an equidistant BS. Two detectors are positioned next to the BS:

$$\phi_{\gamma u} = p|1\rangle_u + q|0\rangle_u, \tag{6}$$

$$\phi_{\gamma v} = p|1\rangle_v + q|0\rangle_v, \tag{7}$$

$$\psi_{A1} = \frac{1}{\sqrt{2}}(iz_1^- + z_1^+), \tag{8}$$

$$\psi_{A2} = \frac{1}{\sqrt{2}}(iz_2^- + z_2^+), \tag{9}$$

where $|1\rangle$ denotes a photon state (with probability p^2), $|0\rangle$ denotes a state of no photon (with probability q^2), $p \ll 1$, and $p^2 + q^2 = 1$.

Since the two sources' radiation is with equal wavelength, a static interference pattern will be manifested by different detection probabilities in each detector. Adjusting the lengths of the photons' paths v and u will modify these probabilities, allowing a state where one detector, D, is always silent due to destructive interference, while all the clicks occur at the other detector, C, due to constructive interference.

Notice that each single photon obeys these detection probabilities only if both paths u and v, coming from the two distant sources, are open. We shall also presume that the time during which the two sources remain coherent is long enough compared to the experiment's duration, hence we can assume the above phase relation to be fixed.

Next, let two spin-$\frac{1}{2}$ atoms be prepared as in Hardy's experiment (Sec. 4 above) and let each "half atom" be placed in one of the possible paths. After the photon was allowed to interact with the atoms, we discard the cases in which absorption occurred (50%), to get:

$$\Psi = \frac{1}{\sqrt{2}^3}(-i|u\rangle z_1^+ z_2^+ - |u\rangle z_1^- z_2^+ + i|v\rangle z_1^- z_2^+ + |v\rangle z_1^- z_2^-). \tag{10}$$

If we now post-select only the cases in which a single photon reached detector D, which means that one of its paths was surely disrupted, we get:

$$\Psi = \frac{1}{4}|d\rangle(z_1^+ z_2^+ + z_1^- z_2^-), \tag{11}$$

which entangles the two atoms into a full-blown EPR state:

$$z_1^+ z_2^+ + z_1^- z_2^-.$$

In other words, tests of Bell's inequality performed on the two atoms will show the same violations observed in the EPR case, indicating that the spin value of each atom depends on the choice of spin direction measured on the other atom, no matter how distant.

The two photon sources, though unrelated, must still be coherent in order to demonstrate interference. Dropping the coherency requirement would make the EPR inversion even more prominent. This has been accomplished by Cabrillo *et. al.* [8] in a different setup, devised for generating pairs of entangled atoms. Their setup involves atoms with three energy levels: two, mutually close "ground" states, $|0\rangle$ and $|1\rangle$, and one excited state $|2\rangle$. Two distant such atoms in $|0\rangle$ state are shone by a weak laser beam tuned to the $|0\rangle \rightarrow |2\rangle$ transition energy. If a detector then detects a single photon of the $|2\rangle \rightarrow |1\rangle$ energy, the entangled state $|1\rangle|2\rangle + |2\rangle|1\rangle$ ensues.

Here, in the absence of coherency, one cannot talk about interference. Still, since only one photon is detected, the uncertainty about the photon's origin suffices to make the two atoms entangled, leading eventually to an EPR state.

Unlike the ordinary EPR generation, where the two particles have interacted earlier, here the only common event lies in the particles' future. These two versions,

one involving coherent light and the other with incoherent light, highlight different peculiarities of the inverse EPR, henceforth termed "RPE." We shall discuss their implications below.

6 Histories for Choice

The "RPE" experiment offers several options for studying the way in which measurement determines a history. Consider, first, its delayed-choice aspect, which can be best demonstrated in the incoherent setup of Cabrillio *et. al.*:

- If the experimenter chooses at the last moment to pull out the BS, then the photon's two possible histories, i.e., "it originated from the right atom" and "it originated from the left atom," become distinguishable. Consequently, the photon's "footprints" become distinguishable too and no entanglement between the atoms will be observed.

- Con versely, inserting the BS will entangle the two atoms, even though their interaction with the photon has taken place earlier. In other words, *what seems to be the generation of uncertainty only in the observer's mind, gives rise to a testable entanglement in reality.* Unlike the delayed-choice experiment, here the history "chosen" leaves observable footprints.

But, in addition to creating uncertainty at the end of the evolution, the coherent version (Fig. 5) gives us the freedom to create uncertainty – or to dissolve it – also at the beginning of that evolution. For even after the photon was detected at D, we can perform two kinds of measurements on the atoms, measurements that will yield conflicting results:

- W e can measure the position of each atom in one out of the two boxes. In this case, one atom must always be found in the intersecting box, while the other must always reside in the non-intersecting box. Consequently, there is only one possible history for the photon now: *It must have taken the path that was not blocked by the atom, never the other, blocked path.* As a result, Bell inequality violations would never be demonstrated by the atoms after this measurement (recall that Bell-inequality statistics cannot be demonstrated on a series of same-spin measurements). Hence, the atoms do not demonstrate non-local correlation.

- On the other hand, we can unite the two boxes of each atom using an inverse magnetic field $-M$, and measure the photon's spin along the z axis. Here, we give up the "which path" information about the photon. Consequently, Bell-inequality violations would be demonstrated in this case, proving that the photon's two possible histories cooperated so as to entangle the two distant atoms.

All these variants are, in essence, erasure experiments. When we insert the BS in the "incoherent RPE" or reunite the atoms in the coherent version, we actually erase the still available information about the photon's two possible histories. Notice, however, that the present erasure experiments (e.g. [9]) demonstrate only the

negative result of this information loss, i.e., the disappearance of the interference pattern. The RPE, in contrast, enables erasure to give rise to a positive result, namely, the entanglement of two distant atoms.

"Nam et ipsa scientia potestas est (for knowledge itself is power)" was an old maxim of the ancient Romans, but quantum mechanics rewards one for cases in which *ignorance* is generated.

7 Admit Backward Causation or Abandon Realism?

The time-symmetry of quantum theory's formalism is well known [10] and has moreover become the cornerstone of some modern interpretations that render "affecting the past" the main characteristic of quantum interaction [11,12]. As early as in 1983, Costa de Beauregard [13] gave a CPT-invariant formulation of the EPR setting that allows a time-reversed EPR. Can we apply such a formulation in our case and assert that the late entangling event, i.e., the detection of the photon, really affects backwards the two histories?

One might argue that our experiment does not really time-reverse the EPR setting because, in order to be sure that Bell's inequality will be violated, the atoms must be measured only after the detection of the entangling photon. Hence, the entangling event still remains in the past of the two correlated atoms. The EPR V shape, so goes the counter-argument, is thus merely flattened rather than turned upside down into a Λ shape.

Notice, however, that the entangling event can lie outside the past light cones of the two atoms' measurements. Here, the argument against backward causation must take the following form: "The two atoms begin to violate Bell-inequality only at the moment the photon was detected at D." This statement is relativistically meaningless. By bringing the entangling event itself into spacelike separation with the entangled particles, we actually render both the normal and inverse EPRs equally possible.

But what does "affecting the past" teach us about the nature of time? This question involves a deeper unresolved issue, that of time's apparent "passage." Adherents of the "Block Universe" model [14], argue that time's passage is only an illusion. Consequently, all quantum mechanical experiments that seem to involve a last minute decision involve no free choice at all. For example, in the EPR, the experimenter's last-moment decision which spin direction to measure, or, in the "delayed choice" experiment, the last-moment decision whether to insert the BS or not, are "already" determined in the four-dimensional spacetime. Within this framework, RPE is just as possible as EPR.

The second alternative is that time has an objective "flow" [15]. Then, the retroactive entangling effect would occur in some higher time once the "Now" has reached the entangling event.

Both views lie at present outside scientific investigation as both can be neither proved nor disproved [a]. Hence, a third and a much easier answer to the problem would be dismissing the entire issue by avoiding any reference to objective reality

[a] However, we have shown elsewhere that Hawking's information erasure conjecture is more consistent with an objective time "passage." See [16]

altogether, as in the Copenhagen Interpretation.

While two of us (AE and SD) tend to the second interpretation and one (AZ) favors the third, we prefer to conclude by pointing out that each side can rely on one of the two giants who have so hotly debated during the first Solvay conferences.

Acknowledgments

We thank Yakir Aharonov, Terry Rudolph and David Tannor for very helpful comments. It is a pleasure to thank the participants of the Workshop on Quantum Measurement Theory and Quantum Information at the Schrödinger Institute in Vienna for enlightening discussions.

References

1. J. A. Wheeler, in *Mathematical Foundations of Quantum Theory*, edited by A. R. Marrow (Academic Press, New York, 1978), pp. 9–48.
2. R. Hanbury-Brown and R. Q. Twiss, Proc. R. Soc. London, Ser. A **242**, 300 (1957).
3. R. Hanbury-Brown and R. Q. Twiss, Proc. R. Soc. London, Ser. A **243**, 291 (1958).
4. P. R. L. and L. Mandel, Phys. Rev. **159**, 1084 (1967).
5. H. Paul, Rev. Mod. Phys. **58**, 209 (1986).
6. A. C. Elitzur and L. Vaidman, Found. of Phys. **23**, 987 (1993).
7. L. Hardy, Phys. Lett. A **167**, 11 (1992).
8. C. Cabrillo, J. I. Cirac, P. Garcia-Fernandez, and P. Zoller, Phys. Rev. A **59**, 1025 (1999), `quant-ph/9810013`.
9. B. G. Englert, M. O. Scully, and H. Walther, Nature **351**, 111 (1991).
10. Y. Aharonov, P. G. Bergman, and J. L. Lebowitz, Phys. Rev. B **134**, 1410 (1964).
11. J. G. Cramer, Rev. Mod. Phys. **58**, 647 (1986).
12. B. Reznik and Y. Aharonov, Phys. Rev. A **52**, 2538 (1995).
13. C. de Beauregard, Phys. Rev. Let. **50**, 867 (1983).
14. H. Price, *Time's Arrow and Archimedes' Point* (Oxford University Press, Oxford, 1996).
15. I. Prigogine, *From Being to Becoming: Time and Complexity in the Physical Sciences* (W. H. Freeman & Co., San Francisco, 1980).
16. A. C. Elitzur and S. Dolev, Found. Phys. Lett. **12**, 309 (1999), `quant-ph/0012081`.

DISCUSSION

Chairman: G. Casati

W. Schleich: Concerning the Elitzur-Vaidman "interaction-free measurement", in 1955, Renninger was trying to publish a paper exactly with the same

picture of interaction-free measurement. There is a footnote there, which tells how the paper was initially rejected and later published due to the influence of Einstein and Born, in "Zeitschrift für Physik".

A. Elitzur: Renninger's idea was quite different. It is better termed "the negative result experiment". There is an extensive review by Vaidman titled "Are interaction-free measurements interaction free?" (quant-ph/0006077). He discusses in details the difference between our work and the earlier ones.

L. Vaidman: Avshalom rightly says that the unique thing about interaction-free measurement is the exchange of roles. Rather than a macroscopic object measuring a microscopic particle, here it is the microscopic particle that measures the larger object, which is the source of the peculiar results.

A. Elitzur: Right. And in this series of works, Hardy and us have completed the circle: both the measuring and the measured objects are quantum-mechanical. The results are even more surprising!

L. Stodolsky: When you say "experiments" do you mean proposals or actual experiments?

A. Elitzur: The interaction-free measurement has long ago been turned from a gedanken experiment into a real experiment by various groups, the most brilliant experiment being performed by Zeilinger and co-workers. The more advanced experiments described in this talk are still gedanken.

L. Stodolsky: I am going to remark on the Hardy experiment. It looks very much to me like the Weizmann experiment with QPC looking at two arms of the interferometer. In this Weizmann experiment it is something about the 2D electron gas. They have the so-called QPC which is a device which measures with varying degrees of sensitivity which path the electron took. You can tune it at different strengths, and you can see interference visibility increasing or decreasing, depending on how strong you have tuned it. I analysed this.

A. Elitzur: The Weizmann experiment (Nature 391:871-874 1998) involved a *macroscopic* detector (the QPC) to measure the electron path. Hardy's aim was different, as well as his method. He used a *single particle* to perform an interaction-free measurement on the particle traversing an MZI. Again, I find this method extremely fruitful. Measure a quantum object not by a macroscopic device but by another quantum object!

R. Chiao: Would you say that experiments of the kind you've described indicate that the uncertainty principle and relativistic locality are somehow connected?

A. C. Elitzur: I have proposed this in a 1992 article ("Locality and indeterminism preserve the second law," Phys. Lett. A167 335) which discussed i) the relativistic prohibition on velocities greater than light, ii) quantum-mechanical indeterminacy, and iii) the thermodynamic prohibition on spontaneous entropy decrease. It turns out that if you violate one prohibition, you end up violating the other two as well. The affinity between the three principles seems to be very, very profound.

PHOTON INDUCED CHAOTIC SCATTERING

L.E. REICHL, AGAPI EMMANOUILIDOU
Center for Studies in Statistical Mechanics and Complex Systems
The University of Texas at Austin
Austin, Texas 78712

We develop a Floquet scattering matrix to describe quantum mechanical behavior of an electron which scatters from an atomic core in the presence of an intense laser field. As the laser intensity is increased, the underlying classical scattering process becomes chaotic. This underlying chaos appears to manifest itself in an interesting form of level repulsion among the eigenphases of the Floquet scattering matrix.

1 Introduction

It is now known that when atomic electrons interact with both the atomic core and with the time-periodic electric field from ultra-high intensity lasers, chaotic structures can be formed in the phase space of the electron [1,2,3]. These chaotic structures can occupy regions of space much larger than the original atomic system, and can stabilize new quasibound states of the electron. While the chaotic structures appear to form a platform to stabilize new states of matter, they can also cause a loss of information about the state of the electron in a scattering process. It is this latter effect that we focus on here.

The fact that chaos in a bounded classical system induces information loss in the corresponding bounded quantum system is now a well known phenomenon (see [4] for a review). Bounded quantum systems which are classically chaotic have an energy level spectrum with the same statistical properties as that of random matrices which are chosen to minimize information. This random matrix type behavior in the quantum spectrum is the result of level repulsion between eigenvalues induced by the underlying chaos and the associated loss of good quantum numbers.

Similar effects occur in scattering problems, although the focus until now has been on the statistical properties of the spacings between partial delay times [5,6]. These are generally due to Fano resonances which are the result of scattering between quanta of a weak applied field and the internal states of an atom, nucleus, or waveguide. These internal states are already exhibiting the effects of underlying chaos, and the scattering process is a means to measure this.

In this paper, we will show a different effect, first observed in [3]. We find that when a very high intensity laser field interacts with an atomic electron, the electron's interaction with the atomic core and laser field induces chaos in the classical electron dynamics. This, in turn, manifests itself in the form of level repulsion between eigenphases of the Floquet scattering matrix for this system. Level repulsion between eigenphases of a random unitary matrix was discussed by Dyson [7], and was later shown to be the result of underlying chaos. Dyson's "circular" random matrix ensembles are based on the assumption that the matrix elements of the unitary matrix are random and uniformly distributed. This is accomplished by assuming that the probability distribution of *independent* matrix elements, $\{S_{i,j}\}$, of the unitary matrix satisfy the condition, $P(\{S_{i,j}\}) = constant$. This distribution minimizes the

Shannon information [8]

$$I(P) = \int P_S(\{S_{i,j}\}) \ln[P_S(\{S_{i,j}\})] d\mu(\bar{S}), \tag{1}$$

where $d\mu(\bar{S})$ denotes the invariant measure of the unitary matrix [9]. We believe that the level repulsion we are observing is due to the underlying classical chaos induced by the external field and leads to loss of information concerning the state of the electron during and after the scattering process.

Much of the theory involved in the derivation of the Floquet scattering matrix can be found in [3]. In the sections below we describe the dynamical system considered here and outline the procedure for deriving a Floquet scattering matrix. We then show the effect of chaos in the scattering process on the eigenphases of the Floquet scattering matrix.

2 Dynamics

We wish to study the dynamics of an electron as it scatters from an attractive short range atomic potential in the presence of a monochromatic electromagnetic radiation field. We assume that the electric field is directed along the x-axis and we consider motion only along the x-axis. The dynamics is governed by the Schrodinger equation which, in atomic units, is given by

$$i\frac{\partial \Psi(x,t)}{\partial t} = \frac{1}{2}\left(-i\frac{\partial}{\partial x} - A(t)\right)^2 \Psi(x,t) + V(x)\Psi(x,t), \tag{2}$$

where $\Psi(x,t)$ is the state of the electron at point x and time t, V(x) is the atomic potential,

$$V(x) = -V_0 e^{-(x/\delta)^2}, \tag{3}$$

$A(t)$ is the vector potential associated with the radiation field and is given by

$$A(t) = \frac{E_0}{\omega}\cos(\omega t). \tag{4}$$

The electric field is $E(t) = -\partial A(t)/\partial t = E_0 \sin(\omega t)$. The potential, $V(x)$, falls off exponentially outside a region of width, $-2\delta < x < 2\delta$.

We can transform to the Kramers-Henneberger (K-H) frame [10,11], which is a reference frame which moves with the electron in the absence of the potential, $V(x)$. In the K-H frame, the asymptotic regions involve free electron states and, in the reaction region, the atomic potential oscillates back and forth along the x-axis with frequency ω. The electron wave function, $\Phi(x,t)$, in the K-H frame can be obtained from $\Psi(x,t)$, via the unitary transformation, U_{KH},

$$\Phi(x,t) = U_{KH}\Psi(x,t), \tag{5}$$

where

$$U_{KH} = \exp\left[\frac{iq^2}{2}\int_{-\infty}^{t} dt'\left(A^2(t') - qA(t')\frac{\partial}{\partial x}\right)\right]. \tag{6}$$

In the K-H frame, the wave function satisfies the Schrödinger equation

$$i\frac{\partial\Phi(x,t)}{\partial t} = -\frac{1}{2}\frac{\partial^2}{\partial x^2}\Phi(x,t) + V(x+\alpha(t))\Phi(x,t), \tag{7}$$

where $\alpha(t) = \alpha_0 \sin(\omega t)$ with $\alpha_0 = \frac{-E_0}{\omega^2}$. Note that although the atomic potential oscillates back and forth along the x-axis, it is still well localized. However, its region of influence now extends over the larger interval, $-2\delta - \alpha_0 < x < 2\delta + \alpha_0$.

The Schrodinger equation has time periodic coefficients and thus satisfies the Floquet theorem. It has solutions of the form

$$\Phi_{\mathcal{E}}(x,t) = e^{-i\mathcal{E}t}\phi_{\mathcal{E}}(x,t), \tag{8}$$

where $\mathcal{E}$ is the Floquet energy, $\mathcal{E} \in [0,\omega)$, and $\phi_{\mathcal{E}}(x,t)$ is a periodic function of time, $\phi_{\mathcal{E}}(x,t) = \phi_{\mathcal{E}}(x,t+T)$. It is useful to expand $\phi_{\mathcal{E}}(x,t)$ in a Fourier series to obtain,

$$\Phi_{\mathcal{E}}(x,t) = e^{-i\mathcal{E}t}\sum_{n=-\infty}^{+\infty}\phi_n(x)e^{-in\omega t}, \tag{9}$$

where $\phi_n(x)$ denote the probability to find the particle in the n^{th} Floquet channel. The Floquet channels are defined as follows. We divide the range of incident energies, E $(0 \leq E \leq \infty)$, into intervals of width ω (in atomic units Planck's constant, $\hbar = 1$) which we call the Floquet channels. Any given incident energy can then be written $E = \mathcal{E} + n\omega$ if the energy lies in the n^{th} channel.

We can now divide the system into three spatial regions: the asymptotic regions I and III with $x \in [x_0, \infty)$ and $x \in (-\infty, -x_0]$, respectively, where the potential can be assumed to be zero; and the reaction region II, $x \in [-x_0, x_0]$, where the potential $V(x+\alpha(t))$ is not zero. The choice of x_0 depends on the value of the parameter α_0.

3 Floquet solution in the asymptotic regions, I and III.

In the asymptotic regions I and III the potential $V(x+\alpha(t))$ is zero and our Floquet solutions consist of a superposition of incoming and outgoing free electron waves. Thus, in regions I and III, we can write

$$\Phi^I_{\mathcal{E}}(x,t) = \sum_{n=-\infty}^{\infty}\phi^I_n(x)e^{-i\mathcal{E}t}e^{-in\omega t}$$

$$= \sum_{n=-\infty}^{\infty} b_n^{out}\frac{e^{ik_n x}}{\sqrt{k_n}}e^{-i\mathcal{E}t}e^{-in\omega t} + \sum_{n=-\infty}^{\infty} b_n^{in}\frac{e^{-ik_n x}}{\sqrt{k_n}}e^{-i\mathcal{E}t}e^{-in\omega t}, \tag{10}$$

and

$$\Phi^{III}_{\mathcal{E}}(x,t) = \sum_{n=-\infty}^{\infty}\phi^{III}_n(x)e^{-i\mathcal{E}t}e^{-in\omega t}$$

$$= \sum_{n=-\infty}^{\infty} a_n^{out}\frac{e^{-ik_n x}}{\sqrt{k_n}}e^{-i\mathcal{E}t}e^{-in\omega t} + \sum_{n=-\infty}^{\infty} a_n^{in}\frac{e^{ik_n x}}{\sqrt{k_n}}e^{-i\mathcal{E}t}e^{-in\omega t}, \tag{11}$$

respectively. Here b_n^{in}, a_n^{in} (b_n^{out}, a_n^{out}) are the probability amplitudes for the incoming (outgoing) electron waves in the nth Floquet channel. The factors, $1/\sqrt{k_n}$, in the wavefunctions in Eqs.(10) and (11) ensure that the Floquet scattering matrix is unitary.

It is important to note that some of these electron waves are propagating and some are evanescent. Propagating Floquet channels have $n = 0, ..., +\infty$ and wavevectors $k_n = \sqrt{2(\mathcal{E} + n\omega)}$. Evanescent Floquet channels have $n = -\infty, ..., -1$ and imaginary wavevectors $k_n = i\sqrt{2|\mathcal{E} + n\omega|}$. The current density for the evanescent channels is zero. In the asymptotic regions, the Floquet channels are not coupled.

4 Floquet solution in the reaction region, II.

The Floquet solutions in the reaction region, II, is much more complicated. The first step is to obtain an equation for $\phi_n(x)$. If we substitute Eq.(9) into Eq.(7). This yields an infinite set of coupled second order differential equations for the Floquet amplitudes, $\phi_n(x)$,

$$-\frac{1}{2}\frac{d^2}{dx^2}\phi_n(x) + [V_0(\alpha_0; x) - (\mathcal{E} + n\omega)]\phi_n(x) + \sum_{\substack{l=-\infty \\ l\neq n}}^{+\infty} V_{n-l}(\alpha_0; x)\phi_l(x) = 0. \quad (12)$$

where

$$V_n(a_0; x) = \frac{1}{2\pi}\int_0^{2\pi} V(x + a(t))e^{in\omega t}d(\omega t)$$

$$= -V_0\frac{i^n}{\pi}\int_0^{\pi} \cos(n\omega t)e^{-(x+a_0\cos(\omega t))^2/\delta^2}d(\omega t), \quad (13)$$

Next, we truncate to a finite number of Floquet channels and take n_e and n_p to be the lower and upper limit of the Floquet channels considered. Thus, $n = -n_e, ..., 0, ..., n_p$ and the total number of Floquet channels (propagating and evanescent) is given by $N_{tot} = n_e + n_p + 1$. The criterion for choosing $n_e$and n_p is based on the behavior of the Floquet scattering matrix and will be discussed below.

Eq. (12) can be written in the following matrix form,

$$\boldsymbol{I}\frac{d^2}{dx^2}\boldsymbol{\phi}^{II}(x) = \boldsymbol{M}(x)\boldsymbol{\phi}^{II}(x), \quad (14)$$

where $\boldsymbol{I}$ is the unit $N_{tot} \times N_{tot}$ matrix, $\boldsymbol{\phi}^{II}(x)$ is the $N_{tot} \times 1$ matrix with matrix elements $\{\phi_n(x)\}$, and $\boldsymbol{M}(x)$ is an $N_{tot} \times N_{tot}$ matrix with elements

$$\boldsymbol{M}_{n,l}(x) = 2(V_{n-l}(\alpha_0; x) - \delta_{n,l}(\mathcal{E} + n\omega)), \quad (15)$$

where $\delta_{n,l}$ is the Kronecker delta and $n, l = -n_e, ..., 0, ..., n_p$.

The general solution of the N_{tot} coupled second order differential equations, Eq.(14), can be written as a linear combination of $2N_{tot}$ linearly independent $N_{tot} \times 1$

column matrices, $\boldsymbol{\chi}_j(x)$, with $j= \ 1,...,2N_{tot}$. The matrix elements, $\{\chi_{n,j}(x)\}$, of these column matrices satisfy Eq.(14), so

$$\frac{d^2}{dx^2}\chi_{n,j}(x) = \sum_{l=-n_e}^{n_p} \boldsymbol{M}_{n,l}(x)\chi_{l,j}(x), \tag{16}$$

where $n = -n_e,...,0,...,n_p$ and $j = 1,...,2N$. It then follows that every channel function $\phi_n(x)$ can be written as a linear combination of $2N$ functions $\chi_{n,j}(x)$ and thus, the wavefunction in the scattering region II is given by

$$\Phi^{II}_{\mathcal{E}}(\ x,t) = \sum_{n=-n_e}^{n_p}\sum_{j=1}^{2N} c_j\chi_{n,j}(x)\ e^{-i\mathcal{E}t}e^{-in\omega t}. \tag{17}$$

In general, the functions, $\chi_{n,j}(x)$, can be obtained numerically using methods described in [3,12].

5 Floquet scattering matrix.

The Floquet scattering matrix ($\boldsymbol{S}$-matrix) connects the amplitudes, $\{a_n^{out}, b_n^{out}\}$, of the outgoing propagating modes with the amplitudes, $\{a_n^{in}, b_n^{in}\}$, of the incoming propagating modes, and therefore it connects Floquet channels with energies that can differ by an integer multiples of ω. The Floquet $\boldsymbol{S}$-matrix is straightforward to derive although there is a considerable amount of algebra involved. We will only describe it here and refer the reader to[3] where it is discussed in great detail. We first note that the wavefunction and its first spatial derivative must be continuous at the boundaries, $+x_0$ $(-x_0)$, between the asymptotic regions I (III), and the reaction region, II. Also, the probability amplitudes a_n^{in} and b_n^{in} of the evanescent modes (for $n < 0$) are zero because of the unbounded character of the exponentials they multiply in the asymptotic regions I and III.

We next introduce the $(n_p+1)\times 1$ matrices $\mathbf{A}^{out}$, $\mathbf{B}^{out}$, $\mathbf{A}^{in}$, and $\mathbf{B}^{in}$, whose matrix elements, $\{a_n^{out}\}$, $\{b_n^{out}\}$, $\{a_n^{in}\}$, and $\{b_n^{in}\}$, respectively, are the probability amplitudes in the propagating Floquet channels. After considerable algebra, we find the Floquet $\boldsymbol{S}$-matrix, that connects the probability amplitudes of the outgoing propagating channels to the probability amplitudes of the incoming propagating channels. We obtain

$$\begin{pmatrix}\mathbf{A}^{out}\\ \mathbf{B}^{out}\end{pmatrix} \equiv \begin{pmatrix}\mathbf{R}' & \mathbf{T}\\ \mathbf{T}' & \mathbf{R}\end{pmatrix}\cdot\begin{pmatrix}\mathbf{A}^{in}\\ \mathbf{B}^{in}\end{pmatrix} \equiv S\cdot\begin{pmatrix}\mathbf{A}^{in}\\ \mathbf{B}^{in}\end{pmatrix}, \tag{18}$$

where the $(n_p+1)\times(n_p+1)$ matrices $\mathbf{R}'$, $\mathbf{R}$, $\mathbf{T}'$ and $\mathbf{T}$ connect propagating modes to propagating modes, but also contain, folded in, contributions from the evanescent modes.

The element $|R_{n',n}|^2$ ($|T_{n',n}|^2$) is the reflection (transmission) probability, for an electron wave that is incident in the propagating channel n from the right, and reflected (transmitted) into the propagating channel n'. Similarly, the elements $|R'_{n',n}|^2$ and $|T'_{n',n}|^2$ are the reflection and transmission probabilities, respectively,

for an electron wave incident from the left in the propagating channel n. The Floquet $\boldsymbol{S}$-matrix is unitary, so the following condition is satisfied

$$\sum_{n'=0}^{n_p} [|R_{n',n}|^2 + |T_{n',n}|^2] = 1, \tag{19}$$

for every incident propagating mode $n = 0, ..., n_p$. The above condition is a statement of conservation of probability.

The criterion we have used for choosing the truncation value, n_p, is that an electron wave incident on the Floquet channel $n = n_p$not be affected by the scattering potential. That is, the transmission coefficient $|T_{n_p,n_p}|^2 = 1$ for all values of the incident energy $E = \mathcal{E} + n_p\omega$.

In all the results discussed here, we choose $V_0 = 0.27035$ a.u. and $\delta = 2$ a.u. For these parameters the potential, $V(x)$, supports only one bound state of energy $E_b = -0.1327$ a.u. in the field-free case. These values of V_0 and δ describe the behavior of a one-dimensional model negative chlorine ion, Cl^-, in the presence of a laser field, and are the same as considered in [13,14,15].

When the time periodic field, $A(t)$, is turned on, the bound state is no longer stable. An electron can always escape the bound state by exchanging photons with the applied field. The bound state becomes a long-lived quasi-bound state, and shows up as a pole of the Floquet scattering matrix in the complex quasi-energy plane[3]. It has been shown in [3,13,14] that at external field amplitude, $\alpha_0 \approx 1.0$, a second quasi-bound state forms and shows up as a second complex pole of the scattering matrix. This new quasibound state appears to be a consequence of the nonlinear atom-field interaction as we will show below. In all subsequent calculations, the frequency of the time periodic field is taken to be $\omega = 0.236$ a.u.

6 Classical Dynamics

The Hamiltonian which describes the classical dynamics of the scattering process (in atomic units) is given by

$$H = \frac{1}{2}(p - A(t))^2 + V(x), \tag{20}$$

and the equations of motion for the particle can be obtained from Hamilton's equations, $\frac{dp}{dt} = -\frac{\partial H}{\partial x}$ and $\frac{dx}{dt} = \frac{\partial H}{\partial p}$. Using strobe plots, it is possible to study the structure of the classical phase space encountered by the particle as it scatters from the potential, $V(x)$, in the presence of the external field. In Figures (1.a)-(1.d), we show a sequence of strobe plots for external field amplitudes $\alpha_0 = 0.1$, 0.7, 3.25, and 5.25, respectively. All the strobe plots are drawn in the Lab frame, but they look exactly the same when they are drawn in the K-H frame except that in the K-H frame the structures are shifted in position by an amount, α_0.

The strobe plots show the position and momentum of a set of trajectories, each with a different initial condition, at time intervals ($t_n = 2\pi(m+1/2)/\omega$, $m = 1, 2, ...$) equal to the period of the external field. Figures (1.a) and (1.b) show a mixture of regular and chaotic dynamics at low incident particle energies. In Figures (1.c)

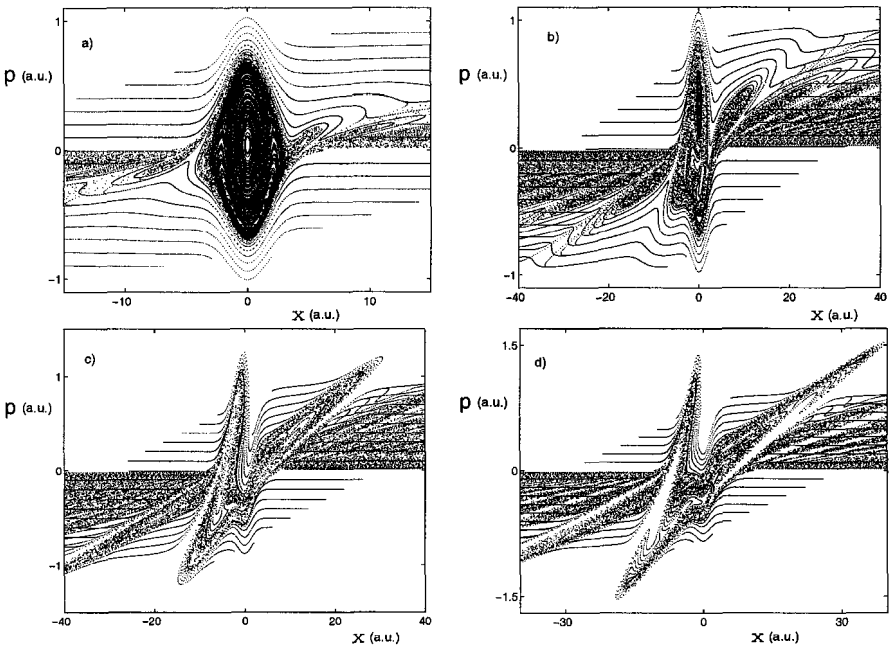

Figure 1: Strobe plots of the classical phase space. The solid lines of trajectories lie at the center of the various channels. (a) $\alpha_0 = 0.1$. (b) $\alpha_0 = 0.7$. (c) $\alpha_0 = 3.25$. (d) $\alpha_0 = 5.25$.

and (1.d), which correspond to stronger driving fields, the dynamics appears to be totally chaotic for low incident energies. In each figure, the various solid lines correspond to different incident Floquet channels. They differ in energy by ω (in atomic units) and show the progress of a series trajectories whose initial energies are chosen to lie at the center of the various channels. As α_0 is increased more and more channels get pulled into the chaotic tangles.

It is important to note that the strobe plots are drawn for values of the position and momentum in atomic units. Since in atomic units the value of Planck's constant, $\hbar = 1$, regions of the strobe plots with unit area can, in principle, support a single quantum state. Figure (1.a) shows the phase space structure for $\alpha_0 = 0.1$. The large regular island in the center of the plot represents the region of phase space dominated by the potential well, $V(x)$. Note that it occupies a unit area of phase space, and this is consistent with the fact that the potential well can support one bound state. However, the regular island is also surrounded by a small degree of chaos. As the field strength increases, the regular region is slowly destroyed and replaced by a wide region of chaotic tangles which spread over increasingly large areas of the phase space. It is apparently these chaotic tangles that dominate the underlying classical phase space when the second quasibound state appears for $\alpha_0 > 1.0$.

7 Quantum signatures of chaos

The Floquet scattering matrix is a $2(n_p+1)\times 2(n_p+1)$ unitary matrix with $2(n_p+1)$ complex eigenvalues, $e^{i\theta_j}$, $(j = 1, 2, ...n_p)$ which lie on the unit circle. Each eigenvalue has associated with it an eigenphase, $-\pi \leq \theta_j \leq \pi$, which is defined modulus 2π. In the limit when $V_0 \to 0$, the matrix elements of the reflection matrices, **R**, all go to zero, and the transmission matrices, **T**. become equal to unit matrices. In this limit, the **S**-matrix has $(n_p + 1)$ eigenvalues, $+1$ and $(n_p + 1)$ eigenvalues, -1. It therefore has $(n_p + 1)$ eigenphases, 0, and $(n_p + 1)$ eigenphases, π.

In Figures (2.a)-(2.d), we plot the eigenphases of the **S**-matrix for the same parameter values as in the respective figures, (1.a)-(1.d). In Fig. (2.a), $\alpha_0 = 0.1$ and $n_p = 6$. While there is a shift away from zero, we see clearly the clustering of eigenphases a distance π apart. Most of the eigenphases are approximately constant as a function of the quasienergy. however, one eigenphase undergoes an abrupt change in value of approximately 2π at a quasienergy, $\mathcal{E} \approx E_b + \omega \approx 0.10$. This is an indication that the electron is delayed significantly while traversing the reaction region, because the slopes of the eigenphases are partial delay times, $\tau_j = \frac{d\theta_j}{d\epsilon}$. Negative slopes indicate that the particle speeds up in traversing the reaction region, and positive slopes indicate that the particle is delayed. Note also that a very rapid change in the eigenphase is an indication that a long lived quasibound state exists at that quasienergy.

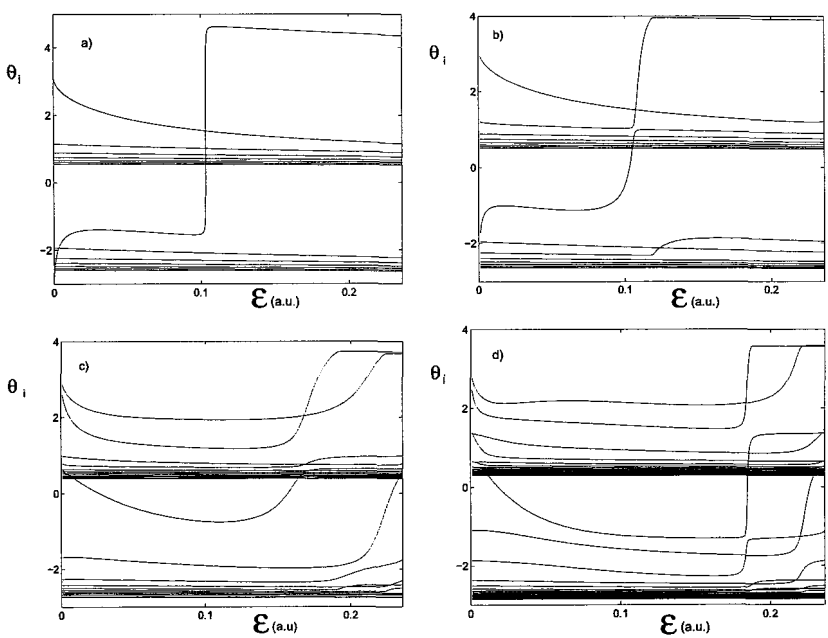

Figure 2: Eigenphases of the Floquet scattering matrix. (a) $\alpha_0 = 0.1$ and $n_p = 6$. (b) $\alpha_0 = 0.7$ and $n_p = 7$. (c) $\alpha_0 = 3.25$ and $n_p = 11$. (d) $\alpha_0 = 5.25$ and $n_p = 19$.

In Figure (2.b) where the external field strength has increased to $\alpha_0 = 0.7$, an interesting phenomenon occurs. There are now three eigenphases involved in the same rapid increase in value of eigenphase, and they appear to share it via a level repulsion. This we believe is a signature of the underlying chaos that can be seen in Figure (2.b). It also indicates that at least three channels have now been affected by the chaos.

For values of the external field strength, $\alpha_0 \gtrsim 1.0$, we expect to see two regions of rapid change in the eigenphase due to the existence of two quasibound states at those field values. In Figures (2.c) and (2.d), we do indeed see those two regions. We now see level repulsion in both of these regions. Also, a larger number of channels appear to be pulled into the chaotic tangles and this is consistent with what is seen in Figures (1.c) and (1.d).

8 Conclusions

Although we have only a few eigenphases undergoing level repulsion, this appears to be the beginning of a process of information loss in the sense of Dyson. The appearance of level repulsion is an indication that good quantum numbers are destroyed locally in the scattering process, and that the scattering process has become a truly random event. Information about the final channels into which the particle is scattered decreases as underlying chaos begins to dominate the scattering process.

Acknowledgments

The authors wish to thank the Robert A. Welch Foundation, Grant No.F-1051 and the Engineering Research program of the Office of Basic Energy Sciences at the U.S. Department of Energy, Grant No. DE-FG03-94ER14405 for partial support of this work. We also thank the University of Texas High Performance Computing Center for use of its facilities.

References

1. W. Chism, D. Choi and L. E. Reichl, Phys. Rev. A. **61**, 054702 (2000)
2. T. Timberlake and L. E. Reichl, Phys. Rev. A **64**, 33404 (2001).
3. Agapi Emmanouilidou and L. E. Reichl, Phys. Rev. A **65**, 33405 (2002).
4. L. E. Reichl, *The Transition to Chaos in Conservative Classical Systems: Quantum Manifestations* (Springer-Verlag, New York, 1992).
5. E. P. Wigner, Phys. Rev. **98**, 145 (1955).
6. F. T. Smith, Phys. Rev. **118**, 349 (1960).
7. F.J. Dyson, J. Math. Phys. **3** 140 (1962); **3** 157 (1962); **3** 166 (1962).
8. Pier A. Mello and Harold U. Baranger, Waves Random Media **9** 105 (1999).
9. L.K. Hua, *Harmonic Analysis of Functions of Several Complex Variables in the Classical Domains*, (American Mathematical Society, Providence).
10. H. A. Kramers, *Collected Scientific Papers* (North-Holland, Amsterdam, 1956), p.272.
11. W. C. Henneberger, Phys. Rev. Lett. 21, 838 (1968).

12. R. Bhatt, B. Piraux, and K. Burnett, Phys. Rev. A 37, 98 (1988).
13. G. Yao and S.-I Chu, Phys. Rev. A 45, 6735 (1992)
14. M. Marinescu and M. Gavrila, Phys. Rev. A 53, 2513 (1996).
15. A. S. Fearnside, R. M. Portvliege, and R. Shakeshaft, Phys. Rev. A 51, 1471 (1995).

DISCUSSION

Chairman: G. Casati

S. Lloyd: Your use of the term quantum information is different from what we normally use. So it seems to me that your discussion of loss of quantum information is different from loss of information due to decoherence.

L. Reichl: Yes, I would say so but how can I answer this? First of all, I am dealing with an open system so there are no stable quantum eigenstates in the sense you are used to. In a bounded system, when a transition to chaos occurs, you can still have energy eigenstates but you can lose all other quantum numbers which identify the state of the system. Here, the only conserved quantity is the Floquet energy. Any quantum numbers that characterized the state in a asymptotic regime are wiped out in the scattering process. So in that sense you lose all information for the system except for that one conserved quantity, the quasienergy.

G. Casati: Basically what you want to say is that in such a situation the exact state is a combination of the exponentially large number of basis states, of computational basis states.

S. Lloyd: Are these states quasistates or the states for the atom?

L. Reichl: No, they are in the neighborhood of the atom but they can have spatial extent much greater than the atomic radius due to interaction with photons from the laser field.

L. Stodolsky: I was just wondering if this is a way of understanding, or is it in some way similar to the mechanism where you create traps with oscillating fields?

L. Reichl: Traps form bounded systems although you can get similar behavior.

G. Casati: If you take an atom which you excite with some periodic field, as you increase the field you increase the ionization, but at some point if you still increase the field you stabilize the system. The ionization probability decreases. This phenomenon can be explained on the classical basis, and it is also true for the quantum basis.

E. C. G. Sudarshan: I don't want to make an elaborate comment but the statement about the rigged Hilbert space is completely unnecessary, unwanted and irrelevant. It is true that you get complex eigenvalues when you go into the complex plane and they have left eigenstates and right eigenstates which are different. There is no rigging necessary.

L. Reichl: The only problem is if you want to understand how the probability of those states is distributed in real space. You have to use some trick because their continuum part blows up very fast, almost exponentially as a function of the spatial coordinates. That's all: it is unbounded.

SOME PROPERTIES OF THREE-PARTY ENTANGLED STATES AND THEIR APPLICATION IN QUANTUM COMMUNICATION

ANDERS KARLSSON[1,a], MOHAMMED BOURENNANE[1,2], IULIA GHIU[1,2], DANIEL LJUNGGREN[1]A ND ANDERS MÅNSSON[1]

[1] *Department of Microelectronics and Information Technology, Royal Institute of Technology (KTH), Electrum 229, 164 40 Kista, Sweden*

[2] *Max-Planck-Institut für Quantenoptik Hans-Kopfermann-Str. 1 D-85748 Garching, Germany*

[3] *Department of Physics, Laboratory of Statistical Physics and Quantum Mechanics, University of Bucharest, PO Box MG-11, R-76900, Bucharest-Măgurele, Romania*

We give a brief overview of work on extending present two-party quantum communication protocols to three-party and multi-party protocols. In particular we discuss the case of three-party protocols and entanglement-assisted transformations between inequivalent classes of three-particle entangled states (GHZ-states and W-states) which are non-interchangeable under local transformations. We furthermore review possible applications of three-party entangled states.

1 Introduction

Entanglement is the key physical resource in most quantum information processes, e.g. quantum teleportation [1], two- or multiparty quantum cryptography [2,3], and quantum computation [4,5]. Moving onwards from two-particle entangled states, much interest has been devoted to three-particle entangled states, notably the Greenberger-Horne-Zeilinger (GHZ) states [6]

$$|GHZ\rangle = 1/\sqrt{2}(|000\rangle + |111\rangle) \tag{1}$$

and their role in generalizations of Bell inequalities, as well as an enabling resource for quantum computation [7,8,9,10,11,12]. Whereas for two-particle states, the possibilities and restrictions of local manipulation of entanglement is known, see e.g. [12,13,14], for three or multipartite entanglement, there still remain unresolved issues concerning both entanglement transformations as well as possible applications in quantum information processing.

Recently, there has been some interest devoted to so called W-states [15], an example being the state

$$|W\rangle = \frac{1}{\sqrt{3}}(|001\rangle + |010\rangle + |100\rangle). \tag{2}$$

An interesting property of this state is that if, say, particle one is traced out, there remains a large degree of entanglement in particle two and three, or if the state of the first particle is measured in the $\{0,1\}$ basis, then either the state of particle two and three is maximally entangled, or in a product state.

Some interesting questions now arise: How can we generate these three-party entangled states, for simplicity thinking only of optics? Secondly, how can we use these states in quantum communication?

[a] Corresponding author: andkar@ele.kth.se, Fax:+46 8 752 12 40

Our paper is organized as follows: In section II, we introduce the two general classes of three-particle entangled states inequivalent under so called SLOCC (stochastic local quantum operations and classical communication between the parties), briefly describe how these states can be generated by optical means, and finish by reviewing single-copy bipartite entanglement optimal manipulation as well as discuss some protocols for conversion of a certain family of the W-states and an EPR-pair (i.e a maximally entangled two-party state) into the state GHZ. In section III we address some possible applications of these states. Finally in section IV we conclude.

2 From two-party to three-party quantum states: the GHZ and W classes

For two-party entanglement, basically one needs only to be concerned with single-particle properties as well as the correlations and entanglement properties between the two parties. However, for multi-party situations it is obviously not that easy. For instance, we may be interested only in the entanglement shared by Alice and Bob, or that of Bob and Charlie, that of Alice and Charlie (the names referring to the three parties or locations), or perhaps in genuine three-party entanglement between Alice, Bob and Charlie.

For genuine three-party entanglement it was shown [15] that states of the GHZ-type and of the W-type are inequivalent in the following sense: if we allow only Stochastic Local quantum Operations and Classical Communications [16], abbreviated SLOCC, then one cannot succeed in transforming states from the GHZ-class to the W-class and vice-versa with a non-zero probability of success. We note that in Refs.[17,18] the optimal distillation of the state GHZ from one copy of an arbitrary tripartite entangled state has been presented.

2.1 Optical generation of GHZ and W states

As has been shown, notably by the Zeilinger group in Vienna and former associates, in optics higher order entanglement can be produced conditionally by suitably mixing EPR-pairs on a beamsplitter [19,20]. By conditional is meant that in some cases the photons do not exit in the desired ports, for instance, two photons may exit in the same port, while we want the photons in different ports. For the sake of comparison let us here illustrate with a conceptually simpler scheme according to Rarity et al. [21], see Fig. 1. Let us use the computational notation and denote horizontally H and vertically V polarized photons as $|H\rangle = |0\rangle$ and $|V\rangle = |1\rangle$ respectively. Now, suppose a single photon in state $|\psi\rangle = (|0\rangle + |1\rangle)/\sqrt{2}$ and an EPR-state of the following form $|EPR\rangle = (|00\rangle + |11\rangle)/\sqrt{2}$ on a polarizing beamsplitter (PBS). As pointed out by Pittman et al. [22] a PBS works as a parity check. If two photons of different polarization are incident on the ports, they will both exit in the same port, but if the polarization is the same, they will exit in different ports. Thus, with the state above incident on the PBS, we have the following states before the PBS $(|000\rangle + |111\rangle)/2$, giving the desired GHZ state correlations, and $(|100\rangle + |011\rangle)/2$, which will give two photons in the same port.

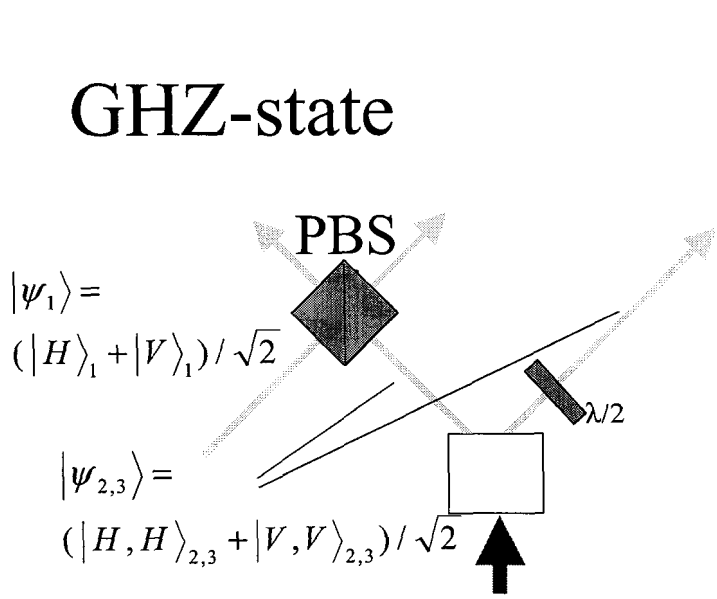

Figure 1: Schematic of GHZ-state generation by optical means. The polarizing beamsplitter (denoted by PBS) transmits one polarization and reflects the other, in the computational basis acting as parity gate. This means that only if the polarizations of the three photons are the same does one get one photon out in each of the exit beams, thereby conditionally (half of the times) giving a GHZ-state.)

In order to generate a W-state, one can use a scheme proposed by Weinfurter[23], see Fig. 2, which is based on a polarization dependent transmission in one arm. In this case one starts with a single photon $|\psi\rangle = |V\rangle = |1\rangle$ and an EPR-state of the following form $|EPR\rangle = (|01\rangle + |10\rangle)/\sqrt{2}$. Going through the setup one finds that the cases with useful three photons at the upper three output are: If photon 2 initially is $|0\rangle$ is $\sqrt{T_v}(|011\rangle + |101\rangle)/2$, and when photon 2 initially is $|1\rangle$ is $\sqrt{2T_H}|110\rangle$. Choosing $T_v = 2T_H$, and adding these two outcomes in superposition renders the useful output state $(|011\rangle + |101\rangle + |110\rangle)/\sqrt{3}$.

As an alternative to direct generation of entangled states, one may consider also using quantum gates[24]. For instance, two quantum CNOT gates can be used to create a GHZ-state. However, as is well-known by anyone in the field, it is very difficult to create efficient quantum gates due to the large non-linearity (optical) that is required. As a side comment, since a quantum CNOT gate also can be used to implement a perfect quantum non-demolition (QND) measurement, the level of difficulty in doing a perfect QND measurement with a signal and a probe both at the single quanta level, and a quantum gate should in many cases (if not always)

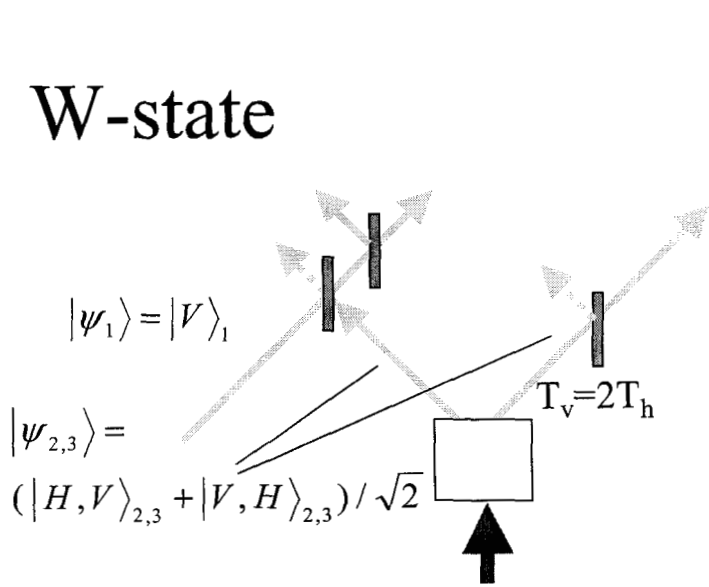

Figure 2: Schematic of conditional W-state generation by optical means. Only when there is one photon in each of the uppermost arms, does one get a useful output. In the first (leftmost) beamsplitter one selects cases when there are two photons going to the next beamsplitter. The rightmost beamsplitter has a polarization dependent transmittance and is used to put equal weights on the terms in the W-state.

be judged as equal. Realizing this, recently several authors have considered using linear optics to do probabilistic quantum gates, c.f. [22]. In many ways this is a very clever and interesting path to explore further.

However, it should be stressed that for many practical schemes just by brute force replacing CNOTs by linear quantum gates, may not be a good idea since the overhead in using EPR-pairs to construct general quantum gates is too big compared to using the more simple schemes presented above. This suggests that linear optical quantum gates, when assembled for a specific task should be "compiled" and reduced to a more simpler set of elementary "building blocks", rather than to use the full gates by themselves.

Finally, it can be noted that if one uses "entanglement with the vacuum" [25], exploring the zero and one Fock states of the photon field, then W-state correlations are easily produced by having a 2/3 transmittance beamsplitter followed by 1/2 transmittance beamsplitter. A W-state is then simply a single photon leaving in either of the three exit beamsplitter ports with equal probability.

2.2 *Inter-conversion the GHZ and W classes*

Let us now move on to discuss the following question: Suppose we have generated one of the above states, then what is the possibility of converting this state into the other type? Of some interest in entanglement transformations has been entanglement catalysis processes [26]. The questions we address here are: Can we perform the transformation between the two inequivalent classes using a "catalysis" state, such as shared Einstein-Podolsky-Rosen (EPR) pairs, quantum states of the form:

$$|\Psi^+\rangle = (|00\rangle + |11\rangle)/\sqrt{2}, \tag{3}$$

and which is the probability of success to transform W-states into GHZ-states and vice-versa by using SLOCC in presence of additional entanglement resources?

Let us then first show, as an illustration, a simple way to convert the state W of Eq.(2) into the state GHZ of Eq.(1) using a single EPR-pair. Suppose the three parties involved, Alice, Bob, and Charlie, share three-particle entanglement of the type W, and at the same time, Alice and Bob share one EPR-pair. To transform the state, first Alice makes a measurement in the computational basis $\{0,1\}$. From Eq.(2) we see that with probability $p = 2/3$, she projects out a two-particle maximally entangled state between Bob and Charlie, and when that happens she also knows it with certainty. Now we have two EPR-pairs, one pair for Alice-Bob and another one for Bob-Charlie. Secondly, Bob can prepare locally the state GHZ, then he teleports [1] the state of one particle to Alice and another one to Charlie by using the shared Alice-Bob and Bob-Charlie EPR-pairs, respectively [16].

Moving onwards to the more general case, let us define the two classes of three-particle entangled states [15], first the GHZ-class:

$$|\psi_{GHZ}\rangle = \sqrt{K}(c_\delta|0\rangle|0\rangle|0\rangle + s_\delta e^{i\phi}|\varphi_A\rangle|\varphi_B\rangle|\varphi_C\rangle), \tag{4}$$

where $|\varphi_A\rangle = c_\alpha|0\rangle + s_\alpha|1\rangle, |\varphi_B\rangle = c_\beta|0\rangle + s_\beta|1\rangle, |\varphi_C\rangle = c_\gamma|0\rangle + s_\gamma|1\rangle$ and K is the normalization factor.

Secondly, the W-class is:

$$|\psi_W\rangle(a,b,c,d) = \sqrt{a}|100\rangle + \sqrt{b}|010\rangle + \sqrt{c}|001\rangle + \sqrt{d}|000\rangle, \tag{5}$$

where $a,b,c > 0, d \geq 0$, and $a+b+c+d = 1$. The state W of Eq. (2) is characterized by: $d = 0, a = b = c = 1/3$. It has been shown that there is not a local operator (invertible or non-invertible) $A \otimes B \otimes C$ (where A, B and C are the local operators of Alice, Bob, and Charlie, respectively) such that:

$$|\psi_W\rangle = A \otimes B \otimes C|\psi_{GHZ}\rangle, \tag{6}$$

where $|\psi_{GHZ}\rangle$ and $|\psi_W\rangle$ belong to the GHZ-class and W-class, respectively [15].

Suppose now that two observers, Alice and Bob, share one copy of a pure bipartite entangled state Ψ_{AB} and that they would like to convert it into another pure bipartite entangled state Φ_{AB}. The greatest probability of success, if the two parties are allowed only to act by LOCC, is [14]:

$$P(\Psi_{AB} \to \Phi_{AB}) = \min_{l \in [1,n]} \frac{\sum_{i=l}^{n} \alpha_i}{\sum_{i=l}^{n} \beta_i}, \tag{7}$$

where α_i and β_i are the Schmidt coefficients of Ψ and Φ defined as,

$$|\Psi_{AB}\rangle = \sum_{i=1}^{n} \sqrt{\alpha_i}|i_A i_B\rangle, \sum_{i=1}^{n} \alpha_i = 1,$$
$$|\Phi_{AB}\rangle = \sum_{i=1}^{n} \sqrt{\beta_i}|i_A i_B\rangle, \sum_{i=1}^{n} \beta_i = 1, \quad (8)$$

where $|i_A\rangle$ and $|i_B\rangle$ are the bases for the quantum system A and B.

In Ref.[26], the catalysis transformation between two bipartite states $|\psi_1\rangle, |\psi_2\rangle$ is defined as follows: Suppose Alice and Bob share an entangled state $|\psi_1\rangle$, that cannot be converted into $|\psi_2\rangle$ by LOCC. A preparator can 'lend' them an entangled state $|\phi\rangle$. If the transformation

$$|\psi_1\rangle \otimes |\phi\rangle \rightarrow |\psi_2\rangle \otimes |\phi\rangle \quad (9)$$

is possible, then this protocol is called entanglement-assisted local transformation or catalysis transformation [26], since the state $|\phi\rangle$ is not consumed. In [27], however, it was shown that such true catalysis transformations between GHZ- and W-states is not possible.

Let us instead show how one can make a transformation using the assistance by an EPR-state, where the entanglement is swapped. Suppose Alice, Bob, and Charlie share a copy of the following W-state (5) :

$$|\psi_W\rangle_{123}(a, a, 1-2a, 0) = (\sqrt{a}|100\rangle + \sqrt{a}|010\rangle + \sqrt{1-2a}|001\rangle)_{123}, \quad (10)$$

where $a \in \left[\frac{1}{3}, \frac{1}{2}\right[$. Here, in order to more clearly see later how the entanglement is transferred, we have introduced indices, such that the three particles are denoted by "1", "2", and "3". Consider that a preparator, Daniel, can send to two of them an EPR-pair, indexed by "4" and "5". They want to transform this state into the state GHZ (1) with the help of the EPR-pair "45"(see Fig. 3):

$$|\psi_W\rangle_{123}(a, a, 1-2a, 0) \otimes |EPR\rangle_{45} \rightarrow |GHZ\rangle_{125} \otimes |00\rangle_{34}. \quad (11)$$

Then the highest probability is equal to '$2a$' and is obtained when the preparator sends the EPR-pair "45" to Alice and Charlie, or to Bob and Charlie. The optimal protocol for achieving the transformation consists in three steps:

(a) Charlie measures his particle "3" in the computational basis. After this measurement, he has to send the outcome to Alice and Bob.

Let us consider that Bob and Charlie share the EPR-pair.

(b) Bob applies a CNOT operation onto his particles, where the particle "2" represents the source, while particle "4" is the target.

(c) Bob measures particle "4" in the computational basis.

To prove this, let the initial state be written as follows:

$$|\phi_i\rangle = |\psi_W\rangle_{123} \otimes |EPR\rangle_{45} = (\sqrt{a}|100\rangle + \sqrt{a}|010\rangle$$
$$+\sqrt{1-2a}|001\rangle)_{123} \otimes \frac{1}{\sqrt{2}}(|00\rangle + |11\rangle)_{45}; \quad (12)$$

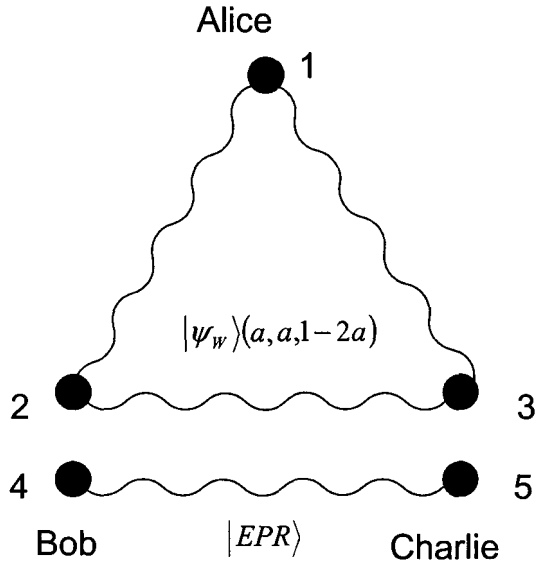

Figure 3: Schematic of the transformation from $|\psi_W\rangle(a,a,1-2a,0)$ into the state GHZ using one EPR-pair (the wavy lines represent the entanglement). The EPR-pair is used to as a mean to transfer the entanglement.

Now, let us compute the probability given by the above protocol:

Step (a): After the measurement, Charlie will obtain the state $|0\rangle_3$ with the probability $2a$, and the state of the whole system will be projected onto:

$$|\phi_a\rangle = \frac{1}{2}(|1\rangle_1|00\rangle_{24}|0\rangle_5 + |1\rangle_1|01\rangle_{24}|1\rangle_5) + \\ + \frac{1}{2}(|0\rangle_1|10\rangle_{24}|0\rangle_5 + |0\rangle_1|11\rangle_{24}|1\rangle_5). \quad (13)$$

Step (b): The CNOT-gate performed by Bob will lead to the following state:

$$|\phi_b\rangle = \frac{1}{2}(|1\rangle_1|0\rangle_2|0\rangle_5 + |0\rangle_1|1\rangle_2|1\rangle_5)|0\rangle_4 + \\ + \frac{1}{2}(|1\rangle_1|0\rangle_2|1\rangle_5 + |0\rangle_1|1\rangle_2|0\rangle_5)|1\rangle_4. \quad (14)$$

Step (c): Regardless of Bob's outcome measurement of particle "4", the final state is local unitary equivalent to the state GHZ. We have obtained the final state

with the total probability $P = 2a$. In[27,28] it was proved that the above local protocol is optimal.

Let us discuss how we can apply the above procedure backwards to go from the GHZ-class to the W-class. Suppose that Alice, Bob, and Charlie share a GHZ-state, and at the same time Alice and Bob share an EPR-pair. One can obtain an EPR-pair shared by Bob and Charlie from the GHZ-state[29] with probability one if Alice performs a measurement in x-basis $|x+\rangle = (|0\rangle + |1\rangle)/\sqrt{2}, |x-\rangle = (|0\rangle - |1\rangle)/\sqrt{2}$:

$$|GHZ\rangle = \frac{1}{\sqrt{2}}\left[|x+\rangle_A \frac{1}{\sqrt{2}}(|00\rangle + |11\rangle)_{BC} + |x-\rangle_A \frac{1}{\sqrt{2}}(|00\rangle - |11\rangle)_{BC}\right]. \quad (15)$$

Bob can prepare locally an arbitrary three-particle entangled state, and by using the two EPR-pairs, the three observers will share the three-particle state. Thus, we have shown in this section how stochastic local operations followed by classical communications assisted by additional entanglement can be used to perform transformations between two states of the two inequivalent classes. How useful these transformations are in practice remains to be seen, and it can be noted that they use CNOTs at some stages, else they have to be realized with a smaller probability of success.

3 Applications of three-party quantum entanglement

Having now discussed some properties of three-party correlated states, let us move on to discuss possible applications. Let us first note that some of the original interest in GHZ-states stemmed from the possibility to obtain a stronger violation of Bell inequalities[6]. Recently, this was studied by Cabello also in conjunction to W-states[30] where proof of Bell's theorem without inequalities valid for both GHZ and W was described. Here we will briefly just review some simple examples of how entanglement can be used for simple multi-party communication and computational tasks.

3.1 Quantum secret sharing

Let us first discuss how three-particle entanglement can be used for secret sharing, as was first shown by Hillary et al. [3]. Secret sharing, a real-life application in classical cryptography, is a process whereby a secret is not entrusted by a single party, but is split between multiple parties who must collaborate to retrieve the secret.

Suppose, Trent, Alice and Bob share one particle each from a three-particle entangled Greenberger-Horne-Zeilinger (GHZ) state[6]

$$|\psi_{GHZ}\rangle = \frac{1}{\sqrt{2}}(|000\rangle_{TAB} + |111\rangle_{TAB}), \quad (16)$$

where the first particle is that of Trent, the second that of Alice and the third that of Bob (in[3], and the discussion above the parties (Trent, Alice, Bob) were denoted (Alice, Bob, Charlie), but we stick here to the common notation from classical

cryptography of denoting the sender in secret sharing by Trent). Now, they then make random measurement, either in the x-direction (defined earlier), or in the y-direction, the y eigenstates defined as

$$|y+\rangle = \frac{1}{\sqrt{2}}(|0\rangle + i|1\rangle), \quad |y-\rangle = \frac{1}{\sqrt{2}}(|0\rangle - i|1\rangle). \tag{17}$$

Now, by re-expressing the GHZ-state in the x and y- eigenstates, as was shown in [3], Alice and Bob can construct a lock-up table that allows them to jointly, but only jointly, determine which was the measurement outcome of Trent. In [31] a similar quantum secret sharing scheme was shown by using a complementary set of two-particle Bell states. This scheme has also been demonstrated in a very elegant experiment by Tittel et al. [32].

3.2 Quantum information splitting with GHZ-states

In [3] classical secret key sharing by quantum methods was also extended to the splitting of quantum information (qubits), which we also have studied in the context of teleportation to two parties [35]. The basic idea is as follows: Trent has a qubit $|Q\rangle = (a|0\rangle + b|1\rangle)$, which he wants to send to either Alice or Bob (both cannot generally have it as that would violate the "no-cloning-theorem"). This may be done using a teleportation procedure, whereby Trent, Alice and Bob initially share a GHZ-state. Next, Trent makes a joint Bell-state measurement on the state $|Q\rangle$ and his particle of the GHZ-state. By communicating the outcome (2 bits) to Alice and Bob, their joint state can be rotated to the split state $|Q\rangle_{s2} = a|00\rangle + b|11\rangle$, where the notation is that of Alice having the first particle and Bob the second particle. From this state, Alice may for instance retrieve $|Q\rangle$ if Bob does a so called quantum erasure measurement in the x basis, and communicates (1 bit) which outcome ($x+$ or $x-$) he obtained. It should be emphasized that the teleportation method is not the only way to achieve the quantum information splitting. By using quantum controlled-NOT gates [24], the quantum information in a qubit can also trivially be split to several parties, e.g. for instance to three parties $|Q\rangle_{s3} = a|000\rangle + b|111\rangle$ by the successive operation of two quantum controlled-NOT gates.

A more general theory of quantum secret sharing (of both classical information and of quantum states) was developed by Cleve et al. [33], and Gottesman [34], who also very elegantly showed the connection between quantum secret sharing and quantum error correction. Expressed simply, quantum error correction coding protects quantum information from decoherence by the environment because the environment does not learn anything about it. Then, for secret sharing replacing the environment with the external parties, a quantum secret can also be kept unknown to the outsider using coding.

It should furthermore be noted, that the concept of using GHZ-states for quantum gate constructions was very elegantly used by Gottesman and Chuang [9] in showing that quantum gates could be constructed using Bell measurements together with entanglement as a resource. Also, the concept of gate teleportation [36] by Nielsen and Chuang, who showed how stochastically teleport a quantum gate from one location to another, has been extremely fruitful for the further devel-

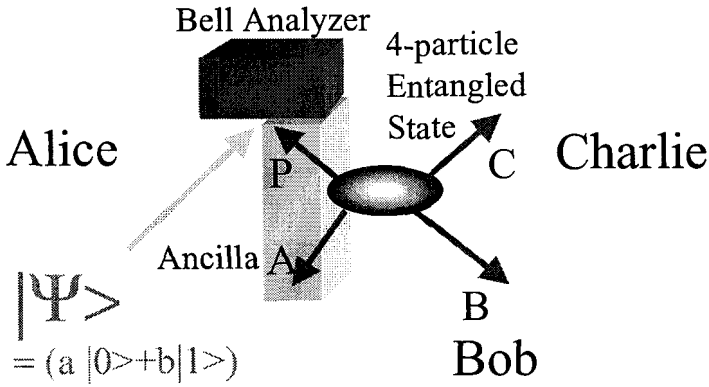

Figure 4: Schematics of 1-2 telecloning. The state to be remotely cloned (telecloned) is subject to a Bell measurement together with the particle P (preparator). If the ancilla particle A is not used, the state is telecloned. By sending along the ancilla, the full quantum state can be recovered at one of the two locations by a joint operation.

opment of linear quantum logic, and generally for the understanding of quantum operations.

3.3 Multi-party quantum teleportation and quantum cloning

Quantum information splitting, of course, is very much related to quantum information cloning [37]. In a much more general context than [35], Murao et al. [38] showed how optimal quantum cloning (approximate copying) could be implemented using teleportation and a specially prepared cloning state. It is interesting to note here that parts of the telecloning state used in a one to two-party cloning is exactly a W-state. Looking in even more detail on the cloning state, such as that to be used in Fig. 4, one finds that this state can be written as:

$$|\Phi_{clone}\rangle = \sqrt{\frac{2}{3}}|GHZ\rangle_{P,A,B,C} + \sqrt{\frac{1}{6}}|EPR\rangle_{P,A}|EPR\rangle_{B,C}. \qquad (18)$$

As shown by Weinfurter and Zukowski [39], this particular state can be generated in optics in a double-pair emission from type-II parametric down-conversion. Quantum telecloning therefore is open for experimental implementations. However, with respect to the implementation of quantum cloning, it should be noted that in many cases there is a direct connection between quantum cloning and amplification, and

it is well known [40] that linear amplifiers (such as those already used in optical networks) can operate at the fundamental quantum limit. Recently, quantum cloning on the single-photon level was shown experimentally by parametric amplification [41] and in an Erbium doped optical amplifier [42].

4 Conclusions

In this paper we have given a brief overview of some (but of course not all) properties and applications of three-party entangled quantum states. It is very clear that if quantum communication in particular, should go beyond point-to-point protocols towards quantum networking, it is crucial that we learn to generate and understand the properties of such multi-party quantum states. We believe a central point for further studies is to find effective schemes in the use of entanglement resources, practical setups for the generation and detection of the states, as well further studies of linear quantum logic.

Acknowledgements

This work was supported by the European IST QuComm project, the Swedish Science Research Council (VR), and the Swedish Institute (SI) through a visiting researcher fellowship.

References

1. C.H. Bennett, G. Brassard, C. Crepeau, R. Jozsa, A. Peres, and W.K. Wooters, Phys. Rev. Lett., vol. 70, pp. 1895-1898 (1993).
2. A. K. Ekert, Phys. Rev. Lett. **67**, 661 (1991).
3. M. Hillary, V. Buzek and A. Bertaiume, Phys. Rev. A **59**, 1829 (1999).
4. P.W. Shor in *Proceedings of the Symposium on the Foundation of Computer Science, 1994, Los Alamonitos, California* (IEEE Computer Society Press, New York 124 (1994).
5. L.K. Grover, Phys. Rev. Lett. **79**, 325 (1997).
6. D. M. Greenberger, M.A. Horne, A. Shimony, and A. Zeilinger, Am. J. Phys., **58** 1131 (1990).
7. L.K. Grover, quant-ph/9704012.
8. J. I. Cirac, A. K. Ekert, S.F. Huelga, C. Macchiavello, Phys. Rev. A **59**, 4249 (1999);
9. D. Gottesman and I.L. Chuang, Nature **402**, 390 (1999).
10. D. Collins, N. Linden, S. Popescu, quant-ph/0005102.
11. J. Eisert, K. Jacobs, P. Papadopoulos, M. B. Plenio, Phys. Rev. A **62**, 052317 (2000).
12. D. Jonathan and M. Plenio, Phys. Rev. Lett. **83**, 1455 (1999).
13. M. A. Nielsen, Phys. Rev. Lett. **83**, 436 (1999).
14. G. Vidal, Phys. Rev. Lett. **83**, 1046 (1999).
15. W. Dür, G. Vidal, and J. I. Cirac, Phys. Rev. A **62**, 062314 (2000).

16. C.H. Bennett, S. Popescu, D. Rohrlich, J.A. Smolin, and A.V. Thapiliyal, Phys. Rev. A **63**, 012307 (2001).
17. O. Cohen, T. A. Brun, Phys. Rev. Lett. **84**, 5908 (2000).
18. A. Acín, E. Jané, W. Dür, and G. Vidal, Phys. Rev. Lett. **85**, 4811 (2000).
19. D. Bouwmeester, J. W. Pan, M. Daniell, H. Weinfurter, and A. Zeilinger, Phys. Rev. Lett., **82**, 1345-1349 (1999).
20. J.-W. Pan, D. Bouwmeester, and H. Weinfurter , Phys. Rev. Lett., **80**, 3891 (1998).
21. J.G. Rarity and P. R. Tapster, Phys. Rev. A, vol. **59**, R35-R38 (1999).
22. T.B. Pittman, B.C. Jacobs, J.D. Franson C, Phys. Rev. A, **64**, 062311 (2001)
23. H. Weinfurter, private communication.
24. A. Barenco, D. Deutsch, A. Ekert, and R. Jozsa Phys. Rev. Lett., vol. **74**, pp.4083 - 4086 (1995)
25. G. Björk, P. Jonsson and L. L. Snchez-Soto, Phys. Rev. A, vol. **64**, art. no. 042106/1-6, 2001.
26. D. Jonathan and M. Plenio, Phys. Rev. Lett. **83**, 3566 (1999).
27. I. Ghiu, M. Bourennane and A. Karlsson, Phys. Lett. A, vol. **287**, no. 1-2, pp. 12-18 (2001).
28. I. Ghiu, M. Bourennane and A. Karlsson, "An upper bound...", unpublished.
29. N. Linden, S. Popescu, B. Schumacher, and M. Westmoreland, quant-ph/9912039 (1999).
30. A. Cabello, Phys. Rev. A **65** 032108 (2002).
31. A. Karlsson, M. Koashi and N. Imoto, Phys. Rev. A, vol. **59**, no. 1, pp. 162-168 (1999).
32. W. Tittel, H. Zbinden and N. Gisin, Phys. Rev. A **63**, 042301 (2001).
33. R. Cleve, D. Gottesman and H.-K. Lo, Phys. Rev. Lett., **83**, 1459 (1999).
34. D. Gottesman, quant-ph/9910067
35. A. Karlsson and M. Bourennane, Phys. Rev. A, vol. **58**, no. 6, pp. 4394-4400 (1998).
36. M. A. Nielsen and I. L. Chuang, Phys. Rev. Lett., vol. **79**, pp. 321-324 (1997).
37. V. Buzek and M. Hillery, Phys. Rev. A **54**, 1844 (1996).
38. M. Murao, D. Jonathan, M.B. Plenio and V. Vedral, Phys. Rev. A, **59**, pp. 156 - 161 (1999).
39. H. Weinfurter, M. Zukowski, quant-ph/0103049
40. Y. Yamamoto and H.A. Haus, Rev. Mod. Phys., vol. **58**, pp. 1001-1019 (1986).
41. A. Lamas-Linares, C. Simon, J. C. Howell, and D. Bouwmeester, Science **296**, 714 (2002).
42. S. Fasel, N. Gisin, G. Ribordy, V. Scarani, H. Zbinden, "Quantum cloning with an optical fiber amplifier" quant-ph/0203056, accepted for publication Phys. Rev. Lett.

DISCUSSION

Chairman: I. Cirac

L. Stodolsky: What are some physical realizations of these high-dimensions states?

A. Karlsson: In the European project I mentioned, QuComm, we talked about it sometimes and I think there is ongoing work, notably by the Geneva group of Gisin on that. The problem experimentally with this is that you have to stabilize all the optics, notably the interferometers. The time-bin entangled states are realized following from a pulse coming in to a beam-splitter where it chooses to go along one of several paths of different propagation lenghts, after which they are again recombined, hence creating a superposition. And then one can apply phases to, or choosing the splitting ratio for the various paths in order to create various entangled states.

ATOMIC AND NUCLEAR INTERFERENCE EFFECTS FOR QUANTUM INFORMATION PROCESSING

OLGA KOCHAROVSKAYA, ALEXEI A. BELYANIN, IGOR MARIYENKO, AND YURI V. ROSTOVTSEV

Department of Physics and Institute for Quantum Studies, Texas A&M University, College Station, TX 77843-4242, USA

Recent experimental and theoretical results demonstrate that both populations and coherence in a system of nuclear spins in solids can be controlled by a laser field with high efficiency. Nearly 100% nuclear polarization can be achieved on a submicrosecond time scale. Both a high speed of the optical excitation of nuclear polarization and long storage times can be achieved simultaneously. The most promising candidates are rare-earth and possibly transition-metal impurities with a large constant of hyperfine interaction.

The purpose of this paper is to demonstrate the potential for nuclear spins in solids as a system of choice for implementation of quantum information processing and quantum computation [1].

Although the current trend in the search for a suitable material system for quantum information technologies is shifted towards single atoms in traps or in the cavity quantum electrodynamics settings, there is little doubt that solid-state based systems will ultimately win this race. This is because only solids can satisfy the demands of scalability, compactness, high density of the information carriers, and compatibility with existing micro- and nanoelectronics technology.

There have been quite a few proposals of solid state systems, most of them dealing with electron spins [2]. Most prominent and frequently mentioned candidates include spins of free carriers and excitons in semiconductors (both in bulk materials and in the nanostructures), electron spins in rare-earth ion impurities and in nitrogen vacancy centers in diamond. The reason why they are so popular is that electron spins can be easily manipulated with lasers and coupled to each other through a variety of interactions existing in solids. Spin states and spin coherence can be efficiently controlled by an optical pumping or by a bichromatic field. The possibility of such a control has been successfully demonstrated in many experiments, from the optical hole burning to electromagnetically induced transparency and slow group velocity of light.

However, the openness to environment is simultaneously a weak point. The lifetime of electron spins and especially the decoherence time are rather short. For semiconductors it is usually shorter than nanosecond, and even for relatively well isolated electron shells in the impurity ions the decoherence time is in the microsecond range.

The system that performs much better in this respect is nuclear spins in solids. They are much stronger shielded from the environment than electron spins, and their lifetime and decoherence time can reach many seconds or minutes. However, so far they received very little attention as candidates for the quantum information processing. There are two reasons for this lack of interest.

First, it is commonly believed that manipulation of nuclear spins with laser

light is very inefficient. There are no nuclear transitions in the optical range, while electronic and nuclear subsystems interact very weakly.

Second, the times needed to induce or change orientation of nuclear spins in solids are notoriously long [3]. In experiments on the optical orientation in semiconductors, optically detected NMR and NQR, the orientation times of many minutes were reported.

The above problems seem to be an inevitable consequence of a good isolation of nuclear spins from the environment. However, in our work it has been demonstrated that both obstacles can be actually overcome, and fast and efficient manipulation of nuclear spins by laser light is possible. Below we outline the general ideas behind the coherent laser control of nuclear spins and illustrate them with specific examples.

As we have already mentioned, the direct driving of nuclear transitions by optical fields seems to be impossible simply because there are no suitable transitions in the optical range. A natural idea is to drive electronic optical transitions and to use various kinds of interactions between electronic and nuclear degrees of freedom in order to affect nuclei. Optical pumping of the nuclear spin polarization have been studied extensively in semiconductors for almost twenty years, see e.g. [3] for the review. Unfortunately, the process is rather slow and inefficient since it involves creation of a nonequilibrium population of polarized electrons in the conduction band, their subsequent capture on shallow impurity centers, the transfer of electron spin polarization to the impurity nuclei, and diffusion of nuclear spin polarization in the lattice. Similar ideas for rare-earth and transition-metal impurities in crystals have been developed even earlier [4]. However, the degree of the nuclear polarization reached in these experiments was of the order of 10%, and laser exposition time was of the order of minutes.

In a recent series of papers we have demonstrated the possibility to manipulate gamma-ray Mossbauer transitions in solids and also to achieve nearly 100% nuclear polarization by means of optical laser pumping [5,6,7,8]. The idea is to employ hyperfine interaction between electrons and a nucleus. Although the coupling between electron and nuclear subsystems is rather weak in energy scale (of order 1 μeV) as compared to the energies of optical electron transitions and especially gamma-ray nuclear transitions, it can lead to a large effect on the nuclei if the electrons are driven resonantly (cf. the analogy with weakly coupled oscillators). Optical orientation of nuclear spins can lead to drastic modification of gamma-ray Mossbauer spectra. This can be seen from the simplest model of a compound electron-nucleus system that involves at least four energy levels (Fig. 1): $|1\rangle = |G, g\rangle$, $|2\rangle = |G, e\rangle$, $|3\rangle = |E, g\rangle$, $|4\rangle = |E, e\rangle$. Here $|G\rangle$ and $|E\rangle$ stand for the ground and excited states of a nucleus and accordingly $|g\rangle$ and $|e\rangle$ stand for the ground and excited states of an electron. In the absence of coupling between nuclear and electronic degrees of freedom, two pairs of transitions 1-2 and 3-4 as well as 1-3 and 2-4 are exactly degenerate (Fig. 1a) since electronic transitions are the same both for the ground and excited nuclear states. If the electron and nuclear systems are not coupled to each other, driving of electronic transitions 1-2 and 3-4 in this fully symmetric degenerate four-level system does not produce any physical effect on γ-ray nuclear transition.

The hyperfine interaction leads to the appearance of the hyperfine structure:

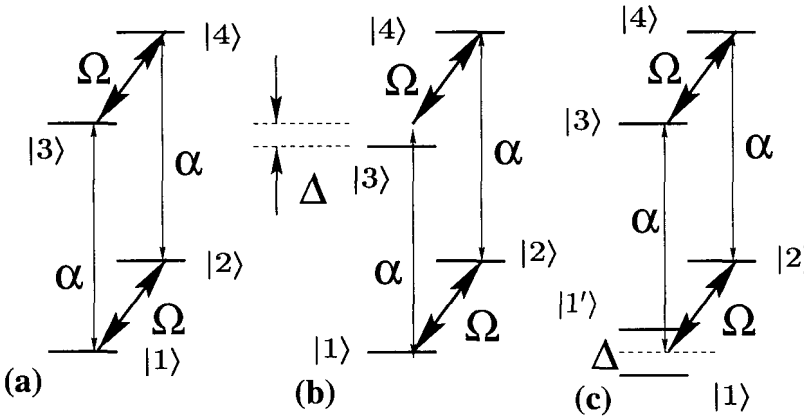

Figure 1. Four-level energy level scheme of the compound nuclear-electron system. In the case of the absence of hyperfine interaction (a), the shift (b) and the splitting (c) of an energy level due to the hyperfine interaction.

a shift and/or a splitting of the electron-nuclear levels (Fig. 1b,c). Below we concentrate on a scheme with a hyperfine splitting of the ground state. In this case, as shown in [11], a frequency-selective or polarization-selective optical driving leads to the redistribution of populations between nuclear spin sublevels. This results in the disappearance of some gamma-ray absorption lines, see Figs. 2. An even more exciting possibility is to employ not only optical pumping of populations of the spin sublevels, but also a spin coherence. This could lead to observation of quantum interference effects on the gamma-ray nuclear transitions, i.e., the effects similar to the electromagnetically induced transparency (EIT), slow group velocity of light, and even lasing without inversion that were intensively studied for the last decade on the atomic transitions [9,10]. As we have recently shown [12], EIT in gamma-rays has been observed for the first time in Mossbauer absorption experiments with $FeCO_3$ [13,14], in which, however, the coherence was created by a magnetic field.

Coming back to the nuclear orientation by means of a resonant driving of electronic transitions, the main problem with solids is that inhomogeneous (and in some cases homogeneous) linewidth typically overlaps the hyperfine structure. Therefore, polarization-selective optical pumping is an imperative. Unfortunately, polarization selection rules in solids are usually not well defined due to the fact that the crystal field of a lattice can essentially influence both the energy levels and the wave functions of the electronic states. However, well-defined polarization rules are possible for paramagnetic-ion doped dielectrics which may result in an almost 100% efficient nuclear orientation via optical pumping and hyperfine interaction [15]. This provides, on the one hand, efficient nuclear-electron entanglement and, on the other hand, transfer of the quantum electronic state to the nuclear state with 100% fidelity. The estimates for $^{231}Pa : Cs_2ZrCl_6$ show that resonant laser driving of the electric dipole-allowed optical transition with the wavelength 411 nm with remarkably low

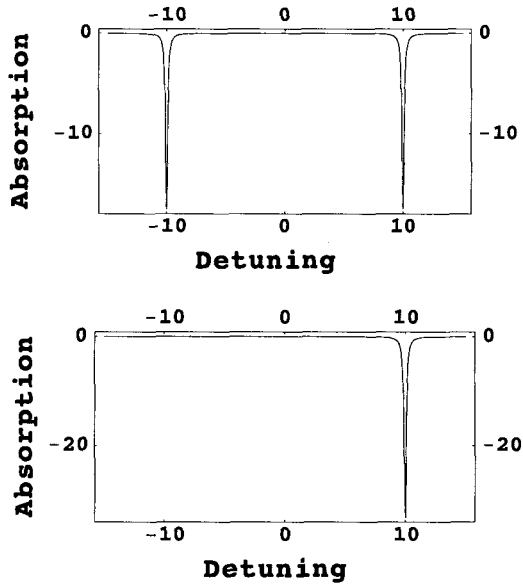

Figure 2. Vanishing of absorption at one of two Mössbauer transitions via optical pumping.

intensity of the order of 100 μW/cm^2 should lead to the depletion of some of the magnetic states up to the level of 0.1% of total population which corresponds to the suppression of resonant absorption up to the level of off-resonant losses.

An alternative to the polarization-selective optical pumping is to use spin coherence and create coherent population trapping by means of, e.g., bichromatic laser field. As was shown in our works [5,6,7], the bichromatic driving of 1-2 and 1'-2 optical transitions in a simple degenerate double-lambda scheme based on the level scheme of Fig. 1c can lead to disappearance of both 1-3 and 1-3' gamma-ray absorption lines even when both optical and gamma-ray lines overlap the hyperfine structure (Fig. 3). This gives us a unique possibility of controllable electron-nuclear entanglement for this case. The first experimental demonstration of a strong spin coherence and coherent population trapping of nuclear spins in solids has been made by Hemmer et al. [16] in Pr^{+3}-doped crystals and N-V centers in diamond. He has obtained almost 100% EIT in the optical absorption by means of a strong bichromatic driving.

Let us now discuss how *fast* we can redistribute a nuclear spin population and build up spin coherence by means of a resonant laser radiation.

To estimate the relaxation time scale of nuclear orientation via optical pumping, let us consider a simple scheme, as shown in Fig. 4. For simplicity, we choose two electron levels having electron moments J_1 and J_2 correspondingly, and nuclear spin I. To get a readable analytic result, we assume the simplest configuration in which the optical pumping is still possible, namely, $J_1 = J_2 = I = 1/2$.

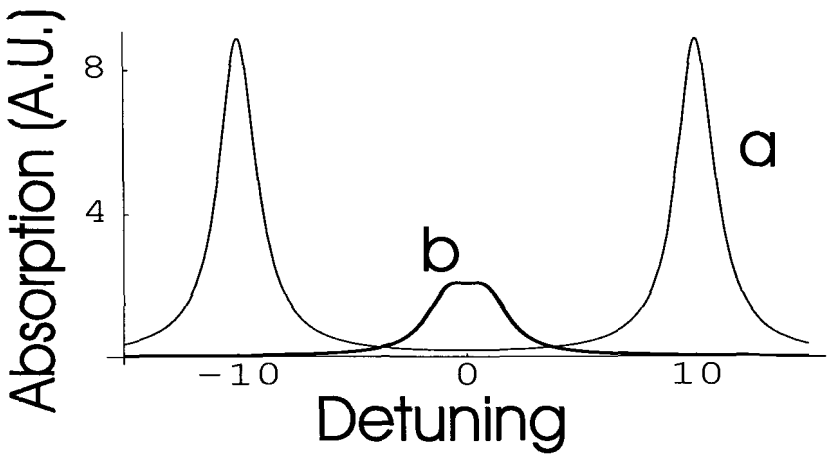

Figure 3. Modification of the Mössbauer absorption spectra for the scheme involving level splitting with increase of the intensity of the driving field: a) $\Omega = 0$; b) $\Omega = 100\gamma_0$.

We choose the direct product of electron and nuclear wavefunctions to be the basis for electron-nuclear states:

$$|J_1, m_1, I, m\rangle = |J_1, m_1\rangle \otimes |I, m\rangle. \tag{1}$$

Then, Hamiltonian can be written as follows:

$$\hat{H} = \hat{H}_0 + \hat{H}_{hf} + \hat{V} + \hat{H}_{bath}. \tag{2}$$

The H_0 is the diagonal part that is related to the energy of electronic and nuclear states without hyperfine interaction between them,

$$\hat{H}_0 = \sum_{J_1 m_1 m} \epsilon_{m_1 m_2 m} |J_1, m_1, I, m\rangle\langle J_1, m_1, I, m|. \tag{3}$$

The interaction part of the Hamiltonian includes the hyperfine coupling between electronic and nuclear subsystems,

$$\hat{H}_{hf} = \hbar\Delta \left(\hat{I}_z \hat{J}_z + \frac{\hat{I}_+ \hat{J}_- + \hat{I}_- \hat{J}_+}{2} \right), \tag{4}$$

where Δ is the constant of hyperfine interaction, and also a part with the external electromagnetic fields,

$$\hat{V} = \hbar \sum_{m_1 m_2 m} \Omega_{m_1 m_2} |J_1, m_1, I, m\rangle\langle J_2, m_2, I, m| + c.c., \tag{5}$$

where $\Omega_{m_1 m_2} = \mu_{m_1 m_2} E_l / \hbar$ is the Rabi frequency for transition $J_1 m_1 \leftrightarrow J_2 m_2$, $\mu_{m_1 m_2}$ is the dipole moment of the transition, E_l is the laser field applied to the

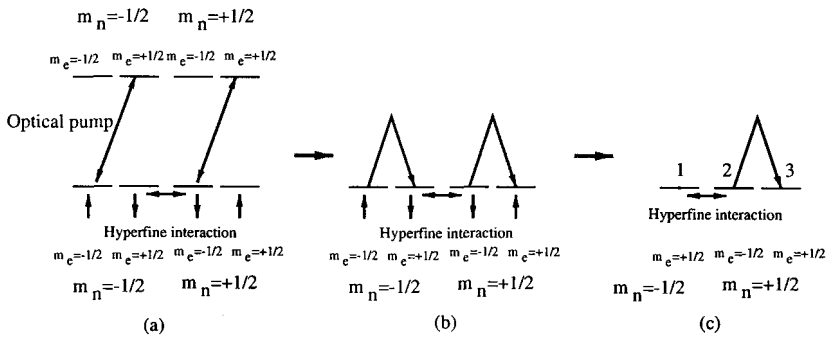

Figure 4. A simple model to demonstrate nuclear orientation via optical pumping. (a) All electronic nuclear levels. (b,c) Simplified systems.

system. To describe different relaxation processes, we take into account coupling with radiation modes and surrounding electrons and nuclei,

$$\hat{H}_{bath} = \hat{V}_s + \hat{V}_e + \hat{V}_n, \tag{6}$$

where

$$\hat{V}_s = \hbar \sum_{m_1 m_2 m} g_k \hat{b}_{m_1 m_2} |J_1, m_1, I, m\rangle\langle J_2, m_2, I, m| + c.c. \tag{7}$$

is the part of Hamiltonian that is responsible for spontaneous relaxation from the electron excited state;

$$\hat{V}_e = \hbar \sum_{m_1 m_2 m} g_e \hat{b}_{m_1 m_2} |J_1, m_1, I, m\rangle\langle J_1, m_2, I, m| + c.c. \tag{8}$$

and

$$\hat{V}_n = \hbar \sum_{m_1 m_2 m} g_n \hat{b}_{m' m} |J_1, m_1, I, m'\rangle\langle J_1, m_1, I, m| + c.c. \tag{9}$$

are the parts of Hamiltonian that are responsible for electronic and nuclear relaxation, respectively. As is easily seen the state basis allows us to consider the relaxation of nuclei independently from the electron relaxation.

Thus, as is seen in Fig. 4a, the optical pump driving the electron transition causes the polarization of the electrons via optical relaxation to the states that are not coupled with the laser field. Consider the most common situation when the relaxation rate on the optical transition, γ_0, is much larger than the electronic and nuclear spin relaxation rates between the components of hyperfine structure, γ_e and γ_n. In this case we can treat an optical drive as a one-directional pump with effective rate γ_0 as shown in Fig. 4b.

Furthermore, the state $|1/2, 1/2\rangle$ is practically empty because of $\gamma_0 \gg \gamma_e, \gamma_n$. Therefore, the simplified system shown in Fig. 4c can be analyzed. Under such conditions, the set of density matrix equations has a form

$$\dot{n}_1 = -\gamma_n n_1 + i\Delta(\sigma_{12} - \sigma_{21}) + \gamma_n n_3 \tag{10}$$

$$\dot{n}_2 = i\Delta(\sigma_{21} - \sigma_{12}) - (\gamma_0 + \gamma)n_2 + \gamma n_3 \tag{11}$$

$$\dot{n}_3 = \gamma_n n_1 + (\gamma_0 + \gamma)n_2 - (\gamma + \gamma_n)n_3 \tag{12}$$

$$\dot{\sigma}_{12} = -\Gamma_{12}\sigma_{12} + i(n_1 - n_2)\Delta \tag{13}$$

where n_1, n_2, n_3 are the diagonal elements of the density matrix corresponding to the populations of corresponding levels $|1\rangle$, $|2\rangle$, and $|3\rangle$; σ_{12} is the nondiagonal element of the density matrix corresponding to the coherence between the levels $|1\rangle$ and $|2\rangle$; $\Gamma_{12} = \gamma_0/2 + \gamma + \gamma_n$, and $\sigma_{21} = (\sigma_{12})^*$. The relaxation rates of such a system can be then found by solving the characteristic equation corresponding to the above set of equations. The resulting set of relaxation constants can be written as follows:

$$\gamma_1 = -2\gamma - \gamma_0 - 2\gamma_n, \tag{14}$$

$$\gamma_2 = -\gamma - \frac{\gamma_0}{2} - 2\gamma_n, \tag{15}$$

$$\gamma_{3,4} = -\gamma - \frac{\gamma_0}{2} - \gamma_n \pm \frac{1}{2}\sqrt{(2\gamma + \gamma_0 - 2\gamma_n)^2 - 16\Delta^2}. \tag{16}$$

When the hyperfine interaction is relatively weak, $2\gamma + \gamma_0 - 2\gamma_n \gg 4\Delta$, the slowest rate corresponding to the relaxation rate of the nuclear polarization is given by

$$\gamma_p = -2\gamma_n - \frac{4\Delta^2}{\gamma_0}. \tag{17}$$

In the opposite case of a strong hyperfine interaction, $2\gamma + \gamma_0 - 2\gamma_n \ll 4\Delta$, all relaxation rates are of the order of γ_0, and the hyperfine interaction results in the resolved splitting of levels.

Using these general expressions, let us estimate the relaxation times for the material systems that are of main interest for us.

It is immediately seen that the situation in popular semiconductors of III-V group is very unfavorable for a fast nuclear orientation. Indeed, for the optically excited electrons in the conduction band the optical relaxation rate is very high, $\gamma_0 \sim 10^{10} - 10^{12}$ s^{-1}, while the constant of hyperfine interaction is relatively small (actually, it is dependent on the electron density and probability of electron localization on the donor centers; see, e.g., the review by Dyakonov and Perel in [3]). The resulting nuclear spin relaxation rate, according to Eq. (17) and [3], is many minutes for free electrons and about 0.1-1 s for the electrons localized at donor centers.

For the rare-earth impurities in crystals, the situation depends on whether we use a dipole-allowed or forbidden transition for the optical pumping. Let us consider two specific examples. $Pr^{3+} : Y_2SiO_5$ has a dipole-forbidden optical transition, and the relaxation rates are $\gamma_0 = 10^4$ s^{-1}, $\gamma_n = 10^{-3}$ s^{-1}, and $\gamma_e = 10^3$ s^{-1}. The intensity of hyperfine interaction is about 10 MHz, so we can conclude that the nuclear polarization can be built up on the time scale of the order of $\gamma_0^{-1} = 0.1$ ms. $Eu^{2+} : CaS$, CaF_2 has a dipole-allowed optical transition, and the relevant relaxation rates are $\gamma_0 = 10^7$ s^{-1} and $\gamma_e = 10^3$ s^{-1}. The intensity of hyperfine

interaction is not known exactly; it is somewhere between 100 MHz and 1 GHz. Since $\Delta \gtrsim \gamma_0$, the nuclear polarization can be obtained on the time scale of the order of $\gamma_0^{-1} = 100$ ns.

In conclusion, recent experimental and theoretical results demonstrate that both populations and coherence in a system of nuclear spins in solids can be controlled by a laser field with high efficiency. Nearly 100% nuclear polarization can be achieved on a submicrosecond time scale. It is crucial for various quantum information applications that we can achieve both a high speed of the optical excitation of nuclear polarization and long storage times simultaneously, in the same material system. The most promising candidates are rare-earth and possibly transition-metal impurities with a large constant of hyperfine interaction. It is quite possible, however, that there are other candidates with a large ratio of Δ^2/γ_0, according to Eq. (17).

The authors are grateful to Rufus Cone, Zameer Hasan, Philip Hemmer, Roman Kolesov, and Suhail Zubairy for valuable discussions. This work was supported by the AFOSR, the DARPA, the Office of Naval Research, the Texas Advanced Technology and Research Programs.

References

1. M. Brooks, Quantum computing and communications, (London ; New York : Springer, 1999).
2. H. Ohno, Science 281, 951 (1998); A. Imamoglu, D.D. Awaschalow, G. Burkard, et al., Phys. Rev. Lett. 81, 4204 (1999); F.T. Chatnock, T.A. Kennedy, Phys. Rev. Lett. 64, 041201 (2001).
3. F. Meier, P.B. Zakharchenya, Optical Orientation, (North-Holland Physics Publishing, North-Holland, 1984).
4. L.F. Mollenau, W.B. Grant, C.D. Jeffries, Phys. Rev. Lett. 20, 488 (1968); G. Lampel, Phys. Rev. Lett. 20, 491 (1968); W.B. Grant, L.F. Mollenau, C.D. Jeffries, Phys. Rev. B 4, 1428 (1971).
5. R. Kolesov, Yu. Rostovtsev, O. Kocharovskaya, Opt. Commun. **179**, 537 (2000).
6. O. Kocharovskaya, Proceedings of International Symposium on Atomic Coherence and Inversionless Optical Amplification, Eds. J.Y. Gao, S.Y. Zhu, Changchun, China, 1995.
7. O. Kocharovskaya, R. Kolesov, Yu. Rostovtsev, Phys. Rev. Lett. **82**, 3593 (1999).
8. O. Kocharovskaya, R. Kolesov, Y. Rostovtsev, Lasing without inversion: a new path to gamma-ray laser, Laser Physics 9, 745 (1999).
9. O. Kocharovskaya and Ya.I. Khanin, Pis'ma Zn. Eksp. Teor. Fiz. **48**, 581 (1988), (Sov. Phys. JETP Lett. **48**, 630 (1988)); S.E. Harris, Phys. Rev. Lett. **62**, 1033 (1989); M.O. Scully, S.Y. Zhu, and A. Gavrieliedes, Phys. Rev. Lett. **62**, 2813 (1989).
10. For reviews of atomic coherence effects see: O. Kocharovskaya, Phys. Rep. **219**, 175 (1992); M.O. Scully, Phys. Rep. **219**, 191 (1992); E. Arimondo in *Progress in Optics XXXV*, ed. by E. Wolf (Elsevier, Amsterdam, 1996), p.257;

S.E. Harris, Phys. Today **50(7)**, 36 (1997); a special issue of Laser Physics **9**, n.4 (1999), Eds. O. Kocharovskaya, P. Mandel, M. Scully; M.O. Scully and M.S. Zubairy, *"Quantum Optics"*, (Cambrige University Press 1997).
11. C.D. Jeffries, Phys. Rev. Lett. 19, 1221 (1967); L.F. Mollenau, W.B. Grant, C.D. Jeffries, Phys. Rev. Lett. 19, 1221 (1967); R. Kolesov, E. Kuznetsova, Phys. Rev. B 63, 184107 (2001).
12. R. Coussement, Y. Rostovtsev, J. Odeurs, G. Neyens, P. Mandel, G. Kozyreff, R. Shakhmuratov, O. Kocharovskaya, Controlling absorption of gamma radiation via nuclear level-crossing, submitted to Phys. Rev. Lett. (2001).
13. R. Coussement, G. Neyens, M. Van Den Bergh and P. Boolchand, Laser Physics **5**, 292 (1995).
14. R. Coussement, G. Neyens, Hyperfine Interact. **107**, 307 (1997).
15. Y. Rostovtsev, A. Belyanin, O. Kocharovskaya, under preparation.
16. M.K. Kim MK, B.S. Ham BS, P.R. Hemmer PR, M.S. Shahriar, J. Mod. Opt. 47, 1713 (2000).

DISCUSSION

Chairman: I. Cirac

L. Accardi: On your last transparency, you had explicit form of interaction Hamiltonian. Can you very quickly comment on various pieces?

O. Kocharovskaya: It involves quadrupole interaction and it produces this splitting, and it involves the interaction with the component which is parallel to the direction of the gradient of electric field and to the direction of propagation of our photons in our experiment, and component of magnetic field which is orthogonal to this, and interaction with (0,0,1), basically.

L. Accardi: Axis Y, what is it in your case, electromagnetic field or not?

O. Kocharovskaya: Electromagnetic field.

L. Accardi: So, how is it related to the bi-parallel and bi-orthogonal thing?

O. Kocharovskaya: What is important for us here is that the component of magnetic field which is orthogonal to the gradient of the electric field produces the coupling between these two anti-crossing levels so, in fact you see, we increase magnetic field and at some point we have this coupling, and everybody was using this level-crossing technique to restore this hyperfine splitting. So we know at which magnetic field it occurs, we know this dependence, we can restore this splitting, but how did they detect it? They detected it by the change of polarization. So this is a typical Mössbauer experiment: we have source, which moves, and it breaks our absorber. So under specific magnetic field, there is a change of polarization, and what one would expect is that if we look for the intensity of the absorbed radiation then we should simply add the intensities from this and from these transitions. They should be added together because we have a crossing of two levels at some point. But it turns out actually that this is not the case. This is what one would have by simply adding these intensities (this point) but it turns out that it is essentially smaller. And why it comes to be smaller? It's because of interference

phenomena which originate from the coupling between these two anticrossing levels via the orthogonal component of the magnetic field. And so, we did the theoretical fit which seems to be very good for this experiment. So we believe it's the first observation of electromagnetically induced transparency in gamma rays.

TROJAN HORSE ATTACKING STRATEGY ON QUANTUM CRYPTOGRAPHY

GUIHUA ZENG *

Modern information processing laboratory (MIPL), Department of Electronic Engineering, Shanghai Jiaotong University, Shanghai 200030, China
Theoretische Quantendynamik, Fakultät für Physik, Universität Freiburg, H.-Herder-Strasse 3, D-79104 Freiburg, Germany

Trojan horse attacking strategy on quantum cryptography is investigated, three aspects are involved. First, the mechanism for the Trojan horse attacking strategy on quantum cryptography as well as classic cryptography is studied. Then the fragility of the quantum cryptographic algorithm employing EPR pairs as key against the Trojan horse attacking strategy is analyzed. To prevent the Trojan horse attacking strategy, an improvement scheme which makes use of non-orthogonal entangled states is proposed, results show the improvement scheme is robust to the Trojan horse attacking strategy without reducing the security on other kinds of attacking strategies.

1 Introduction

In private communication and data security attackers (e.g., adversary and/or ragger) will try to break the employed confidential system for their benefits. To prevent effectively the attacks from obtaining the legitimate information, cryptography has arisen and is employed to prevent the attacks. Cryptography is a subject which is employed for rendering the message secret and creating a cipher by making use of algorithms and protocols so that the attackers can not or can not easily acquire the private information. It plays a very important role in the modern information protection. However, as virtue rises one foot, vice rises ten feet. To break the algorithms and protocols provided in the cryptography, a concomitant subject called cryptoanalysis has also arisen [1].

The so called cryptoanalysis is a science and study of methods of breaking ciphers. Many attacking strategies for converting encrypted messages into plaintext without initial knowledge of the key employed in the encryption have been investigated and used in practice. But, any successes of these strategies completely depend on the drawbacks of the cryptographic system, i.e., cryptosystem. These drawbacks arose from two major causes, i.e., the inappropriate fundamentals, which are employed as a foundation for the scheme, and the imperfection of the cryptosystem's construction. Actually, any improper design will create drawbacks in the cryptosystem and subsequently the attacker can break in principle the scheme by means of these drawbacks. Of course, an absolutely perfect cryptosystem is not possible and not necessary in practice, since such kind of system leads to a huge cost.

Trojan horse attacking strategy (THAS) arose from the drawbacks of construction of the system (e.g., device, computer program, algorithm or protocol *et al.*). When a Trojan horse can be hidden without easy detection in a system, an attacker can make use of this kind of strategy to break the system and then obtain useful

*E-MAIL: GUIHUAZENG@HOTMAIL.COM

information. Unfortunately, this strategy is not only available in classic cryptography but also in the recently proposed quantum cryptography [2,3,4,5,6,8,7,9]. This strategy on the quantum key distribution has been analyzed in [10,6,11], and a scheme for preventing this strategy was proposed in [11].

In this paper we consider the THAS on the quantum cryptographic algorithm, which employs EPR pairs as the symmetrical key. Three aspects will be investigated in this work, including the mechanism, the attacking way on the quantum cryptographic algorithm, and the preventing approach for this attacking strategy. Especially the improvement scheme will be investigated in detail.

This paper is arranged as follows. In Sec. 2, the mechanism for the THAS will be analyzed first. Then in Sec. 3 we will investigate the THAS on the quantum cryptographic algorithm which employs EPR pairs as the key. An improvement scheme for preventing the THAS will be presented in Sec. 4. After these a simple remark will be presented in Sec. 5. Finally a conclusion will be drawn in Sec. 6.

2 Mechanism for Trojan horse attacking strategy

Let us firstly investigate the mechanism for the THAS on cryptography in this section. In essential, all attacking approaches proposed in cryptoanalysis (including classic cryptoanalysis and quantum cryptoanalysis) can be categorized mainly as three kinds of attacking strategies, i.e., the strategy based on fundamentals drawbacks (SFD), the strategy based on obtained information (SOI), and the strategy based on assistant systems (SAS). In the SFD the attacker makes use of fundamentals drawbacks to break the cipher and obtain useful information. As an example, the classic cryptosystem is based on the complexity assumption which has not been proven, thus usually containing a fundamentals drawback. With the development of the mathematics these drawbacks become a means for breaking the cryptosystem [1]. Another example is the attacking approaches presented in quantum cryptography, by far most attacking strategies such as the individual and collective attacks [8] are based on the fundamentals, i.e., quantum laws. Fortunately all proofs are advantaged to the quantum cryptography but not to the cryptoanalysis. While in the SOI the attacker makes use of the leaked information of the cryptosystem, the ciphertext, and/or the obtained parts of plaintext to break the cryptosystem [1]. However, we would like to stress here the SAS, which relies on assistant systems to break the cryptosystem. One of the typical approaches in this situation is the THAS.

To study the mechanism for THAS let us firstly consider what is the Trojan horse in the information protection, since the Trojan horse is the important base in the THAS. In data security the Trojan horse is defined as a small program inserted by an attacker in a computer system. It performs functions not described in the program specifications, taking advantage of rights belonging to the calling environment to copy, misuse or destroy data not relevant to its stated purpose. For example, a Trojan horse in a text editor might copy confidential information in a file being edited to a file accessible to another. More generally, the so-called Trojan horse is a 'robot horse' which can become a part of the legitimate users' systems. Then the 'robot horse' can be surreptitiously exploited by the legitimate authorizations of operation (e.g., measurement,detection *et al.*) to the detriment of

security. For example, break the system via feeding back information to the attacker (e.g., the dishonest manufacturer or even the adversary) or directly destroying the legitimate data. To the legitimate users' system the Trojan horse is actually an additional system with passive effects. Many things, such as devices and small programs inserted in the users' system, probing signals entering the users' system through a public channel *et al*, or even the attacker, can become a Trojan horse. However, we must emphasize that it is impossible for any Trojan horse to play the same role as legitimate users because the Trojan horse is only a small part of the legitimate system.

There are mainly two kinds of Trojan horses, i.e., the pre-lurked Trojan horse and the online Trojan horse. The pre-lurked Trojan horse is a 'robot horse' which is pre-inserted in the legitimate users's system, e.g., programs, apparatuses or even offices. At an appropriate condition the lurked Trojan horse is activated automatically by the legitimate system, and then it feeds back the available information to the attackers, even destroying the users' system. The online Trojan horse is actually a probing signal which may enter the legitimate system without awareness and then back-reflect to the attacker. Both kinds of Trojan horses may be classic as well as quantum. In addition, the Trojan horse may also be a combination of the 'quantum horse' and 'classic horse'.

If a Trojan horse can be inserted successfully in the users' system, the attacker can break the employed cryptosystem and obtain available information by means of the feedback information of the 'robot horse'. This attacking strategy is called THAS. Corresponding to the kinds of the Trojan horses there are two kinds of THASs, i.e., the strategy relying on a pre-lurked Trojan horse and the strategy depending on the probing signal. While the attacking ways may be classic approaches or quantum approaches determined by the features of the employed Trojan horses. For example, if employing a pointer state of the legitimate system as the Trojan horse, or a pre-inserted tiny device as a Trojan hose, which is exploited to detect the quantum state of the qubits as the key, the attacker can obtain useful messages by analyzing the feedback information of the Trojan horses. If sending light pulses (probing signal) into the fiber entering legitimate users's apparatuses, then the attacker can analyze the backreflected light [10]. Of course, without the Trojan horse this strategy can do nothing since the feedback information of the Trojan horse is very important in this attacking strategy. Obviously this strategy is completely different from the strategies which are always involved in the quantum cryptography, e.g., the intercept/resend attack and the entanglement attack [3,5,8,7], where the attacker can directly obtain the information for attacking.

3 Trojan horse attacking strategy on quantum cryptographic algorithm

In this section we consider the THAS on the quantum cryptographic algorithm which employs EPR pairs as the key. Recently, two interesting quantum vernam algorithms based on EPR pairs have been proposed. These algorithms employ EPR pair(s) as the symmetrical keys of the algorithm. In [12] the message is encrypted by means of a quantum controlled-NOT with employment of a symmetrical key which

consisted of one EPR pair and one bilateral rotation. In [13] the message is encrypted with a key which consisted of two EPR pairs. A common feature of the above quantum vernam algorithms is that EPR pairs are applied as a sharing key between the two legitimate users called Alice and Bob. These algorithms are provably secure for the SFD and the SOI. However, they can not circumvent the THAS. In the following we investigate the fragility of these algorithms against the THAS which employs pre-lurked Trojan horse (in this section and the following section we suppose the Trojan horse is a tiny device pre-inserted in Alice's or Bob's apparatus).

To show the fragility of the quantum cryptographic algorithm employing EPR pair(s) as the key against the THAS, we first give a simple description for this kind of algorithm. In general, this kind of algorithm can be summarized generally as follows. Suppose Alice and Bob sharing n EPR pairs as the key $\mathcal{K} = \{|k_1\rangle, |k_2\rangle, \cdots, |k_n\rangle\}$. Each EPR pair can be expressed as,

$$|\Phi_i^+\rangle = \frac{1}{\sqrt{2}}\left(|0_a^i 0_b^i\rangle + |1_a^i 1_b^i\rangle\right) = |k_i\rangle, \tag{1}$$

where subscripts a, b denote Alice's particles $\mathcal{P}_a$ and Bob's $\mathcal{P}_b$ of each EPR pair, $|k_i\rangle$ denotes the i^{th} key element, and $i = 1, 2, \cdots, n$. Denote the plaintext (message) by

$$|\psi^m\rangle = \alpha|0\rangle + \beta|1\rangle, \tag{2}$$

the corresponding particle is expressed as $\mathcal{P}_m$, where $|\alpha|^2 + |\beta|^2 = 1$. Suppose Alice is the sender, then Alice encrypts the qubit $|\psi^m\rangle$ by making use of the quantum controlled-NOT operations on both her EPR particle $\mathcal{P}_a$ (key particle) and the message particle $\mathcal{P}_m$. After that, Alice obtains the ciphertext $|\Psi^c\rangle$, which can be denoted as,

$$|\Psi^c\rangle = C_{mk}^n|k_n\rangle\{C_{mk}^{n-1}|k_{n-1}\rangle\{\cdots\{C_{mk}^1|k_1\rangle|\psi^m\rangle\}\}\}, \tag{3}$$

where C_{mk}^i denotes the i^{th} quantum controlled-NOT gate on $\mathcal{P}_m$ and $\mathcal{P}_a$, the subscript mk denotes the quantum gate operating on the key particle and the message particle. Then Alice sends the ciphertext to Bob via a quantum channel. After receiving the ciphertext $|\Psi^c\rangle$ Bob decrypts the ciphertext by making use of an inverse process controlled under the key. Finally Bob gets the message.

Now let us investigate THAS on the above quantum algorithm. First, we consider the situation of using only one EPR pair as the key. In this case, the key is just the EPR pair, i.e, $|K\rangle = |\Phi^+\rangle$, which can be denoted as,

$$|\Phi^+\rangle = \frac{1}{\sqrt{2}}\left(|0_a 0_b\rangle + |1_a 1_b\rangle\right). \tag{4}$$

Then ciphertext can be expressed as,

$$\begin{aligned} |\Psi^c\rangle &= C_{ma}|\Phi^+\rangle|\psi^m\rangle \\ &= |0_a 0_b\rangle \otimes |\psi^m\rangle + |1_a 1_b\rangle \otimes X_m|\psi^m\rangle. \end{aligned} \tag{5}$$

where X_m denotes the quantum X-gate on the particle $\mathcal{P}_m$. Eq. (5) illustrates that when Alice's and Bob's EPR particles are in the states $|0_a 0_b\rangle$ then the message particle is in the state $|\psi^m\rangle$, otherwise, the state of the message particle is in $X_m|\psi^m\rangle$.

Obviously, if Alice's and Bob's EPR particles can not be disturbed by the attacker, the above algorithm is secure. However, if the attacker can pre-lurk a Trojan horse in Alice's or Bob's apparatus, the legitimate communicators Alice and Bob will not be lucky since the attacker can obtain their useful information through the THAS. This can be done very easily. Suppose the attacker puts successfully a Trojan hose, Υ, e.g., a set of tiny devices which can distinguish the eigenstates states $|0\rangle$and $|1\rangle$(for example a device can recognize the 'bright' and 'dark' pulse) and send feedback information, in Alice's apparatus (this is available since in practice the users are not experts so that they can not easily find the 'robot horse' which is pre-lurked ulteriorly by the dishonest manufacturers), then the key can be written as $|\Phi^+(\Upsilon)\rangle$. Subsequently Alice's encrypting transformation by making use of controlled-NOT yields a ciphertext state, which can be written as,

$$|\Psi_h^c\rangle = |0_a(h_{\shortparallel})0_b\rangle \otimes |\psi^m\rangle + |1_a(h_{\perp})1_b\rangle \otimes X_m|\psi^m\rangle, \tag{6}$$

where $h_{\shortparallel}$ and $h_{\perp}$ are the feedback information of the Trojan horse. After Alice has encrypted her message $|\psi^m\rangle$ using the EPR pair, the Trojan horse is activated automatically. For example, if the attacker pre-lurks measurement bases for the eigenstates states $|0\rangle$ and $|1\rangle$, the Trojan horse only needs to measure Alice's EPR particle. Now the 'horse' feeds back the result $h_{\shortparallel}$ when the measurement result is $|0\rangle$, otherwise the 'horse' feeds back the result $h_{\perp}$. Then, what the attacker needs to do is to wait for Alice's ciphertext $|\Psi^c\rangle$ and the feedback information of the Trojan horse. If the attacker can successfully intercept the ciphertext particle $\mathcal{P}_m$ which is sent to Bob, then the attacker can obtain completely the qubit $|\psi_m\rangle$ by making use of the feedback information $h_{\shortparallel}$ and $h_{\perp}$, and the intercepted particle $\mathcal{P}_m$. For example, if the feedback information shows that Bob's key bit is $|0\rangle$, attacker gets $|\psi^m\rangle$. If the feedback information shows that Bob's key bit is $|1\rangle$, attacker gets $X_m|\psi^m\rangle$. With this knowledge, the attacker can completely obtain the plaintext (message).

In the above we have analyzed the Trojan horse attacking strategy for the situation which makes use of only one EPR pair as a key. For the case of making use of two EPR pairs $|\Phi_1^+\rangle$ and $|\Phi_2^+\rangle$ as the key (see Ref. [13]), the Trojan horse attacking strategy can also be successful. In this case the key can be denoted as,

$$|k_1\rangle = |\Phi_1^+\rangle = \frac{1}{\sqrt{2}}\left(|0_a^1 0_b^1\rangle + |1_a^1 1_b^1\rangle\right), \tag{7}$$

and

$$|k_2\rangle = |\Phi_2^+\rangle = \frac{1}{\sqrt{2}}\left(|0_a^2 0_b^2\rangle + |1_a^2 1_b^2\rangle\right). \tag{8}$$

Suppose the attacker pre-lurks successfully two 'horse' Υ_1 and Υ_2 into Alice's or Bob's devices using the similar ways described above. After Alice's encryption using controlled-X and controlled-Z gates on the key particle and message particle, the ciphertext state can be written as,

$$\begin{aligned}
|\Psi_h^c\rangle &= C_{a_2 m}^Z\{(C_{a_1 m}^X(|\Phi_1^+(\Upsilon_1)\rangle|\psi^m\rangle))|\Phi_2^+(\Upsilon_2)\rangle\} \\
&= \frac{1}{2}|0_a^1 0_b^1(h_{\shortparallel}^1)\rangle\left\{|0_a^2 0_b^2(h_{\shortparallel}^2)\rangle \otimes |\psi^m\rangle + |1_a^2 1_b^2(h_{\perp}^2)\rangle \otimes Z_m|\psi^m\rangle\right\} \\
&+ \frac{1}{2}|1_a^1 1_b^1(h_{\shortparallel}^1)\rangle\left\{|0_a^2 0_b^2(h_{\shortparallel}^2)\rangle \otimes X_m|\psi^m\rangle + |1_a^2 1_b^2(h_{\perp}^2)\rangle \otimes X_m Z_m|\psi^m\rangle\right\}
\end{aligned} \tag{9}$$

where the superscripts '1' and '2' refer to the particles in the pairs $|\Phi_1^+\rangle$ and $|\Phi_2^+\rangle$, $h_{\shortparallel}^1$ and $h_{\perp}^1$ are feedback information of the Trojan horse Υ_1, $h_{\shortparallel}^2$ and $h_{\perp}^2$ are feedback information of the Trojan horse Υ_2. Υ_1 and Υ_2 are associated with Bob's particles. It is clear that the attacker can get the message by the similar way of employing one EPR pair as the key. Therefore, the quantum cryptographic algorithms based on the EPR pairs as keys are fragile against the THAS, although they are provably secure against the other attacking strategies.

Actually, if the possible states of Alice's key particles $\mathcal{P}_a$ (or Bob's key particle $\mathcal{P}_b$) are orthogonal states, any quantum cryptographic algorithm which employs directly such kind of key is not robust to the THAS. Because in such a situation the successful Trojan horse can recognize the possible states of the key particle. For example, while Alice and Bob employ the EPR pair as the key then Alice's or Bob's key particle takes the state $|0\rangle$or $|1\rangle$. Then a proper Trojan horse, e.g., a device which can distinguish the eigenstates $|0\rangle$ and $|1\rangle$, can recognize exactly the state of the key particle as described above. Thus the available feedback information can be obtained by the attacker. Therefore, to prevent the THAS one should use the non-orthogonal states as a sharing key in the symmetrical quantum cryptographic algorithm.

4 Prevent Trojan horse attacking strategy

In this section we will show that the above THAS can be prevented by making use of the non-orthogonal entanglement state as the key. The process is as follows. The legitimate users Alice and Bob create a set of EPR pairs, each pair can be denoted as

$$\begin{aligned} |\Phi^+\rangle &= \frac{1}{\sqrt{2}}(|0_a 0_b\rangle + |1_a 1_b\rangle) \\ &= \frac{1}{\sqrt{2}}(|+_a +_b\rangle + |-_a -_b\rangle), \end{aligned} \tag{10}$$

where $|\pm\rangle = \frac{1}{\sqrt{2}}(|0\rangle + |1\rangle)$. Then Alice or Bob randomly choose a operator from $\{\mathcal{I}, H\}$ to apply on her (his) EPR particles until all EPR pairs have been operated, where $\mathcal{I}$ and H are respectively the unit operation and the Hadamard gate. This operation yields,

$$|\psi_1\rangle = \mathcal{I}|\Phi^+\rangle = |\Phi^+\rangle, \tag{11}$$

and

$$|\psi_2\rangle = \mathcal{H}|\Phi^+\rangle. \tag{12}$$

In bases $|0\rangle, |1\rangle$ and $|+\rangle, |-\rangle$, $|\psi_2\rangle$ can be expressed as,

$$\begin{aligned} |\psi_2\rangle &= \frac{1}{\sqrt{2}}(|1_a +_b\rangle + |0_a -_b\rangle) \\ &= \frac{1}{\sqrt{2}}(|+_a 1_b\rangle + |-_a 0_b\rangle). \end{aligned} \tag{13}$$

After these operations, Alice and Bob obtain a random sequence which consists of $\{|\psi_1\rangle, |\psi_2\rangle\}$. Finally Alice and Bob take this sequence as the key. Since $|\langle\psi_1|\psi_2\rangle|^2 \neq$

0 which means that the states $|\psi_1\rangle$ and $|\psi_2\rangle$ are non-orthogonal, any quantum attacking strategies can not be available [14]. This point is guaranteed by the no-cloning theorem [15]. In the following we will show these properties can also be employed to prevent the Trojan horse attacking strategy.

To the attacker the key $|K\rangle$ is a superposition of $|\psi_1\rangle$ and $|\psi_2\rangle$, i.e.,

$$|K\rangle = c_1|\psi_1\rangle + c_2|\psi_2\rangle. \tag{14}$$

Then the ciphertext state can be written as,

$$\begin{aligned} |\Psi_e^c\rangle &= C_{am}|K\rangle|\psi^m\rangle \\ &= \left(\tilde{\alpha}_k^c|0_a 0_b\rangle + \tilde{\beta}_k^c|0_a -_b\rangle\right) \otimes |\psi^m\rangle \\ &+ \left(\tilde{\alpha}_k^c|1_a 1_b\rangle + \tilde{\beta}_k^c|1_a +_b\rangle\right) \otimes X_m|\psi^m\rangle, \end{aligned} \tag{15}$$

where $\tilde{\alpha}_k^c = c_1/\sqrt{2}$, $\tilde{\beta}_k^c = c_2/\sqrt{2}$. After the encrypting transformation, Alice obtains the ciphertext, i.e., Eq. (15). Then Alice sends the particle $\mathcal{P}_m$ to Bob,

Now let us show how to prevent the Trojan horse attacking strategy. Suppose the attacker lurks successfully a 'horse', Υ, in Bob's apparatus, then the ciphertext state takes,

$$\begin{aligned} |\Psi^c(\Upsilon)\rangle &= C_{am}\left(\alpha^c|\Psi^+(\Upsilon)\rangle + \beta^{c'}|\psi^+(\Upsilon)\rangle\right)|\psi^m\rangle \\ &= \left(\tilde{\alpha}_k^c|0_a 0_b(h_{\shortparallel})\rangle + \tilde{\beta}_k^c|0_a -_b(h_?)\rangle\right) \otimes |\psi^m\rangle \\ &+ \left(\tilde{\alpha}_k^c|1_a 1_b(h_\perp)\rangle + \tilde{\beta}_k^c|1_a +_b(h'_?)\rangle\right) \otimes X_m|\psi^m\rangle, \end{aligned} \tag{16}$$

where $h_?$ and $h'_?$ denote the inconclusive feedback information. Although the key is a superposition state (see Eq. (14)), in each encrypting operation Alice and Bob only choose one state from $\{|\psi_1\rangle, |\psi_2\rangle\}$ as the key element. Accordingly, if the attacker pre-lurks one Trojan horse, e.g., Υ_1 (for $\{|0\rangle, |1\rangle\}$), in Bob's apparatus, then another states, i.e., $\{|+\rangle, |-\rangle\}$ can not be recognized exactly. If the attacker employs two Trojan horses, e.g., 'robot horse' Υ_1 and 'robot horse' Υ_2 (for $\{|+\rangle, |-\rangle\}$), the attacker can find it impossible to get the useful feedback information. Because Alice and Bob's choices for the key are completely random, this makes it impossibile for the Trojan horses Υ_1 and Υ_2 to follow completely the changes of the key elements. In other terms, because there are two pairs random bases, i.e., $\{|0\rangle, |1\rangle\}$ and $\{|+\rangle, |-\rangle\}$ in Alice's and Bob's apparatuses, it is impossible for the the attacker's 'horse' to recognize these bases. Subsequently, the 'horses' are blind and can not give correct feedback information. The security is the same as the BB84 protocol [3].

5 Remark

In the above we have analyzed the fragility of the quantum cryptographic algorithm against the Trojan horse strategy, where the EPR pair(s) are employed as a key. However, we here would like to stress that the quantum key distribution protocols which are implemented by making use of the EPR pair(s) do not suffer this kind of drawbacks. Since in the quantum key distribution the EPR pair carries initially

no information. Especially the users's measurement for obtaining the final key is completely random. This random feature leads the Trojan horse employed in the above section to be of no use [4].

6 Conclusion

In this work, the fragility of the THAS on the quantum cryptographic algorithm implemented by the EPR pairs as the key has been analyzed in detail. It is found that any quantum cryptographic algorithm exploiting set of orthogonal states as the symmetrical key can not circumvent the THAS. To prevent this kind of attacking strategy we proposed a new approach which makes use of the non-orthogonal entangled states. The improvement scheme is robust to the THAS. In addition, the mechanism for the THAS on the quantum cryptography as well as the classic cryptography is also investigated. In any THAS the Trojan horse is very important.

Acknowledgements

This work was supported by the Alexander von Humboldt-Stiftung foundation (Grant no. IV CHN 1069575 STP) and the National Natural Science Foundation of China (Grant no. 60102001).

References

1. B. Schneier, *Applied Cryptography: protocols, algorithms, and source code in C* (John Wiley & Sons, Inc., 1994).
2. S. Wiesner, Sigact News. **15**, 78, (1983).
3. C. H. Bennett, and G. Brassard. *Advances in Cryptology: Proceedings of Crypto'84*, August 1984, Springer-Verlag, 475 (1984).
4. A. K. Ekert, Phys. Rev. Lett. **67**, 661 (1991).
5. C. H. Bennett *et al.*, J. Crypto. **5**, 3 (1992); W. T. Buttler *et al.*, Phys. Rev. Lett. **84**, 5652 (2000).
6. H.-K. Lo and H.F. Chau, Science, **283**, 2050 (1999).
7. M. Hillery, V. Buzek and A. Berthiaume, Phys. Rev. A **59**,1829 (1999); R. Cleve, D. Gottesman, H. -K. Lo, Phys. Rev. Lett. **83**, 648 (1999).
8. P. W. Shor, and J. Preskill, Phys. Rev. Lett. **85**, 441 (2000); D. S. Naik *et al.*, *ibid* **84**, 4733 (2000).
9. G. Zeng, and W. Zhang, Phys. Rev A **61**, 032303 (2000).
10. N. Gisin, G. Ribordy, W. Tittel and H. Zbinden, arXiv: quant-ph/0101098, 19, Jan 2001.
11. J. Larsson, arXiv: quant-ph/0111073, 13 Nov 2001.
12. Y. Zhang, C. Li and G. Guo, Phys. Rev. A **64**, 024302 (2001).
13. D.W. Leung, Quantum information and computation **2** no.1, (2001). See also arXiv: quant-ph/0012077, newest version, 9 Oct 2001.
14. A. Karlsson, M. Koashi, N. Imoto, Phys. Rev. A **59**, 162 (1999).
15. W. K. Wooters and W. H. Zurek, Nature **299**, 802 (1982).

NOTE ON THE EPR–CHAMELEON EXPERIMENT

LUIGI ACCARDI, KENTARO IMAFUKU, MASSIMO REGOLI
Centro Vito Volterra, Università di Roma "Tor Vergata"
email: accardi@volterra.mat.uniroma2.it,
WEB page: http://volterra.mat.uniroma2.it

In the past 20 years quantum probability has challenged the widespread belief that classical macroscopic systems cannot, by local independent choices, produce sequences of data whose correlations violate Bell's inequality. The possibility of such a violation is not a matter of interpretation, but of fact: "local independent choices" means that two separated and non communicating experimenters make measurements but one does not know what the other measures (or even if the other one measures something); correlations are evaluated by means of standard procedures. The present experiment shows that this is not the case: in no way the EPR correlations and related experiments can be considered as a support of the incompatibility of quantum theory with local realistic theories, in particular relativity.

1 Bell's argument

Bell's inequality was proved in the paper [6]. In this paper, while the thesis, i.e. the inequality itself, is clearly stated and correctly proved, the mathematical assumptions from which the thesis follows (and without which the thesis cannot be proved) were not formulated. Bell insisted that his inequality was a consequence of locality, however he did not formulate a clear, formally stated, mathematical theorem from which one could deduce which mathematical property corresponded to locality.

This opened a debate whose goal was to try and establish which these assumptions effectively were. The reader interested in having an idea of the arguments used before quantum probability may consult the famous [9] or [7] or, for the connections with probability [8].

The mathematical formulation, now commonly adopted, of the Bell inequality was first given in [1]. The main result of this paper consists in having realized that the mathematical assumptions on which the validity of the inequality depends are only the following two ones:

(i) that the random variables take values in the interval $[-1, 1]$ (originally Bell considered only the set $\{-1, 1\}$ but shortly after he extended his result to the full interval)

(ii) that all the random variables are defined on a single probability space.

More precisely:

Lemma (1) Let A, B, C be random variables defined on the same probability space $(\Omega, \mathcal{F}, P)$ and with values in the interval $[-1, 1]$. Denote

$$\langle AB \rangle := \int_\Omega A(\omega)B(\omega)P(d\omega)$$

the correlations (mean zero can be assumed without loss of generality). Then the following inequality holds:

$$|\langle AB\rangle - \langle CB\rangle| \leq 1 - \langle AC\rangle \tag{1}$$

The following corollary of (1) (which is equivalence for ± 1-valued observables), due to Clauser, Horne, Shimony, Holt (CHSH).

Corollary (2) Let A, B, A', B' be random variables defined on the same probability space $(\Omega, \mathcal{F}, P)$ and with values in the interval $[-1, 1]$. Then the following inequality holds:

$$|\langle AB\rangle - \langle A'B\rangle + \langle AB'\rangle + \langle A'B'\rangle| \leq 2 \tag{2}$$

Proof. With the replacements $B \to B'$, $C \to -C$, (1) becomes

$$|\langle AB'\rangle + \langle CB'\rangle| = 1 + \langle AC\rangle \tag{3}$$

Adding (1) to (3) and replacing C by A' we get

$$|\langle AB\rangle - \langle A'B\rangle| + |\langle AB'\rangle + \langle A'B'\rangle| \leq 2$$

which implies (2).

The following Theorem is used to establish a connection between Bell's inequality and the predictions of quantum mechanics (cf. [3] for a comparison of the various proofs).

Theorem (4). There cannot exist a stochastic process

$$S_a^{(1)}\ ,\ S_b^{(2)} \qquad a, b \in [0, 2\pi]$$

defined on a probability space $(\Omega, \mathcal{F}, P)$ and with values in the set $\{\pm 1\}$, whose correlations are given by:

$$\langle S_a^{(1)} S_b^{(2)}\rangle = -\cos(a - b) \qquad ; \qquad a, b \in [0, 2\pi] \tag{4}$$

Remark. According to quantum theory the expression in the right-hand side of (4) is the correlation of two spin or polarization observables, along directions a, b, of two quantum particles in singlet state. These correlations have been experimentally confirmed by many experiments since the early days of quantum mechanics and this confirmation has been interpreted by several people as experimental evidence that quantum theory is incompatible with any local realistic classical theory.

The thesis of the present paper

While nobody doubts that the validity of the correlations (4) is a well established experimental fact according to the quantum probabilistic interpretation, the claim that the experimental validity of the correlation (4) is incompatible with a local realistic interpretation of quantum mechanics, is definitively unwarranted both for theoretical (cf. sections 2, 3, 4) and for experimental (cf. Sec. 5 and Appendix) reasons.

Let us briefly comment the experimental aspects of the above mentioned thesis. Bell's main claim in [6] is that: "In a theory in which parameters are added to quantum mechanics, to determine the results of individual measurements, without changing the statistical predictions, there must be a mechanism whereby the setting of one measuring device can influence the reading of another instrument, however remote. Moreover, the signal involved must propagate instantaneously, so that such a theory could not be Lorents invariant (cf. Sec. VI of [6])." The proof he gave of this statement was recalled above: the EPR correlations (quantum mechanics) violate Bell's inequality, but if the result of the measurements are pre-determined by additional parameters and if the theory is local (i.e. it does not involve instantaneous propagation of signals), then it is impossible to violate these inequalities.

It follows that, if one wants to falsify experimentally Bell's statement one must produce a classical macroscopic system which fulfilled the above listed requirements of Bell, i.e.

(i) pre-determination of the results of individual measurements by means of additional parameters (which respect to quantum theory)

(ii) no instantaneous signals

(iii) reproduction of the EPR correlations (the statistical prediction of quantum mechanics)

Our experiment produces such a classical macroscopic system and therefore it falsifies Bell's statement **experimentally**.

Let us describe in more detail our experiment to show that it exactly parallels what happens in the usual EPR type experiments with photons. Just like the start of any EPR type experiment, we start from 3 spatially separated objects:

(i) a central computer C, which plays the role of the source of entangled pairs

(ii) two additional computers A and B which play the role of the two experimental apparata which measure the polarizations of the individual photons.

The central computer C sends randomly pairs of signals. Corresponding to the fact that the source emits randomly pairs of entangled photons. The source of course does not know where the measuring apparata are; it even does not know **if** there are any apparata at all. Thus the photons are emitted a priori in all possible directions with a probability distribution that the theory can predict. Independently of each other the computers A and B choose one space direction, say a and b respectively, for each received photon and compute the values of two binary function, i.e. with values ± 1, say $S_a^{(1)}$, $S_b^{(2)}$. These values depend only on the signal emitted by the source, hence they are pre-determined in the sense of EPR and Bell. Since, by Heisenberg's principle, we cannot follow the trajectory of a photon (or of any other microscopic particle) without altering it, the only way to be sure that two photons come from the same entangled pair is to check time coincidences: if the photons arrive simultaneously, we conclude that they come from the same entangled pair. In fact the probability that two spurious photons are detected simultaneously by

two spatially separated apparata is negligible. In experiments with photons the term "simultaneous" has to be meant in the sense of a very narrow time window. But our experiment can also reproduce the ideal situation in which all apparata involved are 100% efficient. Exactly as in the experiment for photons the statistics is conditioned on coincidences (these topics are further discussed in Sec. 5). We do not know the mechanism of coincidences for individual photons because quantum mechanics does not predict the space-time trajectories of microscopic particles. In our model this mechanism is:

(i) deterministic, i.e. uniquely pre-determined by the hidden parameters

(ii) entirely local.

This is achieved by exploiting the chameleon effect, described in Sec. 2 below. After many iterations of the described procedure the two local computers A, B send back to C the registered values. The correlations are computed exactly as in the case of photons. The classical, deterministic, local dynamical system underlying the computer program has been built in such a way that the correlations are precisely the EPR ones (cf. Sec. 4 below). The computers involved are classical deterministic objects. All the choices are local. No hidden or superluminal signal is involved. All the results are uniquely determined by "additional parameters". Thus all the requirements listed in Bell's paper are fulfilled. The EPR correlations are faithfully reproduced hence Bell's inequality is violated.

In conclusion: our experiment proves in a conclusive way that the appeal to Bell's inequalities to support the claim that quantum theory is incompatible with any local realistic theory is unjustified not only theoretically but also experimentally.

2 Critiques to Bell's analysis

The quantum probabilistic approach offers to the physicists a way out from the "quantum muddle" by criticizing Bell's analysis and proving that:

i) the contradiction, pointed out by Bell, arises only from his implicit postulate that 3 statistical correlations, coming from 3 mutually incompatible experiments, can be described within a single classical probabilistic model

ii) that this implicit postulate is by no means a consequence of locality and reality.

If the implicit postulate (i) is not assumed, then Bell's proof is at fault already in its first step because in the proof of (1) (and the same is true for (2) one must use the apparently obvious identity

$$\langle AB\rangle - \langle CB\rangle = \langle AB - CB\rangle \tag{5}$$

However, by explicitly writing this identity:

$$\int_\Omega A(\omega)B(\omega)P_{a,b}(d\omega) - \int_\Omega C(\omega)B(\omega)P_{c,b}(d\omega) = \int_\Omega \left(A(\omega)B(\omega) - C(\omega)B(\omega)\right) P_{a,c,b}(d\omega) \tag{6}$$

one immediately recognizes that the left hand side is experimentally observable while the right hand side is not. In fact while the pair joint probabilities $P_{a,b}, P_{c,b}, \ldots$

are experimentally observable, there is no reason to postulate, as Bell implicitly does when using formula (5), that the experimentally unobservable, triple joint probabilities $P_{a,c,b}$ exist.

It is well known from classical probability that there are constraints, i.e. the Kolmogorov compatibility conditions, which relate the pair with the triple joint probabilities and which are necessary conditions for the existence of the latter ones. Since the pair correlations are deduced from the pair probabilities and since, when using (5), Bell is postulating a priori the existence of these (experimentally unobservable) triple joint probabilities, the only rational conclusion he can draw from his argument is that the inequality (1) (Bell's inequality) is one of these necessary conditions. Consequently, the experimental violation of this inequality is simply an experimental proof of the fact that the triplet joint probabilities for 3 singlet correlations cannot exist.

This was the critique that, starting from 1981 [1], quantum probability opposed to Bell's argument.

The chameleon effect

One might try to counter this critique by arguing that the existence of the triple probabilities is a consequence of the "realism" assumption.

For example suppose that in a box there are many pairs of balls whose color can be either green or brown. Moreover each ball is either made of glass or of wood and it weights either 10 or 20 grams. The rules of the game are such that you can only measure one observable at the time on each ball (color, weight, material). Thus on each pair we can simultaneously measure at most two observables and we can make an experimental analysis of the joint statistics of all possible pairs of observables ("color-material", "color-weight", ...).

Because of the rules of the game the triple joint probabilities "color-material-weight" are not accessible to experiment.

However the "realism assumption" tells us that any one of the possible triple combinations (color, material, weight) has a definite relative frequency in the box and therefore the pair statistics we observe, is a consequence of this triple statistics which, although unobservable "exists". Consequently, the claim of many authors to postulate the existence of the triple probabilities for the singlet correlations simply amounts to postulating the objective existence of physical properties independently of the observer. This is a realism postulate. Hence, if we exclude superluminal communications (locality) the experimental proof of the non existence of the triple probabilities is equivalent to the experimental invalidation of the realism postulate.

Arguments of this kind are quite reasonable: for example they are at the basis of classical statistical mechanics and it is probable that Einstein had in mind something of this kind when speaking of "objective reality".

According to quantum probability there is a more subtle notion of "objective reality" which gives a better intuition of the behavior of quantum systems (but it is by no means restricted to them). We call the corresponding realism "chameleon realism" as opposed to the "ballot box realism" of classical statistical mechanics.

Suppose that, in the above example, you leave the rules of the game unaltered,

but you replace the pairs of balls by pairs of chameleons and the observables (color, material, weight) by (color on the leaf, color on the wood, weight).

Is it still reasonable to believe that the pair statistics you observe, is a consequence of some (unobservable) triple statistics?

A little thought shows that the answer is: No!

According to quantum probability, quantum systems are much more similar to chameleons (adaptive: we measure the response to an interaction) than to balls (passive: we read what was in the box).

3 Mathematical formulation of the chameleon effect

The attempt to translate in a precise mathematical and physical language the intuitive difference between "ballot boxes" and "chameleons" leads to a natural generalization of von Neumann's measurement theory.

The generalization consists in introducing, in this theory, the notions of locality and causality.

It is widely accepted, since von Neumann's original analysis, that a qualitative analysis of the measurement process should start from the joint (unitary) evolution $u_{S,A}$ (system, apparatus): for simplicity we consider discrete time. Thus, if ψ_o is the initial state of the system, its state at the time of measurement is

$$\psi := \psi_o \circ u_{S,A} \tag{7}$$

Now suppose that we want to measure the observable S_a of the system (say: spin in direction a). Then the apparatus M must be prepared to measure S_a (say: by orienting a magnetic field in direction a). Therefore the interaction Hamiltonian between system and apparatus, hence also the joint dynamics, will depend on a:

$$u_{S,A} := u_{S,A(a)} := u_a \tag{8}$$

In other words: the dynamics of a system depends on the observable we want to measure: this is the chameleon effect. As anybody can see, it is a simple corollary of the standard ideas on measurement theory.

Now suppose that the system, hence the apparatus, is made up of two spatially separated parts: $(1, M_1, 2, M_2)$ and that we measure independently

$$S_a^{(1)} = (S_a \otimes 1_2) \otimes 1_M \qquad (resp.\ S_b^{(2)} = (1_1 \otimes S_b) \otimes 1_M)\ , \quad M = (M_1, M_2)$$

on particle 1 (resp. particle 2). Then, according to the chameleon effect, we will have

$$u_{S,A} := u_{a,b} \tag{9}$$

and, according to quantum (or classical) mechanics, the pair correlations will be

$$\langle S_a^{(1)} S_b^{(2)} \rangle := \psi_o \circ u_{a,b} \left(S_a^{(1)} S_b^{(2)} \right) = \psi_{a,b} \left(S_a^{(1)} S_b^{(2)} \right) \tag{10}$$

This shows that the pair joint probability $P_{a,b}$, corresponding to these correlations, depends on a, b, hence the application of Bell's inequality is impossible. This dependence is called "conceptuality".

However, by considering the mean value of a single particle observable, say $S_a^{(1)}$:

$$\psi(S_a^{(1)}) := \psi_o \left(u_{a,b}(S_a^{(1)}) \right) \tag{11}$$

we see that, for a general dynamics, the mean value of an observable of particle 1 will depend on the measurement we do on particle 2: this means that the EPR locality condition is not satisfied. Thus conceptuality is not enough to guarantee locality.

If we want it to be satisfied, we have to restrict the class of allowed dynamics and also the class of allowed initial states.

The physical arguments which allow defining such restrictions have been discussed in previous papers of the authors (cf. [4] for bibliography). Here we will just state the results.

The EPR locality condition is mathematically expressed by the fact that the local dynamics of each particle is independent of the local dynamics of the other one, in formulae

$$u_{a,b} := u_a \otimes u_b \tag{12}$$

and the causality condition by the fact that the initial state of the particle is independent of the initial state of the apparatus (because the particles cannot know which measurement will be made on them). In formulae:

$$\psi_o := \psi_{1,2} \otimes \psi_{A_1} \otimes \psi_{A_2} \tag{13}$$

However both ψ_{A_1}, ψ_{A_2} may depend on the state of the system 1 (resp. 2) because the local interaction of particle 1 (resp. 2) with the apparatus may depend on the state of the particle at the moment of interaction. With these restrictions one easily computes that the EPR locality condition is satisfied. However (12) and (10) show that the pair joint probabilities, corresponding to pair correlations, still depend on a, b, hence the application of Bell's inequality is still impossible.

This extension of the standard quantum theory of measurement was first proposed in [2]. The experiment discussed in the present conference is a concrete realization of this abstract scheme.

4 Description of the dynamical model

In the present section we construct a dynamical system which simulates locally the EPR correlation (4).

In the idealized dynamical system considered in our experiment we consider only two time instants 0 (initial) and 1 (final) so, in our case, a "trajectory" consists of a single jump. We do not describe the space–time details of the trajectory because we are only interested in distinguishing 2 cases:

- at time 1 the particle is in the apparatus (and in this case it is detected with certainty)
- at time 1 the particle is not in the apparatus (and in this case it makes no sense to speak of detection)

Thus our "configuration space" for the single particle will be made of 3 points: s (source), 1 (inside apparatus), 0 (outside apparatus). Since at time 0 the "position" of both particles is always s, because of the chameleon effect, the position $q_{j,1}$ of particle $j = (1,2)$ at time 1 will depend on the polarization a_j, on the initial state σ and on the state λ_j of the apparatus $M_j (j = 1,2)$:

$$q_{j,1} = q_{j,1}(a_j, \sigma, \lambda_j) \quad ; \qquad j = 1,2,$$

The local, deterministic dynamical law of this dependence is described as followed.

1. The state space of the composite system (particles, apparatus) is

$$\{\text{position space}\} \times \{\text{inner state space}\} \times \{\text{apparatus space}\}$$

$$= \{s, 0, 1\} \times [0, 2\pi]^2 \times [0,1]^2$$

2. The initial state is always of the form

$$(s, s, \sigma_1, \sigma_2, \lambda_1, \lambda_2) \in \{s\}^2 \times [0, 2\pi]^2 \times [0,1]^2$$

i.e. the initial position of both particles is always s.

3. To speak of correlations only makes sense if the deterministic trajectories of both particles end up in the detectors (pre-determination). This means that the statistics is conditioned to the subset

$$\{1\}^2 \times [0, 2\pi]^2 \times [0,1]^2 \tag{14}$$

of the state space.

4. Just by changing the order of the factors the state space can be realized as

$$\{(s_1, \sigma_1, \lambda_1; s_2, \sigma_2, \lambda_2)\} \in (\{s, 0, 1\} \times [0, 2\pi] \times [0,1]) \times (\{s, 0, 1\} \times [0, 2\pi] \times [0,1])$$

Therefore a local deterministic dynamics is uniquely determined by the assignment of two functions $T_{1,a}, T_{2,b}$:

$$(s_1, \sigma_1, \lambda_1; s_2, \sigma_2, \lambda_2) \to (T_{1,a}(s_1, \sigma_1, \lambda_1), T_{2,b}(s_2, \sigma_2, \lambda_2))$$

$$=: (q_{1,a}, s_{1,a}, m_{1,a}; q_{2,b}, s_{2,b}, m_{2,b})$$

where $(q_{1,a}, s_{1,a}, m_{1,a})$ (resp. $(q_{2,b}, s_{2,b}, m_{2,b})$) depends only on $(s_1, \sigma_1, \lambda_1)$ (resp. $(s_2, \sigma_2, \lambda_2)$). Moreover it is convenient to identify the endpoints of both intervals $[0, 2\pi]$ and $[0,1]$, i.e. to identify these intervals to circles so that the functions $q_{j,x}, s_{j,x}, m_{j,x} (j = 1,2, x = a,b)$, as functions of the variables σ, λ can be extended by periodicity to the whole real line (period 2π in σ, period 1 in λ). This allows giving a meaning to formula (17) of [5] in full generality, i.e. without appealing to special choice (11) of the cited paper.

5. With these conventions, for every $a, b \in [0, 2\pi]$, we uniquely specify a deterministic dynamics as follows

$$(s_1, \sigma_1, \lambda_1; s_2, \sigma_2, \lambda_2) \mapsto (q_{1,a}(s_1, \sigma_1, \lambda_1), \sigma_1, \lambda_1; q_{2,b}(s_2, \sigma_2, \lambda_2), \sigma_2, \lambda_2) \quad (15)$$

i.e. the inner state of the particle and of the apparatus do not vary under the evolution, but the position varies according to the law:

$$q_{1,a}(s, \sigma_1, \lambda_1) = \chi_{[0, p_{1,a}(\sigma_1)]}(\lambda_1) \; ; \; q_{2,b}(s, \sigma_2, \lambda_2) = \chi_{[0, p_{2b}(\sigma_2)]}(\lambda_1)$$

$$p_{1,a}(\sigma) = \frac{1}{4}|\cos(\sigma - a)| \quad , \quad p_{2,b}(\sigma) = 1 \quad (16)$$

$$(\chi(x) = 1 \text{ if } x \in I \; , \qquad I = 0 \text{ if } x \notin I)$$

Remember that the initial position of both particles is always s. Therefore it is sufficient to define the dynamics only in this case.

6. For every setting $(a, b) \in [0, 2\pi]^2$ of the apparata, the initial probability distribution $P_{a,b}$ of our deterministic dynamical system is given by:

$$\delta_{s,s_1}\delta_{s,s_2}\frac{1}{2\pi}\delta(\sigma_1 - \sigma_2)\delta(m_{1,a}(\sigma_1, \lambda_1) - m_a)\delta(m_{2,b}(\sigma_2, \lambda_2) - m_b)d\sigma_1 d\sigma_2 d\lambda_1 d\lambda_2 \quad (17)$$

where m_a, m_b are fixed numbers in $[0, 1]$ and

$$m_{1,a}(\sigma_1, \lambda_1) = \frac{4\lambda_1}{\sqrt{2\pi}|\cos(\sigma_1 - a)|}, \quad m_{2,b}(\sigma_2, \lambda_2) = \frac{\lambda_2}{\sqrt{2\pi}} \quad (18)$$

Finally the random variables $S_a^{(1)}, S_b^{(2)}$:

$$\{s\}^2 \times [0, 2\pi]^2 \times [0, 1]^2 \to \{\pm 1\}$$

are defined by

$$S_a^{(1)}(s, \sigma, \lambda) = \text{sgn}\,(\cos(\sigma - a)) \, ; S_a^{(2)} = -S_a^{(1)} \quad (19)$$

It is now a matter if simple calculations (cf. section (2) of[5]) to verify that the correlations

$$\langle S_a^{(1)} S_b^{(2)} \rangle = \int_\Omega S_a^{(1)}(T_{1,a}(s, \sigma_1, \lambda_1)) S_b^{(2)}(T_{2,b}(s, \sigma_2, \lambda_2)) dP_{a,b}(\omega) \quad (20)$$

($\omega = (s, \sigma_1, \lambda_1; s, \sigma_2, \lambda_2)$) are precisely the EPR correlations.

Finally notice that the dynamics (15) is slightly simplified with respect to the one described in[5]. However, due to the choice (11) of[5] this simplification does not change the calculations in the specific case under consideration. For more general classes of models the simplification (15) is convenient because with this choice the state space is mapped into itself by the dynamics and no additional identifications are required.

There is no conceptual difficulty to include in our model the consideration of the space-time trajectory of the particle. This surely would improve the present model, however the main conclusion of our experiment, i.e. the reproducibility of the EPR correlations by a classical, deterministic, local dynamical system, will not change.

5 Comments on the experiment

The realization of the computer simulation of the local dynamical system constructed in the previous section has been qualitatively described in the introduction above and will be discussed in detail in the appendix.

Our goal in this section is to briefly illustrate the conceptual meaning of this implementation.

Recall the basic idea of the chameleon effect: *the local dynamics influences the statistics and since the factorization of the dynamics (12), i.e.* $((1, M_1), (2, M_2))$, *is different from the factorization of the state (13), i.e.* $((1, 2), (M_1, M_2))$, *the result of the local interaction is a global dependence of the final state on the whole measurement setting, i.e.* (a, b).

Now, in any dynamical system, the statistics is determined by the number of trajectories that fall into a pre–assigned region of the state space.

Therefore, by definition, to say that the dynamics influences the statistics, means that the dynamics changes the trajectories of the single particles.

As explained above this change will be local because of the form (12) of the dynamics, but the influence on the statistics will be global because of the form (13) of the initial state.

Here the word "change" has to be interpreted with respect to the trajectories that the particles would have in absence of interaction with the apparatus.

Another important point is that, in all the EPR–type experiments, the two apparata must be spatially separated: if the two apparata were contiguous there might exist communications between them without violating the locality principle.

This obvious fact has an important conceptual consequence, namely that: *in all EPR–type experiments, the statistics is conditioned on those trajectories that lead both particles to interact with the apparatus.*

Now let us forget, for the moment, the quantum mechanical situation and let us concentrate our attention on a classical dynamical system composed, as in our experiment, of two particles and two apparata.

The state space of the particles will consist, as in our experiment, of their space position and of inner degrees of freedom.

The condition that the two apparata are spatially separated implies on a priori selection of the trajectories and this selection is the physical counterpart of the probabilistic operation of conditioning.

Combining this remark with what said before on the local deformation of the trajectories due to interaction with the apparatus, we see that this local deformation can manifest itself only in two ways:

(i) by altering the space trajectories

(ii) by altering the "trajectories" of the inner degrees of freedom.

They are both local effects and they can alter the statistics

(j) by changing the number of pairs of trajectories which end in the influence region of the apparatus

(jj) by altering the response of a single particle to the interaction with the apparatus.

Now, if we want to respect the singlet law, the response of each particle to the apparatus must be pre–determined. Therefore the simplest way to construct a dynamical system which respects the singlet law and realizes the chameleon effect (i.e. the alteration of statistics due to local interactions with the apparatus) is to construct the deterministic dynamics in such a way that the space dynamics of the particles is influenced by the local interaction, while its inner degree of freedom is not.

This is what we have realized with the dynamics (15).

Such a deformation is perfectly compatible with the assumption of an 100 per cent (ideal) efficiency of the detectors. In fact the efficiency is measured by the ratio of the number of detected particles over the number of particles which have interacted with the apparatus.

It would be totally meaningless to take into account, in the determination of the efficiency, also those particles whose space trajectory has brought them so far from the apparatus that no physical interaction between them is conceivable.

Moreover, and this is a possible difference between the classical and the quantum case, the very notion of "total number of pairs emitted by the source" is a totally platonic and in principle unobservable quantity in the quantum case (under the assumption of a neat space separation between the two apparata).

In some, but not all, classical situations this number might be observable, but in a quantum context, where you cannot follow the trajectory of single particles without altering it, this number is quite unobservable.

Appendix –Description of the simulation–

The program and the instruction to run it are available from the web site "http://volterra.mat.uniroma2.it".

1. Let $N \leq N_{tot}$ be natural integers and let

$$\{\sigma_j \ : \ j = 1, \ldots, N\} \tag{21}$$

be the sequence of numbers either deterministically or pseudo-randomly distributed in $[0, 2\pi]$ with good equidistribution properties. (cf. the option D (deterministic) or R (random) that has been inserted in the program of the experiment.) Let $N(\sigma_j)$ $(j = 1, \ldots, N)$ denote a sequence of natural integers such that

$$\sum_{j=1}^{N} N(\sigma_j) = N_{tot}$$

Remark. N_{tot} represents the (physically unobservable) "total number" of entangled pairs emitted by the source. $N(\sigma_j)$ is the number of times that the input σ_j is produced in the sequence (21).

2. For each j from 1 to N, repeat the following 3 operations (a), (b), (c), $N(\sigma_j)$ times

   (a) The central computer sends σ_j to the computers 1 and 2.

   (b) Computer 1 computes the position of particle 1 using the deterministic dynamics and sends back $S_a^{(1)}(\sigma_j)$ $(= 1 \text{ or } -1)$ if the particle is inside the apparatus. It sends back nothing if the particle is outside the apparatus. Computer 2 does the same thing. The deterministic dynamics is such that $S_a^{(1)}(\sigma_j)$ is sent back with probability $p_{1,a}(\sigma_j)$ and $S_b^{(2)}(\sigma_j)$ is sent back with probability $p_{2,b}(\sigma_j)$ where $p_{1,a}, p_{2,b}$ are sufficiently regular probability densities (say piecewise smooth with a finite number of discontinuities in $[0, 2\pi]$.

   Remark. This corresponds in the real experiments, to labeling the local detection time of the photon. When both computers send back a value ± 1, then we say that a *coincidence* occurs. The emergence of this probability in a deterministic context is due to the fact that the dynamics has strong chaotic properties.

   (c) *Only in case of a coincidence, i.e. when the central computer receives the value* ± 1 *from both computers*, the central computer computes the "correlation product" $S_a^{(1)}(\sigma_j) S_b^{(2)}(\sigma_j)$.

3. The central computer computes the correlation as

$$\frac{\text{Sum of all correlation products}}{\text{The total number of coincidences}}. \tag{22}$$

Remark. This is what is done in all experiments and a corresponds to the statement of the problem because, up to now, the EPR correlations have always been interpreted as equal time correlations.

Introducing

$$p(\sigma_j) = \frac{N(\sigma_j)}{N_{tot}} = \frac{1}{2\pi} \tag{23}$$

the expected number of coincidences $\mathcal{N}_{\text{coincidences}}$ and the sum of all correlation products $\mathcal{S}_{\text{correlations}}$ become respectively

$$\begin{aligned}
\mathcal{N}_{\text{correlations}} &= \sum_{j=1}^{N} N(\sigma_j) p_{1,a}(\sigma_j) p_{2,b}(\sigma_j) S_1^{(a)}(\sigma_j) S_2^{(b)}(\sigma_j) \\
&= N_{tot} \sum_{j=1}^{N} p(\sigma_j) p_{1,a}(\sigma_j) p_{2,b}(\sigma_j) S_1^{(a)}(\sigma_j) S_2^{(b)}(\sigma_j) \\
&\to N_{tot} \int_0^{2\pi} d\sigma \; p(\sigma) p_{1,a}(\sigma) p_{2,b}(\sigma) S_1^{(a)}(\sigma) S_2^{(b)}(\sigma) = \frac{N_{tot}}{2\pi} \qquad (24) \\
\mathcal{S}_{\text{coincidences}} &= \sum_{j=1}^{N} N(\sigma_j) p_{1,a}(\sigma_j) p_{2,b}(\sigma_j) = N_{tot} \sum_{j=1}^{N} p(\sigma_j) p_{1,a}(\sigma_j) p_{2,b}(\sigma_j)
\end{aligned}$$

$$\rightarrow N_{tot} \int_0^{2\pi} d\sigma \; p(\sigma) p_{1,a}(\sigma) p_{2,b}(\sigma) S_1^{(a)}(\sigma) S_2^{(b)}(\sigma)$$

$$= -\frac{N_{tot}}{2\pi} \cos(a-b) \tag{25}$$

with the choice in (16) and (19). Thus the correlation defined by (22) is

$$\frac{\mathcal{S}_{\text{correlations}}}{\mathcal{N}_{\text{coincidences}}} = -\cos(a-b) \tag{26}$$

which is exactly the EPR correlation. We underline that, as shown by (24), even if the mechanism of coincidences depends on the setting of the apparatus, the expected number of coincidences (24) is independent of it, in agreement with [10].

References

1. Luigi Accardi: Topics in quantum probability, Phys. Rep. 77 (1981) 169-192
2. L. Accardi: Einstein-Bohr: one all, in: The interpretation of quantum theory: where do we stand? Acta Enciclopedica, Istituto dell'Enciclopedia Italiana (1994) 95–115 Volterra preprint N. 174 (1993)
3. Luigi Accardi, Massimo Regoli: Locality and Bell's inequality. Preprint Volterra, N. 427 (2000) quant-ph/0007005; an extended version of this paper, including the description of the present experiment will appear in the proceedings of the conference "Foundations of Probability and Physics", Vaxjo University, Sweden, November 27 - December 1 (2000), A. Khrennikov (ed.), World Scientific (2001)
4. Luigi Accardi, Massimo Regoli: The EPR correlations and the chameleon effect, discussed during the "Japan-Italy Joint workshop on Quantum open systems and quantum measurement", Waseda University, 27–29 September 2001 Preprint Volterra, N. 487 (2001)
5. L.Accardi, K.Imafuku, M.Regoli: On the EPR–chameleon experiment, Infinite dimensional analysis, quantum probability and related topics, **5** (2002) 1–20, quant-ph/0112067, Volterra Preprint December (2001) N. 494
6. Bell J.S: On the Einstein Podolsky Rosen Paradox Physics **1** 195-200 (1964)
7. Stapp H. P.: Bell's Theorem as a Nonlocality Property of Quantum Theory. Phys. Rev. Lett., **49**, 1470-1474 (1982)
8. Suppes P., Zanotti M.: On the Determinism of Hidden Variable Theories with Strict Correlation and Conditional Statistical Independence of Observables. Logic and Prob. in Quant. Mech., 445-455 (1976)
9. E.P. Wigner: Amer Journ. of Phys. 38 (1970) 1005
10. Alain Aspect, Philippe Grangier, and Gerard Roger: Experimental Realization of Einstein-Podolsky-Rosen-Bohm Gedankenexperiment: A New Violation of Bell's Inequalities, Phys. Rev. Lett. **49**, 91 (1982)

QUANTUM NETWORKS FOR DISTRIBUTED COMPUTATION AND COMMUNICATION

H. J. KIMBLE
Norman Bridge Laboratory of Physics 12-33
California Institute of Technology
Pasadena, California 91125
USA

Although formal discussions of quantum computation and communication involve abstract unitary transformations in Hilbert space, implementations of quantum logic require attention to the dynamical processes of particular physical systems. In the Quantum Optics Group at Caltech, we are attempting to lay the foundations for quantum information science by way of advances on several fronts in optical physics, including cavity quantum electrodynamics.

Cavity quantum electrodynamics (QED) offers powerful possibilities for the deterministic control of atom-photon interactions quantum by quantum[1]. Indeed, modern experiments in cavity QED have achieved the exceptional circumstance of strong coupling, for which single quanta can profoundly impact the dynamics of the atom-cavity system. The diverse accomplishments of this field set the stage for advances into yet broader frontiers in quantum information science for which cavity QED offers unique advantages, including the creation of quantum networks to implement fundamental quantum communication protocols and for distributed quantum computation[2].

The primary technical challenge on the road toward such scientific goals is the need to trap and localize atoms within a cavity in a setting suitable for strong coupling. Beginning with the work of Mabuchi et al. in our laboratory in 1996 [3], several groups have been pursuing the integration of the techniques of laser cooling and trapping with those of cavity quantum electrodynamics (QED)[4]. Two separate experiments in our group have achieved significant milestones in this quest, namely the real-time trapping and tracking of single atoms in cavity QED[5,6,7]. Indeed, Refs. [5,6] represent the first realizations of trapped atoms within a setting of strong coupling in cavity QED.

In both these experiments, the arrival of a single atom into the cavity mode can be monitored with high signal-to-noise ratio in *real time* by a near resonant field with mean intracavity photon number $\bar{n} < 1$. In one experiment, an atom's arrival triggers *ON* an auxiliary field that functions as a far-detuned dipole-force trap (FORT)[6], thereby trapping the atom within the cavity mode with a lifetime $\tau \approx 100$ms, which should be compared to the nanosecond time scale for internal dynamics of the atom-cavity system. We have spent considerable effort to understand the mechanisms that limit the trap lifetime and which heat atomic motion within the FORT[8], with some rather interesting surprises. For example, thermal excitation of the elastic modes of the glass cylinders that form the mirrors of the cavity contributes to parametric heating of axial motion of a trapped atom. Here, $k_B T$ of energy per elastic mode leads to displacement noise for the positions of the two mirror surfaces with spectra density for the length variations $\sim 10^{-17}\mathrm{m}/\sqrt{\mathrm{Hz}}$

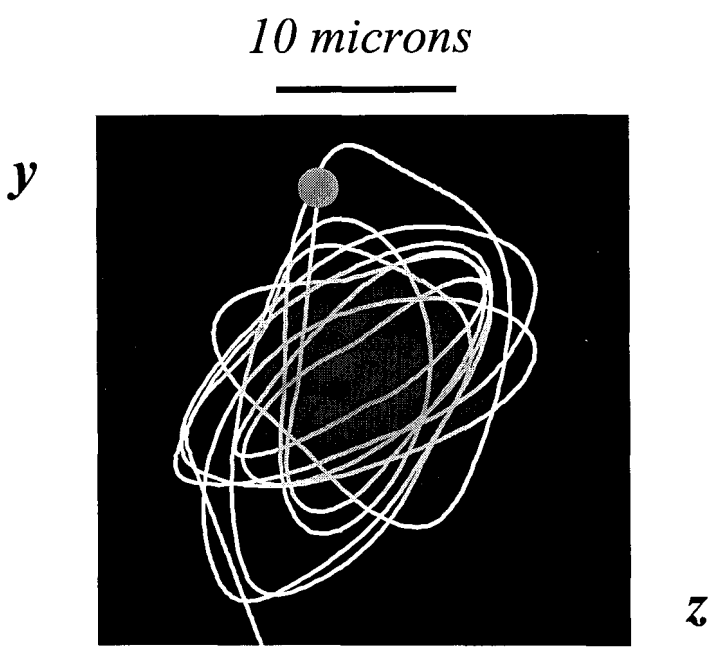

Figure 1. Reconstructed orbit for a single atom bound in orbit by single photons. The orbit is in the $y-z$ plane perpendicular to the cavity axis, with motion along the x-direction of the standing wave estimated to be less than about 60nm. Animated versions of atomic trajectories can be viewed at *http://www.its.caltech.edu/~qoptics/atomorbits/*, and more information found in Refs. [7] and [10].

around 1MHz. We have as well extended the usual free-space theory of laser cooling and trapping to the setting of strong coupling in cavity QED[9].

In a second experiment, we rely upon light forces at the single-photon level to trap a single atom within the cavity mode[5,7,10]. Because an atom moving within the resonator generates large variations in the transmission of a weak probe laser, we have been able to develop an inversion algorithm to reconstruct the trajectories of individual atoms from the cavity transmission, thereby realizing a new form of microscopy. As illustrated in Figure 1, these reconstructions reveal single atoms bound in orbit by the mechanical forces associated with single photons. Over the duration of the observation, the sensitivity is near the standard quantum limit for sensing the motion of a Cesium atom[11].

Beyond quantum information processing with internal atomic states and photons serving as *qubits*, we are also investigating algorithms for continuous quantum variables[12,13,14], including our realization of quantum teleportation for the quadrature amplitudes of a beam of light[15,16,17]. This experiment utilizes squeezed-state entanglement to achieve *unconditional* quantum teleportation. Together with our capabilities for strong coupling in cavity QED, we are striving to realize diverse

new capabilities in quantum information science, including protocols for the teleportation of the wave function of a massive particle[14].

This work is supported by the National Science Foundation, by the Caltech MURI for Quantum Networks administered by the Army Research Office, and by the Office of Naval Research.

References

1. For a recent review, see contributions in the Special Issue of Physica Scripta **T76** (1998).
2. J. I. Cirac, S. J. van Enk, P. Zoller, H. J. Kimble, and H. Mabuchi, Physica Scripta **T76**, 223 (1998).
3. H. Mabuchi, Q. A. Turchette, M. S. Chapman, and H. J. Kimble, Opt. Lett. **21**, 1393 (1996).
4. For a recent review, see G. Rempe, Physics World, **13**, 37 (2000).
5. J. Ye, C. J. Hood, T. Lynn, H. Mabuchi, D. W. Vernooy and H. J. Kimble, IEEE Transactions on Instrumentation and Measurement **48**, 608 (1999).
6. J. Ye, D. W. Vernooy, and H. J. Kimble, Phys. Rev. Lett. **83**, 4987 (1999).
7. C. J. Hood, T. W. Lynn, A. C. Doherty, A.S. Parkins, and H. J. Kimble, Science **287**, 1447 (2000).
8. C. W. Gardiner, J. Ye, C. Nägerl and H. J. Kimble, Phys. Rev. A **61**, 045801 (2000).
9. S. J. van Enk, J. McKeever, H. J. Kimble, and J. Ye, Phys. Rev. A **64**, 013407 (2001).
10. A. C. Doherty, T. W. Lynn, C. J. Hood, and H. J. Kimble, Phys. Rev. A **63**, 013401 (2001).
11. H. Mabuchi, J. Ye, and H. J. Kimble, Appl. Phys. B **68**, 1095 (1999).
12. S. L. Braunstein and H. J. Kimble, Phys. Rev. Lett. **80**, 869 (1998).
13. Samuel L. Braunstein and H. J. Kimble, Phys. Rev. A **61**, 042302 (2000).
14. A. S. Parkins and H. J. Kimble, Journal Opt. B: Quantum Semiclass. Opt. **1**, 496 (1999); quant-ph/9909021; *Frontiers of Laser Physics and Quantum Optics,* eds. Z. Xu et al. (Springer, Berlin, 2000), 132; Phys. Rev. A **61**, 052104 (2000).
15. A. Furusawa, J. L. Sorensen, S. L. Braunstein, C. A. Fuchs, H. J. Kimble, and E. S. Polzik, Science **282**, 706 (1998).
16. Samuel L. Braunstein, Christopher A. Fuchs, and H. J. Kimble, Journal of Modern Optics **47**, 267 (2000).
17. Samuel L. Braunstein, Christopher A. Fuchs, H. J. Kimble, and P. van Loock, Phys. Rev. A **64**, 022321 (2001).

DISCUSSION

Chairman: P. Zoller

L. Wang: What is the resolution in the experiment?

H. J. Kimble: For the actual measurements, the achieved resolution is about

$20\text{nm}/\sqrt{\text{Hz}}$, with this result applying to atomic motion in the plane transverse to the cavity axis. The atom's motion along the axial direction is tightly confined around one particular antinode to within about ± 60nm. Because of the much greater field gradients in the axial direction, the *inferred* sensitivity for observation of motion along the cavity axis is about 10^2 higher, or $0.2\text{nm}/\sqrt{\text{Hz}}$, which we intend to investigate in future experiments. As pointed out in our *Science* article, the current measurements bring us close the standard quantum limit for position measurement.

R. Chiao: Could you summarize what are the relative advantages and disadvantages of using ions and neutral atoms for doing quantum information processing?

H. J. Kimble: In my view, there are two essential features that make trapped ions very attractive for quantum information processing. The first is that the trapping mechanism is essentially independent of the internal atomic state. The second is the remarkable capability to store ions for extremely long times with extraordinarily low heating rates (essentially "forever" on the time scales of the internal dynamics). The achievements by the ion trapping community (e.g., D. Wineland's group at NIST, R. Blatt's group in Innsbruck, and H. Walther's group in Garching) represent spectacular advances, and are the "proof of the pudding" regarding the potential of trapped ions in quantum information science.

On the other hand, there are disadvantages, including that a single atomic charge couples to stray external fields in troublesome ways. With respect to the combination of trapped ions and cavity QED, it is difficult to achieve very small mode volumes (and hence very strong coupling) with the current generation of "macroscopic" ion traps, although this will certainly change with micro-fabricated structures being pursued by various groups. In a similar fashion, the "clock" rates are limited in current structures to about 10^6/sec for schemes based upon the vibrational motion of the ion chain, but might be much larger in smaller structures.

As for neutral atoms, the trapping and state manipulation capabilities for small atomic samples ($N = 1, 2, ...$) are not as well developed as for ions, but there is rapid progress. For example, my group is pursuing a trapping scheme in a far-off resonance trap (FORT) that makes the trapping potential very nearly independent of the relevant internal atomic states for quantum information processing (see also the work by H. Katori et al.). The absence of Coulombic repulsion between neutral atoms leads to a whole set of new possibilities for quantum information processing, as for example, have been investigated by I. Cirac, P. Zoller, and colleagues, by I. Deutsch and P. Jessen, and others.

M. Raizen: Two questions. One: could you say something more about the thermal fluctuations in mirror substrate and what we could do with that? You mentioned some possible manipulations. The other question is: at some point in the future the length of cavity will become capable or less than the thickness of your substrate, mirrors etc. Where does one go technologically from there?

H. J. Kimble: First question first, which relates to the thermal motion of the mirror substrates that form the cavity in our experiments. If one solves for the elastic modes of a cylinder (as was done in the 19$^{\text{th}}$ century by Lord Rayleigh), then equipartition of energy demands that in thermal equilibrium, each of these modes contains $k_B T$ of energy. This energy in turn is a source of stochastic excitation for

each particular normal-mode of the cylinder. In our case, this thermally excited "Brownian" motion leads to motion of the mirror faces, which translates in turn to a noise source for the intracavity field that is employed to trap the atom. This qualitative discussion can be made quantitative, and leads to the noise spectra shown in my presentation, with the theory and experiment matching quite nicely. So, we clearly observe the thermal excitation of the elastic modes of the mirror substrates, and are able to do so with very low probe powers (e.g., the graph shown had about 3μW of transmitted power).

This is all "bad news" for our efforts to trap single atoms in cavity QED, and demands some ways to circumvent the noise that I have discussed, and which we are implementing in the laboratory. The "good news" is that the measurements also suggest some possible new research directions related to the motion of the mirrors themselves, never mind cavity QED for the moment. In this regard, we take our lead from the pioneering work of V. Braginsky, K. Thorne, and colleagues to ask whether it might be possible to access quantum aspects of the motion of the mirrors, including sensing at and beyond the standard quantum limit, exploiting the mirror motion from radiation pressure as a nonlinear mechanism, and implementing feedback control of a macroscopic quantum object. In this regard, we note the beautiful work already performed by A. Heidmann and colleagues (Paris) and S. Schiller et al. (Konstanz), including feedback to cool the motion of a selected elastic mode.

As for your second question, let me reply in two ways. The first is to ask for extrapolations of current technologies to their ultimate limits for advancing the cause of strong coupling. C. Hood, J. Ye, and I have investigated this point in detail for Fabry-Perot cavities in a recent paper in the Physical Review [Phys. Rev. A **64**, 033804 (2001)]; a forthcoming paper with J. Buck addresses this issue for the whispering gallery modes of microspheres. In qualitative terms, the limit for the critical photon number n_0 is of order $10^{-5} - 10^{-6}$ photons. The second reply is to seek out completely new technical avenues for resonators suitable for cavity QED with single atoms. An example of this approach is the pioneering work of H. Mabuchi and A. Scherer at Caltech who are investigating nano-fabricated resonators made from photonic bandgap materials.

L. Vaidman: I just want one more clarification about the experiment you showed in the movie. What is an indirect test of what you showed on screen is correct. So what do you know for sure in some independent test that this is exactly the trajectory? The slide you just showed you said inherent sensitivity whatever was 0.2.

H. J. Kimble: This is a good question, but a couple of things might be confused. First, let me make clear the distinction between our actual measurements related to the radial motion and possible future observations related to the axial motion. This is the point that I addressed in my reply to Professor Chiao, and may relate to the factor of 100 that you mention.

However, the point that I think that you are raising is whether or not there is an independent check that our "atom-cavity microscope" (ACM) is really reliable. That is, can we actually believe that the motion illustrated in the movies that I have shown faithfully mirrors the actual atomic motion? Well, there is in fact no

independent "microscope" with the sensitivity to make such a confirmation. The important thing about our measurements via the cavity field is that they represent an in principle enhancement in our ability to extract real-time information about atomic motion beyond that which would otherwise be possible (e.g., via fluorescence imaging).

However, you should be skeptical (as are we) of such an answer, and that is why we are pursuing another avenue to confirm the validity of the measurements made by our ACM. The basic idea is to perform quantum feedback based upon our *inference* of the atomic motion. If we are faithfully tracking the motion (including the effect of quantum back action), then we should be able to "control" efficiently the atomic motion, including to remove energy and angular momentum and to "watch" as the orbit circularizes and spirals inward. If we have an incomplete or wrong algorithm (e.g., omit the mechanical effects of measurement back action), then we won't be able to control the motion with feedback.

L. Vaidman: This is done or this is in the future?

H. J. Kimble: The results that I have shown related to quantum feedback and orbits that spiral to the origin in the transverse plane are from numerical simulations, with "real" results from the laboratory hopefully coming for the next Solvay conference. But again to your important question of an independent way to confirm our measurements of atomic motion, and again the answer is "no". We are attempting to learn the rules and regulations for optimal state estimation of open quantum systems. How do we confirm that all this fancy stuff that we know about quantum measurement and back action is correct for single, continuously observed quantum systems? Perhaps the only available option is via quantum feedback with various control algorithms.

E. Polzik: You mentioned the possibilities for efficient quantum state exchange by employing single trapped atoms in cavity QED. Do you have vision of how to get there? Do you have a short statement about the same kind of vision for continuous variables?

H. J. Kimble: On a technical front, we have to learn to manipulate the external degrees of freedom for single trapped atoms in the same way that the ion trapping and the lattice communities have demonstrated so spectacularly over the past decade. We must do this with single (or few) atoms within the setting of cavity QED which brings a difficult set of scientific and technical problems. In qualitative terms, our task is coherent control of atomic wave packets, but here we must accomplish this control in the presence of strong coupling for both internal and external degrees of freedom. S. Parkins and I, as well as by now other groups, have investigated several theoretical avenues, and have identified some promising directions to achieve marvellous quantum state manipulations for atomic wave-packet states within the cavity, and thence to and from the external world by way of the cavity mirrors.

GEOMETRIC CONSTRUCTION OF MULTI-BIT QUANTUM GATES

KLAUS MØLMER, ANDERS SØRENSEN and XIAOGUANG WANG[a]
QUANTOP - Danish Quantum Optics Center
Institute of Physics and Astronomy
University of Aarhus
DK-8000 Århus C, Denmark

In the ion trap quantum computer the internal states of trapped ions serve as quantum bits and laser induced collective vibrations of the ions serve to couple the ions and to perform gate operations. We have developed a method to perform gates on different ions by illuminating the ions with bichromatic light. Here, we display a geometric representation of this operation which enables us to extend the method to implement trigonometric functions of operators on the quantum register and to produce gates which may involve a large number of bits in a single operation.

1 Introduction

Starting with the ion trap proposal by Cirac and Zoller [1], a number of proposals for quantum computing exists where gates involving pairs of qubits are implemented by use of the coupling to a harmonic oscillator degree of freedom. In the ion trap, the internal electronic or hyperfine states of the ions are coupled to the collective vibrational degree of freedom due to the recoil during absorption of laser light. In the present paper, we shall use the terminology of the ion trap, but we wish to point out that the ideas and the formalism will also be applicable to other systems such as atoms [2], ions [3] or quantum dots [4] which are localized in an optical cavity and which communicate *via* a single mode of the optical field, and it will apply to an array of Josephson-junction qubits which are coupled by an LC-oscillator mode in an electrical circuit [5].

The outline of the paper is as follows. In Sec. 2, we recall our original bichromatic proposal for two-bit gates, which works even if the vibrational motion of the ions is not kept in its ground state [6]. In Sec. 3, we present a method for faster gate operation, deduced from a geometric interpretation that links the gate operation to the area in the oscillator phase space encircled by laser light induced displacements of the ions. In Sec. 4, we present operations that turn the geometric area into a gate with products of more than two qubit operators, and in Sec. 5 we present examples of applications of the resulting multi-bit gates.

2 Slow two-colour gate

We illuminate two ions with bichromatic light detuned by the same amount above and below atomic resonance, $\omega_j = \omega_{eg} \pm \delta$, $j = 1, 2$. This laser setting provides the

[a]Present address: Institute for Scientific Interchange, I-10133 Torino, Italy

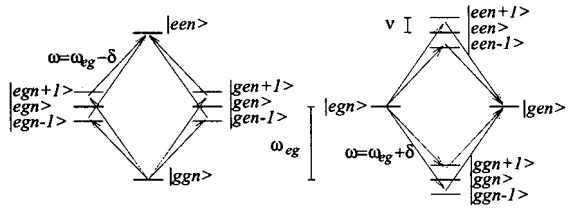

Figure 1: Energy level diagram for two ions with quantized vibrational motion illuminated with bichromatic light. The only resonant transitions are from $|ggn\rangle$ to $|een\rangle$ and from $|egn\rangle$ to $|gen\rangle$. Various transition paths involving intermediate states with vibrational number $n \pm 1$ are identified.

interaction Hamiltonian ($\hbar = 1$)

$$H_{\text{int}} = \sum_{i,j} \frac{\Omega_{ij}}{2} (\sigma_{+i} e^{i(\eta(a+a^\dagger) - \omega_j t)} + h.c.). \tag{1}$$

Ω_{ij} is the Rabi frequency of the interaction between ion i and laser field j. Due to the Coulomb repulsion the ions are coupled, and by selecting the appropriate laser frequencies we may induce the interaction (1) with either the center-of-mass mode or the stretch vibrational mode, represented by the ladder operators a and $a^\dagger$. η is the Lamb-Dicke parameter, which enters because we want the photonic recoil to excite the atomic motion, and σ_{+i} is the spin raising operator describing excitation of ion i.

H_{int} couples the states $|ggn\rangle \leftrightarrow \{|egn \pm k\rangle, |gen \pm k\rangle\} \leftrightarrow |een\rangle$, where the first (second) letter denotes the internal state e or g of the first (second) ion and n, $n \pm k$ is the quantum number for the vibrational mode of the ions in the trap, see Fig. 1. The only energy conserving transitions are between the states $|ggn\rangle$ and $|een\rangle$ and between $|egn\rangle$ and $|gen\rangle$. We choose laser frequencies away from resonances so that no intermediate states $|egn \pm k\rangle$ and $|gen \pm k\rangle$ are populated in the process.

The Rabi frequency $\tilde{\Omega}$ for the transition between $|ggn\rangle$ and $|een\rangle$, via intermediate states m, can be determined by second order perturbation theory,

$$\left(\frac{\tilde{\Omega}}{2}\right)^2 = \left| \sum_m \frac{\langle een|H_{\text{int}}|m\rangle\langle m|H_{\text{int}}|ggn\rangle}{E_{ggn} + \omega_j - E_m} \right|^2, \tag{2}$$

where the laser energy ω_j is the energy of the laser exciting the intermediate state $|m\rangle$. If the laser detuning $\delta$is not too far from the frequency $\nu$of the collective vibration in the trap we may restrict the sum to $|m\rangle = |egn \pm 1\rangle$ and $|gen \pm 1\rangle$, and we get

$$\tilde{\Omega} = -\frac{(\Omega\eta)^2}{\nu - \delta}, \tag{3}$$

where $\Omega = \Omega_{ij}$ is assumed to be the same for both ions and for both laser fields.

Eq. (3) contains no dependence on the vibrational quantum number n. This is due to interference between the paths indicated in Fig. 1. If we take a path involving $|n+1\rangle$, we have a factor of $n+1$ appearing in the numerator ($\sqrt{n+1}$ from raising and $\sqrt{n+1}$ from lowering the vibrational quantum number). In paths

involving $|n-1\rangle$ we obtain a factor of n. Due to the opposite detunings, the denominators in Eq. (2) have opposite signs and the n dependence disappears when the two terms are subtracted. The coherent evolution of the internal atomic state is thus insensitive to the vibrational quantum numbers, and it may be observed with ions in any superposition or mixture of vibrational states. The vibrational state may even change due to heating during the gate as confirmed by Monte Carlo wave function simulations in Ref.[6].

No particularly demanding assumptions are required for the experimental parameters. With a vibrational frequency $\nu/2\pi = 200$ kHz, and Rabi frequencies $\Omega/2\pi$ of modest 20 kHz, a coherent evolution from $|gg\rangle$ to $|ee\rangle$ is accomplished in few ms. Due to our use of off-resonant interactions instead of resonant couplings, however, this time scale is much longer than the time scale possible in the original ion trap proposal [1].

3 Fast two-color gate: an operator "multiplication engine"

In the Lamb-Dicke approximation our bichromatic interaction Hamiltonian has a simple harmonic time dependence in the interaction picture with respect to the atomic and vibrational Hamiltonian

$$H_{\rm int} = -\sqrt{2}\eta\Omega J_y[x\cos(\nu-\delta)t + p\sin(\nu-\delta)t], \tag{4}$$

where we have introduced the dimensionless position and momentum operators for the centre-of-mass vibrational mode $x = \frac{1}{\sqrt{2}}(a+a^\dagger)$ and $p = \frac{i}{\sqrt{2}}(a^\dagger - a)$, and where we have introduced the collective internal state observable $J_y = \frac{\hbar}{2}(\sigma_{y,i} + \sigma_{y,j})$ in terms of Pauli spin matrices for the two ions illuminated.

The exact propagator for the Hamiltonian (4) can be represented by the ansatz

$$U(t) = \mathrm{e}^{-iA(t)J_y^2}\mathrm{e}^{-iF(t)J_y x}\mathrm{e}^{-iG(t)J_y p}, \tag{5}$$

where the Schrödinger equation $i\frac{d}{dt}U(t) = HU(t)$ leads to the expressions $F(t) = -\sqrt{2}\eta\Omega\int_0^t \cos((\nu-\delta)t')dt'$, $G(t) = -\sqrt{2}\eta\Omega\int_0^t \sin((\nu-\delta)t')dt'$, and $A(t) = \sqrt{2}\eta\Omega\int_0^t F(t')\sin((\nu-\delta)t')dt'$.

If $F(t)$ and $G(t)$ both vanish after a period τ, at this instant the propagator reduces to $U(\tau) = \mathrm{e}^{-iA(\tau)J_y^2}$, *i.e.*, the vibrational motion is returned to its original state, be it the ground state or any vibrationally excited state, and we are left with an internal state evolution which is *independent* of the external vibrational state. Note that $(\sigma_y)^2 = 1$ implies that $J_y^2 = \frac{\hbar^2}{4}(2+2\sigma_{y,i}\sigma_{y,j})$, yielding an interaction that couples $|gg\rangle$ and $|ee\rangle$. The timing so that $G(\tau)$ and $F(\tau)$ vanish allows faster gate operation than in Section 2, because we tolerate that the internal state is strongly entangled with the vibrational motion in the course of the gate.

The interpretation of this rather miraculous phenomenon follows a proposal by Milburn [10]: Adjusting the phases of laser fields resonant with side band transitions, one may couple internal state operators to different quadrature components, so as to produce effective Hamiltonians $H_1 = \lambda_1 J_y x$ and $H_2 = \lambda_2 J_y p$. By alternating

square pulse application of the Hamiltonians H_1 and H_2 we obtain by use of the Baker-Hausdorff relation the propagator

$$e^{iH_2\tau}e^{iH_1\tau}e^{-iH_2\tau}e^{-iH_1\tau} = e^{i\lambda_1\lambda_2 J_y^2\tau^2} \tag{6}$$

because the commutator of the oscillator position and momentum is a constant. Since H_1 and H_2 are proportional to the generators for displacements of momentum and position, respectively, the equation (6) shows that after operator valued phase space translations of $\pm\lambda_i J_y\tau$, the oscillator returns to its original state, but an effective Hamiltonian has been synthesized which is the operator product of the internal state parts of H_1 and H_2. A round trip in the oscillator phase space provides a "multiplication engine" for qubit Hamiltonians.

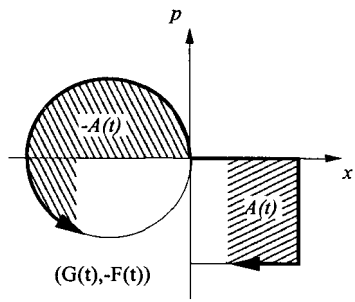

Figure 2: The paths traversed in phase space and a geometric representation of the function $A(t)$ in case of pulsed (rectangular path) and harmonic (circular path) interaction.

The bichromatic and the square pulse operations are both sketched in Fig.(2), where the geometric interpretation of the resulting operation as an area is clearly displayed. The actual spatial displacements are entangled with the internal states, and it is easiest to understand the Figure by considering eigenstates of the relevant internal state operators. All internal states follow similar curves but scaled according to the magnitude of the eigenvalues, hence the encircled area becomes internal operator valued, as in Eqs.(4,5). The shared oscillator degree of freedom thus provides a phase space for geometric excursions, in strong analogy with proposals for quantum gate operation using geometric (Berry) phases related to excursion in spin degrees of freedom [7]. The oscillator offers the special feature, that the phase area does not depend on its initial state, the paths in the Figure do not need to begin and end at the origin in phase space.

In Fig. 3 (a) we show results of the slow gate evolution, which is also described by Eq. (5), but where $F(t)$ and $G(t)$ are always small, so that the internal state is always disentagled from the harmonic oscillator. (The non-zero values of $F(t)$ and $G(t)$ are responsible for the small fast oscillations in the figure). The slow gate may be stopped when $A(t) \approx \tilde{\Omega}t$ has acquired the desired value, irrespective of the current value of $F(t)$ and $G(t)$. In Fig. 3 (b), we show the fast gate operation, where $(\nu - \delta)t = 2 \cdot 2\pi$ at the time $\nu t \approx 250$, where the maximally entangled state $\frac{1}{\sqrt{2}}(|gg\rangle - i|ee\rangle)$ is created.

In comparison with the slow gate, the fast gate is not as tolerant to heating of the ionic motion. For a detailed analysis of error mechanisms and their influence on gate fidelities, see [8].

Incidentally, it turns out [9] that by application of the collective spin operator J_y^2 to a whole string of ions, we may generate a maximally entangled state

$$|\Psi\rangle = \frac{1}{\sqrt{2}}(e^{i\phi_g}|gg...g\rangle + e^{i\phi_e}|ee...e\rangle), \tag{7}$$

for any number of ions, by simply illuminating all ions with the bichromatic light. By use of the fast bichromatic gate this has been demonstrated for 4 ions [11].

4 Trigonometric and multi-bit gates

H_1 and H_2 do not have to involve the same internal state operator J_y. For any commuting operators $\hat{A}$ and $\hat{B}$ it is the product of these operators that appears in place of J_y^2 in Eq. (6). $\hat{A}$ and $\hat{B}$ may for example be operators acting on two different qubits so that a two-qubit gate is produced. A C-NOT gate, for example is obtained by using $\hat{A} = (\sigma_{z,1} + 1)/2$, $\hat{B} = \sigma_{x,2}$and $\lambda_1\lambda_2\tau^2 = \pi/2$.

In combination with single particle qubit operations, the C-NOT gate suffices to produce any unitary operation acting on all the bits [12]. The C^2-NOT or Toffoli gate described in Ref. [12] thus involves 4 one-bit gates and 3 two-bit gates. Experimentally, each gate corresponds to turning on a given Hamiltonian for a certain duration and each gate adds an experimental complication and/or possibility of error. We will now show that one may extend the trick in Sec. 3. to produce higher order gates directly.

According to our geometric interpretation, two operators act as the sides of a rectangle, whose area becomes the product of the two. To produce terms which are products of more than two operators it would thus seem necessary to consider a volume in an even larger phase space, but there is, in fact, no reason that a 2-dimensional area should not be expressible as a product of three terms or more. In Fig. 4, we indicate a trajectory in phase space which follows the outline of a

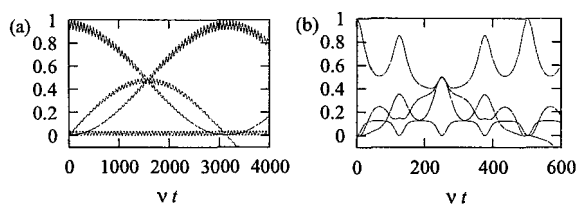

Figure 3: Time evolution of density matrix elements calculated using (5). (a) Pertubative regime (b) Fast gate. The first curve (counting from above at $\nu t \approx 1000$ in (a) and $\nu t \approx 130$ in (b)) represents $\rho_{gg,gg}$, the second is the imaginary part of $\rho_{gg,ee}$, the third is $\rho_{ee,ee}$, and the last curve is the real part of $\rho_{gg,ee}$. In (a) the physical parameters are $\delta = 0.9\nu$, $\eta = 0.1$, and $\Omega = 0.1\nu$. In (b) the physical parameters are $\delta = 0.95\nu$, $\eta = 0.1$, and $\Omega = 0.177\nu$. The parameters in (b) are chosen such that a maximally entangled state $\frac{1}{\sqrt{2}}(|gg\rangle - i|ee\rangle)$ is formed at the time $\nu t \approx 250$.

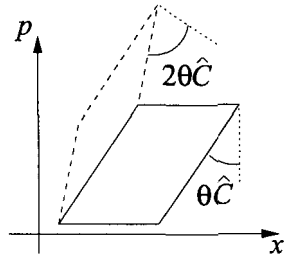

Figure 4: Translations in xp-phase space of the oscillator during gate operation: By application of an interaction proportional to $\hat{C}n$, the displacement along the p-direction in Fig.2 is rotated into another direction given by the angle $\theta\hat{C}$, and the phase space displacements follow the outline of a parallelogram whose enclosed area becomes $\lambda_1\lambda_2\hat{A}\hat{B}\cos(\theta\hat{C})$.

parallelogram, whose area is the product of the lengths *and* of the cosine function of the angle indicated in the figure. In our case, we want this angle to contain an internal state operator, and we hence impose a Hamiltonian $H = \omega\hat{C}n$ to the system, where n is the number operator for the oscillator. This yields, after a time $t = \theta/\omega$, $\exp(i\theta\hat{C}n)x\exp(-i\theta\hat{C}n) = \cos(\theta\hat{C})x + \sin(\theta\hat{C})p$, so that a displacement along the p-axis at this stage is equivalent to a displacement along a direction making the angle $\theta\hat{C}$ with the p-axis (in the $t = 0$ Heisenberg picture). Successive applications of $\lambda_1\hat{A}x$, $\lambda_2\hat{B}p$ and $\omega\hat{C}n$, thus produces the geometric area $\lambda_1\lambda_2\hat{A}\hat{B}\cos(\theta\hat{C})$, *i.e.* an operator involving a product of three internal state operators.

We now consider the outcome of applying an interaction which may be described by

$$H(t) = u(t)\hat{A}x + v(t)\hat{B}p + s(t)\hat{C}n, \tag{8}$$

where $\hat{A}$, $\hat{B}$ and $\hat{C}$ are commuting operators acting on the internal states of the atoms, and u, v, and s are arbitrary functions of time. With this Hamiltonian the time dependent Schrödinger equation for the propagator $idU(t)/dt = H(t)U(t)$ has the solution

$$U = \mathrm{e}^{-i\hat{W}(t)}\mathrm{e}^{-in\hat{S}(t)}\mathrm{e}^{-ix\hat{U}(t)}\mathrm{e}^{-ip\hat{V}(t)}, \tag{9}$$

with

$$\begin{aligned}
\hat{S}(t) &= \hat{C}\int_0^t s(t')dt' \\
\hat{U}(t) &= \int_0^t \hat{A}u(t')\cos(\hat{S}(t')) - \hat{B}v(t')\sin(\hat{S}(t'))dt' \\
\hat{V}(t) &= \int_0^t \hat{B}v(t')\cos(\hat{S}(t')) + \hat{A}u(t')\sin(\hat{S}(t'))dt' \\
\hat{W}(t) &= \int_0^t \hat{U}(t')[\hat{B}v(t')\cos(\hat{S}(t')) + \hat{A}u(t')\sin(\hat{S}(t'))]dt'.
\end{aligned} \tag{10}$$

In the xp-phase space the net action of the propagator is to perform translations $(x,p) \to (x + \hat{V}(t), p - \hat{U}(t))$ followed by a rotation by an angle $\hat{S}(t)$ around the

origin. Since the functions $\hat{U}$, $\hat{V}$, and $\hat{S}$ involve the internal state operators $\hat{A}$, $\hat{B}$, and $\hat{C}$, the translation and rotation is entangled with the internal states of the bits. We now generalize the trick applied in the previous section to ensure that $\hat{U}$, $\hat{V}$, and $\hat{S}$ vanish after a certain time τ, such that the harmonic oscillator is returned to its initial state and we are left with an internal state evolution operator $\exp(-i\hat{W}(\tau))$. As expected from our geometrical analysis, the expression for $W(\tau)$ in (10) contains products of $\hat{A}$, $\hat{B}$ and trigonometric functions of $\hat{C}$.

For a single qubit operator, expressed in terms of Pauli spin matrices, we have $\sin(\theta\sigma) = \sin(\theta)\sigma$, and we can thus produce three-bit gates directly. Consider three bits which are subject to the time independent Hamiltonian

$$H = \Omega\left(\frac{\sigma_{z1} + \sigma_{z2} + 1}{4\sqrt{M}}x + \sigma_{x3}\left(n - \frac{1}{32M}\right)\right), \tag{11}$$

where M is an integer. After a duration $\tau = M2\pi/\Omega$ the propagator (9) reduces to $\exp(-i\pi[(\sigma_{z1} + \sigma_{z2} + 1)^2 - 1]\sigma_{x3}/16) = \exp(-i\pi(\sigma_{z1} + 1)(\sigma_{z2} + 1)\sigma_{x3}/8)$, which is exactly the Toffoli gate. In the ion trap quantum computer this gate can be achieved by applying a single pulse of suitably directed and detuned fields to the ions.

5 Applications of $\cos(\theta\hat{C})$

Rather than the product of three operators, we have in the general case the product of two operators and a trigonometric function of the third one. This raises the question of applicability of such a product. It is rather cool to have so easy access to such a complicated operation, and one may imagine direct applications of periodic operator functions for the manipulation of enlarged codewords for qubits which encode $|0\rangle$ and $|1\rangle$ onto states with, e.g., 0, 6, 12 and 18 excitations and with 3, 9, 15 and 21 excitations, respectively [13].

Here, we shall outline some ideas making explicit use of the trigonometric function for quantum computing. Our basic idea is that access to trigonometric functions of a bounded operator implies access to any function of the operator by Fourier transformation.

The projection operator on the space where all bits are in the $|1\rangle$ state can be expressed as product of single particle projection operators $\prod_{l=1}^{n}(\sigma_{lz}+1)/2$. We now observe that if and only if all qubits are in the $|1\rangle$ state, the product $\prod_{l=1}^{n_c}\frac{(\sigma_{lz}+1)}{2}$ is equal to unity, but also the sum $\hat{J}_z - J = \sum_{l=1}^{n_c}\frac{(\sigma_{jz}-1)}{2}$ only vanishes in that state.

We now use the Fourier transform $\sum_{k=1}^{m}\cos(2\pi\frac{k}{m}N) = m\delta(N \bmod m)$ which can also be applied to operators so that:

$$\prod_{l}^{n}\frac{(\sigma_{lz}+1)}{2} = (n+1)^{-1}\sum_{k=1}^{n+1}\cos\left(\frac{2\pi k}{n+1}(\hat{J}_z - J)\right). \tag{12}$$

We can thus implement the projection operator on the state where all qubits are in the $|1\rangle$ state. More interestingly, we can apply NOT-operations to a selected subset of qubits before and after the projection operator, which will then produce

the projection operator on any desired state of the register, and we can choose to apply such a projection to only a subset of the qubits. We still have room to choose operators $\hat{A}$ and $\hat{B}$, and implement for example a NOT operation on one qubit controlled by a specific state of the other qubits.

To implement the unitary operator which can be written on the form $\exp(-i\mu\hat{A}\cos(\theta\hat{C}))$, where $\hat{A}$ and $\hat{C}$ are internal state operators, we follow the construction of the parallelogram in Fig.4. First, we apply a Hamiltonian proportional to $\hat{A}p$ which performs a translation along the x-axis. Then a Hamiltonian $H \sim \hat{C}n$ makes a rotation by an angle θ, and we perform a translation along the p-axis. By using the operator identity (12) we can devise a C^{n_c}-NOT gate by following the outline of $n_c + 1$ such parallelograms, one after the other. By rotating each parallelogram, so that the first linear displacement is precisely opposite of the last displacement of the previous parallelogram, we can save half of the operations, as indicated in Fig.4. Note that the sum over l implicit in the $\hat{J}_z$ term in Eq. (12) just amounts to illuminating several qubits instead of a single qubit at a time.

In 1997, Grover presented a search algorithm [14] that identifies the single value x_0t hat fulfills $f(x_0) = 1$ for a function $f(x)$ provided, *e.g.*, by an oracle (all other arguments lead to vanishing values of the function). If x is an integer on the range between 0 and $N - 1 = 2^n - 1$, the search algorithm is able to find $x_0$aft er on the order of $\sqrt{N}$ evaluations of the function. Grover's algorithm has been demonstrated on NMR few qubit systems [15]. In the following we show how our proposal can be used to implement the search algorithm.

The quantum algorithm first prepares an initial trial state vector populating all basis states with equal probability. For demonstration purposes, the function $f(x)$ can be encoded by letting the state of the register undergo a transformation where the amplitude of the x_0 component changes sign and all other amplitudes are left unchanged. This step can be implemented by writing x_0 in binary form, $b_0b_1b_2...b_{n-1}$, $b_i = 0$ or 1, and by applying the unitary operator

$$U_f = \exp\left(i\pi\Pi_{i=0}^{n-1}\left(\frac{\sigma_{iz} + 2b_i - 1}{2}\right)\right). \tag{13}$$

The crucial step in Grover's algorithm is the 'inversion about the mean', where the amplitude with the sign changed will grow in comparison with the other amplitudes. The inversion about the mean is given by the unitary matrix [14]

$$U_G = \frac{2}{N}M - I, \tag{14}$$

where I is the $N \times N$ identity matrix, and M is the $N \times N$ matrix with unit elements in all positions.

In the standard binary basis, the matrix M couples all states to any other state, and it can be written as the tensor product $\Pi_{i=0}^{n-1}(\sigma_{ix} + 1)$, where the single qubit operators $\sigma_{ix} + 1$ are 2×2 matrices with unit elements in all positions. A straightforward calculation shows [16] that $\exp((i\pi/N)M) = I - \frac{2}{N}M$, which apart from an irrelevant global phase yields precisely the inversion about the mean. The inversion about the mean is therefore produced directly by the action of the following

multi-particle operator

$$U_G = \exp\left(i\pi\Pi_{i=0}^{n-1}\left(\frac{\sigma_{ix}+1}{2}\right)\right), \tag{15}$$

where we used $N = 2^n$.

Both U_f and U_G can be implemented effectively using (12). To implement the function (13), it is easiest to first invert all the bits, which have the value zero in x_0, so that U_f on that state should encode only unit bit values, *i.e.*, precisely the operator described in (12). After application of this simple U_f, the qubits encoding the value zero should be flipped back again. All qubits should then have their $\sigma_x$comp onents rotated into the z-direction, to use again the operation in (12) to implement U_G, which is the same operator, defined for the x-components of the spins.

Further examples of specific gate construction and of the use of trigonometric gates are presented in [17].

6 Conclusion

In summary, we have presented a technique to produce multi-bit gates in quantum computers where all qubits are coupled to a joint harmonic oscillator degree of freedom. We have derived general expressions, and we have exemplified the method by suggestions for the generation of C^n-NOT gates and a complete Grover search algorithm. It is known how to make C^2-NOT and C^3-NOT gates by means of one- and two-bit gates, but it is difficult to make a theoretical comparison of these implementations with our proposal, since we build up the desired one-, two- and multi-bit interactions continuously in time.

The essential operation in the Grover search (15) is implemented without individual access to the qubits and, *e.g.*, in the ion trap it is much easier to implement the Hamiltonian $H = \sum_i(\sigma_{iz} - 1)n$ than just a single term $H = (\sigma_{iz} - 1)n$ in that sum. In addition, it is an experimental advantage to apply as few control Hamiltonians as possible, since imprecision in timing accumulates if many operations are needed.

A recent preprint [18] has addressed the achievements of so-called 'concurrent quantum computing', in which access to multi-bit interaction Hamiltonians of the form $\Pi_i\sigma_{z,i}$ is assumed, where the number of terms in the product can be chosen at will. That paper presents ideas for Grover's and Shor's algorithm, without suggesting a practical means to implement the interaction. We believe that our paper provides a proposal for such implementation.

A feature of our proposal worth mentioning is that all operations are expressed as unitary gates acting on the qubit degrees of freedom. The oscillator is certainly important, but at the end of the gates the qubits actually decouple from the oscillator. One consequence is that the initial state of the oscillator does not even have to be specified. It can be in the ground state, an excited state, or even in an incoherent mixture of states, possibly entangled with environmental degrees of freedom, as long as this entanglement does not evolve during gate operation. In this way our proposal differs significantly from the recent proposal of hybrid computing [19],

where the oscillator degrees of freedom take active part in the calculation. The commutator relations for the oscillator operators were crucial for our argument: as shown in [8], a finite dimensional 'data-bus' cannot provide operators having a non-vanishing c-number commutator as x and p or a and $a^\dagger$. If, however, the qubits interact with a finite dimensional system, which is in a known initial state, this may be used just the same way (*e.g.*, in an eigenstate of the angular momentum operator J_z, the commutator of J_x and $J_y$is a c-number).

References

1. J. I. Cirac and P. Zoller, Phys. Rev. Lett. **74**, 4091 (1995).
2. X. Maitre *et al.*, Phys. Rev. Lett. **79**, 769 (1997); P. W. H. Pinkse, *et al.*, Nature **404**, 365 (2000); C. J. Hood *et al.*, Science **287**, 1447 (2000).
3. G. R. Guthörlein *et al*, Nature **414**, 49 (2001); J. Pachos and H. Walther, quant-ph/0111088.
4. A. Imamoglu, et al., Phys. Rev. Lett **83**, 4204 (1999).
5. Yu. Makhlin *et al*, Nature **386**, 305 (1999).
6. A. Sørensen and K. Mølmer, Phys. Rev. Lett. **82**, 1971 (1999).
7. J. Jones *et al*, Nature **403**, 869 (2000); G. Falci *et al*, Nature **407**, 355 (2000); L.-M. Duan *et al*, Science **292**, 1695 (2001).
8. A. Sørensen and K. Mølmer, Phys. Rev. A **62**, 022311, (2000).
9. K. Mølmer and A. Sørensen, Phys. Rev. Lett. **82**, 1835 (1999).
10. G. Milburn, quant-ph/9908037.
11. C. A. Sackett, *et al.*, Nature **404**, 256 (2000).
12. A. Barenco et al, Phys. Rev. A **52**, 3457 (1995).
13. D. Gottesman, A. Kitaev, and J. Preskill, Phys. Rev. A **64**, 012310 (2001).
14. L.K. Grover, Phys. Rev. Lett. **79**, 325 (1997).
15. I. L. Chuang *et al*, Phys. Rev. Lett. **80**, 3408 (1998); J. A. Jones *et al*, Nature **393**, 344 (1998).
16. X. Wang, A. Sørensen and K. Mølmer, Phys. Rev. Lett. **86**, 3907 (2001).
17. X. Wang and P. Zanardi, Phys. Rev. A **65**, 032327 (2002).
18. F.Yamaguchi *et al*, quant-ph/0005128.
19. S. Lloyd, quant-ph/0008057.

DISCUSSION

Chairman: P. Zoller

L. Stodolsky: I think I understood that you essentially use what is mathematically $SU(2)$ and then sort of higher spins on SU(2) for this geometric phase arguments.

K. Mølmer: I actually use the harmonic oscillator phase space and the associated mathematical group of translations, not rotations as $SU(2)$.

L. Stodolsky: But, you are using the result, I think, that the geometric phase does not depend on any particular representation of $SU(2)$, something, we actu-

ally showed a long time ago. I want to make a remark that people in this field might be interested in the fact, that you can use, let's say, $SU(3)$. If you use a three-dimensional phase space you can have more information than in the spin 1 representation of $SU(2)$ and the geometric phase will be different.

K. Mølmer: I am not sure if I fully understand your proposal. Let me make a remark about an important property of the harmonic oscillator phase space in contrast to the rotation groups which have only finite representations: the trick that we are using really needs the commutator of my operators, x and p, to be a c-number. And this can only happen for operators acting on an infinite-dimensional Hilbert space! If you use the rotation group, any finite representation of that will not give you this particular commutator. That's not to say that we cannot use finite-dimensional quantum degrees of freedom as 'data-bus' to communicate the interaction between qubits. It just means that in this case you have to start with a well-known state of your 'bus system', if you are in an eigenstate of the commutator in question, it is effectively a c-number. In the oscillator case, in contrast, I can start in any point in phase space and I automatically return to the same point at the end of the gate.

L. Stodolsky: Still I think my remark may be relevant, maybe not for your talk if you are using qubits, but for generalizations to some representation of $SU(2)$.

K. Mølmer: I agree that you can invoke geometrical pictures also for finite dimensional representations. In fact this is what we do if we use interwining qubits to communicate between spatially remote qubits. So I don't disagree with what you say.

S. Lloyd: The oscillators from most applications we can use are in a thermal state. Could you comment on how realistic is this in terms of say ion traps, if you can do that?

K. Mølmer: We cannot allow the trap to be in just any thermal state, because when we are writing our Hamiltonian, we use an approximation that relies on the excursions of the particles being smaller than the wavelength of the radiation. You have to cool your ions by laser cooling or other means to have an average excitation n_{th} which is small enough, for example 10 if your trap is tight enough. Our proposal also works for cavity QED experiments where the vibrational motion is replaced by the cavity field, which also has to be restricted to not too large numbers. The group of Dave Wineland uses these methods in ion traps. We have made complete calculations, that I did not show in my talk, of the reduction in gate fidelity when you take finite temperatures and heating into account. Due to the increase in the number of vibrational modes in the trap, this admittedly becomes a more and more serious problem, the more particles you have in the trap.

L. Accardi: I understand mathematically your commutation trick, but this coupling of $\sigma_y$wit h x on the one side, and the p on the other side, can you deduce that from some physically fundamental interaction? Because otherwise there is a realisability problem. Can you implement?

K. Mølmer: I know I was going a little bit fast during the talk. Using radiation we can excite the atomic state and this is represented by the σ_x operator which couples the ground and excited state. If the radiation has a frequency which is higher than the atomic transition frequency by exactly the trap frequency, then you will at

the same time resonantly excite the center-of-mass motion in the trap, so therefore you have both the atomic excitation and the $a^\dagger$ acting on the motional state. The corresponding de-excitation process introduces a, and x and p appear as suitable combinations of these two terms. Of course, you need a spatially dependent coupling to actually couple different motional states, but the laser field has a wavelength, and hence such a dependence. In fact, the laser wavelength is related to the photon momentum, and this offers the picture of the atom being excited and spatially kicked by the photon recoil at the same time. Hamiltonians of the kind that I have discussed have indeed been made in the experimental ion trapping groups.

BELL'S INEQUALITIES

KARL GUSTAFSON*
Department of Mathematics, University of Colorado, Boulder, CO 80309-0395 USA

Much of the Bell Theory for quantum mechanics may be placed within a general operator trigonometry which I developed independently about 35 years ago. From that mathematical viewpoint, certain issues in the Bell theory are seen as "just geometry".

1 Introduction and Conclusions

Many issues combine for consideration when speaking of Bell's Inequalities: non-locality, realism, hidden variables, incompatible measures, wave function collapse, other. Each of these issues then may be viewed from several viewpoints: historical, theoretical, physical, experimental, statistical, communicational, cryptographical, and mathematical. Here I will stress the latter viewpoint. In particular, I will show that much of the Bell theory for quantum spin probabilities may be placed within a general operator trigonometry which I developed independently about 35 years ago. From that mathematical viewpoint, much of the Bell theory is "just geometry".

In Section 2 I will provide some background for the issues and the viewpoints surrounding Bell's Inequalities. Much has been written/published on these matters so here I will just present a few key facts and some bibliography for the interested reader. In Section 3 I will quickly expose the key aspects of my operator trigonometry which enable one to embed much of the Bell theory within it. In Section 4 I further explore the improved geometrical understandings of the Bell theory from the trigonometric and mathematical viewpoint. Sections 5 and 6 present very brief coments on probabilistic and physical understandings. Section 7 contains additional remarks prompted by a referee.

As in my presentation at the 22nd Solvay Conference on Physics (Delphi, Greece, 24-29 November, 2001), I will state the principal conclusions now. First, from the operator trigonometry we have the following key geometrical fact:

Theorem 1.1 *Let x, y, z be any 3 nonzero vectors in a real or complex Hilbert space of any dimension. We take $\|x\| = \|y\| = \|z\| = 1$ for convenience. From $\langle x, y\rangle = a_1 + ib_1$, $\langle y, z\rangle = a_2 + ib_2$, $\langle x, z\rangle = a_3 + ib_3$, define angles $\phi_{xy}, \phi_{yz}, \phi_{xz}$ in $[0, \pi]$ by $\cos\phi_{xy} = a_1$, $\cos_{yz} = a_2$, $\cos\phi_{xz} = a_3$. Then there holds the general triangle inequality*

$$\phi_{xz} \leqq \phi_{xy} + \phi_{yz} \tag{1.1}$$

The following conclusions follow from the Theorem and related considerations to be discussed in the rest of this paper.

Corollary 1.1 *Much of the Bell (1965), Wigner (1970), Accardi (1982), Gudder–Zanghi (1984), Herbert–Peres (1993), Williams–Clearwater (1998), Khrennikov*

*ALSO AT INTERNATIONAL SOLVAY INSTITUTES FOR PHYSICS AND CHEMISTRY, 1050 BRUSSELS, BELGIUM

(2000), others, considerations are contained in the above Theorem.

Corollary 1.2 *The Bell–Wigner inequality is a necessary condition for a Kolmogorovian probability model to apply to those situations. The Accardi–Gustafson inequality is a necessary condition for a quantum mechanical probability model to apply to those situations*

Corollary 1.3 *From the mathematical viewpoint of this paper, one cannot argue "nonlocality" on the basis of violation of Bell's Inequality.*

2 Bell Theory

One can take the Bell Theory back to the early days of quantum mechanics and its interpretations. Although quantum mechanics "works", some of its fundamental theoretical underpinnings are not fully understood to this day. Bell's inequalities attempted to remove some of this confusion by providing "tests" of the validity of certain assumptions of quantum mechanics. However, it seems that Bell's inequalities also added to the confusion in some ways. Following is just a sketch of some of the related developments in this story. The reader may find a huge literature on these matters elsewhere.

The 1935 paper [1] of Albert Einstein, Boris Podolsky and Nathan Rosen was a *gedankenexperiment* which purported to demonstrate that quantum mechanics cannot provide a complete description of reality. According to the extensive account [2] of Jammer, although much of the actual EPR paper [1] was written by Podolsky, the origins of this paper go back to 1930 when Niels Bohr 'defeated' Einstein's earlier *gedankenexperiment* presented at the Sixth Solvay Congress in Brussels in 1930, an important episode in in the famous ongoing debate between the two which had begun already ten years earlier in 1920. To better present his view, Einstein then, along with Richard Tolman and Podolsky, wrote a paper [3] with another *gedankenexperiment* which argued that if one accepted quantum mechanic's uncertainty principle, then one could not even predict the past, let alone the future. Also Einstein sharpened his arguments by shifting attention away from direct attacks on the uncertainty principle itself but instead with more focus on logical paradoxes which would follow from it [4]. Moreover Einstein modified his photon box *gedankenexperiments* with their paradoxical consequences to the more clear-cut two particle *gedankenexperiment* which appears in the 1935 EPR paper [1]. Erwin Schrödinger immediately agreed with the EPR argument, reformulated it, and came up with his own *gedankenexperiment* now known as his half-dead half-alive cat [5].

The conclusion of the groundbreaking paper[1] was: "While we have thus shown that the wave function does not provide a complete description of the physical reality, we left open the question of whether or not such a description exists. We believe, however, that such a theory is possible." Thus the emphasis in [1] was on inadequacies of a theory in which all information is in the wave function. In 1951 David Bohm [6] responded by reformulating the EPR argument to one expressed more simply in terms of spin functions, and presented an argument that "no theory of mechanically determined hidden variables can lead to all of the results of the quantum theory." Nonetheless Bohm then introduced his version of such a hidden variable theory. This was like earlier semiclassical hydrodynamical or pilot wave

quantum models, except for two new features. First, the existence of a quantum mechanical potential, shall we say among all of the particles in a considered ensemble ψ, was assumed. Second, each particle trajectory will be well-posed if you know its initial condition. But because the initial position could not be experimentally measured, it is a hidden variable.

In 1964 Bell [7] presented his famous inequality and exhibited certain quantum spin measurement configurations whose quantum expectation values could not satisfy his inequality. Bell's analysis assumes that physical systems, e.g. two measuring apparatuses, can be regarded as physically totally separated, in the sense of being free of any effects one from the other. Thus his inequality could provide a 'test' which could be failed by measurements performed on correlated quantum systems. In particular it was argued in [7] that local realistic hidden variable theories could not hold. However, the exact nature of hidden variables as viewed by Bell is unclear from [7].

As is well known the 1982 physical experiments of Aspect *et al.* [8] demonstrated that beyond any reasonable doubt the Bell inequalities are violated by certain quantum systems, and papers continue to appear with further demonstrated violations.

In a 1970 paper [9], Wigner simplified and clarified in several ways the argument of Bell. Wigner assumed that all possible measurements are predetermined, even if they involve incompatible observables, and moreover any measurement on one of two apparatuses does not change the preset outcomes of measurements on the other apparatus. Thus the meanings of locality and realism are made more clear and both assumptions are present in the model setup. It is helpful to imagine, for example, that the 'hidden variable' is just the directional orientation of each of the two apparatuses, each of which can be thought of as just a three-dimensional possibly skew coordinate system, for example. Then two spin 1/2 particles are sent to the apparatuses, each to one, both coming from a common atomic source, with perfect anticorrelation and singlet properties. Nine measurements are then needed to simultaneously measure the direction vectors $\omega_1, \omega_2, \omega_3$ of the two spins. Each spin has two possible values $1/2 \equiv +$, $-1/2 \equiv -$, so each measurement can permit four relative results: $++$, $--$, $+-$, $-+$. Therefore there are 4^9 possible outcomes. Wigner then assumes that the spins are not affected by the orientation of the particular measuring apparatus. This reduces the outcomes to 2^6 possibilities. For example, if the hidden variables are in the possibility domain $(+,-,-,;-+-)$, then the measurement of the spin component of the first particle in the ω_1 direction will yield value spin $= +$, no matter what direction the spin of the second particle is measured.

Although Wigner [9] doesn't state any theorems, I would now like to formalize his argument into theorem form here because it will be helpful later on in this paper. I will, however, use Wigner's notation.

Theorem 2.1 *In the above setup, let $\theta_{12}, \theta_{23}, \theta_{31}$ be the angles between the three directions $\omega_1, \omega_2, \omega_3$. Then the probability that the spin component of particle 1 in the ω_i direction and the spin component of particle 2 in the ω_k direction both measure $+$ or both measure $-$ is $\frac{1}{2}\sin^2\left(\frac{\theta_{ik}}{2}\right)$. Otherwise the probability of measurements $+-$ or $-+$ is $\frac{1}{2}\cos^2\left(\frac{\theta_{ik}}{2}\right)$.*

Proof: The singlet state is assumed to be spherically symmetric so that the total

probability of the first particle's spin being in the opposite direction is also 1/2. The probability that the measurement of the spin component of the first particle in the ω_i direction and the measurement of the spin component of the second particle in the ω_k direction are both of the same sign is $\frac{1}{2}\sin^2(\theta_{ik}/2)$ because otherwise the probability is $\frac{1}{2}\cos^2(\theta_{ik}/2)$ and these two conditional probabilities must be equal and add to 1. The fact that such quantum spin probabilities are given trigonometrically as $|\langle\psi(\omega_i),\psi(\omega_k)\rangle|^2 = \cos^2(\theta_{ik}/2)$ in terms of the angle θ_{ik} between directions ω_i and ω_k is a special property of spin systems and for example the Eulerian angle representation for $SU(2)$, see, e.g. ([10], p. 225). ■

Wigner [9] states that one can obtain these conditional quantum probability expressions "by direct calculation" but does not provide it and instead offers roughly the above argument, but with no mention as to the origin of his particular trigonometric expressions. Of course we all know that quantum probabilities within a Hilbert space model become inner products which for normalized state vectors become cosines, but I want to emphasize here the particular nature of these particular spin models which give such particular trigonometric expressions, because those will tie directly my earlier general operator trigonometry to those quantum spin probabilities.

Bell's inequality [7] gave a necessary condition for the existence of a classical, e.g. Kolmogorovian, probability model for a given set of correlation functions. This inequality was not satisfied by all of the possible quantum mechanical correlations of two-spin systems in a singlet state. Wigner [9] corrected the posing of Bell's question, to place the issues squarely within a quantum mechanical Hilbert space, and with the issues directed at appropriate quantum mechanical conditional probabilities. In 1982 Accardi and Fedullo [11] went further. Let $A, B, C, \ldots$ denote observable entities with possible real values $a_\alpha, b_\beta, c_\gamma, \ldots$ respectively. Let $P(A = a_\alpha \,|B\, = b_\beta)$ denote the conditional probability that observable A has value a_α given that observable B has value b_β, likewise for the other observables. It is assumed that all of these conditional probabilities are symmetric, e.g. $P(A = a_\alpha \mid B = b_\beta) = P(B = b_\beta \mid A = a_\alpha)$. Restrict attention to the case of three observables and two possible obtainable values each. Then the conditional probabilities $P(A \mid B), P(B \mid C), P(C \mid A)$ are said to satisfy a two-dimensional Hilbert space model (real or complex) if for each observable A, B, C there exists an orthonormal basis $\{\phi_\alpha\}, \{\psi_\beta\}, \{\chi_\gamma\}$ within the Hilbert space such that the conditional probabilities are given (e.g., in quantum mechanical sense) by $P(A\,|B\,) = |\langle\phi_\alpha, \psi_\beta\rangle|^2$, likewise the others. Let p, q, r be any three (potential conditional probabilities) numbers in the interval $(0, 1)$: we comment that it is easier not to have to consider the degenerate cases at the ends of that interval, and let $|\langle\phi_1, \psi_1\rangle|^2 = p$, $|\langle\psi_1, \chi_1\rangle|^2 = q$, $|\langle\chi_1, \phi_1\rangle|^2 = r$. Then Accardi and Fedullo [11] proved the following result.

Theorem 2.2 *In the above setup, p, q, r admit a complex Hilbert space model if and only if $|p+q+r-1| \leqq \pm 2(pqr)^{1/2}$, and a real Hilbert space model iff $p+q+r-1 = \pm 2(pqr)^{1/2}$.*

Proof: See the details in [11]. I have chosen to state the theorem in the way it is expressed in Gudder and Zanghi [12] where a simpler proof is given. In [12] it is noted that their approach allows to consider also the case of four or more events. ■

I will return to the Bell Theory in later sections of this paper. There are many aspects I will not discuss at all. But the next step in the logical development from my perspective is to connect some of the above considerations to my operator trigonometry.

3 Trigonometric Theory

Here I want to place the Bell–Wigner–Accardi et al. theory of quantum probabilities for spin systems into what I regard to be its natural and more general setting: that of my operator trigonometry [13,14,15,16,17]. The key link to this connection between the abstract operator trigonometry and the quantum probability theory comes by noting that Accardi and Fedullo's ([11], Proposition 3, Eq. (19)), namely

$$\cos^2\alpha + \cos^2\beta + \cos^2\gamma - 1 \leqq 2\cos\alpha\cos\beta\cos\gamma \tag{3.1}$$

a necessary and sufficient condition for the angles α, β, γ of a quantum spin model in a 2-dimensional complex Hilbert space, is precisely the same as (see, e.g., Gustafson and Rao [14], Lemma 3.3-1, equation (3.3-3)) the operator trigonometry relation

$$1 - a_1^2 - a_2^2 - a_3^2 + 2a_1a_2a_3 \geqq 0 \tag{3.2}$$

for the real cosines a_1, a_2, a_3 of the angles between arbitrary unit vectors in any complex Hilbert space. The angles of inequality (3.1) are related to transition probability matrices $P(A \mid B), P(B \mid C), P(C \mid A)$ for three observables A, B, C which may take two values. The angles of (3.2) are related to a triangle inequality for general operator angles within the general operator trigonometry. Moreover, Wigner's version, ([9], Eq. (3)) of Bell's inequality, namely

$$\frac{1}{2}\sin^2\frac{1}{2}\theta_{23} + \frac{1}{2}\sin^2\frac{1}{2}\theta_{12} \geqq \frac{1}{2}\sin^2\frac{1}{2}\theta_{31} \tag{3.3}$$

is also a special instance of the general operator trigonometry. By this I mean, as will be shown below, that Wigner's expression (3.3) may be inserted into my operator trigonometry in such a way as to transparently violate (3.1) for certain angles.

There are many parts of the operator trigonometry (see [13], [14], [15], [16], [17] and citations to the earlier work therein) that are interesting in other scientific domains but are not needed here. So I will skip them all. The principal entities of the operator trigonometry are the angle $\phi(A)$ which measures the maximal turning capability of an operator A, the associated entities $\cos\phi(A)$ and $\sin\phi(A)$, and the antieigenvectors $x_\pm$ which are most turned by A. In some sense the operator trigonometry can be viewed as extending the Rayleigh–Ritz theory of operator eigenvectors and eigenvalues to a larger theory also including operator antieigenvectors and antieigenvalues. However, important for our purposes here is a very small piece of the operator trigonometry, the following 'micro' triangle inequality (Gustafson and Rao, 1971, see [14]) for arbitrary unit vectors x, y, z in a Hilbert space. Let $\langle x, y\rangle = a_1 + ib_1$, $\langle y, z\rangle = a_2 + ib_2$, $\langle x, z\rangle = a_3 + ib_3$, and define the angles $\phi_{xy}, \phi_{yz}, \phi_{xz}$ in $[0, \pi]$ by $\cos\phi_{xy} = a_1, \cos\phi_{yz} = a_2, \cos\phi_{xz} = a_3$. For the

proof below let us also recall the Gram matrix

$$G = \begin{bmatrix} \langle x,x\rangle & \langle x,y\rangle & \langle x,z\rangle \\ \langle y,x\rangle & \langle y,y\rangle & \langle y,z\rangle \\ \langle z,x\rangle & \langle z,y\rangle & \langle z,z\rangle \end{bmatrix} \tag{3.4}$$

A Gram matrix is positive semidefinite in any number of dimensions, and definite iff the given vectors are linearly independent.

Theorem 3.1 *For arbitrary unit vectors x, y, z in a real or complex Hilbert space, one has*

$$\phi_{xz} \leqq \phi_{xy} + \phi_{yz}. \tag{3.5}$$

Proof: It suffices to show

$$\cos\phi_{xz} \geqq \cos(\phi_{xy} + \phi_{yz}) \tag{3.6}$$

which by the sum formula for cosines is equivalent to

$$\sqrt{1-a_1^2}\,\sqrt{1-a_2^2} \geqq a_1a_2 - a_3. \tag{3.7}$$

The desired result (3.5) follows trivially when the right side of (3.7) is negative. In the other case we need

$$(1-a_1^2)(1-a_2^2) \geqq (a_1a_2 - a_3)^2, \tag{3.8}$$

which is equivalent to (3.2). But for unit vectors the determinant of the Gram matrix (3.4) becomes

$$|G| = \begin{vmatrix} 1 & a_1 & a_3 \\ a_1 & 1 & a_2 \\ a_3 & a_2 & 1 \end{vmatrix} = 1 + 2a_1a_2a_3 - (a_1^2 + a_2^2 + a_3^2) \geqq 0 \tag{3.9}$$

which gives (3.2), hence (3.6), hence (3.5). ∎

Now we may give [18],[19],[20],[21] an explicit connection between the operator trigonometry and the quantum probabilities.

Theorem 3.2 *The Accardi–Fedullo quantum probability inequality (3.1) and Theorem 2.2 above are special instances of the operator trigonometry. The Wigner quantum probability inequality (3.3) and his other spin probability configurations (see below) are special violations of the operator trigonometry. In this sense the operator trigonometry provides a natural quantum trigonometry.*

Proof: Clearly (3.1) is a special instance of (3.2) and hence of the operator trigonometry. In the same way all of the quantum spin inequalities in the Accardi–Fedullo theory [11] may be seen within the operator trigonometry. We admit to being vague about the details (as Wigner was in [9]) so we don't try to examine every detail of this statement here. Stated another way, the point we contend is: these inequalities are a direct mathematical consequence of the Hilbert space structure, without any additional physical ideas involved. ∎

To continue the proof of Theorem 3.2, let us turn next to Wigner's inequalities. It is useful to explicitly follow their order of appearance and his analysis of them in his paper [9]. As we outlined in the previous section, Wigner reformulates Bell's set up and reduces the outcomes to 2^6p ossibilities, e.g., the instance in which the hidden variables are in the domain $(+,-,-;-,+,-)$ that we mentioned above. Then he shows that these 64 possibilities can be grouped by sixteens, with most terms cancelling, e.g., see his argument to obtain the expression [9, Eq. (2)]. In the first of the four resulting spin measurement possibilities, i.e., that of ++ for first particle in direction ω_1 and second particle ω_3, he then arrives (assuming joint probability factorization ([9], Eq. (1)), an assumption Bell also made) at the conclusion that the "hidden parameters can reproduce the quantum mechanical probabilities only if the three directions $\omega_1, \omega_2, \omega_3$ in which the spins are measured are so situated that $\frac{1}{2}\sin^2\frac{1}{2}\theta_{23} + \frac{1}{2}\sin^2\frac{1}{2}\theta_{12} \geqq \frac{1}{2}\sin^2\frac{1}{2}\theta_{31}$", inequality (3.3) above. Then to make the point very clear, he specializes to the case in which the three directions $\omega_1, \omega_2, \omega_3$ in 3 space are coplanar and with ω_2 bisecting the angle between $\omega_1$and ω_3. Then $\theta_{12} = \theta_{23} = \theta_{31}/2$ and inequality (3.3) becomes

$$\sin^2\left(\frac{1}{2}\theta_{12}\right) \geqq \frac{1}{2}\sin^2(\theta_{12}) = 2\sin^2\left(\frac{1}{2}\theta_{12}\right)\cos^2\left(\frac{1}{2}\theta_{12}\right) \tag{3.10}$$

from which $\cos^2(\frac{1}{2}\theta_{12}) \leqq 1/2$ and hence $\theta_{31} = 2\theta_{12} \geqq \pi$. Thus the condition (3.3) necessary for appropriate quantum mechanical spin probabilities for the hidden variable theories is violated for all $\theta_{31} < \pi$. Wigner then asserts (without giving the details) that the same conclusion may be drawn for all coplanar directions.

Let us now look at this conclusion and its extension to all coplanar directions from the operator trigonometric perspective. The Gram determinant G (3.4) vanishes if and only if the three directions are coplanar, no matter what their frame of reference. Then we may write the equality in (3.9) as follows

$$(1 - a_1^2) + (1 - a_2^2) - (1 - a_3^2) = 2a_3(a_3 - a_1a_2) \tag{3.11}$$

or in the terminology of (3.3)

$$\begin{aligned} &\sin^2\left(\tfrac{1}{2}\theta_{12}\right) + \sin^2\left(\tfrac{1}{2}\theta_{23}\right) - \sin^2\left(\tfrac{1}{2}\theta_{13}\right) \\ &= 2\cos\left(\tfrac{1}{2}\theta_{13}\right)\left[\cos\left(\tfrac{1}{2}\theta_{13}\right) - \cos\left(\tfrac{1}{2}\theta_{12}\right)\cos\left(\tfrac{1}{2}\theta_{23}\right)\right]. \end{aligned} \tag{3.12}$$

Nonquantum probability violation (3.3) in the coplanar case is equivalent to the right side of (3.12) being nonnegative. Since all half-angles do not exceed $\pi/2$, except for the trivial case when $\frac{1}{2}\theta_{13} = \pi/2$, the nonnegativity of (3.12) means that of its second factors. By choosing the direction ω_2 to be the "one in between" among the half-angles, we can without loss of generality assume that $\frac{1}{2}\theta_{12} + \frac{1}{2}\theta_{23} = \frac{1}{2}\theta_{13}$. the required nonnegativity of (3.12) then reduces by the elementary cosine sum formula to

$$\cos\left(\frac{\theta_{12}+\theta_{23}}{2}\right) \geqq \frac{1}{2}\left[\cos\left(\frac{\theta_{12}+\theta_{23}}{2}\right) + \cos\left(\frac{\theta_{12}-\theta_{23}}{2}\right)\right] \tag{3.13}$$

i.e., $\cos((\theta_{12}+\theta_{23})/2) \geqq \cos((\theta_{12}-\theta_{23})/2)$, which is false for positive θ_{23}. This completes Wigner's omitted argument and is the meaning of coplanar quantum probability violation.

Wigner considers two other configurations for quantum nonprobability violation, namely ([9], Eqs. (6) and (7), respectively)

$$1 - \frac{1}{2}\left(\sin^2\frac{1}{2}\theta_{12} + \sin^2\frac{1}{2}\theta_{23} + \sin^2\frac{1}{2}\theta_{31}\right) \geqq 0 \tag{3.14}$$

and

$$\frac{1}{2}\left(\sin^2\frac{1}{2}\theta_{12} + \sin^2\frac{1}{2}\theta_{23} - \sin^2\frac{1}{2}\theta_{31}\right) \geqq 0. \tag{3.15}$$

As Wigner notes, (3.15) gives (3.3), and moreover, the positivity of the three cyclically interchanged versions of (3.15), plus that of (3.14), is a necessary and sufficient condition for the possibility to interpret the spin measurements in the ω_i directions on a singlet state in terms of hidden variables.

How do these look from the operator trigonometric perspective, using only the Gram matrix and cosine sums? Using from (3.9) the general Grammian expression

$$|G| = (1 - a_1^2) + (1 - a_2^2) + (1 - a_3^2) + 2(a_1a_2a_3 - 1) \tag{3.16}$$

immediately (3.14) and (3.15) become, respectively

$$a_1a_2a_3 - \frac{1}{2}|G| \geqq 0 \tag{3.17}$$

and

$$2a_3(a_1a_2 - a_3) \geqq 0. \tag{3.18}$$

We note that (3.16) brings us more quickly to (3.18) which is the same as (3.12) and (3.15) but now for arbitrary directions. Also (3.16) expresses the positivity of (3.14) in a more delicate manner (3.17) which includes the degree of linear independence of the ω_i directions. Thus the operator trigonometry perspective makes more precise both qualitatively and quantitatively the arguments of Wigner [9] and more importantly, when his angles violate Theorem 3.1.

We return to Accardi and Fedullo [11]. This was an important paper which not only advanced Wigner's treatment [9] of the Bell theory but also clarified the statistical meaning of the complex numbers in quantum mechanics, a longstanding question. In addition [11] stressed the notion of statistical invariants to determine whether probability models were Kolmogorovian or not. As we did with Wigner [9], we wish to look closely at some details in [11] while ignoring some larger picture considerations.

Accardi and Fedullo [11] emphasize conditional probabilities, also called transition probabilities, in contrast to Bell's [7] arguments with correlations and Wigner's [9] arguments with configuration combinatorics. Conditional probabilities

$$P(A = a_\alpha \mid B = b_\beta), \quad P(B = b_\beta \mid C = c_\gamma), \quad P(C = c_\gamma \mid A = a_\alpha) \tag{3.19}$$

are assumed to satisfy symmetry conditions

$$P(A = a_\alpha \mid B = b_\beta) = P(B = b_\beta \mid A = a_\alpha), \text{etc.} \tag{3.20}$$

and are said to admit a Kolmogorovian probability model if there exists a probability space $(\Omega, \mathcal{O}, \mu)$ and for each observable A, B, C a measurable partition $A_\alpha, B_\beta, C_\gamma$, of Ω such that for each observable outcome α, β, γ

$$P(A = a_\alpha \,|B \, = b_\beta) = \frac{\mu(A_\alpha \cap B_\beta)}{\mu(B_\beta)}. \tag{3.21}$$

The transition probabilities (3.19) are said to satisfy a complex Hilbert space probability model if there exists a complex Hilbert space $\mathcal{H}$ such that for each observable A, B, C there exists an orthonormal basis $(\phi_\alpha), (\psi_\beta), (\chi_\gamma)$ such that for each α, β, γ

$$P(A = a_\alpha \,|B \, = b_\beta) = |\langle \phi_\alpha, \psi_\beta \rangle|^2. \tag{3.22}$$

Real Hilbert space versions are also defined the same way. We refer the reader to [11] for more details.

Limiting discussion to three observables taking only two values, the conditional probabilities (3.19) may be represented by the following transition probability matrices

$$\begin{aligned} P = P(A \,|B\,) &= \begin{bmatrix} p & 1-p \\ 1-p & p \end{bmatrix} = \begin{bmatrix} \cos^2(\alpha/2) & \sin^2(\alpha/2) \\ \sin^2(\alpha/2) & \cos^2(\alpha/2) \end{bmatrix} \\ Q = P(B \,|C\,) &= \begin{bmatrix} q & 1-q \\ 1-q & q \end{bmatrix} = \begin{bmatrix} \cos^2(\beta/2) & \sin^2(\beta/2) \\ \sin^2(\beta/2) & \cos^2(\beta/2) \end{bmatrix} \\ R = P(C \,|A\,) &= \begin{bmatrix} r & 1-r \\ 1-r & r \end{bmatrix} = \begin{bmatrix} \cos^2(\gamma/2) & \sin^2(\gamma/2) \\ \sin^2(\gamma/2) & \cos^2(\gamma/2) \end{bmatrix}. \end{aligned} \tag{3.23}$$

As in [11] we assume for simplicity $0 < p, q, r < 1$, $0 < \alpha, \beta, \gamma < \pi$. Some reasonable probability completeness and positivity assumptions are made and then it is shown [11] that P, Q, R of (3.23) admit a Kolmogorovian probability model if and only if the inequality

$$|p + q - 1| \leqq r \leqq 1 - |p - q| \tag{3.24}$$

holds. We will not pursue the classical probability issues here.

For conditions for a quantum mechanical spin system to have a complex Hilbert space model existing, the Pauli matrices

$$\sigma_1 = \begin{bmatrix} 0 & 1 \\ 1 & 0 \end{bmatrix}, \quad \sigma_2 = \begin{bmatrix} 0 & -i \\ i & 0 \end{bmatrix}, \quad \sigma_3 = \begin{bmatrix} 1 & 0 \\ 0 & -1 \end{bmatrix} \tag{3.25}$$

and spin operators $\sigma \bullet a = \sigma_1 a_1 + \sigma_2 a_2 + \sigma_3 a_3$ for $a = (a_1, a_2, a_3)$ a real 3 vector of norm 1 are considered. A spin model for the transition probabilities (3.23) is said to exist if there exist three normalized 3 vectors a, b, c such that the the orthonormal bases $\psi_\alpha(a), \psi_\beta(b), \psi_\gamma(c)$ realize the matrices P, Q, R of (3.23) in the sense of (3.22). In this way the question of the existence of a Hilbert space probability model is reduced to the question of the existence of three norm-1 vectors a, b, c such that

$$\begin{aligned} |\langle \psi_1(a), \psi_1(b) \rangle|^2 &= \cos^2 \tfrac{1}{2}\theta_{ab} \\ |\langle \psi_1(a), \psi_2(b) \rangle|^2 &= \sin^2 \left(\tfrac{1}{2}\theta_{ab}\right) \end{aligned} \tag{3.26}$$

where $\cos\alpha = \cos\theta_{ab}$, $\cos\beta = \cos\theta_{bc}$, $\cos\gamma = \cos\theta_{ac}$ link the angles of (3.23) to the angles θ between the sought-for directions a, b, c. The setup is the same as in Wigner [9] but the setting is now framed specifically in terms of competing classical or nonclassical probability models. In particular, it is shown ([11], Proposition 3, Corollary 6, Theorem 3.2) that such vectors a, b, c exist if and only if

$$\cos^2\alpha + \cos^2\beta + \cos^2\gamma - 1 \leqq 2\cos\alpha\cos\beta\cos\gamma. \tag{3.27}$$

Immediately we recognize that (3.27) is the condition for the nonnegativity of our Gram determinant. In other words, (3.27) is always satisfied for any three normalized direction vectors in a complex Hilbert space, with equality holding if and only if those vectors happen to be coplanar. In other words, the operator trigonometry provides the natural geometrical model for the quantum probability theory. That is an emphasized main outcome of this paper.

We may express the above determinations as follows.

Theorem 3.3 *The Accardi–Fedullo inequalities and Theorem 2.2 are properties of a real or complex Hilbert space independent of any additional physical or probabilistic ideas involved. Moreover the fact that equality is the rule for the real Hilbert space case is just due to the fact that the real Hilbert space is isomorphic to* $\mathbb{R}^2$ *and all vectors in there are coplanar.*

Proof: As we have shown above, all of these inequalities may be expressed in terms of the Grammian matrix being a positive semidefinite Hermitian operator, with determinant given by (3.9). As shown in ([11], Theorem 10), a P, Q, R transition matrix real Hilbert space model can occur iff the three direction vectors $\omega_1, \omega_2, \omega_3$ are coplanar, viz., the Grammian $|G| = 0$. One could conclude the same by eliminating the σ_2 spin matrix degree of freedom from (3.25). With respect to [12] the meaning is that of no allowed phase α or β. ■

In the same way we may say

Theorem 3.4 *The geometrical meaning of the important triangle inequality (3.5) of Theorem 3.1 is that of adjacent real angles created by adjacent vectors in an arbitrary preHilbert space of any dimension.*

Proof: Given any three unit vectors x, y, z, they determine as above Theorem 3.1 three real angles $\phi_{xy}, \phi_{xz}, \phi_{yz}$ between these adjacent vectors. For the complex case one may reconstruct three real vectors $\tilde{x}, \tilde{y}, \tilde{z}$ from the real angles $\phi_{xy}, \phi_{xz}, \phi_{yz}$ defined by the real part of the complex inner product. ■

4 Augmentation of Geometrical Understandings

The next three sections of this paper extend my previous discussions and advance earlier understandings of what is really going on with Bell's Inequalities. Again no attempt at completeness is made. In fact I will just select a few of the better books that treat Bell Theory, and then provide my own alternative understandings. Because of time limitations for this conference paper deadline I will restrict my treatment here to three understandings: geometrical, probabilistic, physical. From these discussions will follow Corollaries 1.1, 1.2, 1.3.

In the paper up to this point I have stressed that much of the Bell theory, when it is placed into my operator trigonometry, takes on a much more geometrical nature

than was heretofore recognized. I plan to extend that "quantum trigonometry" in coming papers. In this section I will (A) note a few literature citations as to triangle inequalities and comment on those, (B) treat Bell's inequalities as equalities, (C) comment on Bell's original inequality from a mathematical perspective.

(A) Triangle inequalities. A number of authors have noticed resemblances or analogies to triangle inequalities in Bell-type arguments. My contribution presented in this paper may be stated: one need not resort to "analogies". There is a fundamental Hilbert space triangle inequality (Theorem 1.1) which explains much of the Bell theory.

For example, Wigner [9] and Accardi and Fedullo [11] make statements "have the form of triangle inequalities for three sides" and "equivalent to a couple of inequalities which are necessary and sufficient conditions...to be adjacent angles of a tetrahedron in R^3," respectively. However the general Hilbert space inequality (1.1) was not glimpsed. Moreover as we have seen in the previous section, Wigner's [9] 'triangle inequality' is sometimes in violation of the true Hilbert space fundamental triangle inequality of Theorem 3.1.

Williams and Clearwater [22] in a very useful and accessible book on quantum computing state ([22], p. 194), "or more simply

$$P_{v_1 h_2} + P_{v_2 h_3} \geqq P_{v_1 h_3} \tag{4.1}$$

which is Bell's Inequality. Note the similarity to a 'triangle inequality' where the two 'sides' are longer than the longest 'side'. Also in analogy to this triangle inequality we should note that it applies to Euclidean space and that Bell's Inequality applies only to worlds with local interactions." I will come back to (4.1) later, but for now the point is that (4.1) is not 'analogous' to a triangle inequality, we know from my discussion in Section 3 above that (4.1) may in some instances violate my basic triangle inequality (1.1). To verify this, note that (4.1) is equivalent [22, p. 195] to Wigner's formulation (3.3).

Khrennikov ([23], p. 5937) states "to consider Bell's inequality (and its generalizations) as analogues of the inequality for the sum of angles in a triangle. The latter inequality gives the possibility to find the right geometry to describe some physical phenomena." The point I am making in this paper is that I can show in many instances that the 'right geometry' has indeed already been found: my operator trigonometry. Let me hasten to add here that in this paper I have not been attempting generality so when I say 'Bell inequality' I mean just one of them, without distinguishing whether it be Wigner, CHSH, Cirelson generalization. The trigonometric details for each of these will be worked out systematically elsewhere.

(B) Bell Equalities. It is interesting to render Bell inequalities, equalities. Then one may express analytically exactly the "violation zones". I earlier [21] mentioned this in terms of the Grammian expressions such as (3.9). Here let me proceed somewhat differently. Again without a full development, I proceed via an example. Consider the nice treatment of Bell's Inequalities in Bohm ([24], pp. 347–354). A very large number of particles in the spin singlet state are considered. Let $\mathbf{a}, \mathbf{b}, \mathbf{c}, \mathbf{d}$ be four arbitary chosen unit vector directions in the plane orthogonal to the two beams produced by the source. Let $v_i(\mathbf{a})$ and $v_i(\mathbf{d})$ be the "hidden" predetermined values ± 1 of the spin components along $\mathbf{a}$ and $\mathbf{d}$, respectively, of particle 1 of the ith

pair, similarly $w_i(\mathbf{b})$ and $w_j(\mathbf{c})$ for particle 2 values along directions $\mathbf{b}$ and $\mathbf{c}$. Then the average correlation value for particle 1 spins measured along $\mathbf{a}$ and particle 2 spins measured along $\mathbf{b}$ is

$$E(\mathbf{a},\mathbf{b}) = \frac{1}{N}\sum_{i=1}^{N} v_i(\mathbf{a}) w_i(\mathbf{b}) \tag{4.2}$$

In the same way one considers the average correlation values $E(\mathbf{a},\mathbf{c})$, $E(\mathbf{d},\mathbf{b})$, $E(\mathbf{d},\mathbf{c})$ and adding up all pairs as i runs from 1 to N one arrives at the Bell inequality

$$|E(\mathbf{a},\mathbf{b}) + E(\mathbf{a},\mathbf{c}) + E(\mathbf{d},\mathbf{b}) - E(\mathbf{d},\mathbf{c})| \leqq 2. \tag{4.3}$$

Demanding this estimate hold as well for quantum mechanical expectations $E(\mathbf{a},\mathbf{b}) = -\mathbf{a}\cdot\mathbf{b}$, one has ([24], p. 349)

$$\begin{aligned} |\mathbf{a}\cdot\mathbf{b} + \mathbf{a}\cdot\mathbf{c} + \mathbf{d}\cdot\mathbf{b} - \mathbf{d}\cdot\mathbf{c}| &= |\mathbf{a}\cdot(\mathbf{b}+\mathbf{c}) + \mathbf{d}\cdot(\mathbf{b}-\mathbf{c}| \\ &\leqq |\mathbf{a}||\mathbf{b}+\mathbf{c}| + |\mathbf{d}||\mathbf{b}-\mathbf{c}| \\ &= \sqrt{2+2\cos\phi} + \sqrt{2-2\cos\phi} \end{aligned} \tag{4.4}$$

where ϕ is the angle θ_{bc} (a notation I will use below) between $\mathbf{b}$ and $\mathbf{c}$. Then one observes that the last expression is maximized to value $2\sqrt{2}$ when $\theta_{bc} = \pi/2$, and "any configuration sufficiently 'near' to" the directions providing this maximal violation of Bell's inequality will also violate it.

Wishing now to preserve equality in the above so that we may analytically express what we may call the 'violation boundaries, violation regions', starting from (4.4) we have

$$\begin{aligned} |\mathbf{a}\cdot\mathbf{b} + \mathbf{a}\cdot\mathbf{c} + \mathbf{d}\cdot\mathbf{b} - \mathbf{d}\cdot\mathbf{c}| &= |\mathbf{a}\cdot(\mathbf{b}+\mathbf{c}) + \mathbf{d}\cdot(\mathbf{b}-\mathbf{c})| \\ &= |\|b+c\|\cos\theta_{a,b+c} + \|b-c\|\cos\theta_{d,b-c}| \\ &= |(2+2\cos\theta_{bc})^{1/2}\cos\theta_{a,b+c} \\ &\quad +(2-2\cos\theta_{bc})^{1/2}\cos\theta_{d,b-c}| \end{aligned} \tag{4.5}$$

Squaring this expression and writing everything quantum trigonometrically,

$$\begin{aligned} |\mathbf{a}\cdot\mathbf{b} + \mathbf{a}\cdot\mathbf{c} + \mathbf{d}\cdot\mathbf{b} - \mathbf{d}\cdot\mathbf{c}|^2 &= (2+2\cos\theta_{bc})\cos^2\theta_{a,b+c} \\ &\quad +(2-2\cos\theta_{bc})\cos^2\theta_{d,b-c}) \\ &\quad +2(4-4\cos^2\theta_{bc})^{1/2}\cos\theta_{a,b+c}\cos\theta_{d,b-c} \\ &= 4\cos^2(\theta_{bc}/2)\cos^2\theta_{a,b+c} \\ &\quad +4\sin^2(\theta_{bc}/2)\cos^2\theta_{d,b-c} \\ &\quad +4\sin^2\theta_{bc}\cos\theta_{a,b+c}\cos\theta_{d,b-c}. \end{aligned} \tag{4.6}$$

In the above I used two standard trigonometric halfangle formulas. Now substituting the standard double angle formula $\sin\theta_{bc} = 2\sin(\theta_{bc}/2)\cos(\theta_{bc}/2)$ into the above we arrive at

$$|\mathbf{a}\cdot\mathbf{b} + \mathbf{a}\cdot\mathbf{c} + \mathbf{d}\cdot\mathbf{b} - \mathbf{d}\cdot\mathbf{c}|^2 = 4[\cos\theta_{bc}/2)\cos\theta_{a,b+c} + \sin(\theta_{bc}/2)\cos\theta_{d,b-c}]^2 \tag{4.7}$$

and hence the quantum *Bell equality*

$$|\mathbf{a}\cdot\mathbf{b}+\mathbf{a}\cdot\mathbf{c}+\mathbf{d}\cdot\mathbf{b}-\mathbf{d}\cdot\mathbf{c}|= 2|\cos(\theta_{bc}/2)\cos\theta_{a,b+c}+\sin(\theta_{bc}/2)\cos\theta_{d,b-c}|. \quad (4.8)$$

We may also write the righthand side of (4.8) as twice the absolute value of the two-vector inner product

$$\mathbf{u}_1\cdot\mathbf{u}_2\equiv(\cos(\theta_{bc}/2),\sin(\theta_{bc}/2))\cdot(\cos\theta_{a,b+c},\cos\theta_{d,b-c}) \quad (4.9)$$

to arrive at the *Bell equality*

$$|\mathbf{a}\cdot\mathbf{b}+\mathbf{a}\cdot\mathbf{c}+\mathbf{d}\cdot\mathbf{b}-\mathbf{d}\cdot\mathbf{c}|= 2(\cos^2\theta_{a,b+c}+\cos^2\theta_{d,b-c})^{1/2}|\cos\theta_{u_1,u_2}|. \quad (4.10)$$

The right sides of these two Bell equalities (4.8), (4.10) isolate the "classical probability factor" 2 from the second factor, which may achieve its maximum $\sqrt{2}$. That the latter maximum is consistent with the third factor in (4.10) also achieving its maximum value 1 may be seen as follows. Fix any directions $\mathbf{b}$ and $\mathbf{c}$. Then choose $\mathbf{a}$ relative to $\mathbf{b}+\mathbf{c}$ and choose d relative to $\mathbf{b}-\mathbf{c}$ so that $\cos^2\theta_{a,b+c}=1$ and $\cos^2\theta_{d,b-c}=1$, respectively. Now we may choose the free directions $\mathbf{b}$ and $\mathbf{c}$ to maximize the third factor to $\cos\theta_{u_1,u_2}=\pm1$. But that means the two-vectors $\mathbf{u}_1$ and $\mathbf{u}_2$are colinear and hence

$$\begin{aligned}\mathbf{u}_1&=(\cos(\theta_{bc}/2),\sin(\theta_{bc}/2))=2^{-1/2}(\cos\theta_{a,b+c},\cos\theta_{d,b-c})\\&=2^{-1/2}(\pm1,\pm1)\end{aligned} \quad (4.11)$$

and thus the important angle θ_{bc} is seen to be $\pm\pi/2$. More to the point, the above Bell equality allows one to exactly trace out the "violation regions" analytically in terms of the trigonometric inner product condition $1\leqq|\mathbf{u}_1\cdot\mathbf{u}_2|\leqq\sqrt{2}$. From this point of view, there are no Bell inequalities. Each should be replaced with a Bell equality.

Let me summarize the above. One started with a classical probability correlation definition (4.2) and derived a Bell inequality $|\cdots|\leqq2$. The "equality" version of this classical probability version would be in the individual terms

$$|v_i(a)(w_i(b)+w_i(c))+v_i(d)(w_i(b)-w_i(c))|=2 \quad (4.12)$$

On the other hand, inserting the quantum correlation definition into the left side of (4.3) results (4.4) in the Bell inequality $|\cdots|\leqq2\sqrt{2}$. My equality version (4.10) of this becomes the vector trigonometric identity

$$|\cos\theta_{ab}+\cos\theta_{ac}+\cos\theta_{bd}-\cos\theta_{dc}|=2(\cos^2\theta_{a,b+c}+\cos^2\theta_{d,b-c})^{1/2}|\cos\theta_{u_1,u_2}|. \quad (4.13)$$

It could be useful to call (4.13) the quantum spin correlation identity. But it is just a mathematical result in vector trigonometry.

In retrospect, one may view my expression (3.12) as a Bell equality, or perhaps more appropriately named, a Wigner–Gustafson identity. The left side is Wigner's expression which from (3.3) he wanted to be nonnegative. The right side tells you when, and when not, that will be the case. What Wigner imagined to be a 'triangle inequality' is now corrected to an identity which does indeed correspond to a true geometric triangle inequality (3.5).

(C) Elementary Inequalities. Accardi [25] (with some attribution to the renowned and recently deceased statistician G. Watson) makes the point that Bell's original inequality follows from just an elementary Kolmogorov probability property inserted into a very elementary real number inequality. In this subsection I want to quickly look at the latter. Remember that Bell's original inequality was expressed [26] as

$$|P(\mathbf{a},\mathbf{b}) - P(\mathbf{a},\mathbf{c})| \leqq 1 + P(\mathbf{b},\mathbf{c}) \tag{4.14}$$

Here I wish to consider the situation rather generally, $\mathbf{a}$, $\mathbf{b}$, $\mathbf{c}$ are to be general vector directions in some Hilbert space, and P is to be some/any probabilistic, stochastic, statistical, correlational, expected value, entity in the real interval $[-1,1]$. To connect to (4.14) we prepare the following elementary inequality: I don't know its full history so I make no comment on that here.

Lemma 4.1 *Let a,b,c be arbitrary real numbers in $[-1,1]$. Then*

$$ab - bc + ac \leqq 1 \tag{4.15}$$

Proof: A short proof which however considers several cases was given in [25]. Here for completeness I give an alternate proof. From $b^2 \leqq 1$ and $c^2 \leqq 1$ we have $b^2(1-c^2) \leqq 1 - c^2$ and hence $b^2 + c^2 \leqq 1 + b^2c^2$. Adding $2bc$ to both sides of the latter and multiplying by $a^2 \leqq 1$ we therefore have

$$a^2(b^2 + c^2 + 2bc) \leqq b^2 + c^2 + 2bc \leqq 1 + b^2c^2 + 2bc \tag{4.16}$$

i.e.,

$$a(b+c)^2 \leqq (1+bc)^2 \tag{4.17}$$

Taking the positive square root we have

$$a(b+c) \leqq |a||b+c| \leqq 1 + bc \tag{4.18}$$

I note that there would appear to be some additional advantage to this proof if one wants to consider extending the inequality to complex numbers or to other settings, which I will not pursue here. ■

The point to be made now is that whenever one can express the stochastic entities $P(\cdot,\cdot)$ in a Bell inequality (4.14) by a factored form $P(\mathbf{a},\mathbf{b}) = ab$ with the real numbers a,b,c in the interval $[-1,1]$, then the Bell Inequality is just an instance of the general mathematical inequality (4.15) of Lemma 4.1. To obtain his model Bell assumed that the joint probability of the detection of events A and B at two "separated" left and right measuring apparatuses was the product of separate conditional probabilities

$$p^{LR}(A, B \,|\mathbf{a}\,, \mathbf{b}, \lambda) = p^L(A \,|\mathbf{a}\,, \lambda) p^R(B \mid \mathbf{b}, \lambda) \tag{4.19}$$

It is this factorization which essentially renders Bell's expression (4.14) into the elementary general inequality (4.15).

A second instance in which reduction to Lemma 4.1 is possible is the treatment by Peres [27] of the measurement process on macroscopic bodies when considering ensemble averages $K_{ij} = 1 - \langle a_i a_j \rangle$t aken over consecutive time intervals. Let a_j

denote the value at time t_j of a dichomatic variable A with values ± 1. Then for three consecutive times one has

$$(a_1 + a_3)a_2 \leqq 1 + a_1 a_3 \tag{4.20}$$

Quoting [27, p. 427] "This equation does not assume any specific dynamical law, but only the possibility of performing *noninvasive measurements*: the value of a_3 on the right hand side (with no measurement of a_2) is the same as that on the left hand side (when there is a measurment of a_2)." But by Lemma 4.1 we know (4.20) is always true, independent of any physical assumptions.

One may also consider the ensemble averages K_{ij} defined above. From (4.20) one then obtains [27] the Peres–Herbert [28] inequality

$$K_{13} \leqq K_{12} + K_{23} \tag{4.21}$$

which we may write as

$$\langle a_1 a_2 \rangle + \langle a_2 a_3 \rangle \leqq 1 - \langle a_1 a_3 \rangle \tag{4.22}$$

The point now is: depending on whether or not you can factor the ensemble correlations $\langle a_i a_j \rangle$, you will be able to, for example, (i) reduce to Lemma 4.1 or (ii) violate (4.22).

5 Augmentation of Probabilistic Understandings

There is a huge literature on probabilistic issues related to Bell's inequalities and I will not even attempt to cite that literature. See [23,26,29-33] and many current papers. I will only examine one basic conceptual probabilistic issue as it seems relevant within the frame of this present paper. This issue could be stated as the question: where is the "error" in Bell's inequality? To prosecute this point and to save time I will follow the treatment of ([22], pp. 190–196). I have already referred to this in Section 4(A), e.g., see the Bell inequality (4.1). Let us follow the derivation of (4.1). Let a Polarizer 1 with orthogonal axes h_1 and v_1 (think: horizontal and vertical) be inclined at angle θ_1 to the horizontal, likewise Polarizer 2 with axes h_2 and v_2 inclined at angle θ_2 to the horizontal, let θ_{12} be the angle between the polarizers. Let P_{xy} denote the probability of detecting a photon along the x and y axes, respectively, of the two detectors. Then (as in Wigner [9] for example, which [22] is to some extent following, among others) for a given wavefunction ψ the measurement probabilities for the 4 possible outcomes are

$$\begin{aligned} P_{v_1 v_1} &= \tfrac{1}{2}\cos^2\theta_{12}, P_{v_1 h_2} = \tfrac{1}{2}\sin^2\theta_{12} \\ P_{h_1 v_2} &= \tfrac{1}{2}\sin^2\theta_{12}, P_{h_1 h_2} = \tfrac{1}{2}\cos^2\theta_{12} \end{aligned} \tag{5.1}$$

Now add the third polarizer with axes h_3 and v_3 at angle θ_3 to the horizontal. Now to quote [22] "We can write down the following relationships from straightforward probability arguments,

$$\begin{aligned} P_{v_1 h_2} &= P_{v_1 h_2 v_3} + P_{v_1 h_2 h_3} \\ P_{v_2 h_3} &= P_{v_1 v_2 h_3} + P_{h_1 v_2 h_3} \\ P_{v_1 h_3} &= P_{v_1 v_2 h_3} + P_{v_1 h_2 h_3} \end{aligned} \tag{5.2}$$

$\cdots$. From these relations it follows that

$$P_{v_1 h_2} \geqq P_{v_1 h_2 h_3}$$
$$P_{v_2 h_3} \geqq P_{v_1 v_2 h_3} \tag{5.3}$$

from which it follows

$$P_{v_1 h_2} + P_{v_2 h_3} \geqq P_{v_1 h_2 h_3} + P_{v_1 v_2 h_3} \tag{5.4}$$

or more simply

$$P_{v_1 h_2} + P_{v_2 h_3} \geqq P_{v_1 h_3} \tag{5.5}$$

which is Bell's Inequality".

For the examining of the above let us recall the *Axiom of Composite Probabilities*

$$P(X) = P(A_1) \cdot P(X \mid A_1) + P(A_2) \cdot P(X \mid A_2) \tag{5.6}$$

which states an additivity of probabilities of disjoint events and is equivalent under other rather reasonable conditions to *Bayes Axiom* $P(A \mid B) = P(A \cap B)/P(B)$. The *Axiom of Composite Amplitudes*

$$\begin{aligned} \psi(A = a \mid C = c) = {} & \psi(A = a \mid B_1 = b_1) \cdot \psi(B_1 = b_1 \mid C = c) \\ & + \psi(A = a \mid B_2 = b_2) \cdot \psi(B_2 = b_2 \mid C = c) \end{aligned} \tag{5.7}$$

states an additivity of wave function amplitudes and follows from Bayes Axiom but does not need Bayes Axiom for its validity. Keeping these two axioms in mind, let us see how "Bell's conclusion errors" are made. The basic spin probability assumption (5.1) is essentially the fundamental quantum probability projection rule I discussed in Section 4(B), plus a less obvious intrinsic assumption of spherically equidistributed equally likely outcomes. The "straightforward probability arguments" (5.2) are the axiom of composite probabilities (5.6) above. In (5.3) we have assumed that probabilies are non-negative as we drop them. The last step (5.4) to (5.5) again uses the axiom of composite probabilities (5.6) plus a less obvious switching of measuring instrument order.

But we know that the Bell Inequality (5.5), i.e., (4.1), is the same as Wigner's (3.3), which we know violates the fundamental Hilbert space triangle inequality (1.1) for certain angular configurations. Therefore we conclude that the axiom of composite probabilities is not consistent with the standard quantum probability (Projection) rule.

It would be interesting therefore to derive "Bell tests" just from the axiom of composite amplitudes. One could then examine the consistency of the fundamental projection postulate of quantum mechanics with those new Bell relations, and with reality.

6 Augmentation of Physical Understandings

There is a huge literature on the physical and metaphysical interpretations of Bell's inequality and related theory and experiments. See the already cited references [29,30,31,32,33]. I hope to elsewhere address a number of those issues from the perspective that I have developed in this paper. Here I will make only three comments.

The first is that since the operator trigonometry provides a new and correct mathematical setting for much of the Bell theory, I would assert that one correct physical understanding of the Bell inequalities is that of basic Hilbert space geometry, more specifically, the geometry of Euclidean and Unitary spaces, more specifically, that of a classical but new vector trigonometry.

The second comment is that the principal connection to physics in the above development is our belief that quantum correlations are given by the quantum probability rule: for two normalized vectors $\mathbf{u}$ and $\mathbf{v}$, the probability that a quantum system prepared in state $\mathbf{u}$ will successfully pass a test for state $\mathbf{v}$ is $|\mathbf{u}\cdot\mathbf{v}|^2 \equiv \cos^2\theta_{u,v}$. The quantum probability rule generally states that the expectation value of an observable A which has been determined experimentally as the arithmetic mean $\langle A\rangle$ of a large number of trials, should correspond theoretically to $Tr(AW)$ where W is the statistical operator describing the state of the system. For pure states this quantum probability rule becomes, operationally and loosely: the expected value is the projection onto the state. For the spin zero singlet state in the Bell situation the expected correlation value is $E(a,b) = -\mathbf{a}\cdot\mathbf{b} = -\cos\theta_{ab}$. From this ansatz alone and my Bell equalities above, one divides vectors $\mathbf{a}$, $\mathbf{b}$, $\mathbf{c}$, $\mathbf{d}$ into 'satisfaction' and 'violation' regions in whatever Hilbert space you want to take your direction vectors from.

From this viewpoint, I would prefer that the multitude of physical experiments over the years since [8] which have found various physical quantum mechanical configurations in which "Bell's inequality" is violated, be restated as showing that my Bell's Identity is achieved by those physical configurations for which the right hand side is between2 and $2\sqrt{2}$. But we know the latter is just vector geometry. So what these physical experiments really have shown is various verifications of the quantum probability rule. To repeat and indeed overstate my point, rather than seeking "Bell inequality violations", it would be more interesting to seek "quantum probability rule violations". This, because the quantum probability rule is a far-reaching assumption, an ansatz, which in the sense of my presentation in this paper, reduces much of quantum mechanics to a vector trigonometry. Thus one should seek some quantum physical situation which could result in physical measurements for which there obtains a right-hand-side greater than $2\sqrt{2}$.

As a third comment, let me make a final assertion (Corollary 1.3) which seems relevant in view of the developments of this paper: one cannot argue either locality or nonlocality on the basis of satisfaction or violation of Bell's Inequality. Bell's Inequality, notwithstanding the key and very important role it has played in the evolving scientific revolution of quantum mechanics, is seen in retrospect as a "red herring": a diversion distracting attention away from the real issue [34]. Unlike political red herrings, the original intent of Bell and consequent investigators was genuine. However, from my viewpoint, the real issue as concerns nonlocality in quantum physics is the projection rule. This "probability" rule is fundamental to Von Neumann quantum mechanics. It is also fundamental to my quantum trigonometry. It is surely true for the latter, i.e., geometrically. Is it true for the former?

7 Concluding Remarks

I have used the terms Bell Inequalities and Bell Theory in a very general sense. I tried to make that very clear in the first sentence of the Introduction. There I also tried to make clear that the contribution in this paper would emphasize a very limited viewpoint: mathematical. Nonetheless I would like to add the following comments.

As I indicated at the beginning of Section 3, I discovered the link between my operator trigonometry and the quantum probability when I read the Accardi–Fedullo paper [11]. That is one reason why (after a few years) I decided in Corollary 1.2 to call this inequality (3.1), (3.2) the Accardi–Gustafson inequality, to distinguish it from what I also referred to in Corollary 1.2 as the Bell–Wigner inequality. It is pointless to argue any historical priorities between the operator trigonometry and the quantum probability inequalities because the discovery contexts were entirely different. However it should be mentioned that the operator trigonometric version predates the quantum probability version by about ten years. See the historical account in [15].

In contrast, as I tried to make clear in Section 4, Bell's original inequality (4.14) and Wigner's related inequality (3.3), (4.1) are different from the Accardi–Gustafson inequality. Because they were both derived from what has been seen in retrospect to be questionable use of physically appropriate probability theory, both Bell's and Wigner's inequalities are flawed geometrically, although in different ways. In Section 4 I created the term Bell Equalities to emphasize that I can nonetheless embed Bell-type and Wigner-type inequalities into my operator trigonometry so that we may try to determine precisely the 'violation regions' and their causes.

In so doing we are then able to identify the historical errors in their physical derivations. This is the main point of Section 5. In that section I also very quickly without elaboration recall some basic axioms of probability. A referee has pointed out that I should not be so quick to say which implies which (e.g., especially vis a vis Bayes axiom). For a more complete examination of the latter I refer the reader to [34], where it is emphasized that "the nonvalidity of Bayes' axiom is really universal for quantum theory and that all the interpretive problems of this theory arise from an unjustified application of this axiom." It should be pointed out that in the same sense in his fundamental paper [35] Accardi opened up the important alternative of "quantum probability" as a way to resolve many of these paradoxical aspects of quantum theory which as we have seen are often caused by careless mixing of classical and nonclassical probability axioms. The paper [36] was a turning point in the debate on Bell's inequalities, and shifted attention from 'realism' and 'locality', to the underlying assumed probabilistic models.

One of the conclusions of Section 6 is that of serous questioning of Von Neumann's projection rule. I am far from the first to do so and from the book [36, p. 188] I quote "the projection rule is to be considered as a purely mathematical tool and no physical meaning should be ascribed to it."

Acknowledgement

A referee was especially helpful.

References

1. Einstein, A., Podolsky, B. & Rosen, N. (1935). Can quantum mechanical description of reality be considered complete?, *Phys. Rev.* 47, 777-780.
2. Jammer, M. (1974) *The Philosophy of Quantum Mechanics*, John Wiley & Sons, New York.
3. Einstein, A., Tolman, R. & Podolsky, B. (1931). Knowledge of past and future in quantum mechanics, *Phys. Rev.* 37, 780–781.
4. Einstein, A. (1932). Uber die Unbestimmtheitsrelation, *Zeitschrift für Angewandte Chemie* 45, 23.
5. Schrödinger, E. (1935). Die gegenwärtige Situation in der Quantenmechanik, *Die Naturwissenschaften* 23, 807–812, 824–828, 844–849.
6. Bohm, D. (1951). *Quantum Theory*, Prentice Hall, New Jersey.
7. Bell, J. (1964), On the Einstein–Podolsky–Rosen paradox, *Physics* 1, 195–200.
8. Aspect, A., Dalibard, J. & Roger, G. (1982). Experimental test of Bell's inequalities using time-varying analyzers, *Phys. Rev. Letters* 49, 1804–1807.
9. Wigner, E. (1970). On hidden variables and quantum mechanical probabilities, *Amer. J. Phys.* 38, 1005–1009.
10. Miller, W. (1972). *Symmetry Groups and Their Applications*, Academic Press, New York.
11. Accardi, L. & Fedullo, A. (1982). On the statistical meaning of complex numbers in quantum mechanics, *Lett. Nuovo. Cim.* 34, 161–172.
12. Gudder, S. & Zanghi, N. (1984). Probability models, *Nuovo Cim.* B 79, 291–301.
13. Gustafson, K. (1997). *Lectures on Computational Fluid Dynamics, Mathematical Physics, and Linear Algebra*, World Scientific, Singapore.
14. Gustafson, K. & Rao, D. (1997). *Numerical Range*, Springer, Berlin.
15. Gustafson, K. (1996). Commentary on: *Topics in the Analytic Theory of Matrices*, Section 23, Singular Angles of a square matrix, in *Collected Works of Helmut Wielandt*, vol. 2, eds. Huppert, B. & Schneider, H. (De Gruyters, Berlin), 356–367.
16. Gustafson, K. (1999). A computational trigonometry and related contributions by Russians Kantorovich, Krein, Kaporin, *Computational Technologies* 4, No. 3, 73–83.
17. Gustafson, K. (2001). An unconventional computational linear algebra: operator trigonometry, in *Unconventional Models of Computation, UMC'2K*, eds. I Antoniou, C. Calude, M. Denneen (Springer, London), 48–67.
18. Gustafson, K. (1999). The geometry of quantum probabilities, in *On Quanta, Mind, and Matter. Hans Primas in Context*, eds. H. Atmanspacher, A. Amann, U. Mueller-Herold, (Kluwer, Dordrecht), 151–164.
19. Gustafson, K. (1999). The trigonometry of quantum probabilities, in *Trends in Contemporary Infinite Dimensional Analysis and Quantum Probability*, eds. L. Accardi, H. Kuo, N. Obata, K. Saito, S. Si, L. Streit, (Italian Institute of Culture, Kyoto), 159–173.
20. Gustafson, K. (2000). Quantum trigonometry, *Infinite Dimensional Analysis, Quantum Probability, and Related Topics* 3, 33–52.

21. Gustafson, K. (2001). Probability, geometry, and irreversibility in quantum mechanics, *Chaos, Solitons and Fractals* 12, 2849–2858.
22. Williams, C. P. and S. Clearwater (1997). *Explorations in Quantum Computing*, Springer, New York.
23. Khrennikov, A. (2000). A perturbaton of CHSH inequality induced by fluctiations of ensemble distributions, *J. Math. Physics* 41, 5934–5944.
24. Bohm, A. (1993). *Quantum Mechanics, Foundations and Applications*, Springer, New York.
25. Accardi, L. (1988). Foundations of quantum mechanics: a quantum probabilistic approach, in *The Nature of Quantum Paradoxes*, eds. Tarozzi, G. & Van der Merwe, A. (Kluwer, Dordrecht), pp. 257–323.
26. Jammer, M. (1991). John Stewart Bell and the debate on the significance of his contributions to the foundations of quantum mechanics, in *Bell's Theorem and the Foundations of Modern Physics*, eds. A. Van der Merwe, F. Selleri, G. Tarozzi (World Scientific, Singapore), 1-23.
27. Peres, A. (1993). *Quantum Theory, Concepts and Methods*, Kluwer, Dordrecht.
28. Herbert, N. (1975). Cryptographic approach to hidden variables, *Amer. J. Phys.* 43, 315–316.
29. Afriat, A. and F. Seleri (1999). *The Einstein, Podolsky, and Rosen Paradox*, Plenun Press, New York.
30. Van der Merwe, A., Selleri, F., & Tarozzi, G., Eds. (1991). *Bell's Theorem and the Foundations of Modern Physics*, World Scientific, Singapore.
31. Mermin, D. (1985). Is the moon there when nobody looks? Reality and the quantum theory, *Physics Today*, April, 38–47.
32. Maudlin, T. (1994). *Quantum Non-Locality and Relativity*, Blackwell, Oxford.
33. d'Espagnat, B. (1995). *Veiled Reality: An Analysis of Present-Day Quantum Mechanical Concepts*, Addison–Wesley, Reading, MA.
34. Accardi, L. (1984). The probabilistic roots of the quantum mechanical paradoxes, in *The Wave–Particle Dualism*, eds. S. Diner, D. Fargue, G. Lochak, F. Selleri (D. Reidel Publishing, Dordrecht), 297–330.
35. Accardi, L. (1981). Topics in quantum probability. *Physics Reports* 77, 169–192.
36. Namiki, M., Pascazio, S. and Nakazato, H. (1997). *Decoherence and Quantum Measurements*, World-Scientific, Singapore.

DISCUSSION

Chairman: P. Zoller

E. C. G. Sudarshan: I have two comments to make. One is that I completely agree with you that in fact it (Bell's Inequality) is unrelated to non-locality. It is very popular but quite often negligable. Second, I will ask the question in the following manner: can I have simultaneous quantum measurement distribution for all the three measurements?

K. Gustafson: That is a question people have looked at. The answer is gen-

erally no.

E. C. G. Sudarshan: What happens is that the non-measured but implied probability can be negative even though all measured probabilities are positive.

K. Gustafson: I don't know about that but in my opinion it is certainly not related to Bell's inequality.

SYSTEMS AND SUBSYSTEMS IN QUANTUM COMMUNICATION

V.V. BELOKUROV, O.A. KHRUSTALEV, V.A. SADOVNICHY AND O.D. TIMOFEEVSKAYA

M.V. Lomonosov Moscow State University

1 Introduction

Recent progress in quantum communications has caused a great interest in the problems connected with divisions of quantum systems into subsystems and reunifications of subsystems into a joint system.

Although general theory of such processes was proposed in 1927 [1], so far, a subtraction of a subsystem is often described in a primitive ("visual") manner, in terms of wave functions with comments a-la "reduction of wave packets".

It makes the explanation of quantum properties of subsystems look rather vague. As an example, we quote the classical paper [2] on the photon teleportation experiment.

The important property of an entangled pair is that as soon as a measurement on one particles projects it, say, onto $|\leftrightarrow>$ *the state of the other one is determined to be* $|\updownarrow>$*, and vice versa. How could a measurement on one of the particles instantaneously influence the state of the other particle, which can be arbitrary far away? Einstein, among many other distinguished physicists, could simply not accept this "spooky action at a distance". But this property of entangled states has been demonstrated by numerous experiments.*

These problems can be solved in the framework of von Neumann's density matrix formalism. The natural notion of "reduced density matrix" appears from the general definition of the density matrix. It is this operator that is the most adequate to associate with the notion of state of a subsystem.

While analyzing various experiments it often appears necessary to describe the state of a selected subsystem when the exact value of some observable associated with the subsystem is additional to the first one.

For these purposes in the next section we define the notion of **conditional density matrix**.

Although operators with the same title were defined previously (e.g., [5]), they supposed the very special structure of the Gilbert space of the total system and their forms were absolutely different from the form of our operator.
Our construction intimately related to von Neumann's ideas has a more general nature and a more simple structure.

2 Conditional density matrix

Consider two systems S_1 and S_2. The joint system is denoted as S_{12}.

The principal question that we want to answer here is how the states of the subsystems (or component systems) are related to the states of the joint system, and vice versa.

Let ρ_1 and ρ_2 be the density matrices of the systems S_1 and S_2.

If at least one of the states ρ_1 or ρ_2 is pure (i.e. ${\rho_i}^2 = \rho_i$) then these states determine the state of the compound system S_{12} uniquely:

$$\rho \quad = \quad \rho_1 \otimes \rho_2$$

If the state of the system S_{12} is ρ_{12} then the state of the system S_1 is determined by the following equation:

$$\rho_1 \quad = \quad Tr_2\ (\rho_{12}).$$

Now we can define the conditional density matrix.

If the state of the system S_{12} is ρ_{12} then the state of the system S_1 (upon the condition that the system S_2 is in the pure state ρ_2, ${\rho_2}^2 = \rho_2$) is

$$\rho_{1/2} \quad = \quad \frac{Tr_2\ (\rho_2\ \rho_{12})}{Tr\ (\rho_2\ \rho_{12})}.$$

Analogous operators were constructed with the help of some artificial procedures [3,4].

3 Example: Orthopositronium

As an example we consider orthopositronium - the system consisting of an electron and a positron. The total spin of the system is equal to zero. In this case the nonrelativistic approximation is valid and the state vector of the system is represented in the form of the product

$$\Psi(\vec{r}_e, \sigma_e; \vec{r}_p, \sigma_p) \quad = \quad \Phi(\vec{r}_e, \vec{r}_p)\ \chi(\sigma_e, \sigma_p).$$

The spinorial wave function is equal to

$$\chi(\sigma_e, \sigma_p) \quad = \quad \frac{1}{\sqrt{2}}\ (\chi_{\vec{n}}(\sigma_e)\ \chi_{(-\vec{n})}(\sigma_p) \ - \ \chi_{\vec{n}}(\sigma_p)\ \chi_{-\vec{n}}(\sigma_e)).$$

Here $\chi_{\vec{n}}(\sigma)$ and $\chi_{(-\vec{n})}(\sigma)$ are the eigenvectors of the operator that projects spin onto the vector $\vec{n}$:

$$(\vec{\sigma}\vec{n})\ \chi_{\vec{n}}(\sigma) \quad = \quad \chi_{\vec{n}}(\sigma),$$

$$(\vec{\sigma}\vec{n})\ \chi_{(-\vec{n})}(\sigma) \quad = \quad -\ \chi_{(-\vec{n})}(\sigma).$$

The spinorial density matrix of the system is determined by the operator with the kernel

$$\rho(\sigma; \sigma') \quad = \quad \chi(\sigma_e, \sigma_p)\ \chi^*(\sigma'_e, \sigma'_p),$$

The spinorial density matrix of the electron is

$$\rho_e(\sigma, \sigma') \quad = \quad \sum_{\xi} \chi(\sigma, \xi)\ \chi^*(\sigma', \xi) \quad =$$

$$\frac{1}{2}\ (\chi_{\vec{n}}(\sigma)\ \chi_{(-\vec{n})}(\sigma') \ + \ \chi_{\vec{n}}(\sigma)\ \chi_{(-\vec{n})}(\sigma')) \quad = \quad \frac{1}{2}E(\sigma, \sigma').$$

In this state the electron is completely unpolarized.

If there is a polarization filter on the way of the electron the latter will pass through it with the probability independent of the filter orientation. The same fact is valid for the positron if its spinorial state is measured independently of the electron spinorial state.

Now let us consider a quite different experiment. Namely, the positron passes through the polarization filter and the electron polarization is simultaneously measured. The operator that projects the positron spin onto the vector $\vec{m}$ (determined by the filter) is given by the kernel

$$P(\sigma,\sigma^{'}) \quad = \quad \chi_{\vec{m}}(\sigma)\ \chi^{*}_{\vec{m}}(\sigma^{'}).$$

Now the conditional density matrix of the electron equals to

$$\rho_{e/p}(\sigma,\sigma^{'}) \ = \ \frac{\sum_{(\sigma,\sigma^{'})}\chi_{\vec{m}}(\sigma)\ \chi^{*}_{\vec{m}}(\sigma^{'})\ \chi(\sigma_e,\sigma^{'})\ \chi^{*}(\sigma^{'}_e,\sigma)}{\sum_{(\xi,\sigma,\sigma^{'})}\chi_{\vec{m}}(\sigma)\ \chi^{*}_{\vec{m}}(\sigma^{'})\ \chi(\xi,\sigma^{'})\ \chi^{*}(\xi,\sigma)}.$$

The result of the summation is

$$\rho_{e/p}(\sigma,\sigma^{'}) \quad = \quad \chi_{(-\vec{m})}(\sigma)\ \chi^{*}_{(-\vec{m})}(\sigma^{'}).$$

Thus, if the polarization of the positron is somehow determined then the electron appears to be polarized in the direction opposite to that of the positron.

4 Teleportation

In the Innsbruck experiment on a photon state teleportation, the initial state of the system is the result of the unification of the pair of photons 1 and 2 being in the antisymmetric state $\chi(\sigma_1,\sigma_2)$ with summary angular momentum equal to zero and the photon 3 being in the state $\chi_{\vec{m}}(\sigma_3)$ (that is, being polarized along the vector $\vec{m}$). The joint system state is given by the density matrix

$$\rho(\sigma,\sigma^{'}) \quad = \quad \Psi(\sigma)\Psi^{*}(\sigma^{'}),$$

where the wave function of the joint system is the product

$$\Psi(\sigma) \quad = \quad \chi(\sigma_1,\sigma_2)\ \chi_{\vec{m}}(\sigma_3).$$

Considering then the photon 2 only (without fixing the states of the photons 1 and 3) we find the photon 2 to be completely unpolarized with the density matrix

$$\rho(\sigma_2,\sigma^{'}_2) \ = \ Tr_{(1,3)}\ \rho(\sigma_1,\sigma_2,\sigma_3;\sigma_1,\sigma^{'}_2,\sigma_3) \ = \ \frac{1}{2}\ E(\sigma_2,\sigma^{'}_2).$$

However, if the photon 2 is registered when the state of the photons 1 and 3 has been determined to be $\chi(\sigma_1,\sigma_3)$ then the state of the photon 2 is given by the conditional density matrix

$$\rho_{2/\{1,3\}} \quad = \quad \frac{Tr_{(1,3)}\ (P_{1,3}\ \rho_{1,2,3})}{Tr\ (P_{1,3}\ \rho_{1,2,3})}.$$

Here $P_{1,3}$ is the projection operator

$$P_{1,3} \quad = \quad \chi(\sigma_1,\sigma_3)\ \chi^{*}(\sigma_1,\sigma_3).$$

To evaluate the conditional density matrix it is convenient to preliminary find the vectors

$$\phi(\sigma_1) \quad = \quad \sum_3 \chi^*_{\vec{m}}(\sigma_3)\ \chi(\sigma_1, \sigma_3)$$

and

$$\theta(\sigma_2) \quad = \quad \sum_1 \phi^*(\sigma_1)\ \chi(\sigma_1, \sigma_2).$$

The vector θ equals to

$$\theta(\sigma_2) \quad = \quad -\frac{1}{2}\ \chi_{\vec{m}}(\sigma_2)$$

and the conditional density matrix of the photon 2 appears to be equal to

$$\rho_{2/\{1,3\}} \quad = \quad \chi_{\vec{m}}(\sigma_2)\ \chi^*_{\vec{m}}(\sigma_2^{'}).$$

Thus, if the subsystem consisting of the photons 1 and 3 is forced to be in the antisymmetric state $\chi(\sigma_1, \sigma_3)$ (with total angular momentum equal to zero) then the photon 2 appears to be polarized along the vector $\vec{m}$.

5 Pairs of polarized photons

Now consider a modification of the Innsbruck experiment. Let there be two pairs of photons (1, 2) and (3, 4). Suppose that each pair is in the pure antisymmetric state χ. The spinorial part of the density matrix of the total system is given by the equation

$$\rho(\sigma, \sigma^{'}) \quad = \quad \Psi(\sigma)\ \Psi^*(\sigma^{'}).$$

The wave function of the total system is the product of the wave functions of the subsystems

$$\Psi(\sigma) \quad = \quad \chi(\sigma_1, \sigma_2)\ \chi(\sigma_3, \sigma_4).$$

If there are polarization filters that transform states of the photons 2 and 4 into the states with definite polarization $\chi_{\vec{m}}(\sigma_2)$ and $\chi_{\vec{s}}(\sigma_4)$ then the wave function of the system is transformed into

$$\Phi(\sigma) \quad = \quad \chi_{\vec{n}}(\sigma_1)\ \chi_{\vec{m}}(\sigma_2)\ \chi_{\vec{r}}(\sigma_3)\ \chi_{\vec{s}}(\sigma_4).$$

Here $\vec{n}$, $\vec{m}$ and $\vec{r}$, $\vec{s}$ are pairs of mutually orthogonal vectors.

Now the conditional density matrix of the pair of photons 1 and 3 is

$$\rho_{(1,3)/(2,4)}(\sigma, \sigma^{'}) \quad = \quad \Psi(\sigma_1, \sigma_3)\ \Psi^*(\sigma_1^{'}, \sigma_3^{'}).$$

The (conditional) wave function of the pair is the product of wave functions of each photon with definite polarization

$$\Psi(\sigma_1, \sigma_3) \quad = \quad \chi_{\vec{n}}(\sigma_1)\ \chi_{\vec{r}}(\sigma_3).$$

6 Quantum realization of Vernam communication scheme

Modification of the character of correlation as a result of polarization of one of the pair of entangled photons can be used in communication schemes. We are not going to describe this scheme in detail. Instead we recall only the main idea of the Vernam communication scheme [6]. In this scheme, Alice encrypts her message (a string of bits denoted by the binary number m_1) using a randomly generated key k. She simply adds each bit of the message with the corresponding bit of the key to obtain the scrambled text ($s = m_1 \oplus k$, where $\oplus$ denotes the binary addition modulo 2 without carry). It is then sent to Bob, who decrypts the message by subtracting the key ($s \ominus k = m_1 \oplus k \ominus k = m_1$). Because the bits of the scrambled text are as random as those of the key, they do not contain any information. This cryptosystem is thus provable secure in the sense of information theory. Actually, today this is the only provably secure cryptosystem!

Although perfectly secure, the problem with this security is that it is essential that Alice and Bob possess a common secret key, which must be at least as long as the message itself. They can only use the key for a single encryption. If they used the key more than once, Eve could record all of the scrambled messages and start to build up a picture of the plain texts and thus also of the key. (If Eve recorded two different messages encrypted with the same key, she could add the scrambled text to obtain the sum of the plain texts: $s_1 \oplus s_2 = m_1 \oplus k \oplus m_2 \oplus k = m_1 \oplus m_2 \oplus k \oplus k = m_1 \oplus m_2$, where we used the fact that $\oplus$ is commutative.) Furthermore, the key has to be transmitted by some trusted means, such as a courier, or through a personal meeting between Alice and Bob. This procedure may be complex and expensive, and even may lead to a loophole in the system.

With the help of pairs of polarized photons we can overcome the shortcomings of the classical realization of the Vernam scheme. Suppose Alice sends to Bob pairs of polarized photons obtained according to the rules described in the previous section. Note that the concrete photons' polarizations are set up in Alice's laboratory and Eve does not know them. If the polarization of the photon 1 is set up by a random binary number p_i and the polarization of the photon 3 is set up by a number $m_i \oplus p_i$ then each photon (when considered separately) does not carry any information. However, Bob after obtaining these photons can add corresponding binary numbers and get the number m_i containing the information ($m_i \oplus p_i \oplus p_i = m_i$).

In this scheme, a secret code is created during the process of sending and is transferred to Bob together with the information. It makes the usage of the scheme completely secure.

References

1. J. von Neumann, Gött. Nach. pp. 1–57, 245 – 272, **1927**. See, also, J. von Neumann, Mathematische Grundlagen der Quantenmechanik, Berlin, 1932.
2. D. Bouwmeester, J.-W. Pan, K. Mattle, M. Eibl, H. Weinfurter, A. Zeillinger, Nature, **390**, pp. 577–579, **1997**.
3. K-H Fitchtner, M. Ohya, Quantum Teleportation with Entangled States given by Beam Splittings, quant-ph/9912083, 1999.

4. M. Koniorczyk, T. Kiss, J. Jansky, Teleportation: from probability distributions to quantum states, J. Phys. A (Math. Gen.) **34**, pp. 6949–6955, 2001.
5. L.B. Levitin, Chaos, Solitons and Fractals, **10**, n. 10, pp. 1651–1656, 1999.
6. G. Vernam, Cipher printing telegraph systems for secret wire and radio telegraph communications, J. Am. Inst. of Electrical Engineers, **45**, pp. 109-115, **1926**.

QUANTUM ENHANCEMENTS TO CHANNEL CAPACITY

SETH LLOYD
d'Arbeloff Laboratory for Information Systems and Technology,
Department of Mechanical Engineering, Massachusetts Institute of Technology,
Cambridge, Massachusetts 02139

Communication channels are physical systems that transfer information from one place to another. Like all physical systems, communication channels are governed by the laws of quantum mechanics. Quantum mechanics is known to bound the capacity of bosonic channels such as optical fibers or free-space electromagnetic communication: a single transverse mode of the electromagnetic field can communicate a number of bits per second proportional to the square root of the power invested in communication. This paper investigates the capacity of a variety of quantum channels, and shows that enhancements in channel capacity can be obtained by coupling together the information degrees of freedom in quantum channels. So, for example, by coupling together modes in a multimode optical fiber, one can in principle obtain a significant enhancement of the capacity of the fiber for fixed power over the same fiber with uncoupled modes.

Inquiries into the fundamental physical limits to communication date back a half century at least. Because of the central importance of electromagnetic methods for communication with the more recent emphasis on optical communication, with most of these efforts have focused on the bosonic channel [1–22]. Communication channels, like all physical systems, are at bottom quantum mechanical, and their physical limits are calculated using the laws of quantum mechanics. Quantum mechanics provides limitations to the rate of communication via the introduction of quantum noise and fluctuations. However, quantum mechanics can also provide opportunities for enhancement of channel capacity. A variety of results suggest that certain enhancements in channel capacity can be obtained by exploiting techniques of quantum information processing [23–26]. For example, quantum systems can be correlated with eachother in ways that classical systems cannot, a feature known as entanglement. It has been speculated that entanglement might be used enhance the capacity of quantum communication channels [24–28]. Perhaps the best known example of the use of entanglement to enhance communication capacity is that of super-dense coding [25], in which two parties who initially possess an entangled state can send two bits of classical information by sending a single quantum bit. In addition, shared prior entanglement may enhance the transmission capacity of quantum channels in the presence of noise [28]. In general, the amount by which entanglement can enhance communication is not known. Schumacher and Westmoreland [26] and Kholevo [27] have shown that sending an entangled state down parallel noiseless quantum channels does not in general enhance their capacity.

A recent paper by the author [29] investigates the question of whether it is possible to enhance the capacity of communication channels by coupling together their information-bearing degrees of freedom in a way that induces entanglement. Communication channels are physical systems, and physical systems can be coupled together. The resulting, composite system typically exhibits different behavior from a collection of uncoupled systems. In contrast to [24–28], which augment communication capacity by sending entangled states down uncoupled channels, or by ex-

ploiting pre-existing entanglement, this paper investigates the situation in which information-propagating degrees of freedom are coupled via a nonlinear dynamics to induce an entangled state in the process of transmission. Indeed, references [26-27] suggest that such a coupling may be necessary to obtain an enhancement of noiseless channel capacity via entanglement. Since one possible coupling is no coupling at all, if one allows the possibility of engineering entangling couplings between electromagnetic modes or spin chains, one cannot do worse than the unentangled case. The question is, how much better can one do? As [29] shows, for fixed power, M coupled, entangled spin chains or modes of the electromagnetic field can in principle transmit information at a rate at least $\sqrt{M}$ times greater than M uncoupled, unentangled chains or modes. The couplings are nonlinear, entangling couplings, and are likely to prove hard to engineer. But the potential rewards in increased communication capacity are large.

To understand how quantum mechanics allows enhancements of communication capacity, first review the case of unentangled parallel quantum channels. In particular, it is well established [1-22] that the broadband bosonic channel (a single transverse mode of the electromagnetic field) with power P can transmit $C_{1q} = \alpha\sqrt{P/\hbar}$ bits per second, where $\alpha = \sqrt{\pi/3}(1/\ln 2)$. A similar result holds for propagation of information down spin chains. (The power P is equal to the energy E used to transmit the information, divided by the total time t over which the transmission takes place: as noted in [8,17], this energy need not be dissipated in the course of transmission.) As a consequence [1], if the power is spread amongst M unentangled broadband bosonic channels, each with power P/M, the rate of communication is $C_{Mc} = \sqrt{M}C_{1q}$. This is the best known rate for power-limited communication using M unentangled channels, though it is not proven to be the limiting rate. For noiseless channels, however, references [26-27] imply that this rate cannot be surpassed merely by entangling the states of the channels while leaving their dynamics unchanged. By contrast, in [29] the author showed that if one couples together M spin chains or tranverse modes of the electromagnetic field to induce entanglement between the modes in the course of propagation, then using power P one can send information from A to B at a rate $C_{Mq} = \sqrt{2/\pi(1-2^{-M})}M\sqrt{P/\hbar} \approx MC_1 = \sqrt{M}C_{Mc}$. That is, for a fixed power, dynamics that entangle chains or modes can in principle outperform by a factor of $\sqrt{M}$ dynamics that leave the chains or modes unentangled.

To analyze the effect of an entangling dynamics on information propagation, we use a simpler channel model than the bosonic channel— the 'qubit' channel. The qubit channel immediately generalizes to channels consisting of spin chains and to modes of the electromagnetic field.

The qubit channel transmits a quantum bit from A to B. Suppose that A and B each possess a two-state quantum system, or 'qubit.' A's qubit holds the quantum state $|\psi\rangle$ which is to be transmitted to B, whose qubit is initially in the state $|0\rangle$. The two states $|0\rangle$ and $|1\rangle$ of the qubits are assumed to be degenerate, so that no energy is required to store the qubit. The qubit channel can be used either to transmit classical information - $|\psi\rangle = |0\rangle$ or $|1\rangle$ - or to transmit quantum information - $|\psi\rangle = \alpha|0\rangle + \beta|1\rangle$. The dynamics of the channel should transfer the information from A's qubit to B's qubit. After the transfer has taken place, B's qubit is in

the state $|\psi\rangle$ and A's qubit is in a standard state such as $|0\rangle$. The sole restriction placed on dynamics of the channel is that it obeys the rules of quantum mechanics: the time evolution of A's qubit and B's qubit, together with their environment and whatever interaction they use to transfer the information, is a unitary, Hamiltonian dynamics. (An arbitrary strictly positive time evolution can be embedded in such dynamics [30].) This requirement bounds the rate of reliable information transmission down the qubit channel for any possible dynamics given limited power.

Note that we are taking a different approach here from references [24–28]: rather than taking the dynamics of the channel as fixed, and attempting to improve its capacity by encoding information cleverly in quantum states, we are looking at all possible quantum channels operating between A's qubit and B's qubit, and investigating restrictions over all possible dynamics that can be used to transfer information from A to B. This would seem at first to be a quite ambitious goal: how can we restrict all possible dynamics? But in fact, all quantum dynamics obey the Margolus-Levitin theorem, which implies that when B's qubit is rotated by π, the average energy of the complete system above its ground state is $E \geq \pi\hbar/2\Delta t$, where Δt is the time over which the transfer takes place [31]. In [29], the Margolus-Levitin theorem is used to show that the maximum rate at which information can be sent down the qubit channel is $C_{1q} = 1/\Delta t = (2/\sqrt{\pi})\sqrt{P/\hbar}$. This result holds for any dynamics that reliably transfers the qubit from A to B. In other words, the power-limited capacity of the qubit channel differs from that of the broadband bosonic channel by a constant of order unity.

Note, as above, that the energy applied during transmission need not be dissipated: it is merely the energy invested in the propagation of information and can in principle be recovered after transmission. In fact, existing quantum logic devices can swap information from one place to another at rates given here, with minimal dissipation during the transfer process.

The bound C_{1q} applies to the reliable transmission of a single bit. If one accepts unreliable or noisy transfer, then the transfer time can be less than $\Delta t = \pi\hbar/4E$, as one does not have to rotate the state of A and B by the full angle π to transform them into an orthogonal state. This feature, together with the use of error correcting codes, can be used to enhance the rate of transfer of information for a given energy. In addition, if one is willing to send less than a full bit of information by sending a 0 with a higher probability, one can decrease the energy per transmission time Δt. The maximum rate of information transmission for such noisy implementations is currently unknown.

A simple example of an interaction that attains the qubit capacity limit [1] is the application of a 'swap' operation: $S|\psi\rangle_A|\phi\rangle_B = |\phi\rangle_A|\psi\rangle_B$ for all $|\psi\rangle, |\phi\rangle$. Clearly, the swap operator performs the desired transfer, and as shown in [29], attains power/capacity limit of the qubit channel. It does so coherently and without dissipation in principle. As noted above, existing quantum logic devices can swap information from one place to another at rates very close to this limit [35–37].

The proof that swap attains the desired limit C_{1q} relies on the properties of the swap operator [29]: S is unitary, $S^2 = 1$, consequently S is also Hermitian, $S = S^\dagger$. It is straightforward to show that $e^{i\pi S/2} = iS$. The proof that swap attains the desired power-limited information transfer rate for the qubit channel

uses S as a Hamiltonian, and applies this Hamiltonian for a time necessary to effect the information transfer.

The 'swap' picture of quantum information transmission assumes a direct transfer of A's qubit to B over a time $\Delta t \geq d(AB)/c$, where $d(AB)$ is the distance between A and B. To look at propagation effects, consider the case in which A's and B's qubits are coupled by an intervening chain of qubits $A_1 B_1 A_2 B_2 \ldots A_n B_n$, where A has access to A_1 and B has access to B_n. Here, it can be shown [29] that the transmission of information from A to B by repeated swapping down the chain of qubits comes within $\sqrt{2}$ of the the power/capacity limit C_{1q} .

Now turn to the case of multiple qubit channels that can be coupled to eachother during the course of propagation. It is here that entanglement leads to a significant enhancement in power-limited transmission rate. Clearly, M uncoupled qubit channels can transmit information at a rate $\sqrt{M}$ greater than a single quantum channel using the same power P merely by dividing the power equally amongst the channels [1]. Each channel now transmits at a rate $(2/\sqrt{\pi})\sqrt{P/M\hbar}$ giving an overall rate of transmission $C_{Mc} = (2M/\sqrt{\pi})\sqrt{P/M\hbar} = (2/\sqrt{\pi})\sqrt{MP/\hbar} = \sqrt{M}C_{1q}$. This rate enhancement is the best known enhancement for parallel unentangled channels and holds for both the bosonic channel and for the qubit channel. Because of the square root dependence of transmission rate on power, both the qubit and broadband bosonic channel are more efficient at a lower power. As a result, one improves performance by dividing up information and power among the different channels.

The goal of the present work is to show that one can improve on the unentangled transmission rate C_{Mc} by engineering interactions that entangle the qubit channels in the process of transmission. The goal of the M-channel transfer is to enact the $2M$-qubit analog of the swap above: $S_{1\ldots M} = S_1 S_2 \ldots S_M$, where S_1 is the swap operator on the first of A and B's qubit channels, S_2 is the swap operator on the second, etc. The $2M$ qubit swap $S_{1\ldots M}$ swaps A's M qubits with B's M qubits and has the same properties as the 2-qubit swap above (Hermitian, squares to one, etc.). An obvious way to perform the $2M$-qubit swap is just to apply M two-qubit swaps. I.e., one applies the Hamiltonian $S_1 + S_2 + \ldots + S_M$ for an amount of time required to perform the transfer in each of the channels. Since $e^{i\pi(S_1+S_2+\ldots+S_M)/2} = i^M S_1 S_2 \ldots S_M$, this method clearly effects the transfer. It is straightforward to verify that this method attains the unentangled transfer limit C_{Mq} above.

But the unentangled limit can be surpassed by the following method. $S_{1\ldots M}$ is Hermitian and can be applied as a Hamiltonian. It is easy to verify that $e^{i\pi S_{1\ldots M}/2} = iS_{1\ldots M}$: accordingly, applying the $2M$-qubit swap operator as a Hamiltonian also swaps the qubits. But it does so more efficiently than swapping the qubits one by one. In fact, in [29] it is shown that the transmission rate for applying the $2M$-qubit swap Hamiltonian is $C_{Mq} = 1/\Delta t = \sqrt{2(1-2^{-M})P/\pi\hbar}$. Comparing C_{Mq} with C_{Mc} we see that using the $2M$-qubit swap operator as a Hamiltonian gives an enhancement in transmission rate of $\sqrt{M}$ over swapping the qubits one by one.

In addition, applying the Hamiltonian $S_{1\ldots M}$ necessarily entangles the M qubit channels (except in some very simple cases as when the message being transmitted is $00\ldots0$). For example, if A's input state is $|b_M\rangle = |b_1 \ldots b_M\rangle$, then at time $\Delta t/2$ (halfway through the controlled flipping operation) A and B's qubits are in the

state $(e^{-i\pi/4}/\sqrt{2})(|b_1 \ldots b_M\rangle_A|00\ldots0\rangle_B + i|00\ldots0\rangle_A|b_1 \ldots b_M\rangle_B)$. Transferring M bits down M uncoupled, unentangled quantum channels using the same power as a single qubit channel takes $\sqrt{M}$ times longer than transferring the information down coupled, entangled channels. Unentangled transfer corresponds to the application of M two-qubit swap operations with Hamiltonian $S_1 + \ldots S_M$ as opposed to the $2M$-qubit swap Hamiltonian $S_{1\ldots M} = S_1 S_2 \ldots S_M$, and takes $\sqrt{M}$ times the energy of the entangled swap. As a result, the coupled, entangled channels have a capacity of at least $\sqrt{M}$ times the capacity of the uncoupled, unentangled channels.

Perhaps the most remarkable aspect of this result is that the use of entanglement allows the transfer of M bits in the same time and using the same power that it takes to transfer a single bit. In some sense, that it is just as easy in terms of power and energy to rotate $2M$ bits from one state to another as it is to rotate 2 bits from one state to another should not be surprising: no two states in Hilbert space are more than angle of π apart. Accordingly, if one can effect arbitrary evolutions on the M-qubit channel Hilbert space, M bits can be transferred using the same power and time as one bit. Effectively, the coupling between the channels allows them to transmit information in the form a 'super-boson' with 2^M internal states. The $\sqrt{M}$ enhancement afforded by exploiting entanglement is typical of quantum information processing and arises from essentially the same source as the $\sqrt{M}$ enhancements in quantum search [32] and quantum positioning [33].

Of course, enacting the necessary Hamiltonian $\tilde{S}_{1\ldots M}$ is likely to prove experimentally difficult. To attain the $\sqrt{M}$ enhancement of channel capacity allowed by entanglement, an M-qubit entangling operation must be used. The single qubit channel swap operator between A and B can be written $S = \sigma_x^A \sigma_x^B + \sigma_y^A \sigma_y^B + \sigma_z^A \sigma_z^B$, and the corresponding operator for swapping particles such as photons between A and B is $a_A a_B^\dagger + a_A^\dagger a_B$. The M-channel swap operator $S_{1\ldots M}$ is the product $S_1 S_2 \ldots S_M$ of the individual swap operators, and corresponds to interaction operators of the form $\sigma_x^1 \sigma_x^2 \ldots \sigma_x^M$ for spin qubits and $a_{A1} a_{B1}^\dagger \ldots a_{AM} a_{BM}^\dagger + H.C.$ for particle modes. That is, M'th order nonlinear interactions are required to attain the entanglement-enhanced channel capacity presented here. Enacting the proper entangling coupling is likely to prove experimentally difficult, but if such coupling can be enacted, substantial gains in quantum channel capacity can be obtained. Whether or not the potential gains afforded by entanglement can be realized in experimentally feasible quantum optical systems acting over significant distances remains an open question.

Acknowledgements

The author would like to thank Vittorio Giovannetti, Lorenzo Maccone, Hermann Haus, Jeff Shapiro, and Franco Wong for inspiration and for helpful discussions. This work was supported by ARDA via NRO and by the ARO under a MURI program.

References

1. C.M. Caves, P.D. Drummond, *Rev. Mod. Phys.* **66**, 481-537 (1994).

2. J.P. Gordon, in *Advances in Quantum Electronics*, J.R. Singer ed., (Columbia, New York, 1961), p. 509.
3. D.S. Lebedev, L.B. Levitin, *Dok. Akad. Nauk SSSR* **149**, 1299; *Sov. Phys. Dokl.* **8**, 377 (1963).
4. D.S. Lebedev, L.B. Levitin, *Inf. Control* **9**, 1 (1966).
5. H. Marko, *Kybernetik* **2**, 274 (1965).
6. H. Takahasi, in *Advances in Communication Systems, Vol. 1*, A.V. Balakrishnan, ed., (Academic, New York 1965), p. 227.
7. J.I. Bowen, *IEEE Trans. Inf. Theory* **IT-13**, 230 (1967).
8. R. Landauer, J.W.F. Woo, in *Synergetics*, H. Haken, ed., (Tuebner, Stuttgart 1973), p. 97.
9. C.W. Helstrom, *Proc. IEEE* (Lett.) **62**, 139 (1974).
10. H.P. Yuen, J.H. Shapiro, *IEEE Trans. Inf. Theory* **IT-24**, 657 (1978).
11. J.H. Shapiro, H.P. Yuen, J.A. Machado Mata, *IEEE Trans. Inf. Theory* **IT-25**, 179 (1979).
12. H.P. Yuen, J.H. Shapiro, *IEEE Trans. Inf. Theory* **IT-26**, 78 (1980).
13. L.B. Levitin, *Int. J. Th. Phys.* **21**, 299 (1982).
14. J.B. Pendry, *J. Phys. A* **16**, 2161 (1983).
15. Y. Yamamoto, H.A. Haus, *Rev. Mod. Phys.* **58**, 1001 (1986).
16. B.E.A. Saleh, M.C. Teich *Phys. Rev. Lett.* **58** 2656 (1987).
17. R. Landauer, *Nature 335*, 779 (1988).
18. J.D. Bekenstein, *Phys. Rev. A* **37**, 3437 (1988).
19. J.D. Bekenstein, M. Schiffer, *Int. J. Mod. Phys. C* **1**, 355 (1990).
20. Schiffer, *Phys. Rev. A* **43**, 5337 (1991).
21. H.P. Yuen, M. Ozawa, *Phys. Rev. Lett.* **70**. 363 (1992).
22. B.E.A. Saleh, M.C. Teich, *Proc. IEEE* **80**, 451 (1992).
23. A.S. Kholevo, *Probl. Peredachi Inf.* **9**, 3 (1973) [*Probl. Inf. Transm. (USSR)* **9**, 177 (1973)].
24. E.H. Lieb, M.B. Ruskai, *J. Math. Phys.* **14**, 1938 (1973).
25. C.H. Bennett, S.J. Wiesner, *Phys. Rev. Lett.* **69**, 2881 (1992).
26. B. Schumacher, M.D. Westmoreland, *Phys. Rev. A* **56**, 131 (1997).
27. A.S. Kholevo, *IEEE Trans. Inf. Theory* **44**, 269 (1998).
28. C.H. Bennett, P.W. Shor, J.A. Smolin, A.V. Thapliy, 'Entanglement-Assisted Capacity of a Quantum Channel and the Reverse Shannon Theorem,' arXiv: quant-ph/0106052.
29. S. Lloyd, *The power of entangled quantum channels,* submitted to Nature, ArXiv/quant-ph/0112034.
30. A. Peres, *Quantum Theory: Concepts and Methods*, (Kluwer, Hingham, 1995).
31. N. Margolus, L.B. Levitin, L.B., in *PhysComp96*, T. Toffoli, M. Biafore, J. Leao, eds. (NECSI, Boston, 1996); *Physica D* **120**, 188-195 (1998).
32. Grover, L.K., in *Proceedings of the 28th Annual ACM Symposium on the Theory of Computing* (ACM Press, New York, 1996), pp. 212-218.
33. V. Giovannetti, S. Lloyd, L. Maccone, *Nature* (2001).
34. Turchette, Q.A., Hood, C.J., Lange, W., Mabuchi, H., Kimble, H.J., *Phys. Rev. Lett.*, **75**, 4710-4713 (1995).
35. Monroe, C., Meekhof, D.M., King, B.E., Itano, W.M., Wineland, D.J., *Phys.*

Rev. Lett., **75**, 4714-4717 (1995).
36. Cory, D.G., Fahmy, A.F., Havel, T.F., in *PhysComp96, Proceedings of the Fourth Workshop on Physics and Computation*, T. Toffoli, M. Biafore, J. Leão, eds., (New England Complex Systems Institute, Boston, 1996).
37. Gershenfeld, N.A., Chuang, I.L. *Science* **275**, pp. 350-356 (1997).

DISCUSSION

Chairman: M. Raizen

N. Sourlas: Is there a simple formula for the case when you have probability of losing certain number of bits during transfer?

S. Lloyd: The question is: is there a simple formula for what will happen if there is a probability for losing certain number of bits in transfer? This is a really good question and I don't have something like that. But let me make few comments. One is that stuff like this is really going to be hard to do quantum mechanically. It is impossible to do classically and hard to do quantum mechanically. And often this kind of systems is very susceptible to noise, so decoherence will kill you. This kind of transmission is really messed up by noise, and indeed the fact that you have very entangled state in the process of transmission suggests that the enhancement will be disturbed by loss.

My guess is that this transfer will be $\sqrt{N}$ more sensitive to noise than classical transfer. That's a typical kind of price that you have to pay for this kind of things. Interestingly, however, if you can use error-correcting codes there are cases in which noise actually enhances the communication capacity. So I can actually do better if I'm allowed to use error-correcting codes.

G. Leuchs: Quantum dense coding is also a communication scheme which uses entanglement. What could you say about that?

S. Lloyd: Very good question. I'm glad that you asked. The result I dervied is much better than quantum dense coding in terms of the channel improvement. Quantum dense coding gives you a factor of 2 in the communication rate. The result that I derived gives an improvement of the square-root of the number of parallel channels. If you have a million modes, for example, you could get a thousand-fold improvement. Of course, I'm assuming Apollo-like power to entangle these photonic channels; so it is not surprising that I can do much better in terms of transmission. Indeed, I did not derive absolute information theoretic for the channel capacity, but the argument in terms of angles rotating in Hilbert spaces is a very powerful one and I would be very surprised if you will get more than a few bits more than this bound I've derived.

ENTANGLEMENT, KINETIC ENERGY AND THE QUANTUM FICTITIOUS POTENTIAL

J. BOTERO[1,2], M. A. CIRONE[1], J. P. DAHL[1,3], A. DELGADO[1,4] and W. P. SCHLEICH[1]

[1] *Abteilung für Quantenphysik, Universität Ulm, D-89069 Ulm, Germany*

[2] *Escuela Colombiana de Ingenieria, AA14520 Bogota, Colombia*

[3] *Chemical Physics, Department of Chemistry, Technical University of Denmark, DTU 207, DK-2800 Lyngby, Denmark*

[4] *Department of Physics and Astronomy, University of New Mexico, Albuquerque, New Mexico 87121, USA*

We discuss the average kinetic energy of N non–interacting quantum particles in its dependence on N. For a peculiar entangled state, the kinetic energy increases quadratically with N, in contrast to its behavior in simple thermodynamics.

1 Introduction

Entanglement as a resource is the common theme of quantum information, quantum computation and quantum cryptography. Moreover, entanglement marks one of the most essential differences between classical and quantum physics. In the present paper we draw attention to an unusual effect originating from entanglement: the average kinetic energy of N non–interacting but appropriately entangled particles depends quadratically on N. We refer to this effect as dimensional enhancement of kinetic energy [1].

The quadratic behavior of the kinetic energy, rather than the linear dependence familiar from simple thermodynamics [2], is reminiscent of superradiance [3], where the intensity of light radiated from N dipoles is N^2 times the intensity of a single one, rather than N. This superradiance effect is due to constructive interference between the individual dipoles. Similarly, we can trace the kinetic–energy enhancement back to interference of matter waves.

Our paper is organized as follows: In Sec. 2 we show that the average kinetic energy of the multiparticle system consists of two contributions: (*i*) the para–radial kinetic energy [1] corresponding to the square of the radial momentum operator [4], and (*ii*) the potential energy corresponding to the quantum fictitious force [5]. We dedicate Sec. 3 to the evaluation of the average kinetic energy of a system of N particles in three different quantum states: (*i*) a product state, (*ii*) a simple entangled state, and (*iii*) an unusual entangled state. We conclude in Sec. 4 with a brief summary.

2 Formulation of the problem

We start our discussion by first deriving expressions for the average kinetic energy of N non-relativistic particles of identical mass, M, in three space dimensions. Here, we concentrate on the motional degrees of freedom, but do not take into account the internal structure of the particles. Hence, we deal with a $D = 3N$ dimensional

configuration space, and the wave function $\Psi = \Psi(x_1, x_2, \ldots, x_D)$ depends on D coordinates.

2.1 *Average kinetic energy*

We recall that the kinetic-energy operator,

$$\hat{T} = -\frac{\hbar^2}{2M}\Delta^{(D)}, \tag{1}$$

is determined by the Laplacian [6]

$$\Delta^{(D)} = \frac{\partial^2}{\partial r^2} + \frac{D-1}{r}\frac{\partial}{\partial r} + \frac{\hat{\Lambda}^2}{r^2}, \tag{2}$$

in D dimensions. Here $r = (x_1^2 + x_2^2 + \cdots + x_D^2)^{1/2}$ denotes the radius in the D–dimensional hyperspace. The operator $\hat{\Lambda}^2$, which involves derivatives with respect to the $D-1$ angles of hyperspace, is proportional to the angular momentum operator in configuration space [7].

Hence, the average kinetic energy

$$\langle \hat{T} \rangle = -\frac{\hbar^2}{2M}\int_0^\infty dr\; r^{D-1} \int d\Omega_D\; \Psi^* \Delta^{(D)} \Psi \tag{3}$$

of the particles described by Ψ involves the Laplacian, Eq. (2), and integrations over the hyperradius r and the solid angle Ω_D in the D-dimensional hyperspace.

The dimensional enhancement effect is most conspicuous for s-states, that is, when the wave function depends on the hyperradius r only. In this case, the wave function is completely symmetric under exchange of coordinates of the particles, corresponding to a bosonic state.

For an s–state of wave function $\Psi = \Psi(r)$ the angular part of the Laplacian, that is, the operator $\hat{\Lambda}^2/r^2$ does not contribute to the integral. Moreover, it is useful to introduce the radial wave function u via the relation

$$\Psi(r) = \frac{1}{\sqrt{S_D}} \frac{u(r)}{r^{\frac{D-1}{2}}}, \tag{4}$$

where S_D denotes the total solid angle in D dimensions, and $u(r)$ is normalized.

When we recall the action of the Laplacian on the wave function

$$\Delta^{(D)}\Psi(r) = \frac{1}{\sqrt{S_D}} \frac{1}{r^{\frac{D-1}{2}}} \left[-\frac{\partial^2}{\partial r^2} + \frac{(D-1)(D-3)}{4r^2} \right] u(r) \tag{5}$$

the average kinetic energy defined by Eq. (3) takes the form

$$\langle \hat{T} \rangle \equiv T = T_r + T_V. \tag{6}$$

Here we refer to the contribution

$$T_r = \int_0^\infty dr\; u^*(r) \left[-\frac{\hbar^2}{2M}\frac{d^2}{dr^2} \right] u(r) \tag{7}$$

as the *para–radial kinetic energy*[1,4].

Furthermore, the contribution

$$T_V = \int_0^\infty dr\ V_Q(r)|u(r)|^2 \tag{8}$$

results from the *quantum fictitious potential*[5]

$$V_Q(r) = \frac{\hbar^2}{2M}\frac{(D-1)(D-3)}{4r^2}. \tag{9}$$

We conclude by emphasizing that for an s–state the kinetic energy may be said to be purely radial in hyperspace.

2.2 *Quantum fictitious potential*

Since the potential V_Q defined in Eq.(9) is proportional to the square of Planck's constant, it is a quantum potential with no classical analogue. Moreover, V_Q depends inversely on the square of the hyperradius. This feature reminds us of the classical centrifugal potential, which gives rise to the non-inertial, that is, fictitious centrifugal force. Indeed, for $D \geq 4$ the potential V_Q given by Eq. (9) is positive and thus corresponds to a repulsive force. This property suggests the name *quantum centrifugal potential*. In accordance with this, some authors[8] combine it with the contribution from $\hat{\Lambda}^2$, giving rise to the centrifugal potential. This combination, however, conceals the fact that it is a genuine part of the radial kinetic energy.

We note that for $D = 2$, the potential V_Q is negative corresponding to an attractive force. This centripetal force is unique to two dimensions and counterintuitive to the classical notion of the centrifugal force always being repulsive. To capture this contradiction, we have coined the phrase *quantum anti-centrifugal potential* for the potential V_Q in the case of $D = 2$. In Refs.[9] and[10] we have focused on consequences of this attractive potential. However, in the present work we concentrate on the repulsive case corresponding to $D \geq 4$.

We recognize that one and three dimensions are also special: the potential V_Q vanishes.

3 Wave functions

The dimension D of configuration space enters the quantum fictitious potential V_Q quadratically. Hence, the total kinetic energy resulting from T_V could in principle be quadratic in D. We recall that in the case of N particles in three space dimensions, we deal with a $D = 3N$ dimensional configuration space. Consequently, for $N \gg 1$, the strength $S \equiv (D-1)(D-3) = (3N-1)(3N-3) \simeq 9N^2$of the quantum non-inertial potential, is quadratic in the number of particles. According to Eq. (8), the same argument may hold for the contribution T_V to the kinetic energy. However, this feature strongly depends on the form and, in particular, on the D-dependence of the radial wave function u, as we show in the present section.

3.1 *Product wave function*

We start our discussion with the wave function

$$\Psi_0(r) = \varphi(x_1)\varphi(x_2)\cdots\varphi(x_D) = \left(\frac{\kappa^2}{\pi}\right)^{\frac{D}{4}} e^{-\frac{1}{2}\kappa^2 r^2}, \tag{10}$$

describing the state of a Bose-Einstein condensate of $N = D/3$ non-interacting particles in an isotropic magnetic trap at zero temperature [11]. The value of κ is determined by the harmonic potential of the trap. The wave function Ψ_0 is a product of normalized one–dimensional Gaussians

$$\varphi(x) = \left(\frac{\kappa^2}{\pi}\right)^{\frac{1}{4}} e^{-\frac{1}{2}\kappa^2 x^2}, \tag{11}$$

and does therefore not show any entanglement.

When we substitute the radial wave function u_0 corresponding to Ψ_0 into the expressions Eqs.(7) and (8) for the para–radial kinetic energy and the potential energy, and perform the integrals we arrive at

$$T^{(0)} = \frac{D}{2}\epsilon, \tag{12}$$

where we have introduced the kinetic energy $\epsilon \equiv (\hbar\kappa)^2/(2M)$.

Since $D = 3N$, we find indeed the familiar thermodynamic result

$$T^{(0)} = \frac{3}{2}N\epsilon \tag{13}$$

with the average kinetic energy being proportional to the number of particles. This result holds true for quantum states describing non–interacting and non–entangled particles.

3.2 *Entangled wave function*

Our second N-particle wave function, $\Psi_1(r)$, is constructed by retaining the wave function $\varphi(x)$ for $D-1$ space directions, while taking a wave function of the form $x^2\varphi(x)$ for the last direction. Symmetrization by forming the coherent sum $\sum_{i=1}^{D} x_i^2 \exp(-\frac{1}{2}\kappa^2 r^2)$, and subsequent normalization gives

$$\Psi_1(r) = \mathcal{N}_1(D) r^2 e^{-\frac{1}{2}\kappa^2 r^2}, \tag{14}$$

where the normalization constant $\mathcal{N}_1$dep ends on D.

In this case, the average kinetic energy

$$T^{(1)} = \left(\frac{D}{2} - 2 + \frac{8}{D+2}\right)\epsilon \tag{15}$$

has a more complicated dependence on the dimension D of configuration space. This feature is due to entanglement combined with the fact that the wave functions $\varphi(x)$ and $x^2\varphi(x)$ are non–orthogonal.

We note that for $D = 2$, the kinetic energies of the two states Ψ_0 and Ψ_1 are identical. However, for larger values of D, the kinetic energy of the entangled wave function Ψ_1, Eq.(14), is always below that of the product state. For a large number of particles, that is for large values of D, we approach the expression Eq.(12) corresponding to a product wave function.

3.3 Enhancement

We now turn to a rather unusual wave function. It is motivated by the requirement that the radial wave function u should be independent of the number of dimensions. However, quantum mechanics drastically restricts the set of possible states. Indeed, we recall from Eq.(4) that the radial wave function u has to be divided by $\sqrt{r^{D-1}}$ in order to provide the wave function Ψ. Hence, all derivatives of u must vanish at $r = 0$, in order that a proper $\Psi(r)$ may be constructed for any D.

The function

$$u_2(r) = \mathcal{N}_2 \exp\left[-\frac{1}{2}\left(\frac{\beta}{r} + \kappa r\right)\right] \tag{16}$$

fulfills this requirement. Here, β and κ are parameters and the normalization constant $\mathcal{N}_2$ can be expressed [1] in terms of the modified Bessel function of first order K_1[12].

Since the wave function $u_2(r)$ is independent of the dimension D, but the quantum fictitious potential is quadratic in D, the average kinetic energy must be quadratic in D. Indeed, when we substitute the wave function u_2 into the definitions Eqs. (7) and (8) of the energies T_r and T_V, and perform the integrations, we arrive at

$$T_r^{(2)} = \frac{1}{2\sqrt{\beta\kappa}} \frac{K_2(2\sqrt{\beta\kappa})}{K_1(2\sqrt{\beta\kappa})}\, \epsilon \tag{17}$$

and

$$T_V^{(2)} = \frac{(D-1)(D-3)}{4\beta\kappa}\, \epsilon, \tag{18}$$

where K_2 denotes the modified Bessel function of second order [12].

The para-radial contribution $T_r^{(2)}$ is independent of D. In contrast, $T_V^{(2)}$ involves D, and hence the number N of particles quadratically. This enhancement results from the quantum centrifugal potential and reflects the constraint that, as we squeeze more particles into the state, we do not alter the radial wave function u_2. Indeed, u_2 is independent of D, and thus independent of N. Forcing additional particles into this state leads to a strong increase in energy.

4 Summary

We have analyzed the kinetic energy of N non-interacting particles in free space. We have found an unusual entangled quantum state for which the average kinetic energy increases quadratically with the number of particles. This enhancement of kinetic energies is due to the wave nature of the atoms. It results from the form of the Laplacian in D dimensions, giving rise to the quantum fictitious potential.

Is this quadratic dependence on N the ultimate increase or is another asymptotic behavior possible? Does the degree of entanglement determine the deviation from the linear dependence? How does the analytic behavior of the wave function determine the asymptotics? Three questions that indicate that this research topic is by no means exhausted. To provide detailed answers goes beyond the scope of this paper. Here we can only indicate hints for further studies.

Starting with the last question, we note that the wave function u_2, Eq.(16), is non–analytic at the origin. It cannot be expanded into a Taylor series but into a Laurent series. All derivatives at the origin vanish. This feature is crucial in order to ensure the appropriate behavior of the wave function Ψ at the origin for all dimensions. We conjecture that there are many other wave functions besides u_2t hat satisfy this criterion and in this way lead to different power laws. In order to address the second question we need a meaningful measure of entanglement for continuous variable. This question is still in debate. Our example may provide some new insight into this problem.

In conclusion, we mention that the enhancement effect can also be interpreted[5] as a consequence of the commutation relation between the operators of the radial unit vector and the momentum in hyperspace. Indeed, the commutation relation provides via the uncertainty relation a lower bound of the kinetic energy which under appropriate conditions is quadratic in the number of dimensions.

Acknowledgments

One of us (WPS) is most grateful to I. Antoniou for organizing an exciting and stimulating conference in the splendid historic surroundings of Delphi. We thank G. Alber, E. Arimondo, I. Białynicki-Birula, F. Bopp, M. Mussinger, K. Vogel, W. Wonneberger and J. Yngvason for many fruitful discussions. J. B. and J. P. D. gratefully acknowledge the support of the Alexander von Humboldt–Stiftung. Moreover, the work of A. D. and W. P. S. is partially supported by the DAAD and the Deutsche Forschungsgemeinschaft, respectively. M. A. C. and W. P. S. are grateful for the financial contributions of the European Commission through the IHP Research Training Network QUEST and the IST project QUBITS.

References

1. W. P. Schleich and J. P. Dahl, Phys. Rev. A **65**, 052109 (2002).
2. See, for example, R. C. Tolman, *Relativity, thermodynamics, and cosmology* (Clarendon, Oxford, 1934).
3. R. H. Dicke, Phys. Rev. **93**, 99 (1954).
4. For a more detailed discussion of the subtleties associated with the concept of radial kinetic energy, see J. P. Dahl and W. P. Schleich, Phys. Rev. A **65**, 022109 (2002).
5. I. Białynicki–Birula, M. A. Cirone, J. P. Dahl, T. H. Seligman, F. Straub and W. P. Schleich, Fortschr. Phys. **50**, 599 (2002).
6. A. Sommerfeld, *Partielle Differentialgleichungen der Physik* (Geest & Portig, Leipzig, 1947); *Partial Differential Equations in Physics* (Academic Press,

New York, 1949).
7. J. Avery, *Hyperspherical Harmonics. Applications in Quantum Theory* (Kluwer, London, 1989).
8. D. R. Herschbach, in: *Dimensional Scaling in Chemical Physics*, p. 61, edited by D. R. Herschbach, J. Avery and O. Goscinski (Kluwer, Dordrecht, 1993).
9. M. A. Cirone, G. Metikas, and W. P. Schleich, Z. Naturf. **56a**, 48 (2001); M. A. Cirone, J. P. Dahl, M. Fedorov, D. Greenberger and W. P. Schleich, J. Phys. B. **35**, 191 (2002); M. A. Cirone, K. Rzązweski, W. P. Schleich, F. Straub and J. A. Wheeler, Phys. Rev. A **65**, 022101 (2002).
10. I. Białynicki-Birula, M. A. Cirone, J. P. Dahl, M. Fedorov, and W. P. Schleich, arXiv:quant-ph/0110116 (to appear in Phys. Rev. Lett.); I. Białynicki-Birula, M. A. Cirone, J. P. Dahl, R. F. O'Connell, and W. P. Schleich, to appear in J. Optics B: Quantum and Semiclassical Optics.
11. See, for example, G. Baym and C. J Pethick, Phys. Rev. Lett. **76**, 6 (1996).
12. M. Abramowitz and I. Stegun, *Handbook of Mathematical Functions* (National Bureau of Standards, Washington, 1964).

DISCUSSION

Chairman: M. Raizen

E. Yarevsky: You consider only s-waves. Actually it means that you have already introduced some special non-local interaction. If you would consider p or d-waves, you would have some other interaction. So it is some special kind of interactions that you have considered.

W. Schleich: Fine, I agree with every statement that you have made. If you would have a p-wave, you would see similar effects but they would not be surprising because p corresponds to angular momentum, and that just rises the angular momentum of the wave by a constant. The point here is that there is no rotation in this wave function; there is absolutely no angular momentum. The attraction is only due to the wave nature of that particular wave function. And of course you can say, yes, I have introduced a particular interaction, but the interaction is because – and I agree with you – of this s-wave. But what's wrong with that?

E. Yarevsky: Actually the problem is that if you have these particles, you cannot restrict yourself only to s-waves, because a real wave function has projections on different components.

W. Schleich: Here, I disagree with you because that is a matter of preparation, and I can prepare a wave function that is in this $s = 0$ state. There is absolutely no doubt in my mind.

L. Stodolsky: For easier understanding: you are introducing a sort of Hamiltonian.

W. Schleich: No, there is no need to show Hamiltonians. There are only two free particles, there is nothing more than that. But there are two parts to the problem: one part is kinematics, and the other is dynamics. In the problem with the N^2-dependence it is the kinematics that matters, so I don't need to know the

Hamiltonians.

L. Stodolsky: You need the Hamiltonians to do the calculations.

W. Schleich: That's what we did. We did the calculation and we found this effect. That's not so trivial because these particles live in a space of large dimensions.

L. Stodolsky: How do these high dimensions come in?

W. Schleich: That's exactly where the dynamics comes in. When you talk about two entangled particles, then you have to take the Hamiltonian into account in the dynamic part, and indeed, that's just a Hamiltonian of two free particles. I agree, there is nothing more.

L. Stodolsky: What's wrong with two particles?

W. Schleich: The point is, that if you look at any textbook, you might find such discussions for Gaussians. But I'm emphasizing the present wave function is not a Gaussian.

L. Stodolsky: No forces, just two free particles?

W. Schleich: That's right. They are prepared in a very specific case. They are not Gaussians, these are wave packets that have a node at the origin. You wouldn't see the effect if you would just take Gaussians. The attraction as well as the N^2-effect depends crucially on that particular wave function.

H. Kimble: Would you see the effect with a Bose-Einstein condensate?

W. Schleich: No! A Bose-Einstein condensate in its most elementary description would be a product state of Gaussians.

LONG DISTANCE QUANTUM COMMUNICATION

LUMING DUAN[1], M. LUKIN[2], P. ZOLLER[2], AND J. I. CIRAC[3]
[1] *Institute for Theoretical Physics, University of Innsbruck Technikerstrasse 25-2, A-6020 Innsbruck, Austria*
[2] *Physics Department, University of Harvard, Cambridge, MA, US*
[3] *Max-Planck Institut für Quantenoptik, Hans-Kopfermann Str. 1, D-85748 Garching, Germany*

We show how one can use atomic ensembles in order to construct quantum repeaters. This may allow for quantum communication over long distances.

1 Introduction

Quantum communication is an essential element required for constructing quantum networks, and it also has the application for absolutely secret transfer of classical messages by means of quantum cryptography [1] The central problem of quantum communication is to generate nearly perfect entangled states between distant sites. Such states can be used, for example, to implement secure quantum cryptography using the Ekert protocol [1], and to faithfully transfer quantum states via quantum teleportation [2]. All the known realistic schemes for quantum communication are based on the use of the photonic channels. However, the degree of entanglement generated between two distant sites normally decreases exponentially with the length of the connecting channel due to the optical absorption and other channel noise. To regain a high degree of entanglement, purification schemes can be used [3]. However, entanglement purification does not fully solve the long-distance quantum communication problem. Due to the exponential decay of the entanglement in the channel, one needs an exponentially large number of partially entangled states to obtain one highly entangled state, which means that for a sufficiently long distance the task becomes nearly impossible.

To overcome the difficulty associated with the exponential fidelity decay, the concept of quantum repeaters can be used [4]. In principle, it allows to make the overall communication fidelity very close to the unity, with the communication time growing only polynomially with the transmission distance. In analogy to a fault-tolerant quantum computing [5,6], the quantum repeater proposal is a cascaded entanglement purification protocol for communication systems. The basic idea is to divide the transmission channel into many segments, with the length of each segment comparable to the channel attenuation length. First, one generates entanglement and purifies it for each segment; the purified entanglement is then extended to a longer length by connecting two adjacent segments through entanglement swapping [2,7]. After entanglement swapping, the overall entanglement is decreased, and one has to purify it again. One can continue the rounds of the entanglement swapping and purification until a nearly perfect entangled states are created between two distant sites.

To implement the quantum repeater protocol, one needs to generate entanglement between distant quantum bits (qubits), store them for sufficiently long time

and perform local collective operations on several of these qubits. The requirement of quantum memory is essential since all purification protocols are probabilistic. When entanglement purification is performed for each segment of the channel, quantum memory can be used to keep the segment state if the purification succeeds and to repeat the purification for the segments only where the previous attempt fails. This is essentially important for polynomial scaling properties of the communication efficiency since with no available memory we have to require that the purifications for all the segments succeeds at the same time; the probability of such event decreases exponentially with the channel length. The requirement of quantum memory implies that we need to store the local qubits in the atomic internal states instead of the photonic states since it is difficult to store photons for a reasonably long time. With atoms as the local information carriers it seems to be very hard to implement quantum repeaters since normally one needs to achieve the strong coupling between atoms and photons with high-finesse cavities for atomic entanglement generation, purification, and swapping [8,9], which, in spite of the recent significant experimental advances [10,11,12], remains a very challenging technology.

To overcome this difficulty, Ref. [13] proposes a very different scheme to realize quantum repeaters based on the use of atomic ensembles with the ΛII-level configuration. The laser manipulation of the atomic ensembles, together with some simple linear optics devices and moderate single-photon detectors, do the whole work for long-distance quantum communication. The setup is much simpler compared with the single-atom and high-Q cavity approach discussed in the previous chapter. To achieve this, the scheme makes significant advances in each step of entanglement generation, connection, and applications, with each step having built-in entanglement purification and resilient to the realistic noise. As a result, the scheme circumvents the realistic noise and imperfections, and at the same time keeps the overhead in the communication time increasing with the distance only polynomially, as long as the atomic coherences survive the whole process. In this paper, we will review the realization of quantum repeaters and long-distance quantum communication following the approach in Ref. [13].

2 Entanglement generation

To realize long-distance quantum communication, first we need to entangle two atomic ensembles within the channel attenuation length. The entanglement generation scheme described here is based on single-photon interference at photodetectors, and is fault-tolerant to realistic noise. This scheme is an extension of a proposal first proposed in [14,15] to entangle single-atoms. The extension was made in [13] to entangle atomic ensembles with significant improvements in the communication efficiency thanks to the collective enhancement of the signal-to-noise ratio for many-atom ensembles.

The system is a sample of atoms prepared in the ground state $|1\rangle$ with the ΛII-level configuration (see Fig. 1). It can be shown that one can define an effective single-mode bosonic annihilation operator a for the cavity output signal (it is called the forward-scattered Stokes signal in the free space case). After the light-atom interaction, the signal mode a and the collective atomic mode $s \equiv \left(1/\sqrt{N_a}\right) \sum_i |1\rangle_i \langle 2|$

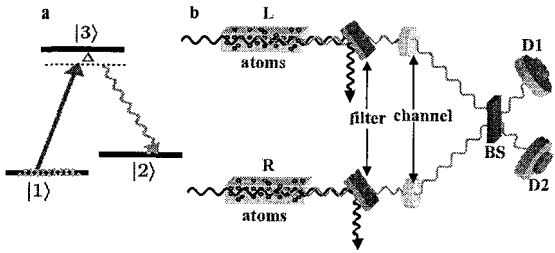

Figure 1. (1a) The relevant level structure of the atoms in the ensemble with $|1\rangle$, the ground state, $|2\rangle$, the metastable state for storing a qubit, and $|3\rangle$, the excited state. The transition $|1\rangle \rightarrow |3\rangle$ is coupled by the classical laser with the Rabi frequency Ω, and the forward scattering Stokes light comes from the transition $|3\rangle \rightarrow |2\rangle$. For convenience, we assume off-resonant coupling with a large detuning Δ. (1b) Schematic setup for generating entanglement between the two atomic ensembles L and R. The two ensembles are pencil shaped and illuminated by the synchronized classical laser pulses. The forward-scattering Stokes pulses are collected after the filters (polarization and frequency selective) and interfered at a 50%-50% beam splitter BS after the transmission channels, with the outputs detected respectively by two single-photon detectors D1 and D2. If there is a click in D1 *or* D2, the process is finished and we successfully generate entanglement between the ensembles L and R. Otherwise, we first apply a repumping pulse to the transition $|2\rangle \rightarrow |3\rangle$ on the ensembles L and R to set the state of the ensembles back to the ground state $|0\rangle_a^L \otimes |0\rangle_a^R$, then the same classical laser pulses as the first round are applied to the transition $|1\rangle \rightarrow |3\rangle$ and we detect again the forward-scattering Stokes pulses after the beam splitter. This process is repeated until finally we have a click in the D1 *or* D2 detector.

are in a two-mode squeezed state with the squeezing parameter r_c proportional to the interaction time t_Δ. If the interaction time t_Δ is very small, the whole state of the collective atomic mode and the signal mode can be written in the perturbative form

$$|\phi\rangle = |0_a\rangle |0_p\rangle + \sqrt{p_c} S^\dagger a^\dagger |0_a\rangle |0_p\rangle + o(p_c), \quad (1)$$

where $p_c = \tanh^2 r_c$ is the small excitation probability and $o(p_c)$ represents the terms with more excitations whose probabilities are equal or smaller than p_c^2. The $|0_a\rangle$ and $|0_p\rangle$ are respectively the atomic and optical vacuum states with $|0_a\rangle \equiv \bigotimes_i |1\rangle_i$. There is also a fraction of light from the transition $|3\rangle \rightarrow |2\rangle$ emitted in other directions which contributes to spontaneous emissions. It can be shown that the contribution to the population in the collective atomic mode s from the spontaneous emissions is very small for many-atom ensembles due to the collective enhancement of the signal-to-noise ratio for this mode.

Now we show how to use this setup to generate entanglement between two distant ensembles L and R using the configuration shown in Fig. 1. Here, two laser pulses excited both ensembles simultaneously, and the whole system is described by the state $|\phi\rangle_L \otimes |\phi\rangle_R$, where $|\phi\rangle_L$ and $|\phi\rangle_R$ are given by Eq. (1) with all the operators and states distinguished by the subscript L or R. The forward scattered Stokes signal from both ensembles is combined at the beam splitter and a photodetector click in either D1 *or* D2 measures the combined radiation from two samples, $a_+^\dagger a_+$ or $a_-^\dagger a_-$ with $a_\pm = \left(a_L \pm e^{i\varphi} a_R\right)/\sqrt{2}$. Here, φ denotes an unknown difference of the phase

shifts in the two-side channels. We can also assume that φ has an imaginary part to account for the possible asymmetry of the setup, which will also be corrected automatically in our scheme. But the setup asymmetry can be easily made very small, and for simplicity of expressions we assume that φ is real in the following. Conditional on the detector click, we should apply a_+ or a_- to the whole state $|\phi\rangle_L \otimes |\phi\rangle_R$, and the projected state of the ensembles L and R is nearly maximally entangled with the form (neglecting the high-order terms $o(p_c)$)

$$|\Psi_\varphi\rangle_{LR}^{\pm} = \left(S_L^\dagger \pm e^{i\varphi} S_R^\dagger\right)/\sqrt{2}\,|0_a\rangle_L\,|0_a\rangle_R\,. \tag{2}$$

The probability for getting a click is given by p_c for each round, so we need to repeat the process about $1/p_c$ times for a successful entanglement preparation, and the average preparation time is given by $T_0 \sim t_\Delta/p_c$. The states $|\Psi_r\rangle_{LR}^{+}$ and $|\Psi_r\rangle_{LR}^{-}$ can be easily transformed to each other by a simple local phase shift. Without loss of generality, we assume in the following that we generate the entangled state $|\Psi_r\rangle_{LR}^{+}$.

As will be shown below, the presence of the noise modifies the projected state of the ensembles to

$$\rho_{LR}(c_0,\varphi) = \frac{1}{c_0+1}\left(c_0\,|0_a0_a\rangle_{LR}\langle 0_a0_a| + |\Psi_\varphi\rangle_{LR}^{+}\langle\Psi_\varphi|\right), \tag{3}$$

where the "vacuum" coefficient c_0 is determined by the dark count rates of the photon detectors. It will be seen below that any state in the form of Eq. (3) will be purified automatically to a maximally entangled state in the entanglement-based communication schemes. We therefore call this state an effective maximally entangled (EME) state with the vacuum coefficient c_0 determining the purification efficiency.

3 Entanglement connection through swapping

After the successful generation of the entanglement within the attenuation length, we want to extend the quantum communication distance. This is done through entanglement swapping with the configuration shown in Fig. 2. Suppose that we start with two pairs of the entangled ensembles described by the state $\rho_{LI_1} \otimes \rho_{I_2R}$, where ρ_{LI_1} and ρ_{I_2R} are given by Eq. (3). In the ideal case, the setup shown in Fig. 2 measures the quantities corresponding to operators $S_\pm^\dagger S_\pm$ with $S_\pm = (S_{I_1} \pm S_{I_2})/\sqrt{2}$. If the measurement is successful (i.e., one of the detectors registers one photon), we will prepare the ensembles L and R into another EME state. The new φ -parameter is given by $\varphi_1+\varphi_2$, where φ_1 and φ_2 denote the old φ-parameters for the two segment EME states. As will be seen below, even in the presence of the realistic noise and imperfections, an EME state is still created after a detector click. The noise only influences the success probability to get a click and the new vacuum coefficient in the EME state. In general we can express the success probability p_1 and the new vacuum coefficient c_1 as $p_1 = f_1(c_0)$ and $c_1 = f_2(c_0)$, where the functions f_1 and f_2 depend on the particular noise properties.

The above method for connecting entanglement can be cascaded to arbitrarily extend the communication distance. For the ith ($i = 1, 2, \cdots, n$) entanglement

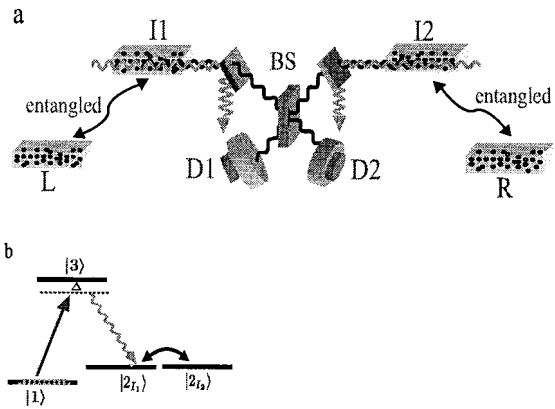

Figure 2. (2a) Illustrative setup for the entanglement swapping. We have two pairs of ensembles L, I_1 and I_2, R distributed at three sites L, I and R. Each of the ensemble-pairs L, I_1 and I_2, R is prepared in an EME state in the form of Eq. (3). The excitations in the collective modes of the ensembles I_1 and I_2 are transferred simultaneously to the optical excitations by the repumping pulses applied to the atomic transition $|2\rangle \rightarrow |3\rangle$, and the stimulated optical excitations, after a 50%-50% beam splitter, are detected by the single-photon detectors D1 and D2. If either D1 *or* D2 clicks, the protocol is successful and an EME state in the form of Eq. (3) is established between the ensembles L and R with a doubled communication distance. Otherwise, the process fails, and we need to repeat the previous entanglement generation and swapping until finally we have a click in D1 or D2, that is, until the protocol finally succeeds. (2b) The two intermediated ensembles I_1 and I_2 can also be replaced by one ensemble but with two metastable states I_1 and I_2 to store the two different collective modes. The 50%-50% beam splitter operation can be simply realized by a $\pi/2$ pulse on the two metastable states before the collective atomic excitations are transferred to the optical excitations.

connection, we first prepare in parallel two pairs of ensembles in the EME states with the same vacuum coefficient c_{i-1} and the same communication length L_{i-1}, and then perform the entanglement swapping as shown in Fig. 2, which now succeeds with a probability $p_i = f_1(c_{i-1})$. After a successful detector click, the communication length is extended to $L_i = 2L_{i-1}$, and the vacuum coefficient in the connected EME state becomes $c_i = f_2(c_{i-1})$. Since the ith entanglement connection need be repeated in average $1/p_i$ times, the total time needed to establish an EME state over the distance $L_n = 2^n L_0$ is given by $T_n = T_0 \prod_{i=1}^{n} (1/p_i)$, where L_0 denotes the distance of each segment in the entanglement generation.

4 Entanglement-based communication schemes

After an EME state has been established between two distant sites, we would like to use it in the communication protocols, such as quantum teleportation, cryptography, and Bell inequality detection. It is not obvious that the EME state (3), which is entangled in the Fock basis, is useful for these tasks since in the Fock basis it is experimentally hard to do certain single-bit operations. In the following we

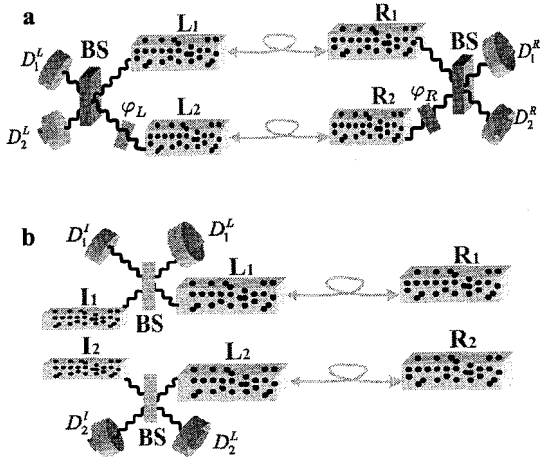

Figure 3. (3a) *Schematic setup for the realization of quantum cryptography and Bell inequality* detection. Two pairs of ensembles L_1, R_1 and L_2, R_2 (or two pairs of metastable states as shown in Fig. 1(b)) have been prepared in the EME states. The collective atomic excitations on each side are transferred to the optical excitations, which, respectively after a relative phase shift φ_L or φ_R and a 50%-50% beam splitter, are detected by the single-photon detectors D_1^L, D_2^L and D_1^R, D_2^R. We look at the four possible coincidences of D_1^R, D_2^R with D_1^L, D_2^L, which are functions of the phase difference $\varphi_L - \varphi_R$. Depending on the choice of φ_L and φ_R, this setup can realize both the quantum cryptography and the Bell inequality detection. (3b) Schematic setup for probabilistic quantum teleportation of the atomic "polarization" state. Similarly, two pairs of ensembles L_1, R_1 and L_2, R_2 are prepared in the EME states. We want to teleport an atomic "polarization" state $\left(d_0 S_{I_1}^\dagger + d_1 S_{I_2}^\dagger\right)|0_a 0_a\rangle_{I_1 I_2}$ with unknown coefficients d_0, d_1 from the left to the right side, where $S_{I_1}^\dagger, S_{I_2}^\dagger$ denote the collective atomic operators for the two ensembles I_1 and I_2 (or two metastable states in the same ensemble). The collective atomic excitations in the ensembles I_1, L_1 and I_2, L_2 are transferred to the optical excitations, which, after a 50%-50% beam splitter, are detected by the single-photon detectors D_1^I, D_1^L and D_2^I, D_2^L. If there two clicks, one at D_1^L or D_1^I and another one at D_2^L or D_2^I, the protocol is successful. A π-phase rotation is then performed on the collective mode of the ensemble R_2 conditional on that the two clicks appear in the detectors D_1^I,D_2^L or D_2^I,D_1^L. The collective excitation in the ensembles R_1 and R_2, if appearing, would be found in the same "polarization" state $\left(d_0 S_{R_1}^\dagger + d_1 S_{R_2}^\dagger\right)|0_a 0_a\rangle_{R_1 R_2}$.

will show how the EME states can be used to realize all these protocols with simple experimental configurations.

Quantum cryptography and the Bell inequality detection are achieved with the setup shown by Fig. 3a. The state of the two pairs of ensembles is expressed as $\rho_{L_1 R_1} \otimes \rho_{L_2 R_2}$, where $\rho_{L_i R_i}$ $(i = 1, 2)$ denote the same EME state with the vacuum coefficient c_n if we have done n times entanglement connection. The φ-parameters in $\rho_{L_1 R_1}$ and $\rho_{L_2 R_2}$ are the same provided that the two states are established over the same stationary channels. We register only the coincidences of the two-side detectors, so the protocol is successful only if there is a click on each side. Under this condition, the vacuum components in the EME states, together with the state

components $S_{L_1}^{\dagger} S_{L_2}^{\dagger} |\text{vac}\rangle$ and $S_{R_1}^{\dagger} S_{R_2}^{\dagger} |\text{vac}\rangle$, where $|\text{vac}\rangle$ denotes the ensemble state $|0_a 0_a 0_a 0_a\rangle_{L_1 R_1 L_2 R_2}$, have no contributions to the experimental results. So, for the measurement scheme shown by Fig. 3, the ensemble state $\rho_{L_1 R_1} \otimes \rho_{L_2 R_2}$ is effectively equivalent to the following "polarization" maximally entangled (PME) state (the terminology of "polarization" comes from an analogy to the optical case)

$$|\Psi\rangle_{\text{PME}} = \left(S_{L_1}^{\dagger} S_{R_2}^{\dagger} + S_{L_2}^{\dagger} S_{R_1}^{\dagger}\right) / \sqrt{2} \, |\text{vac}\rangle \, . \tag{4}$$

The success probability for the projection from $\rho_{L_1 R_1} \otimes \rho_{L_2 R_2}$ to $|\Psi\rangle_{\text{PME}}$ (i.e., the probability to get a click on each side) is given by $p_a = 1/[2\,(c_n + 1)^2]$. One can also check that in Fig. 3, the phase shift ψ_Λ ($\Lambda = L$ or R) together with the corresponding beam splitter operation are equivalent to a single-bit rotation in the basis $\left\{ |0\rangle_\Lambda \equiv S_{\Lambda_1}^{\dagger} |0_a 0_a\rangle_{\Lambda_1 \Lambda_2} \, , \;\; |1\rangle_\Lambda \equiv S_{\Lambda_2}^{\dagger} |0_a 0_a\rangle_{\Lambda_1 \Lambda_2} \right\}$ with the rotation angle $\theta = \psi_\Lambda / 2$. Now, it is clear how to do quantum cryptography and Bell inequality detection since we have the PME state and we can perform the desired single-bit rotations in the corresponding basis. For instance, to distribute a quantum key between the two remote sides, we simply choose ψ_Λ randomly from the set $\{0, \pi/2\}$ with an equal probability, and keep the measurement results (to be 0 if D_1^Λ clicks, and 1 if D_1^Λ clicks) on both sides as the shared secret key if the two sides become aware that they have chosen the same phase shift after the public declare. This is exactly the Ekert scheme [1] and its absolute security follows directly from the proofs in [16,17]. For the Bell inequality detection, we infer the correlations $E(\psi_L, \psi_R) \equiv P_{D_1^L D_1^R} + P_{D_2^L D_2^R} - P_{D_1^L D_2^R} - P_{D_2^L D_1^R} = \cos(\psi_L - \psi_R)$ from the measurement of the coincidences $P_{D_1^L D_1^R}$ etc. For the setup shown in Fig. 3a, we would have $|E(0, \pi/4) + E(\pi/2, \pi/4) + E(\pi/2, 3\pi/4) - E(0, 3\pi/4)| = 2\sqrt{2}$, whereas for any local hidden variable theories, the CHSH inequality [18] implies that this value should be below 2.

We can also use the established long-distance EME states for faithful transfer of unknown quantum states through quantum teleportation, with the setup shown by Fig. 3b. In this setup, if two detectors click on the left side, there is a significant probability that there is no collective excitation on the right side since the product of the EME states $\rho_{L_1 R_1} \otimes \rho_{L_2 R_2}$ contains vacuum components. However, if there is a collective excitation appearing from the right side, its "polarization" state would be exactly the same as the one input from the left. So, as in the Innsbruck experiment [19], the teleportation here is probabilistic and needs posterior confirmation; but if it succeeds, the teleportation fidelity would be nearly perfect since in this case the entanglement is equivalently described by the PME state (4). The success probability for the teleportation is also given by $p_a = 1/[2\,(c_n + 1)^2]$, which determines the average number of repetitions for a successful teleportation.

5 Noise and built-in entanglement purification

We next discuss noise and imperfections in the schemes for entanglement generation, connection and applications. In particular we show that each step contains built-in entanglement purification which makes the whole scheme resilient to the realistic noise and imperfections.

In the entanglement generation, the dominant noise is the photon loss, which includes the contributions from the channel attenuation, the spontaneous emissions in the atomic ensembles (which results in the population of the collective atomic mode s with the accompanying photon going to other directions), the coupling inefficiency of the Stokes signal into and out of the channel, and the inefficiency of the single-photon detectors. The loss probability is denoted by $1-\eta_p$ with the overall efficiency $\eta_p = \eta_p' e^{-L_0/L_{\rm att}}$, where we have separated the channel attenuation $e^{-L_0/L_{\rm att}}$ ($L_{\rm att}$ is the channel attenuation length) from other noise contributions η_p' with η_p' independent of the communication distance L_0. The photon loss decreases the success probably for getting a detector click from p_c to $\eta_p p_c$, but it has no influence on the resulting EME state. Due to this noise, the entanglement preparation time should be replaced by $T_0 \sim t_\Delta/(\eta_p p_c)$. The second source of noise comes from the dark counts of the single-photon detectors. The dark count gives a detector click, but without population of the collective atomic mode, so it contributes to the vacuum coefficient in the EME state. If the dark count comes up with a probability p_{dc} for the time interval t_Δ, the vacuum coefficient is given by $c_0 = p_{dc}/(\eta_p p_c)$, which is typically much smaller than 1 since the Raman transition rate is much larger than the dark count rate. The final source of noise, which influences the fidelity to get the EME state, is caused by the event that more than one atom are excited to the collective mode S whereas there is only one click in D1 or D2. The conditional probability for that event is given by p_c, so we can estimate the fidelity imperfection $\Delta F_0 \equiv 1 - F_0$ for the entanglement generation by

$$\Delta F_0 \sim p_c. \tag{5}$$

Note that by decreasing the excitation probability p_c, one can make the fidelity imperfection closer and closer to zero with the price of a longer entanglement preparation time T_0. This is the basic idea of the entanglement purification. So, in this scheme, the confirmation of the click from the single-photon detector generates and purifies entanglement at the same time.

In the entanglement swapping, the dominant noise is still the losses, which include the contributions from the detector inefficiency, the inefficiency of the excitation transfer from the collective atomic mode to the optical mode [21,22], and the small decay of the atomic excitation during the storage [21,22]. Note that by introducing the detector inefficiency, we have automatically taken into account the imperfection that the detectors cannot distinguish the single and the two photons. With all these losses, the overall efficiency in the entanglement swapping is denoted by η_s. The loss in the entanglement swapping gives contributions to the vacuum coefficient in the connected EME state, since in the presence of loss a single detector click might result from two collective excitations in the ensembles I_1 and I_2, and in this case, the collective modes in the ensembles L and R have to be in a vacuum state. After taking into account the realistic noise, we can specify the success probability and the new vacuum coefficient for the ith entanglement connection by the recursion relations $p_i \equiv f_1(c_{i-1}) = \eta_s\left(1 - \frac{\eta_s}{2(c_{i-1}+1)}\right)/(c_{i-1}+1)$ and $c_i \equiv f_2(c_{i-1}) = 2c_{i-1} + 1 - \eta_s$. The coefficient c_0 for the entanglement preparation is typically much smaller than $1-\eta_s$, then we have $c_i \approx (2^i - 1)(1-\eta_s) = (L_i/L_0 - 1)(1-\eta_s)$, where L_i denotes the communication distance after i times entanglement connection. With the

expression for the c_i, we can easily evaluate the probability p_i and the communication time T_n for establishing a EME state over the distance $L_n = 2^n L_0$. After the entanglement connection, the fidelity of the EME state also decreases, and after n times connection, the overall fidelity imperfection $\Delta F_n \sim 2^n \Delta F_0 \sim (L_n/L_0)\,\Delta F_0$. We need fix ΔF_n to be small by decreasing the excitation probability p_c in Eq. (5).

It is important to point out that our entanglement connection scheme also has built-in entanglement purification function. This can be understood as follows: Each time we connect entanglement, the imperfections of the setup decrease the entanglement fraction $1/(c_i+1)$ in the EME state. However, the entanglement fraction decays only linearly with the distance (the number of segments), which is in contrast to the exponential decay of the entanglement for the connection schemes without entanglement purification. The reason for the slow decay is that in each time of the entanglement connection, we need to repeat the protocol until there is a detector click, and the confirmation of a click removes part of the added vacuum noise since a larger vacuum components in the EME state results in more times of repetitions. The built-in entanglement purification in the connection scheme is essential for the polynomial scaling law of the communication efficiency.

As in the entanglement generation and connection schemes, our entanglement application schemes also have built-in entanglement purification which makes them resilient to the realistic noise. Firstly, we have seen that the vacuum components in the EME states are removed from the confirmation of the detector clicks and thus have no influence on the fidelity of all the application schemes. Secondly, if the single-photon detectors and the atom-to-light excitation transitions in the application schemes are imperfect with the overall efficiency denoted by η_a, one can easily check that these imperfections only influence the efficiency to get the detector clicks with the success probability replaced by $p_a = \eta_a / \left[2\,(c_n+1)^2\right]$, and have no effects on the communication fidelity. Finally, we have seen that the phase shifts in the stationary channels and the small asymmetry of the stationary setup are removed automatically when we project the EME state to the PME state, and thus have no influence on the communication fidelity.

The noise not correctable by our scheme includes the detector dark count in the entanglement connection and the non-stationary channel noise and set asymmetries. The dark counts decrease the fidelity linearly with the number of segments L_n/L_0, and the non-stationary noise as well as the asymmetries decrease it by the random walk law $\sqrt{L_n/L_0}$. For each time of entanglement connection, the dark count probability is about 10^{-5} if we make a typical choice that the collective emission rate is about 10MHz and the dark count rate is 10^2Hz. So this noise is negligible even if we have communicated over a long distance (10^3 the channel attenuation length $L_{\rm att}$ for instance). The non-stationary channel noise and setup asymmetries can also be safely neglected for such a distance. For instance, it is relatively easy to control the non-stationary asymmetries in local laser operations to values below 10^{-4} with the use of accurate polarization techniques [20] for Zeeman sublevels (as in Fig. 2b).

6 Scaling of the communication efficiency

We have shown that each of our entanglement generation, connection, and application schemes has built-in entanglement purification, and as a result of this property, we can fix the communication fidelity to be nearly perfect, and at the same time keep the communication time to increase only polynomially with the distance. Assume that we want to communicate over a distance $L = L_n = 2^n L_0$. By fixing the overall fidelity imperfection to be a desired small value ΔF_n, the entanglement preparation time becomes $T_0 \sim t_\Delta / (\eta_p \Delta F_0) \sim (L_n/L_0)\, t_\Delta / (\eta_p \Delta F_n)$. For an effective generation of the PME state (4), the total communication time $T_{\rm tot} \sim T_n / p_a$ with $T_n \sim T_0 \prod_{i=1}^{n} (1/p_i)$. So the total communication time scales with the distance by the law

$$T_{\rm tot} \sim 2\,(L/L_0)^2 \,/\, (\eta_p p_a \Delta F_T \Pi_{i=1}^{n} p_i)\,, \qquad (6)$$

where the success probabilities p_i, p_a for the ith entanglement connection and for the entanglement application have been specified before. The expression (6) has confirmed that the communication time $T_{\rm tot}$ increases with the distance L only polynomially. We show this explicitly by taking two limiting cases. In the first case, the inefficiency $1 - \eta_s$ for the entanglement swapping is assumed to be negligibly small. One can deduce from Eq. (6) that in this case the communication time $T_{\rm tot} \sim T_{\rm con}\,(L/L_0)^2\, e^{L_0/L_{\rm att}}$, with the constant $T_{\rm con} \equiv 2t_\Delta / \left(\eta_p' \eta_a \Delta F_T\right)$ being independent of the segment and the total distances L_0 and L. The communication time $T_{\rm tot}$ increases with L quadratically. In the second case, we assume that the inefficiency $1 - \eta_s$ is considerably large. The communication time in this case is approximated by $T_{\rm tot} \sim T_{\rm con}(L/L_0)^{[\log_2(L/L_0)+1]/2+\log_2(1/\eta_s-1)+2} e^{L_0/L_{\rm att}}$, which increases with L still polynomially (or sub-exponentially in a more accurate language, but this makes no difference in practice since the factor $\log_2(L/L_0)$ is well bounded from above for any reasonably long distance). If $T_{\rm tot}$ increases with L/L_0 by the mth power law $(L/L_0)^m$, there is an optimal choice of the segment length to be $L_0 = mL_{\rm att}$ to minimize the time $T_{\rm tot}$. As a simple estimation of the improvement in the communication efficiency, we assume that the total distance L is about $100L_{\rm att}$, for a choice of the parameter $\eta_s \approx 2/3$, the communication time $T_{\rm tot}/T_{\rm con} \sim 10^6$ with the optimal segment length $L_0 \sim 5.7L_{\rm att}$. This result is a dramatic improvement compared with the direct communication case, where the communication time $T_{\rm tot}$ for getting a PME state increases with the distance L by the exponential law $T_{\rm tot} \sim T_{\rm con} e^{L/L_{\rm att}}$. For the same distance $L \sim 100L_{\rm att}$, one needs $T_{\rm tot}/T_{\rm con} \sim 10^{43}$ for direct communication, which means that for this example the present scheme is 10^{37} times more efficient.

7 Summary

In summary, in this section we explained the recent atomic ensemble scheme for implementation of quantum repeaters and long-distance quantum communication. The proposed technique allows to generate and connect the entanglement and use it in quantum teleportation, cryptography, and tests of Bell inequalities. All of the elements of the scheme are within the reach of current experimental technology,

and have the important property of built-in entanglement purification which makes them resilient to the realistic noise. As a result, the overhead required to implement the scheme, such as the communication time, scales polynomially with the channel length. This is in remarkable contrast to direct communication where the exponential overhead is required. Such an efficient scaling, combined with a relative simplicity of the proposed experimental setup, opens up realistic prospectives for quantum communication over long distances.

References

1. Ekert A., *Phys. Rev. Lett.*, **67** (1991) 661.
2. Bennett C. H., Brassard G., Crepeau C., Jozsa R., Peres A., and Wootters W. K. *Phys. Rev. Lett.*, **70** (1993) 1895.
3. Bennett C. H., Brassard G., Popescu S., Schumacher B., Smolin J. A., and Wootters W. K. *Phys. Rev. Lett.*, **76** (1996) 722.
4. Briegel H. J., Dur W., Cirac J. I., Zoller P., *Phys. Rev. Lett.*, **81** (1998) 5932; Dur W., Briegel H. J., Cirac J. I., Zoller P., *Phys. Rev. A*, **59** (1999) 169.
5. Knill E., R. Laflamme R., and Zurek W. H., *Science*, **279** (1998) 342.
6. Preskill J., *Proc. R. Soc. Lond. A*, **454** (1998) 385.
7. Zukowski M., Zeilinger A., Horne M. A., and Ekert A., *Phys. Rev. Lett.*, **71** (1993) 4287.
8. J. I. Cirac, P. Zoller, H. J. Kimble, and H. Mabuchi, *Phys. Rev. Lett.* **78**, 3221-3224 (1997).
9. S. J. Enk, J. I. Cirac, and P. Zoller, *Science* **279**, 205-207 (1998).
10. Ye J., Vernooy D. W., and Kimble H. J., *Phys. Rev. Lett.*, **83** (1999) 4987.
11. Hood C. J., Lynn T. W., Doherty A. C., Parkins A. S., and Kimble H. J., *Science* **287** (2000) 1447.
12. Pinkse P. W. H., Fischer T., Maunz T. P., and Rempe G., *Nature*, **404** (2000) 365.
13. Duan L.-M., Lukin M. D., Cirac J. I., and Zoller P., quant-ph/0105105, to appear in *Nature*.
14. Cabrillo C., Cirac J. I., G-Fernandez P., and Zoller P., *Phys. Rev. A*, **59** (1999) 1025.
15. S. Bose, P. L. Knight, M. B. Plenio, and V. Vedral, *Phys. Rev. Lett.* **83**, 5158-5161 (1999).
16. Lo H. K. and Chau H. F., *Science*, **283** (1999) 2050.
17. Shor P. W. and Preskill J., *Phys. Rev. Lett.*, **85** (2000) 441.
18. Clauser J. F., Horne M. A., Shimony A., and Holt R. A., *Phys. Rev. Lett.*, **23** (1969) 880.
19. Bouwmeester D., Pan J.-W., Mattle K., Eibl M., Weinfurter H., Zeilinger A., *Nature*, **390** (1997) 575.
20. Budker D., Yashuk V., and Zolotorev M., *Phys. Rev. Lett.*, **81** (1998) 5788.
21. Liu C., Dutton Z., Behroozi C. H., and Hau L. V., *Nature*, **409** (2001) 490.
22. Phillips D. F., Fleischhauer A., Mair A., and Walsworth R. L., and Lukin M. D., *Phys. Rev. Lett.*, **86** (2001) 783.

DISCUSSION

Chairman: A. Ekert

L. Accardi: When you extend your argument from single ion trap, two level, to N two-level systems, you produce entangled pairs or an entangled chain of N?

J. Cirac: Entangled pairs. One entangles the first two ions in an EPR state. Then one takes a second ion in the same trap and an ion somewhere else, and then creates another entangled pair. Now, one performs a joint measurement between these two ions in the same trap, and automatically what one has is that the first and the last ions become entangled.

L. Accardi: So you have to know which atom on the chain has emitted the photon, or it is not necessary?

J. Cirac: Yes.

L. Wang: In terms of keeping fidelity to a certain value such that you can do the repeating, what's the maximum loss I can tolerate in a fibre?

J. Cirac: The loss does not affect the fidelity, it is something independent. The loss means that the photon does not arrive so you have to repeat the procedure more times. So, if there is no phase change in a fibre but there is a bit of loss on the way, then you have to repeat it more times. The problem is that, of course, if you go to very long distances then you have to wait for a very long time, an exponential time with respect to the length. So it is better go to a short distance and wait for shorter times. And the fidelity would be 1. Now, what may happen is that there are not only losses, but also some other errors, in the fibre. This may damage your fidelity.

L. Wang: That's my question: how long a distance do I have to implement a repeater? I mean that's one kilometre, or that's one centimetre?

J. Cirac: 10 kilometres.

L. Wang: The second question quickly is: if I want to do only quantum key distribution, I don't need entanglement. What about that?

J. Cirac: Yes, you don't need entanglement but the problem is that you must use fault tolerant error correction. But in that case the error rate cannot be larger than 10^{-4}, so it is better do this with entanglement, with our protocol.

S. Lloyd: I have a question concerning these collective modes. How sensitive are these collective modes to the position of the detector?

J. Cirac: This is a Raman transition, and what we are using is that the laser and the detected photon propagate along the same direction. What counts now is that the relative k is basically zero, corresponding to a hyperfine transition. It is of the order of centimetres. So we can move the detectors over centimetres and nothing will happen.

L. Stodolsky: In the discussion, when you have the correlations, and that manifold does not go into the detector. They all cancel out somehow. So my question is: at the end, will I have the same result as if I have only one atom from ensemble A and one atom from ensemble B, and then average over all pairs?

J. Cirac: You will get the result. I mean, you can think there are N collective atomic modes, which are coupled to the electromagnetic field. And now what happens is that there is one of these last modes which is relevant - this is the one

coupled to the atomic collective modes - and the other ones are not relevant. Not relevant in the sense that you are not going to measure them, so that you will trace them out. But they don't interfere with the relevant modes. But of course, I didn't prove this fact in the talk; one has to read the paper to see how this works.

L. Stodolsky: So why do you need this collective language?

J. Cirac: Well, you need the collective language because otherwise you have to use a single atom. So the important point here is that we can get exactly the same as if we would have a single atom, but having many atoms. You don't have to make the effort of the isolating, cooling an atom, and all that. This is the claim.

UNIVERSAL QUANTUM COMPUTATION WITH JOSEPHSON JUNCTIONS

K. CH. CHATZISAVVAS*, C. DASKALOYANNIS†, C. P. PANOS‡
Physics Department, Aristotle University of Thessaloniki, 54124 Thessaloniki, Greece

An implementation method of a gate in a quantum computer is studied in terms of a finite number of steps evolving in time according to a finite number of basic Hamiltonians, which are controlled by on-off switches. As a working example, the case of a particular implementation of the two qubit computer employing a simple system of two coupled Josephson junctions is considered.

1 Introduction

In classical computing the programming is based on commands written in the machine language. Each command is translated into manipulations of the considered device, obtained by electronic switches. In quantum computation quantum mechanics is employed to process information. Although there are differences between classical and quantum computers, the programming in both cases should be based on commands, and a part of these commands is realized by quantum gates.

Initially, one of the leading ideas in quantum computation was the introduction of the notion of the universal gate [1]. Given the notion of a universal set of elementary gates, various physical implementations of a quantum computer have been proposed [2]. Naturally, in order for an implementation to qualify as a valid quantum computer, all the set of elementary gates have to be implemented by the proposed system. This property is related to the problem of controllability of the quantum computer. The controllability of quantum systems is an open problem under investigation [3].

Recently [4,5], attention was focused on the notion of encoded universality, which is a different functional approach to the quantum computation. Instead of forcing a physical system to act as a predetermined set of universal gates, which will be connected by quantum connections, the focus of research is proposed to be shifted to the study of the intrinsic ability of a given physical system, to act as a quantum computer using only its natural available interactions. Therefore the quantum computers are rather a collection of interacting cells (e.g. quantum dots, nuclear spins, Josephson junctions etc). These cells are controlled by external classical switches and they evolve in time by modifying the switches. The quantum algorithms are translated into time manipulations of the external classical switches which control the system. This kind of quantum computer does not have connections, which is the difficult part of a physical implementation. Any device operating by external classical switches has an internal range of capabilities, i.e. it can manipulate the quantum information encoded in a subspace of the full system of Hilbert space. This capability is called encoded universality of the system [4].

*E-MAIL: KCHATZ@AUTH.GR
†E-MAIL: DASKALO@AUTH.GR
‡E-MAIL: CHPANOS@AUTH.GR

The notion of the encoded universality is identical to the notion of the controllability [3] of the considered quantum device. The controllability on Lie groups from a mathematical point of view was studied in [6,7,8,9,10,11]. The controllability of atomic and molecular systems was studied by several authors, see review article [3] and the special issue of the *Chemical Physics* vol. 267, devoted to this problem. In the case of laser systems the question of controllability was studied by several authors and recently in [10,11]. In the present paper we investigate the conditions in order to obtain the full system of Hilbert space by a finite number of choices of the values of the classical switches. As a working example we use the Josephson junction devices in their simplest form [12,13,14,15], but this study can be extended in the case of quantum dots or NMR devices.

In this paper the intrinsic interaction of a system operating as a universal computer is employed instead of forcing the system to enact a predetermined set of universal gates [4]. As a basic building block we use a system of two identical Josephson junctions coupled by a mutual inductor. The values of the classical control parameters (the charging energy $E_c$and the inductor energy E_L) are chosen in such a way that four basic Hamiltonians, H_i,$(i = 1, \ldots, 4)$ are created by switching on and off the bias voltages and the inductor, where the tunneling amplitude E_J is assumed to be fixed. Our procedure allows the construction of any one-qubit and two-qubit gate, through a finite number of steps evolving in time according to the four basic Hamiltonians. Using the two Josephson junctions network a construction scheme of four steps for the simulation is presented in the case of an arbitrary one-qubit gate, and of fifteen steps, for the simulation of a fundamental two-qubit gate. The main idea of this paper is the use of a small number of Hamiltonian states in order to obtain the gates.

Each fundamental two-qubit gate U is represented by a *command* containing 15 *letters* i.e. the fifteen steps mentioned above. Each letter consists of a binary part (the states of the on-off switches), which determines the basic Hamiltonian used, and a numerical part corresponding to the time interval.

Our proposal can be generalized for N-qubit gates $(N > 2)$ belonging to the $SU(2^N)$. In that case $N + 2$ basic Hamiltonians are needed to implement such a gate. The generalization of these ideas is under investigation.

The paper is organized as follows: In section 2 we present for clarity reasons the formalism of Josephson junctions one-qubit devices. In section 3 we apply the formalism to two qubit gates and simulate two-qubit gates and the possible N-qubit generalizations are discussed. In section 4 the results are summarized. Finally in the Appendix A, the essential mathematical feedback is provided.

2 One-qubit devices

The simplest Josephson junction one qubit device is shown in Fig 1. In this section we give a summary of the considered device. The detailed description and the complete list of references can be found in the section II of the detailed review paper [16]. The device consists of a small superconducting island ("box"), with n excess Cooper pair charges connected by a tunnel junction with capacitance C_J and Josephson coupling energy E_J to a superconducting electrode. A control gate

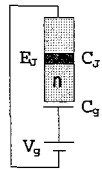

Figure 1. One qubit device

voltage V_g (ideal voltage source) is coupled to the system via a gate capacitor C_g.

The chosen material is such that the superconducting energy gap is the largest energy in the problem, larger even than the single-electron charging energy. In this case quasi-particle tunneling is suppressed at low temperatures, and a situation can be reached where no quasi-particle excitation is found on the island. Under special condition described in [16] only Cooper pairs tunnel coherently in the superconducting junction.

The voltage V_g is constrained in a range interval where the number of Cooper pairs takes the values 0 and 1, while all other coherent charge states, having much higher energy, can be ignored. These charge states correspond to the spin basis states:

$|\uparrow>$ corresponding to 0 Cooper-pair charges on the island, and

$|\downarrow>$ corresponding to 1 Cooper-pair charges.

In this case the superconducting charge box reduces to a two-state quantum system, *qubit*, with Hamiltonian (in spin 1/2 notation):

$$H = \frac{1}{2}E_c\,\sigma_3 - \frac{1}{2}E_J\,\sigma_1 \tag{1}$$

where

$$\sigma_3|\uparrow>=|\uparrow>, \quad \sigma_3|\downarrow>=-|\downarrow>$$

and

$$\sigma_1|\uparrow>=|\downarrow>, \quad \sigma_1|\downarrow>=|\uparrow>$$

In this Hamiltonian there are two parameters the *bias energy* E_c and the *tunneling amplitude* E_J. The bias energy E_c is controlled by the gate voltage V_g of Fig 1, while the tunneling amplitude E_J here is assumed to be constant i.e. it is a constant system parameter. The tunneling amplitude can be controlled in the case of the tunable effective Josephson junction, where the single Josephson junction is replaced by a flux-threaded SQUID [16], but this device is more complicated than the one considered in this paper.

The Hamiltonian is written as:

$$H = \frac{1}{2}\Delta E(\eta)(\cos\eta\,\sigma_3 - \sin\eta\,\sigma_1) \tag{2}$$

where η is the mixing angle

$$\eta \equiv \tan^{-1}\frac{E_J}{E_c}$$

The energy eigenvalues are

$$E_{\pm} = \pm \frac{\Delta E(\eta)}{2}$$

and the splitting between the eigenstates is:

$$\Delta E(\eta) = \sqrt{E_J^2 + E_c^2}$$

The eigenstates provided by the Hamiltonian (1), are denoted in the following as $|+>$ and $|->$:

$$\begin{aligned} |+> &= \cos\tfrac{\eta}{2}\,|\downarrow> + \sin\tfrac{\eta}{2}\,|\uparrow> \\ |-> &= \sin\tfrac{\eta}{2}\,|\downarrow> - \cos\tfrac{\eta}{2}\,|\uparrow> \end{aligned} \tag{3}$$

To avoid confusion we introduce a second set of Pauli matrices $\vec{\rho} = (\rho_1, \rho_2, \rho_3)$, which operate in the basis $|+>$, $|->$, while reserving the $\vec{\sigma}$ operators for the basis of $|\uparrow>$ and $|\downarrow>$:

$$\begin{aligned} \rho_3 &= |+><+| - |-><-|, \\ \rho_1 &= |+><-| + |-><+|, \\ \rho_2 &= i|-><+| - i|+><-| \end{aligned}$$

In the proposed model we assume that the device of Fig 1 has a switch taking two values 1 and 0, corresponding to the switch states *ON* and *OFF*. This switch controls the gate voltage V_g, which takes only two values either $V_{\rm id}$ or $V_{\rm deg}$, where the first one corresponds to the *idle Hamiltonian*, while the second one corresponds to the *degenerate Hamiltonian*.

The *idle* point can be achieved for a characteristic value of the control gate voltage $V_g = V_{\rm id}$, corresponding to a special value of the bias energy and to the phase parameter $\eta = \eta_{\rm id}$. At this point the energy splitting $\Delta E(\eta)$ achieves its maximum value, which is denoted by ΔE.

For simplicity reasons we reserve the symbol $E_c$for the bias energy corresponding to the idle point and by definition, the Hamiltonian at the *idle point* then becomes:

$$H_{\rm id} = \frac{E_c}{2}\sigma_3 - \frac{E_J}{2}\sigma_1 = \frac{1}{2}\Delta E\,\rho_3 \tag{4}$$

At the *degeneracy* point $\eta = \frac{\pi}{2}$ the energy splitting reduces to E_J, which is the minimal energy splitting. This point is characteristic for the material of the Josephson junction and corresponds to a special characteristic choice of the control gate voltage $V_g = V_{\rm deg}$.

$$H_{\rm deg} = -\frac{E_J}{2}\sigma_1 = -\frac{E_J}{2}\left(\sin\eta_{\rm id}\rho_3 - \cos\eta_{\rm id}\rho_1\right) \tag{5}$$

The system is switched in the state *OFF* (or 0) corresponding to the *degenerate* Hamiltonian (5) during a time interval t_1, then the system is switched to the state *ON* (or 1) i.e. the *idle* Hamiltonian (4) during a time interval t_2 and it comes back to the initial *degenerate* Hamiltonian during the time t_3 etc. The general form [22] of the evolution operator is:

$$U = \mathrm{e}^{-it_4 H_{\rm id}}\,\mathrm{e}^{-it_3 H_{\rm deg}}\,\mathrm{e}^{-it_2 H_{\rm id}}\,\mathrm{e}^{-it_1 H_{\rm deg}} \tag{6}$$

The operators $H_{\rm id}$ and $H_{\rm deg}$ and their commutator

$$[H_{\rm id}, H_{\rm deg}] = i\frac{E_c E_J}{2}\sigma_2$$

form a (non-orthogonal) basis of the algebra $su(2)$. Therefore the pair $H_{\rm id}$, $H_{\rm deg}$ generates $su(2)$ by taking these elements and all their possible commutators and their linear combinations. That means that the combination of four terms as in equation (6) for all the four time intervals $\{t_1, t_2, t_3, t_4\}$ cover all the matrices belonging in $SU(2)$.

Thus we conclude that every 2×2 matrix U in $SU(2)$ can be achieved by a device as in Fig 1, with manipulation of the binary switch permitting to the Hamiltonian two possible states i.e. the *idle* one and the *degenerate* one. The gate U corresponds to a *command*, each command is constituted by (three) letters, each of them having the form of a pair

$$\{e, t\}, \quad e = 0\,(OFF),\ \text{or}\ 1\,(ON),\ \text{and}\ 0 \le t < \infty$$

i.e. the command corresponding to equation (6) is analyzed in the following (at most four [22]) letters:

U
$\{0, t_1\}$
$\{1, t_2\}$
$\{0, t_3\}$
$\{1, t_4\}$

The one qubit gates are 2 × 2 unitary matrices belonging to the group U(2). Each element in the group $U(2)$ can be projected up to one multiplication constant to an element of group $SU(2)$. Evidently the elements generated by the evolution operator (6) belong to $SU(2)$. Throughout this paper we shall use projections of $U(2^N)$ matrices in $SU(2^N)$, using the symbol "$\mapsto$" to denote this projection. Let us consider the fundamental one qubit gates or commands NOT, $\sqrt{\rm NOT}$, Hadamard, Phase Shift and their $SU(2)$ projections:

$$\text{NOT} = \begin{pmatrix} 0 & 1 \\ 1 & 0 \end{pmatrix} \mapsto i\sigma_1 = \mathrm{e}^{-i\frac{\pi}{E_J}H_{\rm deg}} \in SU(2),$$

$$\sqrt{\text{NOT}} = \frac{1}{\sqrt{2}}\begin{pmatrix} \mathrm{e}^{-i\frac{\pi}{4}} & \mathrm{e}^{i\frac{\pi}{4}} \\ \mathrm{e}^{i\frac{\pi}{4}} & \mathrm{e}^{-i\frac{\pi}{4}} \end{pmatrix} \mapsto$$
$$\mapsto \frac{1}{\sqrt{2}}\left(\mathbb{I} + i\sigma_1\right) = \mathrm{e}^{-i\left(\frac{\pi}{2E_J}\right)H_{\rm deg}}$$

$$\text{Had} = \frac{1}{\sqrt{2}}\begin{pmatrix} 1 & 1 \\ 1 & -1 \end{pmatrix} \mapsto \frac{i}{\sqrt{2}}\left(\sigma_1 + \sigma_3\right) =$$
$$= \mathrm{e}^{-it_3^{\rm h}H_{\rm deg}}\,\mathrm{e}^{-it_2^{\rm h}H_{\rm id}}\,\mathrm{e}^{-it_1^{\rm h}H_{\rm deg}}$$

where

$$t_1^{\rm h} = t_3^{\rm h} = \frac{2\left(\cos^{-1}\left[\sqrt{\frac{E_J+E_c}{2E_c}}\right] + \frac{\pi}{2}\right)}{E_J},$$

$$t_2^{\mathrm{h}} = \frac{2\left(\sin^{-1}\left[\frac{\Delta E}{\sqrt{2}E_c}\right] + \pi\right)}{\Delta E}$$

and

$$\mathrm{PhS} = \begin{pmatrix} 1 & 0 \\ 0 & \mathrm{e}^{i\phi} \end{pmatrix} \mapsto \cos\tfrac{\phi}{2}\,\mathbb{I} - i\sin\tfrac{\phi}{2}\,\sigma_3 = \\ = \mathrm{e}^{-it_3^{\mathrm{ph}} H_{\mathrm{deg}}}\,\mathrm{e}^{-it_2^{\mathrm{ph}} H_{\mathrm{id}}}\,\mathrm{e}^{-it_1^{\mathrm{ph}} H_{\mathrm{deg}}}$$

where

$$t_1^{\mathrm{ph}} = t_3^{\mathrm{ph}} = \\ = \frac{2\left(\cos^{-1}\left[\frac{1}{2}\sqrt{2 - \frac{\sqrt{2}\,\Delta E\sqrt{-1+\frac{2E_c^2}{\Delta E^2}+\cos\phi}}{E_c\cos\frac{\phi}{2}}}\right] + \frac{\pi}{2}\right)}{E_J},$$

$$t_2^{\mathrm{ph}} = \frac{2\left(\sin^{-1}\left[\frac{\Delta E\,\sin\frac{\phi}{2}}{E_c}\right]\right)}{\Delta E}$$

The above formulas imply the following analysis of these commands in letters (Table 1).

NOT	$\sqrt{\mathrm{NOT}}$	Had	PhS
$\{0, \pi/E_J\}$	$\{0, \pi/2E_J\}$	$\{0, t_1^{\mathrm{h}}\}$	$\{0, t_1^{\mathrm{ph}}\}$
$--$	$--$	$\{1, t_2^{\mathrm{h}}\}$	$\{1, t_2^{\mathrm{ph}}\}$
$--$	$--$	$\{0, t_3^{\mathrm{h}}\}$	$\{0, t_3^{\mathrm{ph}}\}$

Table 1. Letter Analysis of One-qubit gates

The above analysis of a quantum gate in letters is rather trivial in the one qubit case and it was presented for clarity reasons, but the similar construction is far from evident and quite complicated in the N-qubit case.

3 Two-qubit devices

In order to perform one and two qubit quantum gate manipulations in the same device, we need to couple pairs of qubits together and to control the interaction between them. For this purpose identical Josephson junctions are coupled by one mutual inductor L as shown in Fig 2. The physics and the detailed description of the coupled Josephson junctions are discussed and reviewed in [16]. For $L = 0$ the system reduces to a series of uncoupled, single qubits, while for $L \to \infty$ they are coupled strongly. The ideal system would be one where the coupling between different qubits could be switched in the state *ON* (or state '1') by applying an induction via a constant value inductor L and in the state *OFF* (or state '0') corresponding to $L = 0$ and leaving the qubits uncoupled in the *idle* state.

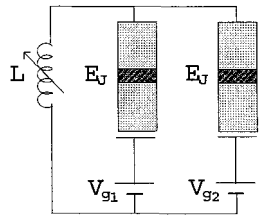

Figure 2. Two qubit device

The Hamiltonian for a general two-qubit system is written:

$$\begin{aligned} H &= H_1 + H_2 + H_{\text{int}} = \\ &= \tfrac{1}{2}E_{c_1}\,\sigma_3^{(1)} - \tfrac{1}{2}E_{J_1}\,\sigma_1^{(1)} + \\ &\quad + \tfrac{1}{2}E_{c_2}\,\sigma_3^{(2)} - \tfrac{1}{2}E_{J_2}\,\sigma_1^{(2)} - \tfrac{1}{2}E_L\,\sigma_2^{(1)}\,\sigma_2^{(2)} \end{aligned} \tag{7}$$

For an explanation of the formalism used in this section see Appendix A.

In the case of two identical junctions we have $E_{J_1} = E_{J_2} = E_J$, since the tunneling amplitude of the junction is a system parameter, depending on the material. Under these conditions the two coupled Josephson junctions Hamiltonian will be controlled by the following control parameters : E_{c_1}, E_{c_2}, E_L, which will be called *switches*. The first two parameters are controlled by the gate voltages V_{g_1}, V_{g_2}, while the last parameter is related to the inductor switch L. In the proposed model each of the parameters E_{c_1}, E_{c_2} can have two values 0 or E_c. The first is the state '0' (or OFF) corresponding to the *degenerate* one qubit state, while the other one is equal to E_c (ON or '1' state) corresponding to the one qubit *idle* state. Also the parameter E_L takes two values. The one is $E_L = 0$ (OFF or '0' state) corresponding to an uncoupled two qubit state and the other one has a fixed value (ON or '1' state). For the sake of simplicity we use the symbol E_L for this induction amplitude. Using this combination of parameter values or binary switches values, we can obtain the following four fundamental states of the Hamiltonian (7):

H_1: where both of the junctions are in the idle state ($E_{c_1} = E_{c_2} = E_c$), while they are uncoupled ($E_L = 0$).

$$H_1 = \frac{1}{2}E_c\,(\sigma_3^{(1)} + \sigma_3^{(2)}) - \frac{1}{2}E_J\,(\sigma_1^{(1)} + \sigma_1^{(2)}) \tag{8}$$

This Hamiltonian corresponds to the switches choice $(E_{c_1}, E_{c_2}, E_L) \rightarrow (1, 1, 0)$.

H_2: where both of the junctions are in the degenerate state ($E_{c_1} = E_{c_2} = 0$), while the two qubits are coupled.

$$H_2 = -\frac{1}{2}E_J\,(\sigma_1^{(1)} + \sigma_1^{(2)}) - \frac{1}{2}E_L\,\sigma_2^{(1)}\sigma_2^{(2)} \tag{9}$$

corresponding to the switch choice $(0, 0, 1)$.

H_3: where the first junction is in degeneracy ($E_{c_1} = 0$), the second is in the idle state ($E_{c_2} = E_c$) and they are uncoupled ($E_L = 0$).

$$H_3 = \frac{1}{2} E_c \sigma_3^{(2)} - \frac{1}{2} E_J (\sigma_1^{(1)} + \sigma_1^{(2)}) \tag{10}$$

corresponding to the switch choice $(0, 1, 0)$.

H_4: where the first junction is in the idle state ($E_{c_1} = E_c$), the second is in the degeneracy ($E_{c_2} = 0$) and they are uncoupled ($E_L = 0$).

$$H_4 = \frac{1}{2} E_c \sigma_3^{(1)} - \frac{1}{2} E_J (\sigma_1^{(1)} + \sigma_1^{(2)}) \tag{11}$$

corresponding to the switch choice $(1, 0, 0)$.

These four Hamiltonian forms are linearly independent and they can generate the su(4) algebra by repeated commutations and linear combinations. For a detailed discussion see the discussion in Appendix A, equation (25). Any elementary two-qubit gate, which is represented by a unitary 4×4 matrix $U \in$SU(4), can be constructed as follows:

$$\begin{aligned} U = {} & e^{-iH_{k_n} t_n} \dots e^{-iH_{k_1 5} t_{15}} e^{-iH_{k_1 4} t_{14}} \dots e^{-iH_{k_6} t_6} \cdot \\ & \cdot e^{-iH_{k_5} t_5} e^{-iH_{k_4} t_4} e^{-iH_{k_3} t_3} e^{-iH_{k_2} t_2} e^{-iH_{k_1} t_1} \end{aligned} \tag{12}$$

At the k-th step the device is put at one of the Hamiltonian states H_1, H_2, H_3 or H_4b y appropriate manipulations of the switches during a time interval t_k, $k = 1, 2, \dots, n$.

From a physical point of view any two qubit quantum gate can be obtained by n time steps. The maximum number of steps is a large finite number equal to 5449 [22]. In practice the fundamental two bit gates can be calculated by 15 steps. Each gate, corresponding to the 4×4 matrix U, is associated to a *command*. Each command consists of a number n *letters* or steps, each of them being a collection of 4 numbers $\{e_1, e_2, \ell, t\}$ of the following form for a command:

letter $\Leftrightarrow \{e_1, e_2, \ell, t\}$			$0 \le t < \infty$
$e_1 = 0$	if $V_{g_1} = V_{\text{deg}}$	$\Rightarrow$	$E_{c_1} = 0$
$= 1$	if $V_{g_1} = V_{\text{id}}$	$\Rightarrow$	$E_{c_1} = E_c$
$e_2 = 0$	if $V_{g_2} = V_{\text{deg}}$	$\Rightarrow$	$E_{c_2} = 0$
$= 1$	if $V_{g_2} = V_{\text{id}}$	$\Rightarrow$	$E_{c_2} = E_c$
$\ell = 0$	if $L = 0$	$\Rightarrow$	$E_L = 0$
$= 1$	if $L \neq 0$	$\Rightarrow$	$E_L \neq 0$

We shall show that any fundamental two-qubit gate U corresponds to a *command*, which contains 15 letters and is presented in Table 2, for the choice of parameters used by the experimentalists in their proposed Josephson junction models [12,13,14,15]. Each *letter* is the codified command which indicates the state of the binary switches and the time interval.

We should notice that the succession of switch states follows a cyclic pattern. This regularity might facilitate the manipulation of the coupled junction device.

Let us now give some numerical simulations of the proposed model for some fundamental quantum gates essential for the quantum computation (we use these

U
$\{1,1,0,t_1\}$
$\{0,0,1,t_2\}$
$\{0,1,0,t_3\}$
$\{1,0,0,t_4\}$
$\{1,1,0,t_5\}$
$\{0,0,1,t_6\}$
$\{0,1,0,t_7\}$
$\{1,0,0,t_8\}$
$\{1,1,0,t_9\}$
$\{0,0,1,t_{10}\}$
$\{0,1,0,t_{11}\}$
$\{1,0,0,t_{12}\}$
$\{1,1,0,t_{13}\}$
$\{0,0,1,t_{14}\}$
$\{0,1,0,t_{15}\}$

Table 2. Letter analysis of a command (gate) U

gates multiplied with a proper constant because the corresponding matrices should be elements of the $SU(4)$ group). These gates are:

1. The CNOT gate. Probably the most important gate in quantum computation:

$$\text{CNOT} = \begin{pmatrix} 1\,0\,0\,0 \\ 0\,1\,0\,0 \\ 0\,0\,0\,1 \\ 0\,0\,1\,0 \end{pmatrix} \mapsto$$

$$\mapsto \frac{e^{i\frac{\pi}{4}}}{2}\left(-\sigma_3^{(1)}\sigma_1^{(2)} + \sigma_3^{(1)} + \sigma_1^{(2)} + \mathbb{I}\otimes\mathbb{I}\right) \in SU(4)$$

2. The SWAP gate, which interchanges the input qubits:

$$\text{SWAP} = \begin{pmatrix} 1\,0\,0\,0 \\ 0\,0\,1\,0 \\ 0\,1\,0\,0 \\ 0\,0\,0\,1 \end{pmatrix} \mapsto$$

$$\mapsto \frac{e^{i\frac{\pi}{4}}}{2}\left(\sigma_1^{(1)}\sigma_1^{(2)} + \sigma_2^{(1)}\sigma_2^{(2)} + \sigma_3^{(1)}\sigma_3^{(2)} + \mathbb{I}\otimes\mathbb{I}\right)$$

3. The QFT_4 gate, the gate of the Quantum Fourier Transform (the quantum version of the Discrete Fourier Transform), for 2 qubits. A very useful gate for

the implementation of several quantum algorithms (e.g. Shor's algorithm):

$$\mathrm{QFT}_4 = \frac{1}{2}\begin{pmatrix} 1 & 1 & 1 & 1 \\ 1 & i & -1 & -i \\ 1 & -1 & 1 & -1 \\ 1 & -i & -1 & i \end{pmatrix} \mapsto$$

$$\mapsto \frac{e^{i\frac{3\pi}{8}}}{2\sqrt{2}}(\sigma_1^{(1)}\sigma_3^{(2)} + \mathbb{I}\otimes\mathbb{I}) + \frac{e^{-i\frac{\pi}{8}}}{2\sqrt{2}}(\sigma_1^{(1)} + \sigma_3^{(2)}) +$$
$$+\frac{e^{i\frac{\pi}{8}}}{2}(\sigma_2^{(1)}\sigma_2^{(2)} + \sigma_3^{(1)}\sigma_1^{(2)})$$

4. A conditional Phase Shift. This gate provides a conditional phase shift $e^{i\phi}$ on the second qubit (adds a phase to the second qubit):

$$\mathrm{PhShift} = \begin{pmatrix} 1 & 0 & 0 & 0 \\ 0 & 1 & 0 & 0 \\ 0 & 0 & 1 & 0 \\ 0 & 0 & 0 & e^{i\phi} \end{pmatrix} \mapsto$$

$$\mapsto \frac{i\sin\frac{\phi}{4}}{2}(\sigma_3^{(1)}\sigma_3^{(2)} - \sigma_3^{(1)} - \sigma_3^{(2)}) +$$
$$+\frac{1}{4}(3e^{-i\frac{\phi}{4}} + e^{i\frac{\phi}{4}})\,\mathbb{I}\otimes\mathbb{I}$$

In our analysis we consider this phase to be $\phi = \frac{\pi}{2}$.

In the simulations of this paper, the energies are assumed to take the following values:

$$E_c = 2.5\,K = 3.45\,10^{-23}\,J,$$

$$E_J = 0.1\,K = 0.138\,10^{-23}\,J,$$

$$E_L = 0.1\,K = 0.138\,10^{-23}\,J$$

i.e. the time scale is of the order of 10^{-11} sec . The numerical value corresponding to the idle state is chosen to conform to the available experimental data [20], and to keep in the range of different experimental propositions [15,17,18,16,19].

Each fundamental gate or command U_{gate} is approximated by an evolution operator $U(t_1, t_2, \ldots, t_{15})$ of the form (12). This simulation is equivalent to the analysis of the command U_{gate} to letters in conformity with Table 2. The efficiency of our simulation is defined by a *test function*, f_{test}. It is a function of 15 time variables:

$$f_{test}(t_1, t_2, \ldots, t_{15}) =$$
$$= \sum_{i,j=1}^{4} |(U_{\mathrm{gate}})_{ij} - (U(t_1, t_2, \ldots, t_{15}))_{ij}|^2 = \qquad (13)$$
$$= ||U_{\mathrm{gate}} - U||^2$$

Actually, f_{test} is the norm deviation of our simulation. The optimum, is obviously the nullification of this norm, $f_{test} = 0$. In fact we apply a minimization procedure and we calculate the time values, which minimize f_{test}. The numerical results are shown in Table 3.

CNOT	SWAP	QFT_4	Phase Shift($\phi = \frac{\pi}{2}$)
{1, 1, 0, 102.7757}	{1, 1, 0, 700.5872}	{1, 1, 0, 710.2581}	{1, 1, 0, 110.7116}
{0, 0, 1, 158.8193}	{0, 0, 1, 205.2390}	{0, 0, 1, 084.8635}	{0, 0, 1, 902.6813}
{0, 1, 0, 909.9617}	{0, 1, 0, 139.7456}	{0, 1, 0, 159.4397}	{0, 1, 0, 120.3082}
{1, 0, 0, 130.0504}	{1, 0, 0, 199.3881}	{1, 0, 0, 142.5689}	{1, 0, 0, 397.8240}
{1, 1, 0, 300.7220}	{1, 1, 0, 130.4966}	{1, 1, 0, 133.2760}	{1, 1, 0, 109.4998}
{0, 0, 1, 143.9878}	{0, 0, 1, 115.8947}	{0, 0, 1, 653.3505}	{0, 0, 1, 175.8195}
{0, 1, 0, 101.0584}	{0, 1, 0, 110.9584}	{0, 1, 0, 133.4825}	{0, 1, 0, 521.3209}
{1, 0, 0, 900.5691}	{1, 0, 0, 200.5504}	{1, 0, 0, 924.2883}	{1, 0, 0, 122.5053}
{1, 1, 0, 151.5296}	{1, 1, 0, 120.2794}	{1, 1, 0, 173.8055}	{1, 1, 0, 102.2305}
{0, 0, 1, 083.4085}	{0, 0, 1, 784.0008}	{0, 0, 1, 633.4525}	{0, 0, 1, 795.3231}
{0, 1, 0, 161.0839}	{0, 1, 0, 798.0702}	{0, 1, 0, 701.2262}	{0, 1, 0, 108.9077}
{1, 0, 0, 901.9591}	{1, 0, 0, 129.1358}	{1, 0, 0, 131.3048}	{1, 0, 0, 198.7137}
{1, 1, 0, 699.3097}	{1, 1, 0, 501.6780}	{1, 1, 0, 849.6562}	{1, 1, 0, 159.0513}
{0, 0, 1, 191.4272}	{0, 0, 1, 130.0444}	{0, 0, 1, 128.8483}	{0, 0, 1, 888.0009}
{0, 1, 0, 101.2086}	{0, 1, 0, 160.2219}	{0, 1, 0, 150.0286}	{0, 1, 0, 100.7132}
$f_{test} = 2.9 \times 10^{-6}$	$f_{test} = 9.5 \times 10^{-8}$	$f_{test} = 1.0 \times 10^{-7}$	$f_{test} = 1.2 \times 10^{-7}$

Table 3. Letter analysis of Two-Qubit Gates

In our numerical examples we use an approximation of the time parameters to the fourth decimal digit. Respectively we calculate the value of the test function. Taking into consideration three more decimal digits the test function f_{test} attains values of the order of 10^{-10}. It is a matter of intensity of the numerical algorithms used to find the minimum of the test function ($f_{test} = 0$) and convention of the number of decimal digits of the time parameters to succeed the optimal simulation. Indeed time parameters can not be determined with absolute precision in an implementation scheme for quantum computation.

The construction of the one-qubit gates with the two-qubit Josephson device of Fig 2 is possible. That is gates of the form $\mathbb{I} \otimes W$ and $W \otimes \mathbb{I}$, where $W \in SU(2)$, Fig 3, which are simulated by the same device.

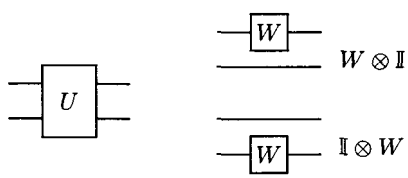

Figure 3. Two-qubit and one-qubit gates in two qubit networks

The construction scheme comes as follows:

$$U = \mathrm{e}^{-it_4 H_1} \mathrm{e}^{-it_3 H_4} \mathrm{e}^{-it_2 H_1} \mathrm{e}^{-it_1 H_4} \tag{14}$$

where H_1 and H_4 are special forms of the Hamiltonian (7), rewritten in the idle basis and $t_1, \ldots, t_4$ the time duration of each step. Obviously:

$$H_1 = \left(\tfrac{1}{2} E_c \sigma_3^{(1)} - \tfrac{1}{2} E_J \sigma_1^{(1)}\right) + \\ + \left(\tfrac{1}{2} E_c \sigma_3^{(2)} - \tfrac{1}{2} E_J \sigma_1^{(2)}\right) = \tfrac{\Delta E}{2} (\rho_3^{(1)} + \rho_3^{(2)})$$

$$H_4 = \left(\tfrac{1}{2} E_c \sigma_3^{(1)} - \tfrac{1}{2} E_J \sigma_1^{(1)}\right) - \tfrac{1}{2} E_J \sigma_1^{(2)} = \\ = \tfrac{\Delta E}{2} \left(\rho_3^{(1)} + \tau^{(2)}\right)$$

where

$$\tau = -\frac{E_J}{\Delta E} \sigma_1$$

It can easily be shown that:

$$U = \mathrm{e}^{-it_{tot} \frac{\Delta E}{2} \rho_3} \otimes \\ \otimes \mathrm{e}^{-it_4 \frac{\Delta E}{2} \rho_3} \mathrm{e}^{-it_3 \frac{\Delta E}{2} \tau} \mathrm{e}^{-it_2 \frac{\Delta E}{2} \rho_3} \mathrm{e}^{-it_1 \frac{\Delta E}{2} \tau}$$

Setting the total time

$$t_{tot} = \sum_{i=1}^{4} t_i = \frac{4k\pi}{\Delta E} \quad , k \in \mathbb{N}$$

the previous relation is written as:

$$U = \mathbb{I} \otimes \mathrm{e}^{-it_4 \frac{\Delta E}{2} \rho_3} \mathrm{e}^{-it_3 \frac{\Delta E}{2} \tau} \mathrm{e}^{-it_2 \frac{\Delta E}{2} \rho_3} \mathrm{e}^{-it_1 \frac{\Delta E}{2} \tau}$$

The right hand side of the last relation is a 2×2 SU(2) matrix depending on 3 independent time parameters t_1, t_2, t_3, since the fourth time parameter t_4 is specified from the demand that total time is assumed to be fixed. By an appropriate choice of these three time parameters any gate U of the above form can be constructed. So any command of the form $U = \mathbb{I} \otimes W$, which corresponds to an one qubit gate can be constructed by at most four steps. Therefore any command $\mathbb{I} \otimes W$ can be analyzed in at most four letters. We simulate numerically the proposed model for the following one-qubit gates, $\mathbb{I} \otimes$ (NOT), $\mathbb{I} \otimes$ (Had), $\mathbb{I} \otimes (\sqrt{\mathrm{NOT}})$ and $\mathbb{I} \otimes$ PhS:

$$\mathbb{I} \otimes \mathrm{NOT} = \begin{pmatrix} 0 & 1 & 0 & 0 \\ 1 & 0 & 0 & 0 \\ 0 & 0 & 0 & 1 \\ 0 & 0 & 1 & 0 \end{pmatrix} \mapsto \mathbb{I} \otimes (i\sigma_1) \in SU(4)$$

$$\mathbb{I} \otimes \mathrm{h} = \frac{1}{\sqrt{2}} \begin{pmatrix} 1 & 1 & 0 & 0 \\ 1 & -1 & 0 & 0 \\ 0 & 0 & 1 & 1 \\ 0 & 0 & 1 & -1 \end{pmatrix} \mapsto \mathbb{I} \otimes \left(\frac{i}{\sqrt{2}} (\sigma_1 + \sigma_3)\right)$$

$$\mathbb{I}\otimes\sqrt{\mathrm{NOT}}=\frac{1}{\sqrt{2}}\begin{pmatrix}\mathrm{e}^{-i\frac{\pi}{4}} & \mathrm{e}^{i\frac{\pi}{4}} & 0 & 0\\ \mathrm{e}^{i\frac{\pi}{4}} & \mathrm{e}^{-i\frac{\pi}{4}} & 0 & 0\\ 0 & 0 & \mathrm{e}^{-i\frac{\pi}{4}} & \mathrm{e}^{i\frac{\pi}{4}}\\ 0 & 0 & \mathrm{e}^{i\frac{\pi}{4}} & \mathrm{e}^{-i\frac{\pi}{4}}\end{pmatrix}\mapsto$$
$$\mapsto\mathbb{I}\otimes\left(\frac{1}{\sqrt{2}}(\mathbb{I}+i\sigma_1)\right)$$

$$\mathbb{I}\otimes\mathrm{PhS}=\begin{pmatrix}1 & 0 & 0 & 0\\ 0 & \mathrm{e}^{i\phi} & 0 & 0\\ 0 & 0 & 1 & 0\\ 0 & 0 & 0 & \mathrm{e}^{i\phi}\end{pmatrix}\mapsto\mathbb{I}\otimes\left(\cos\frac{\phi}{2}\,\mathbb{I}-i\sin\frac{\phi}{2}\,\sigma_3\right)$$

The case of the gates of the form $U=W\otimes\mathbb{I}$ can be similarly treated by using basic Hamiltonians $H_1$and H_3.

$$\begin{aligned}H_1&=\left(\tfrac{1}{2}E_c\,\sigma_3^{(1)}-\tfrac{1}{2}E_J\,\sigma_1^{(1)}\right)+\left(\tfrac{1}{2}E_c\,\sigma_3^{(2)}-\tfrac{1}{2}E_J\,\sigma_1^{(2)}\right)\\&=\tfrac{\Delta E}{2}(\rho_3^{(1)}+\rho_3^{(2)})\end{aligned}$$

$$\begin{aligned}H_3&=-\tfrac{1}{2}E_J\,\sigma_1^{(1)}\left(\tfrac{1}{2}E_c\,\sigma_3^{(2)}-\tfrac{1}{2}E_J\,\sigma_1^{(2)}\right)\\&=\tfrac{\Delta E}{2}\left(\tau^{(1)}+\rho_3^{(2)}\right)\end{aligned}$$

where

$$\tau=-\frac{E_J}{\Delta E}\sigma_1$$

The equivalent construction scheme is:

$$U=\mathrm{e}^{-it_4H_1}\mathrm{e}^{-it_3H_3}\mathrm{e}^{-it_2H_1}\mathrm{e}^{-it_1H_3} \tag{15}$$

Obviously,

$$U=\mathrm{e}^{-it_4\frac{\Delta E}{2}\rho_3}\mathrm{e}^{-it_3\frac{\Delta E}{2}\tau}\mathrm{e}^{-it_2\frac{\Delta E}{2}\rho_3}\mathrm{e}^{-it_1\frac{\Delta E}{2}\tau}\otimes$$
$$\otimes\mathrm{e}^{-it_{tot}\frac{\Delta E}{2}\rho_3}$$

Setting the total time

$$t_{tot}=\sum_{i=1}^{4}t_i=\frac{4k\pi}{\Delta E},\quad k\in\mathbb{N}$$

the previous relation is written as:

$$U=\mathrm{e}^{-it_4\frac{\Delta E}{2}\rho_3}\mathrm{e}^{-it_3\frac{\Delta E}{2}\tau}\mathrm{e}^{-it_2\frac{\Delta E}{2}\rho_3}\mathrm{e}^{-it_1\frac{\Delta E}{2}\tau}\otimes\mathbb{I}$$

It is apparent that the numerical results for a simulation of an one-qubit gate should be the same regardless of its form, $\mathbb{I}\otimes W$ or $W\otimes\mathbb{I}$. Thus the numerical results concerning the time parameters presented in Table 4 should be the same for the simulation of the corresponding gates NOT $\otimes\,\mathbb{I}$, Had $\otimes\,\mathbb{I}$, $\sqrt{\mathrm{NOT}}\otimes\mathbb{I}$, PhS $\otimes\,\mathbb{I}$.

Here it must be noticed that usually in order to achieve the construction of one qubit gates a more complicated technique is usually proposed. In this method the Josephson junctions are "neutralized" by appropriate annihilation of the tunneling amplitude E_J by using SQUID techniques [17,16].

$\mathbb{I} \otimes \mathrm{NOT}$	$\mathbb{I} \otimes \mathrm{Had}$	$\mathbb{I} \otimes \sqrt{\mathrm{NOT}}$	$\mathbb{I} \otimes \mathrm{PhS}$
$\{1,0,0,133.6621\}$	$\{1,0,0,113.3151\}$	$\{1,0,0,115.7315\}$	$\{1,0,0,114.9978\}$
$\{1,1,0,104.2929\}$	$\{1,1,0,111.1253\}$	$\{1,1,0,114.3695\}$	$\{1,1,0,109.2394\}$
$\{1,0,0,102.2461\}$	$\{1,0,0,109.4076\}$	$\{1,0,0,100.0236\}$	$\{1,0,0,115.3838\}$
$\{1,1,0,111.8267\}$	$\{1,1,0,118.1799\}$	$\{1,1,0,121.9033\}$	$\{1,1,0,112.4068\}$
$f_{test} = 1.5 \times 10^{-8}$	$f_{test} = 1.5 \times 10^{-8}$	$f_{test} = 3.4 \times 10^{-9}$	$f_{test} = 1.5 \times 10^{-9}$

$\mathrm{NOT} \otimes \mathbb{I}$	$\mathrm{h} \otimes \mathbb{I}$	$\sqrt{\mathrm{NOT}} \otimes \mathbb{I}$	$\mathrm{PhS} \otimes \mathbb{I}$
$\{0,1,0,133.6621\}$	$\{0,1,0,113.3151\}$	$\{0,1,0,115.7315\}$	$\{0,1,0,114.9978\}$
$\{1,1,0,104.2929\}$	$\{1,1,0,111.1253\}$	$\{1,1,0,114.3695\}$	$\{1,1,0,109.2394\}$
$\{0,1,0,102.2461\}$	$\{0,1,0,109.4076\}$	$\{0,1,0,100.0236\}$	$\{0,1,0,115.3838\}$
$\{1,1,0,111.8267\}$	$\{1,1,0,118.1799\}$	$\{1,1,0,121.9033\}$	$\{1,1,0,112.4068\}$
$f_{test} = 1.5 \times 10^{-8}$	$f_{test} = 1.5 \times 10^{-8}$	$f_{test} = 3.4 \times 10^{-9}$	$f_{test} = 1.5 \times 10^{-9}$

Table 4. Letter analysis of one-qubit gates in two qubit networks

4 Summary

The traditional approach to quantum computing is the construction of elementary one-qubit and two-qubit gates (universal set of quantum gates) which are connected by quantum connections and can represent any quantum algorithm [21]. A different view is employed in the present paper, proposed in [4,5] under the name of encoded universality. According to this, we do not force the system to act as a predetermined set of universal gates connected by quantum connections, but we exploit its intrinsic ability to act as a quantum computer employing its natural available interaction.

Thus, any one-qubit and two-qubit gate can be expressed by two identical Josephson junctions coupled by a mutual inductor. This can be realized by a finite number of time steps evolving according to a restricted collection of basic Hamiltonians. These Hamiltonians are implemented using the above system of junctions by choosing suitably the control parameters, by switching on and off the bias voltages and the mutual inductor. The interaction times of the steps are calculated numerically.

Each *command* consists of a series of *letters* and each letter of a binary part (the values of the switch characterizing the Hamiltonian) and a numerical part (the interaction time).

The generalization to N-qubit gates is currently under investigation. In this case we need $N + 2$ basic Hamiltonians in order to represent the corresponding N-qubit gate. The structure of commands is an open problem. However by using the techniques described in [21,22], the number of letters can be reasonably reduced in the N-qubit case. The application of the same methodology for other devices as quantum dots and NMR are under investigation.

Appendix

A Minimal generating set of the su(2^N) - algebra

Let us consider the su(2) algebra in the adjoint representation. This algebra representation is a three dimensional vector space with basis the 2×2 Pauli matrices:

$$\sigma_3 = \begin{pmatrix} 1 & 0 \\ 0 & -1 \end{pmatrix}, \quad \sigma_1 = \begin{pmatrix} 0 & 1 \\ 1 & 0 \end{pmatrix} \quad \text{and} \quad \sigma_2 = \begin{pmatrix} 0 & i \\ -i & 0 \end{pmatrix}$$

therefore

$$\text{su}(2) = \text{span}(\sigma_3, \sigma_1, \sigma_3)$$

This su(2) algebra in the adjoint representation is generated by the following 2×2 hermitian matrices:

$$\sigma_3 = \begin{pmatrix} 1 & 0 \\ 0 & 1 \end{pmatrix} \quad \text{and} \quad \sigma_1 = \begin{pmatrix} 0 & 1 \\ 1 & 0 \end{pmatrix}$$

because

$$[\sigma_3, \sigma_1] = 2i\sigma_2$$

The adjoint representation of the algebra su(2^2) is the vector space spanned by the 15 matrices

$$\text{su}(2^2) = \text{span}(\sigma_i^{(1)}, \sigma_i^{(2)}, \sigma_i^{(1)}\sigma_j^{(2)}, i,j = 1,2,3) \tag{16}$$

where

$$\sigma_i^{(1)} = \sigma_i \otimes \mathbb{I}, \quad \sigma_i^{(2)} = \mathbb{I} \otimes \sigma_i, \quad \sigma_i^{(1)}\sigma_j^{(2)} = \sigma_i \otimes \sigma_j$$

the adjoint representation of the su(2^2) algebra can be generated by linear combinations and successive commutations of the following 4 elements:

$$\sigma_3^{(1)}, \quad \sigma_3^{(2)}, \quad \sigma_1^{(1)} + \sigma_1^{(2)}, \text{ and } \sigma_2^{(1)}\sigma_2^{(2)} \tag{17}$$

This is indeed true because all the elements of the basis (16) can be generated by repeated commutations of the elements (17), because for $k = 1,2,3$:

$$\begin{aligned} \sigma_2^{(k)} &= \tfrac{i}{2}\left[\sigma_1^{(1)} + \sigma_1^{(2)}, \sigma_3^{(k)}\right], \\ \sigma_1^{(k)} &= \tfrac{i}{2}\left[\sigma_3^{(k)}, \sigma_2^{(k)}\right] = \\ &= \tfrac{1}{4}\left[\sigma_3^{(k)}, \left[\sigma_3^{(k)}, \sigma_1^{(1)} + \sigma_1^{(2)}\right]\right] \end{aligned} \tag{18}$$

The elements $\sigma_k^{(1)}\sigma_\ell^{(2)}$ can be generated by commutating the generators $\sigma_m^{(i)}$ with $\sigma_2^{(1)}\sigma_2^{(2)}$. One illustrative example is the construction of the element $\sigma_1^{(1)}\sigma_3^{(2)}$, by using the generators (17):

$$\begin{aligned} &\sigma_1^{(1)}\sigma_3^{(2)} = \tfrac{1}{4}\left[\sigma_1^{(2)}, \left[\sigma_3^{(1)}, \sigma_2^{(1)}\sigma_2^{(2)}\right]\right] = \\ &= \tfrac{1}{16}\left[\left[\sigma_3^{(k)}, \left[\sigma_3^{(k)}, \sigma_1^{(1)} + \sigma_1^{(2)}\right]\right], \left[\sigma_3^{(1)}, \sigma_2^{(1)}\sigma_2^{(2)}\right]\right] \end{aligned} \tag{19}$$

In the case of the adjoint representation of the algebra su(2^3), we can work following a similar methodology. The adjoint representation algebra su(2^3) is a vector space spanned by the following 63 matrices:

$$\begin{aligned} \mathrm{su}(2^3) = \mathrm{span}(&\sigma_i^{(1)}, \sigma_i^{(2)}, \sigma_i^{(3)}, \sigma_i^{(1)}\sigma_j^{(2)}, \\ &\sigma_i^{(1)}\sigma_j^{(2)}\sigma_k^{(3)}, i,j,k = 1,2,3) \end{aligned} \tag{20}$$

where

$$\sigma_i^{(1)} = \sigma_i \otimes \mathbb{I} \otimes \mathbb{I}, \quad \sigma_i^{(2)} = \mathbb{I} \otimes \sigma_i \otimes \mathbb{I} \quad \sigma_i^{(3)} = \mathbb{I} \otimes \mathbb{I} \otimes \sigma_i$$

The above elements can be generated by repeated commutations of the following 5 matrices:

$$\begin{gathered} \sigma_3^{(1)}, \quad \sigma_3^{(2)}, \quad \sigma_3^{(3)}, \\ \sigma_1^{(1)} + \sigma_1^{(2)} + \sigma_1^{(3)}, \text{ and} \\ \sigma_2^{(1)}\sigma_2^{(2)} + \sigma_2^{(1)}\sigma_2^{(3)} + \sigma_2^{(2)}\sigma_2^{(3)} \end{gathered} \tag{21}$$

The linear terms $\sigma_i^{(k)}$ can be easily generated by formulas as in equation (18). The quadratic terms $\sigma_i^{(k)}\sigma_j^{(\ell)}$ are generated by manipulations slightly more complicated than in the case of equation (19). Let us take the example of the generation of the element $\sigma_1^{(1)}\sigma_3^{(2)}$, then we must perform the following commutation actions:

$$\begin{aligned} &\sigma_2^{(1)}\sigma_1^{(2)} + \sigma_1^{(2)}\sigma_2^{(3)} = \\ &= \tfrac{i}{2}\left[\sigma_3^{(2)}, \sigma_2^{(1)}\sigma_2^{(2)} + \sigma_2^{(1)}\sigma_2^{(3)} + \sigma_2^{(2)}\sigma_2^{(3)}\right] \\ &\sigma_1^{(1)}\sigma_1^{(2)} = \tfrac{i}{2}\left[\sigma_3^{(1)}, \sigma_2^{(1)}\sigma_1^{(2)} + \sigma_1^{(2)}\sigma_2^{(3)}\right] \\ &\sigma_2^{(2)} = \tfrac{i}{2}\left[\sigma_3^{(2)}, \sigma_1^{(1)} + \sigma_1^{(2)} + \sigma_1^{(3)}\right] \\ &\sigma_1^{(1)}\sigma_3^{(2)} = \tfrac{i}{2}\left[\sigma_2^{(2)}, \sigma_1^{(1)}\sigma_1^{(2)}\right] \end{aligned} \tag{22}$$

Therefore all the quadratic terms can be generated by the elements (21). Let us now generate a cubic term of the algebra as the element $\sigma_3^{(1)}\sigma_2^{(2)}\sigma_1^{(3)}$. This element is generated by the commutation elements $\sigma_3^{(1)}\sigma_3^{(2)}$ and $\sigma_1^{(2)}\sigma_1^{(3)}$, which are generated previously:

$$\sigma_3^{(1)}\sigma_2^{(2)}\sigma_1^{(3)} = \frac{i}{2}\left[\sigma_3^{(1)}\sigma_3^{(2)}, \sigma_1^{(2)}\sigma_1^{(3)}\right]$$

By induction we can prove the following proposition:

Proposition A.1 *The adjoint hermitian representation of the algebra su(2^N), i.e the set of hermitian traceless $2^N \times 2^N$ can generated by the algebra of Lie-polynomials of the set:*

$$\mathcal{A}_N = \left\{ \sigma_3^{(1)}, \sigma_3^{(2)}, \ldots, \sigma_3^{(N)}, \sum_{k=1}^{N} \sigma_1^{(k)}, \sum_{i<j}^{N} \sigma_2^{(i)}\sigma_2^{(j)} \right\} \tag{23}$$

The set $\mathcal{A}_N$ of the generators has $N+1$ elements, we should point out that this number is much smaller than the number $4^N - 1$, which is the dimension of the

algebra su(2^N). Therefore, large Lie algebras can be generated by using a relatively small number of elements.

Let us now construct the group SU(2^N). For the sake of simplicity we start the discussion with the SU(4) case, i.e with the set of unitary 4×4 matrices with determinant equal to 1.

Let us consider four linearly independent elements, which are given by the formulas:

$$\begin{aligned} H_1 &= \tfrac{1}{2}E_c\,(\sigma_3^{(1)} + \sigma_3^{(2)}) - \tfrac{1}{2}E_J\,(\sigma_1^{(1)} + \sigma_1^{(2)}) \\ H_2 &= -\tfrac{1}{2}E_J\,(\sigma_1^{(1)} + \sigma_1^{(2)}) - \tfrac{1}{2}E_L\,\sigma_2^{(1)}\sigma_2^{(2)} \\ H_3 &= \tfrac{1}{2}E_c\,\sigma_3^{(2)} - \tfrac{1}{2}E_J\,(\sigma_1^{(1)} + \sigma_1^{(2)}) \\ H_4 &= \tfrac{1}{2}E_c\,\sigma_3^{(1)} - \tfrac{1}{2}E_J\,(\sigma_1^{(1)} + \sigma_1^{(2)}) \end{aligned} \tag{24}$$

Starting from this system we can reconstruct the elements (17) because:

$$\begin{aligned} \sigma_3^{(1)} &= \tfrac{2(H_1 - H_3)}{E_c} \\ \sigma_3^{(2)} &= \tfrac{2(H_1 - H_4)}{E_c} \\ \sigma_1^{(1)} + \sigma_1^{(2)} &= \tfrac{2(H_1 - H_3 - H_4)}{E_J} \\ \sigma_2^{(1)}\sigma_2^{(2)} &= \tfrac{2(H_3 + H_4 - H_1 - H_2)}{E_L} \end{aligned} \tag{25}$$

These relations prove that the su(4) algebra can be generated by combinations and successive commutations of the four elements $\{H_1, H_2, H_3, H_4\}$.

References

1. D. Deutsch, "Quantum Theory, the Church-Turing principle and the Universal Quantum Computer", Proc. Roy. Soc. London A **400**, 97-117 (1985).
2. S. Braunstein, H. -K. Lo, Editors, "Experimental proposals for Quantum Computation", Fort. Phys. **48**, 765-1138 (2000).
3. H. Rabitz, R. de Vivie-Riedle, M. Motzkus, K. Kompa, "Whither the future of controlling quantum phenomena? ", Science **288**, 824-828 (2000).
4. D. P. DiVincenzo, D. Bacon, J. Kempe, D. A. Lidar, K. B. Whaley, "Encoded Universality in physical implementations of a Quantum Computer", LANL e-print **quant-ph/0102140**.
5. D. P. DiVincenzo, D. Bacon, J. Kempe, G. Buckard, K. B. Whaley, 2000, "Universal quantum computation with exchange interaction", Nature (London) **408**, 339-342, **quant-ph/0005116**.
6. V. Jurdjević, H. Sussmann, "Control systems on Lie groups", J. Diff. Eq. **12**, 313-329 (1975).
7. V. Ramakrishna, M. V. Salapaka, M. Dahleh, H. Rabitz, A. Peirce, "Controllability of molecular systems", Phys. Rev. A **51**, 960-966 (1995).
8. V. Ramakrishna, "Control of molecular systems with very few phases", Chem. Phys. **267**, 25-32 (2001)
9. N. Khaneja, S. J. Glaser, "Cartan decomposition of $Su(2^N)$ and control of spin systems", Chem. Phys. **267**, 11-23 (2001), **quant-ph/0010100**.

10. H. Fu, S. G. Schirmer, A. I. Solomon, "Complete Controllability of finite-level quantum systems", J. Phys. A: Math. and Gen. **34**, 1679-1690 (2001), **quant-ph/0102017**.
11. S. G. Schirmer, H. Fu, A. I. Solomon, "Complete controllability of quantum systems", Phys. Rev. A **63**, 025403 (2001), **quant-ph/0010031**.
12. Y. Nakamura, C. D. Chen, J. S. Tsai, "Spectroscopy of energy-level splitting between two macroscopic quantum states of charge coherently cuperposed by Josephson coupling", Phys. Rev. Lett. **79**, 2328-2331 (1997).
13. D. V. Averin, "Adiabatic quantum computation with Cooper pairs", Sol. St. Comm. **105**, 659-664 (1998), **quant-ph/9706026**.
14. D. V. Averin, "Solid-state qubits under control", Nature (London) **398**, 748-749 (1999).
15. A. Shnirman, G. Schön, Z. Hermon, "Quantum manipulation of small Josephson junctions", Phys. Rev. Lett. **79**, 2371-2374 (1997), **quant-ph/9706016**.
16. Y. Makhlin, G. Schön, A. Shnirman, "Quantum state engineering with Josephson junction devices", Rev. Mod. Phys. **73**, 357-400 (2000), **cond-mat/0011269**.
17. Y. Makhlin, G. Schön, A. Shnirman, "Josephson junction qubits with controlled couplings", Nature (London) **398**, 305-307 (1999), **cond-mat/9808067**.
18. Y. Makhlin, G. Schön, A. Shnirman, "Josephson junction qubits and the readout process by single electron Transistors", LANL e-print **cond-mat/9811029**.
19. Y. Nakamura, Yu. A. Pashkin, J. S. Tsai, "Coherent control of macroscopic quantum states in a single-Cooper-pair box", Nature **398**, 786 (1999), **cond-mat/9904003**.
20. Y. Nakamura, J. S. Tsai, "Quantum-state control with a single-Cooper-pair box", J. Low Temp. Phys. **118**, 765-779 (2000).
21. A. Barenco, Ch. H. Bennett, R. Cleeve, D. P. DiVincenzo, N. Margolus, P. Shor, T. Sleator, J. A. Smolin, H. Weinfurter, "Elementary gates for quantum computation", Phys. Rev. A **52**, 3457-3467 (1995), **quant-ph/9503016**.
22. D. D'Alessandro, "Uniform Finite Generation of Compact Lie Groups and universal quantum gates", (2001) LANL e-print **quant-ph/0111133**.

DISCUSSION

Chairman: A. Ekert

S. Lloyd: I have two comments. The first comment is that let's be careful with Josephson junction devices. The fabrication tolerances are not so great, so assuming things like degeneracy for a couple of bits, that is very difficult to make actual bits that are actually degenerated. The next comment or question is that there is a difference between universal quantum code and universal quantum computations. It was shown a long time ago that if you have almost any interaction between quantum bits, it allows you to construct quantum logic gates and then performs

universal quantum control. So in that case it is not a conjecture. The problem is that just being able to do any unitary calculations does not mean that you are able to do the same two-qubit operation in an efficient fashion. You know, the fact that you can do any $CNOT$ operation could take 2^N operations to do a two-qubit operation. So I was wondering, in your scheme where you have everything coupled with everything else in these Josephson devices, what guarantee to you that you are actually able to perform two-qubit operations or quantum logic operations by this kind of quantum machine language?

C. Daskaloyannis: First of all, we consider the "idealized" Josephson junction, proposed by the experimentalists, as a working example. We could take as working examples another device like quantum dots or other solid state devices, but these proposals have not yet been confirmed by experiments. In order to design a machine language, i.e. the appropriate sequence of letters, for a quantum computer one must specify some device. We do not propose any device, but we study the quantum computing capabilities of devices which are composed of identical elementary parts controlled by binary parameters. Also, the choice of control parameters is not unique, one could propose another choice of binary control parameters. These choices are constrained by the internal structure of the device. The proposed model is flexible, and our discussion does not depend really on the choice of the device. In our discussion the quantum byte has a binary part and a continuous bit. With this choice we can construct any gate. We have studied a minimal configuration which is not necessarily the most economic one. Specially in the Josephson N-qubit device we can show that any elementary CNOT or two-qubit gate can be constructed by N+1 steps.

P. Stamp: You are assuming that in those models that you use, as you said, one of the terms is variable and the other is constant. But then you have more complicated schemes which have more letters and I really want to ask: have you some feeling for how much you can reduce the time of computation by increasing the length number of letters?

C. Daskaloyannis: At this moment, we consider a minimal construction scheme, which can implement any gate. We do not have any idea how the computational time could be reduced by increasing the number of q-bits.

STATISTICAL MECHANICS APPROACH TO ERROR-CORRECTING CODES

NICOLAS SOURLAS

Laboratoire de Physique Théorique de l' Ecole Normale Supérieure *
24 rue Lhomond, 75231 Paris CEDEX 05, France.
e-mail: sourlas@lpt.ens.fr

I will review the relationship between error-correction codes and certain mathematical models of spin glasses. I will show that there is a one to one relationship between error correcting codes and spin glass models. Minimum error probability decoding is equivalent to finding the magnetisation of the corresponding spin system. Convolutional codes correspond to one-dimensional spin systems and Viterbi's decoding algorithm to the transfer matrix algorithm of Statistical Mechanics.

I will also show how the recently discovered (or rediscovered) capacity approaching codes (turbo codes and low density parity check codes) can be analysed using statistical mechanics. Turbo codes correspond to two coupled spin chains, while low density parity check codes are spin models on a diluted random graph. It is possible to show, using statistical mechanics, that these codes allow error-free communication for signal to noise ratio above a certain threshold. This threshold, which corresponds to a phase transition in the spin model, depends on the particular code, and can be computed analytically in many cases.

The mathematical theory of communication[1,2] is probabilistic in nature. Both the production of information and its transmission are considered as probabilistic events. A source is producing information messages according to a certain probability distribution. Each message consists of a sequence of K bits $\vec{\sigma} = \{\sigma_1, \cdots, \sigma_K\}$, $\sigma_i = \pm 1$ and it is assumed that the probability $P_s(\vec{\sigma}) \equiv \exp -H_s(\vec{\sigma})$ of any particular sequence $\vec{\sigma}$ is known. According to Shannon the information content of the message is $-\ln P_s(\vec{\sigma})$ and the average information of the source is given by

$$-\sum_{\vec{\sigma}} P_s(\vec{\sigma}) \ln P_s(\vec{\sigma})$$

The messages are sent through a transmission channel. In general there is noise during transmission (which may have different origins) which corrupts the transmitted message. If a $\sigma = \pm 1$ is sent through the transmission channel, because of the noise, the output will be a real number J, in general different from σ. Again, the statistical properties of the transmission channel are supposed to be known. Because of the noise during the transmission, there is a loss of information. The channel capacity C is defined as the maximum information per unit time which can be transmitted through the channel. The maximum is taken over all possible sources.

For reasons of simplicity, we will assume in the following that all the source symbols are statistically independent and that the noise is independent for any

*UMR 8549, Unité Mixte de Recherche du Centre National de la Recherche Scientifique et de l' Ecole Normale Supérieure.

pair of bits ("memoryless channel"). In the case of a memoryless channel and of a gaussian noise, Shannon[1,2]calculat ed the channel's capacity

$$\mathcal{C} = \frac{1}{2}\log_2(1 + \frac{v^2}{w^2})$$

where $v^2/w^2$is the signal to noise power ratio.

Under the above assumptions, communication is a statistical inference problem. Given the transmission channel's output and the statistical properties of the source and of the channel, one has to infer what message was sent. In order to reduce communication errors, one may introduce (deterministic) redundancy into the message ("channel encoding") and use this redundancy to infer the message sent through the channel ("decoding"). The algorithms which transform the source outputs to redundant messages are called error-correcting codes. The inverse of the redundancy (see later for a precise definition) is called the rate R of the code.

The famous Shannon coding theorem[1,2] states that for infinite long messages, it is possible to communicate error free, provided the rate of the code is smaller than the channel capacity. For practical purposes it is also required that the computational complexity of the code (the amount of computation required both for encoding and decoding) is not very large. It must be possible to encode and decode in a reasonable amount of time. A code which is very good for very long messages of length N but requires an exponential in N decoding time is obviously not very interesting.

Until recently there were no known codes of reasonable computational complexity allowing communication with a very small error, for noise level not too far from capacity. This situation changed drastically with the recent discoveries of the "capacity approaching" codes. First came the discovery of turbo codes by Berrou and Glavieux[3] and later the rediscovery of low density parity check codes[4], first discovered by Gallager[5,6], in his thesis, in 1962. Both turbo codes and low density parity check (LPDC) codes are based on random constructions. Because of this randomness, it is not easy to analyse them with the traditional methods of communication theory.

I have shown some time ago[7,8,9,10] that there is a mathematical eqivalence of error-correcting codes to some theoretical spin-glass models.

I will explain later that it is possible to use this equivalence with spin glasses, to study the properties of these capacity approaching codes using the methods of statistical mechanics developed in the study of disordered systems.

Let me start by fixing the notations. Each information message consists of a sequence of K bits $\vec{u} = \{u_1, \cdots, u_K\}, u_i = 0$ or 1. The binary vector $\vec{u}$ is called the source-word. Encoding introduces redundancy into the message. One maps $\vec{u} \to \vec{x}$ by encoding. $\vec{u} \to \vec{x}$ has to be a one to one map for the code to be meaningful. The binary vector $\vec{x}$ has $N > K$ components. It is called a code-word. The ratio $R = K/N$ which specifies the redundancy of the code, is called the rate of the code. One particularly important family of codes are the so-called linear codes. Linear codes are defined by

$$\vec{x} = G\vec{u}$$

G is a binary (i.e. its elements are zero or one) $(N \times K)$ matrix and the multiplication is modulo two. G is called the generating matrix of the code. Obviously by construction all the components x_i of a code-word x are not independent. Of all the 2^N binary vectors only $2^K = 2^{NR}$, those corresponding to a vector $\vec{u}$, are codewords. Codewords satisfy the linear constraints (called parity check constraints) $H\vec{x} = 0$ (modulo two), where H is a $(K \times N)$ binary matrix, called the parity check matrix. The connection with spin variables is straightforward. $u_i \to \sigma_i = (-1)^{u_i}$, $x_i \to J_i = (-1)^{x_i}$. It follows that $u_i + u_j \to \sigma_i \sigma_j$ and

$$J_i = (-1)^{\sum_j G_{ij} u_j} = C^i_{k_1 \cdots k_i} \sigma_{k_1} \cdots \sigma_{k_i} \tag{1}$$

The previous equation defines the "connectivity matrix" C in terms of the generating matrix of the code G. Similarly one can write the parity check constraints in the form:

$$(-1)^{\sum_j H_{lj} x_j} = 1 \ \to M^l_{k_1 \cdots k_l} J_{k_1} \cdots J_{k_l} = 1 \tag{2}$$

This defines the "parity constraint matrix" M in terms of the parity check matrix H of the code.

Codewords are sent through a noisy transmission channel and they get corrupted because of the channel noise. If a $J_i = \pm 1$ is sent, the output will be different, in general a real number J_i^{out}. Let us call $Q(\vec{J}^{out}|\vec{J})d\vec{J}^{out}$ the probability for the transmission channel's output to be between $\vec{J}^{out}$ and $\vec{J} + d\vec{J}^{out}$, when the input was $\vec{J}$. The channel "transition matrix" $Q(\vec{J}^{out}|\vec{J})$ is supposed to be known. We will assume that the noise is independent for any pair of bits ("memoryless channel"), i.e.

$$Q(\vec{J}^{out}|\vec{J}) = \prod_i q(J_i^{out}|J_i) \tag{3}$$

Knowing the noise probability i.e. $q(J_i^{out}|J_i)$, the code (i.e. in the present case of linear codes knowing the generating matrix G or the parity check matrix H) and the channel output $\vec{J}^{out}$, one has to infer the message that was sent. The quality of inference depends on the choice of the code.

We will now show that there exists a close mathematical relationship between error-correcting codes and theoretical models of disordered systems. To every possible information message (source word) $\vec{\tau}$ we can assign a probability $P^{source}(\vec{\tau}|\vec{J}^{out})$, conditional on the channel output $\vec{J}^{out}$. Or, equivalently, to any code-word $\vec{J}$ we can assign a probability $P^{code}(\vec{J}|\vec{J}^{out})$.

Because of Bayes theorem, the probability for any code-word symbol ("letter") $J_i = \pm 1$, $p(J_i|J_i^{out})$, conditional on the channel output J_i^{out}, is given by

$$p(J_i|J_i^{out}) \ = \ \frac{q(J_i^{out}|J_i)}{\sum_{J_i} q(J_i^{out}|J_i)}$$

It follows that

$$\ln p(J_i|J_i^{out}) \ = \ c1 \ + \ \ln q(J_i^{out}|J_i) \ = \ c2 \ + \ h_i J_i \tag{4}$$

where $c1$ and $c2$ are constants (non depending on J_i) and

$$h_i = \frac{1}{2} \ln \frac{q(J_i^{out}|+1)}{q(J_i^{out}|-1)} \tag{5}$$

The two previous equations illustrate the well known fact that the most general function of a variable $J = \pm 1$ is a linear function (because $J^{2k} = 1$, $J^{2k+1} = J$). h_i which will play the role of an external field (see eq. (8) below) or of a coupling constant (see equ. (10)), is called in coding theory the log-likelihood or the "extrinsic information".

It follows that

$$P^{code}(\vec{J}|\vec{J}^{out}) = c \prod_l \delta(M^l_{k_1 \cdots k_l} J_{k_1} \cdots J_{k_l}; 1) \exp\left(\sum_i h_i J_i\right) \tag{6}$$

where c is a normalising constant. The Kronecker δ's enforce the constraint that $\vec{J}$ obeys the parity check equations (Equ. (2)), i.e. that it is a code-word. The δ's can be replaced by a soft constraint,

$$P^{code}(\vec{J}|\vec{J}^{out}) = const \exp\ [u \sum_l M^l_{k_1 \cdots k_l} J_{k_1} \cdots J_{k_l} + \sum_i h_i J_i\ ] \tag{7}$$

where $u \to \infty$. We now define the corresponding spin Hamiltonian by:

$$-H^{code}(\vec{J}) = \ln P^{code}(\vec{J}|\vec{J}^{out}) = u \sum_l M^l_{k_1 \cdots k_l} J_{k_1} \cdots J_{k_l} + \sum_i h_i J_i \tag{8}$$

There are two models of memoryless channel noise, i.e. of $q(J_i^{out}|J_i)$, that are extensively studied. The first is the "gaussian channel" for which the output J^{out} can take any real value and

$$q(J_i^{out}|J_i) = c \exp - \frac{(J_i^{out} - J_i)^2}{2w^2}$$

where w^2 is the variance of the gaussian noise and c a normalising constant. The other is the " binary symmetric channel ", for which the output is a binary variable, i.e. $J^{out} = \pm 1$, and

$$q(J_i^{out}|J_i) = (1-p)\delta_{J_i^{out}, J_i} + p\delta_{J_i^{out}, -J_i}$$

i.e. every symbol J_i is transmitted without error with probability $1-p$ and is flipped with probability p. For the gaussian channel the field h_i is given by (see equation (5)) $h_i = J_i^{out}/w^2$, while for the binary symmetric channel $h_i = \frac{1}{2} J_i^{out} \ \ln((1-p)/p)$.

Alternatively, one may proceed by solving the parity check constraints

$$J_i = C^i_{k_1 \cdots k_i} \sigma_{k_1} \cdots \sigma_{k_i}$$

by expressing the codewords in terms of the sourcewords.

$$P^{source}(\vec{\sigma}|\vec{J}^{out}) = const.\ \exp\left(\sum_i h_i C^i_{k_1 \cdots k_i} \sigma_{k_1} \cdots \sigma_{k_i}\right) \tag{9}$$

where the h_i's are given as before. The logarithm of $P^{source}(\vec{\sigma}|\vec{J}^{out})$,

$$H^{source}(\vec{\sigma}) = -\ln P^{source}(\vec{\sigma}|\vec{J}^{out}) = -\sum_i h_i C^i_{k_1 \cdots k_i} \sigma_{k_1} \cdots \sigma_{k_i} \tag{10}$$

In equation (10), and in equation (8), the h_i's, are known because the channel output is known (see equation (5)). They are known numbers once the channel output is known.

We imagine the case where we transmit the *same* word a large number of times. Because of the randomness of the noise, every time we will get a different channel output, although the input was the same. We will consider the *ensemble* of all these transmissions and the ensemble of the resulting outputs. This is completely analogous to the case of disordered magnetic systems, where in every sample the positions of the magnetic ions is fixed, but one considers the ensemble of samples obtained with the same experimental procedure (i.e. exactly the same chemical composition, exactly the same concentrations, etc). In statistical mechanics one computes the average value of an observable in this ensemble. There are two reasons for doing this. The first reason is that "good" observables, as for example the magnetization per spin, the energy per spin etc, are "self-averaging". An observable is called self-averaging if its probability distribution over the ensemble of samples becomes a delta function when the size of the sample becomes large. (This property of self-averaging has been recently studied by probabilists and they proved it in several cases. They call it concentration of the measure.) The other reason is that we have developed the tools of computing analytically the ensemble average. Without averaging we are unable, up to now, to perform any analytical computation.

Viewed in this way, the Hamiltonian defined in equation (8) is the Hamiltonian of a spin system with multispin interactions with infinite ferromagnetic coupling and a random external magnetic field, while the Hamiltonian in equation (10), is a spin glass Hamiltonian. I will show later that the error probability per bit is simply related to the magnetization of the corresponding spin model (at the appropriate temperature, see later). It follows that the error probability per bit is self-averaging.

We have given two different statistical mechanics formulations of error correcting codes. One in terms of the souceword probability P^{source} and the other in terms of the codeword probability P^{code}.

Because of the one to one correspondence between codewords and sourcewords, the two formulations are equivalent. In practice however it may make a difference. It may be more convenient to work with P^{source} rather than P^{code}, depending on the case. For the case of turbo codes (see later) it will be more convenient to define another probability, the "register word" probability.

It follows that the most probable symbol sequence ("word maximum a posteriori probability" or "word MAP decoding"), i.e. the symbol sequence that maximises the probability P^{source} or P^{code} (depending on the case), is given by the ground state of this Hamiltonian (H^{code} or H^{source}). Instead of considering the most probable symbol sequence, one may only be interested in the most probable value τ_i^p of the i'th symbol or "bit" τ_i[9,10,11], ignoring the values of the other symbols ("symbol MAP decoding"). The sequence of the most probable symbols does not necessarily coincide with the most probable sequence. Because $\tau_i = \pm 1$, the probability p_i for $\tau_i = 1$ is related to the average of τ_i m_i, by $p_i = (1 + m_i)/2$.

$$m_i = \frac{1}{Z} \sum_{\{\tau_1 \cdots \tau_N\}} \tau_i \exp -H(\vec{\tau}) \quad Z = \sum_{\{\tau_1 \cdots \tau_N\}} \exp -H(\vec{\tau}) \quad \tau_i^p = \text{sign } (m_i) \quad (11)$$

In the previous equation m_i is obviously the thermal average at temperature $T = 1$. It is amusing to notice that $T = 1$ corresponds in spin glasses to Nishimori's temperature[14].

When all messages are equally probable and the transmission channel is memoryless and symmetric, i.e. when $q(J_i^{out}|J_i) = q(-J_i^{out}| - J_i)$, the error probability is the same for all input sequences. It is enough to compute it in the case where all input bits are equal to one, i.e. when the transmitted code-word is the all zero's code-word. In this case, the error probability per bit P_e is $P_e = \frac{1-m^{(d)}}{2}$, where $m^{(d)} = \frac{1}{N}\sum_{i=1}^{N} \tau_i^{(d)}$ and $\tau_i^{(d)}$ is the symbol sequence produced by the decoding procedure.

This means that it is possible to compute the bit error probability, if one is able to compute the magnetization in the corresponding spin system.

Let me give a simple example of an $R = 1/2$ "convolutional" code. From the N source symbols (letters) u_i's we construct the $2N$ code-word letters x_k^1, x_k^2, $k = 1, \cdots, N$.

$$x_i^1 = u_i + u_{i-1} + u_{i-2} \ , \quad x_i^2 = u_i + u_{i-2} \tag{12}$$

It follows that

$$J_k^1 = \sigma_k \sigma_{k-1} \sigma_{k-2}, \quad J_k^2 = \sigma_k \sigma_{k-2} \tag{13}$$

$$C^{(1,k)}_{i_{k_1} i_{k_2} i_{k_3}} = \delta_{k,i_{k_1}} \delta_{k,i_{k_2}+1} \delta_{k,i_{k_3}+2} \ , \quad C^{(2,k)}_{i_{k_1} i_{k_3}} = \delta_{k,i_{k_1}} \delta_{k,i_{k_3}+2} \tag{14}$$

The corresponding spin Hamiltonian is

$$-H = \frac{1}{w^2} \sum_k J_k^{1,out} \tau_k \tau_{k-1} \tau_{k-2} + J_k^{2,out} \tau_k \tau_{k-2} \tag{15}$$

Here I assumed a Gaussian noise. In that case, Equ. (5) reduces to $h_k = J_k^{out}/w^2$, where w^2 is the variance of the noise. This is a one dimensional spin glass Hamiltonian. In fact it is easy to see that convolutional codes correspond to one dimensional spin systems. Their ground state can be found using the $T = 0$ transfer matrix algorithm. The $T = 0$ transfer matrix algorithm corresponds to the Viterbi algorithm in coding theory. For symbol MAP decoding, one can use the $T = 1$ transfer matrix algorithm. The $T = 1$ transfer matrix algorithm is the BCJR algorithm in coding theory[15].

I have illustrated above the mathematical correspondence between disordered spin systems and error correcting codes. Using this correspondence it has been possible to analyse both LPDC codes and turbocodes using the methods of statistical mechanics. Most of the results have been obtained with the "replica" method. (For a lucid exposition of this method see reference [16]). This is a method developed in the context of spin-glass theory and which has not yet been made rigorous. Within the "replica" method there are approximation schemes. The simplest is the replica symmetric approximation. For symbol MAP decoding, i.e. for the temperature $T = 1$, there are very strong arguments that replica symmetry is not broken. It is outside the scope of the present paper to explain the replica method.

To fix the notations, let me remind that Gallager's low density parity check (k, l) codes are defined by choosing at random a sparse parity check $K \times N$ matrix

H as follows. H has N columns (we consider the case of codewords of length N). Each column of H has k elements equal to one and all other elements equal to zero. Each row has l non zero elements.

It is convenient to use graphical representations (slightly different from Tanner's graphical representation used in coding theory) to represent the interaction terms appearing in the Hamiltonian. Each spin is represented by a point in the graph. The spins which are multiplied by the same coupling are connected by a line. It follows from equation (8) that Gallager's k, l codes correspond to random "diluted" (sparse) graphs. Such models are called diluted spin models with l-spin infinite strength ferromagnetic interactions in an external random field. It is known that in the case of extreme dilution, one can analyse these models in the mean field approximation. Very sparse graphs have locally a tree structure, i.e. there are no loops of short length. In such a graph with N vertices, the size of the typical loop is known to be $\ln N$. This is the reason why one can apply mean field in this case.

Gallager[5,6] proposed an approximate iterative decoding algorithm for LDPC codes. This is an iterative computation of the log-likelihood (or extrinsic information or cavity field, according to the terminology) $h_i(t)$, where t is the iteration time. The probability $p(\sigma_i)$ of the spin σ_i is related to h_i by $p(\sigma_i) = \exp(h_i)/cosh(h_i)$. $h_i(0)$ is given by equ. (5). At $t = 1$ one considers the interaction of σ_i with its neighbors σ_j on the graph. Let us remind that the interaction (see equ. (8) where the limit $u \to \infty$ has to be taken) imposes the product of the spins present in an interaction term to be equal to plus one. Taking into account this information, together with the values of $h_j(0)$, one computes $h_i(1)$. It easy to imagine how this procedure can be iterated. At time t one takes into account the information coming from all the spins which are up to distance t on the graph. It is hoped that this procedure will converge to a fixed point for $p(\sigma_i)$ after a reasonable number of iterations. It is obvious that this number of iterations will depend on the amount of noise. If the noise is too strong there will be no convergence.

This updating of $h_i(t)$, which today is called the sum-product algorithm, would be exact in a graph without loops. It is approximate because of the presence of loops on a random graph. It is worth noticing that decoding with the sum-product algorithm is equivalent to "solving" the corresponding spin model, i.e. computing the local magnetizations, by iteration of the Thouless Anderson Palmer[17] (TAP) equations, which invented fifteen years later in the context of mean field spin glasses. A more general derivation for spin glasses, called the cavity method, was later developed by Mézard, Parisi and Virasoro[18]. The same algorithm was rediscovered recently in computer science, where it is called the belief propagation algorithm.

As we saw, low density parity check codes are based on a random construction, a random parity check matrix more precisely. We will see that the same is true for Turbo Codes, a random permutation in that case. By the same random construction, for example in Gallager's case matrices with fixed k and l, we can construct several codes, i.e. there exist several random matrices even if k and l are fixed. In order to be able to use statistical mechanics, we have to consider the ensemble of codes defined by these matrices and compute the average error probability per bit in this ensemble. This is justified because it can be shown a posteriori that the error probability per bit is self-averaging.

Low density parity check codes have been analysed using Statistical Mechanics methods by Kabashima Kanter and Saad[19,20] in the replica symmetric approximation. More recently Montanari[21] was able to go beyond replica symmetry. He established the entire phase diagram of LDPC codes. For $k,\ l \to \infty$ with rate $R = 1 - k/l$ fixed, he showed that k, l codes can be analysed without replicas, similarly to the random energy model of Derrida[22]. There is a phase transition in this model, which occurs at a critical value of the noise n_c. Phase transitions can appear only in the infinite volume limit (the thermodynamic limit), i.e. in the limit of strings of symbols of infinite length. $n_c$separates a zero error phase, i.e. a phase with a magnetization equel to one, from a high error phase. It turns out that n_c, in this limit, coincides with Shannon's channel capacity. For finite k and l Montanari found an exact one step replica symmetry breaking solution. He computed the location of the phase transition, i.e. the critical value of the noise n_c for which the phase transition occurs. n_c is given in terms of an implicit equation which has to be solved numerically. n_c has a simple asymptotic expansion for large k, l and fixed rate R. For the binary symmetric channel with error probability p, the first term of the asymptotic expansion for the threshold $p_c(k,l)$ is

$$p_c(k,l) = p_c^0 - \frac{1-R}{2(\ln(p_c^0) - \ln(1-p_c^0))}(1-2p_c^0)^{2k} + O((1-2p_c^0)^{4k})$$

p_c^0 is the threshold for $k,\ l \to \infty$, i.e. the threshold provided by the channel capacity. We see that the approach to the $k,\ l \to \infty$ limit is exponential.

The thresholds above were obtained by maximising the appropriate probabilities. This means that they can only be reached by an optimal (but unknown) decoder. The actual decoder may behave differently.

The only alternative to statistical mechanics to theoretically understand LPDC codes and turbocodes is the method of "density evolution" which was devised by Richardson and Urbanke[23]. This method, applied to Gallager's k, l codes, consists in considering the ensemble of Gallager's codes with fixed k and l and the ensemble of channel outputs, when the input is the all zeros codeword. This method of considering an ensemble of codes and an ensemble of channel outputs is very new in coding theory. It can be considered as the rediscovery by coding theorists of the methods developed in the seventies in the study of disordered systems. Richardson and Urbanke study the probability density $\mathcal{P}(h)$ of the log-likelihoods (or cavity fields) h_i, for this ensemble. As we stated earlier, the sum product decoding algorithm can be viewed as a time evolution process of these h_i's. They study how $\mathcal{P}(h)$ evolves with "time", i.e. when iterating the decoding algorithm. They showed that the probability density converges to the zero error limit provided the noise is less than some value n_c^{bp}. They computed n_c^{bp} performing a local stability analysis of density evolution, starting from the no error regime. n_c^{bp} is not equal to the threshold n_c computed by statistical mechanics for regular Gallager codes, i.e. the decoding is not optimal near the threshold. The reason for this is not yet understood. See the remarks at the end of this paper for a possible explanation.

Turbo Codes also have been analysed using statistical mechanics[24,25]. They are based on recursive convolutional codes. An example of non recursive convolutional code was given in Equ. (12). The corresponding recursive code is given, most

conveniently, in terms of the auxiliary bits b_i, defined below. The b_i's are stored in the encoder's memory registers, that's why I call $\vec{b}$ the the "register word".

$$x_i^1 = u_i,\ x_i^2 = b_i + b_{i-2},\ b_i = u_i + b_{i-1} + b_{i-2} \tag{16}$$

It follows that the source letters u_i are given in terms of the auxiliary "register letters" b_i

$$u_i = b_i + b_{i-1} + b_{i-2} \tag{17}$$

All additions are modulo two.

To construct a turbo code, one artificially considers a second source word $\vec{v}$, by performing a permutation, chosen at random, of the original code-word $\vec{u}$. So one considers $v_j = u_{P(i)}$ where $j = P(i)$ is a (random) permutation of the K indices i and a second "register word" c_i, $c_i = v_i + c_{i-1} + c_{i-2}$. Obviously

$$v_i = c_i + c_{i-1} + c_{i-2} = u_j = b_j + b_{j-1} + b_{j-2},\quad j = P(i) \tag{18}$$

Equ. (18) can be viewed as a constraint on the two register words $\vec{b}$ and $\vec{c}$. Finally in the present example, a rate $R = 1/3$ turbo code, one transmits the $N = 3K$ letter code-word $x_i^1 = u_i$, $x_i^2 = b_i + b_{i-2}$, $x_i^3 = c_i + c_{i-2}$, $i = 1, \cdots, K$. Let's call, as before,

$$J_i^\alpha = (-1)^{x_i^\alpha},\quad \alpha = 1, 2, 3$$

the channel inputs and $J_i^{out,\alpha}$ the channel outputs. In the previous, for reasons of convenience, we formulated convolutional codes using the source-word probability P^{source} and LDPC codes using the code-word probability P^{code}.

The statistical mechanics of turbo codes is most conveniently formulated in terms of the "register words" probability $P^{reg}(\vec{\sigma}, \vec{\tau}|\vec{J}^{out})$ conditional on the channel outputs $\vec{J}^{out}$, where $\tau_i = (-1)^{b_i}$ and $\sigma_i = (-1)^{c_i}$. The logarithm of this probability provides the spin Hamiltonian

$$-H = \frac{1}{w^2} \sum_k J_k^{out,1} \tau_k \tau_{k-1} \tau_{k-2} + J_k^{out,2} \tau_k \tau_{k-2} + J_k^{out,3} \sigma_k \sigma_{k-2} \tag{19}$$

Because of Equ. (18), the two spin chains $\vec{\tau}$ and $\vec{\sigma}$ obey the constraints

$$\sigma_i \sigma_{i-1} \sigma_{i-2} = \tau_j \tau_{j-1} \tau_{j-2},\quad j = P(i) \tag{20}$$

(As previously, we have considered the case of a Gaussian noise of variance w^2.) This is an unusual spin Hamiltonian. Two short range one dimensional chains are coupled through the infinite range, non local constraint, Equ. (20). This constraint is non local because neighboring i's are not mapped to neighboring j's under the random permutation. It turns out that this Hamiltonian can be solved by the replica method.

The equations one gets cannot be solved exactly as in the case of LPDC codes. One can verify that, when the noise is sufficiently weak, zero error probability is a solution of the equations. One can perform a local stability analysis of this zero error probability solution.

One finds a phase transition at a critical value of the noise n_{crit}. For noises less than n_{crit}, it is possible to communicate error free. (For example for the $R = 1/3$

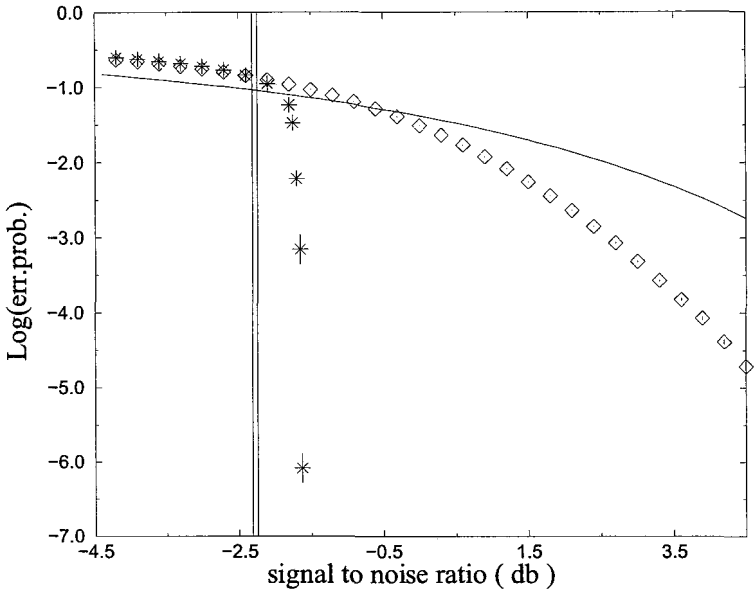

Figure 1. Numerical results for the average error probability per bit of the Turbo Code described in the text (gaussian channel). Stars (*) are obtained for a random permutation, diamonds ($\diamond$) correspond to the identity permutation. The continuous curve corresponds to the uncoded message. The leftmost vertical line is located at the Shannon capacity, while the rightmost one is the threshold computed using statistical mechanics (see text).

Turbo Code we described above we get that the error probability vanishes for signal to noise ratio above $\Theta \simeq -2.240$ db.) In this respect, turbo codes are similar to Gallager's LDPC codes. The statistical mechanical models however, are completely different.

Figure 1 shows the results of a numerical simulation for the Turbo Code presented above. The bit error probability vanishes above a certain value of the signal to noise ratio, but the value of this threshold seems to be slightly different from the one we obtain from our equations. This disagreement could have different origins. One possibility is that the true threshold is different from that provided by the local stability analysis (possibility of a first order phase transition. Local stability analysis assumes there is a second order transition). Another possibility is that the turbodecoding algorithm does not find the optimal configuration for this code (possibility of a "dynamical transition"). It was explained above that the algorithm tries to find the configuration which maximises the appropriate probability function. It may happen that this function has a large number of local maxima

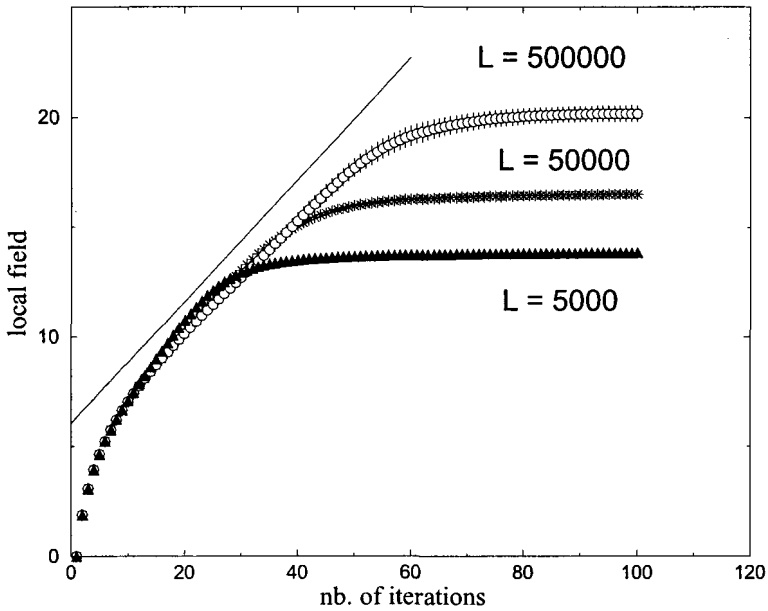

Figure 2. The dynamics of the turbo decoding algorithm in the low-noise regime. Triangles, diamonds and circles represent the average extrinsic information as a function of the number of iterations for different sizes ($L = 5000, 50000, 500000$) of the source message. Notice that the saturation after a large number of iterations is a finite size effect. The slope of the straight line describes the asymptotic behavior for an infinitely long message and is obtained analytically from the KPP equation.

and that the algorithm is trapped in one of them. A third possibility is that when close to the threshold, convergence becomes extremely slow and that one should run the algorithm for an infinite time to reach the correct threshold. (This is called "aging"). It would be interesting to understand which of the above scenaria occurs.

Let me also mention that, under some reasonable assumptions, the iterative decoding algorithm for turbo codes (turbodecoding algorithm), can be viewed[25] as a time discretisation of the Kolmogorov, Petrovsky and Piscounov equation[26]. It is known that this KPP equation has traveling wave solutions. The velocity of the traveling wave, which is computable analytically, corresponds to the convergence rate of the turbodecoding algorithm. The agreement with numerical simulations is excellent, as this is illustrated in Figure 2.

I would like to conclude by pointing out some open questions.

As it was emphasised above, belief propagation decoding is expected to work in the absence of loops. For random graphs the typical loop length $L \sim \log N$, where N is the number of vertices. For $N = 10^6$, $L \sim 10$. However it is known empirically that, in the case of a not very weak noise, one has to iterate t times the decoding algorithm with $t >> L$ ($t \sim 150$ is a typical value), i.e. in practice one

cannot ignore the presence of loops. It is not known why the algorithm works in the presence of loops as it does in practice.

We saw that there is a phase transition both in LDPC codes and in Turbo Codes. What is the order of the phase transition? This question is particularly relevant for turbo codes where we assumed a second order transition. Without this assumption we are unable to compute the signal to noise threshold above which communication is error free.

Using statistical mechanics we computed the properties of infinite systems, i.e. infinite message length in the case of error correction codes. In practice of course all messages have finite length. In some applications this length is short. What are the finite size effects? We know from the theory of phase transitions that near a phase transition finite size effects can be very important. Is there finite size scaling? The answer will depend on the order of the phase transition.

It is empirically known that the number of iterations required for the decoding algorithm to converge increases dramatically as the noise increases and one gets close to the phase transition. How does the decoding complexity behave as one approaches the zero error noise threshold? Is there a critical slowing down, as it is usually the case for physical systems near a phase transition? As it was said before, the decoding algorithms both for LDPC codes and turbo codes are heuristic and there are not known results as one approaches the phase transition.

It is well known that disordered systems often exhibit a "glassy" behaviour. This means that below a certain temperature they get trapped in metastable states and do not reach equilibrium in any finite time. Is there a glassy phase in decoding? In other terms, do the heuristic decoding algorithms reach the threshold of optimum decoding (which we computed by equilibrium statistical mechanics) in a finite number of iteration steps, or is there a (lower) noise "dynamical" threshold ("dynamical" transition in the language of disordered systems) where the decoding algorithm gets trapped in metastable states? In that case the decoding algorithm would be unable to reach optimal performance as computed by equilibrium statistical mechanics.

I hope that at least some of the above questions will be answered in the near future.

References

1. Shannon, C. E., A Mathematical Theory of Communication, *Bell Syst. Tech. J.* 27, 379 and 623 (1948)
2. Shannon, C. E. and Weaver W., A Mathematical Theory of Communication, (Univ. of Illinois Press, 1963)
3. C. Berrou, A. Glavieux, and P.Thitimajshima. Proc.1993 Int.Conf.Comm. 1064-1070
4. MacKay, D. J. C. Neal, R. M. *Elect. Lett.* 33, 457 (1997)
5. Gallager, R. G. *IRE Trans. Inform. Theory* , IT-8, 21 (1962)
6. Gallager, R. G. *Low-Density Parity-Check Codes* , MIT Press, Cambridge MA (1963)
7. Sourlas, N., *Nature* 339, 693 (1989)

8. Sourlas, N., in *Statistical Mechanics of Neural Networks*, Lecture Notes in Physics 368, ed. L. Garrido, Springer Verlag (1990)
9. Sourlas, N., Ecole Normale Supérieure preprint (April 1993)
10. Sourlas, N., in *From Statistical Physics to Statistical Inference and Back*, ed. P. Grassberger and J.-P. Nadal, Kluwer Academic (1994) p. 195.
11. Ruján, P., *Phys. Rev. Lett.* 70, 2968 (1993)
12. Nishimori, H., *J. Phys. Soc. Jpn.*, 62, 2973 (1993)
13. Sourlas, N., *Europhys. Lett.* 25, 169 (1994)
14. Nishimori, H., *Progr. Theor. Phys.* 66, 1169 (1981)
15. L. Bahl, J. Cocke, F. Jelinek, and J. Raviv. IEEE Trans.Inf.Theory **IT-20**(1974) 248-287
16. Mézard, M. Parisi, G. Virasoro, M. A. Spin Glass Theory and Beyond, World Scientific (1987)
17. Thouless, D. J. Anderson, P. W. Palmer, R. G. *Phil. Mag.* 35, 593 (1977)
18. Mézard, M. Parisi, G. Viresoro, M. A. *Europhys. Lett.* 1, 77 (1986)
19. Kanter, I. and Saad, D. *Phys. Rev. Lett.* 83, 2660 (1999)
20. Kabashima, Y. Murayama T. and Saad, D. *Phys. Rev. Lett.* 84, 1355 (2000)
21. Montanari, A. *Eur. Phys. J.* B 23, 121 (2001)
22. Derrida, B., Random-energy model: An exactly solvable model of disordered systems, *Phys. Rev.* B24, 2613-2626 (1981)
23. Richardson, T. J. Urbanke, R. L. *IEEE Trans. Inform. Theory* 47, 638 (2001).
24. Montanari, A. Sourlas, N. *Eur. Phys. J.* B 18, 107 (2000)
25. Montanari, A. *Eur. Phys. J.* B 18, 121 (2000)
26. Kolmogorov, A. Petrovsky, I and Piscounov, N. *Moscou Univ. Math. Bull.* 1, 1 (1937)

DISCUSSION

Chairman: E. Polzik

G. Hegerfeldt: How would you get the random matrix H? From random numbers generated by the computer?

N. Sourlas: Yes, there are algorithms to give you this. That is the notion of self averaging. As you said, once you have given these algorithms, this defines for you a family of codes not a single one. And then the point is that the properties of their probabilities are the same with probability one for anyone of the codes in this family.

DIRECT DETECTION OF QUANTUM ENTANGLEMENT

PAWEŁ HORODECKI
Faculty of Applied Physics and Mathematics, Technical University of Gdańsk, 80-952 Gdańsk, Poland.

ARTUR K. EKERT, CAROLINA MOURA ALVES, DANIEL K. L. OI
Centre for Quantum Computation, Clarendon Laboratory, University of Oxford, Parks Road, Oxford OX1 3PU, U.K.

L. C. KWEK
Department of Natural Sciences, National Institute of Education, Nanyang Technological University, 1 Nanyang Walk, Singapore 637616.

DAGOMIR KASZLIKOWSKI
Department of Physics, Faculty of Science, National University of Singapore, Lower Kent Ridge, Singapore 119260.

MICHAŁ HORODECKI
Institute of Theoretical Physics and Astrophysics, University of Gdańsk, 80-952 Gdańsk, Poland.

After playing a significant role in the development of the foundations of quantum mechanics, entanglement has been recently rediscovered as a new physical resource with potential commercial applications, ranging from quantum cryptography to very precise frequency standards. Thus, the detection of quantum entanglement is vital in the experimental context. We present a direct method of detecting the presence of entanglement and we put it in the context of quantum information science.

1 Entanglement

Probably the best way to agitate a group of jaded, but philosophically-inclined, physicists is to buy them a bottle of wine and mention *interpretations of quantum mechanics*. Opening Pandora's box isn't much different, despite the fact that, as far as lip-service goes, the orthodoxy established by Niels Bohr over 60 years ago, known as the "Copenhagen interpretation", still effectively holds sway. It seems that everybody agrees with the formalism of quantum mechanics, but no one agrees on its meaning. Quantum theory, according to the "Copenhagen interpretation", provides merely a calculational procedure and does not attempt to describe objective physical reality. According to Bohr

> There is no quantum world. There is only an abstract physical description. It is wrong to think that the task of physics is to find out how the nature is. Physics concerns what we can say about nature. [a]

[a] Quoted after Aage Petersen in *Niels Bohr: a centenary volume*, eds. A.P. French and P.J. Kennedy, Harvard University Press, 1985.

A very defeatist view indeed, but hardly surprising. The intellectual atmosphere and the philosophy of science at the time were dominated by positivism that emerged in Vienna in the early 1920s. According to this school of thought all statements other than those describing or predicting observations are meaningless [b].

One of the first who found the pragmatic instrumentalism of Bohr unacceptable was Albert Einstein. In 1927 during, the fifth Solvay Conference in Brussels, Einstein directly challenged Bohr over the meaning of quantum theory. This triggered the Bohr-Einstein debate, which lasted almost three decades and which, among many other things, brought quantum entanglement into the remit of modern physics. In early 1935, Einstein, together with Boris Podolsky and Nathan Rosen, published a classic paper which featured a composite quantum system consisting of two distant particles with entangled wave function [1]. The entanglement of the wave function as such was never mentioned in the paper, as the authors focused on the incompleteness of quantum mechanical description of reality. Erwin Schrödinger, at the time a fellow of Magdalen College in Oxford, seems to have been the first to spot it and to realize its importance. In August 1935, the Cambridge Philosophical Society received a paper written by Schrödinger, and communicated by Max Born, titled "Discussion of probability relations between separated system" [2]. The paper was read 28 October 1935. Its opening paragraph states

> When two systems, of which we know the states by their respective representatives, enter into temporary physical interaction due to known forces between them, and when after a time of mutual influence the systems separate again, then they can no longer be described in the same way as before, viz. by endowing each of them with a representative of its own. I would not call it *one* but rather *the* characteristic trait of quantum mechanics, the one that enforces its entire departure from classical lines of thought. By the interaction the two representatives (or ψ-functions) have become entangled...[c]

After playing a significant role in the development of the foundations of quantum mechanics [3], entanglement has been recently rediscovered as a new physical resource with potential commercial applications such as, for example, quantum cryptography [4], better frequency standards [5] or quantum-enhanced positioning and clock synchronization [6]. On the mathematical side, the studies of entanglement have revealed very interesting connections with the theory of positive maps [7,8]. The capacity to generate entangled states is one of the basic requirements for building quantum computers. Hence, efficient experimental methods for detection, verification and estimation of quantum entanglement are of great practical importance. Here, we describe an experimentally viable, *direct* detection of quantum entanglement which has been proposed recently by Horodecki and Ekert [10]. It is efficient and does not require any *a priori* knowledge about the quantum state. In the particular case of two entangled qubits, it provides an estimation of the amount of entanglement. We also discuss it in context of some aspects of quantum information theory.

[b]It is quite amusing to notice that according to this criterion positivism is itself meaningless.
[c]The emphasized "*o*ne" and "*t*he" are due to Schrödinger.

2 Specification of the problem

Suppose we are given n pairs of particles, all in the same quantum state described by some density operator ϱ, which is unknown. We need to decide whether the particles in each pair are entangled or not. From a mathematical point of view we need to assert whether ϱ can be written as a convex sum of product states [12],

$$\varrho = \sum_{i}^{k} p_i |\alpha_i\rangle\langle\alpha_i| \otimes |\beta_i\rangle\langle\beta_i|, \tag{1}$$

with $|\alpha_i\rangle$ and $|\beta_i\rangle$ pertaining to different particles in the pair and $\sum_i p_i = 1$. It is assumed that the Hilbert spaces associated with each particle are of finite dimension d (taken to be the same for the two particles), so that one can always find $k \leq d^2$. If ϱ were known, we could try either to find the decomposition (1) directly or to use one of the mathematical separability criteria [8]. For sufficiently large n, we may indeed start with the quantum state estimation. However, this involves estimating $d^4 - 1$ real parameters of ϱ, most of which are irrelevant in the context of the entanglement detection.

Another possibility is the recourse to a particular class of two-particle observables, called entanglement witnesses, which can detect quantum entanglement is some special cases (see [9,8]). They have positive mean values on *all* separable states and negative on *some* entangled states. Therefore, any individual entanglement witness leaves many entangled states undetected. When ϱ is unknown, we need to check infinitely many witnesses, which effectively reduces this approach to the quantum state estimation. However, if some information about the state is available, the entanglement witnesses approach may be very convenient [11]. In this paper we will focus on the case of unknown ϱ.

3 What are positive maps good for?

In the following we describe a direct method of detecting quantum entanglement without invoking the state estimation.

We construct a measurement, as powerful in detecting quantum entanglement as the best mathematical test based on positive maps [7], which can be performed on all copies of ϱ. The measurement can be viewed as two consecutive physical operations: firstly, we construct a transformation which maps ϱ into an appropriate state ϱ'; secondly, we measure the lowest eigenvalue of ϱ'. This eigenvalue alone serves as a separability indicator.

A convenient starting point for our construction is the most powerful, albeit purely mathematical and not directly implementable in a physical way, separability criterion proposed to date. The criterion is based on mathematical properties of linear positive maps acting on matrices [7]. Let M_d be a space of matrices of dimension d; recall that $\Lambda : M_d \mapsto M_d$ is called positive if $X \geq 0$ implies $\Lambda(X) \geq 0$ (expression $X \geq 0$ means that the matrix X has a nonnegative spectrum). If the induced map $\mathbb{I} \otimes \Lambda$ is also positive, then Λ is called completely positive and, as such, it represents a physically allowed transformation of density operators (here

$\mathbb{I}$ denotes the identity map on an auxiliary system of any dimension). Using this terminology, the separability criterion reads [7]: ϱ is separable iff

$$[\mathbb{I} \otimes \Lambda](\varrho) \geq 0, \tag{2}$$

for all positive but not completely positive maps $\Lambda : M_d \mapsto M_d$ acting on the second particle. In fact, it is sufficient to consider only positive maps Λ such that the maximum of $\mathrm{Tr}\,\Lambda(\varrho)$, over all ϱ, is equal to unity. Other positive maps differ only by a positive multiplicative factor which does not affect the condition (2).

Furthermore, in some cases, instead of scanning all positive maps, we can choose just one. For example, *all* entangled states of two qubits can be detected by choosing Λ to be transposition [13,7]. The snag is that positive maps Λ, such as an anti-unitary transposition and the induced maps $\mathbb{I} \otimes \Lambda$, cannot be implemented in a laboratory. Thus, the criterion (2) tacitly assumes prior knowledge of ϱ. However, there is a way to modify it, so that it becomes experimentally viable and without involving any state estimation.

4 Operational criterium for detecting entanglement

If we mix in an appropriate proportion of $[\mathbb{I} \otimes \Lambda]$ with a depolarizing map, that turns any density matrix into a maximally mixed state, the resulting map can be completely positive This is because the lowest negative eigenvalues generated by the induced map $[(\mathbb{I} \otimes \mathbb{I}) \otimes (\mathbb{I} \otimes \Lambda)]$ can be offset by the positive eigenvalues of the maximally mixed state generated by the depolarizing map. The most negative eigenvalue $-\lambda < 0$ is obtained when $[(\mathbb{I} \otimes \mathbb{I}) \otimes (\mathbb{I} \otimes \Lambda)]$ acts on the maximally entangled state of the form $\frac{1}{\sqrt{d^2}} \sum_{i=1}^{d^2} |i\rangle|i\rangle$, where each state $|i\rangle$ pertains to a d^2 dimensional subsystem, itself is composed of two d dimensional parts. Thus, the map

$$\widetilde{[\mathbb{I} \otimes \Lambda]}(\varrho) = p\frac{I \otimes I}{d^2} + (1-p)[\mathbb{I} \otimes \Lambda](\varrho), \tag{3}$$

is completely positive, therefore physically implementable, when the induced map $[(\mathbb{I} \otimes \mathbb{I}) \otimes \widetilde{(\mathbb{I} \otimes \Lambda)}]$ is positive. This happens for $p \geq (d^4\lambda)/(d^4\lambda + 1)$ [14]. By inserting the threshold value $p = (d^4\lambda)/(d^4\lambda + 1)$ into (3), we can modify the criterion (2) as follows: ϱ is separable iff for all positive maps Λ,

$$\widetilde{[\mathbb{I} \otimes \Lambda]}(\varrho) \geq \frac{d^2\lambda}{d^4\lambda + 1}, \tag{4}$$

i.e. when the minimal eigenvalue of the transformed state $\varrho' = \widetilde{[\mathbb{I} \otimes \Lambda]}(\varrho)$ is greater than $(d^2\lambda)/(d^4\lambda + 1)$. In general, for some maps Λ, the related completely positive maps $\widetilde{\mathbb{I} \otimes \Lambda}$ are not trace-preserving and require postselections in their physical implementations. Maps such as $\widetilde{\mathbb{I} \otimes \Lambda}$ have been referred to as "structural" physical approximations of unphysical maps $\mathbb{I} \otimes \Lambda$ [14].

For example, if we take Λ to be transposition T (the first positive map used for detecting entanglement), we obtain

$$\widetilde{[\mathbb{I}\otimes T]}(\varrho) = \frac{d}{d^3+1} I\otimes I + \frac{1}{d^3+1}[\mathbb{I}\otimes T](\varrho). \tag{5}$$

In the two qubit case, where the partial transposition is a sharp test for entanglement, we obtain,

$$\widetilde{[\mathbb{I}\otimes T]}(\varrho) = \frac{2}{9} I\otimes I + \frac{1}{9}[\mathbb{I}\otimes T](\varrho), \tag{6}$$

which can be represented and implemented as

$$\frac{1}{3}\Lambda_1\otimes\Lambda_2 + \frac{2}{3}\mathbb{I}\otimes\sigma_x\sigma_z\Lambda_1\sigma_z\sigma_x, \tag{7}$$

with the two channels defined as:

$$\Lambda_1(\varrho) = \frac{1}{3}\sum_{i=x,y,z}\sigma_i\varrho\sigma_i, \quad \Lambda_2(\varrho) = \frac{1}{4}\sum_{i=o,x,y,z}\sigma_i\varrho\sigma_i. \tag{8}$$

The map can be implemented by applying selected products of unitary (Pauli) transformations with the prescribed probabilities. Since the map is trace-preserving, any post-selection in experimental realizations is avoided.

Thus, in order to detect entanglement of an arbitrary two-qubit state ϱ, it is enough to estimate a single parameter, i.e. the minimal eigenvalue of $\widetilde{[\mathbb{I}\otimes T]}(\varrho)$. The state ϱ is separable iff this eigenvalue satisfies $\lambda_{min} \geq \frac{2}{9}$. Let us also point out an extra bonus: λ_{min} gives us $-\lambda'$, the most negative eigenvalue of $[\mathbb{I}\otimes T](\varrho)$, which enters the expression for the upper and lower bounds for the entanglement of formation,

$$H\left(\frac{1+\sqrt{1-4\lambda'^2}}{2}\right) \leq E(\varrho)$$
$$\leq H\left(\frac{1+\sqrt{1-4\left(\sqrt{2\lambda'^2+\lambda'}-\lambda'\right)}}{2}\right), \tag{9}$$

where $H(x)$ is the Shannon entropy. The above formulae can be derived from the estimations of the concurrence provided by Verstraete et al [15].

5 Spectrum estimation

Suppose for a moment that $\widetilde{\mathbb{I}\otimes\Lambda}$ is a trace-preserving map, e.g. the transposition case. The first part of our entanglement detection measurement is accomplished by applying $\widetilde{\mathbb{I}\otimes\Lambda}$ to each of the n pairs to obtain n copies of $\varrho' = \widetilde{[\mathbb{I}\otimes\Lambda]}(\varrho)$. Then, following the criterion (4), we need to measure the lowest eigenvalue of ϱ'.

This can be viewed as a special case of the spectrum estimation, and possible approaches depend a lot on particular physical realizations of ϱ'. Here, we provide

two general solutions. The first one, based on quantum interferometry, is conceptually simple and relies on estimating $d^2 - 1$ parameters from which the spectrum of ϱ' can be calculated (this is a significant gain over the state estimation which involves $d^4 - 1$ parameters). The second solution is a joint measurement on all copies of ϱ', which gives directly the estimate of the lowest eigenvalue.

We start with the quantum interferometry, presented here as a quantum network shown in Fig.(1). A typical interferometric set-up for a single qubit — the Hadamard gate, phase shift φ, the Hadamard gate, followed by a measurement — is modified by inserting in between the Hadamard gates a controlled-U operation, with its control on the qubit and with U acting on a quantum system described by some unknown density operator ρ. (N.B. we do not assume anything about the form of ρ; it can, for example, describe several entangled or separable sub-systems.) The action of the controlled-U on ρ modifies the interference pattern by the factor,

$$\mathrm{Tr}\rho U = \mathrm{v}e^{i\alpha}, \tag{10}$$

where v is the new visibility and α is the shift of the interference fringes, also known as the Pancharatnam phase [16]. Formula (10) has been derived, in the context of geometric phases, by Sjöqvist et al. [17].

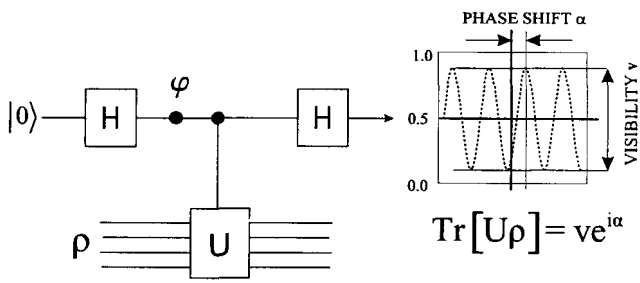

Figure 1. Both the visibility and the shift of the interference patterns of a single qubit (top line) are affected by the controlled-U operation. This set-up allows to estimate $\mathrm{Tr}\, U\rho$, the average value of U in state ρ.

The network can evaluate certain non-linear functionals of density operators. Let us choose ρ to be composed of two subsystems, $\rho = \varrho_a \otimes \varrho_b$, and let U to be the exchange operator V, such that $V\,|\,\alpha\rangle\,|\,\beta\rangle = |\,\beta\rangle\,|\,\alpha\rangle$ for any pure states of the two subsystems. The interference pattern is now modified by the factor $\mathrm{Tr}\, V(\varrho_a \otimes \varrho_b) = \mathrm{Tr}\, \varrho_a\varrho_b$. For $\rho = \varrho \otimes \varrho$, we can estimate $\mathrm{Tr}\,\varrho^2$, which gives us an estimate of $\sum_{i=1}^{m} \lambda_i^2$, where λ_i are the eigenvalues of ϱ. N.B. $\mathrm{Tr}\,\varrho^2$ is real hence there is no need to sweep the phase φ in the interferometer, it can be fixed at $\varphi = 0$.

In general, in order to calculate the spectrum of any $m \times m$ density matrix ϱ we need to estimate $m - 1$ parameters $\mathrm{Tr}\varrho^2$, $\mathrm{Tr}\varrho^3$,... $\mathrm{Tr}\varrho^m$. For this we need the controlled-shift operation. Given k systems of dimension m we define the shift $V^{(k)}$

as

$$V^{(k)} \mid \phi_1\rangle \mid \phi_2\rangle \ldots \mid \phi_k\rangle = \mid \phi_k\rangle \mid \phi_1\rangle \ldots \mid \phi_{k-1}\rangle \,, \tag{11}$$

for any states $\mid \phi\rangle$. Such an operation can be easily constructed by cascading $k-1$ swaps V. This time, if we prepare $\rho = \varrho^{\otimes k}$ the interference will be modified by the factor

$$\mathrm{Tr}\, \varrho^{\otimes k} V^{(k)} = \mathrm{Tr}\, \varrho^k = \sum_{i=1}^{m} \lambda_i^k . \tag{12}$$

Thus, measuring the average values of $V^{(k)}$ for $k = 2, 3 \ldots m$ gives us effectively the spectrum of ϱ. In our case, in particular, we obtain the spectrum (and the lowest eigenvalue) of $\varrho' = \widetilde{[\mathbb{I} \otimes \Lambda]}(\varrho)$ by estimating $d^2 - 1$ parameters $\mathrm{Tr}\, \varrho'^k$, where $k = 2 \ldots d^2$. Again, the phase in the interferometry can be fixed at $\varphi = 0$.

The interferometric scheme described above is conceptually simple and experimentally viable. However, if the simplicity of the implementation is not an issue, we can choose to measure the estimate of the lowest eigenvalue directly. This requires a join measurement on all of the n pairs (see [10] and [18] for further details).

6 Conclusions

Let us summarize our findings. Given n copies of a bipartite $d \otimes d$ system, described by some unknown density operator ϱ, we can test for entanglement either by estimating ϱ and applying criterion (2), or, more directly, by performing the measurements we have just described. The state estimation involves estimating $d^4 - 1$ parameters of ϱ, most of which are of no relevance for the entanglement detection. The optimal state estimations rely on joint measurements on all copies of ϱ. However, one can construct less efficient but simpler state estimation methods which involve measurements only on individual copies. Our more direct, interferometry based, method requires estimations of only $d^2 - 1$ parameters and joint operations on d copies of ϱ'. The most demanding, from the experimental point of view, is our second method. It is a measurement with an outcome which is an estimate of just one parameter, but, like the optimal state estimation, the measurement involves joint operations on all copies of ϱ'. Both direct and indirect entanglement detections have their own merits. Depending on the context, applications, and technologies involved, one can choose one or the other.

There are powerful mathematical tools to test the entanglement in bipartite and some multipartite Gaussian states [25], and the present scheme can be modified to directly detect it. However, in order to modify it efficiently, the present scheme would have to be translated into the language of spectrum of covariance matrix, rather then of the state itself. Those issues are related to more general and interesting questions of inherently quantum decision problems on continuous variables domain [26]. In particular, it would be interesting to consider possible implications of such approach, on the so called quantum Gaussian channels.

Direct entanglement detections can be employed as sub-routines in quantum computation. For example, one may consider performing or not performing a quantum operation on a given quantum system, conditioned on some part of quantum data being entangled or not. In fact, direct entanglement detections can be viewed as quantum computations solving an *inherently quantum* decision problem: given as an input n copies of ϱ, decide whether ϱ is entangled. Here, the input data is quantum and such a decision problem cannot even be even formulated for classical computers. Nonetheless, the problem is perfectly well defined for quantum computers. Finally, let us add that the method presented here can be easily generalized to cover all linear maps tests for *arbitrary* multiparticle entanglement [21] and the so called k-positive map tests detecting Schmidt numbers of density matrices [22]. Modification of the method to the case of two distant labs, under restrictions to local operations and classical communication [8], is possible [24]).

Acknowledgements

A.K.E., L.C.K. and D.K. acknowledge financial support provided under the NSTB Grant No. 012-104-0040, P.H. and M.H. would like to acknowledge support from the EU (EQUIP, contract no. IST-1999-11053), C.M.A. is supported by the Fundação para a Ciência e Tecnologia (Portugal) and D.K.L.O. would like to acknowledge the support of CESG (UK) and QAIP (contract no. IST-1999-11234).

References

1. A. Einstein, B. Podolsky, and N. Rosen. *Physical Review*, 47:777, 1935.
2. E. Schrödinger *Proc. Cam. Phil. Soc*, 31:555–563, 1935.
3. J.S. Bell. *Physics*, 1:195, 1964.
4. A. K. Ekert. Quantum cryptography based on bell theorem. *Physical Review Letters*, 67(6):661–663, 1991.
5. J. J. Bollinger, W. M. Itano, D. J. Wineland, and D. J. Heinzen. Optimal frequency measurements with maximally correlated states. *Physical Review A*, 54(6):R4649–R4652, 1996.
6. V. Giovannetti, S. Lloyd, and L. Maccone. Quantum-enhanced positioning and clock synchronization. *Nature*, 412(6845):417–419, 2001.
7. M. Horodecki, P. Horodecki, and R. Horodecki. Separability of mixed states: Necessary and sufficient conditions. *Physics Letters A*, 223(1-2):1–8, 1996.
8. G. Alber, T. Beth, M. Horodecki, P. Horodecki, R. Horodecki, M. Röttler, H. Weinfurter, R. F. Werner, and A. Zeilinger. *Quantum information: an introduction to basic theoretical concepts and experiments.*, volume 173 of *Springer Tracts in Modern Physics*. Springer, 2001.
9. D. Bruß, J. I. Cirac, P. Horodecki, F. Hulpke, B. Kraus, M. Lewenstein, A. Sanpera. Reflections upon separability and distillability. quant-ph/0110081.
10. P. Horodecki, A. K. Ekert. Direct detection of quantum entanglement quant-ph/0111064
11. O. Gühne, P. Hyllus, D. Bruß, A. K. Ekert, M. Lewenstein, C. Macchiavello, A. Sanperra. Detection of entanglement with few local measurements quant-

ph/0205089
12. R. F. Werner. Quantum states with einstein-podolsky-rosen correlations admitting a hidden-variable model. *Physical Review A*, 40(8):4277–4281, 1989.
13. A. Peres. Separability criterion for density matrices. *Physical Review Letters*, 77(8):1413–1415, 1996.
14. P. Horodecki. From limits of nonlinear quantum operations to multicopy entanglement witnesses and spectrum states estimation. quant-ph/0111036.
15. F. Verstraete, K. Audenaert, J. Dehaene, and D. de Moor. A comparison of the entanglement measures negativity and concurence. quant-ph/0108021.
16. S. Pancharatnam. Generalized theory of interference and its applications. *Proceedings of the Indian Academy of Science*, XLIV(5):247–262, 1956.
17. E. Sjöqvist, A. K. Pati, A. Ekert, J. S. Anandan, M. Ericsson, D. K. L. Oi, and V. Vedral. Geometric phases for mixed states in interferometry. *Physical Review Letters*, 85(14):2845–2849, 2000.
18. M. Keyl and R. F. Werner. Estimating the spectrum of a density operator. *Physical Review A*, 64 (5):052311-1–052311-5, 2001.
19. J. I. Cirac, A. K. Ekert, and C. Macchiavello. Optimal purification of single qubits. *Physical Review Letters*, 82(21):4344–4347, 1999.
20. A. Barenco, A. Berthiaume, D. Deutsch, A. Ekert, R. Jozsa, and C. Macchiavello. Stabilization of quantum computations by symmetrization. *SIAM Journal on Computing*, 26(5):1541–1557, 1997.
21. M. Horodecki, P. Horodecki, and R. Horodecki. Separability of n-particle mixed states: necessary and sufficient conditions in terms of linear maps. *Physics Letters A*, 283(1-2):1–7, 2001.
22. B. M. Terhal, P. Horodecki. Schmidt number for density matrices. *Physical Review A*, 61 (4):040301-040305, 2000.
23. Dirk Bouwmeester, Artur K. Ekert, and Anton Zeilinger. *The physics of quantum information: quantum cryptography, quantum teleportation, quantum computation.* Springer, New York, 2000. Dirk Bouwmeester, Artur K. Ekert, Anton Zeilinger (eds.).
24. P. Horodecki, et al. (in preparation).
25. G. Giedke, B. Kraus, M. Lewenstein, J. I. Cirac, Phys. Rev. Lett. 87: 167904- , 2001; G. Giedke, B. Kraus, M. Lewenstein, J. I. Cirac, Phys. Rev. A, 64: 052303- , 2002; and references therein.
26. S. L. Braunstein and A. K. Pati (eds.), *Quantum Information Theory with Continuous Variables*, Kluwier Academic Publishers, Dodrecht, 2002, in press.

DISCUSSION

Chairman: E. Polzik

L. Accardi: Do you check on an ensemble, because you cannot check on a single system?

A. Ekert: Yes, of course. The experimental scenario I have in mind is that you have N copies of a bipartite system in the same state. Mathematically you have

the N-fold tensor product of this density operator. Then you apply a completely positive map to each of the N systems which generates N copies of a new density operator. Then you have to test for the lowest eigenvalue of this new density operator, and this, in general, involves joint operations on all N systems.

P. Stamp: How to implement the final operator $I \otimes T$ in certain cases in the lab?

A. Ekert: For example, if you take two qubits, then you can look what this completely positive map looks like, and then you can decompose it into a mixture of some dephasing channels, with different probabilities, different randomisations of the channels. Or maybe they are other ways as well.

I. Cirac: Is that completely positive map separable itself? Can it be implemented locally?

A. Ekert: Yes, I think so. Actually what I know it is for the qubit, because I can write it in this way. But for the general case, I don't know.

D. Ellinas: In order to construct the modified criterion you have, do you use the partial transposition only or just any positive operator without being completely positive? Do you use the model with specific partial transposition or any positive map?

A. Ekert: Actually, I use the partial transposition as an example. You can actually take this test, and you can go all the way through and you will get an equivalent test, a more general test, which says: for all maps, and then I put the tilde here and there will be an expression on the r.h.s. So I think it was just easier in this short time to explain the special case of partial transposition. And in fact, if you choose one particular positive map you will be as powerful as partial transposition.

D. Ellinas: So I ask if positivity is sufficient for construction?

A. Ekert: You can choose any map that is positive but not completely positive.

K. Mølmer: I am sure that the chairman will forgive me this question, because in his talk he demonstrated entanglement himself. Can you see a relation between your visibility testing and visibility testing in that experiment?

A. Ekert: Let's put it this way: should E. Polzik be working on this process?

THE THEORY OF NEURAL NETWORKS AND CRYPTOGRAPHY

IDO KANTER[1] and WOLFGANG KINZEL[2]

[1] *Minerva Center and Department of Physics, Bar-Ilan University, Ramat-Gan 52900, Israel*

[2] *Institut für Theoretische Physik, Universität Würzburg D-97074, Germany*

A connection between the theory of neural networks and cryptography is presented. A new phenomenon, namely synchronization of neural networks, is leading to a new method of exchange of secret messages. Two artificial networks being trained by the Hebbian learning rule on their mutual outputs develop an antiparallel state of their synaptic weights. The synchronized weights are used to construct an ephemeral key exchange protocol for the secure transmission of secret data. The complexity of the generation of the secure channel is linear with the size of the network. An attacker who knows the protocol and all details of any transmission of the data finds it difficult to decrypt the secret message.

1 Introduction

The ability to build a secure channel is one of the most challenging fields of research in modern communication. Since the secure channel has many applications, in particular for mobile phone, satellite and internet-based communications, there is a need for fast, effective and secure transmission protocols[1]. Here we present a novel principle of a cryptosystem based on a new phenomenon which we observe for artificial neural networks.

The goal of cryptography is to enable two partners to communicate over an insecure channel in such a way that an attacker cannot understand and decrypt the transmitted message. In a general scenario, the message is encrypted by the sender through a key E_k, and the result, the ciphertext, is sent over the channel. A third party, eavesdropping on the channel, should not be able to determine what the message was. However, the recipient who knows the encryption key can decrypt the ciphertext using his private key D_k.

In a *private-key* system the recipient has to agree with the sender on a secret key E_k, which requires a hidden communication prior to the transmission of any message. In a *public-key* system, on the other side, the key E_k is published and a hidden communication is not necessary. Nevertheless, an attacker cannot decrypt the transmitted message since it is computationally infeasible to invert the encryption function without knowing the key D_k. In a *key-exchange protocol*, both partners start with private keys and transmit – using a public protocol – their encrypted private keys which, after some transformations, leads to a common secret key. In most applications a public-key system is used which is based on number theory where the keys are long integers[1,2].

In this report we suggest a novel cryptosystem. It is a key-exchange protocol which uses neither number theory nor a public key, but is based on a learning process of neural networks: The two participants start from a secret set of vectors $E_k(0)$ and $D_k(0)$ without knowing the key of their partner. By exchanging public information the two keys develop into a common time dependent key $E_k(t) = -D_k(t)$, which is

used to encrypt and decrypt a given message. An attacker who knows the algorithm and observes any exchange of information finds it difficult to reveal the keys $E_k(t)$ and $D_k(t)$. Our method is based on a new phenomenon: Synchronization of neural networks by mutual learning[3].

Simple models of neural networks describe a wide variety of phenomena in neurobiology and information theory[4,5,6]. Artificial neural networks are systems of elements interacting by adaptive couplings which are trained from a set of examples. After training they function as content addressable associative memory, as classifiers or as prediction algorithms.

Two feedforward networks can synchronize their synaptic weights by exchanging and learning their mutual outputs for given common inputs. Surprisingly, synchronization is fast; the number of bits required to achieve perfect alignment of the weights is lower than the number of components of the weights. After synchronization, the synaptic weights define the common time dependent private key $E_k(t) = -D_k(t)$. The complexity of our cryptosystems scales linearly with the size of the network (=number of bits of the keys). With respect to possible attacks, we find that tracking the weights of one of the networks by the attacker is a difficult problem. In summary, from this new biological mechanism one can construct efficient encryption systems using keys which change permanently.

The paper is organized as follows. In section II we speculate on the possible biological meaning of this new bridge between the theory of neural networks and cryptography. In section III the definition of the architecture and the dynamical rules are presented. In section IV the synchronization time between the parties derived from simulations are presented, while in section V the efficiency of a simple attacker is examined. In section VI some possible generalizations of our secure channel are briefly discussed.

2 Possible biological relevance

Synchronization is the subject of recent research in neuroscience[7,8,9,10,11], where, for instance, in experiments on cats and monkeys it was found that the spike activity of neurons in the visual cortex has correlations which depend on the kind of optical stimulus shown to the animal[12]. The phenomenon described here suggests that synchronization can be used by biological neuronal networks or by networks of the immune system to exchange secure information between different parts of an organism.

The interpretation of the synchronization process as a mechanism to build a secure channel is a controversial subject. The need in biological systems for the secure transmission of secret data which is incorporated by a biological mechanism to encrypt and to decrypt a data is in question.

At that point we present our viewpoint on the possibility of such a biological realization. In table I we demonstrate a partial list of operations commonly used by a user of a personal computer (or by human activities in daily life). In comparison we present the implications of the research of modern biology, indicating that similar operations such as 'copy', 'paste', 'insert', 'cut' etc. exist in the activity of a cell and DNA. It is clear that biological operations are restricted to biological

purposes, hence they are very limited in comparison to the variety of options and flags suggested by any primitive software.

A possible conclusion of the above comparison would be the following paradigm. *All operations that can be found at the macroscopic level of human activity can also be found in biological activity on the microscopic level.* Hence, the adaptation of this paradigm indicates that the secure transmission of data also exists on the microscopic activities of a biological system. Encryption and decryption of biological signals should also be found in the microscopic functioning of human activities. The level of security, of course, should be rescaled with the expected capability of a sophisticated biological attacker.

Operation	Computers	Biology
cut	√	√
copy	√	√
paste	√	√
find	√	√
replace	√	√
encrypt	√	???
decrypt	√	???

Table 1: A similarity between functions operated by computers and activities operated by biological systems on the microscopic level.

3 Definition: network and dynamical rules

In the following we introduce and investigate a simple model which shows the properties sketched above. The architecture used by the recipient and the sender is a two-layered perceptron, exemplified here by a parity machine (PM) with K hidden units. More precisely, the size of the input is KN and its components are denoted by x_{kj}, $k = 1, 2, ..., K$ and $j = 1, ..., N$. For simplicity, each input unit takes binary values, $x_{kj} = \pm 1$. The K binary hidden units are denoted by $y_1, y_2, ..., y_K$. Our architecture is characterized by non-overlapping receptive fields (a tree), where the weight from the jth input unit to the kth hidden unit is denoted by w_{kj}, and the output bit O is the product of the state of the hidden units (see Fig. 1). For simplicity we discuss PMs with three hidden units $K = 3$. We use integer weights bounded by L, i.e., w_{kj} can take the values $-L, -L+1, ..., L$.

The secret information of each of the two partners is the initial values for the weights, w^S_{kj} and w^R_{kj}, for the sender and the recipient, respectively. It consists of $6N$ integer numbers, $3N$ of the recipient and $3N$ of the sender. Sender and recipient do not know the initial numbers of their partners, which are used to construct the common secret key.

Each network is then trained with the output of its partner. At each training step, for the synchronization as well as for the encryption/decryption step, a new common public input vector (x_{kj}) is needed for both the sender and the recipient. For a given input, the output is calculated in the following two steps. In the first

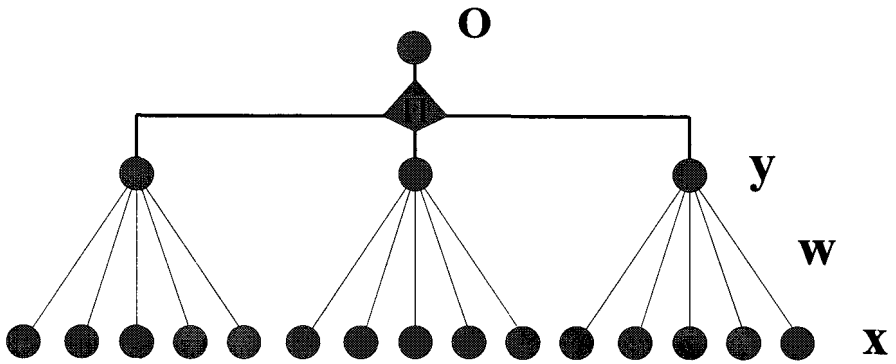

Figure 1: Architecture of the networks: $3N$ input units x are transmitted by three weight vectors w to three hidden units y. The final output bit O is the product of the hidden units.

step, the state of the three hidden units, $y_k^{S/R}, k = 1, 2, 3$, of the sender and the recipient are determined from the corresponding fields

$$y_k^{S/R} = \text{sign}[\sum_{j=1}^{N} w_{kj}^{S/R} x_{kj}] \tag{1}$$

In the case of zero field, $\sum w_{kj}^{S/R} x_{kj} = 0$, the sender/recipient sets the hidden unit to $1/-1$. In the next step the output $O^{S/R}$ is determined by the product of the hidden units, $O^{S/R} = y_1^{S/R} y_2^{S/R} y_3^{S/R}$.

The sender is sending its output (one bit) to the recipient, the recipient is sending its output to the sender and both networks are trained with the output of its partner. In the event that they do not agree on the current output, $O^S O^R < 0$, the weights of the sender/recipient are updated according to the following Hebbian learning rule[6,13]

$$\begin{aligned} \text{if } \left(O^{S/R} y_k^{S/R} > 0\right) \text{ then } w_{kj}^{S/R} &= w_{kj}^{S/R} - O^{S/R} x_{kj} \\ \text{if } \left(|w_{kj}^{S/R}| > L\right) \text{ then } w_{kj}^{S/R} &= \text{sign}(w_{kj}^{S/R})\, L \end{aligned} \tag{2}$$

Only weights belonging to the one (or three) hidden units which are in the same state as that of their output unit are updated, in each of the two networks. Note that by using this dynamical rule, the sender is trying to imitate the response of the recipient and the recipient is trying to imitate that of the sender[16].

There are three main ingredients in our model which are essential for a secure key exchange protocol: Firstly, from the knowledge of the output, the internal representation of the hidden units is not uniquely determined because there is a four fold degeneracy (for the output $+1$ there are four internal representations for the three hidden units $(1,1,1)$, $(1,-1,-1)$, $(-1,1,-1)$, $(-1,-1,1)$). As a consequence, an observer cannot know which of the weight vectors is updated according

to equation (2). Secondly, we have chosen the parity machine since there is a lack of correlation between the state of the hidden unit and the output bit (for output bit 1, for instance, for each hidden unit there are two internal representations with state 1 and two internal representations with state -1). This observation favors the PM over other multilayer networks. Thirdly, since each component is bounded by L, an observer cannot simply invert the sum of equation (2); the network forgets[15].

4 Synchronization process

We find that the two PMs learning from each other are able to synchronize, at least for some parameters K, L and N[16]. Our simulations show that after an initial relatively short transient time the two partners align themselves into antiparallel states. It is easy to verify from our learning rule that as soon as the two networks are synchronized they remain so forever. The number of time steps required to reach this state depends on the initial weight vectors and on the sequence of random inputs, hence it is distributed. Fig. 2 shows the distribution of synchronization time obtained from at least 1000 samples. It is evident that two communicating networks synchronize in a rather short time. The average synchronization time t_{av} decreases with increasing size N of the system (see Fig. 3); it seems to converge to $t_{av} \simeq 410$ for large networks. This observation was recently confirmed by an analytical solution of the presented model[17]. Surprisingly, in the limit of large N one needs to exchange only about 400 bits to obtain agreement between $3N$ components. However, one should keep in mind that the two partners do not learn the initial weights of each other, they are just attracted to a dynamical state with opposite weight vectors.

Note that this fast synchronization, independent of the size of the network, may also serve as an efficient biological mechanism to initialize two networks with the same initial conditions - the strength of the synapses. The number of operations (updates) per bit is very small, ~ 200 for $L = 3$ and only ~ 10 for $L = 1$ where synchronization is achieved after a few dozen steps. In artificial computers one can achieve a similar goal by the synchronization of the initial seed of a random number generator between the two partners. The complexity per bit (among 3N) is governed by the complexity to generate a random number.

As soon as the weights of the sender and the recipient are antiparallel the public initialization of our private-key cryptosystem is terminated successfully and the encryption of the message starts. There are then two possibilities in choosing an algorithm: First, use a conventional encryption algorithm, for example a stream cipher like the well-known Blum-Blum-Shub bit generator[1]. In this case the seed for this pseudo-random number generator is constructed from our weight vector after synchronization. Note that this bit generator is secure: even without a secret message one cannot guess the next bit from a polynomial number of consecutive output bits. Second, use the PM with time–dependent weights itself for a stream cipher by multiplying its output bit with the corresponding bit of the secret data.

In the case of the PM, the complexity of the encryption/decryption processes scales linearly with the size of the transmitted message, whereas the complexity of the synchronization process does not scale with the size of the network. Hence our

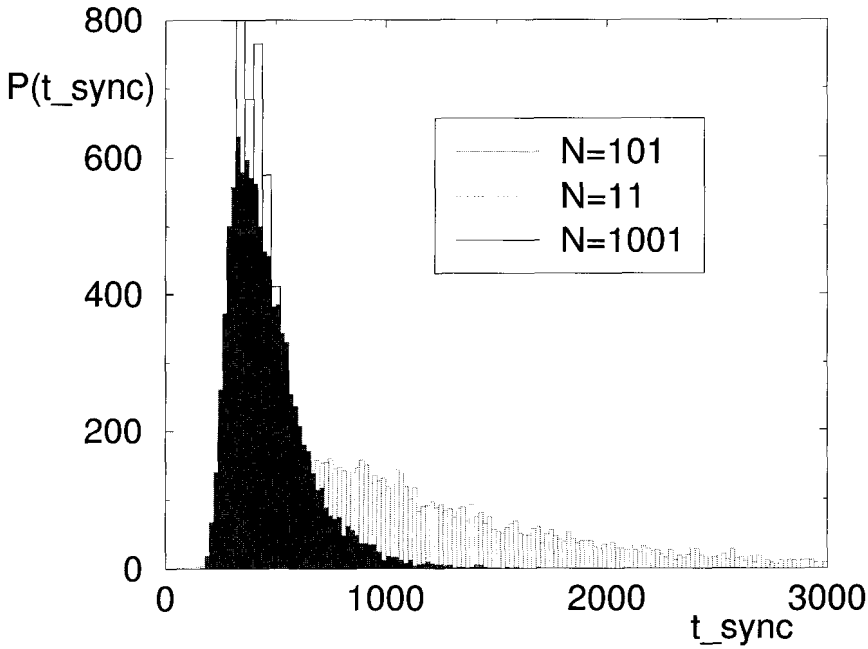

Figure 2: Distribution of synchronization time t_{sync} for three sizes N of the two networks.

construction is a linear cryptosystem[18].

5 An attacker

We now examine a possible attack on our cryptosystem. An attacker eavesdropping on the line knows the algorithm as well as the actual mutual outputs, hence he knows in which time steps the weights are changed. In addition, the attacker knows the input x_{kj} as well. However, the attacker does not know the initial conditions of the weights of the sender and the recipient. As a consequence, even for the synchronized state, the internal representations of the hidden units of the sender and the recipient are hidden from the attacker and he does not know which are the weights participating in the learning step. For random inputs all four internal representations appear with equal probability in any stage of the dynamical process, hence for t training steps there are 4^t possibilities to select internal representations[14].

Therefore, on the time scale of synchronization, the observing network has difficulty in obtaining complete knowledge about the other two networks. We have simulated the following basic attack on our cryptosystem. The architecture of an attacker is identical to the architecture of the partners, the recipient and the sender. The dynamics of this attacker tries to imitate the moves of one of the parties, the

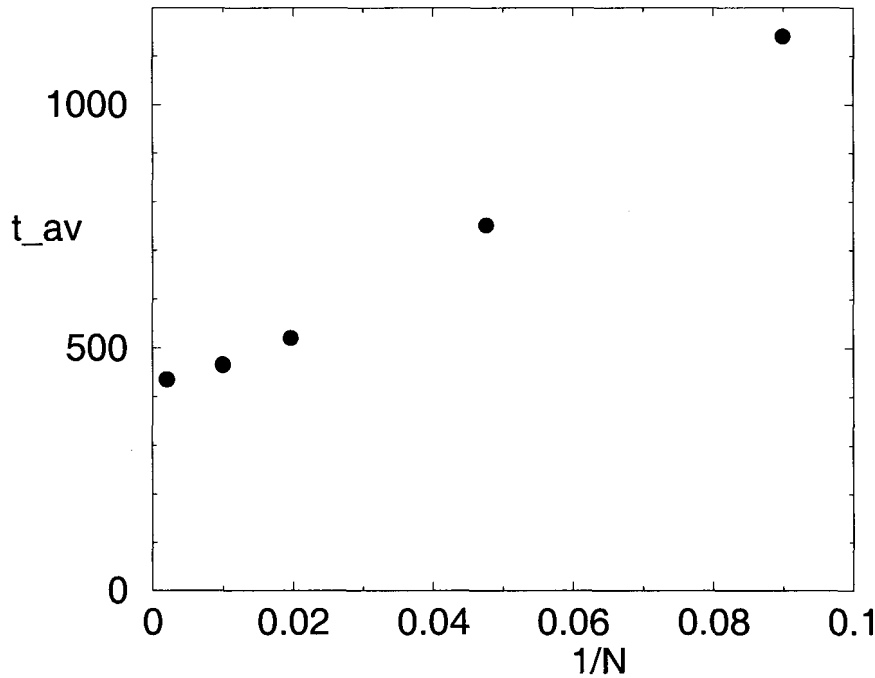

Figure 3: Average synchronization time as a function of $1/N$, for system size $N = 11, 21, 51, 101, 1001$.

sender for instance. The observing network is trained with the input vector and output bit of the sender, and the training step is performed only if sender and recipient disagree with each other[3].

The learning rule may be considered for each component of the weight vectors as a kind of biased random walk with reflecting boundaries. Therefore, for very long times, the observer may take the weight vector of the other network by chance. The distribution of the ratio between the time t_{sync} the sender and recipient need to synchronize and the learning time t_{learn} of this basic attacker needs for complete overlap is shown in Fig. 4. For $N = 101$ the average learning time is a factor of about 125 larger than the corresponding synchronization time. In addition, with increasing system size the tail of the distribution for larger ratios is reduced.

Hence the time to synchronize by chance is very long and in the example discussed here it is of order $O(10^5)$[19]. The heart of our cryptosystem is that synchronization is a much simpler task than tracking by an observer.

Recently the dynamic of such simple attackers was formulated and examined analytically for large networks, $N \gg 1$. The analytical results for the learning time were found to be in agreement with the results of simulations[17].

Possible advanced attacks were recently examined in [20], where it seems that

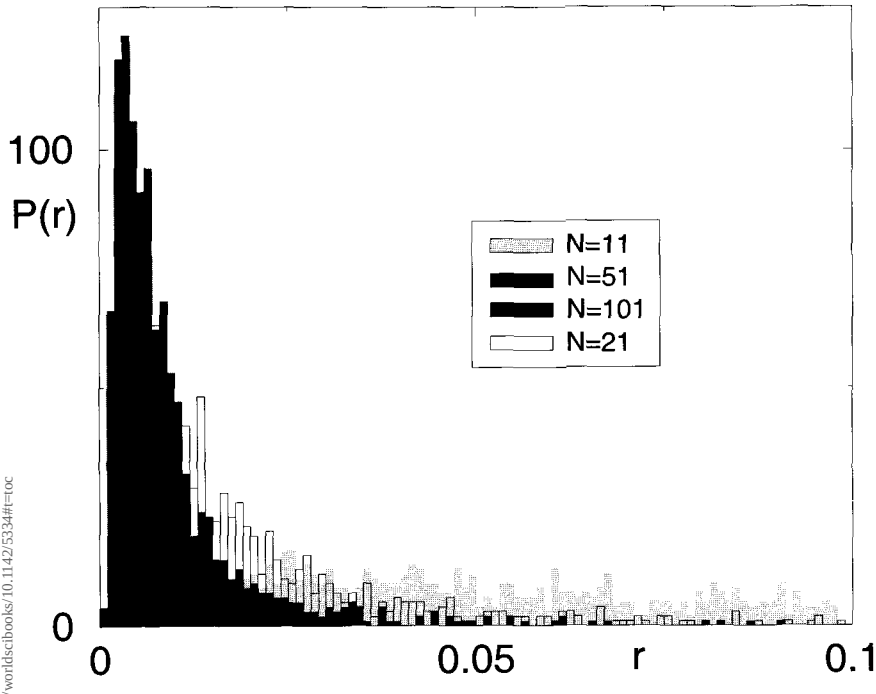

Figure 4: Frequency of the ratio r between synchronization and learning times.

the presented cryptosystem is breakable under an attack based on an ensemble of attackers using more advanced strategies - dynamical rules. The question of whether a practical secure channel based on a public protocol for the synchronization of the parties exists is in question. We would like to conclude this section and to repeat our abovementioned statement that *the required level of security for biological networks should be rescaled with the expected capability of a sophisticated biological attacker.*

6 Generalization

Our key exchange protocol can be generalized in the following directions as is briefly described below.

Bit-Packages: An important issue for the implementation of our cryptosystem is to accelerate the synchronization process from hundreds of time steps to a few dozen while maintaining the security of our channel. Surprisingly, both of these two goals can be achieved simultaneously by sending bit packages (BP). In this scenario the process contains the following steps: (a) The sender and the recipient generate $B > 1$ common inputs. (b) The sender and the recipient calculate the output of their PM for the set of B inputs and store the B sets of the corresponding values y_{ki} $(i = 1, ..., B)$ of the hidden units (the internal representations) (c) The

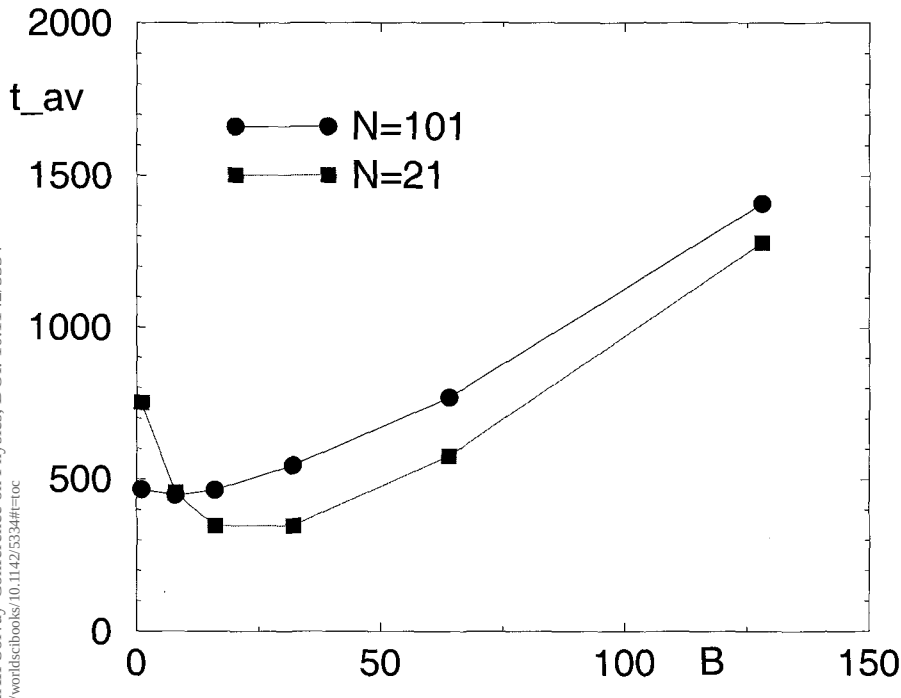

Figure 5: Total number of transmitted bits until synchronization. B is the number of bits in each bit package exchanged between sender and recipient.

transmission of mutual information; the sender/recipient sends a package consisting of B bits ($b_i^{S/R}$) to the recipient/sender. (d) The sender and the recipient update their weights using the same learning rule as for $B = 1$: In the case where bit $b_i^S \neq b_i^R$ the learning process takes place as before using the corresponding internal representations. The synchronization time is dramatically reduced, as shown in Fig. 5. For instance, for $N = 21$, $K = 3$, $L = 3$, synchronization is achieved after 12 bit packages if the size of the package is larger than $B \geq 32$.

Several partners: Up to now we have discussed the scenario of two partners exchanging secret information. But our method can be extended to the case of a pool of several participants sharing secret information. In this case we would like to transmit information among several partners, but only if all of them are available to act cooperatively. The mutual information is the global flow of information, namely the output bits of all participants. Assume that we would like to build a common private key among an even number Q of partners, each of them represented by a PM. In each time step each of the Q partners is exposed to the Q outputs O^1, ..., O^Q. In case $O^q = -O^{q+1}$ for $q = 1$, ..., $Q - 1$ the learning step is performed. In our simulations we find, for instance, that for $N = 61$, $K = 3$ and $L = 3$ for $Q = 4$, 6, 8 the average synchronization time is 640, 1023, 2430 respectively.

Generation of inputs: A common public input can be generated following a public seed number for a random number generator. The main disadvantage of this method is that the number of new random variables necessary to define a common input is of order $O(N)$. A simple way to overcome this difficulty is to shift all of the $3N$ input units one place to the right and to set the left-most input equal, for instance, to the output of the sender[21,22].

Permutation of the weights: In order to increase the security of our channel, one can apply the following types of permutations: (a) To permute a fraction (or all) of the weights belonging to an updated hidden units. (b) A global permutation of weights belonging to an updated hidden unit with weights belonging to other hidden units. (c) The fraction of permuted weights increases as the parties approach synchronization. It is clear that the permutations are following a public protocol, but the internal presentations of the parties are hidden. Our simulations indicate the following main results: (a) Synchronization between the parties is achievable under these classes of permutations, but t_{synch} increases. (b) The overlap between an attacker and one of the parties at the synchronization time is reduced by the permutation among the weights, and the system is more robust with respect to advanced attacks[20].

This work profitted from enjoyable collaborations with Richard Metzler and Michal Rosen-Zvi. The work is supported in part by the German Israel Science Foundation (GIF).

References

1. D. R. Stinson, *Cryptography: Theory and Practice* (CRC Press 1995)
2. R. L. Rivest, A. Shamir and L. Adelman, *Comm. of the ACM* **21**, 120 (1978).
3. I. Kanter, W. Kinzel and E. Kanter *Secure exchange of information by synchronization of neural networks*, Europhys. Lett. **57**, 141 (2002).
4. J. Hertz, A. Krogh, and R. G. Palmer: *Introduction to the Theory of Neural Computation*, (Addison Wesley, Redwood City, 1991)
5. A. Engel, and C. Van den Broeck: *Statistical Mechanics of Learning*, (Cambridge University Press, 2001)
6. M. Opper and W. Kinzel: Statistical Mechanics of Generalization, *Models of Neural Networks III*, ed. by E. Domany and J.L. van Hemmen and K. Schulten, 151-20 (Springer Verlag Heidelberg 1995)
7. M. Castelo-Branco, R. Goebel, S. Neuensehwander and W. Singer, Nature **405**, 685 (2000).
8. A. K. Engel, P. König and W. Singer, Nature **405**, 685 (2000).
9. J. K. Lin, U. Ernst and T. J.Sejnowski, Networks: Computation in Neural Systems **9**, 333 (1998).
10. R. Ritz and T. J.Sejnowski, Artificial Neural Networks -ICANN 97, 7th International Conference Proceedings, Eds by W. Gerstner, A. Germond, M. Hasler and J. D. Nicoud, Springer-Verlag, 1997, page 79.
11. A. Riehle, S. Grun, M. Diesmann and A. Aertsen, Science **278**, 1950 (1997).
12. C. M. Gray, P. König, A. K. Engel and W. Singer, Nature **338**, 334 (1989).
13. M. Biehl and N. Caticha: Statistical Mechanics of On-line Learning and Gen-

eralization, *The Handbook of Brain Theory and Neural Networks*, ed. by M. A. Arbib (MIT Press, Berlin 2001)
14. E. Barkai and I. Kanter, Europhys. Lett. **17**, 181 (1991).
15. J. L. van Hemmen, G. Keller and R. Kühn, Europhys. Lett. **5**, 663 (1988).
16. In fact, such a scenario has recently been studied by R. Metzler, W. Kinzel and I. Kanter, Phys. Rev. E **62**, 2555 (2000), and W. Kinzel, R. Metzler and I. Kanter J. Phys. A **33** L141 (2000), for two perceptrons with continuous weights and normalized weight vectors. However, we find that for such a system an outside observer can find the internal state of both perceptrons by learning the communication. Furthermore, the normalization of the weight vector after each learning step is a non-local operation and is violating the linear complexity of our cryptosystem.
17. M. Rosen-zvi, I. Kanter and W. Kinzel cond-mat/0202350
18. As for the hardware implementation of our cryptosystem, the calculation of the local fields, eq. (1), are similar to a linear filter which can be implemented in parallel using existing technologies. Hence, the complexities of calculating local fields of the hidden units are taken as order $O(1)$ and the synchronization process is of $O(1)$ only.
19. Note that the average learning time for $N = 101$ scales exponentially with L and for $L = 1, 2, 3, 4$, was found in simulations to be equal to $58, 1480, 90380, \sim 10^7$. For a comparison the average synchronization time for $L = 4$ is ~ 950 only. These results indicate that our construction may be secure even as a stream cipher.
20. I. Kanter and W. Kinzel (unpublished).
21. E. Eisenstein, I. Kanter, D. Kessler and W. Kinzel, Phys. Rev. Lett. **74**, 6 (1995).
22. I. Kanter, D. Kessler, A. Priel and E. Eisenstein, Phys. Rev. Lett. **25**, 2614 (1995).

DISCUSSION

Chairman: E. Polzik

An introduction to the discussion

The talk of Ido Kanter concentrated on another type of cryptosystem: secure and linear cryptosystems using error-correcting codes. A public-key cryptosystem procedure based on a Gallager-type parity-check error-correcting code is presented. The complexity of the encryption and the decryption processes scale linearly with the size of the plaintext Alice sends to Bob. The public-key is pre-corrupted by Bob, whereas a private-noise added by Alice to a given fraction of the ciphertext of each encrypted plaintext serves to increase the secure channel and is the cornerstone for digital signatures and authentication. Various scenarios are discussed including the possible actions of an attacker as eavesdropper or as a disruptor. For more details please see Europhys. Lett. 51, 244 (2000).

G. Leuchs: What role does the added noise play?

I. Kanter: The idea is to use error-correcting codes as a cryptosystem. Usually one thinks of the noise in the following way: we prepare the message here, then we transmit it, and noise is somehow added during the transmission. However, in this case, we do not have noise added through the transmission, but Alice adds private noise.

We can use this private noise for identification, signature and so on. Moreover, I would like to emphasize here that the cryptosystem should be considered not only as decryption and encryption, but also in terms of other tasks of the secure channel such as stamping, signature and authentication which are no less important than encryption and decryption. The second point I would like to stress to the community here is the need to think about an attacker which, besides eavesdropping over the channel, can also act as a disruptor. I cannot be certain that all the cryptosystems presented during this conference are robust against an attacker acting as a disruptor.

G. Leuchs: So Bob has to know the noise, that private noise?

I. Kanter: No. Bob uses the decoder to split the message (signal) and noise. In addition we can use the private noise, for instance, in order to add more information, because it is not a random noise. The purpose of the noise is to hide the information, and the amount of noise should be less than the channel capacity.

G. Zeng: Do you think this is the case when you use quantum bits?

I. Kanter: I'm not sure. I have thought about it but I think one should try to find the quantum interpretation of the two matrices in the Gallager code. At the moment I don't know the interpretation.

A. Ekert: My comment is that McEliece proposed cryptosystems resulting in a kind of quantum immune. It is not obvious how to attack them with the current knowledge about quantum algorithms.

I. Kanter: I agree. By the way, the cryptosystem I proposed was first suggested by McEliece. The complexity of the encryption/decryption processes is of order N^2 since McEliece used dense matrices. It's not so easy to choose sparse matrices such that the inverse matrices are sparse, too.

This page intentionally left blank

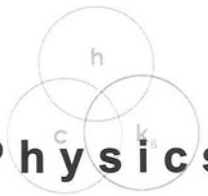

The Physics of Communication

Proceedings of the XXII Solvay Conference on Physics

This volume presents the state of the art in the research on new possibilities for communication and computation based on quantum theory and nonlocality, as well as related directions and problems. It discusses challenging issues: decoherence and irreversibility; nonlocality and superluminosity; photonics; quantum information and communication; quantum computation.

World Scientific
www.worldscientific.com
5334 hc

ISBN 981-238-449-9
9 789812 384492